



Composites in Civil Engineering



International Institute for FRP in Construction (IIFC)

CICE 2006

December 13-15, 2006

Miami, Florida, USA

Editors:

Amir Mirmiran, Florida International University
and Antonio Nanni, University of Miami

Copyright © 2006

To contact the editors:
Amir Mirmiran
Department of Civil and Environmental Engineering
Florida International University
10555 West Flagler Street, Suite 3600
Miami, Florida 33174
Tel (305) 348-3055
Fax (305) 348-2802
E-mail: mirmiran@fiu.edu

All rights reserved, including rights of reproduction and use in any form or by any means, including making of copies by any photo process, or by any electronic or mechanical device, printed or written or oral, or recording for sound or visual reproduction or for use in any knowledge or retrieval system or device, unless permission in writing is obtained from the editors.

The papers in this volume have been peer reviewed by individuals who are expert in the subject areas of the papers. However, the statements or opinions expressed in each paper are solely those of the individual authors. The editors are not liable for any loss or damage caused by any potential error or omission in each paper, whether such error or omission is the result of negligence or any other cause. Any and all such liability is disclaimed herein.

The proceedings includes a copy protected CD attached on the back cover. The CD contains the conference papers. Adobe Acrobat Reader® is needed. No other special installation is required. More detailed information is available on the CD as readme text file.

Printed in the United States of America
First Printing: November 2006

ISBN: 0-615-13586-2

Preface

Applications of fiber reinforced polymer (FRP) composites in civil engineering has increased significantly in recent years, both for the strengthening of existing structures and for new construction. The *Third International Conference on Composites in Civil Engineering* (CICE 2006) is the official conference of the International Institute for FRP in Construction (IIFC). The aim of this conference is to provide an international forum for all concerned with the application of FRP composites in civil engineering to exchange recent advances in both research and practice. The first of this series of conferences was held in Hong Kong in 2001, followed by one in Australia in 2004.

This conference is also sponsored by the American Concrete Institute (ACI), the American Society of Civil Engineers (ASCE) and its Structural Engineering Institute (SEI), the Canadian Society for Civil Engineers (CSCE), and the Intelligent Sensing for Innovative Structures (ISIS) Canada Research Network.

A total of 179 papers are included in this volume, covering a range of topics including bond and development, bridge applications, bridge decks, composite and hybrid systems, confinement issues, creep and sustained loads, fatigue and durability issues, design guides, FRP reinforcing bars, health assessment, masonry structures, modeling, novel applications, prestressing applications, repair of columns, repair techniques, retrofit of slabs, seismic applications, shear retrofit, and strengthening of concrete and metal structures. The technical papers in this volume not only address analytical and experimental work, but also cover field applications, and design and construction guidelines.

The papers in this volume are authored by experts in the field from 28 different countries around the world, including Australia, Belgium, Brazil, Canada, Chile, China, Czech Republic, Denmark, France, Germany, Hong Kong, Iran, Ireland, Israel, Italy, Japan, Malaysia, the Netherlands, Oman, Poland, Portugal, Saudi Arabia, South Korea, Sweden, Switzerland, Turkey, United Kingdom, and the US.

This volume of valuable reference articles would not have been possible without the help, dedication, and collaboration of numerous individuals. First and foremost, we thank the authors for meeting our various submittal deadlines, allowing this document to represent the most current work on the subject from around the world. We would also like to thank the Organizing Committee and the International Advisory Committee of the conference for their relentless efforts in making this conference a reality. It is also important to thank the Executive Committee and the Council of the International Institute for FRP in Construction (IIFC) for their support throughout this process.

The conference is co-organized by the Florida International University and the University of Miami. Sincere thanks to Ms. Dora Hernandez, Ms. Lilia Silverio,

Ms. Rui Zheng, Mr. Bin Li, and Mr. Yilei Shi for their assistance with the various aspects of the daunting task of putting together this conference and the proceedings.

The Editors
Amir Mirmiran, Florida International University
and Antonio Nanni, University of Miami

Miami, Florida
December 2006

Conference Organization

Conference Chairs

Amir Mirmiran	Florida International University	Miami, Florida
Antonio Nanni	University of Miami	Miami, Florida

Organizing Committee

M. Arockiasamy	Florida Atlantic University	Boca Raton, Florida
S. Azhar	Auburn University	Auburn, Alabama
J. Busel	American Composites Manufacturers Association	Arlington, Virginia
R. El-Hacha	University of Calgary	Calgary, Canada
A. Fam	Queen's University	Kingston, Canada
H.R. Hamilton	University of Florida	Gainesville, Florida
R. Sen	University of South Florida	Tampa, Florida
M. Shahawy	SDR Engineering, Inc.	Tallahassee, Florida
L. Spainhour	Florida State University	Tallahassee, Florida
L. Zhao	University of Central Florida	Orlando, Florida
Z.Y. Zhu	URS Corporation	Miami, Florida
R.F. Zollo	University of Miami	Miami, Florida

International Advisory Committee

B. Bakht	JMBT Structures Research Inc.	Canada
C.E. Bakis	Pennsylvania State University	USA
L.C. Bank	University of Wisconsin-Madison	USA
N. Banthia	University of British Columbia	Canada
J.F. Chen	University of Edinburgh	UK
E. Cosenza	Università Federico II	Italy
M. Erki	Royal Military College	Canada
H. Fukuyama	Building Research Institute	Japan
K. Ghavami	Pontificia universidade Catolica/PUC-Rio	Brazil
I. Harik	University of Kentucky	USA
L. Hollaway	University of Surrey	UK
V.M. Karbhari	University of California, San Diego	USA
T. Keller	Swiss Federal Institute of Technology Lausanne	Switzerland
P. Labossière	Université de Sherbrooke	Canada
Z.T. Lu	Southeast University	China
A. Machida	Hokkaido University	Japan
U. Meier	European Maritime Pilots' Association	Switzerland
M. Mottavalli	University of Tehran	Iran

A. Mufti	University of Manitoba	Canada
K. Neale	Université de Sherbrooke	Canada
D.J. Oehlers	University of Adelaide	Australia
S. Rizkalla	North Carolina State University	USA
S. Saiidi	University of Nevada, Reno	USA
L. Taerwe	Ghent University	Belgium
B. Taljsten	Skanska Company	Sweden
K.H. Tan	National University of Singapore	Singapore
J.G. Teng	Hong Kong Polytechnic University	China
T. Triantafillou	University of Patras	Greece
T. Ueda	Hokkaido University	Japan
G. Van Erp	University of Southern Queensland	Australia
P. Waldron	University of Sheffield	UK
Z.S. Wu	Ibaraki University	Japan
L.P. Ye	Tsinghua University	China
Q.R. Yue	National Diagnosis and Rehabilitation of Industrial Building Research Center	China
X.L. Zhao	Monash University	Australia

TABLE OF CONTENTS

Preface

Conference Organization

Keynote Papers

The Prognosis of FRP Composites in Construction from a Worldwide Perspective 1
Len Hollaway

Future of FRP in Far EAST 11
Ueda Tamon

Part I. Bond and Development

Bond Tests on Concrete and Masonry Blocks Externally Bonded with FRP 17
Francesca Ceroni and Marisa Pecce

Cohesive-Bridging Zone Model of the FRP-Concrete Interface Debonding 21
Jialai Wang

Constitutive Model for Time Dependent Bonding and Debonding along FRP-Concrete Interface 25
Hesham M. Diab and Zhishen Wu

Debond Characteristics of Carbon Fiber Laminates for Bridge Rehabilitation 29
M. Arockiasamy, M. Sivakumar and M. Shahawy

Debonding of CFRP Laminates Externally Bonded to Concrete Specimens at Low and High Temperatures 35
Ernst Lucas Klamer, Dick Hordijk and Cees S. Kleinman

Effects of Bond Configurations on Flexural Response of RC Beams Externally Strengthened with CFRP Sheets 39
Jiangguo Dai, Keisuke Sumiyoshi, Tamon Ueda, Hiroshi Yokota and Yasuhiko Stao

Environmental Sensitivity and Defect Criticality in FRP Bond to Concrete Through a Fracture Mechanics Approach 43
Rajiv Navada and Vistasp M. Karbhari

Improving the Bonding and Ductile Behavior of FRP Strengthened RC Beams 47
H. Fatemi, A. Davaran and J. Esmaili

Intermediate Crack Debonding Analysis of Reinforced Concrete Beams Strengthened with Externally Bonded FRP Plates 51
Luciano Ombres

Evaluation of FRP Bond Specifications for Development Lengths <i>Nathan Newman, Ashraf Ayoub and Abdeldjelil Belarbi</i>	55
Practical Use of Pull-off Strength Testing (ASTM D4541) for Assessing Quality of FRP-to-concrete Bond <i>Kent A. Harries</i>	59
Prediction of Bond Failure of Concrete Prisms Bonded with FRP Composites <i>H. Toutanji, P. Saxena and L. Zhao</i>	63
Strength Model for Intermediate Crack Debonding in FRP-Strengthened Concrete Members Considering Adjacent Crack Interaction <i>J. F. Chen, J. G. Teng and J. Yao</i>	67
Study on Bond Characteristics of CFRP/Steel Double-Lap Shear Joints at Subzero Temperature Exposure <i>Ahmed Al-Shawaf, Riadh Al-Mahaidi and Xiao-Ling Zhao</i>	71
The Mechanism of Effect of Structural Span on Intermediate Crack-induced Debonding <i>Hemdan Okasha Ahmed Said and Zhishen Wu</i>	75
Strain Rate Effects on Strength of Unidirectional FRP Fabrics and Bond to Concrete <i>M. Saiid Saiidi, Rita Johnson and E. Manos Maragakis</i>	79
Bond Behavior of CFRP Strengthened Full-Scale Prestressed Concrete Bridge Girders <i>O. Rosenboom and S. Rizkalla</i>	83
Bond Characteristics of GFRP Post-Installed Anchors <i>Ehab A. Ahmed, Ehab F. El-Salakawy and Brahim Benmokrane</i>	87
Effect of Adhesive Modulus on the Monotonic and Fatigue Behavior of Externally Bonded CFRP Strips <i>Kent A. Harries, Andrew Zorn and Benjamin Reeve</i>	91
Experimental Study on the Local Bond Behavior of NSM-FRP Bars to Concrete <i>Donatella Galati and Laura De Lorenzis</i>	95
 Part II. Bridge Applications	
A Case Study of Life Cycle Cost Based on a Real FRP Bridge <i>Itaru Nishizaki, Nobufumi Takeda, Yoshio Ishizuka and Takumi Shimomura</i>	99
Structural Rehabilitation of an Off-System Bridge Using External Bonded CFRP Laminates <i>Nestore Galati, Andrea Rizzo and Antonio Nanni</i>	103

Enhancement of Shallow Depth Patches for Concrete Bridges using FRP Overlays <i>Golrokh Nossoni, Ronald S. Harichandran and Rigoberto Burgueño</i>	107
Experimental Study on Prestressed Concrete Girders Strengthened with CFRP Tapes at Different Bridge Repair Stages <i>Arkadiusz Mordak and Zbigniew Manko</i>	111
Feasibility Study of Thermoplastic Wrap for Bridge Protection <i>Nasim Uddin, John D Purdue and Uday Vaidya</i>	115
Field Tests of Prestressed Concrete Beams of Road Bridge Spans Strengthened by CFRP Tapes <i>Zbigniew Manko and Arkadiusz Mordak</i>	119
Blast Mitigation of A Concrete Arch Bridge Using Composites <i>Achille Devitofranceschi, Domenico Asprone, Andrea Prota, Renato Parretti and Antonio Nanni</i>	123
Performance of FRP Retrofitted Bridges under Blast Loading <i>Rui Zheng and Amir Mirmiran</i>	127
Design and Analysis a 10-m FRP Deployable Bridge <i>R. G. Wight, M.A. Erki, C. T. Shyu, R. Tanovic and A. Xie</i>	131
Response of No-Name Creek FRP Bridge to Static Loads, Moving and Impact Traffic Loads <i>Eric Zhou, Youqi Wang, David Meggers and Jerry Plunkett</i>	135
 Part III. Bridge Decks	
Behaviors of New Generation of FRP Bridge Deck with Outside Filament-wound Reinforcement <i>Peng Feng and Lieping Ye</i>	139
Tests of a FRP Deck Panel at Very Cold Temperatures <i>Z. John Ma and Usha Choppali</i>	143
Static and Fatigue Testing of Innovative All-Composite Bridge Deck Slab <i>René J. Roy, Mathieu Robert, Brahim Benmokrane, Ahmed S. Debaiky and Hossein Borazghi</i>	147
Rapid Construction of Concrete Bridge Deck Using Prefabricated FRP Reinforcement <i>Fabio Matta, Antonio Nanni, Thomas E. Ringelstetter and Lawrence C. Bank</i>	151
Testing of an FRP Deck System for Moveable Bridges <i>Lei Zhao, Jignesh S. Vyas and Marcus Ansley</i>	155

Part IV. Composites Systems

Urban Light Transport (ultra) Guideway Project <i>Thanongsak Imjai, Maurizio Gaudagnini, Kypros Pilakoutas and Peter Waldron</i>	159
Composite Sandwich Wall Panels for Building Applications <i>Waleed Shawkat, Hart Honickman and Amir Fam</i>	163
Behavior of Jute/Epoxy Composite Curved I-Beam under Bending Loading <i>Asad A. Khalid</i>	167
Load Carrying Capacities of Pultruded FRP Sheet Piling <i>Yixin Shao and Fabien Darchis</i>	171
A Case Study on Life-cycle Assessment of Environmental Aspect of FRP Structures <i>Hirokazu Tanaka, Hitoshi Tazawa, Morio Kurita and Takumi Shimomura</i>	175

Part V. Confinement Issues

Axial Behavior of Circular Columns Confined with Fiber-Reinforced Polymer Jackets <i>Azadeh Parvin and Aditya S. Jamwal</i>	179
CFRP Confined Ultra High Strength Concrete Columns <i>Adnan R. Malik and Stephen J. Foster</i>	183
Strengthening of Short Circular RC Columns with FRP Jackets: A Design Proposal <i>T. Jiang and Jin-Guang Teng</i>	187
Experimental Study on Concrete Columns Strengthened with CFRP Sheet Confinement under Eccentric Loading <i>Shuangyin Cao, Denghu Jing and Ning Sun</i>	193
Influence of Radius of Corners in Concrete Columns Confined with FRP Sheets <i>Giuseppe Campione, Nunzio Miraglia and Maurizio Papia</i>	197

Part VI. Creep and Sustained Loads

Serviceability of High Strength Concrete Beams with Internal FRP Reinforcement Under Sustained Load <i>Shawn P. Gross, Joseph Robert Yost and Jonathan V. Crawford</i>	203
Deformational Behavior of FRP Confined Concrete Under Sustained Compression <i>Rajeev Kaul, R. Sri Ravindrarajah and Scott T. Smith</i>	207
Long-Term Behavior of CFRP Laminates: An Experimental Study <i>Francesco Ascione and Geminiano Mancusi</i>	211

Creep Tests on GFRP Pultruded Shapes Stiffened with Carbon Fiber Sheets <i>Marina Bottoni, Claudio Mazzotti and Marco Savoia</i>	215
 Part VII. Design Guides	
A Design Procedure of FRP Confining Systems for Upgrade R/C Columns <i>Angela Di Nardo, Ciro Faella and Roberto Realfonzo</i>	219
Design and Manufacturing of Low Cost Thermoplastic Composite Bridge Superstructure <i>Nasim Uddin, Abdul Moeed Abro and Uday Vaidya</i>	223
Italian Design Guidelines for the Strengthening of Existing Civil Constructions Using Externally Bonded Fiber Reinforced Polymers <i>Luigi Ascione, Andrea Benedetti, Antonio Borri, Angelo Di Tommaso, Luciano Feo, Roberto Frassine, Gaetano Manfredi, Giorgio Monti, Antonio Nanni, Maurizio Piazza, Carlo Poggi and Elio Sacco</i>	227
Large-Size Reinforced Concrete Columns Strengthened with Carbon FRP: Validation of Existing Design Guidelines <i>Silvia Rocca, Nestore Galati and Antonio Nanni</i>	231
Torsion Design of CFRP Plated RC Members <i>Adrian K. Y. Hii and Riadh Al-Mahaidi</i>	235
Analysis and Design of FRP Reinforced Concrete Columns <i>Ching Chiaw Choo and Issam E. Harik</i>	239
Probabilistic Design of FRP Strengthening of Concrete Structures <i>Anders Carolin</i>	243
Thresholds of Construction Anomalies in FRP Repair Systems <i>Baris Yalim, Serhat Kalayci and Amir Mirmiran</i>	247
Static and Dynamic Performance of FRP Deck Bridges under Vehicle Loading and Implications in Design <i>Y. Zhang and C. S. Cai</i>	251
Load and Resistance Factor Design for FRP Strengthening of Concrete Structures <i>Rebecca A. Atadero and Vistasp M. Karbhari</i>	255
Czech Guidelines for Strengthening of Concrete Bridges by Composites <i>Miroslav Černý</i>	259

Part VIII. Durability Issues

- Deterioration Mechanism of Bond between CFRP Plate and Concrete in Moist Environment 263
Zhenyu Ouyang and Baolin Wan
- Durability Approach for GFRP Rebars 267
Andre Weber
- Durability Assessment of Adhesives and Reinforcement at the FRP-Wood Interface 271
Gary M. Raftery, Annette M. Harte and Peter D. Rodd
- Durability of Steel Members Strengthened by CFRP Strips under Mechanical and Environmental Loading 275
Pierluigi Colombi, Giulia Fava and Carlo Poggi
- Effect of Surface Deterioration on Stress Transfer between Concrete and FRP Laminate 279
Amnon Katz

Part IX. Fatigue Issues

- Fatigue Behavior of Externally Bonded Steel Fiber Reinforced Polymer (SFRP) for Retrofit of Reinforced Concrete 283
Kent A. Harries and Patrick L. Minnaugh
- Fatigue Performance of Concrete Bridge Deck Slabs Reinforced with Glass FRP Composite Bars 287
Amr El Ragaby, Ehab El-Salakawy and Brahim Benmokrane
- Fatigue Process of Adhesively Bonded Joints from Pultruded GFRP Adherends 291
Ye Zhang and Thomas Keller
- Prediction of the Extended Fatigue Life of Strengthened Bridge Deck with FRPs 295
Hongseob Oh, Jongsung Sim and Minkwan Ju
- Static and Fatigue Investigation of Bridge Deck Cantilevers 299
Chad Klowak, Aftab Mufti and Baidar Bakht

Part X. FRP Bars

- Environmental Considerations in Using FRP Rebars in Concrete Pavements 303
Amnon Katz
- Evaluation of Crack Widths in Concrete Flexural Members Reinforced with FRP Bars 307
Charles E. Bakis, Carlos E. Ospina, Timothy E. Bradberry, Brahim Benmokrane, Shawn P. Gross, John P. Newhook and Ganesh Thiagarajan

The Performance of Curved Non-Ferrous Reinforcement for Concrete Structures <i>Thanongsak Imjai, Maurizio Gaudagnini, Kypros Pilakoutas and Peter Waldron</i>	311
Flexural Testing of Spun-Cast Hollow Concrete Pile Sections Reinforced with CFRP Grid and Bars <i>Antonis Petrou Michael and H. R. Hamilton III</i>	315
Use of GFRP Bars as Reinforcement for Concrete Bridge Deck Slabs <i>Brahim Benmokrane, Ehab El-Salakawy, Sherif El-Gamal and Amr El-Ragaby</i>	319
Optimization of Braided Reinforced Composite Rods <i>Cristiana Gonilho Pereira, Raul Figueiro, Said Jalali and Mário de Araújo</i>	323
 Part XI. Health Assessment	
Nondestructive Evaluation of FRP Bonding by Shearography <i>F. Taillade, M. Quiertant and C. Tourneur</i>	327
Structural Health Monitoring in Cold Climate of a CFRP Strengthened Concrete Hollow Box Girder Bridge <i>Björn Täljsten and Arvid Hejll</i>	331
Structural Health Monitoring of Degrading Concrete Beams in a Laboratory Environment <i>Markus Bergström and Björn Täljsten</i>	335
Debonding Detection in CFRP Strengthened RC Beams Using Active Sensors <i>Seung Dae Kim, Chi Won In, Kelly E. Cronin, Hoon Sohn and Kent Harries</i>	339
 Part XII. Hybrid Systems	
Experimental Study on FRP-Concrete Hybrid Beams <i>Tianhong Li, Peng Feng and Lieping Ye</i>	343
Hybrid Bonding of FRP Laminates to Reinforced Concrete Structures <i>YuFei Wu and Yue Huang</i>	347
Hybrid FRP-Concrete Sandwich Bridge Deck <i>Thomas Keller, Erika Schaumann and Till Vallée</i>	351
Hybrid Square FRP/Steel Grid Tube Confined Concrete Cylinders <i>Manu John and Guoqiang Li</i>	355
Structural Characterization of Composite Sandwich Panel with Hybrid FRP-Steel Core for Bridge Decks <i>Hyo Seon Ji, Byung Jik Son and Z. John Ma</i>	359

Part XIII. Masonry Structures

- Characterization of Masonry Wallettes and Shear Triplet Specimens Retrofitted with GFRP Compoistes 363
S. Suriya Prakash and P. Alagusundaramoorthy
- FRP Composite Reinforcements on Masonry Vaults: Effectiveness and Reliability 367
Alessandro Baratta and Ottavia Corbi
- On the Reinforcement of Masonry Walls by Means of FRP Provisions 371
Alessandro Baratta and Ileana Corbi
- Strengthening Masonry Arches with Composites 375
Giulio Castori, Antonio Borri, Skip Ebaugh and Paolo Casadei
- Prioritized FRP Research for Concrete and Masonry Structures 379
Max Porter and Kent Harries

Part XIV. Modeling

- An Analytical and Numerical Investigation of Debonding Problems in Beams Strengthened with Composite Materials 383
Domenico Bruno, Fabrizio Greco and Paolo Lonetti
- Numerical Analysis of Two-way Concrete Slabs with Openings Strengthened with CFRP 387
Piotr Rusinowski, Ola Enochsson and Björn Täljsten
- Numerical Modeling of FRP Shear Strengthened RC Beams Using Compression Field Theory 391
Zhe Qu, Xinzheng Lu, Lieping Ye, Jianfei Chen and John Michael Rotter
- Numerical Simulation of Bond Deterioration between CFRP Plate and Concrete in Moisture Environment 395
Zhenyu Ouyang and Baolin Wan
- Numerical Study on Masonry Load Bearing Walls Retrofitted with FRP Composites 399
S. Suriya Prakash and P. Alagusundaramoorthy
- Modeling of RC Square Hollow Piers Wrapped with CFRP 405
Gian Piero Lignola, Andrea Prota, Gaetano Manfredi and Edoardo Cosenza
- Prediction of failure Loads of FRP Pultruded profiles Using Closed-form Equations 409
Linda M. Vanevenhoven, Carol K. Shield and Lawrence C. Bank

Theoretical Study on Spalling Resistance of FRP Sheets Bonded to Bent Concrete Surface <i>Hong Yuan and Renhuai Liu</i>	413
Theory of a New Method for Externally Anchored FRP Band Pre-Stressed Reinforcement <i>Jing Zhuo and Tangning Li</i>	417
Post-Buckling Behavior of FRP Composite Thin-Walled Members <i>Nuno Freitas Silva, Nuno Silvestre and Dinar Camotim</i>	421
Fatigue Crack Growth Simulation for CFRP Bonded Steel Plates using Boundary Element Method <i>Hongbo Liu, Xiao-Ling Zhao and Riadh Al-Mahaidi</i>	425
Nonlinear Finite Element Modeling of RC Beams Strengthened with Different CFRP Schemes <i>Rajai Z. Alrousan, Mohammad A. Alhassan and Mohsen A. Issa</i>	429
Finite Element Analysis of FRP Debonding from Concrete Undergoing Global Mixed Mode I/II Loading <i>Baolin Wan and Zhenyu Ouyang</i>	433
Finite Element Modeling of FRP Shear Strengthened RC Beams <i>O. F. A. Ootom, S. T. Smith and S. J. Foster</i>	437
A Finite Element Analysis on Shear and Normal Stresses in Adhesively-Bonded Joints of Composite Structures <i>Luciano Feo and Francesco Ascione</i>	441
Finite Element Modeling of FRP-Filament Winded Poles <i>R. Masmoudi and H. Mohamed</i>	445
 Part XV. Novel Applications	
Advanced Grid Stiffened FRP Tube Encased Concrete Cylinders <i>Guoqiang Li and Dinesh Maricherla</i>	449
Applicability of Fiber Reinforced Plastics to Hydraulic Gates <i>Tomonori Tomiyama and Itaru Nishizaki</i>	453
Stressed Arch Modular Deployable Composite Shelters Concept and Development <i>T. Omar, G Van Erp and P. W. Key</i>	457
Evaluation of Epoxy Encapsulated Timber Piles <i>Nakin Suksawang, Hani Nassif, Ozgul Ozkul, Ali Maher and Abbas Sarmad</i>	461

Part XVI. Prestressing Applications

- CFRP Prestressing Tendons: Solution Uptake and Swelling Effects 467
Paul Scott and Janet Lees
- Experimental Study on Behaviors of Concrete Beams Strengthened with External Prestressing CFRP Tendons 471
Zhi Fang and Hongfang Li
- Post-strengthening of Prestressed Concrete Beams Using Unstressed and Prestressed CFRP Strips 475
Mohammad Reza Aram, Masoud Motavalli and Christoph Czaderski
- Reinforcement Technology by Prestressed Carbon Fiber Reinforced Plastics (CFRP) 479
Shouping Shang, Yongjun Jin, Hui Peng, Ming Wang and Qiaojuan Leng
- Wedge Anchorage for Loaded or Prestressed FRP 483
Stefan L. Burtscher

Part XVII. Repair of Columns

- Evaluation of the Carrying Capacity of RC Columns Strengthened with Composite Materials 487
Emmanuel Ferrier, Marc Quiertant and Patrice Hamelin
- Large-size Reinforced Concrete Columns Strengthened with Carbon FRP: Experimental Evaluation 491
Silvia Rocca, Nestore Galati and Antonio Nanni
- Parametric Analysis of Shape Effects in Concrete Columns Confined with FRP 495
Ricardo Carrazedo and João Bento de Hanai
- Slenderness Effects on Circular FRP-Wrapped Reinforced Concrete Columns 499
Jason Fitzwilliam and Luke A. Bisby
- Theoretical Model for FRP-Confined Circular Concrete-filled Steel Tubes Under Axial Compression 503
Jin-Guang Teng and Y. M. Hu

Part XVIII. Repair Techniques

- Methodological Considerations for Reinforced Concrete Structures Repair Using Posttensioned CFPR Strips 507
José Antonio Bellido de Luna del Rosario
- Physico-chemical and Mechanical Behavior of Fiber Reinforced Repair Mortars 511
Amjad Mallat and Abdenour Alliche

Severely Damaged URM Walls Retrofitted with FRP Strips Subjected to Out-of-Plane Loading	515
<i>C. R. Willis, Q. Yang, R. Seracino, S. H. Xia and M. C. Griffith</i>	
Supporting Conditions Effects in the Out-of-plane Behavior of URM Walls Strengthened with Externally Bonded FRP Strips	519
<i>Ehab Hamed and Oded Rabinovitch</i>	
Two Dimensional Evaluation of Patch Repairs of Structural Elements	523
<i>Sameer Hamoush, Maurice McNeal and Hisham Abdul-Fattah</i>	
Part XIX. Retrofit of Slabs	
Analysis of Debonding Failures in FRP-Strengthened Concrete Beams and Slabs	527
<i>Kenneth W. Neale, U. A. Ebead, W. Elsayed, H. Abdel Baky and A. Godat</i>	
Australian Generic Retrofitting Guideline for Plating RC Beams and Slabs	531
<i>Deric John Oehlers</i>	
Indirect Crack Control Procedure for FRP-Reinforced Concrete Beams and One-Way Slabs	535
<i>Carlos E. Ospina and Charles E. Bakis</i>	
Strengthening of Precast Prestressed Hollow Core Slabs with CFRP Sheets	539
<i>M. K. Rahman, A. H. Al-Gadhib, J. Mohiuddin and M .H. Baluch</i>	
Use of Carbon-Fiber Reinforced Polymers in Slab-Column Connection Repair	543
<i>Widianto, Ying Tian, Jaime Argudo, Oguzhan Bayrak and James O. Jirsa</i>	
Part XX. Seismic Applications	
Seismic Retrofit of Large Scale Circular RC Columns Wrapped with CFRP Sheets	547
<i>G. Wu, Z. S. Wu, Z. T. Lv and D. S. Gu</i>	
Seismic Retrofitting of Reinforced Concrete Columns by Continuous Fiber Rope with Concrete Jacket	551
<i>Takumi Shimomura, Nguyen Hung Phong, Akihiro Matsumoto, Kenzo Sekijima and Kyuichi Maruyama</i>	
Seismic Performance of Hybrid FRP-Concrete Pier Columns	555
<i>Yilei Shi, Bin Li, Amir Mirmiran, and M. Saiid Saiidi</i>	
Experimental Study of FRP Wrapping for RC Bridge Under Seismic Loads	559
<i>Éric St-Georges, Nathalie Roy, Pierre Labossiere, Jean Proulx and Patrick Paultre</i>	
Use of CFRP to Strengthen Poorly Detailed Reinforced Concrete Beams	563
<i>Insung Kim, James O. Jirsa and Oguzhan Bayrak</i>	

Residual Behavior of FRP Retrofitted RC Columns after being subjected to Earthquake Damage <i>Bo Shan, Yan Xiao and Zhengyu Huang</i>	567
Estimation of the Ductility of Web-bonded FRP Beams for Assessment of Strengthened RC Exterior Joints <i>S. S. Mahini and H.R. Ronagh</i>	571
Part XXI. Shear Retrofit	
Parameters Influencing the Behavior of RC Beams Strengthened in Shear with Externally Bonded FRP <i>Omar Chaallal and Abdelhak Bousselham</i>	577
Calculating the Thickness of FRP Jacket for Shear and Torsion Strengthening of RC T-Girders <i>A. Deifalla and A. Ghobarah</i>	581
Calibration of Eurocode-like Equation for the Concrete Contribution to the Shear Capacity of FRP RC Members <i>Raffaello Fico, Andrea Prota, Renato Parretti, Gaetano Manfredi and Antonio Nanni</i>	585
Ductility and Shear Strength Enhancement by Fiber Sheet with Large Fracturing Strain <i>Ueda Tamon, Dhannyanto Anggawidjaja, Senda Mineo, Nakai Hiroshi and Jiangguo Dai</i>	589
Application of Newly Developed GFRP Stirrups for Shear Reinforcement of Concrete Beams <i>Jongsung Sim, Cheolwoo Park, Sungjae Park and MinKwan Ju</i>	593
Repair of Corrosion Damaged Concrete Beams without Shear Reinforcement using Carbon Fiber Reinforced Polymers Sheets <i>Abdullah Al-Saidy</i>	597
Shear Retrofit of Low Strength Reinforced Concrete Short Columns with GFRP Composites <i>Alper Ilki, Idris Bedirhanoglu, Ismail Hakki Basegmez, Cem Demir and Nahit Kumbasar</i>	601
State-of-Practice of FRP Strengthened RC Girders in Shear <i>Abdeldjelil Belarbi, Ashraf Ayoub and Sang-Wook Bae</i>	605
Strengthening of Concrete Beams in Shear with Mineral Based Composites Laboratory tests and theory <i>Björn Täljsten, Katalina Orosz and Thomas Blanksvärd</i>	609

Analytical Prediction of Debonding Failures in RC Beams Strengthened in Shear with NSM FRP Reinforcement 613
Andrea Rizzo and Laura De Lorenzis

Part XXII. Strengthening

Flexural Behavior of Reinforced Concrete Beams Strengthened with Near Surface Mounted CFRP Strips 619
Renata Korynia

Strengthening Choices for the Repair and Retrofit of Concrete Bridge Structures with FRP 623
J. M. Eyre, T. J. Ibell and A. Nanni

Natural Fiber Composites for Strengthening of Glued-laminated Timber in Tension Perpendicular to Grain 627
Alann André, Helena Johnsson and Anders Carolin

Prestressed SRP and CFRP Sheets for Strengthening Concrete Beams 631
Daniel B. Prentice and Gordon Wight

Flexural Strengthening of 48-year Old Pedestrian Bridge Reinforced Concrete Girders 635
Raafat El-Hacha

Strengthening of RC Beams with Prestressed Near Surface Mounted CFRP Rods 639
Moataz Badawi and Khaled Soudki

Strengthening of Steel Bridges Under Low Frequency Vibrations 643
L. Zhang, L. C. Hollaway, J. G. Teng and S. S. Zhang

Structural Strengthening with Externally Bonded SCRP (Steel Cord Reinforced Polymer) 649
Wine Figeys, Luc Schueremans, Dionys Van Gemert and Kris Brosens

Worlds First Bridge with Sprayed FRP Strengthening: Revisited 653
N. Banthia, R. C. Tennyson and A. Mufti

Analysis of Post-tensioned Concrete Road Bridge Beams Strengthened by CFRP Tapes Using FEM Under Static Load 657
Arkadiusz Mordak and Zbigniew Manko

A Review of FRP-Strengthened RC Beam-Column Connections 661
S.T.Smith and R. Shrestha

Anchorage of Carbon Fiber Reinforced Polymer Sheets with and without Height Transition 665
Sarah L. Orton, James O. Jirsa and Oguzhan Bayrak

Effect of FRP U-jacketing Anchorage on FRP-Concrete Interfaces under Fatigue Loading	669
<i>Kentaro Iwashita, Zhishen Wu, Takashi Ishikawa and Yasumasa Hamaguchi</i>	
FRP Upgrade of Concrete Girders to Support Flood Loads	673
<i>Abdelhakim Bouadi, Eric Green and Narendra Gosain</i>	
Tests on FRP-strengthened Timber Joints	677
<i>K. I. Crews and S. T. Smith</i>	
Recent Developments on the Use of Inorganic Polymer for High Temperature/High Strength Composites	681
<i>James Giancaspro and P.N. Balaguru</i>	
The Influence of Fatigue and Aggressive Environment on the Performance of RC Beams Reinforced with CFRP Materials	685
<i>Marco Arduini, Mariano Romagnolo and Antonio Nanni</i>	
Bond Strength of Carbon Fiber Reinforced Polymers on Concrete and Masonry	689
<i>Umit Serdar Camli and Baris Binici</i>	
Compressive Stress-Strain Models of FRP-Confined Concrete	693
<i>Mingxue Liu and Jiaru Qian</i>	
Accelerated Replacing and Construction of Concrete Bridge Decks Using Thin CFRP Stiffened Plates	697
<i>Lijuan Cheng</i>	
Part XXIII. Strengthening of Metals	
Bending Strength of CFRP-strengthened Circular Hollow Steel Sections	701
<i>J. Haedir, M. R. Bambach, X.L. Zhao and R. Grzebieta</i>	
Bond and Splice Behavior of High Modulus CFRP Materials Bonded to Steel Structures	705
<i>M. Dawood and S.Rizkalla</i>	
CRFP-Aluminum Alloy Composite Structures: A New Type of Composite Structures in Future	709
<i>Lieping Ye, Peng Qian and Peng Feng</i>	
Experimental Study on CFRP-Aluminum Alloy Composite Pipes Under Axial Compressive Load	713
<i>Peng Qian, Lieping Ye and Peng Feng</i>	
Rehabilitation of Cracked Aluminum Structures with GFRP Composites Considering Fatigue	717
<i>Chris P. Pantelides and Justin D. Nadauld</i>	

Effectiveness of Different Composite Materials for Repair of Steel Bridge Girders <i>Amr Shaat and Amir Fam</i>	721
Experimental and Numerical Analysis of the Structural Response of FRP-Strengthened Cold-Formed Steel Columns <i>Ben Young, Nuno Silvestre and Dinar Camotim</i>	725
Experimental and Numerical Study of the Debonding Mechanisms in Steel Beams Strengthened by CFRP Strips <i>Pierluigi Colombi, Paolo Dubini, Giulia Fava and Carlo Poggi</i>	729
Experimental Study on Fatigue Behavior of Tensile Steel Plates Strengthened with CFRP Plates <i>Yun Zheng, Lieping Ye, Xinzheng Lu and Qingrui Yue</i>	733
Preliminary Bond-Slip Model for CFRP Sheets Bonded to Steel Plates <i>S. Fawzia, X.L. Zhao, R. Al-Mahaidi and S. H. Rizkalla</i>	737
Flexural Strengthening of Composite Steel-Concrete Girders Using Advanced Composite Materials <i>Raafat El-Hacha and Nora Ragab</i>	741

Keynotes*

*Keynote papers that are available at the time this volume went to press.

THE PROGNOSIS OF FRP COMPOSITES IN CONSTRUCTION FROM A WORLD WIDE PERSPECTIVE

L C Holloway
University of Surrey, Guildford, Surrey, UK.

ABSTRACT

Advanced polymer composites (APC) have hitherto been utilized predominately in the aerospace and marine industries but for the last three decades there has been a growing awareness amongst civil/structural engineers of the importance of the unique mechanical and in-service properties of these materials together with their customized fabrication technologies. These extraordinary properties of APCs have enabled researchers and engineers to innovate and produce techniques in manufacture and design that can be used in the civil engineering infrastructure ranging from the strengthening of reinforced concrete, metallic materials, and the seismic retrofitting of bridges and columns to the use in replacement bridges decks and in the new bridge and building structures. Their lightness, corrosion resistance, potentially high overall durability, tailorability and high specific attributes enable them to be used in areas where the conventional construction materials might be restricted. In spite of these excellent characteristics there are many engineers who are still not convinced of the potential of advanced polymer composites.

This paper will illustrate the advantageous position in which the APC composites industry currently finds itself and how this situation might be further exploited. The discussion will cover a review of APCs in terms of (i) The innovation concept developments of the advanced polymer composite material over the last three decades. (ii) The durability concerns and the reliability of field tests (iii) Addition of additives to improve performance of the APCs in construction. There seems to be no justification for resistance to its use in construction providing the material is understood and designed correctly.

KEYWORDS

Polymer composites, durability, additives, infrastructure rehabilitation, hybrid constructions.

1. INTRODUCTION

Thirty years ago the construction industry, generally, was considered as a low technology, low skill and labour intensive compared with most other industries; this fact was highlighted in a UK report, Latham Report (1994). It is therefore not surprising that the polymer/composites industry did not show interest in the civil engineering industry where the possibility of utilizing new materials and therefore market opportunities were not visible to potential investors. The technological revolution in materials and processing in all other sectors of the manufacturing industry had largely by-passed the construction industry. The mismatch between research investment and construction expenditure meant that construction proceeded on a scale with an inadequate understanding of many aspects such as deterioration mechanism for structures and this often meant that due allowance was not made for practical repair and maintenance. Consequently, when in the early 1970, the initial inception of fibre reinforced polymer (FRP) composites into the building industry was introduced as a semi-load bearing structural material it was hailed by a few engineers as a breakthrough for the FRP composites industry. However, it was reviled by many as an architectural gimmick which would not last. Understandably, during that early period, the progress of the advanced polymer composite (APC) material for civil engineering applications was slow but over the last two decades its utilisation has gained momentum. Currently major structural systems are being constructed completely from APCs or the APCs are used in combination with the more conventional civil engineering materials to form hybrid structures where the component parts of the structural system are used advantageously. Many civil engineers are now convinced of the value of the APC material but still a percentage of engineers require assuring of its potential capabilities. In addition, they do not accept it as being a potential competitor to the conventional heavier construction materials.

All scientific and engineering inventors are keen to exploit their findings and will sometimes make far reaching claims which, at the time, cannot be justified; the initial inventors/users of the 1970s structural FRP systems were no exception. Currently, inventors within the composites field are more restrained in their claims, due possibly to a greater understanding of the material and an upsurge in litigation attitudes. Unfortunately, the claims made during the early 1970s, with no justification, did the FRP composites industry a great deal of harm which was difficult to overcome. Furthermore, during this period small fabricators, consisting of one or two operatives, set themselves up as experts, and were mainly involved in the manufacture of components for load bearing or semi-load-bearing infill panels; these were the systems used at that time and made by the hand lay-up method which is rather primitive by present day standards. These fabricators paid little or no attention to the curing procedure of the composites and as a consequence these units were inadequately cured and within a short period of time, in practical use, commenced to degrade. However, the larger and experienced fabricators manufactured large structural buildings such as Mondial House on the banks of the River Thames and the American Express Building, Brighton, UK, both built in 1974 and currently are showing no signs of deterioration.

This paper illustrates the advantageous position, in which the APC industry currently finds itself, but it discusses some perceived problems. It indicates the skepticism of some civil engineers to the new developments in FRP composites for construction, whether these skepticisms are justified and how this situation might be overcome with further initiatives, exploitations and design codes in the future. The analysis covers the possibilities and realization of APC material. These points are illustrated by introducing the material and potential in terms of (i) Innovations and concept developments, (ii) Durability and long term testing requirements, (iii) Addition of additives to improve a particular property.

2. INNOVATIONS AND CONCEPT DEVELOPMENTS.

2.1 Introduction

The utilization of FRP as a substitute for the more conventional materials must be resisted, unless there is a definite advantage in its use. An example where the APC has taken the initiative is in the rehabilitation of structural members; this topic will be raised late in the paper. Ideally, the FRP material should be designed and used in situations best suited to its properties and material characteristics; this implies innovations and indeed throughout the world a considerable effort is being exerted by researchers examining ways of utilizing composites either as 'all composite' structures or in combination with the more conventional civil engineering materials. This section will demonstrate *some* of the FRP composite concepts which have been developed over the past 30 years and which give an indication of the methodology that should be applied to FRP composite concept developments if the material is to become one of the leading materials of the 21st Century. Composites do have disadvantages and these, of course, must be taken into account when developing a new system; often these disadvantages can be made into 'stepping stones' in the development of a system which is not affected by these disadvantages. The disadvantages can be broadly divided into three groups as:

- (i) Costs compared with other materials used in construction. In this context it must be emphasized that the volume and amount of FRP material used in a similar form of construction is small compared with the conventional material of civil engineering, therefore, they cannot be compared on a weight basis. Nevertheless, cost can still be a problem and innovative ways of forming structural systems must be developed. Examples will be given later where it has been a decided advantage to use APC due to their advantageous long term properties. The whole life costing must be considered in structural work.
- (ii) Fire is a problem with civil engineering structures which are designed as thin systems. On off-shore oil installations FRP are used as fire barriers because of the relative thick composite systems used; is there a possibility here for civil engineering?
- (iii) APCs must be used as tension components. Due to the thin laminates used in construction buckling is a major problem.

2.2 The Building Block System

The gradual implementation of innovative research and construction programmes, since the 1970s, has successfully demonstrated the potential of FRP composites technology for use in construction. This revolution in the use of FRP structural material commenced in the mid-1970s with the building of 'all-composites' construction such as the wet lay-up (hand laminated) randomly orientated glass fibre reinforced polyester polymer (GFRP) composite classroom at Preston Lancashire, UK. The idea was to develop a system which could speed the construction process by using light weight large building blocks to construct the structure. In this example an icoshedron geometrical shape was



Figure 1a Manual fabrication of Building Block GFRP Class Room Lancashire UK

Figure 1b Mechanized fabrication of Building Block Bonds Mill Bridge Gloucester UK.

used for the overall structure and the flat surfaces of the icoshedron were again folded by using four number three sided 'pyramids'. This folded plate structure gained stiffness by the folded nature of its geometrical shape. Experimental tests to destruction were undertaken on coupon specimens made from pristine GFRP composite material and on the building blocks of the structure (the large pyramidal units). To resist fire, 50 mm thick integral skin phenolic foam units were fitted into the building block units; fire tests at the Building Research Establishment, UK were carried out on an assembled four building block unit. The tests showed that the structural unit had over one half hour fire resistance. It was felt at the time that the material and the building block system were very satisfactory for utilization in construction; indeed a whole school system was designed. At that time little thought had been given to the durability of the material, however, field analysis tests undertaken on this structure over the past 35 years have shown that the material has suffered no degradation. In the 1980s the building block system was mechanized when the Maunsell Plank (the building block) was developed by Maunsell Structural Plastics (now Faber Maunsell) and used to form the Aberfeldy bridge in Scotland over the river Tay. The Plank was manufactured by the pultrusion technique and the only manual operation associated with the erection of the bridge was to effect the bonding together of the building blocks and the fabrication of the bridge. The building block (Maunsell Plank) was also used in box beam form (10 plank units) to fabricate Bonds Mill Bridge. This mechanized building block system demonstrated that the idea was sound but it exposed a failing in attitude of civil engineers to readily accept new ideas. From past experience new materials and structural concepts will take twenty or more years to become accepted by the civil engineering industry.

It can be concluded that the building block technique is an ideal procedure to readily produce 'all FRP composite' structures quickly, efficiently and utilizing only a limited number of different structural units.

2.3 The Improvements in Polymers for the Composite Construction

Since the 1970s polymers have been modified and improved for various uses in construction. To some extent this has made the understanding of the material more difficult as every time a new formulation is introduced, a new set of characterization curves have to be produced. Consequently, obtaining information on its long term characteristics are difficult to obtain quickly. In the development of FRP composites for construction, very often the civil engineering industry has drawn upon the knowledge and experience of the aerospace industry to improve the composite materials and manufacturing technologies. Generally the material that has been used to form the civil engineering construction components has been the two part resin and a curing agent system; the resins were initially polyester but these have largely been replaced by the vinylester and epoxy resins. Recently, the pre-impregnated (prepreg) material, which is widely used for patching in the aircraft industry, has been of interest to construction as it has advantages over the two part component material. It is realized, however, that there are subtle differences between the material requirements and the manufacturing technologies for these two industries, but it is the ingenuity and innovation of the material scientist and civil engineer who have modified/changed the polymer component of the composite, the curing procedure and the way in which the final product is utilized to suit the particular civil engineering requirements. This characteristic of being able to tailor the material to meet any desired specification at the time of designing the structural component is a decided advantage over the more conventional civil engineering materials which are normally restricted to specific strength/stiffness values. A new technique for the fabrication of a carbon fibre pre-impregnated with an epoxy polymer, (the material/system, (the prepreg) manufactured by Advanced Composites Group Ltd. Heanor, Derbyshire, UK), was initially introduced into the aerospace industry, the material has been modified considerably for use in the civil engineering industry This innovative system with a film adhesive compatible with the matrix of the composite can be used to upgrade a

concrete or metallic structural member; the polymer is cured at 65⁰C applied for 16 hours under a vacuum assisted pressure of 1 bar. The advantage of this material and the curing system is that the adhesive film is used in conjunction with the prepreg, both can be fabricated in the factory or on site and around members of any geometric shape. The system has been used for the strengthening of metallic structures (Garden 2004) and for the fabrication of the 'Duplex' composite/concrete Spanish bridge beam system, which will be described in Section 2.4.2. The compaction (for minimum voids), the film adhesive system (curing simultaneously with the matrix material of the composite for greater interpenetration contact) and factory or site fabrication method (to provide the upgrading material with an ideal fit to the structure) implies that a high quality composite/bonding system can be employed.

Because of the structural advantages of the technique mentioned above it is possible that this system will be the preferred one for retrofitting structural members in the future.

2.4 Combining Composite/Concrete Material

Concrete, steel and timber have been the prominent materials utilized in the construction industry for many decades and this situation is likely to continue to be the case for the next decade or so, however, advanced materials and in particular the advanced polymer composites have been combined with the more conventional materials for over a decade and the combination have produced a new generation of composite structures which outperform structural systems using individual conventional materials only. This section will discuss these combinations which have been used and new system which are entering the construction industry; these combinations have been developed through the imaginative skills of the civil engineers.

2.4.1 The rehabilitation of degraded bridges or the upgrading to improve the loading capacity of the bridge.

During the late 1980s research and innovation was directed towards systems using FRP composites in conjunction with the more conventional civil engineering materials. In these systems the two dissimilar materials were used to their greatest structural advantage. Initially, structures using this concept tended to be those requiring rehabilitation because of (i) degradation to the parent material due the hostile environment in which the structure was situated, (ii) a change of use of a structural building and (iii) an increase in loading capacity of a bridge or structural building. It was found that the utilization of FRP material in this latter example helped to solve the numerous challenges facing the civil engineer. It has been reported in publications many times that a large number of bridges throughout the world have been classified as functionally obsolete or structurally deficient and require some form of maintenance or major rehabilitation to restore them to their original structural condition. There are many examples of upgraded structures that can be cited Hollaway (2007) and where FRP composites have been successfully used. Although this technique, over the short period of time in which it has been in existence, has been shown to be satisfactory, the long term durability of the joint has yet to be proven.

2.4.2 Structures manufactured from composites and concrete as new structural systems.

The procedures used to upgrade structures were the forerunners of a future technique to combine FRP composites and concrete. This innovative idea was first introduced by Triantafillou and Meier (1992) and the basic concept of this construction has been developed independently by a number of researchers Van Urp *et al* 2003, Canning *et al* (2000), Hulatt *et al* (2003). It consists of placing the bulk concrete in the compression part of a rectangular or Tee section beam and the FRP composite in the tension zone; this latter to resist flexural and shear forces on the beam. As the FRP composite can only be used in relatively thin plate form the interior of the tension part of beams may require a 'permanent shuttering' constructed from, say, a foamed polymer. The advantages of this new concept are a considerable reduction in beam weight, high load carrying capacity and good fatigue behaviour. Researchers at the University of Southern Queensland, Australia have expanded the development into the construction industry where two or three bridges have been built using this technique. From the research work on the combined FRP composite/concrete member (duplex system), undertaken at the University of Surrey UK, an example of a bridge constructed using this system has been erected by NECSO Entrecanales Cubiertas, Madrid, Spain using the material of Advanced Composites Group Ltd. Heanor, Derbyshire, UK. The beam element utilizes the high compressive strength of the concrete and the high tensile strength of carbon fibre; the manufacturing method is by the pre-impregnated FRP technology, using a cure temperature of 65⁰C for 16 hours and a vacuum assisted pressure of 1 bar. The benefits of this system is in the significant cost savings provided due to the lower weight and reduced through life cost of the beam. The opportunities for this technology are remote site installations and refurbishment of infrastructure in developing countries or war regions.

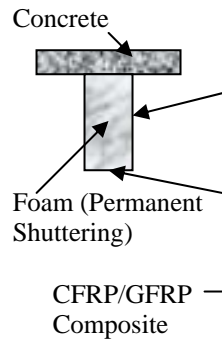


Figure 2a Testing of 5.5 m exp. Beam

Figure 2b Construction of Bridge

NECSO Entrecanales Cubiertas/ACG Bridge, constructed in Spain

Research engineers at the University of Southern Queensland have developed a fibre/polymer composite system that can replicate the appearance and integrity of hardwood timber for the replacement of timber rail and road bridges. The researchers claim that the material stores more carbon dioxide than it release, and it is virtually maintenance-free; researches are now investigating the possibility of making the polymers used in the structure from plant oils rather than fossil fuel oils thus providing a renewable source

Concrete filled steel tubes have been in existence for some time and a variation of this form is two concentric steel tubes with the space between them filled with concrete. Hybrid members in the form of a double skin tube composed of a steel inner tube, a GFRP composite outer tube and a concrete infill in the space between the two tubes has recently been introduced by the research team at The Hong Kong Polytechnic University; the member can be employed as a column or beam. The advantages of this hybrid member over the earlier versions are: (a) The hybrid member exhibits a high degree of ductility. (b) The hybrid section has good corrosion protection, (c) The positioning of the inner steel tube towards the tension zone of the beam provides substantial improvements in flexural stiffness, ultimate load and crack resistance, (Yu *et al* 2006).

2.4.3 Reinforced concrete using FRP rebars.

Over recent years there have been published research papers that have indicated a number of potential problems with this method of using FRP technology as internal reinforcement to concrete and in particular if the fibre used in the composite is a glass fibre. It has been reported by Bank, L. C. and Gentry, R.T. (1995), Sen, et al (2002) and Bank et al, (1998) that accelerated laboratory test results of GFRP in a simulated concrete pore water solution of high pH values and at elevated temperatures up to 80⁰C have indicated that there is a decrease in the tensile, shear and bond strengths,; these results would suggest that there is a case for not using GFRP rebars in concrete, Uomoto (2000). However, Tomosawa and Nakatsuji (1997) have shown that after 12 months exposure to alkaline solutions at temperature between 20⁰-30⁰C, and Clarke and Sheard (1998), likewise, after 2 years exposure to a tropical climate on a test platform off the Japanese coast, have reported that there had been no material or physical deterioration to the GFRP composite. Furthermore, Sheard et al (1997) reported that the overall conclusions of the work of the EUROCRETE project were that GFRP is suitable in a concrete environment. ISIS Canada Research Network of Centers of Excellent, and associated Universities, in Canada, are undertaking long term field exposure analysis and laboratory tests on samples of five GFRP reinforced concrete structures across Canada to provide information on the reliability of GFRP rebar materials, which had been incorporated into a concrete situated in the natural environment for 5 to 8 years. To date no degradation of the GFRP rebars have been recorded. This would indicate that the results from accelerated tests of FRP composite materials should be treated with caution by engineers reading technical papers on this topic and that a thorough understanding of the accelerated test exposure conditions, procedures and reasons for the chemical reactions must be understood.

The prognosis for the utilization of FRP rebars looks encouraging and the indications are that FRP rebars can be used safely over many years.

2.5 Bridge deck replacement.

Many bridges have superstructures of reinforced concrete or steel beams supporting a concrete deck. Typically a concrete deck has a 25-40 year life span. In areas of the world where it is necessary to use deicing salts during the winter period, salt solution enters cracks or percolates through the running surface of the bridge to the reinforced concrete with the possibility of corroding the steel reinforcement. When this deck requires replacement an

innovative and cost effective way of undertaking this task is to replace the bridge deck by high quality factory made FRP components which can be delivered to site and would then be fabricated in an area adjacent to the bridge. The whole bridge deck component can then be lifted in place by a light crane. The advantages of the FRP deck over the conventional one are cost, ease of application, lightweight, high strength and high performance, chemical and corrosion resistant, rapid project delivery and largely factory manufactured. This system has been utilized in the USA for a number of years and was introduced into Europe in 2004, when the old West Mill Bridge, Gloucester, UK. was dismantled and replaced with FRP beams and GFRP ASSET deck system. It may be concluded that the innovative deck system for small to medium span bridges will become one of the major replacements for bridge decks within the foreseeable future.

2.6 Joining FRP composite materials to similar or dissimilar materials.

The chemistry of adhesive systems is generally not well understood by the civil engineer and advice is normally sort from the adhesive manufacturers. Epoxy resins are the best known and most widely used resins for the manufacture of the structural adhesives. There are only a few commercial epoxy resins but a wide range of curing agents, including amines and acid anhydrides which can polymerize these resins. Structural adhesives can be both cold cured, used on construction sites and hot cured, used in a factory environment; all are cross-linked. Ideally the cold cure adhesives should be post cured at an elevated temperature for a limited time depending upon the value of the temperature of cure. All amorphous polymers have a glass transition temperature (T_g) and during service it is unacceptable for the temperature of the adhesive to oscillate above and below the T_g , indeed, the temperature of service should not be taken beyond 20°C below the T_g .

There is a lack of information on the durability and long term physical and mechanical characteristics of adhesive polymers; this area must be investigated urgently.

Generally, the civil engineer does not use the adhesive film when designing large structural systems but a unique technique to the civil engineering industry has been demonstrated by Photiou *et al* (2006) and Zhang *et al* (2006) and has been shown practically by Garden, (2004) that an excellent bond can be achieved between an FRP prepreg composite and the structural steel member (or other general civil engineering material) using a film adhesive compatible with a prepreg matrix of the FRP composite (a composite system is discussed in Section 2.4.2); both of which are cured simultaneously under a vacuum assisted pressure at a slightly elevated temperature. This fabrication procedure and cure method provides an almost void free joint. The joint using the adhesive film has a greater degree of quality control over that of the two part adhesive joint. The thickness of the joint and the curing procedure can readily be controlled. In addition, the film adhesive, due to its thinness (approximately 0.1 mm), has a much reduced free surface area for any moisture or salt solution to enter, thus giving it a better durability characteristic.

The optimum composite joint design is the one capable of distributing stresses over a wide area rather than concentrating them at a point. Adhesively bonded joints can satisfy this requirement; however, most of the adhesive joints have a brittle failure. There have been many attempts to join FRP composite tubular members together when skeletal structures are being fabricated; these structures are in the form of a double layer skeletal roof system, a crane, etc. Three examples are mentioned here of innovative systems which have been developed and involve mechanical fixing for transmitting tensile and compressive forces, such as (i) the clip on fasteners developed by W. Brandt Goldworthy & Associates, Inc. The Snap Joint technology is a similar concept to that used by Kliptico, developed before the Second World War by an Australian firm, as a toy construction kit; structures were formed from a series of steel members which clipped/snapped together. The pultruded composite member (or other manufactured rigid member) which is to be joined to another member by the Snap Joint technology method has one end shaped as a 'fir-tree', and therefore has a large load bearing area, is snapped into another structural member. The 'fir tree' end of the joint is slotted along its longitudinal length to provide enough lateral flexibility to be able to compress when entering the part to be joined. A hole is drilled into the section at the end of the slot to inhibit the crack propagation along the length of the pultruded member. In order to make this joint concept successful, the fibre architecture of the 'fir tree' end must be designed in such a way that the load bearing surfaces have high interlaminar shear strength capacity. (ii) A specially designed exterior end cap with fins to mate with a slotted cover plate to mechanically join other skeletal members at a node point of either an axially loaded member or at skeletal joints. The interior of the end cap has a concentric tube threaded on its outside surface. The precise amount of adhesive is poured between this threaded side and the threaded inside of the end cap thus enabling the adhesive to work its way around the threads as the pultruded, or similar, member is inserted into the annulus (iii) The 'energy' loaded joint to deploy a skeletal structure, this system is described in Fanning and Hollaway (1993) These fixings do not involve bolting through the FRP composite member but uses adhesives to bond the end cap to the tensile/compressive member (item 2) and the energy loaded joint to the structural member (item 3). Figure 3 illustrates the system.



Figure 3a Structure Half Deployed



Figure 3b Structure Fully Deployed

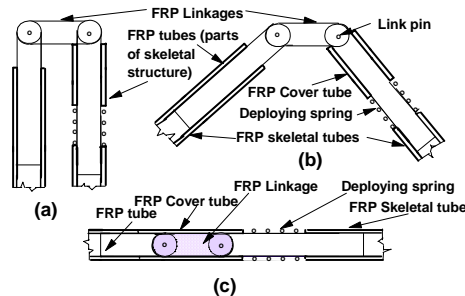


Figure 3c Joint Mechanism

3 DURABILITY AND LONG TERM TESTING OF FRP COMPOSITES

The above mentioned examples of innovative FRP composite structural systems may be considered the early successes of FRP in construction, but the composite material must resist environmental attack over the life of the structure. With conflicting durability test results from research laboratories many of which are derived from accelerated tests and unrealistic elevated temperatures to accelerate the degradation, there remains some uncertainty over the durability of composites. Exposure to high and low temperature variations, moisture and salt solution ingress, ultra-violet rays from the sun and fire will all lead to reduced mechanical performance. A further concern is the durability of ambient-cured systems as these have a relatively low glass transition temperature and may not reach their full polymerization if they have not been post cured before use, thereby, making them more susceptible to degradation. It should be remembered, however, that all engineering materials are sensitive to environmental changes in different ways and those adverse factors mentioned above will not be unique to the FRP materials. Indeed, composite materials do offer some significant durability advantages over the more conventional construction materials; these include superior corrosion and fatigue resistance. These advantageous properties must be exploited further in the future utilization of composite materials.

The only reliable way of estimating durability of composites is to undertake monitoring of the structure over time or field tests. In 2004, ISIS, Canada Research Network of Centres of Excellence, Mufti et al (2005) Mufti et al (2005), Mufti et al (2005), commenced an investigation into five GFRP reinforced concrete structures to provide information on the reliability of GFRP materials, which had been incorporated into a concrete situated in the natural environment for 5 to 8 years. To undertake this task, core specimens of the GFRP reinforcement were removed from the structures, which were located across Canada from east to west; giving a wide coverage of varying natural environmental conditions. These specimens were analyzed to determine any degradation of the E glass fibre and vinyl ester polymer rebars used in the concrete structures. The overall conclusions of the ISIS researchers were that, up to that time, no degradation of the GFRP flexural tension reinforcement had taken place and that the material is durable and compatible with concrete; the tests are continuing.

ADDITION OF ADDITIVES

The polymers that are exposed to natural weathering will deteriorate over time but the degree of deterioration will be dependent upon a number of factors. These may be listed as (i) The type of resin used. (ii) The ultra-violet component of the sunlight and the orientation of the composite relative to the rays of the sun. (iii) The environment

into which the polymer is situated. (iv) Additives which are mixed with the polymer. The additives in the form of particles or chemicals, if used, are mixed with the resin at the time of manufacture of the polymer and the purpose of adding these is to (a) impart fire resistance, (b) to resist the uptake of moisture, (c) to accelerate the cure of the polymer. These additives are impurities with respect to polymer and will affect its mechanical properties.

Probably the most severe attack on the composite is the ingress of moisture. Composite systems can be engineered to provide resistance against diffusion of moisture and aqueous solutions into them, but moisture eventually will diffuse into all organic polymers leading to changes in mechanical and chemical characteristics. The primary effect of diffusion is through hydrolysis and plasticization. This process may cause reversible and irreversible changes to a polymer. The characteristic of the polymer, which may occur, is a lowering of the T_g value and in a composite causing deleterious effects to the fibre/matrix interface bond resulting in a loss of integrity.

Possible solutions for the reduction of diffusion through the polymer is to :-

- (i) apply a protective coating/gel coat on to the system,
- (ii) cure the product at an elevated temperature,
- (iii) utilize factory made composites, such as the pultrusion technique; these composites are manufactured at temperatures of 120⁰C-140⁰C. This ensures low void content, virtually full cure, high levels of overall integrity,
- (iv) use an appropriate sizing/finishes on the fibres of the composites.

An innovative procedure which is being developed for enhancing the resistance of ingress of moisture and aqueous solutions into the polymer is by the addition of nano-particles into it. This innovation by material scientists and engineers could be a major enhancement to the utilization of advanced polymer composites in construction, particularly adhesives.

Chemically treated layered silicates (clays) can be mixed with polymer matrix materials to form a nano-composite in which clay layers are evenly distributed through the material. Research has shown that these high aspect ratio clays alter the properties of the composite by a number of mechanisms, to increase the strength and fire resistance and to reduce permeability. However, as with all new material systems claims and counter-claims have been made and the literature shows that there are a number of conflicting reports as to the percentage improvements that nano-composites can achieve. This might be due to different polymers or curing agents being used in the research or different nano-composites being employed. As in all research it is vital to confirm (i) precisely the materials used viz. the type of clay used, and the surfactant that is mixed into the clay, (ii) the temperature and length of time of mixing of the clays to the polymer, (iii) the type of epoxy polymer that is specified, and (iv) that no chemical additives have been introduced into the polymer before introducing the nano-composites into the resin, [additives are often introduced into the resins by manufacturers of polymers for construction]. Before nano-composite materials can be seriously used in the construction field there are still many questions to be answered, i.e. what will be the extended life-time of the structure if the material is used? Will the material be relevant to on-site wet lay-up processing, or will the use of it be restricted to factory produced products? Will the production of nano-composites be financially viable to civil engineers? One of the advantages in the utilization of nano-composites in civil engineering will be: (i) The improvement in the inter-laminar shear failure of adhesives, (ii) The barrier property improvement of composites and polymers in the construction industry. Both of these items will be of particular relevance to the rehabilitation of structural members. Although nano-particles in FRP composites will reduce the permeability of the pristine polymer and thereby improve the boundary properties, eventually the ingress of solutions will penetrate the FRP composites. It will be realized that all man-made materials do have a finite life and FRP polymer composites are no exception but it is hoped that the improvements that can be made by the addition of nano-particles to civil engineering composites will improve and extend their performance considerably.

THE EUROPEAN UNION SPHERE

The European Commission Joint Research Centre, 2006, has stated that precise EU market share figures for the composite market are difficult to obtain due to its high fragmentation. Furthermore, the composites' market is included with the plastics sector; indeed European Union's statistical data base, the Statistical Office of the European Administration (EUROSTAT), does not collect segregated figures for the composites industrial sector. This logic is also applied by individual Member States. A survey by French Ministerial Organization Service des Études et des Statistiques Industriels (SESSI, 2004), based on the EUROSTAT data, estimated that the composite sector represents 5% (equivalent to €7 billion) of the total EU plastics market, which is estimated to be worth €140 billion. These figures equate to those issued by the Department of Trade and Industry, UK, (DTI, 2001) which estimated the overall revenue of the EU composites industry at €5 billion and was expected to grow by 3.8% annually; these figures were based on figures obtained for 1998. Projecting this figure forward for the market turnover in 2004 would be of the order of €6 billion, a figure very similar to that of the French government. It is

estimated that the industrial sector uses 10% of FRP (e.g. Pressure vessels, piping, chimney, chemical plant applications), and the transportation sector uses 32%; nearly 65% of the total composites market. However, the SSSI report has stated that European market share for plastics exports during the years 1990s and into 2000 fell from 62% to 48% and over the same period the Asian share of the market increased from 12% to 21%. By contrast the USA market use of FRP in Transportation and Construction has grown substantially over the past two decades which indicates a growing importance of the FRP market, in spite of the fact that the USA composites industry has faced many of the problems with which its European counterparts have had to cope. A number of organizations in Europe have been formed to promote the use of composites in construction, including COBRE (based in the Netherlands) and the Network Group for Composites in Construction.(based in the UK) but their funding cannot be compared with that of equivalent programmes currently running in the USA.

The slow development of codes of practice in Europe incorporating advanced composite materials in civil engineering is still seen as a barrier for its more extensive use. The European Commission Joint Research Centre is in the process of presenting to the EU Commission justification for drawing up new codes and standards for the use of FRP composites in civil engineering. Currently, designers rely upon best practice design guidelines, developed by bodies as (i) the International Federation for Structural Concrete (fib) Task Group 9.3, (ii) European Committee for Standardisation, prEN 1504, (iii) CIRIA for the strengthening of steel members, (Cadei *et al.* 2004), or (iv) the American codes issued by the ASCE and ACI. Without codes of practice there will be little motivation to expand the use of FRP composite materials for the European construction sector with the result that the resistance to its use by skeptics will continue.

OBSERVATIONS

The advanced polymer composite material is a unique system and must be designed in such a way as to take full advantage of its extraordinary properties. This implies that innovative ideas must be employed to ensure that its advantageous properties are used to the full. All the examples that have been given in this paper have been dependent upon innovative ideas, which have related to the uniqueness of the material. Currently, and into the foreseeable future, the paper has suggested that the most efficient way of using the APC material is in conjunction with the more conventional materials. The structural component formed from this combination, then uses to the full the advantageous properties of the composite and those of the joining material.

When the whole life costing of a structural unit is taken into account the manufactured composite system will generally be more economical than that made by conventional materials and for the design/build/maintain contracts, composites should be at an advantage. Construction materials have an important role to play in sustainable development through their energy performance and durability, as this determines the energy demand of buildings throughout their lifetime. By developing the use of materials and their combinations, significant improvements of the environment and quality of life can be achieved.

There are currently, some limitations to the use of composites, some of these can be overcome with further research and development (e.g. durability) and some which, at the moment, cannot be overcome (e.g. fire) but research eventually may be able to solve this problem. For instance, it has been claimed by some researchers that a large percentage increase can be achieved in fire properties of composites by incorporating exfoliated nano-particles into the pristine polymer of the composite. If this is economically feasible for the construction industry then other additives which are to be incorporated into the polymer can be included, after the addition of the nano-particles, to impart other particular properties to the composite.

As more results from field tests become available, it is clear that the prognosis for the durability of composite materials, over the life span of a civil engineering structure, shows that the APC is much more durable than had been first realized from laboratory accelerated tests and in many instances is more durable than the conventional civil engineering materials. There seems to be no logical justification for not using composites in construction; indeed the examples given in this paper have indicated the material has considerable advantages in certain applications. However, one must realize that it cannot be used for every type of construction, it must be used sensibly and its limitations must be fully realised.

REFERENCES

Bank, L. C. and Gentry, R.T. (1995) 'Accelerated test methods to determine the long-term behaviour of FRP composite structures: Environmental effects', *Journal of reinforced Plastics and Composites*, Vol 14, pp559-587.

Bank, L. C., Gentry, R.T., Barkatt, A., Prian, L., Wang, F and Mangla, S. R. (1998). 'Accelerated aging of pultruded glass/vinylester rods', *Proceeding 2nd International Conference on Fibre Composites in Infrastructure (ICCI)*, (1998), Vol 2, pp423-437.

Canning, L, Holloway, L. and Thorne, A.M. (2000) 'An investigation of the composite action of an FRP/concrete prismatic beam', *Jnl. Construction and Building Materials*, Vol. 13, Elsevier Ltd. pp417-426.

Cadei, J M C., Stratford, T J. Hollaway, L C. and Duckett, W G. (2004). ‘Strengthening Metallic Structures Using Externally Bonded Fibre-reinforced Polymers’ *CIRIA,RP 645, Publication No. C595, CIRIA, London.*

Clarke, J. L. and Sheard P., (1998). ‘Designing durable FRP reinforced concrete structures’, Proceedings 1st International Conference on Durability of Fibre reinforced polymer (FRP) Composite for Construction (CDCC 1998), Sherbrooke, Quebec, Canada, (1998), pp 13-24.

European Committee for Standardisation, prEN 1504. *Products and systems for the protection and repair of concrete structures; Part 1, General scope and definitions; Part 2, Surface protection; Part 3, Structural and non-structural repair; Part 4, structural bonding; Part 5, Concrete injection; Part 6, Grouting to anchor reinforcement or to fill external voids; Part 7, Reinforcement corrosion prevention; Part 8, Quality control and evaluation of conformity; Part 9, General principles for use of products and system; Part 10, Site application of products and systems and quality control of the work.*

European Commission Joint Research Centre European Lab. for Structural Assessment Institute for the Protection and security of Citizen

Fanning, P. and Hollaway, L C (1993) ‘A case study in the design and analysis for a 5 m deployable composite antenna’. In *Composite Engineering Vol 3 No 11*, pp 1007-10232

fib, (2001). ‘Externally bonded FRP reinforcement for RC structures’ Bull. No 14, Technical Report prepared by Task Group 9.3 Lausanne’

Garden, H. (2004). ‘Refurbishment of Steel Building Using FRP Material’ MSc Module, Department of Civil Engineering, University of Surrey, April 2004.

Hollaway, L C. (2007) ‘Field Survey Applications’ Chapter 12 ‘Durability of Composites for Civil Structural Applications’ Ed. V Karbhari, Publishers Woodhead Publishing Ltd. To be published in 2007.

Hulatt, J., Hollaway, L. & Thorne, A. (2003), ‘Short term testing of a hybrid T-beam made from a new prepreg material’ *ASCE Journal of Composites for Construction*, Vol 7, No. 2 pp 135-145. ISSN 1090-0268

Latham Report (1994) *Government / Industry Review of Procurement and Contractual Arrangements. In, The UK Construction Industry* [HMSO, London, 1994

Mufti, A., Benmokrane, B., Boulfiza, M., Bakht, B. and Breyy, P. (2005). ‘Field study on durability of GFRP Reinforcement’ International Bridge Deck Workshop, Winnipeg, Manitoba, Canada. April 14-15, 2005.

Mufti, A., Onofrei, M., Benmokrane, B., Banthia, N., Boulfiza, M., Newhook, J., Bakht, B., Tadros, G. and Brett, P. (2005) ‘Durability of GFRP reinforced concrete in field structures’, 7th International Symposium on Fiber Reinforcement for Reinforced Concrete Structures (FRPRCS-7), New Orleans Louisiana, USA, November 7-10, 2005.

Mufti, A., Onofrei, M., Benmokrane, B., Banthia, N., Boulfiza, M., Newhook, J., Bakht, B., Tadros, G. and Brett, P. (2005) ‘Report on the studies of GFRP durability in concrete from field demonstration structures’. Proceedings of the Composites in Construction 2005 - 3rd International Conference, eds. Hamelin et al 2005, Lyon, France, July 11-13, 2005.

Photiou, N.K., Hollaway, L.C., and Chryssanthopoulos, M.K. (2006) ‘Selection of CFRP systems for steelwork upgrading’ In press *ASCE Journal of Materials in Civil Engineering*, September/October.

Sen, R., Mullins, G. and Salem, T. (2002). ‘Durability of E-glass/Vinylester Reinforcement in alkaline solution’, *ASI Structural journal* Vol 99, pp 369-375.

Tomosawa, F and Nakatsuji, T (1997) ‘Evaluation of ACM reinforcement durability by exposure tests’, Non-metallic (FRP) reinforcement for concrete structures, Proceedings 3rd International Symposium, Sapporo, (1997) Vol. 2, pp139-146.

Triantafillou, T.C. and Meier, U. (1992) ‘Innovative design of FRP combined with concrete’, Proceedings 1st Int. Conf. Advanced Composite Materials for Bridges and Structures (ACMBS). Sherbrooke, Que., pp491-499.

Sheard, P., Clarke, J.L., Dill, M., Hammersley, G. and Richardson, D. (1997). ‘EUROCRETE – Taking account of durability for design of FRP reinforced concrete structures’- non-metallic (FRP) reinforcement, for concrete structures, Proceedings of 3rd International Symposium, Sapporo, (1997), Vol 2, pp 75-82.

Uomoto, T. (2000). ‘Durability of FRP as reinforcement for concrete structures’ *Advanced Composite Materials in Building and Structures 3rd International Conference*, Ottawa, Ontario, Canada, (2000) pp3-14.

Van Erp, G., Cattell, C and Heldt, T. (2003). ‘Fiber Composites in Civil Engineering – An opportunity for a novel approach to traditional reinforced concrete concepts’ *Proc. Conference in Civil Engineering – Challenges of Concrete Construction VI – Composite Materials in Concrete*, Held at University of Dundee 5-11 September 2003.

Yu, T., Wong, Y L, Teng, J G, Dong, S.L. and Lam, E S S. (2006) ‘Flexural behaviour of hybrid FRP-concrete-steel double skin tubular members’ Accepted for publication *Journal of Composites for Construction*, ASCE.

Zhang L, Hollaway, L C, Teng J-G and Zhang, S S. (2006) ‘Strengthening of Steel Bridges under Low Frequency Vibrations’ Accepted for presentation at CICE 2006, Florida, USA.

FUTURE OF FRP IN FAR EAST

UEDA Tamon
(Professor, Hokkaido University, Sapporo, Japan)

ABSTRACT

This paper briefly introduces the present situation and future of FRP in construction in the Far East, namely Japan, Korea and China, which is a major contributor to FRP in construction in the world. The present situation includes statistics, practical applications, major researches and guidelines/standards. Future directions of FRP in construction in the Far East are presented.

KEYWORDS

FRP reinforcement, FRP shape, Far East, practical application, research, design guideline, standard

1. INTRODUCTION

The Far East including Japan, Korea and China is a major region in the world to produce fibers, which are used for fiber reinforced polymer (FRP) in construction. Japan is a country to produce 17,600 ton of PAN type carbon fiber, which is three quarters of the world production in 2003 (Ishihara and Shibaya 2005). Japan produced 23,000 ton of para-aramid fiber, which is equivalent to USA production of 22,700 ton in 2003 (Ishihara and Shibaya 2005). In 2003 Far East produced 1,250,000 ton of glass fiber (350,000 ton in Japan, 250,000 ton in Taiwan, 150,000 ton in Korea and 500,000 ton in China) which is more than one third of the world production, 3,200,000 ton (Tazawa 2004). China is a major country for FRP products which produced 1,740,000 ton in 2004, while Japan produced 342,000 ton in 2004 (JRPS 2006). FRP in construction shared 32 % of the FRP production in China and 18 % in Japan. Japan is the pioneer country to implement guidelines and standards for FRP reinforcement for concrete (JSCE 1997 and JSCE 2001), while Korea is a leading country to introduce FRP bridges (Kim 2005)

This paper briefly introduces the recent situation and future of FRP in construction in the Far East, namely Japan, Korea and China. FRP in construction means FRP reinforcement for concrete and FRP shape. Types of fiber in FRP include carbon, aramid, glass and some new types of fiber.

2. FRP IN JAPAN

As the pioneer country for application of FRP as reinforcement for concrete and geo structures, Japan has been leading the world in terms of amount of FRP reinforcement used and number of application cases. The amount of FRP rods and cables does not show increase recently. One of its popular applications is ground anchor. FRP sheet, however, shows increase in its amount used and application cases (see Figure 1). Mostly they are with carbon fibers and over 70% of the total cases are for seismic retrofitting of both bridges and buildings. Construction cost of seismic retrofitting with FRP jacketing has become competitive to steel and concrete jacketing (Ueda 2005).

Photo 1 shows a typical example of seismic retrofitting by CFRP sheet, in which the reduction in construction cost due to the lightness was the reason for its application. Recently FRP sheet application for repairing deteriorated concrete surface to prevent concrete pieces from falling apart is getting popular. A good application example of FRP reinforcement for concrete was seen in pedestrian bridge in the ocean (Photo 2). This concrete bridge is steel-free due to severe corrosive environment. Application of FRP shape to actual structures in Japan can be seen in only two cases. One is GFRP pedestrian bridge under severe corrosive environment due to salt attack in Okinawa (Photo 3), and the other is strengthening of existing reinforced concrete bridge deck by adding GFRP beams underneath.

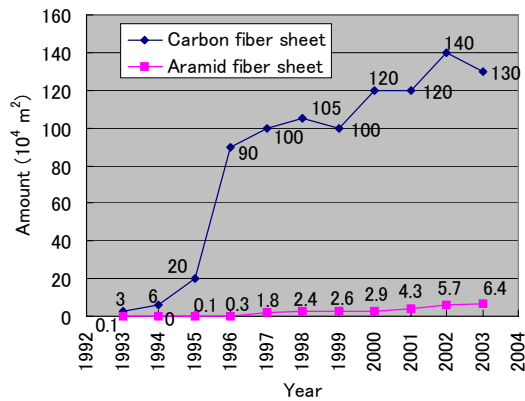


Figure 1: FRP Sheet Amount Used in Japan



Photo 1: Seismic Retrofitting by CFRP Sheet



Photo 2: Steel-free Concrete Bridge with FRP Reinforcement



Photo 3: First FRP Bridge in Japan

Japan is also a pioneer to introduce guidelines and standards for design, materials and construction. The followings are the first in the world for FRP rod/cable as concrete reinforcement and FRP sheet for retrofitting concrete structures for which the English versions are available:

- Recommendation for design and construction of concrete structure using continuous fiber reinforcing materials, which includes quality specifications and test methods (JSCE 1997)
- Recommendation for upgrading of concrete structures with use of FRP sheets which includes test methods (JSCE 2001)

Japan is chairing ISO/TC71/SC6 “Non-traditional reinforcing materials for concrete structures”, which has been drafting standard testing methods for FRP rod/cable/gird and sheet.

In Japan research on FRP in construction is not as active as in the past. However, there are still innovative studies going on and the followings are examples:

- Prestressing technique with PBO sheet for strengthening bridges
- Seismic retrofitting by fiber sheet (PAF sheet and PET sheet) with high fracturing strain
- Hybrid FRP beam consisting of hybrid C-GFRP flanges and GFRP web as a government funded project

3. FRP IN KOREA

In Korea major practical applications of FRP in construction are external bonded FRP sheet and FRP bridge deck. Disastrous accidents in early 1990’s, which were the collapse of Sung-Su Bridge over Han River and of Sam-Pung Department Store, made engineers and researchers in civil engineering start paying serious attention to repair/retrofit of infrastructures. Maintenance works has been keeping 26 % or more of the overall construction works since 2003. One of the repair/retrofit methods used is external bonding with FRP.

Statistics on papers published in the Proceedings of Korea Concrete Institute since 1997 shows steady increase in number of papers on FRP and reached 10.4 % of the total number in 2005. Among the papers on FRP 82.5 % were

related to strengthening, while papers on FRP structural member were 14.6 %. Most popular research target was carbon fiber (59 %) followed by glass fiber (30 %) and FRP sheet (58 %) followed by FRP plate (18 %).

A loading test on actual concrete bridge girders, which was severely deteriorated and retrofitted by external bonded FRP as shown in Photo 4, was carried out in order to verify the proposed standard guidelines. On the other hand, seismic retrofitting technique for piers using FRP wrapping automation device is under development (Photo 5). The wrapping and gluing glass fiber is done automatically by the device. Since this process secures the continuity of the fiber, the confinement stress can be effectively provided. This technique has been applied in the seismic retrofit of two bridges; Seomjin Bridge on a national highway and a bridge on the 88 expressway.



Photo 4: Retrofit of RC Highway Bridge Girder by External Bonded FRP



Photo 5: Seismic Retrofit of RC Highway Bridge Pier by Automated GFRP Wrapping Machine

In Korea there are 8 bridges with FRP deck, two of which are under construction. Six of them are with steel girder, while the remaining two are with concrete girder (see Photo 6). The first one, Beoncheon Bridge of Junbu Expressway was constructed in 2001 with a span of 8 m, while Nucha Bridge in Busan under construction is the largest in the world with a length of 300 m.



Photo 6: Gwanghyang Harbor Bridge (FRP Deck with Steel Plate Girder)

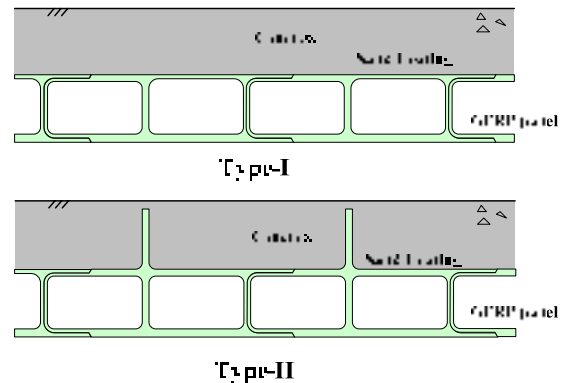


Figure 2: FRP-Concrete Composite Deck

There are various researches on FRP in construction as follows:

- Sheet of basalt fiber produced by molten basalt for better fire resistance
- Near surface mounted method using T-shape CFRP plate
- Wedge-type mechanical anchor for CFRP plate
- FRP-concrete composite deck as “BRIDGE 200” project from 2002 to 2006 (see Figure 2)
- Concrete-filled FRP composite column (cast-in-place type and precast type)

- Hybrid GFRP rod with fiber optic as sensing element and winded glass fiber for bonding (see Figure 3)

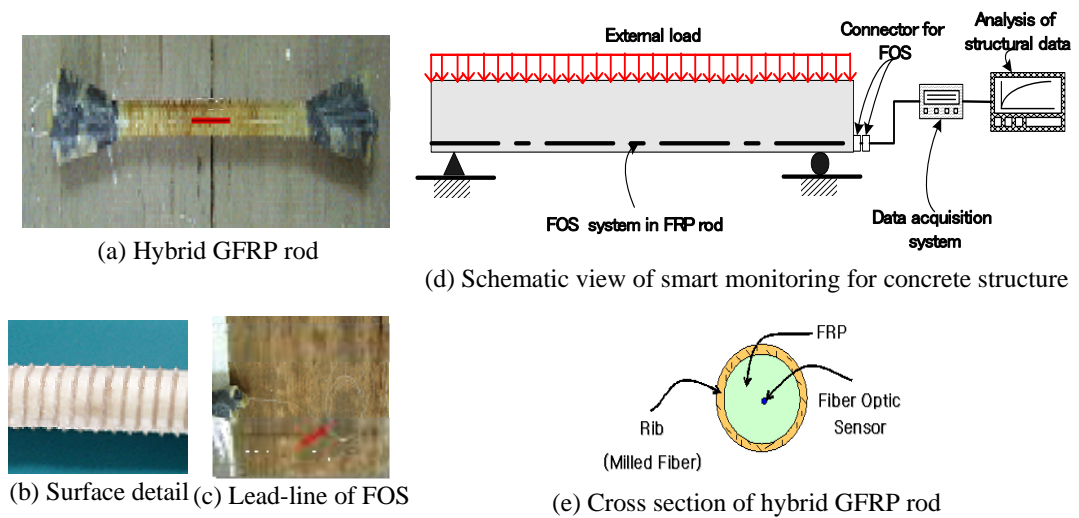


Figure 3: Hybrid GFRP Rod with Fiber Optic Sensor (FOS)

4. FRP IN CHINA

In China, as the country where a FRP bridge was constructed for the first time in the world, there are various practical applications. The first FRP bridge was constructed in Miyun, Beijing in 1982. It is a highway bridge consisting of six GFRP sandwich beams with a span of 20.7 m and still in good service condition (see Photo 7). A recent example of bridge with FRP is a cable stayed bridge with a length of 51.5 m where the stayed cables are CFRP (Photo 8). The cable stayed bridge was constructed in Zhenjiang, Jiangsu in 2004, in which 8 pairs of CFRP cables were used.

Other examples are working platforms and backwater panels. A 10,000 m² GFRP working platform was completed at a mine in Gansu Province, which consists of FRP frame structures with connecting steel bolts and 12m height. GFRP backwater panels, which are pultruded GFRP sandwich panels, have been installed on river bank about 40 km long in the flood season.



Photo 7: World First Highway FRP Bridge in Beijing (photographed by Feng Peng and Ye Lieping)



Photo 8: CFRP Cable Stayed Bridge in Jiangsu (photographed by Ye Zhang)

Typical researches on FRP are as follows:

- FRP-bonding behaviors of FRP strengthened RC elements

- Behaviors of FRP confined concrete columns
- Anchorage system and dynamic behavior of CFRP cables
- High-performance FRP bridge decks
- Long-span FRP woven web structures (Photo 9)
- FRP-aluminum hybrid structural elements (Photo 10)
- FRP-concrete hybrid bridge decks

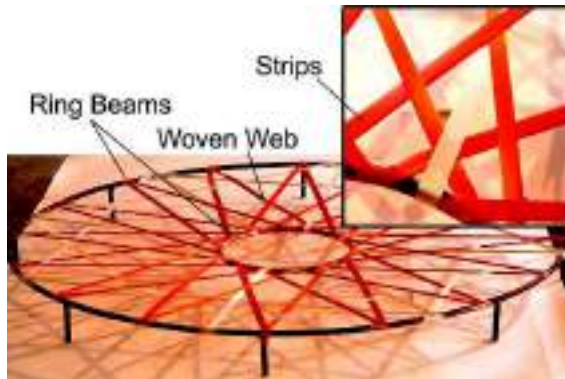


Photo 9: Long-span FRP Woven Web Structures



Photo 10: FRP-aluminum Hybrid Structural Element

Chinese market of FRP in construction is quite active recently. The production of FRP in construction shared 32 % of the total FRP production of 1,740,000 ton in 2004, which was similar to that in USA and much greater than in Japan. In the recent decade, approximately 10,000,000 m² of FRP sheets were used to strengthen RC structures, which is comparable to the amount used in Japan for the same period.

For more reliable application of FRP, governments in China have introduced and will introduce relevant guidelines as follows:

- Technical specification for strengthening concrete structures with carbon fiber reinforced polymer laminate, CECS 146:2003, published in 2003
- Design code for strengthening concrete structure, GB 50367-2006, published in 2006 (including the chapters of FRP materials and FRP strengthening)
- Code for applications of advanced fiber reinforced polymer composites in construction (in drafting), including FRP strengthening concrete elements and masonry structures, FRP bar reinforced concrete elements, FRP prestressed concrete elements, and FRP-concrete hybrid elements

Further information is also available in previous papers (Ye 2003 and Ye 2004).

5. FUTURE FOR FRP IN CONSTRUCTION AND CONCLUDING REMARKS

Japan Society of Civil Engineers (JSCE) set up Committee on Utilization of Innovative Structural Materials in 2004 upon the request of a group of companies lead by Shimizu Corporation and Toray Industries Inc. The Committee, chaired by the author, presented the final report in which the following points were presented for market enhancement for FRP in the near future (JSCE 2006):

(1) Shield Tunnel Segments: Trial design calculation of FRP-concrete composite segment and FRP segment were made for a small size tunnel for swage and a large size tunnel for highway. In order to utilize high strength of FRP, limit state design method is preferable to allowable stress design method. Segment thickness can be reduced by applying FRP in comparison with conventional RC and steel segments. Trial LCC calculation showed that FRP-concrete composite segment with thin layer of FRP (0.2 mm) would be more economical than RC segment for the small size sewage tunnel.

(2) Bridge and Pedestrian Decks: As a substitute of steel bridge deck, FRP bridge deck showed slight increase in the initial cost but reduced the construction time. A FRP bridge deck substituting concrete bridge deck could reduce the construction time significantly. A new type of hybrid FRP beam consisting of hybrid C-GFRP flanges and GFRP web was considered for a pedestrian deck and showed possibility of significant reduction in

construction time. For the cases where construction time is limited, FRP deck and beam would provide a feasible solution.

(3) Coastal and Harbor Structures: CFRP sheet pile could be a feasible structural element for coastal and harbor structures. However, strength under impact should be investigated further. For a life cycle shorter than 50 years high initial cost with the CFRP sheet pile cannot be a better solution than conventional steel sheet pile even after maintenance cost for the steel sheet pile is considered. Reduction in production cost of the CFRP sheet pile and in construction cost due to the lightness of CFRP sheet pile should make it more feasible.

(4) LCC and Environmental Impact: Since FRP is a highly durable material under corrosive environment, trial LCC comparison was made for a pedestrian bridge situated under severe salt attacking environment. A FRP bridge with special features to reduce initial cost, which were obtained through the experience of constructing the first FRP pedestrian bridge in Japan, gave a better LCC than a prestressed concrete bridge with epoxy coating of steel reinforcements. Estimated emission of CO₂ in the case of the FRP pedestrian bridge is less than that in the case of the PC bridge because the emission during construction in the former case can be reduced due to the smaller sub-structure and the lighter super-structure.

The high material cost in comparison with conventional materials, such as concrete and steel, is the primary obstruction for FRP application in construction. In order to overcome this drawback, we need more precise cost estimation with consideration of the lightness of material and LCC, which is different from the conventional cost estimation way. Development of rational design method for FRP may be also a way to ease the material cost barrier. Both precise cost estimation and rational design method could enlarge FRP market for durable structures and architectural structures as seen in Korea and China. Another suggested direction is to explore new inexpensive fiber materials, which may not have high strength/stiffness but other good features such as high fracturing strain.

6. ACKNOWLEDGMENT

Chapter 3 was prepared based on the information provided by Prof SIM Jongsung of Hanyang University, Korea, Dr PARK Cheolwoo of Kangwon National University, Korea and Dr KIM Byun-Suk of Korea Institute of Construction and Technology, while Chapter 4 was prepared based on the information provided by Prof YE Lieping and Dr FENG Peng of Tsinghua University, China. The author would like to show his sincere gratitude for kindly providing him the related information for this paper.

7. REFERENCES

- Ishihara, H. and Shibaya, M. (2005). "Present situation of super fiber and technology for production of textile". *Journal of Textile Engineering*, The Textile Machinery Society of Japan, Vol.58, No.1 (in Japanese).
- Japan Reinforced Plastics Society (JRPS). <http://www.jrps.or.jp/index.html> (in Japanese).
- JSCE Committee on Utilization of Innovative Structural Materials (2006). *Utilization of Innovative Structural Materials for Civil Engineering Fields*, JSCE (in Japanese)
- JSCE Research Committee on Continuous Fiber Reinforcing Materials (1997). "Recommendation for design and construction of concrete structure using continuous fiber reinforcing materials". *Concrete Engineering Series*, Japan Society of Civil Engineers, No.23.
- JSCE Research Committee on Upgrading of Concrete Structures with FRP Reinforcement (2001). "Recommendation for upgrading of concrete structures with use of FRP sheets". *Concrete Engineering Series*, Japan Society of Civil Engineers, No.41.
- Kim, B. S., Cho, J. R. and Kim, S. T. (2005). "Korean research and application status of FRP in bridges". *Proceedings of KCI-ACI Joint Seminar*.
- Tazawa, H. (2004). Document prepared for JSCE Committee on Utilization of Innovative Structural Materials (in Japanese).
- Ueda, T. (2005). "FRP for Construction in Japan", *Proceedings of JSCE-CICHE Joint Seminar on Concrete Engineering in Mongolia*, 19 May 2005, Ulan Batar, pp.54-68.
- Ye, L. P., Feng, P., Lu, X. Z., Qian, P., Lin, L., Huang, Y.L. and Hu, W.H. (2004). "FRP in China: the state of FRP research and design guidelines in construction". *Proceedings of 2nd International Conference on FRP Composites in Civil Engineering (CICE2004)*, Adelaide, Australia, pp.109-119.
- Ye, L. P., Feng, P., Zhang, K., Lin, L. and Hong, W.H. (2003). "FRP in civil engineering in China: Research and applications". *Proceedings of the 6th International Symposium on FRP Reinforcement for Concrete Structures (FRPRCS-6)*, Singapore, World Scientific, pp.1401-1412.

Part I. Bond and Development

BOND TESTS ON CONCRETE AND MASONRY BLOCKS EXTERNALLY BONDED WITH FRP

Francesca Ceroni

(Assistant Professor, Department of Engineering, University of Sannio, Benevento, Italy)

Marisa Pecce

(Full Professor, Department of Engineering, University of Sannio, Benevento, Italy)

ABSTRACT

The paper is a preliminary presentation of a study focused on definition of the bond properties of carbon and glass fibers externally bonded to strengthen concrete and masonry elements. An experimental program is now in progress starting from the analysis of previous bond tests: monotonic and cyclic loads will be applied on concrete and masonry specimens according to a pull-out test procedure considering various configurations of FRP sheets, anchorage systems, environmental temperature. Comparisons of available experimental tests with existing debonding formulations are developed to check their effectiveness.

KEYWORDS

FRP laminates, bond behavior and strength, testing procedure, concrete, masonry.

1. INTRODUCTION

Different strategies can be pursued in repair and strengthening of existing structures. Innovative techniques based on Fibre Reinforced Plastic (FRP) materials appear to be interesting alternatives to traditional solutions; along with high structural effectiveness, composite materials are light and easy to install, their application does not imply loss of space and, in some cases, it can be performed without interrupting the use of the structure. However high strength of FRP can not be used since interface failures is typical issue of FRP composites. Therefore strength and stress distribution of bond between FRP are central aspects especially at the anchorage or at discontinuities as cracks in concrete structures or mortar joints in masonry structures. Generally debonding occurs in the support materials characterized by a lower tensile strength, so that bond strength is strictly related to the tensile strength of the support material and to the bond stress distribution at the interfaces, that depends on stiffness of adhesive and fibres. Cracks and irregularities of the surface could represent weak points for the bond behavior due to concentration of stresses. For this reasons the bond strength in applications on masonry elements is more difficult to prevent due to greater variability and uncertainty of masonry characteristics, to the irregularities caused by mortar joints or unevenness of the surface. In general no standard procedure has been developed to evaluate the bond strength, even if a lot of schemes have been proposed and tested by various researchers (Yao et al., 2005). The bond law in terms of shear stress-slip at the interface is usually assumed bilinear (Lu et al., 2005); the experimental calibration of the factors is essential and particularly difficult for defining the descending branch of this bilinear law. Furthermore in seismic retrofitting cyclic bond stresses at the interface have to be considered, therefore it is necessary to analyze the bond strength degradation and the efficiency of anchorage systems under cyclic loads to evaluate the effective performances.

In this paper a summary of experimental results obtained by the authors with different loading patterns is reported, comparing the experimental maximum loads and the theoretical ones given by various formulations. A wide experimental program in progress is described, aimed to examine the bond behavior under cyclic loads and temperature effects, evidencing also the effect of various type of anchorage systems, for FRP applications on concrete and masonry.

2. THE EXPERIMENTAL PROGRAM

2.1 Results of previous experimental tests

Experimental tests have been realized according to different test procedures (Pecce et al., 2003) to investigate the bond behavior at the interface between masonry or concrete and FRP laminates. In the following the results of experimental tests already carried out are summarized and the experimental program planned is presented.

2.1.1 Bond tests on concrete specimens

Tensile tests were realized on concrete blocks connecting two concrete prisms on two opposite sides by one carbon sheet with various bonded lengths and a fixed width of 100mm. On one side the laminate is anchored with a transversal sheet in

order to have the peeling on the other side where strain gauges are glued. Tensile load is applied by gripping steel bars embedded at the ends of the concrete prisms. Four carbon FRP wet lay up products were used: the fiber thickness was variable between 0.130 and 0.165mm and the Young's modulus of fibers was 230GPa, as declared by producers, while the concrete strength defined by compressive tests on cubes was 25MPa. Beam tests were also realized according to the beam-test scheme usually carried out to evaluate bond properties of steel bars in concrete elements. Two prisms were linked at the bottom side by FRP sheets and the two blocks are connected at the top by a steel hinge allowing rotation. The load was applied in two points. Two carbon FRP wet lay up products were used with fiber thickness of 0.130 and 0.165mm and Young's modulus of 230GPa, while the concrete strength defined by compressive tests on cubes was 29MPa. In Table 1 the following geometrical properties of specimens are reported: width, B, height, H, and length, L, of specimen, width and bonded length of fibers, B_f and L_b. The experimental failure modes and the maximum loads are also reported and the last ones are compared with various theoretical debonding loads (fib bulletin 14, 2001; Chen & Teng, 2001; CNRDT200/2004) reported in the following in terms of maximum tensile load (N) or tensile stress (f):

- 1) fib bulletin 14 (2001): $N_{fa,max} = \alpha c_1 k_c k_b b \sqrt{E_f t_f f_{ctm}}$ $\alpha = 0.9, c_1 = 0.64, k_c = 0.67, c_2 = 2$
- 2) Chen & Teng (2001): $N_{fa,max} = 0.427 \beta_p \beta_L b_f L_e \sqrt{f'_c}$; $L_e = \sqrt{E_f t_f / \sqrt{f'_c}}$; $b_L = 1$ for $L_b > L_e$, $\beta_L = \sin \frac{\pi L}{2L_e}$ for $L_b < L_e$
- 3) CNR DT200/2004 (2004): $f_{idd} = \frac{1}{\gamma_{f,d} \sqrt{\gamma_c}} \sqrt{2E_f \Gamma_{FK} / t_f}$; $\Gamma_{FK} = 0.03 k_b \sqrt{f_{ck} f_{ctm}}$; $k_b = \sqrt{(2 - b_f / b) / (1 + b_f / 400)}$

The safety factors for debonding failure, $\gamma_{f,d}$, and for concrete, γ_c , are assumed equal to 1 in order to compare the provisions with the experimental results. For tensile tests a variability of failure loads is registered varying the products used with a tendency to increase at growing the bonded length. The average test-to-predicted bond strength ratio and its standard deviation are respectively 1.14 and 0.34, 1.01 and 0.44, 1.06 and 0.31 for formulations 1), 2) and 3) for tensile tests, while are 1.83 and 0.22, 1.57 and 0.18, 1.67 and 0.20 for beam tests. The experimental results are strongly under estimated when beam test is used, due to type of concrete crushing involving a larger volume of material. The considered formulas give comparable results, if the safety factors for design are not considered; besides it would be specified if the average or characteristic values of parameters have to be introduced.

Table 1. Experimental tests on concrete specimens strengthened with CFRP

Specimen	Test	B [mm]	H [mm]	L [mm]	B _f [mm]	L _b [mm]	F _{max} [kN]	Failure	Fib bulletin 14 [kN]	Chen & Teng [kN]	CNR DT-200/2004 [kN]
C5_1	Tensile	150	150	300	100	50	12.9	DB	10.0	12.0	10.8
C5_2	Tensile	150	150	300	100	50	7.3	P	10.0	12.0	10.8
C5_3	Tensile	150	150	300	100	50	7.3	DB/P	9.5	11.6	10.3
C5_4	Tensile	150	150	300	100	50	9.5	P	10.0	12.0	10.8
C10_1	Tensile	150	150	300	100	100	16.8	DB/P	12.5	15.8	13.5
C10_2	Tensile	150	150	300	100	100	18.3	P/CR	12.5	15.8	13.5
C10_3	Tensile	150	150	300	100	100	15.2	DB	11.1	14.0	12.0
C10_4	Tensile	150	150	300	100	100	14.3	DB/P	12.5	15.8	13.5
C15_1	Tensile	150	150	300	100	150	12.5	DB/P	12.5	15.8	13.5
C15_2	Tensile	150	150	300	100	150	15.3	DB	12.5	15.8	13.5
C15_3	Tensile	150	150	300	100	150	7.4	DB	11.1	14.0	12.0
C15_4	Tensile	150	150	300	100	150	22.5	P/CR	12.5	15.8	13.5
C10_1c	Beam test	150	150	230	100	100	19.7	SH	11.7	14.6	12.8
C15_1	Beam test	150	150	230	100	150	25.0	SH	11.7	14.6	12.8
C15_1c	Beam test	150	150	230	100	150	20.6	SH	11.7	14.6	12.8
C10_2	Beam test	150	150	230	100	100	21.8	SH	13.2	16.5	14.6
C10_2c	Beam test	150	150	230	100	100	20.7	SH	13.2	16.5	14.6
C15_2	Beam test	150	150	230	100	150	27.3	SH	13.2	16.5	14.6
C15_2c	Beam test	150	150	230	100	150	25.7	SH	13.2	16.5	14.6

DB = superficial debonding, P = debonding with concrete detachment, CR = concrete failure, SH = shear failure of block

2.1.2 Bond tests on tuff specimens

Various types of set-up were used to solve difficulties into applying a tensile load to tuff stones. First tensile tests (specimen TC1-TC5 in Table 2) were performed gripping the tuff blocks through articulated systems of steel plates. In one of the set-up, stones were in tension together with fibers (TC5), while in two different ones the laminates were in tension and the stones were compressed using 2 (TC1 & TC2) or 1 blocks (TC3 & TC4). In tensile tests having the tuff blocks in compression, debonding occurred with detachment of the not compressed stone thickness; when masonry was in tension the tuff blocks crashed in tension. Finally beam-tests were performed, with the same scheme described above; in some

cases fibers were anchored with transversal sheets at both ends. The mean experimental compressive strength of tuff is 3.3MPa and the Young's modulus is 1850MPa. Carbon and glass wet-lay up systems were used having thickness of 0.167mm and 0.111mm respectively. The elastic modulus were 230 and 74GPa according to manufacturer's indications. In Table 2 the geometrical properties of specimens are reported: width, B, height, H, and length, L, of specimen, width and bonded length of fibers, B_f and L_b, number of layers, n, and fiber type, anchorage system. The experimental failure modes and loads are also reported and compared with the theoretical formulation suggested by (CNR DT200-2004):

$$4) f_{fdd} = \frac{1}{\gamma_{f,d} \sqrt{\gamma_m}} \sqrt{\frac{2E_f \Gamma_{FK}}{t_f}} ; \Gamma_{FK} = c_1 \sqrt{f_{mk} f_{mfm}} \quad c_1=0.015. \text{ The safety factors for debonding failure, } \gamma_{f,d}, \text{ and for}$$

masonry, γ_m , are assumed equal to 1 in order to compare the provisions with the experimental results. It is interesting to noticed that the failure loads of tuff specimens are comparable with the values of concrete, even if the tensile strength of tuff is about 10% of concrete: this leads to suppose that probably for masonry elements the distribution of stress and the failure mode are able to involve greater amount of material. Moreover the theoretical provisions are too much conservative respect to the experimental results, so that the main parameters affecting the strength should be reviewed.

Table 2. Experimental tests on tuff specimens strengthened with CFRP and GFRP

Specimen	Set-up	B [mm]	H [mm]	L [mm]	B _f [mm]	L _b [mm]	n	Fiber	Anchorage	F _{max} [kN]	Failure	CNR DT-200/2004 [kN]
TC1	Tensile test	200	260	400	100	200	1	C	No	10	DB	3.5
TC2	Tensile test	200	260	400	100	200	1	C	No	17	DB	3.5
TC3	Tensile test	240	110	400	100	200	1	C	No	23	DB	3.5
TC4	Tensile test	240	110	400	100	200	1	C	No	17	DB	3.5
TC5	Tensile test	240	110	400	100	200	1	C	No	15	TM	3.5
TC10_1	Beam test	185	110	185	100	100	1	C	No	11.8	SHT	3.5
TC15_1	Beam test	185	110	185	100	150	1	C	No	14.9	SHT	3.5
TC20	Beam test	250	110	315	100	200	1	C	No	17.8	SHT	3.5
TC10a_1	Beam test	185	110	185	100	100	1	C	CFRP sheet	15.8	SHT	3.5
TC10_2	Beam test	190	110	175	100	100	1	C	No	11	SHT	3.5
TC10a_2	Beam test	190	110	175	100	100	1	C	CFRP sheet	14.7	SHT	3.5
TC15_2	Beam test	190	110	175	100	150	1	C	No	13.5	SHT	3.5
TC15a	Beam test	190	110	175	100	150	1	C	CFRP sheet	16.0	SHT	3.5
TG10_1	Beam test	185	110	185	100	100	1	G	No	10.5	SHT	1.6
TG10a_1	Beam test	185	110	185	100	100	1	G	GFRP sheet	18.2	SHT	1.6
TG10_2	Beam test	190	110	175	100	100	1	G	No	12.6	SHT	1.6
TG15	Beam test	190	110	175	100	150	1	G	No	16.7	SHT	1.6
TG10a_2	Beam test	190	110	175	100	100	1	G	GFRP sheet	15.0	SHT	1.6
TG15a	Beam test	190	110	175	100	100	1	G	GFRP sheet	18.6	SHT	1.6
TG20	Beam test	250	110	315	100	200	1	G	No	9.6	TF	1.6

SHT = Shear failure of stone, TF = Tensile fracture of fiber, DB = superficial debonding, TM = Tensile fracture of masonry, C = Carbon; G = Glass

2.2 The experimental program in progress

The experimental program in progress comprises concrete and masonry blocks externally bonded with carbon and glass FRP sheets having bonded lengths of 100 and 150mm. The load scheme is an asymmetric pull-out test where the tensile load is transferred to the laminate by gripping the end of FRP sheets and applying compression to the concrete/masonry block included in a steel frame (Figure 1). This loading pattern seems to be the best one to calibrate the bond strength and law (Yao et al., 2005). Carbon and glass wet-lay systems will be used having thickness of 0.165mm and 0.343mm respectively. The elastic modulus are 230 and 81GPa according to manufacturer's indications. In Table 3 the following geometrical properties of specimens are reported: width, B, height, H, and length, L, of specimen, width and bonded length of fibers, B_f and L_b, number of layers, n, and fiber type, anchorage system and special treatment before or during the test. Effects of width, bonded length, anchorage system, number of layers, temperature treatment (specimens will kept at a fixed temperature before performing the test) and cyclic loads will be considered.

3. CONCLUSIONS

The lack of a standard experimental procedure for bond test both for concrete and tuff specimens implicates different results depending on the loading pattern and the specimen geometry, especially for masonry. Beam tests on concrete specimens give higher experimental bond strength respect to the tensile tests due to the shear failure mode of concrete blocks (Yao et al., 2005). Based on these previous experiences and a literature review, a new experimental program has been planned adopting the same set-up for concrete and masonry specimens (single shear test set-up with strengthened

element in compression) that should give more stable results with failure modes related to bonding behavior varying parameters. Parallel tests on concrete and tuff specimens will be performed to check the difference in bond behavior considering that the failure loads of realized test resulted quite comparable, even if the two materials have a very dissimilar strength. This will be useful also to check the effectiveness of the formulations predicting the delamination loads. The available data evidence that the theoretical formulations are safe in most cases for concrete, even if the role of the safety factors is very important; the Italian code gives good provisions for concrete specimens in tension and too much safe predictions for masonry elements.

4. REFERENCES

- Chen J. F., Teng J. G. Anchorage strength models for FRP and Steel Plates bonded to concrete. Journal of structural Engineering, ASCE, Vol. 127, No. 7, July 2001.
- CNR DT 200/ 2004. Istruzioni per la Progettazione, l'Esecuzione ed il Controllo di Interventi di Consolidamento Statico mediante l'utilizzo di Compositi Fibrorinforzati, 2005 (in italian).
- Fib Bulletin 14. FRP as Externally Bonded Reinforcement of R.C. Structures: Basis of design and safety concept, 2001, TG9.3.
- Yao J., Teng, J.G., Chen J.F. Experimental study on FRP-to-concrete bonded joints. Composites: Part B: Engineering, 36 (2005), Elsevier, pp. 99–113.
- Lu, X.Z., Teng, J.G., Ye, L.P., Jiang, J.J. Bond–slip models for FRP sheets/plates bonded to concrete. Engineering Structures, 27 (2005), Elsevier, pp. 920–937.
- Pecce M., Ceroni F., Manfredi G., Prota A. Tests and modelling on bond of FRP laminates. JCI International Symposium on Latest Achievement in Technology and Research on Retrofitting Concrete Structures, Interface Mechanics and Structural Performance, July 2003 – Kyoto, Japan, pp. 95-99.

Table 3. Experimental tests in progress on concrete and masonry specimens

Specimen	Material	B [mm]	H [mm]	L [mm]	B _r [mm]	L _b [mm]	n	Fiber	Anchorage	Treatment
2 specimens	CR	150	150	400	100	150	1	C	No	No
+ three tests using anchorage systems at the end (FRP sheet, FRP bar, FRP fan)										
2 specimens	CR	150	150	400	100	100	1	C	No	No
+ two test using anchorage systems at the end (FRP sheet)										
2 specimens	CR	150	150	400	50	150	2	C	No	No
2 specimens	CR	150	150	400	50	150	2	C	FRP sheet	No
2 specimens	CR	150	150	400	100	150	1	C	No	80°
2 specimens	CR	150	150	400	100	150	1	C	No	60°
3 specimens	CR	150	150	400	100	150	1	C	No	Cyclic load
+ three tests using anchorage systems at the end (FRP sheet, FRP bar, FRP fan)										
2 specimens	CR	150	150	400	100	150	1	G	No	No
+ three tests using anchorage systems at the end (FRP sheet, FRP bar, FRP fan)										
2 specimens	CR	150	150	400	100	100	1	G	No	No
2 specimens	CR	150	150	400	100	100	1	G	FRP sheet	No
2 specimens	CR	150	150	400	50	150	2	G	No	No
2 specimens	CR	150	150	400	50	150	2	G	FRP sheet	No
2 specimens	CR	150	150	400	100	150	1	G	No	80°
2 specimens	CR	150	150	400	100	150	1	G	No	60°
3 specimens	CR	150	150	400	100	150	1	G	No	Cyclic load
+ three tests using anchorage systems at the end (FRP sheet, FRP bar, FRP fan)										
2 specimens	T	250	110	370	100	150	1	C	No	No
+ three tests using anchorage systems at the end (FRP sheet, FRP bar, FRP fan)										
2 specimens	T	250	110	370	100	150	1	C	No	80°
2 specimens	T	250	110	370	100	150	1	C	No	60°
3 specimens	T	250	110	370	100	150	1	C	No	Cyclic load
+ three tests using anchorage systems at the end (FRP sheet, FRP bar, FRP fan)										
2 specimens	T	250	110	370	100	150	1	G	No	no
+ three tests using anchorage systems at the end (FRP sheet, FRP bar, FRP fan)										
2 specimens	T	250	110	370	100	150	1	G	No	80°
2 specimens	T	250	110	370	100	150	1	G	No	60°
3 specimens	T	250	110	370	100	150	1	G	No	Cyclic load
+ three tests using anchorage systems at the end (FRP sheet, FRP bar, FRP fan)										

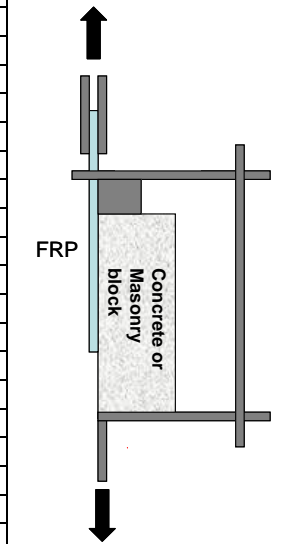


Figure 1. Experimental set-up for asymmetric pull-out test

CR = Concrete, T = Tuff, C = Carbon, G = Glass

COHESIVE –BRIDGING ZONE MODEL OF THE FRP-CONCRETE INTERFACE DEBONDING

Jialai Wang

(Assistant Professor, The University of Alabama, Tuscaloosa, Alabama 33487-0205, USA)

ABSTRACT

Debonding along the FRP-concrete interface can lead to premature failure of the structures. In this study, a combined cohesive/bridging zone model is presented to simulate the debonding procedure between the FRP and concrete interface. The crack processing zone of the interface is modeled by a cohesive zone model and the particle interlocking zone of the interface is modeled by a bridging zone model. Closed-form solutions of interfacial stress, FRP stress and ultimate load of plated beam are obtained for a typical single-lap specimen. Excellent agreements with experimental results have been achieved by this model, which verifies the validation of the proposed novel bond-slip law.

KEYWORDS

Cohesive zone model; Fiber reinforced polymer; Strengthening; Concrete; Debonding

1. INTRODUCTION

Experimental studies have shown that the stress deformation relationship of the FRP-concrete interface is nonlinear (Chajes et al. 1995; Bizindavyi and Neale 1999; Dai et al. 2005;). By considering a nonlinear bond-slip law, it is possible to model the whole debonding process of FRP-concrete interface as demonstrated recently by Yuan et al. (2004). In existing cohesive zone debonding models (Yuan et al. 2004, Wang 2006), a simple bi-linear bond stress-slip law is used frequently. As observed in experimental studies (Leung and Tung 2006) the FRP-concrete interface debonding has two different failure stages, i.e., a crack processing (damaging) stage of the bond followed by a particle bridging (interlocking) stage until the surfaces of the FRP plate and concrete substrate are fully separate. Due to the different failure mechanisms at crack processing and bridging stage, the stress-slip law should be different. In this study, a novel nonlinear bond stress-slip law is proposed, in which two different linearly softening laws are employed in to simulate these two stages separately.

2. COHESIVE/BRIDGING ZONE MODEL OF INTERFACE DEBONDING

Consider a simply-supported reinforced concrete beam (RC beam) reinforced by an FRP plate subjected to pointed loads and/or uniform distributed load, as shown in Fig. 1(a). To simplify the analysis, only a flexural crack existing at the mid-span of the concrete beam is considered in this study. Since a symmetric load is applied, only half of the structure needs to be analyzed (Fig. 1(b)). The geometry of the cross-section of the plated beam is shown in Fig. 1(a). Both the concrete beam and FRP plate are modeled as linear elastic simple beams (beam 1 and 2 in Fig. 1, respectively). Therefore, the constitutive laws for these two beams read:

$$N_i = C_i u_i', \quad M_i = -D_i w_i'' \quad i = 1, 2 \quad (1)$$

where N_i and M_i are axial forces and bending moments of beam i ($i = 1, 2$), respectively; u_i and w_i are axial and vertical displacements of beam i ($i = 1, 2$), respectively; C_i and D_i are axial and bending stiffnesses of beam i ($i = 1,$

2), respectively; and $C_i = E_i b_i h_i$, $D_i = E_i I_i$; E_i is the Young's modulus of beam i ($i = 1, 2$); b_i and h_i are width and height of beam i ($i = 1, 2$); I_i is the moment of inertia of the beam i ($i = 1, 2$).

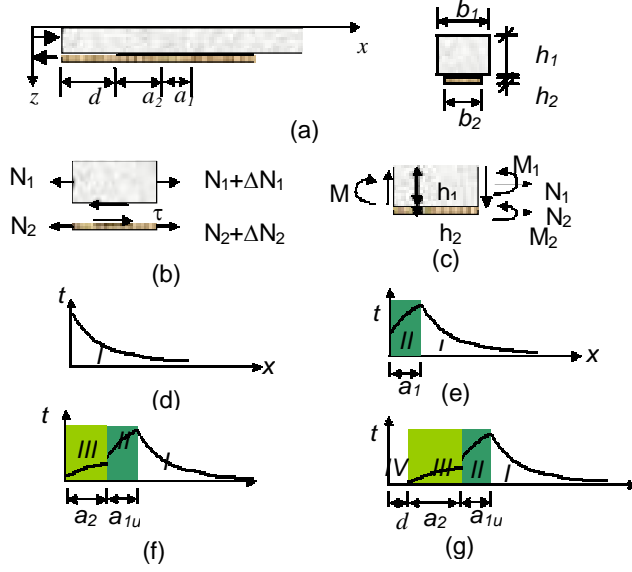


Fig. 1. Interfacial stress of FRP-plated concrete beam .

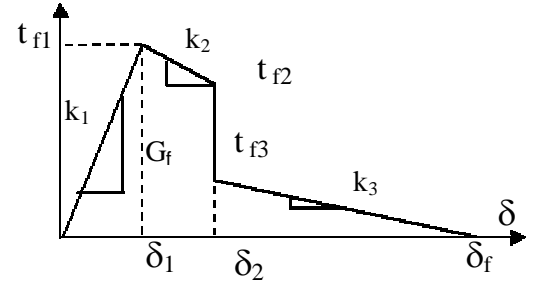


Fig. 2. Cohesive/bridging bond-slip model

Beam 2 is bonded to Beam 1 through the FRP-concrete interface layer which is modeled as a large fracture processing zone with a nonlinear bond-slip law as demonstrated in many experimental studies (Bizindavyi and Neale 1999). Based on the different failure stages of the interface, the whole FRP-concrete interface can be divided into four different zones as shown in Fig. 1 after full debonding occurs. Two different linearly softening laws are employed in this study to simulate the cohesive zone (Zone II) and bridging zone (Zone III) separately. Correspondingly, the proposed bond stress-slip law has four segments as shown in Fig. 2. This non-linear relationship can be described by the following equation:

$$\tau = \begin{cases} \tau_{f1} \frac{\delta}{\delta_1} & \delta < \delta_1 \\ \tau_{f1} - \frac{\tau_{f1} - \tau_{f2}}{\delta_2 - \delta_1} (\delta - \delta_1) & \delta_1 \leq \delta < \delta_2 \\ \tau_{f3} - \frac{\tau_{f3}}{\delta_f - \delta_2} (\delta - \delta_2) & \delta_2 \leq \delta < \delta_f \\ 0 & \delta_f \leq \delta \end{cases} \quad (2)$$

The slip along the interface δ (relative axial displacement of the top of the FRP plate and the bottom of the concrete beam) and given by:

$$\delta = (u_1 - Y_1 w_1' - u_2 - Y_2 w_2') \quad (3)$$

Y_1 and Y_2 are the distances from the bottom of beam 1 and the top of beam 2 to their respective neutral axis. From the point of view of CZM, such a nonlinear relationship is a material property of the FRP-concrete interface.

Under external load, interfacial shear stress is developed along the FRP-concrete interface. Four debonding stages shown in Fig. 1(d) to 1(g) are analyzed as follows.

Stage I: Linearly elastic stage

By assuming the FRP plate and concrete beam have the same curvature (Smith and Teng 2001; Rasheed and Pervaiz 2002), the governing equation of shear stress along the interface of FRP-concrete can be obtained as:

$$\tau'' = \frac{\tau_f}{\delta_1} \left(\frac{1}{C_1} + \frac{1}{C_2} + \frac{(Y_1 + Y_2)^2}{(D_1 + D_2)} \right) b_2 \tau + \frac{\tau_f}{\delta_1} \frac{Y_1 + Y_2}{D_1 + D_2} M' \quad (4)$$

Considering constant bending Moment M in conventional single-lap specimen, the shear stress and axial force of the FRP plate in this stage can be expressed as:

$$\tau = Ae^{-\lambda_1 x}, \quad N_2 = N_{20} + \int_0^x b_2 (\Delta\tau + \tau_c) dx = N_{20} + \frac{b_2 A}{\lambda_1} e^{-\lambda_1 x} \quad (5)$$

Where $\lambda_1 = C_\lambda \sqrt{\frac{\tau_{f1}}{\delta_1}}$, $C_\lambda = \sqrt{b_2 \left(\frac{1}{C_1} + \frac{1}{C_2} + \frac{(Y_1 + Y_2)^2}{D_1 + D_2} \right)}$, $C_\tau = \frac{Y_1 + Y_2}{(D_1 + D_2) C_\lambda^2}$, $N_{20} = b_2 C_\tau M$.

Stage II: Elastic-softening stage

If the load is increased after reaching the elastic limit, part of the interface turns to soften with the slip and two regions along the interface are formed (Fig. 1 (e)):

Region I: Linearly Elastic Region ($\delta = \delta_I$):

$$\tau = \tau_{f1} e^{-\lambda_1 (x-a_1)}, \quad N_2 = N_{20} + \frac{b_2 \tau_{f1}}{\lambda_1} e^{-\lambda_1 (x-a_1)} \quad (6)$$

where a_1 is the softening zone size.

Region II: Linearly Softening Region ($\delta_I < \delta = \delta_2$):

$$\tau = \tau_{f1} \cos(\lambda_2 (x - a_1)) + \frac{\lambda_2}{\lambda_1} \tau_{f1} \sin(\lambda_2 (x - a_1)), \quad N_{2s} = N_{20} - \frac{b_2}{\lambda_2} \left(\sin(\lambda_2 (x - a_1)) - \frac{\lambda_2}{\lambda_1} \cos(\lambda_2 (x - a_1)) \right) \tau_{f1} \quad (7)$$

where $\lambda_2^2 = \frac{\tau_{f1} - \tau_{f2}}{\delta_2 - \delta_1} \left(\frac{1}{C_1} + \frac{1}{C_2} + \frac{(Y_1 + Y_2)^2}{D_1 + D_2} \right) = \frac{k_2}{k_1} \lambda_1^2$

Stage III: Elastic-softening-bridging Stage

In this stage, three different zones exist on the FRP-concrete interface, as shown in Fig. 1(f). The interface shear stress and the axial force of the FRP plate in Zone I and II can be obtained by shifting the abscissas of corresponding solution in Stage II by a bridging zone size a_2 .

Zone I: Elastic zone:

$$\tau = \tau_{f1} e^{-\lambda_1 (x-a_{1u}-a_2)}, \quad N_{2e} = N_{20} + \frac{b_2 \tau_{f1}}{\lambda_1} e^{-\lambda_1 (x-a_{1u}-a_2)} \quad (8)$$

Zone II: Softening zone:

$$\tau = \tau_{f1} \left(\cos(\lambda_2 (x - a_{1u} - a_2)) + \frac{\lambda_2}{\lambda_1} \sin(\lambda_2 (x - a_{1u} - a_2)) \right), \quad N_{2s} = N_{20} - \frac{b_2}{\lambda_2} \left(\sin(\lambda_2 (x - a_{1u} - a_2)) - \frac{\lambda_2}{\lambda_1} \cos(\lambda_2 (x - a_{1u} + a_2)) \right) \tau_{f1} \quad (9)$$

Zone III: Bridging zone:

$$\tau = \tau_{f3} \cos(\lambda_3 (x - a_2)) + \frac{\lambda_3}{\lambda_2} \tau_{f1} \left(\sin(\lambda_2 a_{1u}) + \frac{\lambda_2}{\lambda_1} \cos(\lambda_2 a_{1u}) \right) \sin(\lambda_3 (x - a_2)),$$

$$N_2 = N_{20} + \frac{b_2}{\lambda_3} \left(-\sin(\lambda_3 (x - a_2)) \right) \tau_{f3} + \frac{\lambda_3}{\lambda_2} \tau_{f1} \left(\sin(\lambda_2 a_{1u}) + \frac{\lambda_2}{\lambda_1} \cos(\lambda_2 a_{1u}) \right) \cos(\lambda_3 (x - a_2)) \quad (10)$$

where $\lambda_3^2 = \frac{\tau_{f3}}{\delta_f - \delta_2} \left(\frac{1}{C_1} + \frac{1}{C_2} + \frac{(Y_1 + Y_2)^2}{D_1 + D_2} \right) = \frac{k_3}{k_2} \lambda_2^2$

Stage IV: Elastic -softening-bridging-debonding stage

If the load is increased after reaching the debonding limit, full debonding occurs along the interface (Fig. 1 (g)) and propagates a distance d from the location of the pull end. In this zone, the interface shear stress is zero. Therefore N_1 and N_2 are constants. The stress distribution within zones I, II, and III can be obtained by simply shifting d in abscissas in that of elastic -softening-bridging stage. Following the same procedure

3 EXPERIMENTAL VERIFICATION

As verification, the FRP stress calculated by the present analytical solutions for a single-lap shear test in Fig. 1(a) are compared with experimental result (Pan and Leung 2006) and presented in Fig.3. The parameter in bond stress-slip law shown in Fig. 2 are chosen as $k_1 = 153 \text{ MPa/mm}$, $\tau_{f1} = 5.2 \text{ MPa}$, $k_2 = 4 \text{ MPa/mm}$, $\tau_{f2} = 4.62 \text{ MPa}$, $\tau_{f3} = 1.25 \text{ MPa}$, $k_3 = 0.56 \text{ MPa/mm}$. The total fracture energy $G_f = 2.2 \text{ N/mm}$. Fig. 3 shows the present analytical model has achieved good agreements with experimental results, which validates the novel bond-slip model of this study.

4. CONCLUSIONS

In this study, a novel cohesive/bridging zone model is proposed to simulate the FRP-concrete interface debonding. This new model uses two different softening laws to describe the nonlinear bond stress-slip law of the FRP-concrete interface at cohesive zone and bridging zone, respectively. Closed-form solutions of the interfacial stress, the axial force of FRP plate for different debonding stages. The validation of this model is verified by excellent agreements with experimental data achieved by the new bond stress-slip law. The cohesive/bridging zone model in this study provides an efficient and effective way to analyze more general FRP-concrete interface debonding.

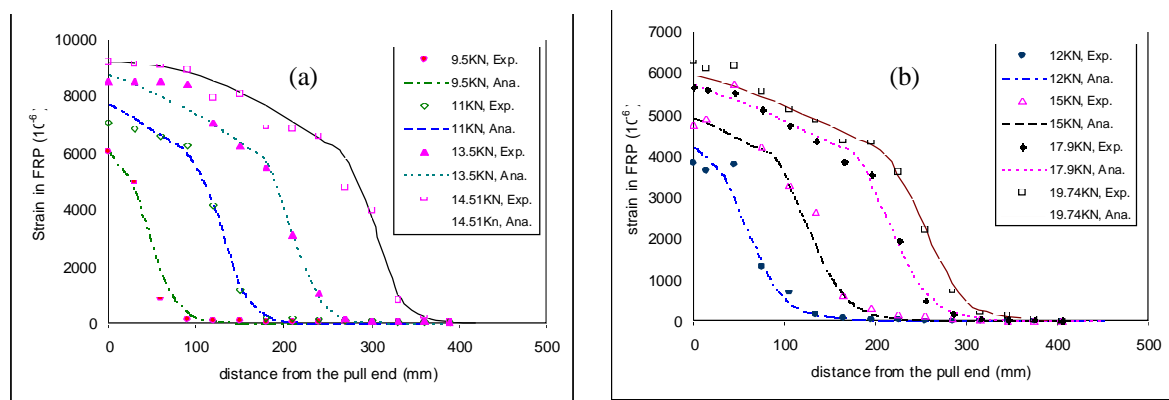


Fig. 3. Comparison between the present solution and experimental result (Pan and Leung 2006): (a) CFRP thickness = 0.22 mm ; (b) CFRP thickness = 0.44 mm

REFERENCES:

- Bizindavyi, B.L. and Neale, K.W., (1999). "Transfer Lengths and bond strengths for composites bonded to concrete". *Journal of composites for construction* 3, 153-160.
- Chajes, M.J., Januszka, T.F., Mertz, D.R., Thomson Jr., T.A., Finch Jr., W.W., (1995). "Shear strengthening of reinforced concrete beams using externally applied composite fabrics". *ACI Structural Journal* 92, 295-303.
- Dai, J., Ueda, T., Sato, Y., (2005). "Development of the Nonlinear Bond Stress-Slip Model of Fiber Reinforced Plastics Sheet-Concrete Interfaces with a Simple Method". *Journal of Composites for Construction* 9, 52-62.
- Leung, C.K.Y., and Tung, W.K. (2006). "Three-parameter model for debonding of FRP plate from concrete substrate". *Journal of Engineering Mechanics* 32, 509-518.
- Pan, J. and Leung, C.K.Y. (2006). "Debonding along the FRP-concrete interface under combined pulling/peeling effects". *Engineering Fracture Mechanics*. in press.
- Rasheed, H.A., and Pervaiz, S.,(2002). "Bond slip analysis of fiber-reinforced polymer-strengthened beams". *Journal of Engineering Mechanics* 128, 78-86.
- Smith, J.G., and Teng, J.,(2001). "Interfacial stresses in plated beams". *Engineering Structure* 23, 857-871.
- Taljsten, B., (1996). "Strengthening of concrete prisms using the plate bonding technique". *International Journal of Fractures* 82, 253-266.
- Wang, J. (2006). "Cohesive zone model of intermediate crack-induced debonding of FRP-plated concrete beam". *International Journal of Solids and Structures*. (in press).
- Yuan H., Teng, J.G., Seracino, R., Wu, Z.S., and Yao, J., (2004). "Full-range behavior of FRP-to-concrete bonded joints". *Engineering Structures* 26, 553-565.

CONSTITUTIVE MODEL FOR TIME-DEPENDENT BONDING AND DEBONDING ALONG FRP-CONCRETE INTERFACE

Hesham Diab

PhD Candidate, Ibaraki University, Hitachi, Ibaraki, Japan

Zhishen Wu

Professor, Ibaraki University, Hitachi, Ibaraki, Japan

ABSTRACT

The time-dependent behavior of FRP-concrete interface is big common for concrete structures strengthened with externally bonded fiber reinforced polymer (FRP) sheets or plates. This paper is devoted in developing a new nonlinear viscoelastic model for studying the long-term behavior of FRP-concrete interface. The model has the ability to describe creep behavior of FRP-concrete adhesive layer and creep fracture propagation along the FRP-concrete interface. The creep of FRP-concrete interface is taken into account by using Maxwell's generalized rheological model through a step-by-step time increment model. The nonlinear time-dependent behavior of adhesive layer depends on the time-dependent degradation of the bond strength and fracture energy. The proposed model has been calibrated by using the results of the double lab shear creep test specimens to verify its validity. The results demonstrate the reliability of the proposed models and their capability to predict the time-dependent propagation of debonding. The results show also the ability of this model to predict a wide range of the creep fracture not only under low sustained loading but also under high sustained loading.

KEYWORDS: FRP-concrete interface, Creep fracture Propagation, Nonlinear viscoelastic model

1. INTRODUCTION

For realistic predictions of the long-term behavior of structures externally strengthened by FRP sheets not only the instantaneous response of FRP-concrete interface under static loadings, but also the influence of long-term deterioration processes is of important. In this case it has been shown, that basic creep strongly affects the serviceability of concrete structures and contributes to a reduction of lifetime and carrying capacity. Although in the last two decades great achievements have been directed to understand the bonding and debonding behavior of FRP-concrete interface and develop different evaluation methods based on bond strength (Wu et al. 2002), it is difficult till now to understand and model the creep fracture at FRP-concrete interface. The present study extends the capability of linear viscoelastic model presented by the authors to simulate the interfacial time-dependent debonding along FRP-concrete interface. This new model has the ability to predict and to evaluate the initiation of micro-cracks and formation of a macro-crack i.e predicts the creep Fracture propagation at FRP-concrete interface. A model able to reproduce these nonlinear effects is described in the following part of this contribution in combination with the previously linear viscoelastic model (Wu, and Diab, 2005).

2. OBJECTIVES AND FORMULATION OF CONSTITUTIVE RELATION

The previous rheological model describes satisfactorily the creep of FRP-concrete interface for low sustained loads i.e. under the debonding limit. This previous model describes only a single feature of the much complex behavior of FRP-concrete interface. As time increases the shear stress along FRP-concrete interface decreases due to stress relaxation function that completely define an ideal viscoelastic material which means the debonding will not occur after the short-term loading based on the bond strength criteria. Recent creep experimental tests show that the FRP-concrete interface behaves in a much complex manner than viscoelastic behavior. The creep of the adhesive leads to initiate and increase the debonding along FRP-concrete interface. This result restricts the applicability of linear viscoelastic model to fully represent the real behavior of FRP-concrete interface especially under high sustained loads. Therefore, modifications that allow for creep fracture in the linear viscoelastic model are necessary. Clearly

Studies of the fracture test data of concrete structures strengthened with FRP sheet showed that the debonding models with softening shear stress-slip relation are inevitable for describing the FRP-concrete interface. Although the interfacial fracture energy is affected by the mechanical property of adhesive and by the concrete strength, it is difficult to say that it affected by time. Based on this discussion, a modified constitutive relation must satisfy the following requirements:

1. The constitutive relation must be reduced to that for linearly viscoelastic aging creep and it should predict when the micro crack is initiated, If the initial load is under the debonding limit.
2. In the absence of creep (e.g., for very fast deformation), the constitutive relation must reduce to an algebraic bond-slip relation which describes softening behavior.
3. The fracture energy of FRP-concrete interface remains constant and does not depend on the time.

Requirement 1 is crucial. It makes it difficult to use debonding failure models which depend only on the bond strength criteria without any external equation because the shear stress descends with time due to the relaxation function. Therefore, a new factor should be considered for the bond failure model coupling with linear relaxation to attain the requirement 1. The rheological model for describing the nonlinear behavior and for attaining the previous requirements can be effectively be represented through a series of analogical models shown in Figure 1(a). A system with N Maxwell's chains that models the increment in creep and elastic slip is placed in series with an element that schematizes the softening model. The softening element describes the softening diagram after attaining the micro debonding, and their respective deformations, s^e , s^c and s^p must be added. So we may write (see Figure 1(a))

$$S = S^e + S^c + S^p \quad (1)$$

where S , S^e , S^c and S^p = total, elastic, creep and softening slip deformation at FRP-concrete interface element respectively.

The increment in elastic and creep slip deformation has been presented in our previous research (Wu, and Diab, 2005) for linear viscoelastic behavior of FRP-concrete interface.

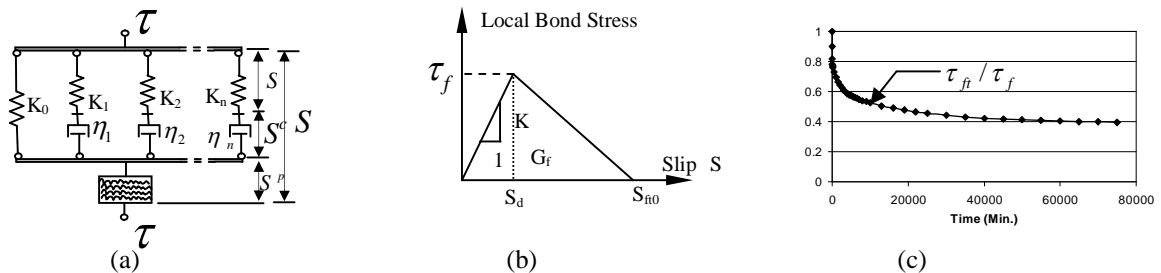


Figure 1. A nonlinear viscoelastic model, Linear Model and time-dependent behavior of maximum shear stress

Most of debonding models for representing short-term behavior of FRP-concrete interface depend on the bond stress criteria, which is difficult to use solely for time-dependent models as mentioned before. Therefore, a new factor should be added to these types of debonding models.

2.1 Fictitious Bond Stress Criteria Model (FBCM)

For the present investigation, a new interfacial debonding model was developed that attempts to combine bi-linear debonding model shown in Figure 1(b) with time-dependent bond strength. The new fictitious bond stress criteria model (FBCM) depends on the assumption that the bond strength is decreased with time and the fracture energy is being constant with time where the fracture energy is represented by the area under the $\tau - s$ curve. The form of bond strength time-dependence equation is taken to be,

$$\frac{\tau_{ft}}{\tau_f} = \sum_{i=0}^n \alpha_i \left[\frac{\lambda_i}{\Delta t} \left(1 - e^{-\frac{\Delta t}{\lambda_i}} \right) \right] \quad (2)$$

where n is the number of terms of the series, λ_i are the relaxation times, Δt is the time increment, α_i is a coefficient define the percent of reduction of the bond stress within each relaxation time, and τ_f, τ_{ft} are bond strength and time-dependent bond strength respectively,

One important point in choosing the parameters of equation 2 is that this equation must be able to realistically model the time-dependent maximum bond stress where the FRP-concrete interface will be initiated to debonding if the time-depend shear stress increased than this value at a generic time. These parameters depend on the time-

dependent parameters of concrete, adhesive and FRP sheets. From experience, The best way to find these parameters (n, α_i, λ_i) is by solving the linear viscoelastic problem i.e. neglecting debonding and then drawing the time-dependent maximum shear stress for FRP-concrete interface as shown in Figure 1(c), from this relation, the relaxation times and reduction coefficient can be obtained as discussed in the previous work.

Base on the requirement 3, the fracture energy which is represented by the area under the curve is being constant and the maximum time-dependent slip is calculated as follows:

$$s_{ft} = \frac{\tau_f}{\tau_{ft}} \cdot s_{ft_0} \quad (3)$$

where s_{ft_0} and s_{ft} are maximum slip at instantaneous load (t_0) and maximum time-dependent slip at time (t).

It should be pointed out that the value s_{ft_0} is very important to be obtained based on the fracture energy and maximum bond strength. The slope of the linear softening part depends on this value, so the small value of s_{ft_0} leads to high slope which allows the debonding to evolve quickly and causes difficulties due to the rapid debonding. However, the different values of s_{ft_0} based on the same fracture energy and different bond strengths lead to the same result. It is clear that the exponential form of equation 2 is physically motivated. At short-term loading, Δt should be equal zero and in turn the requirement 2 will be attained and due to the linear viscoelastic model the interfacial bond stress descends with time and the bond strength is also reduced with time which means requirement 1 will be attained.

3. CALIBRATION OF THE PROPOSED MODEL

The proposed model (FBCM) is calibrated by using the experimental results obtained from double lap shear test specimens (S23, S16.8, S14 and S9.8, where S23 means that the sustained load is 23 kN) carried out at Ibaraki University (Takeshi, 2006). A two-dimensional FE analysis is carried out to simulate the experimental specimens using a commercially available FE code DIANA. The details of the prism specimens are schematically shown in Figure 2. The FRP-concrete interface is represented by an interface element (L8IF) with zero thickness. Using supplied subroutine mechanism offered by DIANA, The long-term behavior of adhesive is represented by the proposed nonlinear viscoelastic model and the linear viscoelastic behavior of the material is represented by a Maxwell chain formed by five rheological elements in parallel. The relaxation times (λ), given in minutes, are selected according to (Wu and Diab, 2006), based on actual linear experimental results. The values adopted are $\lambda_0 = \infty$, $\lambda_1 = 14.4$, $\lambda_2 = 1440$, $\lambda_3 = 14400$ and $\lambda_4 = 144000$, and the values of stiffness are $\alpha_0 = 0.12$, $\alpha_1 = 0.4$, $\alpha_2 = 0.24$, $\alpha_3 = 0.2$ and $\alpha_4 = 0.04$ (where $\alpha_n = K_n / K$) and K is the total interfacial.

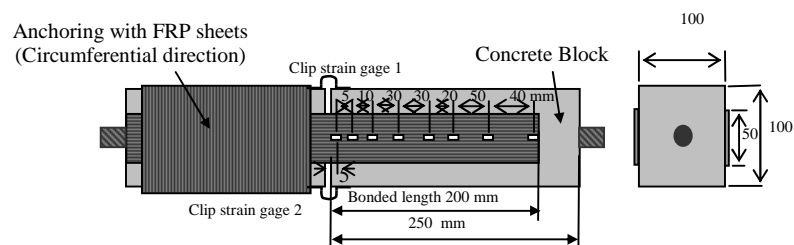


Figure 2 Detail of FRP sheet-concrete bonding joints (Double-lap shear test)

3.1 Comparison between Experimental and Analytical Results

The time-dependent maximum bond strength equation of all specimens is represented by equation (4) which is obtained based on the previous illustration

$$\frac{\tau_{ft}}{\tau_f} = 0.4 + 0.2 e^{-t/14.4} + 0.2 e^{-t/1440} + 0.12 e^{-t/14400} + 0.08 e^{-t/144000} \quad (4)$$

The fracture energy of FRP-concrete interface is obtained by changing the value of the maximum slip s_{ft_0} until obtaining a good agreement between numerical and experimental results while the initial maximum bond strength remains constant then a comparison between experimental and numerical fracture energy is done. A comparison

between experimental fracture energy obtained based on (JSCE, 2001) and that obtained from the proposed model is shown in Figure 3(a). The proposed model gives a high accuracy at low and high sustained loads as shown in Figure 3(b) which represents time-dependent displacement with semi logarithmic scale for S23 and S16.8 (82 and 60% of their static capacity, where the static capacity was 28 kN). Figure 3(c) and 3(d) show the time-dependent FRP strain distribution along bonded FRP sheet. The results demonstrate the ability of the proposed model to simulate the creep fracture propagation along FRP-concrete interface. It should be mentioned that the divergence between numerical and experimental strain at time zero for S14 is a result of a macro crack occurred at concrete block due to static load which it is not considered in this study, where concrete behaves in elasticity. Although it seems that the creep of FRP-concrete interface stopped after 22930 minutes at the specimen S9.8, the numerical model gives a small increasing at FRP strain as shown in Figure 3(d), more experimental study is needed to confirm this observation.

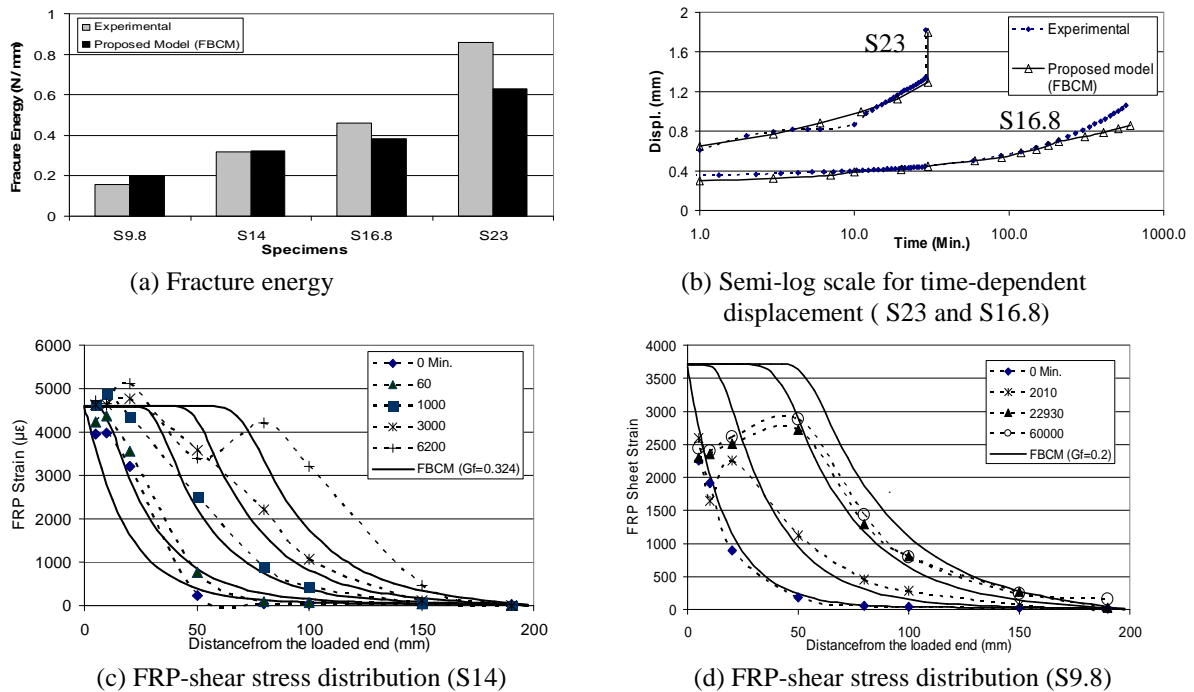


Figure 3. Comparisons between numerical results for Model (FBCM) with experimental results from double-lap shear test

4. CONCLUSION

From the analysis presented above, the following conclusions may be drawn:

- The proposed model seems to be able to predict the debonding and creep fracture propagation along FRP-concrete interface.
- By using the fictitious bond stress criterion model (FBCM), the propagation of the fracture process zone along FRP-concrete interface can be numerically simulated for high and low sustained loads.

5. REFERENCES

- Japan society of Civil engineers (JSCE) (2001). "Recommendations for Upgrading of Concrete Structures with Use of Continuous Fiber sheet." *Concrete Engineering Series 101*.
- Takeshi Sasaki (2006). "Study on creep behavior of FRP sheets and FRP-concrete interface." Graduated paper (supervised by Prof. Wu, Z. S.), Ibaraki University.
- Wu, Z. S., and Diab, H. M. (2005). "Interfacial constitutive model for long term behavior of FRP-concrete adhesive." *Proceedings of International Symposium on Innovation & Sustainability of Structures in Civil Engineering*, Southeast University, China, pp. 1757-1769.
- Wu, Z. S., and Diab, H. M. "Constitutive model for time-dependent behavior of FRP-concrete interface". *Journal of Composites for Construction*, ASCE. (Primarily accepted)
- Wu, Z. S., Yuan, H., and Niu H. (2002). "Stress transfer and fracture propagation in different kinds of adhesive joints." *Journal of Engineering Mechanics*, ASCE, Vol. 128, 562-573.

DEBOND CHARACTERISTICS OF CARBON FIBER LAMINATES FOR BRIDGE REHABILITATION

M. Arockiasamy

(Professor and Director, Center for Infrastructure and Constructed Facilities, Florida Atlantic University, Boca Raton, Florida, USA)

M. Sivakumar

(Senior Design Engineer, PTE Strand Co Inc., Hialeah, Florida, USA)

M. Shahawy

(President, SDR Engineering, Tallahassee, Florida, USA)

ABSTRACT

Recent bridge inspection statistics nation wide show that more than a third of the United States' half million highway bridges are either "structurally deficient" or functionally obsolete". Bridge components are exposed to deterioration effects because they are directly subjected to environmental conditions, corrosive action, accidental vehicular impacts, and cyclic load variations. This may cause defects in concrete bridges including cracking, scaling, spalling, leaching, chloride contamination, delamination and partial or full depth damage, and lead to posting load restrictions on the use of bridges. Retrofit and rehabilitation is essential in order to restore the bridge to its original design load carrying capacity.

Fiber reinforced polymer (FRP) composites are increasingly being used for the repair and strengthening of deteriorated concrete structural components through adhesive bonding of prefabricated strips/plates and the wet lay-up of fabric. Concrete structural elements strengthened with FRP reinforcement can fail in different ways. Bond failure modes have attracted the attention of the designers besides the classical failure modes, such as reinforcing steel rebar fracture, concrete crushing, or shear failure. The objective of the present study is to evaluate the interfacial bond strength between the FRP composite strip, adhesive and the concrete under harsh exposure conditions-namely simulated tidal conditions and freeze-thaw exposure. The bond strength is experimentally determined by the peel test and the results compared with those based on finite element stress analysis. The fracture toughness for debonding is evaluated and expressed as the critical strain energy release rate.

KEYWORDS

Debond, Carbon Fiber Laminates, Bridge Rehabilitation

1. INTRODUCTION

The deterioration and critical need for renewal of civil infrastructure has recently been the focus of considerable discussion among the researchers in North America, Europe and Japan. The repair of concrete beams by the external bonding of a steel/ composite plate is an effective method to protect concrete and restore a part of the stiffness of the structure (Meier, et al. 1991; Arockiasamy, et al. 1995). Whether the plate repair is of steel or advanced composite material, the plate is typically bonded to the concrete using an adhesive. The corrosion of the steel plates continues to be a problem. The effect of adverse environmental conditions on the externally bonded steel plates can be overcome by using FRP materials which have the distinct advantages of strength, non-corrosive properties and ease of application with limited interruption to traffic.

The fiber-reinforced polymer (FRP) composite laminates have been used to strengthen an aging single-span reinforced- concrete T-beam bridge in the state of New York (Hag-Elsafi, et al, 2001). Load tests were conducted to evaluate effectiveness of the strengthening system and investigate its effect on structural behavior, and tests results were compared with those obtained using classical analysis. The load test was repeated to monitor in-service performance of the system after two years of service (Hag-Elsafi, et al, 2004). Further inspection using an infrared thermography camera did not show any significant delamination in the system.

Beside the classical failure modes, such as steel fracture, concrete crushing or shear failure which can appear in normal RC and PC members, bond failure modes have to be taken into account in a concrete member strengthened with externally bonded reinforcement (Blaschko M. et al., 1998). These bond failures can occur in the interface between the externally bonded reinforcement and the concrete body. The following are the possible bond failure modes: • i) FRP peeling-off at the outermost flexural crack in the uncracked anchorage zone, • ii) FRP peeling-off at flexural cracks in the maximum bending area, • iii) FRP peeling-off at flexural cracks between the outermost crack and the maximum bending area, • iv) FRP peeling-off caused by shear cracks and • v) FRP peeling-off caused by the unevenness of the concrete surface.

The susceptibility of open sandwich beams (concrete/adhesive/steel) was investigated to static fracture by crack propagation along the adhesive layer, using linear elastic fracture mechanics (Anandarajah, A. and Vardy A. E., 1985). This study was focused on a simply supported beam with four point loadings. It was found that beams constructed with a suitable adhesive should not be at risk from such failure, whether they were conventionally reinforced beams strengthened by an externally bonded plate or plain concrete beams reinforced solely by an external plate. In addition, it was reported that the beams were relatively insensitive to the thickness of the adhesive bond layer.

The present study evaluates the interfacial bond strength between the FRP composite strip, adhesive and the concrete under harsh environmental exposure. Interface crack propagation and peeling of FRP laminate from concrete was investigated in the experimental work (Baker, W. A., 1999). Multiple specimens were tested using a specially designed test fixture for characterizing the concrete/FRP laminate debond fracture. The compliance and critical load for crack propagation were obtained for each specimen. The experimental results are compared with those based on finite element stress analysis. The fracture toughness for debonding is expressed as the critical strain energy release rate.

2. FRACTURE ENERGY

The energy balance approach can be used to find the adhesive fracture energy, G_c . The energy criterion for fracture describes quasi-static crack propagation as the conversion of the work done, W_d , by the external force and the available elastic energy stored in the bulk of the specimen, U , into surface free energy, γ_m . The relationship may be written as

$$\frac{d}{da}(W_d - U) \geq \gamma_m \cdot \frac{d}{da}A \quad (1)$$

where dA is the increase in surface area associated with an increment of crack growth, da . For a crack propagating in a lamina of width, b , Eq. (1) becomes

$$\frac{1}{b} \left[\frac{d}{da}(W_d - U) \right] \geq \gamma_m \quad (2)$$

Bonded structures exhibiting bulk linear-elastic behavior, i.e., away from the crack tip regions, obey Hooke's Law. G_c may be expressed as:

$$G_c = \frac{F_c^2}{2 \cdot b} \cdot \frac{d}{da}C \quad (3)$$

where F_c is the load at the onset of crack propagation and C is the compliance of the structure and is given by displacement/load, i.e., v/F_c . The compliance function, C , will be determined by experimental data obtained by the debond tests and regression analysis.

3. EXPERIMENTAL SETUP

Twenty seven concrete blocks were made from a commercially available 5,000 psi ready-mix concrete. After an initial curing period of seven days, CFRP composite plates were then bonded to the top of the concrete blocks. An initial crack was then introduced to these specimens i) at the concrete-epoxy interface, ii) through mid-thickness of epoxy layer, and iii) at the epoxy-CFRP plate interface. The test specimens were grouped into three categories of nine specimens each based on exposure conditions. One group consisted of only control specimens and the other two were subjected to freeze-thaw and simulated tidal conditions. The tidal conditioning was simulated exposing the specimens to alternative wet/dry cycles of 24hrs for 100 days. A similar cycle was adopted to expose the specimens to freeze-thaw conditioning by placing the specimen in the freezer (-10°F to 0°F) for 24 hours and then removed and allowed to thaw for another 24 hours at room temperature.

The bond strength of the CFRP plate-epoxy-concrete interface is evaluated using the peel test. The test method was adapted from the peel tests that have been used extensively for composite materials. The specimen was fixed to a tilted base (tilt angle ψ) and vertical load applied at the end of the plate as shown in Figure 1.

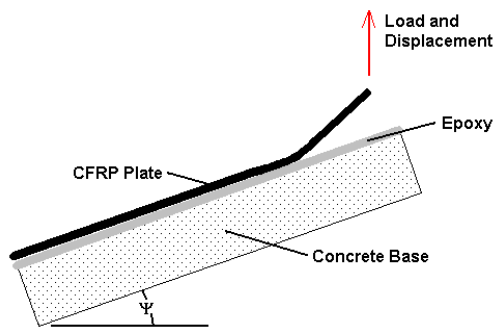


Fig. 1 – Specimen configuration

The specimen was loaded at a constant displacement rate of about 1.5 mm/min until the crack propagates and arrests at a new crack length. The specimen was then fully or partially unloaded. This procedure was repeated until the top plate becomes totally separated from the concrete. By this process, several compliance and critical loads for crack propagation data points were obtained for each specimen, and from this data the fracture energy, G_c was then calculated from Eq. 3 above.

4. RESULTS, DISCUSSIONS AND CONCLUSIONS

The load vs. displacements and corresponding crack lengths were recorded and graphs generated for critical load, compliance and fracture energy for each crack length. Typical graphs shown in Fig. 2 represent the data for specimens with initial crack locations at the CFRP/epoxy interface. Similar graphs were generated for the specimens with initial cracks through the epoxy and concrete/epoxy interface (Baker, W. A., 1999). The overall test results show that the control specimen exhibited a slightly higher average fracture energy compared with the specimens exposed to tidal simulation and the freeze/thaw specimens. From the peel test data, no significant difference between fracture energies of the control and tidal specimens can be deduced. However, the freeze/thaw action had an adverse effect on the fracture energy of the specimens.

A scanning electron microscope (SEM) was used to examine the surface of the epoxy-CFRP interface after debonding to further evaluate the effect of the harsh environmental conditions on the bond. The micrographs from the SEM at 25,000volts and 1000X showed no discernable difference between the control and conditioned

specimens. Based on the limited data, it can be stated that the composite structural system was not adversely affected by harsh environmental conditions.

A finite element model (FEM) was developed using four node plane strain elements and analyzed to obtain compliance vs. crack length relationship. Fig. 4 shows the comparison of the experimental results and good correlation with the values from the FEM model and the beam theory. The compliance calculation using beam theory was made for a fixed ended beam with load applied perpendicular to the longitudinal beam axis, whereas the compliance based on the FEM model and the experiment was for a force applied at a 20° tilt angle. The significant difference between the compliance values at higher crack lengths can be attributed to the effect of the tilt angle.

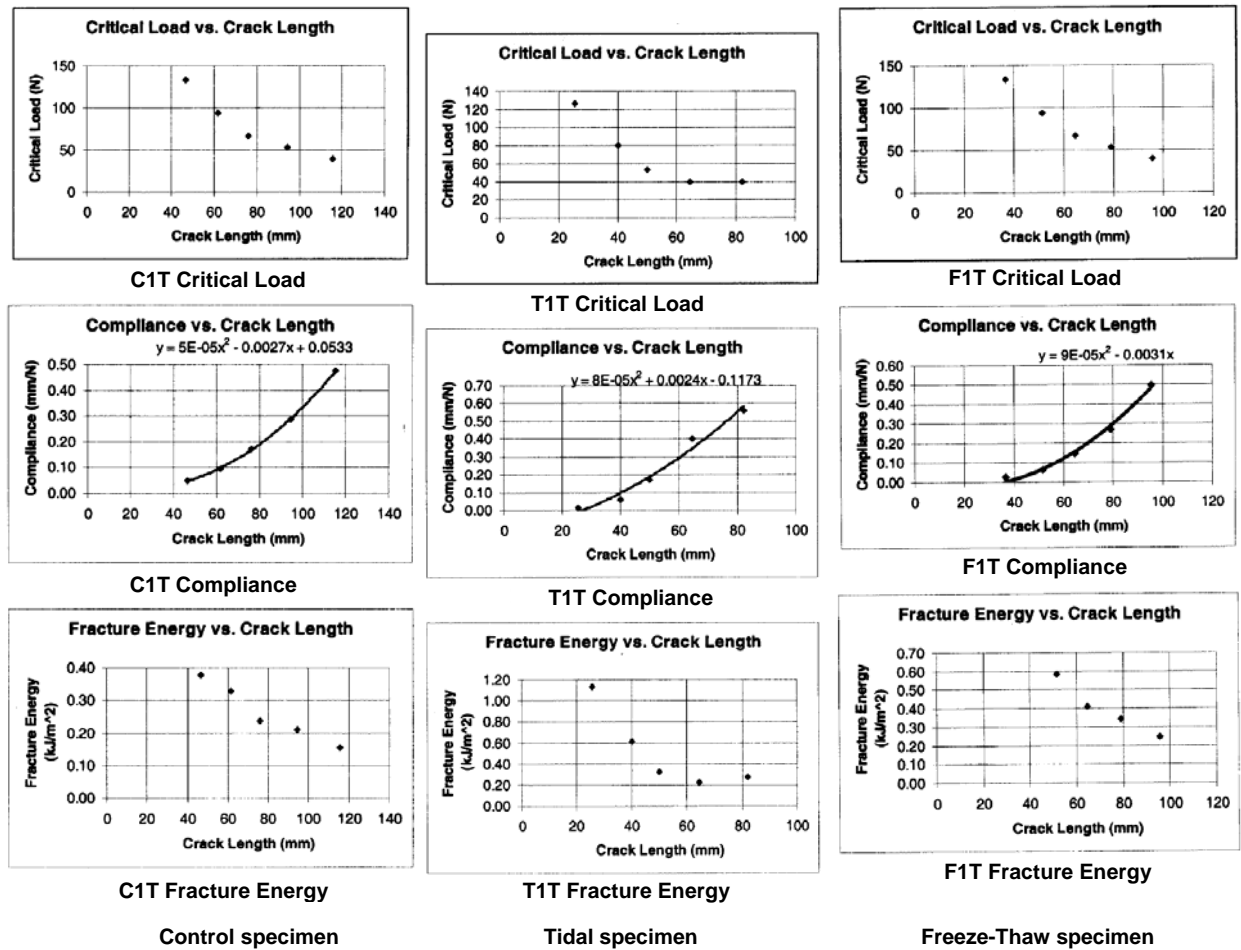


Fig. 2 – Critical load, compliance and fracture energy for each crack length



Fig. 3 – The micrographs from the SEM at 25,000volts and 1000X

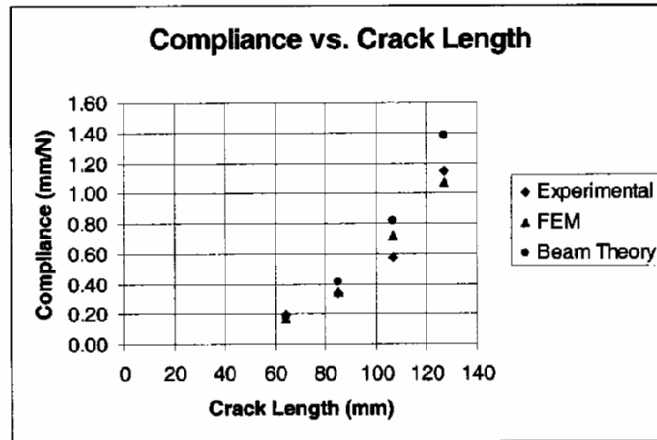


Fig. 4 – Comparison of experimental and analytical results

REFERENCE

- Anandarajah, A. and Vardy A. E., (1985). "A theoretical investigation of the failure of open sandwich beams due to interfacial shear fracture". *The Structural Engineer*, Vol. 63, No. 4, pp 85-92.
- Arockiasamy, M., Sowrirajan, R., and Zhuang, M.,(1995). "Behavior of beams prestressed or strengthened with fiber reinforced plastic composites", Proceedings of the IABSE Symposium, San Francisco, CA, pp 997-1002.
- Baker, W. A., (1999). "Debond of CFRP laminate bonded with concrete exposed to harsh environmental conditions", MS thesis, Florida Atlantic University, Boca Raton, FL.
- Blaschko M., Niedermeier, R. and Zilch, K.,(1998). "Bond Failure Modes of Flexural Members Strengthened with FRP". *Second International Conference on Composites in Infrastructure, (ICCI '98)* Vol 1. pp 315-327.
- Hag-Elsafi,O., Alampalli, S., Kunin, J.,(2001). "Application of FRP laminates for strengthening of a reinforced-concrete T-beam bridge structure". *Composite Structures* 52. pp 453-466.
- Hag-Elsafi,O., Alampalli, S., Kunin, J.,(2004). "In-service evaluation of a reinforced-concrete T-beam bridge FRP strengthening system". *Composite Structures* 64. pp 179-188.
- Meier, U., and Kaiser, H., (1991). "Strengthening of structures with CFRP laminates", *Proceedings of the Specialty Conference on Advance Composite Materials in Civil Engineering Structures*, ASCE, Las Vegas, NV, pp 224-232.

DEBONDING OF CFRP LAMINATES EXTERNALLY BONDED TO CONCRETE SPECIMENS AT LOW AND HIGH TEMPERATURES

Ernst L. Klamer

(Ph.D. Researcher, Eindhoven University of Technology, Eindhoven, The Netherlands)

Dick A. Hordijk

*(Professor, Eindhoven University of Technology, Eindhoven, The Netherlands and
Director, Adviesbureau ir. J.G. Hageman B.V., Rijswijk, The Netherlands)*

Cees S. Kleinman

(Professor, Eindhoven University of Technology, Eindhoven, The Netherlands)

ABSTRACT

This paper presents the results of an experimental investigation into the influence of temperature on small scale concrete specimens, strengthened with externally bonded Carbon Fiber Reinforced Polymers (CFRP). Debonding of the CFRP, due to high shear stresses in the concrete at the interface with the adhesive, governs the failure of these specimens at room temperature. Temperature changes however will affect the bond properties of the CFRP-adhesive-concrete joint, both due to the significant difference in the Coefficient of Thermal Expansion (CTE) between concrete, adhesive and CFRP and due to the change of the material properties with increasing temperatures. Both effects can affect the load level at which debonding occurs. Especially the adhesive shows a significant decrease in strength and stiffness when the temperature reaches the glass transition temperature (T_g). To investigate the influence of temperature on the debonding of externally bonded CFRP, two different test setups were used; a double-lap shear test setup and a three point bending test setup. Test results have shown that a change in temperature affected both the failure load and the type of failure, especially when the T_g of the adhesive was reached.

KEYWORDS

Carbon Fiber Reinforced Polymers, Temperature, Thermal stresses, Debonding, Bond

1. INTRODUCTION

One of the strengthening techniques that has become increasingly popular in the construction industry lately, is the strengthening with externally bonded reinforcement based on Carbon Fiber Reinforced Polymers (CFRP). This strengthening technique has proven to be a cost-effective and durable solution to strengthen existing (reinforced) concrete structures. By now, guidelines have become available and numerous applications have been realised world wide. Despite these developments, some questions have still remained unanswered. One of these questions that has received very little attention so far is the effect of the ambient temperature on the debonding behavior of externally bonded CFRP. Temperature changes will cause thermal stresses due to the significant difference in the coefficient of thermal expansion (CTE) between concrete and CFRP and will change the properties of the applied materials, like the strength and stiffness of the adhesive. Both effects can affect the load level at which debonding occurs.

So far, only limited research has been carried out into the influence of temperature on the debonding of externally bonded CFRP. Experimental results from literature (Tadeu and Branco, 2000; Di Tommaso et al., 2001; Blontrock, 2003; Wu et al., 2005) have shown that the influence of temperature can be significant. However, based on the reported failure loads as function of the temperature no distinctive conclusions can be drawn. It is also not known to what extent the applied test setup had influenced the results and to what extent thermal stresses had developed during the heating of the specimens. The aim of this project was therefore to further investigate the influence of temperature on the debonding behavior of CFRP, externally bonded to concrete specimens.

2. EXPERIMENTS

Two different types of experiments, double-lap shear tests and a three point bending tests, were carried out. Each test set-up was carried out with two different concrete grades ($f_{cm,cube} = 40.1 \text{ N/mm}^2$ and 70.8 N/mm^2) to investigate the influence of the concrete strength. The specimens were tested in the temperature range from -20°C till 100°C .

2.1 Double-lap Shear Tests

The double-lap shear test specimens were produced in two series, one for each concrete grade, of twelve specimens each. To be able to connect the specimen to the tensile testing machine, a steel threaded rod (M20 for the low and M24 for the high strength concrete specimens) of about 1 m length was placed into the center of the specimens (Figure 1). The specimens, including the rod, were cut in half after curing of the concrete. Two CFRP laminates (Sika CarboDur S512) of $50 \times 1.2 \times 650 \text{ mm}^3$ were then bonded to two opposite sandblasted surfaces with a two-component epoxy adhesive (SikaDur-30). 25 mm at each side of the saw cut remained unbonded to prevent local stress concentrations near the saw cut (Figure 1). Before testing, the specimens were heated in the oven for 12 hours.

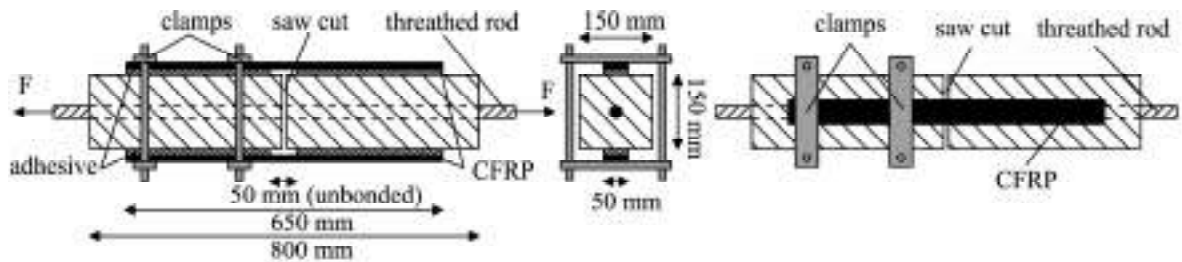


Figure 1: Double-lap Shear Test Setup

The double-lap shear test specimens were tested in a 250 kN tensile testing machine, by pulling the two parts away from each other. Steel clamps were applied at one side of the specimen, to make sure that debonding of the CFRP was initiated at the other side. In this way, strain gauges, which measured the strain distribution over the length of the CFRP, had to be applied on only one side. All specimens were packed with isolation. The temperature of the concrete surface and the adhesive were measured during the experiment and varied with a maximum of 3°C .

2.2 Three Point Bending Tests

The three point bending test specimens were also produced in two series, one for each concrete grade, of twelve specimens each. The concrete specimens were cut at midspan till half the height of the beam to create an initial bending “crack” (Figure 2). The specimens spanned 750 mm, were supported at one fixed hinge support and one roller support and were loaded at midspan. No internal reinforcement was applied. One CFRP laminate ($25 \times 1.2 \times 650 \text{ mm}^3$) was applied to the sandblasted soffit of the specimens. 25 mm at each side of the saw cut remained unbonded to avoid local stress concentrations. The three point bending test specimens were tested in a 100 kN testing machine. The specimens were not isolated during the tests, in order to have a clear sight on the specimens. The temperature of the concrete surface and adhesive were measured during the tests and varied with a maximum of 5°C . Steel clamps were applied to make sure debonding occurred at one side, which reduced the number of needed strain gauges.

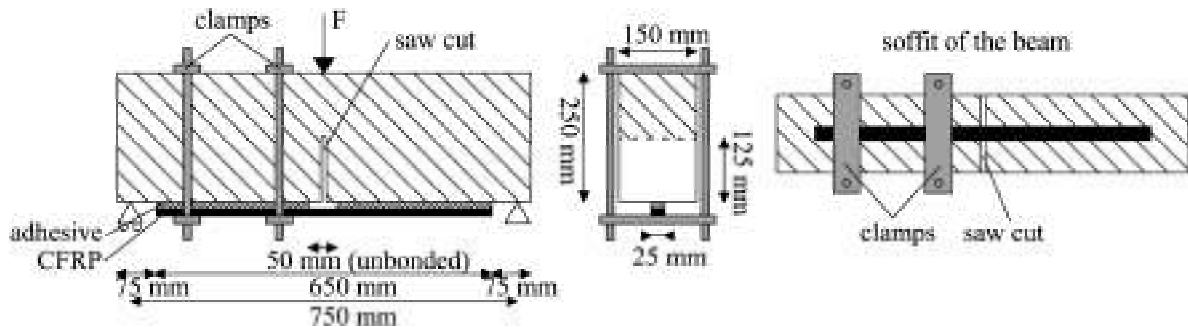


Figure 2: Three Point Bending Test Setup

3. TEST RESULTS

3.1 Failure of the specimens

Both the double-lap shear tests and the three point bending tests failed by debonding of the CFRP laminate due to high shear stresses in the concrete-adhesive interface. This was followed by a bending crack at midspan in case of the three point bending tests. Debonding was initiated at the loaded end near the saw cut and propagated towards the end of the laminate. The specimens which were tested at temperatures from -20°C till 50°C failed in an explosive way by failure of the concrete at the interface with the adhesive, leaving a small layer of concrete (1–3 mm) attached to the adhesive (Figure 3). The specimens that were tested at temperatures of 50°C and higher also failed at the interface between the adhesive and concrete, but no concrete remained attached to the adhesive (Figure 4).



Figure 3: Failure in the Concrete at 20°C

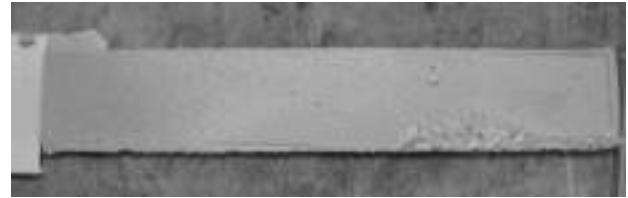


Figure 4: Failure in the Adhesive at 70°C

3.1 Failure Load – Temperature Relation

Figure 5 and Figure 6 show the measured failure loads as a function of the applied temperature for both concrete grades, respectively for the double-lap shear tests and for the three point bending tests. Two linear regression lines were plotted in each figure to give an impression of the tendencies. Basically, two different temperature zones can be distinguished, first a zone in which the failure load increased with increasing temperature (zone 1), followed by a zone in which the failure load decreased with increasing temperature (zone 2).

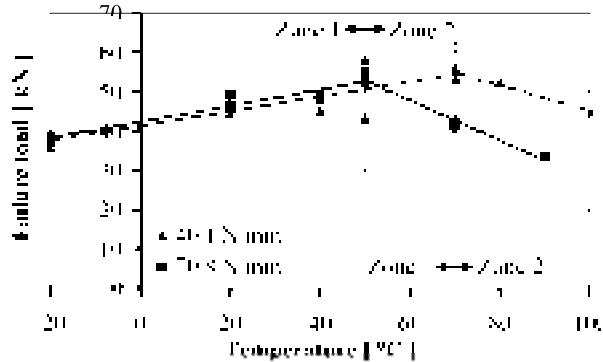


Figure 5: Failure Load Double-lap Shear Tests

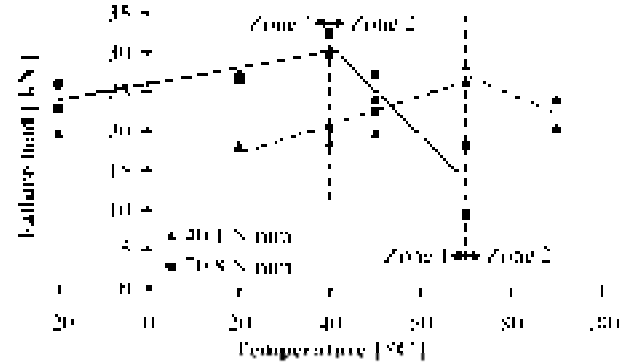


Figure 6: Failure Load Three Point Bending Tests

3.3 Influence of Temperature on the Failure Load

It was expected that debonding was initiated at the loaded end of the CFRP laminate due to the high shear stresses in the concrete at the interface with the adhesive. Increasing the temperature was expected to affect the shear stress distribution in the concrete due to three important effects (Figure 7): (1) The development of thermal stresses due to the difference in CTE between concrete and CFRP; (2) the reduced adhesive stiffness; and (3) the reduced bond strength of the concrete-adhesive interface (Klamer, 2006). These temperature related properties were used in a Finite Element Analysis to simulate the shear stress distribution of the double-lap shear tests at 20°C and 70°C.

The difference in CTE between concrete ($\alpha_c = \pm 10 \times 10^{-6} / ^\circ\text{C}$) and CFRP ($\alpha_f = \pm 0 \times 10^{-6} / ^\circ\text{C}$) caused an initial shear stress distribution in the concrete at the interface with the adhesive, when increasing the temperature ((1) in Figure 7). By subsequently loading the specimen, first the initial shear stresses had to be compensated at the loaded end ($\tau_{0kN,70^\circ\text{C}}$). The difference in CTE between concrete and CFRP therefore had a positive influence on the failure load.

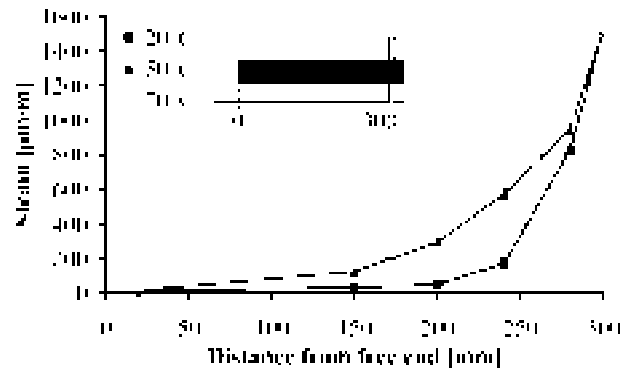
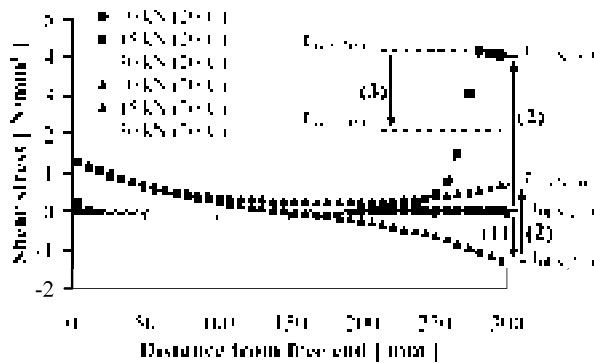


Figure 7: Shear Stress in the Concrete-Adhesive Interface. Figure 8: Measured Strain in the CFRP at 30 kN

The second effect was the reduction of the Young's modulus of the adhesive when increasing the temperature (Klamer, 2005). As a result, the strain in the CFRP laminate, at the same external load, became more equally distributed over the length of the CFRP laminate (Figure 8). A more equal strain distribution implied that the normal stress in the CFRP was transferred to the concrete more equally. The increase in shear stress at the loaded end, when applying an external load, will therefore be smaller at 70°C ($\Delta\tau_{70^\circ\text{C}}$) compared to the increase at 20°C ($\Delta\tau_{20^\circ\text{C}}$) ((2) in Figure 7). The reduced adhesive stiffness therefore had a positive influence on the debonding load.

The third effect however was the bond strength of the concrete-adhesive interface. At temperatures near or above T_g , the concrete surface bond strength was significantly reduced ((3) in Figure 7) and governed over the positive influence of the reduced adhesive stiffness and the difference in CTE. The reduced bond strength therefore explains the decreasing failure load with increasing temperatures in zone 2 after the initial increasing failure load in zone 1.

4. CONCLUSIONS

The experimental results have shown that temperature affected the load at which debonding was initiated, but also affected the type of failure. Basically three effects of temperature were expected to have affected the debonding load: (1) The difference in CTE between concrete and CFRP; (2) the reduced Young's modulus of the adhesive at elevated temperatures; and (3) the reduced bond strength of the concrete-adhesive interface at elevated temperatures.

5. ACKNOWLEDGEMENTS

The authors are indebted to the Dutch Ministry of Transport, Public Works and Water Management that supported this investigation and SIKA Nederland BV for supplying the CFRP laminates and the adhesive free of charge.

6. REFERENCES

- Blontrock, H. (2003). "Analyse en modellering van de brandweerstand van betonelementen uitwendig versterkt met opgelijmde composietlaminaten". Ph.D. thesis, Ghent University, Ghent, Belgium. (In Dutch).
- Di Tommaso, A., Neubauer, U., Pantuso, A., and Rostásy, F.S. (2001). "Behavior of adhesively bonded concrete-CFRP joints at low and high temperatures". *Mechanics of Composite Materials*, Vol. 37, No. 4, pp. 327-338.
- Klamer, E.L., Hordijk, D.A., and Janssen, H.J.M. (2005). "The influence of temperature on the debonding of externally bonded CFRP". *Proceedings of 7th symposium on Fiber Reinforced Polymer Reinforcement for Concrete Structures*, Editors: C.K. Shield, J.P. Busel, S.L. Walkup and D.D. Gremel, Kansas City, pp. 1551-1570.
- Klamer, E.L. (2006). "The influence of temperature on concrete structures strengthened with externally bonded CFRP, Experimental Research". O-2006.04, Eindhoven University of Technology, Eindhoven, The Netherlands.
- Tadeu, A.J.B., and Branco, F.J.F.G. (2000). "Shear tests of steel plates epoxy-bonded to concrete under temperature". *Journal of Materials in Civil Engineering*, Vol. 12, No. 1, pp. 74-80.
- Wu, Z.S., Iwashita, K., Yagashiro, S., Ishikawa, T., and Hamaguchi, Y. (2005). "Temperature effect on bonding and debonding behavior between FRP sheets and concrete". *J. Society of Material Science*, Vol. 54, No. 5, pp. 474-480.

EFFECTS OF BOND CONFIGURATIONS ON FLEXURAL RESPONSE OF RC BEAMS EXTERNALLY STRENGTHENED WITH CFRP SHEETS

Jianguo Dai

(Researcher, LCM Research Center, Port and Airport Research Institute, Yokosuka, Japan)

Keisuke Sumiyoshi

(Graduate student, Division of Built Environment, Hokkaido University, Sapporo, Japan)

Tamon Ueda

(Professor, Division of Built Environment, Hokkaido University, Sapporo, Japan)

Hiroshi Yokota

(Director General, LCM Research Center, Port and Airport Research Institute, Yokosuka, Japan)

Yasuhiko Sato

(Associate Professor, Division of Built Environment, Hokkaido University, Sapporo, Japan)

ABSTRACT

This paper investigates experimentally how various bond configurations influence the flexural response of FRP-strengthened RC beams. A total of seven beams (200×200×2200mm) were tested. One was the reference without strengthening. Two were strengthened with CFRP sheets using hard and soft adhesive bonding, respectively, along the whole test span. The remaining four were applied a combination of hard and soft adhesives but in two different ways. One way is to use the soft adhesive at the flexure-dominating zone only and another is to use it for the shear-dominating zone only. Pair tests were conducted for these four specimens under both normal and low temperature (-10°C). It is revealed that a sole use of soft adhesive improves the ultimate member strength and ductility but leads to a loss of stiffness. Using the soft adhesive at the flexure-dominating zone can not improve the member strength but improve the member ductility only. However, use of hard adhesive at the flexure-dominating zone and the soft one for the remaining parts can improve the member strength and ductility while avoiding loss of member stiffness. This test program provides an in-depth understanding of the debonding mechanisms in the FRP-strengthened RC beams. In addition, it is verified that a low temperature of -10°C does not influence the global flexural response of FRP strengthened beams using the combined bonding system.

KEYWORDS

FRP, adhesive bonding, flexural strengthening, bond configuration

1. INTRODUCTION

Flexural strengthening of functionally deficient RC members is a main application of FRP strengthening technology. Since stress transfer between the external FRP and existing RC members is usually achieved through adhesive bonding, appropriate selection of adhesives plays a critical role in optimizing the mechanical and durability performance of the strengthened system. Unfortunately, the issue of how to achieve optimized macro-bond performance remains unsolved up to date. As has been widely known in the FRP flexural strengthening cases, premature interface debonding causes a sudden drop of loads and loss of ductility of the whole composite system except when additional mechanical anchorages are available at the end of FRP. This debonding occurs often at a low stress level in the FRP when an epoxy adhesive with high elastic modulus is chosen to be the bonding material. A fewer researchers tried to use a flexible adhesive with low elastic modulus for the FRP flexural strengthening application [Maeda et al, 2001, Sato et al. 2002]. They found that the flexible bonding can improve greatly the

flexural strength, ductility and the strain level in FRP at the ultimate stage. However, it is noticed that the flexible bonding system hardly contribute the strength and stiffness enhancement before steel reinforcement yields. This is not favored when the serviceability strengthening is also required. With the aim to consider simultaneously the factors of strength, stiffness, ductility, and also, the utilizing efficiency of FRP materials, this study tries to find an optimized bond configuration for the flexural strengthening while providing an in-depth understanding of the debonding mechanism.

2. TEST PROGRAM

A total of 7 RC beams were designed to fail in flexure in this test program. Each beam has the section area of 200×200 mm and was longitudinally and transversely reinforced with 2D13mm and D6@75mm, respectively (see Fig.1). The yielding strengths of the longitudinal and transverse reinforcement are 370 and 356MPa, respectively. As shown in Table 1, among the seven beams SP-1(0-0-0) was the reference beam and the remaining six were strengthened with 0.334mm thick CFRP sheets. The elastic modulus and tensile strength of the CFRP sheets are 230GPa and 3430MPa, respectively. Two types of bonding adhesives EE2000 and HP-430 were used. EE2000 is a hard adhesive that has an elastic modulus of 1.95GPa and HP-430 is a soft adhesive with an elastic modulus less than 50MPa. Four types of bond configurations were applied (SP-2 to SP-5 in Table 1) that correspond to specimens H-H-H, S-S-S, H-S-H, and S-H-S, respectively. Description of these different bond is shown in Fig.1, where ‘‘H’’ and ‘‘S’’ mean the hard and soft adhesives, respectively. Concept for this design is based on the presumption that that soft bond around the flexure-dominating zone can increase the beams’ rotation and delay the mid-span debonding while soft bond at the shear-dominating zone can increase the interface slip and bond force transfer. The thickness of adhesive layer was kept 0.5mm for all strengthened beams. Specimens SP-6 and SP-7 had the same test variables with SP-4 and SP-5 but they were put in a low-temperature chamber for two weeks before test but after the curing to investigate the bond performance under low temperature, which is a popular environmental concern in Hokkaido. Specimens SP-1 and SP-2 were from a previous test (Dai et al. 2005). Their concrete strength was 33MPa. Concrete strength of the remaining beams was 30MPa.

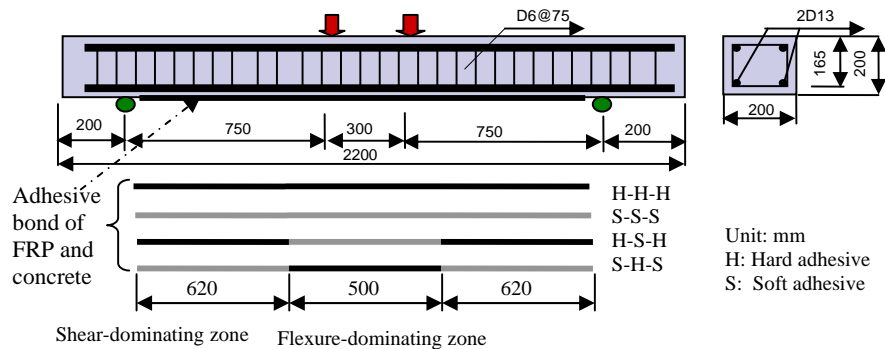


Figure 1: Beam dimensions, bonding configurations and loading arrangement

Table 1 Arrangement of specimens and test results

No	Test Code	P_y (kN)	P_u (kN)	δ_y (mm)	δ_u (mm)	$\epsilon_{frp,max}$ (μs)	Temperature	Failure description
SP-1	0-0-0	40.2	44.1	4.08	25.7	-	20°C	Concrete failure after steel yields
SP-2	H-H-H	61.6	109.0	5.79	16.4	7,170	20°C	FRP peeling (failure at concrete side)
SP-3	S-S-S	48.6	114.5	4.95	25.6	12,004	20°C	FRP peeling (failure in the adhesive layer)
SP-4	H-S-H	49.2	104.4	4.8	18.2	8,810	20°C	FRP peeling (failure at concrete side)
SP-5	S-H-S	54.1	120.3	5.26	25.1	11,216	20°C	FRP peeling (failure in the adhesive layer)
SP-6	H-S-H LT	N/A	103.5	N/A	18.0	N/A	-10°C	FRP peeling (failure at concrete side)
SP-7	S-H-S LT	N/A	117.0	N/A	27.1	N/A	-10°C	FRP peeling (failure in the adhesive layer)

Note: P_y : load at the yielding of steel reinforcement; P_u : the maximum load capacity; δ_y : deflection at the yielding of steel reinforcement; δ_u : the ultimate deflection; $\epsilon_{frp,max}$: the maximum strain observed in FRP; and f_c : concrete strength. N/A: unclear yielding load and deflection since gages on the FRP sheets and steel reinforcement were incorrectly recorded in the chamber.

3. TEST RESULTS AND DISCUSSION

3.1. Load-Deflection Response

Figures 2 and 3 shows load-deflection curves of all tested beams. The yield and ultimate load and deflection are presented in Table 1 as well. It is clear that all strengthened beams have greater member stiffness and ultimate member strength than the reference one (see Fig.2). Test beams H-H-H and H-S-H have similar ultimate strength. On the other hand, test beams S-S-S and S-H-S have similar ultimate strength. So the bond properties of adhesives at the shear-dominating zone determine the efficiency in strength enhancement. As shown in Table 1, the maximum strains in the FRP sheets in the cases of H-H-H, H-S-H, S-S-S and S-H-S are 7170 , 8810 , 12004 , and 11216μ , respectively, meaning that the efficiency of utilizing FRP's strength is much improved by using soft adhesives at the shear-dominating zone. Interestingly, test beams H-H-H and S-H-S have similar member stiffness before steel yields. So have the test beams H-S-H and S-S-S. This comparison indicates that the bond at the flexure-dominating zone determines the strengthening efficiency in terms of member stiffness. The hard interface bond seems favorable for the flexure-dominating area. The ductility performance sequence is: $S-H-S \approx S-S-S > H-S-H > H-H-H$, indicating that the interface slip capacity at both flexure and shear zones influence the ductility but the latter's influence is much greater. Therefore, it is a good choice to combine the hard bond between FRP and concrete at mid-span area for the stiffness enhancing purpose and the soft bond at anchorage areas for the strength and ductility enhancing purpose. Figure 3 shows the effects of low temperature. The global flexural responses of FRP strengthened beams under 20°C and -10°C do not show noticeable differences at the whole loading stage.

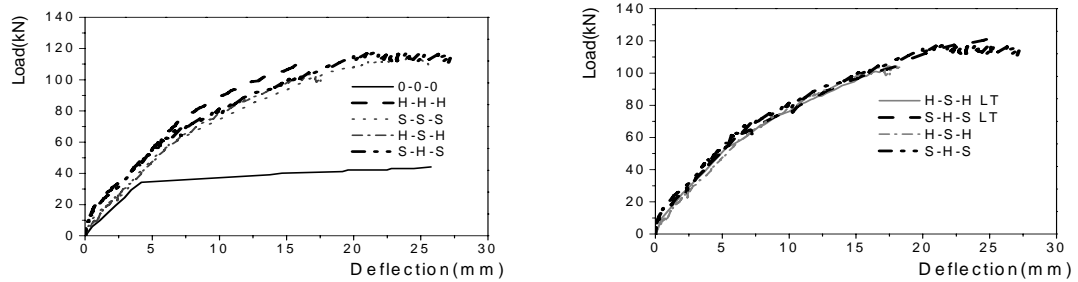


Figure 2: P- δ curves: effects of bond configuration Figure 3: P- δ curves: effect of temperature

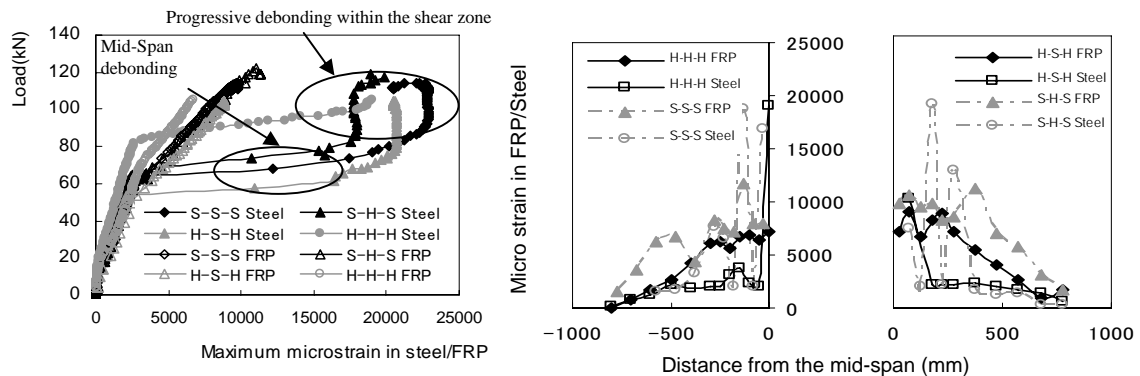


Figure 4 Strain development in FRP/steel Figure 5 Strain profile in FRP/steel at failure

3.2 Strain Development and Distribution in the FRP Sheets and Steel Reinforcement

Figure 4 indicates development of the maximum strains observed in the FRP and steel at the flexure zone. Strains in both steel and FRP increase with the load and strains in the FRP are larger before the steel yields. In the contrast, strains in the steel are much greater than that in FRP after the steel yields. This can be understood as the occurrence of mid-span debonding between the FRP and concrete that is triggered by the yielding of steel. Clearly, this mid-span debonding is not the critical factor to cause the ultimate failure of FRP strengthened RC beams although it occurs first. It does not stop the continuing increase of strain in FRP (see Fig.4). After this mid-span debonding period, stress concentration in the mid-span can be released. Rapid increase of the maximum strain in the steel stops and but strains in the FRP increase further. As a result, the debonding between FRP and concrete propagated stably

in the shear-dominating zone, where the steel has not yet yielded. A substantial increase of member strength is observed during this period (see Fig.4). Soft adhesive in the shear zone allows more increase of strain in the FRP since it can accommodate larger interface slip and opening ability until a critical debonding. Figure 5 presents the strain distributions in the FRP and steel for the peeled side of each beam at the ultimate stage. It is shown that different bonding adhesives hardly influence the strain distribution pattern in the flexural zone at the ultimate stage. However, use of the soft adhesive in shear zone [see S-S-S and S-H-S in Fig. 5] corresponds to a wider-range steel yielding area that brings more member ductility. Moreover, the average strain gradients of FRP within the shear zone are comparatively large. Hence using soft adhesives brings higher average bond stresses along the shear span, which may be related to the increased number of cracks within the shear span.

3.3 Failure Mode and Debonding Mechanisms

All beams failed due to the peeling of CFRP sheets at one side as shown in Fig.6. However, the FRP/concrete interfaces failed at concrete side and in adhesive layer, respectively, when the hard and soft adhesives were used in the shear-dominating zone. In all the cases, the peeled FRP sheets were attached with some cover concrete at the mid-span zone. In the case that the amount of cover concrete is small, a horizontal crack at the height of steel reinforcement is yet visible (see S-H-S and H-S-H in Fig.6). As mentioned in the last section the FRP/concrete interface at the mid-span debonds right after the steel yields to keep the deformation compatibility. These horizontal debonding cracks were consequently attributed to the further yielding of steel reinforcement. The impact from energy release of FRP induced spalling of concrete cover. In the shear-dominating zone, the peeling of FRP from concrete in all tested beams are related to a major flexure-shear crack hence a critical factor for the ultimate failure is the interface deformation ability at the tip of a major diagonal flexural-shear crack. Hence a comprehensive mix-mode bond modeling for FRP/concrete interface and the discrete modeling of concrete fracture are needed to simulate the above-two different failure mechanisms. Fig.6 also shows that soft bond in the shear zone allows development of more cracks (see S-S-S and S-H-S) compared to hard adhesive case at the ultimate stage. This should be considered when numerical simulation based on crack spacing is performed for bond strength prediction.

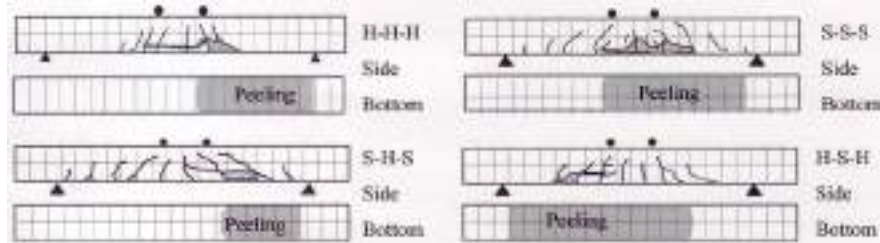


Figure 6 Failure modes of tested beams

4. CONCLUSIONS

1. A further insight into the whole-range debonding mechanisms of FRP strengthened RC beams in flexure is provided. It is found that concrete cover failure at the mid-span area is not closely related to the bond of FRP/concrete interface but the yielding of steel. The ultimate failure of strengthened beams occurs far beyond the mid-span debonding between FRP sheets and concrete. The interface deformation capacity at the tip of a major flexural-shear crack is confirmed to be a critical factor dominating the ultimate strength and ductility.
2. Combined use of soft and hard adhesives at the shear and flexure-dominating zones, respectively, seems to give an optimized flexural response. More studies are needed to analyze the effective bond length of FRP to concrete with multi-cracks, so that an optimum proportion of hard to soft adhesive bonding lengths can be formulated.
3. The strengthened beams show no difference in their flexural response under low temperature of 20°C and -10°C.

5. REFERENCES

- Maeda, T.; Komaki, H.; Tsubonai, K. and Murauei, K.(2001), Strengthening Effects of CFRP Sheet Bonding using Soft Resins, *Proceedings of the Japan Concrete Institute*, Vol.23, No.1, pp.817-822(in Japanese)
- Sato, Y., Ito, T., Komaki, H. and Maeda, T. (2002), Flexural Behaviors of Reinforced Concrete Beams Strengthened by CFS with Soft Layer, *Proceedings of the Japan Concrete Institute*, Vol.24, No.2, pp.1375-1380(in Japanese)
- Dai, J.G., Ueda, T., Sato, Y. and Ito, T. (2005), Flexural Strengthening of RC Beams Using Externally Bonded FRP Sheets through Flexible Adhesive Bonding, *Proceedings of the International Symposium on Bond Behavior of FRP in Structures (BBFS 2005)*, Edited by J.F. Chen and J.G. Teng, Hong Kong, China, pp.213-221.

ENVIRONMENTAL SENSITIVITY AND DEFECT CRITICALITY IN FRP BOND TO CONCRETE THROUGH A FRACTURE MECHANICS APPROACH

Rajiv Navada

(University of California San Diego, La Jolla, CA 92093-0085, USA)

Vistasp M. Karbhari

(University of California San Diego, La Jolla, CA 92093-0085, USA)

ABSTRACT

Although fiber reinforced polymer (FRP) composites are extensively used for the rehabilitation of concrete infrastructure there is a critical lack of information regarding the effect and criticality of defects, both from a short-term perspective and as related to long term durability making assessment of these difficult. This paper reports on the use of a fracture based methodology for determination of criticality and discusses some results based on defect type and exposure.

KEYWORDS

Bond, Fracture energy release rate, defect, effect, criticality..

1. INTRODUCTION

Although fiber reinforced polymer (FRP) composites are increasingly being used in the form of externally bonded reinforcement for the rehabilitation of deteriorating and/or under-strength concrete structures, there are still a number of issues that have not been resolved and are hence being addressed either through use of excessive caution or through inordinately high factors of safety. Predominant on this list are the issues of durability and the criticality of defects. While a body of research is being conducted on the former topic, the latter has still to be addressed in an integrated fashion. Although a series of recent publications has provided lists of potential defects and an assessment of techniques to identify them (Kaiser and Karbhari, 2003; Kaiser and Karbhari, 2004; Kaiser et al, 2004), and guidelines for repair of a range of defects were recently published (Mirmiran et al, 2004) there is a singular lack of understanding related to the criticality of defects and the effect of these defects on the integrity of the rehabilitation scheme.

Since most rehabilitations are expected to provide significant periods of service it is important that the effect of defects be clearly determined so as to provide the engineer with guidance as to whether a defect found during inspection has to be immediately treated, or can be monitored for a period of time, or merely neglected as being non-critical and aesthetic in nature. In addition, it is important that the effect of environmental exposure on the system be assessed since this could have an accelerative effect on the progression of growth of the defect, and hence on its criticality. In this paper a fracture based approach to the assessment of criticality of defects is outlined and some results are discussed providing initial guidance both to effects of defects and to effects of environmental exposure.

2. APPROACH AND METHODOLOGY

In an attempt to simulate the growth of separation between the externally bonded FRP and the concrete substrate (which could occur within the concrete, within the adhesive layer, between layers of FRP, or in combinations thereof) a method initially proposed by Yamaguchi et al (1999) and modified by Kaiser (2002) is used in the current investigation. The test setup essentially consists of a concrete beam with a central notch over which the FRP layer is bonded. When loaded as shown in Figures 1(a) and (b) a mixed mode condition is imparted at the two crack tips thereby closely simulating actual field conditions for crack progression. An additional advantage of the method is

that two interfacial regions, one on either side of the central notch can be studied simultaneously enabling multiple tests under similar conditions, as well as providing a means for direct comparison of effects of defects occurring along the bonded length of the FRP composite. Details on the test method, including the use of a video monitoring system capable of accurately recording crack growth along the four edges (Figure 2) are provided by Kaiser (2002) and hence will not be repeated herein.

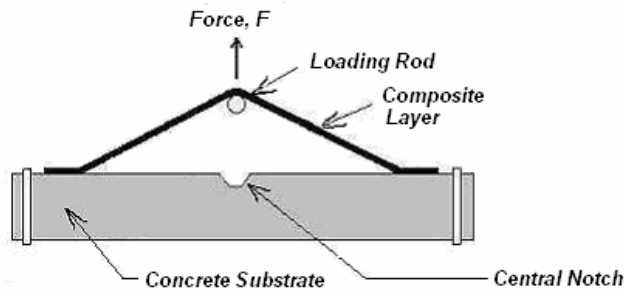


Figure 1(a): Schematic of Test Set-up

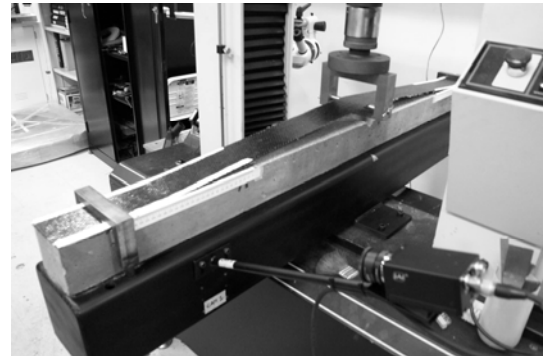


Figure 1(b): Test Setup Showing Progression of Interfacial Crack

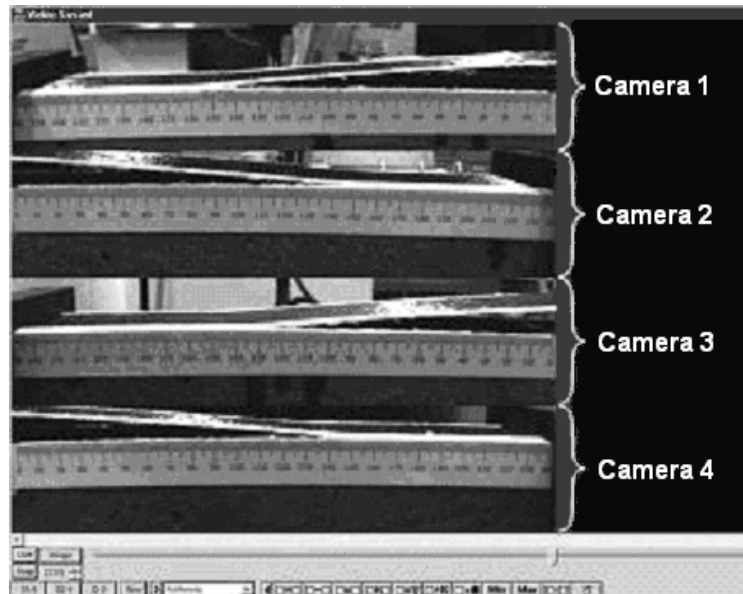


Figure 2: Typical Images of Crack Growth Obtained By the Cameras

In the current set of experiments strips of unidirectional carbon fabric were laid-up on the concrete beams and impregnated with an epoxy resin having a viscosity of 700-900 cps, leaving a central unbonded region of 374.7 mm on either side of the central notch. This gap both ensured that crack progression was stable and that the effect of the notch (used for placement of the rod to cause peel as in Figure 1) on propagation was minimized. Two layers of the fabric were placed and the specimens were allowed to cure under ambient conditions for 4 days prior to testing.

In order to assess the effect of defects arising from conditions related to bonding specimens were tested after application of both inadequate primer and excessive primer (with the latter representing the case where the excessive application of primer resulted in a discernable resin rich layer at the interface), in the presence of a moisture saturated substrate (equivalent to 4% moisture measured at the surface), and with a variety of debonds and delaminations at the interface. Specimens were also tested after exposure for periods of 30 and 60 days to (a) heat at 65°C, (b) freeze at -10°C, (c) immersion in water at 23°C and (d) ponding (representative of conditions where the top of the concrete was exposed to water which was allowed to seep in towards the FRP-concrete interface. For the purpose of the current investigation a uniform and constant level of 2 mm of water was maintained on the top surface of the specimen, i.e in contact with the concrete on the face opposite to the FRP).

3. ANALYTICAL DEVELOPMENT

As shown in Figure 1, the CFRP is loaded by means of a loading rod which is inserted in the notch in the concrete beam. From a force balance and use of trigonometric relations the potential energy stored can be determined by integrating the forces with respect to Δ under the condition that peel length, a , remains constant (wherein E_{11} is the Young's Modulus of Elasticity of the composite membrane, ε is the strain in each of the arms, F is the vertical Force in each arm and can be expressed as $S \sin \theta$, where θ is the peel angle, a is the peeled distance on either side, Δ is the vertical displacement of loading arm $x = \Delta/a$, $\alpha = s/a$ and $S = E_{11}Bt$ as shown in Figure 3) and using the initial condition that at $\Delta=0$, $U_s=0$ as

$$U_s = E_{11}Bt \left[\frac{\Delta^2 + s^2 + 3a^2}{2a} - \sqrt{(a-s)^2 + \Delta^2} - \sqrt{(a+s)^2 + \Delta^2} + \frac{\sqrt{\{(a+s)^2 + \Delta^2\}\{(a-s)^2 + \Delta^2\}}}{2a} \right]$$

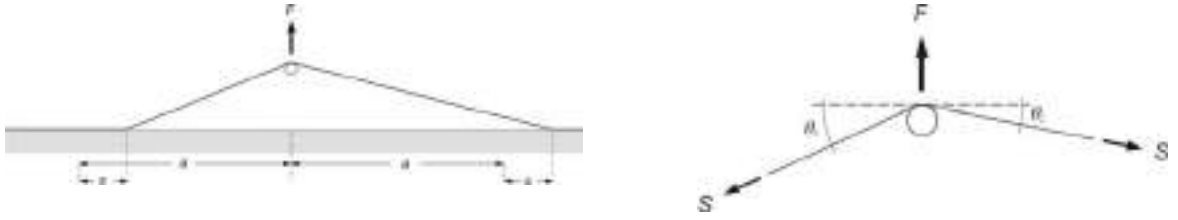


Figure 3: Geometry and force balance

Finally, fracture toughness can be calculated by differentiating the equation for potential energy with respect to the average peel distance, a , under the condition that membrane displacement, Δ , remains constant, resulting in

$$G = - \frac{dU}{2Bda} \Big|_{\Delta=const}$$

$$G = \frac{1}{4} E_{11}t \left[x^2 + \alpha^2 - 3 + \sqrt{(1+\alpha)^2 + x^2} \sqrt{(1-\alpha)^2 + x^2} + \frac{(1+\alpha) \left\{ 2 - \sqrt{(1-\alpha)^2 + x^2} \right\}}{\sqrt{(1+\alpha)^2 + x^2}} + \frac{(1-\alpha) \left\{ 2 - \sqrt{(1+\alpha)^2 + x^2} \right\}}{\sqrt{(1-\alpha)^2 + x^2}} \right]$$

This represents the “slip” case as defined by Kaiser (). Under constraints of the test fixture if the slip were restricted, the strain in the two arms of the composite membrane would be different. This would cause the strain energy stored in the two arms and hence the fracture energy release rates (FERR's) for the two arms to be different such that $S_1 = \varepsilon_1 E_{11}Bt$ and $S_2 = \varepsilon_2 E_{11}Bt$ leading to the generalized form of

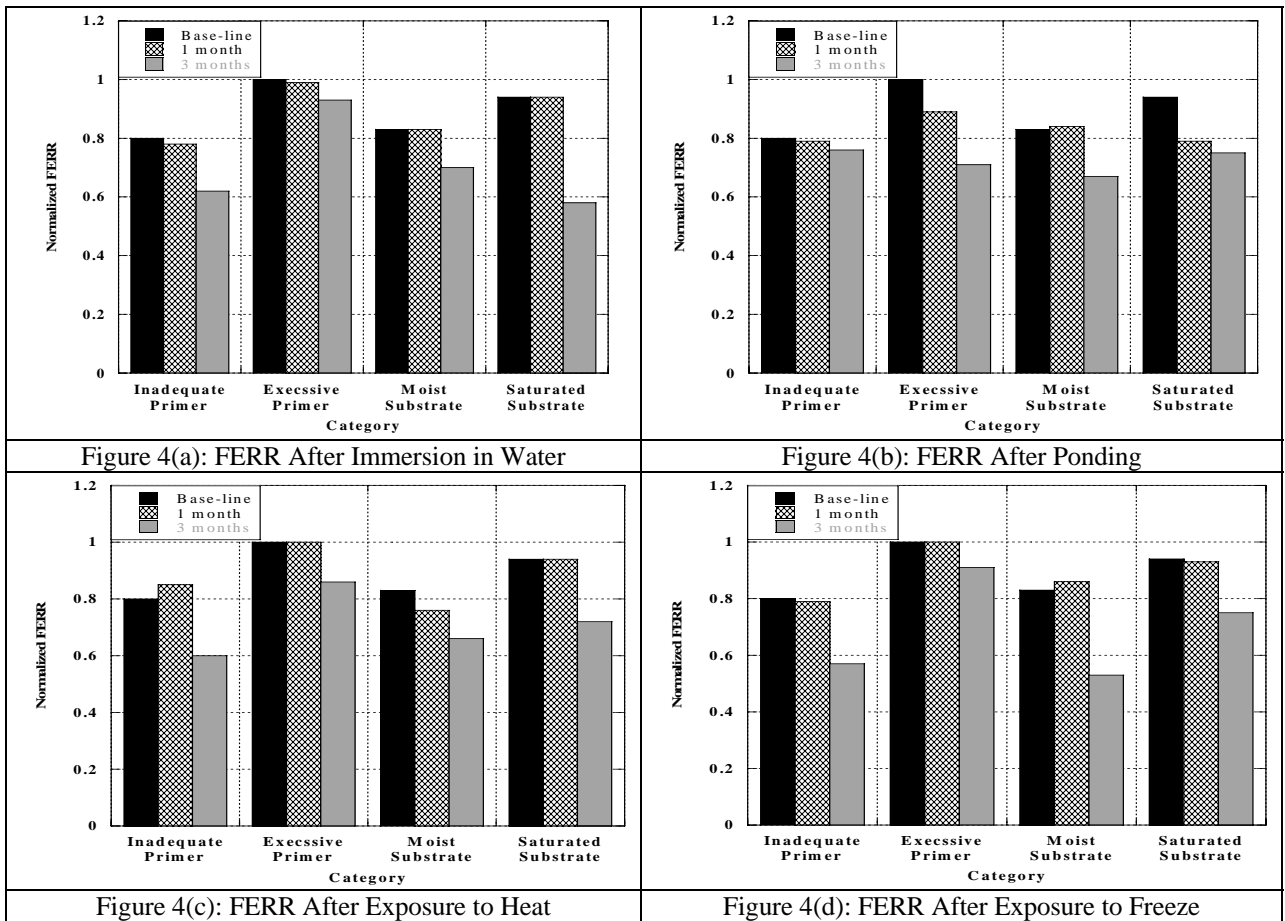
$$G = E_{11}t \left[-1 + \left\{ \left(-\sqrt{a^2 + \Delta^2} - \frac{a^2}{\sqrt{a^2 + \Delta^2}} \right) / a \right\} - \left\{ \left(-a\sqrt{a^2 + \Delta^2} + \frac{\Delta^2}{2} \right) / a^2 \right\} \right]$$

Using this equation it is possible to get 2 values of FERR per concrete specimen, one from each side of the notch. It should be noted that for this case the result of the differentiation for G involves the division by B instead of $2B$ as in the earlier case.

4. RESULTS AND DISCUSSION

Due to space restrictions only representative results are presented herein. For ease of comparison results in Figures 4(a)-(d) results are shown as normalized values with the base-line being the defect free specimen set. Thus lower values represent greater levels of deterioration. As can be seen there is a substantial effect of exposure on FERR. It is interesting to note that there is a pronounced effect of freeze primarily in cases where the substrate has moisture prior to application of the FRP. Further it can be seen that gradients, as compared to saturation, of moisture are more deteriorative, as could be expected from a thermo-elastic perspective. It is interesting to note that approximate relationships can also be derived through such experiments to assess effects of defects. The effect of length of a delamination was seen to affect FERR in linear fashion till a limiting size when the length equaled the width of the fabric strip. This trend can be simply expressed as

$$\text{Normalized FERR} = 1 - 0.64(\text{Delamination width})$$



5. SUMMARY

This study provides a methodology for the comprehensive assessment of the effect and criticality of defects and environmental exposure. The use of the fracture mechanics approach ensures that it is amenable to scaling to allow results obtained on small specimens to be later appropriately scaled to field structures providing a means for development of inspection and defect criticality guidelines.

6. ACKNOWLEDGEMENTS

The authors gratefully acknowledge the support of SCCI and the Oregon Department of Transportation.

6. REFERENCES

- Kaiser, H. and Karbhari V.M. (2003), "Identification of Potential Defects in the Rehabilitation of Concrete Structures With FRP Composites," *International Journal of Materials and Product Technology*, 19[6], pp. 498-520.
- Kaiser, H. and Karbhari V.M. (2004), "Non-Destructive Testing Techniques for FRP Rehabilitated Concrete: I – A Critical Review," *International Journal of Materials and Product Technology*, 21[5], pp. 349-384.
- Kaiser, H., Karbhari V.M. and Sikorsky, C. (2004), "Non-Destructive Testing Techniques for FRP Rehabilitated Concrete: II – Assessment," *International Journal of Materials and Product Technology*, 21[5], pp. 385-401.
- Mirmiran, A., Shahawy, M., Nanni, A. and Karbhari, V.M., (2004) "Bonded Repair and Retrofit of Concrete Structures Using FRP Composites: Recommended Construction Specifications and Process Control Manual," NCHRP 514, Transportation Research Board of the National Academies,
- Yamaguchi, K., I. Kimpara, and K. Kageyama (1999), Evaluation of Debonding Energy Release Rate of Externally Bonded FRP Sheets for Rehabilitation of Infrastructures, in Proceedings of ICCM-12, Paris, France.
- Kaiser, H.(2002), Assessment of Defect Criticality and Non-destructive Monitoring in CFRP-rehabilitated Civil Structures, Masters Thesis Department of Structural Engineering, UCSD: La Jolla. p. 264.

IMPROVING THE BONDING AND DUCTILE BEHAVIOR OF FRP STRENGTHENED RC BEAMS

H. Fatemi,

Graduate student, the University of Tabriz, Tabriz, E. Azerbaijan, IRAN

A. Davaran,

Assistant Prof., the University of Tabriz, Tabriz, E. Azerbaijan, IRAN

J. Esmaili

Assistant Prof., the University of Tabriz, Tabriz, E. Azerbaijan, IRAN

ABSTRACT

Fiber reinforced polymer (FRP) is one of the most commonly used materials for strengthening and repairing of the concrete structures. Debonding between fiber and concrete is a common failure mode, which is brittle and abrupt. In this paper, it has been shown that adding the U-shaped FRP layers in the orthogonal direction to longitudinal FRP, extended upward to the beam's web, can improve the ductile behavior of the RC beam. A new and effective detailing for providing end-anchorage of FRP is proposed which easily can be constructed. Flexural behavior of several RC beams strengthened with the FRP by different arrangement of the U-shaped orthogonal reinforcing FRP were studied experimentally and the effectiveness of each arrangement has been verified.

KEYWORDS:

FRP, debonding, RC beams, ductility

1. INTRODUCTION

Fiber reinforced polymers (FRP) are progressively used for repairing and retrofit of reinforced concrete (RC) structures. The flexural weakness or defects of RC beams are tackled normally with gluing FRP plates to the tension face of the beam, Figure 1. Among the versatile types of the fibers, carbon textiles with higher tensile

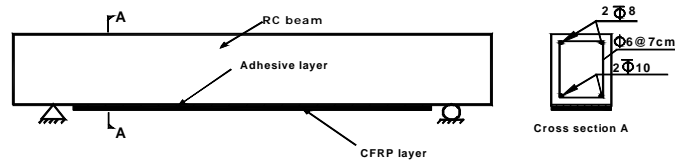


Figure 1. RC Beam Strengthened with FRP

strength is commonly preferred, because of easy handling and performance. Many researchers have studied the behavior of simply supported beams strengthened with carbon FRP (CFRP) attached to the bottom face of beam, (Smith and Teng 2002) and (Buyukozturk et al, 2004). Several important failure modes, observed experimentally are shown in Figure 2. These well-known modes are:

(a) Rupture of FRP in tension, (b) Shear failure near the supports or concentric force, (c) Crushing of concrete in compression and, (d) Debonding of the FRP or splitting of concrete cover.

The debonding mode can be separated to three groups, as indicated in (Smith and Teng 2002). These are:

(d1) Cover splitting of concrete cover attached to FRP, (d2) debonding of the FRP and glue from the concrete skin and, (d3) debonding of the FRP because of concrete cracks in the intermediate part of beam.

An extensive description of debonding modes has been verified by (Oehlers and Seracino 2004). Many analytic-empiric formulas have been proposed based on different theories to explain the debonding failure mode by the aforementioned references. Recent test results have shown that debonding has an abrupt nature, so a rapid

decrease of the strength is usually observed immediately after the ultimate load is attained. Promotion of bonding strength and formation of some ductile behavior can be viewed as important goals in this regard. In this paper, an innovative method for anchoring of CFRP for strengthening of beams is presented. In addition, the effects of adding U-shaped FRP, which are orthogonal to the longitudinal fibers and extended upward to the beam's web are investigated.

2. MATERIALS AND GEOMETRY AND METHODS

In this research, seven lightly reinforced concrete simply supported beams are verified experimentally. The first four specimen are aimed to observe the ductile behavior by adding some U-shaped, specially detailed FRP orthogonal to main FRP. Moreover, the last three specimens are tested to verify an innovative anchorage detailing.

2.1. Geometrical Property of Specimens

All the seven beams have a dimensions of 150x200x1200 millimeters (mm.). See Figure 1. The top and bottom reinforcing steels are two No. 8 and two No. 10 REBARS (having diameters of 8 and 10 mm.), respectively. Loop stirrups with 6 mm. in diameter at 70.mm spacing are used for shear reinforcing. This reinforcing complies with minimum demands of ACI 318-99 .The difference between flexural and shear nominal load bearing capacity of the strengthened beam, provides a wide variation rang for verifying the debonding force. So getting a detailing to cause the debonding strength moves up toward the upper limit of shear failure load, was thought to be a good plan. It can be mentioned that the U-shaped FRP could also increase the shear strength in some cases, which must be taken into account. The concrete cover of tension and compression reinforcement are 35 mm. and 30 mm., respectively. All the other size and spacing parameters are depicted in the Figures 1 and 3.

2.2. Physical properties of the material

The compressive strength of the cylindrical samples of the concrete was about 20.6 Mpa. The yield strength of the longitudinal and transverse rebar was 344 and 275 Mpa, respectively. The carbon fiber textiles used was SIKAWRAP-Hex230 C and the epoxy for gluing the fibers had a grade of SIKADUR 330, both manufactured by the SIKA-co of the Switzerland. The tensile strength, modules of elasticity, and one layer thickness of carbon fibers were 3650 Mpa, 231000 Mpa and 0.12 mm, respectively.

2.3. Methods of Strengthening of the Specimens

The four specimens of the first group have been made as follows:

A0: a specimen with no CFRP, **A1**: having two layers of CFRP with dimension of 150 mm. x 900 mm., **A2U**: having two layers longitudinal CFRP and one U-shaped transverse (150mm width) attached to each end of the longitudinal CFRP and **A3X**: having two layers of longitudinal CFRP and one crossed shaped transverse (150mm x 500mm) CFRP at each end. These specimens have been shown in Figure 2. The other three specimens in the second group are made as follows: **B1**: specimen with two longitudinal and one U-shaped transverse CFRP at each end, **B2AN**: specimen with two layers of CFRP and two anchoring CFRP at a distance of 240 mm. from each end and **B3AN**: specimen similar to **B2AN** but the distance of the anchoring CFRP from each end was 140 mm. The anchor detail is made of following steps. First, a slit with a width a little less than concrete cover is prepared. Then the end of longitudinal FRP is wrapped around a coupled of 10 mm rebar which is smeared with glue. Finally, they are placed into the slit and then the finished face is smoothed by extra sikadure31/41. The slit is covered by two layered U-shaped CFRP, as shown in Detail 1 of Figure 2.

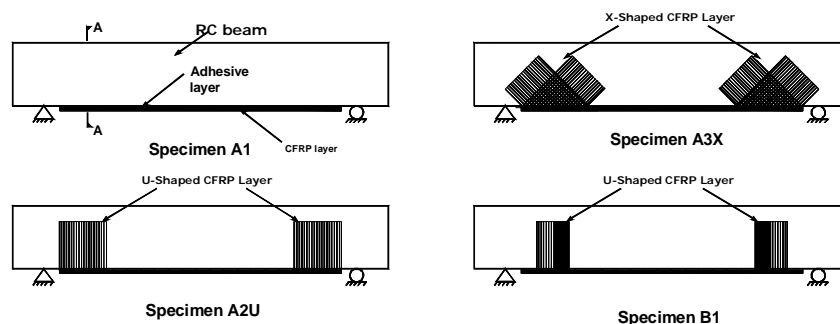


Figure 2. The Different Arrangement of Specimens

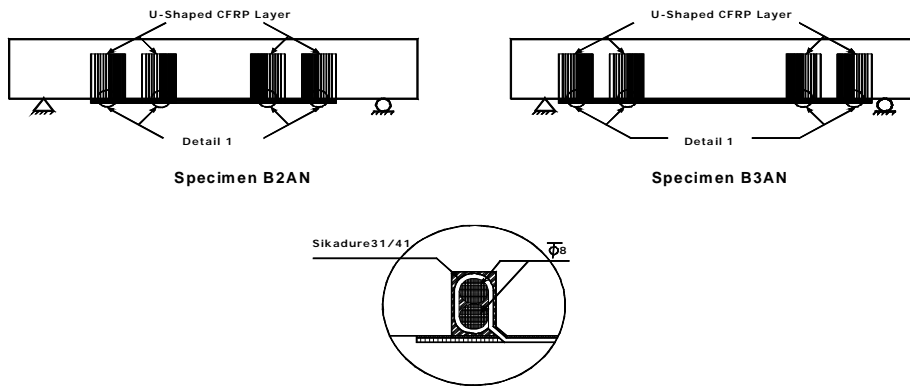


Figure 2(Continued). The Different Arrangement of Specimens

2.4. Test Setup

Every seven specimen was loaded by a universal testing machine. The loading method is shown in Figure 3. The points A and C have 100mm distance from beam's end. The two moving support A and C, compressed the specimen against the fixed support B. It was not seen any local concrete crushing near the supports in this tests.

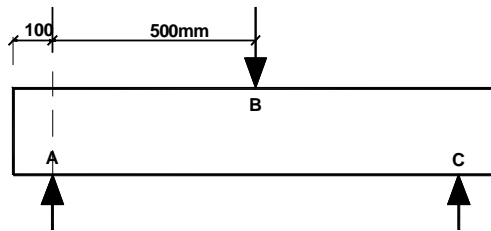


Figure 3. The Loading Setup

3. RESULTS

The load-displacement graphs of the first group have been traced in Figure 4. The load setting view and observed failure mechanisms have been shown in Figure 6. The load-displacement behavior of the second group has been shown in Figure 5. A new observed failure mode for specimen **B2AN** and **B3AN** of the second group are indicated in Figure 6. In this mode the lateral cover splitting followed by bottom face splitting of the concrete cover was observed. The initiation of lateral cover separation can be attributed to the considerable tensile force, which is produced by the U-shaped CFRP at the anchoring zones.

The broader area of the separation zone is thought to be the main reason for the increased load capacity of the specimens **B2AN** and **B3AN** in second group. It is evident that the proposed anchoring detail can drastically raise the load capacity in comparison to traditional bonding method such as one used in specimen **B1**.

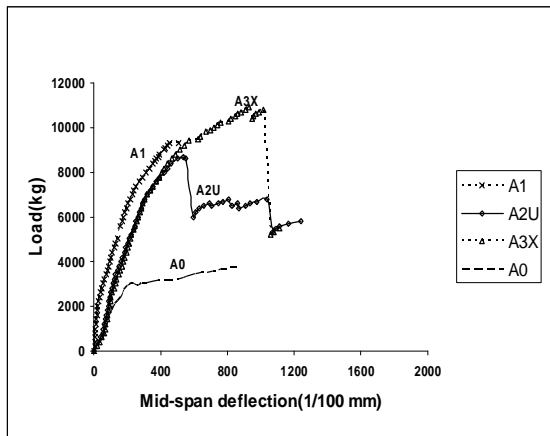


Figure 4. Comparison of 1st Group

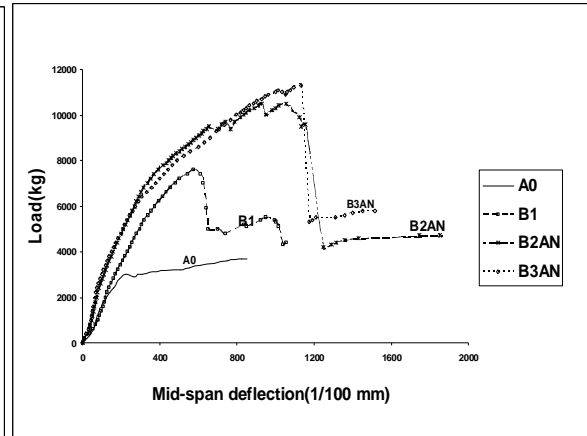


Figure 5. Comparison of 2nd Group



(a) Load Setting View



(b) End Cover Splitting, A1



(c) Intermediate Debonding, A2X



(d) Side cover Splitting, B2AN



(e) Side cover Splitting, B3AN



(f) Shear Failure Between, B3AN

Figure 6. Observed Failure modes

4. CONCLUSION

Eight simply supported RC beams were investigated experimentally. Some observed results could be mentioned as follow:

- a) Using the U-shaped transverse CFRP can partly remove the abrupt and brittle nature of the debonding failure mechanism, but further researches are needed to confirm the results.
- b) An innovative and simple anchoring detailing for multi layer CFRP is proposed. This method can postpone the end debonding mechanism and considerably increase the load bearing capacity of simple RC beams. Extensive experimental and analytical works are required to characterize the proposed method.
- c) Using the U-shaped end anchorage causes the intermediate debonding precedes the end debonding mechanism.
- d) The presence of anchorage leads to the shear failure to occur near that zone.

5. REFERENCES

- Smith S. T. and Teng J. G. (2002). "FRP-strengthened RC beams. I: review of debonding strength models". Engineering Structures, Vol. 24, pp 385-395.
- Buyukozturk O., Gunes O. and Karaca E. (2004). "Progress on understanding debonding problems in reinforced concrete and steel members strengthened using FRP composites". Construction and Building Materials, Vol. 18, pp 9-19.
- Oehlers D. J. and Seracino R. (2004). Design of FRP and Steel Plated RC Structures, 1st edition, Elsevier Ltd.

INTERMEDIATE CRACK DEBONDING ANALYSIS OF REINFORCED CONCRETE BEAMS STRENGTHENED WITH EXTERNALLY BONDED FRP PLATES

Luciano Ombres

Associate Professor, Department of Structural Engineering, University of Calabria, Rende (CS), Italy

ABSTRACT

The present paper concerns with intermediate crack debonding failure modes in FRP strengthened reinforced concrete beams; a theoretical non linear model derived from a cracking analysis based on slip and bond stress is adopted to predict the stresses and strains distributions at the failure. The analysis refers to beams with multiple cracks; an analytical form of the local bond-slip law is, also, considered. In order to validate the effectiveness of the model, a comparison between theoretical predictions and experimental results available in the literature, is carried out. Results of a numerical analysis, varying geometrical and mechanical parameters involved in the physical problem are, also, presented and discussed.

KEYWORDS

Crack Debonding, Reinforced Concrete, FRP

1. INTRODUCTION

The behaviour of reinforced concrete structures strengthened with externally bonded Fiber Reinforced Polymers (FRP) plates is governed from debonding failure modes that, as well known, can drastically reduce their flexural capacity. Debonding failures can take place at the ends of the FRP plates in presence of high stresses at the interface between the FRP and the concrete or away from the ends of the bonded FRP plates when they are induced by flexural or flexural-shear cracks. The first failure modes have been extensively studied and many models of analysis have been proposed; on the contrary, the second type of failure, commonly named Intermediate Crack-induced debonding failure (IC debonding failure), has received less attention especially from a theoretical point of view.

The mechanism of IC debonding is related to the formation of cracks at the tensile side of the concrete elements. When a crack is formed in the concrete, the tensile stresses released by the cracked concrete are transferred to the FRP plate; consequently high local interfacial stresses between the FRP plate and the concrete are induced near the crack. Further increase of the applied loading produce an increase both in the tensile stress in the plate and in the interfacial stress between the FRP plate and the concrete near the crack. When the interfacial stress achieves the critical values, debonding initiates and then propagates away from the crack. The IC debonding can occur in presence both of a single flexural crack and of multiple cracks; in the last situation a succession of plate debonding between adjacent cracks can occur simultaneously with a sudden failure of the beams.

The IC debonding is governed by the FRP-to-concrete bond-slip behaviour, which, generally, is affected by elastic deformations and microcracking; the interfacial debonding is likely to occur near the crack intersection immediately after flexural cracking.

Even if the IC debonding represents the most common failure mode in reinforced concrete structures strengthened with externally bonded thin FRP plates, there is a lack of research on this topic and a limited number of models are available in the technical literature; among those the models proposed by Niu and Wu, Chen and Teng and Liu, Oehlers and Seracino.

Niu and Wu (Niu and Wu, 2001) developed a methodology for predicting the debonding failure load due to flexural cracks in FRP-strengthened reinforced concrete beams based on the fracture energy criterion; the debonding failure load is established by combining the reinforced concrete beam theory with the solution from the simple shear test.

The model proposed by Chen and Teng (Teng et al. 2003) is based on the similarity between the IC debonding failures and those in simple shear tests; a bond strength model is combined with a simple section analysis for predicting the strength of beams and slabs, which fail by IC debonding. The maximum force that the bonded FRP can take is expressed as.

$$P = \alpha \beta_f \beta_L \sqrt{f_c} b_f L_e, \text{ where } L_e = \sqrt{\frac{E_f t_f}{\sqrt{f_c}}}; \quad \beta_f = \sqrt{\frac{2 - b_f/b_c}{1 + b_f/b_c}}; \quad \beta_L = \begin{cases} 1 & \text{if } L \geq L_e \\ \sin(\pi L/2L_e) & \text{if } L \leq L_e \end{cases} \quad (1)$$

and b_c =concrete width, $b_f t_f$ and E_f = FRP width, thickness, and elastic modulus, respectively, L = bond length; f_c = concrete compressive strength, α = calibration factor to account for any difference between the behaviour of a beam failed by IC debond and a shear-lap specimen failed by interfacial debond. The α -value proposed by Chen and Teng on the basis of experimental results is 0.4. Recently, an experimental study carried out by Pham and Al-Mahaidi (Phan and Al-Mahaidi, 2006) on CFRP retrofitted reinforced concrete beams, indicates that α can be taken as 1.04.

A discrete crack model based on partial interaction theory has been developed by Liu, Ohlers and Seracino (Liu et al., 2005) to analyse the IC debonding behaviour of plated members; the model takes into account slip at both the plate/concrete and bar/concrete interfaces. Through the model the maximum plate strain reached and the strain at debonding failure can be determined.

In the present paper, a theoretical non linear model derived from a cracking analysis, founded on slip and bond stresses, is adopted for the analysis of the debonding induced from intermediate flexural cracks in FRP reinforced concrete beams. The analysis refers to beams in which a multiple cracking takes place. An analytical form of the bond-slip laws at the interfaces FRP-to- concrete and steel rebars –to-concrete are used. Through the model the strains and stresses in the concrete element between two contiguous cracks for any loading level can be evaluated. The IC debonding occurs when the strains and stresses in the cracked element reach the values that correspond to the failure condition at the interface FRP-to- concrete. To validate the model, a comparison between theoretical predictions, experimental results available in the literature, and predictions of others theoretical models, is made. Obtained results put in evidence as the predictions of the proposed model are in good agreement with those experimental.

2. THE NON-LINEAR MODEL

The model, derived from a cracking analysis based on slip and bond stress, refers to a beam element between two consecutive cracks (block) subjected to a constant bending moment higher than the first cracking bending moment. The analysis refers to the stabilized crack formation phase and considers two limit cracking configurations corresponding to the maximum and minimum crack spacing that bound all possible cracking configurations. The following equations are used to solve the structural problems:

i) *Equilibrium conditions on the cross-sections (translational and rotational)*

$$\int_{\Omega_c} \sigma_c d\Omega_c + \sum_{i=1,n} \omega_{ri} \sigma_{ri} = 0$$

$$\int_{\Omega_c} \sigma_c y d\Omega_c + \sum_{i=1,n} \sigma_{ri} y_i \omega_{ri} = M$$
(2)

where Ω_c is the concrete area, ω_{ri} is the area of the i^{th} reinforcement (FRP sheet, steel rebars); y_i is the distance between the neutral axis of the cross section and the centroid of the i^{th} reinforcement.

ii) *Strain compatibility between two points, initially fully bonded, belonging to the steel rebar and the concrete*

$$u'_s(z) = \frac{du_s}{dz} = \varepsilon_s(z) - \varepsilon_{ct}(z) \quad (3)$$

and to the FRP sheet and the concrete

$$u'_r(z) = \frac{du_r}{dz} = \varepsilon_r(z) - \varepsilon_{ct}(z) \quad (4)$$

where $u_s(z)$ is the slip between the concrete and the steel rebar; $\varepsilon_s(z)$ and $\varepsilon_{cts}(z)$ are strains of the steel rebar and the concrete in tension at the level of the steel rebars, respectively; $u_r(z)$ is the slip between the concrete and the FRP sheet; $\varepsilon_r(z)$ and $\varepsilon_{ct}(z)$ are strains of the FRP sheet and the concrete at the tensile side of the cross-section, respectively;

iii) *Longitudinal stress equilibrium of the concrete reinforcements:*

$$\sigma_s' = \frac{d\sigma_s(z)}{dz} = \frac{4}{d_b} \tau_s(z) \qquad \sigma_r' = \frac{d\sigma_r(z)}{dz} = \frac{1}{t_f} \tau_r(z) \qquad (5)$$

where d_b is the steel rebar diameter; t_f is the thickness of the FRP sheet; $\sigma_s(z)$ and $\sigma_r(z)$ are tensile stresses in the steel rebar and the FRP sheet respectively; $\tau_s(z)$ and $\tau_r(z)$ are bond stresses between steel rebar and concrete and FRP sheet and concrete, respectively.

The equations 2-5 furnish a system of differential equations that cannot be solved in closed form because the inhomogeneity of the boundary conditions; as a consequence a numerical solution is required being impossible to solve the mathematical model in a closed form (Aiello and Ombres, 2004). The utilized numerical procedure is founded on the finite differences method, by dividing the space between two cracks in $n-1$ discrete elements with small length Δz . An iterative procedure that transforms the problem of limit conditions in the iterative solution of an initial value problem is adopted (Aiello and Ombres, 2004).

2.1. Limit conditions for the IC debonding

The following limit conditions have to be imposed to evaluate the occurrence of the IC debonding:

- At the halfway, for symmetry, the slip between FRP/concrete and steel rebar/concrete is equal to zero;
- At the distance l_b from the midway, immediately before the crack formation, that is when the tensile strain in the concrete is equal to zero, at the FRP/concrete interface the slip is maximum and the bond stress is zero. These conditions are the most favourable to the IC debonding failure.

2.2. The load at IC debonding failure

The numerical procedure developed considering initial values allows evaluating strains, stresses and loading value corresponding to the IC debonding. For an assigned load, the procedure starts evaluating strain and stress distribution at the halfway by equilibrium conditions (2) and imposing the limit value $u_r=u_s=0$. Therefore it is possible to evaluate, by means of equations (2)-(5), the stress and strain distribution at the edge cross section of the first discrete element contiguous to the halfway; subsequently, the procedure is extended to every contiguous discrete elements. The limit values at the distance l_b from the midway are attained iteratively; the iteration is made varying the external load. The procedure halts when the IC debonding failure conditions are reached.

3. COMPARISON WITH THEORETICAL AND EXPERIMENTAL RESULTS

Theoretical predictions of the proposed model are compared with experimental results and with predictions of other theoretical models available in the literature. In particular the database of experimental results reported in (Teng et al., 2003) are considered together with predictions of the Niu and Wu (Niu and Wu, 2001) and the Chen and Teng (Teng et al., 2003) models. These models, as previously mentioned, are based on the similarity between IC debonding failures and those in shear tests on FRP-to-concrete bonded joints; analytical relationships are obtained combining a simple section analysis of concrete beam with the solution from the shear test. Both models do not consider the local bond-slip FRP-to-concrete. The proposed model requires an explicit bond-slip relationship that adequately describes the effective interaction between the reinforcements (FRP sheets and steel rebars) and the concrete. In the analysis the bond-slip law between the FRP and the concrete is expressed by the Ueda et al. model (Ueda et al., 2005), while the well-known Bertero-Popov-Eligheausen model is adopted for the bond-slip law between the steel rebars and the concrete. Results of the comparison in terms of shear force at the IC debonding failure are reported in the Table 1. The analysis of results evidences, as predictions of the proposed model are in very good agreement with experimental results; the mean value, the standard deviation and the coefficient of variation of the ratio V_{pred}/V_{exp} are equal to 0.9588, 0.09678 and 0.0982, respectively.

Table 1. Shear force at the IC debonding failure: theoretical - experimental comparison

Beam designation (Teng et al, 2003)	Experimental (kN)	Chen and Teng (kN)	Niu and Wu (kN)	Proposed (kN)
A1	72,80	65,52	65,77	80,59
A2	84,90	67,96	68,31	85,68
A7	86,10	65,25	64,00	77,52
C1	77,20	65,52	65,77	79,49
B2	148,00	96,07	94,79	137,75
4	14,80	11,37	12,99	15,15
5	15,30	13,51	16,29	16,07
6	14,00	14,45	13,84	13,12
7	12,80	12,53	9,47	13,43
8	18,70	17,20	12,03	20,41
B3u	17,00	11,85	13,73	20,65
B4u	17,25	12,22	12,45	17,90
B5u	17,30	10,61	14,17	17,48
B1u	30,00	31,93	24,24	28,27
B3	27,60	25,71	23,37	25,40
B4	26,30	25,57	24,73	25,79
B5	34,90	33,63	31,97	29,53
B6	34,80	33,69	29,17	29,59
B7	29,60	29,31	28,20	27,44
B8	30,80	29,03	28,12	28,17

4. CONCLUDING REMARKS

The results of the analysis, allow to draw the following concluding remarks:

- The predictions of the model are in very good agreement with experimental results and in some cases more accurate than models usually adopted for the analysis of the IC debonding failure;
- The local bond slip law is fundamental for the IC debonding mechanism; consequently, a reliable structural analysis imposes the use of prediction models founded on the local bond-slip law like the proposed model.

Further comparisons with experimental and numerical results are needed for a better validation of the model that seems to be very useful for the accurate prediction of the IC debonding failure of FRP-strengthened reinforced concrete beams.

5. REFERENCES

- Aiello, M.A. and Ombres, L. (2004). "Cracking and deformability analysis of reinforced concrete beams strengthened with externally bonded carbon fiber reinforced polymer sheets". *Journal of Materials in Civil Engineering*, ASCE, Vol. 16, No 5, pp. 392-400.
- Liu, I., Oehlers, D.J., and Seracino, R. (2005). "FRP plated reinforced concrete hinges: partial interaction numerical simulation". *Proceedings of the Third International Conference Composites in Construction-CCC05* Editors: P. Hamelin, D. Bigaud, E. Ferrier and E. Jacquelin, Lyon, France, pp. 69-76.
- Niu, H. and Wu, Z. (2001). "Interfacial debonding mechanism influenced by flexural cracks in FRP-strengthened beams". *Journal of Structural Engineering*, Vol. 47A, pp. 1277-1288
- Pham, H.B., and Al-Mahaidi, R. (2006). "Prediction models for debonding failure loads of carbon fiber reinforced polymer retrofitted reinforced concrete beams". *Journal of Composites for Constructions*, ASCE, Vol. 10, No 1, pp. 48-59.
- Teng, J.G., Smith, S.T., Yao, J. and Chen, J.F. (2003). "Intermediate crack-induced debonding in RC beams and slabs". *Construction Building and Materials*, Vol. 17, pp. 447-462.
- Ueda T., Dai J.G., and Sato Y. (2005). "Development of nonlinear bond stress slip model of fiber reinforced plastics sheet-concrete interfaces with a simple method", *Journal of Composites for Constructions*, ASCE, Vol. 9, No 1, pp. 52-62.

EVALUATION OF FRP BOND SPECIFICATIONS FOR DEVELOPMENT LENGTHS

Nathan Newman

(Graduate Research Assistant, University of Missouri-Rolla, Rolla, Missouri, United States)

Ashraf Ayoub

(Assistant Professor, University of Missouri-Rolla, Rolla, Missouri, United States)

Abdeldjelil Belarbi

(Distinguished Professor, University of Missouri-Rolla, Rolla, Missouri, United States)

ABSTRACT

This paper presents an analytical study performed on concrete girders reinforced with FRP bars with the goal of evaluating current ACI-440 design equations for bond development length. The analytical model is based on finite element formulation of anchored bar problems with inelastic constitutive laws for the corresponding materials. The bond stress-slip behavior between FRP bars and concrete was calibrated from experimental data obtained from a large database set of over 50 test specimens available in the literature. A large number of analytical simulations were conducted in order to investigate the effect of different parameters on the development length. These parameters include: bar type (GFRP, CFRP), bar strength, bar modulus of elasticity, bar diameter, surface coatings, concrete strength, and confinement. The analytical study concluded by proposing a new equation for development length that accounts for the effect of these parameters.

KEYWORDS

Bond, FRP, Development Length

1. INTRODUCTION

In more recent years, the use of FRP bars as reinforcement in concrete has grown due to its corrosion resistance, fatigue resistance, magnetic transparency, and lightweight properties (Okelo and Yuan, 2005). However, the knowledge of the properties of FRP and its behavior with respect to concrete are limited. This presents a problem when deriving design equations, specifically when searching out a reliable equation for the bond development length of FRP bars embedded in concrete. The lack of understanding of this material is reflected in that essential design equations and the ability to accurately design structures using FRP are inadequate. The equation for the development length of steel bars in concrete can not be directly applied to FRP bars due to several obvious differences in material properties and surface variations between the two products, but more importantly the differences in their respective bond failure mechanisms prevent this. This is due mainly to their material properties, specifically their stress-strain relationships. Steel generally displays an elastic region with a large plastic region in its stress-strain curve. This plastic region contributes ductility to the bond system on behalf of the reinforcement during loading. However, the stress-strain relation for FRP displays a large elastic region immediately followed by ultimate failure with no preceding warning. There is no plasticity in the FRP reinforcement; therefore, all of the ductility of the system comes from the bond behavior due to the interaction of the FRP and the concrete. It is important to ensure that the FRP is protected and does not yield, but rather the bond. Doing this causes the bond system failure to better resemble the failure mode of the bond and not that of the FRP. In order to derive a length of embedment which satisfies this ideal scenario for a set condition, numerical modeling was used. Using one-dimensional finite element analysis, the behavior of the FRP bond with concrete was analyzed, and used to derive a more accurate design equation for the development length of a straight FRP bar embedded in concrete.

2. APPROACH

For the duration of the study, no new physical testing (such as direct pullout testing) was to be conducted. However, data needed to be obtained through other means. This was done by contacting a plethora of researchers whom had done similar testing and by gathering test data from various journal articles and papers. A sizable database of specimens was thereby accumulated. Each specimen's stress-slip behavior of the FRP to concrete bond was documented and their respective parameters were obtained and recorded. In order to find the required development length for an FRP bar, the ACI 440.1R-03 equations for development length were first used to find an embedment length which would expectantly fall close to the actual development length. This calculated length was used in the numerical model as the embedment length for the respective specimen. The analysis was run using a computer model, and the f_{FRP} stress versus slip relationship for the setup was plotted. From this graph, the maximum achieved stress in the FRP bar was found. The embedment length of each specimen for a set diameter was varied until the defined development length criterion was met. The embedment length used to achieve the criterion was then taken as the development length of the specimen for that exact diameter. In this manner, the development length of all of the specimens and their variations were found. The results were then analyzed to develop a design equation.

3. CRITERION FOR DEVELOPMENT LENGTH

In order to establish a criterion for determining an acceptable value for development length, the original criterion for steel was examined. It was found that the criterion for steel is based on achieving a slightly magnified value of the yield stress for steel in the bar. By doing this, the bar is pushed beyond its elastic range and into plastic deformation and thereby ensuring ductility in the system. Since FRP does not present a plastic deformation range, an alternate criteria was needed. It was decided upon to use a reduction factor to lower the FRP ultimate tensile stress to a level which would allow the bond to fail before the bar failed. Since FRP fails in an abrupt fashion without warning, it is desirable to have bond failure first. The criterion used to obtain an acceptable development length for steel was a target stress in the steel bar of $1.25f_y$ (Jirsa and Lutz, 1979). The reciprocal of this factor was taken in order to apply it to FRP as a reduction factor. It was decided to use a reduction factor of $0.8f_{pu}$ for the FRP development length criterion. This value was then compared with the model results. When the maximum axial stress achieved in the bar matches $0.8f_{pu}$, the coinciding embedment length for that particular case is taken as the required development length for the respective specimen. An ideal bond relationship between FRP embedded bars and concrete is shown in Figure 1. From this diagram it can be seen that the FRP is protected and that the ductility is provided by the bond. The ductility comes from the bond hardening slope just prior to bond yielding. The criterion defined for this testing would be met when the maximum stress in the FRP achieved is equal to $0.8f_{pu}$.

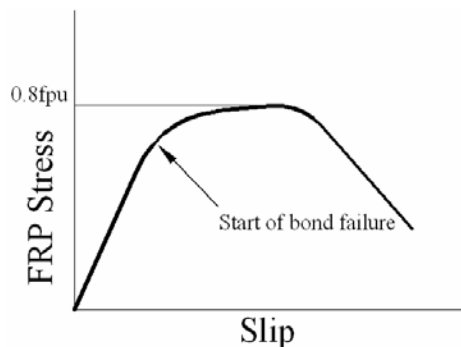


Figure 1: Proposed FRP Stress-Slip Relationship Controlled by Bond Failure

4. MODEL

The analytical model used in this project is based on a one-dimensional finite element formulation of an anchored bar with inelastic constitutive laws for the materials involved. A total of six elements with seven nodes are taken for each bar specimen. The program is displacement controlled, so either one end was pulled a set distance for a pullout test, or one end was pulled while the other end was pushed a set distance for a push-pull test. This displacement was

a fixed preset variable. The program was arranged around the following variables: modulus of elasticity of the bar, ultimate tensile strength of the bar, bond behavior for the corresponding specimen, diameter of the bar, and the embedment length.

In order to depict the behavior of bond, the following constitutive model was used. The bond stress versus displacement plot for a given specimen was described by three key points. These points are illustrated in Figure 2. Using these points, the essential components concerning the bond properties are addressed. These include FRP/bond stressing and yielding, and bond failure.

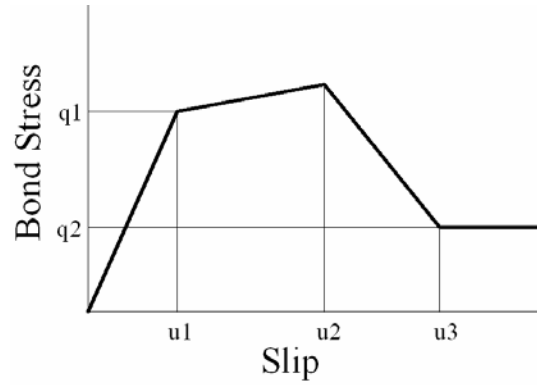


Figure 2: Idealized Bond Stress-Slip Relationship

5. NUMERICAL RESULTS

The ACI 440.1R-03 equations were used to calculate suggested development lengths using the following equations:

$$l_{bf} = K_2 \frac{d_b^2 f_{fu}}{\sqrt{f'_c}} \quad \text{Eq (1)}$$

$$l_{bf} = \frac{d_b f_{fu}}{2700} \quad \text{Eq (2)}$$

The corresponding development length for a set condition were found to be; 30 inches using the ACI 440.1R-03 Eq. 2, and 58 inches using the ACI 440.1R-03 Eq. 1, taking an average value for the suggested K_2 factors (ACI, 2003). The numerical simulation was run using both of the acquired development lengths, the results are shown below in Figure 3 along with the development length which was found using the criterion previously defined. The development length found using the criteria was 17 inches for this test specimen.

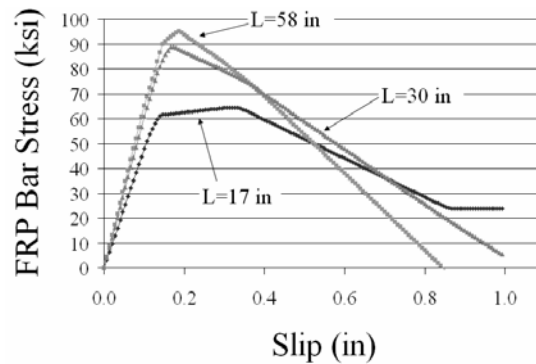


Figure 3: Stress-Slip Relationships for Various Embedment Lengths

From Figure 3 it can be seen that the development length of 17 inches is the more viable length which exhibits a bond hardening region. From this region comes the desired ductility. The plots of specimens with 30 and 58 inches both fail due to rupture of the FRP bar.

Figure 4 displays several stress-slip curves for three different embedment lengths. Each of these specimens is pullout failure controlled due to the bond hardening region found at the peak of each curve, however, only one meets the criterion. The f_{pu} of each of these specimens is the same at 80ksi, which gives a target f_{frp} of 64ksi. The specimen having an embedment length of 17 inches peaks at approximately 64 ksi and therefore satisfies our criterion and is taken to be the development length for the set condition of its parameters.

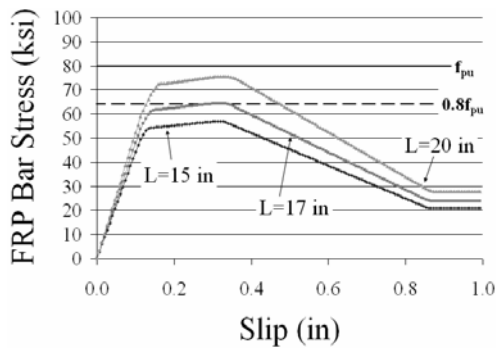


Figure 4: Comparison of Stress-Slip Relationship in terms of Embedment Length and Stress Level Criteria

6. CONCLUDING REMARKS

This study attempts to approach the evaluation of the FRP bond from a different perspective than steel. The failure mechanism and criteria are based around preserving the ductility of the bond when using FRP. Using a wide spread of data, the effect of differing parameters were investigated via the use of finite element analysis. The work is currently in progress, and will result in a set of proposed design equations for development length that considers the effect of the different parameters investigated.

7. REFERENCES

- ACI (2003). "Guide for the Design and Construction of Concrete Reinforced with FRP Bars," American Concrete Institute.
- Jirsa, James O. and Lutz, LeRoy A. (1979). "Rationale for Suggested Development, Splice, and Standard Hook Provisions for Deformed Bars in Tension". *Concrete International*, July, pp 47-61.
- Okelo, Roman and Yuan, Robert L. (2005). "Bond Strength of Fiber Reinforced Polymer Rebars in Normal Strength Concrete". *Journal of Composites for Construction*, May/June, pp 203-213.

PRACTICAL USE OF PULL-OFF STRENGTH TESTING (ASTM D4541) FOR ASSESSING QUALITY OF FRP-TO-CONCRETE BOND

Kent A. Harries

(Assistant Professor, Department of Civil and Environmental Engineering, University of Pittsburgh)

ABSTRACT

Many researchers report, and many practitioners specify, pull-off strength testing (ASTM D4541 or similar) as a quality assessment measure for bonded FRP retrofit procedures. Such testing techniques were not originally developed for bonded FRP applications typical of civil infrastructure and require careful application and interpretation of results. Nonetheless, pull-off strength testing has a variety of applications including substrate assessment, FRP installation quality assessment and assessment of bond degradation due to environmental exposure. A variety of experimental data are presented representing laboratory and field applications of pull-off testing of FRP applications. Guidance for the use of pull-off testing is provided.

KEYWORDS

Adhesive, Debonding, Pull-off testing, Surface preparation, QC/QA

1. INTRODUCTION

The quality, integrity and overall performance of bonded FRP retrofit systems is largely dependent on adhesion of the FRP system to the concrete substrate. Although a great deal of research has been conducted focusing on bond behavior, and a number of methods for assessing this have been proposed, few may be practically adapted for *in situ* quality control/assurance (QC/QA) or acceptance testing. The essence of a sound QC/QA method includes a) simplicity of application; b) the ability to be rapidly deployed with minimal preparatory work; c) easily understood acceptance criteria; and d) excellent repeatability ensuring integrity of data. The existing ASTM Standard D4541 *Standard Test Method for Pull-Off Strength of Coating Using Portable Adhesion Testers* (2002) provides such a method which is well suited to acceptance testing of bonded FRP systems.

2. ASTM D4541 DIRECT TENSION TESTING

The ASTM D4541 test method was developed to assess the adhesion of overlays for concrete repair. Guidance for this application is found in ICRI (2004). Overlay repairs, however, differ from bonded FRP applications in a number of crucial ways. The ASTM D4541 test method is, nonetheless, appropriate for the qualitative and quantitative assessment of bond quality of a bonded FRP system.

The ASTM D4541 test method involves adhering a rigid disk (or dolly) to the surface of the FRP to be tested (Figs. 1(a) and (b)). The test sample is isolated from the surrounding FRP by a circular hole produced using a core drill. Using a pull-off test apparatus (an example is shown in Fig. 1(c)), the disk is subject to direct tension. Failure occurs through the weakest plane within the depth of the test sample. Seven failure (Fig. 2) are possible in a bonded FRP system. The implications of each failure mode are discussed below. If bond is sound, the method will result in a cohesive failure in the concrete substrate (Failure Mode G) and thereby provide a lower bound value for the adhesive bond strength. If the bond capacity is deteriorated the failure mode, failure surface and pull-off strength can all provide insight into the bond behavior and deterioration mechanism. Classification of the failure allows qualitative assessment of the degradation and may help to identify the nature of the degradation. Pull-off strength, assuming it is no longer governed by the substrate concrete, may be a surrogate quantitative measure of bond degradation.

2.2 ASTM D4541 Test Apparatus and Procedure

Five test apparatus types are recognized in ASTM D4541. Comparison of results from one apparatus to the next is inappropriate (ASTM 2002). Only a Type I *Fixed Alignment Adhesion Tester*, as defined by ASTM D4541, is appropriate for assessing FRP bond. Such an apparatus uses 50 mm (or larger) disks. All other apparatus types permitted use smaller disks (usually 20 mm) and are suited to assessing the adhesion of coatings (such as paint systems) where the substrate is not expected to be the weak plane. Because the weak plane is expected to be in the concrete substrate, a test area having a diameter greater than twice the maximum aggregate size is suggested. Vaysbund and McDonald (1999) assessed the field performance of three commercially available testers. A DYNA Z15 tester (Fig. 1(c)) was used in the present work. With this unit, the entire test process is easily executed by one person and testing may be carried out in any orientation (downhand, horizontal (Fig 1(c)), or overhead).

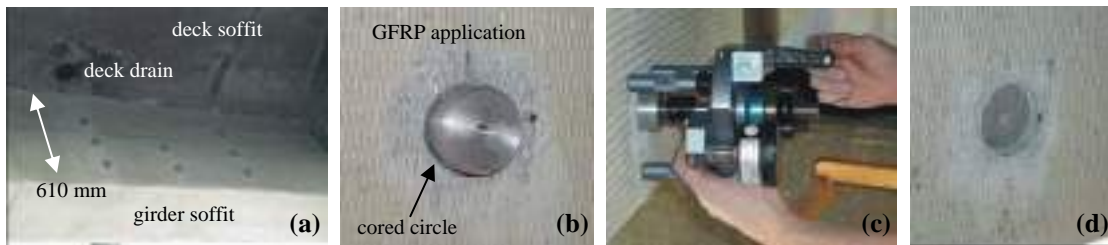


Figure 1: Pull-off test application: a) view of application on web of reinforced concrete interstate girder; b) 50 mm rigid disk; c) manually operated pull-off test apparatus; d) Failure Mode G. (Harries 2001)

In the ASTM D4541 test procedure, providing a cored circle around the perimeter of the test sample is considered optional. This cored circle must be provided for useful results to be obtained for FRP system. Without the core, load spreading from the rigid disk is likely and a greater region of bonded material is engaged. The extent of this region is a function of the FRP system thickness, flexural properties and through-thickness shear properties (Harries et al. 2004). In drilling the core it is important not to exert stresses (dominantly torsional) on the test sample. This is best accomplished using a smooth (no teeth) diamond core drill. For a concrete repair application, Vaysbund and McDonald (1999) recommend that the core extend a minimum of 25 mm or twice the disk diameter into the substrate material. Although no parametric study has been conducted on bonded FRP applications, it is known that the typical debonding plane is located within the concrete immediately adjacent the adhesive. For this reason, the author proposes that only a minimum penetration into the concrete substrate, equal to the greater of 6 mm or the sum of the FRP and adhesive thickness, is required. Bonding the rigid disk to the FRP is easily accomplished using any manner of high-strength adhesive. The author typically uses a two-part “5-minute” epoxy with excellent success.

3. INTERPRETATION OF PULL-OFF TEST FAILURE MODES

Seven failure modes possible in a pull-off test conducted on a bond FRP system are shown in Figure 2. Combinations of these modes (with the exception of Mode F) are generally unlikely.

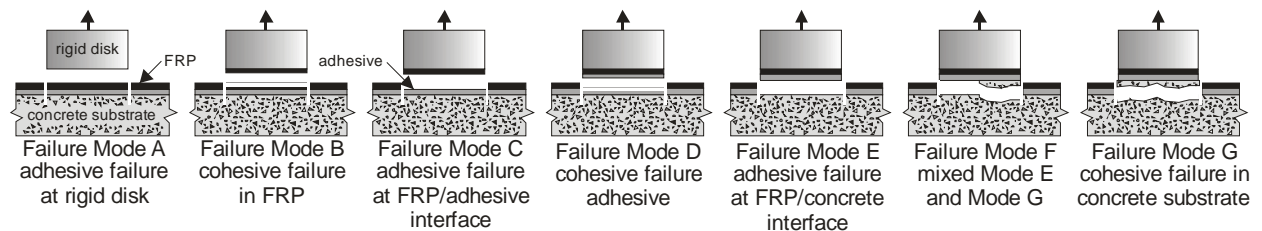


Figure 2: Pull-off failure modes for FRP applications.

Failure Mode A: adhesive failure at rigid disk provides little information beyond a lower-bound pull-off capacity for the system tested. Mode A is an indication of the use of an inappropriate adhesive system for fixing the test disk.

Failure Mode B: cohesive failure in FRP is an indication of poor through-thickness properties of the FRP. Such failures are observed largely due to incomplete wet-out of the fibers or plies comprising the FRP. Figure 4 shows a Mode B failure which occurred between plies of a multi-ply wet layed-up GFRP installation (Harries 2001). Mode B

failures have also been observed in preformed CFRP strip materials having a too high fiber volume ratio (Reeve 2005). Such failures may also result from environmental degradation of the FRP material itself.

Failure Modes C and E: adhesive failure at either adhesive interface is an indication of poor adhesion properties which may result from a) improper selection (matching) of adhesive for adherand materials; b) contamination of adhesive; c) improper or incomplete cure of adhesive; d) contamination or improper preparation or cleaning of adherand surfaces; or e) environmental degradation. In the author's experience, Mode E is more common than Mode C; this is believed to reflect the greater variability in concrete surface preparation and the greater likelihood of contamination of this interface during installation.

Failure Mode D: cohesive failure in adhesive is unlikely to be observed in conventional FRP applications. If observed, Mode B is an indication of very poor adhesive properties likely resulting from contamination, incomplete cure or environmental degradation. In these cases, however, Modes C or E are more likely.

Failure Mode F: mixed cohesive failure in substrate and adhesive failure at the adhesive/substrate interface is commonly observed in FRP pull-off tests (Fig. 3). It is generally believed that this failure initiates in the concrete substrate. The failure plane in concrete is circuitous; if it reaches the adhesive/concrete interface, the failure plane is likely to follow the interface plane resulting in a mixed mode failure. It is typically observed that such a failure propagates through the concrete on one "side" of the disk and through the interface on the other (Fig. 4), supporting the described behavior. It is rare to have a mixed mode failure with the concrete failure interspersed with the interface failure across the area of the disk. Mode F failures are reported with their proportions of each failure mode.

Failure Mode G: cohesive failure in concrete substrate is the desired failure mode, representing a sound FRP-adhesive system. This is not to say that a Mode G failure is will meet acceptance criteria, but rather that the concrete substrate – as the least controllable constituent – should be the "weak link" in the bonded FRP system. An initially degraded substrate or poor surface preparation will lead to low Mode G pull-off strength values. The extent of aggregate failure (as opposed to failure through only the cement paste) should be noted.

3.1 Lower-bound test results and acceptance criteria

If the pull-off test is being used as a QC/QA method having a minimum specified pull-off strength as an acceptance criteria, it would seem reasonable to accept any failure mode whose capacity exceeds the acceptance criteria. Such an approach must be used with great caution. For example, a Mode A failure that exceeds the acceptance criteria may be considered to be a valid test although unseen damage in the remainder of the bonded system may exist making such an inclusion ill-advised. Modes B and D, although exceeding an acceptance criteria suggest flaws or poor preparation of the constituent materials of the bonded system. Modes C and E, similarly, suggest poor surface preparation or contaminated interfacial surfaces. Pull-off strength acceptance criteria is limited by the tensile capacity of the substrate concrete. In most applications, this substrate will consist of the paste-rich cover concrete located at a formed surface. Estimates of the tensile strength of concrete vary. It is recommended that pull-off strength acceptance criteria not exceed $0.33\sqrt{f_c'}$ (MPa).

4. APPLICATIONS OF PULL-OFF STRENGTH TESTING

Pull-off strength testing has been used by the author in a number of studies largely to establish QA/QC of bonded FRP systems. In such cases, samples are selected at random from areas of the FRP application not affecting the performance of the retrofit. In all studies a protocol ensuring that the concrete age exceeds 56 days and the FRP system has cured for at least 7 days is followed. All samples are prepared with a smooth (no teeth) diamond core barrel. The left side of Fig. 3 shows one such QA/QC program (for the beams reported in Harries et al. 2006). This program assessed a CFRP application using two different adhesive types. As seen in Fig. 3, generally excellent pull-off strength values were found for the high-modulus adhesive (average pull-off strength = $0.58\sqrt{f_c'}$) while acceptable results (average = $0.52\sqrt{f_c'}$), although with significantly greater variability, were found for the low-modulus adhesive. As reported in Fig. 3, most failures were Mode G, giving a good degree of confidence to this testing. Pull-off strength testing has been used to study the effect of environmental exposure (Malvar et al. 2003) and initial surface condition (Wan et al. 2006) on bonded FRP applications. One such study is reported by Harries et al. (2004) and shown in the middle section of Fig. 3. In this study, pull-off testing of an epoxy-based concrete pipe lining system was conducted for cases where the substrate was surface dry and where it was saturated. It can be seen in Fig. 3 that the epoxy applied to the saturated surface had essentially the same pull-off strength (average = $0.43\sqrt{f_c'}$) although the failure mode changed from F and G in the dry application to E in the saturated application. This result indicates some retarding effect on the adhesion due to the presence of water on the substrate for the material used.

Finally, Harries (2001) reports a small field study using pull-off testing to assess the *in situ* quality of a five-year old GFRP application on the exterior girder of an Interstate overpass. This application is shown in Fig. 1. Not only was the *in situ* pull-off capacity of interest, but also the effect of a road drain was questioned. As shown in Fig. 1, three test samples were taken beneath the road drain and the remaining samples in regions unaffected by the drain. The results are shown on the right side of Fig. 3. In this study, the pull-off strength results were relatively low (average $=0.38\sqrt{f'_c}$) and no effect was seen due to the presence of the road drain. The results from this study were inconclusive and would suggest that a low “guaranteed” pull-off strength be adopted. The highest test results were Mode A failures – indicating that the adhesive used to secure the disks was barely adequate. Additionally a Mode B failure (Fig. 4) was observed between laminates of the multi-ply hand layed-up GFRP application. Investigation of all disks indicated excessively thick resin layers between often dry GFRP fibers. This observation clearly indicates poor quality GFRP installation where wet-out was not ensured and may indicate inadequate rolling or working of the GFRP sheets or sagging of the sheets during installation due to excessive resin.

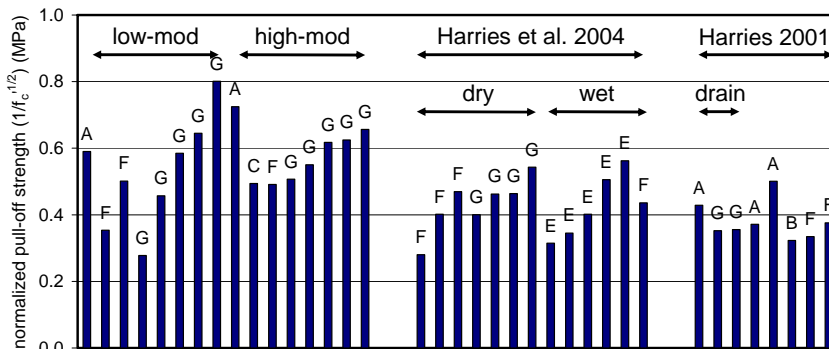


Figure 3: Pull-off strength results.

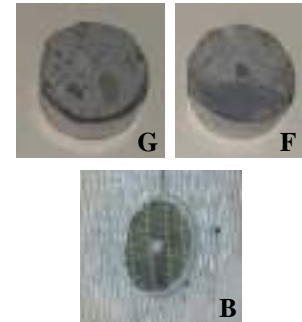


Figure 4: Representative failure modes.

5. CONCLUSIONS

ASTM D4541-type direct tension testing is easily adopted for QC/QA and other investigative applications of bonded FRP systems. For applications to concrete, a Type 1 (ASTM 2002) pull-off test apparatus is used and the sample should be core-drilled for reliable results to be obtained. Careful interpretation of the failure modes and resulting disks can provide significantly more qualitative information than simply the pull-off strength. Representative examples of QC/QA and surface preparation and environment exposure studies are presented, illustrating the potentially wide applicability of this simple test technique.

6. REFERENCES

- American Society for Testing and Materials (ASTM) (2002) *D4541-02 Standard Test Method for Pull-Off Strength of Coatings Using Portable Adhesion Testers*, ASTM, West Conshohocken, PA.
- International Concrete Repair Institute (ICRI) (2004) *Guideline No. 03739 Guide to Using In-Situ Tensile Pull-Off Tests to Evaluate Bond of Concrete Surface Materials*, ICRI, Des Plaines, IL.
- Harries, K.A. (2001) *In Situ Tests on FRP Retrofit Application: 1585 Northbound Bridge over SC85 Southbound in Spartanburg SC*, report to South Carolina Department of Transportation, October 2001. 5 pp.
- Harries, K.A., Reeve, B. and Zorn, A. (2006) “Effect of Adhesive Modulus on the Monotonic and Fatigue Behavior of Externally Bonded CFRP Strips” *Proceedings of the 3rd International Conference on FRP Composites in Civil Engineering (CICE 2006)* Miami, December 2006.
- Harries, K.A., Young, S., McNeice, D. and Warren, D. (2004) “Sprayed Epoxy Composite Materials for Structural Rehabilitation” *Proceedings of the 10th Underground Construction Technology Conference*, Houston, Jan. 2004.
- Malvar, L.J., Josji, N.R., Beran, J.A. and Novinson, T. (2003) “Environmental Effects on the Short-Term Bond of Carbon Fiber-Reinforced Polymer (CFRP) Composites” *ASCE Journal of Composites for Construction*, Vol. 7, No. 1, pp 58-63.
- Reeve, B. (2005) “Effect of Adhesive Stiffness and CFRP Geometry on the Behavior of Externally Bonded CFRP Retrofit Measures Subject to Monotonic Loads” *M.Sc. Thesis*, University of Pittsburgh. December 2005.
- Vaysburd, A.M. and McDonald, J.E. (1999) “An Evaluation of Equipment and Procedures for Tensile Bond Testing of Concrete Repairs” *Technical Report REMR-CS-61*, US Army Corp of Engineers, Washington, DC.
- Wan, B., Petrou, M.F. and Harries, K.A. (2006) “Effect of the Presence of Water on the Durability of Bond Between CFRP and Concrete” *Journal of Reinforced Plastics and Composites*, Vol. 25, No. 8, pp 875-890.

PREDICTION OF BOND FAILURE OF CONCRETE PRISMS BONDED WITH FRP COMPOSITES

H. Toutanji

(Professor, University of Alabama in Huntsville, Huntsville, AL, USA)

P. Saxena

(Graduate Research Assistant, University of Alabama in Huntsville, Huntsville, AL, USA)

L. Zhao

(Graduate Research Assistant, University of Alabama in Huntsville, Huntsville, AL, USA)

ABSTRACT

The use of fiber reinforced polymer (FRP) for strengthening concrete structures has grown rapidly during the past few years. In spite of exhibiting superior properties, the safety of usage is questionable as FRP undergoes brittle debonding failures. Amongst the reported failure modes of FRP strengthened concrete beams, there has been limited research in terms of intermediate crack induced interfacial debonding and fewer strength models are developed for predicting such failures. It is suggested that conducting a simple shear test on the FRP bonded to concrete substrate can simulate this type of failure mode. This paper is a study of the existing experimental and analytical work done to understand the failure mode of FRP bonded concrete. Twelve specimens were tested to study the influence of concrete strength and the amount of FRP on the ultimate load capacity of FRP-concrete bond under direct shear. Existing experimental work was collected from literature and consists of an extensive database of 351 concrete prisms bonded to FRP and tested in direct shear. The analytical models from various sources are applied to this database and the results are presented.

KEYWORDS

FRP, Bond, Inorganic Epoxy, Bond length, Anchorage strength models.

1. INTRODUCTION

The concern with the use of FRP is the premature debonding failure. The aim of this study is to review and compare the existing studies and predictive models on the FRP-to-concrete bond. Of the various premature failure modes exhibited by FRP strengthened RC beams, intermediate crack induced debonding is a less commonly reported failure mode. It however has a significant control over the strength of a major portion of the FRP strengthened beam (Smith and Teng 2002). Few strength models focus on predicting midspan debonding. It is suggested in many studies (Teng et al. 2003, Chen and Teng 2001, Seracino 2001) that conducting a simple shear test on the FRP bonded to concrete substrate can simulate this type of failure mode. Hence, a model based on a simple shear test may predict intermediate crack induced debonding accurately. This paper presents an experimental study of 12 specimens of FRP-to-concrete bonded prisms. An inorganic epoxy was used for bonding FRP sheets to the concrete surface. This gave an excellent opportunity to compare the models even with specimens having a different epoxy system. Further, anchorage strength models from various sources are applied to an extensive database of 351 specimens collected from literature and tested in single or double shear tests.

2. EXPERIMENTAL PROGRAM AND RESULTS

The pull out test specimens consisted of a concrete prism bonded with FRP strips by an inorganic epoxy. The concrete prism had a dimension of 200 mm × 200 mm with a thickness of 130 mm. Concrete cylinders made from

the same batches were cast and tested according to ACI provisions. Also, the average modulus of elasticity of concrete E_c was obtained as 33.5 GPa. Commercially available carbon fiber sheets with unidirectional plain weave were used. The thickness of each layer of the carbon fiber is 0.165 mm measured by a dial caliper. Yarn fiber type T300C, 3K was used. Its properties obtained by conducting a FRP coupon test are listed in Table 1.

Table 1. Properties of Inorganic Epoxy and CFRP

	Ultimate Strain (%)	Tensile Strength (MPa)	Compressive Strength (MPa)	Modulus of Elasticity (GPa)
Inorganic Epoxy	0.6	-	23.6	4.1
CFRP	0.006	660	-	110

The surface preparations for concrete included roughening and sandblasting, followed by rinsing with a water jet. The prepared surface was primed with inorganic epoxy. The carbon fiber sheet was also impregnated with the epoxy and was placed on the marked bonding area of 50 mm × 100 mm. They were left at room temperature for at least 3 days for the matrix to fully dry. Each layer of fiber sheet had the same length. The thickness of bonded FRP sheet was also measured after curing with a dial caliper. Five strain gages were installed on the FRP before testing at an interval of 20 mm to monitor the strain distribution along the bond length, as shown in Figure 1. Loading and strain information was obtained by a data acquisition system. The load cell and strain gauges were scanned at a time interval of 1 second, recording the load-strain relation for each specimen.

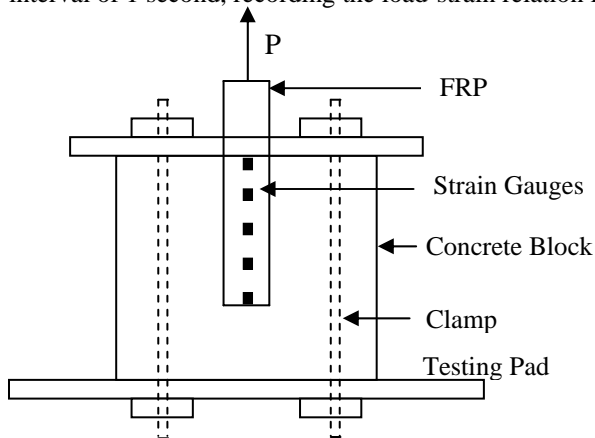


Figure 1: Shear Test Set-up

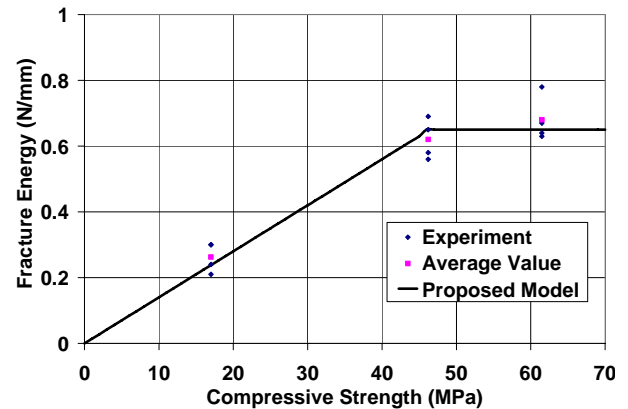


Figure 2: Variation of Fracture Energy

The concrete strength, experimental loads, and failure modes for all the specimens are listed in Table 2. The modes of failure primarily observed are concrete shearing (CS) and fiber delamination (DL). Since the failure was initiated due to either shearing of concrete (CS) or the fracture of concrete edge (initiation of DL mode of failure), it is reasonable to assume the dependency of fracture energy on concrete strength. Zhao (2005) in his study compared the experimental load to the bond failure load proposed by Taljsten (1996) and plotted the interfacial fracture energy per unit area of the joint G_f (N/mm) with respect to the compressive strength of the concrete (MPa), as shown in Figure 2. Zhao (2005) proposed a simple bilinear relationship between the variation of fracture energy and concrete strength, as

$$G_f = \begin{cases} 0.014 f'_c & 0 \leq f'_c \leq 46.2 \text{ MPa} \\ 0.65 & f'_c \geq 46.2 \text{ MPa} \end{cases} \quad (1)$$

and

$$P_u = b_f \sqrt{2G_f t_f E_f} \quad (2)$$

Equations (1) and (2) can be used together to find the ultimate debonding load P_u of the FRP-to-concrete bond. Specimens were divided into three groups, namely, Group I, II and III according to the concrete compressive strengths of 17.0 MPa, 46.2 MPa and 61.5 MPa, respectively. Further specimens in each group were numbered based on the layers of carbon fiber sheet. Numbers 1, 2, 3, and 4 corresponded to three, four, five, and six number of carbon fiber layers, respectively. A significant increase in the ultimate load was noted with an increase in the number of carbon fiber sheets for group I. However, for groups II and III there was a slight increase in the ultimate load between 5 and 6-layered fiber bonded concrete substrate. Also, an increase in the ultimate load was noted with an increase in the concrete strength.

Table 2. Experimental Results

Specimen	I-1	I-2	I-3	I-4	II-1	II-2	II-3	II-4	III-1	III-2	III-3	III-4
Concrete Strength (MPa)	17.0	17.0	17.0	17.0	46.2	46.2	46.2	46.2	61.5	61.5	61.5	61.5
No. of Layers	3	4	5	6	3	4	5	6	3	4	5	6
Experimental Load (kN)	7.56	9.29	11.64	12.86	12.55	14.25	17.72	18.86	13.24	15.17	18.86	19.03
Failure Mode	CS	CS	DL									

3. ANALYTICAL REVIEW

Various models readily available in different studies were collected to predict the bond strength of FRP-to-concrete bonded specimens. The models were collected from the studies of Chen and Teng (2001), Lu et al. (2005), Adhikary and Mutsuyoshi (2001), and Dai et al. (2005) and were categorized according to the consideration of effective bond length. The effective bond length is defined as the length beyond which any increase in the bond length of the fiber cannot increase the anchorage load. To ascertain the extent of usefulness of shear test for predicting midspan debonding in flexurally strengthened RC beams, an extensive database consisting of 351 rectangular concrete prisms bonded with FRP plates tested in single and double shear tests was developed. These specimens were collected from experimental studies conducted or reported by Zhao (2005), Adhikary and Mutsuyoshi (2001), Sharma et al. (2006), Seracino (2001), Yao et al. (2005), Fu-quan et al. (2001), Chen and Teng (2001), Lu et al. (2005), and Nakaba et al. (2001). The following conditions were applied to the prisms in order to include them in the database:

1. It was not preloaded or precracked,
2. It did not have any form of external anchorage between the concrete and FRP sheet or plate, and
3. It was not devised or subjected to any physical condition in order to induce a particular failure mode.

Different models were applied to the database to study the predictability. The experimental versus predicted load was plotted for each of the models and statistical analysis was carried out. Figure 3 shows the scatter of the modified bond strength model by Chen and Teng (2001). This model predicts the best results in terms of average experimental-to-predicted bond strength ratio (1.58) and percentage of unsafe design (2.5%). Most of the specimens lie in the safe zone, for this model providing conservative yet efficient predicted debonding loads. Zhao’s (2005) model based on the interfacial fracture energy gave an average bond strength ratio of 1.314 and 21% unsafe design as shown in Figure 4. While most of the specimens lie in the safe zone, they are highly scattered.

The model by Dai et al. (2005) highly overestimates the bond strength for most of the test data as seen in Figure 5, with a large number of specimens lying in the unsafe zone. The average experimental-to-predicted bond strength ratio is found to be 0.673 and the percentage of unsafe design is 94%.

Based on the tests conducted on the FRP bonded concrete prisms and the comparative study of all the models, a pattern is observed in the results. It implies that some of the better predicting models could be used as a basis for developing a model for intermediate crack induced debonding. This could be achieved by applying the model to beams tested in bending and checking the validity through modifications.

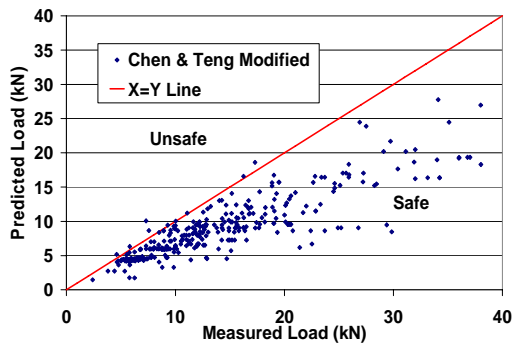


Figure 3: Chen and Teng’s Modified Model

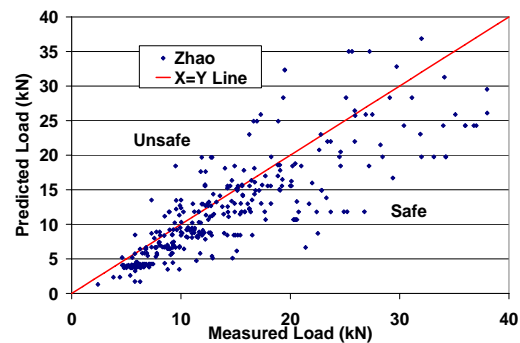


Figure 4: Zhao’s Model

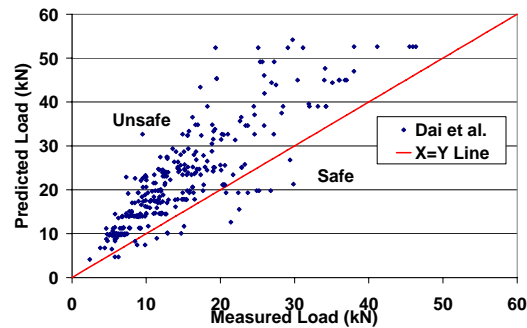


Figure 5: Dai et al.'s Model

4. CONCLUSIONS

With a consideration of balance between the average ratio of predicted to experimental bond strength and percentage of safe design, models by Chen and Teng, Khalifa et al., Yang et al., and Lu et al. are effective in predicting the bond strength. Lu et al.'s model is dependent on several parameters that require lengthy calculations. Interfacial fracture energy based models by Zhao, and Yuan and Wu are also recommended with emphasis on Yuan and Wu's model. Since none of the models considered, had any parameter dependent on the properties of the epoxy, it was not possible to infer the effects of epoxy on the bond strength in the current study. Empirical models underestimate the bond strength and have a scattered load prediction. It was also found that the underestimation of bond strength is mainly the reason for attaining a low percentage unsafe design (<10%) for some of these models. The models that overestimate the bond strength (average experimental-to-predicted bond strength ratio < 1) were usually found to have a very high percentage of unsafe design (65~95%) as well.

5. REFERENCES

- Adhikary, B. B., and Mutsuyoshi, H. (2001). "Study on the bond between concrete and externally bonded CFRP sheet." *Proc., 6th Int. Symp. on Fiber Reinforced Polymer Reinforcement for Concrete Structures (FRPRCS-5)*, Vol. 1, pp 371-378.
- Chen, J. F., and Teng, J. G. (2001). "Anchorage strength models for FRP and steel plates bonded to concrete." *Journal of Structural Engineering*, Vol. 127, No. 7, pp 784-791.
- Dai, J., Ueda, T., and Sato, Y. (2005). "Development of the nonlinear bond stress-slip model of fiber reinforced plastics sheet-concrete interfaces with a simple method." *Journal of Composites for Construction*, Vol. 9, pp. 52-62.
- Fu-quan, X. U., Jian-guang, G., and Yu, C. (2001). "Bond strength between CFRP sheets and concrete." *Proc., FRP Composites in Civil Eng.*, Vol. 1, pp. 357-364.
- Khalifa, A., Gold, W. J., Nanni, A., and Aziz, A. (1998). "Contribution of externally bonded FRP to shear capacity of RC flexural members." *Journal of Composites for Construction*, Vol. 2, No. 4, pp. 195-203.
- Lu, X. Z., Teng, J. G., Ye, L. P., and Jiang, J. J. (2005). "Bond-slip models for FRP sheets/plates bonded to concrete." *Engineering Structures*, Vol. 27, No. 6, pp. 920-937.
- Nakaba, K., Toshiyuki, K., Tomoki, F., and Hiroyuki, Y. (2001). "Bond behavior between fiber-reinforced polymer laminates and concrete." *ACI Structure Journal*, Vol. 98, No. 3, pp. 359-367.
- Seracino, R. (2001). "Axial intermediate crack debonding of plates glued to concrete surfaces." *Proc., FRP Composites in Civil Eng.*, Vol. 1, pp. 365-372.
- Sharma, S. K., Ali, M. S. M., Goldar D., and Sikdar, P. K. (2006). "Plate-concrete interfacial bond strength of FRP and metallic plated concrete specimens." *Composites Part B*, Vol. 37, No. 1, pp. 1-10.
- Smith, S. T., and Teng, J. G. (2002). "FRP-strengthened RC beams I: review of debonding strength models." *Engineering Structures*, Vol. 24, No. 4, pp. 385-395.
- Taljsten, B. (1996). "Strengthening of concrete prisms using the plate bonding technique." *International Journal of Fracture*, Vol. 82, pp. 253-266.
- Teng, J. G., Smith, S. T., Yao, J., and Chen, J. F. (2003). "Intermediate crack-induced debonding in RC beams and slabs." *Construction Building and Materials*, Vol. 17, No. 6-7, pp. 447-462.
- Yao, J., Teng, J. G., and Chen J. F. (2005). "Experimental study on FRP-to-concrete bonded joints." *Composites Part B*, Vol. 36, No. 2, pp. 99-113.
- Zhao, L. (2005). "Characterizations of RC beams strengthened with carbon fiber sheets." Ph.D. thesis, University of Alabama in Huntsville, Alabama, USA.

STRENGTH MODEL FOR INTERMEDIATE CRACK DEBONDING IN FRP-STRENGTHENED CONCRETE MEMBERS CONSIDERING ADJACENT CRACK INTERACTION

J.F. Chen

(Lecturer, Institute for Infrastructure and Environment, Edinburgh University, Edinburgh, UK)

J.G. Teng

(Chair Professor of Structural Engineering, Department of Civil & Structural Engineering,
The Hong Kong Polytechnic University, Hong Kong, China)

J. Yao

(Professor, Department of Civil Engineering, Zhejiang University, Hangzhou, China)

ABSTRACT

Intermediate crack (IC) debonding is a common failure mode in RC beams strengthened by bonding an FRP plate to the tension face. Such a debonding failure initiates in the high moment region and propagates towards a plate end. This paper presents a new strength model for IC debonding failures. This strength model is based on a recent analytical solution for interfacial debonding between concrete and externally bonded FRP and considers the interaction between two adjacent cracks in an explicit manner. This enables factors such as the effect of load distribution to be automatically considered. Other factors such as the internal reinforcement on IC debonding behaviour can also be accounted for if their effect on cracking spacing is properly captured through an appropriate crack spacing equation.

KEYWORDS

FRP, concrete beam, strengthening, interface, IC debonding.

1. INTRODUCTION

The performance of the FRP-to-concrete interface in providing an effective stress transfer is of crucial importance in reinforced concrete (RC) structures strengthened with externally bonded fibre reinforced polymer (FRP) plates (or sheets). A number of failure modes in FRP-strengthened RC members are directly caused by interfacial debonding between the FRP and the concrete. One of these failure modes, commonly referred to as intermediate crack debonding (IC debonding) (e.g. Teng *et al.* 2003; Lu *et al.* 2006), involves debonding of the FRP plate which initiates at a major crack where the plate is under high tension and propagates along the FRP-to-concrete interface towards a stress-free end of the plate.

The stress state of the FRP-to-concrete interface in an IC debonding failure may be compared with that in a simple pull-off test specimen in which a plate is bonded to a concrete prism and is subjected to tension. However, a key difference exists: in a normal RC beam with a tension-face FRP plate, the FRP plate spans over a series of cracks, and as a result, the propagation of debonding from the initiation crack to the adjacent crack depends not only on the tensile force in the FRP plate at the initiation crack but also that at the adjacent crack. The effect of this adjacent-crack interaction has been considered in a recent model by Lu *et al.* (2006) for RC beams bonded with a tension face FRP plate developed based on finite element results. This paper presents an alternative IC debonding strength model, which accounts for adjacent-crack interaction in an explicit manner.

2. ANALYTICAL MODEL FOR ADJACENT-CRACK INTERACTION

The behaviour of the FRP-to-concrete interface between two adjacent cracks (Figure 1) may be approximated by a simple model as shown in Figure 2. The model is similar in geometry to a simple pull-off test. Their chief difference lies in that both ends (i.e. at both cracks) of the FRP plate are subjected to tension in the present model. Several recent studies have been conducted to investigate the behaviour of such a bonded joint model (Schilde and Seim, 2004, Teng *et al.* 2006, Chen *et al.* 2005, 2006). Teng *et al.* (2006) presented an analytical solution for this bonded joint (Figure 2) based on a bilinear local bond-slip model between the FRP and the concrete but the solution is involved and does not provide an explicit expression for the ultimate load. Chen *et al.* (2006) subsequently developed a simpler analytical solution for the same FRP-to-concrete bonded joint model (Figure 2) based on a linearly softening bond-slip model (i.e. neglecting the ascending branch in the bilinear bond-slip model). They produced a simple yet fairly accurate solution in comparison with that given in Teng *et al.* (2006).

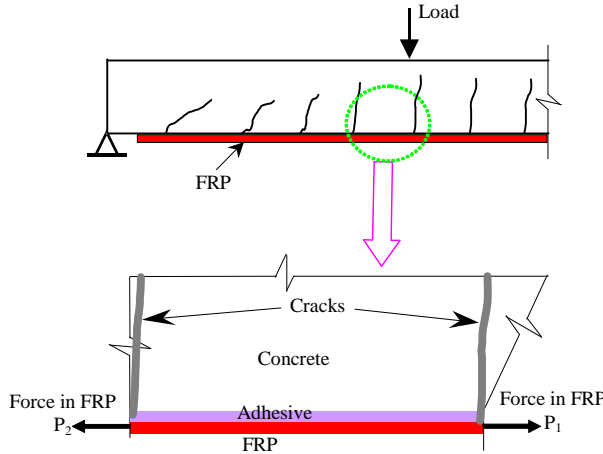


Figure 1: Intermediate crack debonding in FRP-plated RC beams

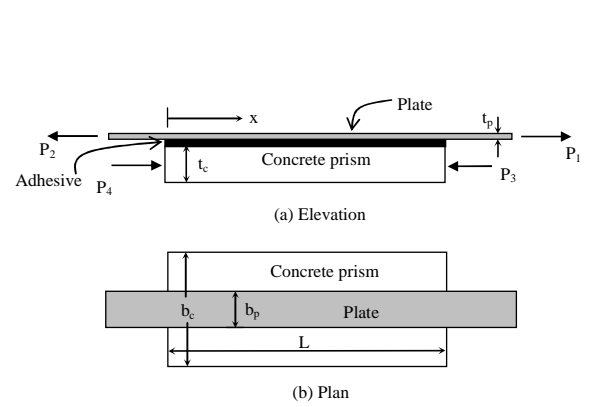


Figure 2: FRP-to-concrete bonded joint model between two adjacent cracks

The FRP-to-concrete bonded joint model (Figure 2) investigated by Teng *et al.* (2006) and Chen *et al.* (2006) is subjected to the following loading: the plate is subjected to two tensile forces, P_1 at the right end and P_2 at the left end with $P_1 \geq P_2 \geq 0$; the concrete prism is subjected to two forces P_3 and P_4 which can be either tensile or compressive; and all these forces remain proportional throughout the loading process. The width and thickness of the plate are b_p and t_p respectively, and those of the concrete prism are b_c and t_c respectively, which are all constant along the length. The length of the bonded part of the plate (i.e. bond length) is L . The elastic moduli of the plate and the concrete are E_p and E_c respectively.

If the tensile deformation of the concrete is neglected, which is usually conservative (Teng *et al.* 2006), Chen *et al.*'s (2006) solution leads to the following expression for the ultimate load at the right end of the plate for the FRP-to-concrete bonded joint:

$$P_{1,u} = \begin{cases} b_p \sqrt{2G_f E_p t_p} (1 - \beta^2)^{-1/2} & \text{if } L \geq a_u \\ b_p \sqrt{2G_f E_p t_p} \sin(\lambda L) [1 - \beta \cos(\lambda L)]^{-1} & \text{if } L < a_u \end{cases} \quad (1)$$

where

$$\beta = \frac{P_2}{P_1} \quad (2a)$$

$$a_u = \frac{1}{\lambda} \arccos \beta \quad (2b)$$

$$\lambda^2 = \frac{\tau_f^2}{2G_f} \frac{1}{E_p t_p} = \frac{\tau_f}{\delta_f} \frac{1}{E_p t_p} \quad (2c)$$

in which τ_f is the peak shear stress of the linearly softening FRP-concrete bond-slip model, δ_f is the slip value when the interfacial shear stress reduces to zero which signifies the shear fracture (or debonding or macro-cracking) of a local bond element and $G_f = \tau_f \delta_f / 2$ is the fracture energy of the interface.

3. NEW IC DEBONDING STRENGTH MODEL

It is significant to note that when $P_2 = 0$ (i.e. $\beta = 0$, the plate is subjected to a tensile force at the right end only), and Eq. (1) reduces to the solution given by Yuan *et al.* (2001) for a simple pull-off test of an FRP-to-concrete bonded joint. It is also noted that Yuan *et al.*'s (2001) solution was the basis for Chen and Teng's (2001) bond strength model for the simple pull-off test. Following the same procedure as employed in Chen and Teng (2001), a new IC debonding strength model considering the interaction between two adjacent cracks is thus proposed as follows based on Eq. (1). The model is expressed in terms of the maximum (i.e. ultimate) stress in the plate at its right end for convenience of design application. The maximum tensile force in the plate at the right end can be easily obtained by multiplying the maximum plate stress by the cross sectional area of the plate $b_p t_p$.

The ultimate stress in the plate at the critical crack where debonding initiates is then given by

$$\sigma_{IC} = \alpha \beta_\sigma \beta_w \beta_L \sqrt{\frac{E_p \sqrt{f'_c}}{t_p}} \quad (3)$$

where f'_c is the cylinder compressive strength of concrete. The coefficient β_σ reflects the effect of the ratio between the plate stresses at the adjacent crack and the critical crack α_σ ; the coefficient β_w reflects the effect of the difference between the width of the plate b_p and the width of the concrete prism (the width of the beam) b_c ; and the coefficient β_L reflects the effect of the bond length. They are found from

$$\beta_\sigma = \begin{cases} \frac{1}{\sqrt{1-\alpha_\sigma^2}} & \text{if } L \geq L_e \\ \frac{1}{1-\alpha_\sigma \cos \frac{\pi L}{2L_e}} & \text{if } L < L_e \end{cases} \quad (4)$$

$$\beta_w = \begin{cases} \frac{b_p + 2\delta}{b_p} & \text{if } b_p + 2\delta < b_c \\ \frac{b_c}{b_p} & \text{if } b_p + 2\delta \geq b_c \end{cases} \quad (5)$$

$$\beta_L = \begin{cases} 1 & \text{if } L \geq L_e \\ \sin \frac{\pi L}{2L_e} & \text{if } L < L_e \end{cases} \quad (6)$$

The effective bond length in Eq. 4 is given by

$$L_e = \frac{2}{\pi} \sqrt{\frac{E_p t_p}{f'_c}} \arccos \alpha_\sigma \quad (7)$$

which reduces to the effective bond length equation in Chen and Teng's (2001) model when the stress ratio α_σ equals zero. If both the internal reinforcement and the external reinforcement do not vary along the beam length, the plate stress at the critical crack where IC debonding initiates σ_{IC} and that at the adjacent crack in the direction of IC debonding propagation σ_{adj} may be approximately related to the bending moments M_{IC} and M_{adj} at these locations. That is

$$\alpha_\sigma = \frac{\sigma_{adj}}{\sigma_{IC}} \approx \frac{M_{adj}}{M_{IC}} \leq 1 \quad (8)$$

It may be noted that in Chen and Teng's (2001) bond strength model, $\beta_w = \sqrt{(2-b_p/b_c)/(1+b_p/b_c)}$. Eq. (5) is used here instead to better reflect the width ratio effect. Further details will be published separately. Based on a test database collected from the literature, $\delta=10$ mm may be adopted. Both b_p and b_c should be in mm in Eq. (5). Because of this new expression for β_w , the coefficient α in Eq. (3) needs to be reduced from 0.427 to 0.315 as the best-fit value, and from 0.315 to 0.25 as the 95 percentile lower bound value for design use. It should also be noted that the bond length L in this model should be taken as the distance between the crack where IC debonding initiates and the adjacent crack in the direction of debonding propagation.

4. COMPARISON WITH TEST DATA

The above model has been compared with the test results of 18 cantilever slab specimens reported in Yao *et al.* (2005) which failed due to IC debonding in the concrete with a thin layer of concrete attached to the FRP plate after debonding. The remaining four specimens reported in Yao *et al.* (2005), which failed by either debonding at the adhesive-concrete interface with little concrete attached to the FRP plate or concrete crushing, were excluded in this comparison. Using the crack spacings and crack positions observed in the tests, the predictions from the present model are in close agreement with the test results. The ratio of the test value to the prediction has an average value of 1.02 with a CoV of 26.6% for the bending moment. The corresponding values for the axial strain of the FRP are 1.01 and 26.1% respectively. More details of these comparisons and further comparisons with other test data can be found in Chen *et al.* (2006).

5. CONCLUSIONS

This paper has presented a new strength model for IC debonding failure in RC beams bonded with a tension-face FRP plate based on an analytical solution for a simple FRP-to-concrete bonded joint model between two adjacent cracks. The new strength model was found to show close agreement with a set of test data. An important feature of the new model is that it considers the interaction between two adjacent cracks in an explicit and rigorous manner. This feature enables factors such as the effect of load distribution to be automatically considered. The effects of other factors such as the type and amount of internal tensile reinforcement can also be reflected if their effect on crack spacing is properly captured by an appropriate crack spacing equation.

6. ACKNOWLEDGMENTS

The authors gratefully acknowledge the financial support provided by the Research Grants Council of the Hong Kong Special Administrative Region, China (Project No: PolyU 5173/04E), the Natural Science Foundation of China (Project No: 50378084), and Edinburgh University, UK.

7. REFERENCES

- Chen, J.F., Yuan, H. and Teng, J.G. (2005). "Analysis of debonding failure along a softening FRP-to-concrete interface between two adjacent cracks", *Proc., International Symposium on Bond Behaviour of FRP in Structures (BBFS2005)*, Chen & Teng (eds), 7-9 Dec., Hong Kong, pp103-111.
- Chen, J.F., Yuan, H. and Teng, J.G. (2006). "Debonding failure along a softening FRP-to-concrete interface between two adjacent cracks in concrete members", *Engineering Structures*, accepted for publication.
- Chen, J.F. and Teng, J.G. (2001). "Anchorage strength models for FRP and steel plates bonded to concrete", *Journal of Structural Engineering*, ASCE, 127(7), 784-791.
- Chen, J.F., Teng, J.G. and Yao, J. (2006). "Strength model for IC debonding in FRP-plated concrete members", *In preparation*.
- Lu X.Z., Teng J.G., Ye L.P. and Jiang J.J. (2006). "Intermediate crack debonding in FRP-strengthened RC beams: FE analysis and strength model", *Journal of Composites for Construction*, ASCE, accepted for publication.
- Schidle, K. and Seim, W. (2004). "Experimental and numerical investigations of bond between CFRP and concrete", *Proc., 2nd Int. Conference on FRP Composites in Civil Engineering*, 8-10 Dec., Adelaide, Australia, 381-387.
- Teng, J.G., Smith, S.T., Yao, J. and Chen, J.F. (2003). "Intermediate crack-induced debonding in RC beams and slabs", *Construction and Building Materials*, 17(6-7), 447-462.
- Teng, J.G., Yuan, H. and Chen, J.F. (2006). "FRP-to-concrete interfaces between two adjacent cracks: theoretical model for debonding failure", *International Journal of Solids and Structures*, 42, in press.
- Yao, J., Teng, J.G. and Lam, L. (2005). "Experimental study on intermediate crack debonding in FRP-strengthened RC flexural members", *Advances in Structural Engineering*, 8(4), 365-396.
- Yuan, H., Wu, Z.S. and Yoshizawa, H. (2001). "Theoretical solutions on interfacial stress transfer of externally bonded steel/composite laminates", *Journal of Structural Mechanics and Earthquake Engineering*, JSCE, 18(1), 27-39.

STUDY ON BOND CHARACTERISTICS OF CFRP/STEEL DOUBLE-LAP SHEAR JOINTS AT SUBZERO TEMPERATURE EXPOSURE

Ahmed Al-Shawaf, Riadh Al-Mahaidi and Xiao-Ling Zhao
(*Department of Civil Engineering, Monash University, Victoria 3800, Australia*)

ABSTRACT

This paper addresses the effect of subzero environmental exposures on the bond characteristics between CFRP and steel plates. A series of tensile tests were conducted on CFRP/steel plates specimens joined together in double-lap shear joints and subjected to 20°C, 0°C, -20°C, and -40°C environmental exposures. Normal modulus (240 GPa) unidirectional carbon fibre plies were used in strengthening the epoxide matrix. The aim of the current experimental work is to determine the debonding strength, elongation development and lap-shear stress and slip variation under subzero exposures. This will help in establishing the feasibility of using CFRP in retrofitting steel structures at extremely cold environments.

KEYWORDS

CFRP (Carbon Fibre Reinforced Polymer), Debonding Failure, Double-Lap Shear, Effective Bond Length, Subzero temperature.

1. INTRODUCTION

The adoption of FRP composite laminates in strengthening aged steel structures has acquired some acceptance recently as an alternative to traditional strengthening methods by virtue of their advantages, amongst which are high stiffness-to-weight-ratio, enhanced fatigue life, corrosion resistance, controllable thermal properties and faster field application. However, the utilization of this methodology depends on the FRP/steel durability, which usually varies according to the nature of environment and the overall properties of the reinforcing fibres, resin matrix, adhesive interface and the fabrication and conditioning techniques.

In terms of subzero environments, considerable work has been conducted on the behaviour of concrete structures strengthened with FRP sheets subjected to cold climate conditions (Baumert, Green et al.,1996), (Rivera, Karbhari et al.,1999),(Neale, Labossiere et al.,2001), (Karbhari,2002).Throughout all previous studies, FRP/concrete bond-related issues have been experimentally investigated, concluded and recommendations were proposed for adopting this retrofitting methodology under such climates. Nevertheless, when it comes to steel adherends, the majority of the concrete practice design guidelines can not be superimposed due to micro/macrosstructural differences between both materials (Fawzia, Al-Mahaidi et al.,2004a). Literally, more than 90% of past FRP literature under subzero conditions has concerned itself with the area of environmental degradation and development of databases of test results for specific composite materials, especially those utilized in aeronautical applications (Springer,1981). On the other hand, a very limited number of experimental investigations were addressing mainly the bond durability of the CFRP/steel interface at subzero exposures intended for civil applications (Karbhari and Shulley,1995),(Colombi, Fanesi et al.,2005). However, these works adopted different matrix resins, fibres, and fabrication, conditioning and experimentation procedures than the present work. This paper reports the results of a series of double strap shear tests conducted at Monash University in order to characterise the debonding phenomena between wet lay-upped CFRP and steel plate specimens loaded statically in axial tension under ambient and subzero temperatures. The prime objective of the current study is to investigate and provide some feedback data on the short-term effect of subzero conditions, encountered in civil infrastructure applications (i.e. retrofitting bridges, petroleum industry structures...etc), on bond strength. Brief discussions are presented on failure modes, joint capacity, strain distribution along joint effective bond length and effect of temperature on specimens' lap-shear stress and slip.

2. EXPERIMENTAL PROGRAM

2.1. Materials

For the fabrication of the wet lay-up CFRP laminates, normal modulus unidirectional carbon fibre sheets were used with a nominal modulus of elasticity of 240 GPa, tensile strength of 3800 MPa, and thickness of 0.176 mm. Araldite 420 A/B (epoxy adhesive) was chosen as the resin matrix and adhesive interface at the same time since wet lay-up method was adopted. Mild steel plates with a 350 MPa yield strength, and nominal thickness of 4.85 mm were used in the current test program.

2.2. Specimens Geometry, Test Setup and Thermal Conditioning

The proposed overall dimensions for the double-doubler joint-specimens (refer to Figure 1) were decided according to the load-frame gripping system and the internal space of the environmental chamber used for composite-specimens' conditioning. A steel rig for producing the whole eight specimens to be tested in the

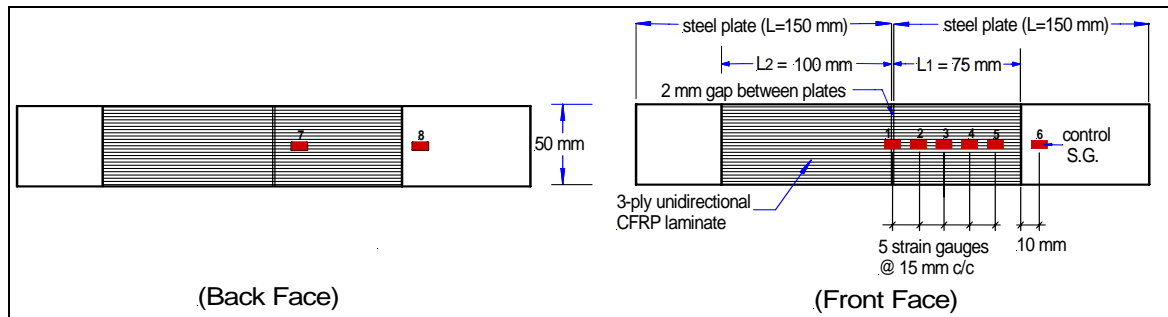


Figure 1: Geometry of Double-Doubler CFRP/Steel Specimen Showing Strain Gauges Positioning

program in a single sample was devised. The aim was to attain the maximum possible consistency and alignment for the specimens and also to have a flat composite outer surface for a reliable strain gauging. Traditional mechanical surface-pretreatment of the main steel plates were followed according to the epoxy-manufacturer's data sheet before applying the first epoxy layer on both faces. These included cleaning, degreasing, abrading and final degreasing. Three unidirectional carbon fibre plies were applied consecutively on both faces of the steel plates. The sample was then cured for 14 days at room temperature and post-cured for 4 hours at 50°C. Cutting into the predetermined specimens' geometry was achieved by means of a water-jet cutting machine. Before testing, foil strain gauges were attached to CFRP outer surfaces as depicted in Figure 1. All specimens were thermally aged inside an environmental chamber and tested individually in direct tension with a screw driven load frame under displacement control (2 mm/min). The current test method has a good conformance with both ASTM standard (D3528-96) and (D5868-01). However, main dissimilarity is due to the adoption of wet lay-up FRP composite. For each target temperature (viz. 20°C, 0°C, -20°C and -40°C), two specimens were tested. Once the target temperature, measured by a thermocouple attached to the CFRP surface, was attained; an extra ten minute period was allowed to ensure specimen's thermal stabilisation before the onset of the test. The soaking time at each temperature was later validated using an experimental calibration procedure similar to the one described in ASTM: D3528.

3. RESULTS AND DISCUSSION

3.1. Failure Patterns



Figure 2: Typical Failure Modes for Double-Doubler CFRP/Steel Specimens (Edge Views)

The prevailing failure mode for the CFRP/steel specimens tested at all present temperatures' range (i.e. from 20 → -40 °C) was found to be, as expected, complete debonding failure at the interface intermixed with minor patches of CFRP fibre-tear failure which could be interpreted as an indication of good steel surface preparation. As illustrated in Figure 2, the failure occurred at the shorter bondline (i.e. effective bond length) which is equal

to 75 mm. This failure was found similar to those observed from previous tests on CFRP/steel adherends ,(Colombi, Fanesi et al.,2005) at ambient temperatures.

3.2. Ultimate Load Capacity

The plot of the applied load with the joint strain readings for specimens tested at (20°, 0°, -20°, -40°C) are shown in Figure 3 . This figure reveals explicitly the irrelevancy of the short-term subzero exposure within the current temperature range on the lap-shear joint capacity, as all the CFRP specimens failed between (70-75) KN with no specific trend. It also depicts a general tendency of higher composite strains with temperature increase.

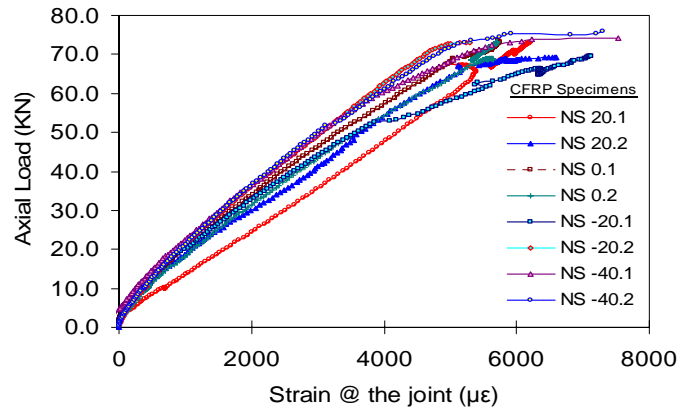
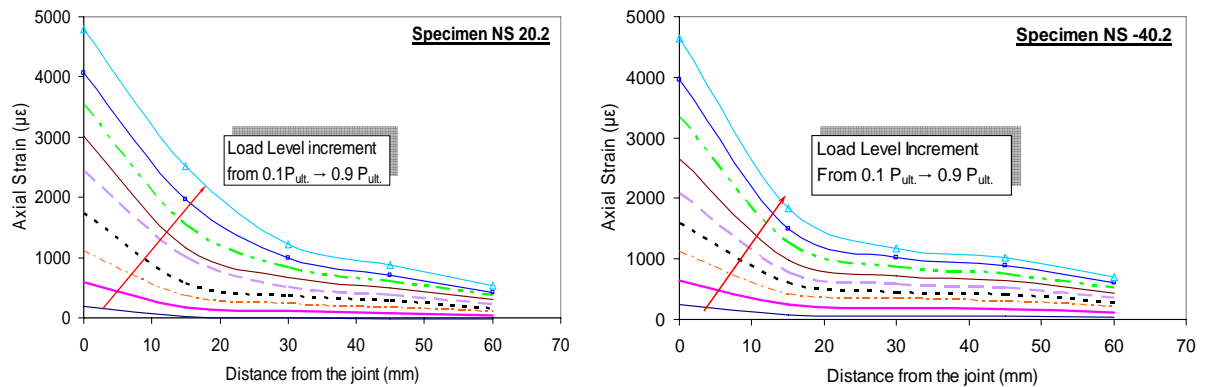


Figure 3: Axial Load vs. Strain at the Joint for Subzero Exposures (i.e. strain gauge no. 1, ref, Figure 1)

3.3. Strain Distribution, Lap-Shear Stress and Slip relations

The strain distribution along the effective bond length was captured by the strain gauge readings at the surface of the CFRP laminate. These readings are plotted with the distance from the joint under two exposures (i.e. 20°C and -40°C) at different load levels as shown in Figure 4. Close examination of Figure 4 (a) and (b) reveals that for the same load ratio, the slope of the strain curves for the (-40°C) exposure is steeper than that of the (20°C) ones. This means that the shear (bond) stress values are higher in the subzero temperature exposure. This could be attributed to the effect of increased embrittlement and stiffness of the subzero-aged adhesive.



a : Exposure Temperature= 20°C

b : Exposure Temperature = - 40 ° C

Figure 4 : Strain Distribution along Effective Bondline for Increasing Load Level

The effect of adhesive increased stiffness at subzero temperature-exposure is further emphasised in Figure 5. It shows plots of slip values vs. lap-shear stress for all CFRP/steel specimens (two at each temperature). The maximum lap-shear stress occurs close to the joint (i.e. at 7.5 mm) which is believed to be due to changes in the rheological and mechanical properties of the adhesive at subzero temperatures and the relatively short effective bond length. A systematic and considerable increase in the maximum lap-shear stress is evident when the exposure temperature dropped from (20°C) to (-40°C). All curves plateaued and lap-shear stresses declined after attaining their maximum values. The exception to this is the (-40°C)-exposure specimens, where it is conceived that the effect of growing embrittlement due to the extreme subzero exposure has prevented the lap-shear stress

from exhibiting this plateau with the current, relatively short effective bond length, and thus, any shifting in the maximum lap-shear stress away from the joint.

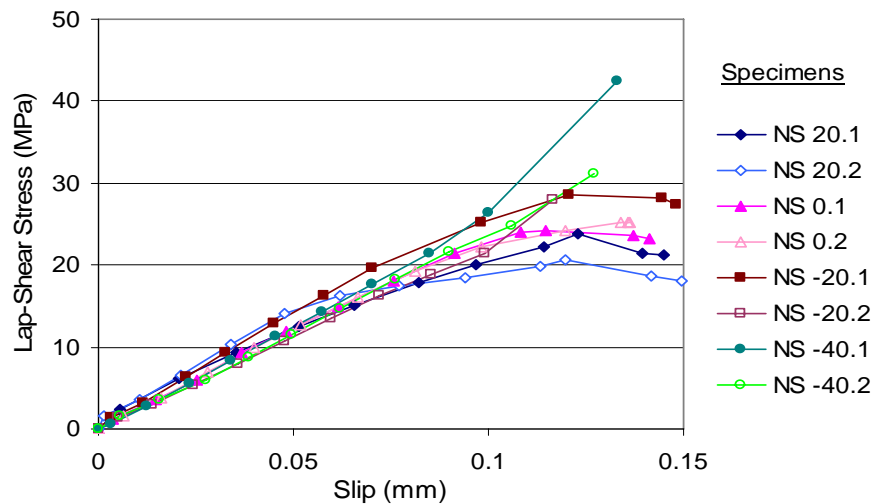


Figure 5 : Slip (at 7.5 mm from joint) vs. Lap-Shear Stress at Experimental Subzero Temperatures

4. CONCLUSIONS

Tensile experiments on subzero preconditioned CFRP/steel plates double-lap joints were conducted to investigate the short-term interfacial bond characteristics. The following conclusions can be drawn based on the limited test results:

- The devised rig for fabricating wet lay-up CFRP/steel plate main sample and the water-jet cutting method have proved to yield high specimen's reproducibility and thus good experimental consistency. As such, it is recommended for such applications.
- The predominant failure mode encountered at all current short-term thermal exposure was an adhesive/steel interface debonding failure.
- The short-term subzero exposure seemed to have insignificant effect on the lap-shear strength of the CFRP/steel composite.
- The well-known embrittlement and ductility reduction phenomena of FRP composites at low temperatures seemed to be responsible for decreasing strain, and consequently increasing lap-shear stress values of the CFRP/steel specimens with temperature decrements from 20°C to -40°C.

5. REFERENCES

- Baumert, M.E., Green, M.F. and Erki, M.A. (1996). "Low temperature behaviour of concrete beams strengthened with FRP sheets", *CSCE Annual Conference*, Alberta, Canada, pp 179-190.
- Colombi, P., Fanesi, E., Fava, G. and Poggi, C. (2005). "Durability of steel elements strengthened by FRP plates subject to mechanical and environmental loads", *CCC2005: Third international conference composites in construction*, Lyon, France.
- Fawzia, S., Al-Mahaidi, R., Zhao, X.L. and Rizkalla, S. (2004a), Comparative study of failure mechanisms in steel and concrete members strengthened with CFRP composites, in *Developments in Mechanics of Structures and Materials*, A. J. Deeks and H. Hao, London, Balkemea Publishers: pp 71-76.
- Karbhari, V.M. (2002). "Response of fiber reinforced polymer confined concrete exposed to freeze and freeze-thaw regimes". *Journal of Composites for Construction*, Vol. 6, No. 1, pp 35-40.
- Karbhari, V.M. and Shulley, S.B. (1995). "Use of composites for rehabilitation of steel structures - determination of bond durability". *Journal of Materials in Civil Engineering*, Vol. 7, No. 4, pp 239-245.
- Neale, K.W., Labossiere, P. and Theriault, M. (2001). "FRPs for strengthening and rehabilitation: Durability issues", *Composites in Construction: A reality*, American Society of Civil Engineers, Capri, Italy, pp 102-109.
- Rivera, J., Karbhari, V.M. and Dutta, P.K. (1999). "Effects of extended freeze-thaw exposure on composite wrapped concrete cylinders". *International SAMPE Symposium and Exhibition (Proceedings)*, Vol. 44, No. pt 2, p 2231.
- Springer, G.S. (1981). *Environmental effects on composite materials*, Technomic Pub. Co., Westport, CT / USA.

THE MECHANISM OF EFFECT OF STRUCTURAL SPAN ON INTERMEDIATE CRACK-INDUCED DEBONDING

Hemdan SAID

(Ph. D. Candidate, Ibaraki University, Hitachi, Ibaraki, Japan)

Zhishen WU

(Professor, Ibaraki University, Hitachi, Ibaraki, Japan)

ABSTRACT

In the current paper, a finite element analysis based on the smeared crack model and interfacial fracture mechanics has been carried out to focus upon the effect of structural span on the intermediate crack-induced debonding. Considering that for structures with multi distributed cracks, local debonding at some points does not mean a complete debonding failure, the mechanism of debonding has been explained from the macroscopic point of view. Based on this consideration, it has been shown that at the same levels of midspan bending moments of FRP-strengthened girders with same cross section, as the span length increases, the gradient of FRP stress distribution decreases. This implies that interfacial shear stress along the FRP-concrete interface decreases and consequently the possibility of debonding decreases.

KEYWORDS

FRP sheets, Debonding; Smeared crack; Fracture mechanics; Span effect.

1. INTRODUCTION

Premature failure due to intermediate crack-induced debonding (IC debonding), which limits the full utilization of the material potential, has been observed to be the most dominant failure mode in FRP-strengthened structures. Till date, Extensive research has been carried out for investigating the IC debonding and studying different parameters which affect it (e.g. Triantafillou, 1992; Täljstén, 1997; Wu et al. 1998; Wu and Niu, 2000; and Wu & Yin, 2002). Through these researches, it has been recognized that debonding in flexural structures is affected by many parameters such as flexural cracks spacing, amount and properties of FRP sheets, and mechanical properties of the adhesive layer. Another important parameter which is observed to affect the debonding behavior is the span of FRP-strengthened structures with same cross section. Limited research has dealt with this issue (Wu and Said, 2005 and Wu et al. 2006). In previous study, Wu and Said, (2005) have shown that the effective bonding length increases with the increase of structural span. This implies relieving shear stresses by transferring them over a larger length. Wu et al., (2006) observed experimentally and confirmed numerically that for large spans, shear stress along the FRP-concrete interface decreases and consequently the failure mode may shift from intermediate crack-induced debonding to the rupture of FRP sheets. Based on the previous discussion, it is believed that the span length of an FRP-strengthened structure has a significant effect on the interfacial shear stress distribution at the FRP-concrete interface and consequently on the IC debonding. Till now, the mechanism of such effect is still ambiguous and need to be clarified. In the current study, a finite element analysis based on the smeared crack model and interfacial fracture mechanics is performed to explain the mechanism of span effect on the IC debonding. First, details of the finite element modeling have been discussed briefly. Second, the mechanism of span effect has been explained by carrying out numerical simulation of a general kind of structures. Finally, span effect in different code provisions has been discussed.

2. PROBLEM STATEMENT

It is observed from the available experiments of FRP-strengthened girders that girders with large spans may fail due to FRP rupture before debonding. On the other hand, because most of the available guidelines and code provisions for predicting debonding failure are based on experiments and analyses of small-size structures, they may not be

appropriate for application to large-scale ones and need to be modified. Understanding deeply the failure mechanism associated with the IC debonding is of great importance for introducing powerful guidelines lead to developing safe and economic design methods. Therefore, the current study focuses upon clarifying the mechanism of the effect of structural span on the IC debonding, which may be useful in future for updating the current design guidelines.

3. FINITE ELEMENT MODELLING

As a structural model, the full-scale girder shown in Fig. 1 is considered. The selected girder is a general kind of structures with an I-shape section and it is widely used in the field applications for bridge construction. During analyses, clear spans ranging from 10m to 30m are considered while cross sectional dimensions and reinforcement are kept unvaried. For all different spans, girders are considered to be strengthened with 3 layers of FRP sheets. Thickness and width of each layer is 0.128mm and 300mm respectively. The FRP amount has been selected to give different failure modes (IC debonding or FRP rupture) for different spans. Although this type of girders is usually prestressed in the practical applications, no prestressing of strands or FRP sheets has been considered in the current simulation for comparing accurately among different spans. For accurate simulation, it is necessary to establish appropriate models for considering propagation of cracks in concrete, bond-slip behavior between reinforcing bars and concrete, and bonding behavior along the adhesive layer. In the following sections, the adopted concrete cracking, material, interfacial and structural models have been presented.

3.1. Concrete Cracking Model

The rotating smeared crack model is adopted to simulate the initiation and propagation of cracks where the tensile behavior is modeled by a simplified linear softening curve.

3.2. Material Models

The response of concrete in compression is modeled by the pre-defined parabolic curve given by the software. The parabolic curve is based on fracture energy in compression by the definition of the crack band width of the element. Concrete compressive strength and modulus of elasticity are considered as 58 MPa and 33.9 GPa respectively. Steel reinforcing bars are considered as a linear elastic-perfectly plastic material. The elastic-perfectly plastic behavior is modeled by Von Mises yield criterion with a yielding stress of 300 MPa and Young's modulus of 200 Gpa. Strands are considered as a linear elastic-perfectly plastic material with strain hardening. The elastic-perfectly plastic behavior is modeled by Von Mises yield criterion with a yielding stress of 1730 MPa. FRP sheets in general behave in a linear elastic manner up to rupture. The modulus of elasticity and the tensile strength are considered as 240 GPa and 4.0 GPa, respectively.

3.3. Interfacial Models

The linear softening model shown in Fig. 2 is adopted to simulate the mode-II fracture of the adhesive. In this model, when the local bond stress attains the local bond strength τ_f , micro-debonding is initiated and followed by a decrease in the local bond stress until it becomes zero where macro-debonding is formed. The slope of the ascending branch represents the interfacial stiffness k_s , while the area under the curve represents the mode II fracture energy G_f^b . The values of τ_f , k_s , and G_f^b are chosen to be 4.0 MPa, 80 MPa/mm, and 0.4 MPa.mm respectively. On the other hand, the interfacial behavior between concrete and reinforcing bars is modeled according to (CEB-FIP model code 1990).

3.4. Structural Model

Due to symmetry, only half of each girder has been analyzed with appropriate boundaries. Girders have been solved under 3-point loading using the load control in combination with the arc-length control. Concrete is modeled by 4-node plane stress elements, steel bars and FRP sheets are modeled by 2-node linear truss elements connected to concrete by zero-thickness line interface elements. In order to accurately compare the behavior of different-span girders, initial stresses due to own weight of girders are neglected.

4. VALIDATION OF THE MODEL

The validity and rationality of the finite element model has been checked by investigating the suitable mesh and by comparing with some experimental results. Due to the limited space, it is not available to present these comparisons here. Detailed validation and comparisons can be referred to in Wu et al. (2006).

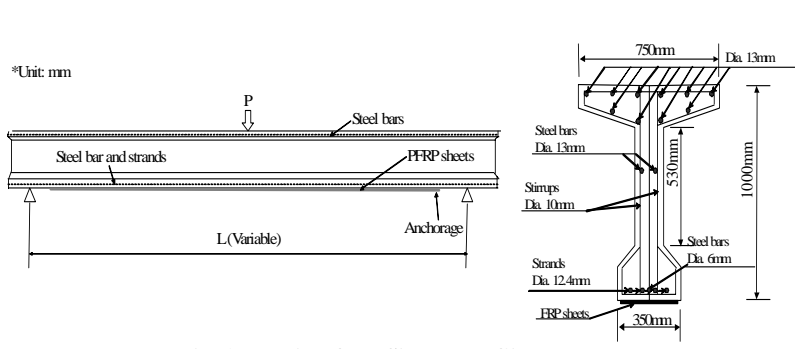


Fig. 1: Details of the Simulated Girders.

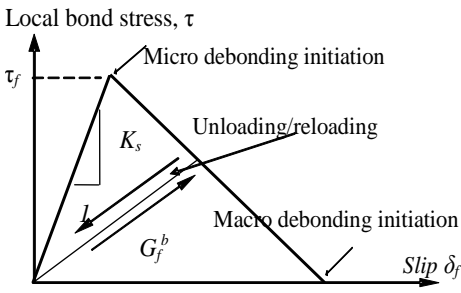


Fig. 2: Linear softening model for FRP-concrete interface.

5. NUMERICAL SIMULATION AND DISCUSSION

As stated previously, the main purpose of the current research is to clearly show the mechanism of the effect of span on the IC debonding. Therefore, three girders having spans within the field application range of 10m, 20m, and 30m are simulated. All the simulated girders have the same cross sectional dimensions and reinforcement as shown in Fig. 1. Therefore, results of the different spans are compared at the same levels of midspan bending moments. Results are discussed for the case of multi distributed cracks from both microscopic and macroscopic points of view. From the microscopic point of view, Fig. 3 shows a comparison among the shear stress distributions of the simulated girders at the same level of midspan bending moment before the initiation of micro debonding. It is clear from this figure that as the span length decreases, the local bond stress tends to be higher; this implies an increase in the possibility of micro debonding and consequently an increase in the possibility of macro debonding. This result can also be confirmed by drawing the shear stress distributions for the three girders at a bending moment corresponding to the initiation of macro debonding of the 10m-girder as shown in Fig. 4. This figure illustrates that macro debonding initiated for the 10m-girder around mid-span, while no debonding in 20m and 30m girders occurred. The shear stress distribution of the first element attained macro debonding of the 10m-girder is shown in Fig. 5. It should be noted that for structures with multi distributed cracks, local debonding at some points does not mean a complete debonding failure. Therefore, the mechanism of debonding will be further explained from the macroscopic point of view. Herein, the FRP stress distributions for different spans have been drawn in Fig. 6. This figure illustrates that at the same level of midspan bending moments, FRP stresses at midspan are approximately equal for different spans. It is clear that as the span length increases, the gradient of the FRP stress distribution decreases which means a reduction in the interfacial shear stress and hence the possibility of debonding decreases. Let us assume that the gradient of FRP stress distribution of the 20m-girder or the 30m-girder increases to the same level of the gradient of the 10m-girder. This requires a higher level of midspan bending moment which causes a

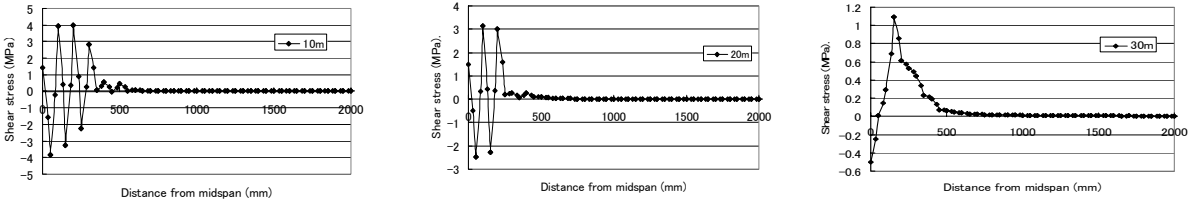


Fig. 3: Shear Stress Distributions for Different Spans at the Same Level of Midspan Bending Moment before Micro Debonding.

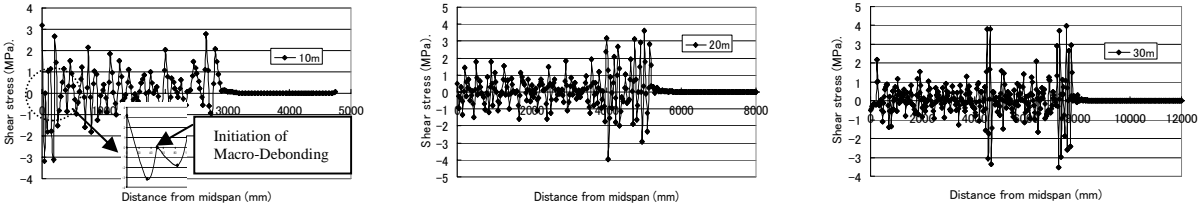


Fig. 4: Shear Stress Distributions for Different Spans at a Level of Midspan Bending Moment Corresponding to the Initiation of Macro Debonding of the 10m-Girder.

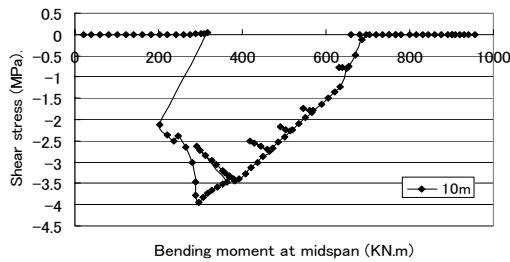


Fig. 5: Shear Stress Distribution of the First Element Attained Macro Debonding of 10m-Girder

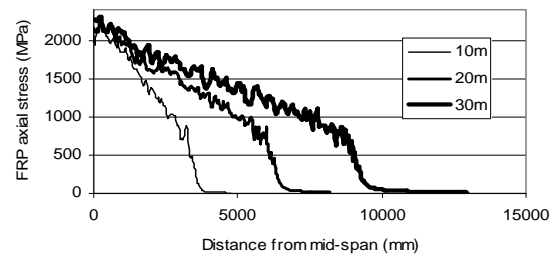


Fig. 6: FRP Stress Distributions for Different Spans at the Same Level of Midspan Bending Moment

higher level of midspan FRP stress. In other words, for same levels of gradient of FRP stress distributions which means same levels of interfacial shear stresses for girders with same cross section, the midspan bending moments of girders having longer spans should be higher than those of girders having shorter ones. This implies that values of the maximum FRP stress of long-span girders are higher than those of short-span ones under same conditions of interfacial shear stresses. Therefore, long-span girders may have a debonding failure at higher levels of maximum FRP stress than those of short-span ones and in some cases they may fail due to FRP rupture before attaining the critical values of interfacial shear stresses. It is worth mentioning, for the case of a single localized crack, the situation is analogous to the simple shear test and hence the structural span has no effect on debonding in this case.

6. SPAN EFFECT IN DIFFERENT CODE PROVISIONS

By reviewing the most famous code provisions for predicting debonding, it is noticed that the ACI 440.2R-02 code, which adopts a reduction factor in the FRP ultimate strain, does not take the span effect into account. On the other hand, although both of the JSCE and the FIB codes do not consider the span effect directly, they take it into account indirectly. This is because both of the JSCE and the FIB codes are based on the difference in FRP stress between two successive flexural cracks. Therefore, more quantitative investigations are required for updating these codes.

7. CONCLUSION

In the current research, a numerical simulation has been carried out for studying the effect of span of FRP-strengthened structures on the intermediate crack-induced debonding and for explaining clearly the mechanism. Based on the rotating smeared crack model and interfacial fracture mechanics, girders with different spans and same cross section have been analyzed. FRP stress distributions as well as shear stress distributions for the different spans are compared at the same levels of bending moments. It is found that for FRP-strengthened structures with multi distributed cracks, as the span increases, the gradient of FRP stress distribution decreases and consequently local shear stresses along the FRP-concrete interface decreases. Therefore, long-span girders may have a debonding failure at higher levels of maximum FRP stress than those of short-span ones and in some cases they may fail due to rupture before attaining the critical values of interfacial shear stresses. Based on this conclusion; more quantitative investigations are required for updating the current code provisions for accurate prediction of debonding failure of large scale structures.

REFERENCES

- CEP-FIP Model Code (1990).
- Täljsten, B. (1997). "Strengthening of beams by plate bonding", *ASCE Journal of Materials in Civil Engineering*, 9(4), pp. 206-212.
- Triantafillou, T. C., and Plevis, N., (1992). "Strengthening of RC Beams with Epoxy-Bonded FRP Composite materials", *Materials and Structures*, V. 25, pp. 201-211.
- Wu, Z. S., Matsuzaki, T., and Tanabe, K., (1998). "Experimental study on fracture mechanism of FRP-reinforced concrete beams", *Proceeding of JCI Symposium on Non-metallic FRP Reinforcement for Concrete Structures*, pp. 119-126.
- Wu, Z. S. and Niu, H. D. (2000). "Study on Debonding Failure Load of RC Beams Strengthened with FRP Sheets", *Journal of Structural Engineering*, Vol. 46A, pp.1431-1441.
- Wu, Z. S. and Said, H. (2005). "Debonding in FRP-strengthened flexural members with different shear-span ratios", *7th International Symposium on FRP Reinforcement for Concrete Structures (FRPRCS-7)*, USA, pp. 411-426.
- Wu, Z. S., Said, H., and Iwashita, K. (2006). "Performance evaluation of strengthened structures with prestressed PBO fiber reinforced polymer sheets", *Annual Meetings and Symposium (IABSE 2006)*, Budapest, Hungary, (accepted).
- Wu, Z. S. and Yin, J. (2002). "Numerical analysis on interfacial fracture mechanism of externally FRP-strengthened structural member", *JSCE Journal of Material, Concrete Structures and Pavements*, 55(704), pp. 257-270.

STRAIN RATE EFFECTS ON STRENGTH OF UNIDIRECTIONAL FRP FABRICS AND BOND TO CONCRETE

M. Saiid Saiidi

Professor, University of Nevada, Reno, Nevada, USA

Rita Johnson

Staff Engineer, Stantec, Reno, Nevada, USA

E. Manos Maragakis

Professor, University of Nevada, Reno, Nevada, USA

ABSTRACT

As part of a study towards the development of fiber reinforced polymer (FRP) seismic restrainers, the effect of dynamic loading on the tensile strength and bond properties of unidirectional glass and carbon fiber fabrics was studied. The bond studies concentrated on the FRP bond to concrete. Nearly 120 samples were tested at strain rates of up to 100,000 $\mu\epsilon/\text{sec}$. The data showed that the tensile strength of FRP fabrics is insensitive to strain rate. In contrast, bond strength is increased with strain rate as a logarithmic function. An equation developed based on the regression analysis of the bond data is presented.

KEYWORDS

Dynamic tests, Fiber reinforced polymer, FRP/concrete bond, Strain rate

1. INTRODUCTION

Seismic restrainers are used to prevent excessive relative movements of bridge superstructures. They are mostly made of steel cables, rods, or occasionally, plates. The potential use of fiber reinforced polymer (FRP) fabrics as seismic restrainers was investigated in an exploratory study at the University of Nevada, Reno. The study consisted of material testing, development of FRP restrainers, and shake table testing of the restrainers. Because seismic restrainers are subjected to dynamic loading, the effects of strain rate on the tensile and bond strength of FRP was investigated. This article presents a brief summary of the study of the materials. More details are provided in (Johnson et al., 2005).

2. STRAIN RATE STUDIES

Past research has shown that material strength generally increases at higher strain rates. For example at 50,000 $\mu\epsilon/\text{sec}$, concrete compressive strength increases by approximately 25% (Kulkarni and Shah 1998). In steel, loading at a high rate results in the yield stress increasing by 10 to 20 percent (Paulay and Priestley 1992). The reason for the increase of strength at higher strain rates is believed to be from the extremely localized yielding due to enhanced bond among the molecules at high rates. Shake table testing of steel restrainers has shown that strain rate in the restrainers may reach 100,000 $\mu\epsilon/\text{sec}$ (Camargo-Sanchez et al). Past studies on FRPs and bond to concrete have been under static loads. The effect of strain rates on FRP fabrics and FRP bond to concrete has not been studied.

2.1 Tensile Strength of FRP Specimens

A test plan was developed to assess the strain rate effect on the strength of unidirectional FRP fabrics tested in tension in the fiber direction. Eighty, 25.4 mm wide, 305 mm long glass and carbon fabric strips were tested in an

MTS load frame testing machine at various strain rates. The FRP material properties are listed in Table 1. The maximum strain rate that could be applied was 100,000 $\mu\epsilon/\text{sec}$. All the material tests were conducted at a static rate and five constant dynamic strain rates of 1,000, 5,000, 10,000, 50,000, and 100,000 $\mu\epsilon/\text{sec}$. A minimum of three specimens were tested at each rate. One-half of the samples were tested without any coating but the remaining samples were coated with a silicon elastomer, Sylgard 184. This coating was used to serve as a matrix for the fabrics while maintaining their flexibility. Because the application of FRP in this study was for seismic restrainers, it was essential that the fabrics maintained their flexibility and buckled out of plane when subjected to compression. This would avoid overstressing the bonded area. Past research has shown Sylgard coated FRPs can undergo large deformations while maintaining their strength and durability (Luo and Mitra 1999). The end segments of the strips were coated with epoxy to facilitate clamping by the grips in the testing machine. Figure 1 shows a typical test setup.

Table 1 – FRP Material Properties

	Fiberglass Composite	
	Design	Specified
Ultimate Tensile Strength in Primary Direction	460 MPa	575 MPa
Elongation at Break	0.58 kN/mm width	0.75 kN/mm width
Tensile Modulus	2.2%	2.2%
Laminate Thickness	20.9 Gpa	26.1 Gpa
Primary Fiber	1.3 mm	1.3 mm
	Glass	
	Carbon Fiber Composite	
	Design	Specified
Ultimate Tensile Strength in Primary Direction	745 MPa	876 MPa
Elongation at Break	0.75 kN/mm width	0.89 kN/mm width
Tensile Modulus	1.2%	1.2%
Laminate Thickness	61.5 Gpa	72.4 Gpa
Primary Fiber	1.0 mm	1.0 mm
	Carbon	



Figure 1: FRP Strip Test Setup



Figure 2: FRP-Concrete Bond Test Setup

The measured tensile strengths for different strain rates and fibers were evaluated to determine the influence of strain rate. Table 2 shows the results for CFRP samples. The table shows data for both the uncoated and coated CFRP specimens. It can be seen that the FRP strength showed considerable scatter and that no consistent trend could be observed in the data with respect to the effect of strain rate. A similar pattern of response was observed in GFRP specimens. The tensile strength of the coated samples was always greater than that of the uncoated specimens, indicating the binding action of the coating material that better mobilized the fibers. The rupture of the uncoated strips was always at the edge fibers and was controlled only by a few fibers. In coated fibers a larger number of fibers were ruptured. Nonetheless, increasing strain rate did not appear to affect the strength of the FRP samples regardless of coating.

The insensitivity of FRP laminate strength to strain rate may be attributed to the mechanism by which the strength is provided. It is well known that FRP fabric strength is always lower than the strength of the constitutive fibers because of the presence of the matrix. Because of the relatively low modulus of elasticity of the matrix, high strain rates are unlikely to affect the matrix strength. In materials such as steel and concrete, the bond among the molecules is sensitive to strain rate and hence dynamic loading increased the capacity.

Table 2 – Measured Data for CFRP Samples

Rate ($\mu\text{s}/\text{sec}$)	25.4 mm Fabric Strips				25.4 mm Elastomer Coated Fabric Strips				Carbon Bond Tests (25.4 mm strips)			
	Strip #	Max Force (kN)	Strength (MPa)	Ave Stress (MPa)	Strip #	Max Force (kN)	Strength (MPa)	Ave Stress (MPa)	Strip #	Max Force (kN)	Max Ave Bond Stress (Strength) (MPa)	Ave Bond Strength (MPa)
Static	1	11.73	469	454	1	20.92	824	766				4.06
	2	7.38	295		2	19.32	761		3	8.72	4.50	
	3	15.12	610		3	18.59	732		4	6.67	3.45	
	4	10.91	441		4	18.99	748		5	8.18	4.23	
5000	8	14.66	586	563	8	22.59	889	796	9	9.34	4.83	4.80
	9	13.74	607		9	20.21	796		10	10.85	5.61	
	10	12.43	496		10	17.84	702		11	7.65	3.95	
10000	11	14.27	572	533	11	18.61	733	710			0.00	5.29
	12	13.91	531		12	19.52	769		12	12.01	6.21	
	13	13.31	496		13	17.50	689		13	8.81	4.55	
					14	16.49	649		14	9.88	5.10	
50000	14	11.82	448	485	15	18.82	741	739	15	8.54	4.41	5.02
	15	14.27	510		16	17.26	679		16	7.25	3.75	
	16	11.26	496		17	20.24	797		17	13.34	6.89	
100000	17	13.28	517	567	18	17.05	671	661	18	9.61	4.96	4.95
	18	14.11	600		19	17.09	673		19	8.85	4.57	
	19	16.12	586		20	16.24	639		20	10.28	5.31	

2.2 Bond Strength

FRP restrainers that were developed as a part of the larger study were to be attached to concrete by epoxy resin. Bond strength to concrete is a function of the strength and stiffness of the epoxy resin, the bond area, and strength of concrete (Teng et al 2001). Typical static bond strength tests have shown that failure occurs in the form of near surface shear in concrete. The effect of dynamic loading on bond strength was studied by testing 40 single-lap, FRP-concrete bond specimens (Fig. 2). Twenty specimens consisted of GFRP strips and the other 20 of CFRP. The specimens were loaded such that the eccentricity of the load was near zero. The middle 203 mm portion of the FRP strips that were not attached to either the grips or bonded to the beams were coated with the flexible elastomer. A 279 mm x 102 mm x 12.7 mm steel plate was anchored to the concrete beams to attach the beams to the grips in the testing machine. A minimum of three specimens per strain rate (static; 1,000; 5,000; 10,000; 50,000; 100,000 $\mu\text{s}/\text{sec}$) for each of the glass and carbon FRP/concrete bond specimens were tested until failure.

An effective bond length of 69 mm and 76 mm was used for the GFRP and CFRP strips, respectively. The bond lengths were purposely made shorter than what was necessary to develop the full strength of the composite strips to force bond failure (Teng et al 2001). The surface area of concrete was prepared using standard procedures for bond preparation, the details of which are presented in (Johnson et al. 2005).

Bond failure occurred typically in concrete near the interface with FRP strips regardless of the strain rate (Fig. 3). The right three columns in Table 2 list the bond test results for CFRP specimens. The average measured static bond strength of the samples was 3.7 MPa for the GFRP specimens and 4.06 MPa for the CFRP specimens. The fact that these strengths are close confirms that concrete strength controls FRP/concrete bond strength. The bond strength data in Table 2 show that bond strength is improved as strain rate increases. This is attributed to the sensitivity of concrete shear strength to strain rate. The shear strength of concrete is a function of its compressive strength and the compressive strength is known to increase with strain rate (Kulkarni and Shah 1998). Because the bond strength is controlled by concrete properties and not the fiber type, the entire bond test data were combined (Fig. 4) and a regression analysis was conducted. The amplification factor for bond strength as a function of strain rate was found to be: $0.052 \ln(\text{strain rate}) + 0.736$. Based on this equation at a strain rate of 50,000 $\mu\text{s}/\text{sec}$ the bond strength

increases by approximately 25%. Because bond failure is undesirable and for added conservatism, the increase in bond strength under dynamic loading was neglected in the design of the seismic restrainers.



Figure 3: Typical Bond Failure

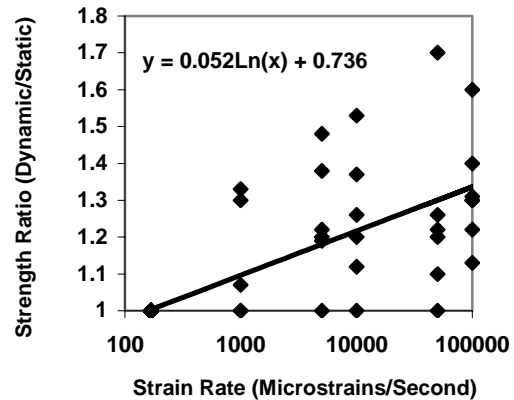


Figure 4: Effect of Strain Rate on Bond

3 CONCLUSIONS

The data discussed in this article demonstrated that the tensile strength of unidirectional GFRP and CFRP fabrics is independent of the strain rate of up to 100,000 microstrains per second. The effect of higher rates was not studied. In contrast, the bond strength of FRP fabrics to concrete was found to depend on the strain rate. An equation representing the trend in the data was developed based on regression analysis of the combined data for GFRP and CFRP specimens. Even though the bond strength improves under dynamic loading, it is recommended that the bond design for seismic restrainers be based on the static bond strength for a conservative design.

4 ACKNOWLEDGEMENTS

This study was funded by the National Cooperative Highway Research Program, Innovations Deserving Exploratory Analysis (NCHRP-IDEA) with supplemental funds from the Nevada Department of Transportation (NDOT). The authors are indebted to S. Luo, P. LaPlace, P. Lucas, and R. Nelson of UNR for their advice and assistance. E. Fyfe and S. Arnold of the Fyfe Co. are thanked for donating the FRP fabrics and the epoxy resins.

5 REFERENCES

- Camargo-Sanchez, F., Maragakis, E. M., Saiidi, M., Elfass, S., (2004) "Seismic Performance of Bridge Restrainers at In-Span Hinges", Civil Engineering Department, Report N. *CCEER 04-04*, University of Nevada Reno.
- Johnson, R., Saiidi, M. and Maragakis, E., (2005) "A Study of Fiber Reinforced Plastics for Seismic Bridge Restrainers," Center for Civil Engineering Earthquake Research, Department of Civil Engineering, University of Nevada, Reno, Nevada, Report No. CCEER-05-2.
- Kulkarni, S. M. and Shah, S. P., (1985) "Response of Reinforced Concrete Beams at High Strain Rates," *ACI Structural Journal*, 95 (6), 705-715.
- Luo, S. Y., and Mitra, A., (1999) "Finite Elastic Behavior of Flexible Fabric Composite under Biaxial Loading," *Journal of Applied Mechanics*, 66, 631-638.
- Nakaba, K., Kanakubo, T., Furuta, T., Yoshizawa, H., (2001) "Bond Behavior between Fiber-Reinforced Polymer Laminates and Concrete," *ACI Structural Journal*.
- Paulay, T., and Priestley, M.J.N., (1992) Seismic Design of Reinforced Concrete and Masonry Buildings, John Wiley and Sons, USA.

BOND BEHAVIOR OF CFRP STRENGTHENED FULL-SCALE PRESTRESSED CONCRETE BRIDGE GIRDERS

Owen Rosenboom

(PhD Candidate, North Carolina State University, Raleigh, NC, USA)

Sami Rizkalla

(Distinguished Professor, North Carolina State University, Raleigh, NC, USA)

ABSTRACT

This paper presents the bond characteristics of carbon fiber reinforced polymer (CFRP) flexural strengthening systems for prestressed concrete. Two large-scale prestressed concrete bridge girders were strengthened with externally bonded CFRP precured strips and tested monotonically to failure. Both girders failed due to FRP debonding propagating from intermediate flexural cracks. The main test variable considered in the experimental program was the amount of FRP debonding mitigation provided. Test results show that using transverse anchorage wraps along the length of the girder can increase the debonding strains of the longitudinal CFRP strips by over 20 percent. The full program with testing of five girders is described along with preliminary analytical results.

KEYWORDS

Reinforced concrete, prestressed concrete, FRP, debonding.

1. INTRODUCTION

Strengthening concrete structures with CFRP materials is becoming attractive solution to strengthen existing bridges. While the flexural failure modes due to concrete crushing and FRP rupture are well known (Rosenboom et al., 2006), the bond behavior of large-scale plated structures can still not be predicted with confidence. For long-span FRP plated reinforced concrete, with the longitudinal strengthening extending to near the supports, the common failure mode is interface debonding propagating from flexural cracks around midspan towards the supports. Various analytical models have been proposed to predict the strain in the FRP at debonding including fracture based models (Teng et al., 2000) and models based on mechanics (Sebastian 2002).

As part of an extensive research project funded by the North Carolina Department of Transportation examining the cost-effectiveness and value engineering of CFRP repair and strengthening for prestressed concrete, a study has been initiated to determine the bond characteristics of CFRP strengthening systems for prestressed concrete. Two girders were strengthened with CFRP precured strips and tested to failure, which occurred due to FRP debonding propagating from the midspan region. The main test variable examined was the amount of debonding mitigation provided. Test results show that debonding strain could be increased with a properly designed anchorage system.

2. EXPERIMENTAL PROGRAM

2.1 Test Girders and Strengthening Configuration

Two 45 year-old 9140 mm long prestressed concrete test girders were extracted from a bridge and delivered in good condition prior to strengthening with no visible cracks. Both girders were prestressed with ten 1723 MPa stress-relieved strands with an average prestressing force of 71.7 kN per strand measured experimentally. The strand configuration consisted of both straight and harped prestressing strands as shown in Figure 1. Concrete core samples were taken after testing and the average concrete compressive strength for both girders was 61.4 MPa. For both girders the main longitudinal CFRP strengthening was two CFRP precured strips ($A_{FRP}=119 \text{ mm}^2$), having a

modulus of elasticity of 164.8 GPa and a tensile strength of 2800 MPa. The strips were bonded to the concrete with a high-modulus, high-strength 2-part structural adhesive with a shear modulus of 1.03 GPa provided by the manufacturer. Transverse wet lay-up CFRP sheet “U-wraps” 152 mm wide were provided on each web at a spacing of 914 mm along the length of girder EB1S. Similar U-wraps were provided for girder EB1SB on *one side only*, to study the bond characteristics without U-wraps. The 1.3 mm thick U-wrap material was also tested, and the modulus of elasticity was found to be 51.7 GPa with an ultimate tensile strength of 710 MPa. The CFRP was installed according to NCHRP Report 514 (Mirmiran et al. 2004) under simulated field conditions by experienced contractors.

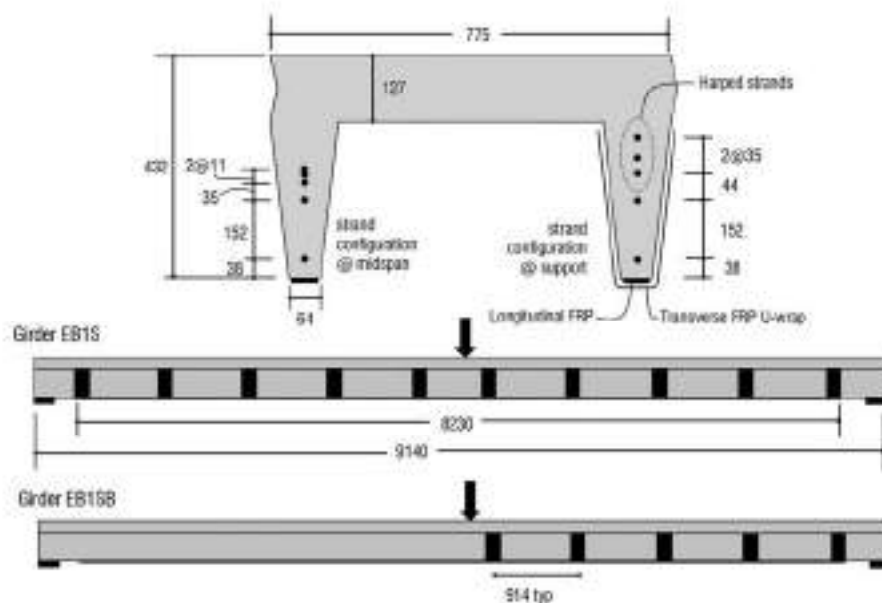


Figure 1: Girder cross-section and strengthening configuration (in mm)

2.2 Test Setup and Instrumentation

The girders were supported by concrete blocks and tested using a 490 kN actuator in 3-point bending with 216 mm elastomeric bearing pads provided on each side. Displacement was measured through the use of potentiometers at midspan and at the support sections. Strain gauges were used to measure concrete compressive strain and were also applied to the longitudinal CFRP along the length of the girder to measure FRP tensile strains for girder EB1SB. Each girder was loaded up to the cracking load then unloaded to determine the effective prestressing force, and then the girder was loaded at a rate of 2.5 mm per minute up to failure.

3. TEST RESULTS

The cracking load of girder EB1S was 57 kN. The effective prestress force per strand, determined from crack re-opening load, was found to be 72.1 kN. At yielding of the prestressing strands (at a load of 102.3 kN), numerous flexural cracks had formed around midspan at a stabilized spacing of approximately 100 mm. Near failure the flexural cracks bifurcated at the bottom of the web due to the plating constraint. Failure occurred due to intermediate crack debonding which propagated from the midspan towards the supports at a load level of 176 kN. The experimentally measured debonding strain at failure was 0.0122 mm/mm, 72 percent of the ultimate strain measured from tensile tests. The interface along which the debonding propagated was mixed: in certain locations around midspan the failure surface was the concrete paste layer just above the longitudinal CFRP, whereas closer to the supports the failure surface was either at the CFRP-adhesive interface or within the strip (interlaminar failure).

The cracking load of girder EB1SB, with debonding mitigation on one side only, was 57.8 kN. From the crack re-opening load, the effective prestress force was determined to be 71.2 kN. The behavior of this girder was similar to

girder EB1S before and after cracking and yielding of the prestressing strands, which indicates that the presence of the U-wraps did not influence flexural cracking. The girder failed due to intermediate crack debonding at a load level of 161.9 kN as shown in Figure 2b, with an experimentally measured debonding strain of 0.0100 mm/mm, which is 59 percent of the tensile strength of the CFRP. The debonding initiated near midspan on the side without U-wraps and propagated towards the support. The failure interface initially was the concrete paste layer at the bottom of the web and then shifted to the CFRP-adhesive interface towards the supports. The increase in FRP strain at debonding due to the presence of the U-wraps at 914 mm spacing was 22 percent higher. The load versus deflection curves for girders EB1S and EB1SB along with a control girder described in Rosenboom et al. (2005) are shown in Figure 2a. The increase in ultimate load compared to the control girder was 19.3 percent for girder EB1SB and 9.6 percent for girder EB1S. The measured axial tensile strain in the externally bonded CFRP strip versus the distance along the beam is shown in Figure 3a.

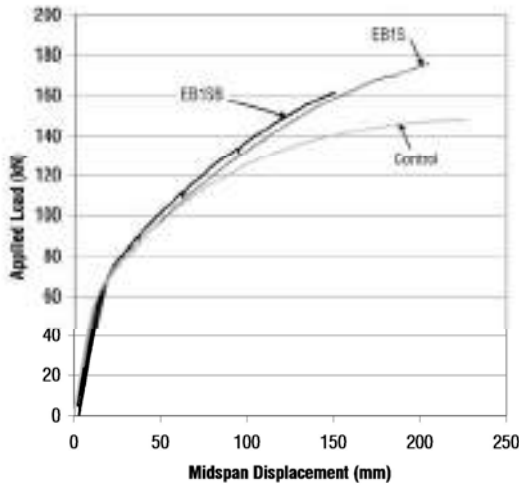


Figure 2a: Load-deflection behavior of tested girders



Figure 2b: debonding failure of girder EB1SB

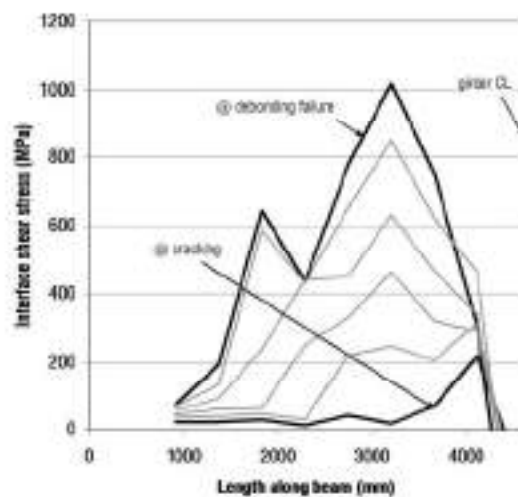
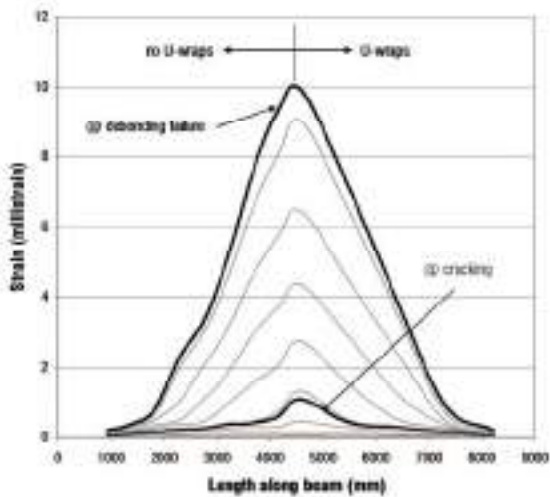


Figure 3a: Length along beam v. tensile strain in FRP Figure 3b: Length along beam v. interface shear stress

4. ANALYTICAL MODELING

There are several behaviors of prestressed concrete that make strengthening with externally bonded CFRP is more effective than regular reinforced concrete. The effective prestress force in the beam imposes an initial compressive strain in the beam soffit that is present regardless of whether the beam is propped during strengthening. This initial strain in the beam soffit is directly translated into extra CFRP force that can be developed prior to debonding failure compared to what is traditionally developed for a reinforced concrete beam. Most of the developed models assume that the member is already cracked at the time of strengthening, which is rare for typical prestressed concrete

members. Even if the prestressed concrete member has been subjected to overloading conditions during its service life and is cracked at the time of strengthening, the prestressing force will promote crack closure increasing the debonding strains of the CFRP at failure.

From equilibrium of the axial forces along the length of a plated beam the interface shear stress (τ_i) can be determined by the following equation:

$$\tau_i = t_p E_p \frac{d\varepsilon_p}{dx}$$

where t_p and E_p are the thickness and modulus of elasticity of the plate and ε_p is the axial strain in the plate along the length of the beam, x . Application of this equation to the measured strain values for girder EB1SB are shown in Figure 3b. The predicted strain gradient in the externally bonded FRP material along the beam can be found by conducting a moment-curvature analysis of the section assuming flexural failure. Since the axial strain gradient is an important factor affecting the bond behavior, the stress-strain characteristics of the longitudinal steel reinforcement becomes very important. Stress relieved prestressing strands, with a less abrupt transition from elastic to plastic behavior than regular reinforcing steel, place less of a demand on the interface shear stress in this transitional zone along the beam. At the plate termination point a different state of stress exists, with shear and normal stresses acting together due to many factors including the abrupt termination of the plate. At a large distance away from the termination point, peeling stresses become smaller in magnitude, and are influenced mainly by aggregate interlock once debonding propagates. Therefore, an assumption can be made that intermediate crack debonding is mainly due to mode II interface shearing stresses, not an interaction between shear and normal stresses.

Future tests will include three additional prestressed concrete C-Channel girders to examine the effect of the number of CFRP layers and the type of CFRP material (pre-cured or wet lay-up). In each case the tensile strains along the length of the girder will be measured and used to identify failure criteria to an analytical model which will be presented at the conference.

5. CONCLUSIONS

As part of a comprehensive research project sponsored by the North Carolina Department of Transportation, five prestressed concrete bridge girders are considered to evaluate the bond behavior and performance of CFRP strengthening systems. Test variables include the amount of CFRP material, type of CFRP system (pre-cured or wet lay-up), and presence of transverse U-wrap anchorage. The test results of two girders are presented in this paper showing that increases in debonding strain of 22 percent can be achieved through the use of transverse wet lay-up CFRP U-wrap anchorage.

6. ACKNOWLEDGEMENTS

The authors would like to thank the North Carolina Department of Transportation for funding this research, and for numerous industry partners for supplying materials and labor for FRP installation. The authors would also like to thank the dedicated staff at the Constructed Facilities Laboratory.

7. REFERENCES

- ACI Committee 440, (2002) "Design and Construction of Externally Bonded FRP Systems for Strengthening Concrete Structures (ACI 440.2R-02)", ACI Manual of Concrete Practice, American Concrete Institute.
- Mirmiran, A., Shahawy, M., Nanni, A., Karbhari, V., "Bonded Repair and Retrofit of Concrete Structures Using FRP Composites," NCHRP Report 514, 2004.
- Rosenboom, O.A., Rizkalla, S., (2006) "Flexural Behavior of Aged Prestressed Concrete Girders Strengthened with Various FRP Systems", accepted for publication in Construction and Building Materials.
- Sebastian, W.M. (2002a) "Sensitivities of strength and ductility of plated reinforced concrete sections to preexisting strains," Journal of Structural Engineering, V. 128, No. 5, pp. 624-636.
- Teng, J.G., Chen, J.F., Smith, S.T., Lam, L. (2002) FRP Strengthened RC Structures, John Wiley and Sons, Ltd, England.

BOND CHARACTERISTICS OF GFRP POST-INSTALLED ANCHORS

Ehab A. Ahmed

(Ph. D. Candidate, University of Sherbrooke, Sherbrooke, Quebec, Canada)

Ehab F. El-Salakawy

(Canada Research Chair Professor, University of Manitoba, Winnipeg, Manitoba, Canada)

Brahim Benmokrane

(NSERC Research Chair Professor, University of Sherbrooke, Sherbrooke, Quebec, Canada)

ABSTRACT

This paper addresses the bond behavior of GFRP post-installed adhesive anchors embedded in plain concrete. A total of 15 sand-coated GFRP V-ROD bars of 25.4 mm diameter (#8) were tested at different embedment lengths ranging from $5d_b$ (127 mm) to $15d_b$ (381 mm). The anchors were installed in wet holes using epoxy based adhesive (HIT RE 500). The experimental results indicated the adequate performance of this type of post-installed GFRP adhesive anchors. The capacity of these anchors is achieved at a considerably smaller embedment length.

KEYWORDS

Bond, GFRP, Anchor, Adhesive.

1. INTRODUCTION

The resistance to corrosion and chemical attack, high strength-to-weight ratio, and ease of handling of FRP rods make them a better alternative to steel reinforcement in concrete members subjected to severe environmental conditions. The adhesive anchor generally consists of a reinforcing bar inserted into a drilled hole in hardened concrete with a structural adhesive acting as a bonding agent between the concrete and the reinforcing bar (Cook et al. 1992). The post-installed anchors can be driven in almost any desired position in hardened concrete by installing in holes drilled into concrete. These anchors are usually needed for strengthening and rehabilitation of deteriorated concrete structures or even attaching a structural concrete element to an existing concrete structure. The load-transfer mechanism of adhesive anchor is different than that of cast-in-place one. For adhesive anchor, the load is transferred through the adhesive to the concrete along the entire embedded portion of the anchor. This load-transfer depends on the strength of the adhesive-bar bond, the adhesive-concrete bond, and also on the extent to which the adhesive impregnates the concrete surrounding the drilled hole (Cook et al. 1992). Although the use of these post-installed adhesive anchors provides greater flexibility in design and strengthening of concrete members, their behavior is less understood than that of the cast-in-place anchors.

The bond strength of post-installed FRP anchors depends on the mechanical properties of the FRP bars, the adhesive, and the concrete. The high strength and low modulus of elasticity as well as the differences in the properties of the fiber material and the matrix may lead to different bond characteristic from those of steel bars (Wang et al. 1999). Additionally, the behavior of post-installed FRP anchors seems to be more complex because it is dependent on the adhesive-bar interface, adhesive-concrete interface, as well as the surface and material properties.

To experimentally investigate the behavior of GFRP adhesive anchors, an extended experimental program was planned. The program included two different diameters, 15.9 mm and 25.4 mm as well as two different types of adhesive; epoxy based and cement based. The anchors were tested with different embedment lengths ranging from $5d_b$ to $15d_b$; where d_b is the bar diameter. The details of the test program are shown in Table 1. This paper presents the results of the completed portion of that program; series 1, group I. The FRP bars and the adhesives used in this study were manufactured by Pultrall Inc. (2005) and Hilti Inc. (2005), respectively.

2. EXPERIMENTAL STUDY

2.1. Test Specimens

This research includes tension testing of 15 sand-coated GFRP V-ROD adhesive anchors of 25.4 mm diameter. The used adhesive, Type HIT RE 500, is a high strength epoxy based adhesive specially designed for fastening into solid base materials in a wide range of material temperatures ranging from 49°C down to -5°C. It may be also used in underwater fastening for oversize holes up to two times the bar diameter but with a maximum of 76 mm hole diameter (Hilti Inc. 2005). The specifications of this adhesive are shown in Table 2.

Table 1: Details of Test Specimens

Series	Adhesive Type	Diameter (mm)	Embedded Length (mm)			No. of Samples	
			5 d _b	10 d _b	15 d _b		
Series 1	Group I	Epoxy based	25.4	127	254	382	3×5=15
	Group II	Cement based	25.4	127	254	382	3×5=15
Series 2	Group I	Epoxy based	15.9	79.5	159	238.5	3×5=15
	Group II	Cement based	15.9	79.5	159	238.5	3×5=15

The test specimens included three different embedment lengths 5d_b, 10d_b, and 15d_b with five replicate samples each. Table 2 gives the details of the test specimens. The FRP bars were cut to the desired length then steel tubes were installed on the FRP bars (using epoxy grout) at one end keeping the other end free to be driven into the concrete. Each bar is designated by a set of symbols and numbers to be uniquely identified. As an examples for G#25-5D-E4; the first letter G denotes glass, #25 denotes the bar diameter in mm, 5D denoted the embedded length in bar diameter multiplications, E4 denotes the fourth sample out of the five replicates with epoxy adhesive.

Table 2: Material Specifications (Hilti 2005)

Adhesive	Compressive strength (MPa)	Tensile strength (MPa)	Modulus of elasticity (MPa)	Bond Strength (MPa)	Absorption (%)	Resistance (Ω/m)
HIT RE 500	82.7	43.5	7032	12.4	0.06 %	6.6×10 ¹³

Concrete slabs with dimensions of 3450×1750×400 were cast using ready-mixed normal weight concrete (type V, MTQ). After casting, the concrete slabs were cured with water for 14 days and stored out the laboratory for 6 weeks before installing the FRP anchors. Layout of the GFRP anchors was made in accordance with ASTM E 488-96. To install the FRP anchors, holes were drilled using rotary hammer pits. The holes were cleaned by wire brushes and compressed water as this type of epoxy performs adequately in moisture. After cleaning the holes on the inside, the two-component adhesive package was installed in the dispenser then injected into the holes. Consequently, the bars were pushed into the holes in a screwing fashion. The installed specimens were stored out the laboratory for another five months. During this period, the specimens were subjected to real environmental conditions as wet-dry cycles, freeze-thaw cycles and temperature variation. The concrete cylinders were kept in the same conditions and its compressive strength at the day of testing was 45 MPa.

2.2. Test Set-up and Procedure

A test set-up, in accordance with the requirements of the ASTM E 488-96, was used (Figure 1). The test bars were pulled using a hydraulic jack connected to a manual pump. Each anchor was instrumented with one LVDT to measure the bar displacement at different loading stages. Not to break it, the LVDT was removed at approximately 80% of the expected failure load. The loading pump and the LVDT were connected to a data acquisition system to continuously record data up to the anchor failure.

2.3. Test Results and Discussion

The test results are presented in Table 3 while the failure modes are shown in Figure 2. For bars with small embedment length (5d_b), the mode of failure was concrete failure (concrete cone or concrete damage followed by bar pull-out). Additionally, in case of concrete failure, severe damage was observed in the concrete around the anchors. However, for bars with greater embedment lengths (10d_b and 15d_b), the mode of failure was bar rupture.

From the test results, there was no significant difference between anchors with $10d_b$ and $15d_b$ embedment lengths in terms of maximum load and mode of failure. As a result, $10d_b$ seems to be enough development length. Gesoglu et al. (2005) conducted an experimental study on the post-installed steel adhesive anchors of 12 and 16 mm diameter with embedment length ranged from $3.3d_b$ to $10d_b$ in normal-strength, high-strength and steel fiber-reinforced concretes. In this study, the steel bar failure of the 16 mm diameter adhesive anchors was achieved at an embedment length of $10d_b$ in normal-strength, high-strength, and steel-fiber reinforced concretes.

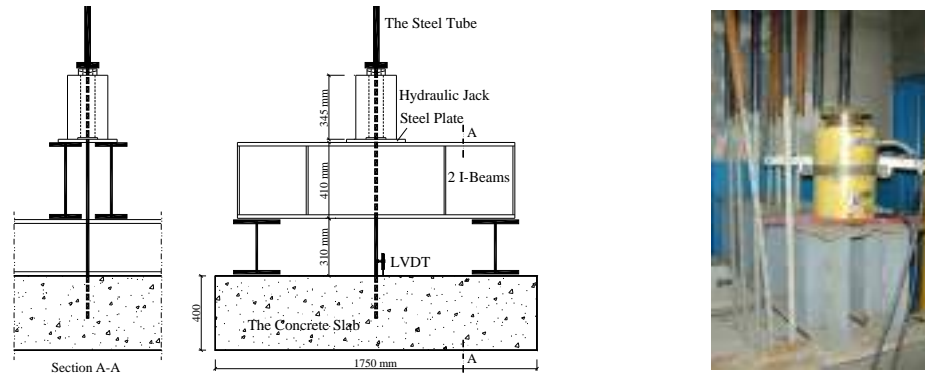


Figure 1: Test Set-up

At the maximum load of each test, the corresponding bond stress was calculated using the following equation:

$$\tau = \frac{F_u}{\pi d_o l_e} \quad (1)$$

where τ is the bond stress (MPa); F_u is the maximum load (N); d_o is the bar diameter (mm) and l_e is the embedded length (mm). Comparing the obtained values listed in Table 3 to the listed one in Table 2, it can be noticed that all of these values are lower than the epoxy adhesive bond capacity reported by the manufacturer. Gesoglu et al. (2005) reported that the maximum bond stress for the $10d_b$ steel anchors was 11.9 MPa for anchors in normal-strength concrete, 12.15 MPa in normal-strength steel fiber reinforced concrete, 12.75 MPa in high-strength plain concrete, and 12.85 MPa in high-strength steel-fiber reinforced concrete.

Table 3: Test Results of GFRP Anchors Series 1, Group I

Designation	Load (kN)	L_e (mm)	Stress (MPa)	Bond Stress (MPa)	Av. Bond Stress (MPa)	SD	COV	Mode of Failure
G#25-5D-E1	110	127 (5 d_b)	217.2	10.61	10.59	0.504	0.190	Concrete
G#25-5D-E2	107		211.3	10.32				Concrete
G#25-5D-E3	105		207.3	10.13				Concrete
G#25-5D-E4	117		231.0	11.28				Concrete
G#25-5D-E5	80	Affected by the nearby ones						Concrete
G#25-10D-E1	250	254 (10 d_b)	493.6	12.34	10.85	0.941	0.708	Rupture
G#25-10D-E2	211		416.6	10.42				Rupture
G#25-10D-E3	227		448.2	11.21				Rupture
G#25-10D-E4	207		408.7	10.22				Tube
G#25-10D-E5	204		402.8	10.07				Rupture
G#25-15D-E1	206	382 (15 d_b)	406.8	6.62	7.07	0.483	0.187	Rupture
G#25-15D-E2	220		434.4	7.07				Rupture
G#25-15D-E3	231		456.1	7.43				Rupture
G#25-15D-E4	239		471.9	7.68				Rupture
G#25-15D-E5	205		404.8	6.59				Rupture

Although all GFRP anchors with embedded depth of $5d_b$ failed by concrete damage, a one piece cone was not obtained. This may be due to the high brittleness of the concrete with relatively high compressive strength.

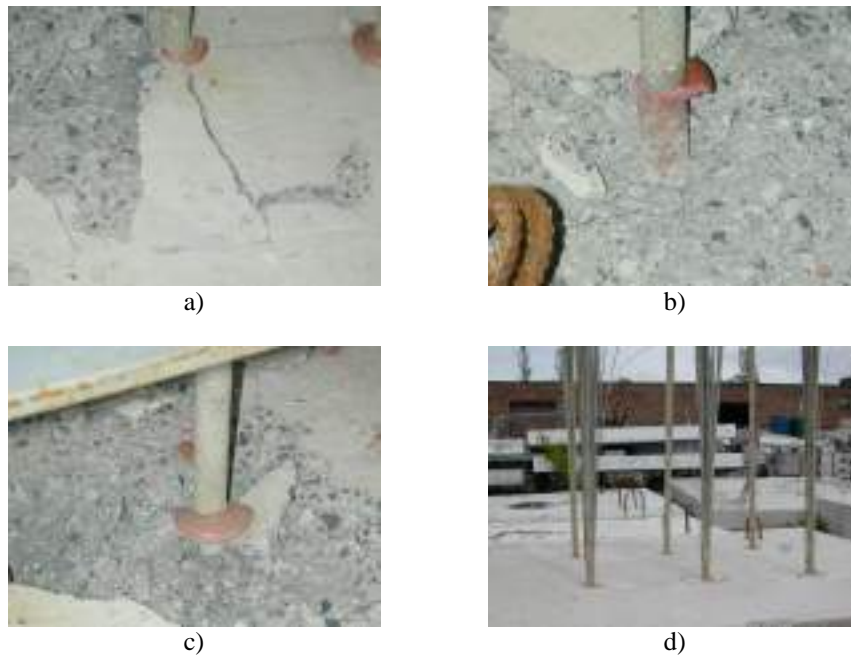


Figure 2: Failure Modes the Test Specimens

3. CONCLUDING REMARKS

An experimental study on the behavior of GFRP post-installed adhesive anchors was conducted using sand-coated GFRP V-ROD bars driven into plain concrete slabs using epoxy based adhesive with different embedment lengths (5, 10, and 15 times the bar diameter). The installed specimens were left out the laboratory for five months. During this period, the specimens were subjected to real environmental conditions as wet-dry cycles, freeze-thaw cycles and temperature variation. Based on the test results the following conclusions can be drawn:

1. Although the anchor installation was performed according to the recommendations of ASTM E-488-96, the corresponding ASTM spacing was not sufficient to prevent the overlapping of the concrete failure at smaller embedded depths.
2. There is no significant difference between the anchors with $10d_b$ and $15d_b$ embedment length in terms of capacity and mode of failure for all the tested specimens.
3. The $10d_b$ (254 mm) embedded length for the sand-coated GFRP V-ROD bars of 25.4 mm diameter seems to be enough to provide ample strength of the GFRP bars.
4. The used epoxy adhesive functioned properly in wet and partially submerged conditions provided that the holes are clean and free of loose sand or concrete particles.

4. REFERENCES

- ASTM E 488-96. (1996). "Standard Test Methods for Strength of Anchors and Masonry Elements." ASTM International, West Conshohocken, PA, USA, pp. 65-72.
- Cook, R.A., Collins, D.M., Klingner R.E., and Polyzois D. (1992). "Load-Deflection Behavior of Cast-in-Place and Retrofit Concrete Anchors." *ACI Structural Journal*, Vol. 89 No. 6, pp. 639-649.
- Gesoglu, M., Özturan, T., Özel, M., and Güneyisi E.(2005). "Tensile Behavior of Post-Installed Anchors in Plain and Steel Fiber-Reinforced Normal-and High-Strength Concretes." *ACI Structural Journal*, Vol. 102 No. 2, pp 224-231.
- Hilti Inc. (2005). Product Technical Guide, <http://www.ca.hilti.com>.
- Pultrall Inc. (2005). Product Technical Specifications, <http://www.Pultrall.com>.
- Wang, Z., Goto, Y., and Joh, O. (1999). "Bond Strength of Various Types of Fiber Reinforced Plastic Rods." *Fourth International Symposium on Fiber Reinforced Polymer Reinforcement for Reinforced Concrete Structures*, Editors: C.W. Dolan, S.H. Rizkalla, and A. Nanni, *ACI SP-188-93*, pp. 1117-1130.

EFFECT OF ADHESIVE MODULUS ON THE MONOTONIC AND FATIGUE BEHAVIOR OF EXTERNALLY BONDED CFRP STRIPS

Kent A. Harries

(Assistant Professor, Department of Civil and Environmental Engineering, University of Pittsburgh, USA)

Andrew Zorn

(Engineer, DMJM Harrie, Pittsburgh, PA, USA)

Benjamin Reeve

(Field Engineer, American Bridge International, Coraopolis, PA, USA)

ABSTRACT

This study investigates the effect of adhesive modulus on the bond behavior of externally bonded fiber reinforced polymer (FRP) composite materials used for repair of reinforced concrete elements under both monotonic and cyclic fatigue loading conditions. Eighteen moderate-scale beam specimens having externally bonded carbon FRP (CFRP) retrofits are tested. Different commercially available adhesive systems are used to bond the CFRP in otherwise identical applications. The deleterious effects of fatigue loading on FRP-to-concrete bond are also identified.

KEYWORDS

Adhesive, Debonding, Fatigue, Flexure

1. INTRODUCTION

Oehlers (2005) presents a summary of five “generic” debonding mechanisms observed in FRP-concrete systems: Plate End (PE); Critical Diagonal Crack (CDC); Flexural Intermediate Crack (FIC); Shear Intermediate Crack (SIC); and, Axial Intermediate Crack (AIC). In reinforced concrete beams having relatively long shear spans and those where the PE mode has been effectively mitigated, debonding of the FRP initiates at flexural (FIC) and/or flexural/shear (SIC) cracks near the region of maximum moment. Under loading, these cracks open and induce high interfacial shear stress accompanied by a small amount of peeling causing delamination, which propagates across the shear span in the direction of decreasing moment. The following parameters have been identified as affecting bond behavior. In many cases, opinions vary on the specific effect and considerably more study is required to understand and quantify these parameters: a) concrete tensile strength; b) adhesive mechanical properties; c) effective bond length of FRP; d) member scale and size; e) concrete section geometry; f) member loading geometry, duration and rate; g) FRP retrofit geometry; and h) environmental and mechanical exposure. The present work focuses on the effect of adhesive material properties and the nature of the applied loading: monotonic or fatigue.

1.1 Adhesive Properties

For the desired performance of a member to be realized, the FRP retrofit must be effectively bonded to the concrete member's tension face. Stiffer adhesives are viewed as being superior since they transmit stress across the FRP-concrete interface in a more efficient manner. Stiffer adhesive systems however are associated with debonding failure of the FRP at lower stress/strain levels and thus result in a less efficient use of the FRP material itself. A flexible adhesive improves the performance of the retrofit by relieving stress/strain concentrations in the FRP while adequately transmitting stresses between the FRP and concrete substrate. In general, reducing the shear stiffness of the adhesive layer results in greater interfacial ductility and higher fracture energy. This study considers two commercially available adhesive systems having shear moduli differing by about a factor of two.

2. EXPERIMENTAL PROGRAM

Eighteen reinforced concrete beams having externally bonded carbon fiber reinforced polymer (CFRP) strip flexural retrofits are reported. The beams are 254 mm deep, 152 mm wide and are supported over a simple span of 4540 mm.

All beams have 3 - #4 primary reinforcing bars. The internal steel had yield and ultimate strengths of 429 MPa and 667 MPa, respectively. Twenty-eight day concrete compressive strength determined from cylinders was 23.3 MPa.

A commercially available 100 mm wide by 1.4 mm thick CFRP strip was used to retrofit sixteen of the beams (the remaining two beams were unretrofit control (C) specimens). In all cases, the CFRP was extended to within 100 mm of the beam supports. The CFRP has a reported tensile strength of 2792 MPa, modulus of 155 GPa and rupture strain of 0.018. Eight beams were retrofit using commercially available low modulus “Adhesive L”; the remaining eight were retrofit using commercially available high modulus “Adhesive H”. Material properties of the adhesive systems are given in Table 1. In all cases the adhesive bondline was approximately 1.6 mm thick.

Table 1: Manufacturer reported material properties of adhesive.

	tensile strength (ASTM D638)	tensile modulus (ASTM D638)	elongation at rupture (D638)	shear strength (ASTM D732)	bond strength ASTM (C882)
Adhesive L	14 MPa	2.2 GPa	0.063	21 MPa	18 MPa
Adhesive H	25 MPa	4.5 GPa	0.010	25 MPa	22 MPa

As shown in Figure 1, the CFRP strips were applied in widths of 25 mm, 51 mm and 102 mm. Four beams were provided with each CFRP geometry: two each applied with the L and H adhesive system, respectively. Specimen designation (given in inch units) is shown in Figure 1.

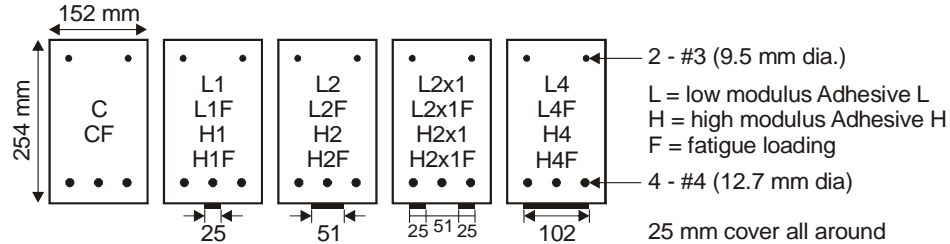


Figure 1: Test specimen and CFRP retrofit geometry.

All beams were tested in three point flexure over a 4540 mm simple span. Applied load, midspan displacement and coincident reinforcing bar and CFRP strains were recorded. One series of nine specimens was tested under increasing monotonic load to failure (L and H specimens). The second series (designated LF and HF) was tested under cyclic fatigue loading conditions. The applied load at midspan was cycled between 4.45 kN to 22.24 kN at rate between 1.2 and 1.7 Hz (depending on the test). This fatigue stress level was selected to result in fatigue life of the unretrofit control specimen CF of approximately $N = 500,000$ cycles. This fatigue regime resulted in fatigue-induced reinforcing bar rupture in five of the nine fatigue specimens (CF, L1F, H1F, L2x1F and H2F). The remaining specimens (L2F, H2x1F, L4F and H4F) were cycled to $N = 2,000,000$ and subsequently tested under increasing monotonic load to failure. These latter specimens are considered to be “runout” specimens having undergone 2 million cycles of fatigue conditioning. A complete description of the test programs reported here are found in Reeve (2005) and Zorn (2006).

3. EXPERIMENTAL RESULTS

A summary of experimental results for all specimens is provided in Table 2. The ultimate deflection is defined as that corresponding to a post-peak load of 80% of the peak load attained. Displacement ductility is defined as the ratio of the ultimate displacement to that at general yield. For the specimens undergoing fatigue loads, data is given for the first post-cracking cycle ($N = 2$) and the final recorded cycle ($N = N_f$). The reinforcing bar stress range is determined from the recorded strain range and assumes $E_s = 200$ GPa. The secant stiffness is the slope of the line between the load and displacement at the lower (4.45 kN) and upper (22.24 kN) limits of the applied fatigue loading.

In all cases, the CFRP strain corresponding to debonding is determined by careful analysis of the CFRP and reinforcing bar data as described by Reeve (2005). Debonding can only be identified as it propagates past at the discrete locations of the strain gauges. For this reason, the strains reported should be interpreted as the *greatest CFRP strain observed while still bonded to the concrete*, and thus are believed to represent a lower-bound on the strain to initiate debonding.

Table 2: Summary of Key Results.

Specimen		increasing monotonic load to failure								
		C	L1	H1	L2	H2	L2x1	H2x1	L4	H4
maximum load (kN)		31.0	39.8	37.7	44.3	43.4	45.5	45.2	51.8	49.2
ultimate deflection (mm)		78.2	84.9	61.2	56.9	55.3	64.7	56.1	72.2	47.4
displacement ductility		2.61	2.48	1.83	1.70	1.60	1.89	1.70	1.91	1.33
CFRP strain at debond ($\mu\epsilon$)		n.a.	5300	2900	6688	3550	7878	3200	4540	2850
Specimen		fatigue loading (cycling from 4.45 to 22.24 kN)								
		CF ¹	L1F	H1F	L2F	H2F	L2x1F	H2x1F	L4F	H4F
N=2	rebar stress range (MPa)	241	247	239	207	199	207	220	174	175
	secant stiffness (kN/mm)	1.43	1.43	1.42	1.71	1.53	1.56	1.63	1.89	1.71
final cycle, N _f		329324	400892	424422	2M	1128006	447695	2M	2M	2M
N=N _f	rebar stress range (MPa)	n.a.	231	250	240	217	230	251	201	196
	secant stiffness (kN/mm)	n.a.	1.34	1.33	1.35	1.37	1.42	1.38	1.56	1.48
Specimen		increasing monotonic load to failure following N = 2000000								
		fatigue-induced reinforcing bar rupture				fatigue-induced reinforcing bar rupture				
maximum load (kN)		45.5				45.3				
ultimate deflection (mm)		67.3				51.3				
displacement ductility		2.05				1.45				
CFRP strain at debond ($\mu\epsilon$)		4300				3909				

¹due to a power failure, Specimen CF was loaded to failure at N = 329,324 prior to fatigue-induced reinforcing bar rupture.

Figure 3 summarizes the load-displacement relationship for the nine monotonic tests conducted and Figure 4 presents a representative example of the load-deflection response of a fatigue specimen (L4F) showing the 2,000,000 cycles of fatigue conditioning and the subsequent monotonic test to failure.

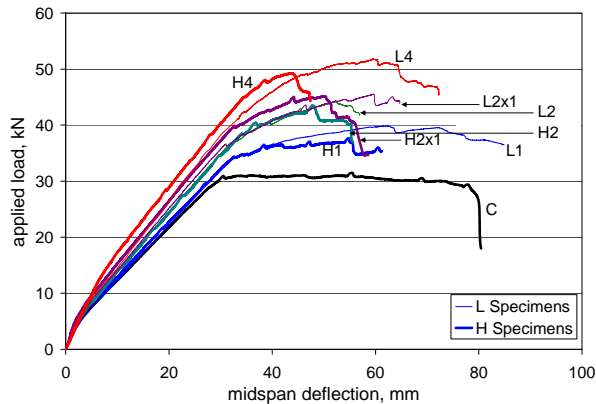


Figure 3: Load deflection behavior of monotonically loaded specimens.

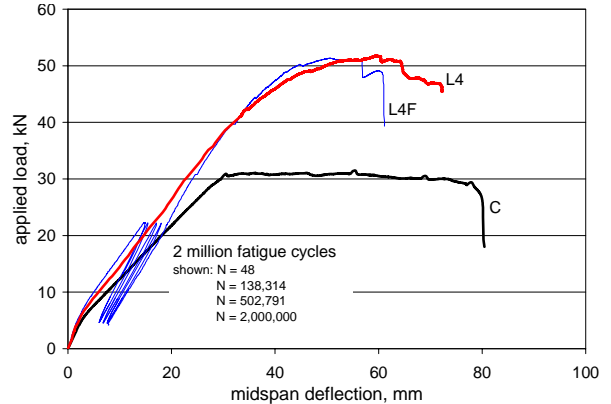


Figure 4: Representative load deflection behavior of Specimens L4 and L4F.

3.1 Performance of Monotonically Loaded Specimens

As is typically observed for externally bonded FRP retrofit applications, the application of the CFRP increases the capacity of the beam although the incremental increase in strength decreases with increasing CFRP area. Similarly the displacement ductility decreases with increasing CFRP area as the section reinforcing ratio increases.

As can be seen in Table 2, the load carrying capacity of the specimens tested is not affected by either the adhesive type (L or H) or the 2,000,000 cycle fatigue conditioning. The ultimate displacement and thus displacement ductility is improved with the softer adhesive system (L). Fatigue conditioning generally results in a reduction in the ultimate displacement and thus ductility of the monotonically loaded beam.

3.2 Performance of Fatigue Loaded Specimens

In all cases, the stress range in the reinforcing steel increases with continued fatigue cycling. This increase is proportional to the observed fatigue life (N_f) and is not affected by the amount of CFRP applied. Similarly, the degradation of secant stiffness is affected by fatigue life. In most cases, the softer adhesive (L) appears to result in a

greater stress range and/or stiffness degradation. This is believed to result from the marginally less efficient stress transfer affected by the softer adhesive requiring the internal reinforcing steel to carry proportionally greater stress.

4. DEBONDING OF EXTERNALLY BONDED CFRP

FIC debonding was the primary mode of failure for all monotonically loaded specimens. At the very least, local debonding was evident in all fatigue specimens except L2F. In the specimens that experienced fatigue-induced reinforcing bar rupture (L1F, H1F, H2F and L2x1), this debonding was caused by the energy release of the reinforcing bar and remained localized near the rupture location. Minor debonding was visually identified in runout specimens H2x1F, L4F and H4F. The debonding in these cases did not propagate beyond a strain gauge location and thus no specific debonding strain may be identified. Nonetheless, the CFRP strains in the region immediate adjacent the observed debonding ranged from only 1545 to 2285 $\mu\epsilon$.

4.1 Effect of Adhesive Stiffness

In FRP retrofit design, the mitigation of debonding is typically addressed through stress and/or strain limits applied to the FRP material. Although, recommendations from various international standards documents vary considerably, all are based on a function of the FRP axial modulus (E_f) and all neglect adhesive line properties. The results of this study show the dramatic effect of adhesive modulus on the CFRP debonding strain. In all cases, the softer adhesive (L) has a higher strain at initiation of debonding and may thus be interpreted as resulting in a more efficient use of the bonded CFRP. This beneficial effect is most pronounced for thinner CFRP strips (L1 and L2x1, each having 25 mm strips).

4.2 Effect of Fatigue Conditioning

In all cases reported, the monotonic tests conducted following 2,000,000 cycles of fatigue conditioning experienced lower strains at debonding than did their monotonically tested counterparts. The superior behavior of softer adhesive (LF) is significantly less pronounced following fatigue conditioning.

5. CONCLUSIONS

The following primary observations and conclusions were drawn from this study:

1. Due to the long shear span, the primary failure mode of all monotonically loaded specimens was FIC debonding. Some FIC debonding was evident during fatigue loading of all specimens except L2F.
2. As observed in most similar studies, the addition of CFRP material increased the load carrying capacity and reduced the displacement capacity (ductility) of the beams. The incremental effect, in each case, is reduced with increasing CFRP area.
3. The stress range in the internal reinforcing steel in the fatigue loaded specimens was observed to increase proportionally with the number of cycles of fatigue loading. Similarly the secant stiffness of the fatigue load cycle degrades with fatigue life. Both effects are marginally worse in the specimens having the lower modulus adhesive (LF specimens).
4. CFRP strains corresponding to the initiation of debonding are significantly greater in the specimens having the low modulus adhesive (L and LF specimens). The improved behavior is more pronounced in those specimens having thinner CFRP strips (L1 and L2x1).
5. The effect of 2,000,000 cycles of fatigue conditioning appears to significantly reduce the previously described beneficial effect on debonding strain of using a lower modulus adhesive.

The results of the present study indicate the need to address: a) the effect of the mechanical properties of the adhesive system used; and b) the development of reduction factors for adhesively bonded FRP systems subject to fatigue loading in developing and updating design guidelines for externally bonded FRP systems.

6. REFERENCES

- Oehlers, D.J. (2005) "Generic Debonding Mechanisms in FRP Plated Beams and Slabs" *Proceedings of the International Symposium on Bond Behavior of FRP in Structures*, December 7-9, 2005, Hong Kong. pp 353-44.
- Reeve, B. (2005) "Effect of Adhesive Stiffness and CFRP Geometry on the Behavior of Externally Bonded CFRP Retrofit Measures Subject to Monotonic Loads" M.Sc. Thesis, University of Pittsburgh. December 2005.
- Zorn, A. (2006) "Effect of Adhesive Stiffness and CFRP Geometry on the Behavior of Externally Bonded CFRP Retrofit Measures Subject to Fatigue Loads" M.Sc. Thesis, University of Pittsburgh. April 2006.

EXPERIMENTAL STUDY ON THE LOCAL BOND BEHAVIOR OF NSM-FRP BARS TO CONCRETE

Donatella Galati

(PhD Candidate, Department of Innovation Engineering University of Lecce, Lecce, Italy)

Laura De Lorenzis

(Assistant Professor, Department of Innovation Engineering University of Lecce, Lecce, Italy)

ABSTRACT

Near-surface mounted (NSM) fiber-reinforced polymer (FRP) reinforcement has proven effective for strengthening reinforced concrete (RC) structures and is gaining increasing attention. The NSM reinforcement is installed by grooving the surface of the member to be strengthened and embedding FRP bars or strips in the grooves with an appropriate binder. In this paper bond tests conducted on short NSM-bar anchorages are presented and results are evaluated to determine the effect of the test variables on local bond-slip behavior and development capacity. Parameters of the present study are the groove depth and width to depth ratio and the mechanical properties of the groove-filling epoxy. During the tests, conducted with a direct shear setup using a specifically suited pulling machine, the loaded-end and free-end slips and the strain distributions in the transverse plane were monitored. The local bond-slip curves obtained from the tests are modelled analytically and used to predict the capacity of a previous series of long bond length specimens characterized by the same other test variables.

KEYWORDS

Bond, fiber-reinforced polymers, near surface mounted reinforcement, pull-out testing, slip

1. INTRODUCTION

This work follows up to a previous experimental study on long bond length NSM bar anchorages (De Lorenzis and Galati 2006), and reports test results on short NSM bar anchorages focusing on the same test variables, i.e. groove depth and width to depth ratio and mechanical properties of the groove-filling epoxy. Beside gaining more test data on the influence of the mentioned variables, the objectives of this investigation were to verify the consistency in failure modes between short and long bond length specimens and to calibrate a local bond-slip relationship based on average bond stress and slip measurements on the short bond length specimens, evaluating whether the use of such local bond-slip relationship would allow an accurate prediction of the ultimate load of long bond length specimens. These results would validate the use of local bond-slip laws from short bond length specimens for prediction of quantities of design interest for strengthening with NSM reinforcement.

2. TEST PROGRAM AND MATERIALS

This paper presents results from a total of 24 NSM joints, see Table 1. The test variables were the groove size and width to depth (w/d) ratio and the mechanical properties of the groove-filling epoxy. Two commercially available epoxies, labeled as "a" and "b", were selected for their significantly different values of tensile strength and modulus of elasticity. Square grooves of two different sizes were evaluated, corresponding to ratios of groove depth d to actual bar diameter $d_{b,a}$ (indicated as k in Table 1) equal to 1.5 and 2.0. For a given groove depth, three different w/d ratios were evaluated, equal to 0.75, 1.00 and 1.25. All joints had a bond length l_b of 37.5 mm, corresponding to 5 times the nominal diameter of the bar d_b , and sufficiently short to consider bond stresses and slips uniformly distributed along the bond length and hence to allow the evaluation of the local bond-slip behavior of the joints. The specimen codes in Table 1 are structured as follows: two initial digits, corresponding to the groove width in mm, are followed by two digits corresponding to the groove depth in mm; then the type of epoxy is reported (a or b), and finally the letters A, B, C indicate different repetitions tested to control the experimental scatter.

The grooves were saw-cut onto the surface of the concrete blocks and then the bar was installed therein. The joints were instrumented with two LVDTs, to monitor slip of the NSM bar with respect to the concrete at the loaded and at the free end of the bond length. Strain gages were also applied to the outer surface of the epoxy, in the direction perpendicular to the bar axis. Testing was conducted in displacement-control mode with a direct pull-out setup, using a portable pulling machine suitable for in-situ testing.

The NSM joints tested in this program were constructed on two concrete blocks, having an average compressive strength of 41.2 and 46.3 MPa and an average splitting tensile strength of 2.3 and 2.7 MPa, respectively. Type-a epoxy had a direct tensile strength of 18.6 MPa (ASTM D 638M), a compressive strength of 46.3 MPa, an elastic modulus of 4150 MPa (ASTM D 695M). Type-b epoxy had a direct tensile strength of 22.8 MPa, a compressive strength of 83.4 MPa, an elastic modulus of 12870 MPa.

The round carbon FRP (CFRP) bars used in this study are spirally wound with a carbon fiber tow and sand coated, having a nominal diameter d_b of 7.5 mm and an actual diameter $d_{b,a}$ of 8.0 mm. The experimental tensile strength is 2214 MPa and the modulus of elasticity is 145.7 GPa. For more details see De Lorenzis and Galati (2006).

3. TEST RESULTS

The main test results are reported in Table 1 and Figures 1 and 2. The Table reports the ultimate load of the joints, P_{max} , the average bond strength at the bar-epoxy interface $\tau_{avgp} = P_{max}/(\pi d_b l_b)$, the loaded-end and free-end slips at peak load, s_{lep} and s_{fep} , and the failure mode.

For all specimens with type-a epoxy, the primary bond failure mechanism was slip at the bar-epoxy interface. Post-failure observations revealed that a very thin layer of epoxy was still visible on the surface of the bar, indicating that failure had resulted from cohesive shear failure in the epoxy. For specimens 12-12/a longitudinal splitting cracks in the epoxy paste and inclined cracks in the concrete adjacent to the groove became visible after the peak load, and widened during the descending branch of the load - slip curves. For joints 12-16/a, bond failure occurred by a combination of slip at the bar-epoxy interface and inclined cracking of the concrete adjacent to the groove. Joints 16-16/a and 20-16/a failed at the bar-epoxy interface with no visible cracks in the concrete or in the epoxy. Type-b epoxy has a tensile strength 23% larger and a modulus of elasticity 210% larger than type-a epoxy. This difference in the epoxy properties caused the average bond strength to increase significantly (Table 1) and in some cases (specimens 12-12 and 16-16) led to a different failure mode. Joints 12-12/b failed abruptly by formation of inclined cracks in the concrete adjacent to the groove before the shear strength of the epoxy was reached. Slip at the bar-epoxy interface occurred only after the peak load under decreasing bond stresses. For joints 12-16/b and 16-16/b, failure occurred by a combination of slip at the bar-epoxy interface and inclined cracking of the concrete. Only joints 20-16/b failed at the bar-epoxy interface with no visible cracks in the concrete.

Figure 1 illustrates the curves giving the average bond stress at the bar-epoxy interface versus loaded- and free-end slips. Only one representative repetition per type of specimen was selected for the sake of clarity.

For specimens 12-12/b and 12-16/b the gain in strength compared with the same specimens with type-a epoxy was accompanied by a more abrupt decrease of the bond stress after failure. For all the other joints the average bond-slip behaviour is characterized by a stiff initial ascending branch, followed by a rather smooth softening branch that indicates a pseudo-ductile nature of bond failure at the bar-epoxy interface. Besides, for all specimens the average bond stresses in the post-peak phase increase as the groove dimensions (i.e. both k and w/d) increase, due to the higher degree of confinement of the bar-epoxy interface. Hence increasing the groove dimensions, while not significantly improving the bond strength, yields a significant increase of the fracture energy of the joint, and this implies that the bond failure load of long bond length specimens will also increase.

Figure 2 shows the transverse strains measured on the epoxy cover at two different locations versus the applied load for selected specimens (strain 1 and 2 are located at a distance of 12.5 mm and 25 mm from the loaded end, respectively). Tensile strains are taken as positive and the curves are limited to the pre-failure phase. All curves display the same general trend. As illustrated in Figure 2, the use of a larger w/d ratio appears to delay the phase where tensile strains are developed in the cover and to reduce the maximum transverse strains at the peak load, indicating that the larger groove dimensions increase the transverse stiffness of the cover of the NSM bar. It is also evident that using type-b epoxy causes a marked reduction in the slope of the strain-load curves, and a substantial reduction of the transverse tensile stresses at peak load. Similar conclusions can be drawn on the effect of k ratio.

4. ANALYTICAL MODELING

As mentioned earlier, the local bond stress-slip relationship is here approximated by the average bond stress-slip relationship of the short bond length specimens. For all specimens the ascending branch of the bond-slip law is well interpreted by the Bertero-Popov-Eligehausen (BPE) relationship, that is $\tau = \tau_m (s/s_m)^\alpha$ valid for $0 \leq s \leq s_m$, where τ is the local bond stress, s the local slip, τ_m and s_m are bond stress and slip at the peak point, and α is a parameter that varies between 0 and 1. The descending branch of the bond-slip law can be described by an equation formally

identical with the exception that a parameter α' varying between -1 and 0 is used in place of α . Parameters τ_m , s_m , α and α' , calibrated by best fitting of the experimental results, are reported in Table 2, where τ_m is taken equal to the average bond strength and s_m is evaluated as the average between loaded-end and free-end slips at the peak point. As previously noted, the local bond strength is weakly affected by the groove dimensions, whereas a dramatic increase in the joint fracture energy G_f (here evaluated at a slip of 3 mm) is observed.

Table 1: Test program and results

Specimen	w/d	k = d/ d _{b,a}	Measured w/d	Measured k	P _{max} (kN)	τ_{avgp} (MPa)	S _{lep} (mm)	S _{fep} (mm)	Failure mode
12-12/a/A	1.00	1.50	1.05	1.47	11.5	13.02	0.31	0.13	BE-C+LC +SP
12-12/a/B	1.00	1.50	1.06	1.50	10.9	12.34	0.23	0.10	BE-C+LC + SP
12-12/a/C	1.00	1.50	1.03	1.45	11.4	12.90	0.20	0.05	BE-C+LC +SP
12-12/a/AVERAGE					11.3	12.75	0.25	0.09	BE-C+LC +SP
16-16/a/A	1.00	2.00	0.93	2.00	11.7	13.24	0.35	0.23	BE-C
16-16/a/B	1.00	2.00	1.07	1.95	12.2	13.81	N/A	0.32	BE-C
16-16/a/C	1.00	2.00	0.97	2.04	14.0	15.84	0.30	0.16	BE-C
16-16/a/AVERAGE					12.6	14.30	0.32*	0.24	BE-C
12-16/a/A	0.75	2.00	0.78	1.98	11.1	12.56	N/A	0.37	BE-C+ SP
12-16/a/B	0.75	2.00	0.70	2.04	14.1	15.96	0.52	0.34	BE-C+ SP
12-16/a/C	0.75	2.00	0.78	1.92	11.1	12.56	N/A	0.29	BE-C+ SP
12-16/a/AVERAGE					12.1	13.69	0.52*	0.33	BE-C+ SP
20-16/a/A	1.25	2.00	1.20	2.00	12.5	14.15	0.53	0.29	BE-C
20-16/a/B	1.25	2.00	1.21	2.02	12.3	13.92	0.42	0.35	BE-C
20-16/a/C	1.25	2.00	1.34	1.96	11.1	12.56	N/A	0.40	BE-C
20-16/a/AVERAGE					12.0	13.54	0.47*	0.35	BE-C
12-12/b/A	1.00	1.50	1.01	1.52	21.5	24.33	N/A	0.23	SP
12-12/b/B	1.00	1.50	0.96	1.47	20.4	23.09	N/A	0.17	SP
12-12/b/C	1.00	1.50	1.00	1.45	17.3	19.58	0.29	0.17	SP
12-12/b/AVERAGE					19.7	22.33	0.29*	0.19	SP
16-16/b/A	1.00	2.00	1.01	1.97	24.3	27.50	N/A	0.18	BE-C+ SP
16-16/b/B	1.00	2.00	1.03	1.96	24.8	28.07	0.16	0.08	BE-C+ SP
16-16/b/C	1.00	2.00	1.08	1.94	23.0	26.03	0.20	0.15	BE-C+ SP
16-16/b/AVERAGE					24.0	27.20	0.18*	0.14	BE-C+ SP
12-16/b/A	0.75	2.00	0.82	1.91	17.3	19.58	0.33	0.22	BE-C+ SP
12-16/b/B	0.75	2.00	0.74	1.95	22.1	25.01	0.16	0.14	BE-C+ SP
12-16/b/C	0.75	2.00	0.77	1.96	18.0	20.37	0.24	0.19	BE-C+ SP
12-16/b/AVERAGE					19.1	21.65	0.24	0.19	BE-C+ SP
20-16/b/A	1.25	2.00	1.10	2.14	23.5	26.60	0.41	0.30	BE-C
20-16/b/B	1.25	2.00	1.18	2.07	21.3	24.11	N/A	0.22	BE-C
20-16/b/C	1.25	2.00	1.21	2.08	23.7	26.82	0.54	0.31	BE-C
20-16/b/AVERAGE					22.8	25.84	0.47*	0.28	BE-C

Note: BE-C = failure at the bar-epoxy interface - cohesive shear failure in the epoxy; LC = longitudinal cracking of the epoxy; SP = splitting failure by fracture in the concrete along inclined planes; N/A = not available; * average of available data.

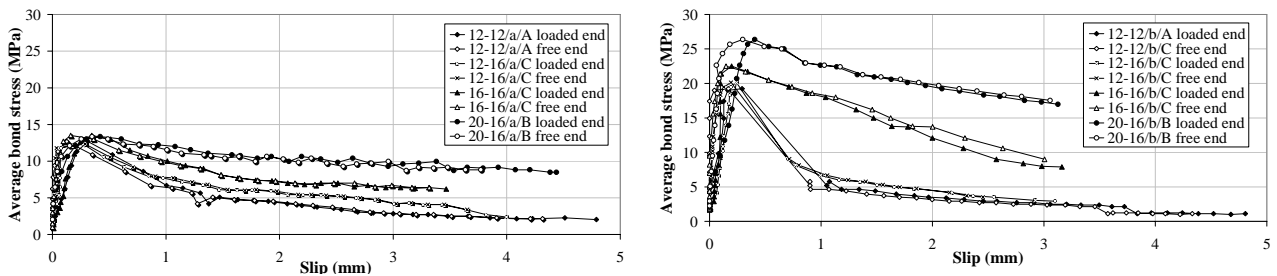


Figure 1: Average bond stress-slip curves

From the calibrated local bond–slip relationship, Figure 3 shows the predicted bond failure load as a function of the bond length. For the tested NSM systems, anchorage and economic efficiency suggest the use of 16x16 mm grooves, i.e. square grooves with a k ratio of 2. This yields a development length of about 55 d_b and 30 d_b when using type-a and type-b epoxy, respectively. Figure 3 also reports the experimental data obtained by De Lorenzis and Galati (2006) for specimens with 24-diameter bond length, which appear in reasonably good agreement with theoretical predictions. Note that curves of specimens 12-12 and 12-16 and those of specimens 16-16 and 20-16 are rather close to each other, in agreement with the values of parameters α and α' reported in Table 2.

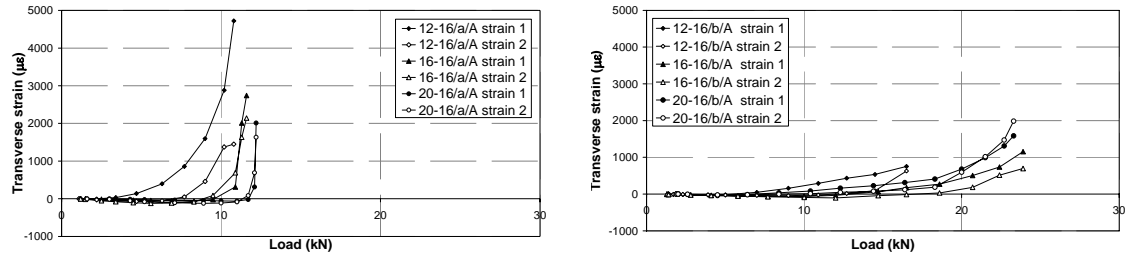


Figure 2: Transverse strain-load curves

Table 2: Calibrated parameters in the local bond– slip relationship

Specimen	Type-a epoxy					Type-b epoxy				
	τ_m (MPa)	s_m (mm)	α	α'	G_f (N/mm)	τ_m (MPa)	s_m (mm)	α	α'	G_f (N/mm)
12-12	12.8	0.17	0.45	-0.54	19.56	22.3	0.21	0.19	-0.82	20.35
12-16	13.7	0.43	0.18	-0.63	22.69	21.7	0.22	0.45	-0.65	23.28
16-16	14.3	0.28	0.21	-0.18	30.67	27.2	0.16	0.34	-0.26	51.67
20-16	13.5	0.41	0.21	-0.18	32.27	25.8	0.33	0.38	-0.16	60.30

5. CONCLUSIONS

The following main conclusions can be drawn: when using type-a epoxy, failure is controlled by slip at the bar-epoxy interface, due to cohesive shear failure in the epoxy; if type-b epoxy is used, failure may occur by concrete cracking for small groove sizes; the failure modes of short bond length specimens are consistent with those of long bond length specimens (De Lorenzis and Galati 2006) which validates the analytical approach used in this study, consisting in calibrating the local bond-slip law based on short bond length data; increasing the groove dimensions does not heavily affect the local bond strength, but significantly enhances the fracture energy of the joint; as a consequence, the bond failure load of long bond length joints increases; for the tested NSM systems, anchorage and economic efficiency suggest the use of 16x16 mm grooves, i.e. square grooves with a k ratio of 2.

The approach used in this study is suggested as a protocol for characterization of different NSM systems. While a general formulation of a local bond-slip law appears unfeasible, calibration of a local bond-slip law based on short bond length testing appears a simple yet reliable procedure to predict the anchorage length of a given NSM system.

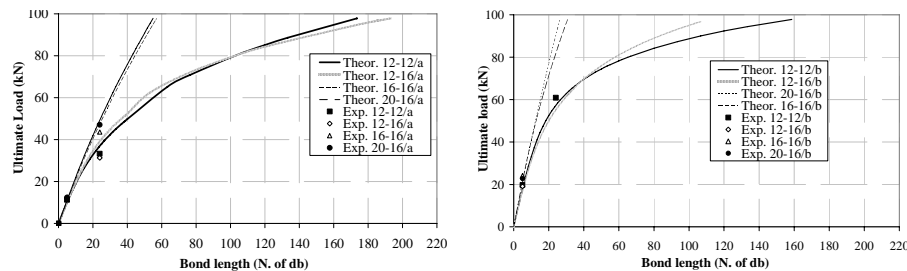


Figure 3: Theoretical and experimental bond failure load as a function of the bond length

REFERENCES

De Lorenzis, L., and Galati D. (2006), “Effect of Construction Details on the Bond Performance of NSM FRP Bars in Concrete”, Proceedings FIB Congress 2006, Naples, Italy, CD-ROM.

Part II. Bridge Applications

A Case Study of Life Cycle Cost based on a Real FRP Bridge

Itaru Nishizaki

(Team Leader, Public Works Research Institute, Tsukuba, Ibaraki, Japan)

Nobufumi Takeda

(Group Leader, Obayashi Corporation, Kiyose, Tokyo, Japan)

Yoshio Ishizuka

(Group Leader, Shimizu Corporation, Koto-ku, Tokyo, Japan)

Takumi Shimomura

(Associate Professor, Nagaoka University of Technology, Nagaoka, Niigata, Japan)

ABSTRACT

In this paper, the authors considered and calculated Life Cycle Cost (LCC) of FRP and Pre-Stressed Concrete (PC) footbridges based on an actual FRP footbridge constructed in Japan. Three types of PC bridges and two types of FRP bridges were set as model cases. The result suggests that FRP bridges have the competitive edge in spite of their initial cost and are more efficient when durability is required in severely corrosive environments.

KEYWORDS

FRP, PC, footbridge, life cycle cost

1. INTRODUCTION

FRP has some excellent properties as a structural material. Its application to bridges offers a possibility to solve problems that bridges made of conventional materials are facing today such as corrosion and damages incurred early in the life-cycle of a structure. Presently, FRP's unit price is usually rather more expensive than that of other conventional materials. This may increase the initial cost of the FRP superstructure and is one of the obstacles deterring widespread use of the material in FRP bridges.

In order to evaluate the benefit of using FRP in bridges, it is important to consider FRP's life cycle cost (LCC) including the cost for maintenance. There has been some research¹⁾⁻³⁾ on the cost benefit of FRP structures; however, because some of those studies begin with the design of the structures and include many suppositions, the LCC estimates of FRP structures are not so reliable.

With this in mind, the authors tried to evaluate the LCC of an actual FRP footbridge, remaining as faithful to actual conditions as possible. The case study is based on an FRP footbridge constructed in Okinawa, Japan, in 2000. It is called "Okinawa Road Park Bridge" and is pictured in Figure 1.



Figure 1: View of the Okinawa Road Park Bridge

2. THE STRUCTURES FOR THE CASE STUDY

A FRP footbridge and PC footbridge crossing a 4-lane road were considered as the case models. The bridges are located close to the seashore and severely affected by sea salt. The main girders of the FRP footbridge are made of hand lay-up FRP; pultruded FRP is used for the stiffeners, decks, and floor systems. Both types of FRP were made of glass fiber and vinylester resin. Parts of the FRP footbridge were made in several factories within the Tokyo area, assembled in a factory in Tokyo Bay, and then shipped to Okinawa. Wall type piers and steel pipe pile foundations were used in the substructure for both bridges.

Table 1: Model cases of FRP and PC bridges

	FRP bridges	PC bridges
Concept	Two span girder bridge with GFRP C-girders	Single span deck girder bridge with hollow post-tension concrete beams
Length	37.8m	36.0m
Span	19.7m+17.2m	35.0m
Width	4.3m	4.3m
Live load	350kgf/m ² for main girders	
	500kgf/m ² for decks	

3. CALCULATION METHOD OF LCC

Direct construction costs of the initial cost and the maintenance cost for both FRP and PC bridges were calculated based on the design reports for both bridges. LCC was obtained by the equations:

$$L_{FRP\ bri.} = I_{FRP\ bri.} + M_{FRP\ bri.}$$

$$L_{PC\ bri.} = I_{PC\ bri.} + M_{PC\ bri.}$$

L: Life-cycle cost
I: Initial cost
M: Maintenance cost

We did not calculate the cost for disuse neither did we consider the discount rate to discount future costs to the base year. Initial costs were calculated for both the superstructure and substructure. Maintenance costs were calculated only for the superstructure. The authors tried to set realistic suppositions in situations where no data existed. In this study, the authors made some assumptions for unknown conditions and simplified the calculation. Hence the values of the costs in this study do not indicate the real values of the Okinawa Road Park Bridge itself.

4. RESULTS

4.1 Initial costs

4.1.1 PC footbridges

Five types of superstructure were roughly designed for the PC footbridges. A deck girder footbridge with hollow post-tension concrete beams was selected after considering multiple viewpoints, including economy, workability, structure, view, and maintenance. Table 2 shows the model cases of the PC footbridge. CASE-1 is the base case with two types of corrosive protected cases added. CASE-2 adopts epoxy resin coated reinforcing bar and PC tendon. CASE-3 also adopts coated bar and tendon, with the addition of a paint coating on the concrete surface. The calculated the initial cost of each superstructure is: 48,240,000JPY, 50,620,000JPY and 54,370,000JPY respectively. As regards the substructure, two piers (Pier 1 and Pier 2) were roughly designed for each of three alternatives. The best results are shown in Table 2. The total cost of the substructure was 10,130,000JPY.

4.1.2 FRP footbridges

The initial cost of FRP bridges is roughly divided into three categories: (1) materials, (2) assembly, and (3) mold for hand lay-up. Table 3 shows the initial cost of FRP bridges. The initial cost of the FRP superstructure was 73,600,000JPY. The base model case (CASE-4) of the FRP footbridge has some special points, for example, it is the first real FRP footbridge in Japan and it is located on the seashore, suggesting that it may be possible to reduce its initial cost. The authors considered a modified case (CASE-5) for FRP bridges so as to reduce its initial cost. These modifications were: (1) change of handrail to aluminum, (2) change of design in the joint part of main girders, and (3) sharing of mold by two bridges. The result of the modified initial cost became 62,350,000JPY.

Table 2: Model cases of PC bridges and initial costs

(Unit: 1000JPY)

	CASE-1	CASE-2	CASE-3
Corrosion protection for the superstructure	None	Coated reinforcing bars Coated PC tendon	Coated reinforcing bars Coated PC tendon Surface coating
Initial cost for the superstructure	48,240	50,620	54,370
Substructure system	Pier 1: 6 Steel pipe piles (ϕ 600mm-9mm, L=17.5m) Pier 2: 4 Steel pipe piles (ϕ 600mm-12mm, L=20.0m)		
Initial cost for the substructure	10,130		
Total Initial costs	58,370	60,750	64,500

Table 3: Model cases of FRP bridges and initial costs

(Unit: 1000JPY)

	CASE-4	CASE-5
Modified points for the superstructure	Standard FRP bridge based on the real bridge	(1) Aluminum handrail (2) Change of joint parts of the main girders (3) Sharing the mold by 2 bridges
Initial cost for the superstructure	73,600	62,350
Substructure system	Pier 1: 2 Steel pipe piles (ϕ 500mm-9mm, L=15.0m) Pier 2: 4 Steel pipe piles (ϕ 500mm-9mm, L=18.0m) Pier 3: 2 Steel pipe piles (ϕ 500mm-9mm, L=12.0m)	
Initial cost for the substructure	6,910	
Total Initial costs	80,510	69,260

There are three piers (Pier 1, Pier 2, and Pier 3) for the substructure of the FRP footbridge. When comparing the two pile systems, driven steel pipe piles and PHC (Pretensioned Spun High Strength Concrete) piles with installation by inner excavation, the steel pipe piles substructure showed better results in this case.

Comparing the total costs including both the superstructure and substructure, the difference of the initial cost of the modified FRP footbridge (69,260,000JPY) was only 10% higher than the initial cost of the corrosion protected PC footbridge. This result suggests FRP bridges have significant competitive power even when considering the initial cost.

4.2 Maintenance costs

4.2.1 PC footbridge

Inspection and repair are the main maintenance considerations for bridges. Only the costs for repair were considered in this study. The costs for inspection were omitted because it seems there are not large differences in the inspection of PC and FRP bridges.

For the PC bridges, the authors estimated the penetration of chloride ion into the concrete after the construction, and the repair was set when the concentration of chloride ion at steel reinforcing bars reached 1.2 kg/m^3 . Replacement of covering concrete and surface coating was selected as the repair method for the PC bridges. The life of the surface coating which protects against chloride ion penetration was set at 15 years and 30 years, and repair of the surface coating was calculated in these intervals. Table 4 shows the results of the repair costs.

4.2.2 FRP footbridge

Since the Okinawa Road Park Bridge is relatively new, there is not enough information on its repair and maintenance requirements. However, five years after its construction, stainless steel bolts were replaced because of corrosion due to the severely corrosive environment. This amounted to 1,000,000JPY. We therefore considered the same scale of repair may be required at the same interval within a severely corrosive environment and set the repair

cost for an FRP footbridge at 1,000,000JPY at 5-year intervals. In the modified case of FRP footbridges, the repair cost was also modified by adopting highly durable bolts. The cost is 3,500,000JPY and the repair interval was set at 40 to 50 years.

Repainting is the major repair concern for FRP footbridges. There will be no corrosion for FRP structures caused by weak points of painting such as edges or bolt parts like a painted steel structure because FRP does not corrode. Hence, we set the repainting interval based on the decrease of thickness caused by the deterioration of the painting material. The repainting interval was set at about 120 years based on the thickness (75 μm) and the material (fluorine resin paint) of the paint. The repainting cost was calculated and the result was 5,600,000JPY including the scaffolding for repainting.

4.3 LCC

Table 4 shows the results of initial cost, maintenance cost and LCC for both PC and FRP footbridges. At 50 years, LCC of the FRP footbridge was 90,510,000JPY; this is lower than the 50-year LCC of the PC footbridge without corrosion protection. The lowest 50-year LCC was that of the PC footbridge with epoxy resin coated reinforcing bar and PC tendon (CASE-2). However, the modified FRP footbridge (CASE-5) showed the lowest 100-year LCC among our five cases. These results suggest that FRP footbridges are more efficient when longer life is required in severely corrosive environments.

Table 4: LCC results of both PC and FRP footbridges

(Unit: 1000JPY)

	CASE-1	CASE-2	CASE-3		CASE-4	CASE-5
			Repair interval: 15 years	Repair interval: 30 years		
Initial cost for superstructures	48,240	50,620	54,370		73,600	62,350
Initial cost for substructures	10,130	10,130	10,130		6,910	6,910
Total the initial costs	58,370	60,750	64,500		80,510	69,260
Maintenance cost for 30 years	24,500	0	18,000	9,000	6,000	3,500
Maintenance cost for 50 years	42,500	0	27,000	9,000	10,000	3,500
Maintenance cost for 100 years	69,500	24,500	54,000	27,000	20,000	7,000
50 years LCC	100,870	60,750	91,500	73,500	90,510	72,760
100 years LCC	127,870	85,250	118,500	91,500	100,510	76,260

5. CONCLUSION

In this paper, the authors considered and calculated the LCC of FRP and PC footbridges, faithfully considering actual conditions based on a real FRP footbridge constructed in Japan. The result suggests that FRP bridges has a competitive edge over other types of construction in spite of its initial cost and that FRP footbridges are more efficient when longer life is required in severely corrosive environments.

6. ACKNOWLEDGEMENTS

This study was carried out as a part of the activity of “The committee for applications of advanced structural materials” of the Japan Society of Civil Engineering (JSCE) from 2004 to 2006. The authors also thank the government of Okinawa prefecture for their cooperation in providing the information on the plans and designs of the FRP and PC footbridges.

7. REFERENCES

- 1) Meiarashi, S., Nishizaki, I. and Kishima, T. (2002). “Life-Cycle Cost of All-Composite Suspension Bridge.” *Journal of Composites for Construction*, 6 (4), 206-214.
- 2) Ehlen, M. A. (1999). “Life-cycle costs of fiber-reinforced-polymer bridge decks.” *J. Mater. Civ. Eng.*, 11(4), 224-230.
- 3) Nystrom, H. E., Watkins, S. E., Nanni, A., and Murray, S. (2003). “Financial viability of fiber reinforced polymer (FRP) bridges.” *Journal of Management in Engineering*, 19(1), 2-8.

STRUCTURAL REHABILITATION OF AN OFF-SYSTEM BRIDGE USING EXTERNALLY BONDED CFRP LAMINATES

Nestore Galati

(Research Engineer, University of Missouri - Rolla, Rolla, Missouri, USA)

Andrea Rizzo

(PhD Candidate, University of Lecce, Lecce, Italy)

Antonio Nanni

(Professor and Chair, University of Miami, FL, USA)

ABSTRACT

This paper presents the use of Fiber Reinforced Polymers (FRP) laminates for the flexural strengthening of a concrete bridge superstructure. The system consists of Carbon Fiber Reinforced Polymers (FRP) laminates bonded onto the concrete surface in order to provide the necessary flexural reinforcement for the deck. The bridge superstructure selected for this project is a 4-span reinforced concrete (RC) slab. The bridge is located on Route 0039 in Washington County, Missouri - USA. The bridge analysis was performed for maximum loads determined in accordance to AASHTO Design specification, 17th edition. The strengthening scheme was designed in compliance with the ACI 440.2R-02 design guide.

KEYWORDS

Mechanically Fastened Fiber Reinforced Polymers (MF-FRP) Laminates, Load Rating, Finite Elements Modeling

1. INTRODUCTION

Fiber-reinforced polymer (FRP) materials have emerged as a practical alternative for construction, renovation and strengthening of bridges with significant cost and time savings over conventional methods. Advantages of FRP materials are that they resist corrosion, long outlive conventional materials, and have high strength-to-weight ratio. It has been shown that in this technical area nowadays the engineer has different tools available in order to find the optimal solution to each problem: manual lay-up FRP and SRP laminates, adhered pre-cured FRP laminates, near surface mounted (NSM) FRP bars and, finally, MF-FRP laminates (Lopez et al. 2004).

This paper reports the use of Fiber Reinforced Polymers (FRP) laminates for the flexural strengthening of a concrete bridge superstructure. The system consists of Carbon FRP laminates produced by MAPEI Corporation bonded onto the concrete surface in order to provide the necessary flexural reinforcement to the deck. The bridge superstructure selected for this project is a 4-span reinforced concrete (RC) slab. The bridge is located on Route 0039 in Washington County, MO. The bridge analysis was performed for maximum loads determined in accordance to AASHTO Design specification, 17th edition. The strengthening scheme was designed in compliance with the ACI 440.2R-02 design guide.

2. DESCRIPTION OF THE BRIDGE

Bridge No. 0390006 (see Figure 1), located in Washington County (Route 0039), MO. The bridge is actually load posted to a maximum weight of 4.5 ton_{SI} (5 ton). The total length of the bridge is 17.8 m (58 ft) and the total width of the deck is about 4.3 m (14 ft). The structure is a 4-span continuous reinforced concrete (RC) slab having 178 mm (7 in) thickness. From visual observations, the guardrail along the longitudinal North edge was found damaged with concrete spalling and exposed steel reinforcement. No visible traces of steel rebar corrosion were observed. Even though the concrete substrate was found sound, as a consequence of the insufficient amount of longitudinal

reinforcement, the deck was visibly cracked at mid-span and corresponding to the piers. Piers and abutments appeared in good conditions.

The geometry of the bridge is summarized in Table 1. Figure 2 and Figure 3 show the longitudinal and plan view of the bridge. Figure 3 also shows the position from where the concrete cores were extracted, and the longitudinal and transverse steel reinforcement of the deck.



Figure 1: Bridge No. 0390006

The details of the bridge reinforcement and material properties were unknown at the time of strengthening due to the unavailability of plans. As a consequence, at the onset of the project, these properties were determined in-situ, based on visual and Non Destructive Testing (NDT) evaluation. Three concrete cores were drilled and tested in compliance with ASTM C39 and ASTM C42. The average concrete compressive strength f_c was found to be 20.0 MPa (2900 psi). The location of the steel reinforcement was accurately detected with a rebar locator. The steel mechanical properties were determined by testing three specimens cut from exposed bars according to ASTM A615 and ASTM A955. The average yield steel strength, f_y , was found to be 512 MPa (74.2 ksi). More details can be found in Rizzo et al. (2005).

Table 1: Geometry of the Bridge

<i>Span</i>	D1	D2	D3	D4
Clear Span, l_c (in the Traffic Direction)	4147 mm (13 ft 7 1/4 in)	4178 mm (13 ft 8 1/2 in)	4451 mm (14 ft 7 1/4 in)	4204 mm (13 ft 9 1/2 in)
Design Length, l_d (in the Traffic Direction)	4350 mm (14 ft 3 1/4 in)	4382 mm (14 ft 4 1/2 in)	4655 mm (15 ft 3 1/4 in)	4407 mm (14 ft 5 1/2 in)
Deck Height, H_d (Average Value)	190 mm (7 1/2 in)	184 mm (7 1/4 in)	178 mm (7 in)	190 mm (7 1/2 in)
Skew, α	48° (between Support and Traffic Direction)			
Roadway Width, W_r	4267 mm (14 ft)			
Curb-to-Curb Roadway Width, W_{rc}	3988 mm (13 ft 1 in)			
Overlay Height, H_o	12.7 mm (0.5 in)			

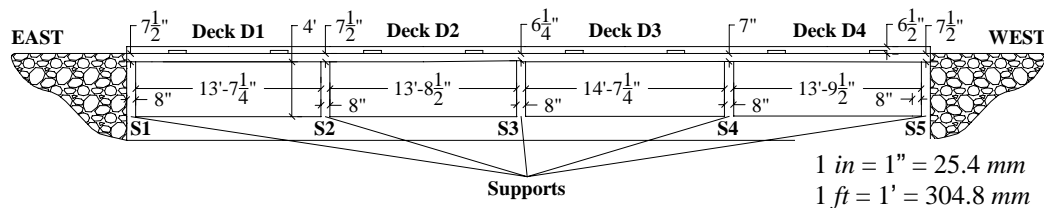


Figure 2: Longitudinal View of the Bridge

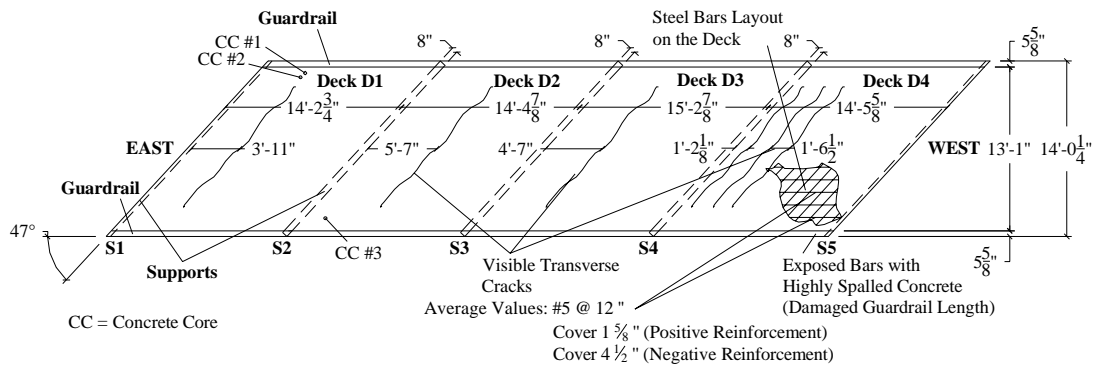


Figure 3: Plan View of the Bridge

3. BRIDGE ANALYSIS AND FRP STRENGTHENING DESIGN

The analysis of the bridge was performed according to the MoDOT Bridge Manual, 1996: the assumed load configurations were consistent with the AASHTO Specifications (AASHTO 2002). The structural analysis of the bridges was performed using design truck and lane loads having geometrical characteristics and weight properties as suggested in AASHTO, 2002 Article 3.7.4. An H15-44 truck load was considered as design load since it generated the maximum load configuration compatible with the shear capacity of the structure: in fact, for “slab” bridges the FRP strengthening can only be used to increase the flexural capacity.

Since the FRP strengthening system does not allow increasing the flexural capacity of the deck in the negative moment region, the analysis was conservatively conducted by neglecting the flexural continuity of the deck over the supports. This led to model the deck as a simply-supported slab between two consecutive supports. This led to model the deck as a simply-supported slab between two consecutive supports.

FRP laminate design was carried out according to the principles of ACI 440.2R-02 (ACI 440 in the following). The properties of concrete, steel and FRP laminates used in the design are summarized in Table 2. The concrete and steel properties were obtained by testing of samples. The guaranteed design material properties of the FRP laminates were determined experimentally as part of a companion experimental program (Rocca et al., 2006).

The ϕ factors used to convert nominal values to design capacities are obtained as specified in AASHTO (2002) for the as-built and from ACI 440 for the strengthened members. Figure 4 details the longitudinal flexural strengthening, while Figure 5 details the moment capacity of the unit slab along its length. More details regarding bridge analysis and design can be found in Rizzo et al. (2005). The CFRP laminates were applied by a certified contractor in accordance to manufacturer’s specification. The strengthening of the bridge was completed in 48 hours without traffic disruption.

The theoretical load rating (Cai and Shahawy, 2003) was calculated for four different truck types, mandatory by Missouri Department of Transportation according to the Manual for Condition of Bridges (ASSHTO, 1996). A detailed description of these trucks can be found in Rizzo et al. (2005). By comparing the load rating calculations before and after strengthening it was showed that the FRP strengthening allowed increasing the posting load of the bridge from 4.5 ton_{SI} (5 ton) to 14.5 ton_{SI} (16 ton).

Table 2: Bending Moments and Shear Forces per Unit of Bridge Deck

Concrete	Steel		FRP - LAMINATES		
Compressive Strength [MPa] ([psi])	Yield Strength [MPa] ([psi])	Modulus of Elasticity [GPa] ([ksi])	Tensile Strength [MPa] ([ksi])	Modulus of Elasticity [GPa] ([ksi])	Thickness [mm] ([in])
41.4 (6000)	455.0 (66)	200.0 (29000)	2700 (390)	230 (33000)	0.167 (0.007)

3. CONCLUSIONS

Conclusions based on the retrofitting of the bridge utilizing FRP materials can be summarized as follows:

- The FRP externally bonded system showed to be a feasible solution for the strengthening of the bridge;
- As a result of FRP strengthening, the load posting of the bridge was increased from 4.5 ton_{SI} (5 ton) to 14.5 ton_{SI} (16 ton), corresponding to a 320% enhancement.

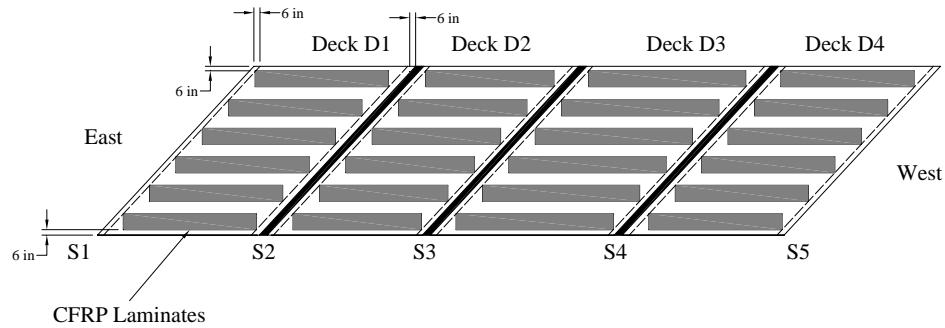


Figure 4: Strengthening of the Deck: Plan View

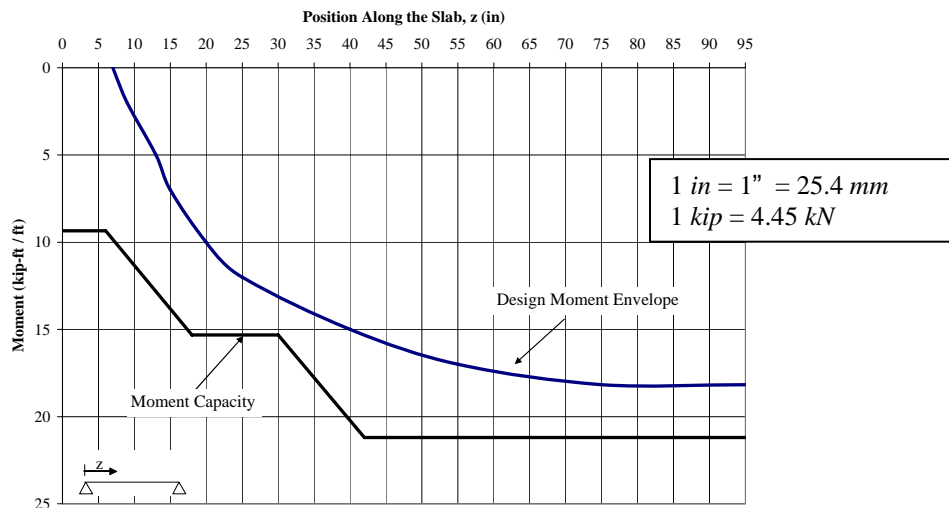


Figure 5: Diagram of the Capacity of the Deck at the Ultimate Load Conditions

4. REFERENCES

- AASHTO, 1996, LRFD Bridge Design Specifications, Second Edition, American Association of State Highway and Transportation Officials, Washington, DC.
- AASHTO, 2002, Standard Specifications for Highway Bridges, 17th Edition, American Association of State Highway and Transportation Officials, Washington, DC.
- ACI Committee 440, 2002, Guide for the Design and Construction of Externally Bonded FRP Systems for Strengthening Concrete Structures (440.2R-02), American Concrete Institute, Farmington Hills, MI.
- Cai, C. and Shahawy, M. (2003). "Understanding Capacity Rating of Bridges from Load Tests" Practice Periodical on Structural Design and Construction. ASCE. Vol. 8. No 4. pp. 209-216
- Lopez, A. and Nanni, A., (2004). "Validation at a Large Scale of FRP Technology for Bridges Strengthening", Submitted to Concrete International – ACI.
- MoDOT Bridge Load Rating Manual. Missouri Department of Transportation, Jefferson City, Missouri, 1996, pp 4.1-4.28
- Rizzo, A.; Galati, N. and Nanni, A., (2005). "Strengthening of Bridge No. 390006 Route 0039 - Washington County, MO" CIES Report 04-055-d, University of Missouri-Rolla, Rolla, MO, USA.
- Rocca, S., N. Galati, and A. Nanni, (2006). "Experimental and Analytical Evaluation of Large-Size Reinforced Concrete Columns Strengthened with FRP", Report UTC-142, University of Missouri-Rolla, Rolla, MO, USA.

ENHANCEMENT OF SHALLOW DEPTH PATCHES FOR CONCRETE BRIDGES USING FRP OVERLAYS

Golrokh Nossoni

(Graduate Research Assistant, Michigan State University, East Lansing, MI, USA)

Ronald S. Harichandran, Ph.D., P.E

(Professor and Chairperson, Michigan State University, East Lansing, MI, USA)

Rigoberto Burgueño, Ph.D.

(Associate Professor, Michigan State University, East Lansing, MI, USA)

ABSTRACT

The use of fiber reinforced polymer (FRP) fabrics applied as overlays on top of traditional patching materials was investigated to provide more durable patches on concrete structures. FRP overlays provide the benefits of keeping the patch in place for a longer period, restraining the diffusion of moisture and chloride ions, especially when patches are cracked, and reducing further damage to the concrete element. Finite element (FE) models were developed to assess the damage on the patching material due to shrinkage, corrosion, and mechanical load. The demands from the numerical studies were used to evaluate suitable FRP fabrics and their configurations. It was found that a layer of bidirectional glass FRP is adequate for shallow depth patching applications. Experiments are being conducted to validate this result.

KEYWORDS

Shallow depth patch, Shrinkage, Cracking, Bond Strength, Debonding, FRP, Delamination

1. INTRODUCTION

Shallow depth surface patches, used to repair damaged concrete bridge elements typically crack extensively soon after application. These patches can be classified into two primary groups: cementitious mortars (CM) and polymer modified cementitious mortars (PM). Cracking and full or partial delamination of the patching material from the concrete substrate is generally unavoidable. The cracking and delamination is related to many factors and the primary factor is the shrinkage of the repair material at an early age. The tensile strength, modulus of elasticity of the repair material at an early age, and structural characteristics govern the effect of restrained shrinkage (Yuan et al., 2003). Restrained shrinkage results in the development of various stresses which can lead to premature failure of the patch. Failure modes include vertical cracking due to direct tension and delamination due to interfacial stresses. The problem is further exacerbated if the repaired structure is subjected to an aggressive environment, where cracks provide free access for intrusion of chloride ions and diffusion of carbon dioxide (Baluch et al., 2002). The choice of an optimum repair material should be based on the best compromise of required properties, and may also be influenced by the availability of materials and technical experience, and other constraints, such as the application technique and construction environment. But even with patching materials that are highly compatible with concrete, the repair typically lasts only for a few years. Most of the research done in this area has focused on improving the compatibility between the concrete substrate and the patching material to prevent cracking, but finding reliable criteria for the required parameters is difficult. To minimize this problem and improve the performance and durability of shallow depth surface patches on concrete substrates, the use of an FRP overlay as a secondary reinforcement is investigated in this study. The additional reinforcement can hold the patching material in place and prevent its premature failure. Finite element simulations of the proposed patching system under shrinkage, corrosion and mechanical loads are reported in this paper. Experimental studies to corroborate numerical predictions are currently underway.

2. NUMERICAL EVALUATION OF PATCH REPAIRS WITH AND WITHOUT FRP

Two- and three-dimensional finite element analyses (FE) were conducted using the general-purpose ABAQUS program (version 6.3). 2-D models were used to study the effect of restrained shrinkage, mechanical load, and corrosion on the repair material and concrete substrate when the FRP overlay was not used. 3-D models were used to select optimally configured layers of FRP on damaged patches. The analyses were conducted on models with the geometry, boundary conditions, and loading to be used for the experimental specimens. Simply supported beams with dimension of 16" × 4" × 3" are being used in mechanical load and shrinkage tests, and beams with dimension of 12" × 6" × 6" are being used in the corrosion test. Both beam geometries have a cavity of dimension 4" × 3" × 0.625" and 4" × 5" × 0.625", respectively, on the bottom side. Full bonding was assumed between all interfaces, but some interfaces were allowed to separate using a node-by-node approach to simulate crack propagation and debonding. Reinforced concrete was modeled as an elastic-plastic material, and the patch materials were assumed to be elastic. The physical and mechanical properties of the patch and FRP materials used in the FE models are given in Table 1.

Table 1: Patch and FRP Materials used in Finite Element Analyses

Patching Materials				FRP				
Material	Type	Elastic Modulus (psi)	Shrinkage Strain (μ ϵ)	Material	Type	Fiber Orientation	E ₁₁ (psi)	Thickness (in.)
Material 1	PM	2.0E+6	350	FRP 1	Glass	Unidirectional	3.47E+6	0.05
Material 2	PM	2.0 E+6	1410	FRP 2	Glass	Chopped	1.17E+6	0.04
Material 3	PM	3.6 E+6	800	FRP 3	Glass	Bidirectional	2.47E+6	0.013
Material 4	PM	2.5 E+6	760	FRP 4	Carbon	Unidirectional	1.02E+7	0.02
				FRP 5	Carbon	Bidirectional	6.60E+4	0.01

First 2-D analyses were performed to determine the most likely location of cracks in the patching material. Subsequently, exhaustive 3-D analyses considering different crack patterns were performed. In all the analyses only one layer of the FRP overlay was considered. For uni-directional FRP, the fibers would normally be oriented in the longitudinal direction for mechanical load and in the transverse direction for the corrosion load. However, since only one layer of FRP overlay is considered and the load carried by the FRP is expected to be low, all analyses for uni-directional FRP were performed twice with fibers oriented in the transverse and longitudinal directions, respectively, to determine whether the load normal to the fibers could be carried by the matrix alone.

2.1 Failure Modes

Failure modes in the patching material include vertical cracking and bond failure, while failure modes in the FRP overlay include rupture of the fibers or matrix, and bond failure between the patch and the FRP overlay. The potential for bond failure was assessed through a debonding index (DI):

$$F_b = \sqrt{(\sigma_{ii} / \sigma_n)^2 + (\tau_{ij} / \tau_n)^2} \quad (1)$$

where τ_n = shear bond strength, σ_n = tensile or compression strength of the patch material, and τ_{ij} and σ_{ii} are the shear and normal stresses acting on the bond interface, respectively. The influence of normal stresses along the FRP bond was neglected.

The potential for tension cracking was evaluated using the magnitude of the principal tension stress. A tension cracking failure index (TCI) was defined as:

$$F_t = \sigma_{p \max} / f_t \quad (2)$$

where $\sigma_{p \max}$ = maximum tension principal stress, and f_t = tensile strength of the patch material. Rupture in the fibers or matrix of the FRP can be evaluated using the same concept. A fiber/matrix rupture index (F/MRI) was defined as:

$$F_r = \sigma_{ii} / f_{ultimate} \quad (3)$$

where σ_{ii} = stress in the direction of fibers or matrix, and $f_{ultimate}$ = ultimate tensile strength of the fibers or matrix depending on the FRP orientation. Failure is assumed to occur when any of the above functions exceed unity.

2.2 Simulation of Load Effects

Since the research focus is on the post-shrinkage behavior of the patch material, a complex diffusion-based technique (Baluch et al., 2002) is not considered necessary. Shrinkage strains were applied as a uniform initial strain in the patch material and the time-dependency of shrinkage was neglected. The mechanical load was limited to that which produced a strain demand of $0.2\varepsilon_y$ in the steel reinforcement. Figure 1(a) shows the TCI-values due to shrinkage at critical locations along the depth of the patch calculated using 2-D analysis. The figure indicates that all patching materials other than Material 1 are expected to crack. After the first crack opens, additional tensile cracks are likely to open at random locations and prevent debonding on the bond surfaces. However, under the mechanical loads debonding failure is most likely.

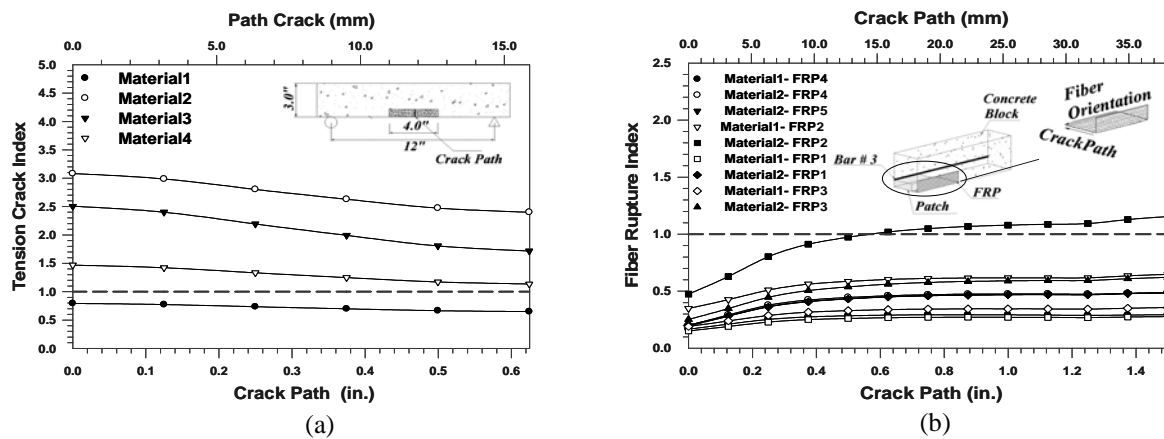


Figure 1: (a) TCI along the most critical path; and (b) FRI along the crack path in the FRP

The two patch materials that had the best and worst performance in the 2-D analyses (Materials 1 and 2) were used to evaluate the behavior of the shallow repairs with FRP overlays using 3-D analyses. The calculated values of the FRI in the critical model are shown in Figure 1(b). In this model a single crack was introduced in the patch material along the transverse direction at the most likely location, and the model was analyzed under combined shrinkage and mechanical loads. As Figure 1(b) shows, only one of the selected FRP overlays (chopped glass FRP2) fails due to the applied load when used with patching material 2. Uni-directional FRPs had fibers oriented in the longitudinal direction. Analyses of uni-directional FRP with fibers oriented in the transverse direction showed that the matrix is not strong enough to carry the applied load in the longitudinal direction and would therefore crack.

When reinforcement bars corrode, the corroded steel swells to about 4 to 6 times its initial volume. However, some of the corrosion products are likely to fill pore voids within the concrete. The expansion due to corrosion was estimated by calibration with available experimental data for FRP wrapped concrete cylinders subjected to accelerated corrosion (Baiyasi, 2000). Based on this calibration, an expansion strain of $17,500 \mu\varepsilon$ was applied to the entire cross section of the #4 bar. Figure 2(a) shows the TCI along different paths due to corrosion for the worst patching materials, calculated using a 2-D model. It clearly indicates that the first crack is likely to open along Path 1.

Based on the results from 2-D analyses, a vertical pre-opened crack was introduced in the 3-D model radiating downward from the bar. The model was studied under combined shrinkage and corrosion loads with fibers oriented in the transverse direction. Only the patch material having the highest shrinkage (Material 2) was considered. Figure 2(b) shows the FRI along the crack path and indicates that the chopped glass FRP overlay (FRP 2) is expected to fail. The other FRP overlays do not fail under this combined load. Analyses with unidirectional fibers oriented in the longitudinal direction showed that the matrix could not sustain the stresses in the transverse direction and that fibers oriented in the transverse direction would be necessary.

Figure 3 shows the DI-values calculated to evaluate the state of the bond between the FRP overlay and the patching material. It was assumed that bond failure initiates in the patching material. The calculated DI-values transverse to the crack path for critical models indicate that there will be debonding near the crack location over a 0.2-0.3 in. length for some FRP overlays (left side of Figs. 3(a) and (b)), and debonding near the patch/concrete interface at the ends of the patch over a 0.1-0.2 in. length for two overlays (right side of Figs. 3(a) and (b)).

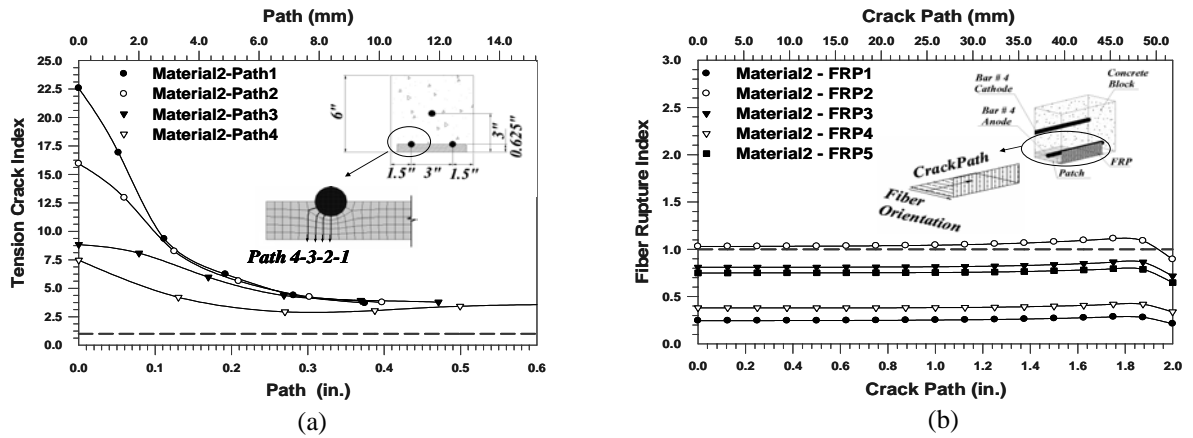


Figure 2: (a) TCI along different paths; and (b) FRI along the crack path in the FRP overlay

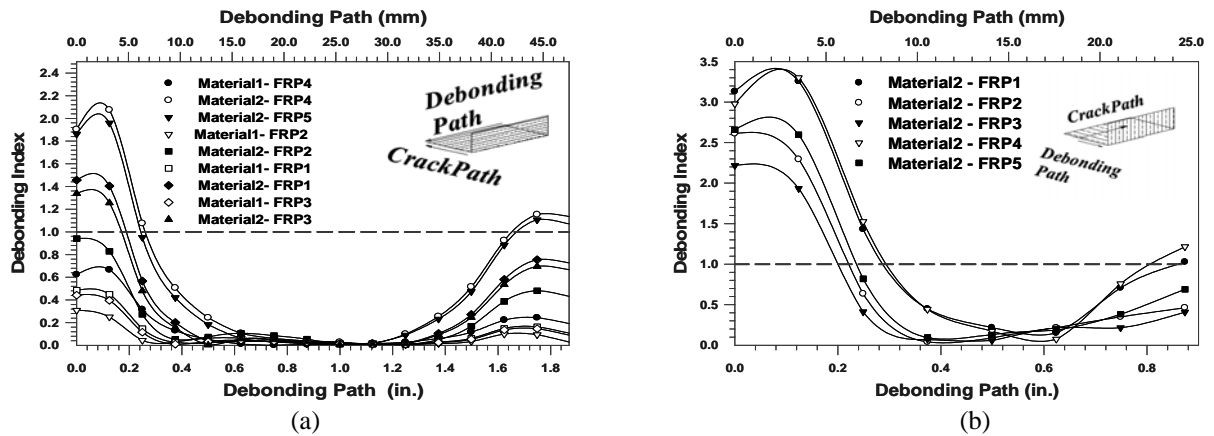


Figure 3: DI along the transverse crack path for: (a) model shown in Figure 1(b); and (b) model shown in Figure 2(b)

3. CONCLUSIONS

Analytical results for mechanical, shrinkage, corrosion, and combined loading effects on patch repairs with an FRP overlay show that one layer of uni-directional fabrics (FRP 1 and FRP 4), with fibers oriented either along the transverse or longitudinal direction, are insufficient to withstand the combined load. One layer of the chopped glass fabric (FRP 2) also is inadequate. However, one layer of the bi-directional fabrics (FRP 3 and FRP 5) is sufficient to resist all loading effects with either of the patching materials considered. Since glass FRP is more economical than carbon FRP, one layer of FRP 3, or any other bi-directional glass reinforced FRP with similar mechanical properties, should be an effective solution for use as an overlay for improving the performance and durability of shallow depth patches in concrete structures.

4. REFERENCES

- Baiyasi, M. I. (2000). "Repair of corrosion-damaged columns using FRP wraps." *Ph.D. Thesis*, Michigan State University, East Lansing, Michigan.
- Baluch, M. H., Rahman, M. K., and Al-Gadhib, A. H. (2002). "Risks of cracking and delamination in patch repair." *Journal of Materials in Civil Engineering*, July/August, pp 294-302.
- Yuan, Y., Li, G., and Cai, Y. (2003). "Modeling for prediction of restrained shrinkage effect in concrete repair." *Cement and Concrete Research*, Vol. 33, No. 3, pp 347-352.

EXPERIMENTAL STUDY ON PRESTRESSED CONCRETE GIRDERS STRENGTHENED WITH CFRP TAPES AT DIFFERENT BRIDGE REPAIR STAGES

Arkadiusz Mordak

(M.Sc., Ph.D. Student, Cracow Technical University, Cracow, Poland)

Zbigniew Manko

(Professor of Civil & Structural Engineering, Wrocław University of Technology, Wrocław, Poland)

ABSTRACT

This paper presents the results of the research on a five-span prestressed concrete road bridge under static load performed at different stages of its repair. All bridge spans become reinforced by CFRP tapes glued on bottom flanges of main beams, and external flat steel stirrups, as well as overlaid a new concrete deck layer. The main aim of the conducted bridge repair was to increase its load capacity to 300 kN (class C) according to the Polish Loads Standard (PN-85/S-10030). The results obtained during the research at different stages of repairs were conducive to determining the behavior of the analyzed span structure under static loads, which allowed for an assessment of the efficiency of the strengthening, as well as establishment of guidelines for future reference concerning this type of strengthening in the engineering practice.

KEYWORDS

Bridges, Prestressed concrete beam, CFRP tapes, Field tests, Static loads, Repair stages

1. INTRODUCTION

This paper presents research on the concrete spans with the prestressed main beams of the road bridge on the Nysa Klodzka River situated in Paczkow (Opole Province, at 72+536 km along the road no. 328 Stanowice – Paczkow). The research was conducted at different stages of the repair works, that is, before performing the main research on static and dynamic field load tests (acceptance inspections), which was aimed to determine the efficiency of the applied repairing methods. Before the repair, the bridge load capacity determined in expertise was classified as class E, that is 150 kN according to the Polish Loads Standard (PN-85/S-10030), mainly due to a very poor technical condition of the load-carrying structure of all bridge spans, resulting mostly from transverse cracks in the main beams (Figure 1). The main aim of the repair was to increase the object load capacity to class C (300 kN).

The aim of the conducted research was to determine the behavior of the chosen spans structures subjected to considerable static loads at various indirect stages (phases) of the performed bridge repair. The research allowed to find out on which elements of the load-carrying structure of span the biggest forces were exerted during the progress of repair works on one half of the bridge. It is quite an important problem not only in terms of construction works safety but also of vehicles and people using the non-repaired part of the bridge is concerned. Furthermore, there is also a possibility of overloading some structure elements, like e.g. main beams.

It should be added that it is a relatively rare activity to perform research on a bridge or its elements during the repair works. The inspection of spans and analysis of the obtained results performed each time after the accomplishment of repairs allow determining the influence of the same load on the quality and durability of this object in the process of strengthening as well as the efficiency and purposefulness of this process.

The final results of the bridge acceptance inspection (PN-S-10040, 1999), conducted after the complete repair under the trial static and dynamic load (Manko and Mordak, 2002), allowed a comprehensive evaluation of the efficiency of the main beams strengthening by applying CFRP tapes. Moreover, it enabled a comprehensive evaluation of the change of the spans structures behavior under the same load during different stages of repair works, simultaneously with the standard traffic running on the second, then non-repaired half of the bridge which included I, II and V spans.

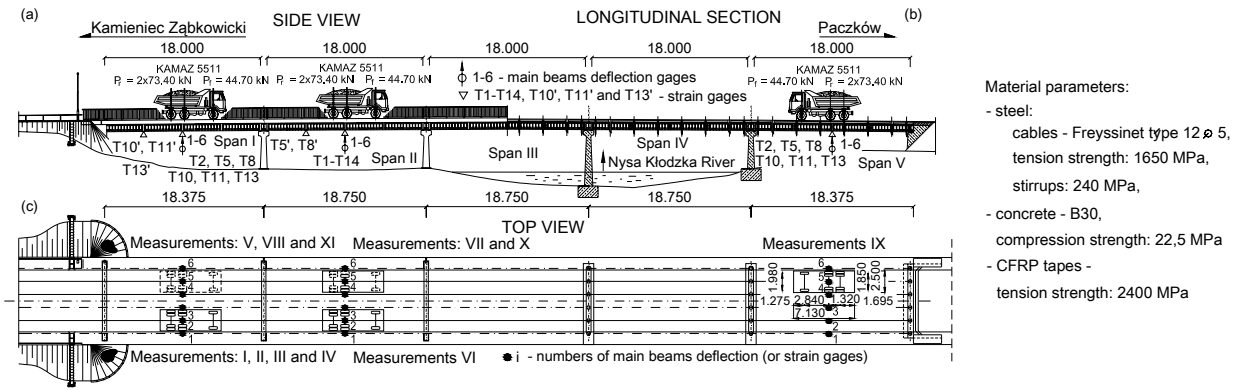


Figure 1: Post-tensioned concrete road bridge: (a) side view from headwater and (b) longitudinal section, (c) top view – technical parameters of truck type KAMAZ 5511 and load distribution on bridge spans during particular stage of field tests, and extensometers localization on strengthening strips during field research

2. RESULTS OF RESEARCH AND DISCUSSIONS

The strengthening of the particular bridge spans was accomplished by gluing the tapes made of carbon fibers CFRP (three for each beam) to the bottom flanges of the main beams and constructing an additional reinforced concrete deck plate of variable thickness 0.12–0.185 m and adding the outer stirrups in the form of steel flats of 5×50 mm section, with axial base by every 0.35 m (Manko and Mordak, 2002; Schoenrad 1998).

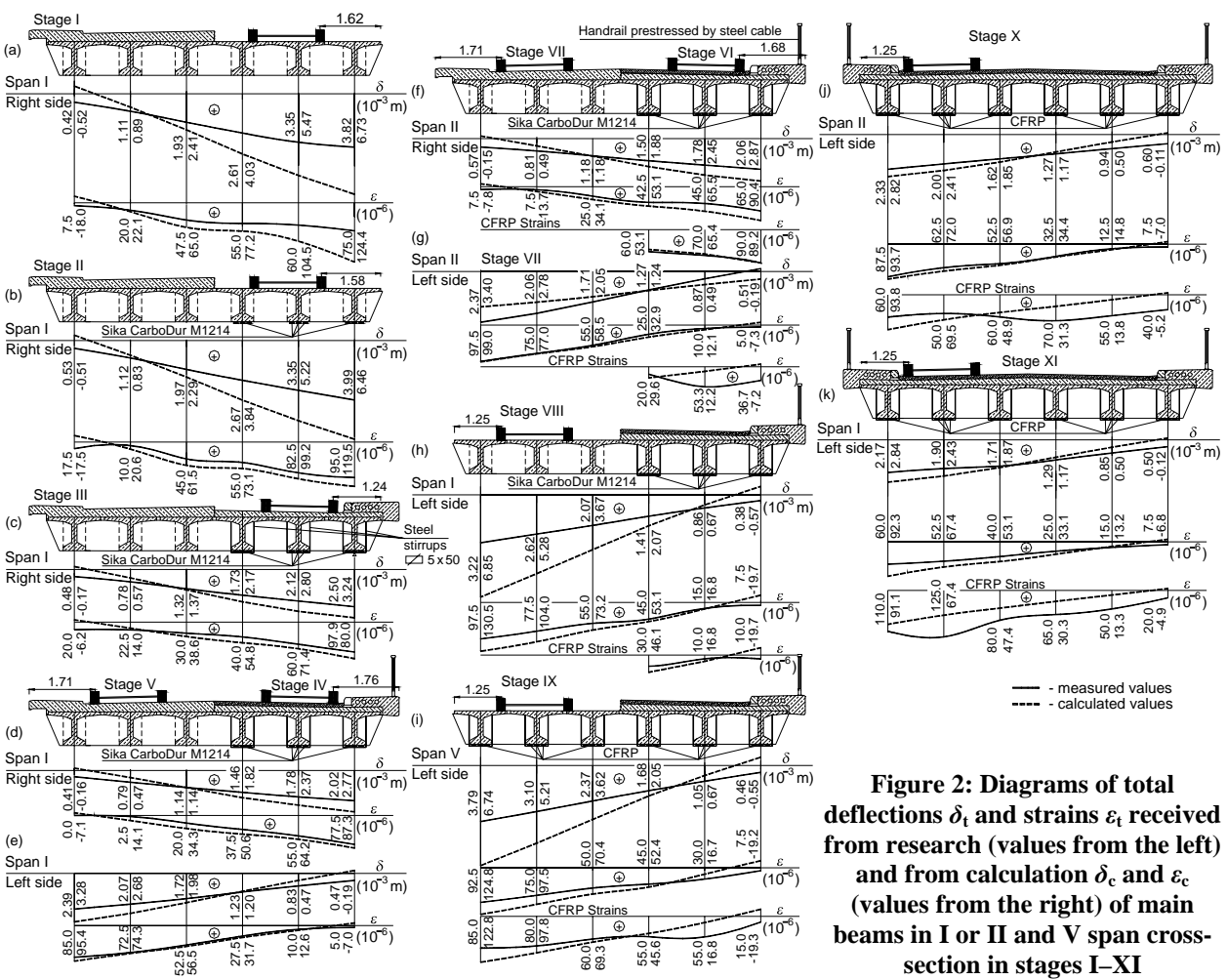


Figure 2: Diagrams of total deflections δ_t and strains ϵ_t received from research (values from the left) and from calculation δ_c and ϵ_c (values from the right) of main beams in I or II and V span cross-section in stages I–XI

The research was conducted at 11 different stages during the bridge repair. Figure 1 shows the load scheme on the tested spans at different stages with the measurements points localization. The following sizes were made:

- six main beams deflections,
- vertical and horizontal displacements of the chosen expansion and fixed bearings, made by dial indicators with 1×10^{-5} m accuracy,
- strains (indirectly – normal stresses) in the main beams, which were performed by strain gages (extensometers) and mechanical indicators,
- strains in the strengthening tapes in half and 1/4 of the effective span of the main beams, and
- strains in the outside stirrups in bearing zones and in midspan, which were performed by strain gages.

The measured permanent deflections of the particular main beams differ inconsiderably among each other, and are not proportional to elastic deflections and do not exceed permissible values ($\delta_{perm} = l_t / 800 = 18.00 / 800 = 22.50 \times 10^{-3}$ m). The relations of the main beams permanent deflections to their total deflections were established on the basis of diagrams shown in Figure 1 and in Table 1.

The maximum total main beams deflections; measured during the research under static load at different stages of bridge repairs, oscillate between 2.02×10^{-3} m and 3.99×10^{-3} m.

The average deflection values of spans cross-sections were smaller than calculated ones in all cases. For the possible load schemes to execute during the repair works, average measured correspond to calculated elastic deflection relations for particular stages were as follow: I – 0.696, II – 0.752, III – 0.895, IV – 0.904, V – 0.925, VI – 0.906, VII – 0.900, VIII – 0.588, IX – 0.702, X – 0.991, XI – 0.969. The measured main beams deflection distributions in span cross-sections were different than calculated ones. It is proved that a real torsional stiffness of the bridge was higher than assumed in static calculations.

The differences between the initial and the final readings found in measurements were approximately the same in all spans and examined main beams cross-sections. It may prove that they were rather a result of new bearings settlement or under bearing joints and possible insignificant reading errors of the measurement instruments, and only to a minimal rate of permanent strains of the prestressed main beams. Prestressed concrete spans structure should not indicate bigger permanent strains, however old bearings became replace by new ones, previously not loaded with such significant loads. This might have resulted in the occurrence of some insignificant settlements and differences in readings under proportionally heavy static load.

Table 1: Values of total (upper row) and permanent (bottom row) deflections and strains of the main beams

Stage of research	Date of measurement	Deflections δ_t and δ_p in (10^{-3} m)						Strains ε_t and ε_p in (10^{-6})					
		Main beam number											
		B1	B2	B3	B4	B5	B6	B1	B2	B3	B4	B5	B6
I	30.08.2001 (span I)	3.82	3.35	2.61	1.90	1.11	0.56	37.50	57.5	47.5	52.5	35.0	25.0
		-0.05	-0.05	-0.07	-0.19	-0.17	-0.32	0.0	0.0	-20.0	5.0	-7.5	0.0
II	10.09.2001 (span I)	3.99	3.35	2.67	1.97	1.12	0.53	132.5	82.5	95.0	85.0	100.0	80.0
		0.14	0.16	0.15	0.11	0.02	-0.06	80.0	25.0	45.0	25.0	82.5	47.5
II	20.10.2001 (span I)	2.50	2.12	1.73	1.33	0.78	0.48	150.0	135.0	95.0	85.0	47.5	0.0
		0.13	0.11	0.06	0.02	-0.05	-0.01	97.5	25.0	40.0	0.0	2.5	0.0
IV	10.11.2001 (span I)	2.02	1.78	1.46	1.14	0.79	0.41	57.5	30.0	80.0	107.5	57.5	20.0
		-0.03	-0.05	-0.08	-0.04	-0.07	-0.15	20.0	27.5	37.5	-5.0	22.5	7.5
V	10.11.2001 (span I)	0.47	0.83	1.23	1.72	2.07	2.39	5.0	7.5	32.5	135.0	117.5	87.5
		0.04	0.02	0.01	-0.01	-0.05	-0.03	0.0	-2.5	22.5	-5.0	-7.5	2.5
VI	17.11.2001 (span II)	2.06	1.78	1.50	1.18	0.81	0.57	120.0	45.0	72.5	17.5	0.0	32.5
		0.09	0.02	0.03	0.02	-0.16	-0.16	55.0	2.5	45.0	2.5	-7.5	25.0
VII	17.11.2001 (span II)	0.51	0.87	1.27	1.71	2.07	2.37	20.0	15.0	25.0	75.0	30.0	97.5
		0.08	0.04	0.00	0.00	-0.05	-0.01	2.5	-2.5	0.0	2.5	-5.0	2.5
VIII	16.02.2002 (span I)	0.38	0.86	1.41	2.07	2.62	3.22	17.5	55.0	45.0	55.0	107.5	72.5
		-0.08	-0.21	-0.19	-0.28	-0.38	-0.53	-5.0	37.5	-2.5	10.0	30.0	15.0
IX	08.03.2002 (span V)	0.46	1.05	1.68	2.37	3.10	3.79	7.5	40.0	45.0	50.0	75.0	92.5
		-0.02	-0.09	-0.12	-0.16	-0.14	-0.14	7.50	-2.5	5.0	0.0	25.0	15.0
X	18.05.2002 (span II)	0.60	0.94	1.27	1.62	2.00	2.33	27.5	52.5	77.5	103.5	182.5	87.5
		-0.02	-0.03	-0.01	-0.02	-0.01	0.00	12.5	37.5	22.5	69.0	182.5	52.5
XI	25.05.2002 (span I)	0.50	0.85	1.29	1.71	1.90	2.17	-32.5	75.0	25.0	60.0	82.5	60.0
		-0.08	0.02	0.06	0.13	0.00	0.06	-32.5	75.0	2.5	50.0	2.5	2.5

3. CONCLUSIONS

The practical experiments of the performed bridge spans research under static load at different stages of its repairs and also conducted observations of their structure interaction together with the comprehensive analysis of the results obtained from measurements and their comparison to calculated ones allow to formulate the following conclusions of the general character (Manko and Mordak, 2002; Meier and Deuring, 1991; Täljsten, 2004):

1. The span structures with the post-tensioned prestressed concrete main beams strengthened by CFRP tapes and outer stirrups in the form of steel flat did not arouse any reservations as far as the sizes of section forces, displacements and strains obtained from the research and calculations are concerned. Deflection and strain values of the main beams obtained from the measurements did not raise any doubts, as far as the strength and carrying capacity in tested spans, in behavior and interaction of the bridge at 11 repair stages are concerned. As the most loaded span structure elements, which need a detailed study and analysis, one should consider the elements of the bridge deck plate where stresses due to their direct load with stresses due to their interaction with main beams and crossbeams sum up.
 2. A satisfactory agreement of main beam deflections in all of the tested spans was obtained in comparison with calculated ones in all cases for each repair stages (stiffness of elements, layers thickness, etc.). This shows correctness of assumptions taken for calculation and static-strength analysis of these spans or also the correctness of assumed analytical structure model with their real behavior at particular repair stages.
 3. In most cases of tested main beams sections and elements of superstructure (deck plate) in the analyzed spans at the different repair stages of the bridge, the deflections and strains (and normal stresses which were calculated on their basis) during field load tests have had an elastic nature. Even without consideration of bearing settlements and displacements, they have appeared mostly smaller than the calculated ones. The noticed some minimal values of permanent displacements were partially the permanent deflections of the main beams and to some extent reading errors and errors of measuring devices.
 4. The grid model of variable load-capacity structure which was assumed for the first calculation at different repair phases depending on layers and strengthening tapes seems to be sufficient tool to determine the deflections and strains in tested structures on an engineering level (what it shows also in the presented juxtaposition of the obtained results – Table 1). To complete the detailed analysis of interaction between particular pavement layers and structure components and the assumed strengthening manner it is necessary to use more complex model which should reflect better a real interaction in a such type of span structures at the considered repair stages of the bridge, especially on the contact section of concrete and CFRP tapes.
 5. Normal stresses in tapes (which were calculated on the basis of strain values) show unambiguously that their load-capacity used was only in about 5–10%. However, no strains were noticed in outer stirrups, but the small strain gages movements are contained in a range of reading accuracy or measuring device errors. A job that can be ascribed them could be connected with the protection against to the delamination of tapes (together with lag of reinforcement bars), what was often happened in the strengthening solutions (Manko and Mordak, 2002).
 6. The differences in the expected deflections and strains of main beams in the relation to those obtained from measurements after the repair of one half of the bridge span proves that there was a good interaction between a new bridge deck layer and pavement layers of the roadway. However, the application of strengthening of main beams with CFRP tapes and outer stirrups did not bring about the significant changes in deflections and strains values of main beams. The efficiency of the strengthening work was assessed as poor because of the lower level of stresses.
- In the fact, above summary and main conclusions refer to the structures of the tested span elements of preset geometric characteristics, particular element stiffness, and determined effective spans. However, it may be stated that spans strengthening constructed by lamels and steel outer stirrups is not the best solution as far as this type of structures are concerned, mostly from the economical point of view. In order to use expensive CFRP tapes to a higher extent, one should install on the beams already known prestressing devices for CFRP tapes (Täljsten, 2004).

4. REFERENCES

- Manko, Z., and Mordak, A. (2002). "Submitting Project and Report on Static and Dynamic Trial Load of Prestressed Road Bridge over Nysa Klodzka River along National Road no. 382 Stanowice – Paczkow in km 72.536 in Paczkow after its Repair." *Scientific-Research Center for the Development of Bridge Industry MOSTAR*, Wroclaw, Poland.
- Schoenrad, Z. (1998). "Technical Design of Bridge Repair over Nysa Klodzka River along National Road no. 382 Stanowice – Paczków in Paczków in km 72.536." *Technical-Engineering Office KARO*, Poznan, Poland.
- Täljsten, B. (2004). *FRD Strengthening of Existing Concrete Structures Design Guidelines*. Division of Structural Engineering, Luleå, Sweden.
- Meier, U., and Deuring, M. (1991). *The Application of Fiber Composites in Bridge Repair*. *Strasse und Verkehr*, H. 9, S. 7–11.

FEASIBILITY STUDY OF THERMOPLASTIC WRAP FOR BRIDGE PROTECTION

Nasim Uddin

(Associate Professor, Department of Civil Engineering at University of Alabama, Birmingham, Alabama, USA)

John D Purdue

(Graduate Student, Department of Civil Engineering at University of Alabama, Birmingham, Alabama, USA)

Uday Vaidya

(Associate Professor, Department of Materials Engineering at University of Alabama, Birmingham, Alabama, USA)

ABSTRACT

The research focused on the effects of low velocity impact loading on high strength concrete confined by a prefabricated polypropylene jacket and comparing the results with similar specimens confined by carbon fiber. In order to accomplish this, both static and dynamic load tests were performed. Concrete cylinders were used for static loading. Twelve concrete cylinders were prepared for static load testing; three were plain concrete and used as control specimens, three were wrapped with one layer of unidirectional carbon fiber, and six were confined by the polypropylene pipe. The thickness of the polypropylene wrap was machined to different thicknesses; three 3 mm and three 6 mm. The cylinders were standard 152 mm x 305 mm. Cylinders were loaded to failure in uniaxial compression using a Tinius-Olsen Universal Testing Machine. Impact testing was performed using four 152 mm x 914 mm columns. The columns consisted of one control sample; one carbon fiber wrapped, and two (one of each thickness) wrapped with polypropylene. Impact testing was conducted using an Instron drop-tower testing machine.

KEYWORDS

Thermoplastic composite, polypropylene jacket, low velocity impact.

1. INTRODUCTION

Concrete bridge piers are designed to withstand large compressive axial loads, but often fail under eccentric out-of-plane loads, such as those created by an impact, earthquake or explosion. In the wake of recent terrorist attacks, such loading is of increased concern. Retrofitting the piers with continuous-fiber-reinforced thermoplastic (CFRTP) polymers could reduce vulnerability to these loads. Presently, fiber-reinforced thermoset polymers are used to add stiffness and tensile strength of concrete bridge members, but there has been no effort made to use thermoplastic composites for damage containment in structures such as bridges because of perceptions of high cost and expensive manufacturing. This study explored thermoplastic composite material produced in continuous pultruded form to produce a cost-effective split product form of directionally oriented glass fiber in polyurethane (or polypropylene) thermoplastic matrix for a representative bridge column. Two split halves will encapsulate the column with on-site mounting feasibility. The advantage of using pre-fabricated thermoplastic forms is they can be **thicker than conventional thermoset wraps** (such as presently used in bridge structures, only from a standpoint of enhancing stiffness/tensile strength). It is envisioned that under impact from unknown threats such as collisions from trucks/trailer or blasts, the structure have progressive failure potential, in place of catastrophic fracture presently witnessed. The tape and pultruded thermoplastic form has flexibility to accommodate curvatures encountered as part of the structure, and can be used either alone (only to suppress catastrophic failure) or in conjunction with conventional thermoset wraps if ductility improvement is also needed. An example of the concept is shown in Fig. 1. The split halves can be connected by a combination of thermoplastic tape wraps around the halves and a secondary mechanical reinforcement. Furthermore, the rate of strain induced on the structure is severe. The polypropylene/glass is expected to enhance failure strain of concrete structures by several orders of magnitude.

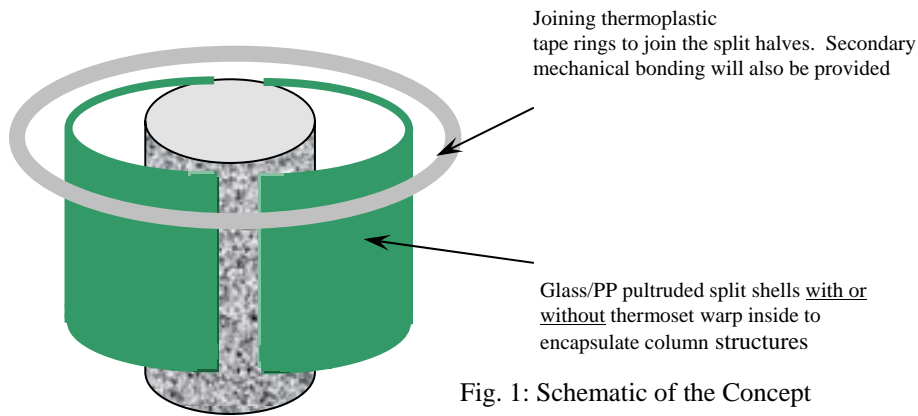


Fig. 1: Schematic of the Concept

Preliminary guidelines for field implementation of polypropylene jacket (PP) wrap systems are shown below: (1) Existing RC columns can be strengthened using prefabricated PP or glass reinforced PP (glass/PP) shells. They can be fabricated in half circles, half rectangles, circles with a slit in continuous rolls, so that they can be opened and placed around columns (Figure 1). Two half shells of PP or glass/PP plate rolled to a radius of 0.5 to 1.0 in. (12.5 to 25 mm) larger than the column radius can be positioned over the area to be retrofitted and the vertical seams may be site-welded (using ultrasonic welding) to provide a continuous tube with a small annular gap around the column. For effective confinement to be achieved, a full contact between the column and the PP or glass/PP shell is essential. This can be ensured by either bonding the shell to a thermoset wrap bonded to the pier (if ductility improvement is needed); otherwise bonding the shell to the column using adhesives, or injecting shrinkage-compensated cement grout or mortar into the space between the shell and the column; (2) Prefabricated PP or glass/PP shells can be used as a stay-in-place forms for a precast modular bridge pier system for new bridge pier construction. The work will compare the effects of dynamic loading of this type of confinement with the most common composite strengthening technique to date, carbon fiber wrapping. Two series of tests will be performed in this research: uniaxial compression testing of cylinders and impact loading of columns. The first letters are used to denote the type of specimen, “Cy” for cylinder and “Co” for columns. The second letter establishes the confinement type, “N” for plain samples, “C” for carbon FRP, and “P” for polypropylene wrapped cylinders. The next letter denotes the type of concrete “B” for high strength. The first number in the scheme is for the confinement thickness (mm) or number of plies. Finally, the last number represents the sample number. The Research Objectives:

- To investigate the effects of static loading on the polypropylene wrapped concrete cylinders and compare with carbon fiber wrapped cylinders.
- To compare the energy absorption characteristics of columns confined by PP and carbon fiber reinforced polymer (CFRP).

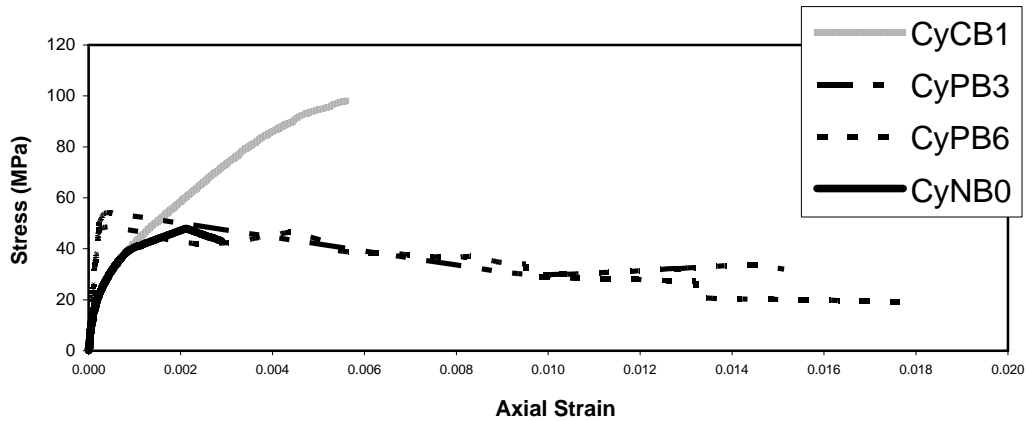
2. STATIC COMPRESSION LOADING

The purpose of the uniaxial compression tests of the concrete cylinders was to evaluate static loading phenomena such as the effect on axial strength and strain capabilities. For this study, two variables were investigated: confinement material (polypropylene and carbon fiber (for reference)) and thickness of the polypropylene confinement. The average compressive strength of the concrete was 58.6 MPa. The cylinders were grouped as follows: three control specimens; three 3 mm and three 6 mm thick polypropylene; and, finally, three 1-ply unidirectional carbon fiber. Unidirectional SikaWrap Hex 103C was used for the CFRP, with Sikadur 300 used for the bonding agent to the concrete surface. The fibers were oriented such that they provided reinforcement in the hoop direction (perpendicular to the applied compression load). After preparing the concrete surface and the carbon fiber, the material was rolled onto the cylinders. George Fischer beta (β)-PP was used for the polypropylene and came in the following dimensions: 140 mm outer diameter, 13 mm wall thickness, and 5 m in length. This material was chosen since it had many desirable characteristics, some of which are high impact strength, abrasion resistance, low weight, and a sizable operating temperature range making it ideal for load bearing applications. Since the polypropylene reinforcement is meant to act as passive reinforcement, the material was machined down from its original 13 mm wall thickness to the two thicknesses previously mentioned. Table 1 below gives the material properties for the two types of confinement. Comparison of the compression test data is presented in Fig. 1, and a summary is presented as follows: (1) *Effect of Confinement Thickness*. No appreciable differences in load-bearing and/or uniaxial concrete compressive strength were observed for the 3 mm or 6 mm polypropylene jackets. This may be due to the high strain capacity within the PP, which masks the influence of the wall thickness (within the 3

Table 1. Mechanical Data for Reinforcing Materials

	Tensile strength (MPa)	Tensile modulus (GPa)	Elongation (%)	Nominal thickness (mm)
SikaWrap Hex 103C	958	73	1.33	1
β -PP	30	2.0	120	3 & 6

Note: β -PP = beta-nucleated polypropylene.

**Fig. 1.** Comparison of stress versus strain for cylinders (averaged values)

mm – 6 mm wall thickness range considered here); (2) *Progressive failure potential*. Both PP thicknesses illustrated a significant improvement in deformability when compared to the unconfined concrete. This enhancement is comparable and much higher to the improvements of the CFRP wrapped cylinders; (3) *Compressive Strength*. As expected, neither series of polypropylene jacketing could produce a significant increase in compressive strength. This was due to the ability of this material to bulge and dilate. As mentioned before, axial strengthening applications are not the intended application of this material, however resistance to transverse loads is expected which is directly related to sustaining higher compressive strains; (4) *Stress-Strain Response*. The stress-strain response of the PP confined concrete is multi-linear in nature, and the mode of failure of PP wrapped specimens reflects a progressive mode of specimen failure relative to a specimen, for example, CFRP jacket which had failed by sudden rupture of all the fibers in a region of the jacket. The bulging of pp jacket, on the other hand, was concentrated along the upper gage length, though some also occurred within the bottom regions to a much less extent. No separation or debonding from concrete surface occurred along the PP. In term of normalized strain data given by the ratio $\varepsilon_{tu}/\varepsilon_{t0}$ (strain at failure of the confined cylinder by strain of the unconfined cylinder), the 3 mm PP jacket produced an average ratio of 8.4, and the 6 mm PP jacket yielded an average ratio of 9.6, which is impressive when compared with the 15.6 average ratio of the glass/PP confinement reported in earlier research (www.UTCA.org). The modes of failure observed during these tests varied depending on the confinement. The PP confined samples exhibited a barreling effect. The ability to dilate considerably allowed the confined concrete to crush and compact inside the PP jacket. While this dilation was drastic, yielding of the polypropylene is evident in only a few places on the samples, and only one sample showed signs of material failure. Failure of the CFRP wrapped cylinders occurred due to fiber rupture near midheight.

3. LOW VELOCITY IMPACT LOADING

Low velocity impact testing was conducted using a total of four concrete columns: one control specimen, one CFRP confined, and two confined by a PP wrap of 3 mm and 6 mm thicknesses. All columns tested were 152 mm x 914 mm. In an effort to illustrate a similar loading situation as would be seen in reality, the columns were placed horizontally inside a testing jig and subjected to axial compression. The system used for impact testing was an Instron Model 8250 drop-weight impact machine with an instrumented striker (tup) assembly. A flat striker was used for this test and had an impact area of 76 mm x 102 mm. For this study, the impact weight was 246 N. The hammer (tup) contained an internal load cell, which was used to record the contact load between the falling assembly and the column during the impact event. The load cell was rated for a maximum load of just over 44 kN.

A drop height of 30 cm was used for all tests, since the combination of this height and the weight of the striker assembly produced loading close to that of the maximum allowed by the load cell. Deflection, velocity, and energy absorption were recorded using the DynaTup software that accompanied the Instron drop-tower. All samples were impacted from a height of 30 cm in an effort to keep the load cell free from damage. Due to the limitations of the drop-tower machine, the impact loading can be classified as low velocity impact or velocity less than 10 m/s (Bartus 2003). Average impact velocity for these tests was 2.4 m/s. A summary of test data is given in Table 2, and fig. 2.

Table 2. Summary of Impact Test Results

Specimen ID	Peak load (kN)	Maximum deflection at midspan (mm)	Maximum strain	Change in strain (%)
CoNB0	38	3.38	0.0024	---
CoCB1	45	2.72	0.0047	143
CoPB3	36	4.52	0.0057	147
CoPB6	34	5.00	0.0058	148

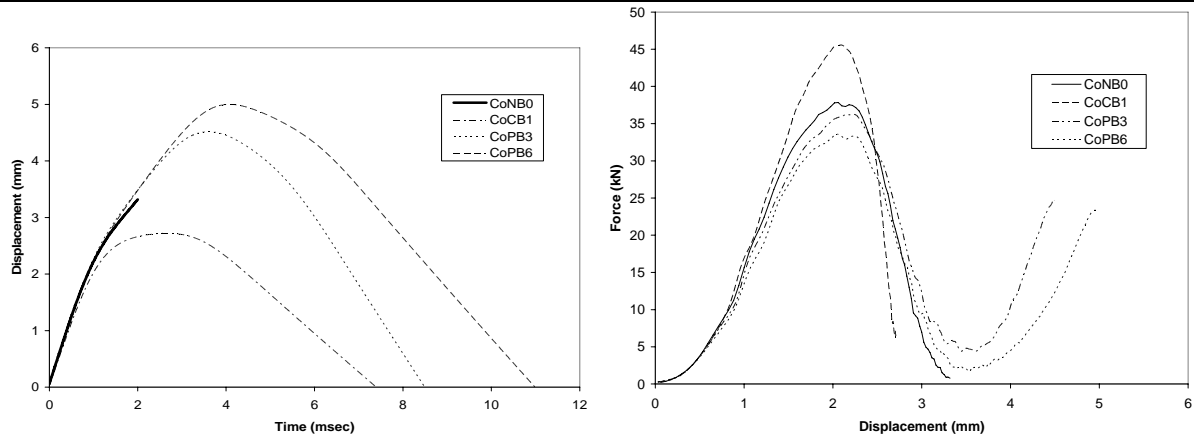


Figure 2. Comparison of load versus displacement; and displacement versus time for tested columns

The impact tests were conducted to assess the energy absorption capacity of three concrete columns strengthened by PP confinement, a carbon/epoxy confined and one unconfined control specimen. From the test results, the following conclusions were made: (1) Peak loading of the columns varied based on the stiffness of the confinement. Since the PP confined columns were the least stiff, they also exhibited the desirable least peak loading from the impact resistant design perspectives; (2) Deflection of the PP confined columns was greater than the unconfined and CFRP wrap columns. This is very favorable given that the time this displacement occurred was nearly six times greater than that of the plain specimen; (3) Transverse flexural strain values recorded across the middle gage length showed that PP wrap strain demonstrates an increase in capability of approximately 145% over the unconfined concrete; (4) Energy absorption of the polypropylene was significantly higher to that of the carbon fiber confinement. Energy absorption for 3 mm PP wrap was higher than that of 6 mm wrap which can be attributed to the lower stiffness of the former. Polypropylene wrap produced higher deflection than the CFRP wrap column and unconfined column. This effect was due to the ability of the material to compress and further absorb the energy from impact; and (5) though failure was not possible for the PP wrapped specimens, the above results demonstrated that the usage of a thermoplastic prefabricated wrap has the potential to suppress the catastrophic failure due to the threat of impact.

4. CONCLUDING REMARKS AND ACKNOWLEDGEMENT

This study explored and demonstrated the potential of thermoplastic composite material (e.g., Polypropylene) produced in continuous pultruded form to suppress catastrophic failure for a representative bridge column. However much more studies are required before any definitive conclusions can be made regarding this issue. We gratefully acknowledge the financial support of UTCA under the director Dr. Danial S. Turner.

5. REFERENCES

Vaidya U., Husman G. and Gleich K. (2004). "Design and manufacture of woven reinforced glass/polypropylene composites for mass transit floor system". *Journal of Composite Materials*, Vol. 38, No. 21, pp 1949-1972.

FIELD TESTS OF PRESTRESSED CONCRETE BEAMS OF ROAD BRIDGE SPANS STRENGTHENED BY CFRP TAPES

Zbigniew Manko

(Professor of Civil & Structural Engineering, Wrocław University of Technology, Wrocław, Poland)

Arkadiusz Mordak

(M.Sc., Ph.D. Student, Cracow Technical University, Cracow, Poland)

ABSTRACT

The paper is presented the method, scope, results and their analysis of the research, and the main conclusions drawn from static field load tests performed on a five-span prestressed concrete road bridge after its repair. The bridge with the effective spans of 18.00 m is located over the Nysa Klodzka river in Paczkow (Poland). All bridge span beams became reinforced by CFRP tapes glued on bottom flanges of main beams as well as overlaid a new concrete deck layer. The main aim of the conducted bridge repair was to increase its load capacity to 300 kN (class C) according to the Polish Loads Standard (PN-85/S-10030). The results obtained during the research of the bridge after its repair at field load tests were conducive to determining the behavior of the analyzed span structure under static loads, which allowed for an assessment of the efficiency of the strengthening, as well as establishment of guidelines for future reference concerning this type of maintenance in the engineering practice.

KEYWORDS

Road bridge, Prestressed concrete beam, Field load test, CFRP strips, Static loads

1. INTRODUCTION

The paper is described the research method and the results of measurements and calculations of the static load test, as well as the analysis of the obtained results of a five-span road bridge with the prestressed concrete main beams of the *Plonsk* type reinforced by CFRP tapes and with a new concrete deck slab (Figures 1 and 2). The bridge over the Nysa Klodzka River is situated in Paczkow (Upper Silesia Province – Poland).

Before the repair, the bridge load capacity determined in expertise was classified as class E, that is 150 kN according to the Polish Loads Standard (PN-85/S-10030), mainly due to a very poor technical condition of the load-carrying structure of all bridge spans, resulting mostly from transverse cracks in the main beams. The main aim of the repair was to increase the object load capacity to class C (300 kN).

The aim of the tests was to determine the behavior of the road bridge spans and supports structure under known load in order to prove the validity of the design assumptions made in the calculations and analyses of the spans and in the load test program. It was to evaluate and determine the real rigidity and the load capacity of the bridge spans after their repair, particularly the flexural rigidity of the strengthening main beams directly integrated with the deck slab and the road surface.

The tests were directed to recognize the response behavior of the span structures of the old bridge under the determined load in order to verify the assumptions made in the design (Schoenradt 1998) as well as to determine the actual load capacity of the object (Manko and Mordak, 2002). It applied mainly to the assessment of the actual stiffness of the prestressed beams, the deck plate and supports (Figure 2). The load tests were specifically intended to investigate whether and to what extent span and deck elements interact, namely if there is any extra reserve of load capacity in the bridge spans. It is manifested in smaller deflection and normal stress values in the main beams and tapes, obtained from measurements carried out in the considered sections, in relation to calculated values obtained on the same service load (PN-77/S-10040, PN-85/S-10030, PN-91/S-10042, PN-S-10040, 1999). Thus, the assumptions concerning the statical scheme and the calculated model of the structure also were verified.

The main conclusions ascertain whether the bridge can be admitted to normal service and with what, if any, post-construction recommendations. The conclusions from this research can be useful for the engineering practice, particularly in the area of the test load of strengthening bridges by FRP, because a number of identical spans were tested.



Figure 1: General side view from the direction of the headwater of the road bridge: (a) localization of four trucks on tested span II (load scheme IIS) and (b) bottom view on the beams strengthening by CFRP tapes

2. BRIEF DESCRIPTION OF BRIDGE STRUCTURE

The tests were carried out on the five-span road bridge. Each span consists of six main beams integrated with the new reinforced concrete deck slab of B30 concrete class. The total width of the individual spans is constant along the bridge length and it is 9.94 m (Figure 2). The total length of the bridge is 98.60 m. The effective length of each of the spans is 18.00 m. The particular spans are simple-supported and made from *Plonsk* type prefabricated prestressed concrete beams of length, L , of 18.50 m and are integrated with the RC deck slab over interior supports. The bridge was designed to serve under the I class load (300 kN) in accordance with the PN-66/B-02015 (or C according to the PN-85/S-10030). The span interior crossbeams are made as prestressed concrete. The tests covered spans I and II (Figure 1). The bridge supports are in the form of massive concrete piers and abutments on spread foundation, fixed in a reinforced concrete footing. The foundation rests directly on the virgin soil. The span main beams rest always on single-roller and fixed steel bearings (Figure 1). The roadway was covered with bituminous pavement, 0.09 m thick, with incorporated insulation of an average thickness 0.01 m (Figure 2). The usable width of the bridge amounts to 9.50 m, which includes the 7.00 m wide roadway and a 1.25 m sidewalk on each side.

The strengthening of the particular bridge spans was accomplished by gluing the CFRP tapes made of carbon fibers (three for each beam) to the bottom flanges of the main beams. Additional by constructing a new reinforced concrete deck plate of variable thickness 0.12–0.185 m as well as adding the outer stirrups in the form of steel flats of 5×50 mm section, with axial base by every 0.35 m (Manko and Mordak, 2002; Schoenrad 1998).

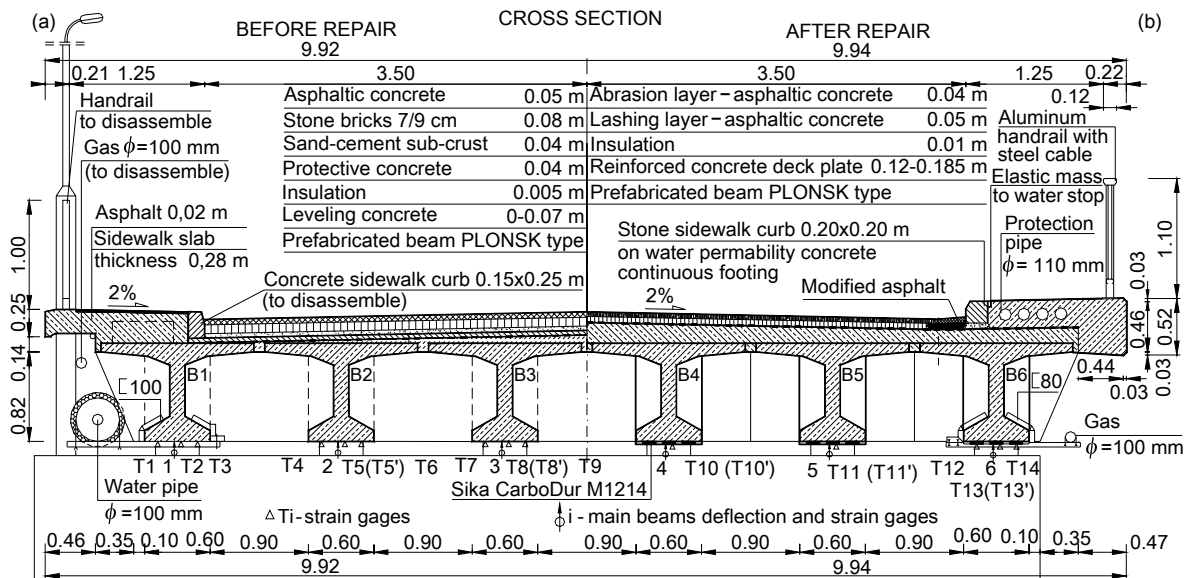


Figure 2: Cross-section of spans and localization of measurement points: (a) before and (b) after, its repair

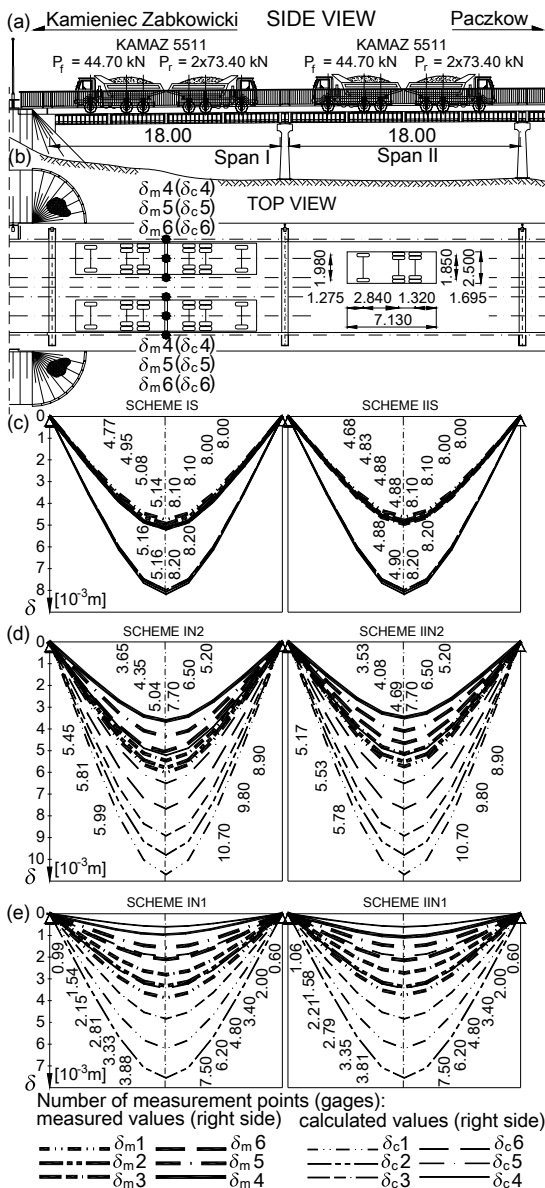


Figure 3: Prestressed concrete road bridge and load cases distribution on bridge during field test: (a) side view from headwater, (b) top view – technical parameters of truck type KAMAZ 5511, and displacements of all tested main beams of the bridge on span length obtained from measurement and calculation for load schemes: (c) IS & IIS, (d) IN2 & IIN2 and (e) IN1 & IIN1

The measured permanent deflections of the particular main beams differ inconsiderably among each other and are not proportional to elastic deflections as well as they do not exceed permissible values (less than 20% of elastic deflections or strains). The relations of the main beams permanent deflections to their total deflections and strains were established based on diagrams shown in report by Manko and Mordak (2002). The differences between the initial and the final readings found in measurements were approximately the same in all spans and examined main beams cross-sections. It may prove that they were rather a result of new bearings settlements or under bearing joints and possible insignificant reading errors of the measurement instruments, and only to a minimal rate of the permanent strains of the prestressed main beams. This might have resulted in the occurrence of some insignificant settlements and differences in readings under proportionally heavy static load.

3. RESEARCH SCOPE AND APPROACH

The static field load tests of the bridge included following measurements (Figure 2):

- six main beams deflections (load-carrying structure) at their midspan by dial indicators with 1×10^{-5} m accuracy;
- vertical and horizontal displacements of the chosen expansion and fixed bearings by dial indicators with 1×10^{-5} m accuracy;
- strains (stresses) in the main beams, which were performed by strain gages (extensometers) and mechanical indicators;
- strains in the strengthening tapes in half and 1/4 of the effective span of the main beams;
- strains in the outside stirrups in bearing zones and in midspan, which were performed by strain gages;
- vertical displacements in selected intermediate supports and abutments, and
- confirmation dimensions of each element of the span structure taken during a general bridge inspection (the technical condition of the span and support structures was inspected prior to, during and after the finish of the testing).

The static load tests were conducted for two nonsymmetrical and one symmetrical load schemes. All the measurements specified by the test loading program were taken exclusively under a static load (Manko and Mordak, 2002). Four trucks of the KAMAZ 5511 type loaded by soil dump with the total weight of 191,50 kN, were used in the tests (Figure 3).

4. TESTS RESULTS AND ANALYSIS

The final results of bridge acceptance inspection (PN-S-10040, 1999), conducted after the complete repair under the trial static and dynamic load, allowed for a comprehensive evaluation of the efficiency of the main beams strengthening by applying CFRP tapes (Figure 3). The maximal total main beams deflections measured during the research under static load, oscillate between 1.37×10^{-3} m and 5.99×10^{-3} m (Table 1). The average deflection values of span cross-sections were smaller than calculated ones in all cases and did not exceed permissible values ($\delta_{perm} = L / 800 = 18.00 / 800 = 22.50 \times 10^{-3}$ m). For the possible three load schemes to execute after the repair works average measured correspond to calculated elastic deflection relations were as follow: IS – 0.629, IIS – 0.598, IN2 – 0.560, IIN2 – 0.540, IN1 – 0.517, IIN1 – 0.508. The measured main beam deflection distributions in span cross-sections were different than calculated ones. It is proved that a real torsional stiffness of the bridge was higher than assumed in the static calculations.

Table 1: Results of total δ_m and ε_m (upper row) and calculated δ_c and ε_c (bottom row) deflections and strains of main beams of studied spans at the midspan for all load schemes by measurement and calculation

Span number	Load scheme number		Deflections δ_m and δ_c in (10^{-3} m)						Strains ε_m and ε_c in (10^{-6})					
			Main beam number											
			B1	B2	B3	B4	B5	B6	B1	B2	B3	B4	B5	B6
I	IS	measured	4,77	4,95	5,08	5,16	5,14	5,16	315	350	310	340	190	185
		calculated	5,04	5,47	5,74	5,77	5,55	5,18	347	334	324	326	337	351
	IN1	measured	3,81	3,55	2,79	2,21	1,58	1,06	180	130	160	175	10	100
		calculated	5,33	4,54	3,52	2,26	1,00	0,17	211	163	138	115	91	77
	IN2	measured	5,99	5,81	5,45	5,04	4,35	3,65	455	410	325	300	160	120
		calculated	6,93	7,26	7,06	5,93	4,14	2,08	401	377	355	333	308	266
II	IIS	measured	4,68	4,83	4,90	4,88	4,88	4,88	230	200	345	370	115	335
		calculated	5,04	5,47	5,74	5,77	5,55	5,18	347	334	324	326	337	351
	IIN1	measured	3,65	3,19	2,63	2,06	1,37	0,88	180	120	160	150	20	75
		calculated	5,33	4,54	3,52	2,26	1,00	0,17	211	163	138	115	91	77
	IIN2	measured	5,78	5,53	5,17	4,69	4,08	3,53	315	270	355	355	100	290
		calculated	6,93	7,26	7,06	5,93	4,14	2,08	401	377	355	333	308	266

5. CONCLUSIONS

The practical experience gained from the testing of the road bridge and the observations concerning the behavior of the structure of post-tensioned prestressed concrete beams of the *Plonsk* type made during the tests, as well as the analysis of the results obtained from the measurement and their comparison with the calculated values leads to specific conclusions as to the real behavior of the structure of the individual spans of the bridge and allows one to form the following general conclusions (Manko and Mordak, 2002):

1. In the light of the tests that were carried out, the structures of the bridge span and supports did not raise any doubts. The deflections of the main beams are principally elastic. The minimal permanent displacements that were discovered are in part residual deflections of the main beams and partly caused by the bearings settlement of piers.
2. The measured deflections and average strains values were considerably lower than the expected (calculated) ones and the permissible ones for all the tested spans. This indicates higher rigidities of the span structures – probably due to better interacting and integration with the RC deck slab and the road surface. This applies to all the main beams in the tested span. In all, five almost identical spans made up of *Plonsk* type beams have been analyzed and therefore, the conclusions as to the behavior of such typical structures can have major practical importance.
3. On the basis of the static tests that were carried out permission could be given for the bridge to be subjected to dynamic tests during the entrance and the exit of a dynamic load and then the bridge could be admitted to normal service. A close inspection of the span and supports of the bridge as well as the supplementary and verifying measurement did not reveal any damage to the structural components or their joints in the considered spans.
4. Normal stresses in tapes (which were calculated on the basis of strain values) show unambiguously that their load-capacity was used only in about 5–10%. However, no strains were noticed in outer stirrups, but the small strain gages movements are contained in a range of reading accuracy or measuring device errors. A job that can be ascribed them, could be connected with the protection against to the delamination of tapes (together with a lag of reinforcement bars), what was often happened in the strengthening solutions (Manko and Mordak, 2002).

In the fact, above summary and conclusions refer to the structures of the tested span elements of preset geometric characteristics, particular element stiffness, and determined effective spans. However, it may be stated that spans strengthening constructed by lamels and steel outer stirrups is not the best solution as far as this type of structures are concerned, mostly from the economical point of view. In order to use expensive CFRP tapes to a higher extent, one should install on the beams already known prestressing devices for CFRP tapes.

4. REFERENCES

- Manko, Z., and Mordak, A. (2002). "Submitting Project and Report on Static and Dynamic Trial Load of Prestressed Road Bridge over Nysa Klodzka River along National Road No. 382 Stanowice – Paczkow in km 72.536 in Paczkow after its Repair." *Scientific-Research Center for the Development of Bridge Industry MOSTAR*, Wroclaw, Poland.
- Schoenrad, Z. (1998). "Technical Design of Bridge Repair over Nysa Klodzka river along National Road No. 382 Stanowice – Paczkow in Paczkow in km 72.536." *Technical-Engineering Office KARO*, Poznan, Poland.

Blast mitigation of a concrete arch bridge using composites

Achille Devitofranceschi¹, Domenico Asprone², Andrea Prota², Renato Parretti² and Antonio Nanni^{2,3}

¹ ANAS S.p.A., Direzione Centrale Progettazione, Rome, Italy

² Department of Structural Analysis and Design, University of Naples "Federico II", Naples, Italy

³ Department of Civil, Architectural and Environmental Engineering, University of Miami, Coral Gables, FL, USA

ABSTRACT

Blast mitigation has recently become a critical need for public infrastructure because the probability of explosions is no longer linked to accidental reasons only. In the spring of 2005, an international project regarding blast mitigation started under the coordination of the University of Missouri – Rolla and the participation of the University of Naples "Federico II" and two Italian firms, ANAS, owner of the Italian highway network, and AMRA, a research center of excellence. The objective of the project was to investigate a real structure under blast loading conditions; the team had the opportunity to study and test to collapse a recently dismissed long-span reinforced concrete arch bridge in southern Italy.

The first phase of the project has been focused on a detailed structural analysis of the bridge performed via a finite element modeling of the structure anticipated by static/dynamic materials characterization. The conducted numerical modal analysis was validated by in-situ vibrodyne tests. This allowed the calibration of the model later used for blast loading analysis.

At this time, two mitigation techniques using composites have been proposed to protect the piers of the bridge. These solutions will be modeled and tested on the structure under blast loads.

KEYWORDS

Blast mitigation, bridge, composites, FRP, pier, reinforced concrete, SRP.

1 INTRODUCTION

The Tenza Viaduct (Figure 1), located in southern Italy, was built in the sixties as part of the Salerno-Reggio Calabria Highway and was open to traffic until two years ago. The highway owner ANAS had planned to change the geometry of the route, since it no longer respects current safety requirements. Accordingly, the bridge was closed to traffic as it belonged to a substituted portion of the highway.

The Tenza Viaduct consists of three different structures, one main span and two approaching spans. The main span is an open spandrel arch structure that is 120 m long and 50 m deep. The bridge deck and its wall piers are supported by a ribbed, solid slab, and fixed-fixed arch. Each 30 m long approaching span is supported by multiple wall piers of different heights. Each individual pier is made of two reinforced concrete (RC) columns connected over their entire height by a RC wall.

The Viaduct was built during the economic growth after the Second World War and although no record exists on the method used for its construction, wood formworks were probably used, as that was a very common practice at that time. In the eighties, the bridge was rehabilitated to meet seismic code requirements. The retrofitting consisted of RC encasement of both piers and arch cross-sections (Nanni et al. 2006).

2 TRADITIONAL BRIDGE ASSESSMENT AND CHARACTERIZATION

The objective of the first phase of the project was to obtain a detailed knowledge of the structure and its behavior. A traditional investigation was performed using: a) static and dynamic characterization of materials; b) a modal

analysis; and c) field validation through vibrodyne testing. Static analysis under gravity and seismic loads was conducted on a FEM model of the structure.



Figure 1: The Tenza Viaduct

2.1 Material characterization

The objective of this campaign was to obtain complete quasi static and dynamic characterization of the materials of the Tenza Viaduct.

First of all, four types of materials were identified:

- The original concrete, used in the sixties when the bridge was built;
- The concrete used for piers and arches rehabilitation;
- The original steel, lightly ribbed, used as reinforcement of the original concrete;
- The modern ribbed steel bars used as reinforcement of the rehabilitated concrete.

For each of these materials several specimens were taken from the structure. Tensile tests of steel specimens as well as compression and ultrasonic tests of concrete specimens were conducted. The collection of the specimens intended to be representative of the whole structure: arch, deck, piers and girders.

The original concrete had an average cylindrical strength of 34 MPa for the arch and 46 MPa for the deck; the rehabilitated concrete had an average cylindrical strength of 31 MPa. Ultrasonic tests were performed before conducting the concrete compressive tests and results were related to the cylindrical strength.

For the steel specimens standard tensile tests were performed and stress-strain curves collected recording yielding strengths of 400 and 490 MPa and ultimate strengths of 593 MPa for original and rehabilitated specimens, respectively.

Moreover, in order to obtain a mechanical characterization of concrete and steel under high dynamic loading rates, tests were performed in the DynaMat Laboratory of the University of Applied of Southern Switzerland using three modified Hopkinson Bars (Cadoni et al., 2000). Stress – strain relationships under different strain rate were evaluated under tensile loads. The strain rate ranged between 10^{-4} and 10^{+1} s^{-1} for the concrete and between 10^{-4} and 10^{+2} s^{-1} for the reinforcing steel. The results show that:

- At high strain-rate, the new concrete seems to have a better behavior than the original one. An increment of tensile strength varying from 100% to 400% was found. This implies also an increase of pseudo-ductility and energy absorption capability with increasing strain-rate.
- The reinforcing steel is also strain-rate sensitive both in terms of stress and strain. As an example, the yielding stress grows more than 60% from the quasi-static regime to the impact one ($>500 \text{ s}^{-1}$), while the failure strength increases its value less than 20%. Ultimate strain and failure strain have an increment of 50%.

The results provide information about the influence of dynamic loads on the constitutive behavior of materials aged in an existing structure and they will be used in structural analyses accounting for strain rate effects.

2.2 FEM model

Considering that the bridge is substantially made of three different structures (central arch and approaching spans), three different numerical models were elaborated. The geometry of the models was obtained from the original drawings of the structure and verified with a 3D laser scanner survey (Figure 2). The values of the elastic properties of the structure were based on the results of the material characterization tests.

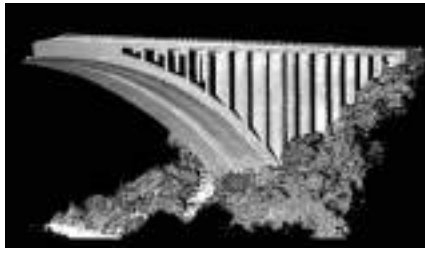


Figure 2: Bridge resulting from the application of the laser scanner

The three models were built using SAP2000 and Straus7 software (Figure 3) (Computers and Structures, Inc., 2004; G+D Computing, 1999). For each of them static and modal analyses were performed. The results show that the first two vibration periods of the central structure are longitudinal (1.08 Hz) and transversal (1.45 Hz), while the first vibration periods of the approaching spans correspond to local modes.



Figure 3: FEM models for arch bridge and approaching spans

The numerical analytical results were verified through a field vibration test conducted using both wind action and a mechanical vibrodyne giving harmonic excitations. Accelerometers distributed on the structure recorded the data obtained during the test. Frequency and LMS (Least Mean Square) analyses of the results confirmed a transversal mode of vibration with a frequency of 1.35 Hz, within 10 per cent difference of the predicted value.

3 MITIGATION TECHNIQUES

The mitigation of blast action on the bridge has been focused on the piers since they appear, in the hierarchy of the structure, the most critical elements. The typical pier has a “I” cross section (Figure 4) with a 300 mm web thickness, a 500 mm flanges thickness, and a 600 to 1,000 mm variable width; the overall height is 3 m. The planned mitigation technique of the bridge can not avoid modifying the shape of the cross section to obtain more compactness to resist blast loading. In fact, the “I” cross section appears vulnerable to shock actions due to local weakness. The planned mitigation technique will provide the filling of the section with light-weight shrinkage-free concrete to obtain a rectangular shape. The filler will also have a sacrificial protection for the web.

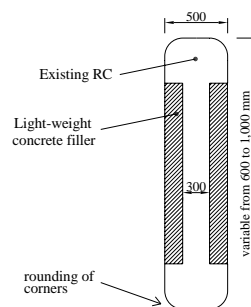


Figure 4: Pier cross section

After rectangular cross section has been realized and the corners are rounded, FRP reinforcement is applied to the contour as externally bonded system due to the promising results displayed by such strengthening technique for blast mitigation (Lawver et al., 2003; Lu et al., 2005).

A first technique calls for the use of Carbon Fiber Reinforced Polymer (CFRP) fabrics, which has shown good results in the literature (Muszynski and Purcell, 2003; Hegemier et al., 2006). This solution also provides an increase to the seismic performance of the structure.

A second technique consists in the application of a multilayered material system made by foam (metallic or polymeric) sandwiched by a Steel Reinforced Polymer (SRP) system (Hardwire LLC, 2002) (Figure 5). In this case, the jacket has also an energy dissipation function that has shown interesting potential in preliminary numerical simulations. The possibility of using this technique for noise mitigation of bridge decks is of interest and currently under consideration.

More detailed information on the mitigation strategy will be orally provided at the conference.

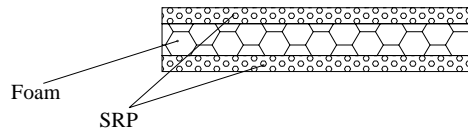


Figure 5: Multilayer technique

4 CONCLUSIONS

The paper presented the work conducted to study the possibility of blast mitigation with composites of a highway bridge. Blast loading is becoming of relevant importance in design procedures of highway infrastructures and composites show interesting characteristics in this field. A traditional analysis of the structure was performed and two different solutions were proposed. Numerical modeling will be used for prediction and blast testing will be conducted to obtain validation and further ideas for blast mitigation design of existing structures.

5 ACKNOWLEDGMENTS

The authors are grateful to Technical Support Working Group (TSWG) for funding support to this project under Contract Number N4175-05-R-4828.

6 REFERENCES

- Cadoni E. et al. (2000) High strain-rate tensile concrete behaviour, *Magazine of Concrete Research*, **52**, No.5, Oct., 365-370.
- Computers and Structures, Inc. "CSI Analysis Reference Manual For SAP2000®, ETABS®, and SAFE™" Berkeley, California, USA September 2004
- G+D Computing, "THEORETICAL MANUAL – Straus7", Sydney, Australia, 1999
- Hegemier, G.A., Seible, F., Rodriguez-Nikl, T., Arnett, K. (2006), "Blast Mitigation of Critical Infrastructure Components and Systems" *Fédération Internationale du Béton, Proceedings of the 2nd International Congress*, June 5-8, 2006 – Naples, Italy
- Lawver, D., Daddazio, R., Oh, G.J., Lee, C.K.B., Pifko, A.B., Stanley, M. (2003), "Composite Retrofits of Reinforced Concrete Slabs to Resist Blast Loading," 74th Shock and Vibration Symposium, San Diego, CA.
- Lu, B., Silva, P., Nanni, A., Baird, J. (2005), "Retrofit for Blast-Resistant RC Slabs with Composite Materials," 7th International Symposium on Fiber-Reinforced Polymer Reinforcement for Concrete Structures, FRPRCS-7, Kansas City, MO, pp. 1345-1359.
- Muszynski, L.C., Purcell, M.R. (2003), "Composite Reinforcement to Strengthen Existing Concrete. Structures against Air Blast," *Journal of Composites for Construction*, ASCE, Vol. 7, No. 2, pp. 93-97.
- Nanni A, Asprone D, Ayoub A, Baird J, Filangieri A, Galati N, Kiger S, Marianos W, Prota A, Quintero R, Wang M, and Wei J. "Blast Testing and Research-Bridge at the Tenza Viaduct". Final Report Task 1 of TSWG Contract Number N4175-05-R-4828, University of Missouri-Rolla, Rolla, MO, U.S.A., 2006.
- Hardwire LLC, "What is Hardwire", www.hardwirellc.com, Pocomoke City, Maryland, 2002.

PERFORMANCE OF FRP RETROFITTED BRIDGES UNDER BLAST LOADING

Rui Zheng

(Ph. D Student, Florida International University, Miami, FL, USA)

Amir Mirmiran

(Professor and Chair, Florida International University, Miami, FL, USA)

ABSTRACT

The use of FRP system to harden the bridges under blast loading has been suggested by a number of studies. This paper considers the material characteristics of concrete, steel and FRP at low and high strain rates, and proposes an analytical technique to convert the three dimensional time-consuming blast loading analysis into a unidirectional study, maintaining high level of fidelity and accuracy. The study shows the benefits of the use of FRP for hardening bridge substructures.

KEYWORDS

FRP, Blast Loading, Dynamic Analysis, Repair and Retrofit, Hardening.

1. INTRODUCTION

Stay-in-place fiber reinforced polymer (FRP) forms have been used for columns, piles, and girders in recent years. The use of FRP composite laminates for retrofitting concrete structural members has been shown to be very successful in restoring or increasing the strength of the members. However, there is little research on the behavior of FRP-confined columns under blast loadings.

The response of a structure subjected to blast loading is complicated and depends on the mass, geometry, and material properties of the structure, as well as the pressure magnitude of the impact loading. The materials of concrete, steel and FRP have different properties in strength and ductility when the loading rate changes. This paper considered the material characteristics of concrete, steel and FRP at low and high strain rates.

At present, most analytical work on blast loading is focused on 3-D finite element analysis with very complicated modeling schemes, accuracy of which depend significantly on the fineness of the mesh, and with significantly high cost of computation. This paper presents the details of an ongoing study on the behavior of FRP-confined columns under blast loading using an equivalent unidirectional analysis with high level of fidelity and accuracy and low computing cost.

2. MATERIAL MODELLING

2.1 Material Modeling at Low Strain Rate

The steel-confined concrete core is modeled after Mander et al. (1988), with an energy-based failure criterion, which equates the energy absorbed in concrete core with the maximum energy stored in the spiral steel reinforcement. The FRP-confined concrete core is modeled after Samaan et al. (1998), with a bi-linear empirical equation and a concrete failure criterion based on the FRP tube rupture in the lateral direction. Both models are cast into the modified Kent-Park model (Scott et al. 1982), which is characterized with a tri-linear curve to fit the concrete stress-strain

responses of the two models. Tensile strength of concrete is neglected for simplicity. The typical hysteretic stress-strain response of concrete core is shown in Fig. 1(a).

The steel reinforcement is simulated as an elasto-plastic material with a tri-linear hysteretic model, as shown in Figure 1(b). Based on earlier coupon tests (Shao 2004 and Zhu 2004), the stress-strain curve for the FRP tube in the longitudinal direction is defined as below, and shown in Figure 1(c):

$$\sigma = (\varepsilon / ABS(\varepsilon)) \times \left(-21.2 + \sqrt{451 + 638,143 \times ABS(\varepsilon)} \right) \quad ABS(\varepsilon) \leq 0.05 \quad [\text{in MPa}] \quad (1)$$

$$\sigma = (\varepsilon / ABS(\varepsilon)) \times \left(-3.08 + \sqrt{9.49 + 13,423 \times ABS(\varepsilon)} \right) \quad ABS(\varepsilon) \leq 0.05 \quad [\text{in ksi}] \quad (2)$$

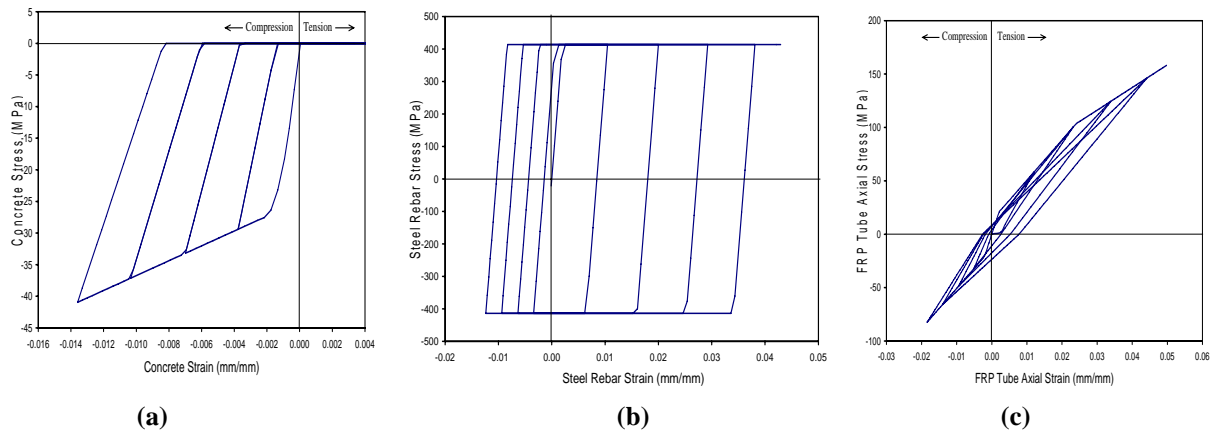


Figure 1: Typical Hysteretic Stress-Strain Curve of Model for (a) Concrete, (b) Steel and (c) FRP

2.2 Material Modeling at High Strain Rate

Concrete, steel and FRP generally show higher strength and ductility at higher loading rates. For the unconfined and steel-confined concrete, Scott et al. (1982) reported that both the peak stress and the post-peak descending slope were affected by the strain rate. The dynamic effect is introduced to the concrete model with dynamic increase factor K_d . The study recommended a constant value of 1.25.

There are few reports regarding the FRP-confined concrete performance under high strain rate. Zhang (2003) stated that the strength for FRP confined concrete is a function of strain rate, as shown in the following equation.

$$f_c'^d = f_c' (1 + \alpha \lg \dot{\varepsilon} / \dot{\varepsilon}_o) \quad (3)$$

where $f_c'^d$ is the dynamic loaded confined concrete strength; f_c' is confined concrete strength under low strain rate; $\dot{\varepsilon}$ is the strain loading rate; $\dot{\varepsilon}_o$ is the standard strain loading rate (10^{-5} 1/s); α is sensitivity index of concrete strength to loading rate, which is a function of confining ratio ξ . Confining ratio is defined as:

$$\xi = \frac{\sigma_f \cdot t}{f_c \cdot r} \quad (4)$$

where σ_f is the FRP rupture stress; t is the external FRP thickness; f_c is unconfined concrete strength under low strain rate; and r is concrete cylinder radius.

The concrete model is therefore modified for the high rate of loading. For this study, the loading rate is at the scale of 10^{-5} 1/s. The FRP-confined concrete model under high and low strain rates are plotted in Figure 2(a).

Steel also shows higher strength and ductility under high strain rate. Soroushian and Choi (1987) proposed a steel model considering various loading rates. The following equation showed that the increment of steel yielding stress is proportional to the logarithm function of the strain rate.

$$\frac{f_y'}{f_y} = \left(-0.451 \times 10^{-6} f_y + 1.46 \right) + \left(-9.20 \times 10^{-7} f_y + 0.0927 \right) \log_{10} \dot{\epsilon} \quad (\text{in MPa}) \quad (5)$$

The ultimate capacity and ultimate strain of the steel material follow the same trend, as follows:

$$\frac{f_p'}{f_p} = \left(-6.83 \times 10^{-6} f_y + 1.72 \right) + \left(-1.37 \times 10^{-6} f_y + 0.144 \right) \log_{10} \dot{\epsilon} \quad (\text{in MPa}) \quad (6)$$

$$\frac{\epsilon_u'}{\epsilon_u} = \left(-8.93 \times 10^{-6} f_y + 1.4 \right) + \left(-1.79 \times 10^{-6} f_y + 0.0827 \right) \log_{10} \dot{\epsilon} \quad (\text{in MPa}) \quad (7)$$

In this study, steel material is modeled with elastic material and linear strain hardening up to failure. The steel model at low and high strain rates are plotted in Figure 2(b).

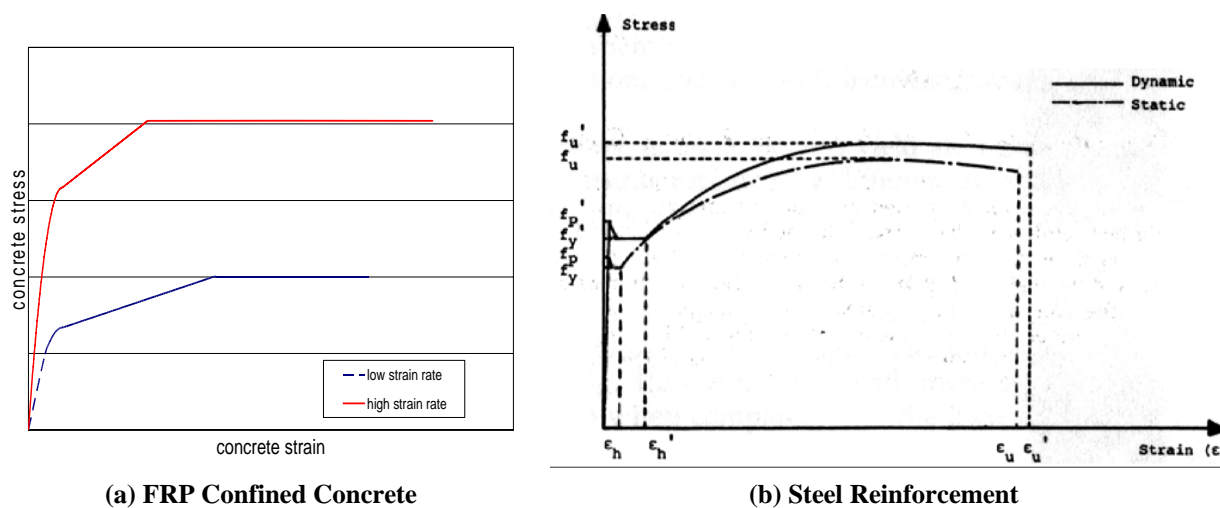


Figure 2: FRP Confined Concrete Stress-Strain Curve under Various Strain Rates for (a) FRP Confined Concrete and (b) Steel Reinforcement

For FRP materials under high strain rate, no literature has been found to provide a definite statement. However, Kuksenko and Tamuzs (1981) reported that the FRP material does not have significant strength increase under high loading rate. Therefore, the FRP model did not include the dynamic effect in this analysis.

3. SIMPLIFIED BLAST ANALYSIS WITH HIGH FIDELITY

Both the conventional reinforced concrete (RC) column and the concrete-filled FRP tube sections are discretized into layers. For each section, material models are adopted from the constitutive material models under high strain rate. Each section is analyzed separately to generate its own moment-curvature response.

In order to simplify the blast analysis with high fidelity and no loss of accuracy, this study incorporates the concept of equivalent section with pseudo materials. The equivalent section was proposed to transform the existing section geometry into an I-shaped section, where the web thickness is considered to be negligible (Figure 3), and the entire section is lumped into two flanges with limited thickness, thus limited stress variation along the flange thickness. Since the material is only present at the two tips of the section, there is no strain or stress gradient in the section. With the concept of equivalent section, the section performance is fingerprinted by the pseudo material defined at the two flanges. In order to produce exactly the same sectional moment-curvature response, the stress-strain curve of the pseudo material is defined based on the moment-curvature response of the actual cross section.

The blast analysis is then conducted on a line element along the column with the pseudo materials using ANSYS®. The study takes significantly less time than the finite element analysis of a complete three-dimensional mesh.

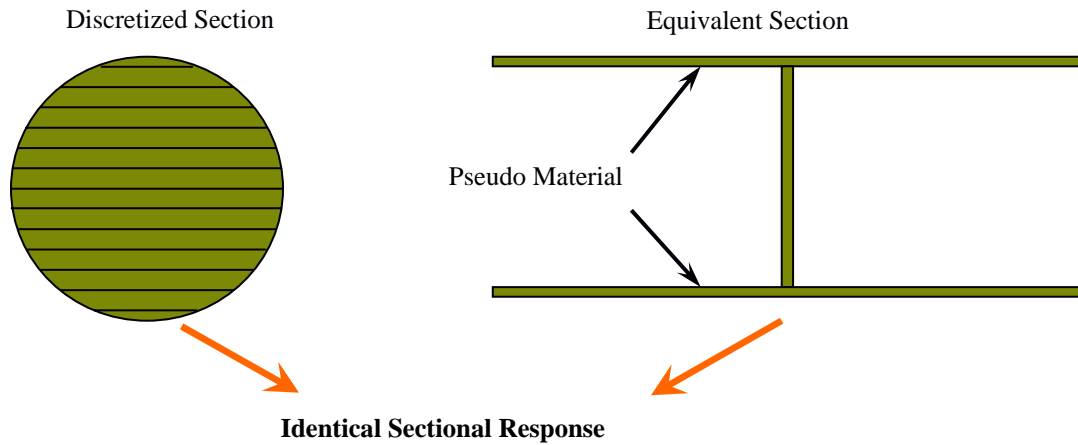


Figure 3: Illustration of the Equivalent Section Concept

4. Blast Analysis

Figure 4 shows the blast loading chosen for this study. A full blast analysis was carried out to compare the performance of pier frames made of either RC or CFFT columns. The study generated a number of results in terms of stresses and deflections of the two systems, as well as the safe distance from the blast loading for the bridge substructure. The study did not include any blast pressure on the bridge deck as it was assumed that the blast pressure is exerted directly on the bridge column. The study showed superior performance of the CFFT columns over equivalent RC columns. It also verified that the simplified method of analysis works quite well for blast loading.

ATF	VEHICLE DESCRIPTION	MAXIMUM EXPLOSIVES CAPACITY	LETHAL AIR BLAST RANGE
	COMPACT SEDAN	500 Pounds 227 Kilos <i>(In Trunk)</i>	100 Feet 30 Meters
	FULL SIZE SEDAN	1,000 Pounds 455 Kilos <i>(In Trunk)</i>	125 Feet 38 Meters
	PASSENGER VAN OR CARGO VAN	4,000 Pounds 1,818 Kilos	200 Feet 61 Meters

Figure 4 : ATF Vehicle Bomb Size Matrix

5. REFERENCE

Kuksenko, V.S., and Tamuzs, V.P. (1981). "Fracture Micromechanics of Polymer Materials." Springer, Hingham, Ma.

Mander, J., Priestley, M., and Park, R. (1988). "Theoretical Stress-Strain Model for Confined Concrete". *Journal of Structural Engineering*, ASCE, Vol. 117, No. 8, 1988, pp. 1804-1826.

Samaan, M., Mirmiran, A., and Shahawy, M. (1998). "Model of Concrete Confined by Fiber Composites". *Journal of Structural Engineering*, ASCE, Vol. 124, No.9, 1998, pp. 1025-1031.

Scott, B.D., Park, R., and Priestley, M. (1982). "Stress-Strain Behavior of Concrete Confined by Overlapping Hoops at Low and High Strain Rates." *ACI Journal*, Vol. 79, No.1, pp. 13-27.

Shao, Y., and Mirmiran, A. (2004). "Nonlinear Cyclic Response of Laminated Glass FRP Tubes Filled with Concrete". *Composite Structures*, Elsevier Science Ltd., Vol. 65, No. 1, 2004, pp. 91-101.

Soroushian, P., and Choi, K. (1987). "Steel mechanical properties at different strain rates." *Journal of Structural Engineering*, ASCE, Vol. 113, No. 4, pp.663-672.

Zhang, B., Pan, J., and Jiang, H. (2003) "Computation of strength for FRP confined concrete under fast loading." *Journal of Harbin Institute of Technology*, Vol. 35, No. 8, pp.958-961.

Zhu, Z. (2004). "Joint Construction and Seismic Performance of Concrete-Filled Fiber Reinforced Polymer Tubes". Ph.D. Dissertation, North Carolina State University, Raleigh, N.C., 2004.

Design and Analysis a 10-m FRP Deployable Bridge

R.G. Wight, MA. Erki, C.T. Shyu, R. Tanovic, A. Xie
*Royal Military College of Canada, PO Box 17000, Station Forces
Kingston, Ontario, Canada K7K 7B4*

ABSTRACT

The Canadian Forces are replacing many of their tracked vehicles with wheeled vehicles in a move towards a “primarily wheeled Army”. However, there is a loss of cross-country mobility associated with this change, which creates a need for lightweight, inexpensive, short span bridges. Owing to its favourable properties, FRP was the target material for the construction of these bridges. A structural concept, adapted to the material properties of commercially available glass FRP (GFRP) pultruded products, is presented. A 10 m span full-scale box-beam was built from commercially available GFRP pultruded sections that were bonded throughout to form a tapered box-beam, with a width of 1.22 m and a height at mid-span of 0.9 m, plus 0.04 m (1.575 in.) for a ribbed GFRP panel for the wearing surface. The box-beam represents a single track of a double-track bridge, whose tracks are to be lightly laced together. The design considered the concepts for modular assembly, methods of transporting, launching and recovering of the structure. The design of a hinge at mid-span to accommodate these features was a major focus. Finite element analysis of the design was used to predict deflection behaviour.

KEYWORDS

Pultruded structural shapes, short span bridge, fibreglass

1. INTRODUCTION

Both the Canadian Forces (CF) and a wide range of Canadian and international non-government organizations (NGOs) have an intense interest in cross-country mobility in settings where infrastructure may have been badly damaged by conflict or natural disaster. The ability to deliver humanitarian aid so as to maintain order and civil society is hugely dependent upon timely restoration of mobility and access. Hence, there exists a need for lightweight, inexpensive, short-span bridges. Owing to its favourable properties, such as high strength to weight ratio, corrosion-free characteristics, high degree of free formability and good fatigue resistance, fibre reinforced polymer (FRP), and in particular glass FRP (GFRP), is the target material for the construction of such bridges.

The concrete/FRP structural research group at the Royal Military College of Canada has developed an expertise in the use of GFRP for short span bridges and their related design issues since 1994 (Erki et al., 1994; Erki et al., 1995; Yantha et al, 1995; Erki et al., 1997; Tanovic et al., 1998). With a view to designing the 10-m full-scale GFRP bridge, a 4.8 m span prototype gap crossing aid was first built using commercially available GFRP pultruded sections that were bonded throughout to form a tapered box-beam, with a width of 1.2 m and a height at mid-span of 0.5 m, plus a 0.04 m (1.575 in.) thick ribbed GFRP panel for the wearing surface (Wight et al., 2004a; Wight et al. 2004b; Heffernan et al. 2004, Wight et al. 2005). The goal was roll-on/roll-off capability, with minimal terrain preparation for deployment of the bridge. Experience with the design, construction and testing of the 4.8 m prototype tapered box-beam confirmed that a gap-crossing aid consisting of built-up box beam components would fulfill the need for transportable, lightweight, short span bridges.

2. DESCRIPTION OF THE BRIDGE

A 10-m span full-scale box-beam was designed and built using commercially available GFRP pultruded sections that were bonded throughout to form a tapered box-beam, with a width of 1.22 m and a height at mid-span of 0.9 m, plus 0.04 m (1.575 in.) for a ribbed GFRP panel for the wearing surface. The box-beam represents a single track of a

double-track bridge, whose tracks are to be lightly laced together. As for the 4.8 m prototype, the low rigidity of GFRP was compensated for by maximizing the moment of inertia at mid-span for the 10-m gap crossing aid. However, unlike the 4.8 m prototype, the 10-m gap crossing aid has two slopes on either side of the mid-span, because with only one slope the large change in angle at mid-span would have been impractical for vehicles. At the quarter-span the height of the box-beam is 0.75 m, and at mid-span it is 0.9 m. The 10-m gap crossing aid consists of three longitudinal beams in parallel, two for the outer faces and one on the centreline of the box. The top and bottom flanges of the beams consist of a pair of back-to-back hollow tube sections ($50.8 \times 50.8 \times 6.4$ mm), spaced by a 6.4 mm thick flat plate section for the web. The three beams are tied together at their tops and bases by two flat plates that make up, respectively, the top and bottom plates of the box-beam. A ribbed decking is further bonded to the top plate to stiffen it and to provide a wearing surface for the vehicle. The full structure would consist of two of these box-beams for the two wheel tracks of the vehicle. The two box-beams would be lightly laced together with bolted GFRP sections. The global dimensions are shown in Figure 1.

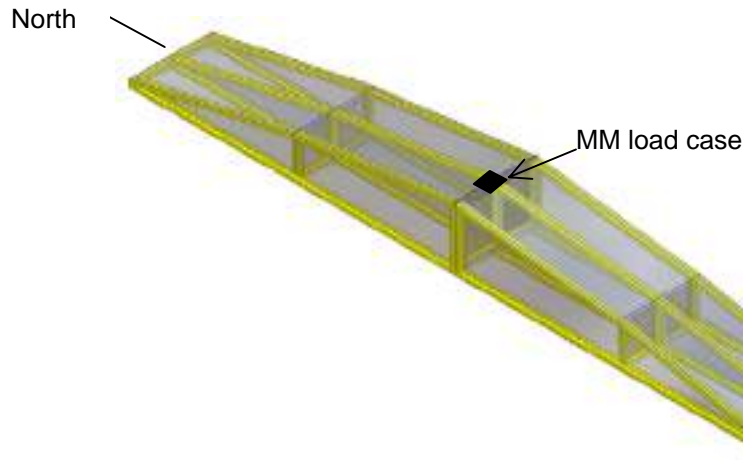


Figure 1: Tapered beam single trackway of the 10-m FRP deployable bridge

The bridge was designed for the Military Load Class (MLC) 30, which in accordance with NATO specifications represents two standardized vehicles, namely a tracked vehicle of 27.22 Tonnes and a wheeled vehicle of 30.84 Tonnes. The design of the 10-m box-beam considered concepts for modular assembly, methods of transporting, launching and recovering of the structure. The design of a hinge at mid-span to accommodate these features was a major focus. Several hinge prototypes, including hybrid FRP/steel hinges, were designed, constructed and tested, before arriving at a proposed solution. Finite element analysis of the design was used to finalize the global design details of the structure. The bridge will be tested in the laboratory, under quasi-static and dynamic loading, and in the field using a moving vehicle. This paper presents design considerations, including the design of the mid-span hinge, finite element analyses for the static loading, and the construction sequence used to build the bridge. Test results will be presented at the conference.

The GFRP materials used are all pultruded sections that were purchased from Creative Pultrusions Inc. The materials were from the 1625 series for the rectangular tubes, the 1625 series for the flat sheets and Flowgrip Flooring for the decking/wearing surface. The hollow tubes and plates consist of alternating layers of randomly oriented fibres and unidirectional fibre rovings in a vinyl ester resin matrix for the hollow tubes and an isophthalic polyester resin matrix for the flat plate. The amount of glass fibre by weight for these sections is between 45 and 50%. The material properties of the GFRP components are shown in Table 1.

To allow ease of transportation and launching, the 10-m gap crossing aid was designed to be in two halves, joined by a hinge attached to the bottom plate at mid-span. The hinge will be predominately in tension. Two main systems were considered, namely a hinge fabricated using carbon FRP (CFRP) sheets wound around a steel hinge pin and an all-steel hinge. The CFRP option required that the CFRP sheets be bonded to the bottom plates of the box-beam. The all-steel hinge was also bonded to the bottom plate, but with the option of lightly bolting the steel plates to the bottom plate of the box-beam to prevent premature failure due to prying. It is expected that prying will occur due to unavoidable eccentricities, in spite of measures taken to reduce these. Also, in the all-steel hinge, consideration was given to whether the center of the steel pin would be placed concentrically or eccentrically with respect to the

thickness of the bottom plate of the box-beam. The system with the pin positioned below the bottom plate of the box-beam would allow less encumbered folding of the box-beam.

Table 1. Material properties of the GFRP components

Component	Property (coupon values)	Units	Values
Tube	Modulus of elasticity	GPa	22
	Poisson's ratio	-	0.35
	Density	Mg/m ³	1.90
Plate	Modulus, of elasticity (LW*)	GPa	12.4
	Modulus of elasticity (CW*)	GPa	6.9
	Poisson's ratio (LW)	-	0.32
	Poisson's ratio (CW)	-	0.28
	Density	Mg/m ³	1.90
Deck	Modulus, of elasticity (LW*)	GPa	20.7
	Modulus of elasticity (CW*)	GPa	10.35
	Poisson's ratio (LW)	-	0.32
	Poisson's ratio (CW)	-	0.28
	Density	kg/m ²	14.65

*LW: lengthwise parallel to the unidirectional fibre rovings;
 CW: crosswise perpendicular to the unidirectional fibre rovings

Ultimately, even though the CFRP hinge would be a lightweight option, it was not favoured, because it had lower failure strength than the all-steel hinge. This lower strength was a result of premature debonding failure of the CFRP sheets from the FRP substrate. Also, it is expected that the impact and dynamic loading of the hinge in service would exacerbate the debonding problem. Uncertainty regarding this could not be adequately addressed. Also, there was uncertainty regarding quality control during fabrication of the CFRP hinge, protection of the hinge from damage in service, and reparability of any damages incurred by the CFRP hinge in service.

For the all-steel hinge, the steel pin was fitted into a steel tube that was welded to the steel plates of the hinge. In tests, welding failure never governed the maximum load obtained. Bonding was used to attach the steel plates of the hinge to the FRP substrate, representing the bottom plate of the FRP box-beam. Pliogrip adhesive with a metal primer worked well in this application. General observations were that for the all-steel hinge, the geometric eccentricity of the steel pin (the centre of the pin placed below the bottom plate) greatly reduced the maximum strength obtained for the hinge, owing to the prying resulting in debonding of the steel plates from the FRP substrate at low loads. The hinge design chosen for the 10-m gap crossing aid is the all-steel hinge with the pin placed as nearly as possible concentrically with the mid-depth of the bottom plate. This design resulted in a hinge strength that was at least 20% greater than provided by the box-beam design. Construction sequence of the 10-m gap crossing aid consisted of (a) assembly of one of the "half-webs" for half of the box-beam; (b) assembly of the three half-webs with internal diaphragms; (c) bonding of the bottom plate on the three half-webs; (d) central hinge in disassembled position. Figure 2 shows part of the construction sequence.



Figure 2: Part of the construction sequence of the 10 m gap crossing aid; (a) bonding of the bottom plate on the three half-webs; (b) central hinge in disassembled position.

3. ANALYSIS

The finite element method, using LUSAS software, was used to analyze the static response of the 10-m FRP gap-crossing aid. Three analyses were done for the tapered beam assuming (a) no mid-span hinge and without the ribbed decking; (b) no mid-span hinge but with the ribbed decking, and (c) with the mid-span hinge and the ribbed decking. For analysis (c), the two halves of the tapered beam were connected at the extreme top and bottom elements only, neglecting as a first approximation the contact problem over the two faces of the adjoining halves. The critical loading case considered was that of a patch load (MM) of 125kN (over 90% of the design vehicle load) at the mid-span apex of the box-beam, as shown in Figure 1. The vertical displacements for the three analyses are (a) 49.2 mm, (b) 26.9 mm, and (c) 61.1 mm. The ribbed decking added considerable stiffness to the displacement behaviour, but the introduction of a hinge resulted in significantly higher displacements compared to the analysis without the hinge but with the ribbed decking (i.e. (b)).

4. SUMMARY AND CONCLUSIONS

The design of a 10-m full-scale FRP gap-crossing aid has been completed, with consideration given to the concepts for modular assembly, methods of transporting, launching and recovering of the structure. The design of a hinge at mid-span to accommodate ease of transportation and launching was a major focus. Several hinge prototypes, including hybrid FRP/steel hinges, were designed, constructed and tested, before arriving at the proposed solution to use an all-steel hinge. Finite element analysis of the design was used to finalize the global design details of the structure. Deflections that normally govern the design of FRP structures were acceptable.

5. REFERENCES

- Erki, M.A., Yantha, P.J., Green, M.F., Johansen, G.E. and Wilson, R. (1994). Dynamic Response of an FRP Military Vehicle Bridge. *Fourth International Conference on Short and Medium Span Bridges*, 8-11 August, Halifax, Nova Scotia.
- Erki, M.A., Yantha, P., Green, M.F., Johansen, G.E., Wilson, R., and Mauer, D. (1995). Experimental Behaviour of a Reinforced Plastic Vehicle Bridge. *Proceedings of the Composite Institute's 50th Annual Conference & EXPO'95*, Feb 1995, pp. 11E1-5.
- Erki, M.A., Tanovic, R., Penstone, S.R., Johansen, G.E., and Wilson, R. (1997). Fatigue Evaluation of FRP Roadway Bridges, *Recent Advances in Bridge Engineering*, ed. U. Meier and R. Betti, Zurich, pp. 193-201.
- Heffernan, P.J., Wight, R.G., Shyu, C.T., Tanovic, R., Erki, M.A. 2004. Rapidly Deployable, Portable, GFRP Vehicle Bridge Development Project. *Proceedings of the 11th European Conference on Composite Materials*, Rhodes, Greece. CD ROM.
- Tanovic, R., Erki, M.A., Penstone, S. (1998). "Fatigue Behaviour of Pultruded FRP Components for Short and Medium Span Bridges", *5th International Conference on Short and Medium Span Bridges, SMSB-V*. Calgary. (CD).
- Tanovic, R., Erki, M.A., Johansen, G.E., and Wilson, R. (1997). Extreme and Fatigue Traffic Loading of a Reinforced Plastic Vehicle Bridge, *Proceedings of the Annual Conference of the CSCE*, Sherbrooke, Quebec, Vol. 6, pp. 61-70.
- Wight, R.G., Shyu, C.T., Tanovic, R., Erki, M.A., and Heffernan, P.J. (2004a). Short-span deployable GFRP Tapered Box-Beam Bridge. *4th International Conference on Advanced Composite Materials in Bridges and Structures*, Calgary, Alberta, 20-23 July, CD-ROM.
- Wight, R.G., Shyu, C.T., Tanovic, R., Erki, M.A., and Heffernan, P.J. (2004b). Deployable Tapered Box-beam Bridge. *Advanced Polymer Composites for Structural Applications in Construction. ACIC 2004* (ed. Hollaway, L.C., Chryssanthopoulos, M.K., Moy, S.S.J.) Woodhead Publishing Limited, Cambridge, England. pp. 428-433
- Yantha, P., Green, M.F., Erki, M.A., Johansen, G.E., and Wilson, R. (1995). Dynamic Testing of an FRP Vehicle Bridge. *Proceedings of the SEM/IMAC Conference*, Nashville, Tennessee, Feb 1995, pp. 11E:1-5.

RESPONSE OF NO-NAME CREEK FRP BRIDGE TO STATIC LOADS, MOVING AND IMPACT TRAFFIC LOADS

Eric Zhou and Youqi Wang
*Department of Mechanical and Nuclear Engineering
Kansas State University
Manhattan, Kansas*

David Meggers
*Kansas Department of Transportation
Topeka, Kansas*

Jerry Plunkett
*Kansas Structural Composites Inc.
Russell, Kansas*

ABSTRACT

In this paper, the field tests are conducted to investigate the response of the first composite bridge in the US to the static load, moving traffic load and impact traffic loads. Static results were compared to previous results. Dynamic responses of the bridge to dynamic traffic loads were measured and are presented in this paper. A detailed discussion is presented.

KEYWORDS:

FRP Bridge, Impact Traffic Load, Moving Traffic Load, Field Tests

1. INTRODUCTION AND GENERAL DESCRIPTION OF FIELD TESTS

No-Name Bridge is the first all composite road bridge in the United States. It was built by Kansas Structural Composites Inc. in Russell, Kansas in 1996. Fig.1 is a schematic illustration of the bridge. It is a single span and self-supporting glass-fiber reinforced composite bridge. Three composite panels comprise the bridge. The panels are supported by steel I-beams which rest on the creek banks. There is a freestanding test platform for long term monitoring beneath the bridge. Fig.2 is a schematic drawing of the three bridge panels. Panel length is 23'3". Bridge width is 27'9". Interlocking joints connect the panels side by side. Previously, two static field tests had been conducted on Nov. 19, 1996 and May 18, 1997, respectively. On September, 2004, field tests were conducted to examine the response of No-Name Creek Composite Bridge to static loads, moving traffic loads, and impact traffic loads. A AASHTO (American Association of State Highway Transportation) type 3 truck was used to apply load to the bridge. Truck dimensions and load distribution are shown in Fig.3. Total weight was 70340 lbs., shared by front wheels and rear wheels. Load supported by front wheels was 16320 lbs.; load supported by rear wheels was 54020 lbs. Three laser sensors were mounted on the test platform. When the truck moved through the bridge, deflection data were transferred to a computer. Specified maximum sensor error is 50 μ . Four kinds of loads were applied during the tests:

1. Static load tests: the truck rested on the middle span location of the bridge
2. Creep load tests: the truck moved through the bridge as slow as possible
3. Dynamic traffic load tests: the truck moved through the bridge at controlled speeds, and,
4. Impact load tests: the truck moved over an obstacle at controlled speeds. When the truck passed over the obstacle, an impact load was applied to the bridge.

Static results were compared to previous results. Dynamic responses of the bridge to dynamic traffic loads were measured and are presented in this paper.

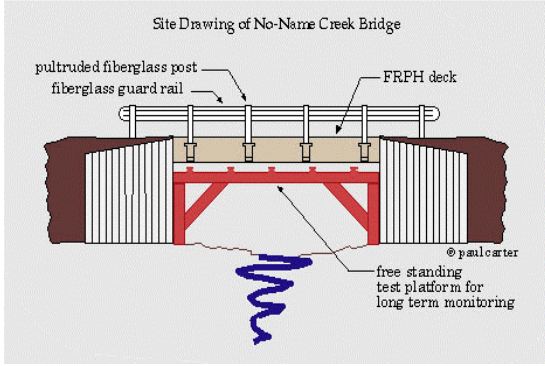


Fig.1 No-name creek bridge

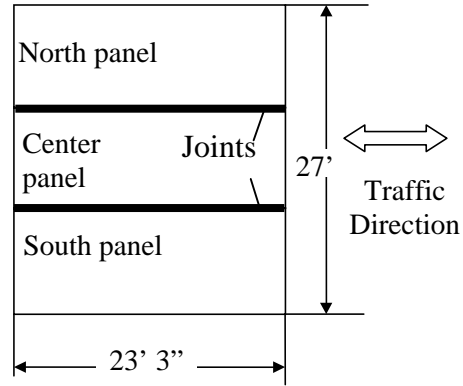


Fig.2 Schematic drawing of bridge panels

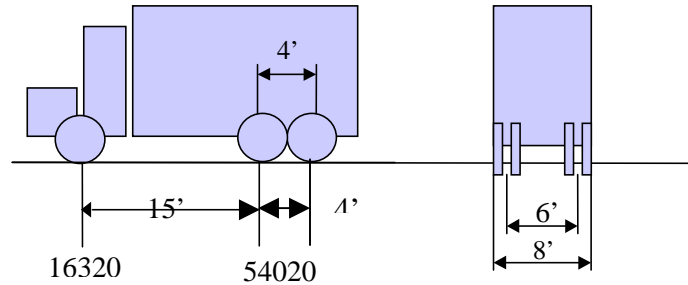


Fig.3 Dimensions of the loading truck

2. TEST DETAIL AND TEST RESULT ANALYSIS

Bridge deflection was measured in four kinds of loads: static truck load, creeping truck load, moving truck load with controlled speed and obstacle induced impact truck load.

2.1 Static Tests

Five static load tests were conducted. In static tests, the truck was loaded on one panel. Mid-span deflections of all panels were measured. This allowed us to evaluate

- (i) Load transfer between panels and
- (ii) Rigidity of bridge panels.

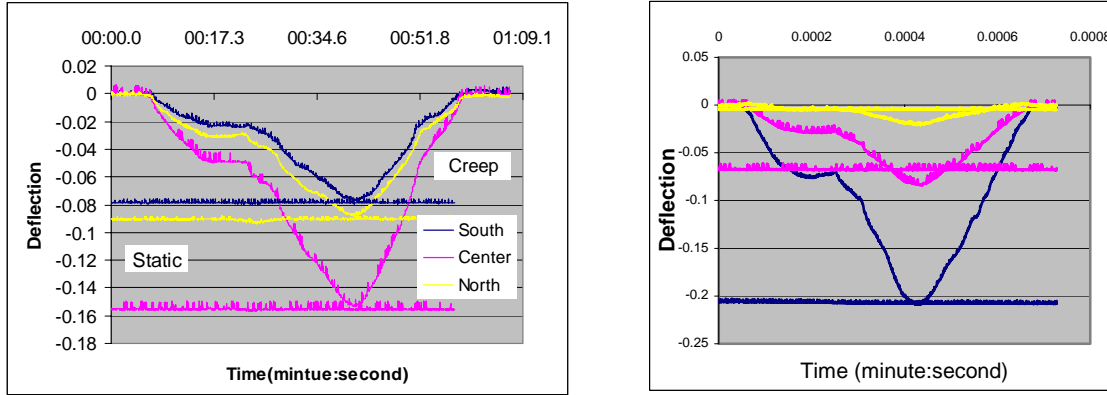
Refer to Table 1. The first column of the table shows truck locations. The second, fourth and sixth columns show the mid-span deflections of each panel. The third, fifth and seventh columns show load fractions supported by each panel.

Table 1. Results from static tests

Truck Location	North Panel		Center Panel		South Panel		Rigidity(EI) (lb.in ²)
	Deflection (in)	Load Fraction	Deflection (in)	Load Fraction	Deflection (in)	Load Fraction	
North panel	0.2567	0.7296	0.0878	0.2496	0.0073	0.0208	5.78E+10
Center panel	0.0878	0.2736	0.1547	0.4822	0.0783	0.2442	6.33E+10
South panel	0.0041	0.0146	0.0669	0.2416	0.2060	0.7437	7.34E+10

2.2 Creep Test

Four creep tests were conducted on the center and south panels. For the creep tests, the truck moved through the bridge as slow as possible. Deflections of mid-span and 1/4 span points were recorded as the truck moved through the bridge. Thus, an influence curve was derived. Fig. 4 shows the two influence curves from two creep tests. Three horizontal curves were taken from the previous static tests.



4-a Test 1: Creep test on center panel

4-b Test-2: Creep test on south panel

Fig.4 Influence curves in mid-span positions

2.3 Moving Traffic Dynamic Tests

In moving traffic dynamic tests, the truck moved through the bridge at five controlled speeds: 5 miles/hour, 10 miles/hour, 20 miles /hour, 30 miles/hour and 35 miles/hour. Similar to static and creep tests, four groups of tests were conducted. In the first and third groups of tests, the truck moved through the center panel. In the second and fourth groups of tests, the truck moved through the south panel. Fig.5 shows mid-span deflection of the center panel under a moving traffic load in the first group of tests. One sees deflection varied insignificantly when the speed was lower than 20 miles/hour. It began to increase significantly afterwards. Similar results were achieved in the other groups of tests. In addition, ratios between dynamic tests and static tests are calculated and are defined as dynamic factors. Fig.6 shows the dynamic factors from the first and third groups of tests.

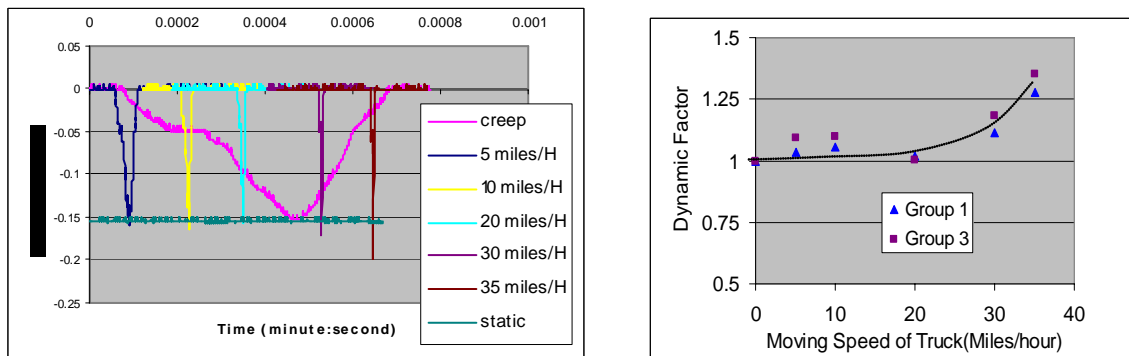


Fig.5 Mid-span deflection in moving traffic tests

Fig.6 Dynamic factors

2.4 Impact Tests

For impact tests, a 2”x 6” wood stud was placed onto the middle of the bridge. The truck drove over the wood stud. Similar to dynamic tests, four groups of tests were conducted. Fig.6 shows results from the first group of tests on the center panel. Deflection increases with increasing moving speed. Impact effect cannot be neglected even when speed is very slow. A similar phenomenon was observed in other groups of tests. The impact factors are shown in Fig.7. The impact induced the south panel vibration as shown in Fig.8.

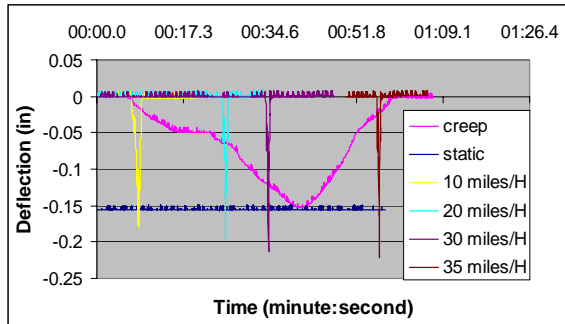


Fig.6 Mid-span deflection under impact loading

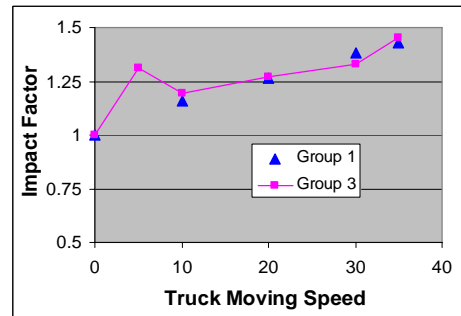


Fig.7 Dynamic factor

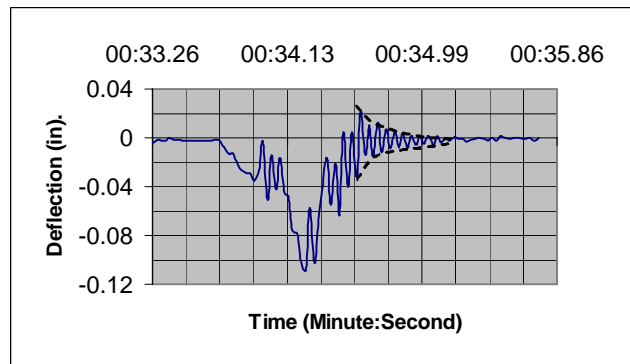


Fig.8 Impact induced south panel vibration (Truck speed: 30 miles/hour, loading: center panel)

3. CONCLUSIONS

Several conclusions are reached through these field tests:

1. Two static tests were conducted in 1996 and 1997. It were found that the rigidity of bridge panels were 6.72×10^{10} lb. in² and 5.93×10^{10} lb. in². In this field test, 6.48×10^{10} lb. in² of the static rigidity was derived. This indicates that there has been no significant change of bridge rigidity after 8 service years.
2. Bridge response to traffic load with a speed lower than 20 miles/hour is similar to static load. Dynamic effect can be neglected. Deflection increases with increased traffic speed after traffic speed reaches 20 miles/hour. When traffic speed reaches 35 miles per hour, bridge deflection increases approximately 30%.
3. Bridge deflection increases with traffic speed in impact tests. Impact effect cannot be neglected even when speed is slow. When traffic speed reaches 35miles per hour, deflection increase approximately 45%.
4. Impact load may trigger significant free vibration of south panels. Free vibration was found in impact tests with traffic speed of 30miles and 35 miles per hour. Frequency approximates 18.6 Hz.

Part III. Bridge Decks

BEHAVIORS OF NEW GENERATION OF FRP BRIDGE DECK WITH OUTSIDE FILAMENT-WOUND REINFORCEMENT

Peng Feng

(Lecturer, Dept. of Civil Engineering, Tsinghua Univ., Beijing, China)

Lieping Ye

(Professor, Dept. of Civil Engineering, Tsinghua Univ., Beijing, China)

ABSTRACT

OFR (outside filament-wound reinforcement) is an effective configuration to improve the performance of FRP bridge decks. It can enhance the transverse stiffness of FRP decks and restrict the swelling and disspreading trends of the FRP components to increase the ultimate load and deformation capacity of FRP decks. The new generation of FRP bridge deck with OFR, named HD deck, was designed. Four HD decks were manufactured and tested in static and fatigue loads. The results show that the HD decks satisfy the demands of China Bridge Design Codes. The efficiency of OFR was verified. Based on the results, the reinforcement mechanism was analyzed.

KEYWORDS

Corrosion resistance, fatigue, light-weight superstructure, debonding, failure simulation.

1. INTRODUCTION

Many different types of FRP bridge decks have been designed and investigated in the last decade as their favorable characters, such as corrosion resistance, light weight and convenient installation (Karbhari et al, 2000; Brown and Zureick, 2001; Stone et al, 2001; Luke et al, 2002; Williams et al, 2003; Keller and Schollmayer, 2004). It was found in the experimental studies of FRP decks that the FRP longitudinal strength, which is much higher than the strengths in shear, transverse and inter-layer, was not utilized efficiently in most cases. The observed failure characteristics, including cracking, fiber breaking, debonding and delaminating, have the corresponding maximum load respectively. The damage always occurs in the mode with the lowest ultimate load: the strength failure in weak direction, such as crack in fiber direction and delaminating, or the assembly failure between components, such as debonding, slip and pullout. To prevent these failure modes and improve the performance of FRP decks, the configuration of OFR (outside filament-wound reinforcement) was presented (Feng et al, 2004). As the outside filament-wound layers enhance the transverse stiffness of the surface of FRP decks and restrict the swelling and disspreading trend of the components, the ultimate load and deformation capacity can be increased obviously with the failure mode changing. Based on this concept, the new generation of FRP bridge deck with OFR was designed, named HD deck. Four HD decks with different OFR layers were tested, among which three were loaded in static and one in fatigue load. And the behavior of HD decks was simulated with finite element software. Based on the results, the reinforcing efficiency of OFR is investigated.

2. HD DECKS

The HD deck is composed of four filament-wound square tubes, two pultruded plates and the OFR layer, as shown in Figure 1. HD decks will be laid on girders in parallel with Z-shaped connectors to form the superstructure of bridges as illustrated in Figure 2. The square tube made of 4400Tex E-glass fiber roving and epoxy resin is wound in $\pm 45^\circ$. Its average thickness is 8mm and the fiber volume ratio is 60.5%. The thickness of the face plate is 12mm which is made of E-glass 4400Tex fiber roving, fabric and mat with vinyl ester resin. They are assembled together and glued with epoxy resin. Then the deck is wound with the fiber filaments dipped in resin in the cross-angle $\pm \theta$.

The OFR layer is made of the same material as the tubes. The mechanical properties of plates and tubes were determined by tests, which are listed in Table 1.

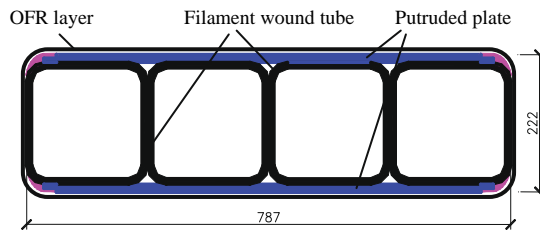


Figure 1: HD Deck Section

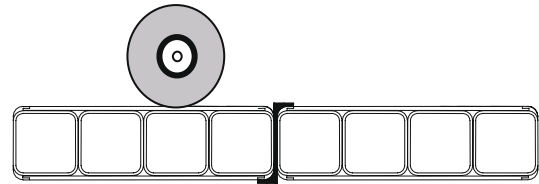


Figure 2: HD Decks in Bridge

Table 1: Material Properties of HD Decks

	Modulus / GPa			Poisson ratio	Strength/ MPa		
	Longitude	Transverse	Shear		Longitude	Transverse	Shear
Plate	31.84	17.41	5.79	0.213	>304 (tension)	57.4	48.0
Tube	23.96	23.96	9.33	0.483	191(compress)	-	-

3. EXPERIMENTAL STUDY OF HD DECKS

Four HD decks with difference OFR layer thickness or cross angle manufactured for the tests, including three for static tests and one for fatigue test, as listed in Table 2. All decks were simply supported. There were two kinds of loading conditions as shown in Figure 3: the central point of 200×200mm area to simulate the wheel load and the four-point line bending to estimate their stiffness.

Table 2: Tested HD Decks

Specimens	Length/m	Span/m	OFR	Load cases
HD0	3.0	2.8m	None	Case 1: four-point line bending to 350kN Case 2: central point to failure
HDW3	3.0	2.8m	±85° 3mm	Case 1: four -point line bending to 350kN Case 2: central point to failure
HDW5	3.0	2.8m	±85° 5mm	Case 1: central point to 630kN Case 2: four -point line bending to failure
HDW3-60	3.0	2.8m	±60° 3mm	Fatigue: central point to 20-100kN 2000000 times Static: central point to 150kN 9 times

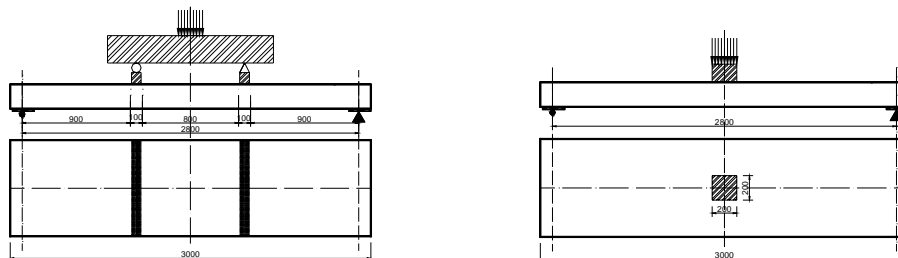


Figure 3: Four-point Line Load and Central Point Load

3.1 Static Load Tests

For HD0 without OFR, the tubes and bottom plate debonded suddenly when the central load reached 485kN as shown in Figure 4(a). There was an obvious gap between the bottom plate and the tubes. Before the failure, HD0

was linear elastic, and the ultimate deflection was 30.1mm. Under the central load of 70kN, which is the design wheel load, the deflection was 4.11mm (span/681). HDW3 deck failed in the punching under the load position as shown in Figure 4(b). The fibers around the loading pad were cut and broke. The maximum load was 618kN with a deflection of 52.5mm after a short ductile process. Comparing with HD0, HDW3 had a 26.4% increase of the load capacity. Its deflection under the design load was 3.97mm that indicates the stiffness was improved a little by OFR. HDW5 didn't fail when the load went to 632kN which is higher than the maximum value of HD0 and HDW3 under the same load pattern. It had a 3.35mm deflection under the design load. After unloading of Case 1, HDW5 was loaded to failure at 1737kN in Case 2. The deck deformed obviously before failure, and broke suddenly at 1737kN. The fiber under the left load point was crushed and fractured as shown in Figure 4(c). In this failure mode, FRP is utilized effectively although it failed in brittle. Comparing these tests, it is shown that the ultimate strength increase obviously with the OFR layer thickness. The effects of OFR can enhance the ultimate load capacity and make the failure process more ductile.



Figure 4: Failure Modes of HD Decks

3.2 Fatigue Load Test

The HDW3-60 was tested in fatigue to simulate the traffic loads. The load was applied periodically from 20kN to 100kN for 2 million times. After 5k, 20k, 50k, 100k, 800k, 1.2M, 1.6M and 2M times, a static load of 150kN was applied once to get the stiffness of the deck. During the loading process of 7 days, no obvious failure was observed, the deck deformed and bounced periodically under the cyclic load. After loading, there was a residual deflection of 0.3mm. The stiffness deterioration of HDW3-60 in the test is illustrated in Figure 5, which are lower than 7% and correspond linearly with the logarithm of load times.

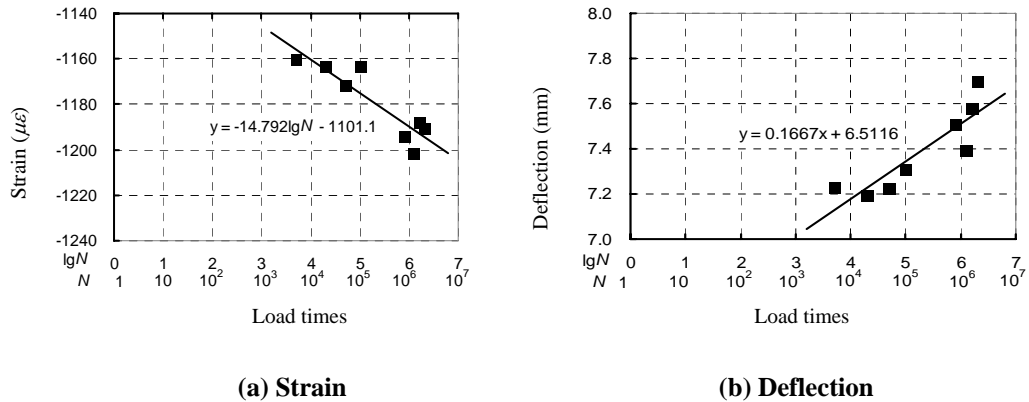


Figure 5: Changes of HDW3-60 with Load Times

3.3 Test Analysis

The stiffness of FRP deck is the control parameter in design. All tested HD decks satisfy the request of Heavy Truck-20 in China Bridge Design Code: the deflection is less than span/600 (4.67mm) under a wheel load of 70kN. The differences of their bending stiffness and shear stiffness determined by four-point line tests are no more than 10.8% to each other. It means that the OFR layer with a thickness less than 5mm doesn't affect the stiffness of the decks obviously. However, the ultimate load and the deformation capacity are improved considerably, which can be seen from the deflection-load curves in Figure 6.

The transverse strains in OFR disclose the reinforcing mechanism. Figure 7 shows the transverse strain distribution of deck surface of HD0 and HDW3 in midspan. When the load is 200kN, which is lower than the half of the ultimate strength of HD0, the strains (the left parts) in these two decks are almost same. But when the load closes to the failure load, the difference (the right parts) at the section corner and near the loading pad can be seen where the strains in HDW3 are much higher than those in HD0. Hence, the OFR layers enhance the inner deck at the corner mainly, which is also verified by FEA (finite element analysis).

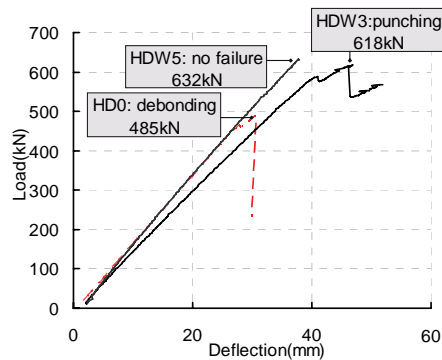
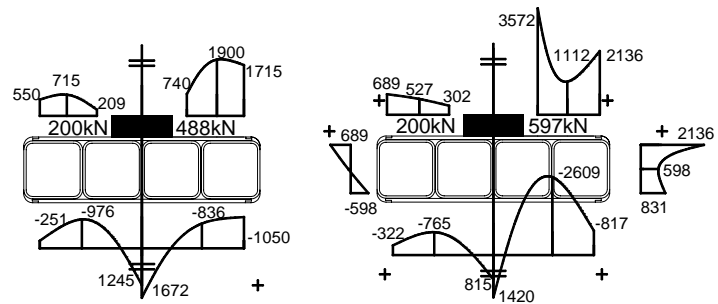


Figure 6: Load-deflection Curves of Tests



(a) HD0

(b) HDW3

Figure 7: Transverse Strain Distribution of Deck Surface

4. CONCLUSIONS

New FRP bridge deck with OFR is design and studied. Four HD decks were tested in static and fatigue loads. The conclusions can be summarized as below: (1) the HD deck with OFR has high bearing strength and low stiffness deterioration; (2) the OFR layer is very effective to enhance the strength and the deformation capacity of FRP bridge deck; (3) OFR layers act at the corner of section mainly.

5. ACKNOWLEDGEMENTS

The authors are very appreciated to Chinese Natural Science Fund to support the key Program of FRP application in civil engineering in China (No. 50238030) and the National High Technology Research and Development Program of China (863 Program) (No. 2001AA336010).

6. REFERENCES

- Brown, R.T., Zureick, A.H. (2001). "Lightweight composite truss section decking". *Marine Structures*, Vol.14, pp115-132.
- Feng, P., Ye, L.P., Zhang, L.W., et al. (2004). "Experimental study of outside filament winding reinforced FRP bridge decks". *Proc. 4th International Conference on Advanced Composite Materials in Bridges and Structures*, Calgary, Alberta, Canada, (CD-ROM).
- Karbhari, V. M., Seible, F., Burgueno, R., et al. (2000). "Structural characterization of fiber-reinforced composite short- and medium-span bridge systems". *Applied composite materials*, Vol.7, No.2-3, pp151-182.
- Keller, T., Schollmayer, M. (2004). "Plate bending behavior of a pultruded GFRP bridge deck system". *Composite Structures*, Vol.64, pp285-295.
- Luke, S., Canning, L., Collins, S., et al. (2002). "Advanced composite bridge decking system – Project ASSET". *Structural Engineering International*, No.2, pp76-79.
- Stone, D, Nanni, A, Myers, J. (2001) "Field and laboratory performance of FRP bridge panels". *Proc. International Conference Composites in Construction*, Porto, Portugal, pp701-706.
- Williams, B., Shehata, E., Rizkalla, S. H. (2003). "Filament-wound glass fiber reinforced polymer bridge deck modules". *Journal of Composites for Construction*, Vol.7, No.3, pp266-273.

TESTS OF A FRP DECK PANEL AT VERY COLD TEMPERATURES

Z. John Ma, Ph.D., P.E.

(Associate Professor, University of Tennessee, Knoxville, Tennessee, USA)

Usha Choppali

(Project Engineer, Tendon Systems LLC, Columbus, Georgia, USA)

ABSTRACT

The FRP deck panel with an overall geometry of 2.134m x 0.340m x 0.178m was cyclically tested under a three-point loading setup in a cold room. During a three-month testing period, the temperature of the cold room was changed from 26^oC to 0^oC, -20^oC, -31^oC, back up to 27^oC, then to -38^oC, and finally to -55^oC. In addition to the experimental program, the Classic Beam Theory (CBT) method and the Finite Element (FE) method were used to predict the panel behavior at room temperatures. Based on this research, the following conclusions were made: (1) The low-temperature stiffness was about 3.8% higher than at the high temperature as long as the low temperature was above a certain degree; (2) When the temperature was lowered from -20^oC to -55^oC, the low-temperature stiffness decreased 11.5% comparing with the stiffness at room temperatures. This degradation in stiffness could not be recovered by raising the panel temperature; (3) Very cold temperature exposure resulted in matrix hardening, matrix microcracking and fiber-matrix debonding as demonstrated by the AE testing data at different temperatures; and (4) At the room temperatures, the FRP panel showed a little stiffer performance than both the CBT method and the FE method would predict.

KEYWORDS

FRP deck panels, very cold temperatures, cycling test, stiffness degradation, Acoustic Emission

1. INTRODUCTION

Fiber-Reinforced Polymer (FRP) composites, used in various applications and environments, are often chosen over conventional materials for their durability. However, there remains a “durability gap” for FRP composites (Karbhari, et al., 2003). Based on a recent study performed by Dutta et al. (2002), it was observed that the low-temperature (-30^oC) stiffness in the load-deflection curves was higher than at the high temperature (50^oC). In cold regions like Alaska, the temperature during the winter season may go well below -50^oC. It is difficult to do cast-in-place concrete for bridge decks in winter. As a result, the use of the FRP composites to replace existing, deteriorated bridge deck systems offers a very attractive alternative in cold regions. The paper presented here focused mainly on the study of the behavior of the FRP deck panel at very cold temperature (below -50^oC) cycling combined with a service load cycling.

2. EXPERIMENTAL PROGRAM

The FRP deck panel specimen was obtained from Kansas Structural Composites Inc. (KSCI), Kansas. It had an overall geometry of 2.134m in length, 0.340m in width, and 0.178m in thickness. The specimen was of sandwich type construction with a vertical corrugated core and was manufactured using the wet lay-up method, as discussed by Plunket (1997). The core of the panels was 152.0mm high and consisted of corrugated cells of 2.5mm thick in the form of honeycomb structure having a standard geometry of 51.0mm and amplitude of 102.0mm wave length. Also, the edge lengths were covered with two layers of 85.0 grams of chopped strand mat. According to the manufacture’s data, the top and bottom plates, of thickness 13.0mm, were composed of several layers of unidirectional, bi-directional and chopped E-glass fibers. Both polyester and vinyl ester resin will be used as matrix in the testing program. However, polyester resin was used as matrix in the specimen reported here. Figure 1 shows

the specimen and the testing setup. The sensor instrumentation can also be seen in the figure. The testing was conducted using a self-equilibrating structural steel frame in a cold room. The cold room is 4.3m by 4.3m in size and was designed to provide a low temperature of -70°C . Figure 2 shows the control panel of the cold room while one of tests was in progress. It was decided to use the service load level of 35.6 kN to test the specimen at various temperatures. At each temperature, the specimen was loaded up to 35.6 kN at a loading rate of 2.2 to 4.4 kN per minute. Figure 3 shows the loading and temperature cycling history of the experiment. The detailed testing program was reported elsewhere (Ma et al., 2006).



Figure 1: Three-Point Bending Test Setup



Figure 2: Control Panel of the Cold Room

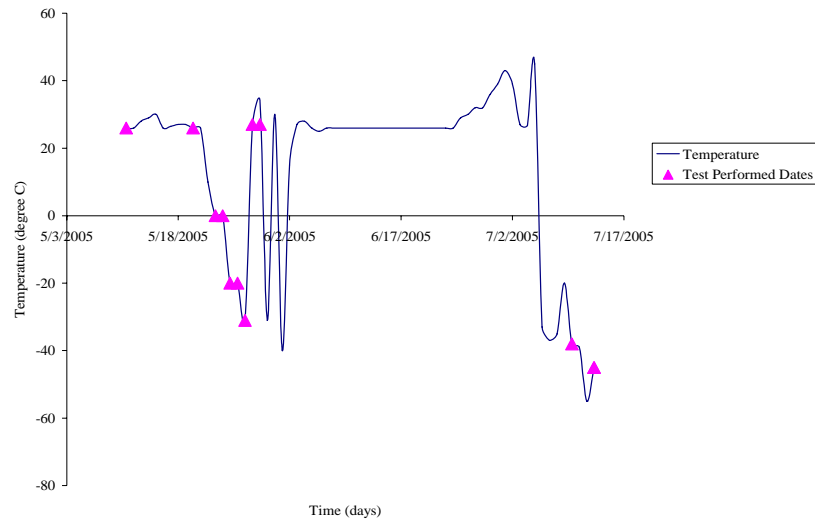


Figure 3: Loading and Temperature Cycling History

3. BAVIOUR OF THE FRP PANEL AT 26°C

After the first stage of room temperature test, it was decided to perform an analysis of the specimen to compare the result from the experiment with the available material data from the manufacturer of the specimen. To achieve this objective, two methods were used: the Classic Beam Theory (CBT) and Finite Element Modeling. In the CBT method, assume that the flexure rigidity for all of the core sheets is the same and all three layers are firmly bonded together. The second assumption was also made that cross-sections which are plane and perpendicular to the longitudinal axis of the unloaded panel remain so when bending takes place. Besides the CBT method, the panel was also modeled and analyzed by the finite element analysis program ABAQUS with a three dimensional deformable shell model. The FE model consists of top and bottom flanges connected by a sandwich core as shown in Figure 4. Figure 5 shows the comparison of the strain between the test result and the FE prediction. Similar to the deflection, the test result showed stiffer performance.

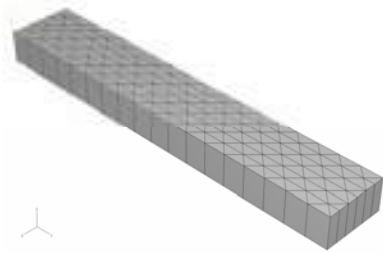


Figure 4: FE Model of the Panel

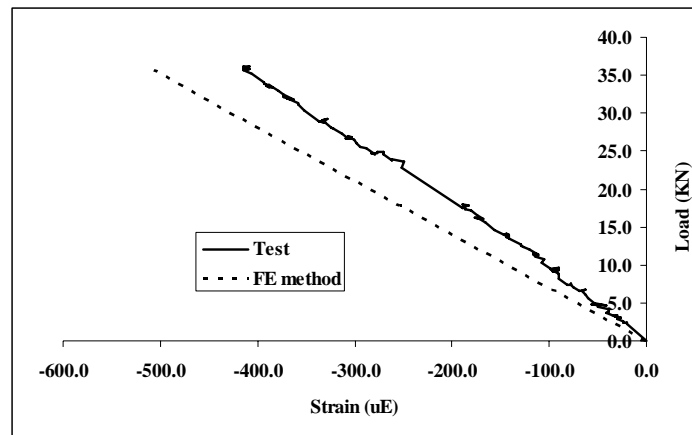


Figure 5: Load vs Strain

4. IMPACT OF THE VERY COLD TEMPERATURE CYCLING

After the first stage room temperature testing, the temperature of the cold room was lowered from 26⁰C to 0⁰C as shown in Figure 3. The panel was tested at 24 hours and 48 hours from the time of lowering the temperature. The data points in Figure 6 shows the relationship between the applied load and the deflection of the panel at mid-span. Figure 6 also shows that the panel stiffness, as represented as the slope of the trend line, is 10.82 KN/mm. The load vs. deflection curve for tests at other temperatures has the same pattern as shown in Figure 6, but with different stiffness values. Figure 7 shows a comparison of the panel stiffness at different temperatures. Please note that the testing conditions remained the same throughout the experiment. The only variable in each data set of the experiment was the temperature. Referring to Figure 7 for the test performed at 26⁰C, a stiffness of 10.42 KN/mm was obtained. As the temperature was lowered to 0⁰C, a static loading test was performed at the 24th hour and the stiffness value attained was 10.82 KN/mm. Another static testing was performed at the 48th hour at the same temperature, and the stiffness value was decreased to 10.59 KN/mm. When the temperature was further lowered to -20⁰C, the stiffness was found to be 10.60 KN/mm at the 24th hour. Until this stage of testing, the panel had been subjected to the temperature change of 46⁰C and four cycles of loading and unloading static tests. At the end of the 4th cycle loading test, the panel stiffness increased the maximum of about 3.8% as the temperature decreased from 26⁰C to 0⁰C and further to -20⁰C. However, when the panel was kept in the -20⁰C for another 24 hours the stiffness did not further increase. Instead, it decreased 5.0% comparing with the stiffness at room temperature. When subjecting the panel to further colder temperature as cold as -55⁰C, the panel stiffness showed a gradual decrease, and stabilized around the value of 9.22 KN/mm. When comparing with the stiffness at original room temperature, it decreased 11.5%. Most importantly, this degradation in stiffness could not be recovered by raising the panel temperature, as shown in Figure 7. Figure 8 shows an example comparison of the AE testing data at different temperatures. On comparing the two figures [(a) and (b)], it is seen that more activity happened at -31⁰C. There was also more energy at -31⁰C. A higher amplitude range (50-60 dB) was observed at -31⁰C when compared to a temperature of 26⁰C. Please note that in Figures 8 (a) and (b) the longer the time of observation the greater is the load applied on the specimen.

5. CONCLUSIONS

The following conclusions were made: (1) The low-temperature stiffness was about 3.8% higher than at the high temperature as long as the low temperature was above a certain degree (about -20⁰C under the testing condition presented in the paper); (2) When the temperature was further lowered from -20⁰C to -55⁰C, the low-temperature stiffness did not further increase. Instead, it decreased 11.5% when comparing with the stiffness at the original room temperature. Most importantly, this degradation in stiffness could not be recovered by raising the panel temperature; (3) Very cold temperature exposure resulted in matrix hardening, matrix microcracking and fiber-matrix debonding as demonstrated by the AE testing data at different temperatures; and (4) At the room temperatures, the FRP panel showed a little stiffer performance than the CBT and the FE methods would predict.

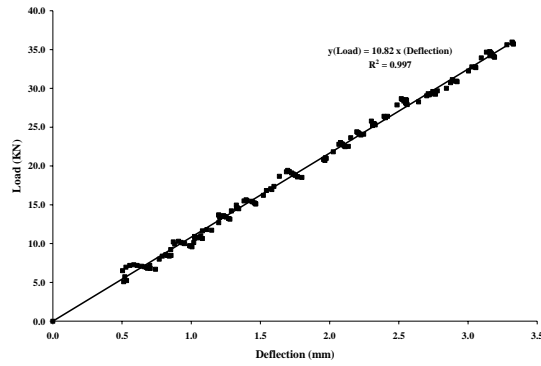


Figure 6: Load vs Deflection at 0°C (24 hours test)

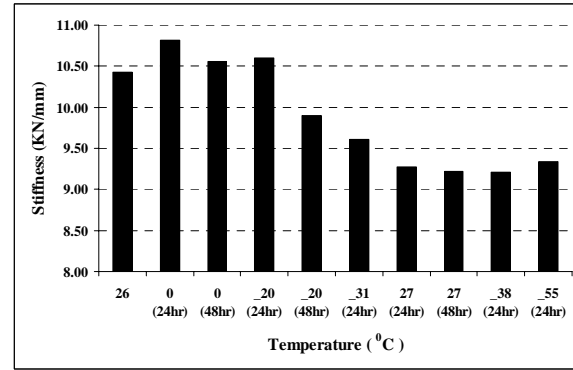
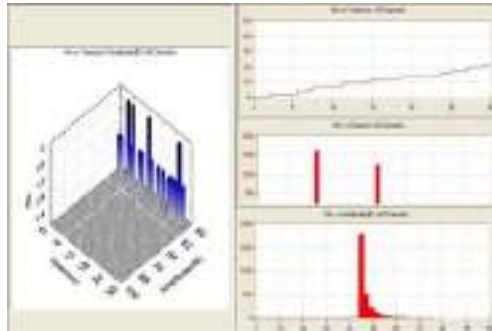
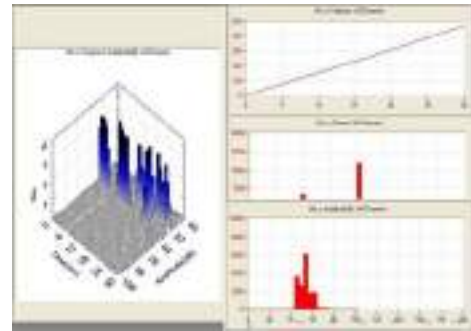


Figure 7: Stiffness vs Temperature and Time



(a) at 26 °C



(b) at -31 °C

Figure 8: Overview of the AE Data at Different Temperatures

6. ACKNOWLEDGEMENT

The test specimen was provided by the KSCI, and we thank Dr. Jerry Plunkett of KSCI for his technical contribution and support. Partial financial support for this study is received from the National Science Foundation – NSF CAREER program (CMS – 0343865) and the Department of Civil and Environmental Engineering at the University of Alaska Fairbanks.

7. REFERENCES

- Dutta, P.K., S.C.Kwon, G.Dullel, and R. Lopez-Anido (2002), “Fatigue Evaluation of Composite Bridge Decks,” In proceedings, 10th U.S.Japan Conference on Composite Materials, September 16-18, 2002, Stanford University, Stanford, C.A., DEStech Publications, 336-344.
- Karbhari, V.M., et al. (2003), “Durability Gap Analysis for Fiber-Reinforced Polymer Composites in Civil Infrastructure,” *Journal of Composites for Construction*, Vol. 7, No. 3, August 2003, pp. 238 – 247.
- Ma, Z. J., Choppali, U., and Li, L., (2006), “Cycling Tests of a Fiber-Reinforced Polymer Honeycomb Sandwich Deck Panel at Very Cold Temperatures,” *International Journal of Materials and Product Technology (IJMPT)*, Vol. 26 (in press).
- Plunket, J. D. (1997), “Fiber-reinforced Polymer Honeycomb Short Span Bridge for Rapid Installation,” IDEA Project Report, November.

STATIC AND FATIGUE TESTING OF INNOVATIVE ALL-COMPOSITE BRIDGE SLAB

René J. Roy

Ph. D. Candidate, Department of Civil Engineering, University of Sherbrooke, Sherbrooke, Quebec, Canada

Mathieu Robert

Ph. D. Student, Department of Civil Engineering, University of Sherbrooke, Sherbrooke, Quebec, Canada

Brahim Benmokrane

NSERC Research Chair Professor in Innovative FRP Composite Materials for Infrastructures, Department of Civil Engineering, University of Sherbrooke, Sherbrooke, Quebec, Canada

Ahmed S. Debaiky

Fellow NSERC Industrial Postdoctoral Researcher, A.S. Composites Inc., Boucherville, Quebec, Canada

Hossein Borazghi

President, A.S. Composites Inc., Boucherville, Quebec, Canada

ABSTRACT

In the context of the state of deterioration of North America's bridges, researchers have been working on improving the performance of current designs. All-FRP bridge slabs have attracted increased interest since the mid 90s. These slabs offer notable advantages over traditional reinforced concrete slabs. These advantages include lighter weight, better durability and faster installation among others. This research focuses on the development of a thermoplastic fiber reinforced polymer (FRP) bridge slab for the replacement of wood logs that are part of the deck structure of a popular steel/timber bridge design. Different structural profiles have been explored through finite element analysis and two slab prototypes have been fabricated. These full-scale prototypes have dimensions of approximately 3200mm×1200mm×250mm and cover two lateral spans. Both prototypes were tested under concentrated static loading and one was subjected to above two million cycles of loading. The slab deflection and FRP laminate stress levels under loading were recorded. The retention of the slab rigidity was monitored at regular intervals during cyclic fatigue loading. No significant rigidity loss was observed during this period.

KEYWORDS

Bridge, deck, FRP, thermoplastic, fatigue

1. INTRODUCTION

The U.S. Federal Highway Administration estimated that close to 30% of the 588 288 bridges in the United States either have a deficient structure or their capacity is obsolete (Busel, 2002). Some of these bridges are located in regions prone to harsh weather conditions, particularly Nordic regions where de-icing salts are commonly used to keep roads functional. As a result, these bridges tend to deteriorate faster. FRP materials are known to be immune to corrosion that affects steel rebars present in reinforced concrete bridge slabs. Along with resistance properties in the same range as steel, FRP composites represent a better alternative for bridge materials. The concept of all-FRP bridge slabs in place of reinforced concrete slabs has been investigated by various researchers and companies (Market Development Alliance, 2000). Many field projects have been realized in the United States since the mid 90s. These slabs had different section profiles composed of FRP laminates either produced by pultrusion, hand lay-up or vacuum assisted molding. This project focuses on the development of an FRP replacement bridge slab for a steel/timber bridge application where the current deck structure includes staggered timber logs. These timber logs

need replacement after about 15 years. With the actual deck design, the steel girders are also exposed to fluid spillage from the bridge surface and this increases their rate of deterioration.

2. DETAILS OF THE EXPERIMENTAL PROGRAM

2.1 Design Parameters

The replacement slab is to be installed in similar conditions as the existing timber logs; hence the span length (L) was kept to 1450 mm for this design. It has been observed through experimentation on this bridge type that the wheel load of a truck axle is supported by three consecutive timber logs. To mirror this, the width of the FRP slab was set to an equivalent of 1200 mm. The thickness of the new slab would match the timber log at 203 mm if the actual wearing surface is kept or it may be increased if a thinner wearing surface is chosen, up to a total of 299 mm including the wearing surface. The prescribed truck axle service load is established from the Canadian Highway Bridge Design Code at 110.25 kN per wheel (CHBDC, 2000). The length of the slab was chosen as to cover two spans to reproduce continuity. The truck axle load is to be applied in two concentrated areas (2×110.25 kN) separated by 1800 mm center to center as prescribed by the code. The loads are centered from the middle support, in this way creating the maximum negative moment over this support. The maximum deflection criterion under the service load was set to $L/400$, and maximum stress in the FRP to 30% of its ultimate strength.

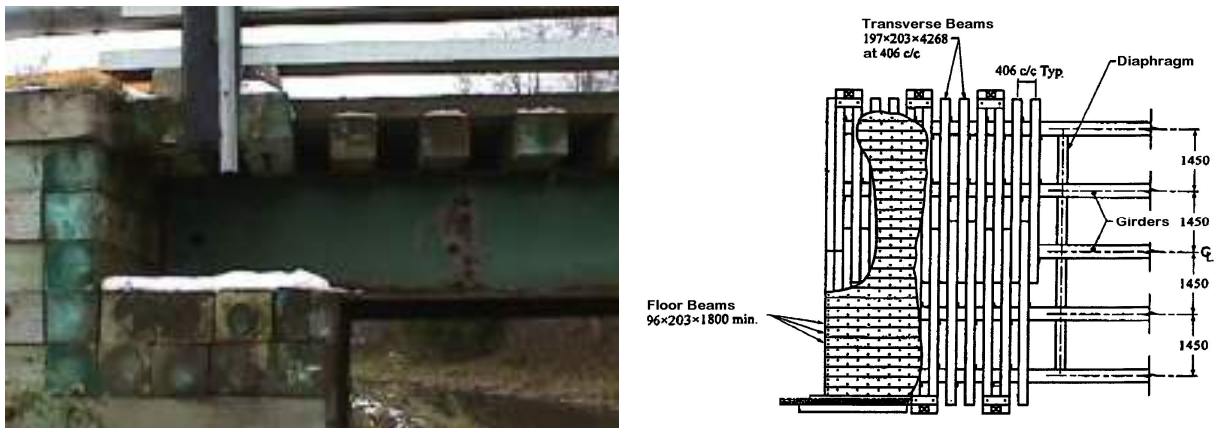


Figure 1 Actual Steel/Timber Bridge Deck.

2.2 Structural Design and Prototype Fabrication

Glass fiber reinforced polypropylene was chosen as a candidate material for a bridge slab. It was used in the form of commingled glass and polypropylene fibers 0°/90° weaved fabrics sold under the commercial name TwinTex® (Saint-Gobain Vetrotex, 2006). Its properties are listed in Table 1.

Table 1 TwinTex® 60% Mass Fiber Material Properties (Robert, 2006).

Tensile Modulus	Tensile Strength	Flexural Modulus	Flexural Strength
12 GPa	229 MPa	11 GPa	189 MPa

Different section profiles made of shaped FRP panels were considered with regard to structural efficiency and ease of fabrication. It was chosen to fill the hollow spaces in the section with polyurethane foam to increase rigidity and help prevent buckling of the FRP laminates in the profile. The polyurethane foam considered had a density of about 3.5 lbs/ft^3 for a modulus of elasticity taken at 10 MPa. These section geometries were modeled for finite element analysis with the SAP2000® software (Computers and Structures, 2006). The FRP laminates were approximated as straight line where needed and the laminate junctions were idealized as fixed (no slip). The model used linear 4-node shell elements for the FRP laminates and linear 8-node elements for the polyurethane foam. From the simulation results, two section geometries were chosen to be fabricated as prototype slabs for testing (Figure 2). These geometries produced satisfactory deflection results for 4-5 mm thick laminates and were judged suitable for simple

fabrication. These prototype slabs were made as an assembly of FRP components joined together by bolts. The FRP components were fabricated by vacuum bag molding in an oven at 180°C. Electrical strain gages were installed on the FRP laminates at various locations in the slabs. Once all the FRP components were assembled (Figure 3), one end of the slab was blocked and the liquid polyurethane foam mix was poured in the cavities by gravity for foaming.

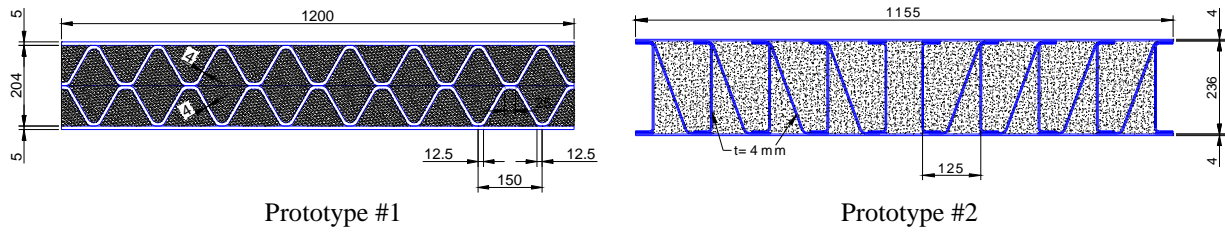


Figure 2 Section Profile Geometries Chosen for Prototype Fabrication.



Figure 3 Prototype #2 During Construction.

2.3 Test Set-up and Cyclic Fatigue Loading Regime

Both prototypes were subjected to a static loading in the laboratory using a 500 kN hydraulic jack. Strains in the FRP laminates were recorded and linear variable differential transformers (LVDT) were used to measure the slab deflection. The slabs rested on three I-beams separated by 1450 mm reproducing the bridge girders. The load was applied equally on two 600 mm × 250 mm steel plates lying on rubber pads. Prototype #2 was further subjected to cyclic loading using two 500 kN hydraulic jacks. The load cycles had a sinusoidal pattern with amplitude from 15 kN to 110.25 kN at a rate of 1 Hz for an initial two million cycles. After these two million cycles the top load limit was doubled to 220.5 kN until failure after 1500 cycles. Figure 4 shows the fatigue test set-up and loading regime.

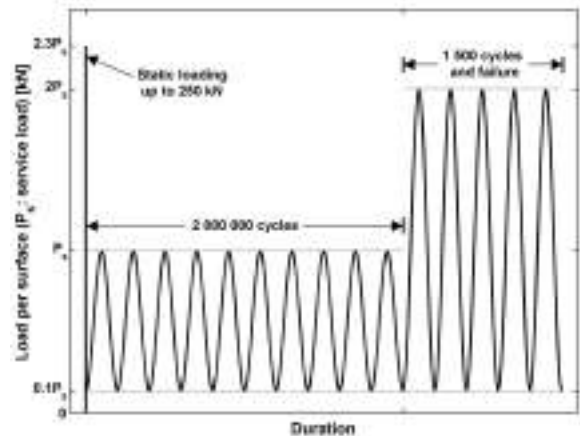


Figure 4 Fatigue Test Set-up and Cyclic Fatigue Loading Regime.

3. TEST RESULTS AND OBSERVATIONS

Both prototype supported a load of 500 kN without any major visible damage resulting. Recorded FRP strains were low with both prototypes, with the maximum representing 25% of ultimate capacity. Prototype #1 had a deflection of $L/180$ at the service load which was greater than the design criteria. Lower than initially planned polyurethane foam rigidity with excessive local deflection around the loading areas were identified as the cause of this defect in rigidity. The slab was then loaded to failure with two 500 kN hydraulic jacks and supported an ultimate load of 780 kN. The failure mode was punching in the loading area. Prototype #2 had a better deflection of $L/382$ under service load, which is in the range of the $L/400$ design criteria. It was therefore chosen for fatigue testing. The test was stopped every 100,000 cycles to perform a recorded static loading whose results are presented in Figure 5. The results show that there was little rigidity loss due to fatigue cyclic loading. Alteration of the polypropylene texture was slightly visible in small regions of the top FRP panel close to the loading areas. After about 300,000 cycles of loading this alteration gradually became more apparent. It later developed into small cracks in the polypropylene matrix. At about the 1,500,000 cycle mark the top FRP panel locally kinked in the region of one of these cracks, close to the end of the slab. We evaluate that these cracks were promoted by the initial static loading, which went up to 2.3 times the service load. When the cyclic load upper limit was doubled, a crack opened in the whole FRP top panel, with fiber ruptures, and developed. The slab failed in a punching style due to this crack after 1,500 cycles.

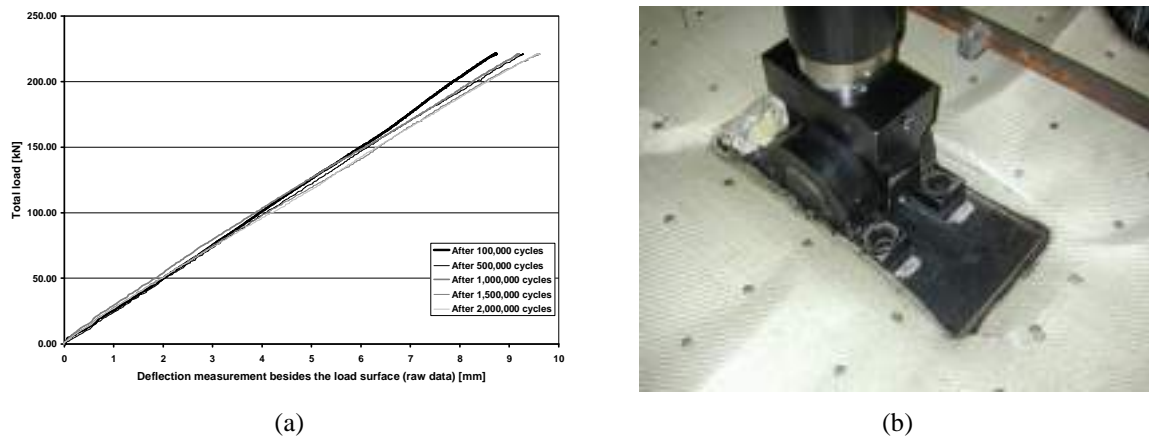


Figure 5 Prototype #2: (a) Slab Deflection Under Static Loading During the Fatigue Test; (b) Failure Mode.

4. CONCLUSIONS

The experiments conducted in this research lead to the following conclusions:

1. Stress levels remain low in the FRP laminates for all practical loading conditions and the designed slabs are able to withstand a load higher than the factored design load.
2. Deflection under the service load for prototype #2 is $L/382$ and is in the range of the design criteria.
3. No significant loss of rigidity was recorded on prototype #2 during the two million cycles of load at 2×110.25 kN.
4. The mode of failure of the slabs is punching in the loading area and this doesn't represent a catastrophic failure.

5. REFERENCES

- Busel, J.P. (2002). "Engineered FRP bridge decks solutions for the future", SAMPE Journal, vol. 38, no 5, September/October 2002, p. 46-48.
- CHBDC (2000) Canadian Highway Bridge Design Code, Standards Council of Canada, Ottawa, Canada.
- Computers and Structures (2006). SAP2000 software, www.csiberkeley.com, Berkeley, California, USA.
- Market Development Alliance (2000). "Product Selection Guide: FRP Composite Products for Bridge Applications", American Composites Manufacturers Association (ACMA), Arlington, VA., USA.
- Robert, M. (2006). "Durabilité du composite polymérique de polypropylène renforcé de fibres de verre", Ms. thesis, Department of Civil Engineering, Université de Sherbrooke, Sherbrooke, Quebec, Canada.
- Saint-Gobain Vetrotex (2006). "Twintex Woven Products Data Sheets", www.twintex.com, Chambéry, France.

RAPID CONSTRUCTION OF CONCRETE BRIDGE DECK USING PREFABRICATED FRP REINFORCEMENT

Fabio Matta

(Graduate Research Assistant, University of Missouri-Rolla, Rolla, MO, USA)

Antonio Nanni

(V. & M. Jones Professor, University of Missouri-Rolla, Rolla, MO, USA)

Thomas E. Ringelstetter

(Graduate Research Assistant, University of Wisconsin-Madison, Madison, WI, USA)

Lawrence C. Bank

(Professor, University of Wisconsin-Madison, Madison, WI, USA)

ABSTRACT

The development of durable structural systems for accelerated bridge construction is key to reducing the economic and social costs associated with replacement operations on a large scale. This paper reports on the field application of stay-in-place reinforcing panels, entirely made of glass fiber reinforced polymer components and specifically developed for the rapid construction of concrete bridge decks. The salient features of the system are illustrated, along with significant research and development outcomes. The five-day construction of the cast-in-place deck and open-post rail of Bridge 14802301 in Greene County, MO, is documented, and the major outcomes outlined. The project demonstrates how lightweight and noncorrosive FRP reinforcement is a practical alternative to steel, with the potential of versatile structural forms that add relevant constructibility and economic advantages.

KEYWORDS

Bridge Deck, Fiber Reinforced Polymers, Accelerated Bridge Construction.

1. INTRODUCTION

During the last four years, increasing investments have been made to support the research and development of innovative technologies for accelerated bridge construction, primarily under the sponsorship of the Federal Highway Administration (FHWA), the American Society of State Highway and Transportation Officials (AASHTO Technology Implementation Group), and the Transportation Research Board (TRB Task Force on Accelerating Innovation in the Highway Industry). Emphasis has been placed on improving safety and minimizing traffic disruption while enhancing quality and durability. The issue arises from the urgent need of upgrading and maintaining a significant portion of the bridge inventory while facing inevitable budget restrictions. Redecking operations are rather frequent, since corrosion of steel reinforcement is a major instrument of degradation in reinforced concrete (RC) decks and safety appurtenances. In the case of off-system bridges, cost-benefit analysis, contractors know-how and equipment availability typically result in the adoption of either partial or full-depth cast-in-place (CIP) technologies. The most popular solution limits the use of prefabricated elements to standardized partial-depth precast prestressed concrete panels as structural stay-in-place (SIP) forms between the girders, with CIP concrete topping, as opposed to traditional removable plywood forms. SIP steel metal deck forms, with a full-depth CIP configuration that eliminates the problem of reflective cracks, are less attractive due to three major drawbacks: a) safety concerns due to risks of accidental damage of relatively thin metal sheets, resulting in local buckling problems under wet concrete load; b) corrosion issues under aggressive environments; c) efficient inspection of the underside of the deck is complicated.

In the project presented herein, an innovative prefabricated glass Fiber Reinforced Polymer (FRP) SIP reinforcement

has been selected to construct the replacement deck of Bridge 14802301 in Greene County, MO. Corrosion resistant FRP reinforcement gratings and SIP form plates are integrated into very large-size modular panels. The structural form takes advantage of FRP composites tailorability and lightweight to provide improved constructibility, resulting in enhanced construction speed and safety.

2. PREFABRICATED STAY-IN-PLACE FRP REINFORCEMENT

2.1 Description and Detailing

The FRP SIP panels are prefabricated assembling off-the-shelf pultruded glass/vinylester components, typically used in floor grating applications in corrosive environments, into a three-dimensional grating made of two (top and bottom) layers (Figure 1). The main load-carrying elements are 38 mm I-bars, spaced at 100 mm on-center, which run continuously in the direction perpendicular to traffic (transverse). Both shape and spacing of the I-bars have been thought to allow ease of walking over the three-dimensional assembly. Three-part cross rods, spaced at 100 mm on-center and running through pre-drilled holes in the I-bars web in the direction parallel to traffic (longitudinal), provide shrinkage and temperature reinforcement, enhance the in-plane rigidity of each reinforcing layer, and constrain the core concrete to ensure mechanical compatibility with the structural I-bars. Top and bottom reinforcing layers are integrated using two-part vertical connectors that space them at 100 mm on-center. The two components forming the connectors are shaped to be epoxy-bonded to the I-bars and then fastened together. The formwork consist of 3.2 mm thick and 1.22 m long plates that are epoxy-bonded to the I-bars in the bottom layer.

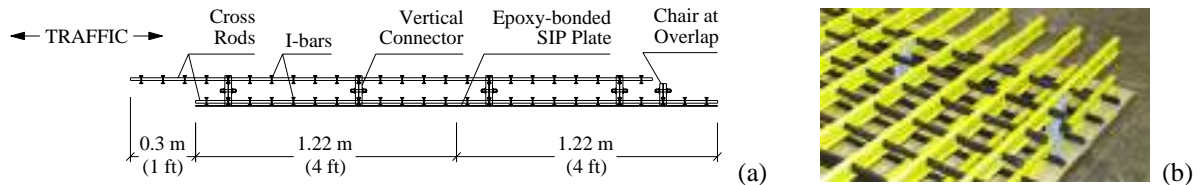


Figure 1: Prefabricated FRP SIP Reinforcement Panels: Longitudinal Section (a) and Close-up (b)

The system concept, detailing and construction procedure have been addressed to improve constructibility by introducing original solutions when needed, and constantly seeking input from practitioners. Each SIP panel has a width of 7.06 m, a typical length of 2.44 m (Figure 1(a)), and a weight of about 409 kg (23.7 kg/m²). The width corresponds to that of the bridge deck minus 127 mm per side, to allow a traditional drip edge notch to be formed on-site. The use of large-size and lightweight panels allows easy placement of the SIP reinforcement on the bridge girders with single picks of a crane at four anchorage points. Hence, both time-consuming and labor-intensive setting/removing of plywood forms and tying of rebars are eliminated. Adjacent panels are connected in a non-mechanical fashion by means of 0.30 m overlaps, formed by offsetting the top and bottom grating layers (Figure 1(a)), thereby preserving a degree of continuity in the longitudinal direction (Figure 1(a) and Figure 2(a)). 3.2 mm thick strips are inserted to cover the SIP plate-to-plate butt joints in order to prevent concrete leaking during casting (Figure 2(b)). When using steel girders, each SIP unit is anchored to the top flanges via stainless steel threaded bolts at every 2.44 m, keeping the bottom reinforcing layer in place with 6.3 mm thick FRP washers (Figure 2(c)). Holes in the SIP plate are drilled on site. When composite action is sought between girders and deck, the panels can be supplied with pre-drilled holes with longitudinal and transverse spacing of 10 cm on-center to accommodate welded shear studs. No cambering of the panels is required to match the roadway crown, which is formed using the finishing machine. The length and layout of the end panels are designed to fit the actual bridge length and accommodate the expansion joints. Since glass FRP is easy to saw-cut, adjustments can be readily made on site (Figure 2(d)).

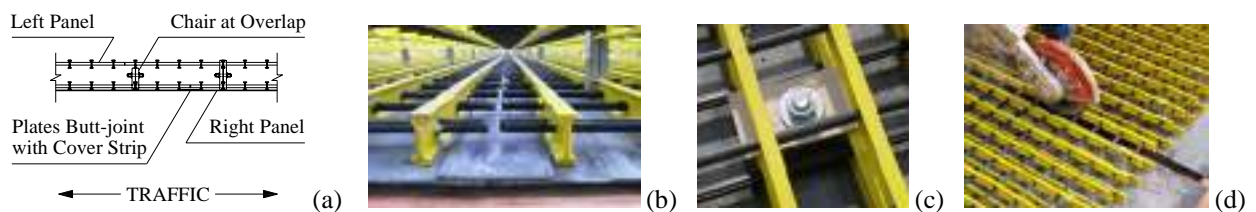


Figure 2: Panel-panel Connection (a, b); Anchoring to Girder (c); End Panels at Expansion Joint (d)

The steel-free reinforcement system is completed with the prefabricated glass FRP rebar cages of a newly designed open post Modified Kansas Corral Rail (Matta and Nanni, 2006). Cut-out pockets in the panels overhang reinforcement facilitate insertion of the post cages at the correct spacing. The continuous top rail reinforcement is made of either 2.44 m or 4.88 m long cages with 1.22 m rebar splices, thought to be rapidly mounted prior to rail forming. Again, the use of lightweight FRP cages greatly simplifies handling and mounting operations, while eliminating on-site rebar tying that is particularly labor-intensive in this case.

2.2 Research and Development

Extensive research and development work during the last 14 years has demonstrated the structural effectiveness of pultruded FRP gratings as internal reinforcement of concrete bridge decks. Two recent pioneer construction projects have been completed in Wisconsin, USA (Bank et al., 2006; Berg et al., 2006). The solution presented herein features the last-generation system, and the first with fully-integrated reinforcement and SIP forms (Ringelstetter et al., 2006). The project Special Provisions included FRP Material Specifications, in compliance with a model specification developed for the FHWA (Bank et al., 2003). Performance Specifications were also defined for the SIP panels by imposing stress and deformation limitations to test panels when simulating typical construction loads, i.e. vertical and lateral loads, in-plane racking, vertical load on overlaps, and wet concrete load (Matta et al., 2005).

The FRP RC open post rail was designed following the ACI 440 guidelines (ACI, 2006) to meet the AASHTO LRFD (AASHTO, 1998) and Standard Specifications (AASHTO, 2002). In the case of the LRFD provisions, where a yield-line approach is recommended to evaluate the equivalent transverse static strength, deformation compatibility was assumed to account for the lack of moment redistribution in FRP RC structures, along with conservative failure scenarios (Matta and Nanni, 2006). In addition, the end posts located at the expansion joints and approach deck, where rail continuity is not provided, were designed to exceed the required crash Test Level 2 strength $F_T = 120$ kN. The deck and rail design was validated through laboratory testing of full-scale deck slabs and rail post/deck connections, which was performed at key steps of the optimization process, and confirmed the significant safety margin of the layout selected for the field implementation (Matta et al., 2005).

3. FIVE-DAY BRIDGE REDECKING

The old Bridge 14802301 (Greene County, MO) slab-on-girder superstructure, built in 1933, was in need of replacement because of severe corrosion-induced degradation of deck and safety appurtenances, and increased load requirements. The load rating was 3.9 t (2004), versus an original design based on a 9.1 t truck load with 30% impact factor. The new superstructure has four symmetrical spans of 11.3 m (exterior) and 10.7 m (interior) length, for a total length of 43.9 m. The cross section comprises four W610×25 steel girders spaced at 1.8 m on-center and acting non-compositely with a 178 mm thick deck. The out-to-out deck and clear roadway width are 7.3 m and 6.7 m, respectively. The girders are continuous over two spans, with a closed expansion joint at the central support.

Transition from research and development to field implementation was conducted in coordination with the manufacturers of the FRP deck and rail reinforcement, and the engineer of record. The construction operations were planned with the contractor parties to minimize the amount of time and work. Construction of the RC deck and railing from the SIP panel installation to rail casting is documented in Figure 3. The job was completed in November 2005 in five days, instead of the typical 2-3 weeks needed for similar steel reinforced bridges built by the contractor. Installation of the deck panels was finalized in six hours during the first day by six workers. During the second day, the 36 rail post cages were mounted, the deck details formed (expansion joints, chamfers, drip edges), and the finishing machine was set. Deck casting and finishing was completed in the third day. The remaining two days were used to mount the open post concrete rail top continuous cages and the formwork, and finally casting.

4. CONCLUSIONS

The first application project of a innovative prefabricated FRP reinforcement for rapid bridge deck construction has been presented. The use of very large-size and lightweight modular stay-in-place panels, comprising a double-layer grating with epoxy-bonded form plates and designed for improved constructibility, eliminates the need of formwork and on-site tying of reinforcing bars. The five-day redecking resulted in over 70% reduction in deck construction time, with a similar reduction in labor cost. Shape and spacing of the reinforcing profiles, devised to facilitate

walking over the three-dimensional assembly, allowed an increase of about 50% in concrete placement productivity while improving safety and working conditions, as confirmed by the field workers.

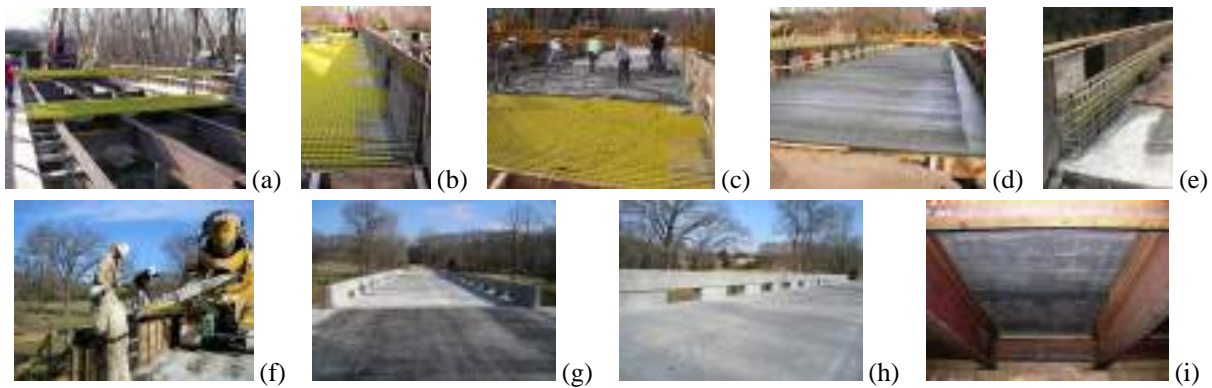


Figure 3: Bridge Redecking Operations: Panels Installation (a); Mounting of Post Cages (b); Deck Casting (c) and Finishing (d); Mounting of Top Rail Cages (e); Rail Casting (f); Finished Superstructure (g-i)

A conservative cost estimate for the deck as-built is \$409/m² (\$38/ft²), of which \$280/m² (\$26/ft²) from the prototype FRP panels delivered to the site. The amount increases to \$483/m² (\$44.9/ft²) including the cost of the open post railing (\$271/m, \$82.6/ft). The competitive potential of the proposed system is also enhanced by the durability of FRP reinforcement, with prospective increased service life and reduced maintenance costs.

5. ACKNOWLEDGEMENTS

The financial support of the US DOT, the UMR UTC on Advanced Materials and NDT Technologies, and the Federal Highway Administration, through the Innovative Bridge Research and Construction Program, is acknowledged. The assistance of Strongwell and Hughes Brothers, industry members of the UMR NSF I-U/CRC “Repair of Building and Bridges with Composites” (RB²C), is also acknowledged. Thanks are due to Greene County, MoDOT, Great River Engineering, Hartman Construction, and Master Contractors LLC, for active support.

6. REFERENCES

- American Association of State Highway and Transportation Officials (1998). *AASHTO LRFD Bridge Design Specifications*, 2nd edition, AASHTO, Washington, DC.
- American Association of State Highway and Transportation Officials (2002). *Standard Specifications for Highway Bridges*, 17th edition, AASHTO, Washington, DC.
- American Concrete Institute Committee 440 (2006). *ACI 440.1R-06 - Guide for the Design and Construction of Concrete Reinforced with FRP Bars*, ACI, Farmington Hills, MI.
- Bank, L.C., Gentry, T.R., Thompson, B.P., and Russell, J.S. (2003). “A Model Specification for FRP Composites for Civil Engineering Structures”. *Construction and Building Materials*, Vol. 17, No. 6-7, pp. 405-437.
- Bank, L.C., Oliva, M.G., Russell, J.S., Jacobson, D.A., Conachen, M.J., Nelson, B., and McMonigal, D. (2006). “Double Layer Prefabricated FRP Grids for Rapid Bridge Deck Construction: Case Study”. *Journal of Composites for Construction*, Vol. 10, No. 3, pp. 204-212.
- Berg, A.C., Bank, L.C., Oliva, M.G., and Russell, J.S. (2006). “Construction and Cost Analysis of an FRP Reinforced Concrete Bridge Deck”. *Construction and Building Materials*, Vol. 20, No. 8, pp. 515-526.
- Matta, F., and Nanni, A. (2006). “Design of Concrete Railing Reinforced with Glass Fiber Reinforced Polymer Bars”, *Proceedings of 2006 ASCE-SEI Structures Congress*, CD-ROM, 9 pp.
- Matta, F., Nanni, A., Galati, N., Ringelstetter, T.E., Bank, L.C., Oliva, M.G., Russell, J.S., Orr, B.M., and Jones, S.N. (2005). “Prefabricated Modular GFRP Reinforcement for Accelerated Construction of Bridge Deck and Rail System”, *Proceedings of FHWA Accelerated Bridge Construction Conference*, pp. 129-134.
- Ringelstetter, T.E., Bank, L.C., Oliva, M.G., Russell, J.S., Matta, F., Nanni, A. (2006). “Development of a Cost-Effective Structural FRP Stay-In-Place Formwork System for Accelerated and Durable Bridge Deck Construction”. *Proceedings of 85th Transportation Research Board Annual Meeting*, CD-ROM #06-2218, 16 pp.

TESTING OF A FRP DECK SYSTEM FOR MOVEABLE BRIDGES

Lei Zhao

Assistant Professor, University of Central Florida, Orlando, Florida, USA

Jignesh S. Vyas

Graduate Research Assistant, University of Central Florida, Orlando, Florida, USA

Marcus Ansley

Chief Structures Research Engineer, Florida Department of Transportation, Tallahassee, Florida, USA

ABSTRACT

Moveable bridges in Florida typically use open steel grid decks due to the weight limitation of 1.2 kN/m^2 . These decks are noisy to ride on, typically less skid resistant than a solid riding surface, and costly to maintain. A new FRP deck system providing a solid roadway surface, satisfying the weight requirements, and having the potential of reducing maintenance cost is being investigated. Fatigue and failure tests were performed on full-size panels in a two-span configuration. Results from the fatigue test showed no signs of degradation after 2 million cycles. The failure tests indicate that a significant factor of safety exists when the AASHTO truck load is considered.

KEYWORDS

FRP composite deck, safety, moveable bridge, fatigue test.

1. INTRODUCTION

It has been reported that approximately 28 percent of America's 600,000 public bridges are either structurally deficient or functionally obsolete (FHWA, 2004). The existing quality of the highway infrastructure has been on a decline, due to insufficient maintenance, heavy loads, unexpected or harsh environmental conditions. This problem has created an urgent need for effective means of structural repair, rehabilitation, and replacement. As a result, there are tremendous opportunities for FRP bridge decks that are corrosion resistant, lightweight, have a high strength to weight ratio and can be easily and rapidly installed. Although FRP material costs are greater than traditional concrete and steel materials, they have shown promise in applications such as decks on moveable bridges, where the advantages of FRP outweigh its high initial costs.

Moveable bridges are bridges across waterways that may lift up or rotate out of the way to allow ships to pass. The weight limitation on the deck for moveable bridges is typically 1.2 kN/m^2 , which makes open steel grid deck the only viable option amongst conventional deck systems. However, these decks present safety and environmental problems, for they are typically less skid resistant than a solid riding surface, create loud noises, and allow debris to fall through the grids. Although the initial cost of construction of a steel grid deck is low, maintenance cost is very high. FRP decks, in comparison, are not only lightweight, but also provide a solid riding surface, which has the potential of improving driving safety, reducing noise levels, and preventing falling debris. Also, the maintenance cost is expected to be significantly lower.

2. DECK SYSTEM DESCRIPTION

The system consists of mainly a pultruded bottom panel and a top plate. The bottom panel, which has four I-sections and a bottom plate, is mechanically fastened to adjacent panels (at their edges) and the top plate (at the top flange of

the I-sections) as shown in the Fig.1. The center-to-center distance between the webs of the I-section is 203 mm. The total deck thickness is 127 mm, which includes a 114-mm-deep bottom panel and a 13-mm-thick top plate.

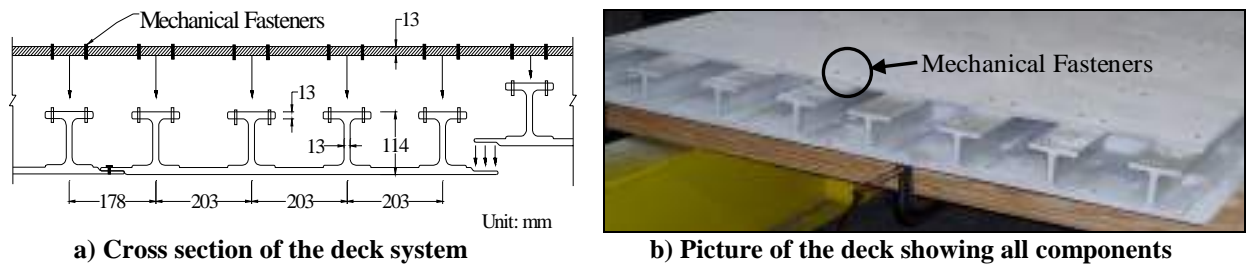


Fig. 1 Deck Assembly

3. TEST SETUP

The prototype deck specimen, which was made of two pultruded sections and top plates, was supported by three steel I-beams that were 1219 mm apart. Loading was applied on top of a polymer-based wear surface that was installed on the top plate of the deck. Fatigue loading was applied simultaneously at locations shown in Fig. 2a up to 80 kN per loading pad. The locations of failure loads in FAIL 1 and FAIL 2 are shown in Fig. 2b. Two failure tests were performed:

- Loading in test FAIL 1 was applied in one span and above two I-beams in the deck (Fig. 2c).
- Loading in test FAIL 2 was applied in the other span and above the center of the web of one of the I-sections in the deck (Fig. 2e).

The deck needed to demonstrate—in both FAIL 1 and FAIL 2—failure loads that are above the AASHTO-required strength of 164 kN. Deflection and strain in the deck during the tests were measured at locations shown in Fig. 2. D0 through D5 and S0 through S13 represent the locations of displacement transducers and strain gages, respectively, mounted on the bottom of the specimen.

4. TEST RESULTS

4.1 Fatigue Test

As shown in Fig. 3a, the progression of the mid-span deflection of the deck stabilized after 1 million cycles, except for one measurement location, D4, where there was a rising trend after 1.0 million cycles. The maximum deflection under the fatigue load grew from 3.7 mm at zero fatigue cycle to 5.2 mm at 2 million fatigue cycles. The long term deflection growth will be studied further and field-monitored on bridges that use this system.

The wear surface showed no signs of cracking or degradation from the fatigue test.

4.2 Failure Tests

The load-deflection and load-strain relations observed from FAIL1 (Fig. 3b) were largely linear-elastic. The peak load and the displacement at the peak load were 370.5 kN and 23.3 mm, respectively. At the peak load, the maximum strain in the bottom plate dropped from 4800 $\mu\epsilon$ to 3500 $\mu\epsilon$ (Fig. 4a), indicating a delamination in the panel. Loading was terminated to avoid damage to the other span, which was to be tested in FAIL 2.

The load-deflection and load-strain relations observed from FAIL 2 (Fig. 3b) were largely linear-elastic up to 313.6 kN, when a load-drop of approximately 12% occurred. When loading continued, the specimen was able to regain the load level of the first peak and eventually failed from web buckling at a load of 396.8 kN and deflection of 48.9mm. The system was able to achieve significant deflection after the first peak. Post-test inspection revealed delamination between the web and the bottom flange of the deck as shown in Fig. 4b. The transverse displacement and strain profiles (Fig.5) indicate that the load is not effectively distributed in the transverse direction. The I-sections directly under the loading pad carried majority of the load.

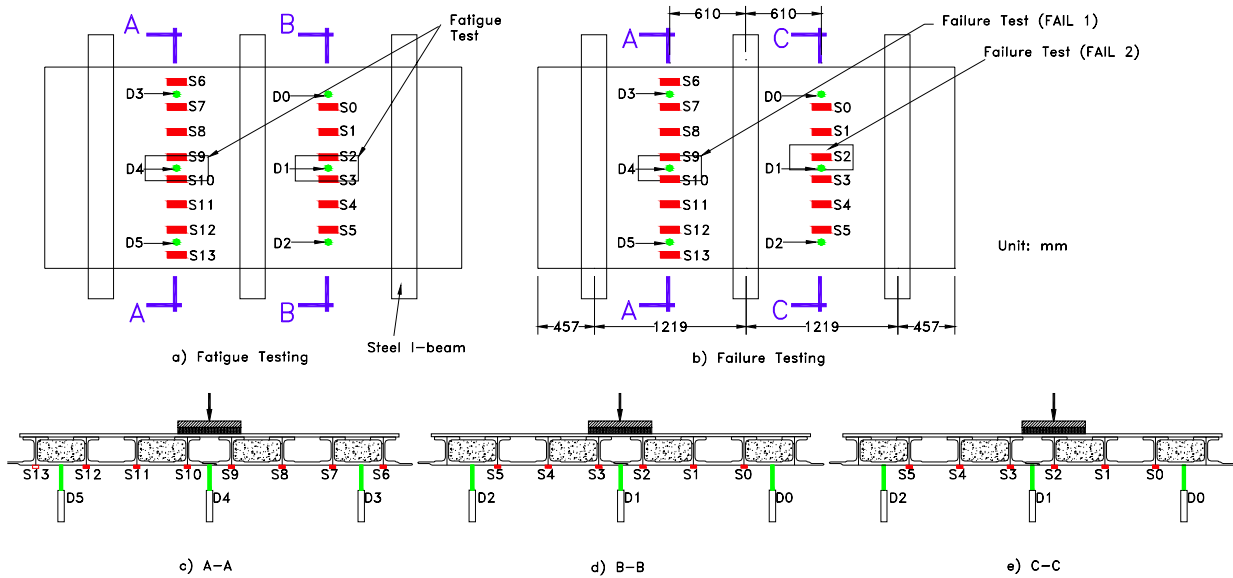


Fig. 2 Loading and Transducer Configuration

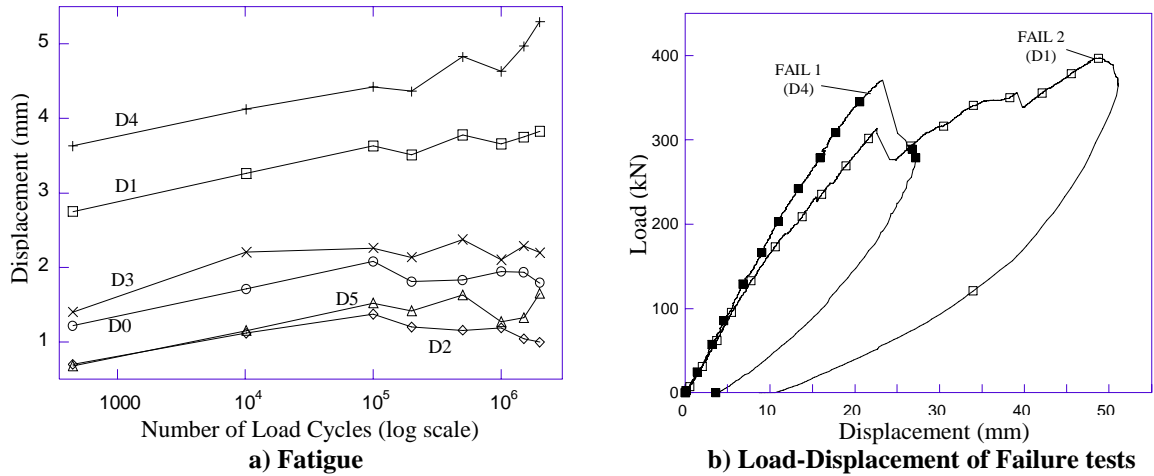


Fig. 3 Overall Displacement Response

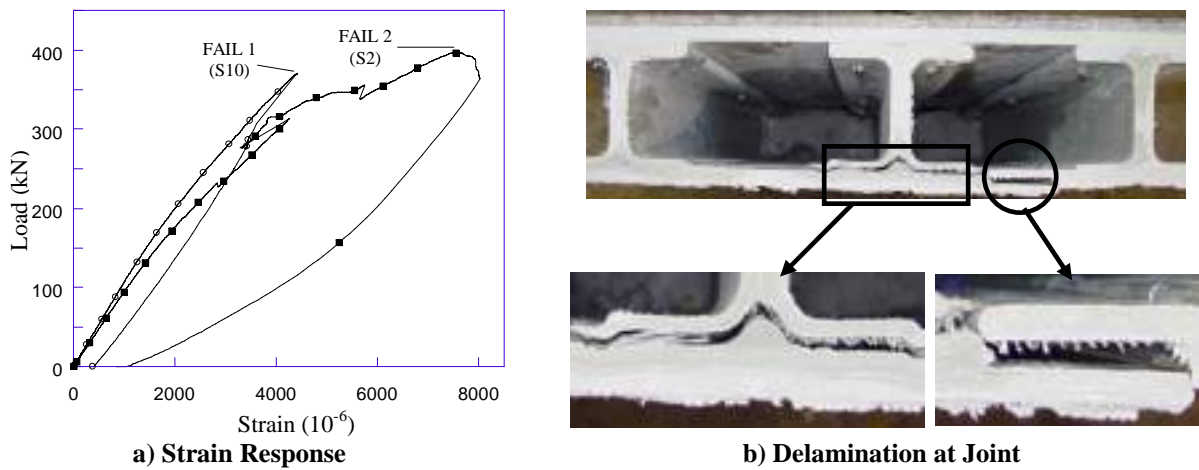


Fig. 4 Strain Response and Failure Mode

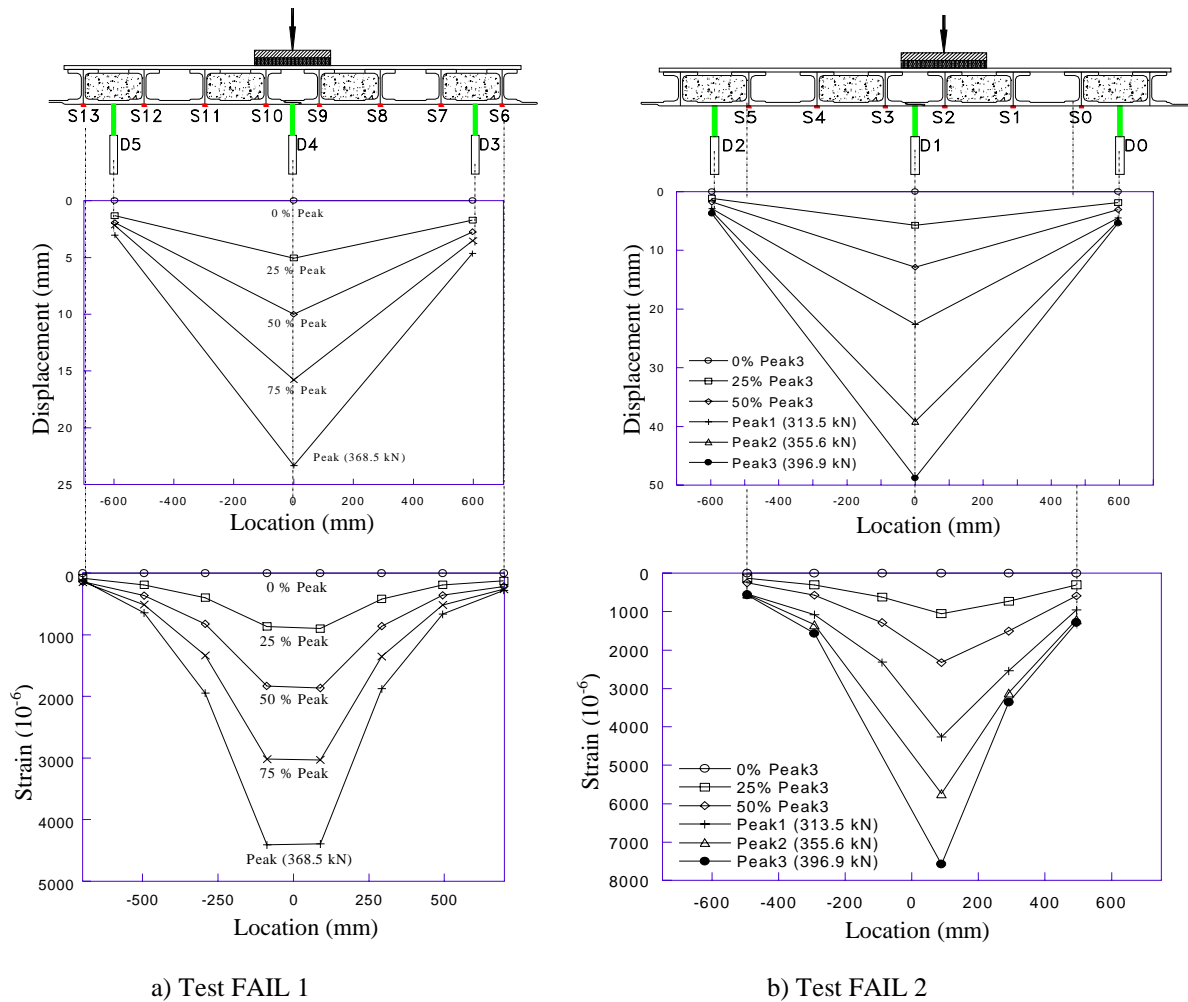


Fig. 5 Displacement and Strain Distribution Profiles

5. CONCLUSION

- The deck system displayed no noticeable signs of degradation after 2 million fatigue cycles. The progression of the deck mid-span deflections, on a log-scale, stabilized after 1 million cycles, except for one location (D4) where deflection showed a slight rising trend. The maximum deflection under the fatigue load was 5.2 mm.
- The peak loads measured from the FAIL 1 and FAIL 2 tests were 370.5 kN and 396.8 kN, respectively, which were 2.3 and 2.42 times the AASHTO requirement for factored load level.
- In FAIL 2, the deck system showed significant deflection capability beyond the first load drop caused by delamination.

6. ACKNOWLEDGEMENT

The authors would like to express their appreciation to Mr. Frank Cobb, Mr. Paul Tighe, Mr. David Allen and Mr. Steve Eudy at the Florida DOT Structures Laboratory for their technical assistance during the testing.

7. REFERENCES

FHWA, "Status of the Nation's Highways, Bridges, and Transit: 2004 Conditions and Performance Report".

Part IV. Composites Systems

URBAN LIGHT TRANSPORT (ULTRA) GUIDEWAY PROJECT

Thanongsak Imjai

(PhD student, Department of Civil & Structural Engineering, Sheffield University, Sheffield, UK)

Maurizio Guadagnini

(Lecturer, Department of Civil & Structural Engineering, Sheffield University, Sheffield, UK)

Kypros Pilakoutas

(Professor, Department of Civil & Structural Engineering, Sheffield University, Sheffield, UK)

Peter Waldron

(Professor, Department of Civil & Structural Engineering, Sheffield University, Sheffield, UK)

ABSTRACT

This paper presents one of the case studies that was examined during the European funded CRAFT RTD Project CurvedNFR. A 6m long concrete plank reinforced with thermosetting FRP bars as longitudinal reinforcement and thermoplastic FRP strips as shear reinforcement was manufactured and tested in the structural laboratory of the University of Sheffield. The use of FRPs allowed the reduction in the required concrete cover (hence a reduction in the overall depth and total weight) and will guarantee the construction of a highly durable structure, thereby minimising the need of structural maintenance. This study shows that current design recommendations for FRP RC structures can be effectively used to predict deflection and crack width of the RC plank at service load. It is also found that serviceability limit state, such as deflection and crack width, control the design criteria.

KEYWORDS

Fibre Reinforced Composite, Reinforced Concrete, Crack width, Deflection

1. INTRODUCTION

The European funded CRAFT RTD project CurvedNFR (2003) was established in 2003 with the aim of developing materials, methodology, and manufacturing process for low-cost, curved fibre reinforced plastics (FRPs) for concrete structures. The ULTra guideway project has been employed as a case study to design and analyse a RC plank using FRPs as internal reinforcements. Important aspects of the project are: 1) analysis of the environmental impact of the infrastructure; 2) visual intrusion from the overhead portions of the structure (Figure 1-right), and 3) evaluation of the durability of the structural elements. A full scale specimen of the RC plank was cast and tested at the University of Sheffield under different load arrangements to simulate the load conditions that the structure will be subjected to during its service life. GFRP thermosetting bars were used as longitudinal reinforcement whilst GFRP thermoplastic strips were used to manufacture the shear reinforcement. The preliminary design of the beam was carried out according to the design recommendations proposed by the ACI 440 committee (ACI 440.1R, 2003). The ULTra project is briefly introduced in the following along with the methodology that was followed for designing and testing the FRP RC plank.

2. ULTRA GUIDEWAY PROJECT

2.1 The ULTra system

Transport by conventional means involves energy use, resource use and emission output which cannot be regarded as sustainable. Current transport is dominated by the car. This provides the flexible personal transport required by

modern forms of cities, but is widely recognised as unsustainable. Current public transport is poorly accepted. Unfortunately, analysis also shows that current forms of public transport offer little, or even negative, benefit in sustainability over the car. A new transport system has been devised to meet the need for transport which is both effective and sustainable. This transport system, ULTra, offers an advanced form of personal transport system that uses a fleet of low power, electrically driven vehicles on a dedicated guideway network of routes (Figure 1).



Figure 1: Driverless automatic ULTra vehicle (left) and overhead portion of the ULTra guideway (right)

In contrast to previous forms of public transport, there is no waiting, no stopping and no transfers within the system. In many circumstances, it can offer better transport than available by other means. ULTra has been designed to demanding sustainability requirements. Typically, ULTra provides a reduction by a factor of 3 in energy use and emissions output over existing forms of transport. ULTra is also complementary to existing forms of transport. By providing a network link to major rail or bus stations, it can improve the attraction of current transport services. Evaluations undertaken for the Department of Transport and supported by recent questionnaire studies, suggest that a comprehensive ULTra system could attract 25-30% of present car drivers. ULTra is now undergoing engineering development funded by the Department of Transport, Local Government and the Regions. It is believed that the system will offer a new approach to public transport with a real prospect of significant gains in effectiveness and sustainability.

2.2 Design concept

The geometry of the cross section of the reinforced concrete guideway has been optimised during the design and an attempt was made to keep the overall depth of the structural elements down to minimal values to reduce visual intrusion (Figure 2). The design process focused on providing sufficient reinforcement to resist the applied loads (Ultimate Limit State Design) and to control deflection and cracking under operating conditions (Service Limit State Design). The design procedure suggested in the ACI 440.3R document was employed to determine the necessary amount of both flexural and shear reinforcement. These include bending and shear design procedures (Imjai et al., 2004). For design considerations, standard sectional analysis was used to determine the flexural properties of the FRP RC section. The RC section was designed to fail due to concrete crushing in compression (over-reinforced section) as the lack of ductility of the composite reinforcement can not provide warning of impending failure. The nominal flexural strength of the section was determined based on strain compatibility, internal force equilibrium, and the mode of failure. According to the design calculations, it is found that the planks under flexural loads can meet the design requirements. The shear capacity of the RC plank provided by 4x10 mm with a spacing of 50 mm thermoplastic composite strips is optimised according to ACI code. It is also found that serviceability limit states such as deflection and crack widths control the design.

3. TEST PROGRAMME

3.1 Beam preparation and material properties

Glass FRP thermosetting Eurocrete bars ($f_{fu}=700$ MPa, $\epsilon_{fu}=0.017$ and $E_f=45$ GPa) were used as longitudinal reinforcing material, and shear reinforcement was provided in the form of links manufactured from FRP thermoplastic Plytron strips ($f_{fu}=720$ MPa, $\epsilon_{fu}=0.019$ and $E_f=28$ GPa) that were produced by Plytron GmbH Ltd. Owing to the physical characteristics of FRP, the overall weight of the reinforcing cage was only about 13.5 Kg, which amounts to about 2% of the total weight of the concrete. By comparison, a similar reinforcing cage made of

steel reinforcement would weight approximately 50 Kg (8% of the total weight of the concrete). The thermoplastic shear links were bent in the laboratory at the University of Sheffield by heating the composite with an air gun at a controlled temperature and shaping it around a custom made mould. The geometry of the specimen is illustrated in Figure 2b along with a schematic view of the cross section showing the reinforcement details.

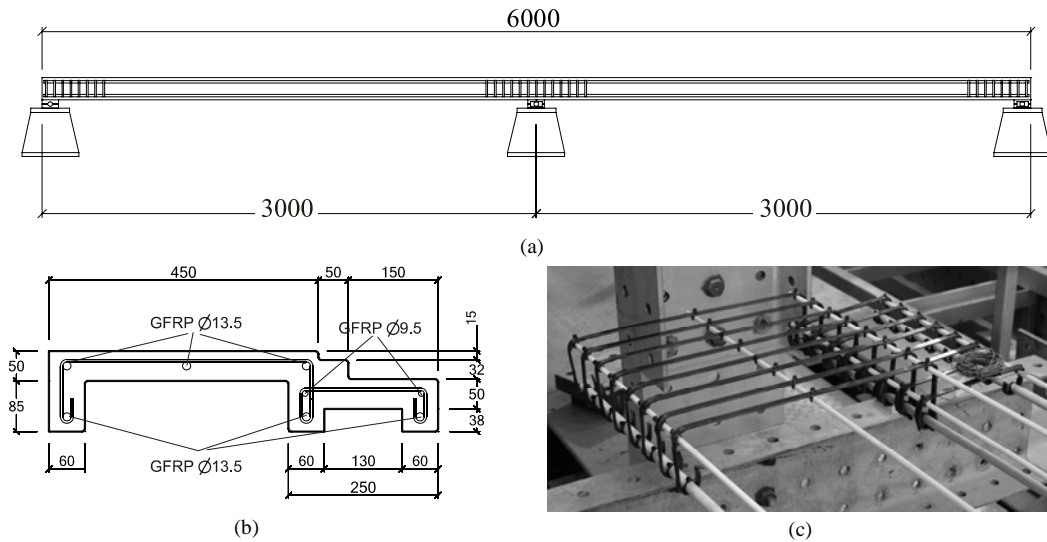


Figure 2: a) Reinforcement arrangement and b) cross section of the ULTra guideway. c) Detailing of the thermoplastic shear reinforcement at one end of the plank

Foil-type electric strain-gauges were positioned at various locations along the flexural and shear reinforcement to monitor variations in strains. The positions where the strain gauges were to be located were accurately marked on each bar and link and the surrounding areas were appropriately prepared to guarantee a successful installation of the gauges. Prior to the application of the gauges on the GFRP bars, glue was used to seal the surface. Cement glue was used to attach the strain gauges to the bars and electrical wires were soldered to the terminal of each gauge for subsequent connection to the data logger. A ready mixed concrete obtained from a local supplier was used to manufacture the test specimens. The specifications of the mix were: concrete C40 with 10 mm maximum aggregate size and cement type OPC with a slump of 100 mm.

3.2 Test set-up

Figure 3 shows the loading patterns to which the beam was subjected during two successive phases of testing. Load case 1 (Figure 3a) was applied to generate the maximum positive bending moment in the RH span, whilst the load case 2 (Figure 3b) was applied to generate the maximum negative moment over the central support. In both cases, the load was applied in increments of about 1 kN. At each load step, cracks were marked and the widths of selected target cracks were measured. Overall deflections of the beam were measured at different locations using several Linear Variable Displacement Transducers (LVDTs).

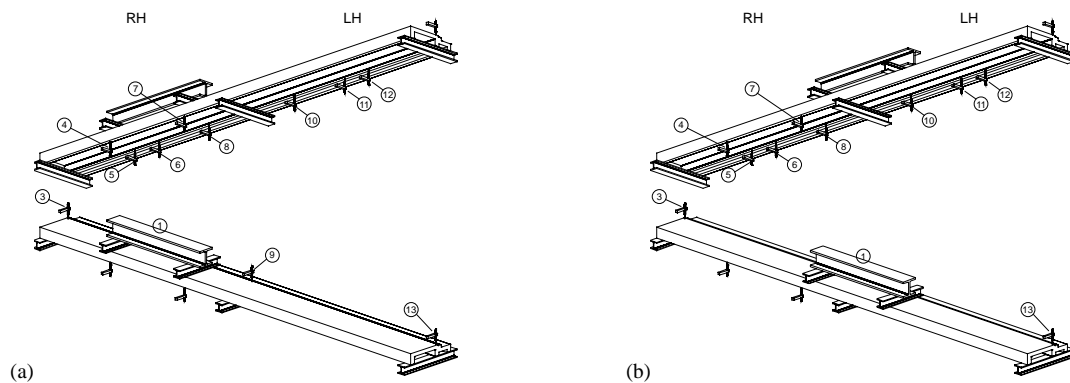


Figure 3: Test set-up and instrumentation for a) load case 1 and b) load case 2

4. DISCUSSION OF THE RESULTS

Three load cycles were performed at load levels corresponding to: a) the load induced by standard passenger-carrying vehicles (service load 1, about 5 kN); b) the load induced by a road sweeper machine (service load 2, about 10 kN); and c) the design load (1.5 times the maximum service load, about 15 kN). In the case of load case 2, the load was further increased to about 50 kN with no severe repercussions on the structural integrity of the beam. The load-displacement behaviours for both load cases are shown in Figure 4. The overall behaviour of the beam and the crack pattern observed during testing confirmed that adequate shear provision was achieved by using the custom made thermoplastic links (see Table 1).

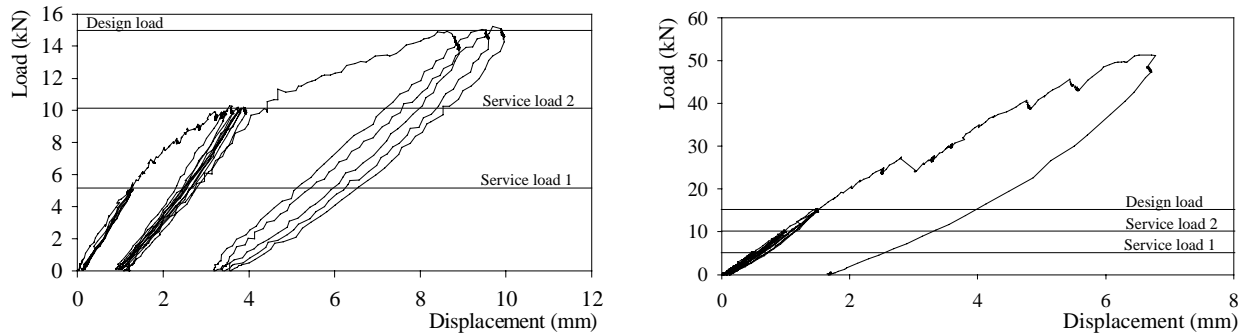


Figure 4: Load-deflection response of ULTra beam: load condition 1 (left) and load condition 2 (right)

Table 1 shows a comparison of the results obtained from the test performed during the first phase of testing (load case 1) with the values predicted according to the recommendations proposed by the American Concrete Institute for the design of concrete structures reinforced with Fibre Reinforced Polymer Reinforcement (ACI 440.1R.03). This table shows clearly that conservative values are generally predicted by the design recommendations and that the tested FRP reinforced beam meets all of the serviceability requirements.

Table 1: Test results and design equation predictions: Load condition 1

Load stage	Serviceability limits		Predicted values		Experimental values	
	Max crack width (mm)	Max deflection (mm)	Max crack width (mm)	Max deflection (mm)	Max crack width (mm)	Max deflection (mm)
Service load 1	0.5	12.5	0.15	4.75	0.10	1.3
Service load 2	0.5	12.5	0.29	9.19	0.25	3.6
Design load	-	-	0.41	11.97	0.35	8.8

5. REFERENCES

- American Concrete Institute (ACI). (2003). "Guide for the Design and Construction of Concrete Reinforced with FRP Bars ACI 440.1R-03", ACI Committee 440, Farmington Hills, MI, USA.
- CurvedNFR (2003). "Cost effective Curved Polymer Composite Rebar". CRAFT RTD European funded project, CRAFT GIST-CT-2002-50365, <http://www.curvednfr.com>
- Imjai T., Guadagnini M., Pilakoutas K., (2004). Case study: *Urban Light Transport (ULTra) guideway Project*, Technical Report, Centre for Cement and Concrete, The University of Sheffield, Sheffield, UK, pp. 23.

COMPOSITE SANDWICH WALL PANELS FOR BUILDING APPLICATIONS

Waleed Shawkat

Master of Science Candidate, Queen's University, Kingston, Ontario, Canada

Hart Honickman

NSERC Undergraduate Researcher, Queen's University, Kingston, Ontario, Canada

Amir Fam

Associate Professor and Canada Research Chair in innovative and retrofitted structures, Queen's University, Kingston, Ontario, Canada

ABSTRACT

This study examines the structural performance of a novel composite panel consisting of a polyurethane foam core sandwiched between two layers of carbon fibre-reinforced polymer (CFRP) skin. Ten panels were tested as one-way slabs, using both four-point bending and three-point bending configurations. The study was intended to examine the consistency and repeatability of test results of similar panels, as well as investigate the effects of shear span-to-thickness ratio, moisture absorption, and the effect of a masonry pattern coating applied to one face of the panel. The flexural strengths and stiffnesses and various failure modes have been evaluated. The panels were also compared to conventional reinforced concrete (RC) panels.

KEYWORDS

Composites, Sandwich Panel, FRP, Polyurethane, Cladding.

INTRODUCTION

The primary purpose of exterior cladding is to provide shelter from rain and snow, as well as providing thermal insulation. It is also responsible for transferring wind loads to the internal skeleton of a building. Since conventional cladding is composed of steel reinforced concrete, corrosion is a major concern especially if the cladding is placed in a harsh environment. The new sandwich panels are polymer based, thus alleviating this concern. Also, they are significantly lighter in weight.

The panels are constructed using a rigid polyurethane foam core sandwiched between two layers of carbon fiber reinforced polymer (CFRP). The CFRP layers resist the tensile and compressive stresses resulting from the flexure induced by wind loading. The polyurethane core resists shear stresses and also contributes to the moment of inertia of the panel's cross section by acting as a spacer that positions the CFRP skins further apart.

In order to fabricate these panels, the CFRP skins are first adhered to the upper and lower faces of a formwork. The polyurethane foam is then injected into the void between the CFRP skins as a two-part liquid. As the two parts of this liquid react, the chemical expands into a foam-like substance, hardens, and adheres to the CFRP skins. Because of this expansion, the polyurethane foam applies pressure to the CFRP skins as it hardens, which helps improve the bond.

Five large panels were trimmed and each was cut in half in order to create ten specimens for testing. Three of the panels were approximately 68 mm thick and had a smooth white marine grade gel-coat applied to the outer surface of the CFRP skins, while the remaining two panels were approximately 55 mm thick and had a masonry-like patterned coating on one face. Table 1 shows partner specimens cut from the same panel.

This paper includes brief description of the test specimens, test parameters, test setups, instrumentation, and test results. The paper also includes evaluation of flexural strength and stiffness of the panels and comparisons with conventional reinforced concrete panels.

TEST SETUPS, INSTRUMENTATION AND PROCEDURES

Specimens #1, 2, 3, 5, 6, 9, and 10 were tested in four-point bending. A span of 1400 mm and width of 300 mm was used for specimens #1, 2, 3, 5, and 6 and a span of 1360 mm was used for specimens #9 and 10 with the full width of 320 mm being loaded using two line loads applied at one and two thirds of the span of the panel. The line loads were applied using two rollers resting on rigid steel strips. Teflon sheets were placed under the steel strip in order to protect the panels from stress concentrations. The specimens were supported along the full width at both ends. Longitudinal strains in the CFRP skins were monitored using four strain gages. They were configured such that there were two strain gages at the mid span of the top face (compression) and an identical setup on the bottom face (tension) of each panel. Mid-span deflections of each panel were monitored using two linear potentiometers.

In order to increase the chances of flexural failure (rather than shear failure) specimens #4, 7, and 8 were tested in three-point bending. A span of 1400 mm was used for specimen #4 and a span of 1360 mm was used for specimens #7 and 8, with loads applied at the midspan of the panels. Instrumentation was similar to the aforementioned tests.

Prior to its flexural test, specimen #6 underwent a water absorption investigation during which it was completely submerged under fresh water for approximately 90 days. The specimen was periodically removed briefly from the water in order to measure its weight so that the water absorption rate could be monitored. This procedure was derived from ASTM C272-01 and ASTM D570-98.

TEST RESULTS, FAILURE MODES AND EFFECT OF VARIOUS PARAMETERS

Table 1 provides a summary of the test types and results in terms of the span (L), the ultimate load (P_u), ultimate moment (M_u), ultimate deflection (δ_u), ultimate strains in the upper and lower CFRP skins (ϵ_u), and failure modes.

As shown in Fig. 1(a), the ultimate loads and deflections of specimens #2 and 3 suggest good consistency within the panel from which they were cut. Both specimens ultimately failed by outward buckling of their upper CFRP skins. The ultimate loads, deflections, and failure modes of specimens #7 and 8, however, were quite dissimilar from each other, see Fig. 1(a). Specimen #7 exhibited outward buckling of its upper skin, whereas specimen #8 exhibited a shear failure within its polyurethane core.

Specimens #1, 2 and 5 were cut from three different panels, yet they were all from the same production batch. A comparison of the load-deflection responses of the three specimens is provided in Fig. 1(a). The ultimate loads and deflections of specimens #1, 2 and 5 suggest significant inconsistencies between the panels. It should be noted that specimens #1 and 5 both failed in shear within the foam at comparable load levels, which suggests comparable quality; whereas specimen #2 failed by CFRP skin buckling in compression at a substantially higher load.

Table 1: Summary of Test Specimens and Results

Specimen	1	2	3	4	5	6	7	8	9	10
Partner	6	3	2	5	4	1	8	7	10	9
Test Type	4-Point	4-Point	4-Point	3-Point	4-Point	4-Point	3-Point	3-Point	4-Point	4-Point
span	mm	1400	1400	1400	1400	1400	1360	1360	1360	1360
width	mm	300	300	300	300	300	319	319	320	320
P_u	kN	5	13.1	14	18.65	6.4	7.7	7.1	4.25	12.6
δ_u	mm	19.4	24.6	24.8	36.3	15.8	30.9	28.9	48.1	51.6
M_u	kN.m	1.17	3.06	3.27	6.53	1.49	1.80	2.41	1.45	2.86
Failure Mode	Foam shear	Skin buckling	flexure	flexure	Foam shear	flexure	flexure	shear	shear	flexure
$\epsilon_{u\ top}$		-1670	-3148	-3180	-6810	-1384	-1740	-2030	-600	-1800
$\epsilon_{u\ bottom}$		1120	2775	2967	5945	1461	1941	3324	2904	4340

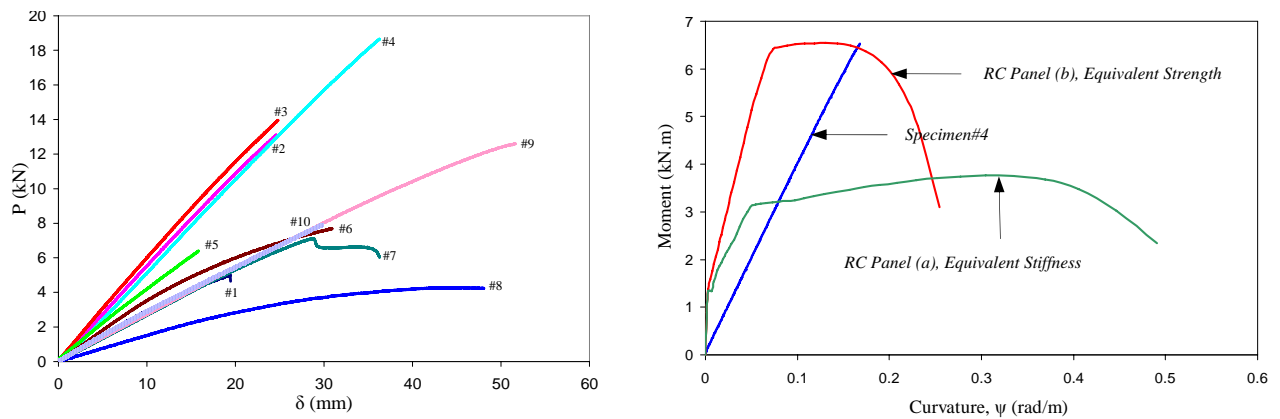
Effect of Shear Span-to-Depth Ratio (a/t)

The effect of shear span (a)-to-depth (t) ratio (a/t) can be studied through specimens #4 and 5. As shown in Table 1, specimen #4 resisted substantially higher moment than specimen #5. This is attributed to their respective failure modes. Specimen #5 failed in shear, whereas specimen #4 was the only specimen in this study to experience a pure flexural strength failure mode by crushing of the upper CFRP skin. Therefore, the maximum strain of the upper skin of specimen #4 represents the compressive failure strain of the CFRP skin since it was utilized to its full capacity. This was certainly a more ideal performance than other specimens that failed prematurely in shear or skin buckling because it demonstrated the true potential of these composite panels. It should be noted that the shear force at ultimate flexural failure of specimen #4 was substantially higher than that of specimen #5 at its shear failure, yet specimen #4 did not fail in shear. This can likely be attributed to poor foam quality, which may have triggered an early shear failure in specimen #5. The performances of specimens #4 and 5, which were cut from the same panel, also indicates a lack of quality consistency within panels.

The effect of (a/t) can also be studied through specimens #7 and 9, although these specimens were cut from different panels. As shown in Table 1, specimen #7 and 9 had somewhat comparable moment resistances despite their dissimilar failure modes. Specimen #7 failed by upper skin buckling, whereas specimen #9 failed in shear. Undulations in the upper skin of specimen #7 (caused by the application of its masonry-pattern coating) may have invited a buckling failure of the upper CFRP skin prior to reaching its compressive strength.

Effect of Moisture Absorption

Comparing specimens #1 and 6, which were cut from the same panel and both were tested under identical four-point bending configuration. Specimen #1 was tested in dry conditions, whereas specimen #6 was submerged in water for about three months and then tested while still wet. A comparison of the load-deflection responses of the two specimens is provided in Fig. 1(a). It is quite interesting to notice that the ultimate load of specimen #6 was higher than that of specimen #1, despite its moisture absorption. It should be noted, however, that failure modes were different. Specimen #1 failed in shear as described earlier, whereas specimen #6 failed by outward buckling of the compression CFRP skin. This failure mode is in fact quite similar to those of specimens #2 and 3, which were tested also in four-point bending but failed at substantially higher loads. The responses in Fig. 1(a) indicate that specimen #6 was also slightly stiffer than specimen #1. It is difficult to assess the effect of moisture on behavior in this case, due to the potential for large variability among the specimens.



(a) Load vs. Deflection for Tested Specimens

(b) Composite Panel vs. Virtual RC Panels

Figure 1: Flexural Behaviour of Wall Panels

Effect of Orientation of Masonry Pattern Coat

Specimens #9 and 10 were produced from the same large panel and were both tested using an identical four-point bending configuration, except that the masonry pattern of specimen #9 was located on the top (in compression), to simulate a wind pressure on a building, whereas that in specimen #10 was located on the bottom (in tension), to simulate a wind suction condition. A comparison of the load-deflection responses of the two specimens is provided in Fig. 1(a). The ultimate loads of specimens #9 and 10 and the deflections at ultimate suggest that having the

masonry pattern in compression certainly has a strengthening effect. Specimen #9 failed in shear within the polyurethane foam as discussed earlier, however specimen #10 failed by buckling of the upper CFRP skin at a lower load. It is clear that the presence of the masonry pattern in compression have prevented the skin buckling in specimen #9 and forced the shear failure mode. Fig. 2 shows a summary of failure modes.



(a) Shear failure



(b) Skin buckling



(c) Skin crushing

Figure 2: Failure Modes

COMPARISON BETWEEN SANDWICH AND REINFORCED CONCRETE PANELS

An analytical model was used to predict the flexural responses of virtual RC panels, designed according to CSA A23.3 to be compared to specimens #4. The RC panels were assumed to be 100 mm thick and reinforced with a single layer of rebar at their mid-thickness. The concrete compressive strength and steel rebar yield strength are assumed 35 MPa and 400 MPa, respectively. The width of the RC panels was assumed equal to that of the composite panels, 300 mm. The objective of this study was to establish the steel reinforcement configuration in the RC panels that would be required to satisfy two different criteria, namely (a) the same flexural stiffness after cracking and (b) the same ultimate moment capacity as the composite panels, see Fig. 1(b).

For the RC panels, Response2000 (Bentz, 2000) was used to establish the moment-curvature responses. It was found that 180 mm² steel reinforcement is needed to satisfy the similar stiffness criterion for RC panel (a). This reinforced ratio is equivalent to 6 No.10/m. RC panel (b), on the other hand, was designed to provide the same moment capacity, by using 390 mm² steel reinforcement, which is essentially 13 No. 10/m. In this case, the stiffness is higher than that of the composite panel and the ductility of the RC panel (b) is substantially lower than that of RC panel (a).

CONCLUSIONS

This study has shown that composite sandwich panels have a great potential and are quite promising as an alternative for reinforced concrete cladding systems. It was noticed that the structural performance is sensitive to the quality of the panel, particularly the integrity of the polyurethane foam core. The following conclusions are drawn:

1. The composite panels tested in this study are 6 to 7 times lighter in weight than conventional reinforced concrete (RC) panels of the same size and are 14 times lighter than a typical 100 mm thick conventional RC panel of the same flexural strength or stiffness.
2. The masonry pattern coat provided a strengthening effect and forced a shear failure mode when positioned in compression (i.e. simulating wind pressure loading), as the flexural strength was substantially higher than that of a panel having the masonry pattern on the tension side (i.e. simulating a wind suction effect), which failed by buckling of the CFRP skin in compression. There was, however, no noticeable effect on the stiffness.
3. The most common failure modes were the outward buckling of the CFRP skin in compression and shear failure within the polyurethane foam core by diagonal tension.

ACKNOWLEDGMENT

The authors wish to acknowledge financial support provided by Res-Precast Inc and Materials and Manufacturing Ontario (MMO).

REFERENCES

- American Society for Testing and Materials, ASTM standards 2005
Bentz, E. (2000) Response 2000, Computer Program for reinforced concrete sections, University of Toronto.
Code for the Design of Concrete Structures for Buildings, Canadian Standard Association (CSA), CSA A23.3-94

BEHAVIOR OF JUTE/ EPOXY COMPOSITE CURVED I-BEAM UNDER BENDING LOADING

Asad A. Khalid

*Department of Mechanical Engineering, Faculty of Engineering,
IIUM International University Malaysia, 53100, Gombak, Malaysia*

ABSTRACT

In this paper experimental work on Jute/ epoxy composite curved beam subjected to four point bending has been carried out. Two, Four, six and eight layers of woven fabric jute/ epoxy composite curved I-beams were fabricated by hand lay-up moulding fabrication process. The test specimen is a continuous Curved I-beam consisting of a central circular 90° region connected by two 200 mm straight legs. The load-displacement response was obtained and the energy absorption values were calculated for all the composite curved I-beams. Glass/ epoxy composite curved beams were also fabricated and tested for comparison purpose. The woven fabric composite curved beams mechanical properties have been obtained from tensile tests. Results from this investigation show that the bending load required for jute/epoxy composite curved I-beams under four point bending was less 21% than glass/ epoxy. The first crushing loads difference between jute and glass/ epoxy fell in the range of 19%-24%. It has been found that the failure mechanism of jute/ epoxy specimens is similar to that of glass/ epoxy. Specimens failed after the initial crushing load localized at the lower part of the beam center region. Then, it followed by the matrix and fiber break. Delamination was also occurred on both materials tested.

KEYWORDS: Bending loading; Jute fiber; Glass fiber; Epoxy; Composite curved beam.

1. INTRODUCTION

Composite materials have a wide range of applications in aerospace, automotive and marine structures, because of their high stiffness and strength with respect to their weight. In addition, composite materials have high corrosion resistance, thermal resistively and considered as non- conductive materials. Since the 1990s, natural fiber composites are emerging as realistic alternatives to glass-reinforced composites in many applications [1]. Natural fibers possess many advantages over glass fibers, such as lower density, lower cost and recycle ability, they are not totally free of problems On the other hand more carbon dioxide neutrality of natural fibers is particularly attractive. So far good number of automotive components previously made with glass fiber composites are now being manufactured using environmentally friendly composites [2]. Natural fibers come from renewable resources and are relatively inexpensive. These fibers are now well recognized to impart good reinforcing capability to composites. While their tensile strengths and moduli are generally inferior to those of polymeric fibers, they often exhibit significantly larger elongation giving them better damage tolerance [3]. Jute Natural fiber is one of the most widely used natural fibers and is very easy cultivated. Jute is a promising reinforcement for use in composite on account of its low cost, low density, high specific strength and modulus, no health risk, easy availability and renews ability. Among all the natural fiber reinforcing materials Jute is

relatively inexpensive and commercially available in the required form [4]. The concept of curved beam construction typically involves stiff and strong face sheets bonded to a thick low-density core. I-beam is widely used in weight reduction. These shapes very often contain curved segments. The simplest case of such a structure, i.e., a curved sandwich beam loaded in pure bending [5].

The main objective of this present investigation is to study the behavior of Jute/ epoxy composite curved I-beam under four point bending. Also to compare the results obtained with glass/ epoxy Curved beam. The comparison will include the effect of bending load on displacement, flexural stress-strain relation, strains at the mid-span of the beam. failure mechanism of the tested composite curved I-beams have been studied also.

2. EXPERIMENTAL WORK

2.1 Materials and Specimens Fabrication

The test specimen was designed based on four-point flexure principle as outlined in ASTM Standard D-6415-99 [6]. Curved I-beams were fabricated by using foam mould covered with sheets of plastics. Hand lay-up molding process has been used to fabricate the specimens. Woven roving jute and glass fibers were used as a reinforced materials and matrix of epoxy resin (Leco 811-563-103) with hardener (Leco 811-563-104) as matrix material with 8:1 ratio, respectively Curved Composite I-beam was of 50 mm height and 50 mm flange width.. The test specimen is a continuous Curved I-beam consisting of a central circular 90° region connected by two 200 mm straight legs tensile test specimens were fabricated also to obtain the required mechanical properties. The mechanical properties for jute/epoxy specimens were $E_{11}=E_{22}= 17.68 \text{ GN/m}^2$, $E_{33}= 8.97 \text{ GN/m}^2$, $G_{13}=G_{23}= 2.86 \text{ GN/m}^2$, $G_{12}= 3.02 \text{ GN/m}^2$, $\nu_{13}=\nu_{23}= 0.24$ and $\nu_{12}= 0.29$. While the properties for the glass/epoxy specimens were $E_{11}=E_{22}= 52.25 \text{ GN/m}^2$, $E_{33}= 12.33 \text{ GN/m}^2$, $G_{13}=G_{23}= 4.2 \text{ GN/m}^2$, $G_{12}= 3.58 \text{ GN/m}^2$, $\nu_{13}=\nu_{23}= 0.25$ and $\nu_{12}= 0.35$. The densities of jute and glass fibers were 1.6 and 2.12 kg/m³ respectively. Samples of the fabricated moulds and composite curved I-beams are shown in Figures 1 and 2 respectively.



Fig. 1. Samples of the fabricated moulds



(a) glass/ epoxy



(b) Jute/ epoxy

Fig. 2. Samples of the fabricated composite curved I-beams

2.2 Test Set-up

A computer controlled servo-hydraulic instron machine type 5582 with a load capacity of 100 kN has been used to perform the quasi static bending load. The crosshead speed was adjusted at 5 mm/min, Figure 3 show the test set-up of the composite I-curved beam under four-point bending. On the other hand, two strain gauges, each of 3 mm gauge length was fixed at the middle of the beam on the bottom and upper surfaces to obtain the longitudinal strain variation. The strains gauges were bonded to the surface of the tube using CN adhesive.

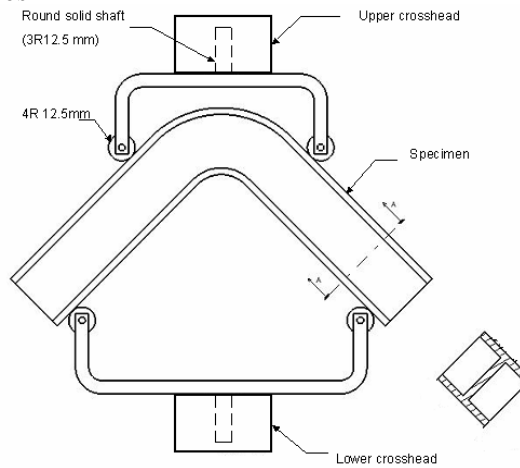


Fig. 3. Test set-up for the curved I-beam

3. RESULTS

Results from this investigation include the load-displacement response for woven roving Jute/ epoxy and glass/ epoxy composite curved I-beams under four point bending. The effect of materials used on initial failure load was investigated. Strain-load relations at the middle surface of the beams were also drawn. Photographs of the tested curved I- beams during loading have been taken to composite tube at the first failure load. Due to the page limitation, results are summarized below.

3.1 Load-displacement

The load displacement relation has been obtained directly from the testing machine. A universal testing machine (Digital Instron Model 8500) with 250 kN load capacity has been used. These tests were all carried out at a speed of 5 mm/min. The effect of number of layers on the initial crushing load is shown in Figure 4. Two, four, six and eight layers of composite curved I -beams were considered for the study. Figure 5 show the strain-load relation up to initial failure of the tested composite curved beams.

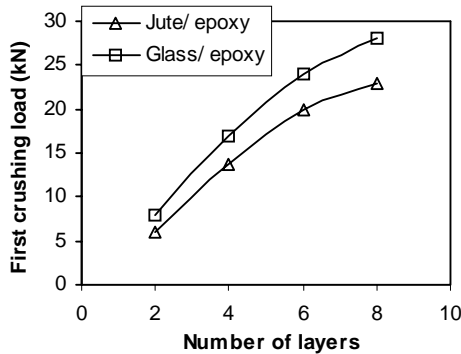


Fig. 4. Effect of number of layers on the first crushing load is shown in

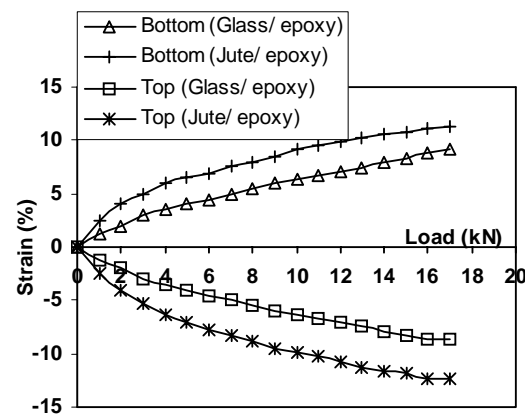


Figure 5. Strain-load relation up to first crushing of the tested composite curved beams

3.2 Failure mechanism

Failure mechanism of the fractured Jute and glass/ epoxy composite curved I-beams under bending have been taken and discussed. A photograph sample of the fractured Jute and glass/ epoxy specimens is shown in Figure 7. As shown from this Figure, Specimens failed after the initial with highly localized stresses at the lower and upper parts of the beam

center region. Then, it followed by the matrix and fiber break. A distinguish delamination was also noticed on both materials tested.



Fig. 6. Photographs of fractured composite curved I-beams under four point bending loading

5. DISCUSSION AND CONCLUSIONS

Composite curved beams were fabricated carefully using hand lay-up method. Three tests were done for each type in order to get better results consistency. Load-displacement graphs and the effect of composite material used have been examined. Longitudinal strains on top and bottom surfaces were examined also and drawn for both materials tested.

The main conclusions that could be drawn from this investigation include:

1. It has been found that for both glass/ epoxy and jute/ epoxy composite curved I-beams, the load increase linearly with displacement until it reaches initial crushing load. The material strength and load decrease after initial crushing load until the final failure of the specimen.
2. Result shows that the first crushing load for the tested glass/ epoxy was higher 20%-31.6% than jute/epoxy beams.
3. Based on the results obtained, it can be concluded that the specific absorption energy (SEA) is slightly higher for glass/ epoxy composite curved I-beam than the jute/ epoxy beams.
4. Failure mechanism of Jute/ epoxy curved beam is similar to the glass/ epoxy curved beams. Fiber break and matrix cracking were found besides fiber fragmentation in the top surface at the mid-span of the beam. Delamination was occurred in the lower surfaces.
5. Jute/ epoxy can be considered for composite structures, as glass/epoxy. While the glass/epoxy beam support loads higher 25% than Jute/ epoxy beams. Further analysis on moisture absorption is needed for both materials.
6. The average percentage of strains for Jute/ epoxy beams were found higher 18% than glass/epoxy beams at the bottom surfaces of the beam. While the difference was 22% at the top surface of the beam.

REFERENCES

1. Joshi S. V., Drzal L. T., Mohanty A. K. and Arora S., Are natural fiber composites environmentally superior to glass fiber reinforced composites, *Composites A*, vol. 35, 2004, 371-376.
2. Paul Wambua, Jan Ivens and Ignaas Verpoest. Natural fibers: can they replace glass in fiber reinforced plastics. *Composites Science and technology*, 63, (2003) 1259-1264.
3. Krishnan Jayaraman and Debes Bhattacharya. Mechanical Performance of wood fiber- waste plastic composite materials.
4. T. Munikenche Gowda, A.C.B. Naidu and Rajput Chaya. 1999, Some mechanical properties of untreated jute fabric-reinforced polyester composites. *Composites A*, 30, 1999, 277-284.
5. Andrew M. Layne and Leif A. Carlson. Test method for measuring strength of a curved sandwich beam. *Experimental mechanics*, vol. 42, No. 2, 2002
6. ASTM standard D 6415-99. Standard test method for measuring the curved beam strength of a fiber-reinforced polymer matrix composite. American society for testing and materials, West Conshohocken (2001).

LOAD CARRYING CAPACITIES OF PULTRUDED FRP SHEET PILING

Yixin Shao

Associate Professor, McGill University, Montreal, Quebec, Canada

Fabien Darchis

Graduate Research Assistant, McGill University, Montreal, Quebec, Canada

ABSTRACT

Buckling initiation and post buckling behaviour of pultruded FRP sheet pilings subject to uniform earth pressure were studied using a finite element method in an attempt to predict the load-carrying capacities of the pilings. The FE predictions were compared with full scale sheet pile tests. It was found that, shell connection model was sufficient to assess the performance of single panel in a connected sheet pile wall. The bifurcation, buckling initiation and post-buckling failure occurred in a close range of loading, suggesting that there existed no post-buckling capacity for the typical installation. With 10% additional materials added either to increase the thickness of the compressive flanges or to create the junction stiffeners between flanges and webs, the buckling resistance of the same profile design could be doubled.

KEYWORDS

Pultruded composites, fiberglass sheet piling, load capacities, buckling.

1. INTRODUCTION

Connected sheet piles are often used as waterfront retaining structures to prevent the erosion of the land. Corrosion resistant FRP sheet piling is finding its way into this unique application. Although pultruded composites have shown excellent tensile capacity, their relatively low elastic moduli and thin walled section design make the FRP sheet piling vulnerable to the local and global buckling. To design a sheet pile section with desired load capacity, understanding the buckling process of FRP sheet pile subject to an earth pressure is essential.

Analytical approaches have been developed to evaluate the buckling of a composite section using the compressive plates restrained by boundary conditions (Kollar, 2003). These approaches require knowledge of the restraints between different plates and the governing equations. They are suited to the estimation of the local buckling in a plate, but difficult to be used to predict the post-buckling behaviour, especially at the presence of nonlinear geometric deformation. Finite element approach appears to be promising in buckling analysis of a complex composite section for pre-buckling, buckling initiation and post-buckling process. FEA calculates directly the load capacity of the structure with exact section shape and takes into account the geometric non-linear deformation. The approach has been successfully employed in assessing the post-buckling behaviour of the pultruded I-beams (Bank and Yin, 1999) and the progressive failure of the pultruded box-beams (Palmer, et al, 1998). This paper is to present a study on the finite element analysis of a pultruded FRP sheet piling subject to a uniform earth pressure using the finite element code of ABAQUS/STANDARD. The main objectives are to evaluate the structural behaviour of the sheet pile panels, including the pre-buckling, buckling initiation and post-buckling performances, and to propose design modifications for enhanced load bearing capacity and serviceability performance of the panel.

2. FINITE ELEMENT MODELING

The earth pressure carried by the sheet pile wall is simulated by a uniform pressure so that the numerical results can be compared with experiments. Fig. 1 shows a simply-supported sheet pile panel loaded by a uniform pressure in a

span of 2.13 m. In experiments, the air pressure was transferred to the panel through the foam inserts. Detailed description of the test setup is given elsewhere (Shao and Shanmugan, 2006). In numerical simulation, the pressure was applied directly to the nodes in vertical direction. The pultruded fibreglass reinforced polyester (FRP) sheet piles are designed and manufactured by IBP Corporation of Canada. The profile of a single unit has a symmetric double-Z cross section, 127 mm deep, 425 mm wide from pin-to-eye connections, and with a wall thickness of 4.7 mm in the top (main) flange and 3.2 mm elsewhere. The mechanical properties are summarized in Table 1. E_{11} , T_{11} and C_{11} are the longitudinal modulus, tensile strength and compressive strength, and E_{22} , T_{22} and C_{22} the transverse modulus, tensile strength and compressive strength, respectively.

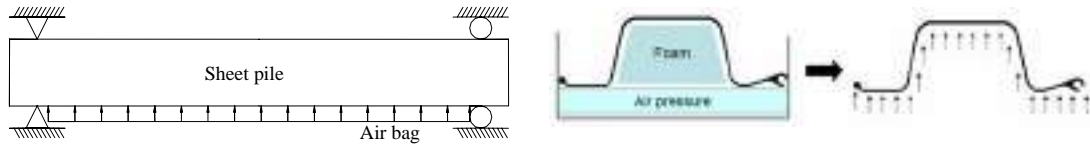


Fig. 1: Sheet pile panel and loading configuration

Nonlinear finite element ABAQUS/STANDARD package was employed with 92000 shell elements to evaluate pre-buckling, buckling initiation and post-buckling of FRP sheet pile under pressure. The nonlinear static analysis was used to establish the probable buckling load, the eigenvalue extraction method to determine the bifurcation load and buckling modes, and the nonlinear static calculation with imperfection and dynamic perturbations to perform post buckling analysis.

Table 1: Material properties

	E_{11} (GPa)	E_{22} (GPa)	ν_{12}	G_{12} (GPa)	T_{11} (MPa)	T_{22} (MPa)	C_{11} (MPa)	C_{22} (MPa)
Top flange	31.4	7.3	0.18	3.1	422	70	314	79
Web	16.1	12.3	0.2	2.7	180	119	178	99
Bottom flange	30.2	7.9	0.18	3.0	298	84	250	66

3. LOAD CAPACITIES BASED ON FEA RESULTS

3.1. Nonlinear Static Analysis and Comparison with Experiments

The sheet pile model with shell connection was progressively loaded by a pressure up to 50 KPa in an increment of 2 KPa. During the monotonically loading, computation stopped at a bifurcation load of 42 KPa after which the solutions to the nonlinear elastic equations were no longer unique. In order to validate the simulation, the pressure-deflection curves and pressure – strain curves of the numerical pre-buckling calculations were compared to the experimental data of single panel tests. They are presented in Figs. 2 and 3. The FEA results agreed well with experimental data. Therefore, the shell-connection model appeared to be sufficient to predict the behaviour of the single panel in a sheet pile wall.

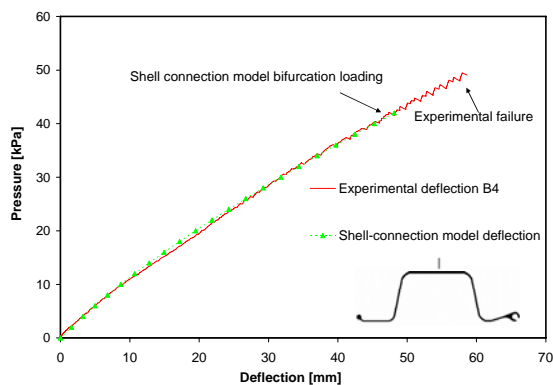


Fig. 2: Comparison of pressure-deflection curves

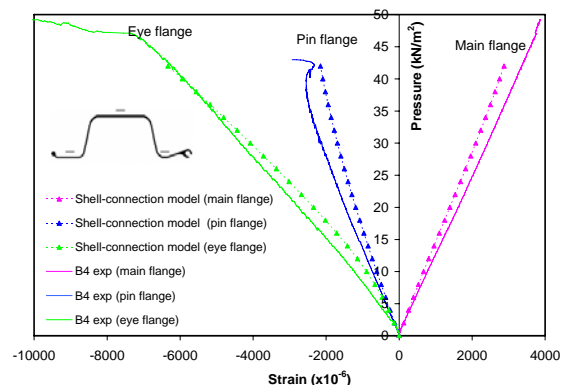


Fig. 3: Comparison of pressure - strain curves

3.2. Buckling Load and the Corresponding Buckling Mode

To determine the buckling loads and their corresponding buckling modes, a buckling extraction calculation was performed on the deformed base state of the panel at 40 kPa. The first mode consisted of combined buckling waves on both pin flange and pin web, whereas the second mode appeared also in combined waves on eye flange and eye web. It was found that the two buckling loads corresponding to the first two buckling modes were so close that it was impossible to predict with certainty which side would buckle first. Experimental results showed that buckling could happen on either side (Shao and Shanmugan, 2006). Fig. 4 compares the FEA first buckling mode with experimental observation. The buckling loads predicted by FEA were about 43 kPa. In experiments, the buckling pressure of the single panels was found in a range of 42 - 48 kPa, with an average of 45 kPa. In the buckling process, eye and pin connections acted as restrained end conditions for bottom flanges: because they were a lot thicker than the bottom flanges, the connections did not participate in the buckling wave. The junction ends (bottom web or flange) played a similar role: the junctions between webs and flanges were restrained end conditions for the adjacent plates.



Fig. 4: Comparison of FEA first buckling mode (left) with experiment (right)

3.3. Post-Buckling Capacity

To investigate the post-buckling capacity of sheet pile after buckling at 43 kPa, post-buckling analysis was performed by introducing geometrical imperfection and by introducing a loading rate. For the first method, the two first buckling modes found by the buckling calculation shown in Fig. 4 were superimposed in the initial geometry. Different levels of perturbation were investigated at 1.0 mm, 0.5 mm and 0.3 mm; the value of which represented the upper bound of the geometric imperfection. As regard to the second method, several loading rates were applied to the panel: 5 kPa/s, 2 kPa/s and 0.3 kPa/s. The last loading rate represented the loading rate in the single panel tests and could be used to simulate the quasi static post buckling curves. The pressure applied ranged from 0 kPa to 60 kPa. Six different calculations, three with imperfection and three with dynamic loading, gave very similar results; in each case, the same post buckling wave pattern appeared at the two junctions (web / pin flange and web / eye flange). Fig. 5 demonstrates the deformed shape and the typical stress distribution in transverse direction (σ_{22}) in web at pin flange and web junction where the compressive stress (σ_{22}) at web first reached to its ultimate compressive strength.

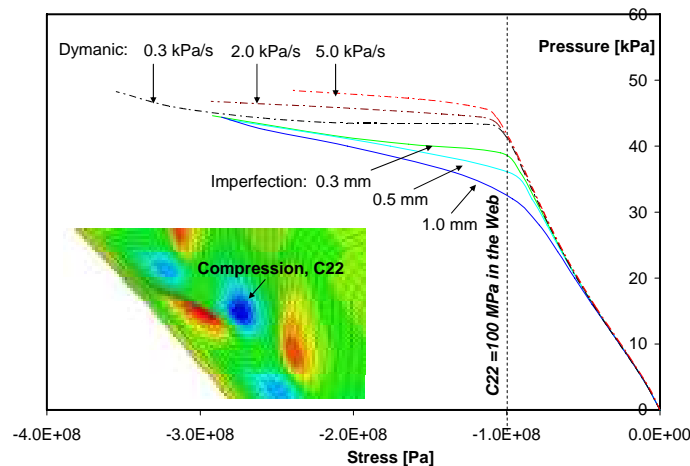


Fig. 5: Mid-section transverse stress distribution (σ_{22}) at junction of pin flange and web

High stress concentrations over small areas appeared after buckling which would lead to localized failure of the panel. At buckling of pin flange, the six curves started to separate and showed distinct buckling behaviours. The more the imperfection was introduced in the panel, the sooner it would buckle. In contrary, the higher the loading rate, the more the resistance to buckling. The perfect static post-buckling curve was assumed to lie between the 0.3 kPa/s curves and the 0.3 mm imperfect curves. After buckling, the sensitivity to imperfection or dynamic loading of the panel disappeared, which was typical of post-buckling of plates, and the curves converged. The post-buckling load capacity was about 39 KPa using imperfection perturbation and 41 KPa using dynamic loading rate and was dominated by transverse compressive strength in web as shown in Fig. 5. The post buckling load was even lower than the buckling load based on finite element analysis, indicating that there was no post-buckling capacity of the sheet pile panel in the installed position.

4. DESIGN MODIFICATION FOR BETTER BUCKLING RESISTANCE

Modifications were proposed for sheet pile design based on two approaches: (1) with added compressive stiffeners (diameter = 15 mm) at the compressive junctions to enhance the restraints on the compressive plates (Fig. 6a) and (2) with the increased thickness (thickness = 4 mm) of two webs and two compressive flanges for better buckling resistance (Fig. 6b). In either case, same amount of 10% additional material was added to the original profile. The buckling load was increased to 93 KPa with added compressive stiffeners and to 66 KPa with increased thickness in compressive members. In comparison with the capacity of 43 KPa in original profile design, the increase was between 100% and 50%.

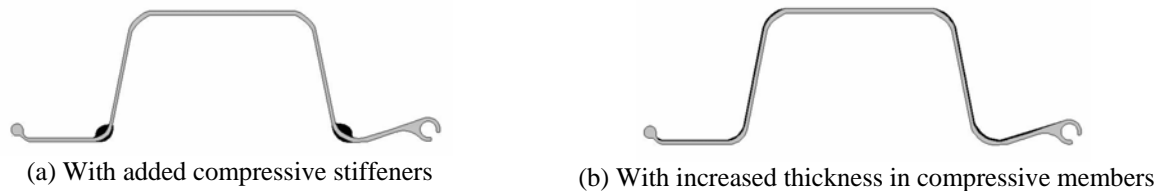


Fig. 6: Modification in sheet pile profile design

5. CONCLUSIONS

A finite element analysis was performed on a sheet pile wall subject to uniform pressure to assess its load capacity. It was found that buckling initiation and ultimate failure happened almost simultaneously at buckling load, suggesting there existed no post-buckling capacity for the sheet pile in the installed position. The pressure-deflection curves were found to exhibit a softening behaviour due to the reduction of the section stiffness. Nonlinear finite element analysis with perturbation function provides an efficient tool for determining the pre-buckling, bifurcation and post-buckling loads of pultruded sheet pilings. The modified profile design with compressive stiffeners or increased thickness in compressive members could double the load capacity.

6. REFERENCES

- Bank, L. C. and Yin, J. (1999), "Failure of Web-Flange Junction in Postbuckled pultruded I-Beams". *Journal of composites for construction*, 3(4), pp 177-184.
- Kollar, L. P. (2003), "Local Buckling of Fiber Reinforced Plastic Composite Structural Members with Open and Closed Cross Sections", *ASCE Journal of Structural Engineering*, 129(11), pp 1503-1513.
- Palmer, D. W., Bank, L. C. and gentry, T. R. (1998), "Progressive Tearing failure of Pultruded Composite Box Beams: Experiment and Simulation", *Composite Science and Technology*, 58, pp 1353-1359.
- Shao, Y. and Shanmugan, J. (2006), "Moment Capacities and Deflection Limits of Composite Sheet Piles", *Journal of Composites for Construction*, in press.

A case study on life-cycle assessment of environmental aspect of FRP structures

Hirokazu Tanaka

(Research Engineer, SHIMIZU CORPORATION, Koto-ku, Tokyo, Japan)

Hitoshi Tazawa

(General Manager, ASAHI GLASS MATEX CO., LTD., Sagami-hara, Kanagawa, Japan)

Morio Kurita

(Group Leader, SHIMIZU CORPORATION, Koto-ku, Tokyo, Japan)

Takumi Shimomura

(Associate Professor, Nagaoka University of Technology, Nagaoka, Niigata, Japan)

ABSTRACT

In this paper, the authors evaluated the amount of carbon dioxide emissions from FRP footbridge and PC (Pre-stressed concrete) footbridge with some reasonable scenarios based on the first FRP footbridge constructed in Japan at 2000. As a result, the total amount of carbon dioxide emissions from FRP footbridge decreased by about 26 percent than that from PC footbridge. This is because the substructure of FRP footbridge was able to be cut down by the superstructure of FRP footbridge which has much lighter weight than that of PC footbridge.

KEYWORDS

FRP structures, Environmental aspect, Amount of carbon dioxide emissions, Case study

1. INTRODUCTION

FRP has some excellent properties as a structural material and has a possibility to solve some problems that the bridges made of conventional materials face today; corrosion in early stage, for example. For spreading use of FRP bridge, it is very important to evaluate an environmental impact properly. There are some studies^{1),2),3)} about the life-cycle assessment of the structures such as buildings and bridges made from concrete and steel, but few studies of FRP bridges. The unit amount of carbon dioxide emissions from FRP is much higher than that from other conventional materials such as concrete and steel. However, FRP bridges have much lighter weight than other conventional materials. This will reduce the total amount of carbon dioxide emissions. The authors tried to evaluate the amount of carbon dioxide emissions from FRP footbridge. We selected the case of "Okinawa Road Park Bridge" constructed at Okinawa in 2000 which is the first FRP footbridge in Japan. We compared this FRP footbridge case with the PC footbridge case which was considered as an alternative plan. The amount of carbon dioxide emissions from the materials and under construction was calculated with some reasonable scenarios. In this study, the authors added some suppositions for unknown condition and made some simplifications for the evaluation, so the amount of carbon dioxide emissions in this study don't indicate the really amount of carbon dioxide emissions of Okinawa Road Park Bridge itself.

2. TARGET STRUCTURE

The target structures to evaluate an environmental impact are FRP footbridge and PC footbridge. FRP footbridge is about 38m in length and about 4.5m in width. The superstructure type of FRP footbridge is two span continuous girder bridges. FRP is made of glass fiber and vinyl-ester resin. PC footbridge is about 36m in length and about

3.5m in width. The superstructure type of PC footbridge is one span post-tension hollow slab girder bridge. The substructure type of FRP footbridge and PC footbridge is wall type pier. The foundation type is steel pipe pile. Figure 1 shows the view of the FRP footbridge.



Figure 1: View of Okinawa Road Park Bridge (FRP footbridge)

3. EVALUATION RANGE

The evaluation range of an environmental impact of FRP footbridge and PC footbridge is shown in Figure 2. In this paper, the materials stage and the construction stage were evaluated. Currently, the only options for disposal and recycling are full recycling of the concrete vs. landfill or incineration of the FRP. But accurate numbers do not exist. So the using stage, the dispose and recycle stage were not evaluated. As for FRP footbridge, the main beam made of hand-lay up FRP and the bridge deck made of pultruded FRP were manufactured in separate factories and transported to Tokyo by land. After the main beam and the bridge deck were assembled in the factory of Tokyo, FRP footbridge was transported to Okinawa by sea.

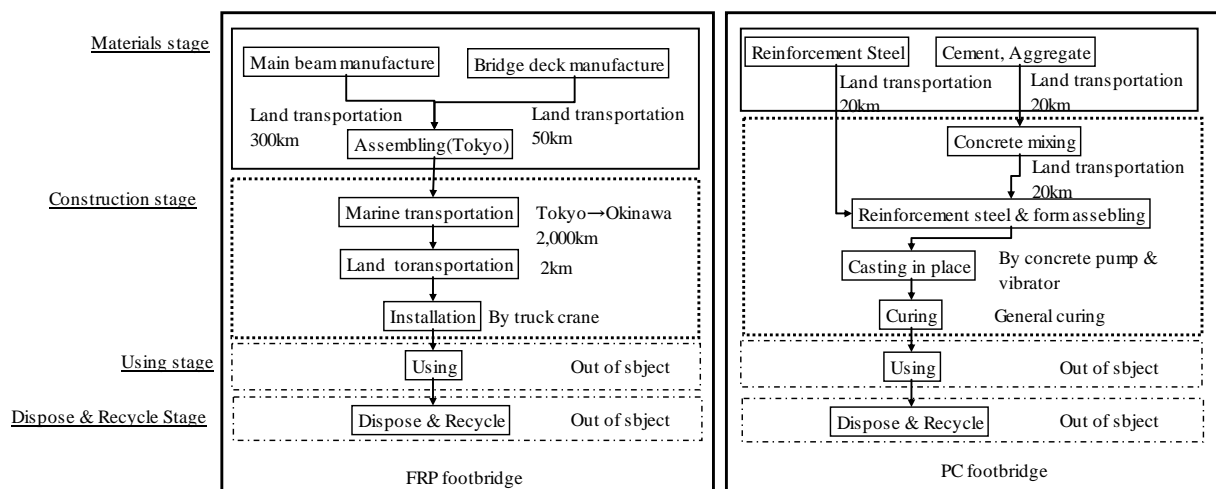


Figure 2: Evaluation Range

4. UNIT OF CARBON DIOXIDE EMISSIONS

The unit amount of carbon dioxide emissions used in this paper is shown in Table 1. The unit amount of carbon dioxide emissions of FRP was referred to the reference⁴⁾. The unit amount of carbon dioxide emissions of concrete, prestressing steel wire, steel pipe pile, and construction of concrete was referred to the committee report⁵⁾. The unit amount of carbon dioxide emissions of transportation was referred to the values⁶⁾ showed on the website of Ministry of Land Infrastructure and Transport in Japan.

Table 1: Unit amount of carbon dioxide emissions

Heading		Unit	Unit amount of carbon dioxide emissions
Materials	FRP(Hand-lay up)	kg	4.97 kgCO ₂ /kg
	FRP(Pultruded)	kg	3.09 kgCO ₂ /kg
	Concrete (Fc27N/mm ²)	kg	0.0918 kgCO ₂ /kg
		m ³	211.1 kgCO ₂ /m ³
	Reinforcement steel	kg	0.755 kgCO ₂ /kg
	Prestressing steel wire	kg	1.31 kgCO ₂ /kg
	Steel pipe pile	kg	1.25 kgCO ₂ /kg
Transportation	Marine transportation	t*km	0.039 kgCO ₂ /t*km
	Land transportation	t*km	0.154 kgCO ₂ /t*km
Construction	Concrete	m ³	39.0kgCO ₂ /m ³

5. EVALUATION RESULT

5.1 AMOUNT OF CARBON DIOXIDE EMISSIONS ON MATERIALS AND CONSTRUCTION STAGE

The amount of carbon dioxide emissions on the materials stage and on the construction stage is shown in Figure 4. On the materials stage, for superstructure, the amount of carbon dioxide emissions from FRP footbridge increased by about 8 percent than that from PC footbridge. This is because the unit amount of carbon dioxide emissions from FRP is much higher than that from concrete, though the weight of superstructure of FRP footbridge is much lighter than that of PC footbridge. For substructure, the amount of carbon dioxide emissions from FRP footbridge decreased by about 50 percent than that from PC footbridge. This is because the substructure of FRP footbridge was able to be cut down, especially the weight of steel pipe pile reduced. On the materials stage, the amount of carbon dioxide emissions from FRP footbridge decreased by about 18 percent than that from PC footbridge. On the construction stage, for superstructure, the amount of carbon dioxide emissions from FRP footbridge decreased by about 80 percent than that from PC footbridge. This is because the work of FRP footbridge under construction was almost the transportation by sea and the amount of carbon dioxide emissions on the transportation by sea is very small. For substructure, the amount of carbon dioxide emissions from FRP footbridge decreased by about 45 percent than that from PC footbridge. This is because the amount of concrete of the substructure of FRP footbridge was much smaller than that of PC footbridge by the weight of superstructure of FRP footbridge being much lighter than that of PC footbridge. On the construction stage, the amount of carbon dioxide emissions from FRP footbridge decreased by about 70 percent than that from PC footbridge.

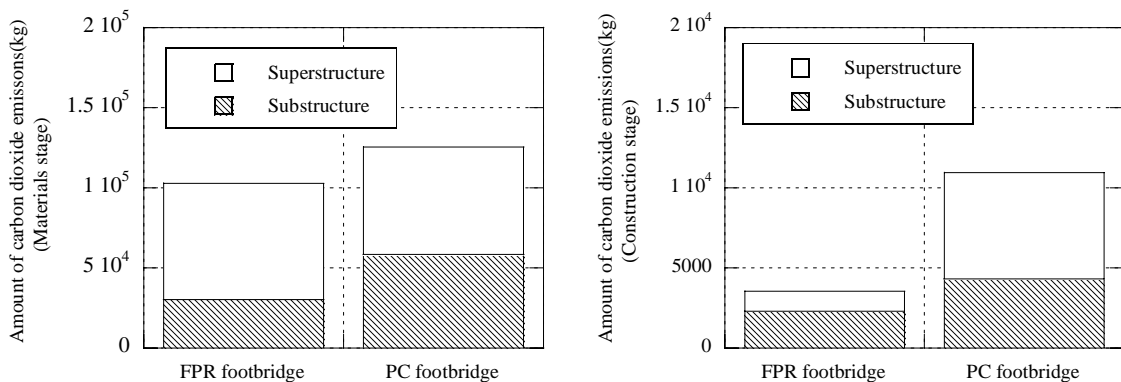


Figure 4: Amount of carbon dioxide emissions on the materials stage and on the construction stage

5.2 TOTAL AMOUNT OF CARBON DIOXIDE EMISSIONS

The total amount of carbon dioxide emissions on the materials stage and the construction stage is shown in Figure 5. The amount of carbon dioxide emissions from FRP footbridge decreased by about 26 percent than that from PC footbridge. Though the unit amount of carbon dioxide emissions from FRP is much higher than that from concrete, the total amount of carbon dioxide emissions on the materials stage and the construction stage of FRP footbridge was smaller than that of PC bridge. This is because the substructure of FRP footbridge was able to be cut down by the weight of superstructure of FRP footbridge which is much lighter than that of PC footbridge.

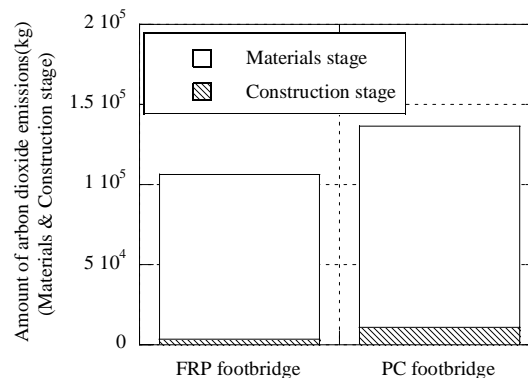


Figure 6: Carbon dioxide emissions on materials and construction stage

6. SUMMARY

- 1) On the materials stage, the amount of carbon dioxide emissions from FRP footbridge decreased by about 18 percent than that from PC footbridge.
- 2) On the construction stage, the amount of carbon dioxide emissions from FRP footbridge decreased by about 70 percent than that from PC footbridge.
- 3) The total amount of carbon dioxide emissions from FRP footbridge on the material and construction stage decreased by about 26 percent than that from PC footbridge. This is because the substructure of FRP footbridge was able to be cut down by the weight of superstructure of FRP footbridge which is much lighter than that of PC footbridge.

7. REFERENCES

- 1) Koji Sakai (2005). "Environmental Design for Concrete Structures". *Journal of Advanced Concrete Technology*, Vol.3, No.1, pp.17-28.
- 2) Kenji Kawai, Takafumi Sugiyama, Koichi Kobayashi and Susumu Sano (2005). "A Proposal of Concrete Structure Design Methods Considering Environmental Performance". *Journal of Advanced Concrete Technology*, Vol.3, No.1, pp.41-52.
- 3) Katz A. (2004). "The environmental impact of steel and FRP reinforced pavements". *ASCE Journal of Composites for Construction*, Vol.8, No.6, pp.481-488.
- 4) Japan Reinforcement Plastic Society (2003). "FRP Whoever Use -FRP handbook-" (In Japanese)
- 5) Japan Society of Civil Engineers (2004). "Environmental impact evaluation of concrete (Part2)" (In Japanese)
- 6) Ministry of Land Infrastructure and Transport (Japan). Data of the unit of carbon dioxide emissions of transportation for 2003, <http://www.mlit.go.jp/sogoseisaku/kankyuu/ondanka1.htm>, 03/21/06. (date accessed)

Part V. Confinement Issues

AXIAL BEHAVIOR OF CIRCULAR COLUMNS CONFINED WITH FIBER-REINFORCED POLYMER JACKETS

Azadeh Parvin

Associate Professor of Civil Engineering, The University of Toledo, OH 43606, USA

Aditya S. Jamwal

Former Graduate Student, The University of Toledo, OH 43606, USA

ABSTRACT

This paper presents a finite-element analysis of the behavior of axially-loaded, small-scale fiber-reinforced polymer (FRP) wrapped concrete columns. Parameters considered were the FRP wrap thickness, and the ply angle orientation with respect to the lateral axis of the column. The finite element analysis results showed considerable increase in the axial compressive strength and ductility of the FRP-confined concrete columns as compared to the unconfined ones. The increase in the wrap thickness resulted in further axial strength and ductility enhancements of the confined columns. Columns confined with the 0° angle ply wrap exhibited the highest axial stress capacity as compared to the columns enhanced with wraps consisted of $\pm 15^\circ$ and $0^\circ/\pm 15^\circ/0^\circ$ ply angles.

KEYWORDS

Column, Confined concrete, Axial load, Fiber-reinforced polymer

1. INTRODUCTION

Fiber reinforced polymer (FRP) wrapping of concrete columns is an ideal technique to increase the strength and ductility of these structural elements. Among the significant parameters that influence the confinement effectiveness of FRP-wrapped concrete columns, wrap thickness or number of FRP layers, and ply angle orientation are noteworthy (Rochette and Labossiere, 2000; Parvin and Jamwal, 2005, 2006). In the present study, effects of the wrap thickness and the ply angle orientation on the performance of small-scale FRP-wrapped circular columns have been investigated using a nonlinear finite element analysis software program (MSC.MARC™ 2001), to gain insight into the behavior of such columns.

2. FINITE ELEMENT ANALYSIS: MODELS, AND SIMULATION RESULTS

Prior to parametric studies, the proposed finite element analysis (FEA) models were validated and calibrated through an experimental study on FRP-wrapped circular columns reported in the literature (Rochette and Labossiere, 2000). The finite element analysis and experimental results were in good agreement and are reported elsewhere (Parvin and Jamwal, 2006).

Using the validated FEA models, the behavior of small-scale FRP-wrapped concrete columns, with various wrap thicknesses, and ply angles under axial loading were investigated. The columns had the dimension of $152.4 \text{ mm} \times 304.8 \text{ mm}$ (6 in \times 12 in). The bottom of the concrete columns was fixed. The axial load was increased incrementally and applied on the top cross-section of the column concrete core and not the FRP jacket. Compression strength of 20.69 MPa (3 ksi) with Poisson's ratio of 0.17 was assigned for the concrete, which was modeled as an isotropic material. Along with the Mohr-Coulomb failure criterion, which has been used for the concrete, isotropic work hardening rule was employed to define the concrete material's plastic behavior. The failure

criterion for the unconfined concrete was the crushing strain of 0.003 and a small strain option unlike the confined concrete, where a large strain option was used for analysis. For all cases, unidirectional E-glass FRP material was used with a modulus of elasticity of 41,370 MPa (6×10^6 psi), a Poisson ratio of 0.24, and a rupture strain of 0.019 along the fiber direction. Since the FRP material was unidirectional, the stiffness in the other direction was negligible. The rupture of the FRP material controlled the failure of the confined column. The unidirectional FRP composite was modeled as an orthotropic material.

Circular column models utilized in the numerical study are presented in Table 1. The template used for labeling the numerical column models leveraged the column shape, the wrap thickness, and the ply angle as follows:

- a) The letter ‘C’ specifies that the column is circular.
- b) The wrap thickness is categorized as 1, 2 and 3 for thicknesses of 1.3 mm (0.051 in.), 2.1 mm (0.083 in.) and 3 mm (0.118 in.), respectively which is represented by the first subscript. The thicknesses of 1.3 mm (0.051 in.), 2.1 mm (0.083 in.) and 3 mm (0.118 in.) correspond to 6, 10 and 14 plies of FRP, respectively.
- c) The ply angles are categorized through the second subscript as 1, 2, and 3 for 0° , $\pm 15^\circ$, and $0^\circ/\pm 15^\circ/0^\circ$, respectively.

As an example, the label or column identifier C11 denotes that the column is a circular with the wrap thickness of 1.3 mm (0.051 in.) and ply angle configuration of 0° .

Table 1: Parametric Case Studies for Circular Columns

Column ID	Wrap Thickness mm (in.)	Ply Angle Configuration		
C11, C12, C13	1.3 (0.051)	0°_6	$\pm 15^\circ_6$	$0^\circ/\pm 15^\circ_4/0^\circ$
C21, C22, C23	2.1(0.083)	0°_{10}	$\pm 15^\circ_{10}$	$0^\circ/\pm 15^\circ_8/0^\circ$
C31, C32, C33	3.0 (0.118)	0°_{14}	$\pm 15^\circ_{14}$	$0^\circ/\pm 15^\circ_{12}/0^\circ$

2.1 FEA Results

The strength and ductility enhancements of wrapped-column models C11 through C33 as compared to the control model C00 are presented in Table 2. Furthermore, the axial stress versus axial and lateral strains are plotted in Figures 1-3 to demonstrate the effects of various wrap thicknesses for each ply angle configuration. The stresses and strains were measured at mid-height of the columns. The circular column with the ply angle of 0° provided the highest axial strength. This increase in axial strength is more visible when the wrap thickness was increased from 1.3 mm (0.051 in.) to 3 mm (0.118 in.). However, the axial strain capacities for the columns with $\pm 15^\circ$ and $0^\circ/\pm 15^\circ/0^\circ$ ply angles are higher than that of columns with 0° ply angle for all the wrap thicknesses. For the columns with 0° and $0^\circ/\pm 15^\circ/0^\circ$ ply angles, the increase in the axial stress was fairly consistent with the increase in the wrap thickness. On the other hand, the same was not true for the column with the ply angle of $\pm 15^\circ$. There was

Table 2: Maximum Axial Stress and Axial Strain for control and FRP wrapped Circular Columns

Case ID	Axial Stress Mpa (ksi)	Axial Strain	% Increase in Axial Stress	% Increase in Axial Strain
C00	20.85(3.024)	0.0033	--	--
C11	40.76 (5.905)	0.0221	95	569
C12	40.28 (5.840)	0.0257	93	679
C13	41.31 (5.990)	0.0246	98	645
C21	48.52 (7.035)	0.0220	133	567
C22	47.58 (6.904)	0.0263	128	697
C23	46.62 (6.765)	0.0272	124	723
C31	58.34 (8.462)	0.0219	180	564
C32	51.48 (7.464)	0.0250	147	658
C33	52.82 (7.659)	0.0246	153	645

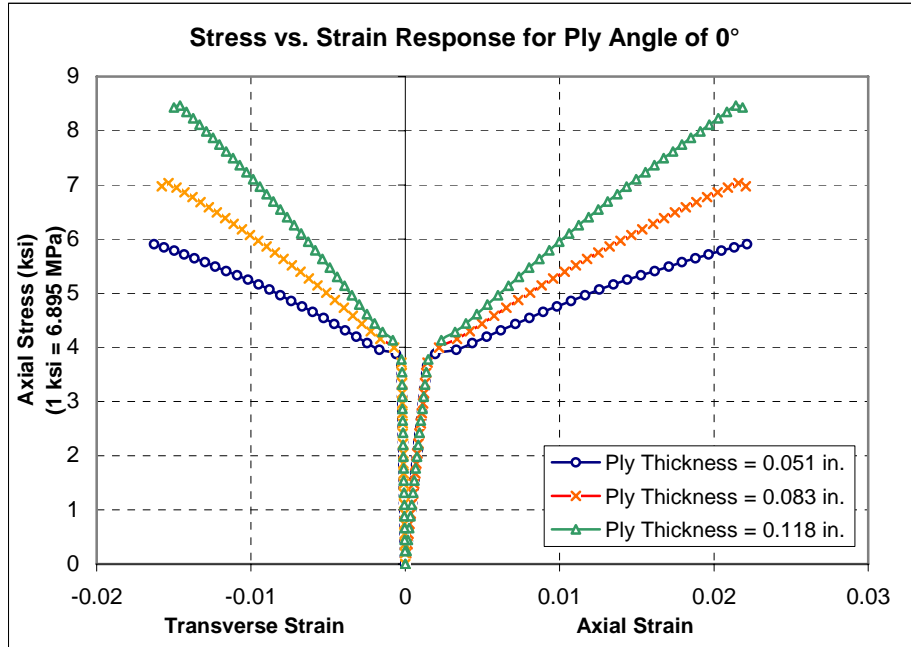


Figure 1: Stress vs. Strain for Ply Angle of 0°

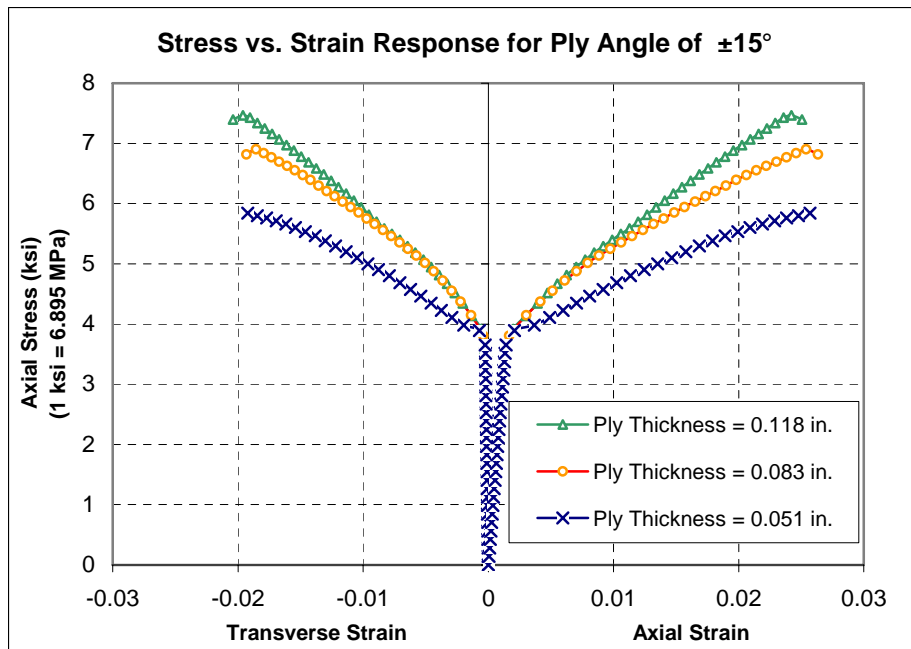


Figure 2: Stress vs. Strain for Ply Angle of ±15°

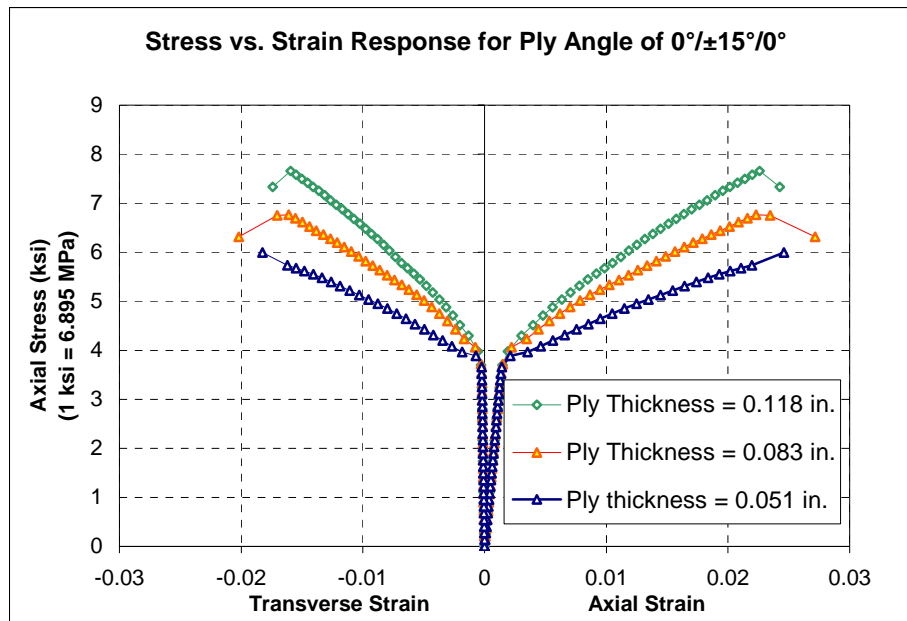


Figure 3: Stress vs. Strain for Ply Angle of $0^\circ/\pm 15^\circ/0^\circ$

an 18% increase in the axial strength when the wrap thickness was increased from 1.3 mm (0.051 in.) to 2.1 mm (0.083 in.) (see axial stresses for model C12 and C22 in Table 2). On the other hand, only 8% gain materialized when the wrap thickness was increased from 2.1 mm (0.083 in.) to 3 mm (0.118 in.) (see axial stresses for model C22 and C32 in Table 2). Regardless of the ply angle configuration, the increase in the wrap thickness resulted in an enhancement in the stiffness as apparent in the slope of second portion of the stress versus strain curves.

3. CONCLUSIONS

In the present study, the effects of various upgrade schemes on axially-loaded FRP-wrapped circular columns were investigated. The following conclusions are drawn:

1. It was observed that the axial stress and strain capacities of the FRP-wrapped concrete column increased by more than 2 to 3 times, and by 5 to 6 times, respectively as compared to the unconfined column.
2. The ply angle of 0° provided the highest axial strength for the FRP wrapped circular columns as compared to ply angles of $\pm 15^\circ$ and $0^\circ/\pm 15^\circ/0^\circ$. However, the ductility provided by the column with the ply angle of 0° was less than that of columns with the ply angles of $\pm 15^\circ$ and $0^\circ/\pm 15^\circ/0^\circ$.
3. The increase in the axial stress carrying capacity is uniform with the increase in the wrap thickness for the column with the ply angle of 0° . The FRP-wrapped circular columns with the ply angles of $\pm 15^\circ$ and $0^\circ/\pm 15^\circ/0^\circ$ provided a non-uniform increase in the axial stress carrying capacity as the wrap thickness was increased. The columns with the ply angle of $0^\circ/\pm 15^\circ/0^\circ$ showed a softening response before failure for the FRP-wrapped columns with higher wrap thicknesses of 2.1 mm (0.083 in.) and 3 mm (0.118 in.).
4. In general, for all the columns, the axial stress carrying capacity increased with the increase in the wrap thickness.

4. REFERENCES

1. MSC.MARC™ 2001. MSC Software Corporation, Palo Alto, CA.
2. Parvin A, Jamwal A S. (2006). "Performance of externally FRP reinforced columns for changes in angle and thickness of the wrap and concrete strength." *Composite Structures*, 73(4), 451-457.
3. Parvin A, Jamwal A S. (2005). "Effects of wrap thickness and ply configuration on composite-confined concrete cylinders." *Composite Structures*, 67 (4), 437-442.
4. Rochette, P., and Labossiere, P. (2000). "Axial testing of rectangular column models confined with composites." *Journal of Composites for Construction*, 4(3), 129-136.

CFRP CONFINED ULTRA HIGH STRENGTH CONCRETE COLUMNS

Adnan R. Malik

(PhD Candidate, The University of New South Wales, Sydney, NSW, Australia)

Stephen J. Foster

(A/Prof., The University of New South Wales, Sydney, NSW, Australia)

ABSTRACT

An experimental investigation was conducted to examine the behaviour of RPC columns confined by CFRP and subjected to concentric and eccentric loadings. All the 17 columns were cast with the concrete mix containing either no fibres or 2% (by volume) of straight steel fibres with a concrete strength of 165 MPa. Experimental data for strength, lateral and axial deformation and the failure mode were obtained for each test. The CFRP confined RPC columns showed improvements in both ultimate compressive strength and ductility compared with unconfined RPC columns. Because of the ultra high strength concrete used in this study, the final failure was sudden and explosive at the point of rupture of the CFRP wrapping.

KEYWORDS

Carbon fibre reinforced polymer, reactive powder concrete, columns, confinement.

1. INTRODUCTION

In recent years, the use of carbon fibre reinforced polymer (CFRP) composites for a variety of structural applications (columns, bridge piers, piles etc.) has been rapidly increasing, mainly because of their superior strength to weight ratio and durability in corrosive environments. The orthotropic behaviour of CFRP makes it a most suitable product for encasing concrete columns and, in particular, in combination with an ultra high strength reactive powder concrete (RPC). The objective of this research is to examine the behaviour of CFRP confined fibre and non-fibre reinforced RPC circular columns without conventional reinforcement tested under concentric and eccentric loading.

2. EXPERIMENTAL PROGRAM

2.1 Test specimens

In this study, 17 RPC columns were tested consisting of 10 CFRP confined steel fibre reinforced RPC (FR-RPC) columns, 6 CFRP confined RPC columns with no steel fibres and one FR-RPC column with no wrapping. The columns were circular; 152 mm in diameter and 1060 mm high. No longitudinal reinforcement was used in any of the columns. The columns tested are identified by load eccentricity, wrap type, existence of steel fibres in the concrete and an identification number for the specimen if the test was repeated. For example, specimen FC35-1 was cast with fibre reinforced RPC, was tested at an initial eccentricity of 35 mm and was wrapped with Type 1 layout carbon fibre polymer sheet. Specimen PC0-2-2 was cast with RPC with no fibres, was tested under concentric loading (0 mm eccentricity), was wrapped with Type 2 carbon fibre sheet and was a repeat test. Column FC0 was control column with no wrap. Details for the columns tested are presented in Table 1.

2.2 RPC mix design and Material properties

The RPC was mixed using locally available materials: 920 kg/m³ of General Portland cement, 920 kg/m³ of Sydney sand, 221 kg/m³ of undensified silica fume, 39 kg/m³ of superplasticizer and 157 kg/m³ of steel fibres for FR-RPC mix. The steel fibres used were high strength straight steel fibres, 13 mm long, 0.2 mm in diameter and had an ultimate tensile strength of 1800 MPa. The water-binder ratio was 0.17. The control specimen properties are

presented in Table 2, where ρ_f is the volumetric ratio of fibres, E_o is the modulus of elasticity, ν is the Poisson's ratio, f_{cm} is the mean compressive cylinder strength, f_{dp} is the double punch tensile strength, f_{sp} is the split cylinder tensile strength, f_{cf} is the flexural tension strength and G_f is the fracture energy.

Table 1: Column Details

Column	Mix	Wrap Type	Load eccentricity (mm)	Column	Mix	Wrap Type	Load eccentricity (mm)
FC60-1	1	1	60	FC10-2	4	2	10
FC35-1	2	1	35	PC60-1	8	1	60
FC20-1	1	1	20	PC35-1	8	1	35
FC10-1	2	1	10	PC20-1	7	1	20
FC0-1-1	3	1	0	PC10-1	7	1	10
FC0-1-2	3	1	0	PC0-1-1	9	1	0
FC60-2	5	2	60	PC0-1-2	9	1	0
FC35-2	5	2	35	FC0	6	-	0
FC20-2	6	2	20				

2.3 FRP material properties and Wrap Details

The CFRP used in this project was MBrace® CF120 and CF530. The resin used for the bonding of CFRP was a two-part epoxy adhesive (MBrace® Staturant). The CFRP was tested in accordance with the ASTM standard D3039 (2005). The mean ultimate tensile strength of three CF120 specimens was 3374 MPa with the strain corresponding to failure load being 0.0145. The elastic modulus was 232 GPa. The columns were wrapped with 4 layers of CFRP. The mechanical properties of the CFRP and epoxy as given by the manufacturer and the wrap details are presented in Table 3.

Table 2: RPC material properties

Mix	ρ_f (%)	f_{cm} MPa	ν	E_o GPa	f_{dp} MPa	f_{sp} MPa	f_{cf} MPa	G_f N/mm
1	2	163	0.13	41.7	8.2	-	26.2	20.7
2	2	165	0.1	42.0	7.7	-	35.4	32.7
3	2	168	0.1	42.6	7.9	-	17.7	14.1
4	2	172	0.13	44.2	7.6	-	26.2	18.4
5	2	168	0.15	42.6	8.7	-	24.7	21.1
6	2	165	0.15	44.2	7.7	-	33.3	28.8
7	0	139	0.13	40.5	3.1	8.0	6.1	0.03
8	0	143	-	-	3.3	8.6	6.4	0.02
9	0	145	0.13	41.0	3.0	8.6	6.0	0.03

Table 3: Mechanical properties of FRP and adhesive and details of CFRP wrapping

FRP and adhesive	Tensile strength (MPa)	Elastic modulus (MPa)	Laminate Structure	Wrap Type 1		Wrap Type 2	
				fibre Sheet	Wrap direction	fibre Sheet	Wrap direction
CF120	3800	240000	Layer1 & Layer 2	CF120	Longitudinal	CF530	Longitudinal
CF530	2650	640000					
Saturant	>50	>3000	Layer3 & Layer4	CF120	Circumferential	CF120	Circumferential

2.4 Test Setup and Instrumentation

The columns testing arrangements and gauging instrumentation are shown in figure 2. The loading was applied via specially designed steel caps clamped to each end of the specimen. To apply the eccentric loading, knife edge end

assemblages were attached to the top and bottom platens of the testing machine. Testing was undertaken using a 5000 kN capacity closed loop servo controlled actuator with lateral displacement used to control the test for eccentrically loaded columns and ram displacement control for the concentrically loaded specimens.

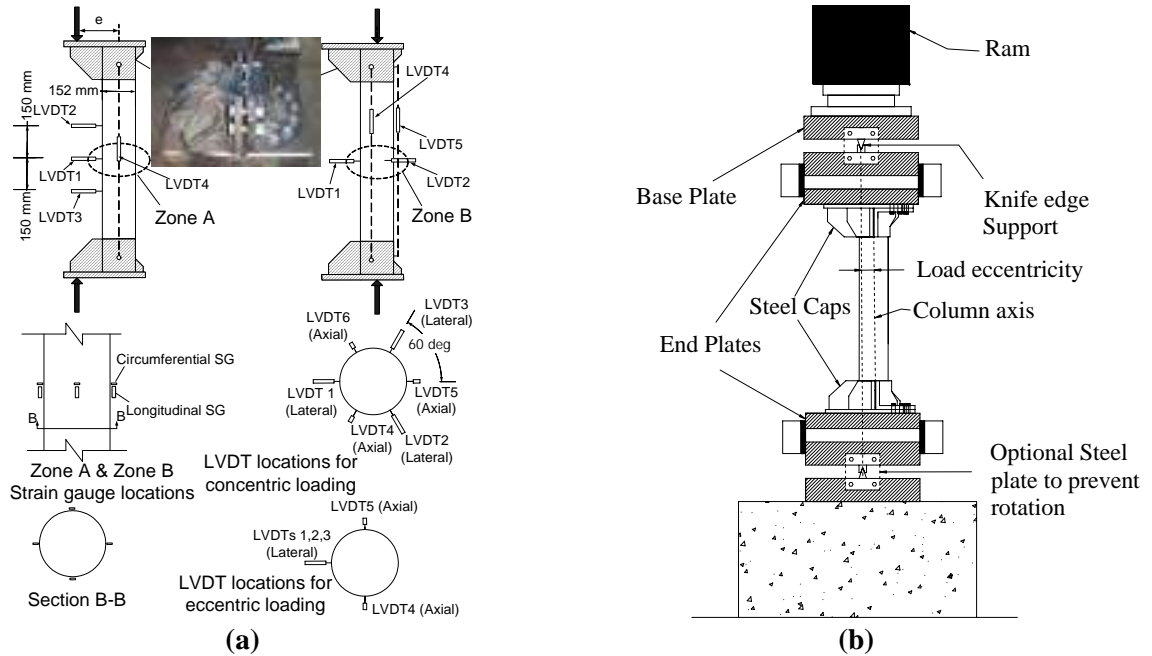


Figure 2: (a) Instrumentation details and (b) Test setup used for column test

3. TEST RESULTS AND OBSERVATIONS

The peak loads, moments at peak load, corresponding lateral displacements at mid height of the specimens, and location of failure zone for the columns tested are given in Table 4.

Table 4: Peak Loads and Corresponding moments and lateral displacements

Column	Failure location [#] (mm)	Peak Load P_u (kN)	Moment at P_u (kNm)	Δ_{mid} at P_u (mm)	Column	Failure location [#] (mm)	Peak Load P_u (kN)	Moment at P_u (kNm)	Δ_{mid} at P_u (mm)
FC60-1	+330	403	35.5	28.2	FC10-2	+230	1912	39.4	10.6
FC35-1	+50	714	38.9	19.4	PC60-1	+328	334	29.8	29.2
FC20-1	+200	1357	46.4	14.2	PC35-1	+238	773	43.4	21.2
FC10-1	+170	2221	42.0	8.9	PC20-1	*	1287	45.2	15.1
FC0-1-1	+150	2971	-	-	PC10-1	+20	1756	38.6	12.0
FC0-1-2	+50	2993	-	-	PC0-1-1	+150	2571	-	-
FC60-2	+330	317	23.3	13.5	PC0-1-2	+160	2495	-	-
FC35-2	-50	833	43.0	16.6	FC0	+200	2510	-	-
FC20-2	-5	1367	47.0	14.4					

Notes: # + is above and - is below column mid height, * test stopped before fibre rupture

For each CFRP confined column tested, snapping sounds were heard near the peak load as the fibres began to rupture; however, there were no visible signs of impending failure on the surface of the wrapping. For columns tested under load eccentricities of 10, 20 and 35 mm, failure occurred when the longitudinal FRP wrapping ruptured in tension and the circumferential wrapping split vertically on the tensile side. Figure 3 shows that the compressive concrete was under a considerable confining pressure towards the end of the test, particularly for the columns with the smaller 10 and 20 mm initial loading eccentricities. In the eccentrically loaded specimens the final failure occurred well beyond the peak loading, as shown in Figure 4. The peak axial loads and corresponding moments for the CFRP confined RPC columns are plotted in Figure 5, together with the axial force bending moment interaction

diagram. The interaction diagram was obtained using an elastic-plastic stress-strain model with a yield stress of $0.85f_{cm}$, elastic modulus of 42.5 GPa and compressive failure strain of 0.005. The figure shows that the peak load is greater than the model calculation. The concentrically loaded columns failed in a sudden and explosive manner and the descending branch could not be captured using the ram displacement control. For CFRP confined specimens tested the failure was characterized by CFRP failing in hoop tension followed immediately by explosive rupture of the RPC. Table 4 shows that the confinement provided to specimen FC0-1-2 increased the failure load by 19% over that of the unconfined specimen FC0.

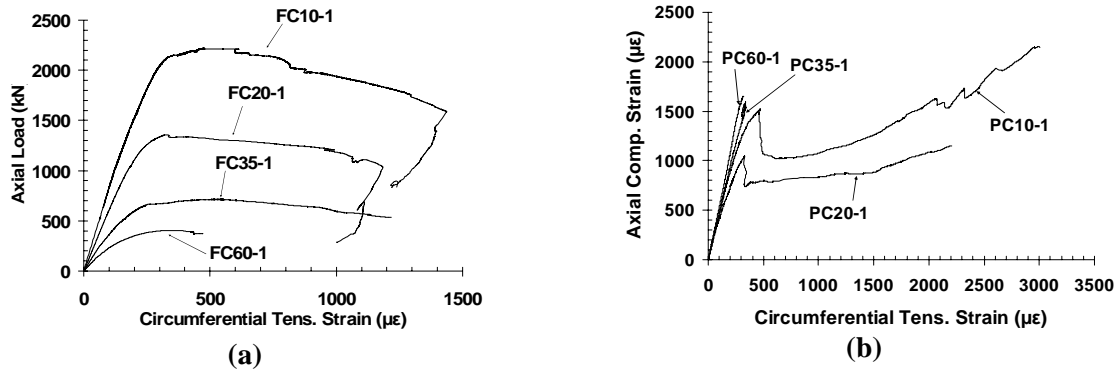


Figure 3. (a) Axial load versus circumferential tensile strain and (b) Axial compressive strain versus circumferential tensile strain.

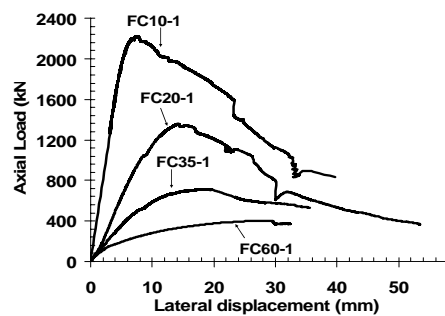


Figure 4. Axial load versus mid height lateral displacement.

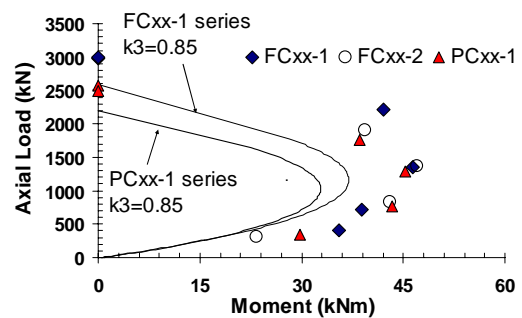


Figure 5. Peak axial loads and corresponding moments for the columns tested.

4. CONCLUSIONS

In this study, 17 RPC columns were tested with 16 confined using CFRP. For the concentrically loaded specimens, failure occurred at or close to the peak loading with little or no residual capacity. The CFRP confinement increased the axial load capacity for concentrically loaded columns by 19% compared with unconfined column. For the eccentrically loaded specimens, the CFRP was shown to be effective in controlling the failure of the specimens with considerable straining occurring beyond the peak loading. There was no evidence, however, that the use of CFRP in the hoop direction significantly increased the strength of the columns. As hoop strains increased, beyond the peak loading, the stresses in the wrapping induced failure of the hoop CFRP and explosive collapse of specimen resulting in a total loss of residual strength. Further investigations are needed to assess the effect of different types and orientations of CFRP sheets to establish general design guidelines for CFRP confined RPC columns.

5. REFERENCES

- ASTM D3039, (2005). "Standard Test Method for Tensile Properties of Polymer Matrix Composite Materials", *ASTM International*.
- Fam, A., Flisak, B., and Rizkalla, S. (2003). "Experimental and analytical modelling of concrete-filled fiber-reinforced polymer tubes subjected to combined bending and axial loads", *ACI Structural Journal*, Vol.100, No.4, pp 499-509.
- Richard, P. and Cheyrezy, M. (1995). "Composition of reactive powder concretes", *Cement and Concrete Research*, Vol. 25, No.7, pp 1501-1511.

STRENGTHENING OF SHORT CIRCULAR RC COLUMNS WITH FRP JACKETS: A DESIGN PROPOSAL

T. Jiang

(PhD Student, The Hong Kong Polytechnic University, Hong Kong, China)

J.G. Teng

(Chair Professor of Structural Engineering, The Hong Kong Polytechnic University, Hong Kong, China)

ABSTRACT

This paper presents a design procedure for FRP jackets for the strengthening of short circular RC columns. The proposed procedure is limited to FRP jackets which are continuous over a strengthened region of the column and possess fibers oriented solely or predominantly in the hoop direction. The design procedure gives due attention to a number of significant issues: (a) the ultimate hoop strain of FRP jacket; (b) the stress-strain model; (c) the slenderness limit for short columns; and (d) the definition of an equivalent stress block for approximate section analysis. The design proposal has been developed within the framework of the Chinese code for the design of concrete structures (GB-50010 2002) for inclusion in the draft Chinese code for the application of FRP composites in construction.

KEYWORDS

FRP, Jackets, Confinement, RC Columns, Design

1. INTRODUCTION

Strengthening of reinforced concrete (RC) columns using fiber-reinforced polymer (FRP) jackets or wraps is now a widely accepted technique. This technique relies on the well-known fact that the compressive strength and ductility of concrete can be substantially enhanced by the confinement from the FRP jacket. This paper presents a design procedure for such FRP jackets which are continuous over a strengthened region of the column and possess fibers oriented solely or predominantly in the hoop direction. The proposed procedure gives due attention to a number of significant issues: (a) the ultimate hoop strain of FRP jacket; (b) the stress-strain model; (c) the slenderness limit for short columns; and (d) the definition of an equivalent stress block for approximate section analysis. The design proposal has been developed within the framework of the Chinese code for the design of concrete structures (GB-50010 2002) for inclusion in the draft Chinese code for the application of FRP composites in construction.

2. ULTIMATE HOOP STRAIN OF FRP JACKET

It is well-known that the hoop rupture strain of FRP jackets confining concrete is significantly lower than that from tensile tests of FRP coupons (Lam and Teng 2004). In the design of FRP jackets, the ultimate hoop strain should be used in assessing the ultimate limit state of the jacket. This ultimate strain should be determined from one of two approaches. For a given FRP system, particularly a new system, a sufficiently large number of FRP-confined concrete cylinder tests should be conducted to find the characteristic value of the ultimate hoop strain. If such tests are not conducted for whatever reason, the characteristic value of the ultimate hoop strain $\varepsilon_{h,rupt}$ should be found from

$$\varepsilon_{h,rupt} = \eta \varepsilon_{frp,rupt} \quad (1)$$

where $\varepsilon_{frp,rupt}$ is the characteristic value of the material ultimate strain of FRP from flat coupon tests conducted according to ASTM D3039/D3039M-00 (2000) or similar specifications, and η is a reduction factor. Based on

recent test results (Xiao and Wu 2000, 2003; Lam and Teng 2003, 2004; Jiang and Teng 2006a), it is suggested that $\eta=0.5$ for CFRP and 0.7 for GFRP.

3. STRESS-STRAIN MODEL FOR FRP-CONFINED CONCRETE

In conventional section analysis of RC columns subjected to eccentric compression, the axial stress-strain curve of concrete is assumed to be the same as that from axial compression tests. The same assumption is also commonly used in the analysis of FRP-confined RC columns (e.g. Teng et al. 2002; Yuan and Mirmiran 2001). Although many stress-strain models have been developed (Teng and Lam 2004), the design-oriented model of Lam and Teng (2003) is believed to be particularly suitable for use in design due to its simplicity and accuracy. The model adopts a simple form (a parabolic first portion which connects smoothly to a linear second portion) which automatically reduces to that for unconfined concrete when no FRP is provided. It is proposed here that this model, incorporating the more accurate expressions for the compressive strength and the ultimate axial strain recently proposed by Teng et al. (2006) be adopted for design use. This refined version of Lam and Teng's model is described by the following expressions:

$$\sigma_c = E_c \varepsilon_c - \frac{(E_c - E_2)^2}{4f'_{co}} \varepsilon_c^2 \quad \text{for } 0 \leq \varepsilon_c < \varepsilon_t \quad (2a)$$

$$\sigma_c = f'_{co} + E_2 \varepsilon_c \quad \text{for } \varepsilon_t \leq \varepsilon_c \leq \varepsilon_{cu} \quad (2b)$$

where σ_c and ε_c are the axial stress and the axial strain respectively, E_c is the elastic modulus of unconfined concrete, E_2 is the slope of the linear second portion, f'_{co} is the compressive strength of unconfined concrete. The transition strain ε_t between the parabolic portion and the linear portion and the slope of the linear second portion E_2 are respectively given by

$$\varepsilon_t = \frac{2f'_{co}}{(E_c - E_2)} \quad ; \quad E_2 = \frac{f'_{cc} - f'_{co}}{\varepsilon_{cu}} \quad (3a); (3b)$$

where f'_{cc} and ε_{cu} are respectively the compressive strength and the ultimate axial strain of confined concrete and are given by

$$\frac{f'_{cc}}{f'_{co}} = \begin{cases} 1 & \text{if } \rho_K < 0.01 \\ 1 + 3.5(\rho_K - 0.01)\rho_\varepsilon & \text{if } \rho_K \geq 0.01 \end{cases} \quad (4)$$

$$\frac{\varepsilon_{cu}}{\varepsilon_{co}} = 1.65 + 6.5\rho_K^{0.8}\rho_\varepsilon^{1.45} \quad (5)$$

where $\rho_K = E_{frp} t / (E_{seco} R)$ is the confinement stiffness ratio and $\rho_\varepsilon = \varepsilon_{n,rup} / \varepsilon_{co}$ is the strain ratio. It should be noted that the confinement ratio f_1 / f'_{co} can be interpreted as a product of ρ_K and ρ_ε ($f_1 / f'_{co} = \rho_K \rho_\varepsilon$). E_{frp} is the elastic modulus of FRP in the hoop direction, t is the thickness of the FRP jacket, R is the radius of the confined concrete core, E_{seco} and ε_{co} are the secant modulus and the axial strain at the compressive strength of unconfined concrete, with $E_{seco} = f'_{co} / \varepsilon_{co}$. When this model is used in a design specification, the model may need small adjustments so that the curve reduces to that for unconfined concrete in a specific national code. In GB-50010 (2002), normal strength concrete is assumed to have $\varepsilon_{co} = 0.002$ and an ultimate strain of 0.0033. As a result, $E_c = 1000f'_{co}$ and the original value of 1.75 for the first item on the right hand side of Eq. (5) in the original model (Lam and Teng 2003; Teng et al. 2006) is replaced by 1.65, so that the stress-strain model for FRP-confined concrete reduces to that for unconfined normal strength concrete adopted by GB-50010 (2002) when no FRP is provided.

4. SLENDERNESS LIMIT FOR SHORT COLUMNS

A comprehensive numerical study (Jiang and Teng 2006b) has recently been conducted to develop a reliable definition of the slenderness limit for short FRP-confined RC columns, in which a computer analysis of slender FRP-confined RC columns was developed using the stress-strain model for FRP-confined concrete in compression described in the preceding section. The analysis is for columns pinned at both ends, and is based on the following

assumptions: (a) the lateral deflection of the column is small in comparison with its length; (b) plane sections remain plane; (c) the concrete does not resist any tension; (d) the steel reinforcement has an elastic-perfectly plastic stress-strain curve; and (e) any confinement from transverse steel reinforcement is negligible. For relatively short columns where material failure occurs before stability failure, the ultimate limit state of the column is reached when the strain at the extreme concrete compression fiber of the critical section reaches the ultimate axial strain of FRP-confined concrete, which is defined by Equation (5). By contrast, for longer columns where stability failure occurs before material failure, the ultimate limit state of the column is characterized by the attainment of the maximum axial load.

The slenderness limit for short RC columns may be defined to ensure that the second order effect leads to only a small amplification of the moment at the critical section or a small reduction (commonly 5% or 10%) of the axial load capacity. In Jiang and Teng's (2006b) study, the latter option was adopted. The slenderness ratio for RC columns is commonly defined as $\lambda = l/r$, where l is the effective length of a column and r is the radius of gyration and $= R/2$ for circular columns. To develop a slenderness limit for FRP-confined RC circular columns, a large parametric study was carried out. Based on the results from this parametric study, the slenderness limit for short FRP-confined RC columns was proposed to be (Jiang and Teng 2006b):

$$\lambda_{crit} = \frac{60 \frac{e_2}{D} (1 - \frac{e_1}{e_2}) + 20}{\frac{f'_{cc}}{f'_{co}} (1 + 0.06 \frac{\epsilon_{h,rup}}{\epsilon_{co}})} \quad (6)$$

where D is the column diameter, and e_1 and e_2 ($e_2 \geq 0$; $|e_2| \geq |e_1|$) are the load eccentricities at the two column ends.

This expression has a clear physical meaning: the numerator defines the slenderness limit for short RC columns without FRP confinement, while the denominator accounts for the effect of FRP confinement. When no FRP confinement is provided and $e_2/D = 0.2$, Equation (6) reduces to $\lambda_{crit} = 32 - 12e_1/e_2$, which is similar to but slightly more conservative than the expression adopted by ACI-318 (2005). Besides, when $e_1/e_2 = 1$, Equation (6) reduces to $\lambda_{crit} = 20$, which is the slenderness limit for short RC columns without FRP confinement given in GB-50010 (2002). Numerical results for the slenderness limit corresponding to a 5% axial load reduction obtained by Jiang and Teng (2006b) are shown in Figure 1. These results are for columns with a longitudinal steel reinforcement ratio ρ_{sc} of 1% and with the circle connecting the centroids of longitudinal reinforcing bars having a radius R_s equal to 70% of the column radius R . Columns experience a larger second order effect when the longitudinal steel reinforcement ratio is smaller and concrete cover is thicker, although the effects of these two parameters are limited. It can be seen from Figure 1 that Equation (6) is conservative for all cases except when the slenderness limit is very small. However, if a 10% loss of axial load capacity is acceptable, numerical results not given here indicated that Equation (6) provides a lower bound prediction for all cases. A 10% reduction in the axial load capacity has been adopted as the criterion for permitted second effects in the existing literature [e.g. CEB-FIP (1993)].

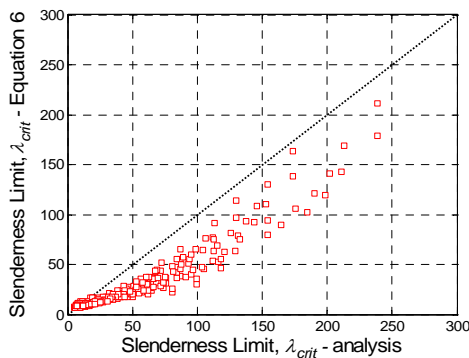


Figure 1: Slenderness Limit for Short Columns

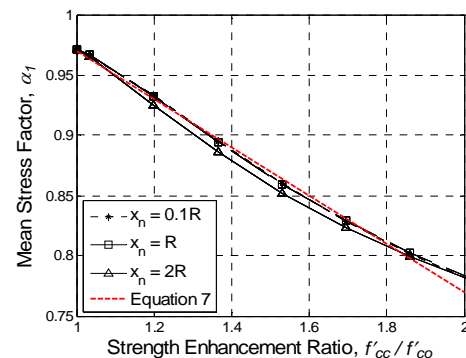


Figure 2: Mean Stress Factor α_1

5. SIMPLIFIED DESIGN EQUATIONS

The strength of a short circular RC column can be found by section analysis. While such section analysis can be conducted using the fiber element approach (e.g. Teng et al. 2002), a simplified approach using an equivalent stress

block is given in GB-50010 (2002). This section presents a similar simplified approach for FRP-confined circular RC columns.

5.1 Stress Block Factors for FRP-confined Concrete

GB-50010 (2002) defines two stress block factors for the compressive concrete in a circular RC section: α_1 which is the mean stress factor and β_1 which is the block depth factor. It recommends that $\alpha_1 = 1$ and $\beta_1 = 0.8$. However, if $\beta_1 = 0.8$ is adopted as the block depth factor for FRP-confined RC columns, a unified and accurate expression for α_1 for different neutral axis depths x_n cannot be obtained. From a trial-and-error process, it was found that when $\beta_1 = 0.9$, the influence of x_n on α_1 can be ignored (Figure 2). The following simple expression can then be proposed for α_1

$$\alpha_1 = 1.17 - 0.2(f'_{cc}/f'_{co}) \quad (7)$$

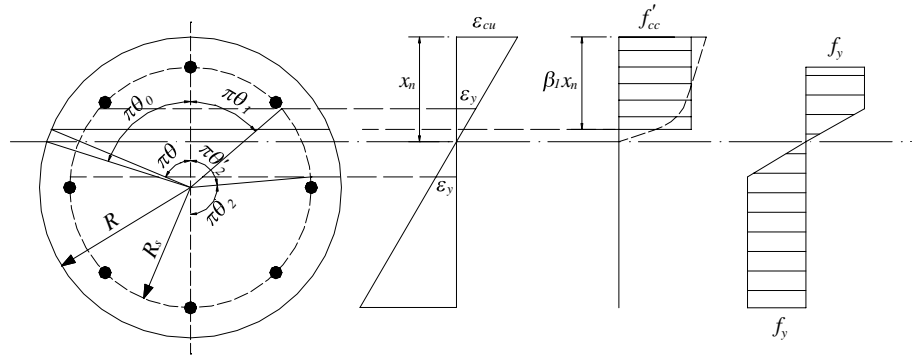


Figure 3: Stresses and Strains over a Circular Section

5.2 Simplified Section Analysis for Design Use

Using the stress block factors proposed above, a simplified section analysis is presented herein, which has been modified from the procedure given in GB-50010 (2002) for the design of circular RC columns. This method is only applicable to columns which have 6 or more evenly distributed longitudinal steel reinforcing bars. As shown in Figure 3, the steel reinforcing bars are smeared into an equivalent steel cylinder of the same total cross sectional area and with longitudinal strength only. $2\pi\theta_0$, $2\pi\theta$, $2\pi\theta_1$ and $2\pi\theta_2$ are respectively the central angles corresponding to the depths of the neutral axis, the equivalent stress block, the yielded compressive steel reinforcement and the yielded tensile steel reinforcement. θ_0 , θ , θ_1 and θ_2 can be calculated from Equation (8) and it is obvious that $\theta_2 = 1 - \theta_1$.

$$\theta_0 = \frac{\arcsin\left[1 - \xi_n(1 + R_s/R)\right]}{\pi} \quad ; \quad \theta = \frac{\arcsin\left[1 - \beta_1 \xi_n(1 + R_s/R)\right]}{\pi} \quad (8a); (8b)$$

$$\theta_1 = \frac{\arcsin\left[R/R_s - (1 - \beta)\xi_n(1 + R/R_s)\right]}{\pi} \quad ; \quad \theta_2 = \frac{\arcsin\left[R/R_s - (1 + \beta)\xi_n(1 + R/R_s)\right]}{\pi} \quad (8c); (8d)$$

where $\xi_n = x_n/h_0$ is the ratio between the neutral axis depth and the effective height of the section h_0 ($h_0 = R + R_s$). β is the ratio between the yield strain of the steel reinforcement to the strain of the ultimate compressive strain of FRP-confined concrete and are given by

$$\beta = \frac{f_y}{E_s \varepsilon_{cu}} \quad (9)$$

The axial load and bending moment carried by concrete can then be calculated from

$$N_c = \alpha_1 f'_{cc} \theta A \left(1 - \frac{\sin 2\pi\theta}{2\pi\theta}\right) \quad ; \quad M_c = \frac{2}{3} \alpha_1 f'_{cc} A R \frac{\sin^3 \pi\theta}{\pi} \quad (10a); (10b)$$

while those carried by the steel reinforcement can be calculated from

$$N_s = f'_y A_s (\theta_1 + k_c) - f_y A_s (\theta_2 + k_t) \quad (11a)$$

$$M_s = f'_y A_s R_s \frac{\sin \pi \theta_1 + m_c}{\pi} + f_y A_s R_s \frac{\sin \pi \theta_2 + m_t}{\pi} \quad (11b)$$

where

$$k_c = \frac{[\xi_n (1 + R/R_s) - R/R_s] \pi (\theta_0 - \theta_1) + \sin \pi \theta_0 - \sin \pi \theta_1}{\pi \beta \xi_n (1 + R/R_s)} \quad (12a)$$

$$k_t = -\frac{[\xi_n (1 + R/R_s) - R/R_s] \pi (\theta_2' - \theta_0) + \sin \pi \theta_2' - \sin \pi \theta_0}{\pi \beta \xi_n (1 + R/R_s)} \quad (12b)$$

$$m_c = \frac{[\xi_n (1 + R/R_s) - R/R_s] (\sin \pi \theta_0 - \sin \pi \theta_1) + \frac{\pi (\theta_0 - \theta_1)}{2} + \frac{\sin 2\pi \theta_0 - \sin 2\pi \theta_1}{4}}{\pi \beta \xi_n (1 + R/R_s)} \quad (12c)$$

$$m_t = \frac{[\xi_n (1 + R/R_s) - R/R_s] (\sin \pi \theta_2' - \sin \pi \theta_0) + \frac{\pi (\theta_2' - \theta_0)}{2} + \frac{\sin 2\pi \theta_2' - \sin 2\pi \theta_0}{4}}{\pi \beta \xi_n (1 + R/R_s)} \quad (12d)$$

Obviously, Equations (11) and (12) are too complex for design use. As a result, the following approximate expressions are proposed:

$$0 \leq \theta_c = \theta_1 + k_c = 1.25\theta - 0.125 \leq 1; \theta_t = \theta_2 + k_t = \max(1.125 - 1.5\theta, 0) \quad (13a); (13b)$$

Using Equation (13), the expressions $\sin \pi \theta_1 + m_c$ and $\sin \pi \theta_2 + m_t$ in Equation (11b) can be numerically approximated by $\sin \pi \theta_c$ and $\sin \pi \theta_t$ respectively. Equation (13) was derived with the assumption of $R/R_s = 1.16$, as was used in developing similar expressions in GB-50010 (2002). This assumption implies unrealistic concrete covers for very large and very small columns, and may render the section analysis slightly un-conservative for small columns. Nevertheless, Equation (13) is still sufficiently accurate for small columns as shown below.

Based on the above simplifications, the design equations can now be written as

$$N_u = \alpha_1 f'_{cc} A \theta \left(1 - \frac{\sin 2\pi \theta}{2\pi \theta} \right) + (\theta_c - \theta_t) f_y A_s \quad (14a)$$

$$M_u = \frac{2}{3} \alpha_1 f'_{cc} A R \frac{\sin^3 \pi \theta}{\pi} + f_y A_s R \frac{\sin \pi \theta_c + \sin \pi \theta_t}{\pi} \quad (14b)$$

where N_u and M_u are the axial load capacity and the moment capacity, respectively.

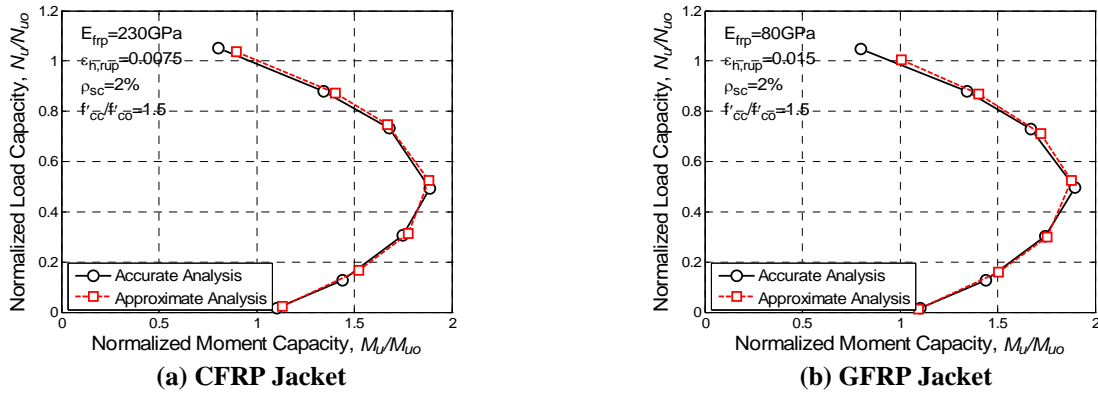


Figure 4: Comparisons between Accurate and Approximate Analyses

5.3 Accuracy of Approximate Design Equations

The predictions of Equation (14) are compared with the results of accurate section analysis in Figure 4 for a 300 mm diameter column wrapped with either CFRP ($E_{frp} = 230\text{Pa}$, $\varepsilon_{h,rup} = 0.0075$) or GFRP ($E_{frp} = 80\text{Pa}$, $\varepsilon_{h,rup} = 0.015$).

The other material properties are: unconfined concrete compressive strength $f'_{co} = 20.1$ MPa, steel yield strength $f_y = 335$ MPa, elastic modulus of steel $E_s = 200$ GPa. The interaction curves are normalized by the axial load capacity N_{uo} (concentric compression) and moment capacity M_{uo} (pure bending) of the column when no FRP confinement is provided. The approximate design equations are seen to provide accurate predictions. Their accuracy is even better for larger columns.

6. CONCLUSIONS

This paper has presented a design procedure for the strengthening of short circular RC columns with FRP jackets which are continuous over a strengthened region of the column and possess fibers oriented solely or predominantly in the hoop direction. The design procedure covers the following aspects: (a) the ultimate hoop strain of FRP jacket; (b) the stress-strain model; (c) the slenderness limit for short columns; and (d) the definition of an equivalent stress block for approximate section analysis. The design proposal was developed within the framework of the Chinese code for the design of concrete structures (GB-50010 2002) for inclusion in the draft Chinese code for the application of FRP composites in construction. The slenderness limit decreases with the confinement ratio, which indicates that FRP-confined RC columns are more prone to the slenderness effect than conventional RC columns. The slenderness limit equation presented in this paper was developed from columns with equal eccentricities at the two ends and are thus unnecessarily restrictive for other cases. Work is currently being conducted by the authors to develop a more accurate expression for such cases. The approximate design equations have been shown to provide close predictions of results from accurate section analysis.

7. ACKNOWLEDGEMENTS

The authors are grateful for the financial support received from the Research Grants Council of the Hong Kong SAR (Project No: PolyU 5059/02E) and The Hong Kong Polytechnic University (Project Codes: RG88 and BBZH).

8. REFERENCES

- ACI-318 (2005). *Building Code Requirements for Structural Concrete and Commentary*, ACI Committee 318.
- ASTM D3039/D3039M-00 (2000). *Standard Test Method for Tensile Properties of Polymer Matrix Composite Materials*, American Society for Testing Materials.
- CEB-FIP (1993). *Model Code 1990*, CEB-Bulletin No. 213/214, Comité Euro-International du Béton.
- GB-50010 (2002). *Code for Design of Concrete Structures*, China Architecture and Building Press, China.
- Jiang, T., and Teng, J.G. (2006a). "Analysis-oriented stress-strain models for FRP-confined concrete", in preparation.
- Jiang, T., and Teng, J.G. (2006b). "Slenderness limits for short FRP-confined RC columns", in preparation.
- Lam, L., and Teng, J.G. (2003). "Design-oriented stress-strain model for FRP-confined concrete", *Construction and Building Materials*, Vol. 17, No. 6-7, pp. 471-489.
- Lam, L., and Teng, J.G., (2004). "Ultimate condition of fiber reinforced polymer-confined concrete", *Journal of Composites for Construction*, ASCE, Vol. 8, No. 6, pp. 539-548.
- Teng, J.G., Chen, J.F., Smith, S.T., and Lam, L. (2002). *FRP-Strengthened RC Structures*, John Wiley and Sons, Inc.
- Teng, J.G., and Lam, L. (2004). "Behavior and modeling of fiber reinforced polymer-confined concrete", *Journal of Structural Engineering*, ASCE, Vol. 130, No. 11, pp. 1713-1723.
- Teng, J.G., Jiang, T., Lam, L., and Luo, Y.Z. (2006). "Refinement of a design-oriented stress-strain model for FRP-confined concrete", in preparation.
- Yuan, W., and Mirmiran, A. (2001). "Buckling analysis of concrete-filled FRP tubes", *International Journal of Structural Stability and Dynamics*, Vol. 1, No. 3, pp. 367-383.
- Xiao, Y., and Wu, H. (2000). "Compressive behavior of concrete confined by carbon fiber composite jackets", *Journal of Materials in Civil Engineering*, ASCE, Vol. 12, No. 2, pp. 139-146.
- Xiao, Y., and Wu, H. (2003). "Compressive behavior of concrete confined by various types of fiber composite jackets", *Journal of Reinforced Plastics and Composites*, Vol. 22, No. 13, pp. 1187-1201.

EXPERIMENTAL STUDY ON CONCRETE COLUMNS STRENGTHENED WITH CFRP SHEETS CONFINEMENT UNDER ECCENTRIC LOADING

Cao Shuangyin

(Professor, Southeast University, Nanjing, Jiangsu, China)

Jing Denghu

(Asst. lecturer, Southeast University, Nanjing, Jiangsu, China)

Sun Ning

(MSC research student, Southeast University, Nanjing, Jiangsu, China)

ABSTRACT

An experimental study of five eccentrically loaded concrete columns confined by unidirectional CFRP sheets is presented. The failure modes, strain distribution at sectional concrete, load capacities, lateral deflections, and strain distribution of CFRP sheets along the circumference were investigated. The results indicated that, via the reinforcement of CFRP sheets, ultimate load capacities of concrete columns were enhanced and ductility of columns was improved. The reinforcing efficiency decreased with the eccentricity increasing. For the column with a comparatively large eccentricity, though the reinforcing efficiency was limited, the failure mode of columns changed from compression to tension. It is also shown that, the plane strain remains, that is, the strain in sectional concrete is linearly proportional to the distance from the natural axis. The strain gradient in CFRP sheet, which is attributes to the non-uniform expansion of concrete, was also observed.

KEYWORDS

Carbon fiber reinforced plastic (CFRP), concrete columns, eccentric loading, strain gradient.

1. INTRODUCTION

The wrap with carbon fiber reinforced plastic (CFRP) sheets can improve compressive performances of concrete columns as a result of concrete core confinement. During the past decades efforts have been increasingly concentrated on studying concrete columns, especially concrete cylinders, under concentric loading (Teng and Chen 2002; Lorenzis and Tepfers 2003; Berthet et al. 2005). However, in field applications, there is no column that is under perfect concentric loading. Several studies on wrapping concrete columns under eccentric loading were conducted with bidirectional CFRP (Chaallal and Shahawy, 2000) or unidirectional CFRP (Parvin and Wang 2001; Li and Hadi 2003). Since the confinement of CFRP sheets to core concrete is passive, nonuniform-confining stress due to uneven dilation of compressive concrete must be considered. Parvin and Wang (2001) have examined the effect of strain gradient on FRP-jacketed concrete prisms, and concluded that the prediction of the ultimate strength depended on the ability of the model to contain the strain value of the FRP jacket. The purpose of this paper is to investigate the performances of rectangular reinforced concrete columns that are subjected to eccentric loading, wrapped with unidirectional CFRP sheets.

2. TEST PROGRAMME

Five test specimens (Fig.1) designed for the study were rectangular cross section of 250mm×250mm and had an overall length of 1350mm. The length between the corbels was 750mm. Steel reinforcement details of the specimens were presented in Fig.1. The actual 28-day concrete cube strength was 24.4 MPa. The columns were wrapped with one layer of unidirectional CFRP sheet with nominal thickness of 0.167mm; the ultimate tensile strength and

Young's modulus of CFRP were 3399 MPa and 235 GPa respectively. The columns were treated with 20mm radius corners. The columns were tested under monotonically increasing axial loads (Fig.2). The load was increased until the significant strength decay was recorded. This decay indicated failure of columns. The specimens of Z1, Z2, Z3, Z4, and Z5 had initial eccentricity of 0, 35, 55, 75, and 115mm respectively. The theoretical balanced condition requires that the initial eccentricity of unconfined column is 130mm according to actual strength of materials. During the test, strains distribution at sectional concrete, lateral deflections, circumferential strains in CFRP sheets and the load were monitored.

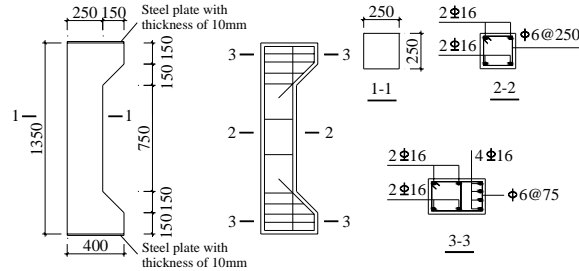


Figure 1: Details of Specimens



Figure 2: The Test Setup

3. EXPERIMENTAL RESULTS AND DISCUSSIONS

For all specimens, failures began with the bulge of CFRP sheets due to the dilation of core concrete (Fig.3a). The fiber broke off in certain corner first, and then the specimen failed in the sides with larger compression by crushing of the concrete near the middle section (Fig.3b, 3c, 3e). At the opposite side, for specimen Z2 with a small initial eccentricity, there were no cracks (Fig.3d), but for specimen Z3, Z4 and Z5, distinct horizontal cracks existed (fig. 3f), the crack width became wider with the increase of initial eccentricity.

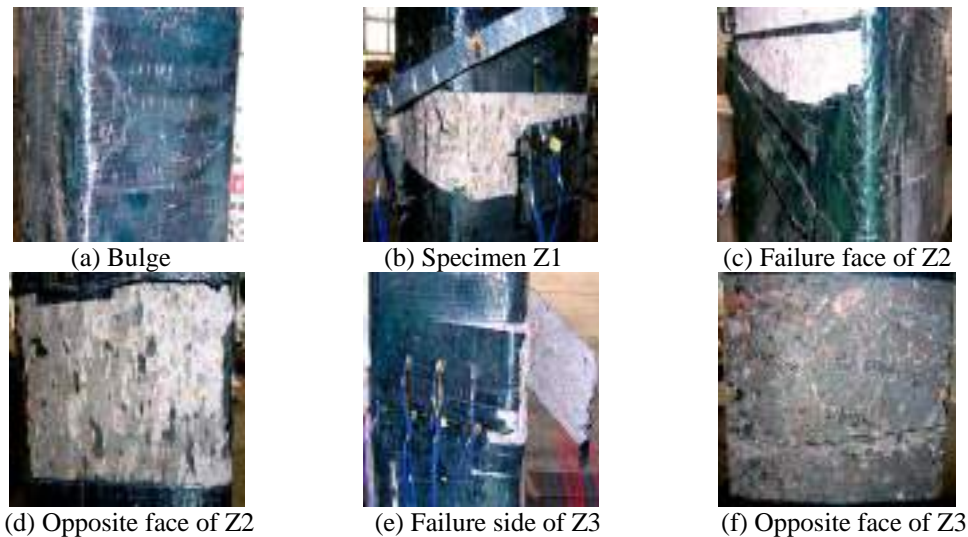


Figure 3: Typical Specimens after Failure

Testing results of five specimens were presented in Table 1, where the capacity of unconfined column was calculated in accordance with concrete theory. The test results indicated that, when the initial eccentricity was smaller than the balance condition, the CFRP confinement was also effective in strengthening concrete columns under eccentric loading. But when the initial eccentricity increased near to the balanced condition (Z5), the enhancement descended drastically. The maximum compressive strain of concrete was up to about 0.005, which was higher than that of unconfined concrete and had no large change as a result of different initial eccentricity (Except column Z2 due to its deviant failure). The maximum tensile strain was up to 35% of ultimate tensile strain of CFRP, which was lower than that of CFRP confining cylindrical concrete due to corner effect and cross section. The strain distributions across the

depth at middle section were displayed in Fig.4. The results showed the strain in the section was linearly proportional to the distance from the natural axis, and this was the same as that in unconfined concrete.

Table 1: Summary of Testing Results

Number of columns	Initial eccentricity (mm)	Deflection (mm)	Capacity (kN)	Compressive strain ($\mu\epsilon$)	Tensile strain ($\mu\epsilon$)	Failure position of CFRP	Enhancement compared to unconfined column	Failure position of columns
Z1	0	—	1975	—	5735	Corner	33.1%	Middle
Z2	35	2.26	1400	-2232	4063	Corner	33.8%	Upside
Z3	55	4.03	1175	-4891	5984	Corner	35.4%	Middle
Z4	75	5.58	1000	-4495	5240	Corner	36.2%	Upside
Z5	115	9.43	650	-5011	5394	Corner	19.2%	Middle

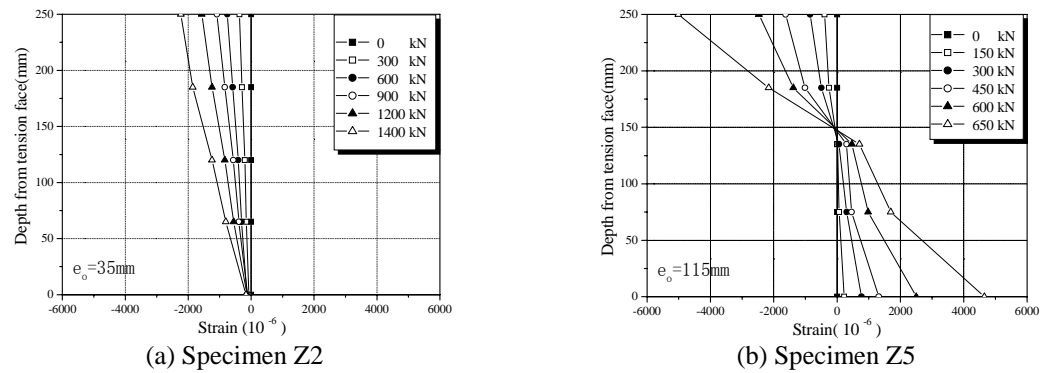


Figure 4: Strain Distribution across the Middle Section

In order to measure the strain distribution of externally confining fiber along the circumference, and so to understand the effectiveness of CFRP confinement in strengthening concrete columns under eccentric loads, strain gauges were bonded in CFRP out layer showed in Fig.5. From the test results showed in Fig.6, it could be seen that the higher the compression in the inner concrete, the greater the strain of external CFRP, and when the inner concrete were in tensile, the strains of CFRP were near to zero, which was similar to the results by Chaallal and Shahawy (2000).

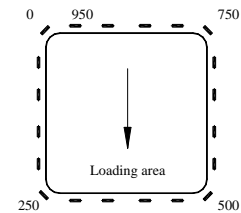
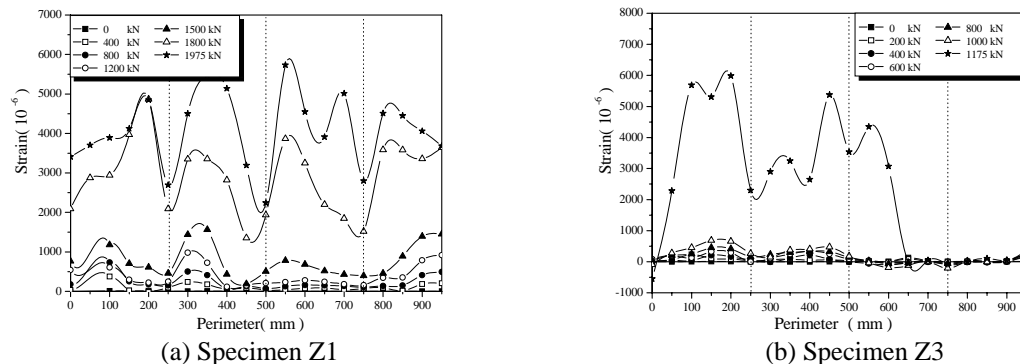
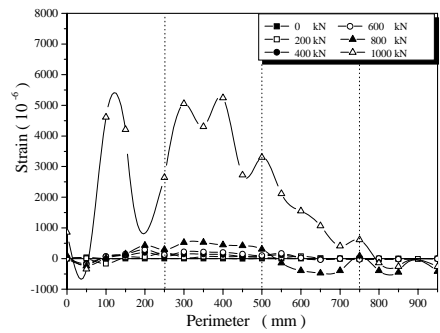


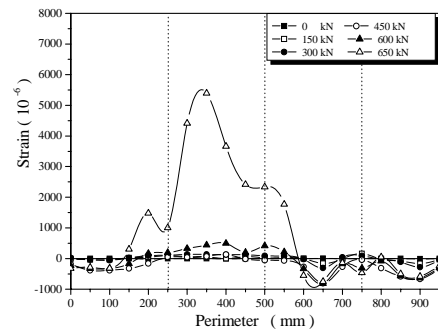
Figure 5: Points of Strain Gauges

The tested load–middle deflection curves were displayed in Fig.7, which indicated that the response consisted of three distinct regions. In the first region, the relation was linear. With the increase of load, a transition zone was entered. Finally, the slope of curve stabilized. Fig.8 showed the comparison of the theoretical $M - N$ curve of the specimens without CFRP confinement and that of the specimens with CFRP confinement. Here second order moments were considered. It could be seen that, for the specimen with an initial eccentricity near to balanced





(c) Specimen Z4



(d) Specimen Z5

Figure 6: Outspread Sketch of Strain of Externally Confining CFRP

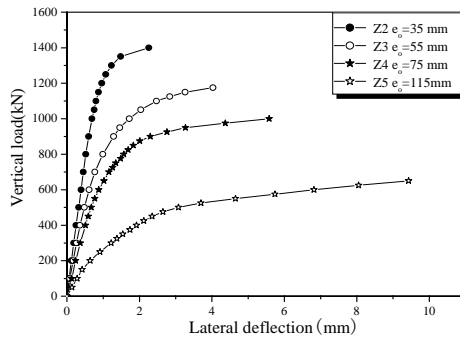


Figure 7: Curve of Load-deflection

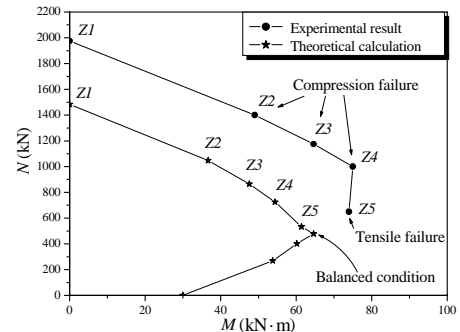


Figure 8: Curve of $M - N$

condition (specimen Z5), though the enhancement was not significant compared to specimens with small initial eccentricity (Z1 to Z4), the failure mode changed from compression to tension after wrapped by CFRP.

4. CONCLUSIONS

The experiment study of five concrete columns wrapped by one layer of unidirectional CFRP sheets under eccentric loading showed that, the CFRP confinement was also effective in strengthening eccentrically loaded concrete columns when the initial eccentricity was comparatively small. With the increase of initial eccentricity near to balanced condition, the reinforcement was not in much effect, but the failure mode of columns changed from brittleness to ductility. Strain gradient in CFRP sheets existed due to the uneven dilation of core concrete, and the assumption that the strain in sectional concrete is proportional to the distance from the natural plan remains.

REFERENCES

- Berthet J. F., Ferrier E., Hamelin P. (2005) "Compressive behavior of concrete externally confined by composite jackets, Part A: experimental study", *Construction and building Materials*, Vol.19, pp 223-232
- Chaallal O., Shahawy M. (2000). "Performance of Fiber-reinforced Polymer-wrapped Reinforced Concrete Column under Combined Axial-flexural Loading", *ACI Structural Journal*, Vol. 97, No. 4, pp 659-668.
- Li J., Hadi M. N. S. (2003) "Behavior of Externally Confined High-strength Concrete Columns under Eccentric Loading", *Composites Structures*, Vol. 62, pp 145-153
- Lorenzis L. D., Tepfers R. (2003) "Comparative study of models on confinement of concrete cylinders with fiber-reinforced polymer composites", *Journal of Composites for Construction*, Vol.7, No.3, pp 219-237
- Parvin A., Wang W. (2001). "Behavior of FRP Jacketed Concrete Columns under Eccentric Loading", *Journal of Composites for Construction*, Vol. 5, No. 3, pp 146-152.
- Teng J. G., Chen J. F., and Smith S. T. (2002). "FRP Strengthened RC Structures", England: John Wiley & Sons, LTD

INFLUENCE OF RADIUS OF CORNERS IN CONCRETE COLUMNS CONFINED WITH FRP SHEETS

Giuseppe Campione

(Associate Professor, University of Palermo, Palermo, Italy)

Nunzio Miraglia

(Assistant Professor, University of Palermo, Palermo, Italy)

Maurizio Papia

(Full Professor, University of Palermo, Palermo, Italy)

ABSTRACT

In the present paper the confinement effects induced in short compressed concrete members externally wrapped with fiber reinforced plastic (FRP) is investigated. Effect of radius of corners and local reinforcements constitute by single strips applied at corners before the continuous wrapping in square cross-sections are considered. The model allows one to evaluate the equivalent uniform confining pressure at ultimate conditions referred to the effective stresses in FRP along the sides of section; consequently, it makes it possible to determine the equivalent confinement pressures exercised by the FRP wraps.

KEYWORDS

FRP; confinement; square cross-section; stress-concentration; sharp corners, smoothed corners; local reinforcement.

1. PROPOSED MODEL

In order to reduce the stress-concentration at the corners of a concrete cross-section wrapped with FRP sheets, two different techniques are available: - the first one is the well know technique (Mirmiran et al. 1998) consisting in smoothing sharp corners with adequate radius of concrete cross-section (see Fig. 1a); - the second one is the reinforcement technique proposed by Campione et al. (2004), consisting in local strengthening at the corner constituted by single strips applied before the continuous wrapping (see Fig. 1b). It has to be observed that the first technique reduces the risk of local failure of fiber at the corners and also increases the equivalent confinement pressures, while the second technique lightly increases the confinement pressures and produces over strength of fibers at the corners, reducing the risk of local failure.

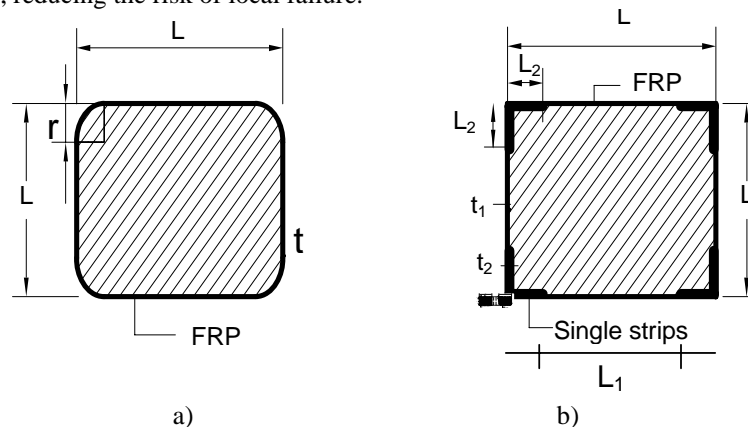


Figure 1: Reinforcing technique at the corners

To explain in a simplified way the confinement effects in the concrete core due to the presence by FRP wraps, which can be pointed out numerically by a finite element approach, a recent model proposed by the authors (Campione et al. 2004) is briefly summarized. It refers to the geometrical model shown in Fig. 2, representing a three dimensional prismatic concrete member having square cross-section of side L with smoothed corners with radius r and eternally wrapped with FRP wraps. The continuous FRP wrap is assumed to be externally applied to the concrete surface with an adequate overlap length and it is not directly axially loaded. If the concrete member is loaded axially and maintains its prismatic shape, it tends to be subjected to axial and lateral strains partially reduced by the presence of the FRP sheet. Therefore, the increase in the bearing capacity of the member is due to the share of normal stress depending on the confinement lateral stresses and a three dimensional model is necessary to consider these effects. It is possible to further simplify the three dimensional model by assuming a plane model (transverse cross-section) and considering, due to the symmetry of the system, only one quarter of the transverse cross-section, as shown in Fig. 2.

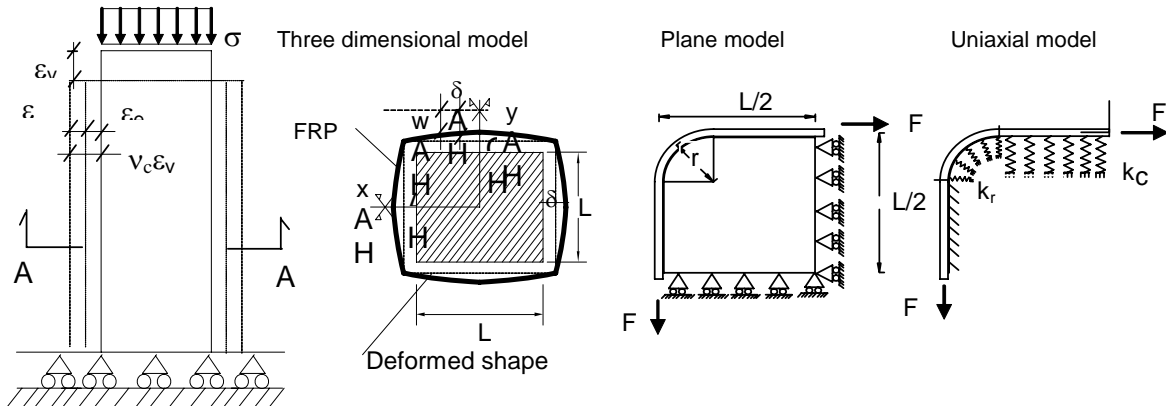


Figure 2: Geometrical model for FRP wrapped prismatic specimens

When lateral expansion occurs in the concrete member, the displacement along the diagonal direction corresponds to the lateral elongations along the two sides of the cross-section. These elongations can be assumed to be produced by two elastic beams (FRP sheets) on uniaxial springs (concrete) and connected at the corners of the cross-section. The elastic beams on elastic springs are stiffened in flexure by including also the effect of axial forces in FRP; nevertheless, because in wrapped cross-section the stresses in FRP are very low with respect to tensile strength of material and very low thickness of reinforcing layers are utilized, the afore mentioned stiffness effect is negligible with respect to the confinement pressures distribution. The membrane effect can be taken into account by imposing that the displacement at the end of the beam (corner of cross-section) is equal to the elongation of the FRP package in the perpendicular direction. To determine the confinement pressures q (interaction between concrete core and FRP wrap acting perpendicular to the lateral concrete surface) it is assumed that the beam behaves as semi-infinite elastic member on elastic springs, subjected to the tensile force F shown in Fig.2. More in details, the two elastic beams having length $L/2 - r$ simulating the FRP package have flexural stiffness proportional to the quantity $E_f t^3/12$, E_f being the modulus of elasticity and t the thickness of the FRP sheet. The elastic springs are considered acting each separately from another and their stiffness takes the presence of the concrete core shell into account. This stiffness can be assumed to be proportional to the stiffness of the confined concrete core. Its value for unit length is $k_v = \frac{E_c}{(L/2 - r) \cdot (1 - 2 \cdot v_c)}$, E_c being the modulus of elasticity of concrete, L the side of the cross-section considered and r the radius of corner of fillet.

The equilibrium equation of the elastic beam of inertia I_f , on elastic springs (see Fig. 2), in term of lateral displacements w , is governed by the following differential equation:

$$\frac{d^4 w}{dx^4} + \frac{k_v}{E_f \cdot I_f} (\delta - w) = 0 \quad (1)$$

Where δ is the lateral displacement of the unconfined concrete specimen and w the actual displacement. If we consider that the elastic beam of length $B/2 - r$ is connected to the perpendicular legs by means of a quarter of

cylinder having axial stiffness $k_r = \frac{E_c}{r \cdot (1 - 2 \cdot \nu_c)}$ by imposing the boundary conditions it is possible to obtain the

$w(x)$ referred to the beam of length $L/2 - r$.

The boundary conditions are: i) the displacement at the tip of the beam is equal to the elongation of FRP along the round fillets and the flat portion plus the radial shortening of concrete cylinder having radius r ; ii) in the same section ($x = 0$ tip of the beam) the rotation is zero. Therefore the following relationships are obtained:

$$w(x=0) = F \cdot \left[\frac{1}{E_f \cdot t} \cdot \left(\frac{L}{2} - r + \frac{\pi \cdot r}{2} \right) + \frac{(1 - 2 \cdot \nu_c)}{E_c} \right] \quad (2)$$

$$\frac{dw}{dx}(x=0) = 0$$

By setting $\beta = \sqrt[4]{\frac{3k_v}{t^3 \cdot E_f}}$ and by integrating the equilibrium equation, Eq. (1), Eq. (2) into account gives the following expressions of the displacement w and of the confinement pressure q :

$$w(x) = \left\{ F \cdot \left[\frac{1}{E_f \cdot t} \cdot \left(\frac{L}{2} - r + \frac{\pi \cdot r}{2} \right) + \frac{(1 - 2 \cdot \nu_c)}{E_c} \right] - \delta \right\} \cdot e^{-\beta x} \cdot \cos(\beta x) + \delta \quad (3)$$

$$q(x) = k_v \cdot (\delta - w) \quad (4)$$

Consequently the resultant of confining pressures along the flat portion proves to be:

$$R = \int_0^{L/2-r} q(x) \cdot dx = k_v \cdot \left\{ \delta - F \cdot \left[\frac{1}{E_f \cdot t} \cdot \left(\frac{L}{2} - r + \frac{\pi \cdot r}{2} \right) + \frac{1 - 2 \cdot \nu_c}{E_c} \right] \right\} \cdot \frac{1}{2 \cdot \beta} \cdot \left[1 - e^{-\beta \left(\frac{L}{2} - r \right)} \cdot \left(\cos \beta \cdot \left(\frac{L}{2} - r \right) - \sin \beta \cdot \left(\frac{L}{2} - r \right) \right) \right] \quad (5)$$

To determine the axial forces in FRP, the equilibrium between the resultant of confinement pressures (in the beam of length $B/2 - r$ plus the contribution due to the circular cylinder) and the force F was imposed, resulting:

$$F = \frac{\frac{k_v}{2 \cdot \beta} \cdot \left[1 - e^{-\beta \left(\frac{L}{2} - r \right)} \cdot \left(\cos \beta \cdot \left(\frac{L}{2} - r \right) - \sin \beta \cdot \left(\frac{L}{2} - r \right) \right) \right] \cdot \delta}{1 + \left[\frac{1}{E_f \cdot t} \cdot \left(\frac{L}{2} - r + \frac{\pi \cdot r}{2} \right) + \frac{1 - 2 \cdot \nu_c}{E_c} \right] \cdot \left\{ \frac{k_v}{2 \cdot \beta} \cdot \left[1 - e^{-\beta \left(\frac{L}{2} - r \right)} \cdot \left(\cos \beta \cdot \left(\frac{L}{2} - r \right) - \sin \beta \cdot \left(\frac{L}{2} - r \right) \right) \right] \right\}} \quad (6)$$

Therefore the equivalent confinement pressure is $f_{1e} = \frac{2 \cdot F}{L}$. In the case of square section ($r=0$) and FRP layers having t_2 thickness and L_2 length at the corners and t_1 thickness in the other part with length $L_1 = L - 2 L_2$, (see Fig 1b), the expression of F force given in Campione et al. (2004).

2. EXPERIMENTAL AND ANALYTICAL VALIDATION

To validate the proposed model two different recent investigations are considered. The first one (Yang et al. 2001) is of experimental nature and it analyses the effect of corner radius on the confinement properties of FRP wraps. In this case unique re-usable aluminum devices were utilised for support of plies of FRP externally bonded. Aluminum device had side of length L and interchangeable corners insert allowing corners of different radius r . Direct tensile test on the devices allows one to force FRP wraps in tension, transmitting stresses around the perimeter of the aluminum devices. Strain measurement along the corners and along the flat portion of the FRP was made allowing one to measure the FRP stress with the variation in the radius of corners. The case of one ply of high strength and low modulus of carbon fiber (ultimate stress 4275 MPa and tensile modulus of 228 GPa) externally bonded to aluminum devices was considered. The variation of maximum stress reached at rupture of FRP with variation in the radius of corners, for $L = 150$ mm was measured. Fig. 3 shows the experimental values (maximum stress is made dimensionless with respect to the ultimate stress measured in circular cross-section, and radius of corner is made dimensionless with respect to the side B). Analytical prediction according to the proposed model (Eq. 6) is also given in the same figure. The analytical results are generated considering for the aluminum device the modulus $E_c = 70$ GPa and the Poisson ratio $\nu = 0.35$. The comparison shows acceptable agreement between analytical and experimental predictions for low values of radius of corners, while for the case of circular cross-section ($r/b = 0.5$) the analytical model provides higher values than the experimental value, which is almost equal to 0.66.

The second case examined refers to the analytical investigation of Karam and Tabbara (2005), in which a refined element model by using the ADINA program was developed, using a nonlinear concrete constitutive law in order to analyze stresses in columns passively confined with FRP wraps. Rectangular and square cross-sections of variable corner radii were investigated. Case here considered is that of concrete member with square cross-section of side $L = 150$ mm externally wrapped with FRP having 1 mm thickness per ply, ultimate strain of 1.5% and modulus of elasticity 105 GPa. Concrete had initial modulus of elasticity of 26 GPa, Poisson ratio 0.18 and strength of unconfined concrete of 30 MPa.

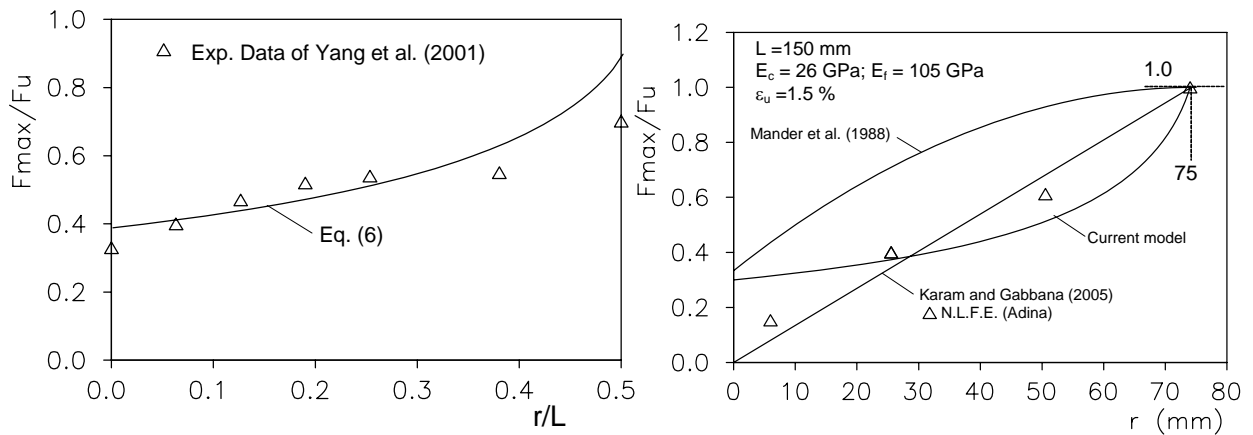


Figure 3: (a, b) Experimental and analytical validation

Results obtained by Karam and Tabbara (2005) by using finite element analysis showed that it is possible to simplify the problem by assuming no friction relations between confining stress and stress in FRP and by assuming FRP as a cable around the corner similar to a pulley. The variation of the stress in FRP with variation in the radius r is almost linear. Fig. 3b shows the variation of ultimate stress reached in FRP at concrete rupture, normalized with respect to the ultimate stress allowable in FRP, with the increase in the radius of corner. In the same graph prediction according to the proposed model, and to the Mander et al. (1988) model and to nonlinear finite element analysis carried out by the Karam and Tabbara (2005) are given. In the Mander et al. (1988) model the actual stress in FRP was taken into account (see Karam and Tabbara 2005) by means of a confinement effectiveness coefficient.

The proposed model is utilised by assuming in Eq. (6) for E_c a value equal to $2/3$ of the initial value, and the Poisson ratio equal to 0.49. It is interesting to observe that the model of Mander et al (1988) overestimates the maximum allowable stress compared with the two other models. The proposed model is the most conservative for high value of radius of corners; moreover, it gives a value of stress in members with sharp corner which is not zero, but essentially depending on the confinement stiffness factor, as observed by Karam and Tabbara (2005).

3. CONCLUSIONS

In the present paper the confinement effects induced in short compressed concrete members by external fiber reinforced plastic (FRP) wrap is investigated. Square cross-sections with round corners are considered. The effect of the increases in the radius of corner in the increase in the allowable stress in FRP at concrete failure was analysed. According with the proposed model it was demonstrated the relation between allowable force in FRP and the radius of corner is not linear and it depends on several factors such as: - fiber type and its thickness and modulus of elasticity; - concrete characteristic (though the modulus of elasticity, and the Poisson ratio of concrete); - dimension of cross-section. Moreover, some other parameters such as the length of the specimens (Campione, 2006) and the premature failure of FRP at the corners due to cutting effects in FRP can reduce drastically the effectiveness of devices and furthers experimental and analytical work is necessary to give more general conclusions.

4. REFERENCES

- Mirmiran, A., Shahawy, M., Samaan, M., EL Echary, H., Mastrapa, J.C. and Pico, O. (1998), "Effect of column parameters on FRP-confined concrete". *J. of Comp. for Constr., ASCE*, Vol. 2, n.4, pp.175-185.
- Mander, J.B., Priestley, M.J.N., and Park, R. (1988), "Theoretical stress-strain model for confined concrete". *Journal of Struct. Engng. ASCE*, Vol. 114 n.8, pp. 1804-1826.
- Yang, X., Nanni, A. and Chen, G. (2001), "Effect of corner radius on the performance of externally bonded FRP reinforcement". *Proc. of FRPRCS5, Non-metallic reinforcement for concrete structures*, Cambridge, UK, July, pp. 16-18.
- Campione G , Miraglia N. and Papia M, (2004), "Strength and strain enhancements of concrete columns confined with FRP sheets". *Structural Engineering and Mechanics*, Vol. 18, n. 6, pp. 769-790.
- Karam G. and Tabbara M. (2005), "Confinement effectiveness in rectangular concrete columns with Fiber reinforced polymer wraps". *J. of Comp. for Constr., ASCE*, Vol. 9, n. 5, pp. 388-396.
- Campione G. (2006)," Influence of FRP wrapping techniques on the compressive behavior of concrete prisms", *Cement & Composite Composites*, Vol.28, n.5, pp. 497-505.

Part VI. Creep and Sustained Loads

SERVICEABILITY OF HIGH STRENGTH CONCRETE BEAMS WITH INTERNAL FRP REINFORCEMENT UNDER SUSTAINED LOAD

Shawn P. Gross

(Associate Professor, Villanova University, Villanova, PA, USA)

Joseph Robert Yost

(Associate Professor, Villanova University, Villanova, PA, USA)

Jonathan V. Crawford

(Staff Engineer, French and Parrello Associates, Wall, NJ, USA)

ABSTRACT

Over the past several years, extensive research has studied the serviceability of concrete members reinforced with internal FRP bars. Numerous experimental tests have been conducted and there exists an extensive body of data in the literature on deflections and crack widths observed during such tests. This work has resulted in the continuous development of design guidelines published by the American Concrete Institute (ACI) Committee 440 and the Canadian Standards Association (CSA). However, there is a relative lack of data on the behavior of flexural members subjected to sustained service-level loading. The ACI and CSA design guidelines clearly indicate the need for additional research in this area, particularly since the design of FRP-reinforced concrete is often governed by serviceability. This paper reports the results of an experimental test program in which six beams (two steel, two GFRP, and two CFRP) were maintained under a constant load for a period of 90 days. Measured flexural crack widths and midspan deflections are reported over the duration of the test period. Measured data is compared to the limited results available from other published studies and to the current ACI and CSA provisions.

KEYWORDS

Serviceability, deflection, crack width, sustained load, high strength concrete

1. INTRODUCTION

A large body of research has demonstrated that the instantaneous service load performance of FRP-reinforced members can be predicted using techniques similar to those used for steel-reinforced concrete, with modifications to account for the lower stiffness of the FRP reinforcement as compared to steel. For example, instantaneous deflections are often computed using a modified form of the well-known Branson effective moment of inertia equation, and crack width estimates are often computed using a modified form of the well-known Gergely-Lutz equation. The same approach – that of using methods developed for steel-reinforced concrete with modification as necessary – has been proposed for time-dependent serviceability behavior, but these proposals have not yet been compared to a large body of research data. The purpose of this study is to complement the small existing database of results on the performance of FRP-reinforced concrete under sustained service level loads.

A few published studies (Brown, 1996; Vijay and GangaRao; 1998; Arockisamy et al., 1998; Gross et al. 2003) have examined the time-dependent deflection of FRP-reinforced beams. These results have generally shown that the deflection increase over time, as a percentage of the initial deflection, is significantly less than the deflection increase suggested by ACI 318 (ACI 318, 2005). For reference, ACI 318 projects increases (ratio of time-dependent to initial deflection) of 100% after three months of sustained loading, 120% after six months, 140% after one year, and 200% for five years or more of sustained load. Brown also compared the results to companion steel-reinforced beams and found the percentage deflection increase to be less for FRP than for steel. On the basis of the limited data available, ACI 440 (ACI 440, 2006) suggests using 60% of the stated ACI 318 values for FRP-reinforced concrete, while the CSA S806 (CSA, 2002) standard for FRP adopts the ACI 318 values without modification.

Additional experimental research (Vijay and GangaRao, 1998; Bakis and Boothby 2004) has suggested that flexural crack widths in FRP-reinforced concrete members increase over time. For example, Bakis and Boothby found that crack widths increased 40% and 60% in indoor and outdoor environments, respectively, for GFRP-reinforced concrete beams under sustained load for three years. However, this time-dependent increase in crack widths is not directly considered by ACI 440 and CSA S806, each of which provides an expression to estimate the probable maximum crack width under full service load. The expressions for each standard are essentially expressions derived for steel-reinforced concrete and are used with simple modification for FRP. The CSA S806 standard implicitly identifies maximum acceptable crack widths of 0.020 in. for exterior exposure and 0.028 in. for interior exposure conditions, and ACI 440 endorses the use of the CSA S806 limits.

2. EXPERIMENTAL TEST PROGRAM

The experimental test program conducted at Villanova University consisted of three pairs of identical beam specimens with details as indicated in Table 1. Each beam measured 4.5 in. wide by 7.25 in. deep in cross-section and all specimens were constructed 74 in. long to allow for a 72 in. testing span with a 4 inch constant moment region. These dimensions were selected after consideration of existing ACI 440 and CSA S806 design provisions, and result in a span-to-depth ratio of approximately 10 such that serviceability criteria do not excessively limit the design efficiency. Reinforcement was chosen such that all beams had similar nominal moment capacities with the same cross-section dimensions. One inch of clear cover was provided for all flexural reinforcement. Beams did not contain transverse shear reinforcement.

All specimens were fabricated in a single pour using high strength concrete with a design compressive strength f'_c of 9000 psi. The concrete mix included 8% silica fume replacement of Portland cement (by weight) and a high-range water reducing admixture. The tested compressive strength of companion cylinders sampled from the beam pour was 8970 psi at 28 days and 9350 psi at 152 days, when the beams were first placed under load. The modulus of elasticity of the concrete at 152 days was 6.77×10^6 psi. Creep tests were also conducted on a single 28 in. long specimen using the procedure outlined in ASTM C512. The creep coefficient for the concrete loaded at 152 days and held under a sustained load for 90 days was found to be 0.51.

Table 1: Test Specimen Details

Specimen	S1 & S2	G1 & G2	C1 & C2
Reinforcement Type	Steel	GFRP – Hughes Bros. Aslan 100	CFRP – Hughes Bros. Aslan 200
f_v (ksi)	60 *	N/A	N/A
f_u (ksi)	N/A	104	356
E (psi)	29.0×10^6 *	5.85×10^6	20.2×10^6
A_r (sq. in.)	0.62 (2 #5)	0.62 (2 #5)	0.20 (2 #3)
ρ / ρ_b	0.46	3.08	3.64
Calculated M_{cr} (kip-in)	28	28	28
Calculated M_n (kip-in)	201	186	195
Applied M_a (kip-in)	70	65	68
Applied M_{sus} (kip-in)	60	56	59
* Assumed value			

Beams were oriented vertically and loaded in pairs in a self-reacting frame as shown in Figure 1. Prior to application of the sustained load, each beam was loaded with a short-term “pre-cracking” load to simulate the effects of live load. Pre-cracking loads (M_a) correspond to 35% of each beam’s respective nominal moment capacity, while sustained loads (M_{sus}) correspond to 30% of the nominal capacity. For each beam pair, the beams were loaded in unison using a hydraulic cylinder for application of the pre-cracking load or a precompressed spring for the sustained load, such that the left beam of each pair experiences tension along the left extreme fiber and the right beam of each pair experiences tension along the right extreme fiber. The spring mechanisms used for sustained loading utilized a set of nuts that could be adjusted to recompress the spring and maintain a constant load as the beams continued to deflect over time. Load for each beam pair was monitored using a load cell connected to a data acquisition system, and deflections were monitored using linear variable differential transducers (LVDTs) mounted to the test fixture. The tests were conducted indoors, but not in a room with constant temperature and relative humidity conditions.

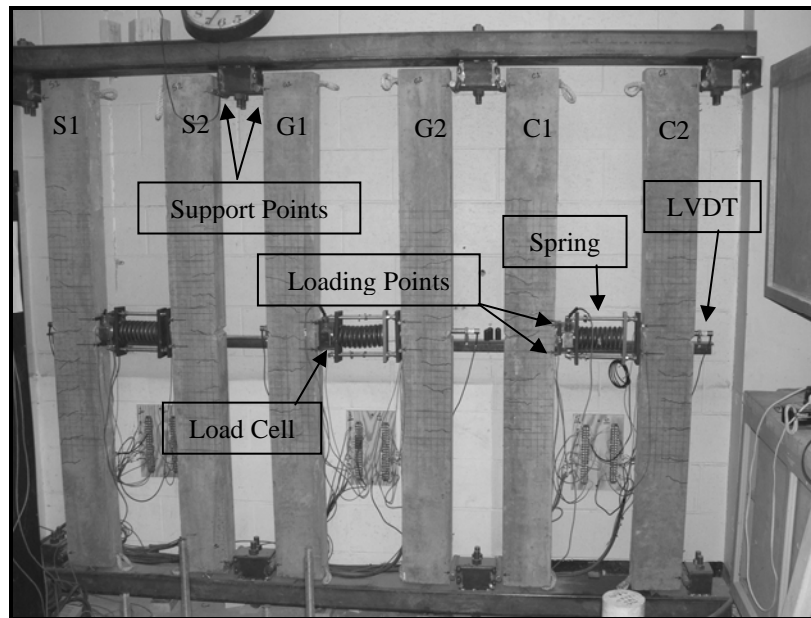


Figure 1: Sustained Load Test Setup

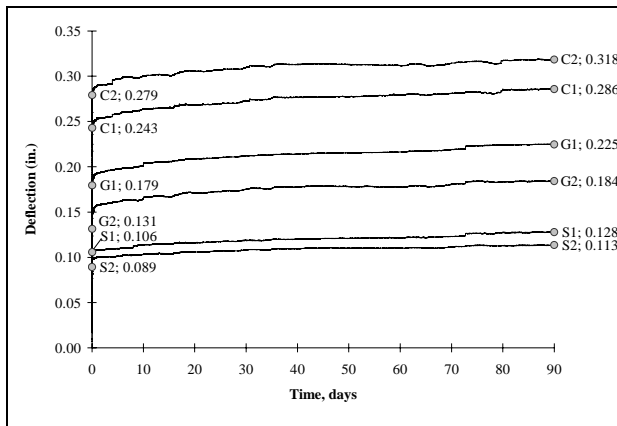


Figure 2: Deflection Test Results

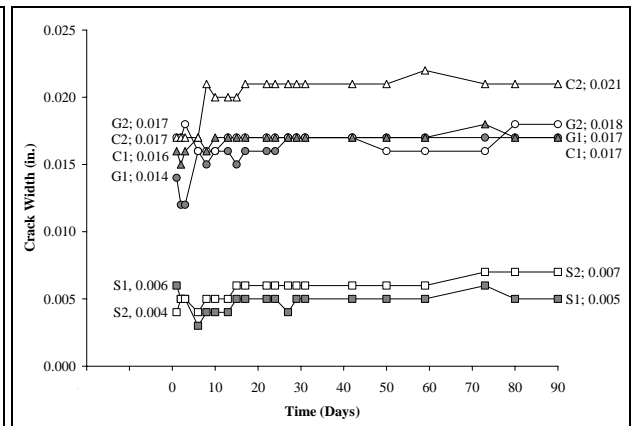


Figure 3: Crack Width Test Results

Table 2: Comparison of Long-Term Deflection Data with Published Results

Source / Specimen	Reinf Type	Time Under Load	$\delta_{\text{long-term}} / \delta_{\text{initial}}$			Ratio – Meas./Pred.		
			Meas. (a)	ACI 440 (b)	CSA S806 (c)	ACI 440 (a)/(b)	CSA S806 (a)/(c)	
Brown (1996)	#10	GFRP	6 mo	0.61	0.72	1.20	0.85	0.51
	#15	GFRP	6 mo	0.92	0.72	1.20	1.28	0.77
Vijay and Gangarao (1998)	T2CR	GFRP	21.5 mo	0.86	0.96	1.60	0.90	0.54
	C1CR	GFRP	12 mo	1.08	0.84	1.40	1.29	0.77
Arockisamy et al. (1998)	B2	CFRP	15.5 mo	1.15	0.90	1.50	1.28	0.77
	B3	CFRP	15.5 mo	0.65	0.90	1.50	0.72	0.43
	B4	CFRP	15.5 mo	0.71	0.90	1.50	0.79	0.47
Current Study	G1	GFRP	3 mo	0.26	0.60	1.00	0.43	0.26
	G2	GFRP	3 mo	0.40	0.60	1.00	0.67	0.40
	C1	CFRP	3 mo	0.18	0.60	1.00	0.30	0.18
	C2	GFRP	3 mo	0.14	0.60	1.00	0.23	0.14
AVERAGE							0.87	0.52

3. RESULTS: DEFLECTIONS

Measured midspan deflections for all beams over the 90 day test period may be seen in Figure 2. All beams behaved similarly, with gradual deflection increases over time. The average deflection increase (ratio of time-dependent to initial) over the test period was found to be 24%, 33%, and 16% for the steel-, GFRP-, and CFRP-reinforced specimens, respectively. These deflection increases for the FRP-reinforced specimens are significantly less than the 100% increase over 90 days predicted by CSA S806 or the 60% increase predicted by ACI 440. The results are compared to selected results from published studies in Table 2. The last two columns in the table indicate that the ACI 440 approach is the more accurate method. However, there is clearly a high degree of variability in the results. The relatively low deflection increases for the beams in the current study, as compared to the other published results, can be explained by low creep coefficient measured for the high strength concrete used to fabricate the beams. However, the larger percentage increase for the GFRP-reinforced specimens (33%) as compared to the steel-reinforced specimens (24%) contradicts the previous findings of Brown (1996) and the underlying principle of the ACI 440 approach.

4. RESULTS: CRACK WIDTHS

Measured maximum crack widths are shown in Figure 3. As expected, the GFRP- and CFRP-reinforced beams exhibited significantly larger crack widths than the steel-reinforced beams. All four FRP-reinforced specimens exhibited maximum crack widths close to the CSA S806 and ACI 440 limit of 0.020 in. for exterior exposure at the end of the 90 day test period. The average crack width increase (ratio of time-dependent to initial) over the test period was found to be 20%, 13%, and 15% for the steel-, GFRP-, and CFRP-reinforced specimens, respectively. These time-dependent increases are consistent with the findings of previous researchers mentioned previously, however it should be noted that almost all of the increase occurred during the first two weeks under sustained load.

5. CONCLUSIONS

This study of FRP-reinforced high strength concrete beams under a 90 day period of sustained loading showed that:

1. Deflections increased by 33% and 16% for the GFRP- and CFRP-reinforced beams, respectively, over the duration of the test period.
2. The existing ACI 440 approach for estimation of time-dependent deflections compared more favorably to the results than the CSA S806 approach, but both significantly overpredicted the time-dependent increase.
3. Crack widths increased by 13% and 15% for the GFRP- and CFRP-reinforced beams, respectively, over the duration of the test period.

6. REFERENCES

- ACI Committee 318 (2005). Building Code Requirements for Structural Concrete (ACI 318-05), American Institute, Farmington Hills, MI.
- ACI Committee 440 (2006). Guide for the Design and Construction of Concrete Reinforced with FRP Bars (ACI 440.1R-06), American Concrete Institute, Farmington Hills, MI.
- Arockiasamy, M., Amer, A., and Shahawy, M. (1998). "Environmental and Long-Term Studies on CFRP Cables and CFRP Reinforced Concrete Beams," *Proceedings of the First International Conference on Durability of Composites for Construction*, B. Benmokrane, and H. Rahman, eds., Sherbrooke, Quebec, pp. 599-610.
- Bakis, C. E.; and Boothby, T. E. (2004). "Evaluation of Crack Width and Bond Strength in GFRP Reinforced Beams Subjected to Sustained Loads," *Proceedings of the Fourth International Conference on Advanced Composite Materials in Bridges and Structures - ACMBS-IV*, Calgary, Canada, CD-ROM
- Brown, V. and Bartholomew, C. (1996). "Long-term Deflections of GFRP-Reinforced Concrete Beams," *Proceedings of the First International Conference on Composites in Infrastructure (ICCI-96)*, Tucson, Ariz., pp. 389-400.
- Canadian Standards Association (2002). Design and Construction of Building Components with Fibre-Reinforced Polymers (CSA S806-02), Canadian Standards Association, Toronto, Ontario, Canada.
- Gross, S.; Yost, J.; and Kevgas, G. (2003). "Time-Dependent Behavior of Normal and High Strength Concrete Beams Reinforced With GFRP Bars Under Sustained Loads," *High Performance Materials in Bridges*, American Society of Civil Engineers, pp. 451-462.
- Vijay, P. V.; and GangaRao, H. V. S. (1998). "Creep Behavior of Concrete Beams Reinforced with GFRP Bars," *Proceedings of the First International Conference (CDCC 1998), Durability of Fiber Reinforced Polymer (FRP) Composites for Construction*, pp. 661-667.

DEFORMATIONAL BEHAVIOUR OF FRP CONFINED CONCRETE UNDER SUSTAINED COMPRESSION

Rajeev Kaul

(Ph.D Candidate, Centre for Built Infrastructure Research, University of Technology Sydney, Australia)

R. Sri Ravindrarajah

(Senior Lecturer, Centre for Built Infrastructure Research, University of Technology Sydney, Australia)

Scott T. Smith

(Senior Lecturer, Centre for Built Infrastructure Research, University of Technology Sydney, Australia)

ABSTRACT

Confining concrete is an effective method to enhance the strength and ductility of reinforced concrete columns. Fibre reinforced polymer (FRP) composites are emerging as a suitable confining material to replace conventional materials such as steel and fibre-reinforced cement composites. Past research on the behaviour of FRP confined concrete in compression is considerable; however, limited research has been reported on the behaviour of confined concrete under sustained compressive loading. This paper reports the preliminary results of an experimental investigation on the deformational behaviour of carbon FRP (CFRP) confined concrete columns under sustained compressive stress levels, corresponding to 40% and 60% of the unconfined concrete compressive strength for up to 150 days. The results show that the creep of confined concrete columns is marginally influenced under moderate sustained stress/strength ratios.

KEYWORDS

Carbon fibre reinforced polymer, CFRP, concrete, confinement, time dependent behaviour, creep

1. INTRODUCTION

Fibre reinforced polymer (FRP) composites have significantly high tensile strength, stiffness and strain capacity compared to concrete. These qualities contribute to the acceptance of FRP as a viable material for strengthening and rehabilitating of concrete structures. In addition, FRP is a durable material in normal exposure conditions and is capable of wrapping any shaped concrete sections. Based on considerable research on the performance of FRP strengthened concrete members under short-term loadings, design recommendations (fib 2001, ACI 2002, Teng et al. 2002) have been published. However, a lack of research on the time-dependent effectiveness of FRP deters a wide-spread usage of FRP (Karbhari et al. 2003). Creep of FRP confined concrete under sustained loading is an important durability parameter in the design of FRP strengthened concrete columns (Smith et. al. 2005), and in some early applications, creep rupture of FRP in strengthened concrete columns has been reported (Naguib and Mirmiran 2002). This paper presents preliminary results of an experimental investigation on the creep behaviour of carbon FRP (CFRP) confined concrete columns, under moderate sustained stress/strength levels.

2. FRP CONFINEMENT TO CONCRETE COLUMNS

Fibre reinforced polymer (FRP) confinement improves the strength and ductility of concrete columns in compression. The strength improvement depends upon the fibre type, thickness and wrapping orientation (Lam and Teng 2003, Matthys et. al. 2005). The FRP, which confines the lateral expansion of concrete, is in tension in the hoop direction and fails in a brittle explosive manner when the concrete is excessively compressed. Research has shown that the tensile strength of FRP in the hoop direction is 10 to 20% lower than that in direct tension (Xiao and Wu 2000), where the ratio of failure hoop strain to that in direct tension is termed as the reduction factor. In FRP confined concrete under sustained compression, concrete experiences compressive creep whereas the FRP is under

sustained tension. As the concrete creeps with time, time-dependent increase in confinement stress in FRP will occur due to load transfer from the low modulus concrete to the relatively high modulus FRP. The interfacial bond stress between FRP and concrete will also experience time-dependent changes. Creep of FRP composite is a combined response of fibres, resin and interfacial behaviour of fibre and the matrix under sustained tension. In addition, the temperature will have a significant influence on the instantaneous and time-dependent deformation of FRP. Naguib and Mirmiran (2002) experimentally investigated the behaviour of glass FRP (GFRP) confined concrete under sustained compression and showed that the effect of confinement on creep of the concrete core is not significant. They also found the ACI 209R-92 (1992) model overestimates the creep of FRP confined concrete and the creep coefficients for the FRP tubes. The difference in the case of FRP wrapped confinement was not however significant. Analytical studies indicated that the creep of FRP wrapped columns is similar to that of sealed concrete.



Figure 1: FRP confined concrete cylinders under sustained compression.

3. EXPERIMENTAL SET-UP AND INSTRUMENTATION

Normal weight medium strength concrete (28-day cylinder strength of 37 MPa) was used in this study. A number of 150 x 300 mm concrete cylinders were cast in standard steel moulds and cured in water at 20°C for 28 days prior to testing. The cylinders were then either confined by wrapping with two layers of unidirectional CFRP formed in a wet lay-up procedure in the hoop direction or unconfined but sealed by coating with epoxy resin used in the formation of the CFRP. The confined and unconfined cylinders were subjected to either short-term uniaxial compressive loading until failure at specified ages or sustained uniaxial compression (up to 150 days) in self-reacting creep rigs, as shown in Figure 1. Each creep rig had a pair of either CFRP confined or unconfined cylinders. The sustained stress intensity corresponded to 40 and 60% of the cylinder strength of the unconfined concrete at the ages of loading (Table 1). The confined compressive strength of the cylinders at the ages of loading is also given in Table 1 (last column in brackets) as well as the sustained stress intensity expressed as a percentage of the cylinder strength of confined concrete. Loads were applied via hand-operated for 40% stress level and electrically-operated hydraulic jacks for 60% stress level and the loads were monitored through calibrated load cells. Periodic load adjustments were made to ensure that appropriate sustained stresses are maintained on the creep cylinders. The confined cylinders loaded were air stored at the uncontrolled laboratory environment for 14 and 32 days respectively after the removal of the cylinders from water curing prior to application of the CFRP.

Table 1: Details of concrete specimens under sustained compressive loading

Creep Rig	Specimen #	Age of concrete at loading	Duration of load	Applied stress level with respect to strength of	
				Unconfined concrete	Confined concrete
No. 3	P3, P4	60 days	150 days	40% (of 42.5 MPa [%])	26% (of 65.0 MPa ^{%%})
No. 4	F3, F4	60 days	150 days		
No. 5	P5, P6	100 days	150 days	60% (of 47.5 MPa [%])	43% (of 65.1 MPa ^{%%})
No. 6	F5, F6	100 days	150 days		

[#] P = Plain unconfined cylinder coated with epoxy resin; F = CFRP confined cylinder

[%] = unconfined compressive strength at age of loading; ^{%%} = confined compressive strength at age of loading

The axial (longitudinal) deformations on both the concrete and CFRP surfaces were measured using a demountable mechanical strain gauge (DEMEC) over a 200mm gauge length. The DEMEC points were mounted on diametrically opposite sides of each cylinder on (i) the concrete surface in unconfined cylinders, or in confined specimens after small holes were drilled through the CFRP, and (ii) on the surface of the CFRP in confined cylinders at a quarter of

the circumferential distance from the concrete DEMEC points. The hoop strain on the CFRP was measured using electrical resistance strain gauges over 67 mm gauge length. Drying shrinkage of companion non-loaded, non-wrapped and non-epoxy coated cylinders, stored in the same room and environment as the creep rigs, was measured throughout the whole duration of the experiment. The creep test was conducted in uncontrolled laboratory environment having the mean temperature and relative humidity of 23°C and 60% respectively. Tension tests were conducted on eight identical two layered, 15 mm wide, 252 mm long and 0.234 mm thick (2 layers of 0.117 mm CFRP nominal thickness sheet) coupons to determine the tensile strength, rupture strain and modulus of elasticity of the CFRP.

4. RESULTS AND DISCUSSION

The mean tensile strength, rupture strain, and modulus of elasticity of the CFRP coupons was 3030 MPa, 1.10 % and 246 GPa with standard deviations of 91 MPa, 0.05 % and 11 GPa, respectively. The mean confined compressive strength of concrete at 28 days was 65.0 MPa compared to 37.0 MPa for the unconfined concrete at the same age. Thus, CFRP confinement increased the cylinder strength by approximately 75%. The sustained stress/strength ratios of the confined cylinders were 26% (at 60 days of age) and 43% (at 100 days of age) which corresponded to 40% and 60% of the unconfined cylinders as given in Table 1. The stress-strain relationships for confined and unconfined concrete in compression indicate that the modulus of elasticity of concrete was not significantly affected by the confinement. The values for the modulus of elasticity, calculated by dividing the applied stress by the instantaneous strain on loading (AS 1012.16 1996) of the creep rigs for the unconfined and confined cylinders were 26.3 GPa and 27.8 GPa at the 40% stress level and 28.9 GPa and 29.4 GPa at the 60% stress level, respectively. Even though the strength of the concrete changes with time (fifth column in Table 1), the strength of the confined concrete cylinder is virtually identical (sixth column in Table 1) as the failure is primarily dependent on the confinement of the CFRP.

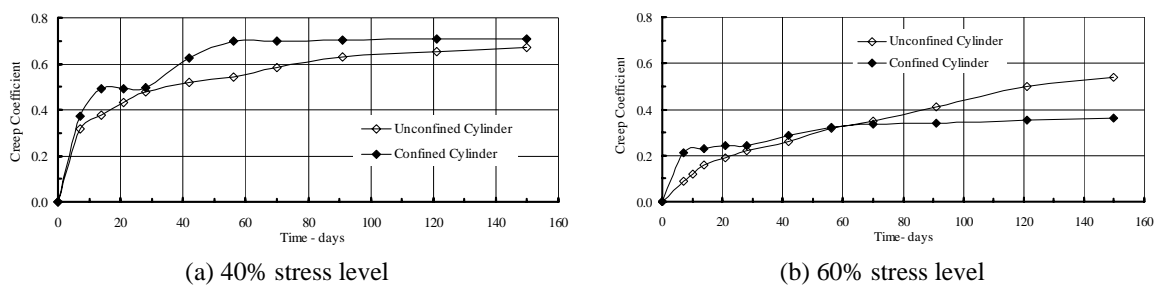


Figure 2: Creep of confined and unconfined concrete: up to 150 days of loading

The time dependent behaviour of loaded concrete is evaluated via its creep behaviour with time. Creep intensity is expressed in terms of creep coefficient which ratio of creep strain to the instantaneous strain on loading. The creep strain is equal to the total strain on the loaded cylinders minus the drying shrinkage strain from non-loaded companion cylinder. Figure 2 shows the development of creep coefficient with time for both confined and unconfined concrete up to 150 days, under both sustained stress levels.

Table 2: Creep coefficient for FRP confined and unconfined concrete

Time (Days)	Creep Coefficient @ 40% Stress Level			Creep Coefficient @ 60% Stress Level		
	Unconfined (Φ_1)	Confined (Φ_2)	Φ_2/Φ_1	Unconfined (Φ_1)	Confined (Φ_2)	Φ_2/Φ_1
28	0.47	0.49	1.04	0.22	0.24	1.09
90	0.62	0.70	1.12	0.41	0.34	0.84
150	0.67	0.70	1.04	0.54	0.36	0.67

The creep coefficient at 150 days for unconfined concrete at the 40% stress level was 0.67 compared to 0.54 for that under 60% stress level. This is partly due to the increase in the age at loading from 60 to 100 days.. With the confined concrete more significant drop from 0.70 to 0.36 was observed after 150 days. Also evident in Figures 2a and 2b is the creep in confined cylinders stabilised earlier than the unconfined cylinders. This is a consequence of the latter having lower concrete stress levels. The rate of creep for the unconfined cylinders increased as the applied stress is increased. This is particularly evident in the unconfined cylinder at 60% loading in which a high stress level

has led to more significant microcracking which may have increased the rate of creep in concrete (Sri Ravindrarajah and Swamy 1989). At both stress levels, the minimally activated FRP is mainly acting as a moisture barrier to the concrete. This was confirmed by small FRP hoop strain measurements. However, when the sustained stress level is greater than the unconfined strength of concrete, the creep response of confined concrete may be influenced by the creep properties of the FRP. Research is in progress to study the creep of confined concrete under high sustained stress levels.

Table 2 summarises the creep coefficients after 28, 90 and 150 days of loading. The ratio of creep coefficient for confined to unconfined concrete was 1.04, 1.12 and 1.04 after 28, 90 and 150 days, respectively at the 40% stress level compared to a more decreasing trend with the ratios at 1.09, 0.84, and 0.67 at 60% stress levels. The increasing creep coefficient of the unconfined cylinder as opposed to the stabilised creep coefficient for the confined cylinders from 90 to 150 days results in a reduction of the ratios in Table 1.

5. CONCLUSION

Compressive strength, modulus of elasticity and creep of concrete confined with 2 layers of CFRP were studied. Concrete cylinders were subjected to constant sustained stress levels, corresponding to 40% and 60% of the unconfined concrete strength at the age of loading of 60 and 100 days, for up to 150 days. The confinement increased the concrete 28-day cylinder strength by 75%. At the stress to strength level of 40%, no significant effect of CFRP on the creep of concrete was noted, however the rate of creep slowed quicker in the confined than the unconfined specimens. Current research is undertaken to investigate the creep of confined concrete under high sustained stress levels. Creep tests on CFRP coupons subjected to different conditions are also being conducted in order to give a better understanding of variations in moisture and temperature in the uncontrolled laboratory conditions, and stress distribution and creep effects in a CFRP confined system. Time-dependent tests will also be conducted on GFRP confined cylinders in the future, where GFRP has been traditionally observed to creep more than CFRP.

6. REFERENCES

- ACI 209R-92 (1992). *Prediction of Creep, Shrinkage and Temperature Effects in Concrete Structures*. American Concrete Institute (ACI), Committee 209, USA.
- ACI 440.2R-02 (2002). *Guide for the Design and Construction of Externally Bonded FRP Systems for Strengthening Concrete Structures*. American Concrete Institute (ACI), Committee 440, USA.
- AS 1012.16 (1996). *Methods of Testing Concrete - Determination of Creep of Concrete Cylinders in Compression*. Standards Australia, Australia.
- fib (2001). *Externally Bonded FRP Reinforcement for RC Structures*. The International Federation for Structural Concrete (fib), Technical Report, Task Group 9.3, Bulletin No. 14, Lausanne, Switzerland.
- Karbhari, V.M., Chin, J.W., Hunston, D., Benmokrane, B., Juska, T., Morgan, R., Lesko, J.J., Sorathia, U. and Reynaud, D. (2003). "Durability gap analysis for fibre-reinforced polymer composites in civil engineering". *Journal of Composite Construction*, Vol. 7, No. 3. pp. 238-247.
- Lam, L. and Teng, J.G. (2003). "Design oriented stress strain model for FRP confined concrete". *Construction and Building Materials*, Vol. 17, pp. 471-489.
- Matthys, S., Toutanji, H., Audenaert, K. and Taerwe, L. (2005). "Axial load behaviour of large-scale columns confined with fibre reinforced polymer composites". *ACI Structural Journal*. Vol. 102, No. 2, pp. 258-267.
- Naguib, W. and Mirmiran, A. (2002). "Time dependent behaviour of fibre reinforced polymer confined concrete columns under axial loads". *ACI Structural Journal*, Vol. 99, No. 2, pp. 142-148.
- Smith, S.T., Kaul, R., Sri Ravindrarajah, R. and Otoom, O.M.A. (2005). "Durability considerations for FRP strengthened RC structures in the Australian environment". *Proceedings (CD-Rom), Australasian Structural Engineering Conference, ASEC*, 11-14 December, Newcastle, Australia.
- Sri Ravindrarajah, R. and Swamy, R.N. (1989). "Load effects on fracture of concrete". *Materials and Structures*, Vol. 22, No. 127, pp. 15-22.
- Teng, J.G., Chen, J.F., Smith, S.T. and Lam, L. (2002). *FRP-Strengthened RC Structures*. John Wiley & Sons, UK.
- Xiao, Y. and Wu, H. (2000). "Compressive behaviour of concrete confined by carbon fibre composite jackets". *Journal of Materials in Civil Engineering*, Vol. 12, No. 2, pp. 139-146.

LONG-TERM BEHAVIOUR OF CFRP LAMINATES: AN EXPERIMENTAL STUDY

Francesco Ascione

(PhD Student, Department of Civil Engineering, University of Rome "Tor Vergata", Rome, Italy)

Geminiano Mancusi

(Assistant Professor, Department of Civil Engineering, University of Salerno, Fisciano, Italy)

ABSTRACT

In this paper the authors present many experimental results on the creep behaviour of CFRP pultruded laminates commonly used for civil structural applications. The study considers both a low stress-state in the laminate, representative of service conditions, and a higher one which is about 70% of CFRP tensile strength. The results here discussed, which only concern the first phase of the experimental study (low stress state), show that creep effects, when high longitudinal normal modulus is considered, can be assumed small.

KEYWORDS

Composite structures, FRP, Pultruded shapes, Long-term behaviour, Creep.

1. INTRODUCTION

Over the past few years, the strengthening of concrete structures with externally epoxy-bonded fiber reinforced polymer (FRP) composites has become increasingly user-friendly among engineers and researchers worldwide (Barbero E., 1998; Barbero E. and Harris J.S., 1998; Holloway L.C. and Leeming M.B., 1999; Ascione L. et.al., 2004). With regard to this technique, one of the most relevant topics is represented by the durability and the reliability, closely related to the time-depending behaviour of fibre-reinforced composite (FRP) materials (Ferry J.D., 1980; Ma C.C.M et.al, 1997; Maksimov R.D. and Plume E., 2001; Triantafillou T.C. and Plevis N, 1994; Petermann J. and Schulte K., 2002). In fact, FRPs are made up of a matrix, highly sensitive to creep, and of purely elastic fibres. When dealing with aged concrete structures, the rate of the viscous deformations in the concrete can be considered equal to zero. Consequently, only FRP creep deformations have to be taken into consideration. A similar problem occurs in the case of the steel-concrete composite structures. In this case, in fact, creep phenomena only concern the concrete component, while the steel component does not flow (CEB-FIP, 1984).

A wrong evaluation of the viscous effects could introduce relevant errors in the design of the structural plating. At the moment, current literature does not provide any final conclusions on this important topic. Furthermore, studies developed in the aeronautic or naval field dealing with the creep properties of composite materials cannot be directly used for civil engineering purposes, mainly due to the different technological processing of these materials. From a more practical point of view, guide-lines and technical codes only introduce stress limitations in order to verify the safety of composite materials when there are viscous effects (JSCE 1997; ACI Committee 440, 2000; CEB-FIP, 2001; CNR DT-200, 2004).

The aim of the paper is to show some experimental results on the creep behaviour of a CFRP laminate investigated by a specific approach, as described below, confirming that such effect can be assumed small if a high value of longitudinal normal modulus of the laminate is considered. The results here discussed belong to the initial phase of a two years long experimental programme currently underway at the University of Salerno.

2. DESIGN OF THE EXPERIMENT

As mentioned above, in order to study the creep behaviour of a CFRP laminate a long term (two years) experimental programme is being carried out.

It concerns a thin CFRP plate bonded to the top flange of a simply supported titanium beam (Ti-6Al-4V). More details are shown in Figs.1a-b. Within this experiment the actual geometrical conditions occurring in the retrofitting of a concrete structure have been simulated. In fact, the behaviour of the beam, made of a high performance titanium alloy, is not time-dependent as is the case of aged concrete structures. Moreover, like FRP, the titanium alloy also exhibits linear elastic response up to very large normal strains. As a consequence, it is possible to evaluate the stresses inside the materials only by measuring corresponding strains at any given time.

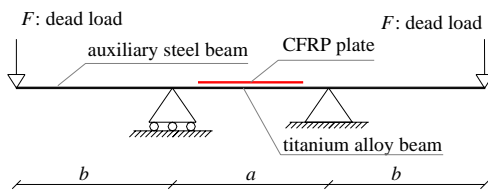


Figure 1.a: Global experimental scheme.

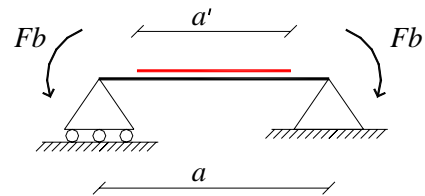


Figure 1.b: Experimental scheme (central bay).

The static scheme adopted by the authors is represented in Fig. 1.a. The total length of the scheme is equal to $7300\text{mm} = a + 2 \cdot b$, where a is the length of the titanium alloy beam (3500mm), while b (1900mm) denotes the length of each lateral rigid auxiliary beam. Last ones are connected to previous by bolted joints (Fig. 2.a). The bond of CFRP plate to titanium alloy beam has been made by using Loctite Multibond 330 adhesive. Finally, the length of the laminate, a' , is equal to 2900 mm.

Dead loads have been applied in symmetry at the free ends of the two rigid auxiliary beams, according to the scheme in Fig.1.a. In particular, a defined number of $1000\text{mm} \times 200\text{mm} \times 10\text{mm}$ steel sheets, about 0,20 kN each one (Fig.2.b), have been used. It is easy to verify: i) constant bending moment ($M = -F \cdot b$) occurs within the supports (Fig. 1.b); ii) no shear stresses arise.



Figure 2.a: Bolted joints.



Figure 2.b: Dead loads.

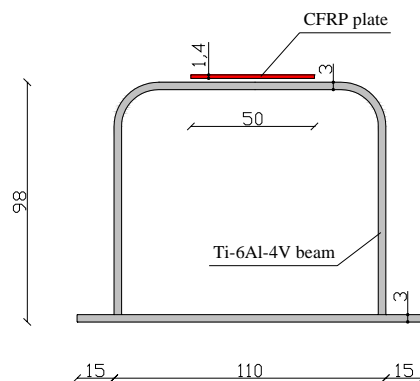


Figure 3: Cross-section of the beam.

The cross-section of the beam, after the CFRP laminate has been bonded, is shown in Fig. 3 (length unit: mm). The most important mechanical properties of the titanium alloy, CFRP and adhesive are described below (Tab.1).

Table 1: Mechanical properties

	Ti-6Al-4V	CFRP	Multibond 330
Longitudinal elastic modulus [N / mm ²]	110000	300000	-
Yield normal stress [N / mm ²]	790 (20°C)	-	-
Ultimate normal stress [N / mm ²]	895 (20°C)	1450	-
Ultimate shear stress [N / mm ²]	-	-	≥16,5
Ultimate normal strain	0,1000	≥0,0045	-

The experimental programme has been divided into two phases, each one performed with a fine control of temperature ($20^{\circ}\text{C} \pm 1^{\circ}\text{C}$) and humidity ($50\% \pm 5\%$):

-1st phase: generation of a low stress state (20% of CFRP tensile strength) in the laminate over a 6-month period. This phase has been completed, with the results obtained by the authors being discussed here for the first time.

-2nd phase: generation of a higher stress level (70% of CFRP tensile strength) over a 18-month period. This phase is still underway.

The strain state evolution is monitored by a continuous data acquisition hardware/software system using 35 strain-gauges applied both to the titanium beam as well as the CFRP plate (Fig. 4.a) at defined positions along the longitudinal axis. Due to the linear elastic response of both materials, stresses can be easily related to strains. An optometric system, OptoNCDT 1401 by $\mu\epsilon$ Micro Epsilon, is used in order to measure the mid-span deflection over time.

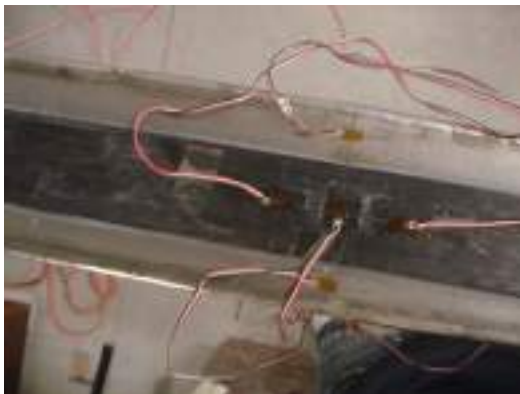


Figure 4.a: Some strain gauges.

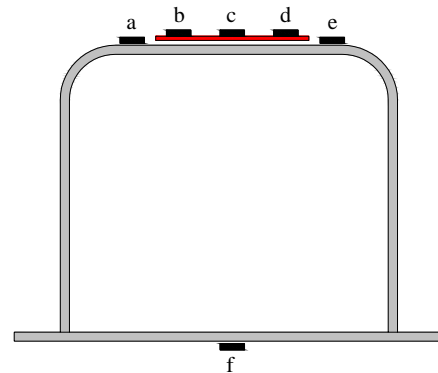


Figure 4.b: Strain-gauges position (mid-span).

3. EXPERIMENTAL RESULTS

In this section the results obtained during the first phase of the experimental programme are discussed.

As indicated above, this phase concerns a continuous monitoring of the stress-strain state over a six-month period. Dead loads have been applied so that the initial stress state in the CFRP laminate is about 20% of its ultimate tensile strength.

The following Fig.5.a shows the values returned by strain-gauges at defined times (every ten minutes) over six months. They refer to the mid-span cross-section (Fig. 4.b). In particular, the cyan, yellow and magenta lines refer to strain-gauges at the top of the CFRP laminate (*b*, *c* and *d* positions), while the blue one refers to the bottom of the CFRP plate. This last value has been established by measuring strains in the titanium alloy, close to the laminate (*a* and *e* positions).

Fig.5.b highlights the evolution of vertical deflection at mid-span cross-section of the beam, evaluated by an optometric sensor applied at the bottom flange (*f* position in Fig. 4.b).

As it can be noted, strains inside the CFRP follow a typical secondary-creep evolution law. The percentage difference is equal to 2,3 % over 180 days (magenta line). On the other hand, strains in the titanium alloy increase exhibiting a percentage difference equal to 1,0 %. Finally, the deflection at mid-span cross-section increases

following a quasi-linear evolution law, characterized by a maximum variation equal to 6,7 % over the whole monitored time.

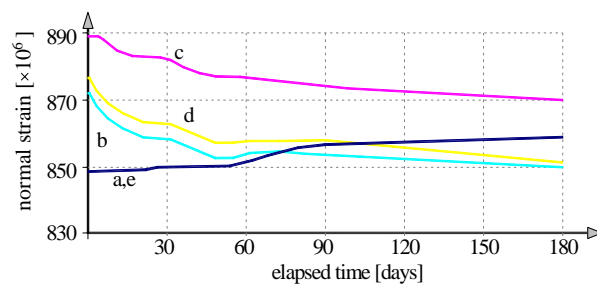


Figure 5.a: Normal strains over time (mid-span).

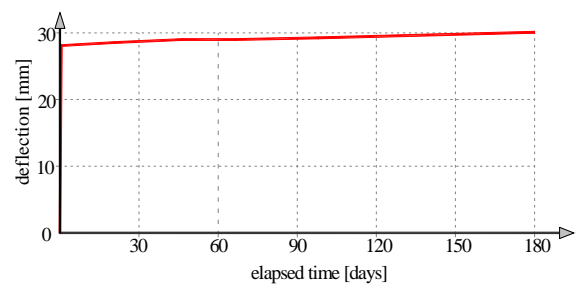


Figure 5.b: Deflection over time (mid-span).

4. CONCLUSIONS

As it is easy to realize, the experimental results show that the investigated CFRP pultruded laminate, characterized by a high longitudinal normal modulus, exhibits small creep strains. In particular, the data obtained have been compared with results of classical creep tests on the same manufactured laminate (Berardi V.P. et al., 2006). Comparisons highlight a less sensitive to creep behaviour and confirm the durability and the reliability of the use of CFRP laminates in structural plating purposes.

5. REFERENCES

- ACI Committee 440 (2000). "Guide for the design and construction of externally bonded FRP systems for strengthening concrete structures".
- Ascione L., Berardi V.P., Mancusi G. (2004). "Time-depending behaviour under sustained loads of Rc beams externally plated with FRP laminates", *Proceedings of IMTCR International Conference*. University of Lecce, Italy.
- Barbero E. (1998). "Introduction to composite material design", Taylor & Francis.
- Barbero E. & Harris J.S.(1998). "Prediction of creep properties from matrix creep data". *Journal of Reinforced Plastics and Composites* 17(4).
- Berardi V.P., Feo L., Giordano A., Ascione F. (2006). "On the creep behaviour of CFRP pultruded laminates: an experimental study", *Proceedings of II FIB International Conference*. Naples, Italy
- CEB-FIP (1984). "Manual on Structural Effects of Time-Dependent Behaviour of Concrete". *Bullettin d'Information* n. 142-142bis.
- CEB-FIP (2001). "Externally bonded FRP reinforcement for RC structures".
- CNR DT-200/2004. "Istruzioni per la Progettazione, l'Esecuzione ed il Controllo di Interventi di Consolidamento Statico mediante l'utilizzo di Compositi Fibrorinforzati. Materiali, strutture di c.a. e di c.a.p., strutture murarie".
- Ferry J.D. (1980). "Viscoelastic properties of polymers". New York: *J. Wiley & Sons*.
- Holloway L.C. & Leeming M.B. (1999). "Strengthening of reinforced concrete structures". *CRC Press*.
- JSCE 1997. "Recommendation for design and construction of concrete structures using continuous fiber reinforcing materials".
- Ma C.C.M., Tai N.H., Wu S.H., Lin S.H., Wu J.F., Lin J.M. (1997). "Creep behaviour of carbon-fiber-reinforced PEEK [+/-45] laminated composites". *Composites: Part B*, 28: 407-417.
- Malvern L.E. (1969). "Introduction to the mechanics of a continuous medium". *Prentice-Hall*.
- Maksimov R.D. & Plume E. (2001). "Long-Term creep of hybrid aramid/glass fiber-reinforced plastics", *Mechanics of Composite Materials* 37 (4).
- Petermann J. & Schulte K. (2002). "The effects of creep and fatigue stress ratio on the long-term behavior of angle-ply CFRP". *Composite Structures* 57: 205-210.
- Triantafillou T.C. & Plevris N. (1994). "Time-dependent behavior of RC members strengthened with FRP laminates". *Journal of Structural Engineering* 120 (3): 1016-1042.

CREEP TESTS ON GFRP PULTRUDED SHAPES STIFFENED WITH CARBON FIBER SHEETS

Marina Bottoni

(PhD Student, University of Bologna, Bologna, Italy)

Claudio Mazzotti

(Associate Professor, University of Bologna, Bologna, Italy)

Marco Savoia

(Full Professor, University of Bologna, Bologna, Italy)

ABSTRACT

Preliminary results of an experimental campaign on creep deformation of pultruded GFRP-shapes subject to long-term loadings are presented. Both tension and shear tests have been performed, for the duration of about three months. Some specimens have been stiffened by FRP carbon sheets, in order to reduce creep deformation.

KEYWORDS

pultruded shapes, creep, carbon fibers, composites

1. INTRODUCTION

As well known, verification against deformability is the most important design requirement for composite pultruded shapes, due to their very high strength-to-modulus ratio. Moreover, in the case of glass fibers, creep deformation due to long-term loading can be significant when compared with elastic deformation, and must then be taken into account.

The subject of the research is the creep strain evolution of GFRP-pultruded shapes subject to long-term loadings (Figure 1), for which few contributions can be found in the literature (Mottram, 1993, McClure and Mohammadi, 1995, Shao and Shanmugam, 2004, Berardi et al. 2006).

Since deformation of structural elements is due to both longitudinal and shear strains, two different creep functions have been experimentally evaluated. With this aim, uniaxial tension and pure shear tests have been performed on specimens extracted from flanges of pultruded GFRP beams. Long-term tests have been conducted in a climate room at 20°C temperature and RH of 60 percent.

Some specimens have been also stiffened by gluing unidirectional carbon fibers with 0° fiber orientation with respect to longitudinal direction for specimens in tension, and two-directional ±45° CFRP sheets on specimens under shear (Figure 2). The effect of CFRP stiffening in reducing long-term deformation of pultruded elements has been investigated.

2. GFRP PULTRUDED SPECIMENS FOR LONG -TERM TESTS

Specimens used for long-term tests have been extracted from pultruded plate elements or from flanges and web of wide-flange pultruded beams. Plates and beams have different mechanical properties, whereas thickness of all pultruded specimens is 9.53 mm. They are made of E-glass longitudinal fibers embedded in a polyester matrix. From failure tests on pultruded plate elements, tensile strength of 79.5 MPa and elastic modulus $E = 9.69$ GPa have been obtained. Specimens extracted from plates and flanges have been subject to long-term tension test, whereas specimens obtained from beam webs have been used for tests on long-term shear behavior. Some specimens for both tension and shear tests have been also strengthened by using externally glued carbon fiber sheets. With more details,

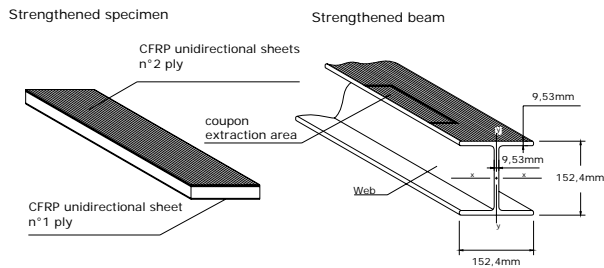


Figure 1: Extraction of specimens from beam flanges.



Figure 2: Two frames for creep tests on specimen.

four unstiffened specimens extracted from plates have been used for long-term tension tests. Two different widths have been adopted, in order to test the effect of stress level on creep strain evolution with time: two specimens were 46 mm wide and 245 mm long, while the remaining two were 65 mm wide and 335 mm long. Four specimens have been stiffened by externally gluing FRP carbon sheets. Two specimens obtained from plates are 31 mm wide and 245 mm long while other two (obtained from beam flanges) are 44 mm wide and 335 mm long. They have different dimensions with respect to unstiffened specimens in order to prescribe the same stress level to pultruded elements, calculated by homogenization criteria based on linear elastic behavior.

As for long-term shear tests, two specimens 120 mm × 220 mm (extracted from beam web) have been prepared. Two additional specimens (from beam web), with same dimensions, have been stiffened with CFRP sheets.

Strengthening of pultruded elements subject to tension tests (Figure 1) has been done with three unidirectional plies of carbon fiber sheets, glued to pultruded specimens (two on one side and one on the other side) extracted from beam flanges and plates. Carbon sheets with fibers content 320 g/m² and longitudinal elastic modulus equal to 240 GPa (according to producer data) have been used. Moreover, specimens for shear tests have been strengthened by means of one ply of two-directional sheets with ±45° fiber orientation on both sides (carbon fiber sheets with fiber content 200 g/m² in each direction and longitudinal elastic modulus of 240 GPa).

As for the application of the reinforcement, an epoxy resin has been applied to pultruded specimen, followed by a carbon fiber sheet; then, epoxy in excess has been taken away by using a roller. This procedure has been repeated for each layer. Specimens have been then wrapped in a cotton fabric and a thicker plastic tissue, in order to adsorb exceeding resin; finally, they were watertight sealed with a nylon sheet and void was created by means of an autoclave. Curing of specimens, at environmental temperature, was five days long.



Figure 3: Instrumentation and load transmission for tension tests.

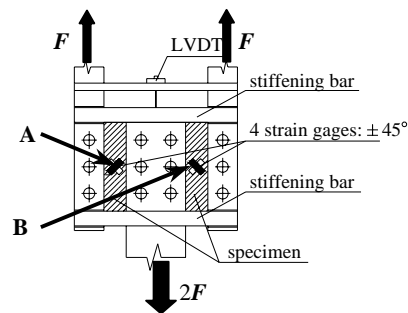


Figure 4: Instrumentation and load transmission for shear tests.

3. EXPERIMENTAL SET-UP FOR LONG -TERM TESTS

Experimental setups for both kinds of long-term tests (tension and shear) are based on the leverage system of Figure 2, giving a constant load with time. Load is applied by means of a number of steel weights suspended from the longer lever arm and is transmitted to specimen chains attached at the shorter lever arm. Amplification factor equal to 8.12 was determined with a load cell before testing. Each frame system has two specimen chains, carrying 50 percent of applied load each, through another leverage system.

Specimens used for tension test have their extremities glued to two steel plates, which are then bolted to other steel plates connecting different specimens (Figure 3); each specimen belonging to one of two chains of the frame is subject to 8893 N axial loading. Specimens for shear test have steel plates glued to their extremities and to their middle portion, where other steel elements are bolted, so that both panels of specimens are subject to uniform shear stresses. Each chain has two specimens, which are subject to 9393 N shear force (Figure 4). The adopted mechanical system is similar to that recommended in standard ASTM D4255 for shear tests on composites.

In tension tests, deformations are measured by means of two longitudinal strain gauges placed on two faces of specimens (Figure 3). For shear-loaded specimens (Figure 4), two strain gauges are placed on both sides with $\pm 45^\circ$ orientation with respect to longitudinal direction. From strain gauge measures, assuming a state of pure shear in panels A and B, shear strain is $|\gamma|=2|\epsilon|$, where ϵ is the average of experimental strains from a couple of strain gauges.

4. EXPERIMENTAL RESULTS

Figures 5-6 show experimental results obtained from tension test on specimens obtained from pultruded plates; each series of data in Figure 5 represents the mean behavior obtained from two identical specimens during the loading phase. In order to compare results of unstiffened and stiffened (with CFRP sheets) specimens, load per unit width is reported (instead of tensile stress) versus axial strain. Linear regression analysis of experimental data gives, as expected, an high degree of correlation in all cases (coefficient of least-square procedure $R^2 \approx 0.996$). Slope of each line then gives the equivalent rigidity $(E \cdot s)_{eq}$ for unstiffened and stiffened specimens, being E the longitudinal Young modulus and s the specimen thickness. As expected, strengthening by using carbon sheets reduces remarkably axial deformability. With reference to specimens with small width, stiffness increase due to CFRP sheets is about 2.5 times.

With reference to long-term tests, ratio between longitudinal creep strain and elastic strain (creep coefficient) is reported in Figure 6 (mean value from two identical specimens). Applied long-term load corresponds to 25 percent and 8 percent of composite strength, respectively, for small and large unstiffened specimens. Unstiffened specimens show approximately the same creep behavior (difference less than 5 percent): creep strain is more than 25 percent of elastic strains after 100 days of loading. Moreover, slope of curves at that time is still appreciable and a significant growth of strains with time can be expected. Stiffening of pultruded elements by means of carbon fiber sheets provides for a strong reduction of delayed deformation (more than 50 percent for small specimens - see Figure 6).

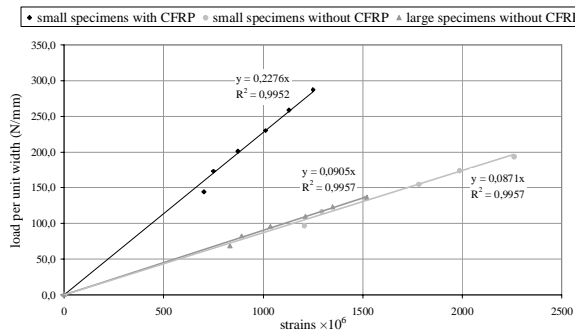


Figure 5: Tension tests – strain measures during loading phase of specimens extracted from plates.

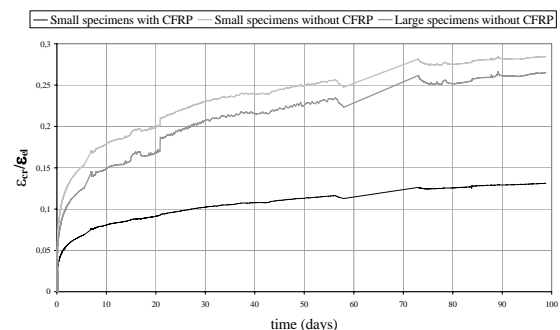


Figure 6: Tension test – creep coefficient of specimens extracted from plates.

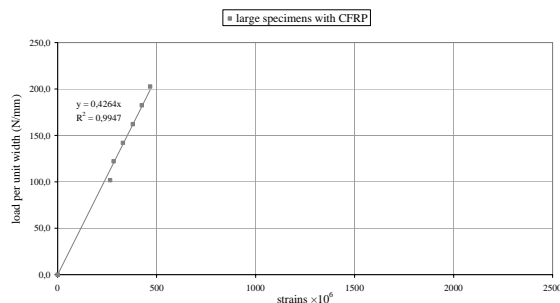


Figure 7: Tension tests – strain measures during loading phase of specimens extracted from beam flanges.

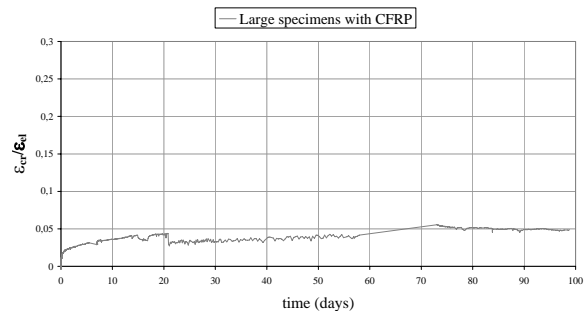


Figure 8: Tension test – creep coefficient of specimens extracted from beam flanges.

Moreover, slope of curve after 100 days is small, suggesting a smaller strain increase with time with respect to unstiffened specimens.

Figures 7-8 show instantaneous and long-term behavior of specimens obtained from beam flanges and stiffened with CFRP; equivalent stiffness is much higher than that of specimens obtained from plates; analogously, creep coefficient is less than half of that provided by those specimens, probably due to higher fiber content. Moreover, slope of curve after 100 days is almost horizontal.

Finally, figures 9-10 show experimental results obtained from specimens extracted from beam webs under long-term shear tests. In Figure 9, shear force acting on each composite panel (half of force on single chain) is reported vs. shear strains γ ; experimental data obtained during the loading phase have been linearly interpolated. Each experimental data is the average value of four strain gauge measures obtained from a specimen. Data scattering is very limited. Results for unstiffened and stiffened specimens are compared. Slope of curves represents the equivalent stiffness $(GA')_{eq}$, with G shear modulus and A' cross-section area (including shear factor). Shear modulus obtained from unreinforced specimens is about 3.18 MPa, close to value 3.4 MPa provided by the manufacturer. Strengthening by CFRP sheets provided for a 37% increase of equivalent shear modulus. Long-term evolution of creep coefficient under shear (Figure 10) shows an increase with time similar to the case of longitudinal creep strain, for both unstiffened and stiffened specimens. CFRP sheets are very effective also in reducing long-term shear strain (about 50%). After 100 days of loading, shear strains still show a remarkable rate of increase, whereas in the presence of CFRP sheets the slope of curves is significantly reduced.

5. CONCLUSIONS

Creep experimental tests have been performed on pultruded specimens subject to axial and shear forces. Specimens strengthened with carbon fibers sheets were also tested. A significant reduction in longitudinal and shear strains in strengthened specimens was observed, for both instantaneous and long-term behaviour. Creep coefficients in tension were about 0.25-0.3 after three months for unstiffened specimens, and reduced by one half in the presence of CFRP; long term shear deformability was higher with respect to axial one.

ACKNOWLEDGEMENTS

The financial support of C.N.R. - National Council of Research, PAAS Grant 2001, is gratefully acknowledged. The authors would like to thank ECT of Ancona (Italy) for providing specimens for testing.

REFERENCES

- Berardi V., Feo L., Giordano A., Ascione L. (2006), On the Creep Behaviour of CFRP Pultruded Laminates: an Experimental Study, *Proc. 2nd Int. fib Congress*, June 5-8, 2006 – Naples, Italy (on CD), 1-9.
- ASTM D 4255/D 4255M (2001), *Standard Test Method for In-Plane Shear Properties of Polymer Matrix Composite Materials by the Rail Shear Method*.
- Mottram J. T. (1993), Short-and long-term structural properties of pultruded beam assemblies fabricated using adhesive bonding, *Composite Structures*, **25**, 387-395.
- McClure G., Mohammadi Y. (1995), Compression Creep of Pultruded E-Glass-Reinforced-Plastic Angles, *Journal of Materials in Civil Engineering*, **7**(4), 269-276.
- Shao Y., Shanmugam J. (2004), Deflection Creep of Pultruded Composite Sheet Piling, *Journal of Composites for Construction ASCE*, **8**(5), 471-479.

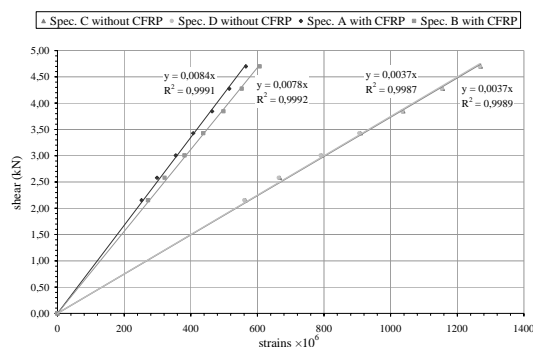


Figure 9: Shear test – strain measures during loading phase of specimens extracted from beam web.

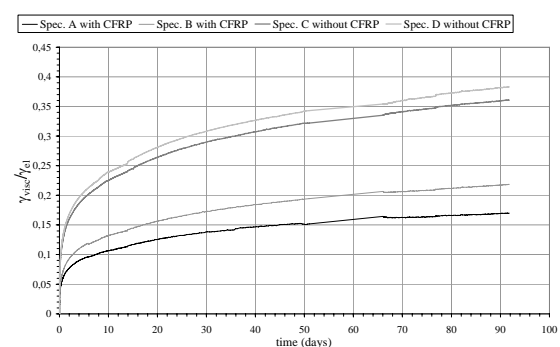


Figure 10: Shear test – creep coefficient of specimens extracted from beam web.

Part VII. Design Guides

A DESIGN PROCEDURE OF FRP CONFINING SYSTEMS FOR UPGRADE R/C COLUMNS

Angela Di Nardo

(Graduate Research Assistant, University of Salerno, Fisciano, Italy)

Ciro Faella

(Full Professor, University of Salerno, Fisciano, Italy)

Roberto Realfonzo

(Associate Professor, University of Salerno, Fisciano, Italy)

ABSTRACT

This paper presents a procedure that allows computing the axial load-bending moment (N-M) interaction curves in case of rectangular R/C columns confined by FRP. At this purpose the constitutive law for the FRP confined concrete in compression adopted by the recently edited guidelines of the Italian National Research Council (CNR, 2005) has been used. This law presents two different branches; the first one parabolic and the second one linear and degenerates in the well-known “parabola-rectangle diagram” (CEN, 2001) when the confinement is absent. The obtained interaction curves are presented in a dimensionless representation ($v-\mu$), which is useful in strengthening interventions design, since it allows representing in a very simple way the dependence on several parameters.

KEYWORDS

R/C columns, FRP, confinement, interaction curves, code provisions.

1. INTRODUCTION

The action of a FRP confining system essentially produces an increment of the strength and of the ultimate strain of compressed concrete; consequently, in case of R/C columns, it provides both an enlargement of the axial force-bending moment (N-M) interaction curve and, mainly, an improvement of the available ductility.

Recently new guidelines have been edited by the Italian National Research Council (CNR-DT200). Such provisions are also aimed at the evaluation of the ultimate curvature and flexural capacity of FRP confined R/C columns: at this purpose the bilinear constitutive relationship proposed in (Faella and Realfonzo, 2002) is introduced in DT200 in order to model the confined concrete under compression (see Figure 1). Assuming $\bar{\varepsilon} = \varepsilon_c / \varepsilon_{c0}$ this law is given by:

$$\text{if } \bar{\varepsilon} < 1: \frac{f_c}{f_{cd}} = (1 + \gamma) \cdot \bar{\varepsilon} - \bar{\varepsilon}^2 \text{ (parabolic branch);} \quad \text{if } \bar{\varepsilon} > 1: \frac{f_c}{f_{cd}} = 1 + (\gamma - 1) \cdot \bar{\varepsilon} \text{ (linear branch)} \quad (1)$$

where:

$$\gamma = \frac{f_{cd} + E_t \cdot \varepsilon_{c0}}{f_{cd}} = \frac{f_{c1}}{f_{cd}} \quad E_t = \frac{f_{ccd} - f_{cd}}{\varepsilon_{ccu}} \quad (2)$$

In Eq.s (1) and (2), f_{cd} and ε_{c0} are respectively the design strength and the corresponding strain (typically assumed equal to 0.2%) of the unconfined concrete, while f_{ccd} is the design confined concrete compression strength and ε_{ccu} its ultimate strain. The Italian guidelines provide for these two parameters the following relations:

$$\frac{f_{ccd}}{f_{cd}} = 1 + 2.6 \cdot \left(\frac{f_{leff}}{f_{cd}} \right)^{2/3} = 1 + 2.6 \cdot f_{l,d}^{2/3} \quad \varepsilon_{ccu} = 0.0035 + 0.015 \cdot \left(\frac{f_{leff}}{f_{cd}} \right)^{0.5} = 0.0035 + 0.015 \cdot \sqrt{f_{l,d}} \quad (3)$$

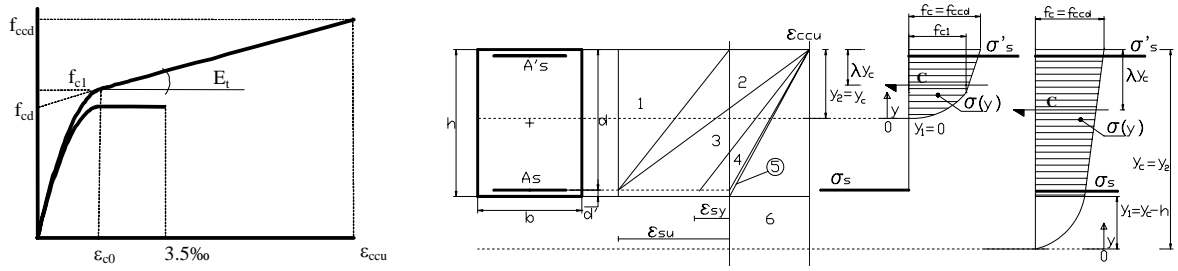


Figure 1: Constitutive law, ultimate regions and stress distribution

where the dimensionless parameter $f_{l,d}$ is given by the ratio of the effective lateral stress produced by the FRP system ($f_{l,eff}$) to the design compression strength of unconfined concrete (according to CNR DT200/2004 the confinement is effective if $f_{l,d} > 0.05$). It is to be observed that for unconfined concrete (i.e. when $f_{l,d} = 0$) the constitutive relationship degenerates in the well known “parabola-rectangle” law (CEN, 2001).

According to the DT200, the effective confinement pressure is given by:

$$f_{l,eff} = \frac{1}{2} \cdot k_{eff} \cdot \rho_f \cdot E_f \cdot \varepsilon_{fd,rid} \quad (4)$$

where: k_{eff} is a coefficient (≤ 1) defined as the ratio of the volume of effectively confined concrete to the volume of the concrete member; ρ_f is the geometric ratio which is a function of section shape and FRP configuration (continuous or discontinuous wrapping); E_f is the FRP Young’s modulus in fibers direction, and $\varepsilon_{fd,rid}$ is the FRP conventional ultimate strain, corresponding to an unacceptable degradation of concrete (which is much lower than the FRP characteristic failure strain under tension ε_{fk}).

2. A PROCEDURE FOR EVALUATING v - μ INTERACTION CURVES

According to the symbols reported in Figure 1, the equilibrium equations which allow computing the ultimate axial force and the bending moment for R/C square or rectangular cross sections are:

$$N_u = b \cdot \int_{y_1}^{y_2} \sigma(y) dy + A_s' \sigma_s' + A_s \sigma_s; \quad M_u = b \cdot \int_{y_1}^{y_2} \sigma(y) \cdot \left(\frac{h}{2} - y_c + y \right) dy + A_s' \sigma_s' \left(\frac{h}{2} - d' \right) - A_s \sigma_s \left(\frac{h}{2} - d' \right) \quad (5)$$

where y_c is the neutral axis depth and steel stresses are assumed positive when the reinforcement is under compression. Equations (5) can be rewritten in a dimensionless form, as follows:

$$v = \frac{N_u}{b \cdot h \cdot f_{cd}} = \xi \psi + \omega' \frac{\sigma_s'}{f_{ys}} + \omega \frac{\sigma_s}{f_{ys}} \quad \mu = \frac{M_u}{b \cdot h^2 \cdot f_{cd}} = \xi \psi (0.5 - \lambda \xi) + \omega' \frac{\sigma_s'}{f_{ys}} (0.5 - \delta') - \omega \frac{\sigma_s}{f_{ys}} (0.5 - \delta') \quad (6)$$

being: $\delta' (=d/h)$ the dimensionless cover; $\xi (=y_c/h)$ the non-dimensional neutral axis depth; f_{ys} the steel yielding strength; $\omega = (A_s \cdot f_{ys}) / (b \cdot h \cdot f_{cd})$ and $\omega' = (A_s' \cdot f_{ys}) / (b \cdot h \cdot f_{cd})$ the steel reinforcements mechanical percentages;

$$\psi = \frac{\int_{y_1}^{y_2} \sigma(y) dy}{y_c \cdot f_{cd}} \quad \text{and} \quad \lambda = 1 - \frac{y_1}{y_c^2 \cdot \psi \cdot f_{cd}} \quad (7)$$

respectively, the ratio of the concrete stress nonlinear diagram area to the rectangular area obtained for a constant concrete stress distribution equal to f_{cd} , and, the ratio to the distance from the extreme compressed concrete fiber of the compressive concrete resultant “C” ($=\xi\psi$) to the depth of the neutral axis (see Figure 1).

In figure 1 the six ultimate regions for a R/C section are also shown; the ultimate state limit is attained when: regions 1 and 2 - the steel strain reaches a limiting value in tension (according to the “Eurocode 2”, $\varepsilon_{su}=0.001$); regions 3 to 6 - the concrete compressive strain is equal to its ultimate value (ε_{ccu} given by Eq.3).

For each of the six regions, the close form solutions of ψ and λ expressions are shown in (Faella et al., 2004), where the Authors assumed the constitutive law reported in Eq. 1.

Figure 2 shows functions $\psi(\xi)$ and $\lambda(\xi)$ obtained by integrating Eq.s 7 for values of $f_{1,d}$ ranging from 0 to 60%; this last value is rarely exceeded in practice. It is possible to observe that in regions 3 to 5 (i.e. for $\xi_{23} \leq \xi \leq 1$) ψ and λ assume constant values (i.e. $\bar{\psi}$ and $\bar{\lambda}$).

The value ξ_{23} - which corresponds to a threshold between regions 2 and 3 - can be evaluated as follows:

$$\xi_{23} = (1 - \delta') \cdot \frac{\varepsilon_{ccu}}{0.01 + \varepsilon_{ccu}} \quad (8)$$

Therefore ξ_{23} also depends on the non-dimensional pressure $f_{1,d}$.

For a generic value of the dimensionless pressure $f_{1,d}$, the simplified trend of the functions $\psi(\xi)$ and $\lambda(\xi)$ is presented in Figure 3a. The analytical expressions of the new relationships are reported in Figure 3b; such relationships depend on the following three coefficients:

$$\bar{\psi} = 1.16 \cdot f_{1,d}^{0.5} + 0.3 \cdot f_{1,d} + 0.8 \quad \bar{\lambda} = 0.437 - 0.05 \cdot f_{1,d} \quad \beta = 0.4 \cdot f_{1,d} + 1.25 \quad (9)$$

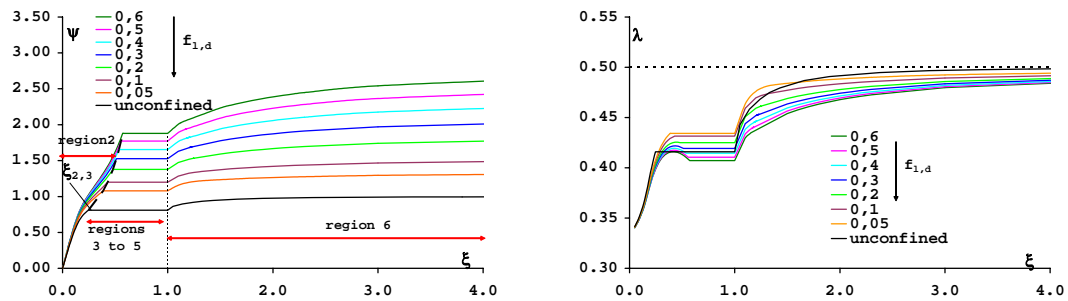


Figure 2: ψ and λ functions versus the neutral axis position

The value $\bar{\psi}$ - assumed by the function ψ in the regions 3 to 5 - was obtained by minimizing the scatters between a polynomial equation (black curve in Figure 3c) - the coefficients of which were obtained imposing $\bar{\psi}=0.8$ for $f_{1,d}=0$ (unconfined concrete) - and the curve obtained from the integration of the Equation 7 (red curve in figure 3c).

The value of $\bar{\lambda}$ - assumed by coefficient λ in regions 3 to 5 - instead, has shown a limited variability within the investigated range of the confinement pressure (red curve in Figure 3d).

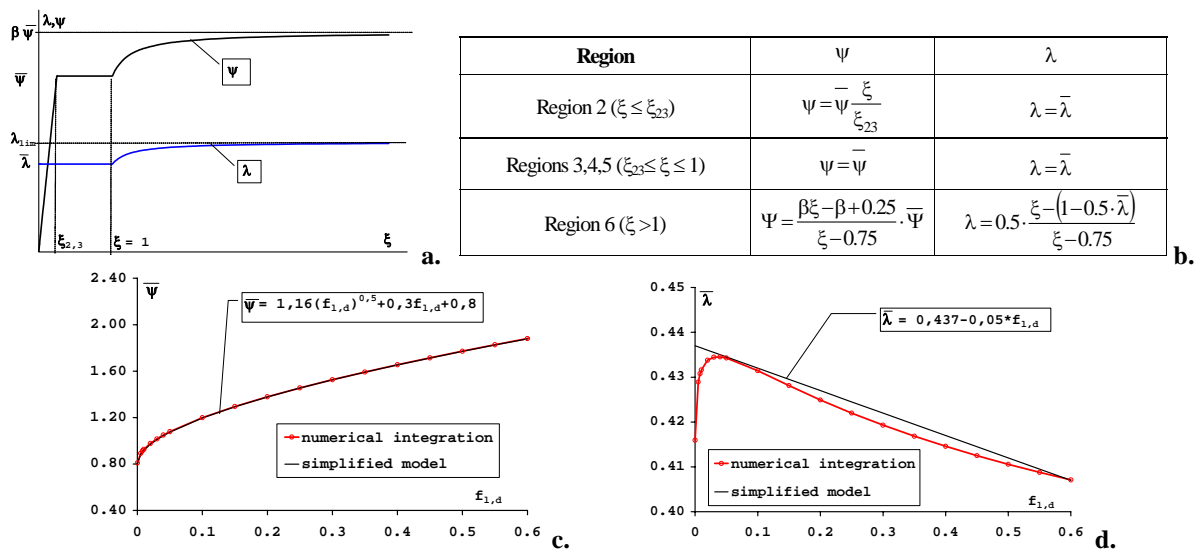


Figure 3: Trend of ψ and λ coefficients – simplified relationships

As shown in the Figure 3d a linear law $\bar{\lambda}(f_{1,d})$ was assumed thus slightly overestimating the values derived from the integration and, consequently, obtaining a conservative estimate in the v - μ curves definition.

3. INTERACTION CURVES AND ULTIMATE CURVATURE

In Figure 4, the v - μ interaction curves obtained from the equilibrium equations (6) and the relationships between v and the dimensionless ultimate curvature ($\phi_{u,d}$) are shown for $f_{1,d}$ ranging between 0 and 60%.

For what concerning the v - μ interaction curves, the ones reported with continuous lines were obtained by the exact solution of integrals contained in Equations 7 (coefficients ψ and λ), while the curves indicated with dotted lines were provided by applying the simplified procedure synthesized in Figure 3; all the curves were obtained for a dimensionless cover (δ') equal to 0.05 and for two symmetrical reinforcement configurations, i.e. $\omega=\omega'=0.1$ and 0.3. Observing the Figure it is evident that the simplified relationships derived for ψ and λ - although they are much simpler - allow obtaining v - μ curves very similar to the exact ones. The major differences between the two models can be observed in the “region 6”, where the simplified model is more conservative.

The ultimate curvature - shown in a dimensionless form in the lower part of the Figure 4 - were obtained by assuming as maximum steel tensile strain a value equal to 4%, according to the seismic Italian code (Ordinanza 3274, 2003) while the ultimate strain of concrete in compression was obtained by applying Equation 3. In the figure the improvement in terms of deformation capacity due to the FRP confinement is evident (note that the curvatures were amplified of a factor equal to 10). The design and/or the safety verifications of FRP confining interventions with the use of the v - μ and v - $(\phi_{u,d})$ diagrams shown in Figure 4 is immediate. Observing the v - μ interaction curves it is possible to evaluate, for each value of v , a threshold value of the non-dimensional confinement pressure; further increments of the confining system stiffness over this value do not produce improvements of strength. In the same way from the v - $(\phi_{u,d})$ diagrams an other threshold of $f_{1,d}$ can be evaluated; further increments of the confinement pressure over this value do not produce improvements of ductility.

Finally, it has to be underlined that the contribute of steel stirrups to the confinement was not considered herein.

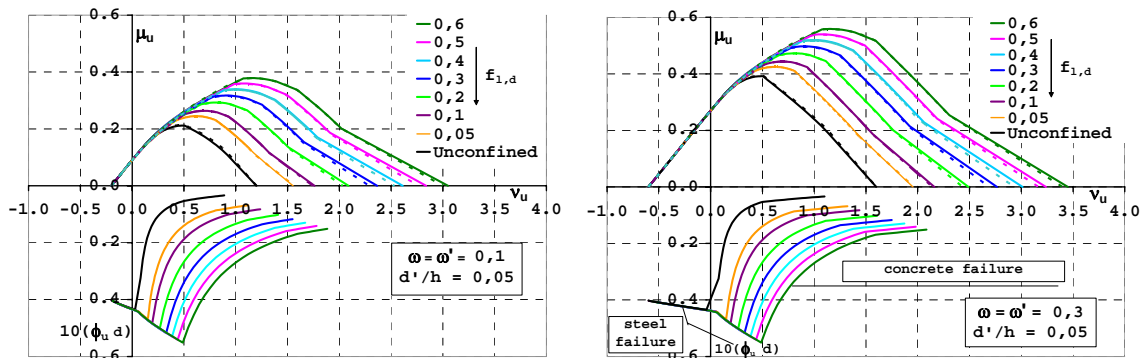


Figure 4: v - μ interaction curves and trends of the nondimensional ultimate curvatures

4. REFERENCES

- CEN, European Committee for Standardization (2001). “Eurocode 2: Design of concrete structures – Part 1: General rules and rules for buildings”, *European Standard, prEN 1992-1*, Brussels, Belgium.
- CNR, National Research Council (2004). “Guide for the design and construction of externally bonded FRP systems for strengthening existing structures (Materials, RC and PC structures, masonry structures)”, *Technical Document CNR-DT 200/2004*, Advisory Committee on Technical Recommendations for Constructions, Rome, Italy.
- Faella C., and Realfonzo R. (2002). “Legami costitutivi del calcestruzzo confinato con FRP”, *Proceedings of the V Italian Workshop on Composite Structures*, Salerno, Italy, November 28-29 (in italian).
- Faella, C., Realfonzo, R., and Salerno N. (2004). “N-M interaction curves of concrete elements confined with FRP systems”, *Proceedings of the International Conference of Restoration, Recycling and Rejuvenation Technology for Engineering and Architecture Application*, Cesena, Italy, June 7-11.
- Ordinanza 3274 (2003), “Norme tecniche per il progetto, la valutazione e l’adeguamento sismico degli edifici”. *Presidenza del Consiglio dei Ministri*, (Italian Seismic Code - in italian).

DESIGN AND MANUFACTURING OF LOW COST THERMOPLASTIC COMPOSITE BRIDGE SUPERSTRUCTURE

Nasim Uddin

(Associate Professor, Department of Civil Engineering at University of Alabama, Birmingham, Alabama, USA)

Abdul Moeed Abro

(Graduate Student, Department of Civil Engineering at University of Alabama, Birmingham, Alabama, USA)

Uday Vaidya

(Associate Professor, Department of Materials Engineering at University of Alabama, Birmingham, Alabama, USA)

ABSTRACT

An integral modular fiber thermoplastic composite bridge structural system is described. The design concept is presented by utilizing high performance thermoplastic material (i.e. Glass/Polypropylene) along with efficient low cost manufacturing process and fabrication techniques. The design is based on detailed finite element analyses to investigate the stiffness and strength of the structural system. To demonstrate the design concept, two bridge deck systems with different spans are modeled. The design concept of both decks presents a unique approach for structurally efficient and low cost bridge deck system.

KEYWORDS

Thermoplastic composite, glass/polypropylene, finite element analyses.

1. INTRODUCTION

The United States of America is facing a major challenge to keep the nation's infrastructure systems in usable condition as large volumes of bridges which were built in the 1960's (the Interstate era) need maintenance, major rehabilitation, or replacement in the near future. A solution to this challenge could be to implement new structural systems using more efficient materials like Fiber Reinforced Composites (Thermoplastics). Thermoplastic composites are relatively new materials in civil engineering applications and lack the history of use in civil infrastructure. Civil applications have often used thermoset composites. Recent progress in low cost thermoplastic materials and fabrication technologies offer new solutions for very lightweight, cost efficient composite structures with enhanced damage resistance and sustainable designs.

Recently, a novel hot melt impregnation technology called DRIFT (Direct ReInforcement Fabrication Technology) (Hartness et al. 2001) has been developed that allows complete impregnation of long fibers with thermoplastic polymers, producing high quality, low cost products that can be made as continuous rods, tapes and pultruded shapes (Hartness et al. 2001). E-glass/PP tapes of 12 mm width and an average layer thickness of 0.6 mm were produced using the DRIFT process. The unidirectional E-glass/PP tape material with a fiber content of 67% by weight (42% by volume) has the tensile strength 87.6 ksi, tensile modulus of 4300 ksi and density of 99 pounds per cubic ft. The hot melt impregnated unidirectional E-glass/PP tape can be woven into a plain weave architecture fabric form through textile weaving operation.

The deck shape (Fig. 1) based on hat-sine rib stiffened design concept is selected by considering various issues such as the processability of the E-glass/PP woven tape, and the practical issues such as tooling, and design flexibility for the prototype studies. The face and the rib portions of the deck floor can be processed through a number of choices, which include thermoforming, double belt press consolidation of the tape forms, reaction injection molding and or extrusion.



Figure 1: Hat-sine reinforced deck shape

2. DESIGN CRITERIA AND DESIGN PROCEDURE

2.1. Applied Loads and Allowable Deflection.

The dead loads are; self weight of the deck (15 psf) and load of wearing surface (5 psf).

The live loads include the three specified types of vehicular loading:

- i) *Design truck load HS20-44*: three axles with loads 32 kips, 32kips and 8 kips. The spacing between the 32 kips axles varies from 14 ft to 30 ft, and is chosen by the designer to produce the maximum effect for shear, moment and deflection.
- ii) *Design tandem*: a pair of 25 kips axles spaced 4 ft apart with transverse spacing of 6ft.
- iii) *Design lane load*: a uniformly distributed load of 640 lbs/ft applied over a 10 ft wide strip.

We use the AASHTO category strength I load combination to compute the ultimate capacity of the bridge i.e.

$$Q = 1.25DC + 1.75(LL + IM). \quad (1)$$

We use the AASHTO service I loading combination for checking the deflection of the bridge design, i.e.

$$Q = LL + IM \quad (2)$$

We use AASHTO specifications 3.6.1.3.2 and 2.5.2.6.2 to adopt the deflection limit of $L/800$ (where L is the span of the bridge). The deflection resulting from the design truck/tandem alone or that resulted from 25 percent of the design truck/tandem taken together with the design lane load should not be greater than the maximum allowed limit. For maximum deflection, the truck or tandem is placed such that the center of gravity of the truck or tandem is on the center of the bridge, i.e. AASHTO arrangement I. We use arrangement II (with the rear axle of the truck or tandem at one end of the bridge) of the truck or tandem load to check for the critical shear stress.

2.2. Design Procedure

The design procedure is based on the finite element analysis which is carried out on Ansys 8.0 software, the composite face and the hat-sine ribs are modeled using the Shell 99 elements. Each element is defined by orthotropic material properties (as defined in Table 1) and ply orientations. The contact region between the face panel and the hat sine stiffened ribs is developed by merging the common nodes and key points. The loading combinations as defined in section 2.1 are applied and based on the combination of least deflection and corresponding stresses, the deck component dimensions (amplitude and wavelength), shape and thickness are determined.

Table 1: Material properties of E-Glass / PP woven tape composite

Property	E-Glass/PP woven tape composite 40 % fiber content by volume
E_X, E_Y, E_Z	1437 ksi, 1437 ksi, 149 ksi
$\nu_{XY}, \nu_{YZ}, \nu_{XZ}$	0.11, 0.22, 0.22
G_{XY}, G_{YZ}, G_{XZ}	184.16 ksi, 108.75 ksi, 108.75 ksi
E_{FIBER}, E_{MATRIX}	10150 ksi, 149 ksi
G_{FIBER}, G_{MATRIX}	4350 ksi, 108.75 ksi

3. DESIGN CASE SUDY, VERFICATION AND COMPARISON.

3.1. Double Lane Bridge Deck System

For the system having 60 ft span bridge deck (Fig. 2), the hat-sine rib dimensions are determined to be optimal at 36 inch depth, 48 inch wavelength and 16 inch contact width with deck component thickness as shown by Fig. 3. The maximum deflection (Fig. 4), ultimate flexural and shear stresses are 0.9 inch, 6366 psi, and 1710 psi respectively.

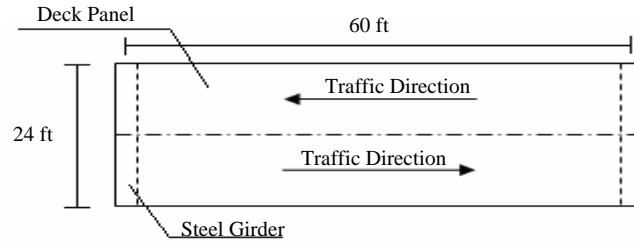


Figure 2: Plan of double lane bridge deck

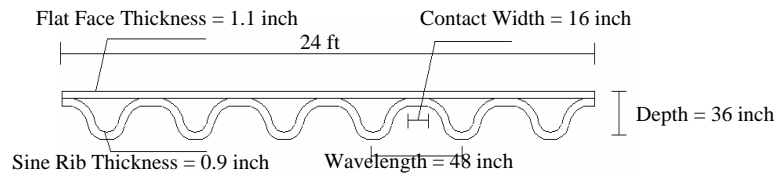


Figure 3: Double Lane Bridge Deck Parameters for Case 1 using Glass / PP

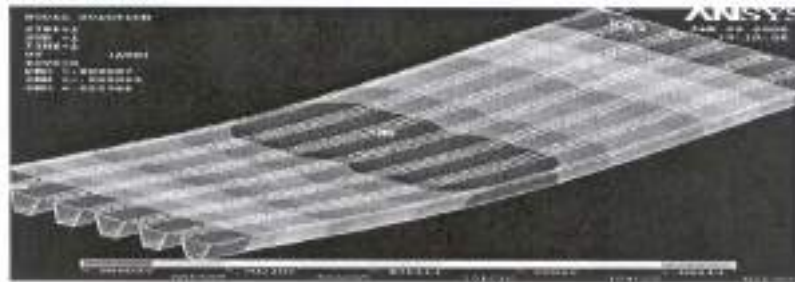


Figure 4: Deflection (inches) for Case 1 of a double lane deck model

3.2. Design Verification

For design verification and accuracy we compare the results of an experiment in which an E-glass/pp panel (Fig. 5) (material properties same as in Table 1) was tested under point loads (500 lbs to 2000 lbs).

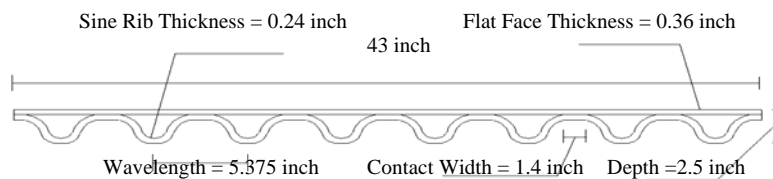


Figure 5: Panel shape and dimensional parameters used in an experiment

By comparing the results (Table 2), the analysis was found to under predict the deflection by 10 to 15 percent. This difference between the analysis and the model could be because of slight imperfectness in contact between the hat sine rib and flat face; it can be avoided by using strengthened bond joining methods like ultrasonic bonding etc.

Table 2: Experimental and Analytical Deflection Comparison

Concentrated Load (lbs)	Maximum Deflection (inches) (Experimental)	Maximum Deflection (inches) (Finite Element Analysis)	Difference (%)
500	0.026	0.023	10.76
1000	0.052	0.046	11.53
1500	0.07	0.06	14.28
2000	0.1	0.085	15

3.3. Comparison with other composite bridge system

We compare the performance of our double lane bridge deck system to the bridge system proposed by Aref and Parsons (2000). A schematic of the cross-section of the bridge system proposed by Aref (2000) consists of seven inner cells encased in an outer shell as shown in Fig. 6.

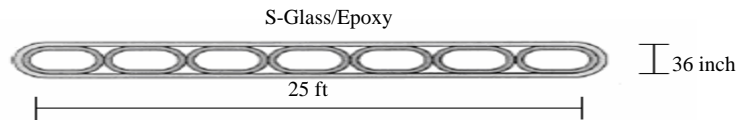


Figure 6. Cross-sections of the S-glass/Epoxy

The performance comparison of both systems is summarized in table 3 based on maximum deflection, failure indices, interface shear stresses, and the self weight of the deck system.

Table 3: Performance comparison between S-glass/epoxy (Aref, 2000) and E-glass/polypropylene (proposed design) deck system

Material	S-glass/epoxy	E-glass/polypropylene
Deflection (inch)	0.9	0.9
Tsai Hill Failure Index	0.24	0.28
Interface σ_{yz} (psi), σ_{xz} (psi)	504, 484	234, 175
Self weight of deck (lbs), DL:LL	67000, 0.46	121500, 0.84

4. CONCLUDING REMARKS AND ACKNOWLEDGEMENT

We have presented the structural system which possesses several special features that contribute to its effectiveness, including the use of curved panels (sine ribs) which provide the nonplanar core configurations to increase the performance of the bridge deck system. We compared our design to one published composite bridge concept proposed by Aref (2000). Although our design has higher self weight which results in higher dead to live load ratio than S-glass/epoxy deck system (Aref, 2000); but our design could result in better low cost deck section based on the manufacturing and material cost comparison. However detailed cost analysis directed towards the manufacturing process and deck material is required before any definitive conclusions can be made regarding this issue.

We gratefully acknowledge the financial support of UTCA under the director Dr. Danial S. Turner.

5. REFERENCES

Aref A.J., Parsons I.D. (2000). “Design and performance of a modular fiber reinforced plastic bridge”. *Journal of Composite*, Part B 31, pp 619-628.
 AASHTO (2004). *AASHTO LRFD Bridge Design Specification*, 3rd edition.
 Hartness T., Husman G., Koeing J. and Dyksterhouse J. (2001). “The characterization of low cost fiber reinforced thermoplastic composites produced by the DRIFT process”. *Journal of Composites*, Part A 32, pp 1155-1160.
 Vaidya U., Samalot F., Pillay S., Janowski G., Husman G. and Gleich K. (2004). “Design and manufacture of woven reinforced glass/polypropylene composites for mass transit floor system”. *Journal of Composite Materials*, Vol. 38, No. 21, pp 1949-1972.

ITALIAN DESIGN GUIDELINES FOR THE STRENGTHENING OF EXISTING CIVIL CONSTRUCTIONS USING EXTERNALLY BONDED FIBRE-REINFORCED POLYMERS

Luigi Ascione, Andrea Benedetti, Antonio Borri,
Angelo Di Tommaso, Luciano Feo, Roberto Frassine,
Gaetano Manfredi, Giorgio Monti, Antonio Nanni,
Maurizio Piazza, Carlo Poggi, Elio Sacco

ABSTRACT

A series of regulatory documents were issued by the National Research Council (CNR) of Italy on the use of FRP for strengthening existing civil constructions. These documents, described in more details in the paper, set for the first time in Italy some standards for production, design and application of FRP for reinforced concrete, masonry, timber and metallic constructions. They are also conceived with an informative and educational spirit, which is crucial for the dissemination, in the professional sphere, of the mechanical and technological knowledge needed for an aware and competent use of such materials.

The documents are the result of a remarkable joint effort of almost all professors and researchers involved in this emerging and promising field, from 15 Italian universities, of the technical managers of major production and application companies, and of the representatives of public and private companies that use FRP for strengthening artifacts. Thus, the resulting FRP codes naturally incorporate the experience and knowledge gained in ten years of studies, researches and applications of FRP in Italy.

KEYWORDS

Design guidelines, Fiber Reinforced Polymers, Existing Civil Constructions, Seismic Strengthening.

1. INTRODUCTION

The peculiar situation of Italy with regards to the preservation of existing constructions, results from the combination of two aspects: a) seismic hazard over the whole of the national territory, recently refined by a new seismic zonation, with medium-high intensity over a large portion of it, the highest expected PGA being 0.35g for a 475 years return period, and b) extreme variety of the built environment, perhaps with no comparison in the entire world.

Construction typology in Italy encompasses examples reckoned as Country's (and world's) historical, architectural and cultural heritage – which include buildings of various function and importance, such as palaces, temples, churches, cloisters, theatres, memorials, city walls, castles, simple dwellings, civil engineering works such as bridges harbours and aqueducts – dating back to more than 2000 years ago, throughout the ancient- middle- modern- and contemporary ages, down to those built in the 20th century.

The first studies on the use of FRP for the rehabilitation of existing civil constructions started in the early 90's by some pioneering groups that were striving to find new solutions to increase the safety of existing constructions, that could compete with the more developed and usual ones of concrete jacketing, steel plating, base isolation, and dissipative bracings.

Over the last ten years the interest has spread so widely and rapidly that FRP composites have now become one of the most active and prolific research fields throughout the country.

As a testimony of the intense activity in Italy in the field of FRP, a series of regulatory documents were issued by the National Research Council (CNR) of Italy on the use of FRP for strengthening structures: Instructions for Design, Execution and Control of Strengthening Interventions by Means of Fibre-Reinforced Polymers: materials, RC structures, prestressed RC structures, masonry structures (CNR-DT200/2004), timber structures (CNR-DT201/2005) and metallic structures (CNR-DT202/2005).

These documents set for the first time in Italy some standards for production, design and application of FRP for the rehabilitation of existing civil constructions. They are the result of a remarkable joint effort of almost all the professors and researchers involved in this emerging and promising field, from 15 universities, to the technical managers of major production and application companies, as well as the representatives of public and private companies that use FRP for strengthening artefacts. Thus, the resulting FRP codes naturally incorporate the experience and knowledge gained in ten years of studies, researches and applications of FRP in Italy.

The aim of the present paper is to present the aforementioned Italian technical codes in order to contribute to their diffusion within the international scientific community.

2. CNR-DT 200/2004

The aim of the Instructions CNR-DT 200/2004 is to draw up a document that can be used for designing, execution and controlling strengthening interventions on structures using fibre-reinforced composites, within the current norms. The document deals with the following issues:

- Materials
- Basic FRP strengthening concepts and particular problems;
- Strengthening concrete and prestressed concrete structures;
- Strengthening masonry.

Within the area of strengthening reinforced concrete structures and prestressed reinforced concrete structures, as well as masonry, specific indications are given relative to constructing in seismic areas according to the most recent norms drawn up both nationally and internationally.

It starts with a description of both the positive and negative aspects of polymeric materials from a didactic perspective as well as including an Appendix (A) which presents several of the mechanical properties, considered to be fundamental in order to fully understand how to use such materials in the structural field. The various peculiarities of these composites are highlighted in comparison to traditionally used isotropic materials, with particular attention being given to joints as well as to how to verify resistance.

The remaining issues are discussed following the usual style of technical documents published by the CNR, in accordance with the approach set out in the Euro-codes. The proposals are distinguished into Principles and Application Rules, with each one being identified by a number and the Principles being labelled with a (P).

The main peculiarities of the CNR-DT 200/2004 help in characterising this document as well as distinguishing it from all the other similar ones published within the international context.

One of the first innovative aspects can be found in the chapter dedicated to the materials to which the technicians of the main companies producing FRP strengthening systems actively contributed. It defines the format of the specific technical product sheets that the very same producers should supply therefore allowing whoever uses them to have the necessary information considered to be indispensable when comparing the various products available on the market.

In both the chapter dealing with the Materials as well as that dedicated to the Basic Strengthening Design Concepts and Particular Problems, the concept of “complete strengthening system” is opportunely introduced. This is another particularity of the CNR-DT 200/2004, that many factors are in play from the moment of executing a FRP strengthening to its success, ranging from the compatibility between each of the single products used to the specific structural substrate to which they must be applied (concrete, masonry, etc.).

The latter consideration is based on the distinction introduced in the document between two types of applications:

- Type-A applications: strengthening system with certification of each component as well as the final product to be applied to a given support;
- Type-B applications: strengthening systems certified for each component only.

For the first type of application, the producer can certify the aforementioned compatibility, with lower partial coefficient values being attributed to the state limit method as well as less severe quality control tests being carried out.

The CNR-DT 200/2004 also gives for the first time specific indications for the use of FRP in seismic areas, in accordance with the most recent literature as well as the most up to date Italian Codes.

Techniques and regulations for executing FRP strengthening interventions are described in the CNR Instructions as well as their subsequent monitoring and relative controls. This was considered a useful aid to designers, works directors and anyone else in deciding when to use FRPs for structural plating.

Another aspect that characterises the CNR-DT 200/2004 is the fact that it organically deals with the main FRP interventions to be carried out on masonry structures, including both simple and double curved.

The other four Appendices of the document include further discussion from a didactic perspective of issues relatively conceptually advanced, ranging from delamination to the behaviour of concrete pillars, strengthened both longitudinally as well as transversely.

3. CNR-DT 201/2005

This document contains the Instructions relative to consolidation interventions of timber structures using fibre-reinforced composites.

The issues dealt with in this document are the following:

- Basic FRP strengthening concepts and particular problems;
- Strengthening of prestressed elements;
- Strengthening of rigid elements;
- Strengthening of thin elements;
- Delamination resistance;
- Fatigue Strengthening;
- Execution, Control and Maintenance.

There are also three Appendices, including several examples of FRP strengthening interventions on structures are described (Appendix A), main bibliographic information (Appendix B) and the reference norms (Appendix C).

This is an informative type of document. It proposes the following objectives: to diffuse within the Technical-Professional community the knowledge acquired on the use of fibre reinforced composite materials in static consolidation of timber structures and to identify the interventions that are effectively appropriate and safe.

Timber is considered to be technically one of the most adapt construction materials with long term load bearing qualities as well as a long applicative history, as highlighted by the elevated durability of the number of structures designed and built.

Over recent years, the ever increasing need for increased resistance and rigidity of both timber and glued lamellate timber structures, has led for number of experiments to be carried out on timber-FRP one in comparison to only wooden ones.

Fibre-reinforced composites offer several evident advantages, being easily applicable and extremely versatile for both restructuring existing structures and designing new ones. These characteristics, due to their attractiveness, have favoured a rapid and widespread diffusion of in strengthening techniques of concrete structures as well as masonry plating through the use of fibre reinforced laminas.

These techniques are now an integral part of the patrimony of many designers as well as proving to be effective tools in rapidly resolving numerous problems.

Even though experiment have been carried out on timber-FRP structures for over the past 15 years, it is a well known fact that the current state of art is not advanced as its concrete counterpart, with it giving a limited number of answers to problems relating to few specific applications.

It is worth noting that up until now no international guide lines have been drawn up for the use of FRP in plating timber structures.

The work carried out so far represents the first step towards a set of design Instructions being drawn up that in the near future, once all the theoretical and experimental studies currently underway have been concluded, will lead to a more complete and universal understanding of the subject area.

In this perspective, the document will be useful in identifying the problems that remain unresolved, allowing the scientific community to concentrate upon them over the next few years.

4. CNR-DT 202/2005

This document contains Instructions relative to the consolidation interventions on metallic structures using fibre reinforced composites.

The issues dealt with in this document are the following:

- Basic FRP strengthening concepts and particular problems;
- Strengthening of prestressed elements;
- Strengthening of rigid elements;
- Strengthening of thin elements;
- Delamination resistance;
- Fatigue Strengthening;
- Execution, Control and Maintenance.

There are two Appendices, one including several examples of FRP strengthening interventions on structures both nationally and internationally, while the other deals with the main bibliographic information.

It is set out as a series of Principles and Application Rules, in accordance with the Euro-codes as previously stated in CNR-DT 200/2004 with the aim of diffusing information within the Technical-Professional community the knowledge acquired on the use of fibre reinforced composite materials in static consolidation of metallic structures as well as identifying the interventions that are effectively appropriate and safe.

It is worth noting that up until now the only international guide lines on the use of FRP plating for metallic structures have been drawn up by an English research agency (CIRIA, 2004) & (ICE, 2001).

The Italian historical architectural patrimony is rich of significant examples of metallic workmanship. They had an important role in the growth of the industrial civilisation as well as giving an impetus to the development of structural theory and the study of material resistance.

As for all types of structures, many metallic structures need to have some sort of restructuring interventions due to design faults, degradation of load bearing elements and variation in use.

Current metallic structure strengthening techniques include either bolting or welding steel plates to the original structure but these can have some negative aspects. The steel plates introduce further weight that must be sustained as well as also being susceptible to corrosion and stress phenomena. Welding can bring about many problems and can sometimes be impractical as in the case of cast iron or steel structures.

Many of the problems associated to traditional techniques can be overcome by using fibre reinforced composites. FRPs have an elevated weight/resistance ratio, higher than steel, are more resistant to corrosion phenomena, if not immune, and are extremely easy to handle.

In the current version of this document reference is made to the CNR-DT 200/2004, in particular to the basic FRP strengthening concepts for prestressed and rigid elements as well as the problems associated to them.

Several aspects regarding delamination and FRP strengthening of metallic framework fatigue damaged are also discussed.

Also this document is useful in identifying the problems that are still unanswered, allowing the scientific community to concentrate upon them over the next few years, with particular attention being given to delamination, the structural behaviour of thin elements with particular reference to eulerian stability, thermal effects (particularly relevant to metal bridges) and prolonged exposure to UV radiation.

4. CONCLUSIONS

The peculiarity of Italy, highly seismic and endowed with a built environment unique in the world, extremely various and rich of cultural value, renders all research in this field a continuous and challenging task.

This nationwide effort has resulted in a series of regulatory documents, that were conceived both for regulating a rapidly growing professional and technical market, as well as for an informative and educational purpose. The documents are deemed of great importance for the dissemination, in the professional sphere, of the physical and technological knowledge necessary to conscious and competent use of FRP in strengthening.

5. REFERENCES

- CNR-DT 200/2004: 'Instructions for design, execution and control of strengthening interventions by means of fibre-reinforced composites: materials, RC structures, prestressed RC structure, masonry' (2004).
CNR-DT 201/2005: 'Instructions relative to consolidation interventions of timber structures using fibre-reinforced composites' (2005).
CNR-DT 202/2005: Instructions relative to consolidation interventions of metallic structures using fibre-reinforced composites' (2005).

LARGE-SIZE REINFORCED CONCRETE COLUMNS STRENGTHENED WITH CARBON FRP: VALIDATION OF EXISTING DESIGN GUIDELINES

Silvia Rocca

(Ph D. Candidate in Civil Engineering, University of Missouri - Rolla, Rolla, Missouri, USA)

Nestore Galati

(Research Engineer, University of Missouri - Rolla, Rolla, Missouri, USA)

Antonio Nanni

(Chair & Professor of Civil Engineering, University of Miami – Coral Gables, Coral Gables, Florida, USA)

ABSTRACT

Current international design guidelines provide predictive design equations for the strengthening of Reinforced Concrete (RC) columns of both circular and prismatic cross-sections by means of FRP confinement and subject to pure axial loading. Extensive studies (experimental and analytical) have been conducted for the case of columns with cross-sections of the circular type, and limited studies have been conducted on the prismatic ones. In fact, the majority of this research has been on small-scale, plain concrete specimens. In this review paper, four international design guidelines are referenced, and a comparative study is presented that is based on the increment of concrete compressive strength and ductility and that, includes the experimental results from six RC columns of different cross-section shapes. The observed outcomes are used to identify and remark upon the limitations beyond the ones specifically stated by each of the guides and to reflect the absence of effects not considered in current models. The purpose of this study is to present a constructive critical comparison of the state-of-the-art design methodologies available for the case of FRP-confined concrete RC columns and to indicate a direction for future developments.

KEYWORDS

Confinement, Ductility, FRP-Strengthening, Prismatic Columns, Reinforced Concrete.

1. INTRODUCTION

The confinement of Reinforced Concrete (RC) columns by means of Fiber Reinforced Polymers (FRP) jackets is a technique being used with growing frequency to seek the increment of load carrying capacity and/or ductility of such compression members. The need for improved strength is the result of higher load capacity demands because of change in the use of the structure or because of more stringent code requirements. Improving ductility stems from the need for energy dissipation, which allows the plastic behavior of the element and, ultimately, of the structure. Ductility enhancement is typically required in existing columns that are subjected to a combination of axial load and bending moment because of a change in code (*e.g.*, to account for seismic provisions) or a correction for design or construction errors (*e.g.*, improper splicing of the longitudinal reinforcement or lack of transverse ties). Extensive work in both the experimental and analytical areas has been conducted on RC columns of circular cross-sections confined with FRP and subjected to pure axial compressive loading. This work has led to the development of several models (the majority being empirical) of two types: design-oriented, where equations are provided to determine the axial compressive strength and the ultimate axial strain (Saaman et al. 1998, Toutanji 1999, Xiao and Wu 2000, among others); and analysis-oriented, which allows the construction of the stress-strain response of the RC column (Spoelstra and Monti 1999, Lam and Teng 2003, among others).

Studies focused on RC columns of non-circular cross-sections have also been conducted; however, such work is limited because the experimental research has primarily been on small specimens of plain concrete due to high cost and lack of high-capacity testing equipment. This situation has been the main reason for overlooking the following

important effects on the element performance that are not accounted for in most of the available models: (a) the size of the cross-sectional area, (b) the dimensional aspect ratio of the cross-sectional area, (c) the presence and possible detrimental effect of longitudinal steel reinforcement instability, (d) the concrete dilation dependant on a pseudo-Poisson ratio, and (e) the contribution of the internal transverse steel reinforcement. In spite of these obstacles, several models have been proposed (Lam and Teng 2003, Maalej et al. 2003, among others) and have become the basis for design provisions. In particular, the predictive equations found in the current design guides are mostly based on approaches created for members of circular cross-section and then modified by a “shape factor” or “efficiency factor.” This factor is intended to account for the geometry of the section and its effect on the confining pressure, which is no longer uniformly applied by the FRP jacket as for the case of circular cross-sections.

2. RESPONSE TO AXIAL LOAD

The purpose of this study is to use pertinent experimental evidence to identify and remark on the differences in the design methodologies used by the existing available design guides on the FRP confinement of RC columns of different cross-sections and subject to pure axial loading. For the purpose of this paper and for the interpretation of experimental results, clear and unequivocal definitions of strength and ductility parameters are necessary:

- f'_{co} and f'_{cc} represent the peak concrete strengths corresponding to the maximum load carried by the RC column for unconfined and confined cases, respectively.
- ϵ_{cu} is the ultimate strain of the unconfined RC column corresponding to $0.85f'_{co}$ (Figure 1(a)). For the confined RC column, ϵ_{ccu} may correspond to one of the following values: a) $0.85f'_{cc}$ in the case of a lightly confined member (Figure 1(b)); b) the failure strain in the heavily confined, softening case when the failure stress is larger than $0.85f'_{cc}$ (Figure 1(c)); or c) heavily confined, hardening case, where ultimate strength corresponds to ultimate strain (Figure 1(d)).

The definition of ϵ_{ccu} at $0.85f'_{cc}$ (or less) is arbitrary, although consistent with modeling of conventional concrete (Hognestad 1951), and such that the descending branch of the stress-strain curve at that level of stress ($0.85f'_{cc}$ or higher) is not as sensitive to the test procedure in terms of speed of loading and stiffness of the equipment utilized.

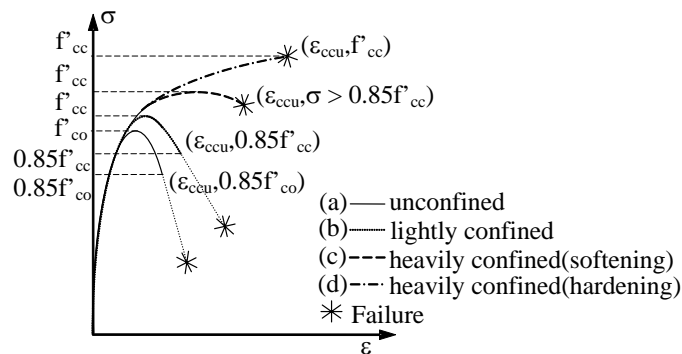


Figure 1: Schematic Stress-Strain Behavior of Unconfined and Confined RC Columns

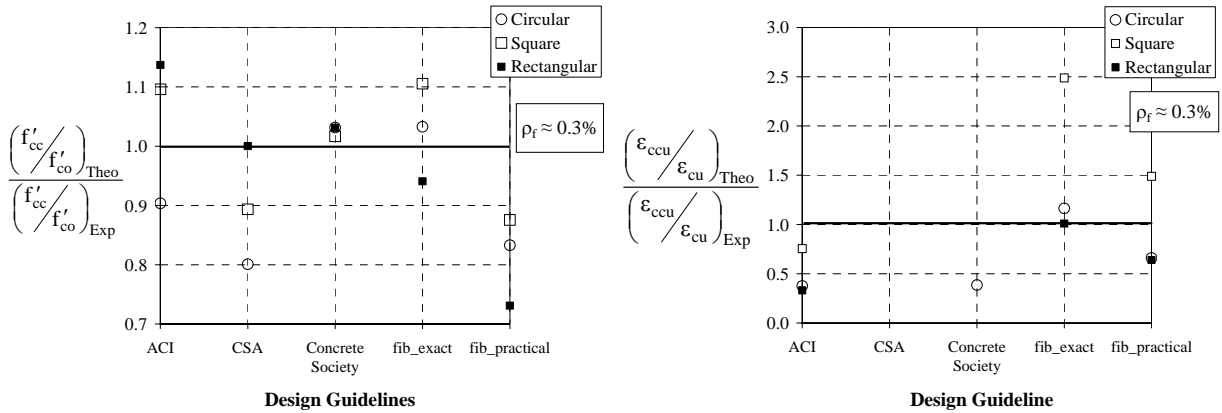
3. COMPARATIVE STUDY

The documents considered in this comparative study are as follows: “Guide for the Design and Construction of Externally Bonded FRP Systems for Strengthening Concrete Structures” reported by the American Concrete Institute (ACI Committee 440.2R-02 2002), “Design and Construction of Building Components with Fibre-Reinforced Polymers” reported by the Canadian Standard Association (CSA S806-02 2002), “Design Guidance for Strengthening Concrete Structures Using Fibre Composite Material” Technical Report 55 by the Concrete Society (TR 55 2004), and “Externally Bonded FRP Reinforcement for RC Structures” Technical Report by the *fédération internationale du béton* (*fib* Bulletin 14 2001). The latter document provides two sets of equations: “exact” and “approximated.”

To evaluate the performance and contrast the different approaches taken by the guidelines for the determination of the compressive strength (f'_{cc}) and the ultimate axial compressive strain for confined concrete (ϵ_{ccu}), a total of six RC

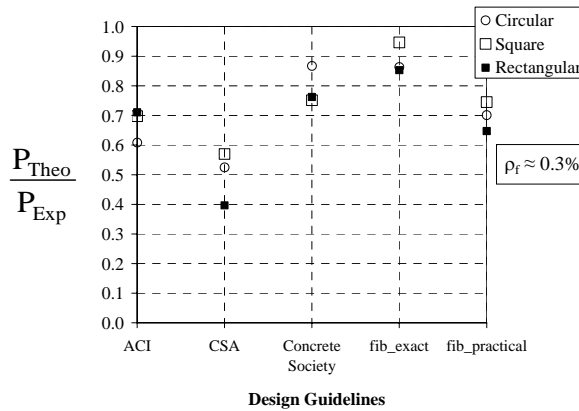
column specimens (three strengthened specimens with their corresponding control units) of different cross-section shapes (circular, square, and rectangular) and equal gross areas (A_g) were selected, designed, constructed, and tested. These specimens were part of a recently-conducted research study on the size-effect of FRP-confined RC columns (Rocca et al., 2006) and in the companion paper are identified as specimens A1 and A2 (circular), C1 and C3 (square), and B1 and B3 (rectangular). This assessment is not intended to be comprehensive, but the three relevant cases presented here indicate the trends of the guidelines under study.

Figure 2(a) shows the accuracy of the different codes with respect to the experimental results in terms of strength enhancement ($[(f'_{cc}/f'_{co})_{theo}]/[(f'_{cc}/f'_{co})_{exp}]$). For the case of circular cross-sections, only the Concrete Society and the “exact” equations by *fib* slightly overestimate the strength enhancement (by approximately three percent). Regarding the prismatic cross-sections, only ACI and the Concrete Society overestimate the strength increase for both square and rectangular sections. The “exact” formulas by *fib* overestimate the strength enhancement for only the square type of cross-section.



(a) Ratio of Theoretical Concrete Compressive Strength Enhancement to Experimental

(b) Ratio of Theoretical Ultimate Axial Deformation Enhancement to Experimental



(c) Ratio of Design Axial Load Capacity to Experimental

Figure 2: Guidelines Performance

Figure 2(b) shows the accuracy of the guidelines in predicting the ultimate axial strain enhancement $\epsilon_{ccu}/\epsilon_{cu}$. A theoretical value of ϵ_{cu} equal to 0.003 was used in the case of ACI, and a value of 0.0035 was used in the cases of the Concrete Society and *fib*. CSA does not provide expressions for the calculation of ϵ_{ccu} . The estimations vary within a range of approximately ± 50 percent of the experimental ratios, with the exception of the value corresponding to the “exact” equations from *fib* for the case of square columns (about 250 percent). In general, the scatter of the predictions was much larger than for the strength enhancement. This may partly be because of the difficulty in accurately representing the effects of parameters such as size and type of aggregates; mix proportions; water/cement ratio; and in the case of confined concrete the stiffness of the FRP jacket.

Figure 2(c) presents the theoretical to experimental ratios of load-carrying capacity of the FRP-strengthened RC columns: P_{theo}/P_{exp} . The theoretical or design values of axial resistance were computed considering the material safety factors and/or the strength reduction factors as required by each guideline. All the predictions appear to be conservative. The results mainly vary in a range from about 60 to 95 percent of the experimentally obtained load-carrying capacity, with the exception of the ratios corresponding to CSA that show a minimum percentage of about 40, which can be considered too conservative.

4. CONCLUSIONS

The limits of applicability of the equations provided by the design guidelines primarily deal with the dimensions of the cross-sections, the side-aspect-ratio (h/b), and loading type (concentric). These limits are the result of the reduced experimental evidence on the area of FRP-confinement of real-size RC columns, which at the same time has not allowed the appropriate implementation of key effects in the current models. These effects have been identified as follows: the instability of longitudinal steel reinforcement, the concrete dilation dependant on the pseudo-Poisson ratio, the contribution of the internal transverse steel reinforcement to the confinement, and an appropriate reduction factor to account for the premature failure of the FRP jacket.

Given the present knowledge, the research community should consider further experimental and analytical work to confirm the basic assumptions and to provide substantial data information to feed and correctly calibrate numerical and analytical models. Although a vast experimental campaign on real-size RC columns following the conventional testing methodology is a choice, the current available sensing technology used in a few dimensionally-relevant specimens represents an innovative alternative testing protocol that would help obtain accurate information and most importantly, would allow the understanding of the physical phenomena. The measurements should be targeted to the strain distribution along the perimeter of the FRP jacket, strain distribution of the longitudinal and transverse steel reinforcement, lateral (outward) deformation of the longitudinal steel bars product of the concrete lateral dilation (bar instability), concrete dilation, and crack propagation detection. A more meaningful interpretation of the experimental data currently available in the literature would become possible once performance phenomena and controlling parameters are fully understood.

5. REFERENCES

- American Concrete Institute, ACI 440.2R-02. (2002). "Guide for the Design and Construction of Externally Bonded FRP Systems for Strengthening of Concrete Structures," American Concrete Institute, Farmington Hills, MI.
- Canadian Standards Association, CSA-S806. (2002). "Design and Construction of Building Components with Fibre-Reinforced Polymers," Ontario, Canada.
- fédération internationale du béton (*fib*). (2001). "Externally Bonded FRP Reinforcement for RC Structures," Bulletin 14, Technical Report, Lausanne, Switzerland.
- Hognestad, E. (1951). "A Study of Combined Bending and Axial Load in Reinforced Concrete Members," Bulletin 399, University of Illinois Engineering Experiment Station, Urbana, IL.
- Lam, L., and Teng, J. (2003). "Design-oriented Stress-Strain Model for FRP-confined Concrete in Rectangular Columns," *Journal of Reinforced Plastics and Composites*, Vol. 22, No. 13, pp. 1149-1186.
- Maalej, M., Tanwongsva, S., and Paramasivam, P. (2003). "Modeling of Rectangular RC Columns Strengthened with FRP," *Cement & Concrete Composites*, Vol. 25, pp. 263-276.
- Rocca, S., Galati, N., and Nanni, A. (2006). "Experimental Evaluation of FRP Strengthening of Large-Size Reinforced Concrete Columns," CIES Report No. 06-63, University of Missouri – Rolla, Rolla, MO.
- Samaan, M., Mirmiran, A., and Shahawy, M. (1998). "Model of Concrete Confined by Fiber Composites," *ASCE Journal for Structural Engineering*, Vol. 124, No. 9, pp. 1025–1031.
- Spoelstra, M. R., and Monti, G. (1999). "FRP-Confined Concrete Model," *ASCE Journal of Composites for Construction*, Vol. 3, No. 3, pp. 143-150.
- The Concrete Society. (2004). "Design Guidance for Strengthening Concrete Structures Using Fibre Composite Material," Technical Report 55, Crowthorne, United Kingdom.
- Toutanji, H. (1999). "Stress-Strain Characteristics of Concrete Columns Externally Confined with Advanced Fiber Composite Sheets," *ACI Materials Journal*, Vol. 96, No. 3, pp. 397–404.
- Xiao, Y., and Wu, H. (2000). "Compressive Behavior of Concrete Confined by Carbon Fiber Composite Jackets," *ASCE Journal of Materials in Civil Engineering*, Vol. 12, No. 2, pp. 139–146.

TORSION DESIGN OF CFRP PLATED RC MEMBERS

Adrian K. Y. Hii & Riadh Al-Mahaidi
(Department of Civil Engineering, Monash University, Victoria 3800, Australia)

ABSTRACT

Since 2001, there have been several experimental investigations in strengthening reinforced concrete members in torsion. However, available tools for torsion design of FRP plated reinforced concrete members are limited and unproven. A database of previous experimental data available in literature was compiled and compared against *fib* Bulletin 14. Modifications consistent with the space truss model were proposed to correct the poor accuracy in predictions of CFRP contribution to strength. Subsequently, a design tool consistent with several national design codes to analyze the full torsional capacity of CFRP plated reinforced concrete beams was validated against the experimental database.

KEYWORDS

Aggregate interlock, CFRP, design methods, reinforced concrete, torsion.

1. INTRODUCTION

A literature survey conducted by the authors (Hii and Al-Mahaidi 2005) found no experimental data for FRP strengthening in torsion reported prior to 2001. Since then, several investigations have been conducted. However, most experiments were exploratory in nature, making the proposal of analytical methods difficult to validate against a single set of tests. Previous researchers have proposed a simple limiting FRP strain value (Ghobarah et al. 2002); (Salom et al. 2004); (Zhang et al. 2001). A more sophisticated design method by *fib* Bulletin 14 (2001) was taken by Ameli et al. (2004) and Panchacharam and Belarbi (2002). However, errors were found in the analysis (Hii and Al-Mahaidi 2005). This paper evaluates the *fib* Bulletin 14 method against a unified database of all available experimental data. Limitations and inconsistencies were identified. Modifications based on current national design codes were then proposed and compared against the same database to observe any improvements in accuracy.

2. EVALUATION OF *fib* BULLETIN 14 GUIDELINES

Based on the assumption of the validity of the truss mechanism, the following equations were provided by *fib* Bulletin 14 to predict the FRP contribution to strength, $T_{n,frp}$:

$$T_{n,frp} = 2\varepsilon_{fd,e} E_{fu} b_f t_f s_f^{-1} A_c (\cot \theta + \cot \alpha) \sin \alpha \quad (1)$$

$$\varepsilon_{fk,e} = k\varepsilon_{f,e} \leq \varepsilon_{max} \quad (2)$$

$$\varepsilon_{fd,e} = \varepsilon_{fk,e} / \gamma_f \quad (3)$$

Where A_c = gross area of concrete section; b_f , s_f , t_f = width, center-to-center spacing and thickness of FRP strips respectively; E_{fu} = Young's modulus for FRP; $k = 0.8$ is used to define the characteristic effective FRP strain, $\varepsilon_{fk,e}$; α = angle between principal fiber orientation and longitudinal axis of member; $\varepsilon_{fd,e}$ = design value of effective fiber strain, $\varepsilon_{f,e}$; $\varepsilon_{max} = 0.005$ (for activation of the aggregate interlock mechanism); γ_f = material safety factor for the FRP (range 1.2-1.5 in *fib* Bulletin 14); and θ = angle of crack to longitudinal axis.

In the case of FRP strips of width b_f and spacing s_f , in Equation 1 t_f is multiplied by b_f/s_f , in effect 'smearing' the strips along the length of member. Although the guidelines require full wrapping around the member cross-section, Panchacharam and Belarbi (2002) and Ameli et al. (2004) observed increases in torsional capacity for both anchored and unanchored U-wraps that were less significant than the equivalent full wrap. Therefore, Equation 1 without the factor 2 was used for specimens strengthened with U-wraps as it was assumed only one full couple exists between fiber strips. Due to the similar cracking mechanisms and lack of available test data, *fib* Bulletin 14 recommended the

adaptation of Triantafillou and Antonopoulos' (2000) shear model. The model assumes the FRP laminates develop an effective strain in the principal material direction at ultimate limit state. Details of the effective strain relationships are located in *fib* Bulletin 14. The *fib* Bulletin 14 guidelines do not explicitly specify the FRP reinforcement ratio, ρ_f , for torsional strengthening. However, it is in the authors' view that applying ρ_f from shear strengthening is inconsistent. A member behaves like an equivalent hollow tube under torsion; thus for completely wrapped specimens, ρ_f for torsion is taken to be equal to t_f/t_c , where t_c is equal to $3A_c/(4p_c)$. p_c is defined as the perimeter enclosing the gross area of concrete. For box-section beams, the smaller of the actual wall thickness or $3A_c/(4p_c)$ is taken as t_c .

Since then, several experimental investigations with externally-bonded CFRP and GFRP on this topic have been carried out by Ameli et al. (2004), Ghobarah et al. (2002), Panchacharam and Belarbi (2002), Salom et al. (2004), and Zhang et al. (2001) in addition to the authors' investigations (Hii and Al-Mahaidi 2004; 2006). Only specimens which failed from FRP debonding or rupture were considered. Specimens which failed from concrete crushing were discarded as the full FRP contribution to strength could not be achieved. Also, beams strengthened with longitudinal strips only were not included as no significant improvement in post-cracking strength was observed in experiments by previous investigators. Closer examination of the effective strain models by Triantafillou and Antonopoulos (2000) were derived from mainly CFRP tests and some AFRP tests (Hii and Al-Mahaidi 2005). Hence, GFRP tests were not considered here since no effective strain model exists. This left thirty relevant CFRP strengthened specimens in the final database. Among the strengthening layouts investigated included varying fiber orientations, as well as full/U-wraps. Varying strip spacings and layers were also investigated. Further details of the database can be found in (Hii and Al-Mahaidi (To be published)).

For comparison purposes, the effective strain, $\varepsilon_{f,e}$, was used throughout this paper. All load, material and safety factors were taken to be unity in this paper. It can be seen from Figure 1(a) that the predicted torsional contribution from CFRP by *fib* Bulletin 14 was generally unsafe by 52%. The crack angle θ was taken to be 45° as it was generally not reported in literature. For the experiments carried out by the authors, a range of crack angles for each specimen was measured (Hii and Al-Mahaidi 2005). The large range found highlighted the importance of the θ parameter. However, the range of values was still generally unsafe. Other parameters should be considered as well for further refinement of *fib* Bulletin 14 guidelines.

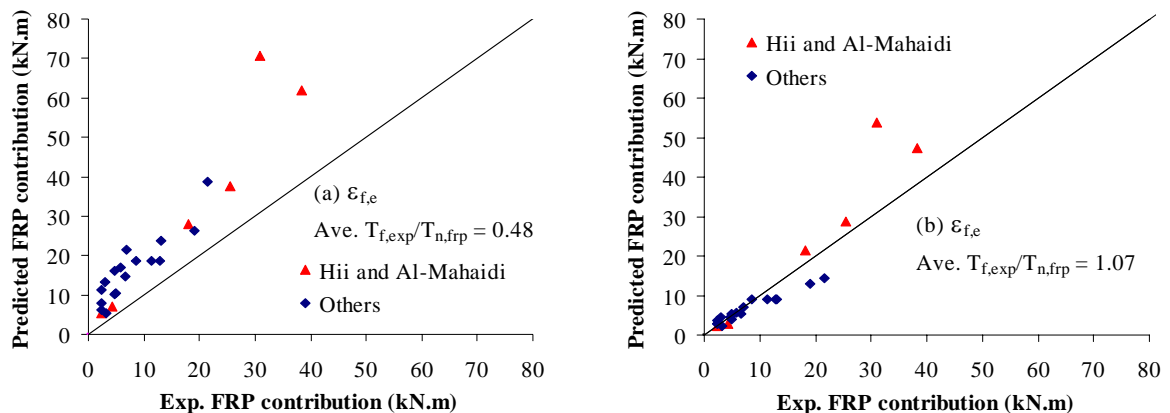


Figure 1: CFRP contribution model verification with $\varepsilon_{f,e}$ for (a) *fib* Bulletin 14; (b) modified to AS3600-2001

3. CFRP CONTRIBUTION TO TORSIONAL STRENGTH

In space truss theory, a solid reinforced concrete member is modeled by an equivalent thin-walled member having the same external dimensions, which consists of concrete compression struts inclined at an angle θ , and transverse and longitudinal reinforcement as tension chords that tie the member together. The shear flow, which is the tangential component of these diagonal compressive stresses, provides the resisting torque. Tests by Hsu and Mo (1985) showed that the shear flow location was independent of the steel bar location, provided the concrete cover was within a certain range to prevent spalling. As expressed in Equation 1 by *fib* Bulletin 14 and previous proposals, the location of the resulting shear flow from the FRP laminates was assumed to be on the concrete surface where the

FRP was externally-bonded. However, the shear flow location is always located at a certain distance below the concrete surface. Hence, Equation 1 is modified to Equation 4 below:

$$T_{n,frp} = 2\varepsilon_{fd,e} E_{fu} A_f s_f^{-1} A_n (\cot \theta + \cot \alpha) \sin \alpha \quad (4)$$

Where A_n = area enclosed by the shear flow path.

For evaluation of the effectiveness in predicting the CFRP contribution only, Equation 4 was modified to be consistent with the Australian Standard AS3600-2001 (SAI 2001). The area enclosed by the shear flow path, A_n , is taken to be equivalent to the area of a polygon with vertices at the centre of the longitudinal bars at the corners of the cross-section. It is immediately obvious in comparing Figure 1(b) with (a) that the improvement in conservativeness was significant; with the average $T_{f,exp}/T_{n,frp}$ values now 1.07 compared to 0.48. The standard deviation was 0.29. In general, the modified method not only gave better predictions of CFRP contribution, but was now consistent with the premise of the space truss model. The full capacity of reinforced concrete beams strengthened with CFRP, T_n , can now be analyzed in the following section.

4. DESIGN PROPOSAL OF CFRP STRENGTHENED RC BEAMS IN TORSION

The full torsional strength of CFRP strengthened reinforced concrete beams, T_n , can be analyzed using the principle of superposition from both the steel, $T_{n,s}$, and CFRP reinforcement, $T_{n,frp}$, as shown in Equation 5:

$$T_n = T_{n,s} + T_{n,frp} \quad (5)$$

It has been shown through photogrammetry measurements by Hii and Al-Mahaidi (2006) that the aggregate interlock between crack faces in concrete were found to increase proportionally with the amount of CFRP bonded. However, the effective strain model by Triantafillou and Antonopoulos (2000) already implicitly accounts for this beneficial effect due to the way it was derived empirically. To maintain consistency with existing codes this was not considered any further. By expanding Equations 4 and 5 to AS3600-2001 form, the final expression is shown in Equation 6. The crack angle θ in AS3600-2001 can either be chosen conservatively as 45° , or to vary linearly from 30° when T_n is equal to the cracking strength, T_{uc} , to 45° when T_n is equal to the maximum torsional capacity before concrete crushing, $T_{u,max}$. For this analysis, Equation 7 (SAI 2001) was used to determine the design crack angle.

$$T_n = \phi 2 A_n (\cot \theta + \cot \alpha) \sin \alpha \left[f_{sy,f} A_{sw} s_t^{-1} + \varepsilon_{fd,e} E_{fu} A_f s_f^{-1} \right] \quad (6)$$

$$\theta = 30^\circ + 15^\circ \left[\frac{T_n - \phi T_{uc}}{\phi T_{u,max} - \phi T_{uc}} \right] \quad (7)$$

Where A_{sw} = area of single stirrup leg; $f_{sy,f}$ = yield strength of stirrups; s_t = center-to-center spacing of stirrups; and ϕ = torsional capacity factor, taken as unity in this investigation.

It must be noted that T_n and θ are coupled in both Equations 6 and 7, which implies an iterative process. However, in design T_n is replaced by applied torque required, so iteration is not required. The average T_{exp}/T_n values for Figure 2(a) were generally conservative at 1.24, where T_{exp} is the experimental torsional capacity of the member. The corresponding standard deviation was 0.34.

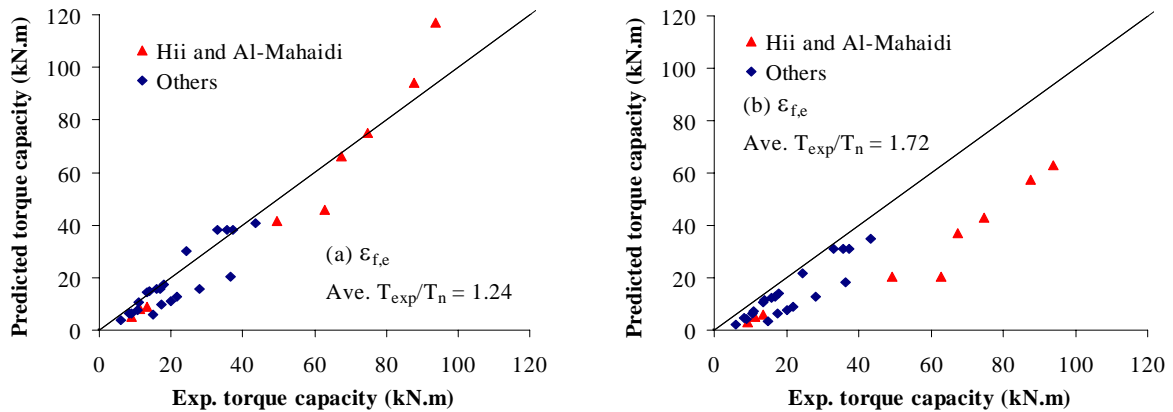


Figure 2: Verification of model for ultimate capacity with $\varepsilon_{f,e}$ modified to (a) AS3600-2001; (b) ACI 318-05

The equation form when adapting the fib Bulletin 14 design method to ACI 318-05 (ACI Committee 318 2005) is similar to Equation 6. However, in ACI 318-05 the area enclosed by the shear flow path, A_n , is taken to be equivalent to 85% of the area enclosed by the centerline of the outermost closed hoops. For design simplicity, the crack angle θ was chosen conservatively as 45° , although more rigorous analysis using the Softened Truss Model algorithm developed by Hsu (1993) is allowed. The average T_{exp}/T_n value for Figure 2(b) was 1.72. The corresponding standard deviation was 0.49. In comparison to AS3600-2001 the predictions by ACI 318-05 were much more conservative. This was mainly due to the fact that a design crack angle of 45° was used in the analysis, which was a conservative assumption. Again, this highlights the importance of the crack angle parameter in design. The empirical definitions of the area enclosed by the shear flow are similar for both design codes. However, differences are more significant for this test series due to the larger specimen sizes, leading to smaller estimates of A_n compared to AS3600-2001. The opposite is true for the smaller scale specimens, due to the concrete cover and size of the steel bars being more significant in comparison to the overall dimensions.

5. CONCLUSIONS

The method for torsional strengthening with FRP in fib Bulletin 14 was compared against a compiled database of available experimental data, and found to be unsafe by 52%. In fib Bulletin 14, the location of the resulting shear flow from the FRP laminates was assumed to be on the concrete surface, which was shown to be inconsistent with the premise of the space truss model. The predictions of FRP contribution were significantly more accurate when the shear flow location was modified to be consistent with AS3600-2001. Through the principle of superposition, the modified equation was then combined with two design codes to analyze the full torsional capacity of CFRP plated reinforced concrete beams. The accuracy of the modified fib Bulletin 14 method was better when adapted to AS3600-2001 compared to ACI 318-05, which was found to be overly conservative. This can largely be attributed to AS3600-2001 taking into account variable crack angles in design. The combination of either design codes with the modified fib Bulletin 14 effective strain model are suitable as a torsion design tool for CFRP plated reinforced concrete members in the future.

6. REFERENCES

- ACI Committee 318. (2005). "ACI 318-05 - Building Code Requirements for Structural Concrete." American Concrete Institute, Michigan, USA.
- Ameli, M., Ronagh, H. R., and Dux, P. F. "Experimental Investigations on FRP strengthening of beams in torsion." *FRP Composites in Civil Engineering - CICE 2004*, Adelaide, Australia, 587-592.
- fib Bulletin 14. (2001). "Externally bonded FRP reinforcement for RC structures." fib - International Federation for Structural Concrete, Lausanne.
- Ghobarah, A., Ghorbel, M. N., and Chidiac, S. E. (2002). "Upgrading Torsional Resistance of Reinforced Concrete Beams Using Fiber-Reinforced Polymer." *Journal of Composites for Construction*, 6(4), 257-263.
- Hii, A. K. Y., and Al-Mahaidi, R. "Torsional Strengthening of Reinforced Concrete Beams Using CFRP Composites." *FRP Composites in Civil Engineering - CICE 2004*, Adelaide, Australia, 551-559.
- Hii, A. K. Y., and Al-Mahaidi, R. "Torsional Strengthening of Solid and Box-section RC Beams Using CFRP Composites." *Composites in Construction 2005 - Third International Conference*, Lyon, France, 59-68.
- Hii, A. K. Y., and Al-Mahaidi, R. (2006). "An Experimental Investigation on Torsional Behaviour of Solid and Box-section RC beams Strengthened with CFRP using Photogrammetry." *Journal of Composites for Construction*, 10(4).
- Hii, A. K. Y., and Al-Mahaidi, R. (To be published). "Torsional Capacity of CFRP Strengthened Reinforced Concrete Beams." *Journal of Composites for Construction*.
- Hsu, T. T. C. (1993). *Unified Theory of Reinforced Concrete*, CRC Press.
- Hsu, T. T. C., and Mo, Y. L. (1985). "Softening of concrete in torsional members - Design recommendations." *ACI Journal*, 82(4), 443-452.
- Panchacharam, S., and Belarbi, A. "Torsional Behaviour of Reinforced Concrete Beams Strengthened with FRP Composites." *FIB Congress*, Osaka Japan.
- SAI. (2001). *AS3600-2001 - Concrete Structures*, Standards Australia International Ltd.
- Salom, P. R., Gergely, J., and Young, D. T. (2004). "Torsional Strengthening of Spandrel Beams with Fiber-Reinforced Polymer Laminates." *Journal of Composites for Construction*, 8(2), 157-162.
- Triantafillou, T. C., and Antonopoulos, C. P. (2000). "Design of Concrete Flexural Members Strengthened in Shear with FRP." *Journal of Composites for Construction*, 4(4), 198-205.
- Zhang, J. W., Lu, Z. T., and Zhu, H. (2001). "Experimental Study on the Behaviour of RC Torsional Members Externally Bonded with CFRP." *FRP Composites in Civil Engineering*, Vol. 1, 713-722.

ANALYSIS AND DESIGN OF FRP REINFORCED CONCRETE COLUMNS

Ching Chiaw Choo

(Research Associate, Kentucky Transportation Center, University of Kentucky, Lexington, Kentucky, USA)

Issam Harik

(Professor, Dept. of Civil Engineering, University of Kentucky, Lexington, Kentucky, USA)

ABSTRACT

Analytical investigations of rectangular concrete compression members reinforced with fiber reinforced polymer (FRP) reinforcing bars were carried out based on the ACI ultimate strength approach. The strength interaction (P - M) relations of reinforced concrete columns with FRP bars were examined and compared to columns with steel bars. The results identified the possibility of premature-compression and brittle-tension failures which were related to the compression and tension ruptures of FRP bars. Brittle-tension failure, when compared with premature-compression failure, was more likely to occur due to low ultimate tensile strain of FRP bars. The study also concluded that the ACI minimum reinforcement ratio limit for steel reinforced concrete columns was not adequate for use in FRP reinforced concrete columns. In this study, design aids have been developed for FRP rectangular concrete columns to determine the minimum required reinforcement ratio ($\rho_{f,min}$) for averting the brittle-tension failure to a failure controlled by concrete crushing; a failure concept used for steel reinforced concrete columns. The proposed approach using $\rho_{f,min}$ enabled the analysis and design of concrete columns reinforced with FRP bars to be carried out in a manner similar to columns reinforced with steel bars based on the ACI 318-05 provisions.

KEYWORDS

Columns, FRP, Analysis, Design, Failure

1. RESEARCH SIGNIFICANCE

In certain applications, FRP bars are favored for their non-corrosive and high-strength properties as evidenced by their use in many concrete constructions. Considerable research efforts have contributed to the understanding of concrete members internally reinforced with FRP composites; of particular interests are the flexural and shear behaviors of FRP concrete members and slabs (Nanni 1993; Almusallam 1997; GangaRao and Vijay 1997; Theriault and Benmokrane 1998; and Deitz, Harik, and Gesund 1999). At present, guidelines for the design and analysis of FRP reinforced concrete members in flexure and shear can be found in ACI440.1R-03 (2003).

With better understanding, particularly the compression attributes, FRP bars can be employed as reinforcement in concrete columns. This analytical study investigates FRP reinforced concrete columns with emphasis placed on the columns' behavior and failure mechanisms. This will ultimately lead to a rational approach – currently not available in guidelines published by ACI (e.g. ACI440.1R-03 2003) – to the design and analysis of concrete columns internally reinforced with FRP bars.

2. STRENGTH OF CONCRETE COLUMNS INTERNALLY REINFORCED WITH FRP BARS

The ultimate strength approach is employed to study the axial load-bending moment strength interaction (P - M) relations of concrete columns internally reinforced with FRP bars. Assumptions pertaining to the analysis of steel reinforced concrete column strength interactions are used. Typical strength interaction ($P_u^* = P_u/bhf_c'$, $M_u^* =$

M_u/bh^2f_c') relations generated for rectangular reinforced concrete columns are presented in Figure 1. The findings and observations related to the behavior of these concrete columns are as follows:

- Based on ACI 318 provisions, the strength interaction relations of steel reinforced concrete columns exhibiting a well-defined *balance* point which signify the transition from a *compression-controlled* region to *tension-controlled* region (Figure 1.a). A balance point is obtained when the outermost concrete fiber reaches an ultimate strain in compression ($\epsilon_c = \epsilon_{cu} = 0.003$) and the outermost steel layer in tension reaches a yield strain ($\epsilon_s = \epsilon_y$), simultaneously.
- Due to a lack of plasticity, the strength interactions of concrete columns internally reinforced with FRP bars do not exhibit a *balance* point; as indicated in Figure 1.b for columns with reinforcement ratios of 5 % and 8 %, respectively. Thus, the failure of these two strength interaction relations is *compression-controlled* defined by concrete crushing.
- *Brittle-tension* failure could potentially occur in FRP reinforced concrete columns when the outermost concrete fiber reaches an ultimate strain in compression ($\epsilon_c = \epsilon_{cu} = 0.003$) and the outermost tension layer of the FRP bars reaches the ultimate strain in tension ($\epsilon_f = \epsilon_{fu}$), simultaneously. This is illustrated by a concrete column reinforced with FRP bars with 1 % reinforcement ratio as shown in Figure 1.b. The 1 % reinforcement ratio is the minimum allowed in ACI318-05 (2005).

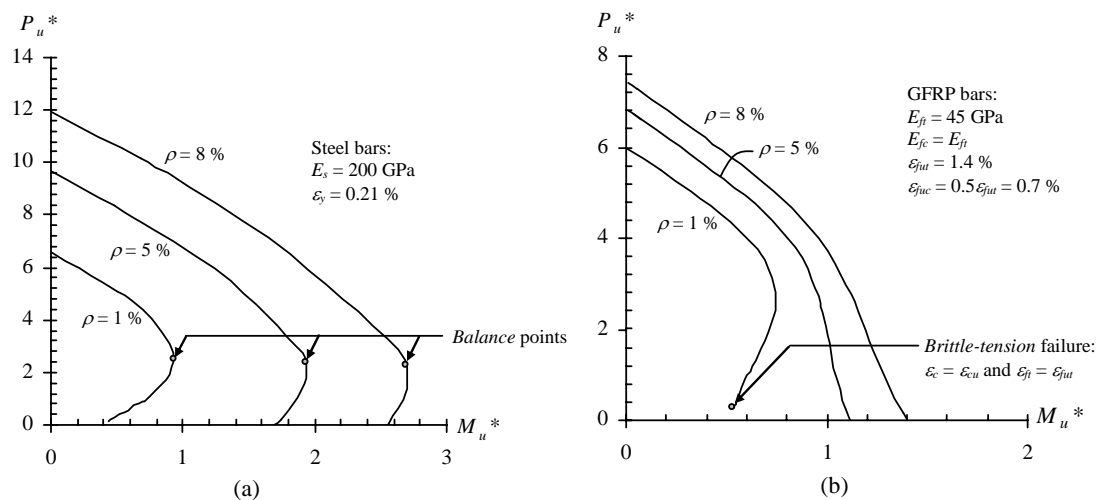


Figure 1: Strength interaction relations of rectangular concrete columns reinforced with: (a) steel bars, and (b) GFRP bars, with a concrete compressive strength (f_c') of 35 MPa.

2.1 Effects of Brittle-Tension or Premature-Compression Failure

Brittle-tension failure could potentially occur due to the low ultimate tensile strain of FRP bars. This can sometimes result in an *incomplete* strength interaction relationship (Figure 1.b). Concrete beam-columns exhibiting brittle-tension failure are incapable of reaching pure flexure (axial load, $P = 0$) prior to the tension FRP reinforcement reaching its ultimate strain and strength. Brittle-tension failure due to tension rupture of FRP bars in concrete columns can be potentially explosive as a large amount of strain energy is suddenly released. Conversely, concrete crushing type failure is more desirable as evidenced by a more progressive and a less catastrophic type failure exhibited by concrete flexural members with FRP bars (Nanni 1993; GangaRao and Vijay 1997; Theriault and Benmokrane 1998).

While not illustrated figuratively, premature compression failure of concrete columns reinforced with FRP bars could happen when compression rupture of FRP bars occurs prior to concrete strain reaching its ultimate (i.e. ACI318 defines maximum usable concrete strain to be 0.003). It is worth pointing out, however, that compression rupture of FRP bars is less likely to occur because the ultimate compression strain of FRP bars is generally greater than the ultimate concrete strain in compression.

3. PREVENTION OF BRITTLE-TENSION FAILURE

From the foregoing, concrete columns internally reinforced with FRP bars if designed to be compression-controlled would have the following advantages: (1) The analysis and design of such columns can be performed based on the ACI code approach; and (2) from a failure standpoint, maintaining compression-controlled failure would be less explosive and more gradual as previously stated.

It appears, from Figure 1, concrete columns reinforced with FRP bars can be safeguarded from brittle tension failure by providing a reinforcement ratio (ρ_f) larger than a minimum ratio designated as $\rho_{f,min}$; the reinforcement ratio required to yield compression-controlled ($\epsilon_c = \epsilon_{cu}$) failure. Naturally, $\rho_{f,min}$ of a concrete column reinforced with specific FRP bars varies with a variety of factors such as properties of the FRP bars, concrete strength, and reinforcement layout. To expedite the determination of $\rho_{f,min}$, design aids (Figure 2) were generated for rectangular concrete columns reinforced with FRP bars independent of the FRP ultimate tensile strain (ϵ_{fu}). Additional aids can be found in Choo (2005). The ordinates in Fig. 2 represent the tensile elastic moduli (E_{ft}) of FRP bars ranging from 35 GPa to 210 GPa, covering most available FRP bars. The abscissas represent the tensile strains (ϵ_{ft}) that will develop at the outermost tensile reinforcing bar layer under pure flexure. As depicted, ϵ_{ft} varies and can be computed for any combination of E_{ft} and ρ shown in the aids. To account for compression elastic moduli (E_{fc}) of FRP bars, different E_{ft}/E_{fc} ratios were also incorporated into these E_{ft} - ϵ_{ft} aids.

To illustrate the use of these aids, the reinforced concrete column internally reinforced with GFRP bar in Fig. 1.b is revisited. Based on the concrete and GFRP properties, the required $\rho_{f,min}$ is approximately 1.3% as shown in Fig. 2.a to avoid brittle-tension failure.

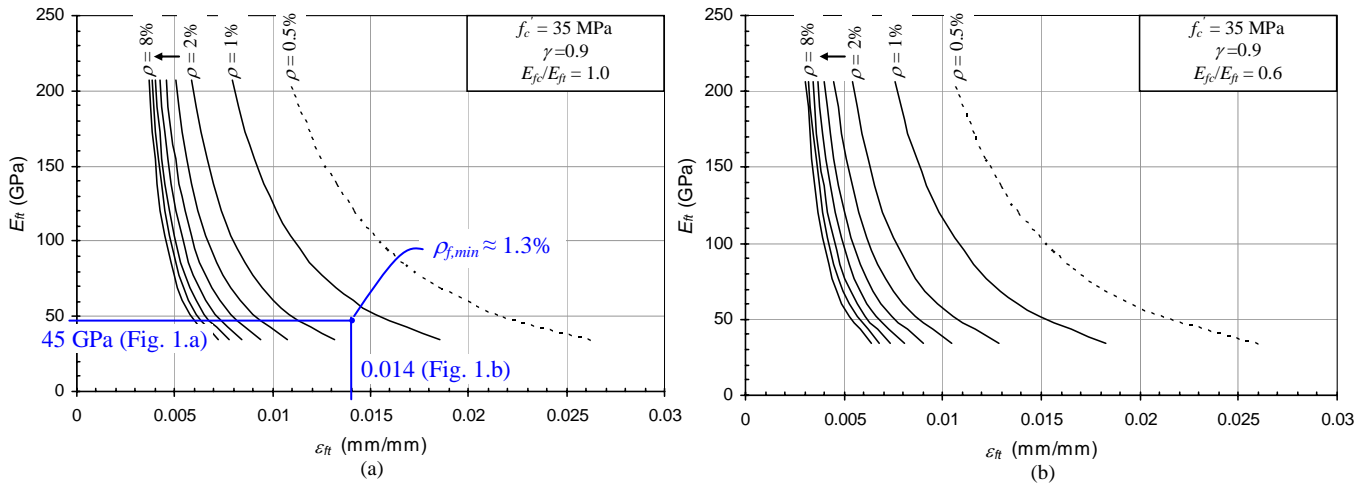


Figure 2: Tensile elastic modulus-tensile strain (E_{ft} - ϵ_{ft}) design aids for rectangular concrete columns reinforced with FRP bars.

3.1 Modification Factors for Concrete and Reinforcement Layout

Note that the aids in Fig. 2 depend on two parameters: concrete strength (f'_c) and the ratio of the distance between the outer layers of rebars to the height of the column cross section in the direction of bending (γ). To account for the increase or decrease of ϵ_{ft} due to concrete strength, a modification factor, α_c , was derived (Choo 2005):

$$\alpha_c = \left(\frac{21 - 0.2f'_c}{14} \right) \geq 1.0 \quad \text{When } 21 \text{ MPa} \leq f'_c < 35 \text{ MPa} \quad (1)$$

$$\alpha_c = \left(\frac{25.25 - 0.15f'_c}{20} \right) \leq 1.0 \quad \text{When } 35 \text{ MPa} \leq f'_c \leq 55 \text{ MPa} \quad (2)$$

To account for γ , a modification factor, α_γ , was derived (Choo 2005):

$$\alpha_\gamma = 1.5 - 0.556\gamma \geq 1.0 \quad \text{when } 0.45 \leq \gamma \leq 0.9 \quad (3)$$

3.2 Modified Ultimate Tensile Strain

To use the aids for other values of the two parameters, the ultimate tensile strain (ϵ_{fut}) of FRP rebar shall be modified as follows:

$$\epsilon_{fut}^* = \epsilon_{fut} \cdot \alpha_c \cdot \alpha_\gamma \quad (4)$$

This modified value, combined with the tensile modulus of elasticity, can then be used to determine a required $\rho_{f,min}$. The introduction of a modified ultimate tensile strain, in fact, permits a quick and efficient way of incorporating other factors in determining $\rho_{f,min}$.

4. CONCLUSION AND DESIGN RECOMMENDATIONS

Strength interaction studies of concrete columns reinforced internally with FRP bars identified the possibility of these failures: (1) premature-compression, and/or (2) brittle-tension failures. These failures are associated with failure of FRP bars prior to concrete crushing, and hence can be potentially disastrous.

Design aids that take material properties and reinforcement layout into consideration were developed for FRP rectangular reinforced concrete columns where a minimum required reinforcement ratio ($\rho_{f,min}$) can be determined and used to prevent brittle tension failure. It can be seen that the introduction of a modified ultimate tensile strain allows a quick and efficient way to incorporate other factors that may influence $\rho_{f,min}$.

Based on the study, it is also observed that the minimum reinforcement ratio limit (1%) set by ACI318 for steel reinforced concrete columns may not be adequate for FRP reinforced concrete columns. The maximum reinforcement ratio limit (8%), however, is still applicable due to the fact that the limit is set to promote constructability and to avoid rebar congestion.

5. REFERENCES

- ACI Committee 318, 2005, "Building Code Requirements for Structural Concrete (318-05) and Commentary (318R-05)," American Concrete Institute, Farmington Hills, MI.
- ACI Committee 440, 2003, "Guide for the Design and Construction of Concrete Reinforced with FRP Bars (ACI 440.1R-03)," American Concrete Institute, Farmington Hills, MI, 42 pp.
- Almusallam, T.H., 1997, "Analytical Prediction of Flexural Behavior of Concrete Beams Reinforced by FRP Bars," *Journal of Composite Materials*, Vol. 31, No. 7, pp. 640-657.
- Choo, C.C., "Investigation of Rectangular Concrete Columns Reinforced or Prestressed Fiber Reinforced Polymer (FRP) Bars or Tendons," PhD Dissertation, University of Kentucky, Lexington, KY, 2005.
- Deitz, D.H., Harik, I.E., and Gesund, H., 1999, "One-Way Slabs Reinforced with Glass Fiber-Reinforced Polymer Reinforcing Bars," *American Concrete Institute*, SP-188-25, 279-286.
- GangaRao, H.V.S., and Vijay, P.V., 1997, "Design of Concrete Members Reinforced with GFRP Bars," *Proceedings of the Third International Symposium on Non-Metallic (FRP) Reinforcement for Concrete Structures (FRPRCS-3)*, Japan Concrete Institute, Sapporo, Japan, Vol. 1, pp. 143-150.
- Nanni, A., 1993, "Flexural Behavior and Design of Reinforced Concrete Using FRP Rods," *Journal of Structural Engineering*, V. 119, No. 11, pp. 3344-3359.
- Theriault, M., and Benmokrane, B., 1998, "Effects of FRP Reinforcement Ratio and Concrete Strength on Flexural Behavior of Concrete Beams," *Journal of Composites for Construction*, Vol. 2, No. 1, pp. 7-16.

PROBABILISTIC DESIGN OF FRP STRENGTHENING OF CONCRETE STRUCTURES

Anders Carolin

(Dr., Luleå University of Technology, Luleå, Sweden)

ABSTRACT

Today, many design proposals exist that address different strengthening issues. Most proposals are derived on assumptions made for designing of new structures and are also based on a deterministic approach where a safety factor is added. The use of probabilistic methods is now extending and the reliability is sometimes calculated afterwards for the strengthened structure. This paper presents how the reliability should be chosen on beforehand when doing design for strengthening of an existing structure, which issues to be considered and also what safety that one can expect from a strengthened structure. Partial coefficients on material properties and loads are used to give a uniform treatment of risk of failure when strengthening of structures. When partial coefficients are chosen the reason for strengthening and the strengthening method may be considered to achieve an optimal strengthening with respect to structural safety and economy. The theoretical basis, the same as for Eurocode, has been used successfully in Swedish design codes for a long time. The results from the analysis indicate that strengthened with CFRP plate bonding has a very desirable effect on structural safety and reduces the risk of failure by considerable proportions.

KEYWORDS

Probabilistic, Design, Retrofitting, Concrete, FRP.

1. INTRODUCTION

The world is complicated. A concrete structure subjected to loading could be seen as a complicated system. By strengthening such a structure, things certainly become complicated. For a long period of time, engineers have tried to make models of the world and the structures in it. This means that simplifications are used to make it possible to describe and estimate how things behave. Models are also quite often used to make predictions. When structures and loads started to be modeled, the idea was to make the bearing capacity the same or higher than the highest known load. Since models are simplifications, a safety factor was then used to make the structure a certain degree stronger to cover for deterioration, model errors, and construction errors. This approach is called deterministic and do not consider distributions in loads, material parameters, and so on. The deterministic approach also gives altering levels of safety for different structures. In a probabilistic approach, uncertainties of loads and bearing capacities of structures are considered in the model. Both bearing capacity of the structure and the load effect have statistical distributions. Failure will occur when the load effect has one of the highest values and load bearing capacity has one of the lowest values, at the same time. Failure is expressed by the probability of load effect becoming larger than load bearing capacity. As an example, failure will not even occur if the load bearing capacity is one of the 1 % lowest cases, if the load effect is just normal. Many codes, e.g. Swedish BBK94 (1994) and Eurocode EN (2002), are based upon reliability and partial coefficients. In normal design by Swedish BBK94 (1994), the lower 5 %-fractal is used as characteristic values, f_k , of the materials. These values are then reduced by partial coefficients, $\eta\gamma_n$, and, γ_m , as presented in Equation 1 and the bearing capacity can then be estimated from the calculated parameters, f_d .

$$f_d = \frac{f_k}{\eta\gamma_n\gamma_m} \quad (\text{Eq. 1})$$

The load effect is taken as a statistical upper limit. Failure occurs when the load effect, S , are higher than the bearing capacity, R , and the probability of failure can be described as the probability of $G < 0$, where G is described by Equation 2.

$$G = R - S \quad (\text{Eq. 2})$$

By law, the yearly probability of failure in Sweden must be 10^{-4} - 10^{-6} or higher, depending on safety class (1, 2 or 3) prescribed by code. These values are directly connected to β -indices in range of 3.72 – 4.75. A structure causing severe consequences if it fails must be design with the lower probability of failure. A structure causing relatively harmless consequences if it fails may be design with a higher probability of failure. The coefficient, γ_m , is considering safety class and varies between 1.0 and 1.2. The partial coefficients $\eta\gamma_n$ together with coefficients on loads have been calibrated so that the demand on yearly probability of failure is met. Model uncertainties, distribution of material properties, and difficulty of construction is considered when $\eta\gamma_n$ is determined. In this paper a favourable aspect for external strengthening regarding structural safety will be addressed.

2. BEARING CAPACITY OF STRENGTHENED STRUCTURE

The load effect depends on many stochastic variables, wind, dynamic load effects, snow, etc. In the case of strengthening, in some cases it can be possible to determine the future load effect more precisely compared to the design of a new structure. It can actually be possible to measure the load effect on a structural member when a load is applied on the structure. Dead-load can be estimated better when the true dimensions can be measured. Loads from support settlements can in some cases be reduced when an old structure is going to be strengthened. This can make the scatter of the load effect narrower. Strengthening with plate bonding with CFRP does not significantly change a structure's dead-load. The load effect on a member in a statically undetermined system can still be altered because of changed stiffness of the studied member. The load effect will, however, not be further discussed here. For a reinforced concrete structure, several stochastic variables affect the load bearing capacity. Concrete properties, steel reinforcement properties, length of internal lever arm, mode of failure and anchorage of reinforcement are all important variables for a structure subjected to flexure. To ensure a ductile failure it is often desired to have an under-reinforced cross-section, which means that the bearing capacity is controlled by amount of strengthening. The flexural bearing capacity for an under-reinforced cross-section can, in its most simplified form, be described as inner lever arm multiplied by the force in the reinforcement as described in Equation 3:

$$R = (d - c)A_s f_{st} \quad (\text{Eq. 3})$$

where d is effective height; c is centre of gravity for the compressive force measure from top of beam; A_s is reinforcement area; and f_{st} is capacity of reinforcement in tension. If a structure is strengthened with externally bonded CFRP, new variables such as composite properties and new failure modes may be added. On the other hand, when a structure is going to be strengthened it is possible to undertake field measurements that can give a more determined description of the existing materials, dimensions and possible defects of the structure. When strengthening is applied the length of the internal lever arm for the composite might be taken as deterministic. The load bearing capacity for a strengthened structure will be dependent on more factors compared to the load capacity of the original structure. The mode of failure may change depending on how much the structure is strengthened. However, to a certain amount the failure mode can be quite reliably described. A normal reinforced concrete member that “fails” by yielding of reinforcement will for a small amount of strengthening fail by fibre rupture, on the assumption that anchorage is sufficient. In analogue of reinforced concrete the bearing capacity of a strengthened reinforce cross-section can be described as Equation 4, where h is the height of the cross-section; A_f is area of strengthening system; ε_f is ultimate strain of fibres; and E_f is modulus of elasticity for strengthening system.

$$R = (d - c)A_s f_{st} + (h - c)A_f \varepsilon_f E_f \quad (\text{Eq. 4})$$

Distribution of variables for reinforced concrete has for example been studied by Jeppsson (2000) and a limited study of strengthening systems has been undertaken by Plevris et al. (1995). Partial coefficients for strengthening have been proposed by Monti and Santini (2002) and Täljsten (2003). For an under-reinforced beam the bearing capacity is mainly limited by the amount of reinforcement. In case of a strengthened beam, reinforcement consists of

both internal steel bars and CFRP. The ultimate capacities of the two materials as well as the two different internal lever arms are independently stochastic. For failure, it is necessary that all variables are at a critical value at the same time. A weak steel bar can be compensated by the composite having its mean value and the structure will have a bearing capacity larger than the load effect. In the same way, a steel bar with medium performance can compensate for a composite that has a performance lower than its 5 % -fractal. The risk for both materials, and therefore the load bearing capacity to be lower than the minimum acceptable level for the strengthened structure, will decrease compared to the non-strengthened structure.

It would be possible to choose partial coefficients so that the probability for failure will be the same for the original structure subjected to original loading and the strengthened structure with the new loading. Since different amounts of strengthening will give different importance to the different stochastic variables, it would imply that the partial coefficient will vary with the strengthening amount. This is not a reasonable situation and it is suggested that the partial coefficient are determined as if the variables for the existing structure are deterministic. This approach will give an additional reliability of the structure that should be seen as an extra security provided by the strengthening system.

3. CALCULATION EXAMPLE

With data on concrete and steel reinforcement from literature, (JCSS PMC, 2001), an ordinary under-reinforced structure was designed deterministically by Equation 3 and partial coefficients from Swedish code. When considering distribution of parameters and a deterministic load, the structure got a probability of failure of $2.05 * 10^{-5}$ calculated by the second-order reliability method (Melchers 1999). Material data for strengthening system was tested (Carolin et al. 2004) and strengthening for an increased load was designed deterministically by Equation 4 with an assumptions on partial coefficients for the strengthening system. The tested CFRP where pultruded laminates with an average modulus of elasticity of 150 GPa. Considerations were given to ensure an under-reinforced cross-section even after strengthening. By setting original structure as deterministic, the increased load as deterministic, and the real distribution of composite parameters, partial coefficients for strengthening system were calibrated. Calibration gave a partial coefficient for fibre rupture of 1.15 and a probability of failure for the strengthened structure of $1.35 * 10^{-5}$. Then, by having all parameters for bearing capacity as stochastic the probability of failure were calculated to $1.23 * 10^{-11}$.

4. ANALYSIS

Two stochastic undetermined load carrying systems give a higher security against failure compared to a single system. The increase in security is dependent on the ratio of influence of each system and the distribution of included parameters. Seeing that the importance of a strengthening system varies, partial coefficients should be determined based on that other reinforcement is seen as deterministic. In cases of an internal steel reinforcement the structural safety of the strengthened structure will increase. It is quite common with material investigations in conjunction of upgrading a structure. For concrete structures in need of strengthening it is quite common to investigate the real compressive capacity of the concrete which then quite often allows increase of reinforcement ratio without changing the failure mode. Even though not as common, real capacity of reinforcement is sometimes investigated. In cases when real material properties are used, it is important that the partial coefficients of the strengthening system will provide the desired and prescribed structural safety together with the partial coefficients on loads. Several design codes for reinforced concrete are based on stress. Design codes on CFRP strengthening are on the other hand often based on strains that are multiplied with a modulus of elasticity. During calibration of partial coefficients, special attention must be given so that the two different approaches harmonize and that distribution of strain and modulus of elasticity are treated correct.

5. DISCUSSION AND CONCLUSIONS

The found partial coefficient is reasonable for a product manufactured in an industrial process like the pultruded laminate studied. For other CFRP products, i.e. hand lay-up composites, it is probably more suitable with higher factors. Täljsten (2003) gives a suggestion on how partial coefficient may be compiled. Nevertheless, partial factors must be calibrated to meet prescribed and desired levels of structural safety. Structures should be designed to fail in

a ductile way or at least with adequate warning signals preceding a potential collapse. One argue against CFRP is that most fibre composites are linear-elastic material without any defined yield plateau. It is important to distinguish between material ductility and structural ductility. A structure with a brittle failure in shear may in fact be strengthened so that the failure mode will change to a more ductile and friendly mode, even when strengthened with a linear elastic material (Carolin, 2003). Failures that might be seen as brittle are: shear failures and anchorage failures. Fibre rupture is also brittle but normally proceeded by large deformations. Since different failure modes are more preferable than others, one solution is to make those more probable than others by design, i.e. make undesired failures less probable as suggested by Pilakoutas et.al. (2002). Different probabilities for failure modes with different brittleness are motivated by that the risk should be constant. By studying risk as the combination of probability and consequence, brittle failures with no warnings may give larger consequences and should therefore have a lower probability of occurring. Different partial factors could be used for different failure modes. A special partial factor for design of anchored could be used. When designing for shear, a special partial factor on shear loads can be applied. It is also possible with different factors on the material depending on studied failure mode.

With deterioration in mind the strategy for strengthening becomes more complicated. Probability of failure is a suitable unit when measuring the performance level of a structure. Since all structures are deteriorating the structural safety will decrease. This implies that structures must be built with certain margins on structural safety and with a lower probability of failure for a new built structure. Uncertainties in construction are normally considered in original design, which then gives the margin for decrease of structural safety caused by deterioration. The structural safety of a new built structure should actually be investigated before deterioration starts.

Finally, loss of strengthening effect must also be considered in design. Structures that may be subjected to vandalism or collision should have the capacity of bearing at least the dead load even if the effect of the strengthening system is lost. Plate bonding is normally relatively sensitive of fire loads and strengthened structures must be able to carry prescribed loads during fire for a certain time. For all cases, structures should be able to carry loads with a prescribed probability with respect to likeliness of certain load combinations at all time.

6. REFERENCES

- BBK 94 (1995). "Boverkets handbok om betongkonstruktioner, BBK 94, Band 1, Konstruktion". Boverket, Stockholm, 185 pp. ISBN 91-7147-235-5 (in Swedish).
- Carolin, A., Täljsten, B., Nilsson, M., Enochsson, O. and Fahleson, C. (2004). "Tillförlitlighetsanalys för reparerade eller förstärkta byggnadskonstruktioner" Luleå University of Technology (in Swedish).
- EN (2002). "Eurocode - Basis of structural design. EN 1990:2002 (E)". CEN, European Committee for Standardization, Brussels, 87 pp.
- Carolin, A. (2003). "Carbon Fibre Reinforced Polymers for Strengthening of Structural Elements", Doctoral Thesis, Luleå University of Technology, 184 pp. <http://epubl.luth.se/1402-1544/2003/18>
- JCSS PMC (2001). Probabilistic Model Code. *Joint Committee on Structural Safety, JCSS*, <http://www.jcss.ethz.ch/JCSSPublications/PMC/PMC.html> (2006-04-15).
- Jeppsson, Joakim (2003): "Reliability-Based Assessment Procedure for Existing Concrete Structures", Doctoral Thesis, Lund University of Technology, 188 pp.
- Melchers, R. (1999): "Structural Reliability Analysis and Prediction", 2nd Ed, John Wiley & Sons, Chichester, UK, 1999, 437 pp. ISBN 0 471 98771 9.
- Monti, G. and Santini, S. (2002): "Reliability-based Calibration of Partial Coefficients for Fiber-Reinforced Plastic" *Journal of Composites for Construction*. August. pp 162-167
- Pilakoutas, K., Neocleous, K. and Guadagnini, M. (2002): "Design Philosophy Issue of Fiber Reinforced Polymer Reinforced Concrete Structures" *Journal of composites for construction*. August, pp. 154-161.
- Plevris, N., Triantafillou, T. and Veneziano, D. (1995): "Reliability of RC Members Strengthened with CFRP Laminates" *Journal of Structural engineering*. July, pp. 1037-1044.
- Täljsten, Björn (2003): "FRP Strengthening of Existing Concrete Structures - Design Guidelines - Second Edition", Luleå University of Technology, ISBN 91-89580-03-6, 230 pp

THRESHOLDS OF CONSTRUCTION ANOMALIES IN FRP REPAIR SYSTEMS

Baris Yalim

(Ph.D. Candidate, Florida International University, Miami, FL, USA)

Ahmet Serhat Kalayci

(Ph.D. Student, Florida International University, Miami, FL, USA)

Amir Mirmiran

(Professor and Chair, Florida International University, Miami, FL, USA)

ABSTRACT

Fiber reinforced polymer (FRP) composites have been used extensively in repair applications over the last two decades. In addition to their high-strength and lightweight properties, important characteristics of FRP systems for structural repair and strengthening applications include their resistance to electro-chemical corrosion, and speed and ease of installation. Therefore, FRP systems can be efficient and economical options to traditional repair methods. However, relationship between the long-term performance of FRP repair systems and their construction processes are not easy to quantify. Moreover, tolerances for most construction anomalies such as surface irregularities and crack widths are not yet based on adequate scientific data. For instance, depending on their state (i.e. shear or flexural) and size, cracks in the concrete may either be left untreated or epoxy injected. The thresholds separating these approaches may depend on technical and economical considerations. This paper presents the current study to evaluate the effect of surface flaws on the performance of wet lay-up FRP systems. Four types of flaws are considered; surface roughness, surface flatness, voids and bug holes, and cracks/discontinuities. Discussions of test results and recommendations are also provided.

KEYWORDS

Surface flaws, FRP repair systems, Reinforced concrete, Construction Guides

1. INTRODUCTION

Many concrete structures that were originally constructed for a specific use may later be renovated or upgraded for a different application due to higher load-carrying capacity requirements or maintenance purposes. As a result, existing structures may need to be retrofitted to meet higher load demands. With over two decades of field applications and research findings, it is generally recognized that the use of FRP systems is efficient and technically reliable for repair and retrofit of concrete structures. Since its first application in Europe and Japan in the early 1980's, use of bonded repair and retrofit of concrete structures with FRP systems has progressively increased to the extent that today it counts for at least 25 federally supported Innovative Bridge Research and Construction (IBRC) projects in the United States (NCHRP 514, 2004). However, there is currently a lack of generally accepted construction specifications and process control procedures for FRP repair systems, making users heavily dependent on specific guidelines from FRP manufacturers. As the FRP technology matures and moves into widespread use, the need has become more urgent than ever to equip users with the means to specify and control the constituent materials and the adequacy of the construction process. The acceptance and use of the FRP repair systems will ultimately depend on the availability of clear design guidelines, installation procedures, and construction specifications (Scalzi et al. 1999). Practical guidelines for such repair techniques are not yet readily available for practicing structural engineers (Shahawy et al. 1996). Thus, the objective of this research is to develop tolerances for surface irregularities and crack widths for bonded repair of concrete structures using FRP composites.

2. TEST SETUP AND PROCEDURE

The test program involves short-term static loading of 45 reinforced concrete beams bonded with FRP sheets. All beams were T-sections with a flexural span of 6.5 ft and target compressive strength of 5 ksi (see Figure 1). A 4-in-wide and 67.5-in-long carbon fiber sheet (SikaWrap Hex 103C) was attached as centered to the bottom of the beam using Sikadur 300 epoxy resin. Additional two 4-in wide fiber sheets were wrapped as U-straps in each shear span to provide anchorage for the FRP system. All beams were tested under three point bending. A self-reaction test frame shown in Figure 1 was designed to accommodate 7-foot-long specimen with 60-kip capacity. The beam was supported on two hinges, with mid-span load applied using an Enerpac hydraulic jack. Each beam was instrumented with three 1.5-in-stroke potentiometers to measure deflections at $\frac{1}{4}$ span points and a strain gauge on the FRP sheet at mid-span of the beam. A 50-kip-capacity Futek load cell measured the applied load.

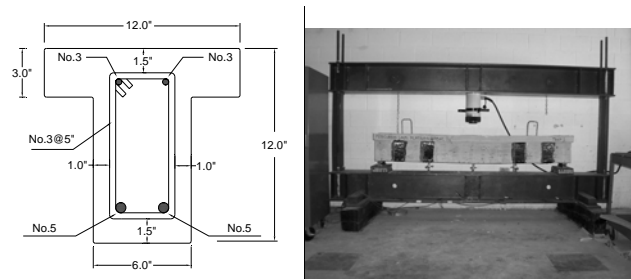


Figure 1: Test Specimen and Test Frame

A total of 9 specimens were tested for the effect of surface roughness. Three concrete surface profiles (CSP) were selected for each three beams, corresponded to CSP 1, CSP 2-3 and CSP 6-9 according to the International Concrete Repair Institute recommendations (ICRI/ACI, 1999). Roughness level of the concrete surface increases from 1 to 9. The intentional roughness levels and surface profiles were developed using grinding and pressure washing after the beam was cured. For surface flatness, a total of 12 specimens were prepared with two different levels of out-of-flatness (1/8 in and 1/16 in over 1 ft length at the mid-span), as peaks and valley, and two duplicates for each case. The intentional out-of-flatness was developed using grinder after concrete was cured. Another 12 specimens were prepared for voids and bug holes with three different void depths (1/4 in, 3/16 in and 1/8 in) and three different void diameters (1/2 in, 3/8 in and 1/4 in). Frequency of voids on the concrete surface was selected as 10% in terms of surface area. Surface voids were created by drilling concrete after it was cured. Finally, 12 specimens were made with three different crack widths (1/8 in, 3/32 in and 1/16 in) and three different crack spacing (1 in, 1.5 in and 2 in).

3. TEST RESULTS & DISCUSSIONS

Figure 2 shows comparisons of load-deflection and load-strain curves, respectively, for all nine beams tested for surface roughness. Mid-span deflections and strains correspond to the peak load. It is clear that the responses are quite similar, regardless of the surface profiles of the beams. All beams typically failed due to FRP debonding at an ultimate load of 30-35 kip with similar mid-span strain and deflection. There is a slight difference between the different surface profiles, as higher roughness translates into a slightly higher capacity. However, the difference is not statistically significant. This may be attributed to the fact that the rougher surface allows for direct bond of FRP sheet to the aggregates. The U-straps proved helpful in anchoring the FRP sheets. The FRP sheets began to peel off as soon as the U-straps ruptured.

In order to evaluate the effect of voids and cracks on FRP repair performance, a statistical method called “Design of Experiment” was utilized. Fundamental purpose of this approach is to determine the relationship between factors affecting a process (surface flaws) and the output of that process (load, displacement and strain).

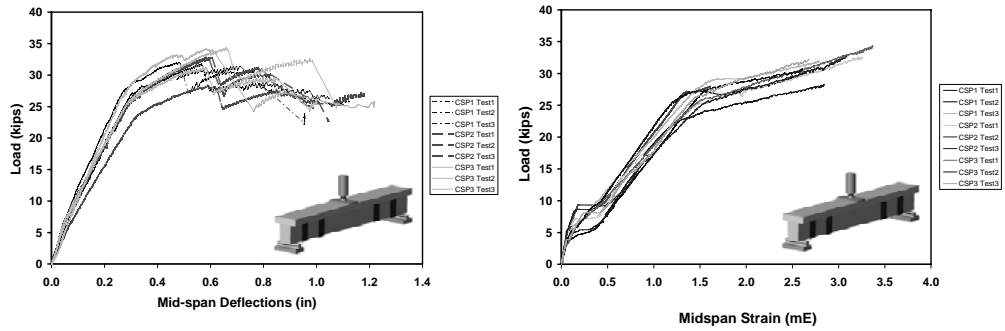


Figure 2: Load-Displacement and Load-Strain Curves for Surface Roughness Specimens

The DOE analysis provides 3D response surface interpolated over test data range. Figure 3 illustrates the variation of each response measure (load, deflection or strain) with a given void depth and diameter. It is also useful to locate the flawless specimen on the surface for comparison. Flawless specimen is shown as a separate layer cutting the surface on various points. In addition to the flawless specimen, several layers were added for each response at different percent reduction of that response measure. This leads to the enhanced determination of the possible specification thresholds for both factors based on each response. Each layer in these graphs cut the response surface at different level such that corresponding void depth and void diameter may be obtained according to the desired percentage of reduction or increase in the response measure. Figure 3b implies that the deflection is more correlated with void diameter than void depth.

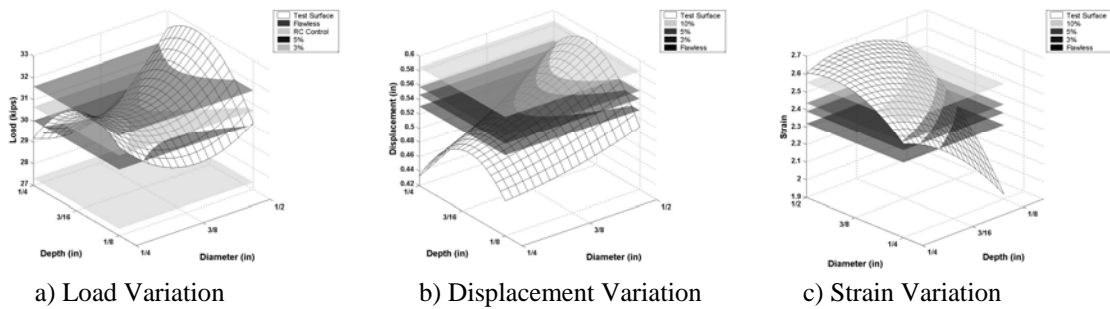


Figure 3: Load-Displacement-Strain Variation with Void Depth and Void Diameter

The DOE approach was again utilized for the evaluation of cracks. Figure 4a shows the load capacity in relation to crack width and spacing. There exists an increasing trend up to 1.5 in spacing. Same conclusion can be drawn in the case of strain, which confirms rise after 1.5 in crack spacing. Similarly, there is substantial drop in the displacement as the spacing becomes larger, particularly when it exceeds 1.5 in. With the available test data, it may be concluded that 1.5 in spacing is the potential limit for existing cracks as far as load capacity, displacement and strain are considered. As the spacing increases the maximum load also increases, as expected. Maximum increase in the ultimate load compared to control specimen (unstrengthened) is about 19% and it occurs for the beams with 3/32 in crack width and 1.5 in crack spacing. Graphs in Figure 4 also imply that crack width does not show a clear correlation with any of the response measures. This may be because of the negligible difference in crack widths. It should be noted that only one test is performed for each crack width and crack spacing. Therefore, it may also be likely that a single test result may affect possible trends or expected correlations.

Load-displacement and load-strain curves for all beams tested for surface flatness are shown in Figure 5. Debonding of longitudinal FRP at the mid-span for the 1/8 in valleys occurs much earlier than that of the control specimens and the 1/16 in valleys. This behavior leads to a plateau at a load level which is about 19% less than the average capacity of control specimens. Average peak load for the 1/16 in valleys is about 4.5% less than that for the control specimens, which is quite reasonable. Failure mode was FRP debonding for all defective specimens as well as control specimens regardless of their out-of-flatness levels.

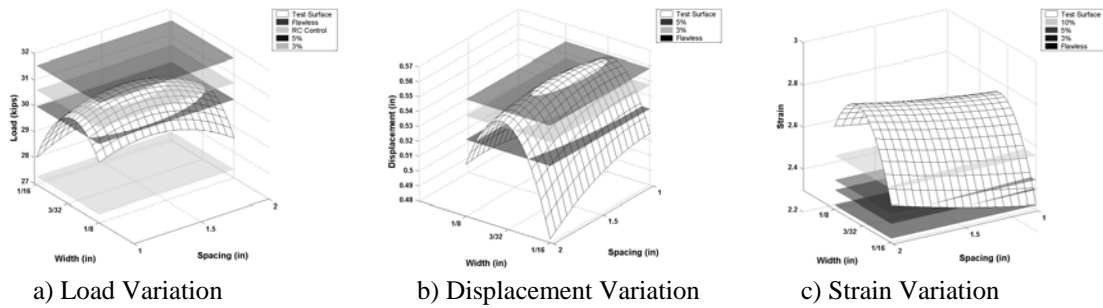


Figure 4: Load-Displacement-Strain Variation with Crack Width and Spacing

Load-strain curves have similar trend until failure. Significant increase in the strain is observed immediately after cracking for the 1/16 in valleys, whereas there is a smooth transition in the strain for the 1/8 in valleys. Average strain values at cracking for the 1/8 in valleys are below those of the control specimens and conversely, average strain values at cracking for the 1/16 in valleys are slightly higher than those of the control specimens. Unlike the valleys, beams with peaks do not have load plateau and their overall behavior is quite similar to that of the control beams which underlines the criticality of valleys in comparison to the peaks. In conclusion, 1/8 in valleys as an out-of-flatness on the concrete surface has significant effect on the composite performance. On the other hand, behavior of the 1/16 in valleys is very similar to that of control specimens. Thus, the 1/16 in should be the controlling threshold for valleys and depressions, and accordingly any valleys or depressions on the concrete surface deeper than 1/16 in measured from 12 in straight edge placed on the surface should be smoothed by grinding or filled using epoxy resin mortar. Peaks on the concrete surface have been found as less critical as compared the valleys of the same size and no threshold is recommended for the peaks at this stage of the research.

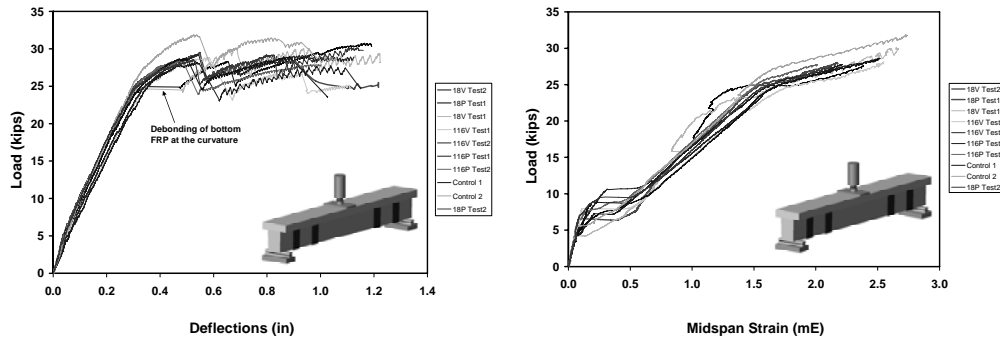


Figure 5: Load-Displacement and Load-Strain Curves for Surface Flatness

4. REFERENCES

- NCHRP 514. (2004) "Bonded Repair and Retrofit of Concrete Structures Using FRP Composites - Recommended Construction Specifications and Process Control Manual." *Report 514*, Mirmiran, A., Shahawy, M., Nanni, A., and Karbhari, V., National Cooperative Highway Research Program (NCHRP), Washington, D.C.
- Scalzi, J.B., Podolny, W., Munley, E., and Tang, B. (1999). "Guest Editorial," *Journal of Composites for Construction*, American Society of Civil Engineers, Vol. 3, No. 3, p. 107.
- Shahawy, M. A., Beitelman, T., Arockiasamy, M., and Sowrirajan, R., (1996) "Experimental Investigation on Structural Repair and Strengthening of Damaged Prestressed Concrete Slabs Utilizing Externally Bonded Carbon Laminates," *Composites, Part B 27B*, pp. 217-224

STATIC AND DYNAMIC PERFORMANCE OF FRP DECK BRIDGES UNDER VEHICLE LOADING AND IMPLICATIONS IN DESIGN

Yin Zhang

Associate Professor, Nanyang Institute of Technology, Nanyang, China; Visiting Scholar, Department of Civil & Environmental Engineering, Louisiana State University, Baton Rouge, Louisiana 70803, U.S.A

C.S. Cai

Associate Professor, Department of Civil & Environmental Engineering, Louisiana State University, Baton Rouge, Louisiana 70803, U.S.A

ABSTRACT

The characteristics of bridges with FRP decks (such as mass, stiffness, and damping) are significantly different from that of the traditional concrete and steel bridges, which may result in a much different performance of FRP bridges from these traditional bridges. For this reason, detailed finite element analyses are used in the present study to investigate the load distribution and the dynamic response of FRP deck bridges. The study is focused on a steel multi-girder bridge and a concrete multi-girder bridge that are modeled using the finite element method to predict the modal characteristics. The present study analyzes the bridge-vehicle interaction based on a three dimensional vehicle-bridge coupled model. The dynamic response of bridges is obtained in the time domain by using an iterative procedure employed at each time step, considering the road roughness of the deck as a vertical excitation to the vehicles. The load distribution and the dynamic response of bridges are compared between the FRP deck and concrete deck bridges. In addition, there are some arguments whether a composite action between the deck and girders should be pursued or if a simple non-composite design should be used. Discussions on this aspect have been made by modeling both the composite and non-composite systems.

KEYWORDS

Fiber Reinforced Polymers; Bridge Deck; Vehicle Bridge Interaction, Dynamic Response, Load Distribution

1. INTRODUCTION

The acceptance of FRP materials in bridge engineering is mainly due to their superior properties such as a high strength-to-weight ratio, better durability, corrosion resistance, and fatigue resistance over steel and concrete materials. An immediate advantage of using an FRP deck to replace a deteriorated concrete deck is the reduction of the superstructure dead load, which results in an increase in the allowable live load capacity. Over the last decade, some FRP bridge deck systems have been proposed, and there is a growing need to understand the behavior of FRP deck bridges. However, very little is known about the lateral distribution of vehicle loads and the dynamic response of bridges with a FRP deck. Therefore, the development of FRP bridge decks has been limited.

The load distribution throughout the bridge deck and the vehicle-induced dynamic impact on bridges are of primary importance in the design of bridges. The load distribution factor and the dynamic impact (or allowance) factor have been used worldwide in bridge design, and extensive experimental and theoretical work has been conducted to determine these factors for bridges with conventional concrete decks. The characteristics of the FRP decks (such as mass, stiffness and damping) are significantly different from those of the traditional concrete and steel decks, which could result in a different performance of FRP deck bridges from the traditional bridges. In the present study, a typical steel multi-girder bridge and a concrete multi-girder bridge with a span length of 60 ft (18.288m) were studied. Connections between an FRP deck to the girders are more difficult than those between a concrete deck and the girders. There are some arguments whether a composite action between the deck and girders should be pursued or if a simple non-composite design should be used. To resolve this issue, the load distribution and the dynamic response were compared in three conditions, namely FRP deck fully composite, FRP deck partially composite, and

concrete deck fully composite with the girders. The dynamic response of the bridge caused by a 3-axle truck was obtained in the time domain by using an iterative procedure employed at each time step. The influence of vehicle velocity as well as bridge surface roughness index on bridge performance was investigated.

2. SIMPLIFIED MODEL OF FRP DECK AND DYNAMIC EQUATION OF MOTION

The FRP bridge decks used in the present study are of a sandwich construction. As shown in Fig. 1, FRP laminates are attached to a closed-cell FRP, honeycomb-type, sinusoidal core, which extends vertically between the two face laminates (or skins). The geometry of this sandwich structure is designed to improve stiffness and buckling response through the continuous support of core elements with the face laminates (Plunkett 1997). Due to the geometrical complexity of this panel configuration, a finite element modeling and analysis for an entire bridge can be very complicated, if not impossible. In this research work, therefore, finite element modeling techniques were employed to develop simplified equivalent properties based on stiffness considerations for this structure. The complex sandwich hollow panel was therefore reduced to a solid orthotropic plate using the equivalent properties derived (Oghumu et al. 2005).

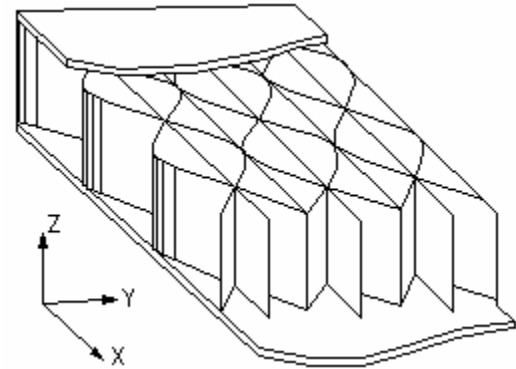


Fig.1 Sandwich Panel Configuration

HS20-44 truck, which is a 3-axle tractor-trailer type, is a major design vehicle in the AASHTO specifications [AASHTO 2002, 2004]. This truck is chosen in this study and is idealized to a vehicle model consisting of two vehicle bodies and 6 wheel bodies. The interaction force between the bridge and the vehicle is dependent on the motion of both the bridge and the vehicle, and that the vehicle displacement is related to the bridge displacement, road surface profile, and position of the vehicle. The equations of motion for the coupled system are written as (Zhang et al. 2006):

$$\begin{bmatrix} M_b \\ M_v \end{bmatrix} \begin{Bmatrix} \ddot{d}_b \\ \ddot{d}_v \end{Bmatrix} + \begin{bmatrix} C_b + C_{bb} & C_{bv} \\ C_{vb} & C_v \end{bmatrix} \begin{Bmatrix} \dot{d}_b \\ \dot{d}_v \end{Bmatrix} + \begin{bmatrix} K_b + K_{bb} & K_{bv} \\ K_{vb} & K_v \end{bmatrix} \begin{Bmatrix} d_b \\ d_v \end{Bmatrix} = \begin{Bmatrix} F_b^r \\ F_v^r + F_v^G \end{Bmatrix} \quad (1)$$

where $\{d_b\}$, $[M_b]$, $[C_b]$, and $[K_b]$ are the displacement vector, mass matrix, damping matrix, and stiffness matrix of the bridge, respectively; $\{d_v\}$, $[M_v]$, $[C_v]$, and $[K_v]$ are the displacement vector, mass matrix, damping matrix, and stiffness matrix of the vehicle, respectively; and $\{F_v^G\}$ = the gravity force vector of the vehicle. It is assumed that the wheels always maintain a point contact with the bridge deck without separation. The equations of motion for the vehicle and bridge are coupled through the interaction force and the terms C_{bb} , C_{bv} , C_{vb} , K_{bb} , K_{bv} , K_{vb} , F_b^r , and F_v^r stem from the contact (interaction) force. The road surface profile was simulated in the space domain, which serves as an input to the vehicle-bridge model.

3. NUMERICAL ANALYSIS OF TYPICAL GIRDER BRIDGE MODELS

One steel girder bridge model and one prestressed concrete girder bridge model were developed. The span length for both bridges is 60ft (18.288m). The two bridges were designed for the HS20-44 loading, and they both consist of five identical girders (with a spacing of 2.29m) which are simply supported. Meanwhile, in order to compare the performance, two types of the bridge decks were used: a honeycomb-type sinusoidal core FRP sandwich panel (see Fig. 1) and a traditional concrete deck. The FRP decks were designed for fully composite or partially composite. The thickness of FRP decks used in these models is 8 in (203 mm), and the deck was simplified as an equivalent orthotropic solid panel, as discussed earlier. The thickness of the concrete decks is 7.5 in (191 mm) for both the steel and prestressed concrete girder bridges.

The bottom-flange stress values at the mid-span of the girders obtained from the FEA were used to calculate the Load Distribution Factors (LDFs). By comparing the two cases of “FRP Deck Fully Comp.” and “FRP Deck Partially Comp.”, it is observed that when the deck and the girders are partially composite, the LDF values are larger, since in this case a smaller portion of loads are shared by the other girders. In other words, bridges with partially composite conditions cannot distribute loads as uniformly as bridges with fully composite conditions. By comparing the two cases of “FRP Deck Fully Comp.” and “Concrete Deck fully Comp.”, it is observed that due to the higher stiffness of the concrete deck, the LDF values of the bridge with concrete deck are smaller than those with the FRP deck. Meanwhile, it is observed that the stress values of concrete girder bridges are smaller than those of steel girder bridges, because concrete girder bridges have a larger stiffness compared to steel girder bridges. LDFs of concrete girder bridges are not as sensitive to deck stiffness as steel girder bridges are.

To investigate the effect of the deck system on bridge dynamic performance, vehicle-bridge interaction analyses of the bridge system with different deck configurations were carried out. The multi-girder bridges were assumed to be at rest before the vehicle entered the bridge. A parametric sensitivity study was conducted to analyze the effect of factors such as road surface condition and vehicle velocity on the bridge dynamic response. The objective was to compare the dynamic performance of the FRP deck bridges (fully composite or partially composite) and the corresponding concrete deck bridges, and find some correlations between the bridge dynamic performance and these parameters. Many investigations have shown that the roughness of a bridge surface is an important factor that affects the dynamic response of bridge structures (Wang et al. 1992). In this study, classification of road roughness based on the International Organization for Standardization was used, and the road surface profile was simulated in the space domain. Two road conditions were considered as inputs to the vehicle-bridge coupled model, namely: (1) road surface condition is good; and (2) road surface condition is poor. Based on these two road conditions and the vehicle velocity of $v = 10\text{m/s}$, 20m/s , or 40m/s , the dynamic responses at the bottom-flange at the mid-span of the center girder were evaluated. Fig. 2 demonstrates the vehicle velocity, road roughness, and displacement relationships of the steel bridge with the three different deck conditions. Due to the page limitation, other results cannot be presented here but are summarized below.

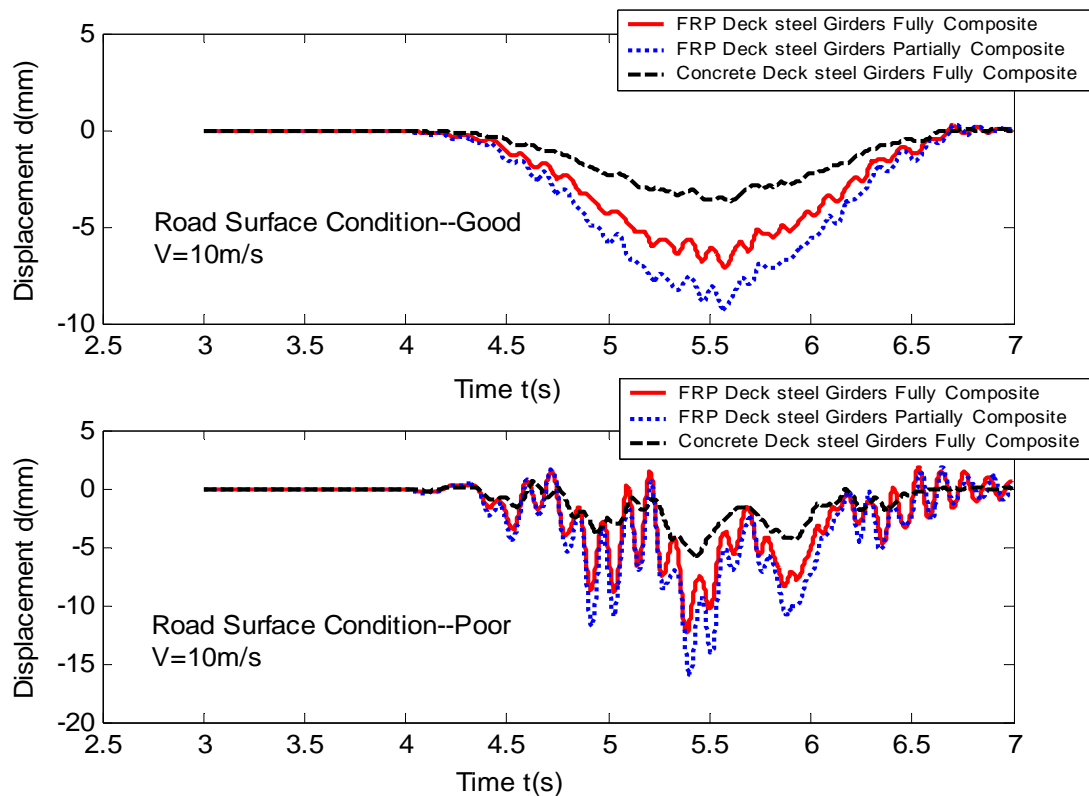


Fig. 2 Displacement Comparison of Steel Multi-Girder Bridge

According to the numerical simulation, deck types have seriously affected the displacement. While the FRP Deck Partially Composite condition results in the largest displacement, the Concrete Deck Fully Composite condition gives the lowest displacement. This observation agrees with that observed for the static loading case as discussed earlier since the deck stiffness is in an ascending order as FRP Deck Partially Composite, FRP Deck Fully Composite, and Concrete Deck Fully Composite. The difference between the FRP Deck Partially Composite and FRP Deck Fully Composite are more pronounced in bridges with steel girders than those with concrete girders. For accelerations, the values of bridges with an FRP deck are far larger than those with a concrete deck, even under a low vehicle velocity condition; the acceleration values of bridges with a FRP deck in the partially composite condition are generally close to the values of those with a FRP deck in the fully composite condition. Under low vehicle velocity (10m/s), the FRP deck in the partially composite condition generally results in a higher acceleration than that of the FRP deck in the fully composite condition. Under high vehicle velocity (40m/s), the trend is just the opposite. The vehicle velocity effect is more pronounced when the road surface condition is poor. Road roughness of a bridge has seriously affected the vehicle's vibrations, thus affecting the vehicle-bridge interaction. It can be seen from the figures that the worse the bridge road condition, the larger the bridge dynamic displacement, and the far larger the bridge dynamic acceleration under the truck load. This situation is more obvious in steel girder bridges. A poor road condition not only influences the bridge's normal operation, it moreover creates a vertical acceleration, which can make the driver uncomfortable and may cause a higher deterioration rate of the bridge. Therefore, maintenance of the bridge road surface in a good condition is very important in reducing the vehicle impact effect. However, the dynamic response of bridges does not increase monotonically with the increase in vehicle velocity. There is a peak value corresponding to a specific vehicle velocity, which is considered as being related to a vehicle induced resonant vibration.

4. CONCLUSIONS

The present study used an equivalent orthotropic solid plate model for the FRP hollow sandwich panel. For both load distribution and dynamic response, bridge deck types have seriously affected the results. The LDF values of FRP deck bridges are larger than those of concrete deck bridges. The dynamic response of FRP deck bridges is also larger than that of the concrete deck bridges. The FRP deck bridges with partially composite conditions have a larger girder distribution and dynamic response than those of the FRP deck bridges with fully composite conditions. Therefore, in order to obtain a better performance, it is necessary to strengthen the connection between the FRP deck and girders through structural measures. However, this is a challenge and usually an expensive requirement for a FRP deck system. If the non-composite condition is preferred for the FRP deck system, then it should be noted that the load distribution and dynamic allowance developed for the full composite condition may not be conservative for the girder design. Road roughness and vehicle velocity all significantly affect the dynamic performance of both the analyzed FRP deck and the concrete deck bridges. The road roughness will greatly affect the vibration of the bridge, even at low vehicle speeds when the surface condition is poor. Acceleration seems to be more sensitive to a poor road condition than to a good road condition with the same vehicle speed, especially for steel girder bridges.

5. REFERENCES

- American Association of State Highway and Transportation Officials (AASHTO) 2002, "Standard Specification for highway bridges," Washington, DC
- American Association of State Highway and Transportation Officials (AASHTO) (2004). "LRFD Bridge Design Specifications," Washington, DC.
- Plunkett, J. D. (1997). "Fiber-Reinforced Polymer Honeycomb Short Span Bridge for Rapid Installation," IDEA Project Final Report, Contract NCHRP-96-IDO30, IDEA Program, Transportation Research Board, National Research Council.
- Oghumu, S. and Cai, C. S., and Zhang, Y. (2005). "Finite Element Modeling and Performance Evaluation for the Development of FRP Bridge Panels." The joint /ASME/ASCE/SES Engineering Mechanics and Materials Conference, June 2005, Baton Rouge, Louisiana.
- Wang TL, Huang DZ, Shahaway M (1992). "Dynamic response of multigirder bridges." Journal of Structural Engineering, ASCE, Vol. 118, No.8, pp 2222-38.
- Zhang, Y., Cai, C. S., Shi, X. M. and Wang, C. (2006) "Vehicle Induced Dynamic Performance Of a FRP Versus Concrete Slab Bridge" J. of Bridge Engineering, ASCE, 11(4), 410-419.

LOAD AND RESISTANCE FACTOR DESIGN FOR FRP STRENGTHENING OF CONCRETE STRUCTURES

Rebecca A. Atadero

(Graduate Research Assistant, University of California, San Diego, La Jolla, CA, USA)

Vistasp M. Karbhari

(Professor, University of California, San Diego, La Jolla, CA, USA)

ABSTRACT

Externally-bonded fiber reinforced polymer (FRP) composites are a maturing technology for the repair and retrofit of existing concrete structures. Current guidelines for the design of FRP strengthening measures do not explicitly consider the uncertainties present in the FRP properties. Load and Resistance Factor Design (LRFD) provides an ideal framework for these considerations and is compatible with existing trends in civil engineering design codes. A recent project has studied the application of LRFD to FRP strengthening schemes. A widely applicable design framework has been proposed using a composite specific resistance factor to consider material variability, and a set of application factors to consider specifics of field manufacture. This paper describes the calibration of resistance factors for the example case of flexural strengthening of T-beam reinforced concrete bridge girders. The calibration considers FRP degradation based on existing durability models and continued degradation of the original structure is modeled by considering general corrosion of the reinforcing steel. Representative girders were selected from a sample of California bridge plans. The reliability was evaluated using simulation and first-order reliability methods.

KEYWORDS

Material Variability, LRFD, Design of Strengthening, Resistance Factors

1. INTRODUCTION

Externally-bonded fiber reinforced polymer (FRP) composites are an increasingly adopted technology for the repair and retrofit of existing concrete structures. In order to encourage the further use of these materials a design code is needed that considers the inherent material variability of the composite, as well as the variations introduced during field manufacture and environmental exposure while in service. Load and Resistance Factor Design (LRFD) provides an ideal framework for these considerations and is compatible with existing trends in civil engineering design codes.

Research into the application of LRFD to FRP strengthening is ongoing. Previous work has assessed the statistical variation in wet layup composite properties (Atadero et al., 2005) and proposed a framework for the application of reliability-based design to FRP strengthening (Atadero and Karbhari, 2005). This framework is based on design values for composite properties that are meant to represent best estimates of the mean values of FRP properties in the field. These design values are found using the mean laboratory predicted values of strength and modulus as the characteristic values, with a set of Application Factors to account for the specifics of field manufacture. A composite specific resistance factor is proposed to account for the variation in the composite properties. This composite specific factor is a function of the COV of the controlling composite property for a particular limit state, and facilitates the application of the proposed procedure to a variety of composite systems displaying different levels of variation. The proposed design framework also makes use of an environmental factor that is specific to the exposure environment and anticipated service life of the strengthening. This paper describes the process used to calibrate preliminary resistance factors for the specific example case of flexural strengthening of reinforced concrete T-beam bridge girders. Complete details may be found in Atadero (2006).

2. CALIBRATION PROCEDURE

The resistance factors were calibrated using a procedure that assumes the load factors have already been determined. For this example the load factors from the *AASHTO Manual for Condition Evaluation and Load and Resistance Factor Rating (LRFR) of Highway Bridges* (2003) were used because the reliabilities found using the AASHTO LRFD (1998) factors were very high. This procedure can be described as a trial and error procedure because designs are first created with many values of the resistance factors, the reliability of all designs is evaluated, and then the pair of factors that results in the smallest difference between the target reliability and the as designed reliability is selected. The procedure is described in further detail in Atadero (2006).

3. RANGE OF CALIBRATION

3.1 Composite Materials

Five different sample materials with properties chosen to represent the anticipated range of properties seen in wet layup CFRP were used for calibration. The assumed properties of these materials are shown in Table 1.

Table 1: Assumed Properties of Sample Materials Used for Calibration

Material	Ultimate Strength MPa (ksi)	Modulus GPa (ksi)	1-Layer Thickness mm (in)	Ultimate Strain mm/mm (in/in)
1	620.5 (90)	51.7 (7500)	1.27 (0.05)	0.012
2	689.5 (100)	61.4 (8900)	1.27 (0.05)	0.011
3	758.4 (110)	58.6 (8500)	1.27 (0.05)	0.013
4	827.4 (120)	59.3 (8600)	1.27 (0.05)	0.014
5	896.3 (130)	68.9 (10000)	1.27 (0.05)	0.013

Time dependent degradation of the composite was modeled using Arrhenius rate relations found in Abanilla (2005). Three conditions were modeled, no degradation, degradation following the model, and degradation following the model, but slowed by a factor of five to better represent field environments.

3.2 Existing Structure

Representative T-beam girders were chosen from an inventory of California bridge plans. These girders were assumed to be deficient due to a loss in reinforcing steel. Three cases were considered, 10, 20 and 30 percent loss. Designs were created to return the girders to the flexural capacity required by the LRFR load factors. The possibility of continuing deterioration of the girder was considered by modeling additional steel loss through a simple corrosion model. Continuing corrosion was considered for each of the three original percentages of loss, resulting in a total of six conditions, three without continuing corrosion, and three with. Design lives of 10, 20, 30, 40, and 50 years were considered.

4. DESIGN OF STRENGTHENING

Trial designs were created for each of the different cases within the extensive range of calibration. The checking equation used for design is shown in Equation 1. In this equation γ_i and L_i are the load factors and load effects, respectively, and R is the nominal resistance as a function of many variables including the FRP contribution, x_{FRP} . The general resistance factor, ϕ , was allowed to take on values of 0.95, 0.9, and 0.85. The composite specific factor, ψ , ranged from 0.95-0.5 in increments of 0.05.

$$\sum_i \gamma_i Q_i \leq \phi R(\dots, \psi x_{FRP}) \quad (1)$$

The design loads were calculated based on the HL-93 load model (AASHTO 1998), using a bridge load analysis program (WSDOT, 2006). The moment resistance of the girders was calculated based on sectional analysis, assuming a linear strain distribution through the depth of the cross-section. The ultimate strength was found when

either the FRP or concrete reached an ultimate strain. The strain limit in the FRP considered the possibility of debonding or composite rupture, and was found to control due to the large area of concrete in the compressive region provided by the T-beams.

5. EVALUATION OF RELIABILITY

The reliability of the trial designs was evaluated using a hybrid procedure whereby the variation in resistance was estimated via Monte Carlo Simulation, and the overall reliability was calculated using first order reliability methods as outlined in Nowak (1999). In this procedure the resistance was modeled as a Lognormal variable with the mean and standard deviation determined through simulation based on a model of resistance (sectional analysis was used in this example) and the individual distributions of variables contributing to resistance. In order to calibrate values of ψ , the composite specific factor, that depend on the COV of the composite, the reliability of each design was evaluated for composite strength COVs of 0.05, 0.10, 0.15, 0.20, 0.25 and 0.30. The components of load were modeled as normal variables following the distributions developed in Nowak (1999). This procedure follows the assumptions used in calibration of the LRFD specifications for design of new bridges, however some of these assumptions (particularly modeling variation in live load) are identified as needing further study.

6. RESULTS AND DISCUSSION

Resistance factors were calibrated for target reliabilities of 2.5, 3.0, and 3.5 for each of the girders and corrosion conditions considered. These reliability indices span the range from the value used for bridge evaluation to that used for design of new bridges. A selection of reliability targets was used to demonstrate the range of possible factors that would be necessary, however it is expected that a code-writing agency would specify this value for the designer.

The calibrated resistance factors were found to be very sensitive to the amount of steel remaining in the section relative to the amount of FRP applied. Due to the range of initial conditions displayed by the girders, comparisons between girders based on the corrosion condition were uninformative. Instead, a common reference value was defined as the amount of steel required to just meet the LRFR load demand for each girder. Different girders at different corrosion conditions were grouped based on the percent of steel loss relative to this reference value. Within each grouping, a range of resistance factors was selected to meet each of the three target reliability indices. Relative losses from 0-30% were considered, with the groups based on 5% increments. As an example, Table 2 shows the factors calibrated for two of the ranges considered. The values of ψ shown in Table 2 are the average of the higher (corresponding to low strength COVs) and lower (corresponding to high strength COVs) values of the range found for each girder and level of corrosion in a particular group. It is important to recognize that this was a strict average, and therefore it can be expected that in using these factors roughly half of designs will fall below the target reliability and roughly half will be above it. The COVs listed in the table refer to the amount of variation seen in the value of the factors, and are provided to give some sense of the amount of variation within a set of factors for a single group, however are not necessary for use in design.

Table 2 shows that as the percent of steel loss relative to the LRFR baseline increases the calibrated resistance factors also increase. This implies that for a fixed value of the resistance factors, as the amount of load carried by the FRP relative to the steel increases, the reliability of the girder increases. From a reliability standpoint, this is attributed to the ability of the steel and FRP to offset weaknesses in each other as more of the load is shared between the two. The change in reliability due to different amounts of steel deficiency poses a difficulty for reliability-based design of strengthening because in real applications it is very rare that the area of remaining steel will be known with a high degree of certainty. Thankfully, conservative designs for high amounts of steel loss can be created using the factors for lower percentages of loss. Table 2 also shows a range of values for ψ . This demonstrates that changes in FRP variability do have the ability to impact the reliability of the girder as a whole, thereby requiring different resistance factors for different levels of variation. The range of COVs considered in this example was quite large, 0.05-0.30, however, it was not impractical; values from 0.12 to 0.23 have been observed by these authors for wet layup samples. Though Table 2 only expresses the range of values, the change in the value of ψ with changes in the strength COV was quite uniform across the different cases considered here. The higher value of the resistance factor generally applies to COVs from 0.05-0.15. Beyond a COV of 0.15, the resistance factor decreases linearly to achieve the low value at a strength COV of 0.30. Tests were also conducted on the effect of changes in the COV of the composite modulus, but they were observed to be much smaller than the effect of changes in the strength COV.

Table 2 : Example of Resistance Factors for Different Target Reliabilities and Different Amounts of Relative Steel Loss

% below steel needed for LRFR	$\beta=2.5$	$\beta=3.0$	$\beta=3.5$
5< , >=10	18 out of 38 cases are too high or no design $\phi=0.95$ Avg $\psi = 0.839-0.732$ COV = 10.0% & 13.0%	$\phi=0.9$ Avg $\psi = 0.831-0.752$ COV = 11.6% & 12.7%	$\phi=0.85$ Avg $\psi = 0.834-0.787$ COV = 9.3% & 9.1%
10< , >=15	21 out of 45 cases are too high or no design $\phi=0.95$ Avg $\psi = 0.870-0.782$ COV = 9.1% & 9.6%	For 15 out of 45 cases $\phi=0.95$ or 0.90 both work. $\phi=0.9$ Avg $\psi = 0.864-0.819$ COV = 9.7% & 9.9%	17 out of 45 cases are too low or no design possible. The rest are evenly split. $\phi=0.85$ Avg $\psi = 0.885-0.840$ COV = 7.5% & 7.6% $\phi=0.90$ Avg $\psi = 0.662-0.626$ COV = 6.9% & 8.3%

Though the remaining area of steel was found to be highly significant, other trends were also observed. In general, only small differences in reliability were present for designs created with different FRP materials. The predicted degradation of the FRP for different design lives was included in the creation of designs, and it was found that there was very little difference in reliability for the different degradation models. Furthermore, designs maintained uniform reliability over different design lives for the cases with no continuing corrosion. For the cases that did consider continuing corrosion, the reliability increased slightly over time, suggesting that the corrosion parameters used in design were slightly more conservative than those used in analysis of reliability.

7. CONCLUSIONS

This paper has described preliminary calibration procedures allowing for the reliability-based design of FRP strengthening with wet layup materials. Results shown here highlight the importance of knowledge regarding the state of the existing structure when the FRP is applied and over time. They also show that the amount of variability in composite properties can impact the reliability of the repaired structure, and should be considered in design.

8. REFERENCES

- Abanilla, M.A.D. (2004). "Physico-Mechanical Characterization of T700 based Carbon/Epoxy Systems for Infrastructure Rehabilitation", Master's Thesis, University of California, San Diego.
- American Association of State Highway Transportation Officials. (1998). *AASHTO LRFD Bridge Design Specifications, Customary U.S. Units*, 2nd edition; AASHTO: Washington D.C.
- American Association of State Highway and Transportation Officials. (2003). *Manual for Condition Evaluation and Load and Resistance Factor Rating (LRFR) of Highway Bridges*; AASHTO: Washington D.C.
- Atadero, R., Lee, L., and Karbhari, V.M. (2005). "Consideration of Material Variability in Reliability Analysis of FRP Strengthened Bridge Decks", *Composite Structures*, Vol. 70, No. 4, pp 430-443.
- Atadero, R.A., and Karbhari, V.M. (2005). "Consideration of Time-Dependent Degradation in the Development of Probabilistic Based Design of FRP Strengthening", *American Society for Composites, Proceedings of 20th Technical Conference*, Editors: F.K. Ko, G.R. Palmese, Y. Gogotsi and A.S.D. Wang, Philadelphia, PA.
- Atadero, R.A. (2006). "Development of Load and Resistance Factor Design for FRP Strengthening of Reinforced Concrete Structures", Ph.D Thesis, University of California, San Diego.
- Nowak, A.S. (1999) *Calibration of LRFD Bridge Design Code*; National Academy Press: Washington D.C.
- Washington State Department of Transportation. Bridge Engineering Software - QConBridge™ Overview. http://www.wsdot.wa.gov/eesc/bridge/software/index.cfm?fuseaction=software_detail&software_id=48 (accessed 2006).

CZECH GUIDELINES FOR STRENGTHENING OF CONCRETE BRIDGES BY COMPOSITES

Miroslav Černý

(Head of Centre for Composites, Klokner Institute, Czech Technical University, Prague, Czech Republic)

ABSTRACT

This paper presents the new Guidelines which have been recently elaborated in the Czech Republic. The Guidelines are focused on strengthening of concrete road bridges by fibre composite strips, mostly based on carbon fibres and epoxy matrices. Methods of strengthening are following: bonding (gluing) of composite strips on concrete surface or impregnating of unidirectional or multidirectional textile by polymeric resin in-situ.

KEYWORDS

Strengthening, Concrete Bridges, Composites, Carbon Fibres, Limit States

1. INTRODUCTION

Many suppliers of carbon fibre sheets are delivering the products, which can be successfully applied for strengthening of RC road bridges. However, in the Czech Republic doesn't exist an unified approach for application and design for strengthening of structures by fibre composites. Since 2001 in the Czech Republic at Czech Technical University (leading by author) has been conducting the work on „Technical Conditions (Guidelines) for Strengthening of Concrete Bridges by Composites“, which has been supporting by Ministry of Transportation of the Czech Republic.

„Technical Conditions“ are oriented to preparation, design and execution of strengthening of road bridges and footbridges from concrete and reinforced concrete by **unprestressed** composites and will serve as groundwork for certification of products for strengthening.

Recently, the „Technical Conditions“ for strengthening of bridges and footbridges from concrete and reinforced concrete on roads by **prestressed** composites are elaborated.

Methodology of design is issuing from the following basic sources:

EN 1991-1 Eurocode 1: Basis of design and actions on structures- Part 1: Basis of design.

EN 1991-3 Eurocode 1: Basis of design and actions on structures- Part 3: Actions on structures: Bridges.

EN 1992-1-1 Eurocode 2: Design of concrete structures- Part 1-1: General rules and rules for buildings

EN 1992-2 Eurocode 2: Design of concrete structures- Part 2: Concrete bridges

EN 206-1: Concrete: Specification, performance, production and conformity

ACI 440.2R-02 (2003) Guide for the Design and Construction of Externally Bonded FRP Systems for Strengthening Concrete Structures

CEB-FIP Technical report (2001): Externally bonded FRP reinforcement for RC structures. Bulletin No. 14

The basic principles involved in Guidelines are presented:

- a) Properties of strengthening elements
- b) Structural requirements, execution and quality control
- c) Recommendations for design

2. PROPERTIES OF STRENGTHENING ELEMENTS

Adhesives, sheets, textile composites and other strengthening elements should have the properties evaluated by the standard test methods. The properties have to be given by the manufacturer or supplier, who should prove that the

tests have been done by the independent testing laboratory according to approved testing methods. The manufacturer should guarantee the quality of products. The control tests of products must be done before the application. The Guidelines include the required properties of products for strengthening of road bridges. The short-term mechanical properties of **adhesives** have to be tested (tensile modulus, tensile strength, fracture strain according to EN ISO 527, bending modulus according to EN ISO 178). Further the short-term mechanical properties of **composite sheets** (tensile modulus, tensile strength, fracture strain according to EN ISO 527) should be tested. Table 1 shows required properties of epoxy adhesive for gluing of carbon fibre sheets.

Table 1: Properties of Epoxy Adhesive (Cerny, 2004)

Properties (at 20 ⁰ C)	Epoxy Adhesive
Density[kg.m ⁻³]	1100- 1700
Tensile E modulus [MPa]	5000
Shear modulus [MPa]	2500
Poisson's ratio[-]	0.2- 0.3
Tensile strength [MPa]	25
Shear strength [MPa]	10- 30
Fracture strain in tension [%]	0.3 – 1
Fracture energy [kJm ⁻²]	0.2- 1.00
Coefficient of thermal expansion [10 ⁻⁶ K ⁻¹]	44- 70
Water absorption:7 days 25 ⁰ C [%w/w]	0.04-0.1

3. STRUCTURAL REQUIREMENTS

Before diagnostic recognition the ordinary or extraordinary inspection of bridge according to standards (Czech Standard 736221) should be done. Further recognition follows according to Technical Conditions (TP 72). It should be recognized: an amount, geometry and type of steel reinforcement including corrosion and the quality of concrete including corrosion. The quality of bonding should be tested according to EN 1542, and by a shear test (test proposed by CTU KI).

4. RECOMMENDATIONS FOR DESIGN

Limit states and design situations (Cerny, 2001)

The design model should consist of a verification of both the **serviceability limit state** and the **ultimate limit state**. The following design situations have to be considered:

- persistent situation, corresponding to the ordinary use of the structure
- accidental situation, corresponding to a loss of strengthening
- special situation (important for **bridges**: stresses due to differences in thermal expansion, cyclic loading, long-term behaviour)

Verification of the ultimate limit state (ULS)

The various failure modes should be considered, assuming (1) full composite action between structural member and strengthening (bonding) and (2) different debonding that may occur.

Load combinations and partial safety factors should be applied. In case of **full bonding**, for the **concrete**, a **parabolic-rectangular diagram**, for the **steel** a **bilinear stress-strain** relationship can be considered.

For **composites** the following stress-strain relationship is considered:

- a) linear for carbon fibre sheets (in tension along fibres)
- b) bilinear for textile composites in warp and fill directions
- c) nonlinear for textile composites in shear

Verification of the serviceability limit state (SLS)

It should be verified that the strengthened structural member behaves adequately in normal use.

The verification involves:

- stresses, these should be limited to prevent steel yielding, damage, excessive creep of concrete and composite
- deformations which may limit normal use of the structure
- cracking which may limit the durability of the structure.

Linear stress-strain diagram is considered for concrete and steel.

For **composites** the following stress-strain relationship is considered:

- linear for carbon fibre sheets (in tension along fibres)
- bilinear for textile composites in warp and fill directions
- nonlinear for textile composites in shear

The following figures illustrate a procedure for evaluation of ULS for rectangular beam in bending, strengthened by a carbon sheet with linear stress-strain relationship (consult CEB-FIP TR, Cerny, 2002):

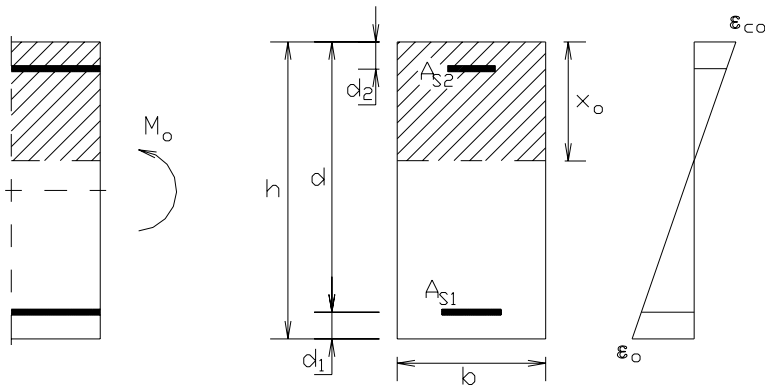


Figure 1: Initial configuration

From the initial configuration an initial strain ϵ_0 at composite level is calculated and used in ULS analysis.

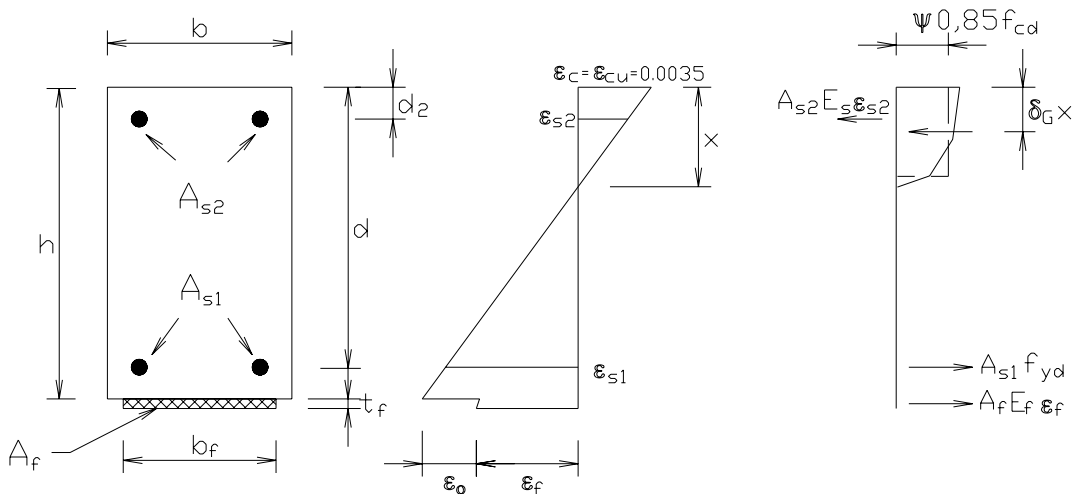


Figure 2: Ultimate limit state in bending

The Figure 2 shows a full composite action when steel yields (f_{yd}) and concrete is crushing (αf_{cd}).

Failure occurs in the critical cross-section at strain limit of steel and failed concrete, composite is not damaged. The design bending moment is calculated on condition of initial strain loaded structure from the method of strain limit by iteration. Some results have been confirmed experimentally (Cerny, 2006). The methodology of design for strengthening is elaborated in Guidelines for bending and shear of a rectangular beam and T beam, some examples are presented in Appendix.

5. CONCLUSIONS

Guidelines "Technical Conditions" allow to enforce unified approach for strengthening, evaluation of materials and design strengthening methods for road RC bridges in the Czech Republic and to achieve more safe and effective strengthening of RC bridges.

6. REFERENCES

- Cerny, M. (2002). "Limit States Design for Structures Externally Reinforced by Composites", *Proceedings of International Symposium on Mechanics of Composites (MC/1)*, Editor: M.Cerny, Czech Technical University, Prague, pp.43-46.
- Cerny, M. (2001). "Limit States Design for Composite Structures", *Proceedings of the International Conference on Composites in Material and Structural Engineering (CMSE/1)*, Editor: M.Cerny, Czech Technical University, Prague, pp.57-58.
- Cerny, M. (2004). „Experimental Evaluation of Carbon Fibre Composites and Adhesives for Strengthening of Engineering Structures“, *3rd Czech /Slovak Symposium „Theoretical and Experimental Research in Structural Engineering“*, CTU Reports, No. 3.
- Cerny, M. (2006). „Testing of RC Beams Strengthened by CFRP Strips“, *4th Czech /Slovak Symposium „Theoretical and Experimental Research in Structural Engineering“*, CTU Reports, No. 3.
- ACI 440.2R-02 (2003) Guide for the Design and Construction of Externally Bonded FRP Systems for Strengthening Concrete Structures, ISBN 0-87031-0887
- CEB-FIP Technical report (2001): Externally bonded FRP reinforcement for RC structures. Bulletin No. 14, ISBN 2-88394-054-1

Part VIII. Durability Issues

DETERIORATION MECHANISM OF BOND BETWEEN CFRP PLATE AND CONCRETE IN MOIST ENVIRONMENT

Zhenyu Ouyang

(Ph.D. Student, Marquette Universit, Milwaukee, WI, USA)

Baolin Wan

(Assistant Professor, Marquette Universit, Milwaukee, WI, USA)

ABSTRACT

This study experimentally investigated the mechanism of deterioration for the bond between CFRP plate and concrete due to moisture attack. The debonding failure in the concrete structures with externally bonded FRP has two major modes: cohesive failure in the concrete surface layer and adhesive failure in the interface between concrete and adhesive layer. A simple experimental approach was developed in this study to directly measure the moisture condition in the interface between concrete and adhesive layer with function of immersion duration in water. Modified Double Cantilever Beam (MDCB) test was used to measure the interfacial fracture energy for the CFRP plate debonding from concrete substrate under Mode I loading. The MDCB specimens were submerged in water for different periods before they were tested. When the value of interface region relative humidity (IRRH) increased, fracture load and fracture energy decreased and failure mode was also changed from cohesive failure to adhesive failure. It was found that the residual thickness of concrete (RTC) on the fracture surface was directly related to the relative humidity in the interface region. When the IRRH was greater than 55%, the value of fracture energy G_f began to decrease significantly with the increase of the IRRH and immersion duration.

KEYWORDS

Bond, CFRP, deterioration, interface region relative humidity (IRRH), residual thickness of concrete (RTC)

1. INTRODUCTION

When reinforced concrete are strengthened with externally bonded fiber reinforced polymer (FRP) composite materials, bond between FRP and concrete for the strengthening system is one of the important factors affecting the structural performance. The debonding failure in the concrete structures with externally bonded FRP has two major modes: cohesive failure in the concrete surface layer and adhesive failure in the interface between concrete and adhesive layer. Normally, it requires larger load and fracture energy to cause concrete cohesive failure than those to cause interface adhesive failure. In ambient environment conditions and with good quality control during application, the performance of the bond between FRP and concrete is good by the evidence that debonding failure happens in concrete. However, when it is exposed to moist environment, the FRP/concrete bond may deteriorate quickly and the failure mode changes from concrete cohesive failure to interface adhesive failure (Wan et al., 2006). It could lose as high as 87% of the gain from CFRP when the CFRP strengthened reinforced concrete beams were exposed to moist environment (Grace and Singh, 2005). Even for very short period when the CFRP bonded concrete specimens were submerged in water, the interfacial energy release rate was reduced 85% after 8 weeks of exposure (Wan et al., 2006). Nguyen et al. (1998) found that there were few water molecule layers at the interface when concrete with epoxy cover was exposed to water for a period. Such water molecule layers seriously decrease the free surface energy of bond interface and create a weakest link in the system. They also change the interface bond stiffness and gradually transfer the debonding failure modes from cohesive failure to adhesive failure. Absorbing water can change the mechanical properties of the adhesive layer. Harmon et al. (2003) found that shear modulus of the bond layer was one of the critical factors which affected the bond performance. Therefore, the changes of bond strength and fracture energy are related to the quantity and distribution of water at the bond interface region.

Almost all of literatures relate the bond deterioration to the moisture condition of surrounding environment and exposure duration. However, even in same moist environment and exposure duration, the actual moist environment in the interface region might be significant different due to different sizes and geometric properties of the specimens, moisture distribution and transportation in concrete. In this research, a simple method was developed to measure the adhesive/concrete interface region relative humidity (IRRH). The relationship between moisture exposure history of the interface and interfacial energy release rate for debonding FRP from concrete was determined. The IRRH value has the potential to be a direct and uniform criterion for the deterioration of the bond between concrete and FRP composites in moist environment.

2. EXPERIMENTAL PROGRAMS

2.1 MDCB Test

The Modified Double Cantilever Beam (MDCB) test was successfully used by Wan et al. (2006) to investigate the water effect on the bond between FRP and concrete. The frame used in this research is the second generation of MDCD test frame as shown in Figure 1. Using this new frame, the loading rate and magnitude can be accurately controlled by a programmable motor. A customized data acquisition system was designed specifically for the MDCB test and was built in the test frame. Therefore, the data can be automatically acquired by connecting this MDCB test frame to any computer.

A ready mixed concrete and commercially available CFRP plate and adhesive were used in this research. The dimension of the concrete specimen was 76 x 76 x 191 mm. The surface of concrete was sand blasted and cleaned by high pressure air before primer was applied. CFRP plate was applied on the concrete surface by standard procedures recommended by the manufacture. The control specimens were tested after they were allowed to cure for 7 days. All other specimens were submerged in distilled water until they were tested. All specimens were tested under Mode I (peeling) load.

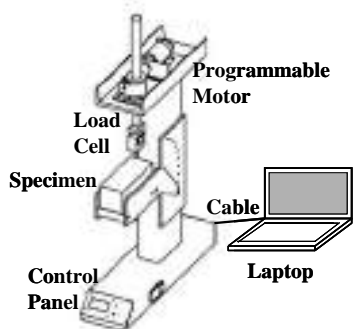


Figure 1: Second generation of MDCB test frame



Figure 2: Measure the Interface region relative humidity (IRRH)



Figure 3: Measure the residual thickness of concrete (RTC)

2.2 Measure the Interface Region Relative Humidity (IRRH)

In order to minimize the disturbance to the moisture content in the concrete at the interface during the test, a plastic tape was used to gradually and carefully cover the debonded area once the peel separation became large enough. After CFRP plate was peeled off from concrete substrate, the fracture surface of concrete was entirely covered by a plastic film immediately. This plastic acted as the original adhesive and CFRP plate to prevent the moisture evaporates from concrete to air. The moisture present in the concrete would evaporate into the space between concrete fracture surface and plastic film until it reached balance. This balanced relative humidity can be approximately considered as the relative humidity in the FRP/Concrete interface region before test. The relative humidity at different locations was measured by an accurate digital hygrometer which had $\pm 3\%$ error according to manufacturer's manual. A short aluminum tube was used as cap to create a small closed space to measure the relative humidity on the fracture surface. The top of the cap was sealed with a rubber washer. A layer of 3-mm-thick water-proof silicone was glued on the bottom wall of the cap. The fully cured silicone was very soft and it could deform with the rough concrete surface when subjected to moderate pressure. Therefore, a closed space was created by the aluminum tube, silicone layer and concrete surface. There was no air convection inside this closed

space and between the space and surrounding air. When the probe was inserted into the cap through the rubber washer, the moisture sensor which located at the end of the probe was placed in this closed and small space as shown in Figure 2. Once the relative humidity reached equilibrium in this small closed space, this R.H. value was recorded as the IRRH.

2.3 Measure the Average Residual Thickness of Concrete (RTC)

Before bonding to the concrete specimens, the thickness of each CFRP plate was measured. After MDCB test finished, the detached plates were measured through a digital coordinate measuring machine (CMM) as shown in Figure 3. For each specimen, about 100 sample points along the entire fracture surface were measured and the average value was calculated. This value was the summation of the thicknesses of CFRP plate, adhesive and residual concrete layer attached on CFRP plate. Each plate was then cut into three coupons along the longitudinal direction of the plate. A high resolution digital microscope was used to measure the adhesive thickness along each edge of these three coupons with 5 mm interval along the longitudinal direction. The adhesive thickness was the average value of those measurements. The difference between the total average thickness from CMM and the sum of CFRP thickness and adhesive thickness was taken as the average residual thickness of concrete (RTC).

3. TEST RESULTS AND DISCUSSION

Energy release rate of each specimen was calculated by following the method developed by Wan et al. (2004) for MDCB test. It was observed in the tests that debonding failure mode changed gradually from cohesive failure in concrete to adhesive failure in interface when immersion duration increased from 2 to 7 weeks. The fracture energy release also decreased with the immersion duration as shown in Figure 4. After the specimens were submerged in water for 7 weeks, the average G_f value was only 22% of the control specimens.

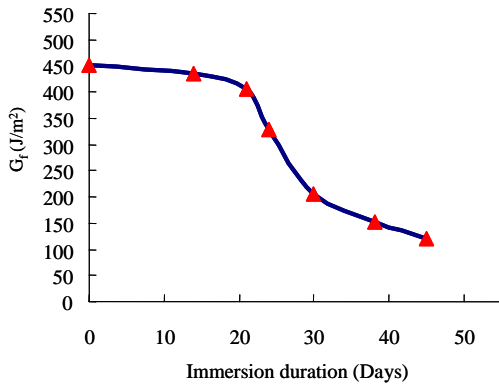


Figure 4: Average fracture energy release rate vs. immersion duration

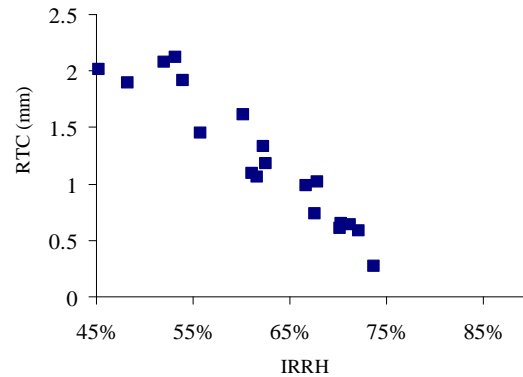


Figure 5: Residual concrete thickness (RTC) vs. interface region relative humidity (IRRH)

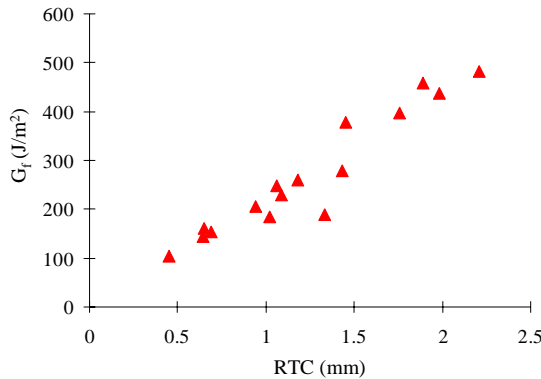


Figure 6: G_f vs. RTC

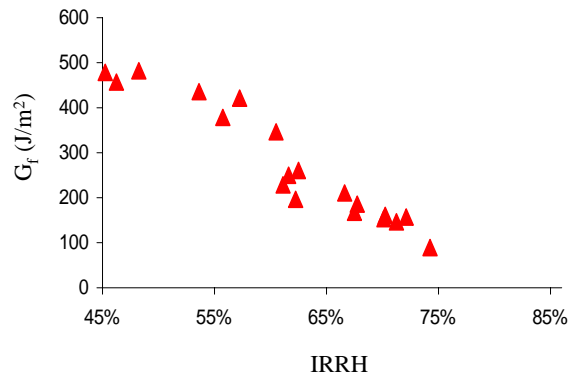


Figure 7: G_f vs. IRRH

It is shown in Figure 5 that the residual thickness of concrete (RTC) on the fracture surface decreased significantly with the increase of the interface region relative humidity (IRRH). When the IRRH was between 45% and 55% which was similar to normal R.H. value in room, the RTC was around 2 mm. When the IRRH was close to 75%, the average RTC was less than 0.5 mm. It is shown in Figure 6 that fracture energy increased with the increase of RTC. The bond fracture energy G_f increased with the increase of RTC when it was less than 2 mm. However, G_f did not change significantly when RTC was greater than 2 mm. The relation between the fracture energy G_f and the IRRH is shown in Figure 7. It is shown that G_f decreased with the increase of IRRH. Such decrease was relatively slow when the IRRH was lower than 55%. When the IRRH value was higher than 55%, the G_f decreased rapidly with the increase of IRRH value and immersion duration. Therefore, the value of IRRH of 55% was the critical value to start the bond deterioration. For the specimens used in this research, it took three weeks to reach this critical humidity in the interface region. If the specimen size was larger or the relative humidity in the environment was lower, it would take longer time to let the interface region to obtain the critical relative humidity value.

When metal, glass or other non-porous materials are glued together with adhesive, the adhesive can only penetrate into a tiny depth and such penetration depth is relatively uniform. However, concrete is a porous material and there are numerous air cavities, capillary pores, gel pores and micro-cracks on the surface. Primer is a low viscosity material and it is easy to penetrate into deeper location in concrete. The contact area between the primer and the walls of the cavities, pores and micro-cracks will significantly increase the bonding area between primer and concrete. The actual bonding area is much larger than the nominal bonding area. Therefore, the bond between primer and the walls of the penetrating path will have significant contribution on the resistance to debond during the peeling test. When specimens are submerged in water, water will penetrate into concrete through the part below primer-saturated concrete much easier and faster than into primer-saturated concrete, adhesive and FRP because of the microcracks and capillary pores in concrete. Therefore, the bottom part of the primer-saturated concrete will reach critical R.H. value for debonding and lose its bonding ability first. After local debonding between pore wall and penetrated primer, the concrete at that part is not gripped during peel test and it will not contribute to the energy dissipation during the global debonding process. Water will continue to penetrate up through the primer-saturated concrete and finally reach the nominal interface between adhesive and concrete. This might be the reason why the RTC and G_f values gradually decrease with the increase of immersion duration as observed in experimental tests.

4. CONCLUSIONS

The following conclusions can be drawn from this research:

1. A simple method was successfully developed to measure the adhesive/concrete interface region relative humidity (IRRH) value. It could be used as a direct and uniform criterion for the deterioration of the bond between concrete and FRP composites in moist environment.
2. The residual thickness of concrete (RTC) on the fracture surface was directly related to the IRRH values
3. When the IRRH value was greater than 55%, the G_f value began to decrease significantly with the increase of IRRH and immersion duration.

5. REFERENCES

- Grace, N.F. and Singh, S.B. (2005). "Durability evaluation of carbon fiber-reinforced polymer strengthened concrete beams: experimental study and design", *ACI Structural Journal*, Vol. 102, No.1, pp40-51.
- Harmon, T.G., Kim, Y.J., Kardos, J., Johnson, T. and Stark, A. (2003)., "Bond of Surface-Mounted Fiber-Reinforced Polymer Reinforcement for Concrete Structures", *ACI Structural Journal*, Vol. 100, No. 5, pp557-564.
- Nguyen, T., Byrd, W. E., Alsheh, D., Aouadi, K., Chin, J. W. (1998). "Water at the polymer/substrate interface and its role in the durability of polymer/glass fiber composites", *Durability of Fibre Reinforced Polymer (FRP) Composites for Construction (CDCC'98)*, 1st International Conference, Canada, pp451-462.
- Wan, B., Petrou, M.F. and Harries, K.A. (2006). "Effect of the presence of water on the durability of bond between CFRP and concrete", *Journal of Reinforced Plastics and Composite*, Vol. 25, No. 8, pp875-890.
- Wan, B., Sutton, M., Petrou, M.F., Harries, K.A. and Li, N. (2004). "Investigation of Bond between FRP and Concrete Undergoing Global Mode I/II Loading," *ASCE Journal of Engineering Mechanics*, Vol. 130, December 2004, pp1467-1475.

Durability Approach for GFRP-Rebars

André Weber

(R &D, Schoeck Bauteile GmbH, Baden-Baden, Germany)

ABSTRACT

Most GFRP-Rebars have been developed, to solve the corrosion problem with bridges and other structures. But one component of these rebars, the glass fibre, is itself susceptible to corrosion in the highly alkaline environment of concrete. The other component of the GFRP-rebar - the resin system - has to provide the protection against diffusion and deterioration.

To begin applications in the past years different accelerated durability tests have been developed and performed. Design and test guidelines as well as first codes have been established in different countries. Now an experience of nearly ten years shows that some rebar systems are stable under certain conditions. In spite of all the benefits the market growth for primary applications is smaller than expected.

There is still a lack of confidence in the new reinforcement technique as a primary reinforcement for buildings and structures. If we do not want to wait 50 years, confidence can only be established by conservative and comprehensible test approaches with broad acceptance in science and by the authorities.

Two different approaches for durability are reviewed from the point of view of safety and the transferability of the results. Basis of the consideration is the international semi-probabilistic safety concept with partial safety factors for load and material. For both approaches results are presented and compared. Furthermore, a defined path from test results to design value of the tensile strength is shown in this paper.

KEYWORDS

Durability, Composite Rebar, Safety Concept, Design Value, Accelerated Durability Test, Extrapolation

1. INTRODUCTION

New materials have acceptance problems, especially if the material is susceptible to attack from its own environment. Long term experience is very limited. Even the significance of 10 years of long term data is low. To get durability results in shorter time two approaches are possibly: Time temperature shifting and extrapolation.

2. SIMPLIFIED APPROACH WITH RESIDUAL STRENGTH

In this first approach the whole service life is projected on the rebar. That means load, time, temperature and alkalinity conditions. To accelerate this test, a higher temperature is chosen for the test. Different authors have developed time/temperature shifting equations. Normally tests are performed over several months at 60°C. The environment can be an artificial concrete pore solution as well as wet concrete. After this test regime the specimen are tested by tensile tests. ACI, ISO, JSCE and CSA have defined different standard test procedures.

Normally the residual strength is reported in relation to the virgin strength. More important regarding the safety theory is the relationship between the residual strength or the load during the test and the design load in the application. This relationship is proposed as a simplified approach for normal conditions by the fib.

But attention: if the conditions change or the testing time is too short an extrapolation is not possible. If, for example, a specimen is loaded for 1 month and the residual strength is 95% and the specimen is loaded for two months and the residual strength is 90% it is not possible to give a value for 3 months or 6 months. A linear

behaviour can not implied. As a specimen deteriorates the load in the residual section rises with every broken fibre, that is the stress in the fibres of the remaining cross section increases. As a result, the deterioration process accelerates. The behaviour is highly nonlinear. There is a certain probability, for example, that the above mentioned specimen is broken after three months.

The approach described above has been selected for the certification process of the Dutch approval authority KIWA. A less clearly specified approach is found in the non-binding section of the Canadian Standard CSA 806. In Annex O the code recommends that the specimens should be loaded with 1.1 times the “design allowable strength” while ageing in an artificial concrete pore solution of pH 12.7 or in concrete.

To meet the internationally accepted safety concept the Canadian approach specifies the test load to be equivalent to a multiple of the design load, that means the specimen is stressed over the testing time with factored loads. The testing time is specified to be 2000h at a temperature of 60°C. For the concrete a high alkaline cement ($\text{Na}_2\text{O} = 1\%$) is used with a water cement ratio higher than 0.45, leading to the highest possible ph value. During the test the concrete is water saturated and cracked, leading to realistic additional bond stresses.

Under the assumption that these conditions are representative of a lifecycle, the conclusion is that the rebar can withstand the design load for the entire service life. After the ageing process the rebar is tested for residual strength. The characteristic value of this tensile strength divided by the material factor has to be higher than the design load. As an example, the results presented in Figure 1 lead to a design value of 350 N/mm² [Weber 04].

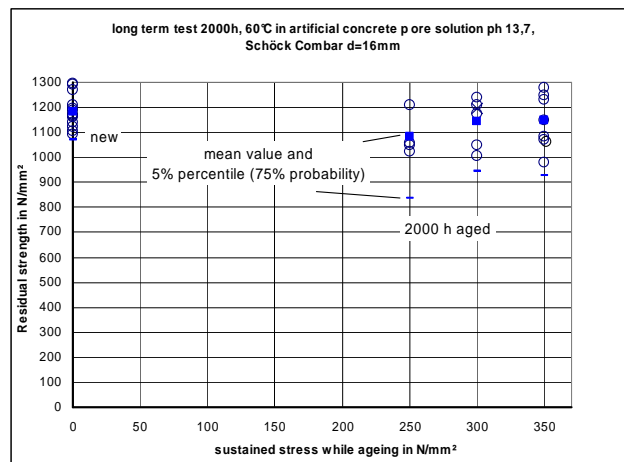


Figure 1 Load influence on Residual Strength of Aged Specimen

This simple approach leads to secure and conservative results for “normal” conditions. This means normal indoor climate or outdoor climate with mean annual temperatures around 10°C. If a more economic design is desired, or conditions differ from these “normal” conditions in central Europe or Northern America, a new approach, which takes the special conditions for each particular application including all the environmental influences into account, has to be chosen.

3. NEW APPROACH BASED ON STRESS RUPTURE TESTS

In the ACI Test Guide [ACI 2004] two different tests are interesting regarding durability. The first is the so called durability test. The second is the so called creep rupture test. It is difficult to understand why creep rupture and durability should be tested separately. Why should creep rupture be tested outside of the concrete environment? Creep rupture tests of GFRP rods show different limits for air, water and concrete [Renaud and Greenwood 2005]. The environment during the creep rupture test is particularly essential to a secure and conservative design value. In addition for the design engineer no second check for creep rupture has to be performed if the design values are secure long term values (including creep rupture) [ACI 2003].

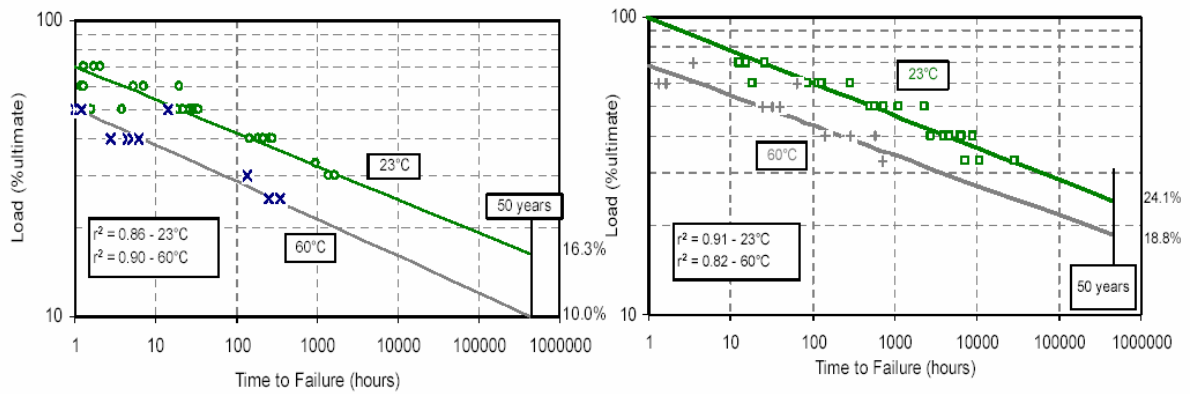


Figure -2 Shape of different stress endurance test curves of two different 6,4mm GFRP rods in cement solution in log/log scale. Examples left for E-glass fibres in UP-resin, right for ECR-glass fibres in UP-resin. (Renaud and Greenwood 2005)

It is clearly to be seen that the slopes of all lines are similar, while the curves are shifted to the left side due to higher temperatures or weaker durability.

It is proposed that FRP should be designed for durability on the basis of a simple design strength equation that multiplies the safety-factored tensile strength by a factor which is linked to various environmental parameters that increase or decrease the factored tensile strength depending on the aggressiveness of the exposure environment and the diameter, as follows. As no value for 1000h load capacity in creep tensile tests is known this value can be estimated from the tensile strength:

$$f_{td} = f_{tk} / \eta_{1000h} / \eta_{env} / \gamma_{frp} \quad (1)$$

simplified to:

$$f_{td} = f_{tk1000h} / \eta_{env} / \gamma_{frp} \quad (2)$$

where:

f_{td} = design value of tensile strength

f_{tk} = characteristic value of tensile strength

f_{tk} = characteristic value of load capacity for 1000h

η_{env} = environmental strength reduction factor

η_{1000h} = environmental strength reduction factor for 1000h sustained load

γ_{frp} = material factor (1,25)

The environmental strength reduction factor η_{env} , is obtained using the following equation. An exponential approach is used, because deterioration is described best by the kinetics of the chemical and physical processes.

$$\eta_{env,t} = 1 / (100\% - R_{10})^n \quad (3)$$

Where R_{10} is the standard reduction of tensile strength in percent per decade due to environmental influence, the exponent n is the sum of the different influence terms: n_{mo} is the term for moisture condition, n_T is the term for temperature and n_{SL} is the term for desired service-life (Table 1). As a rule of thumb $n=3$ for "normal" conditions.

$$n = n_{mo} + n_T + n_{SL} + n_D \quad (4)$$

Table 1: examples for environmental design terms

Material	f_{tk}	f_{1000h}	R_{10}	Moisture Condition	n_{mo}	MAT °C	n_T	Service life in a	n_{SL}	Dia-meter	n_D
	N/mm ²	N/mm ²	%/dec								
CFRP	2000		5	Dry	0	0	0,7	1	-1	Half	0,6
AFRP	2000		10	Outdoor	1	10	1	10	0	Same	0
GFRP 1	1250	1000	18	Wet	2	20	1,4	50	0,7	Double	(-0,6)
GFRP 2	700	300	25			30	2	100	1		

That means for testing that stress rupture tests have to be performed in wet concrete and the basic parameter, the R10 value and the 1000h value, have to be determined with a good probability. For the rebar from figure 1 this is done for different temperatures (fig. 3 and 4). [Weber 2005, Byars 2006].

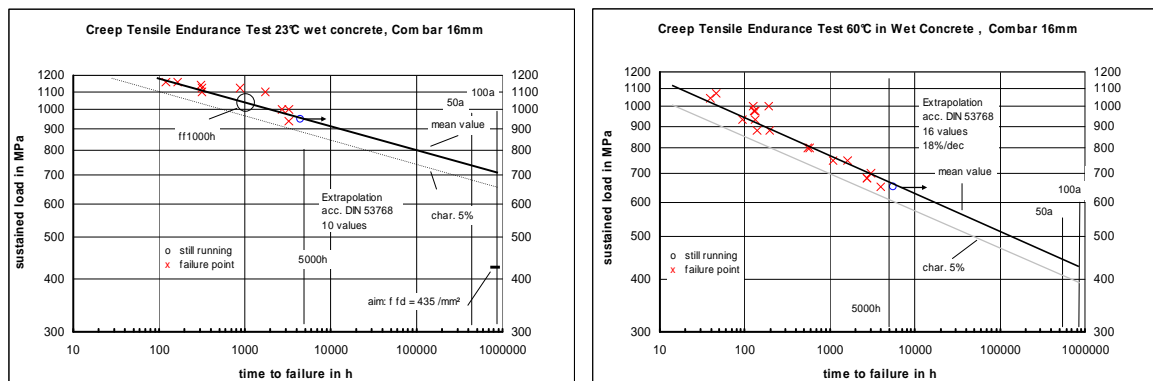


Figure 3 and 4: Stress Rupture Performance of the same Rebar as in fig. 1 for Room Temperature and 60°C

4. DISCUSSION

For specific conditions and especially for normal conditions a durability test under load can lead to secure design values. The assumption is that the whole service life is simulated in an accelerated long term test. The residual strength and the load while testing yield a sufficiently safe design value. Defining the design value solely as a percentage of the virgin strength, however, is not necessarily safe. 10 years of experience in applications under normal conditions without reduction in residual strength will not lead to adequate indications for the following 90 years.

For a detailed environmental design another approach has to be chosen. Time, temperature, humidity and bar diameter have an essential influence on the design value of the tensile strength. The proposed approach does not use time temperature shifting. Based on experimental data as well as on theoretical deterioration kinetics the proposed approach takes all the above mentioned parameters into account leading to secure design values for each and every application. In Canada other values are required than in Florida, while indoor applications need other design values than marine applications.

5. REFERENCES

- [ACI 2003] American Concrete Institute (2003), ACI 440.1R03 “Guide for the Design and Construction of Concrete Reinforced with FRP Bars”, Committee 440,
- [ACI 2004] American Concrete Institute (2004), ACI 440.3R-04 “Guide Test Methods for Fiber-Reinforced Polymers (FRPs) for Reinforcing or Strengthening Concrete Structures, Committee 440
- [CSA 2002] Canadian Standards Association, S806-02 Design and Construction of Building Components with fibre-Reinforced Polymers, Toronto 2002
- [Byars et al. 2006] Byars et al. fib Task Group 9.3. Draft: Design and use of Fibre Reinforced Polymer Reinforcement (FRP) for Reinforced Concrete Structures. FRP Reinforcement for RC Structures. Chapter 3 Durability: Performance and Design, February 2006
- [Renaud and Greenwood 2005] Renaud C and Greenwood M (2005). Effect of Glass fibres and Environments on Long-Term Durability of GFRP Composites Proc. 9. EFUC Meeting Wroclaw PL 11/2005
- [Weber 2004] Weber A. Bewehrungsstäbe aus GFK - Materialverhalten und Anwendungsgebiete, Proceedings. SKZ IBK Symposium, Leipzig 2004
- [Weber 2005] Weber A. GFK-Bewehrung - Bemessung und Anwendung, in Faserverbundwerkstoffe Hrsg.: Dehn, Holschemacher, Tue, Bauwerk Verlag Berlin 2005

Durability Assessment of Adhesives and Reinforcement at the FRP-Wood Interface

Gary M. Raftery (Gary.Raftery@nuigalway.ie),
(*PhD Candidate, Department of Civil Engineering, National University of Ireland, Galway, Ireland*)

Annette M. Harte,
(*Senior Lecturer, Department of Civil Engineering, National University of Ireland, Galway, Ireland*)

Peter D. Rodd,
(*Lecturer, Department of Civil Engineering, National University of Ireland, Galway, Ireland*)

ABSTRACT

Pultruded glass fibre reinforced composites can be used for reinforcing low-grade wood. In composite design, it is imperative that a successful bond is established between the component materials. This paper describes a test program to assess the bond quality between glass fibre reinforced polymers and spruce that contains large juvenile wood proportions. Durability testing involved cycling specimens five times by a vacuum-pressure-soak-drying procedure. Two pultruded reinforcing materials were selected for the study both comprising glass fibres aligned unidirectionally, one in a vinylester resin and the other, in an engineered thermoplastic polyurethane. Bond tests were executed using both wood laminating adhesives and two-part structural epoxies. The tests results show that the bond depends not only on the adhesive in question but also the FRP type. In general, the durability tested specimens failed at equal or lower shear strengths than solid control specimens, ambient tested wood-wood bond specimens or ambient tested FRP-wood bond specimens that were taken from the same plank. Failure modes included wood failure, reinforcement failure and adhesion failure.

KEYWORDS

Fiber Reinforced Plastics, Adhesive Bonding, Durability, Wood

1. INTRODUCTION

Glass fibre reinforced composites are ideally suited to the reinforcement of low-grade glue-laminated timber beams due to their superior mechanical properties, low-weight, ease of handling and corrosion resistance. An adhesive, and surface preparations that permit hygrothermal compliance, are essential to accommodate the shear and peeling stresses that occur at the FRP-wood interface when the wood is subject to fluctuating environmental conditions. The commercial viability of the reinforcement process would be considerably enhanced if a single adhesive system could be used for bonding both the wood laminations and the FRP-wood interface. This would be particularly true if commercial wood laminating adhesives could be utilised at the FRP-wood interface in contrast to more expensive epoxy adhesives which are generally used in FRP-wood connections. Only limited results have been published on bond tests regarding fibre reinforced plastics and low grade wood containing large proportions of juvenile wood. Therefore, this research focuses on quantifying the durability performance of commercially available adhesives when bonding viable reinforcing FRP materials and Irish grown Sitka spruce.

2. TEST PROGRAMME

The experimental programme undertaken involved the assessment of bond via the block shear test and comprised four test phases. These involved the testing of solid shear specimens, ambient wood-wood bonded specimens, ambient FRP-wood bonded specimens and finally durability tested FRP-wood bonded specimens.

Two pultruded fibre reinforced plastic materials were selected for the study comprising glass fibres aligned unidirectionally in a vinyl ester resin (GFRP) and in an engineered thermoplastic polyurethane (FULCRUM). The FRP selection was based on optimising cost versus mechanical properties (tensile modulus and tensile strength). Both FRP materials were stored in the laboratory environment of $65\pm 5\%$ relative humidity and temperature of $20\pm 2^\circ\text{C}$, while wrapped in protective cling-film. All the testing utilised the same batch of Irish grown Sitka Spruce conditioned also in an environment of $65\pm 5\%$ relative humidity and temperature of $20\pm 2^\circ\text{C}$. This is the service environment in which the FRP-reinforced glulam beams are thought most likely to be utilised.

The adhesives examined comprised five conventional wood laminating adhesives and three structural epoxies. All the adhesive manufacturers were confident that their products would form a good bond between the FRP materials and the wood. Two phenol resorcinol formaldehydes (PRFs), a melamine urea formaldehyde (MUF), a polyurethane (PU), and an emulsion polymer isocyanate (EPI) were the wood adhesives selected. In all instances, the instructions stated in the adhesive technical data sheets and the recommendations of the adhesive manufacturers were followed rigidly. For each adhesive and FRP combination under study, five number wood-wood bonded specimens, twenty number ambient tested FRP-wood bonded and ten number durability tested FRP-wood bonded specimens were tested from the same plank. Ten solid shear specimens, which were also cut from the same plank, were directly compared with the results. The solid shear strength test set-up was designed to be consistent with the adhesive bond tested specimens (Okkonen & River, 1989). The bonded assemblies were manufactured and tested with reference to a recognised block shear test standard (ISO, 2001). A solid test specimen width of 40mm was utilized because of a size restraint. Specimen dimensions are illustrated in Figure 1. The thickness of the FRP material, y , was 3mm for the GFRP and 1.2mm for the FULCRUM. A wood backing piece of thickness, x , was used to give a total $(x+y)$ thickness of 20mm.

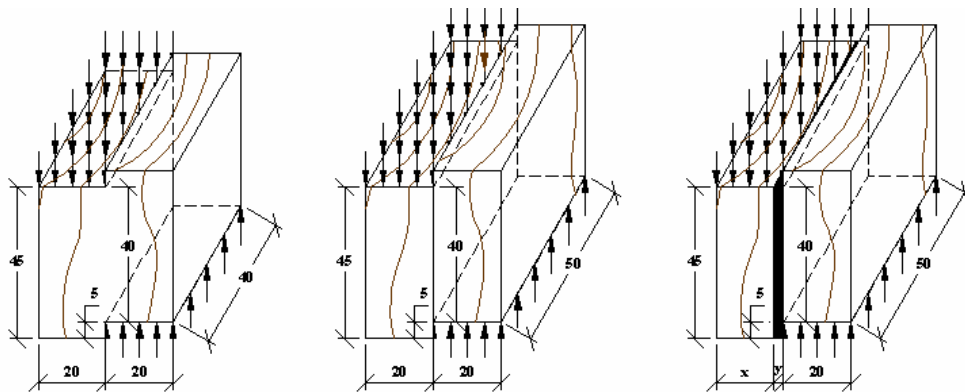


Figure 1: Test Specimens: (a) Solid, (b) Wood-Wood (c) FRP-Wood

Surface preparation of the GFRP material prior to bonding involved gently abrading and then cleaning with methylated spirits. The FULCRUM material was simply wiped clean with methylated spirits because of its inherently rough surface. Clear, defect free wood was carefully selected to promote the highest quality bonding. The wood surface was planed parallel to the grain directly before the bonding process to ensure that the gluing face was uniformly smooth and free from contamination.

The durability test utilised a modified EN 391 procedure (CEN, 2001). FRP-wood test specimens were initially subjected to a vacuum pressure of 70kPa whilst submerged in water followed by pressure soaking at 600kPa. The specimens were subsequently dried for 90 hours in an environmental chamber at $25\pm 5\%$ relative humidity and $35\pm 5^\circ\text{C}$ temperature. The procedure was then repeated five times. Test specimens were finally left to recondition for a minimum of 15 days in an environment of $65\pm 5\%$ relative humidity and a temperature of $20\pm 2^\circ\text{C}$ prior to testing. All specimens were sheared parallel to the grain at constant loading rates such that the test specimen had a target failure time of 60 ± 20 seconds (ISO, 2001). Controlled rate of load was preferred over rate of crosshead displacement as a more progressive application of the load is achieved with the former. A quantitative assessment of the percentage adherend failure, estimated to the nearest five percent of the shear plane area, was executed on each sample. Shear strength of the fractured specimens was calculated based on the assumption of a uniform stress distribution and an instantaneous failure over the theoretical shear plane.

3. EXPERIMENTAL RESULTS AND DISCUSSION

The shear strengths obtained and adherend percentage failure assessments from the tests executed with the GFRP and the FULCRUM material when bonded with the wood laminating and epoxy adhesives are presented in Figures 2-9.

KEY: A=Solid Specimens, B=Ambient tested Wood-Wood Specimens, C= Ambient Tested FRP-Wood Specimens, D=Durability Tested FRP-Wood Specimens, I = Standard Deviation

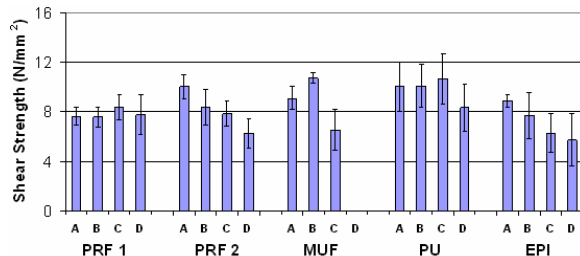


Figure 2: Shear strength vs. Adhesive – GFRP with wood adhesives

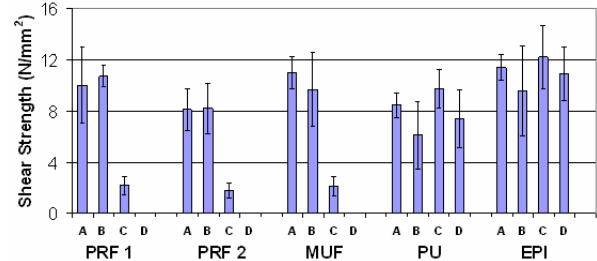


Figure 3: Shear strength vs. Adhesive – FULCRUM with wood adhesives

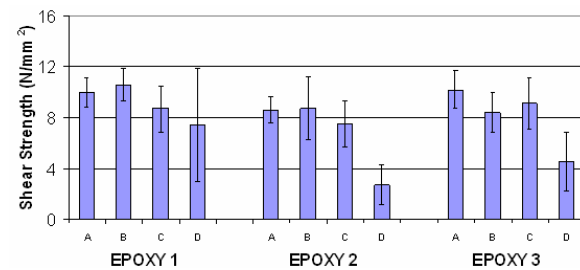


Figure 4: Shear strength vs. Adhesive – GFRP with epoxy adhesives

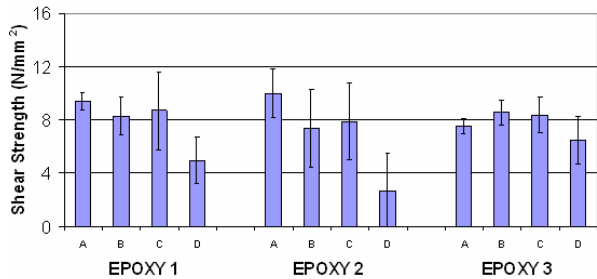


Figure 5: Shear strength vs. Adhesive – FULCRUM with epoxy adhesives

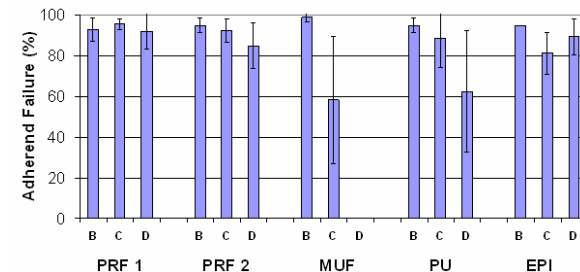


Figure 6: Adherend Percentage Failure vs. Adhesive – GFRP with wood adhesives

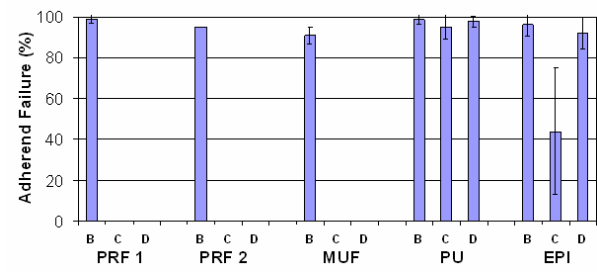


Figure 7: Adherend Percentage Failure vs. Adhesive – FULCRUM with wood adhesives

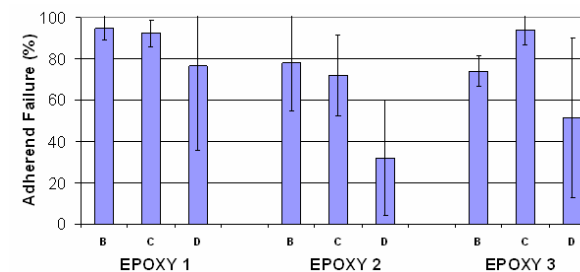


Figure 8: Adherend Percentage Failure vs. Adhesive – GFRP with epoxy adhesives

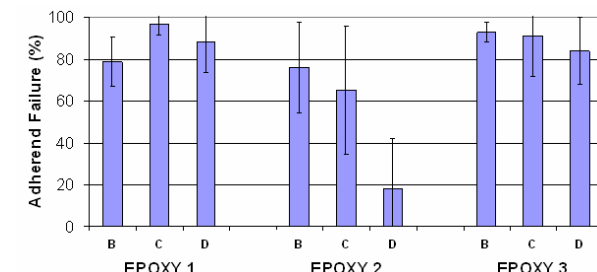


Figure 9: Adherend Percentage Failure vs. Adhesive – FULCRUM with epoxy adhesives

The mean shear strength for PRF 1 bonded GFRP-wood durability tested specimens was marginally higher than for solid specimens and wood-wood bonded specimens from the same board. It also compared well to ambient tested

GFRP-wood bonded specimens. All the MUF bonded durability tested GFRP-wood specimens failed during the moisture cycling procedures. For the remaining wood laminating adhesives, durability tested GFRP-wood bonded specimens failed at lower shear strengths (38% lower for PRF 2, 17% lower for PU and 35% lower for EPI) than those of the solid specimens, ambient tested wood-wood specimens and ambient tested GFRP-wood specimens. With regard to the epoxy bonded GFRP-wood specimens, the durability tested specimens failed at lower shear strengths than the ambient tested GFRP-wood bonded specimens. The difference was particularly significant for Epoxy 2 bonded specimens (60% lower) and Epoxy 3 bonded specimens (55% lower). Adherend failure percentages of the durability tested specimens were favourable (over 80%) for the PRF adhesives and EPI adhesive and compared well with ambient tested wood-wood specimens and ambient tested GFRP-wood specimens. Large variability existed in the results for the PU adhesive which obtained an average failure of 63%. The adherend failure results obtained from the epoxy adhesives were also susceptible to large variations. For example, for Epoxy 3, one specimen failed in adhesion during the moisture cycling while another failed with an adherend failure of 95%.

The PU and EPI adhesives exhibited the highest bond quality for the bond shear strength tests executed with the FULCRUM material when bonding with the conventional wood laminating adhesives selected for the study. In contrast to the tests executed with the GFRP, the PRFs displayed a poor bond quality between the FULCRUM and the wood after being subjected to the hygrothermal stresses of the durability test. It was noted that all samples bonded to the FULCRUM material with both the PRF adhesives and MUF adhesive failed in adhesion while being subjected to the moisture cycling. The durability tested epoxy bonded specimens had lower shear strengths than solid specimens, ambient tested wood-wood specimens and ambient tested FULCRUM-wood specimens from the same plank. Epoxy 3 exhibited the best performance of the three epoxies in terms of strength retention after durability testing. It is believed that Epoxy 2 would exhibit an improved performance if thicker bond lines were used. Due to the premature failure of the PRF and MUF bonded specimens during durability testing, zero adherend percentage failure was assigned to these test samples. The durability tested PU and EPI adhesives displayed excellent adherend percentage failure results with the EPI bonded specimens achieving even better results than the ambient tested FULCRUM-wood specimens. The high percentage adherend failures obtained when bonding with Epoxy 1 and Epoxy 3 showed that strong durable bonds were formed. The average failure for Epoxy 2 bonded FULCRUM-wood specimens were under 20% for the reason above discussed.

4. CONCLUSIONS

Significant differences in the results for the ultimate shear strengths and adherend failures percentages between the two FRP types illustrates that bond integrity depends not only on the adhesive in question but is also substrate specific. In general, the durability tested specimens failed at equal or lower shear strengths than solid control specimens, ambient tested wood-wood specimens or ambient tested FRP-wood specimens taken from the same plank. It is seen that strong durable bonds can be formed at the FRP-wood bond interface when using specific conventional wood laminating adhesives which can exceed the performance of that obtained from bonding with more expensive epoxy adhesives. It is noted that the durability test used in this study is an accelerated aging test and the hygrothermal stresses induced on the tested specimens are considered extreme. The test results provide an excellent assessment of the resistance to hygrothermal stresses at the FRP-wood interface.

5. ACKNOWLEDGEMENTS

The authors would like to sincerely thank COFORD; National Council for Forest Research and Development, Coillte and the Irish Research Council, Science, Engineering and Technology (IRCSET) for sponsorship.

6. REFERENCES

- CEN, European Committee for Standardization (2001), Glued laminated timber, Delamination test of glue lines, EN 391.
- International Organisation for Standardisation (2001), Adhesives; Wood-to-wood adhesive bonds; Determination of shear strength by compressive loading, ISO 6238.
- Okkonen, E. Arnold and River, Bryan H. (1989), Factors affecting the strength of block-shear specimens. *Forest Products Journal* 39 (1):43-50.

DURABILITY OF STEEL MEMBERS STRENGTHENED BY CFRP STRIPS UNDER MECHANICAL AND ENVIRONMENTAL LOADINGS

Pierluigi Colombi

(Associate Professor, Politecnico of Milan, Milan, Italy)

Giulia Fava

(PhD Student, Politecnico of Milan, Milan, Italy)

Carlo Poggi

(Full Professor, Politecnico of Milan, Milan, Italy)

ABSTRACT

CFRP strips are effective both in restoring the lost capacity of damaged steel sections and in strengthening structural members to increase the load-carrying capacity. One of the major points of concern in the use of CFRP strips is related to the durability under various environmental conditions.

The paper discusses experimental results related to steel elements strengthened using CFRP materials. In particular, double side reinforcements and double shear lap joints were quasi-statically tested in tension after exposure to thermal cycles or immersion in salt spray fog or a combination of both. Results of fatigue tests performed on unconditioned double side reinforcements are also presented.

From the analysis of the static tests, it is evident that the salt spray fog conditioning and even more its combination with thermal cycling produced a detrimental effect on the final behavior of the adhesive in transferring loads from the steel to the CFRP. Thermal cycles do not seem to produce particular changes in the adhesive. The fatigue tests showed a significant stiffness reduction of the reinforced bar due to the progressive debonding of the adhesive.

KEYWORDS

CFRP, Steel, Durability, Debonding, Adhesive.

1. INTRODUCTION

Structural rehabilitation of steel structures may be necessary when design and constructional errors have been detected or to increase the load carrying capacity but also in the case of degradation due to corrosion or fatigue damage. The use of fiber reinforced polymer composites as reinforcing elements in a wide variety of constructions posed several questions on the durability of the bond in aggressive environments. The environmental degradation is difficult to evaluate experimentally since laboratory tests are limited in time and may not reflect the real process. This paper presents the results of a series of experiments performed by the authors at the Milan Technical University in order to characterize the bonding properties of epoxy resin used in the reinforcement of steel structures by CFRP strips. Double side reinforcement of continuous steel plates and double side shear lap joints were studied. The specimens were preconditioned by thermal cycles and/or immersion in salt-spray fog environment. The fatigue resistance of continuous reinforcements was also studied.

2. EXPERIMENTAL PROGRAM

The specimens were designed to reproduce the geometry of real applications, such as tension flanges of beams under bending or completely cracked sections repaired by CFRPs. A set of double side reinforcements and double side shear lap joints was preconditioned in salt-spray fog environment and/or subjected to thermal cycles and then tested under tensile loading. Finally, unconditioned double side reinforcements were subjected to fatigue test.

1.1 Materials

The specimens were made with Fe E 275 steel plates. The nominal Young's modulus was assumed equal to 210000 MPa and the tensile strength of (minimum value) 430 MPa with a Poisson ratio equal to 0.3. The specimens were prepared using two pultruded CFRP plates (Sika® CarboDur®). The nominal values of the Young's modulus and the tensile strength are greater than 200 GPa and 2800 MPa, respectively (SIKA Corporation, 2006). The Poisson's ratio of the overlays was assumed equal to 0.3. The overlays were bonded to the steel plates using a thixotropic epoxy resin (Sikadur® 30). The nominal value of the Young's modulus was 12800 MPa while the tensile and shear strengths (after a curing period of 7 days at 35 °C) was 35 MPa and 22.5 MPa, respectively (SIKA Corporation, 2006). The Poisson's ratio of the adhesive was assumed equal to 0.35.

1.2 Specimens Geometry and Preparation

The length of the reinforcing plates was chosen to ensure the full transfer of the stress to the reinforcing strips. The specimen dimensions are reported in Fig. 1.

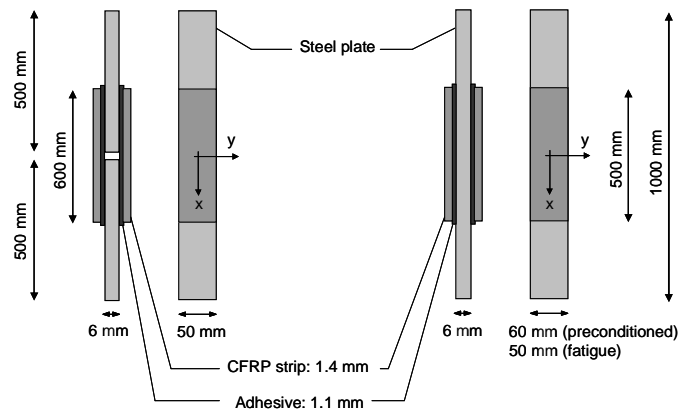


Figure 1 – Double side shear lap joint geometry and double side reinforcement geometry (not to scale).

To prepare the specimens, the steel surfaces were treated by an abrasive disk and degreased by a solvent while FRP plates were sandblasted. The bonding operation was performed just after the surface preparation without using any adhesive promoter (e.g. primer). The specimens for the static tests were artificially aged in an environmental chamber in order to study the environmental effects on bond performance. Salt spray fog with a relative humidity equal to 95 % and a salt concentration (NaCl) of 5 % was used to simulate the effect of high humidity on bond strength in presence of salt, while thermal cycles of 12 hours each between -20 °C (6 hours) and +50 °C (6 hours) were applied to investigate the effect of thermal variations on bond strength. Table 1 summarizes the conditioning treatment for each specimen, where DSR and DSL stand for double side reinforcement and double side shear lap joint, respectively.

Table 1: Description of environmental treatments for each of the specimens under study

Specimen	Specimen type	Thermal Cycles -20 °C (6 h) + 50 °C (6 h)	Salt Spray Fog [H ₂ O] = 95 % ; [NaCl] = 5 %
UC	DSR	---	---
ΔT1	DSR	20 cycles	---
ΔT2	DSR	30 cycles	---
NS1	DSR	---	2 weeks
NS2	DSR	---	3 weeks
NSΔT	DSR	20 cycles	2 weeks (after the thermal cycling)
JUC	DSL	---	---
JNS2	DSL	---	3 weeks
JNSΔT	DSL	20 cycles	2 weeks (after the thermal cycling)

3. STATIC TESTS

Uniaxial tension static tests were performed under displacement control with a constant rate equal to 0.008 mm/sec. Specimens were equipped with strain gauges to monitor the load transfer from the steel to the overlays and to control the bond conditions between the two adherents. Concerning the double side reinforcements, during the loading process a linear response was registered up to the yielding of the steel. Gradual debonding of the CFRP strips was then detected on both sides starting from the ends. Tests were stopped after the complete debonding of both CFRP plates. The inspection of the adherents surfaces revealed perfect interface fracture at the steel-adhesive interface for all the tested specimens. The strain gauge response of specimen preconditioned by thermal cycles is in good agreement with the one of an unconditioned specimen (Colombi and Poggi, 2006), while specimens preconditioned by salt spray fog show an overall lower ductility (Figure 2). In Figure 2 the recorded displacement was normalized with respect to the steel elastic strain at the relevant load level. In particular, the combined effect thermal cycling and salt spray fog had an additional detrimental effect since the thermal cycles produce microcracks in the adhesive promoting then water diffusion (Colombi et al., 2004).

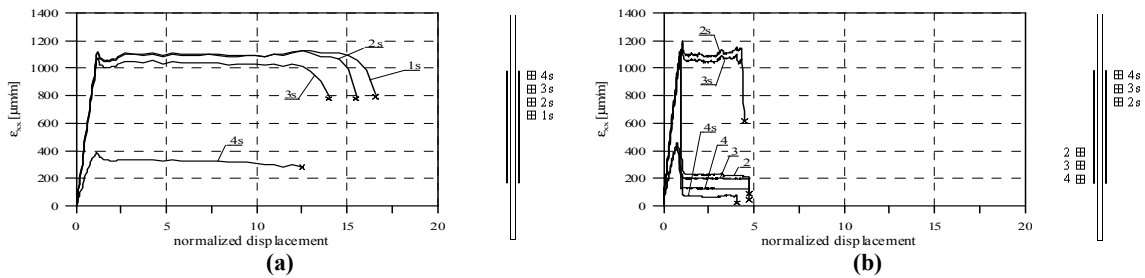


Figure 2 – Axial deformation vs normalized displacement for (a) UC and (b) NSΔT

In the double side shear lap joints, the gradual debonding of the CFRP plate started first from the gap, propagating towards the end of the reinforcement, and then at the strips ends, moving toward the gap. From the analysis of the fracture surface, in the gap zone cohesive delamination of the adhesive layer was observed while interface delamination was recorded at the reinforcement end. At last partial composite delamination was observed in the middle of the joint. A small stiffness reduction and a significant ductility reduction are representative of the bond degradation (Colombi et al., 2005). In Figure 3, specimens JNS2 and JNSΔT showed a relevant ductility reduction.

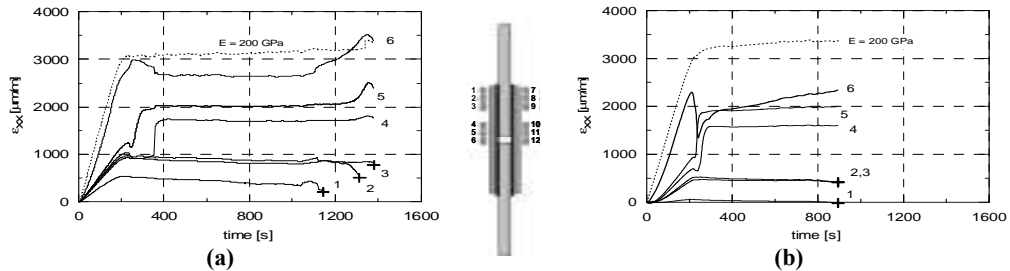


Figure 3 – Axial deformation vs normalized displacement for (a) JNS2 and (b) JNSΔT

4. FATIGUE TESTS

The fatigue tests were performed with an MTS servo-hydraulic closed-loop testing machine under sinusoidal loading control at room temperature. A total of four double side reinforcement specimens were subjected to constant stress range cycles of 83 or 100 MPa calculated in the steel section, while the R ratio was kept equal to 0.4. Therefore the corresponding values of the minimum and maximum loads are 17 kN and 42 kN for $\Delta\sigma = 83$ MPa and 20 kN and 50 kN for $\Delta\sigma = 100$ MPa. As in Figure 4, after 6 million cycles, the specimens subject to a constant stress range of 83 MPa did not present any sign of damage with a stiffness reduction of only 4 %. For $\Delta\sigma = 100$ MPa, failure initiation started at about 0.8 million cycles when CFRP plate debonding initiated on one side and then took place on the opposite one. A fatigue failure mechanism was observed to initiate with CFRP debonding at the plate

ends and propagate along the interfaces (Matta et al., 2004). Based on analytical models (Albat and Romilly, 1998), at end of the CFRP laminate the adhesive shear stresses vary between 4.68 and 11.57 MPa for $\Delta\sigma = 83$ MPa and between 5.51 and 13.78 MPa for $\Delta\sigma = 100$ MPa. Tests were stopped after CFRP debonding reached the midspan on both sides of the specimen, with a stiffness reduction of approximately 15 %. Debonding took initially place at those ends where the thickness of the adhesive appeared to be thin, without affecting the other ends where a more regular adhesive distribution contributes to reduce the stress concentration.

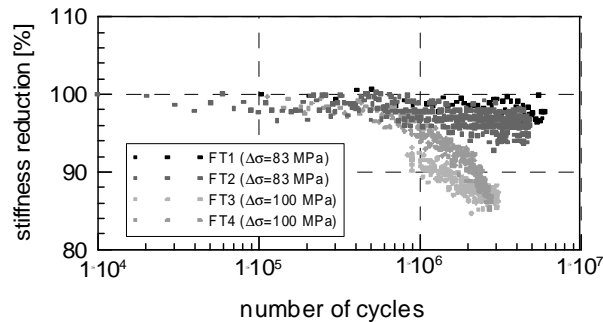


Figure 4 – Reduction in stiffness of retrofitted specimens during fatigue tests

5. CONCLUSIONS

Some of the major issues related to the durability of steel elements retrofitted using FRPs, have been discussed. Both under monotonic and cyclic loading conditions, the failure mechanisms refers to debonding of the CFRP strips in high stress concentration zones, as the plate ends or gap. Regarding the static tests, the thermal cycling of the specimens before testing did not seem to produce particular changes in the adhesive. On the other hand, salt spray fog conditioning and even more its combination with thermal cycling, produced a detrimental effect on the ductility of the specimen. Indeed, moisture or liquid water may infiltrate through micro-cracks in the adhesive at the bond line, leading to premature failure. The fatigue tests showed a significant stiffness reduction of the reinforced bar due to the progressive debonding of the adhesive. Stiffness degradation represents certainly an alert for a subsequent and progressive global failure.

6. ACKNOWLEDGEMENT

The financial support from the research project RELUIS (Italian Network of Seismic Engineering Labs) is gratefully acknowledged. Thanks are also expressed to Sika Italia for supplying the CFRP strips and the adhesive.

7. REFERENCES

- Albat A.M., Romilly D.P. (1998). “A direct linear-elastic analysis of double symmetric bonded joints and reinforcements”, *Composites Science and Technology*, Elsevier, Vol. 59, pp. 1127-1137.
- Colombi P., Fanesi E., Fava G., and Poggi C. (2004). “Steel elements strengthened by FRP materials: durability under mechanical and environmental loads”, *Mechanics of Masonry Structures Strengthened with FRP-materials: Modeling, Testing, Design, Control*, Editors: A. Di Tommaso, University of Venice, Italy, pp. 55-67.
- Colombi P., Fanesi E., Fava G., and Poggi C. (2005). “Durability of steel elements strengthened by FRP plates subject to mechanical and environmental loads” *Proceedings of Third International Conference on Composites in Construction*, Editors: L.R.K. Tiong, University of Lyon, France, pp 291-298.
- Colombi P. and Poggi C. (2006). “Strengthening of tensile steel members and bolted joints using adhesively bonded CFRP plates”, *J. of Constr. and Build. Mater.*, Vol. 20, pp. 22-33.
- Matta F., Karbhari V.M., Tinazzi D., and Vitaliani R. (2004) “Static and fatigue behaviour of steel/CFRP adhesive bonds for the rehabilitation of metallic bridges”. *Mechanics of Masonry Structures Strengthened with FRP-materials: Modeling, Testing, Design, Control*, Editors: A. Di Tommaso, University of Venice, Italy, pp. 411-420.
- SIKA Corporation. (2006). Technical data Sheets <http://www.sika.it/con/con-prod/con-prod-index.htm> 15/03/06

EFFECT OF SURFACE DETERIORATION ON STRESS TRANSFER BETWEEN CONCRETE AND FRP LAMINATE

Amnon Katz
Department of Civil and Environmental Engineering
National Building Research Institute
Technion – Israel Institute of Technology
Haifa 32000, Israel

ABSTRACT

Fiber Reinforced Laminates are widely used to strengthen concrete members suffering from deterioration. Stress transfer between the strengthened concrete and the strengthening laminate depends on the surface quality of the concrete. In the case of deteriorated concrete, stress transfer is complicated due to the gradient in its properties when going from the deteriorated surface to the healthy bulk concrete. This work presents the mechanism of stress transfer between carbon and glass FRP laminates and concrete with deteriorated surface.

Different modes of failure were identified, ranging from horizontal shear of the deteriorated concrete at the surface to diagonal shear of the beam. It was found that a significant amount of stress is transferred by friction within the deteriorated surface, leading to remarkable load-bearing capacities.

Keywords: FRP Laminates, Beam-Strengthening, Concrete, Deterioration

1. INTRODUCTION

Many studies have been conducted to investigate the mechanism of stress transfer between external reinforcement and concrete, first on steel sheet reinforcement (Swamy et. al, 1986; Van-Gemert and Vanden, 1986) and more recently on FRP (Chen et. al., 2001; Xie and Karbhari, 1998; De Lorenzis et al., 2001). These researchers realized the importance of proper stress transfer between the reinforcing system and the concrete.

Models predicting the behavior of externally reinforced beams were developed (Rabinovitch and Frostig, 2000; Mukhopadhyaya and Swamy, 2001), most of which deal with the overall behavior of a beam made of concrete (either cracked or solid) that is considered uniform throughout the cross section. Other studies (Chen et al., 2001; De Lorenzis et al., 2001; Jia et al., 2005), which specifically investigated the bond and stress transfer between external bonded sheets and concrete bodies, also dealt with solid bodies of concrete. According to the model developed by Bizindavyi and Neale (1999), the shear force between the FRP laminate and the concrete is transferred across a zone about 2-3 mm thick, thereby forming a separating zone whose mechanical properties must be taken into account when calculating the mechanism of stress transfer. Some researchers attributed the mechanical properties of this layer solely to the resin used to bond the FRP sheet to the concrete (De Lorenzis et al., 2001), although the properties of the concrete at the surface are generally different from those of the bulk concrete.

FRP laminates are widely used to strengthen concrete structures in various cases in which the surface of the concrete elements is severely deteriorated but the core concrete of such elements remains undamaged. Stress transfer from the surface to the core concrete through layers of varied strength influences the structural behaviour of the element. This study investigated the stress transfer between carbon and glass FRP laminates and the surface of deteriorated concrete beams. Better understanding of the stress transfer in these cases will enable better design for strengthening of concrete elements.

2. EXPERIMENTAL METHOD

Two types of notched concrete beams, 80X150X600 mm, were prepared for this study: solid and layered. The solid beams were made of a single type of concrete throughout the cross section, whereas the layered beams contained a

layer of weak concrete used to simulate the deteriorated surface. The bulk concrete of the solid and layered beams was prepared at three strength levels: 29.7, 46.4 and 76.8 MPa (compressive strength at 28 days), denoted as I, II and III, respectively. Compressive strength of the concrete layer that was used to simulate a deteriorated surface was 13.8 MPa and its tensile strength (determined by a pullout test according to ASTM C1583) was 1.23 MPa. These values are somewhat lower than the minimal values recommended by ACI 440.2 (17 and 1.4 MPa, respectively). An additional layer of concrete was cast between the surface layer and the bulk concrete in order to allow a gradual change in properties between the layers. The deteriorated layer and the intermediate layer were each about 10 mm thick.

After concrete curing, the surfaces to be tested were cleaned and glass or carbon fiber laminates were wet-laid. Additional anchoring wraps were applied on one side of the beam to force failure on the other side only. Bond breakers, 25 mm wide, were used on both sides of the notch to prevent local concentration of stress near the notch. A series of 18 strain-gages was applied to the sides of the beam within the tested zone to monitor strain development in the concrete at different locations and an additional 4 strain-gages were applied on the laminate itself. Figure 1 shows the test setup and arrangement of strain-gages. Most of the results were calculated as the average of three specimens.

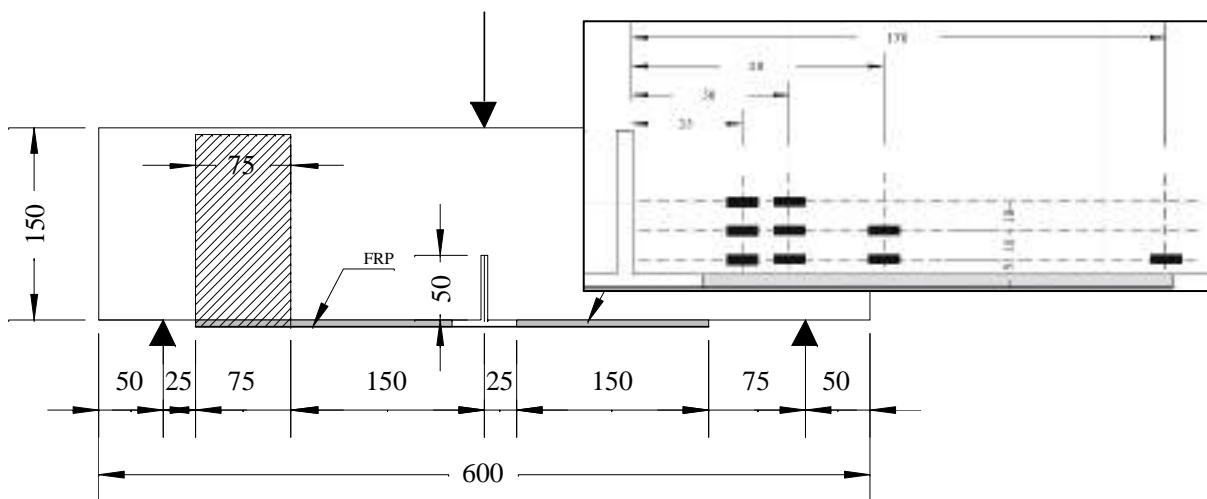


Figure 1: Test setup and strain-gages arrangement (mm).

3. RESULTS

3.1. Modes of Failure and Ultimate Loads

Three modes of failure were identified:

Mode 1: Failure of the bond at the interface between the epoxy layer and the concrete.

Mode 2: Failure of the concrete surface layer.

Mode 3: Failure by shear of the beam. The diagonal crack started close to the end of the laminate.

Failure by Mode 1 was typical to the high-strength (concrete III) solid beams; Mode 3 was typical to layered beams with relatively weak bulk concrete; Mode 2 was typical to all other beams, i.e. solid beams with relatively weak concrete or layered beams with strong bulk concrete. Failure within the concrete layer at the interface was expected to occur in layered beams, due to the weak concrete in this area. However, this type of failure was observed also in solid beams made of Type 1 concrete (30.5 MPa), which is much stronger than the ACI 440.2 recommendations.

Close examination of the specimens that failed by Mode 1 showed some concrete crumbs adhering to the end of the laminate, which indicate that local tensile stresses developed near the end of the laminate, as was analyzed by Rabinovitch and Frostig (2000). It is possible that similar stress development led also to the initiation of a crack near the end of the laminate in the layered beams. This crack begins to develop near the end of the laminate within the weak layer of the surface. When the crack is large enough, the cross section of the beam is reduced and the beam

fails by shear of the "healthy" concrete. If the bulk concrete is strong enough to support this load, failure will occur according to Mode 2.

Figure 2 presents the ultimate load at failure of the tested beams. A decrease in the ultimate load-bearing capacity was seen with layered beams reinforced with carbon laminates as the strength of the bulk concrete increased. All layered beams reinforced with glass laminates exhibited similar ultimate loads regardless of concrete strength. The ultimate load of solid beams reinforced with glass laminate was not affected by concrete strength, and only the high-strength concrete reinforced with carbon laminate exhibited higher ultimate loads compared with the other carbon-reinforced solid beams. Beams reinforced with carbon laminates exhibited somewhat higher ultimate load-bearing capacities than did those reinforced with glass laminates.

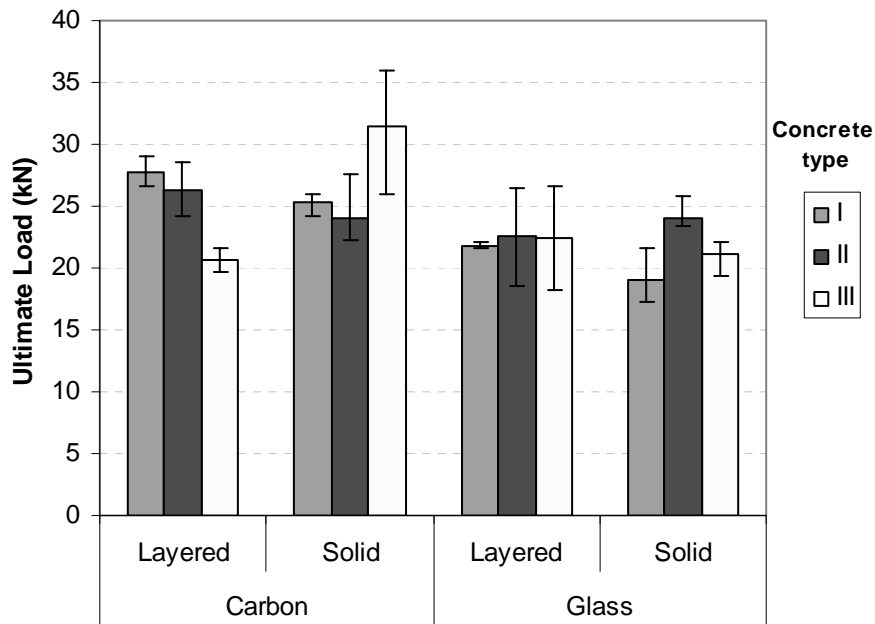


Figure 2: Ultimate load of strengthened beams.

3.2. Strain distribution in concrete layers

Strain development in the concrete layers was measured by a series of strain-gages as seen in Figure 1. Figure 3 presents the strain distribution in a layered beam reinforced by a carbon laminate at two load levels. At low loads, tensile strain begins to develop at some distance from the notch and as the load increases, greater tensile strain develops closer to the notch, until the concrete fails proximate to the notch in the weak layer. Tensile strain begins to develop away from the notch (near SG3/line 1 in Figure 3), however, compression strain was measured closer to the notch (SG2/line 1). Despite debonding in the area close to the notch, strain measured in the laminate indicates that strain continues to increase towards the notch along the unbonded area. This indicates a possible stress transfer between the laminate and the concrete surface by means of a friction mechanism that enables the transfer of a significant amount of load.

4. CONCLUSIONS

The difference between the stiffness of the reinforcing system and that of the concrete surface plays an important role in transferring stresses between the layers. The presence of a weak and soft concrete layer between a layer of stiff laminate (carbon) on one side, and stiff concrete bedding on the other side, may lead to greater concentration of stress in that layer as the stiffness of the bedding concrete increases. As a result, the load-bearing capacity of the beam may decrease.

A significant proportion of the shear stress was transferred by a mechanism of friction at the external concrete layer after initial failure of this layer. Measurements of the longitudinal strain in the layers of concrete indicated a

complicated situation of stress transfer with simultaneous action of external and internal shear forces and moments. A model simulating this stress distribution is currently under development.

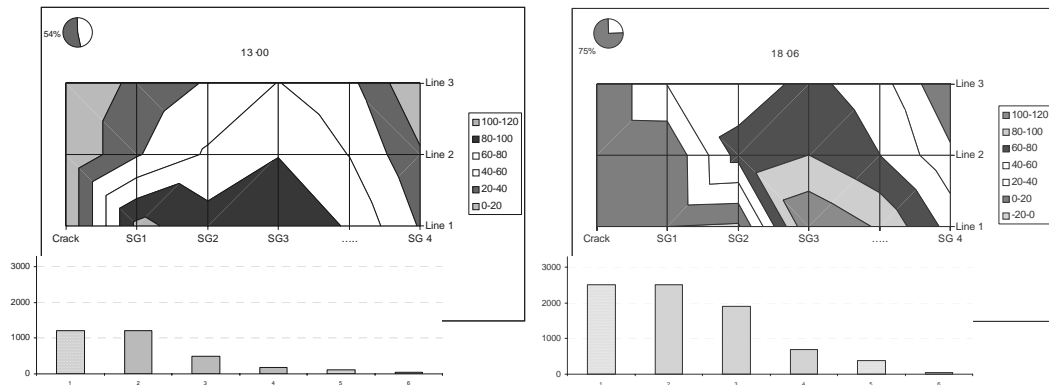


Figure 3: Strain distribution in the concrete layers (area diagram) and along the laminate (bar diagram below) in a layered beam reinforced with carbon laminate (concrete strength II). Load level is indicated at the top of each diagram. Some of the points were calculated by interpolation.

ACKNOWLEDGMENT

This work was partially supported by the Israeli Ministry of Construction and Housing.

REFERENCES

- ACI 440.2R-02, 2002, "Guide for the design and construction of externally bonded FRP systems for strengthening concrete structures", American Concrete Institute, Farmington Hills, MI, USA.
- Bizindavyi, L. and Neale, K. W., 1999, "Transfer lengths and bond strengths for composites bonded to concrete", *Journal of Composites for Construction*, Vol. 3, No. 4, pp. 153-160.
- Chen, J. F., Yang, Z. J., Pan, X. M. And Holt, G. D., 2001, "Effect of test methods on plate-to-concrete bond strength", *Proceedings Fibre-Reinforced Plastics for Reinforced Concrete Structures – FRPRCS-5*, Burgoyne C. J. (Editor), Thomas Telford, London, Vol. 1 pp. 429-438.
- De Lorenzis L., Miller B. and Nanni A., 2001, "Bond of fiber-reinforced polymer laminates to concrete", *ACI Materials Journal*, Vol. 98, No. 3, pp. 256-264.
- Mukhopadhyaya, P. and Swamy N., 2001, " Interface shear stress: a new design criterion for plate debonding", *Journal of Composites for Construction*, Vol. 5, No. 1, pp. 35-43.
- Jia, J., Boothby, T. E., Bakis, C. E., and Brown, T. L., 2005, "Durability evaluation of glass fiber reinforced-polymer-concrete bonded interfaces", *Journal of Composites for Construction*, Vol. 9, No. 4, pp. 348-359.
- Rabinovitch, O. and Frostig, Y., 2000, "Closed-form high-order analysis of RC beams strengthened with FRP strips", *Journal of Composites for Construction*, Vol. 4, No. 2, pp. 65-74.
- Swamy, R. N., Jones, R., and Bloxham, J. W., 1987, "Structural behaviour of reinforced concrete beams strengthened by epoxy-bonded steel plates" *The Structural Engineer*, London, 65A(2), 59–68.
- Van-Gemert, D. and Vanden B. M., 1986, "Long-term performance of epoxy bonded steel-concrete joints", *Proceedings, Adhesion Between Polymers and Concrete*, Chapman & Hall, London, p. 518-527.
- Xie, M. and Karbhari, V. M., 1998, "Peel test for characterization of polymer composite/concrete interface", *Journal of Composite Materials*, Vol. 32, No. 21, pp. 1894-1913.

Part IX. Fatigue Issues

FATIGUE BEHAVIOR OF EXTERNALLY BONDED STEEL FIBER REINFORCED POLYMER (SFRP) FOR RETROFIT OF REINFORCED CONCRETE

Kent A. Harries

(Assistant Professor, Department of Civil and Environmental Engineering, University of Pittsburgh)

Patrick L. Minnaugh

(Graduate Research Assistant, Department of Civil and Environmental Engineering, University of Pittsburgh)

ABSTRACT

Steel fiber reinforced polymer (SFRP) strips comprised of multiple high-strength wires have been introduced into the repertoire of the structural engineer in recent years. The deleterious effects of fatigue loading on FRP-to-concrete bond have been identified in previous studies by the author; therefore the effect of fatigue loading on the bond behavior of SFRP is investigated. Four large-scale beam specimens (4.9 m long) having externally bonded SFRP retrofits are tested. These specimens are paired with unretrofit and CFRP-retrofit companion specimens allowing a number of direct comparisons to be made. Of the SFRP specimens, one is tested in monotonic loading to failure while the remaining three are tested at various fatigue load levels ranging from service load level to an extreme load level. Service load fatigue is cycled for two million cycles and the specimen is then tested monotonically to failure to assess the effects of fatigue on the ultimate performance of the beam. Extreme loading is selected to result in fatigue-induced failure of the internal reinforcing steel.

KEYWORDS

Bond, Fatigue, Retrofit, Steel Fiber Reinforced Polymer (SFRP)

1. INTRODUCTION

Steel fiber reinforced polymer (SFRP) composite materials have been introduced as an alternative to glass and carbon fiber reinforced polymer (GFRP and CFRP) composite materials (Hardwire 2002). Initial research (e.g.: Huang et al. 2005) has indicated that SFRP is comparable to FRP materials as a measure for the flexural retrofit of reinforced concrete members. SFRP is bonded to the tension surface of concrete members and through composite action increases the effective reinforcing in the member active in resisting post-retrofit loads. Like all bonded applications, the effectiveness of SFRP is only realized as long as the bond remains sound. Bond behavior and debonding failures are known to be critical for FRP materials (e.g.: Oehlers 2005). Some retrofit applications may be subject to transient or fatigue load conditions. Previous studies by the author (Harries 2005) have clearly demonstrated the deleterious effects of fatigue loading on FRP-to-concrete bond. Debonding failures have been identified in cases where the transient stress level in bonded CFRP is only 10% to 14% of the material's capacity (Quattlebaum et al. 2005). Additionally, deterioration has been observed in cases where the stress level is as low as 4% of the FRP capacity (Harries and Aidoo 2005). For this reason, the fatigue behavior of SFRP-retrofit concrete sections may also be a concern. This study is believed to be the first to address the fatigue-induced degradation of SFRP performance.

1.1 Steel Reinforced Polymer (SFRP) Material

SFRP consists of high performance steel cord reinforcement embedded in a polymer matrix. The polymer matrix provides continuity to the final composite product and serves as the adhesive to affix the SFRP to the concrete substrate. The steel reinforcement used in this investigation is a high carbon steel cord with a micro-fine brass or AO-brass (Adhesion Optimized) coating. The cord is made by twisting 5 individual wires together - 3 straight filaments wrapped by 2 filaments at a high twist angle (Hardwire 2002). Properties of the SFRP composite and FX adhesive system used are provided in Table 1 along with properties of comparable preformed CFRP strip materials and adhesives specified for the CFRP applications.

Table 1: Manufacturer reported material properties of SFRP, CFRP and adhesives.

	tensile strength	tensile modulus (E_f)	elongation at rupture	thickness (t_f)	width used (b_f)	axial stiffness ($EA = E_f t_f b_f$)
SFRP	1138 MPa	75.5 GPa	0.014	1.2 mm	121 mm	10963 kN
CFRP	2792 MPa	155.1 GPa	0.018	1.4 mm	50 mm	10857 kN
Adhesive FX (SFRP)	31 MPa	not reported	0.025	≈0.8 mm	-	-
Adhesive L (CFRP)	14 MPa	2.2 GPa	0.063	≈1.6 mm	-	-
Adhesive H (CFRP)	25 MPa	4.5 GPa	0.010	≈1.6 mm	-	-

2. EXPERIMENTAL PROGRAM

Four reinforced concrete beams having externally bonded SFRP flexural retrofits are reported. Additionally a number of beams having equivalent CFRP retrofit measures are reported. The beams are 254 mm deep, 152 mm wide and are supported over a simple span of 4540 mm. All beams have 3 - #4 (12.7 mm dia.) primary reinforcing bars. The internal steel had yield and ultimate strengths of 429 MPa and 667 MPa, respectively. Twenty-eight day concrete compressive strength determined from cylinders was 23.3 MPa. Specimen and retrofit geometries are shown in Figure 1. The SFRP and CFRP material properties are reported in Table 1. As shown in Figure 1, the SFRP application was 121 mm wide while the comparable CFRP application was 50 mm wide. These applications are equivalent in terms of axial stiffness (EA) as indicated in Table 1. For the CFRP specimens, the “2” and “2x1” specimens (Fig. 1) performed similarly (Harries et al. 2006); thus both are reported here for a more comprehensive comparison. The SFRP was applied using “Adhesive FX” while the CFRP applications were applied using either “Adhesive L” or “Adhesive H”. Because the SFRP is relatively flexible and “porous”, a thinner and more uniform adhesive bondline (following subtle contours of the substrate concrete) was obtained than in the CFRP applications. Nonetheless, all adhesive systems used were found to perform well.

All beams were tested in three point flexure over a 4540 mm simple span. Applied load, midspan displacement and coincident reinforcing bar and SFRP/CFRP strains were recorded. Specimens reported in Table 2 were tested under cyclic fatigue loading conditions. The applied load at midspan was cycled between the minimum and maximum values shown at rate between 1.2 and 1.7 Hz (depending on the test). Specimens reported in Table 3 were tested under increasing monotonic load to failure. Specimens S4F, L2F and H2x1F did not exhibit a fatigue-induced failure prior to 2,000,000 cycles and were subsequently tested under increasing monotonic load to failure (Table 3). A complete description of the test programs reported here is found in Minnaugh (2006).

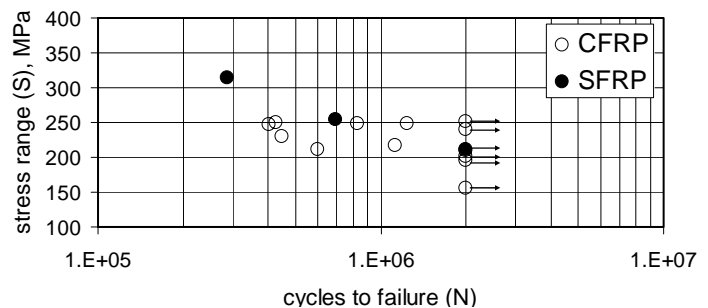
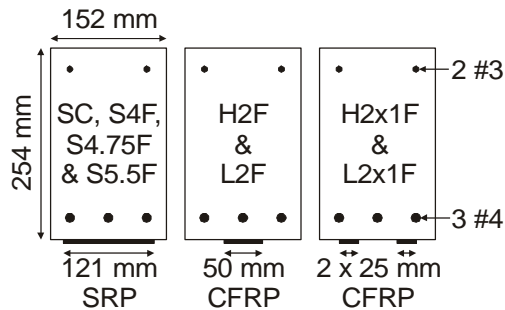


Figure 1: Test specimen and retrofit geometry. Figure 2: S-N behavior of SFRP and CFRP retrofit beams.

3. EXPERIMENTAL RESULTS

Key results from the fatigue and monotonic tests are presented in Tables 2 and 3, respectively. For the fatigue tests, the reinforcing steel and SFRP/CFRP stress ranges (as determined from measured strains using the moduli reported in Table 1 and assuming $E = 200$ GPa for the internal reinforcing steel) and the apparent beam flexural stiffness (determined as the slope of the line between the load and displacement at the lower and upper limits of the applied fatigue loading) at both the initial fatigue cycle ($N = 2$) and at the final measure fatigue cycle ($N = N_f$) is presented. The initial cycle is reported as $N = 2$ since the first cycle, $N = 1$, is required to crack the beam section and thus has a different apparent stiffness. For the monotonic tests, the ultimate deflection is defined as that corresponding to a post-peak load of 80% of the peak load attained. Displacement ductility is defined as the ratio of the ultimate displacement to that at general yield. The SFRP/CFRP debonding strain reported is interpreted as the *greatest SFRP/CFRP strain observed while still bonded to the concrete*, and thus represents a lower-bound on the strain to initiate debonding.

Table 2: Summary of key results from fatigue tests.

Specimen Designation		CF ¹	S4F	S4.75F	S5.5F	L2F	H2F	L2x1F	H2x1F
retrofit/adhesive type (Table 1)		none	SFRP/FX	SFRP/FX	SFRP/FX	CFRP/L	CFRP/H	CFRP/L	CFRP/H
minimum-maximum applied load (kN)		4.5-22.2	4.6-22.1	4.6-25.4	4.5-28.6	4.6-22.2	4.6-22.2	4.5-22.2	4.6-22.2
N=2	rebar stress range (MPa)	241	190	238	286	207	199	207	220
	SFRP/CFRP stress range (MPa)	n.a.	83	98	113	170	188	176	199
	secant stiffness (kN/mm)	1.42	1.77	1.64	1.62	1.70	1.51	1.55	1.61
final cycle, N _f		329324	2M	689671	286306	2M	1128006	447695	2M
N=N _f	rebar stress range (MPa)	n.a.	211	254	315	240	217	230	251
	SFRP/CFRP stress range (MPa)	n.a.	98	85	123	190	206	187	224
	secant stiffness (kN/mm)	n.a.	1.50	1.48	1.48	1.35	1.37	1.42	1.38

¹due to a power failure, Specimen CF was loaded to failure at N = 329,324 prior to fatigue-induced reinforcing bar rupture.

Table 3: Summary of key results from monotonic tests.

Specimen Designation	C	SC	S4F ¹	L2	H2	L2x1	H2x1	L2F ¹	H2x1F ¹
retrofit/adhesive type (Table 1)	none	SFRP/FX	SFRP/FX	CFRP/L	CFRP/H	CFRP/L	CFRP/H	CFRP/L	CFRP/H
maximum load (kN)	31.0	47.4	46.6	44.3	43.4	45.5	45.2	45.5	45.3
ultimate deflection (mm)	78.2	55.8	53.4	56.9	55.3	64.7	56.1	67.3	51.3
displacement ductility	2.61	1.67	1.58	1.70	1.60	1.89	1.70	2.05	1.45
SFRP/CFRP strain at debond (μ ϵ)	n.a.	3000	3170	6690	3550	7880	3200	4300	3910

¹monotonic test following 2,000,000 cycles of fatigue conditioning as described in Table 2.

Figure 2 shows the observed S-N (stress range on internal reinforcing steel – cycles to failure) behavior of the SFRP specimens and a number of CFRP retrofit specimens (including those reported in Table 2) having the same dimensions, reinforcing and retrofit details and loading protocol (Harries et al. 2006; Quattlebaum et al. 2005). As is expected, the fatigue behavior is governed by the behavior of the existing internal reinforcement in all cases. The SFRP specimens have essentially the same behavior as the equivalently retrofit CFRP specimens. As indicated in Table 2, the reinforcing bar stress range increases coinciding with a decrease in apparent beam stiffness as the specimens are subject to fatigue loading (increasing N). The SFRP/CFRP stress range is also seen to increase with cycling, reflecting the continued composite behavior of the retrofit system. The SFRP is less stiff than the CFRP, requiring greater material width to affect the same retrofit stiffness but resulting in lower shear stress being transferred through the adhesive and into the concrete substrate.

Load-displacement relationships for the monotonic SFRP-retrofit control Specimen SC, a representative equivalent CFRP-retrofit Specimen L2 and the unretrofit control Specimen C are shown in Figure 3(a). The SFRP-retrofit specimen exhibits a stiffer flexural response having a marginally greater ultimate capacity. Deflection capacity and ductility are similar to the CFRP retrofit specimen. Similar behavior is observed in the monotonic test of Specimen S4F following two million cycles of fatigue conditioning shown in Figure 3(b). Specimen S4F exhibits essentially identical response to representative CFRP-retrofit Specimen L2F in the initial cycle (N = 1) and through the fatigue conditioning process. The deflection offset following fatigue conditioning is approximately the same, 8 mm, in both cases. In the final monotonic load to failure, SF4 achieves a greater ultimate capacity although exhibits less deformation capacity than L2F. It is noted, however, that L2F exhibited greater deformation capacity than other similar specimens reported in Table 3. Figure 3(c) shows the load deflection cycles for S4.75F and S5.5F. In each case, the ultimate deflection achieved prior to fatigue-induced reinforcing bar rupture was approximately 24 mm. This deflection is approximately the same deflection achieved by Specimen SC at the initiation of reinforcing bar yield and reinforces the observation that the deflection at fatigue failure is well-estimated by the monotonic yield deflection (Quattlebaum et al. 2005).

3.1 Debonding of SFRP/CFRP

No debonding of the SFRP was evident during any stage of fatigue loading. This observation is in contrast to debonding observed during fatigue loading of the CFRP-retrofit specimens identified in Table 2 (Zorn 2006). Due to the greater width of SFRP required to affect the same retrofit, the interfacial shear stress is reduced. As seen in Table

2, even at the greater stress range loading (S4.75F and S5.5F), the SFRP stress remained well below that of the comparable CFRP specimens.

In the monotonic tests reported in Table 3, SFRP debonding is observed at comparably lower strains than in the CFRP specimens. This lower debonding strain is believed to result from the combination of a stiff adhesive and thinner adhesive bondline (Table 1) and reflects the importance of concrete substrate properties on debonding behavior. Nonetheless, the increased beam capacity, similar deflection capacity and no apparent debonding during fatigue conditioning indicate that the SFRP-adhesive system may be tougher than the comparable CFRP system. This latter effect is believed to result from the lower interfacial stresses developed.

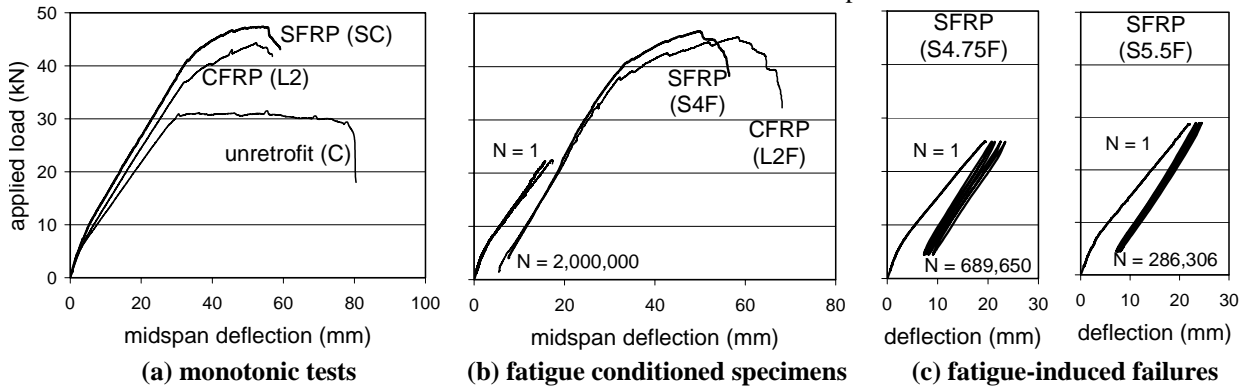


Figure 3: Load-deflection behavior of SFRP and representative companion CFRP specimens.

4. CONCLUSIONS

Steel fiber reinforced polymer (SFRP) flexural retrofit measures were compared with comparable CFRP measures subject to fatigue loading. The following primary observations and conclusions were drawn from this study:

1. SFRP is more axially flexible than CFRP resulting in a greater application width required to affect a comparable retrofit. This results in decreased interfacial stresses and improved fatigue behavior with no evidence of debonding for the (relatively high) stress ranges tested in this program.
2. The SFRP-retrofit specimens are initially stiffer than the comparable CFRP specimens resulting in a marginally increased ultimate capacity. The deformation capacity of comparable systems is, however, essentially the same.
3. A thinner and more uniform adhesive bondline was obtained with the SFRP system. This may account for both the marginally improved global beam behavior and the apparent earlier onset of debonding.
4. The previously-observed deleterious affects of fatigue loading on bonded CFRP systems appear less significant in bonded SFRP systems based on this initial limited study. More study is required to identify an appropriate reduction factor to account for fatigue effects on bonded SFRP systems.

6. REFERENCES

- Hardwire LLC (2002) *www.hardwirellc.com*, Pocomoke City, MD.
- Harries, K.A. (2005) "Fatigue Behavior of Bonded FRP Used for Flexural Retrofit" *International Symposium on Bond Behavior of FRP in Structures (BBFS 2005)*, December 7-9, 2005, Hong Kong. pp 555-560.
- Harries, K.A. and Aidoo, J. (2005) "Deterioration of FRP-to-Concrete Bond Under Fatigue Loading" *International Symposium on Bond Behavior of FRP in Structures (BBFS 2005)*, December 7-9, 2005, Hong Kong. pp 561-566.
- Harries, K.A., Zorn, A. and Reeve, B. (2006) "Effect of Adhesive Modulus on the Monotonic and Fatigue Behavior of Externally Bonded CFRP Strips" *Proceedings of the Third International Conference on FRP Composites in Civil Engineering (CICE 2006)*, December 13-15 2006, Miami, Florida, USA. paper #026.
- Huang, X., Birman, V., Nanni, A. and Tunis, G. (2005) "Properties and potential for application of steel reinforced polymer and steel reinforced grout composites" *Composites Part B*, Vol. 36 pp 73-82.
- Minnaugh, P. (2006) "Performance Characteristics of Steel Reinforced Polymer Composite Flexural Retrofit Measures Subject to Monotonic and Fatigue Loads" M.Sc. Thesis, University of Pittsburgh. December 2006.
- Oehlers, D.J. (2005) "Generic Debonding Mechanisms in FRP Plated Beams and Slabs" *Proceedings of the International Symposium on Bond Behavior of FRP in Structures*, December 7-9, 2005, Hong Kong. pp 353-44.
- Quattlebaum, J., Harries, K.A. and Petrou, M.F. (2005) "Comparison of Three CFRP Flexural Retrofit Systems Under Monotonic and Fatigue Loads" *ASCE Journal of Bridge Engineering*. Vol. 10, No. 6 pp 731-740.
- Zorn, A. (2006) "Effect of Adhesive Stiffness and CFRP Geometry on the Behavior of Externally Bonded CFRP Retrofit Measures Subject to Fatigue Loads" M.Sc. Thesis, University of Pittsburgh. April 2006.

Fatigue Performance of Concrete Bridge Deck Slabs Reinforced With Glass FRP Composite Bars

Amr El-Ragaby

Ph. D. Candidate, Department of Civil Engineering, University of Sherbrooke, Sherbrooke, Quebec, Canada

Ehab El-Salakawy

*Canada Research Chair Professor in Advanced Composite Materials and Monitoring of Civil Infrastructures,
Department of Civil Engineering, University of Manitoba, Winnipeg, Manitoba, Canada*

Brahim Benmokrane

*N SERC Research Chair Professor in Innovative FRP Composite Materials for Infrastructures, Department of Civil
Engineering, University of Sherbrooke, Sherbrooke, Quebec, Canada*

ABSTRACT

Recently, glass FRP (GFRP) bars have been widely used as internal reinforcement for concrete bridge deck slabs subjected to harsh environmental and loading conditions due to their lower cost compared to other kinds of FRPs. There is a lack of data on the performance of FRP-reinforced concrete structural members subjected to cyclic fatigue loading. This research is designed to investigate both the fatigue behavior and life of concrete bridge deck slabs entirely reinforced with GFRP bars. A total of five full-scale deck slabs (3000×2500×200 mm) were constructed and tested under concentrated cyclic loading until failure. Different scheme of variable amplitude cyclic loading as well as different reinforcement types (steel and GFRP), ratios and configurations for top and bottom reinforcement in both directions were investigated. Results are presented in terms of deflections, strains in concrete and FRP bars and crack widths at different levels of cyclic load.

KEYWORDS

Concrete, bridges, deck, FRP, fatigue.

1. INTRODUCTION

Fatigue performance is an important limit state that must be considered by designers of structures subjected to cyclic loading such as bridges. The most susceptible bridge element to fatigue loading is the deck slab since it directly sustains repeated moving wheel loads. FRPs, as non-corrosive materials, have been investigated by researchers as a potential substitute for steel reinforcement in concrete structures to overcome corrosion related problems. FRP materials possess the necessary property of high tensile strength that makes them attractive as structural reinforcement for concrete. The behavior of FRP-reinforced concrete elements is different from those reinforced with steel bars. This is mainly because the FRP materials have relatively low modulus of elasticity, small transverse strength, and different bond characteristics compared to those of steel (ACI 2003). As concrete bridge deck slabs are governed by long-term fatigue endurance and durability of constituent materials, it is necessary to understand the fatigue behavior of such structures especially when using new materials such as GFRP bars. This research is designed to study the fatigue behavior of concrete bridge deck slabs reinforced with different configurations of GFRP bars under fatigue loads.

2. DETAILS OF THE EXPERIMENTAL PROGRAM

2.1. Test Prototypes

The experimental program includes five full-size bridge deck prototypes (2500 mm width, 3000 mm length, and 200

mm thick). Four deck slab prototypes were reinforced with different reinforcement ratios and configurations of GFRP bars and one slab was reinforced with conventional steel bars as a control. Bottom and top concrete covers of 38 mm were used for all slab prototypes. The main bottom transverse GFRP reinforcement for the four GFRP reinforced decks, S1, S2, S3, and S4 was calculated based on the empirical design method recommended by the updated version of Section 16 of the CHBDC, Clause 16.8.7.1 (CSA 2006). This approach results in using 1#19 GFRP @150 mm in the bottom transverse direction with reinforcement ratio of 1.2%. The longitudinal bottom reinforcement for the four slabs consists of 1#16 GFRP @ 200 mm with a reinforcement ratio of 0.6%. For the top reinforcement layer, different configurations and reinforcement ratios were used. For slab S1 and S2, 1#16 GFRP @ 200 was used in both directions with a reinforcement ratio of 0.6% (slabs S1 and S2, had identical bottom and top reinforcement). For S3, a minimum reinforcement ratio of 0.3% was used in both directions, which results in using 1#13 GFRP @ 300 mm in each direction. Slab S4 had no top reinforcement. The control slab S0, reinforced with steel bars, was designed according to the empirical method of the CHBDC, Clause 8.18.4.2 (CSA 2000), which resulted in using 1#10M @ 210 mm in all directions.

2.2. Materials Properties

All test specimens were constructed using normal weight concrete with a targeted 28-day concrete strength of 37 MPa. Following the curing period in laboratory environment (14 days), all deck slab prototypes were stored outdoors in real environmental conditions for at least one year. This was done to simulate the environment that a real bridge will undergo to allow for the formation of concrete cracking that arise mainly from environmental conditions. Also, this storage period helped to stabilize the concrete properties (compressive strength and modulus of elasticity). The average concrete compressive and tensile splitting strengths, obtained from standard tests, were approximately 41 and 3.9 MPa, respectively. In addition to CSA grade 400 steel bars, sand-coated GFRP V-ROD™ (Pultrall Inc. 2004) was used. These GFRP bars are made of high-strength E-glass fibers (73% fiber by volume) with a modified vinyl ester resin, additives, and fillers using a pultrusion process. The GFRP bars have an average modulus of elasticity and ultimate strength of 45 GPa and 700 MPa, respectively.

2.3. Test Set-up and Repeated Fatigue Loading

All slabs were tested under a single concentrated load at the centre of a clear span of 2000 mm. This load was applied through a 75-mm thick steel plate that measures 250 × 600 mm, which is equivalent to the footprint of a wheel as specified by the CHBDC (CSA 2000). The edges of the slabs were partially restrained against lateral displacement using a special arrangement of steel sections and bolts (El-Gamal et al. 2005). Moving vehicular loads were simulated by stationary concentrated load varying cyclically in magnitude. In this research, an accelerated fatigue loading scheme was used. It consists of variable amplitude fatigue loading where all the slabs were subjected to sinusoidal waveform fatigue loading steps. Each step consists of 100,000 cycles with a minimum constant load level and peak variable load levels for each step. The peak loads were equivalent to the multipliers of the load level for fatigue limit state, P_{fls} ($P_{fls} = 87.5 * 1.4 * 1.0 = 122.5$ kN according to Clause 3.5.1 (CSA 2000). If the test prototype completed the last 100,000 at the largest peak load (490 kN) without failure, the test continued at the same peak load level until failure. This fatigue loading scheme was applied to all slabs except slabs S2 and S3. For slab S3, an extra 300,000 cycles at lower peak loads (100,000 at each of 122.5, 153.12 and 214.37 kN peak loads) were applied to the deck slab to assess the effect of cycling at lower peak load levels. For slab S2, 4,000,000 load cycles between a minimum load of 15 kN and a peak load of 122.5 kN at a rate of 4 Hz was applied. This fatigue loading scheme represents twice the fatigue life recommended by many researches for bridge deck slabs (Kumar and GangaRao 1998; Mufti et al. 2005).

3. TEST RESULTS AND OBSERVATION

Any deterioration of the deck slab would be evident from increasing of deflections, strains in reinforcing bars and concrete, crack widths as well as from the loss of deck stiffness with the increase of the number of load cycles or the peak loads. This deterioration will be referred to as damage and the overall progressive deterioration due to the total number of load cycles will be referred to as accumulated damage. These parameters were measured during the monotonic loading tests that were carried out at the end of each fatigue loading step. Figure (1) summarizes the number of cycles that each slab sustained under each fatigue load step until failure. It can be noticed that the steel reinforced slab, S0, has the shortest fatigue life compared to the other tested slabs as it sustained only 300,000 cycles at the first three fatigue loading steps and failed after only 120 cycles at the peak load of 450 kN. Slabs S1, S3 and S4 have similar results although they have different top reinforcement ratios. This similar behavior included slab S3,

which was subjected to additional 300,000 cycles at lower peak loads (100,000 at each peak load of 122.5, 153 and 214 kN). This may indicate that applying repeated loads with amplitude equal or up to 1.75 times the fatigue limit state has insignificant effect on the GFRP-reinforced concrete deck slabs. It should be also noted that after being subjected to 4,000,000 load cycles at the peak load of 122.5 kN, slab S2 did not fail.

Figure (2) shows a comparison between the static responses of the five tested slabs after the 367 kN fatigue load step. All GFRP-reinforced slabs had approximately the same fatigue damage although they have different reinforcement ratios in the top layers. It is clear that the damage accumulated to slab S1 and S4 was similar (both have the same residual deflection and stiffness) although slab S4 had no top reinforcement. Also Slab S3, which was subjected to more load cycles than S1 and S4, had the same accumulated fatigue damage. For the steel reinforced slab S0, it suffered more deterioration with an accumulated damage of about 2.5 times greater compared to the other tested slabs. This was mainly due to the big difference between the modulus of elasticity of steel and concrete and the mechanical bond mechanism, which causes much damage to concrete during cyclic loading.

Similar behavior and changes were observed for the maximum measured strains in reinforcing bars. Figure (3) shows comparisons between the maximum measured strains in the reinforcing bars in the transverse direction following the 183 kN fatigue loading step. Although slab S3 has completed 300,000 cycles (at lower peak load levels) more than slab S1, the difference in the measured strains in the GFRP bars did not exceed 10%. For the GFRP bars, the maximum recorded strain, which was approximately 2400 micro-strain, is still less than 20% of the ultimate strain. For steel, this value was 1700 micro-strain (approximately 85% of the yield strain of the steel). Also, the maximum measured strain in slab S1 was about three times that of slab S2. Figure (4) presents the maximum measured concrete strain in the transverse direction following the 367 kN fatigue loading step. The largest strain of approximately 1250 micro-strain was measured for the steel reinforced slab, S0. While the GFRP-reinforced slab without top reinforcement, S4, recorded the lowest value of about 400 micro-strain.

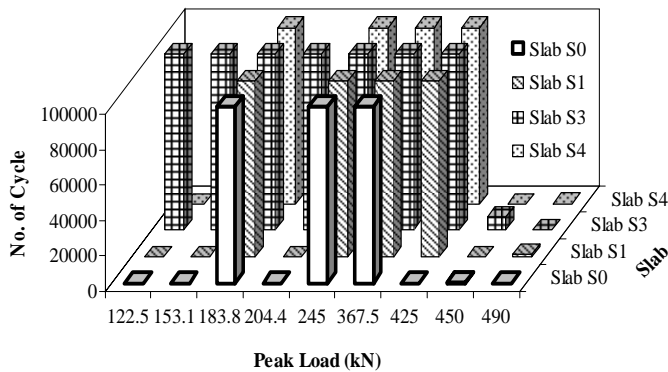


Figure 1. Number of cycles for all slabs to failure

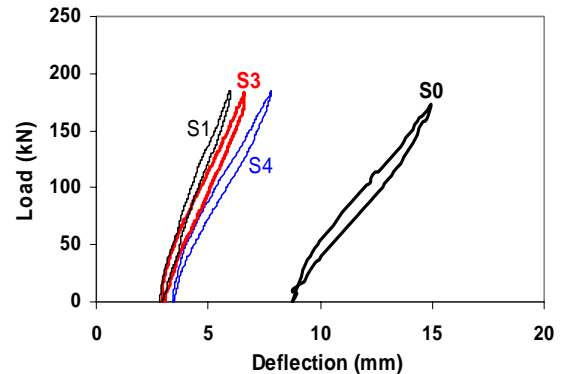


Figure 2. Comparison between static responses after 367 kN fatigue loading steps

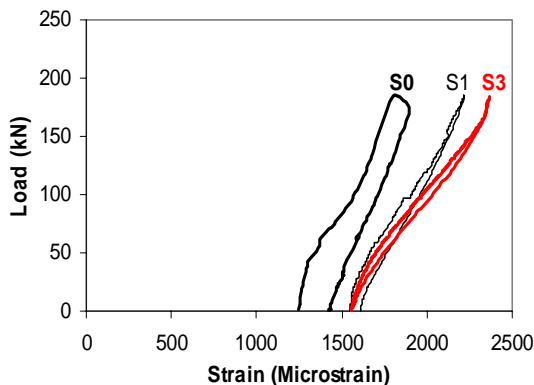


Figure 3. Comparison between transverse bar strains after 183 kN fatigue load step

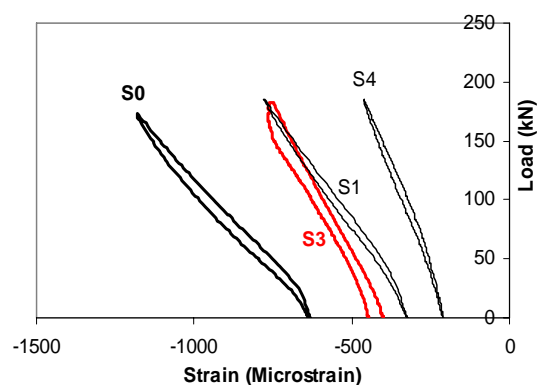


Figure 4. Comparison between compressive strains at top face of concrete after 367 kN fatigue load step

The cracks propagated and grew (became wider) with the increase of the number of load cycles and the peak load. At early stages of fatigue loading, cracks were observed on the bottom face of the deck where some major cracks

FAILURE PROCESS OF ADHESIVELY BONDED JOINTS FROM PULTRUDED GFRP ADHERENDS

Ye Zhang and Thomas Keller
*(Ecole Polytechnique Fédérale de Lausanne EPFL-CCLab,
CH-1015 Lausanne, Switzerland)*

ABSTRACT

Adhesively bonded joints are being used increasingly in civil engineering, especially for joints comprising pultruded glass-fiber reinforced polymer (GFRP) laminates. The layered material architecture, however, leads to a complex delamination failure within the pultruded material, thus necessitating understanding of the progressive failure mechanism of such joints under axial tensile loading. In this work, adhesively bonded joints composed of pultruded GFRP laminates, including double and stepped lap joints, were experimentally investigated. The static strengths of joints were obtained and the failure mechanism was understood. Crack propagation and back face strain gages were successfully employed to identify crack initiation and describe crack propagation, even though the failure mechanism was always brittle. The dominant failure mode for both types of joints was a fiber-tear-off failure that occurred in the mat layers of the GFRP laminates. The critical strain energy release rate was calculated and the resulting values from double lap and stepped lap joints compared very well.

KEYWORDS

Adhesive joints, failure, pultrusion, strength.

1. INTRODUCTION

Adhesively bonded joints are being used increasingly in civil engineering, especially joints composed of pultruded GFRP laminates. Due to the complicated material architecture of pultruded composites, it is important to understand the failure mechanism of the joints under both static and cyclic loading, as well as the progressive failure process considering crack initiation and propagation.

Considerable experience on the mechanical behavior of adhesively bonded FRP joints under static and fatigue loads has already been gathered for aerospace and automotive structures (Abdel-Wahab et al., 2004). However, when these applications are compared with adhesively bonded FRP joints in civil infrastructure, there are essential differences in the manufacturing process, the material architecture, the dimensions of the components and the application environments (Keller and Vallée, 2005). It is therefore urgent to fill the gap of knowledge regarding the fracture behavior of adhesively bonded joints for the civil engineering sector.

In the present work, the quasi-static behavior of adhesively bonded double and stepped lap joints from pultruded GFRP laminates and an epoxy adhesive are investigated. These types of joints are widely used in existing civil engineering structures, an example is shown in Fig. 1.

2. EXPERIMENTAL PROGRAM

Two types of specimens were investigated: balanced double lap joints (DLJ) and stepped lap joints (SLJ), both composed of pultruded GFRP laminates of 50 mm width and 6 or 12 mm thickness. The pultruded GFRP laminates (delivered by Fiberline A/S, Denmark) consisted of E-glass fibers embedded in an isophthalic polyester resin. A two-component epoxy was used (SikaDur 330 from Sika) for the specimens. The adhesive layer thickness was 2 mm. The dimensions and number of the specimens are shown in Fig. 2 and Table 1 respectively.

Four crack propagation gages (HBM/RSD20) were used to detect the crack initiation and propagation in three specimens of each joint type, as shown in Fig. 3 (labeled C) and Table 1. The crack propagation gages consisted of 20 wires, spaced at 1.15 mm intervals, perpendicular to the adhesive layer, and covered almost half of the overlap length. In each specimen, two back face strain gages (D) were placed above the locations where crack initiation was expected to influence the strain response and two more strain gages were used to measure the axial strains (A) outside the joint where the stresses were expected to remain uniformly distributed.

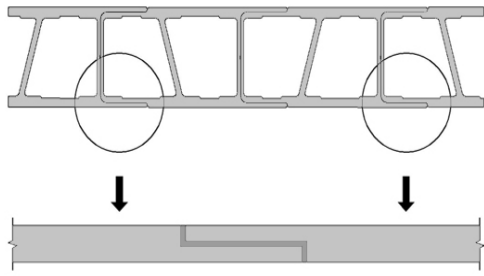


Figure 1: DuraSpan bridge deck with stepped lap joint

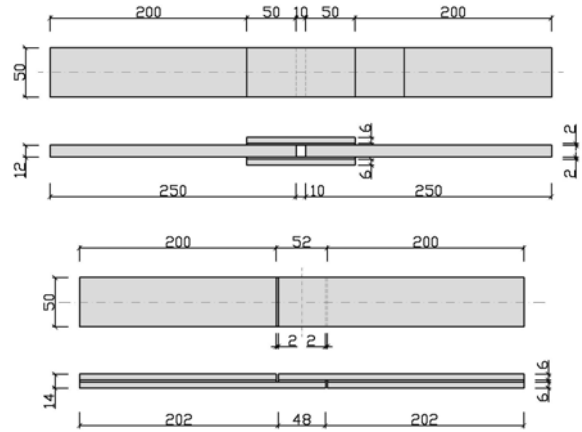


Figure 2: Double lap and stepped lap joint

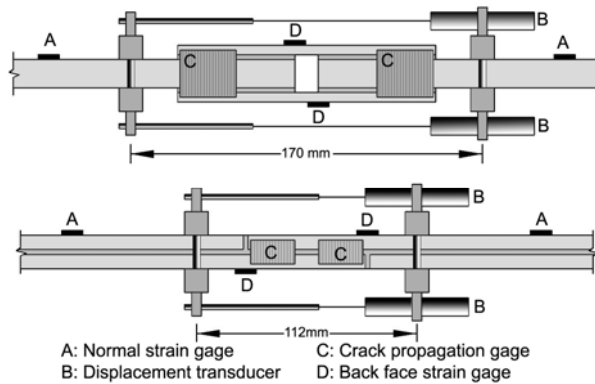


Figure 3: Experimental instrumentation for DLJ (above) and SLJ (below)

Furthermore, two displacement transducers (B) were employed to measure the elongation of the joint. An Instron Universal 8800 hydraulic machine was used to apply the axial force with a displacement rate of 0.5 mm/min for the SLJs and of 1 mm/min for the DLJs.

3. EXPERIMENTAL RESULTS

The double lap joints had an almost linear load-elongation response up to the failure, as shown in Fig. 4, which was very brittle. In contrast, the stepped lap joints exhibited a discontinuous two stage behavior, although the final failure was also brittle. For the SLJs, a failure in the adhesive in the two small gaps perpendicular to the longitudinal adhesive layer occurred, which was followed by a steep decrease of the load. After this first failure, however, the joints continued to sustain an increase in load, although the crack initiation and propagation led to a decrease in overall stiffness. The average static ultimate loads of the double lap and stepped lap joints were 45.6 kN and 10.5 kN respectively (see Table 1).

The typical failure modes of the DLJs and SLJs are shown in Fig. 5. For both types of joints, the dominant failure mode was a fiber-tear-off failure in the GFRP laminates. Failure initiation occurred in the two outer mat layers of the 12 mm laminates below the ends of the outer 6 mm laminates in the DLJs, and in the 6 mm laminates below the (already cracked) small gaps in the SLJs. Failure propagation then occurred in the same mat layers up to final joint failure. Failures were brittle and sudden and their initiation and propagation were normally not observable by the naked eye.

Figure 6 shows typical measured crack gage resistances with increasing load for the DLJs and SLJs. A jump in resistance occurred if one of the twenty wires of one gage was cut. The results from three of the gages on one of the DLJs are shown on the left. The crack initiated simultaneously on both sides of one joint end at a load of 26.9 kN (locations 1 and 2 in Fig. 6, left). The crack then did not grow up to approximately 41.5 kN. Subsequently, it propagated rapidly and cut the remaining gage wires up to final failure. On the other joint edge, crack initiation also occurred at 26.9 kN, but only at one side (3 in Fig. 6).

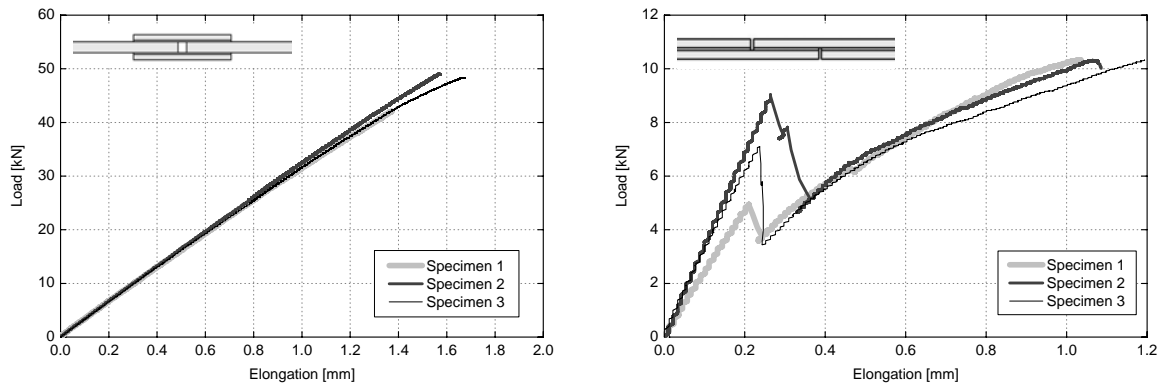


Figure 4: Selected load-elongation curves of DLJ (left) and SLJ (right)

Table 1. Ultimate loads of DLJ and SLJ (* with crack propagation gages)

Specimen	DLJ		SLJ	
	Ultimate load [kN]	Adhesive failure [kN]	Ultimate load [kN]	Adhesive failure [kN]
1 *	42.1	4.9	10.3	
2 *	49.0	9.0	10.3	
3 *	47.5	8.9	11.1	
4	45.1	7.0	10.2	
5	45.9	7.0	10.0	
6	43.7	5.1	10.9	
Average	45.6±2.0	7.0±1.9	10.5±0.5	

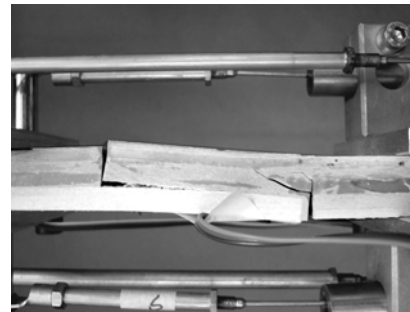
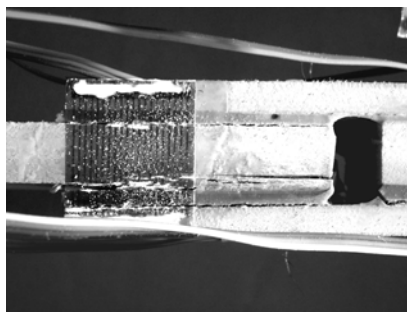


Figure 5: Failure modes of DLJs (left) and SLJs (right) (DLJ with broken crack gage)

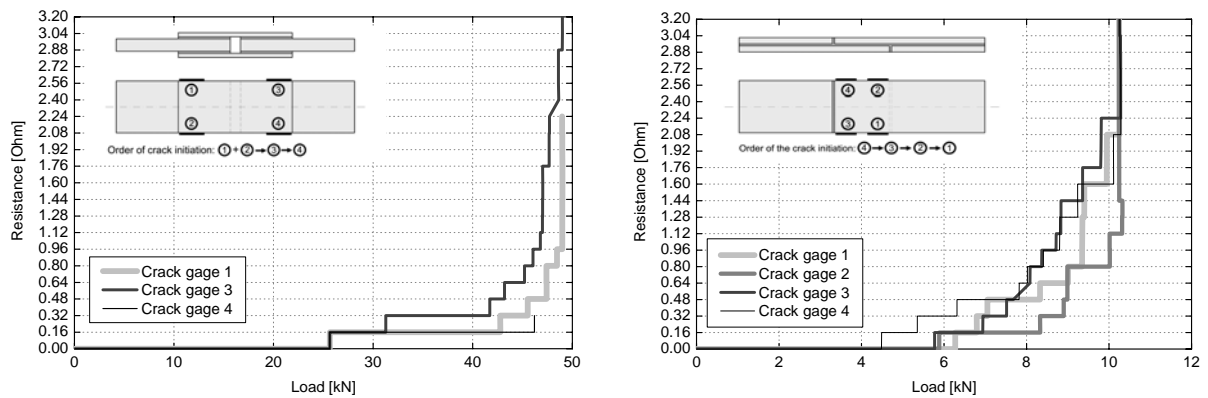


Figure 6: Measured crack propagation gage resistance versus load of typical DLJ (left) and SLJ (right).

Subsequently, only two more points were caught. The cutting of the remaining wires and of the wires of the fourth gage (4 in Fig. 6) could not be recorded due to the too rapid crack propagation, even at a measurement frequency of 800 Hz. For the SLJs, crack initiation in the laminates occurred on each of the four potential locations at a different load (between 4.7 and 6.3 kN). The cracks then propagated at different rates up to the ultimate load. The results from the back face strain gages are shown in Zhang and Keller (in review).

4. DISCUSSION

The dominant failure mode was the same fiber-tear-off failure in the outer mat layers of the laminates for both joint types. Comparing the ultimate loads of both joint types, the average DLJ ultimate load was more than two times higher than the double of that of the SLJ (the double has to be taken to equalize the shear surface). This much higher performance of DLJ was mainly due to the upkeep of a symmetric joint configuration. The adhesive failure in the small SLJ gaps led to a system change from a stepped lap to an asymmetric single lap configuration, showing much smaller stiffness and strength.

The crack initiation in the laminate could be caught by employing both crack propagation gages and back face strain gages. The measured average loads at which crack initiation in the laminates occurred according to crack propagation and back face gage measurements compared very well (see Zhang and Keller, in review).

The critical strain energy release rate values were calculated at a crack length of $a = 25$ mm for each crack, which corresponds to half of the overlap length (Hadavinia et al. 2003). The resulting average values were 804.9 [J/m²] for the DLJs and 721.9 [J/m²] for the SLJs. This small difference is supported by theory, which states that the critical strain energy release rate depends only on the material properties. That is, since the two joint types showed the same failure mode and failed in the same material, their two G_c values must be identical.

5. CONCLUSIONS

Adhesively bonded double and stepped lap joints composed of pultruded GFRP laminates and epoxy adhesives were experimentally investigated under quasi-static axial tensile loading. The following conclusions were drawn:

(1) Double lap joints showed a typical, almost linear behavior under axial tensile stresses, up to sudden and brittle failure. Stepped lap joint showed two stages of failure: adhesive failure in the small joint gap perpendicular to loading and failure of the whole joint. The gap failure changed the joint configuration from stepped lap to single lap with a corresponding decrease in joint stiffness and strength - a major drawback of this joint type. The dominant failure mode for both types of joints was a fiber-tear-off failure, which occurred in the outer mat layers of the GFRP laminates.

(2) Though the dominant failure mode of both types of joints was considered as very brittle and sudden, it was still possible to observe the crack initiation using both crack propagation gages and back face strain gages.

(3) The critical strain energy release rate, G_c , was calculated. The resulting values from double and stepped lap joints compared very well. The experimental results provided useful results to perform a numerical study on the progressive failure process in the next project stage.

6. ACKNOWLEDGEMENTS

The authors would like to thank the Swiss National Science Foundation (Grant No 200021-103866/1), Sika AG, Zurich (supplier of the adhesives) and Fiberline Composites A/S, Denmark (supplier of the pultruded laminates) for the support of this research.

7. REFERENCES

- Abdel-Wahab, M.M., Ashcroft, I.A., Crocombe, A.D., and Smith, P.A (2004). "Finite element prediction of fatigue crack propagation lifetime in composite bonded joints". *Composites Part A*, 35, 213-222.
- Hadavinia, H., Kinloch, A.J., Little, M.S.G., and Taylor, A.C. (2003). "The prediction of crack growth in bonded joints under cyclic-fatigue loading. II. Analytical and finite element studies". *International Journal of Adhesion & Adhesives*, 23, 463-471.
- Keller, T., and Vallée, T (2005). "Adhesively bonded lap joints from pultruded GFRP profiles, Part I: stress-strain analysis and failure modes". *Composites: Part B*, 36, 331-340.
- Zhang, Y., and Keller, T. (in review). "Progressive failure process of adhesively bonded joints composed of pultruded GFRP". *Composites Science and Technology*.

PREDICTION OF EXTENDED FATIGUE LIFE OF STRENGTHENED BRIDGE DECK WITH FRPs

Hongseob Oh

(Professor, Jinju National University, Jinju, Kyoungnam, Korea)

Jongsung Sim

(Professor, Hanyang University, Ansan, Kyeonggi-do, Korea)

Minkwan Ju

(Candidate of PH.D, Hanyang University, Ansan, Kyeonggi-do, Korea)

ABSTRACT

Concrete bridge decks are damaged directly by traffic loads. However almost all fatigue studies on model concrete decks have been performed under a concentrated pulsating load applied at a fixed point. Therefore, a fatigue analysis under a realistically simulated moving load is needed to evaluate the performance of a concrete bridge deck more accurately. In this study, a live load model was used to formulate an approach to calculating extreme load for various time periods. The maximum load effects for time periods from day one to 75 years are derived by extrapolations and simulations. In order to predict the strengthening effect of bridge decks strengthened with one fiber sheet, fatigue tests were performed and probabilistic and reliability analyses on the fatigue of concrete deck were carried out. According to the result of the analysis, strengthened concrete decks are found to have sufficient resistance effect against increasing truck during service life of the bridge.

KEYWORDS

live load model, concrete bridge deck, pulsating load, probability and reliability analysis.

1. INTRODUCTION

Because many previous studies to assess the fatigue performance of FRP strengthened deck panel are limited on the work in the laboratory and tested on the member subjected not the moving wheel loads is similar with real condition of bridge decks but the pulsating loads, it is hard to expect the strengthening effect obtained from the test to real bridge deck, when the verified strengthening techniques based on the test results applied on the real deteriorated bridge decks. These differences of strengthening effect occurred between in field and in laboratory mainly caused by either the workmanship of strengthening or the gap of boundary conditions or loading conditions. Especially, irregularity of traffic loads induced the structural deterioration of deck, including the velocity and the moving route as well as the weight, cannot be simulated in laboratory.

The properties of the decks were typical of bridges for secondary design truck, i.e., DB-18 given by the Korea Highway Bridge Specification. The applied design traffic load for this category is similar to the HS-20 truck in the AASHTO design specification. Fatigue failure of bridge deck gradually progressed not under ultimate loading state but under service loading state, and traffic load provided in design specification is only considered ultimate state to design the load carrying capacity of deck panel. Therefore, the model to simulate fatigue loads for either fatigue analysis or fatigue design of bridge deck need to develop. In this study, authors try to propose the live loading model to assume the real vehicle loads and conduct the fatigue analysis based on the proposed live traffic model. Probabilistic approaches and reliability analysis based on the restricted test results on the strengthened concrete bridge decks is applied to verification of strengthening effect and prediction of extended fatigue life, because fatigue performances on the bridge decks investigated from either laboratory test or real bridge decks are limited and also involved in inevitable uncertainties and extensive variation.

2. LIVE LOADS MODEL

2.1 Axle loads of truck Margins

In this study, the live load model was developed by actually measuring the passing frequency and lane load of the heavy vehicles on the Banpo Great Bridge, Seoul, Korea. Yoon (1996) classified 10 kinds of vehicles in Korea then measured each weight of vehicles. Among the vehicle types, the vehicle types of 5(T2), 6(TT3), 7(ST4), 8(ST5), 9(ST6), and 10(FT5) are classified as heavy vehicles as shown in Fig. 1. In the case of traffic model, TT3 and ST5 truck types were selected as because these types showed more the traffic volume than other truck types. In this study, TT3 truck type was selected because it was investigated that TT3 type showed more traffic volume than ST5 type relatively. To adopt fatigue load to bridge deck, normal and overloaded loading state was considered. For lane load of normal and overloaded state, it was selected as a value of 84.0kN and 133.9kN, respectively. Actually, the upper tail parts of the distribution of axle weights are mainly concerned in the fatigue life of reinforced concrete deck slabs. In this study, ADTT (Average Daily Truck Traffic) provided by Korea Ministry of Construction and Transportation was used to simulate the traffic volume of the bridge designed as 2nd grade. The coefficient of variation is 0.85 based on ASSHTO [1998] with a one way three-lane road. But for considering critical condition of fatigue load, coefficient of variation in this model was selected as 1.0 so that ADTT was acquired as 4,400.

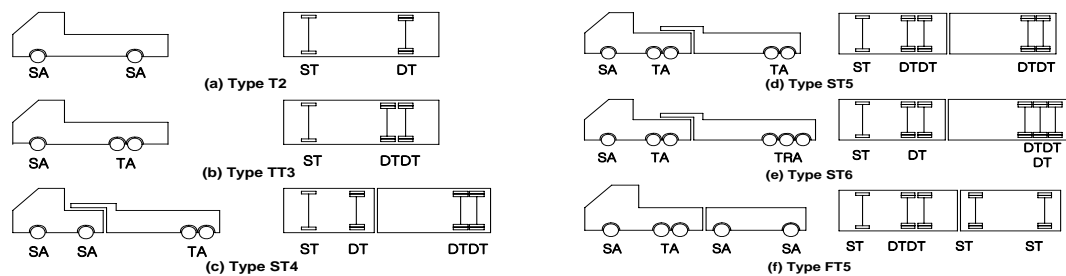


Figure 1: Truck Type [Yoon, 1996]

Table 2: ADTT [Korea Ministry of Construction and Transportation, 2000]

	Passenger Vehicle	Bus	Truck	
			Design Truck	Overloaded Truck
One way traffic	61,477	8,755	11,703	1,600
ADTT	20,326	2,918	3,901	533
			4,434 (approximately 4,400)	

2.2 Live load model

It has been studied that the moving and cyclic load can affect reinforced concrete bridge deck more 4 to 7 times than that of pulsating load. In present, however, only pulsating load has been adopted for fatigue analysis of the bridge deck. Therefore, the live load model for fatigue analysis of the bridge deck was developed by using Type I extreme function adopted actually measured lane load from Table 1. The cumulative distribution function (CDF) of the Type I asymptotic form for the distribution of the largest value, in the classification of Gumbel (1958), is as follows:

$$F_{Y_n}(y_n) = \exp[-e^{-\alpha_n(y_n - u_n)}] \quad (1)$$

where u_n and α_n are, respectively, the location and scale parameters, defined as follows:

u_n = The characteristic largest value of the initial variate X

α_n = An inverse measure of dispersion of X1

The corresponding probability density function (PDF) is

$$f_{Y_n}(y_n) = \alpha_n e^{-\alpha_n(y_n - u_n)} \exp[-e^{-\alpha_n(y_n - u_n)}], \quad -\infty < y_n < \infty \quad (2)$$

In this study, coefficient of variation and average nominal ratio for adopting axle load to extreme function was assumed the value of 0.25 and 1.24 from Nowak (1994). Fig. 3 and 4 shows the result of live load model of axle load for the extreme function and the service life of bridge assumed as 75 years based on Design Specification of Highway Bridge in Korea. Fig. 2(a) and 3(a) indicates the axle load effect of design and overloaded truck as Probability Density Function (P.D.F.) and Fig. 2(b) and 3(b) shows Cumulative Distribution Function (C.D.F.) and this function presents similar shape with Nowak's live load model.

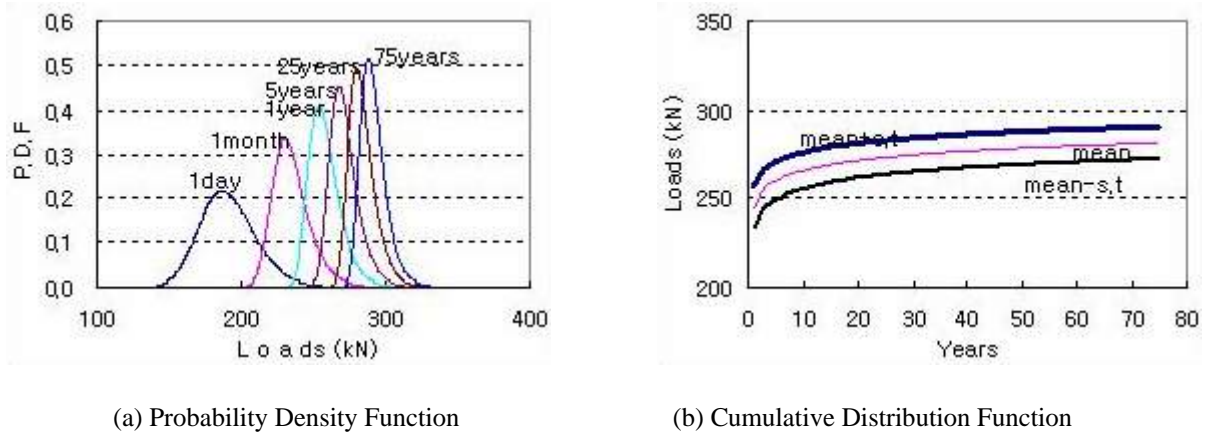


Figure 2: Live load model (normal state tandem load: 84.0kN)

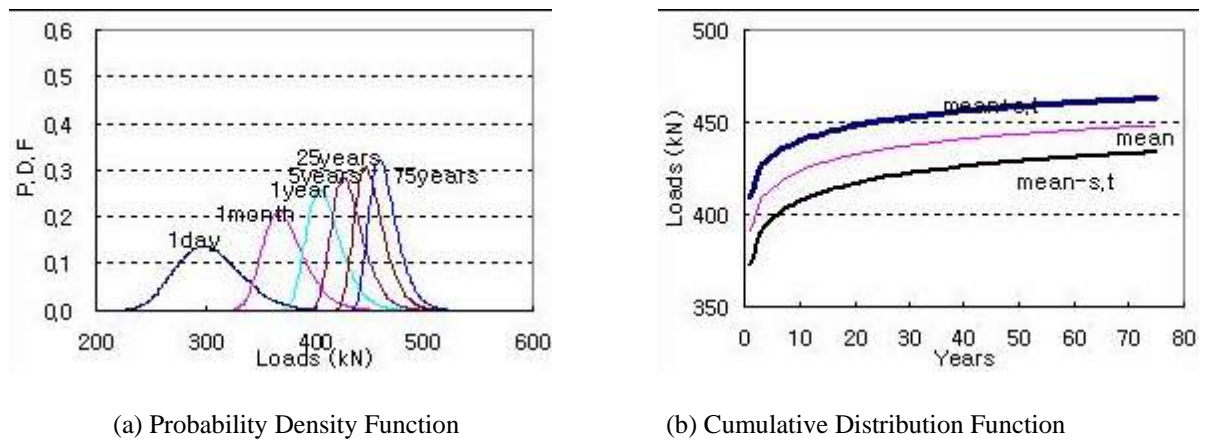


Figure 3: Live load model (overloaded state tandem load: 133.9kN)

3. TEST PROGRAM

The CFS(Carbon Fiber Sheet) and GCFRP(Grid-type Carbon FRP) materials were bonded to the prototype deck panel in an upside-down position. Each fiber sheet was attached to the epoxy-coated surface by pressing it into the epoxy. The GCFS material was first fixed to the concrete surface in an upside-down position using 2.5-cm length anchor bolts spaced every 50 cm. Then the repair mortar suggested by the manufacturer was overlaid on the concrete surface. The nine specimens listed in Table 3 were subjected to cyclic loads to investigate their fatigue failure characteristics. The CON means the unstrengthened reference panel. Fig. 4 and 5 shows test specimens. [Oh, 2001]

Table 3: Stress level

SPECIMENS	CON			CFS			GCFRP		
Stress Level (%)	40	70	90	60	70	80	60	70	80
Loads (kN)	260	450	580	440	510	590	430	500	570

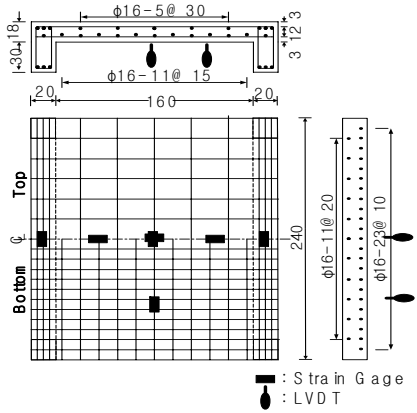


Figure 4: Details of specimen

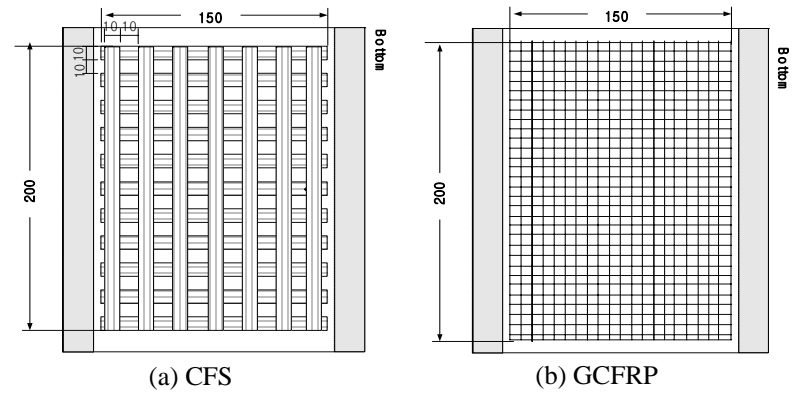


Figure 5: Strengthening details

4. EXPECTATION OF EXTENDED LIFE

To expect the strengthening age of the 2nd grade bridge deck, the rate of increase of overloaded truck passing on the target bridge was assumed as 12% based on ADTT data (see Table 2) in this study. To evaluate the extended life of the bridge deck strengthened with CFS and GCFRP, the target reliability index was assumed as 4.7 and 5.0 for the strengthening or replacement age, respectively. Fig. 6 shows reliability index with the rate of increase 12% from the probability analysis.

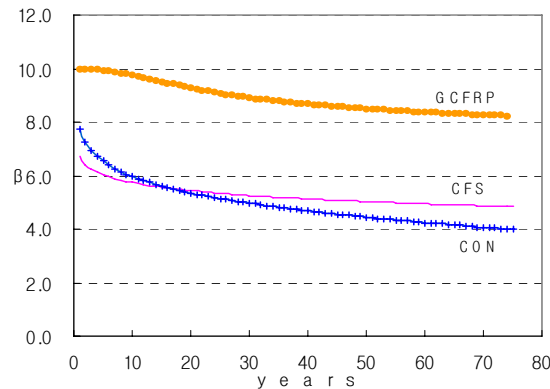


Figure 6: Reliability index (when axle load has the rate of increase 12%)

5. CONCLUSIONS

- (1) It was evaluated that the extended fatigue life of bridge deck strengthened with CFS or GCFRP showed as more 1.2 ~ 1.5 times than that of non-strengthened bridge deck.
- (2) In the case of the strengthening type, GCFRP strengthening method had better reliability index than CFS strengthening method in the point of view for strengthening and extended fatigue life. Therefore, it is evaluated that the GCFRP strengthening method to concrete bridge deck is more effective than CFS strengthening.

REFERENCE

Gumbel, E. J. (1958). *Statistics of Extremes*, Columbia Univ. Press, New York

Nowak, A. S., Yamani, A. S., and Tabsh. (1994). "Probabilistic models for resistance of concrete bridge girders", *ACI structural journal*, Vol. 91, No. 3, pp. 269-276

Oh, H. (2001). "Strengthening Design Method of Bridge Deck Reinforced by Carbon Fiber Sheet", Ph.D. thesis, Hanyang University, Ansan, Korea.

Yoon, S. (1996). "A Study on the Fatigue Behavior and the Fatigue Design of the Reinforced Concrete Deck Slabs of the Composite Bridges", Ph.D. thesis, Seoul National University, Seoul, Korea.

STATIC AND FATIGUE INVESTIGATION OF BRIDGE DECK CANTILEVERS

Chad Klowak

Engineer-in-Training, ISIS Canada Research Network, Winnipeg, MB, Canada

Aftab Mufti

President, ISIS Canada Research Network, Winnipeg, MB, Canada

Baidar Bakht

President, JMBT Structures Research Inc., Scarborough, ON, Canada

ABSTRACT

One solution to the problem of deteriorating bridge decks is to replace or rehabilitate them with innovative technologies such as steel-free bridge decks or decks reinforced with fibre reinforced polymers. Cantilevers are an integral part of bridge decks and this paper outlines test results obtained from static and fatigue destructive testing conducted at the University of Manitoba's W.R. McQuade Heavy Structures Laboratory. The bridge deck contained cantilevers with glass and carbon fibre reinforced polymers (GFRP and CFRP) and conventional steel reinforcement. Experimental results based on the testing of the GFRP and steel reinforced cantilevers (testing on the CFRP cantilever has yet to be completed) indicate that arching-action may be present. However, further experimental investigation is required to better determine bending and arching components in bridge deck cantilever behaviour. The results also indicate that cumulative strain as a result of fatigue may prove to be an issue and may have to be considered in bridge deck design. The paper also concludes that a significant reduction in negative moment reinforcement is feasible and such a reduction would lead to a considerable cost reduction associated with negative moment reinforcement.

KEYWORDS

Cantilever, Bridge Deck, Glass Fibre Reinforced Polymer (GFRP), Static Testing, Fatigue Testing

1. INTRODUCTION

Bridges play an important role in the highway systems around the world and have been adversely affected by age and weathering over the past two decades. The majority of highway bridges have steel reinforced concrete decks supported on steel or concrete girders. Over the years, the weather has taken its toll on these steel reinforced concrete decks. Rainwater and de-icing chemicals applied to bridge deck surfaces to prevent icing of the bridge decks during the winter months have found their way into many concrete decks and caused corrosion of the reinforcing steel (Memon & Mufti, 2004). A solution to the problem of the existing deteriorating bridge decks is to rehabilitate or replace them with innovative technologies such as corrosion-free bridge decks (Mufti et al., 2005). Cantilevers are an integral part of bridge decks and this paper takes a look at the test results obtained from both static and fatigue destructive testing. It outlines the results obtained for a cantilever reinforced with GFRP and discusses those results with respect to deflection and strain.

2. CANTILEVER DETAILS & TESTING SCHEME

Although the bridge deck contained an internal panel that was a second generation steel-free bridge deck this paper will only outline the reinforcement details of the cantilevers. The bridge deck measured 9000 mm in length and 5000 mm in width and was supported on two steel girders (Figure 1). The cantilever overhangs measured 1250 mm

from the center line of the girders to the free edge of the cantilever. The deck was divided into three different panels that, for explanation purposes, we call the GFRP, CFRP, and steel cantilevers. The bottom reinforcement was consistent for all three panels and was comprised of #10 GFRP bars spaced at 200 mm center-to-center in the transverse direction (shorter distance) and #10 GFRP bars spaced at 600 mm center-to-center in the longitudinal direction (longer distance). The top longitudinal reinforcement was also the same for all three panels and consisted of #10 GFRP bars spaced at 600 mm center-to-center. The only difference between the three different panels was the top transverse reinforcement provided to resist the negative moment as a result of applied load near the free edge of the cantilever. The GFRP, CFRP, and steel panels used two #19 GFRP bars spaced at 200 mm center-to-center, two #13 CFRP bars spaced at 200 mm center-to-center, and one 20M steel bar spaced at 200 mm center-to-center respectively.

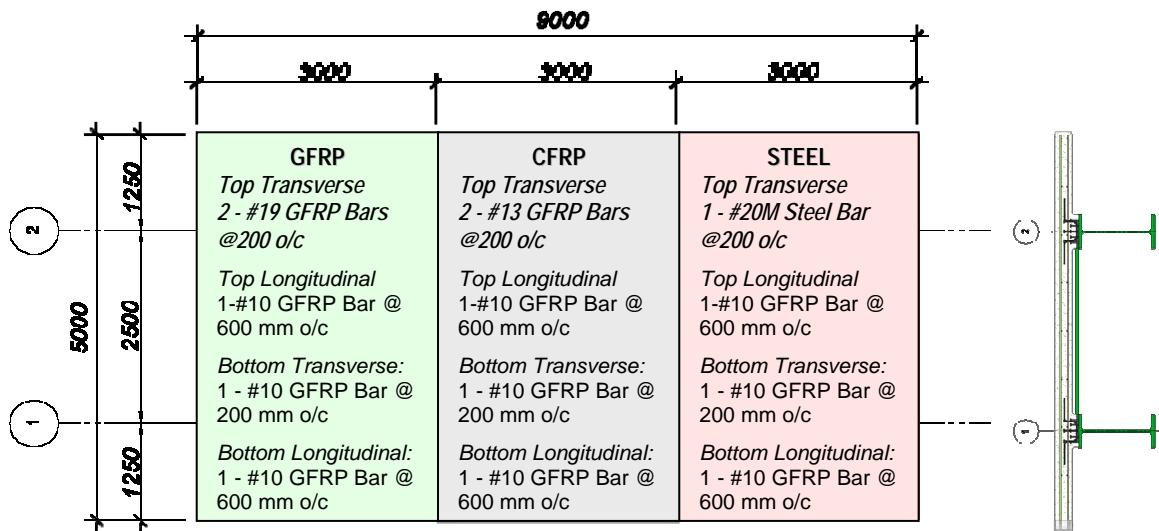


Figure 1: Bridge Deck Cantilever Details

The testing scheme for the cantilevers consisted of six different destructive tests. One of the cantilevers was subjected to three static tests, each of which was conducted on the three different cantilever panels (Figure 2). The static tests were conducted first, in order to determine the ultimate static capacity of each of the cantilevers, before proceeding with the fatigue tests.

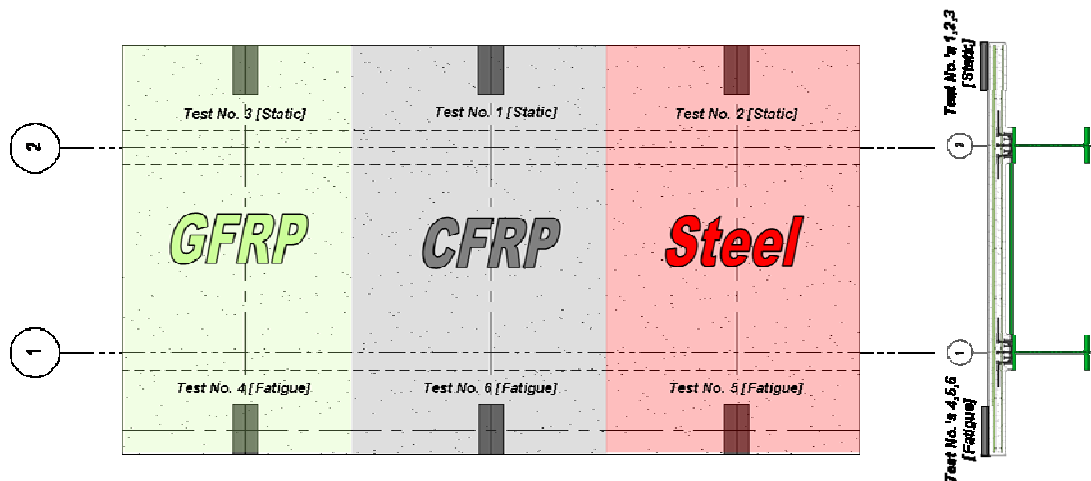


Figure 2: Static & Fatigue Cantilever Testing Scheme

3. GFRP CANTILEVER TEST RESULTS

The experimental results for the GFRP cantilever can be grouped into four different categories. For explanation purposes the results are grouped into those dealing with deflection behaviour and strain behaviour.

3.1 GFRP Cantilever Load Deflection Behaviour

A total of eight displacement transducers were used to monitor deflection for both static and fatigue testing. The results outlined in this paper strictly deal with the displacement transducer placed at the center of the loading plate (Figure 3). The cantilever failed at an ultimate load of 294 kN and a maximum ultimate deflection of 27.2 mm. The applied load for the fatigue testing was 186 kN or approximately 63% of the ultimate load previously determined by the static test. The applied load of 63% is the average of the maximum load measured throughout the entirety of the fatigue test. It is important to note that the ultimate deflection from the fatigue test very closely matches the ultimate deflection measured from the static test. The ultimate fatigue deflection was measured to be 30.1 mm and the deck failed at 104,777 cycles.

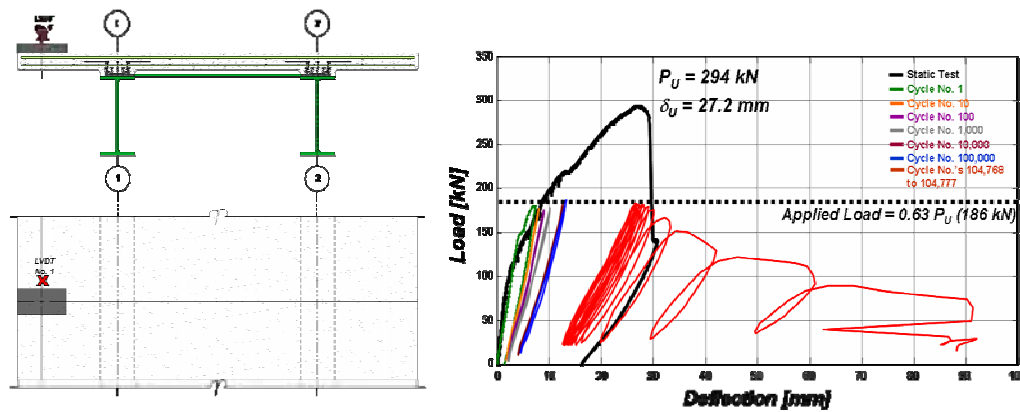


Figure 3: Static & Fatigue Load versus Deflection for GFRP Cantilever

3.2 GFRP Cantilever Load Strain Behaviour

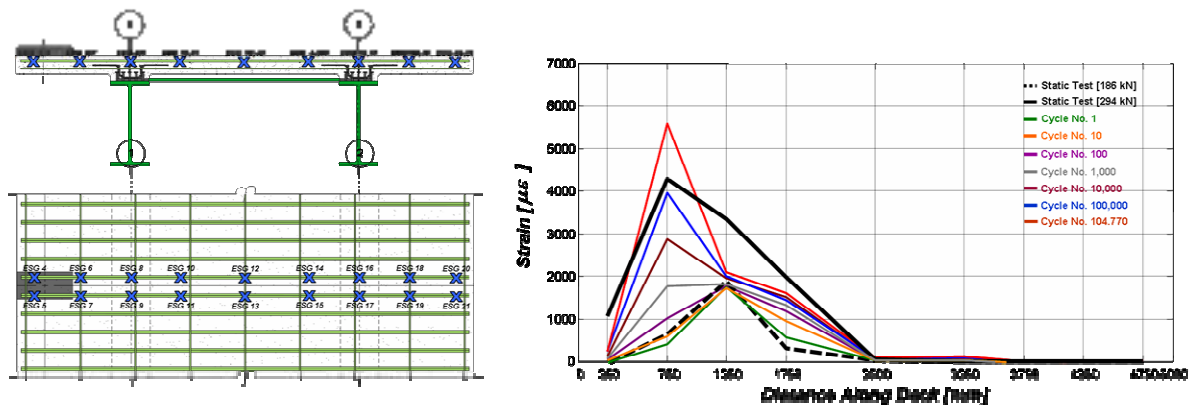


Figure 4: Static & Fatigue Top Transverse GFRP Bar Strain Profile (Note: Center lines of girders occur at distances of 1250 mm and 3750 mm.)

A total of 18 electronic strain gauges were installed on the top transverse GFRP bars in order to provide strain data for the top transverse negative moment reinforcement (Figure 4). The maximum strain at the static load of 186 kN occurs over the girder and is 1900 $\mu\epsilon$ in magnitude; however, at the ultimate load of 294 kN the maximum strain has shifted towards the loading plate and is 4282 $\mu\epsilon$ in magnitude. An important observation is that the strains in the top transverse bar are nearly zero at a distance of 2500 mm from the loaded edge of the cantilever. Looking at the

fatigue strain data it is important to observe that the strain in the top transverse bars remains relatively constant throughout the entire life of the cantilever, however, the strains in the bars much closer to the applied load increase significantly with increased number of cycles. The cumulative strain in the bars over the girder and the cumulative strain in the bars close to the applied load amount to $628 \mu\epsilon$ or approximately 4% and $3142 \mu\epsilon$ or approximately 20% of the ultimate strain of the GFRP bars respectively (Figure 5).

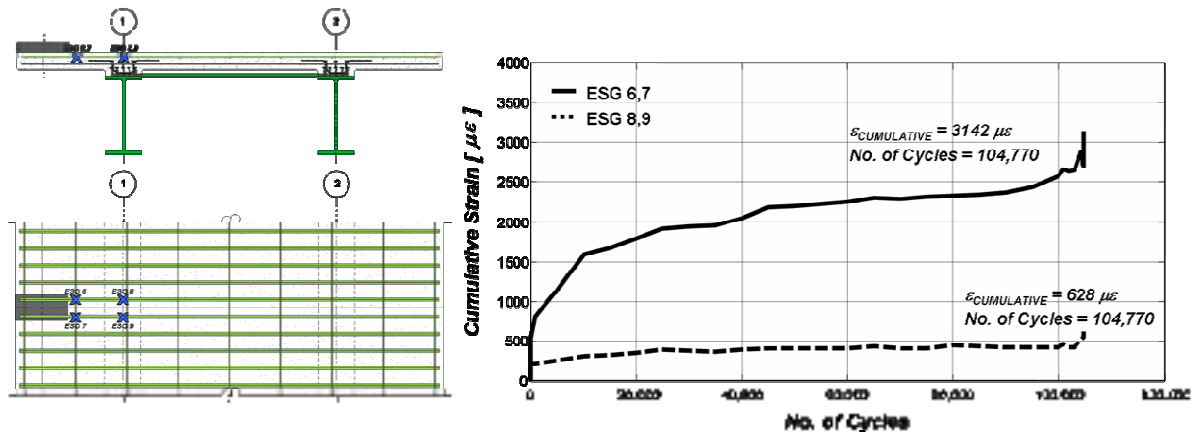


Figure 5: Cumulative Fatigue Top Transverse GFRP Bar Strain

4. CONCLUSIONS & RECOMMENDATIONS

Although this paper only outlines the results obtained from the GFRP cantilever, it is important to briefly discuss the results from the static test conducted on the cantilever with top transverse steel reinforcement in order to make an important point. The static ultimate load for the cantilever with steel reinforcement was recorded as 301 kN. The nominal moment resistance of the cantilever with top transverse GFRP when calculated using conventional design methods was $154 \text{ kN}\cdot\text{m}$ per meter width and the nominal moment resistance of the cantilever with top transverse steel reinforcement was $85 \text{ kN}\cdot\text{m}$ per meter width. If we compare the nominal moment resistance of the two different cantilevers, conventional design methods would suggest that the GFRP cantilever would have a higher ultimate load. The experimental results indicate that the ultimate load of the two cantilevers was the same, suggesting that some arching action may be present in the cantilevers. It is clear from the experimental tests conducted on the bridge deck cantilevers that extensive further experimental investigation is required to gain a better understanding into the bending and arching components of cantilever behaviour. Another conclusion that can be drawn from the experimental tests is that, under fatigue loading conditions, the measured cumulative strain amounted to 20% of the ultimate strain provided by the manufacturer of the GFRP bars. The Canadian Highway Bridge Design Code (CHBDC 2000) limits strain in GFRP bars embedded in concrete to 25% of their ultimate strain under service conditions. Therefore, cumulative strain in GFRP bars may have to be considered in bridge deck design. The final observation that can be made is that the negative moment intensity in the internal panel does not significantly strain the top transverse bars beyond the mid-span of the next adjacent internal panel, suggesting that the bars are not required in this region. Therefore, a 33% reduction by volume is feasible, which could result in a significant cost reduction of the top transverse reinforcement required for negative moment regions in bridge deck cantilevers.

5. REFERENCES

- Canadian Highway Bridge Design Code (CHBDC). (2000). Canadian Standards Association International, Canada.
- Memon, A.H. and Mufti, A.A. (2004). Fatigue behaviour of second generation steel-free concrete bridge deck slab. Proceedings of the Second International Conference on FRP Composites in Civil Engineering (CICE), Adelaide, Australia.
- Mufti, A.A., Memon, A.H. and Klowak, C. (2005) Study of static and fatigue behavior of second generation bridge decks. Proceedings of the International Workshop on Innovative Bridge Deck Technologies, Winnipeg, MB, Canada.

Part X. FRP Bars

ENVIRONMENTAL CONSIDERATIONS IN USING FRP REBARS IN CONCRETE PAVEMENTS

Amnon Katz

*Department of Civil and Environmental Engineering
National Building Research Institute
Technion – Israel Institute of Technology
Haifa 32000, Israel*

Abstract

Introducing reinforcing bars made of fiber-reinforced polymers (FRP) into concrete as a substitute for ordinary steel reinforcing bars may have economic, as well as environmental consequences. A comprehensive approach was used to study the environmental impact of such substitution/replacement, taking into consideration the whole life cycle of the pavement, from cradle to grave, including maintenance activities and changes in concrete technology resulting from the change in rebar type. The deficiencies of the current tools available for the assessment of environmental impacts were also investigated in order to introduce a more reliable model.

It was found that the environmental impact can be reduced significantly at the erection stage due to the possibility of reducing the cement content or the thickness of the concrete layer covering the reinforcing bars, since special protection of the steel against corrosion is no longer needed. During the service life of the pavement, additional environmental impacts are eliminated due to a decrease in the number of required maintenance activities, each of which has direct (materials and construction energy) and indirect (disturbance to traffic) impacts.

Keywords: life cycles assessment, FRP rebar, environmental impacts

1. INTRODUCTION

Fiber-reinforced polymer reinforcing bars (FRP rebars) have emerged in recent years as a substitute for steel bars in concrete. This material is considered to be more durable than conventional steel (Katz et al., 2001; Bank et al., 1998; Umoto and Ohga, 1996) and is, therefore, proposed nowadays as a substitute for steel in structures exposed to aggressive environments, such as marine environments, and in structures exposed to deicing salt chlorides. Recently published design recommendations (ACI 440.1, 2001) indicate that the initial period of uncertainty for this new product is already over and it can now be used more extensively.

The utilization of new products is not always associated with better environmental protection. Sophisticated production processes may sometimes lead to a higher environmental load of a product despite its other beneficial properties. Things become more complicated when the product is highly complex, such as a construction project, in which changing the properties of one material or process may have long-term effects on other materials or processes. Edvardsen and Tollose (2001) concluded that using stainless steel reinforcing bars instead of ordinary steel rebars may lead to an overall reduction in CO₂ emission due to reduced maintenance and repair, despite the increased emission during the production of the bar itself.

Using FRP rebars as a substitute for conventional steel changes an entire set of parameters used in the design of new constructions. Water/cement ratio, minimum cement content, thickness of concrete cover over rebars, and periodical maintenance are all parameters that undergo changes when replacing steel with FRP. The change in these parameters is usually in the direction of less restricting constraints/limitations (Katz, 2004).

The current study describes the change in the environmental impact following the substitution of steel with glass FRP as a reinforcing material for concrete pavement subjected to marine environments.

2. ANALYSING THE ENVIRONMENTAL IMPACTS THROUGHOUT THE WHOLE LIFE CYCLE

2.1. Erection

Protection of steel reinforcing bars in reinforced concrete structures is achieved by lowering the water/cement ratio, increasing the cement content and increasing the thickness of the concrete layer that covers the steel. When FRP rebars are used to replace steel ones, the above stringent requirements can be relaxed. Thus, a higher water to cement ratio can be used, which leads to a lower cement content per concrete unit. The thickness of the non-structural concrete layer that protects the steel can also be reduced, leading to smaller quantities of concrete per unit area of pavement.

In this study, the environmental impacts of steel-reinforced concrete pavement made according to AASHTO concrete Class IV was compared with Class II concrete pavement reinforced with glass fiber-reinforced polymers (GFRP). Table 1 presents the parameters used in this study.

Table 1: Composition and processes for the two pavements.

	Steel-reinforced pavement	FRP-reinforced pavement
Concrete class	Class IV	Class II
Slab thickness	200 mm	165 mm
<u>Concrete composition</u>		
Cement	390 kg/m ³	335 kg/m ³
Water	160 kg/m ³	165 kg/m ³
Gravel	1100 kg/m ³	1205 kg/m ³
Sand	750 kg/m ³	695 kg/m ³
Reinforcement	104 kg/m ³	32.2 kg/m ³
<u>Processing</u>		
Mixing power	9.3 MJ/m ³	9.3 MJ/m ³
Average distance of mineral transport	100 km	100 km
Average distance of reinforcement transport	500 km	1500 km
Average distance of concrete transport	30 km	30 km

2.2. Service-Life Stage

The environmental impact of maintenance activities is divided into two categories: (1) direct impact of construction works, and (2) indirect impact of disturbance to traffic. It was assumed that maintenance activities required for FRP reinforced pavements are at least 50% of those required for steel-reinforced pavements. According to Ehlen (1999) and Ehlen and Marshall (1996), maintenance activities on bridge decks begin on the 28th year after erection and are performed every three years. During each such maintenance activity, 2.5% of the surface is chipped away, reinforcement is repaired and treated with protective paint, and the deck is repaired using new concrete. For steel-reinforced pavement, these assumptions lead to approximately 8 additional maintenance activities over 75 years of service, which are the direct result of steel corrosion (activities resulting from concrete corrosion in both types of pavement were not counted). In such pavements, deterioration of the concrete itself enhances the deterioration of the steel, thus the assumption that 50% of the maintenance activities are a result of steel corrosion only seems conservative.

Direct environmental impacts of the materials and processes were calculated according to the above assumptions. The indirect environmental impact of traffic disturbance (ETD) due to maintenance works was calculated as follows. It was assumed that a slower traffic speed leads to a proportional increase in all environmental impacts, according to Equation 1.

$$ETD = VE \times ADT \times N_c \times \Delta L_{eq} \quad (\text{Eq. 1})$$

where VE = vehicle environmental impact per unit length of road, ADT = average number of cars per day, N_c = duration of traffic disturbance in days, ΔL_{eq} = equivalent additional length of work zone, taking into account the actual length of road affected by the maintenance works, L , and the increased emissions due to the longer time needed to pass this area, calculated as follows:

$$\Delta L_{eq} = L \left(\frac{V_n}{V_a} - 1 \right) \quad (\text{Eq. 2})$$

Where V_n = average normal traffic speed and V_a = average traffic speed in work zone.

2.3. Disposal

Is quite common nowadays to recycle old concrete into aggregate for use in the production of new concrete as well as to recycle all the reinforcing steel. It was, therefore, assumed that ~85% of the concrete could be re-used as aggregate in the production of new concrete (the fine fraction, ~15%, is of minor value). Lacking knowledge on the recycling possibilities of FRP reinforced concrete, it was assumed that all FRP reinforcement and FRP reinforced concrete is not recycled in any way.

3. RESULTS AND DISCUSSION

Data was analyzed using the Eco-indicator 99 method. Environmental impacts were analyzed in light of their impact on human health (years of life lost or years of disability), impact on eco-systems (loss of species over a certain area) and depletion of resources (surplus energy required for their future production). A single score was determined after weighting, grouping and normalization.

Table 2 presents a summary of the analysis performed on the two pavement types. The total environmental load of FRP reinforced pavement was more than 50% lower than that of steel-reinforced pavement. A significant decrease, of approximately 36%, was identified in the erection stage, and resulted mainly from the reduced load of the reinforcement, the lower cement content and the smaller quantity of concrete required due to the reduced slab thickness. Figure 1 presents the environmental load of cement, aggregate, reinforcement, transportation and processes involved in the erection of the two kinds of pavements, together with their relative part of the erection activity. In ordinary steel-reinforced pavement, steel is responsible for 27% of the environmental load; this value is reduced to only 11% for FRP reinforcement. The absolute impact of FRP rebars is only 25% of that of steel rebars of the same diameter. Similarly, the impact of cement was found to decrease by 29%. However, due to the significant decrease in the environmental load of other components, cement still seems to be a significant contributor to the pavement's overall environmental load.

The indirect environmental load resulting from traffic disturbance seems to be the most significant factor during the maintenance stage and is decisively greater than that of the direct maintenance work performed. Thus, an attempt should be made to minimize traffic disturbance during maintenance activities.

Table 2: Summary of the environmental load of the tested pavements (in Eco-indicator 99 points)

Slab type	Erection	Maintenance*	Disposal	Total
Steel-reinforced pavement	179,000	$n \times 13,200$	6,020	291,000
FRP-reinforced pavement	114,000	N/A	7,680	122,000

* $n=8$

The environmental impact of demolishing the pavement is quite small. Despite the larger quantities involved, the impact resulting from the demolition of steel pavement is smaller than that of FRP pavement due to the positive impact of recycling the old concrete (recycling of the steel has already been taken into account in the production of new steel).

Sensitivity analysis was carried in order to study the influence of uncertainties involved in determining the parameters listed above. The following parameters were investigated: effect of concrete thickness (changing concrete class but not concrete thickness), effect of concrete class (changing from Class IV to Class II-bridge), improving the recyclability of the FRP pavement, and the effect of different evaluation methods. All these investigations indicated that the environmental impact of FRP pavement is lower compared with that of steel-reinforced pavement.

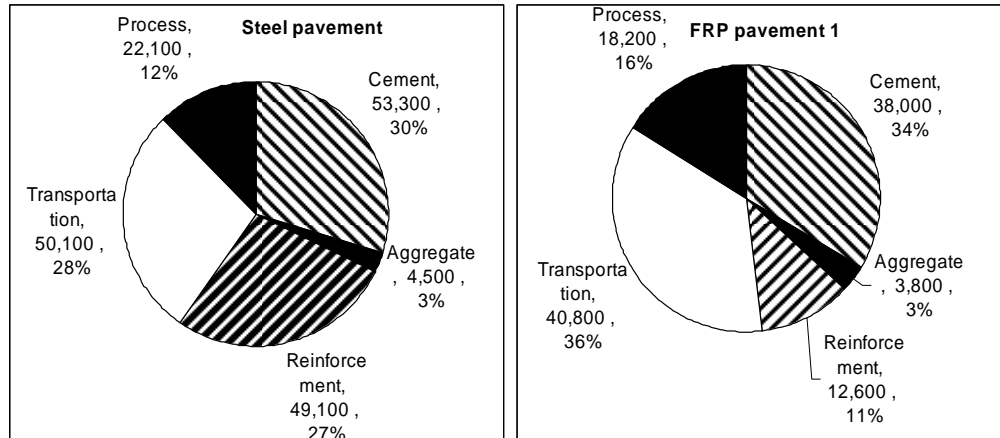


Figure 1: Distribution of the environmental load during the erection stage, for steel- and FRP reinforced pavements, expressed in Eco-points (Eco-indicator 99) and as percentages.

4. CONCLUSIONS

A comparison was made between the environmental impacts of concrete pavement reinforced with steel or FRP bars. It was found that the environmental load might be significantly lower when considering changes in the concrete composition or pavement thickness resulting from better chloride resistance of the FRP rebars. In addition, the environmental impact of the FRP rebar itself is much smaller than that of steel rebar of the same diameter. Sensitivity analysis that examined the effect of different assumptions regarding concrete composition and pavement structure led to the same conclusion. Transportation was found to be an important environmental parameter in the production of concrete due to the large masses of materials involved in the production of concrete pavement.

References

- ACI 440.1R-01, (2001), "Guide for the design and construction of concrete reinforced with FRP bars", American Concrete Institute (ACI), Farmington Hills, MI, USA.
- Bank, L.C., Puterman, M., and Katz, A., (1998), "The Effect of Material Degradation on Bond Properties of FRP Reinforcing Bars in Concrete", *American Concrete Institute (ACI) Materials Journal*, Vol. 95, No. 3, pp. 232-243.
- Edvardsen C. and Tollose K., (2001), "Environmentally "green" concrete structures", Proceedings, FIB symposium *Concrete and Environment*, Berlin, Germany.
- Ehlen M. A., (1999), "Life cycle cost of fiber reinforced polymer bridge decks", *Journal of Materials in Civil Engineering*, Vol. 11, No. 3, pp. 224-230.
- Ehlen M. A. and Marshall H. E., (1996), "The economics of new technology materials: a case study of FRP bridge decking", NISTIR 5864, National Institute of Standard and Technology, Gaithersburg MD 20899, USA, 80p.
- Katz, A., "The environmental impact of steel and FRP reinforced pavements", *ASCE Journal of Composites for Construction*, Vol. 8, No. 6, 2004, pp. 481-488.
- Katz A., Bank L. C. and Puterman M., (2001), "Durability of FRP Rebars After Four Years of Exposure", *Fiber Reinforced Plastics for Reinforced Concrete Structure- FRPRCS-5*, Burgoyne C.J. Editor, Cambridge, Thomas Telford press, UK, pp. 497-503.
- Uomoto, T. and Ohga H., (1996), "Performance of fiber reinforced plastics for construction reinforcement", in Proceedings: *Advanced Composite Materials in Bridges and Structures*, El-Brady et al. Eds., Canadian Society for Civil Engineers, Montreal, Canada, pp. 125-132

EVALUATION OF CRACK WIDTHS IN CONCRETE FLEXURAL MEMBERS REINFORCED WITH FRP BARS

Charles E. Bakis

(Professor, Penn State University, University Park, Pennsylvania, USA)

Carlos E. Ospina

(Senior Engineer, Berger/ABAM Engineers Inc., Federal Way, Washington, USA)

Timothy E. Bradberry

(Support Branch Manager, Bridge Division, Texas Department of Transportation, Austin, Texas, USA)

Brahim Benmokrane

(Professor, Université de Sherbrooke, Sherbrooke, Québec, Canada)

Shawn P. Gross

(Associate Professor, Villanova University, Villanova, Pennsylvania, USA)

John P. Newhook

(Associate Professor, Dalhousie University, Halifax, Nova Scotia, Canada)

Ganesh Thiagarajan

(Assistant Professor, University of Missouri, Kansas City, Missouri, USA)

ABSTRACT

The width of flexural cracks in a concrete member internally reinforced with fiber reinforced polymer (FRP) bars depends on the characteristic of interfacial bond between the reinforcement and concrete. This paper reports the findings of a task group formed under the aegis of ACI Sub-committee 440 H (Reinforced Concrete) to evaluate and compare the effects of bond characteristics in previous and proposed equations for predicting crack widths. Based on the experimental data assembled by the task group, it is shown that the bond coefficient in the proposed equation by Frosch is 19% greater than the bond coefficient in the previous equation attributed to Gergely and Lutz.

KEYWORDS

Crack width, flexure, bond

1. INTRODUCTION

At the October 2004 meeting of Sub-committee H (Reinforced Concrete) of ACI Committee 440 (Fiber Reinforced Polymer Reinforcement), a task group was formed to evaluate the proper value of bond parameter, k_b , for use in a new equation for crack width in flexural members reinforced with deformed FRP bars. Included in the task group's activity were FRP bars reinforced with glass fibers (GFRP), carbon fibers (CFRP) and aramid fibers (AFRP).

The equation for crack width in ACI 440.1R-03 (2003) is referred to as the modified Gergely-Lutz equation:

$$w = 2.2 \frac{f_f}{E_f} \beta k_b \sqrt[3]{d_c A} \quad (1)$$

where w (mm) is the maximum likely crack width at the tension face of a beam or one-way slab (generally taken as the 90-th percentile crack), f_f (MPa) is the stress on the bar calculated by elastic cracked section theory, E_f (MPa) is the longitudinal modulus of elasticity of the bar, β is the ratio of the distance from the neutral axis to the depth where the crack width is measured to the distance from the neutral axis to the centroid of the tensile reinforcement, d_c is the thickness of concrete cover measured from the tension face to the center of the closest reinforcement bar (mm), A is the effective tension area of the concrete surrounding the main tension reinforcement and having the same centroid as that reinforcement divided by the number of bars (mm²), and k_b is a factor that accounts for the bond between a bar and concrete. For uncoated steel bars, k_b is nominally equal to 1. Some typical k_b values for deformed GFRP bars cited in ACI 440.1R-03 are between 0.71 and 1.83. ACI 440.1R-03 suggests that designers assume a value of 1.2 for deformed GFRP bars unless more specific information is available for a particular bar.

At the time this task group was initiated, ACI Committee 440 was considering the adoption of a modified version of the crack width equation by Frosch (1999) in place of the modified Gergely-Lutz equation:

$$w = 2 \frac{f_f}{E_f} \beta k_b \sqrt{d_c^2 + \left(\frac{s}{2}\right)} \quad (2)$$

where s is the bar spacing. The factor 2 in eqn. (2) is used when predicting the maximum crack width. A value of 1.5 is used for the mean crack width and 1.0 for the minimum crack width. Frosch also noted that $k_b=1$ for conventional deformed steel bars and $k_b=2$ for epoxy coated deformed steel bars.

As can be seen, the form of eqn. (2) is different than that of eqn. (1). Therefore, the objective of this task group activity is to recommend an appropriate default value of k_b to use in eqn. (2) when no specific value of k_b has been determined for a particular FRP reinforcing bar.

2. APPROACH

The approach taken in this endeavor is to first collect the available crack width measurements for concrete flexural members reinforced with FRP bars and determine the ratio of k_b for eqn. (2) divided by k_b for eqn. (1) for each crack width measurement. The ratio is computed for the widest flexural crack in a member in experiments where not many crack measurements are available. In data sets where many crack widths are available, the 90th percentile crack width (mean plus standard deviation times 1.28) is used. The ratio resulting from this comparison is then multiplied by the currently recommended default k_b value of 1.2 to arrive at a proposed value of k_b when using eqn. (2). Therefore, the maximum crack width predicted by eqn. (2) with the proposed value of k_b should be no different than that predicted by eqn. (1) with $k_b=1.2$.

Some of the bar strains used in this analysis came from strain gages mounted on the bars while others came from calculations using a cracked elastic section analysis. When strains determined by both methods were provided, only those measured directly with strain gages were used. While eqns. (1) and (2) attempt to relate crack width to bar strain with fixed constants of proportionality, it is often observed in experiments that k_b varies with bar strain. Therefore, it is useful to investigate values of k_b over recommended ranges of bar strains for field applications. For example, according to ACI 440.1R-03 (2003), maximum bar strains in FRP bars subjected to creep and fatigue conditions in non-aggressive environments should be limited to ranges of roughly 2400-6200 $\mu\epsilon$ for GFRP, 2800-9400 $\mu\epsilon$ for CFRP, and 5700-13200 $\mu\epsilon$ for AFRP. The actual maximum limits depend on the particular bars under consideration, as described more fully in ACI 440.1R-03 (2003).

The values of k_b included in the present analysis comprise AFRP, CFRP, and GFRP bars with various types of surface treatments to enhance bond with concrete. Smooth bars and grids were not included in the present analysis. It is expected that k_b values for smooth bars and grids will be larger than those with the types of bars included here.

3. FINDINGS

Table 1 summarizes some key experimental parameters and mean values of k_b for the indicated range of strains for each type of bar. It is noteworthy that mean k_b values reported were often quite scattered for different beams and for any one beam measured at different loads. Much of this scatter within a particular type of bar likely results from inaccuracies involved in the crack width measurements. The maximum value of k_b , for example, could be 50%

greater than the mean value reported. The range of k_b values across different types of bars and different concrete member section properties underscores the need to be conservative when recommending a value of k_b to use when no specific value is available for a particular design application. Further careful analysis of the available data is needed to make definitive statements on the causes for the large variation of k_b found in the various investigations.

Table 1. Summary of flexural crack width experiments and bond parameters, k_b .

Bar Type (source of data)	Surface Treatment	Bar Strain ($\mu\epsilon$)	Mean Gergely-Lutz k_b	Mean Frosch k_b	Ratio of k_b 's, F/GL
Hughes Aslan 100 E-glass/ vinylester (Giernacky, 2002)	Spiral indent, sand coating	2000-2100	0.92	1.10	1.20
Marshall Ind. C-Bar E-glass/ PET-polyester (Trejo et al. 2005)	Molded ribs	1600-4500	1.39	1.72	1.24
Pultrall E-glass/ vinylester (Trejo et al. 2005)	Sand coating	1200-3500	1.07	1.27	1.18
Hughes Aslan 100 E-glass/ vinylester (Trejo et al. 2005)	Spiral indent, sand coating	1100-3600	1.33	1.58	1.19
Marshall Ind. C-Bar E-glass/ PET-polyester (Thériault et al. 1998)	Molded ribs	2300-9000	0.58	0.60	1.03
Marshall Ind. C-Bar E-glass/ PET-polyester (Masmoudi et al. 1998)	Molded ribs	2200-7900	1.00	1.14	1.13
Pultrall E-glass/ vinylester (Newhook, 2000)	Sand coating	2400-4300	0.76	0.84	1.12
Hughes Aslan 200 carbon/ vinylester (Theisz, 2004)	Spiral indent, scrim texture	2400-8800	0.92	1.09	1.19
DFI carbon/ epoxy (Thiagarajan, 2003)	Sand-blasted	1300-9800	1.07	1.16	1.08
Pultrall E-glass/ vinylester (El-Salakawy and Benmokrane, 2004)	Sand coating	1300-3400	0.60	0.67	1.12
Pultrall Carbon/ vinylester (El-Salakawy and Benmokrane, 2004; Kassem, 2004)	Sand coating	1100-3200	0.64	0.79	1.23
Marshall Ind. C-Bar E-glass/ PET-polyester (Kassem, 2004)	Molded ribs	2100-3000	0.83	1.10	1.33
Marshall Ind. C-Bar Carbon/ PET-polyester (Kassem, 2004)	Molded ribs	1300-2800	0.82	1.09	1.32
Arapree Aramid/ epoxy (Kassem, 2004)	Sand coating	3400-4300	0.92	1.22	1.33
Steel (El-Salakawy and Benmokrane, 2004; Kassem, 2004)	Ribbed	800-1200	0.72	0.90	1.26
FRP Maximum			1.39	1.72	1.33
FRP Minimum			0.58	0.60	1.03
FRP Mean			0.92	1.10	1.19
FRP Std. Dev.			0.25	0.31	0.093
FRP CV (%)			27	28	8

Some data for uncoated steel reinforcement bars is included in Table 1 for comparison with data for FRP bars. The k_b values for the steel bars fall within, but near the low end, of the range covered by the FRP bars. The ratio of k_b values for the two equations in the case of steel bars is similar to that found for FRP bars.

Maximum, minimum, mean, standard deviation, and coefficient of variation of k_b values and the ratio of k_b values for only the FRP bars (i.e., excluding steel bars) are given at the bottom of Table 1. For the FRP bars, the mean ratio of the k_b 's for the two equations is 1.19, the maximum 1.33, and the minimum 1.03. Using the mean value of 1.19, the recommended value of k_b to use with FRP bars in eqn. (2) in the absence of more specific data is then

$$k_b = 1.2 \times 1.19 = 1.4 \quad (3)$$

For comparison, the actual values of k_b listed for the various bars when using eqn. (2) ranges from 0.6 to 1.72, with a mean of 1.10. Hence, the recommended value of 1.4 has some built-in conservatism that encompasses most, but not all of the data in Table 1. Equation (2) and the recommended value of k_b shown in eqn. (3) have been incorporated into the latest ACI design guide for concrete reinforced with FRP bars, ACI 440.1R-06 (2006).

4. CONCLUSION

When a specific value of k_b is not known for a carbon or glass FRP reinforcing bar with sand coating, indents, sand-blasted surface, and/or molded ribs to enhance bond with concrete, it is recommended to use a conservative value of 1.4 when using eqn. (2) to predict crack width. The limited amount of data for one type of aramid FRP bar included in this analysis (sand coating) abides by this recommendation as well. Smooth bars and grids are specifically excluded from this recommendation until further analysis on such reinforcements has been carried out.

5. REFERENCES

- ACI 440.1R-03 (2003). "Guide for the design and construction of concrete reinforced with FRP bars." American Concrete Inst., Farmington Hills, Michigan, USA.
- ACI 440.1R-06 (2006). "Guide for the design and construction of structural concrete reinforced with FRP bars." American Concrete Inst., Farmington Hills, Michigan, USA.
- El-Salakawy, E.F., and Benmokrane, B. (2004). "Serviceability of concrete bridge deck slabs reinforced with FRP composite bars," *ACI Struct. J.*, Vol. 101, No. 5, pp. 727-736.
- Frosch, R.J. (1999). "Another look at cracking and crack control in reinforced concrete." *ACI Struct. J.*, Vol. 96, No. 3, pp. 437-442.
- Giernacky, R.G. (2002). "Durability of E-Glass FRP reinforced concrete beams." B.S. Thesis, Dept. of Engineering Science & Mechanics, Penn State University, University Park, Pennsylvania, USA.
- Kassem, C. (2004). "Cracking and load-deflection behaviour of one-way concrete elements reinforced with FRP bars under flexure," Ph.D. Thesis (in French), Dept. of Civil Engineering, Université de Sherbrooke, Sherbrooke, Québec, Canada.
- Masmoudi, R., Thériault, M., and Benmokrane, B., (1998). "Flexural behavior of concrete beams reinforced with deformed fiber reinforced plastic reinforcing rods." *ACI Struct. J.*, Vol. 95, No. 6, pp. 665-675.
- Newhook, J.P. (2000). "The use of fibre reinforced concrete to reduce crack widths in GFRP reinforced concrete beams." *Proc. 3rd Intl. Conf. Advanced Composite Materials in Bridges and Structures*, ACMBS III, Editors: J. L. Humar and A. G. Razaqpur, Canadian Soc. Civil Engineering, Montreal, Quebec, pp. 145-152.
- Theisz, P. (2004). "Properties of high performance concrete beams reinforced with carbon fiber reinforced polymer bars," M.S. Thesis, Dept. of Civil Engineering, Villanova University, Villanova, Pennsylvania, USA.
- Thériault, M., and Benmokrane, B. (1998). "Effects of FRP reinforcement ratio and concrete strength on flexural behavior of concrete beams." *J. Comp. Const.*, Vol. 2, No. 1, pp. 7-16.
- Thiagarajan, G. (2003). "Experimental and analytical behavior of carbon fiber-based rods as flexural reinforcement," *J. Comp. Const.*, Vol. 7, No. 1, pp. 64-72.
- Trejo, D., Aguíñiga, F., Yuan, R.L., James, R.W., and Keating, P.B. (2005). "Characterization of design parameters for fiber reinforced polymer composite reinforced concrete systems." Report FHWA/TX-5/9-1520-3, Texas Transportation Institute, Texas A&M University, College Station, Texas, USA (<http://tti.tamu.edu/documents/9-1520-3.pdf>).

THE PERFORMANCE OF CURVED NON-FERROUS REINFORCEMENT FOR CONCRETE STRUCTURES

Thanongsak Imjai

(PhD student, Department of Civil & Structural Engineering, Sheffield University, Sheffield, UK)

Maurizio Guadagnini

(Lecturer, Department of Civil & Structural Engineering, Sheffield University, Sheffield, UK)

Kypros Pilakoutas

(Professor, Department of Civil & Structural Engineering, Sheffield University, Sheffield, UK)

Peter Waldron

(Professor, Department of Civil & Structural Engineering, Sheffield University, Sheffield, UK)

ABSTRACT

Steel reinforcement in concrete has the tendency to corrode and this process can lead to structural damage. FRP reinforcement represents a viable alternative for structures exposed to aggressive environments and has many possible applications where superior corrosion resistance properties are required. The use of FRP rebars as internal reinforcements for concrete, however, is limited to specific structural elements and does not yet extend to the whole structure. The reasons for this relate to the limited availability of curved or shaped reinforcing elements on the market and their reduced structural performance. Various studies, in fact, have shown that the mechanical performance of bent portions of composite bars is reduced significantly under a multiaxial combination of stresses and that the tensile strength can be as low as 40% of the maximum tensile strength that can be developed in the straight part. In a significant number of cases, the current design recommendations for concrete structures reinforced with FRP, however, were found to overestimate the bend capacity of FRP rebars. This paper presents an overview on the current use of curved reinforcement and discusses the problems related to the performance of curved FRP bars embedded in concrete.

KEYWORDS

Curved FRP bar, tensile strength, bend capacity, corrosion, concrete

1. INTRODUCTION

Fibre Reinforced Polymer (FRP) reinforcement has rapidly emerged as an efficient alternative to conventional steel reinforcement to overcome the problem of corrosion. Owing to its superior durability characteristics, the use of FRP reinforcement can extend the lifespan of concrete structures and reduce the need for maintenance or repair. However, although FRPs are already quite extensively adopted in various sectors of the construction industry (e.g. strengthening and repair of existing structures), their use as internal reinforcement for concrete is limited only to specific structural elements and does not extend to the whole structure. The reason for the limited use of FRPs as internal reinforcement can be partly related to the lack of commercially available curved or shaped reinforcing elements used for shear reinforcement or complex structural connections.

Most of the shaped steel reinforcing bars currently used in concrete structures are provided pre-bent and cut in the factory according to design specifications. These may be supplemented by a small quantity of special one-off shapes bent directly on site. Whether bending occurs on site or at the factory, conventional steel reinforcing bars have a major advantage since, due to their elastoplastic behaviour, they can be easily formed by cold bending, and hence, most detailing needs can be easily met at very low cost.

Existing guidelines for the cold bending of steel reinforcement specify, for mild steel, a bend radius to diameter ratio (r/d) of 2 (for example BS8666:2000), which would induce a maximum strain value of 20% in the material (Figure 1-left). When cold bending FRP bars, however, there are problems associated with the potential buckling of the fibres located in the compression side. Moreover, the typical ultimate strain value of FRP products varies from 1% to 2.5%, hence, the amount of strain that is induced in the fibres needs to be carefully controlled to avoid premature failure of the reinforcing bar. As a result, cold bending of FRP bars requires larger bend radius to diameter ratios than are currently specified for steel reinforcement.

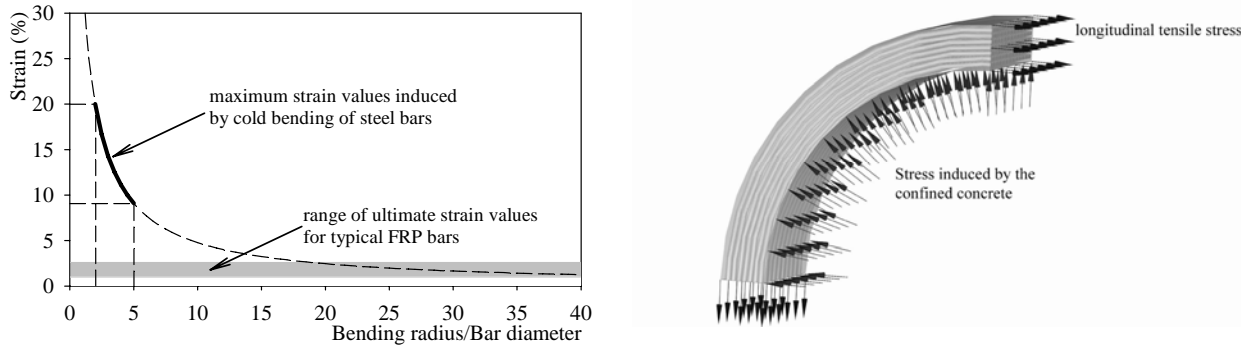


Figure 1: Strain induced in cold bent bar (left) and Longitudinal and transversal stress acting on a FRP bent bar embedded in concrete (right)

In cases where tight radii are needed (i.e. for the manufacture of shear links and hooks), preformed curved bars of FRP are required. The high production costs that are associated with the manufacturing of FRP curved elements, however, have generally reduced the interest in using FRPs for these types of applications. In addition, various studies (Ehsani et al. 1995; Ishihara et al. 1997; Maruyama et al. 1995; Morphy et al. 1997) have shown that the tensile strength of FRP bars can be largely reduced under a combination of tensile and shear stresses. This phenomenon can often become an issue when curved unidirectional composite elements are used as reinforcement in concrete structures (Figure 1-right) and especially when the fibres are designed to carry high tensile stresses, since premature failure can occur at the corner portion of the composite. In fact, tests by different authors have shown that the tensile strength of a bent portion of composite bar can be as low as 40% of the maximum tensile strength that can be developed in the straight part (Ehsani et al. 1995; Maruyama et al. 1995; Morphy et al. 1997).

The reduction in the strength of the composite, therefore, needs to be carefully taken into account since it has a major influence on the maximum value of strain that can be safely sustained by the reinforcement. With all of these issues in mind, the 2 years CRAFT RTD project (CurvedNFR 2003), funded by the European Commission, was carried out with the aim of developing material, methodology and manufacturing process for a low-cost, curved fibre-reinforced plastic (FRP) rebar. The project partnership, which ended in 2005, included 8 specialist SME and 3 RTD organisations across 6 European countries.

2. BEND CAPACITY

The experimental work available in the literature (Ehsani et al. 1995; Ishihara et al. 1997; Maruyama et al. 1995; Morphy et al. 1997; Nagasaka et al. 1989; Nakamura and Higai 1995) indicates that the tensile strength of a bent FRP bar can reduce significantly. The reduction in strength that occurs at the corners of a FRP bar has been quantified using empirical models such as that proposed by the Japan Society of Civil Engineers, which is described by Equation (1) (JSCE 1997). In this equation, the strength of the bent portion, f_{fb} , is expressed solely as a function of the uniaxial tensile strength of the composite, f_{fu} , and the bar geometry (i.e. bar cross-section, d , and bend radius, r).

$$f_{fb} = \left(\alpha \frac{r}{d} + 0.3 \right) f_{fu} \leq f_{fu} \quad (1)$$

The value of $\alpha=0.05$ corresponds to a 95% confidence limit, whilst $\alpha=0.092$ corresponds to a 50% confidence limit.

Equation (1) yields generally a conservative estimate of the maximum strength that can be developed in bent bars and it is currently adopted in the different design recommendations for FRP RC structures proposed by the American Concrete Institute Committee 440 (2003); ISIS Canada (2001) and the Institution of Structural Engineers (1999).

At the University of Sheffield, experimental work has been undertaken on the use of thermoplastic composites to manufacture bars that can be shaped easily to meet any detailing needs. Closed shear links have been produced and used successfully in several applications (Imjai et al. 2004). An extensive series of pullout tests on bent bars embedded in concrete was also conducted and various parameters were investigated (r/d ratio, surface finish, concrete strength). The behaviour of thermoplastic GFRP strips (Plytron; $f_{fu}=720$ MPa; $E_f=28$ GPa) and pre-bent thermosetting GFRP rods (Aslan 100; $f_{fu}=760$ MPa; $E_f=40.8$ GPa) was examined in this experimental programme.

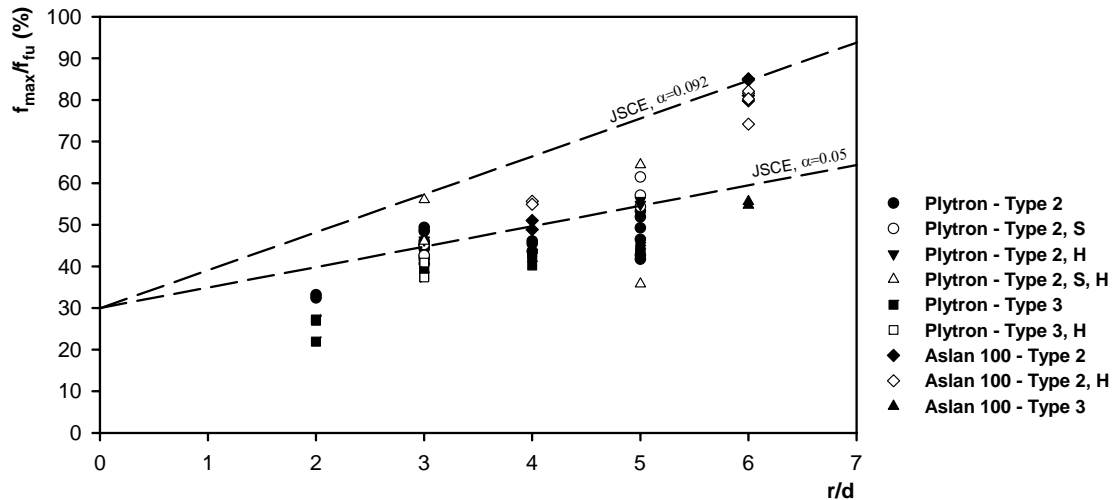


Figure 2: Comparison of test results with predictions according to current design recommendations

The variation in the strength of the bent specimens tested during this research project is shown in Figure 2 and compared to the predictions calculated according to the equation proposed in the JSCE design recommendations (the shaded area demarked by dashed lines). As can be observed, the current design equation does not adequately describe the variation in bend capacity that was observed experimentally. Moreover, whilst the JSCE equation could be used for the design of curved Aslan 100 specimens, it would appear that the same equation could overestimate the bend capacity of the Plytron strip that was used in this study. Sheata *et al.* (2000) have also reported a similar tendency for a commercial type of CFRP reinforcement. In the present study, however, acceptable predictions were obtained for those specimens for which a better bond between the composite and the concrete was ensured either by providing a longer embedment length (Type 2), sand coating the strips (S) or through the use of a high strength concrete (H). Thus, it would appear that the strength of bent bars, depends not only upon longitudinal strength of the composite and the geometry of the bent, but also on the type of fibres, the resin type and manufacturing process.

3. CONCLUSIONS

Based on the experimental work undertaken as part of the CurvedNFR Project, the following conclusions may be drawn:

- (1) Thermoplastic composites seem to offer a valid solution for the manufacturing of bends and complex shapes. The durability of such composites in concrete, however, needs to be investigated.
- (2) The capacity of the bent portion of the composite appeared to be mainly a function of the geometry of the test specimens, namely the bending radius.
- (3) The bend capacity of the test specimens varied between 25% and 85% of the ultimate strength of the composite.

- (4) Values of r/d greater than 4 are required to guarantee a minimum bend capacity of 40% of the ultimate strength of the composite.
- (5) In a significant number of cases, the equation included in the current design recommendations for concrete structures reinforced with FRP was found to overestimate the bend capacity of the Plytron strip.
- (6) The capacity of the bent specimens does not seem to vary linearly with the r/d ratio, as defined in the JSCE equation, and does not appear to be solely a function of the bend geometry. Rather, bond characteristics appeared to be important in controlling the development of stresses along the embedded portion of the composite and in dictating its ultimate behaviour.
- (7) The equation included in the existing design recommendation for predicting the bend capacity of a curved FRP bar does not seem to yield consistent predictions when compared to experimental data. A new predictive model is needed and should be based on a micromechanical approach that takes the mechanical properties of the composite into account.

FRP composite materials need to move from low volume/high technology applications to high volume/relative low technology applications. Before the use of FRPs becomes widely accepted for concrete structures, several significant aspects of the materials have to be examined, including the ability to produce standard reinforcement shapes and the ability to produce large quantities of materials with a consistent quality. All of these aspects are essential if the true potential of FRP reinforcement is to be exploited in civil engineering applications.

4. REFERENCES

- American Concrete Institute (ACI). (2003). "Guide for the Design and Construction of Concrete Reinforced with FRP Bars ACI 440.1R-03", ACI Committee 440, Farmington Hills, MI, USA.
- British Standards Institution (2000), "Specification for Scheduling, Dimensioning, Bending and Cutting of Steel Reinforcement for Concrete", BS8666:2000, BSI, London.
- CurvedNFR (2003). "Cost effective Curved Polymer Composite Rebar". CRAFT RTD European funded project, CRAFT GIST-CT-2002-50365, www.curvednfr.com.
- Ehsani, M. R., Saadatmanesh, H., and Tao, S. (1995). "Bond of Hooked Glass Fiber Reinforced Plastic (GFRP) Reinforcing Bars to Concrete." *Materials Journal*, 122(3), pp. 247-257.
- Imjai, T., Guadagnini, M., and Pilakoutas, K. (2004). "Small-scale and Medium-scale testing for CurvedNFR Project." *ExpR-3*, The University of Sheffield, UK, pp. 13.
- Institution of Structural Engineers (ISE). (1999). Interim Guidance on the Design of Reinforced Concrete Structures Using Fibre Composite Reinforcement, IStructE, SETO Ltd., London.
- ISIS Canada (ISIS). (2001). Manual No. 3 - "Reinforcing Concrete Structures with Fibre Reinforced Polymers (FRPs)", ISIS Canada, Winnipeg, Manitoba, Canada.
- Ishihara, K., Obara, T., Sato, Y., and Kakuta, Y. (1997). "Evaluation of Ultimate Strength of FRP Rods at Bent-up Portion." *Third International Symposium on Non-Metallic (FRP) Reinforcement for Concrete Structures*, Sapporo, Japan, pp. 27-34.
- Japan Society of Civil Engineers (JSCE). (1997). "Recommendation for Design and Construction of Concrete Structures using Continuous Fiber Reinforcing Materials", JSCE, Tokyo, Japan.
- Maruyama, T., Honma, M., and Okamura, H. (1995). "Experimental Study on Tensile Strength of Bent Portion of FRP Rods." *Non-Metallic (FRP) Reinforcement for Concrete Structures. Proceeding of 2nd RILEM symposium (FRPRCS-2)*, pp. 163-176.
- Morphy, R., Sheata, E., and Rizkalla, S. (1997). "Bent Effect on Strength of CFRP Stirrups." *Third International Symposium on Non-Metallic (FRP) Reinforcement for Concrete Structures*, Sapporo, Japan, pp. 19-26.
- Nagasaka, T., Fukuyama, H., and Tanigaki, M. (1989). "Shear Performance of Concrete Beam Reinforced with FRP Stirrups." *Transactions of The Japanese Concrete Institute*, 11, pp. 789-811.
- Nakamura, H., and Higai, I. (1995). "Evaluation of Shear Strength on Concrete Beams Reinforced with FRP." *Concrete Library, JSCE*, 26, pp. 111-123.
- Sheata E., Morphy R. and Rizkalla S. (2000) "Fibre Reinforced Polymer Shear Reinforcement for Concrete Members: Behaviour and Design Guidelines", *Can. J. Civ. Eng./Rev. can. génie civ.* 27(5), pp. 859-872.
- Ueda T., Sato Y., Kakuta Y., Imamura A., and Kanematsu H. (1995). Failure Criteria for FRP rods Subjected to a Combination of Tensile and Shear Forces. *Non-Metallic (FRP) Reinforcement for Concrete Structures. Proceeding of 2nd RILEM symposium (FRPRCS-2)*, pp. 26-23.

FLEXURAL TESTING OF SPUN-CAST HOLLOW CONCRETE PILE SECTIONS REINFORCED WITH CFRP GRID AND BARS

Antonis Petrou Michael

(Post Doctoral Associate, University of Florida, Gainesville, Florida, USA)

H. R. Hamilton III

(Associate Professor, University of Florida, Gainesville, Florida, USA)

ABSTRACT

Corrosion of prestressing steel in precast concrete is a significant problem for bridges constructed in coastal waters. Carbon fiber-reinforced polymer (CFRP) reinforcement has been suggested as a non-corrosive replacement for steel in highly corrosive environments. One drawback, however, is the lack of ductility that CFRP flexural reinforcement provides when the section is taken to its full capacity under extreme events such as earthquakes or barge impacts. This paper covers flexural testing of circular hollow concrete sections constructed using CFRP bars for flexural reinforcement and CFRP grid for concrete confinement. In addition, the pile sections were manufactured using the spun-cast process providing a unique combination of materials and manufacturing processes. Experimental results available from the flexural tests indicated no significant improvement in the ductility of the grid reinforced piles compared to the control piles but that can be attributed to damaged confinement reinforcement and/or failure modes involving shear.

KEYWORDS

Spun-cast piles, CFRP reinforcement, concrete confinement, ductility.

1. INTRODUCTION

The spun-cast method is commonly used to produce prestressed concrete poles for power lines or stadium lighting. They are produced by placing the concrete in a mold and then spinning the mold at high speed for a specific amount of time depending on the size of the pole. The centrifugal force distributes the concrete across the length of the pole while at the same time highly compacts the concrete. Spun-cast poles have higher concrete strengths and less permeability than regular cast concrete poles.

Corrosion of prestressing steel in precast concrete is a problem for bridges in coastal waters. Carbon fiber-reinforced polymer (CFRP) reinforcement has been suggested as a non-corrosive alternative for steel in highly corrosive environments. One drawback, however, is the lack of ductility that CFRP flexural reinforcement provides when the section is taken to its full capacity under dynamic loading events such as earthquakes or barge impacts. In this proposed configuration the piles are designed to fail by crushing the concrete and an improvement in the ductility of the concrete section is sought through concrete confinement. A CFRP grid tied into a circular shape and cast into the concrete in a similar configuration to spiral ties is used as confinement reinforcement.

CFRP grids (with thicknesses of 3 to 4 hundredths of an inch) are used primarily for crack control in concrete structures. Harries and Gassman (2003) conducted tests on reinforced concrete basin knockout panels that employed a light carbon grid to control cracking. The grid reduced cracking of the panel significantly. Shao et al. (2003) used the same light carbon grid to control plastic shrinkage cracking in concrete. They concluded that the plastic shrinkage cracks were reduced by 50% to 65%. Michael et al. (2005) embedded the CFRP in concrete cylinders to provide confinement. Two layers of the CFRP grid were used and it was found that the CFRP grid provided confinement and doubled the concrete crushing strain.

2. PILE MANUFACTURING

Six 38-foot long piles were constructed including three with no grid in the mid-length portion of the pile (spun cast control (SCC) piles) and three with carbon grid over their entire length (spun cast grid (SCG) piles).

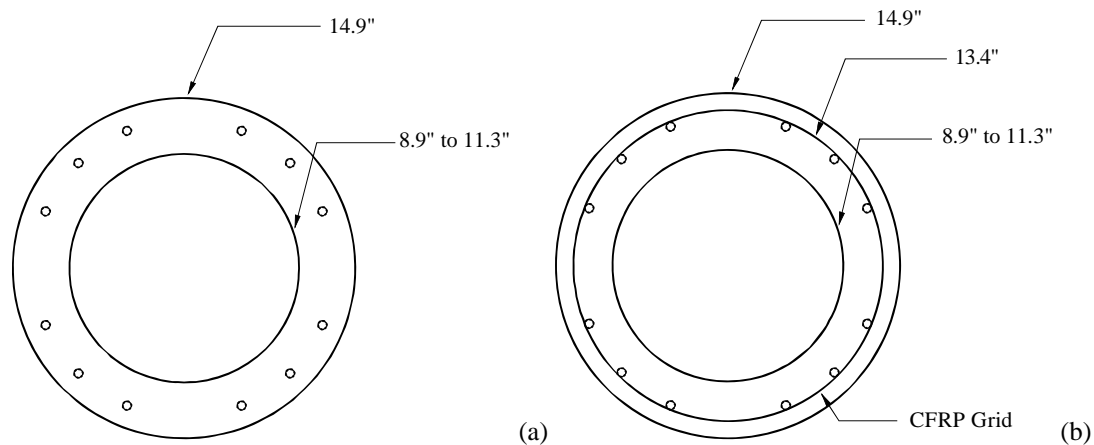


Figure 1: Mid-span cross-section: (a) Control pile and (b) Grid pile

Twelve carbon reinforcing bars with a diameter of 0.375 in. were used as flexural reinforcement for the pile specimens (See Fig.1). A concrete mixture with a specified 28-day compressive strength of 5000 psi and a maximum aggregate size of 0.375 in. was used to manufacture the pile specimens.

The manufacturing process included several steps: (a) Placement of flexural reinforcement, (b) Placement of the CFRP grid, (c) Placement of concrete (See Fig. 2(a)), (d) Sealing of the mold, (e) Spinning of the mold (See Fig. 2(b)), (f) Overnight curing of the pile inside the mold, and (g) Removal of the pile from the mold.



Figure 2: Spun cast pile manufacturing: (a) Concrete Placement and (b) Mold spinning on platform

3. FLEXURAL TESTING

All piles were tested in a simply supported four-point bending configuration (See Fig. 3) in displacement control mode, that is, a constant displacement rate was applied independently of the amount of load. A hydraulic actuator was used to apply the displacement to the piles. The applied displacement was distributed to the two load points using a steel spreader beam. Because the spun-cast pile specimens were circular in cross-section, steel saddles were placed at the end supports to accommodate the shape of the piles and avoid lateral movements. Two more steel saddles were used at the load points for load transfer from the spreader beam to the piles without slippage. The piles were loaded at a rate of 0.01-in. per second. The displacement was applied monotonically until the pile could no longer sustain any load.

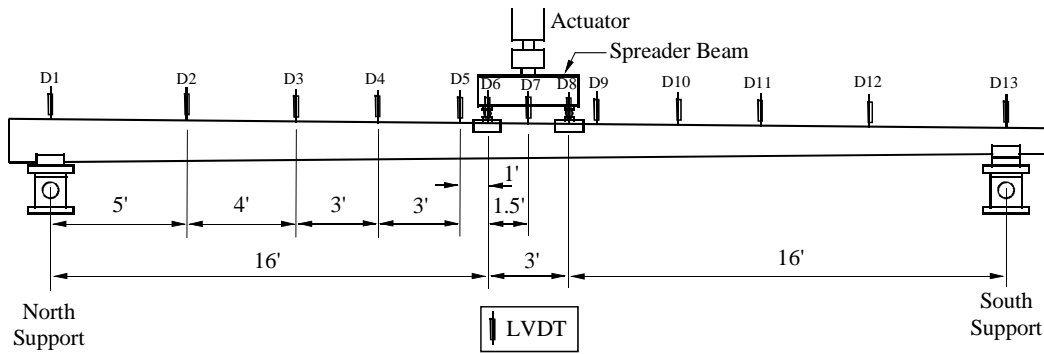


Figure 3: Test set-up

4. RESULTS

The load-displacement curves for all pile specimens were linear to peak load (Fig. 4 (a)). The load-displacement curves for all pile specimens were similar and their behavior non-ductile. Although pile SCG1 had exhibited some post peak behavior it was not significant. This was attributed to the fact that pile SCG1 failed in shear-flexure and therefore the effect of concrete confinement did not contribute to the overall behavior of the pile. Pile SCG3 did not exhibit any post peak behavior and failed in the same manner as pile SCC3. This was not expected because the presence of the CFRP grid as concrete confining reinforcement was expected to result in an improvement in the ductility of the pile. However, it was discovered after the end of the test that the CFRP grid had been badly damaged during construction. The damage resulted in the rupture of the hoop direction strands. The loss of the hoop direction strands resulted in lack of concrete confinement and consequently failure to improve the ductility of the pile.

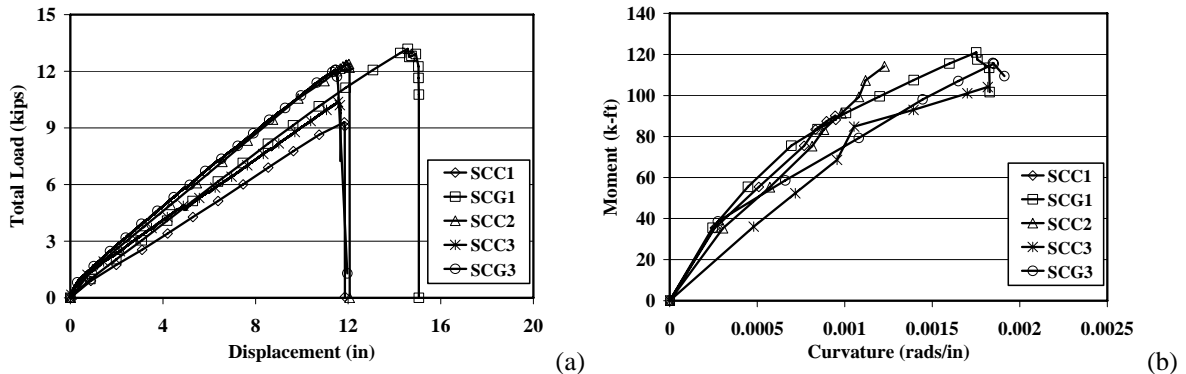


Figure 4: (a) Load-displacement curves and (b) M- Φ curves (Numerical differential method)

The failure of the control piles (SCC1, SCC2 and SCC3) was highly brittle inside the constant moment region. The control piles shattered into pieces (See Fig. 5(a)). Specimens SCG1 and SCG3 also had brittle failures although concrete did not shatter in both cases. The lack of improvement in ductility for these two piles was attributed to the mode of failure for SCG1 (shear-flexure) and to construction mishaps for SCG3 (damage to grid hoop strands). During testing of pile SCG2 a number of significant observations were made. The pile failed in flexure inside the constant moment region adjacent to the south load point. Failure was not abrupt but gradual. Pile SCG2 did not collapse at the end but rather was capable of supporting its own weight and an additional load of approximately 2 kips (See Fig. 5(b)). Unfortunately, a data acquisition malfunction resulted in the loss of the data for this specimen, leaving only video and photographic evidence. This was the type of behavior that was unsuccessfully attempted to duplicate with pile SCG3.

The moment-curvature (M- Φ) curves of all specimens were developed and plotted (See Fig. 4(b)). The numerical differential method was used to calculate the curvature values at various load levels. The numerical differential method calculates the curvature based on the displacement values of adjacent points and therefore any localized

effect such as the formation of a plastic hinge can be detected. The plastic hinge is usually manifested in the form of large increases in the curvature.

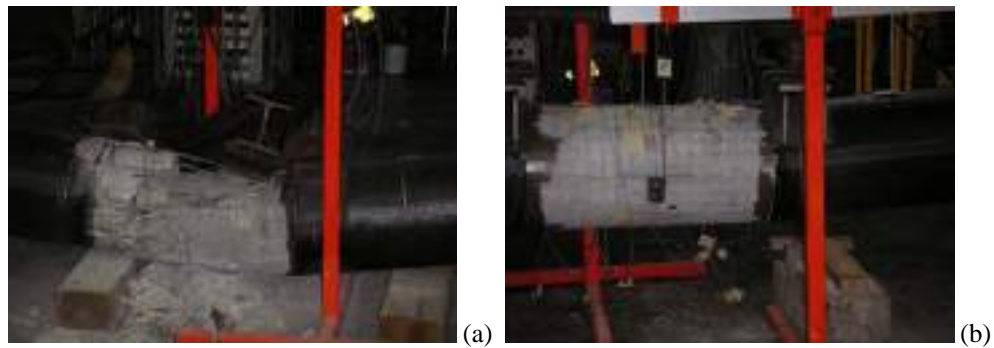


Figure 5: Pile specimens after testing: (a) Control and (b) Grid

It is apparent from the $M-\Phi$ curves that none of the pile specimens formed a plastic hinge. Only specimen SCG1 may have been in the very early stages of plastic hinge formation but the impact on the overall ductility of the pile was minor.

5. CONCLUSIONS

Based on the results presented in this chapter the following conclusions can be drawn:

- The results from the piles indicate that the ductility of the grid piles was not significantly altered. However the visual observations during testing of pile SCG2 indicated a change in the behavior using the CFRP grid as confinement reinforcement and that improvement in ductility of CFRP reinforced pile using concrete confinement might be feasible.
- The tests revealed problems with the manufacturing practice that proved to be very significant in influencing the behavior of the pile specimens. These problems need to be addressed to take advantage of the possible improvement in ductility due to confinement provided by the CFRP grid.
- The results presented in this paper represent a lower bound solution to the ductility problem of spun-cast manufactured CFRP reinforced piles.

6. ACKNOWLEDGEMENTS

This study is sponsored by the Florida Department of Transportation. The authors gratefully acknowledge the contributions of Steve Eudy who set up and ran the data acquisition system, as well as Marc Ansley, Frank Cobb, Tony Johnston, Paul Tighe, and David Allen who helped prepare the specimens and set-up the testing apparatus. The authors would also like to thank Accord Industries, Inc. for manufacturing the piles at cost. The authors thank Jaber Jaber and John French of Accord Industries for their support and help in completing the manufacturing of the piles.

7. REFERENCES

- Harries, K. A. and Gassman, S. L. (2003), "Load tests of reinforced concrete catch basing knockout panels", Department of Civil and Environmental Engineering, University of South Carolina, Report No ST03-01, p. 21.
- Shao, Y., Johnson, C. and Mirmiran, A. (2003), "Control of plastic shrinkage cracking of concrete with TechFab carbon FRP grids", Department of Civil, Construction, and Environmental Engineering, North Carolina State University, Report to Tech-Fab Inc, p. 7.
- Michael, A. P., Hamilton, H. R. III, and Ansley, M. H. (2005). "Concrete confinement using carbon fiber reinforced polymer grid", *7th International Symposium of Fiber-Reinforced Polymer (FRP) Reinforcement for Concrete Structures*, Editors: Carol K. Shield, John P. Busel, Stephanie L. Walkup, and Doug D. Gremel, American Concrete Institute, Kansas City, MO, Vol. 2, pp. 991-1010.

Use of GFRP Bars as Reinforcement for Concrete Bridge Deck Slabs

Brahim Benmokrane ¹, Ehab El-Salakawy ², Sherif El-Gamal ³, and Amr El-Ragaby ⁴

¹ NSERC Research Chair Professor in Innovative FRP Composite Materials for Infrastructures, Department of Civil Engineering, University of Sherbrooke, Sherbrooke, Quebec, Canada

² Canada Research Chair Professor in Advanced Composite Materials and Monitoring of Structure, Dept. of Civil Engineering, University of Manitoba, Winnipeg, Manitoba, Canada

³ Post Doctoral Fellow, Department of Civil Engineering, University of Sherbrooke, Sherbrooke, Quebec, Canada

⁴ Ph. D. Candidate, Department of Civil Eng., University of Sherbrooke, Sherbrooke, Quebec, Canada

ABSTRACT

Six innovative concrete bridges reinforced with FRP bars were recently constructed in North America. Five bridges, Wotton, Magog, Cookshire-Eaton, Val-Alain, and Melbourne Bridges are located in Quebec, Canada, while the sixth one, Morrystown Bridge, is located in Vermont, USA. All the bridges are of girder-type with main girders made of either steel or prestressed concrete with spans ranging from 26.2 to 50.0 m. The deck is a 200 to 230 mm thickness concrete slab continuous over spans of 2.30 to 3.15 m. Glass and carbon FRP reinforcing bars as well as conventional steel were used as reinforcement for the concrete deck slab. The bridges are well instrumented at critical locations for internal temperature and strain data collection using fiber optic sensors. Except Melbourne Bridge, all bridges were tested for service performance using calibrated truckloads. This paper presents the construction details and field testing results of the constructed bridges. The construction procedure and field test results under real service conditions showed very competitive performance to concrete bridges reinforced with steel.

KEYWORDS

Concrete, deck slabs, FRP, strains, deflection, testing.

1. INTRODUCTION

The corrosion of steel reinforcing bars in concrete bridge decks, which leads to excessive cracking, spalling, reduced strength and ultimately loss of structural integrity, constitutes a major problem when measured in terms of rehabilitation costs and traffic disruption (Yunovich and Thompson, 2003). Attempts in recent years to address corrosion-related problems have included the development and assessment of alternatives to conventional steel reinforcement. One of these alternatives, fiber-reinforced-polymer (FRP) composite reinforcement has been used successfully in many industrial applications and, more recently, has been introduced as reinforcement in concrete bridge decks and other structural elements. The use of the non-corrodible FRP bars as reinforcement for concrete bridge decks provides a potential for increased service life, economic, and environmental benefits (Nanni and Faza 2002; El-Salakawy and Benmokrane 2003).

This paper presents new and innovative field applications of FRP bars as reinforcement for the concrete deck slabs of six bridges recently constructed in Canada and USA. The variables in these bridges, which were constructed during 2001 to 2005, are the type of FRP reinforcing bars (glass or carbon), the reinforcement ratio, the area of the bridge deck reinforced with FRP bars, the location, and category of the bridge (traffic volume and frequency of using de-icing chemicals). This paper summarizes the construction details and some of the field testing results of these bridges.

2. DESCRIPTION OF THE BRIDGE DECK SLABS

All the six bridges were built with normal-weight concrete. The concrete for the Morrystown Bridge had an average 28-day compressive strength of 27 MPa, compared to 37 to 52 MPa for the other five Bridges. Sand-coated glass

and carbon FRP bars (Pultrall Inc., Thetford Mines, Quebec) were used in reinforcing the bridge deck slabs of the Wotton, Magog, and Morrystown Bridges in 2001 and 2002. By the end of 2002, in collaboration with the NSERC Industrial Chair at the University of Sherbrooke, Pultrall Inc. was successful in developing new sand-coated glass FRP bars with improved mechanical and durability properties (10-15% and 20-25% more modulus and tensile strength, respectively, compared to those of the old bars). The new glass FRP bars were used in reinforcing the bridge deck slabs of the Cookshire-Eaton, Val-Alain, and Melbourne Bridges.

The design of the concrete deck slab for Wotton and Magog Bridges (Quebec, Canada) was originally made with steel bars. Then, the steel reinforcement was replaced with FRP reinforcement. This design approach led to heavy FRP reinforcement. However, the other four bridges were designed based on serviceability criteria. A maximum crack width of 0.5 mm and allowable stress limits (15 and 30% of the ultimate tensile strength of the material under sustained and service loads, respectively) were used as a controlling design factors. This design approach led to more economic, yet conservative, design.

The six bridges are girder type with the main girders made of either steel or prestressed concrete. The six bridges have different spacing between girders, slab thickness, reinforcement types and ratios. Also, the roads on which the six bridges are located have different functional categories, which mean different traffic volumes and environmental conditions (frequency of using deicing salt). Tables 1 and 2 give some details on these bridges. More details on these bridges can be found elsewhere (El-Salakawy et al. 2003; El-Salakawy et al 2005; Benmokrane et al. 2006).

Table 1. Six concrete bridges reinforced with FRP bars.

Bridge	Total length× total width, m		Deck slab		Traffic	Classification
	Thick, mm	Span, m	Transverse	Reinforcement	V/day	
Wotton	30.6 × 8.90	200	2.60	Glass FRP bars at Top and	< 1000	Rural
Magog	83.7 × 14.1	220	2.85	Carbon FRP bars at Bottom	35,000	Highway
Morrystown	43.9 × 11.30	230	2.36		7,000	Urban
Cookshire-Eaton	52.0 × 13.6	200	2.70	Glass FRP bars at Top and	10,000	Urban
Val-Alain	50.0 × 12.6	225	3.15	Bottom	40,000	Highway
Melbourne	89.4 × 12.5	200	3.15		35,000	Highway

Table 2. Reinforcement details of the concrete deck slab of the six bridges.

Bridge	Bar Type	Transverse Direction		Longitudinal Direction	
		Top	Bottom	Top	Bottom
Wotton (2001)	Steel	No.15M@150 (1.00 %)	No.15M@150 (0.85 %)	No.15M@225 (0.67 %)	No.15M@225 (0.57 %)
	FRP	No.16@150 (Glass-1.00 %)	3 No 10 @ 90 (Carbon-1.50 %)	No.16 @ 165 (Glass-0.90 %)	No.16 @ 165 (Glass-0.76 %)
Magog (2002)	Steel	No.15M@160 (0.82 %)	No.15M@160 (0.70 %)	No.15M@240 (0.55 %)	No.15M@240 (0.47 %)
	FRP	No 16 @ 150 (Glass-0.87 %)	3 No 10 @ 90 (Carbon-1.34 %)	No.16 @ 150 (Glass-0.87 %)	No.16 @ 150 (Glass-0.75 %)
Morrystown (2002)	FRP	No 19 @ 100 (Glass-1.95 %)	No 19 @ 100 (Glass-1.65 %)	No 19 @ 150 (Glass-1.30 %)	No 19 @ 150 (Glass-1.10 %)
Cookshire-Eaton (2003)	FRP	No 19 @ 75 (Glass-3.25 %)	No 19 @ 100 (Glass-2.00 %)	No 19 @ 150 (Glass-1.62 %)	No 19 @ 150 (Glass-1.33 %)
Val-Alain (2004)	FRP	No 19 @ 125 (Glass-1.60 %)	No 19 @ 125 (Glass-1.60 %)	No 19 @ 185 (Glass-1.08 %)	No 19 @ 185 (Glass-1.08 %)
Melbourne (2005)	FRP	No 16 @ 100 (Glass-1.36 %)	No 16 @ 100 (Glass-1.36 %)	No 16 @ 200 (Glass-0.68 %)	No 16 @ 200 (Glass-0.68 %)

3. FIELD TESTING

3.1 Instrumentation of the Bridges

All bridges are similarly instrumented at critical locations for internal temperature and strain data collection using fiber optic sensors (FOS) and thermocouples (Figure 1a). Different types of Fabry-Perot (manufactured by Roctest Ltd., St-Lambert, Quebec) and Bragg Grating (manufactured by Avensys Ltd., Cap. De la Madeleine, Quebec) FOS

were installed on reinforcing bars, embedded in concrete, or glued on the surface of the concrete or steel girders. In addition, during testing, deflections of concrete slabs and girders were measured using a system of rulers and theodolites (Figure 1b).

3.2 Static and Dynamic Load Test

Static and dynamic field tests using calibrated trucks were conducted on the bridges after the completion of construction to evaluate the stress level in the FRP reinforcement, the concrete deck slab, and the girders. The tests were carried out using either a single truck or two trucks simultaneously over the different paths, which are expected to produce the maximum deflections and strains in both the reinforcement and concrete as shown in Figure 1c.

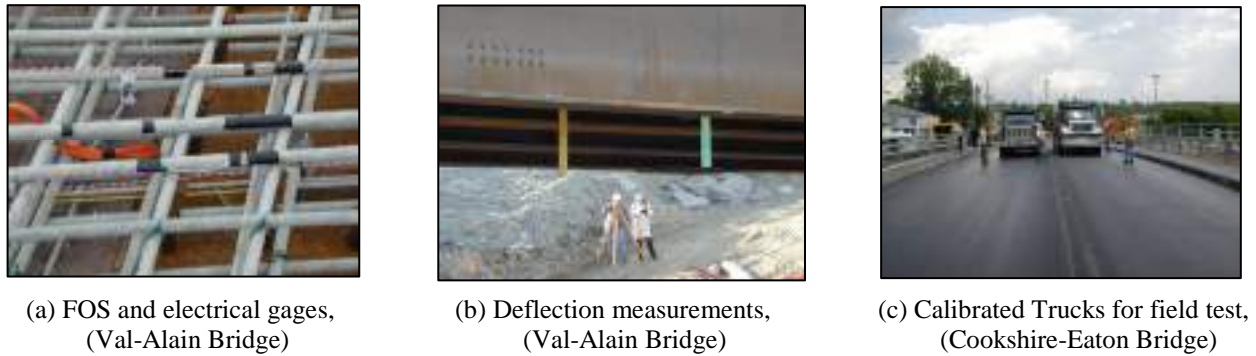


Figure 1. Instrumentation and field load test of the Bridges

4. FIELD TESTING RESULTS

4.1 Strain Measurements

Similar results were obtained for all bridges in terms of maximum measured strains in FRP bars, steel reinforcement, and in concrete. The maximum change in the strain measured in the top and bottom FRP bars (glass or carbon) as the truck moved across the gauge did not exceed 0.5% of the ultimate strain. The maximum concrete compressive strain at the extremes top and bottom surfaces of concrete did not exceed 10 and 30 micro-strain, respectively. Furthermore, the concrete tensile strains were calculated from the tensile strains measured in the FRP bars. The maximum values of tensile strains at the top and bottom surfaces of concrete slab reached 18 and 45 micro strains, respectively. These values were well below the cracking strain of concrete, $\epsilon_{cr} = 112$ to 127 micro strain (for $f_c' = 27$ to 37 MPa and $E_c = 24$ to 29 GPa).

Figures 2a and 2b show the maximum tensile strains measured in top and bottom transverse FRP reinforcement of Val-Alain Bridge against time for different paths at speeds of 5 km/h. For the bottom transverse bars, the maximum measured tensile strain were 53 and 48 micro-strains (compared to 57 for static loading) for speeds of 5 km/h and 50 km/h, respectively. For the top reinforcement, the maximum tensile strains of 22 and 20 micro-strains were recorded for the two simultaneous trucks case at speeds of 5 km/h and 50 km/h, respectively.

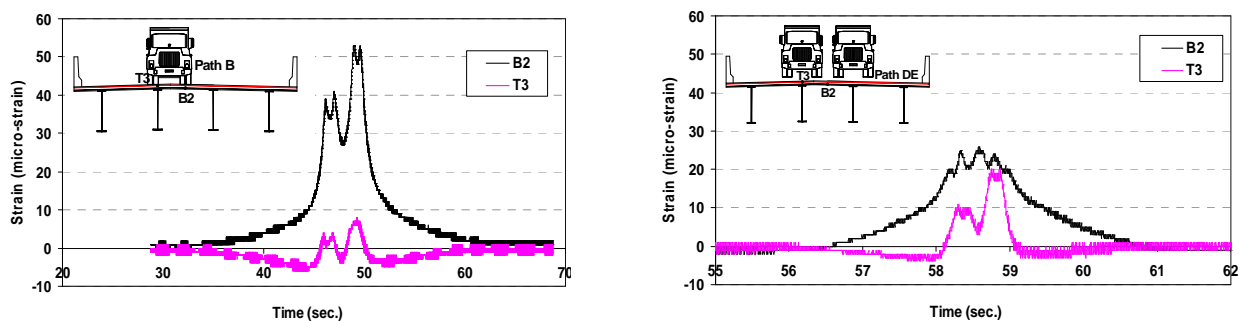


Figure 2. Strains in FRP reinforcement during dynamic load test (Val-Alain Bridge)

4.2 Deflection Measurements

During static tests, deflection of the concrete slabs and steel girders was measured with a theodolite and a system of rulers installed across the mid-span section of the bridge (Figure 1b). The deflection of the concrete deck slab was calculated by subtracting the measured value at the slab position from the average of the values measured on the two girders adjacent to this position. For Morristown Bridge, the single truck traveling over the edge girder (following Path D over girder E, as shown in Fig. 3a) produced the peak deflection of 7.0 mm (L/6270) in that girder. The peak deflection for the middle girders was 8.0 mm (L/5490) measured for the case of the two trucks traveling simultaneously. The maximum measured deflections for the concrete slab were less than 2 mm (S/1180) and were obtained with one truck traveling directly above the measuring point. For Cookshire-Eaton Bridge, as shown in Fig. 3b, the single truck following a certain path B, C, or D (wheel load directly over the girders B, C, or D, respectively) produced a peak deflection of 3.0 mm (L/8680) in the corresponding girder. The peak deflection for the two calibrated trucks traveling simultaneously along Path B-D was 4.0 mm (L/6510) in girder C (Fig. 3b).

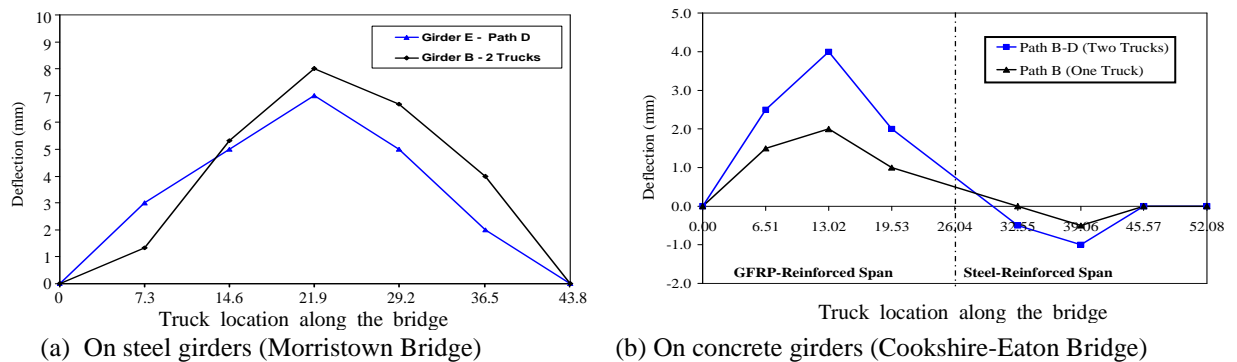


Figure 3. Deflection of girders Vs truck paths and locations

5. CONCLUSIONS

Based on the construction details and the results of the field tests, the following conclusions can be drawn:

1. The serviceability performance of the concrete deck slabs reinforced with FRP bars in terms of strain and deflection was very similar to that reinforced with steel bars.
2. No obstacles to construction were encountered due to the use of the GFRP bars in the two concrete bridge deck slabs. The GFRP bars withstood normal on-site handling and placement with no problems
3. The GFRP-reinforced bridge decks are well performing under very harsh environment. No additional or propagation of cracks, if any, were observed under these severe service conditions
4. During the entire tests, the maximum tensile strains in FRP bars were less than 0.5 % of the FRP ultimate strain. The maximum values of tensile strains in concrete slabs were well below the cracking strain of concrete.

6. REFERENCES

- Benmokrane, B., El-Salakawy, E.F. El-Ragaby, A., and Lackey, T. (2006). Designing and Testing of Concrete Bridge Decks Reinforced with Glass FRP Bars. *ASCE J. of Bridge Engineering*, Vol. 11, No. 2, pp. 217-229.
- El-Salakawy, E.F. and Benmokrane, B. (2003). "Design and Testing of a Highway Concrete Bridge Deck Reinforced with Glass and Carbon FRP Bars". *ACI Special Publication, Field Applications of FRP Reinforcement: Case Studies*, Detroit, Michigan, USA, SP-215-2, pp. 37-54.
- El-Salakawy, E.F., Benmokrane, B., and Desgagné, G., (2003). FRP Composite Bars for the Concrete Deck Slab of Wotton Bridge, *Canadian Journal of Civil Engineering*, Vol. 30, No. 5, October, pp. 861-870.
- El-Salakawy, E.F., Benmokrane, B., El-Ragaby, A., and Nadeau, D. (2005). "Field Investigation on the First Bridge Deck Slab Reinforced with Glass FRP Bars Constructed in Canada." *ASCE Journal of Composites for Construction*, Vol. 9, No. 6, pp. 470-479.
- Nanni, A., and Faza, S. (2002). *Designing and Constructing with FRP Bars: An Emerging Technology*, ACI International, American Concrete Institute, Vol. 24, No.11, Detroit, USA, pp. 29-34.
- Yunovich, M., and Thompson, N. (2003). *Corrosion of Highway Bridges: Economic Impact and Control Methodologies*, ACI International, American Concrete Institute, Vol. 25, No.1, Detroit, USA, pp. 52-57.

OPTIMIZATION OF BRAIDED REINFORCED COMPOSITE RODS

Cristiana Gonilho Pereira

(Researcher, University of Minho, Guimarães, Portugal)

Raul Figueiro

(Professor, University of Minho, Guimarães, Portugal)

Said Jalali

(Associate Professor, University of Minho, Guimarães, Portugal)

Mário de Araújo

(Full Professor, University of Minho, Guimarães, Portugal)

ABSTRACT

This work described the development of braided reinforced composite rods for concrete reinforcement. The research study aims to analyse the influence of braided fabrics geometry on the core reinforced braided fabrics mechanical behaviour. Moreover, this study intends to identify the influence of different fiber types used as core reinforcement and of testing conditions on the mechanical properties of braided fabric composite rods,

KEYWORDS

Concrete, fiber reinforced composite materials, core reinforced braided fabric, core reinforced braided composite rod.

1. INTRODUCTION

Typically, FRP rods are produced by pultrusion, which is a well-known manufacturing method in fabricating FRP products with a constant cross section. In the pultrusion process, the longitudinal fibers are drawn through a resin bath and then passed through a die, which gives the rod its final shape (Kadioglu et al, 2005). Therefore, FRP rods present smooth surface and, when used as internal reinforcement for concrete, the bond at the interface between an FRP rod and concrete is of paramount importance. The bond behaviour will have a direct influence on both the serviceability and ultimate limit. To improve bond behaviour FRP-concrete, a surface treatment is required to introduce deformations on the rod surface, and two different approaches can be considered: deformation of the surface, due to the presence of ribs or indents or providing deformations in the outer resin layer, or surface treatments, such as sand blasting or epoxy-coated sand (Lees, 2001). Besides pultrusion, FRP rods can also be produced using braiding techniques (Soebroto et al, 1990). Braiding is a low cost technique allowing in-plane multiaxial orientation, conformability, excellent damage tolerance and core reinforcement. Moreover, braiding allows the production of ribbed structures and a wide range of mechanical properties may be improved when the core braided fabrics are reinforced with the appropriate type of fibers (Figueiro et al, 2006).

2. EXPERIMENTAL WORK

The current work aims to understand the influence of braided fabrics geometry on the core reinforced braided fabrics mechanical behaviour. A study on the influence of the core reinforcement fiber type on the mechanical properties of the core reinforced braided fabrics and of composite rods has also been undertaken. Moreover, the work aims to understand the influence of testing conditions on the braided reinforced composite rods mechanical properties. The

core reinforced braided fabrics have been produced on a vertical braiding machine. Braided reinforced composite rods have been produced by impregnating the core reinforced braided fabrics on a vinyl ester resin, in a single step.

2.1. Optimal braiding angle of core reinforced braided fabrics

Eight polyester bobbins were used to produce the braided structure and two rovings of glass fiber were used as core reinforcement. The braiding angle varies according to the braided fabric take-up rate. Braiding angles have been measured for each braided fabric produced and tensile tests were carried out. Fabric delivery speed and braiding angle are inversely proportional, as shown in Figure 1.

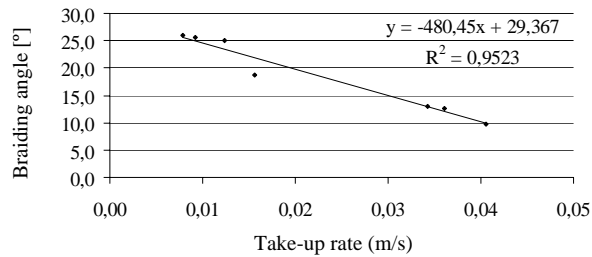


Figure 1: Influence of take-up rate on braiding angle.

Analysing the influence of the braiding angle on the ultimate tensile strength and on the extension at failure, it may be concluded that there is an inflection on the curve. The ultimate tensile strength and the extension at failure increase as the braiding angle increases up to 18.6°. For braiding angles higher than 25°, both the ultimate tensile strength and the extension at failure decrease as the braided angle increases (Figure 2).

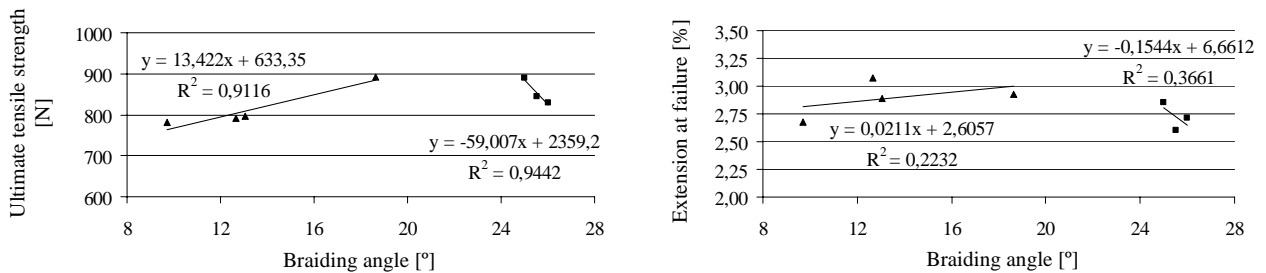


Figure 2: Influence of braiding angle on ultimate tensile strength and on extension at failure (mean values).

Based on the above results, it may be concluded that braided fabrics produced with 8 bobbins of polyester yarn, 2 of them with 4 yarns, and reinforced with 1800 Tex glass fiber roving as core reinforcement, lead to higher values of ultimate tensile strength and higher extensions at failure, when the braiding angles are between 18.6° and 25°.

2. 2. Core reinforced braided fabrics

Core reinforced braided fabrics were produced with a speed of production of 0,0156m/s. Glass, carbon, polyethylene and sisal fibers were used as core reinforcement. Tensile tests were carried out on the different core reinforced braided fabrics for different pre-loading conditions – 25N, 50N and 100N (Figures 4 and 5).

Braided fabrics reinforced with carbon fiber present the highest ultimate tensile stress (Figure 4); this does not seem to be significantly affected by the pre-loading conditions. Braided fabrics reinforced with polyethylene HT fibers present the highest values of extension at failure (Figure 4). The influence of pre-loading on extension is more significant.

As it can be seen in Figure 5, the modulus of elasticity increases when the pre-load is increased from 25 to 100 N. The carbon reinforced fabrics present the highest modulus of elasticity.

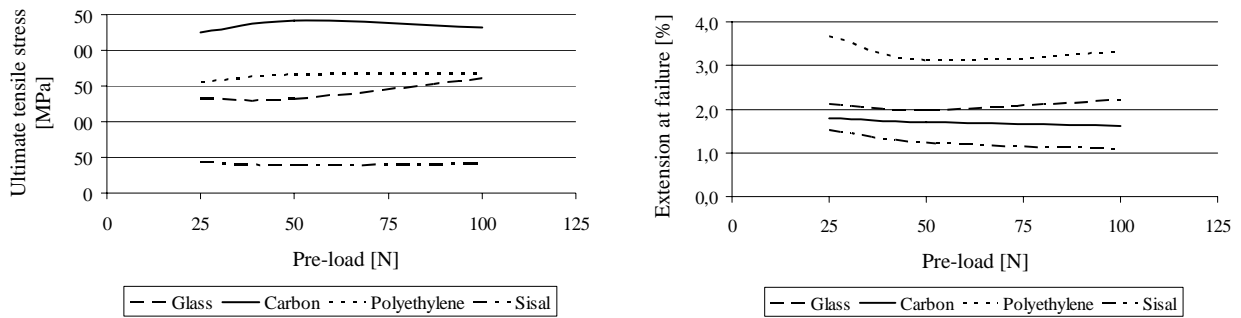


Figure 4: Influence of initial pre-load on the ultimate tensile stress (mean values).

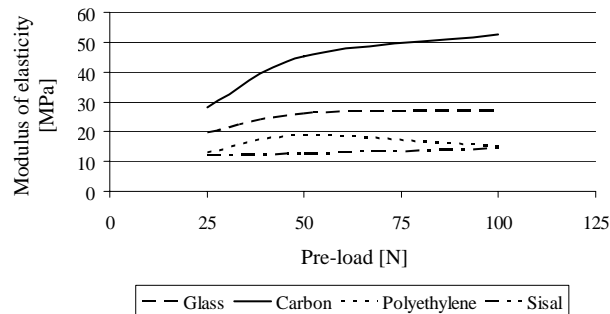


Figure 5: Influence of initial pre-load on modulus of elasticity (mean values).

The effect of initial pre-loading of the core reinforcement braided fabrics presents a significant influence on their modulus of elasticity, as can be seen by analysing the core reinforced braided fabrics tensile behaviour (Figure 6).

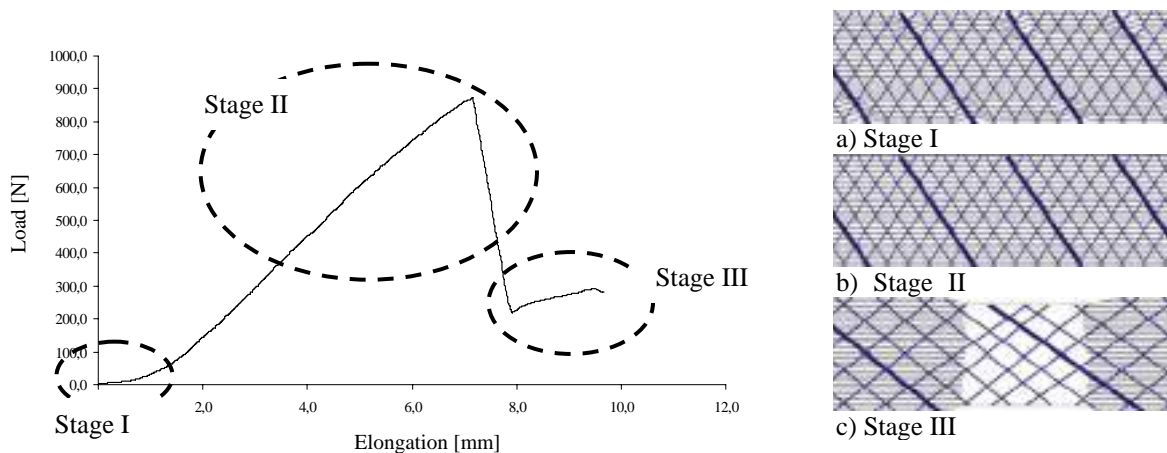


Figure 6: Tensile behaviour of a core reinforced braided fabric.

Three stages can be identified in the load-elongation curve for a core reinforced braided fabric: **Stage I** – The load is supported by the core reinforced fibers; even though, the fibers are not yet completely straight (Figure 6 a)); **Stage II** – The reinforcement fibers are now completely straight and the load is supported by the core reinforced fibers. There is a significant increase in the load required to stretch the reinforcement fibers to the breaking point (Figure 6 b)); **Stage III** – The braided fabric starts to bear the load due breaking of the core reinforcement fibers. Even though braided structures present much better tensile properties comparatively to compressive ones, elongation is much higher than that present by fiber rovings (Figure 6 c)).

2. 3. Braided reinforced composite rods

Braided reinforced composite rods have been produced on a vertical braiding machine with an incorporated impregnation system. Tensile and bending tests were carried out on core reinforced composite rods.

Braided fabric composite rods reinforced with carbon fiber present the highest ultimate tensile stress, on both pre-loading test conditions (Table 4). Regarding to extension at failure and modulus of elasticity, the best results are obtained when core reinforcement fibers are subjected to 25N pre-load. Composite rods reinforced by carbon fibers present significantly higher modulus of elasticity and one of the lowest extensions at failure. Braided fabric composite rods reinforced with carbon fiber present the highest bending stress and significant higher bending modulus (Table 5).

Table 4: Tensile test results for composite rods (mean values).

Pre-load [N]	Reinforcement fiber	Ultimate tensile stress [MPa]	Extension at failure [%]	Modulus of elasticity [GPa]
25	Glass	537,9	4,5	9,7
	Carbon	793,5	3,3	25,0
	Polyethylene	525,3	3,9	8,7
	Sisal	121,8	2,7	4,4
100	Glass	454,5	3,5	9,0
	Carbon	685,7	2,6	23,3
	Polyethylene	473,9	3,9	7,5
	Sisal	114,6	2,3	4,3

Table 5: Bending test results (mean values).

Reinforcement fiber	Bending stress [MPa]	Bending modulus [GPa]
Glass	161,0	5,9
Carbon	351,7	20,3
Polyethylene	115,8	4,1
Sisal	103,0	3,0

3. CONCLUSIONS

It was concluded that for a braided fabric structure there is a braiding angle that promotes the optimized mechanical performance of the core reinforced braided structure and. Analysing the test results obtained it is possible to identify different performances among the different types of core reinforced braided fabrics and the different types of braided reinforced composite rods. The trends in properties of core reinforced braided fabrics are similar to that of composite rods. The mechanical behaviour of the core reinforced braided fabrics is mainly dependent on the core reinforcement performance. It is also concluded that it is necessary to set a pre-tension on the reinforcement fibers to guarantee an optimized mechanical behaviour of core reinforced braided fabrics.

This work is being funded by the Foundation for Science and Technology (Portugal) within POCI PROGRAMME, Project POCI/CTM/6086/2004, “Development of braided reinforced composite elements for concrete reinforcement and monitoring”.

5. REFERENCES

- Fangueiro, R., Sousa, G., Araújo, M., Gonilho Pereira, C., Jalali, S., (2006), “Core reinforced composite armour as a substitute to steel in concrete reinforcement”, International Symposium Polymers in Concrete – ISPIC2006, 2 – 4 April, Universidade do Minho, Guimarães, Portugal.
- Kadioglu, F., Pidaparti, R. M. (2005), “Composite rebars shape effect in reinforced structures”, Composite Structures, No. 67, pp 19-26.
- Lees, J. M. (2001), “Fibre reinforced polymers in reinforced and prestressed concrete applications: moving forward”, Prog. Struct. Engng. Mater., No. 3, pp 122-131.
- Soebroto, H.B., Pastore, C.M., Ko, F.K. (1990), “Engineering design of braided structural fiberglass composite”, Structural Composites: Design and Processing Technology, 6th Annual Conference, Advanced Composites, Detroit

Part XI. Health Assessment

Nondestructive Evaluation of FRP Bonding by Shearography

F. Taillade

(Researcher, Design and Physical Systems Unit - French Public Works Research Laboratory - LCPC, Paris, France)

M. Quiertant

(Researcher, Structural Engineering Unit - French Public Works Research Laboratory - LCPC, Paris, France)

C. Tourneur

(Technical Manager, Freyssinet France, Palaiseau, France)

ABSTRACT

This paper describes the application of shearography to the evaluation of the adhesion of externally bonded fiber-reinforced polymer (FRP) on concrete surface. The principle of the method is first reviewed. Theoretical and experimental analysis of the disbonds is presented. To validate the feasibility of the proposed method, different sizes of defects are simulated by replacing adhesive by TEFLON® discs between the concrete and the carbon epoxy film at known locations of slab type concrete model specimens. To perform shearography analysis, these samples are loaded by vacuum stressing. Presented results show that shearography enables one not only to determine locations and areas of bond defects but also to evaluate the quality of adhesion (assessment of partial debonding).

KEYWORDS

Nondestructive testing, shearography, disbonds, concrete, carbon epoxy, fiber-reinforced polymer, FRP.

1. INTRODUCTION

The strengthening or retrofitting of existing concrete structures must be accomplished according to design and construction guidelines to ensure the durability and long-term performance of the FRP strengthening system (ACI Committee 440, 2002; AFGC, 2003; fib Task Group 9.3, 2001). After being applied, these systems (fibers and resins) have to be evaluated to check their conformance with specifications. The quality-control program must be achieved through a set of inspections and tests. Methods such as acoustic sounding (coin or hammer tap), ultrasonics and thermography are used to detect delaminations (disbonds). These methods are efficient to locate bond defects but are not capable of quantifying evaluating the quality of adhesion of the FRP to the substrate (partial delamination, damage of the resin, bad mechanical property of the resin). Consequently, a shearography nondestructive evaluation (NDE) method for FRP bonding was previously developed by Taillade (Taillade, 2006) and is here applied in the field of the strengthening of concrete structures.

2. PRESENTATION OF THE NONDESTRUCTIVE METHOD

Shearography is a speckle interferometric technique providing full-field and in near-real time quantitative images of structural surface displacements. This technique can be applied to detect the disbonds in a structure composed of a concrete substrate, one layer of adhesive, and one layer of carbon-epoxy composite. Principles of the method are those described by (Hung, 2001) but application proposed by authors is also capable of evaluating the bonding quality between the jacket and the concrete.

2.1 The shearography technique

The principle of an interferometer with a video split, called shearography, is to cause the interference of two waves that had been submitted to nearly the same random fluctuations in optical path during their trajectories between the studied object and the CCD (Charge Coupled Device) matrix. In order to produce this effect, one

conventional technique consists in carrying out a differential measurement of the optical phase φ proportional to the product of the refraction index and the geometrical length along the respective path of each of the two beams. The shearography based on this principle thus causes the interference of two waves coming from two points close to the object A and B and separated by a quantity δ_x ($1 \text{ mm} \leq \delta_x \leq 10 \text{ mm}$). Various devices allow determining this shift, which at times is referred to as the rate of shear; these would include: the Michelson interferometer (see Figure 1 and Leendertz, 1973), glass corner (Hung, 1979), biprism (Hung, 1989), and development defect evaluation (Hung, 1974). The set-up using the Michelson interferometer enables one regulating the rate of shear by simply tilting one of the two interferometer mirrors and then implementing the phase-shift technique (Creath, 1994), by means of translating the other mirror.

In the reference state, φ is equal to φ_s , which represents a random dephasing due to surface roughness and topography of the target object. This random dephasing lies at the origin of the speckle figure that may be observed by examining a rough surface lit by a coherent light source. By assuming that the object undergoes a small deformation, the measured phase becomes: $\varphi_s + \Delta\varphi$, where $\Delta\varphi$ denotes the variation in dephasing between the two states.

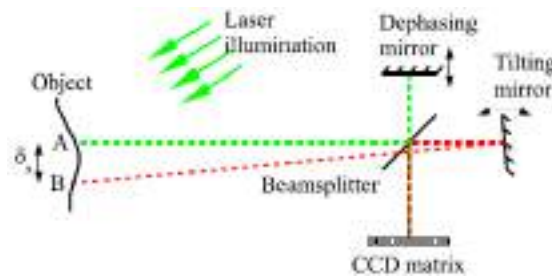


Figure 1: Principle of a shearographic interferometer set-up

In the case of plane waves, for directions of illumination and observation normal to the plate, and with a shear distance δ_x small compared with the characteristic distances over which the deformations occur, the phase difference is expressed at the first order by:

$$\Delta\varphi = \frac{4\pi}{\lambda} \left(\frac{\partial w}{\partial x} \right) \delta_x$$

in which w is the amplitude of the displacements normal to the object surface and λ is the illumination laser wavelength.

By performing an uncertainty budget (Taillade, 2006), we found that the phase difference equivalent to noise is roughly $2\pi/50$ (noise including calibration procedure). Without any particular precaution (in field applications), displacement difference can thus be mapped with a 5 nm uncertainty.

2.2 Excitation method

The partial vacuum (or depression) ΔP is the most employed in nondestructive testing by shearography (Clarady, 1993; Deaton, 1993) to diagnose aircraft structures (Newman, 1991; Bobo, 1991) and the cryogenic tanks of rockets (Burleigh, 1993). It makes it possible to detect very well various kinds of defects and mainly delaminations in composite materials as well as disbonds in the metal structures. The difference in pressure between the blade of air inside the defect and the surface subjected to the stress creates a deformation in the shape of "bump" into defect. The depression which should be applied to obtain a measurable deformation by shearography can be very weak (a few Pascal). It depends primarily on the mechanical characteristics of material analysis (elasticity coefficients) and of width/depth ratio of the defect. To envisage the depression to be applied and to analyze the field of deformation to be measured, we use finite elements models in order to design abacuses usable by the operators. It is then possible to consider that concrete substrate is itself cracked or other producing a particular field deformation. The stressing can be applied by a weak depression to surface study by means of a suction cup.

3. EXPERIMENTATIONS

3.1 Description

Two concrete samples ($300 \times 300 \text{ mm}^2$) have been manufactured (Figure 2). The defects are simulated in replacing adhesive by a TEFLON® disc (width 0.5 mm) between the concrete samples and the carbon epoxy film. Sample n°1 contains four different discs (40, 30, 20, 10 mm dia) and sample n°2 contains four discs with identical 40 mm diameter ($\text{Ø } 40$) with different holes (in number and size represented by the percentage of remaining disc mass) to vary quality of adhesive properties. In the experimental set-up (Figure 3), we show that shearography visualizes deformation through suction cup (Plexiglas® chamber $180 \text{ mm} \times 180 \text{ mm} \times 70 \text{ mm}$ and with 20 mm wall thickness).

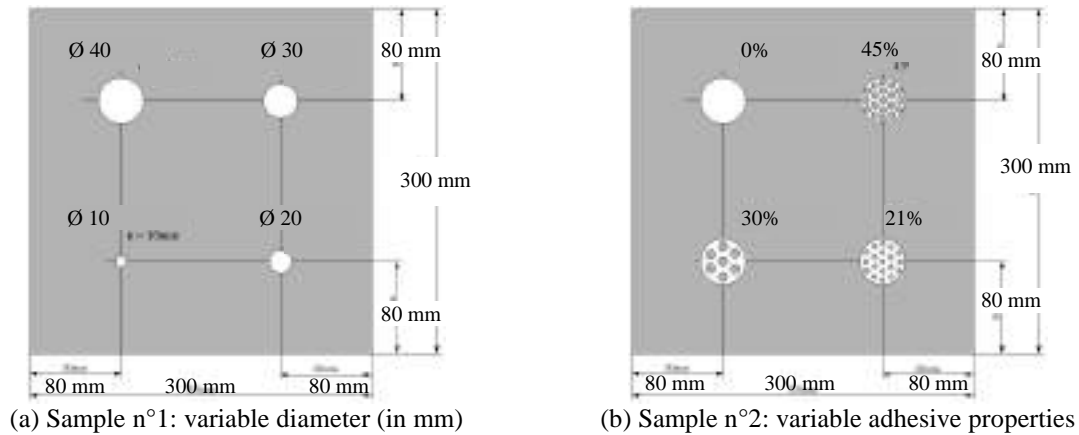


Figure 2: Concrete samples with bonded carbon epoxy film containing different disbands (made of Teflon® discs, size and form variables)

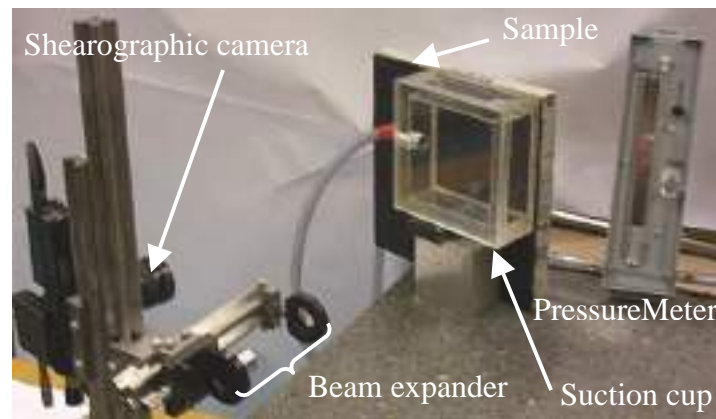


Figure 3: Experimental set-up

3.2 Results

The results obtained with sample n°1 (Figure 4) show the phase difference measured by shearography through suction cup. The applied depression, to visualize defects by shearography, increases when the diameter of defects decreases. The magnitude of pressure is about $100 \text{ hPa} \pm \Delta P/2$ that is not detrimental to structure. With sample n°2, we show (Figure 5) that when the percentage of hole on disc is more important (i.e. when the disbond is less important), it is necessary to impose a more important depression to measure a difference optical phase of the order of 2π . All the results are confirmed by the finite elements analysis.

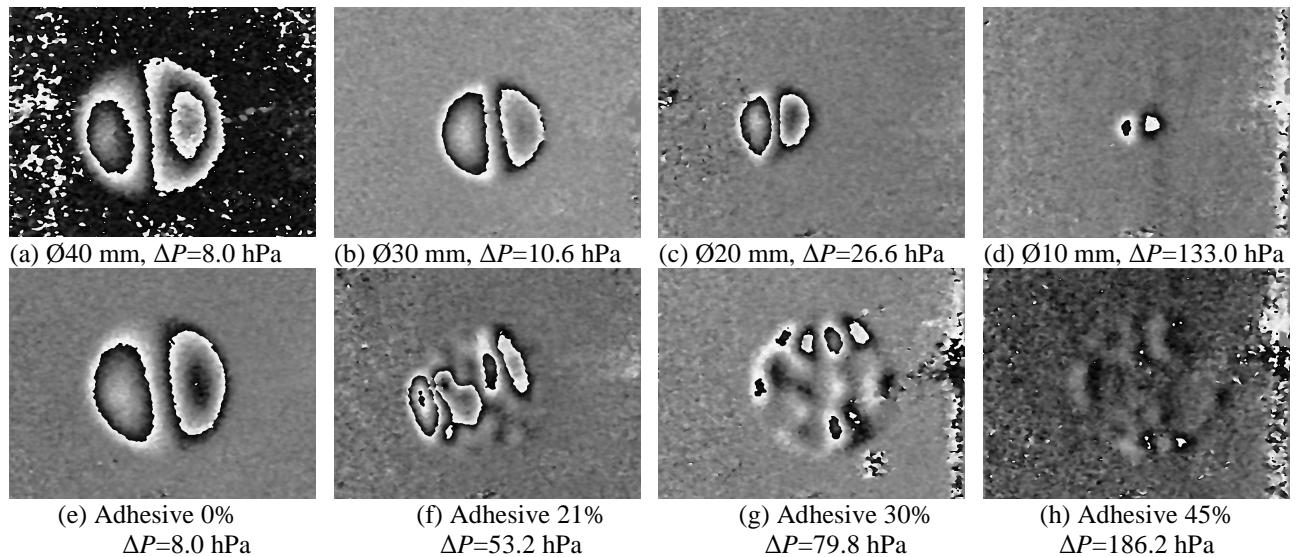


Figure 4 : Measured strain around disbonds of different sizes on sample 1, under different partial vacuum levels (a, b, c, d) and disbonds (40 mm dia) on sample 2 for different adhesive percentage (d, e, f, g)

4. CONCLUSIONS

In this paper, the principle of shearography NDE method is reviewed. An application of this method to the evaluation of the adhesion of externally bonded fiber-reinforced polymer on concrete surface is presented. Results demonstrate that this NDE method enables one to determine not only locations and areas of defects but also to quantify the adhesion in the case of a partial debonding. Moreover, this technology is particularly adapted to field evaluation due to its real time assessment capability and hand portability. This method for local evaluation of bond defects can be complementary to thermography for global and rigorous inspections of repaired structures.

5. REFERENCES

- ACI Committee 440.2R02. (2002). *Guide for the Design and Construction of Externally Bonded Systems for Strengthening Concrete Structures*, ACI, Michigan, U.S.A.
- AFGC. (2003). *Réparation et renforcement des structures en béton au moyen des matériaux composites – Recommandations provisoires*, Bulletin scientifique et technique de l'AFGC. (in French).
- Bobo S. (1991). *Shearographic inspection of a Boeing 737*. Technical report, Federal Aviation Administration.
- Burleigh D. D., Engel J. E. & Kuhns D. R. (1993). "Laser shearographic testing of foam insulating on cryogenic fuel tanks". *Review of Progress in Quantitative Nondestructive Evaluation*, Vol. 12, pp 411-418.
- Clarady J. F. & Summers M. (1993). "Electronic holography and shearography NDE for inspection of materials and structures". *Review of Progress in Quantitative Nondestructive Evaluation*, Vol. 12, pp 381-386.
- Creath K. (1994). Phase shifting holography interferometry. In Rastogi P. K. (ed), *Holographic interferometric*. 68, (Springer Series in Optical Science), pp 109-150.
- Deaton J. B. & Rogowski R. S. (1993). "Electronic Shearography: current capabilities, potential limitations and future possibilities for industrial nondestructive inspection". *Review of Progress in Quantitative Nondestructive Evaluation*, Vol. 12, pp 395-402.
- fib Task Group 9.3. (2001) *Externally bonded FRP reinforcement for RC structures*, fib bulletin 14, Lausanne, Switzerland.
- Hung M. Y. Y. (2001). "Shearography and applications in nondestructive evaluation of structures", *Proceedings of the international conference on FRP Composites in civil engineering 2001*; p. 1723-1730.
- Hung Y. Y. (1974). *Optics Communication*, Vol. 11, No. 2, pp 132-135.
- Hung Y. Y. (1979). *Applied Optics*, Vol. 18, No. 7, pp 1046-1051.
- Hung Y. Y. J. (1989). *Nondestructive Evaluation*, Vol. 8, No. 2, pp 55-67.
- Newman J. W. (1991). "Shearographic inspection of aircraft structure". *Materials Evaluation*, Vol. 49, No. 9, pp 1106-1109.
- Leendertz J. & Butters J. J. (1973). *Phys. E : Sc. Inst.*, Vol. 6, pp 1107-1110.
- Taillade F. (2006). "Metrological Analysis of Shearography". *European Physical Journal – Applied Physics*, to be published.

Structural Health Monitoring in cold climate of a CFRP strengthened concrete hollow box girder bridge

Björn Täljsten

*(Professor, Denmark Technical University, Lyngby, Denmark
Luleå University of Technology, Luleå, Sweden)*

Arvid Hejll

(Tech Lic., Luleå University of Technology, Luleå, Sweden)

ABSTRACT

CFRP (Carbon Fibre Reinforced Polymer)-strengthening with plates and sheets of existing concrete structures is today a well-known method, proven with good results all over the world. However, limited research has been carried out regarding the behaviour of CFRP strengthen structures in cold climates. This paper addresses field testing of a CFRP strengthening pre-stressed concrete hollow box-girder bridge in Stockholm, Sweden, the Gröndals Bridge. Also how the strengthening behaves in cold climate is investigated. Two long term monitoring systems has been installed on a, one traditional system with LVDTs (Linear Vertical Displacement Transducers) mounted over cracks for continuous monitoring and one system with FOS (Fiber Optical Sensors) mounted over cracks and on CFRP-plates. Results show that difference in temperature causes most of the live load. Other results from summer and winter measurements shows that the CFRP plates are not tensioned during winter. A conclusion from this is that the strengthening would have been much more effective if the CFRP would be applied in the winter when the existing structure is contracted due to the temperature effect. Furthermore, the opening of cracks could be followed over time.

KEYWORDS

Structural Health Monitoring (SHM), CFRP Strengthening, cold-climate, strengthening effect

1. INTRODUCTION

To obtain the most out of a measurement program it is important to carry out SHM in a structured way and that a well-planned procedure is followed c.f. (Hejll 2004). When it comes to long term monitoring there are different strategies on how to monitor the structure, e.g. continuous, periodic, automatically triggered and manual triggered. This may be different from one bridge to another and it can also be changed during time. For example, in the beginning of a monitoring project continuously monitoring may be preferable but later the measurements are taken once a week e.g. periodic monitoring or only when traffic passes the bridge e.g. automatically triggered monitoring. One also discusses global and local monitoring. Local monitoring is defined as the monitoring undertaken on a certain part of the structure. It is useful for laboratory tests or for structures with known damages where the defined area is equipped with sensors. To monitor a global behaviour of a structure other parameters are needed, parameters or methods that can provide information of the whole structure. For the Gröndals Bridge a manual triggered long term monitoring method with local monitoring were used for the FOS (Fibre Optic Sensors).

In 2002 a monitoring and strengthening program was launched at the Gröndals Bridge, a large concrete hollow box girder bridge with severe shear cracks in the web were found, just two years after it was opened to tram traffic. The purpose with the monitoring is twofold, firstly to investigate if the crack opening is stable over time and do not propagate, secondly to use and evaluate FOS for monitor crack opening on concrete. In addition to this a comparison between the traditional monitoring technique and the FOS technique has been carried out. Furthermore, we also wanted to use the FOS monitoring to investigate any strengthening contribution from the CFRP plates.

2. STRENGTHENING OF THE BRIDGE

The main span of the Gröndals Bridge is 120 meters with two adjacent spans each of 70 meters. The bridge carries two railway tracks which are placed symmetrically about the cross-section of the bridge. Bridge inspections carried out on the newly built, 2000, Gröndals Bridge revealed extensive cracking in the webs of its concrete hollow box-girder section. The bridge was designed to the currently applicable Swedish codes, BRO 94 and BBK 94. On the basis of these regulations, it was possible to erect the bridge with extraordinarily slender webs. Relatively high shear stresses and principal stresses are generated because of the small web widths although the webs are fully compressed considering the normal stresses caused by longitudinal pre-stressing. Furthermore, the permanent loads on the structure are dominant. As the permanently exerted principal tensile stresses reached the value of the tensile strength of the concrete, shear cracks were finally created. Additionally, restraining bending moments have been superimposed in the webs due to sun radiation. Assuming a linear temperature difference of 10 to 15 K, this, together with the other transverse bending moments, additionally causes vertically directed tensile stresses at the inside of the web amounting to approximately, $\sigma_z = 2$ to 3 MPa. The positions of the cracks in longitudinal direction of the bridge correspond to the areas of the maximum principal tensile stresses. The cracks first appeared after only a few years of service and subsequent inspections showed that the number and size of the cracks were increasing, (James 2004). The cracks widths were between 0.1 – 0.3 mm and for a few isolated cases between 0.4 – 0.5 mm in the most cracked sections. Investigations as to the cause of the cracking suggested that they were due to inadequate web shear reinforcement. The webs have a thickness of 350 mm and a total height of the box girder close to the main span supports of approximately 7.5 m. In addition, the flanges are quite thick; the bottom flange is, at most, about 1300 mm. To increase the safety level of the bridge strengthening was decided. Because of the progressive nature of the cracking combined with wariness for shear cracks, the bridge was temporarily closed for traffic towards the end of 2001 and temporarily strengthened with external steel stays. Final strengthening were carried out with prestressed steel stays in areas with extensive and large cracks and CFRP plates were used in areas with minor or no cracks to limit the number and size of future possible cracking. In this paper only CFRP strengthening are further discussed. The strengthening work was carried out in spring 2003 and the average temperature on the structure at time for strengthening was approximately 15 °C. Before the strengthening work started the concrete surfaces were sandblasted and holes for anchoring the CFRP plates were drilled in the upper and lower flanges. Plates were only placed on the inside of the bridge. The surfaces were thoroughly cleaned with pressurized air and vacuum cleaners. The surfaces to be bonded were treated with a primer for the system to enhance the bond. The CFRP plates were bonded to the surface, i.e. the webs of the structure, with a high quality epoxy adhesive, BPE[®] Lim 567, specific for the strengthening system used. The Young's modulus of the adhesive is approximately 6.5 GPa at 20 °C. Thermal coefficient for the adhesive was approximately $25\text{-}35 \cdot 10^{-6} / ^\circ\text{C}$. The average thickness of the adhesive was 2 mm. A total of 2 500 m of CFRP plates was used for the bridge. The Young's modulus of the plates was 250 GPa with a failure strain of 11% and the thermal coefficient was approximately $6 \cdot 10^{-6} / ^\circ\text{C}$. The CFRP plates have been bonded at an angle of 70° to the horizontal plane. This was in order for the plates to be bonded perpendicular to the direction of the cracks. To enhance the anchorage steel plates with welded steel bars were bonded to the face of the CFRP plates and anchored by epoxy bonding in pre-drilled holes in the top and bottom flanges. The anchorage length was approximately 250 mm.

3. MONITORING

The monitoring systems installed can obviously not capture the effects of the dead load, and consequently only the relative changes with regard to temperature and live load could be recorded. The FOS sensors are of type Bragg grating and at most 7 sensors were written on one fibre, the length of each sensor was approximately 20 mm. Additionally to the FOS system a traditional long-term monitoring system was installed by the Royal Institute of Technology, Sweden, c.f. (James 2004). This system involved the use of LVDT's and temperature sensors in the form of thermocouples, however, in this paper focus is placed on the FOS system. Two temperature sensors were also added to the traditional system and are positioned on the east web of the box girder, one on the inside and one on the outside. The data received from these temperature sensors are used to investigate the effects of temperature on the crack widths. In total, 32 FOS have been installed on the Gröndals Bridge, they are all installed in section A and section B, both on the concrete and on two of the CFRP plates, see Fig. 1. In table 1 the sensors are presented systematically. For the FOS system, the previously mentioned sensors for temperature compensation shall also be included; however, this is not recorded in table 1. The results presented in this paper are mainly from the west side of the bridge, the side that was most warmed by the sun.

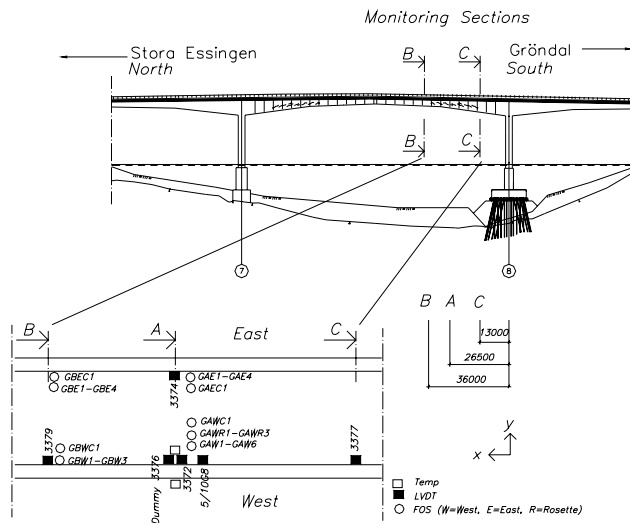


Figure 1. Position of gauges on the Gröndals Bridge.

Section A

Sensor	Measure
GAW1-6	Crack Opening
GWR1-3	Strain Concrete
GAWC1	Strain CFRP
GAE1-4	Crack Opening
GAEC-1	Strain CFRP

Section B

Sensor	Measure
GBW1-3	Crack Opening
GBWC1	Strain CFRP
GBE1-4	Crack Opening
GBEC1	Strain CFRP

Table 1 FOS sensors for monitoring

It is not possible to present all the results from the measurements and therefore only the most interesting findings are presented. However all data from the monitoring up to March 2004 may be found in (James 2004) and (Täljsten and Hejll 2005), where the results from the monitoring are presented for the traditional/ and FOS systems respectively. It was not possible to carry out a continuous FOS monitoring due to the high cost of the system; therefore a periodic monitoring was adopted. It was found that using the chosen FOS system was convenient, in particular for periodic monitoring. The presented results from the monitoring scheme are divided into periodic summer and winter monitoring respectively, on both occasions the monitoring was carried out for approximately 48 hours. FOS sensors were placed over cracks and monitoring is carried out during live loading with trams. The weights of the trams are well defined. The periodic summer monitoring was carried out from the 21st to the 23rd of May 2003. and the periodic winter monitoring was carried out from the 10th to the 12th of March 2005. Fig. 2 and Fig. 3 show selected displacement curves for the FOS monitoring during summer and winter, respectively. With the exclusion of the dead load, it can clearly be seen in both of these curves that it is the temperature on the bridge that has the largest impact on the opening of the cracks and the opening follows a daily variation. GAW3 monitor the largest crack opening, approximately 0.065 mm. On the curve for GAW3 also minor vertical lines can be seen. These lines indicate the passages of the trams and give approximately a crack opening of maximum 0.001 mm. It seems that the effect of the temperature on the opening and closing of the cracks is at least tenfold that of the traffic load. This is confirmed by the traditional monitoring system, where the effect of passing trams is investigated using a sampling rate of 200 Hz, c.f. (James 2004, Sundquist and James 2004).

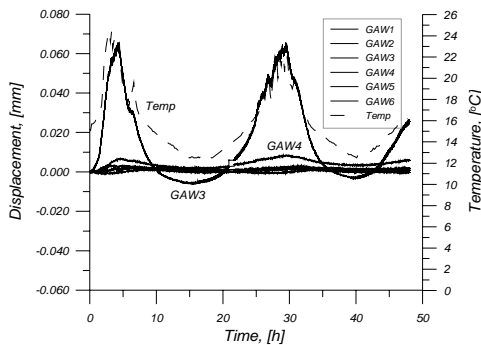


Figure 2. Results from crack-displacement with FOS monitoring system – Summer monitoring

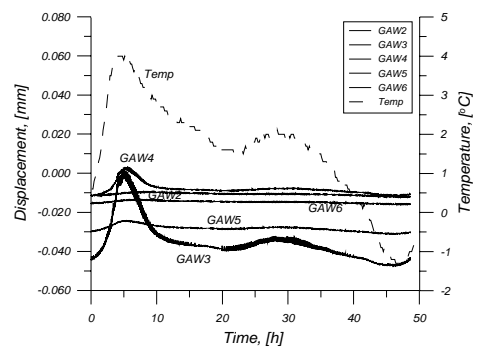


Figure 3. Results from crack-displacement with FOS system – Winter monitoring

For the winter monitoring it can be seen that all cracks are compressed and the opening is negative. In addition to this the crack displacements are fairly small. Furthermore, since the temperature variations for the winter monitoring are considerably less compared to the summer monitoring the changes in crack opening during winter are very small. However, also during winter the displacement curves follow the temperature curves very well. In the figures the effect of the tram traffic can be seen very clear as vertical lines on the displacement curves. The strain values on the CFRP plate on the east side was distinct, both for the summer and winter monitoring, see Fig. 4 to and Fig. 6. These plot shows that the sensor on the plate follows the temperature on the east side very well. Additionally to this it can also be noticed that the plate is under compression during the whole periodic monitoring time period with a maximum measured strain of $-210 \mu\text{str}$ which then correspond to a compressive stress of approximately 55 MPa. The summer monitoring in the CFRP on the west side give a tensile stress in the CFRP plates corresponding to approximately 30 MPa.

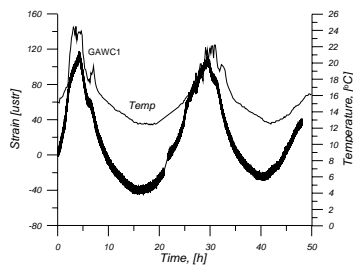


Figure 4. Results from FOS measurement on CFRP– Summer monitoring - West

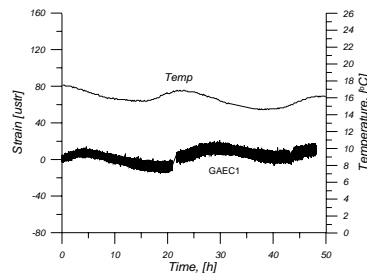


Figure 5. Results from FOS measurement on CFRP– Summer monitoring East

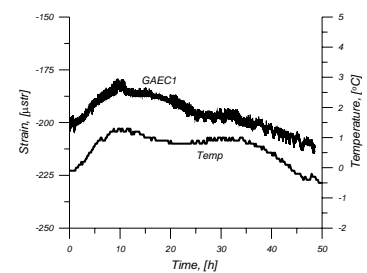


Figure 5. Results from FOS measurement on CFRP– Winter monitoring - East

4. SUMMARY AND CONCLUSIONS

This paper presents both a periodic monitoring from the summer and the winter period and the monitoring shows that the cracks were not propagating and that the openings for the cracks were very small. The largest crack opening measured was approximately 0.06 mm. Furthermore, the temperature effect was at least 10 times larger than the effect from the tram traffic. Comparing the measurements from summer and winter gives the relative effect that the cracks are compressed during the cold period. This is also valid for the measurements on the CFRP plate, which seems to be in tension during the summer and compressed in the winter.

ACKNOWLEDGEMENTS

The research presented in this paper has been funded by several organizations. Here the Development fund of the Swedish Construction Industry (SBUF), Stockholm Transport (SL) and Skanska Sverige AB should be acknowledged. Also City University in London, UK, is acknowledged for their contribution FOS measurements.

REFERENCES

- Hejll, A. 2004 “Structural Health of Bridges”. Licentiate thesis 2004, Division of Structural Engineering, Luleå University of Technology, ISSN 1402-1757/ISRN LTU-LIC—04/46—SE/NR 2004:46
- James G., 2004, Long term health monitoring of the Alvik and Gröndal Bridges, TRITA-BKN Rapport 76, Byggkonstruktion, 2004, Kungliga Tekniska Högskolan, Stockholm, Sweden
- Sundquist, H. and James, G., 2004, Monitoring of shear cracks and the assessment of strengthening on two newly-built light-rail bridges in Stockholm. In *Proceedings of the Second International Conference on Bridge Maintenance, Safety and Management*, IABMAS, Eds. E. Watanabe, D. Frangopol and T. Utsunomiya, Kyoto, Japan, pp 257-258.
- Täljsten B. and Hejll A. (2005). Tvärbanebroarna – Gröndal och Alviksbron: mätning av rörelser med hjälp av fiberoptiska sensorer (FOS), Technical Report, LTU, Luleå, Sweden, Structural Engineering, ISSN 1402-1536/ISRN LTU-TR-05/01-SE/NR 2005:01 (In Swedish).

Structural Health Monitoring of degrading concrete beams in a laboratory environment

Markus Bergström

(PhD student, Luleå University of Technology, Luleå, Sweden)

Björn Täljsten

*(Professor, Technical University of Denmark, Lyngby, Denmark
Luleå University of Technology, Luleå, Sweden)*

ABSTRACT

Much effort has been invested separately on degradation, repair and upgrading of concrete structures. However, few holistic studies including laboratory testing have been performed on the entire cycle during a structures life. Reinforced concrete is the most widely used building material in the world. Normally the life of concrete structures is very long. However, concrete structures possess one drawback; at least in severe environments, the steel reinforcement may corrode. The effects can clearly be seen when the steel reinforcement is attacked by chlorides. The reduced steel cross-section area and loss of bond strength between steel and concrete will lead to increased deformations, cracking and premature ultimate load, thus affecting both the serviceability limit state (SLS) and the ultimate limit state (ULS). Procedures to repair and upgrade the damaged structure are used to increase the structural performance. They follow the structural member of time, a SHM (Structural Health Monitoring) approach is adapted to this project. By applying SHM to a degrading structure it assures that it will keep up to current standards by continuous monitoring, analysing, evaluation and eventually also retrofitting.

KEYWORDS

Structural Health Monitoring (SHM), degradation, corrosion, chloride, curvature, stiffness, life cycle

1. INTRODUCTION

1.1. In general

The current paper is generated from a large research project. The project aim is to experimentally and numerically simulate the behaviour of concrete beams enduring a simulated life cycle procedure. The test program follows the beams from original performance of the intact beam through degradation, repair and upgrading with FRP plate bonding to its original load carrying capacity. Several attributes make this project unique. Amongst these are accelerated corrosion, strain measurement using fibre optic sensors and sustained loading during the entire life cycle. In addition, mid span curvature is monitored using a special test setup.

1.2. Structural Health Monitoring (SHM)

SHM is connected to a continuous method containing monitoring, analysis, assessment and also possible retrofitting of a structure. This way of thinking is important since concrete structures, although appearing stable and solid, are dynamic in terms of changing material properties and internal hard-to-see damages, such as corrosion of steel reinforcement (Hejll, 2005). This project gives the opportunity of applying this way of thinking in the controlled manner of an advanced laboratory test program, presented below.

1.3. Defined life cycle

The simulated life cycle carried out may be divided into seven stages, from a to g, presented in Figure 1 and in the text below the figure, (Horrigmoe, 1998 and Sand, 2001). This may be a normal life cycle for a concrete structure, e.g. a bridge which is located in an environment that is aggressive due to steel corrosion.

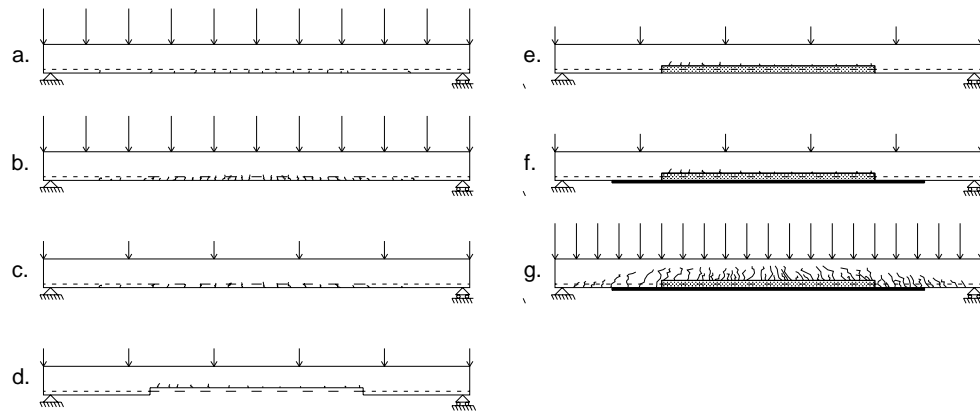


Figure 1. Seven stages create the studied life cycle (Horrigmoe, 1998).

- a. In the initial stage, the beam is subjected to the full service load (SLS), during which cracking in the tension side occurs.
- b. Simultaneously as the serviceability load acts on the beam specimens, accelerated corrosion attacks the tensile flexural reinforcement in mid-span. Thereby, the cross sectional area of the attacked bars and the bond between the bars and concrete is reduced.
- c. The structure is taken out of service, which means that the variable component of the serviceability load is removed. Dead load remains acting on the specimens.
- d. Cracked and chloride contaminated concrete is removed and the tensile reinforcement is exposed over the entire deteriorated region of the beam. The bars are cleaned by sandblasting and will have a permanently reduced cross section
- e. After the concrete is removed the cavity is refilled with a repair mortar. This is strain-free when applied, whereas the neighbouring concrete remains strained and cracked.
- f. After repairing the beam, it is strengthened in flexure using CFRP plates that are applied on the tensioned face of the beam. The strengthening procedure increases the stiffness of the beam, but does not add any significant weight.
- g. The life cycle is closed by finally loading the beams to failure.

2. RESULTS

2.1. Degradation stage

Tensile steel reinforcement was corroded by an accelerated corrosion setup during the 70 day degradation period. The decrease in unit weight due to corrosion was established to be 14% as shown in table 1. Stiffness was meanwhile monitored using a curvature test setup. A 15% reduction in stiffness was observed after 70 days of corrosion, see figure 2.

Table 1. Unit weight and diameter for non-corroded and corroded steel reinforcement bars.

	Unit weight [kg/m]	Diameter [mm]
Non-corroded steel	1,67	16
Corroded steel @ 70 days	1,48	15,1
Reduction	14%	6%

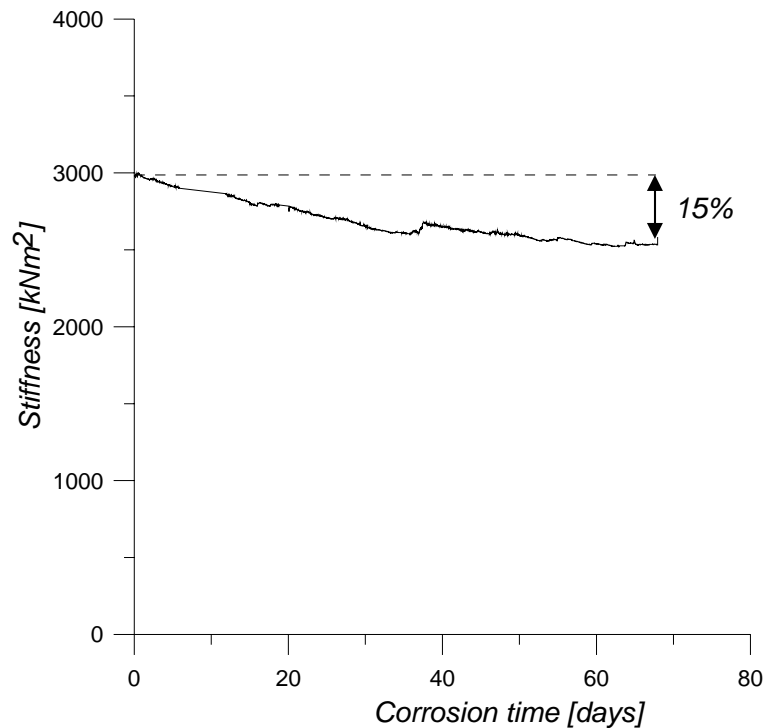


Figure 2. Stiffness measured during the time when corrosion attacked tensile steel reinforcement.

2.2. Life cycle behaviour

FE-calculation (Sand, 2001) has shown that the life cycle behaviour, in terms of the load deflection relation follows a load-deflection path shown by the left part of figure 3. First, the intact beam in stage a) is loaded up to the service load. Deflection increases as corrosion reduces the beam stiffness by reduction of the steel reinforcement content. The concrete beam has to be repaired at a certain corrosion level. The variable load is removed before the repair procedure. This is normally carried out for an existing structure that is taken out of service before being rehabilitated. A further increase of deflection is predicted during the repair procedure as steel reinforcement will move towards the centre of gravity, giving a reduced effective height. This effect arises due to the dead load acting on the beam during removal of damaged concrete. Another mechanism giving increased deflection during repair is that the remaining bond between steel bars and concrete is fully eliminated. It is possible that the repaired beam will need strengthening to reach the capacity of the intact beam again.

The experimental result from the test at LTU is provided in the right part of figure 3. The general appearance of the two graphs corresponds to each other, although no FE-calculation has at this time been carried out for this particular experimental study.

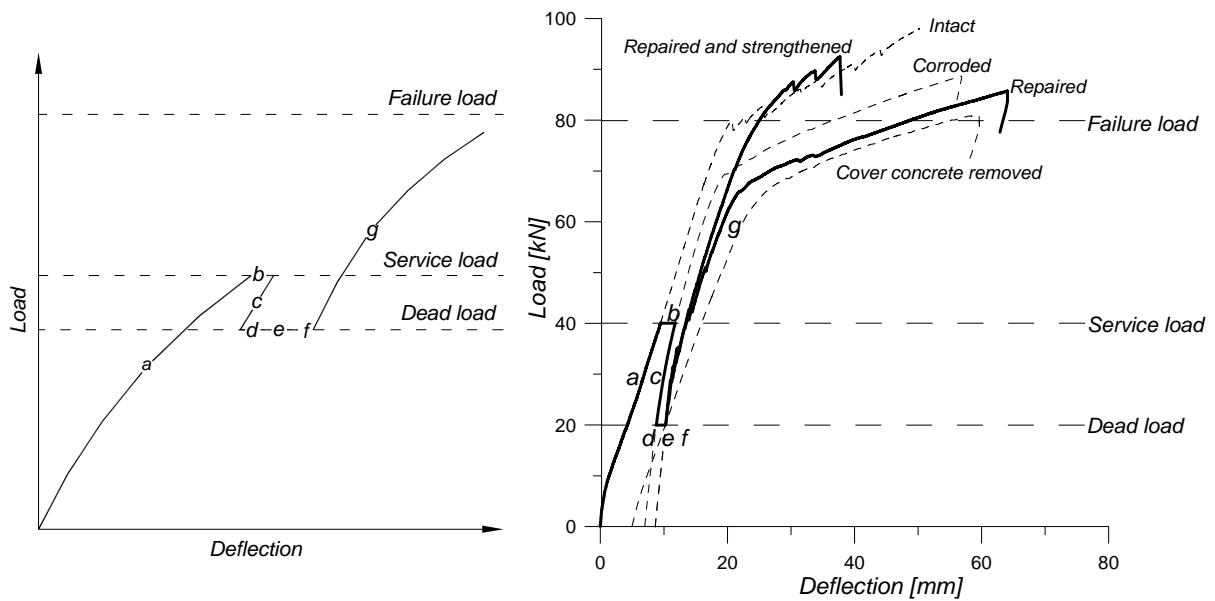


Figure 3. Left: General life cycle behaviour shown by FE-simulation (Sand, 2001). Right: Life cycle behaviour given by bold line, shown by experiment at LTU.

3. CONCLUSIONS

The experimental study has provided promising results to understand the life cycle behaviour of concrete structures during degradation, repair and upgrading. Fundamental mechanisms behind the behaviour are identified. The next step in this study could be to work out principles to minimize the bad influence of these mechanisms, and even take advantage of them. The adaptation of SHM made it possible to monitor the structural behaviour during the different stages.

4. ACKNOWLEDGEMENTS

The research presented in this paper has been funded by several organisations. Here the Development fund of the Swedish Construction Industry (SBUF), Sto Scandinavia AB and Skanska Teknik should be acknowledged.

5. REFERENCES

- Arntsen, B. 2005. "Akselererte korrosjonsforsøk, Forslag til gjennomføring". NORUT Teknologi AS, Narvik, Norway.
- Horrigmoe, G. 1998. "Future needs in concrete repair technology". NORUT Teknologi AS, Narvik, Norway.
- Sand, B. 2001. "Nonlinear finite element analysis of deteriorated and repaired RC beams". NORUT Teknologi AS, Narvik, Norway.
- Täljsten, B. 2004 "FRP Strengthening of Existing Concrete Structures, Design Guidelines". 3rd edition, Luleå University of Technology, Luleå, Sweden.
- Hejll, A. 2005 "Structural Health of Bridges". Licentiate thesis 2004:46, Division of Structural Engineering, Luleå University of Technology, Sweden.

DEBONDING DETECTION IN CFRP STRENGTHENED RC BEAMS USING ACTIVE SENSORS

Seung Dae Kim

(Ph.D. Candidate, Carnegie Mellon University, Pittsburgh, PA, USA)

Chi Won In

(Master Student, Carnegie Mellon University, Pittsburgh, PA, USA)

Kelly E. Cronin

(Undergrad. Student, Carnegie Mellon University, Pittsburgh, PA, USA)

Hoon Sohn

(Assistant Professor, Carnegie Mellon University, Pittsburgh, PA, USA)

Kent Harries

(Assitant Professor, University of Pittsburgh, Pittsburgh, PA, USA)

ABSTRACT

The appropriate bonding condition between substrate reinforced concrete (RC) beams and carbon fiber-reinforced polymer (CFRP) laminates is essential to guarantee the performance of CFRP strips as retrofitting materials. In this study, a theoretical approach and experimental results toward developing a CFRP debond monitoring system are presented. The goal of this study is to understand suitable guided waves propagation in the CFRP-RC structure and to develop a new theoretical framework of nondestructive testing (NDT), in which debonding can be detected without using past baseline data. The concept of time reversal acoustics (TRA), which has been generally applied to body waves, is extended to complex guided waves in CFRP-RC interfacial regions. Several indices sensitive to structural damage are extracted by comparing the known input with the time-reversed signal. Active sensing devices such as lead zirconate titanate (PZT) wafers are used to generate known input waveforms and to measure the time-reversed responses. Two large-scale CFRP-retrofit RC beams, one tested monotonically and the other in a fatigue regime, are used to demonstrate the potential of the proposed debonding monitoring system.

KEYWORDS

active sensing, baseline-free nondestructive testing, debonding, structural health monitoring, time-reversal acoustics.

1. INTRODUCTION

Carbon fiber reinforced polymer (CFRP) composites have become an attractive alternate material for retrofit of civil infrastructures due to their outstanding strength, light weight and versatility. However, the improvement of strength and stiffness in a host structure can only be guaranteed when a reliable bonding condition between the two materials is maintained. Infrared thermography (Levar and Hamilton 2003), Electromechanical (E/M) impedance spectrum (Giurgiutiu et al. 2003), electrochemical impedance spectroscopy methods (Hong and Harichandran 2005) and fiber optic sensing (Ansari 2005) have been previously applied to similar debonding problems. The goal of this study is to ensure the safety and integrity of CFRP strengthened RC structures and to provide early warning of debonding based on real-time nondestructive evaluation testing (NDT). A new NDT technique is developed by applying the concept of time reversal acoustics (TRA) (Fink and Prada 2001) to guided wave propagations within CFRP-strengthened RC beams, and it is based on the premise that "certain types of damage can be instantaneously detected without prior baseline data." This new concept will be extended to develop a NDT system that can be "rapidly" deployed to laboratory specimens or in-field structures and "autonomously" perform local damage diagnoses in the presence of operational and environmental variations that in-service structures encounter.

2. WAVE PROPAGATION AND TIME REVERSAL PROCESS IN CFRP-RC BEAMS

Elastic waves in solid media can be classified into body and guided waves, which are governed by Navier's wave equations (Rose 1999). The guided waves can be further divided into Lamb, Stoneley and Rayleigh waves depending on specific boundary conditions. The various frequency components of Lamb waves travel at different speeds and

attenuate at different rates due to dispersion characteristics. In spite of these unique characteristics, Lamb waves are widely used for defect detection, because they are well guided within two closely spaced boundaries and can travel a long distance with little attenuation. As the thickness of the plate increases, the fundamental symmetric (S_0) and anti-symmetric (A_0) Lamb modes converge to a Rayleigh wave, higher modes merge to a transverse bulk wave, and additional body waves appear. Waves propagation are further complicated in a thin layered thick medium. A CFRP-RC beam is a good example of such a structure with two distinctive thicknesses. Therefore, a conventional Lamb wave approach may not be applicable, and a new approach, which can be used regardless of the complexity of waves, is necessary. To address this issue, a NDT technique based on the TRA concept is proposed. According to TRA, an input signal can be reconstructed at an excitation point (PZT A) if an output signal recorded at another point (PZT B) is reemitted to the original source point (PZT A) after being reversed and scaled in the time domain as shown in Figure 1. If there are certain types of defect along the wave propagation path, time reversibility breaks down and the shape of the restored signal will depart from that of the input signal. By examining the deviation of the restored signal from the known input signal, as shown in Figure 2, certain types of damage can be identified without requiring any previously obtained baseline signals. In reality, the time reversibility does not work well in guided waves due to their multimode and dispersion. To address this issue, a combination of a specific narrowband input waveform and multi-resolution signal processing is employed so that the time reversibility is preserved within an acceptable tolerance for more complex configurations presented in this study (Park et al. 2004).

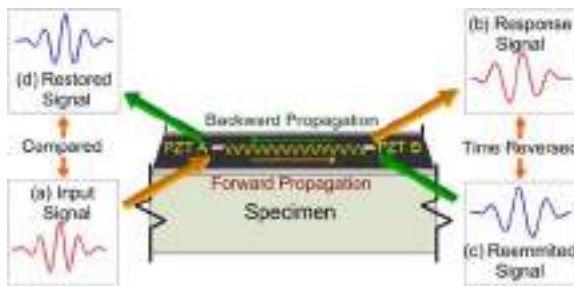


Figure 1: Schematic concept of TRA-based damage identification

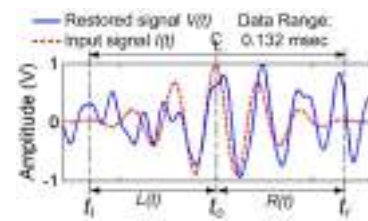


Figure 2: Definition of t_l , t_0 , and t_r

Once the time reversibility of guided waves is achieved, damage classification is based on two damage indices; time reversibility (TR) and symmetry (SYM) indices defined in Equation (1). The TR index compares the waveform of the original input with that of the reconstructed signal, and the SYM index measures the degree of symmetry of the reconstructed signal with respect to the main peak in the middle:

$$TR = 1 - \sqrt{\frac{\left\{ \int_{t_l}^{t_r} I(t)V(t) dt \right\}^2}{\left\{ \int_{t_l}^{t_l} I(t)^2 dt \int_{t_l}^{t_r} V(t)^2 dt \right\}}}, \quad SYM = 1 - \sqrt{\frac{\left\{ \int_{t_0}^{t_l} L(-t)R(t) dt \right\}^2}{\left\{ \int_{t_l}^{t_0} L(t)^2 dt \int_{t_0}^{t_r} R(t)^2 dt \right\}}} \quad (1)$$

where $I(t)$, $V(t)$, $L(t)$ and $R(t)$ denote the known input signal, the main peak, left-hand and right-hand sides of the reconstructed signal, respectively. For the experimental study presented, a 7-peak toneburst signal is used for excitation; t_l , t_r and t_0 represent the starting, ending and center time points of the toneburst signal as defined in Figure 2. The value of the TR and SYM indices become zero when the shape of the main peak in the reconstructed signal is identical to that of the original input signal and symmetric with respect to t_0 .

3. EXPERIMENTAL SETUP AND TEST CASES

The overall configuration and dimension of the test specimens are shown in Figure 3. Four (1 to 4) and eight (5 to 12) strain gauges located on the reinforcing steel and the CFRP strip, respectively as indicated in Figure 3(a). These instruments are used to establish strains and the presence of debonding at the discrete gauge locations. Details of the beam test programs may be found in Reeve (2005) and Zorn (2006). In addition, a total of 15 PZT square wafers (2cm x 2cm x 0.0508cm) were attached on the free surface of the FRP as shown in Figure 3(b). They were used as both sensors and actuators to form an “active” local sensing system. In this study, one PZT wafer was designated as an actuator, exerting a predefined waveform into the structure. Then, the adjacent PZTs became sensors to measure the dynamic strain response signals. This process of guided-wave propagation was repeated for a total of 14 different path combinations (PZTs #1-#2, PZTs #2-#3, ... , and PZTs #14-#15). Data from the active sensing devices were collected at several steps, during which the load was held constant. Two loading cases were investigated in this study (Cases I and II). In Case I, one of the two full-scale specimens was subjected to monotonic loading, and the data were collected at every loading step. The monotonic load was gradually increased until the specimen fully failed. A force-control loading was initially used up to the 5th (40.03kN) loading step and then switched to a displacement-control from the 6th (41.59kN) to the 24th (44.54kN). The other specimen was subjected to fatigue

cyclic loading. In Case II, cyclic loads with a driving frequency of 1.3Hz and the load range of 4.45kN to 22.24kN were applied. The specimen experienced a total of 2,000,000 fatigue cycles over a time period of 16 days. Data were gathered at 24 intermittent steps of loading cycles. During the data collection, the cyclic load was held at 4.45kN.

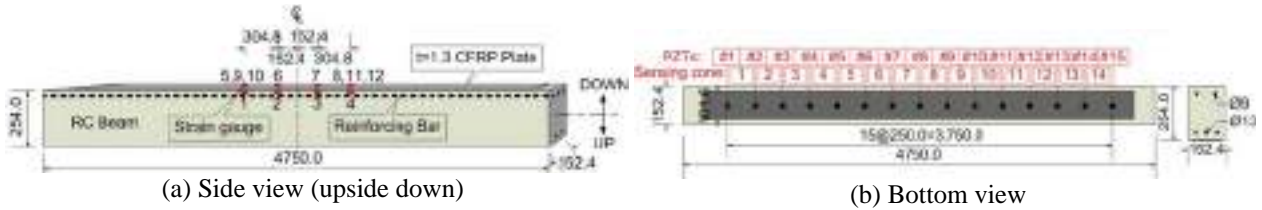


Figure 3: Specimens with attached active sensing devices (all units are in mm)

4. EXPERIMENTAL RESULTS

The monotonic and fatigue load tests (Case I and II) were performed on two beams to introduce debonding between the CFRP layers and the RC beams, and data were periodically collected.

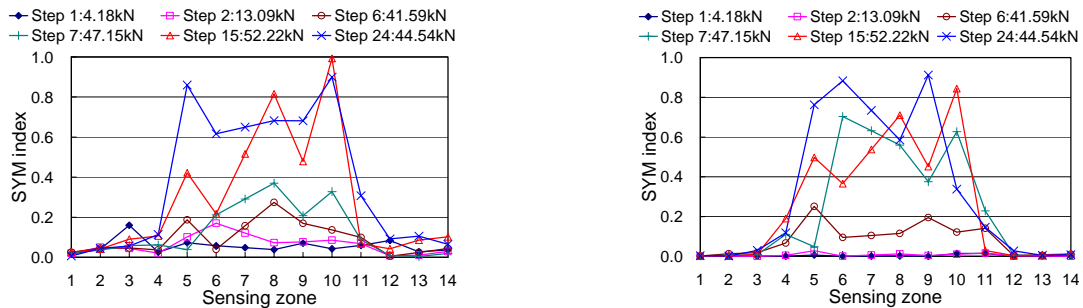


Figure 4: TR and SYM indices along the RC beam measured at selective loading steps (Case I)

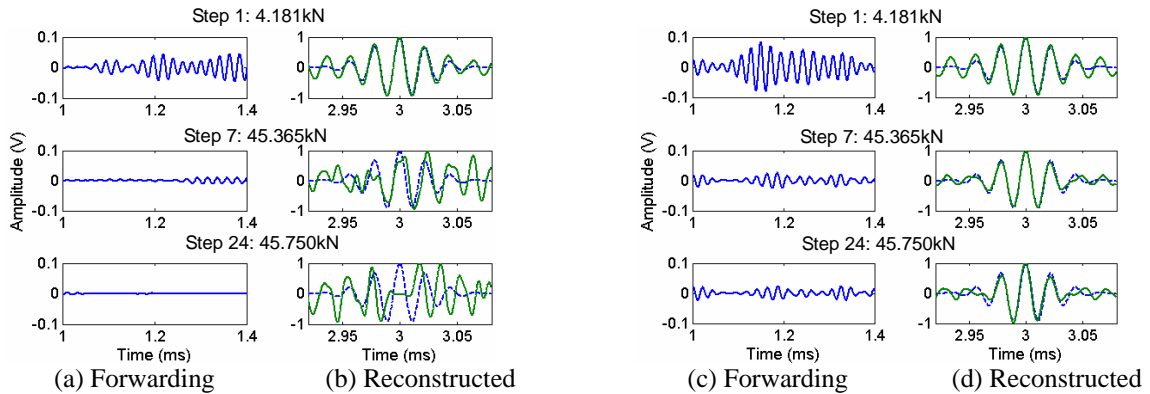
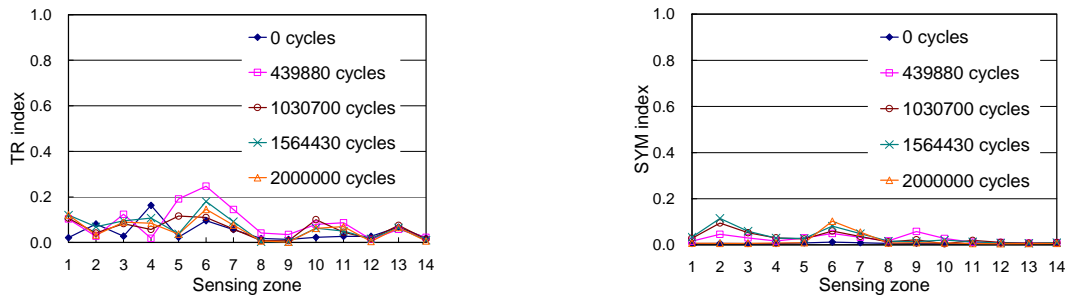


Figure 5: Forwarding and reconstructed signals at sensing zones 10 and 14 (Case I)

The TR and SYM indices at the sensing zones 10 and 14 were examined for the monotonic test (Case I). The values of indices at zone 10 became larger than 0.2 from the 7th loading step as shown in Figure 4. In Figure 4, it is speculated that the initial increase of the indices values at the midspan is not relevant to debonding. A 4.8 mm diameter steel rod embedded in the concrete used to connect the midspan displacement transducer may have affected the indices values. In this study, these TR and SYM outlier values not related to debonding were disregarded. Figure 5 shows the forwarding and reconstructed signals obtained from the sensing zones 10 and 14 at selected loading steps. As the load level increased, the amplitude of the forwarding signal gradually decreased as shown in Figure 5(a). The deviation of the reconstructed signal from the original input signal was observed for the increased load levels, indicating the initiation of debonding near sensing zone 10 in Figure 5(b). On the other hand, no sign of debonding was found near sensing zone 14. This is consistent with the fact that the reconstructed signal in Figure 5(d) did not change much throughout the entire loading steps. However, it should be noted that the forwarding signal continuously changed as loading progressed in Figure 5(c). Overall, the findings from the proposed diagnosis system agree well with the visual inspection and a coin-tapping test results performed after the monotonic loading. The

second specimen was subjected to a fatigue cyclic load (Case II). As shown in Figure 6, there was no sign of CFRP strip debonding during the test nor was any evidence of debonding found from the visual inspection or the coin tapping test after the test. The TR and SYM indices in Figure 6 mostly remained below 0.2 except sensing zone 7.



(a) TR indices at 5 loading cycles (b) SYM indices at 5 loading cycles
Figure 6: TR and SYM indices along the RC beam measured at selective loading cycles (Case II)

5. CONCLUSION

A new real-time monitoring system is developed for detecting debonding of a CFRP layer from a host RC beam. The uniqueness of this approach lies in the fact that debonding can be detected without using previously obtained baseline data. Surface mounted PZT wafers are used to generate and measure complex guide waves within the CFRP-RC coupled structures. Then, two damage sensitive indices are extracted from the measured guided wave signals based on the concept of the TRA. The potential of the proposed method is demonstrated using experimental data obtained from monotonic and fatigue loading tests of the CFRP-RC coupled structures. Using the proposed monitoring system, the location and area of the debonding were successfully identified for the monotonic.

ACKNOWLEDGEMENT

This research was partially supported by an NSF Grant No. CMS-0529208 and Pennsylvania Infrastructure Technology Alliance (PITA) program. The beam test was conducted by Andrew Zorn and Benjamin Reeve in the Watkins-Haggart Structural Engineering Laboratory at the University of Pittsburgh.

REFERENCES

- Ansari, F. (2005). "Fiber optic health monitoring of civil structures using long gage and acoustic sensors." *Smart Mater. and Struct.*, Vol. 14, No. 3, S1-S7.
- Ekenel, M., Stephen, V., Myers, J. J., and Zoughi, R. (2004). "Microwave NDE of RC Beams Strengthened with CFRP Laminates Containing Surface Defects and Tested Under Cyclic Loading." *Proc., 16th World Conference on Nondestructive Testing*, Montreal, Canada. August 30-September 3.
- Fink, M. (1999). "Time-Reversed Acoustics." *Scientific American*, Vol. 281, No. 5, 91-97.
- Fink, M., and Prada, C. (2001). "Acoustic Time-Reversal Mirrors." *Inverse Problems*, 17, R1-R38.
- Giurgiutiu, V., Harries, K.A., Petrou, M.F., Bost, J., and Quattlebaum, J. (2003). "Disbond Detection with Piezoelectric Wafer Active Sensors in RC Structures Strengthened with FRP Composite Overlays." *Earthquake Eng. and Eng. Vibration*, Vol. 2, No. 2, 213-224.
- Hong, S., and Harichandran, R. (2005). "Sensors to Monitor CFRP/Concrete Bond in Beams Using Electrochemical Impedance Spectroscopy." *J. of Composite for Construction*, Vol. 9, No. 6, 515-523.
- Levar, J. and Hamilton, H. (2003). "Nondestructive Evaluation of Carbon Fiber-Reinforced Polymer-Concrete Bond Using Infrared Thermography." *ACI Mater. J.*, Vol. 100, No. 1, 63-72.
- Park, H.W., Sohn, H., Law, K.H., Farrar, C.R., (2004). "Time Reversal Active Sensing for Health Monitoring of a Composite Plate." submitted for *Journal of Sound and Vibration*.
- Reeve, B. (2005). "Effect of Adhesive Stiffness and CFRP Geometry on the Behavior of Externally Bonded CFRP Retrofit Measures Subject to Monotonic Loads." MS Thesis, University of Pittsburgh Department of Civil and Environmental Engineering.
- Rose, L. J. (1999). *Ultrasonic Waves in Solid Media*, Cambridge University Press, New York.
- Zorn, A. (2006). "Effect of Adhesive Stiffness and CFRP Geometry on the Behavior of Externally Bonded CFRP Retrofit Measures Subject to Fatigue Loads." MS Thesis, University of Pittsburgh Department of Civil and Environmental Engineering.

Part XII. Hybrid Systems

EXPERIMENTAL STUDY ON FRP-CONCRETE HYBRID BEAMS

Tianhong Li

(Graduate, Department of Civil Engineering, Tsinghua University, Beijing, China)

Peng Feng

(Lecturer, Department of Civil Engineering, Tsinghua University, Beijing, China)

Lieping Ye

(Professor, Department of Civil Engineering, Tsinghua University, Beijing, China)

ABSTRACT

An innovated form of hybrid deck system is proposed, which is composed of FRP (fiber reinforced polymer) I-shaped profiles, E-shaped profiles and concrete overlay. The E-shaped profiles act as permanent formworks, which make the construction more convenient. Three FRP-concrete hybrid beams and one pure FRP beam were tested. The performance influenced by the depth of concrete and CFRP (carbon fiber reinforced polymer) sheets reinforcement at bottom is studied in comparing. In the tests, the shear cracking failure at the web of the I-shaped profiles is the main failure mode, which was investigated.

KEYWORDS

Permanent framework, corrosion resistance, light-weight structure, shear failure, FRP-concrete structure.

1. INTRODUCTION

The structure deterioration caused by steel corrosion is a considerable problem in civil engineering. The use of FRP (fiber reinforced polymer) is a good approach to solve this problem for its excellent chemical and environmental endurance. Combining FRP and concrete in a reasonable way will benefit the advantages of both the materials and save the cost. So FRP-concrete hybrid structure as shown in Figure 1 is proposed for bridges and floors of buildings.

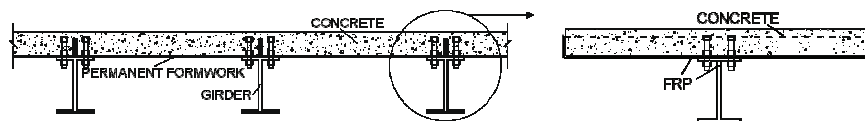


Figure 1: FRP-concrete hybrid structure with permanent formworks

FRP-concrete hybrid beams with different FRP profiles have been studied from 1990s. Deskovic and Triantafillou (1995), Canning et al. (1999) and Hulatt et al. (2004) studied the different GFRP (glass fiber-reinforced polymer) box sections with CFRP(carbon fiber-reinforced polymer) laminate on the tensioned side. Branco et al. (2003) and Nordin and Taljsten(2004) proposed and tested the pultruded GFRP I-profile beams composed with concrete. Fam and Skutezky(2006) proposed rectangular pultruded GFRP tubes filled with concrete combining with concrete slabs. In this paper, the typical element in the proposed hybrid structure system, the FRP-concrete hybrid beam as shown in Figure 1, is investigated. The FRP permanent formworks and FRP girders are included in this system, which is the difference with the aboves. The mechanical concept of this FRP-concrete hybrid beam is similar to that of the steel-concrete composite beams: the bending moment is provided by the concrete under pressure and the FRP profile in tension, and the connectors tranfer the shear force between them. So the compressive strength of concrete and the tensile strength of FRP can be utilized. Its advantages as following: (1) light-weight, which makes transportation and installation more convenient; (2) no needs to remove forms, which may save manual labor and material resources

and accelerate the construction; (3) FRP permanent formworks can act as the reinforcement in transverse; (4) the corrosion resistance of FRP can protect the concrete inside.

In this paper, the mechanical performance of this FRP-concrete hybrid beam is investigated by the tests of three hybrid beams. The stiffness, capacity and failure modes of FRP-concrete hybrid beams are analyzed.

2. TESTS

Four specimens were fabricated and tested, including one pure I-shaped GFRP beam and three hybrid beams. The hybrid beams were composed of I-shaped GFRP beams and E-shaped plates, connected with the combination of steel bolts and epoxy adhesive, and then concrete was cast on the top, as shown in Figure 2. Each specimen had 36 bolts, which are designed to supply full shear transfer without yield. The specimens and the materials' properties are listed in Table 1: H0 is a pure I-shaped GFRP beam, HB is the standard specimen, HB-T has thicker concrete slab, and HB-R has three extra CFRP layers of 0.167mm thick each under the bottom flange. All specimens were simply supported and loaded in four-point bending as shown in Figure 3. The deflections and the slipages were measured with extension indicators, and the strains of FRP and concrete were measured with gauges.

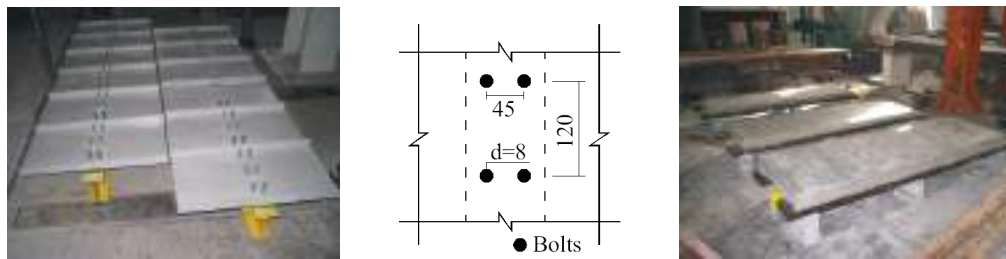


Figure 2: Manufacture of FRP-concrete hybrid beams

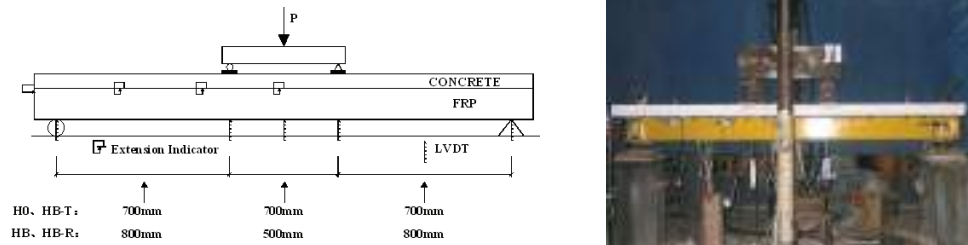


Figure 3: Test setup of simply supported FRP-concrete hybrid beams

Table 1: List of Specimens and Materials Properties

Specimens	h_c /mm	Concrete Strength /MPa	GFRP		CFRP	
			Strength /MPa	Modulus /GPa	Strength /MPa	Modulus /GPa
H0	0	-	650	22	-	-
HB	60	34.0	650	22	-	-
HB-T	110	29.6	650	22	-	-
HB-R	60	28.7	650	22	3500	235

H0 was not expected to be loaded to collapse. The load was applied to 26kN when the midspan deflection reached 16mm, then unload and reload till the midspan deflection was 21mm, 1/100 span when the load was applied to around 34kN. H0 stayed elastic in the whole progress and the deflections of both the two sides were symmetric. No collapse and no cracking sound occurred during the loading, and the deflection disappeared immediately with unloading. For HB, cracking sounds were first heard at the load of 38kN, and the beam suddenly collapsed at 99.2kN with an obvious horizontal crack on the web of FRP beam, while there were no cracks on concrete and no

other failure either. HB-R had the very similar behavior with HB: cracks occurred at 54kN and failed with a horizontal crack on the web under the load of 94.6kN. HB-T had a different phenomenon that some cracks appeared in the lower part of the concrete panel at the midspan at 24kN and in the gaps of the adjoining FRP plates at 34kN. Clacks began to be heard at 50kN till the beam collapsed suddenly at 149kN with the same failure mode. Although all hybrid beams have the same failure mode, the locations of the crack in the webs depend on the thickness of concrete panels in the way that the crack goes close to the concrete panel with the increase of the concrete thickness. The load-deflection curves and the failure modes of the specimens are shown in Figure 4.

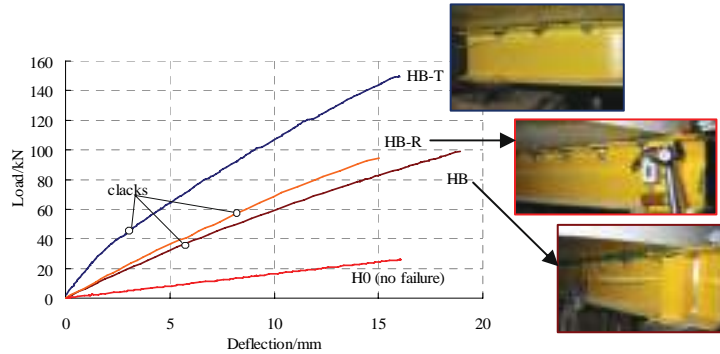


Figure 4: Load-deflection curves and failure modes of test specimens

3. TEST RESULTS AND ANALYSIS

The load-deflection curves clearly show that the bending stiffness of hybrid beams is considerably higher than the pure FRP beam, which can reach up to 4 to 6 times. Among the three hybrid beams, the bending stiffness of HB-T is the highest, which indicates that the increase of the concrete's thickness is effective to enhance the bending stiffness of hybrid beams. Comparing HB and HB-R it can be seen that the CFRP layers in the lower flange have little use in developing the bending stiffness. Strains on the top of concrete and the bottom of FRP beam at the midspan are illustrated in Figure 5. All strains increase almost linearly with the load. The strains of HB-T are smaller than those of the other two at the same load, which indicates that HB-T has the highest rigidity; HB-R and HB have close strain values which means that their rigidity values are almost the same.

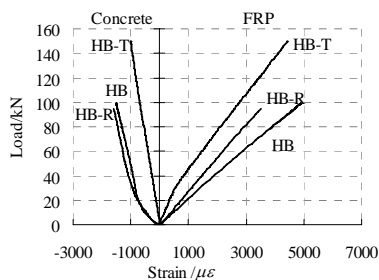


Figure 5: Strains on the top and the bottom of beams

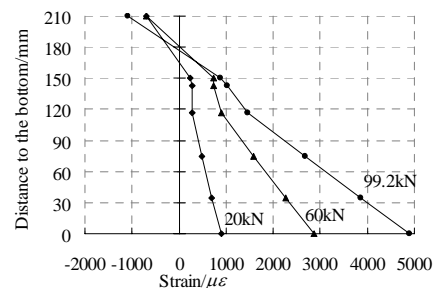


Figure 6: HB strains at midspan

Figure 6 shows the strains of different locations on the midspan cross section of HB. It can be seen that the plane assumption is well satisfied, and so do the other specimens. The slippage between the ribbed plates and the I-shaped beams are measured in the tests, the maximum slippage of HB was 0.15mm, 0.10mm for HB-R and 0.80mm for HB-T. All these indicate that the combination connection gives an excellent shear force transfer.

In the existing experimental researches, the FRP-concrete hybrid beams loaded in bending failed in several possible modes, such as (1) flexural failure by concrete crush (Hulatt et al., 2004; Nordin and Taljsten, 2004); (2) connectors or adjacent concrete failure (Nordin and Taljsten, 2004); (3) concrete panel shear failure (Kavlicoglu, 2001); (4) FRP web shear fracture (Branco et al., 2004). All three hybrid beams in this paper failed in the fourth mode which is resulted by the low shear strength of the pultruded FRP profiles' webs. The shear failure happened too premature

to utilize the tension strength of FRP and the compressive strength of concrete. So it is important to improve the shear strength of the FRP web to enhance the loading capacity of the whole specimen. A short pure I-shaped GFRP beam has been tested to achieve the shear strength of GFRP profile, which was 41.7kN. Since the net section at the seam of two adjacent ribbed plates of the hybrid beams is composed of I-shaped GFRP and a strip of concrete with the thickness of h_c' as shown in Figure 7, it is presented that the increase of the shear capacity of the hybrid beams compared with the pure GFRP beams is provided by the concrete above the ribs. According to the test results, Figure 8 was achieved which shows that the shear strength of hybrid beams corresponds with h_c' linearly.

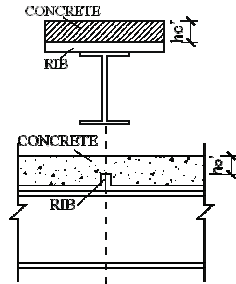


Figure 7: Effective section to bear shear force

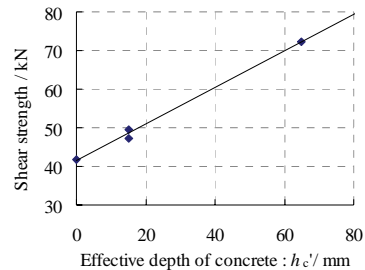


Figure 8: Relation of h_c' and shear strength

4. CONCLUSIONS

An innovative FRP-concrete hybrid deck system with permanent formworks is presented and tested. The following conclusions can be drawn from this study: (1) the bending stiffness of the hybrid beam is related to the concrete slab's thickness, while the CFRP layers bonded on the bottom flange of FRP have little contribution to stiffness; (2) the shear failure of FRP web is a considerable failure mode as it makes it impossible to utilize the strength of FRP and concrete, in which the shear strength increases with concrete slab's thickness.

ACKNOWLEDGEMENTS

The authors are grateful to the Natural Science Foundation of China for their support to the research presented here through a national key project on the application of FRP composites in civil engineering in China (Project No. 50238030).

REFERENCES

- Branco, F.A., Ferreira, J., and Correia, J.R. (2003). "The use of GRC and GFRP-concrete beams in bridge decks". *Proceedings of FRP Composites in Bridge Design and Engineering, COBRAE Conference*, Porto, Portugal
- Hulatt, J.A., Holloway, L.C., and Thorne, A.A. (2004). "A novel advanced polymer composite/concrete structural element". *Proceeding of the Institution of Civil Engineers Structures & Building*, Vol.157, pp 9-17.
- Kavlicoglu, B.M., Gordaninejad, F., Saiidi, M., and Jiang, Y. (2001). "Analysis and testing of graphite/epoxy concrete bridge girders under static loading". *Proceedings of 9th International Conference on Structural Faults and Repairs*, London, United Kingdom.
- Nordin, H., and Taljsten, B. (2004). "Testing of hybrid FRP composite beams in bending". *Composites Part B: engineering*, Vol.35, pp27-33.
- Canning, L., Holloway, L., and Thorne, A.M.(1999). "An investigation of the composite action of an FRP/concrete prismatic beam". *Construction and Building Materials*, Vol. 13, pp417-426.
- Deskovic, N., and Triantafillou, T.C.(1995). "Innovative design of FRP combined with concrete: short-term behavior". *Journal of Structural Engineering*, Vol.121, No.7, pp1069-1078.
- Fam, A. and Skutezky, T.(2006). "Composite T-beams using reduced-scale rectangular FRP tubes and concrete slabs". *Journal of Composites For Construction*, Vol.10, No.2, pp172-181.

HYBRID BONDING OF FRP LAMINATES TO REINFORCED CONCRETE STRUCTURES

Yu-Fei Wu

Assistant Professor, City University of Hong Kong, Hong Kong

Yue Huang

Research student, City University of Hong Kong, Hong Kong

ABSTRACT

This paper reports a new FRP bonding technology that combines the adhesive bonding technology with a new type of mechanical fastening. The new mechanical fastening system does not rely on the bearing to transmit the interfacial shear. Instead, it increases the frictional bond resistance by resisting the separation of the FRP laminate from the concrete substrate. Experimental testing has demonstrated that this new technology can provide a bonding strength that is several times that of the conventional adhesively bonded FRP system.

KEYWORDS

FRP, reinforced concrete, bond, strengthening, retrofitting, testing

1. INTRODUCTION

External bonding of fiber reinforced polymer (FRP) has emerged as one of the most popular methods for structural rehabilitation in recent years (Nanni, 1997; Hollaway and Head, 2001). Up to date, three typical methods of bonding FRP onto concrete structures have been developed. The first and most common method is by adhesively bonding FRP to the external surface of reinforced concrete (RC) members, a method known as externally-bonded FRP or EB-FRP. The second technology is the near-surface mounting (NSM) where the FRP reinforcement is embedded in the cover layer of the concrete structures. The third recent development is the mechanically-fastened FRP (MF-FRP) technique (Bank, 2004), where a special type of FRP strip that has a significant bearing strength is mounted onto the concrete surface by mechanical fasteners. Apart from the above three method, it has been found that anchoring FRP strips at their ends with large anchors, namely end anchorage, can effectively increase both the bond strength and the ductility. Wrapping a longitudinal FRP strip with transverse U shaped FRP strips (U-jackets) has also been found to be effective in delaying the premature debonding. Other methods such as fiber anchors (Lam and Teng, 2001) and interlocking-anchorage with epoxy keys (Grace, 2001) have been investigated to improve the bond capacity as well.

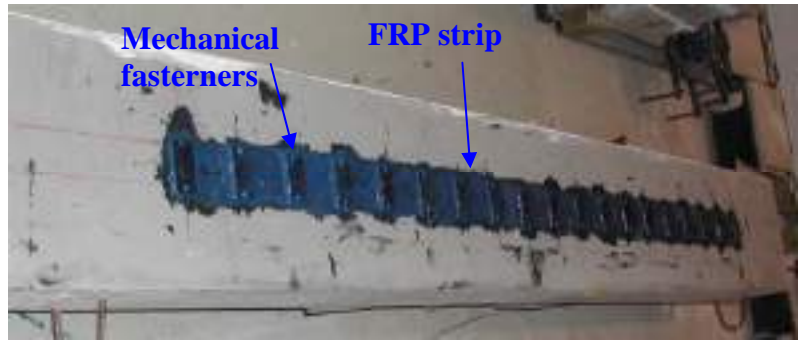
Despite the extensive efforts around the world in recent years in studying the debonding mechanism and in improving the bond strength, the bond remains the weakest link that fundamentally limits the efficacy of the FRP applications. Therefore more effort in finding alternative means of bonding FRP is needed.

2. HYBRID BONDING TECHNOLOGY AND ITS MECHANISM

Careful observations of the debonding process in an EB-FRP beam have revealed that the debonding causes not only a longitudinal slip between the FRP reinforcement and the concrete substrate but also a vertical separation between them. It was this separation that caught the attention of the first author who proposed and developed the new bonding technique by suppressing the separation with a special type of mechanical fastener that is shown in Fig. 1a. This mechanical fastener is composed of a thin steel capping plate that serves to apply normal pressure on the FRP laminate to restrain the vertical separation, and two anchors (concrete nails) that are used to fasten the steel plate onto the concrete substrate.



(a) Mechanical fastener

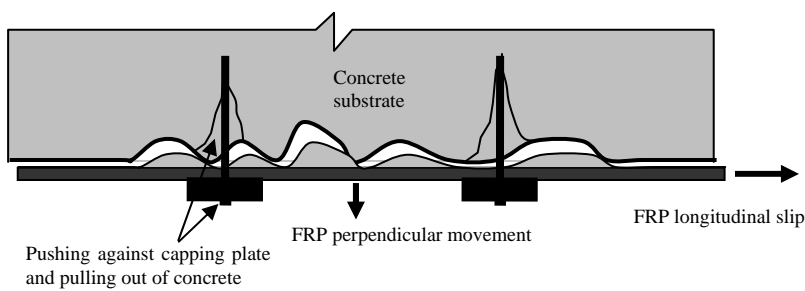


(b) Test specimen (bottom view) after installation of the HB-FRP system

Figure 1: HB-FRP System

This new technique combines the EB-FRP system with the MF-FRP system, and therefore, is named the hybrid bonded FRP (HB-FRP) system. However, the mechanical fasteners in the HB-FRP system work with a very different mechanism from that in the MF-FRP system. No bearing resistance of the FRP is required. Therefore, it is applicable to any commercially available FRP laminates. The application of the HB-FRP system consists of two steps. The first step involves the same procedure as that for an EB-FRP system, by adhesively attaching the FRP laminate onto the surface of the concrete. After the hardening of the adhesive for the EB-FRP, another coat of epoxy resin is applied on top of the FRP strip and the special mechanical fasteners are then installed along the longitudinal direction of the FRP reinforcement at a specified spacing, as shown in Fig. 1b. The installation of each mechanical fastener involves the drilling of two small holes in the concrete and driving the concrete nails into the two pre-drilled holes through the steel capping plate with a hammer, so that the capping plate firmly covers the FRP strip.

Due to the roughness of the debonding surface, any longitudinal slip of the FRP reinforcement against the concrete surface will result in a vertical movement of the FRP strip, as shown in Fig. 2a. This perpendicular movement of the FRP against the fasteners that are firmly embedded into the concrete produces significant vertical pressure on the FRP strip. This vertical pressure in turn causes frictional shear resistance at the interface. Therefore at debonding failure, the fasteners and the concrete around the fasteners will be pushed out by the movement of the vertical separation. This is evident in Fig. 2b where the nail was pushed out vertically from the concrete and a piece of concrete was pulled out by the nail at bond failure. Consequently, the mechanism of the HB-FRP system is completely different from that of the mechanically fastened system where the interfacial shear comes from the bearing of the attached plate/strip on the mechanical fasteners. As the nails did not deform laterally (see Fig. 2b) after debonding failure in the HB-FRP system, it was evident that no significant bearing occurred in the HB-FRP system. Therefore very thin anchors such as normal concrete nails are sufficient in the HB-FRP system.



(a) Frictional shear due to slip



(b) Local debonding failure

Figure 2: Mechanism of the HB-FRP system

3. EVALUATION OF THE HB-FRP SYSTEM

Experimental testing has been performed by the 2nd author to evaluate the HB-FRP system. Tests involved 4 one-way slab members, one strengthened with EB-FRP and the other three by HB-FRP with different FRP thickness.

3.1 Test Specimens

The design details of the RC slab are given in Fig. 3. The specimen with the HB-FRP system is shown in Fig. 4a and the details of the mechanical fastener are shown in Fig. 4b. The specimen with the EB-FRP was identical to that in Fig. 4a except that no mechanical fastener was provided. Properties of the test specimens are given in Table 1. Each ply of FRP had a nominal fiber sheet thickness of 0.165 mm.

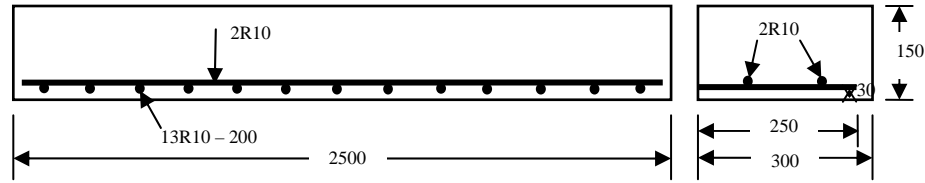
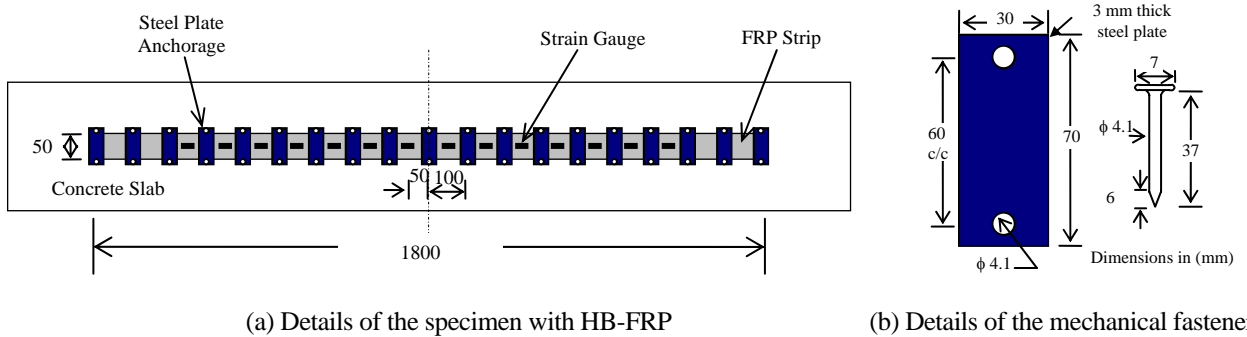


Figure 3: Details of RC Specimen



(a) Details of the specimen with HB-FRP

(b) Details of the mechanical fastener

Figure 4: The HB-FRP system for test specimens

Table 1: Material Properties of the Test Specimens

Specimen	Strengthening Method	Concrete	Steel Bars		FRP Strip		
		Cube Strength (MPa)	Yield Strength (MPa)	Elastic Modulus (GPa)	Tensile Strength (MPa)	Elastic Modulus (GPa)	Ultimate Strain (%)
S1	EB-FRP (2 plies)	80	343	208	4519	257	1.76
S2	HB-FRP (2 plies)	81.2	349	206			
S3	HB-FRP (4 plies)	82	332	208			
S4	HB-FRP (6 plies)	82	346	208			

3.2 Test Results and Discussion

The test setup and the test results are given in Fig. 5. The lowest curve in Fig. 5b gives the response of the member strengthened by the conventional EB-FRP technique, with 2 plies of CFRP. The other three response curves are for members strengthened with the HB-FRP system, with 2, 4 and 6 plies of CFRP, respectively.

The EB-FRP system increased the flexural strength from about 8 kN (calculated) for the un-strengthened member to 17 kN. The failure was by a debonding and complete detachment of the FRP strip from the bottom of the member, which indicated that the bond strength was unable to fully mobilize the tensile rupture strength of the 2-ply CFRP strip. Both the members with the HB-FRP of 2 and 4 plies of CFRP failed by the rupture of the CFRP strip, as shown in Fig. 5c. This clearly indicated that the bond strength with the HB-FRP system was greater than that was needed to fully utilize the material tensile strength of the 4-ply CFRP strip and hence resulted in the rupture of the CFRP strip. The member with a 6-ply CFRP strip failed due to debonding of the strip as shown in Fig. 5d. In this

case, the bond strength of the HB-FRP system was exhausted before the tensile strength of the 6-ply CFRP strip was reached.

From the test result of the conventional EB-FRP strengthened member, it can be seen that the strength increase due to the EB-FRP system was about 9 kN (from 8 to 17 kN). In other words, the EB-FRP system contributed 9 kN of the ultimate load. The ultimate load of the member with the 6-ply HB-FRP system was 70 kN. Taking away the 8 kN contributed by the steel bars, the ultimate load due to the HB-FRP system was 62 kN. This is about seven times ($62/9$) of that contributed by the conventional EB-FRP system. The effectiveness of the HB-FRP system is clearly demonstrated by these test results. Preliminary finite element analyses show that the EB-FRP has only one bond stress block that moves towards the plate end as debonding propagates. However, the HB-FRP system produces many bond stress blocks (one under each mechanical fastener) that increase the total bond resistance many times. Detailed results of the finite element analyses are not included in this paper due to the page length limit. Effort is made at CityU currently to simply the mechanical fastener into a staple, and the mechanical fastening process can be as simple as operating a stapling-machine that is similar to a Powder Actuated Fastening “gun”.

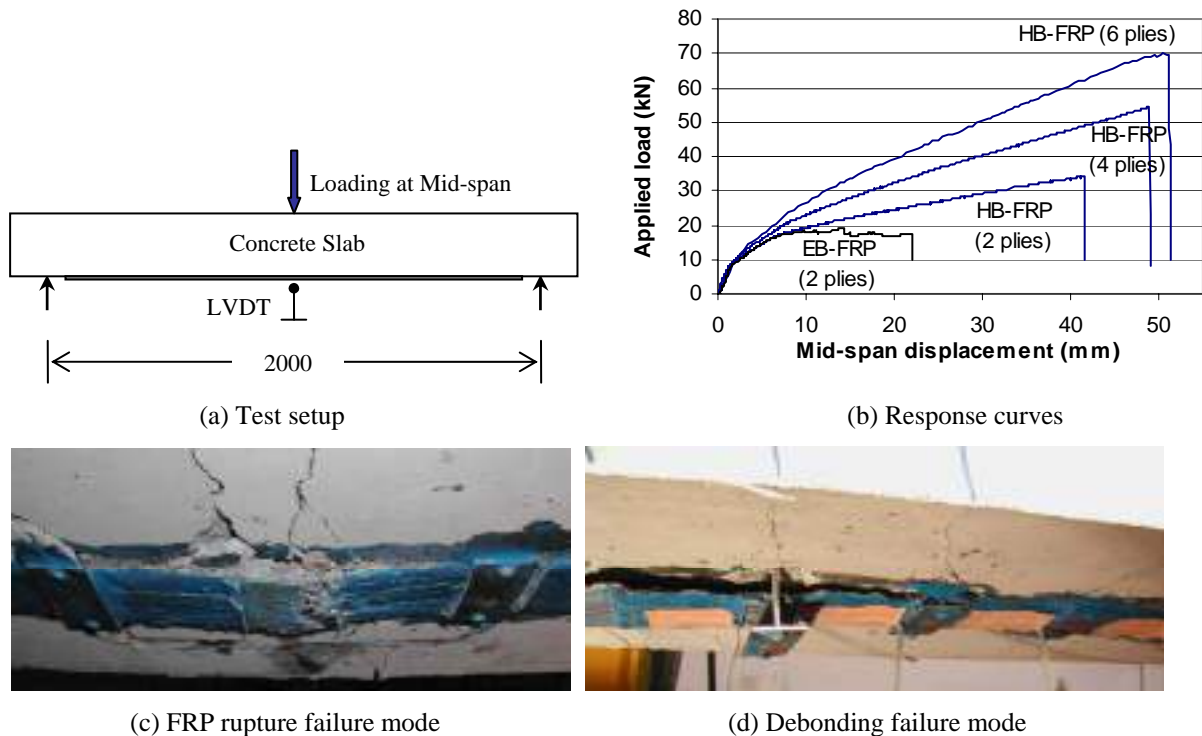


Figure 5: Flexural testing and results

ACKNOWLEDGEMENT

The work described in this paper was fully supported by a grant from the Research Grant Council of the Hong Kong Special Administrative Region, China [Project No. CityU 122106].

4. REFERENCES

- Bank, L.C. Mechanically fastened FRP (MF-FRP) - a viable alternative for strengthening RC members. Keynote Lectures, *Proc. the Second International Conference on FRP Composites in Civil Engineering (CICE 2004)*, 8-10 December 2004, Adelaide, Australia.
- Grace, N.F. Improved anchoring system for CFRP strips, *Concrete International ACI*, 2001; 23(10): 55-60.
- Hollaway, L.C., and Head, P. *Advanced Polymer Composites and Polymers in the Civil Infrastructures*. Elsevier Science, London, UK. 2001.
- Lam, L., and Teng, J.G. Strengthening of RC cantilever slabs bonded with GFRP strips, *Journal of Composite for Construction ASCE*, 2001; 5(4): 221-227.
- Nanni, A. Carbon FRP strengthening: New Technology becomes mainstream, *Concrete International*, 1997; 19(6): 19-23.

HYBRID FRP-CONCRETE SANDWICH BRIDGE DECK

Thomas Keller, Erika Schaumann, Till Vallée
(*Ecole Polytechnique Fédérale de Lausanne EPFL-CCLab,*
CH-1015 Lausanne, Switzerland)

ABSTRACT

This paper presents a new concept for a lightweight hybrid-FRP bridge deck. The sandwich construction consists of three layers: a fiber-reinforced polymer composite (FRP) sheet with T-upstands for the tensile skin, lightweight concrete (LC) for the core and a thin layer of ultra high performance reinforced concrete (UHPFRC) as a compression skin. Mechanical tests on eight hybrid beams were performed with two types of LC and two types of FRP/LC interface: unbonded (only mechanical interlocking of LC between T-upstands) and bonded with an epoxy adhesive. The ultimate loads of the beams increased by 104% on average due to bonding. However, the beam failure mode changed from ductile to brittle. The beams using a LC of 44% higher density exhibited an 81% increase in the ultimate load. The manufacturing of the beams proved to be economic in that epoxy and concrete layers were rapidly and easily applied wet-in-wet without intermediate curing times. The experimental results demonstrated the feasibility of the suggested hybrid bridge deck.

KEYWORDS

Bridge deck, sandwich, hybrid, FRP, lightweight concrete.

1. INTRODUCTION

Fiber-reinforced polymer (FRP) composites have found increased applications in bridge structures in recent years. Applications for strengthening and repair are already well established. A growing number of new bridges have been constructed as all-FRP or hybrid-FRP structures (FRP combined with traditional materials) (Keller, 2006). Several research projects pointed out that the combination of FRP with conventional materials is a promising application of FRP composites in bridge engineering (Deskovic et al. 1995, Hall and Mottram 1998, Canning et al. 1999, Van Erp et al. 2002, Bank et al. 2006).

The hybrid sandwich bridge deck concept suggested in this paper consists of three layers of different materials: FRP composites for the tension skin, lightweight concrete (LC) as a core material and ultra high performance fiber reinforced concrete (UHPFRC) for the compression skin (Fig. 1). The FRP layer, consisting of a 5 mm thick GFRP sheet with T-upstands, also serves as formwork. The fibers in the 30-50 mm thick UHPFRC layer are needed to carry possible local bending moments due to concentrated wheel loads and due to the jointless application (described below). A ductile or at least pseudo-ductile system behavior should be achieved by failure in the top concrete layer and crushing of the lightweight aggregates.

The target total weight of the deck is less than 50% of a normal concrete deck. The FRP layer together with the LC core is easily prefabricated in large elements (approximately 2.50 m x width of the bridge) that are transported to the site and rapidly installed on the main girders. The joints between deck elements as well as between deck and main girders are adhesively bonded. Subsequently, the thin UHPFRC layer is jointlessly cast on site onto the LC core. In regions of negative bending moments, GFRP reinforcement grids are laid into the UHPFRC layer. Since the deck is steel free and the UHPFRC layer is watertight, no waterproofing layer is required and the surfacing is directly applied onto the UHPFRC.

To examine the feasibility of the proposed concept, flexural experiments on hybrid beams were performed. The benefit of a bi-dimensional plate behavior was therefore neglected. The objective of the experiments was to show if a pure mechanical connection between the FRP and LC through the T-upstands is sufficient to provide full composite action or if an additional layer of adhesive is required. Furthermore, the shear capacity of different densities of LC was explored, because no reliable shear properties were available for the LC concretes. To this end, the beams were designed to obtain a shear failure in the lightweight concrete.

2. BEAM DESCRIPTION

The experimental program consisted of eight beams 3600 mm long, 400 mm wide and 200 mm deep (span/15). Figure 1 shows the cross-section of the beams. For the FRP layer, the standard pultruded GFRP element Plank 40HDx500 from Fiberline was used, which was cut to a width of 400mm. Only a 30 mm normal concrete (NC) layer was applied on the top. Lightweight concretes with average densities of 900 and 1300 kg/m³ were used. Furthermore, two types of FRP/LC interfaces were investigated: unbonded (LC directly cast on the FRP) and adhesively bonded (LC cast on wet epoxy adhesive applied between and on T-upstands). Table 1 gives an overview of the four beam configurations and their labeling. For each configuration two beams were examined.

Table 1: Experimental Results at Ultimate Load

Beam	Type of LC	FRP-LC interface	Ultimate Load [kN]	Mid-span deflection [mm]
900-1/2	LC900	unbonded	9.3 / 11.3	11.5-17.3 / 9.4
900E-1/2	LC900	epoxy bonded	31.2 / 30.4	8.7 / 8.1
1300-1/2	LC1300	unbonded	32.1 / 23.3	47.8 / 40.4
1300E-1/2	LC1300	epoxy bonded	42.8 / 50.5	12.3 / 14.1

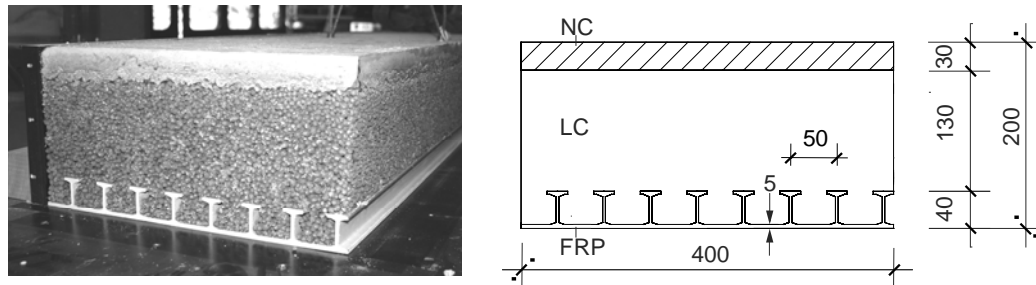


Figure 1: Cross-Section of Hybrid Beams

3. EXPERIMENTAL SET-UP

All beams were simply supported on rollers with a span length of 3000 mm and subjected to three-point bending using a hydraulic jack with a capacity of 200 kN. The load was applied at a constant displacement rate of 1 mm/min. The load was measured with load cells between the jack and the steel plate. For all beams, seven linear voltage displacement transducers (LVDT) were used to measure the deflection of the beams along the span in the centerline and the slippage of the LC and NC from the FRP element at the beam ends. Up to 20 strain gages on the top and at the bottom of the FRP sheet and on top of the T-upstands, and up to 30 Omega gages on the NC and LC concretes were applied to measure the strain distributions through the cross-sections.

4. EXPERIMENTAL RESULTS

4.1 Load-Deflection Response and Failure Mode of Unbonded Beams

The load-deflection curves at mid-span, measured for the unbonded beams with low density LC (beams 900-1, 900-2) and high density LC (1300-1, 1300-2), are shown in Fig. 2. The four beams showed an almost linear-elastic response up to 6.8-11 kN when small vertical cracks first appeared in the tension zone of the LC below the loading plate. The cracks always extended through the LC aggregates. Then the response of all four beams changed.

After first cracking, the load of the beams with high density could be increased significantly up to a first peak (at 31.0 kN for beam 1300-1 and 22.8 kN for 1300-2). The LC started to debond from the FRP sheet (at 20.7 kN for 1300-1 and 17 kN for 1300-2) and the stiffness decreased slightly. Increased slippage at the beam end was measured from this load on. After the first load peak, an oscillating load phase was observed for both beams as the displacement was increased, whereby at each intermediate peak a loud crack was audible. After the oscillating phase, a slight yet steady load increase was observed up to ultimate load. In this last loading phase, a single crack developed slowly through the whole depth of the beam and then horizontally in the LC/NC interface to the loading

plate and on the height of the T-up stands to the support. The LC was further pushed out at one beam end. Upon the sudden drop in load, the crack, which always went through the LC aggregates, reached the support.

The load of the beams with low density LC could only be slightly increased up to the ultimate load after the first cracks were observed (from 6.8 to 9.3 kN for 900-1 and 9.2 to 11.3 kN for 900-2). At ultimate load, debonding of the LC from the FRP sheets started and slippage between LC and FRP could be measured at the beam end. The maximum load of beam 900-1 could be maintained up to a mid-span deflection of approximately 17 mm, after which the load started to decrease slightly up to 34 mm deflection. After this point a sharp drop in the load was observed. The load of beam 900-2 started to decrease slightly immediately after ultimate load up to a mid-span displacement of 32 mm, when also a sharp drop occurred. In this phase, the same failure mechanism developed as described for the unbonded beams with higher density, however, at significantly smaller deflections and lower loads. The ultimate loads of the four unbonded beams and corresponding mid-span deflections are listed in Table 1.

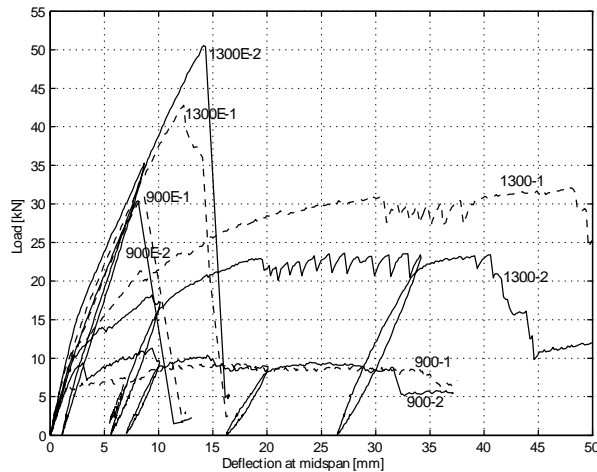


Figure 2: Load-Deflection Response of Unbonded and Bonded Beams

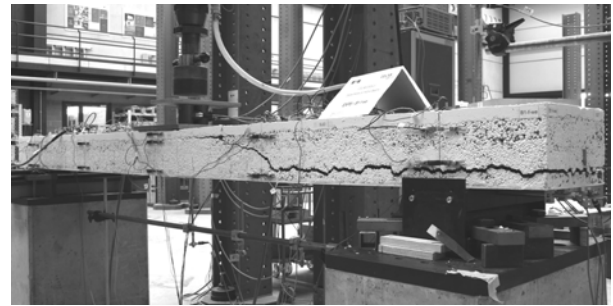


Figure 3: Failure Pattern of Bonded Beam 1300E-2

4.2 Load-Deflection Response and Failure Mode of Bonded Beams

The load-deflection curves at mid-span, measured for the bonded beams with low density LC (900E-1, 900E-2) and high density LC (1300E-1, 1300E-2), are shown in Fig. 2. The responses of all four beams showed a slight yet steady decrease in stiffness up to ultimate failure, which occurred at 31.2/30.4 kN for beams 900E-1/2 and 42.8/50.5 kN for beams 1300E-1/2. First cracks in the tension zone of the LC were observed between 20 and 26 kN for all beams. Subsequently, a multitude of small vertical or slightly inclined cracks developed in the tension zone below the loading plate. At ultimate failure, one of the cracks suddenly grew through the depth of the beam, along the LC/NC interface to the loading plate in one direction and at the height of the FRP T-upstands, just above the LC/FRP interface, to the support and on to the end of the beam in the other direction, as shown in Fig. 3. The epoxy-bonded interfaces remained undamaged. The beams showed no debonding of the LC from the FRP and no slippage at the beam end was measured. After brittle failure, the load dropped and the experiments were stopped. The ultimate loads of the four bonded beams and corresponding mid-span deflections are also listed in Table 1.

5. DISCUSSION

5.1 Influence of Interface Bonding on Flexural Behavior

In the first loading phase, up to 7-11 kN, all eight beams showed almost the same stiffness. At LC concrete cracking, however, the first differences in the behavior of unbonded and bonded beams were seen. While in the LC of the unbonded beams only a few, wide cracks developed with subsequent debonding of the LC from the FRP in the interface, a multitude of small cracks developed in the bonded beams, without debonding of the LC from the FRP. Accordingly, the stiffness of the unbonded beams decreased much more than that of the bonded beams.

After debonding at the LC/FRP interface in the unbonded beams, the composite action between concrete and FRP was partially lost and the FRP sheet participated increasingly in the load transfer with increasing load. Due to this,

the deflections increased considerably up to ultimate failure. The bonded beams, in contrast, showed full composite action up to ultimate failure, which occurred at significantly higher loads and smaller deflections.

The basic failure mode of both beam types was similar, with the exception of two differences. For both beam types, a shear failure in the LC occurred in one beam part. The failure thereby always crossed the LC aggregates. In the unbonded beams, this failure developed slowly and stopped at the support, while the debonded LC was pushed out at the beam end. In the bonded beams, the failure was sudden and brittle and the crack propagated above the T-upstands (in the LC) over the supports up to the beam end. In contrast to the brittle failure of the bonded beams, the unbonded beams showed a very ductile behavior. The oscillating response was interpreted as a slow, progressive failure of the mechanical interlocking between LC and T-upstands, showing a high dissipation of inelastic energy.

5.2 Influence of LC Density on Flexural Behavior

The effect of low versus high density LC on the ultimate load of the unbonded beams was seen to be greater than on the bonded beams (an increase of 169% vs. an increase of 51%, on average). The higher density LC enabled an effective mechanical interlocking between the LC and FRP T-upstands, which could not be developed with the lower density LC.

6. CONCLUSIONS

Experiments on eight hybrid FRP-concrete beams provided useful information about their load carrying behavior and the influence of the two investigated parameters: the FRP/LC interface (unbonded or epoxy bonded) and the type of lightweight concrete (low and high density). The following conclusions were drawn:

- 1) Varying the FRP/LC interface from unbonded to adhesively bonded increased the ultimate load by 104% on average, but changed the failure mode from ductile to brittle.
- 2) Increasing the LC density by 44% increased the ultimate load by 81% on average due to improved mechanical interlocking between LC and T-upstands. The effect was much more pronounced for the unbonded beams (169% increase) than for the bonded beams (51% increase).
- 3) The manufacturing of the beams proved to be rapid and easy. Epoxy, LC and NC were applied wet-in-wet without intermediate curing times within less than 30 minutes per beam. From this point of view the fabrication was very economical.
- 4) The experimental investigation proved the feasibility of the proposed new hybrid bridge deck. Further optimization is possible regarding LC material properties, mechanical FRP/LC interlocking, and local reinforcements over the supports to enable an arch-tie mechanism after concrete cracking.

7. ACKNOWLEDGEMENTS

This research was funded within the project New Road Construction Concept (NR2C) of the 6th European Framework Program. The authors wish to acknowledge the support of Fiberline Composites A/S, Denmark, supplier of the GFRP Plank elements; Sika AG, Zurich, Switzerland, supplier of the epoxy adhesive.

8. REFERENCES

- Canning, L., Holloway, L., and Thorne, A. (1999). "An investigation of the composite action of an FRP concrete prismatic beam". *Construction and Building Materials*, Vol. 13, No. 8, pp. 417-426.
- Deskovic, N., Meier, U., and Triantafillou, T.C (1995). "Innovative Design of FRP Combined with Concrete: short term behavior". *Journal of Structural Engineering*, Vol. 121, No. 7, pp. 1069-1078.
- Van Erp, G.M., Heldt, T., McCormick, L., Carter, D., and Tranberg C (2002). "An Australian approach to fiber composite bridges". *Proceedings of the International Composites Conference ACUN4, Composite Systems: Macro Composites, Micro Composites, Nano Composites*, UNSW Sydney, pp. 145-153.
- Hall, J.E., and Mottram, J.T. (1998). "Combined FRP reinforcement and permanent formwork for concrete members". *Journal of Composites for Constructions*, Vol. 2, No. 2, pp. 78-86.
- Keller, T. (2006). "Emerging markets – FRP composites in bridge superstructures". *8th World Pultrusion Conference, Emerging Markets: Globalization of the Pultrusion Industry*, Budapest, Hungary, (2006).
- L.C. Bank, L.C., Oliva, M.G., Russell J.S., Jacobson D.A., Conachen M., Nelson B, and McMonigal, D. (2006), "Double Layer Prefabricated FRP Grids for Rapid Bridge Deck Construction: Case Study". *Journal of Composites for Construction*, Vol. 10, No. 3, pp. 204-121.

HYBRID SQUARE FRP/STEEL GRID TUBE CONFINED CONCRETE CYLINDERS

Manu John

Graduate Student, Department of Mechanical Engineering, Louisiana State University, Baton Rouge, LA 70803

Guoqiang Li

Assistant Professor, Department of Mechanical Engineering, Louisiana State University, Baton Rouge, LA 70803

ABSTRACT

In this study, a lattice of steel grid tube, which is externally protected by a FRP skin, is used to confine square concrete cylinders. Twenty seven scaled-down square cylinders, which had a height of 308mm, a length of 114.3mm and a width of 114.3mm, were prepared. In order to evaluate the effect of grids on the structural performance of these encased square cylinders, two types of grid tubes were used. Type 1 was prepared with ribs running in the axial direction and Type 2 with ribs in a helical pattern. The specimens were divided into 9 groups. Groups 1 and 5 had grids on one face; groups 2 and 6 had grids on two opposite faces; groups 3 and 7 had grids on three faces and groups 4 and 8 had grids on all the four faces. Among them, Groups 1-4 were made of Type 1 grids and groups 5-8 were made of Type 2 grids. Solid steel tubes, Group 9, which were also wrapped with the same FRP skin, were used to encase concrete cylinders as controls. Uniaxial compression tests were conducted on all the specimens. The effect of the steel grids on the structural behavior was evaluated based on the test results.

KEYWORDS

FRP, grids, concrete confinement, square cylinders.

1. INTRODUCTION

Over the years, steel tube and fiber reinforced polymer (FRP) tube-encased concrete beam-columns have emerged as a novel alternative for rebuilding and new construction of engineering structures (Mirmiran and Shahawy, 1997). This includes manufacturing plants, bridges, high-rise buildings, harbors, water-front fenders, etc. These FRP tube-encased concrete beam-columns possess higher strength and ductility, and they are formwork-free.

In tube encased concrete cylinders, the tube is subjected to a 2-D stress condition - hoop tension and axial compression. This shows a distinct departure from FRP repaired concrete cylinders, where only the hoop tension dominates. Because of the 2-D stress condition, the interfacial bonding strength plays a certain role in carrying the applied axial and transverse loads. Therefore, there is a need to increase the interfacial bonding strength. Recently, a new type of circular steel grid tube that is externally protected by a FRP skin has been developed and tested; the function of the steel grid tube and the FRP skin has been well defined and validated through observation (Li, 2006). A uniaxial compressive load has been used. It is found that, due to the mechanical interlocking developed between the grid tube and the concrete core, both the specific compressive strength and ductility have been increased as compared to solid steel tube confined counterparts. Square steel grid tube encased concrete cylinders were also developed and tested using a four-point bending load configuration. Again, it is found that both the specific bending strength and ductility have been increased (Li et al, 2006). It is well known that stress concentrations exist at the corners in square tube encased concrete cylinders. It is desired to find how the square grid tube behaves if it is subjected to a uniaxial compression. The purpose of this study is thus to investigate the structural behavior of square steel grid tube encased concrete cylinders when they are subjected to a uniaxial compressive load.

2. EXPERIMENTS

2.1 Raw Materials and Specimens Preparation

Type I Portland cement, gravel, natural sand, water, and a superplasticizer DAVA 170 were used to prepare the concrete. The mix design followed ACI Standard 211.1 (“Standard” 1991). The mix ratio by weight was cement: water: coarse aggregate: fine aggregate: admixture = 1: 0.56: 3.80: 2.19: 0.001. To fabricate steel grid tubes, a low carbon steel plate, which had a thickness of 6.35mm, yield strength of 308MPa, and a modulus of elasticity of 200GPa, was obtained. The plate was cut into smaller pieces of 308 mm long by 114.3mm wide steel sheets. Circular holes with a diameter of 25.4mm were drilled through the steel sheets. Once the steel sheets were drilled, they were welded using seam welding to form 308mm high, 114.3mm long, and 114.3 mm wide square cylinders. A steel grid structure is shown in Figure 1.

In order to evaluate the effect of grids on the structural performance of these encased square cylinders, two types of tubes were prepared. Type 1 was prepared with ribs running in the axial direction and Type 2 with ribs in a helical pattern. The encased specimens were divided into 9 groups. Groups 1 and 5 had grids on one face; groups 2 and 6 had grids on two opposite faces; groups 3 and 7 had grids on three faces and groups 4 and 8 had grids on all the four faces. Among them, Groups 1-4 were made of Type 1 grids and groups 5-8 were made of Type 2 grids. Solid steel tubes, Group 9, which were also wrapped with the same FRP skin, were used to encase concrete cylinders as controls. Each group of specimens was weighed individually in order to obtain the specific load-displacement curves. Using a balance, it was found that the weight of a group 1 tube was 5.62 kg; it was 4.96 kg for a group 2 tube, 4.25 kg for a group 3 tube, 3.55 kg for a group 4 tube. For the helical grid tubes the weights were as follows: 5.69 kg for group 5, 5.01 kg for group 6, 4.37 kg for group 7 and 3.66 kg for group 8. The weight for the solid steel tube was 6.38 kg (group 9).

Once the steel tubes were prepared, all of them were wrapped using an ultraviolet (UV) curing E-glass 7715 fabric reinforced vinyl ester composite to form the FRP skin. The hand lay-up technology was used. The 7715 style fiber reinforcement was a unidirectional fabric. In this study, the fiber was aligned along the transverse (hoop) direction to provide the maximum confinement. Each tube was wrapped using two layers of FRP with a 25.4mm overlap. After wrapping, the specimens were moved to a UV-A light source for curing. The details of the UV-A light source can be found elsewhere (Li et.al, 2005). The curing was completed within one hour. Before casting concrete, one end of the tube was capped using a plastic tape. The concrete was then mixed, cast, compacted, finished, and cured for 28 days in a standard wet curing room with 100% relative humidity.

2.2 Compressive Testing

The compression tests were conducted according to ASTM C 39 standard using a FORNEY machine. This machine has a capacity of 2688kN. Each specimen was uniaxially compressed to about 40% of the unconfined concrete strength, and unloaded to guarantee close contact between each component and to reduce errors in displacement measurement. Then, the specimen was reloaded until cylinder failure. The assembled computer data acquisition system can directly record the load–displacement curves. The loading rate was 0.23MPa/s.

3. RESULTS AND DISCUSSIONS

3.1 Axial Load-Displacement Behavior

The specific load (kN/kg) – displacement (mm) curves for each subgroup of specimens are shown in Figure 2. It is seen that the specific load-displacement of grid tube encased concrete cylinders behave similar to the solid steel tube encased concrete counterparts. The load-displacement curves can be generally described by a linear elastic region followed by an almost horizontal curve, which simulates yielding, and a strain hardening region until the peak load is achieved. Once the peak load is reached, the cylinders show a rapid decrease in load as the displacement increases. This is an indication of the structural failure of the cylinders. The reason for this type of structural behavior can be explained as follows. Subjected to a uniaxial compression load, a tensile stress is developed on each face of the square tube along the hoop direction. This type of stress is the highest at the four corners of the tube. The stress concentration at the corners results in yielding and hardening of the welds, similar to a low carbon steel subjected to tension.

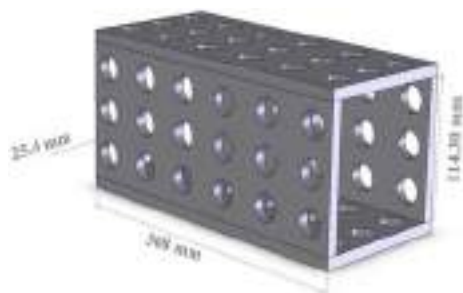


Figure 1: Steel Grid Structure

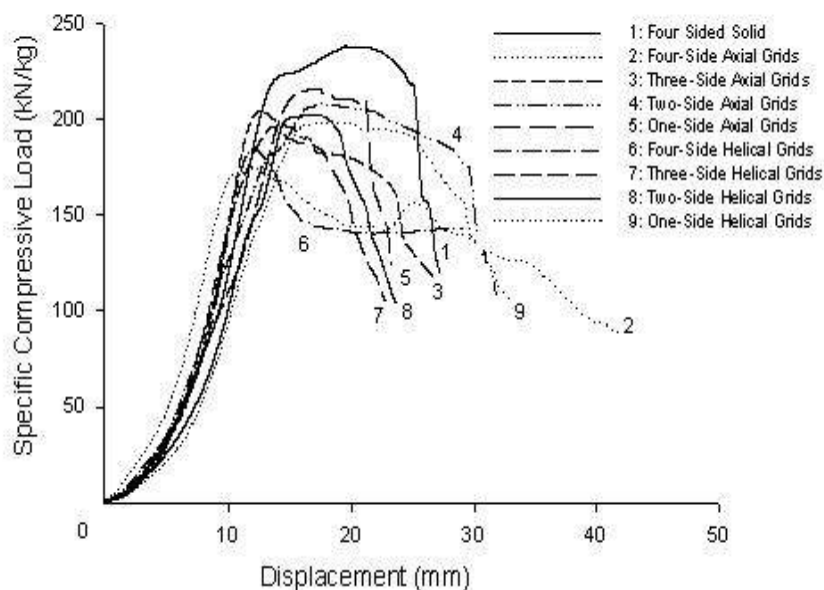


Figure 2: Specific Compressive Load and Displacement of various types of cylinders

3.2 Compressive Strength and Ductility

The specific peak load and the displacement are summarized in Table 1. Comparing the steel grid tube with the solid steel tube, it is seen that the specific axial load of the grid tube is reduced. The reduction becomes larger and larger as the number of grid faces increases, in particular for the axial grid tubes. The reason for this reduction may be due to the fact that the tube and the core carry the load collaboratively. Due to the removal of steel, the stiffness of grid tubes is lower than that of the solid steel tubes. Subject to the same axial load, the concrete core has a higher share of load. As a result, the core expands more laterally. This larger transverse expansion results in larger hoop stress in the tube. Consequently the cylinders with grid tubes fail at a lower axial load.

Table 1: Variation of Specific Load and Displacement with Number of Ribs

Specimen	Peak Specific Load (kN/kg)	Load decrease (%)	Displacement (mm)	Ductility change (%)
Group 9	237.97	-	27.37	-
Group 1	215.76	9.30	23.27	-14.90
Group 2	207.25	12.91	31.82	16.29
Group 3	204.17	14.20	26.61	-2.77
Group 4	174.68	26.60	41.74	52.50
Group 5	198.44	16.61	32.65	19.29
Group 6	202.09	15.07	23.67	-13.52
Group 7	196.13	17.58	22.83	-16.59
Group 8	184.02	22.67	29.82	8.95

Compared with the solid steel tubes, the grid tube encased concrete cylinders show an increase in ductility. This increase becomes more pronounced for the group 4 samples. The reason for this increase in ductility can be explained as follows. For the solid steel tubes and the solid face in steel grid tubes, it can be noticed that local

buckling occurs; see Figure 3. As a result failure occurs abruptly and leads to smaller displacement. On the other hand, for the steel grid faces, no buckling can be seen due to the mechanical interlocking and the support provided by the concrete within the bay area. The failure of the grid faces is mainly due to axial deformation of the bay. Consequently the cylinders with grid tubes possess more ductility.



(a) Solid steel tube locally buckles



(b) Grid face deforms and solid face locally buckles

Figure 3: Failure modes of solid steel face and grid face

Comparing the axial grid tube encased cylinders with helical grid tube encased cylinders, it is found that the axial grid tube leads to a higher reduction in strength and a higher gain in ductility. Depending on the applications, axial grid tube confined cylinders may be more applicable in the case where more ductility is required; on the other hand, helical grid tube encased cylinders may be more proper for the cases where compressive strength is the control factor. It is observed during the testing that the local buckling of the solid steel face or the axial deformation of the grid face is close to the end of the cylinders. For helical steel grid face there is more solid steel at the end of the face than that of the axial grid face. The more solid steel near the end of the face results in higher strength and lower ductility, similar to the solid steel face.

4. CONCLUSIONS

Steel grid tube encased square concrete cylinders are prepared and tested in this study. The test results show that the grid tube encased concrete cylinders behave similarly to the solid steel tube encased control concrete cylinders. Compared to the control specimens, the grid tube encased cylinders have a higher ductility, due to the mechanical interlocking, and a lower strength, due to the reduced stiffness of the steel grid faces. Compared with axial grid tubes the helical grid tubes have a higher compressive strength and a lower ductility, possibly due to a higher amount of solid steel near the end of the helical grid face.

5. ACKNOWLEDGMENT

This study was partially sponsored by the Louisiana Board of Regents and EDO Fiber Science under contract number LEQSF(2004-07)-RD-B-05 and an EDA Fellowship. The encased concrete cylinders were prepared and the tests were conducted in the Concrete Laboratory at the Louisiana Transportation Research Center (LTRC). The support is greatly appreciated.

6. REFERENCES

- Li, G., Torres, S., Alaywan, W., and Abadie, C. (2005). "Experimental Study of FRP Tube-Encased Concrete Columns". *Journal of Composite Materials*, Vol. 39, pp. 1131-1145.
- Li, G. (2006). "Experimental Study of Hybrid Composite Cylinders". *Composite Structures*, (in press) [doi:10.1016/j.compstruct.2005.08.028](https://doi.org/10.1016/j.compstruct.2005.08.028).
- Li, G., John, M. and Maricherla, D. (2006). "Experimental Study of Hybrid Composite Beams". *Construction and Building Materials*, (in press) [doi:10.1016/j.conbuildmat.2005.11.003](https://doi.org/10.1016/j.conbuildmat.2005.11.003).
- Mirmiran, A and Shahawy, M (1997). "Behavior of concrete columns confined by fiber composites", *Journal of Structure Engineering*, Vol 123, pp 583-590.

STRUCTURAL CHARACTERIZATION OF COMPOSITE SANDWICH PANEL WITH HYBRID FRP-STEEL CORE FOR BRIDGE DECKS

Hyo Seon Ji

(Visiting Scholar, The University of Tennessee, Knoxville, Tennessee, USA)

Byung Jik Son

(Assistant Professor, Konyang University, Nonsan-Si, Chungnam-Do, Korea)

Z. John Ma

(Associate Professor, The University of Tennessee, Knoxville, Tennessee, USA)

ABSTRACT

The use of FRP panels for bridge deck is limited, due to the relatively higher cost of the composite materials. A hybrid concept of composite sandwich panel with hybrid FRP-steel core is proposed for highway bridges in order not only to improve stiffness and buckling response but also to be cost-efficiency compared to all FRP decks. The composite sandwich bridge deck system is composed of the hybrid FRP-steel core and the FRP facings. Its structural performance under static loading was conducted, and the ANSYS finite element program was used to predict the panel behaviour. This study is focused on the structural characterization of flexure performance of the composite sandwich panels for bridge decks under static loading. It is found that the presented composite sandwich panel with hybrid FRP-steel core is very efficient for use in bridges. And roughly estimated cost of this composite sandwich deck is \$250/ m², whereas roughly estimated that of an all FRP deck is \$400/m². Therefore, the use of the hybrid composite sandwich deck in bridge construction may be able to compete with the conventional decks.

KEYWORDS

Composite sandwich panel, hybrid FRP-steel core, Cost-efficiency, Finite Element

1. INTRODUCTION

In recent years the interest in using Fibre-reinforced polymer (FRP) in construction field application has significantly increased worldwide. Due to its high specific stiffness and strength, FRP may offer a number of advantages over traditional materials, including environmental durability and ease of construction. The competitiveness of FRP in bridge structures likely falls in the potential for lower life-cycle and installation cost. The first of all FRP short-span bridge in South Korea was installed in May 2002 (Ji et al., 2006). Although many different types of deck systems are currently designed and constructed, the most commonly used type of deck for the slab-on-girder system is a cast-in-place reinforced concrete deck. Recently, compared to conventional materials the application of FRP can significantly improve the performance of bridge deck. However, the use of FRP panels for bridge deck is limited, due to the relatively higher cost of the composite materials. The costs of the bridge decks with different materials are compared such as an estimated cost of \$400/m² for all Glass Fibre-Reinforced Polymer (GFRP) deck, and \$200/m² for all Concrete deck in US dollar. In terms of initial costs, FRP composites are, however, still too expensive to compete with other conventional materials used in civil engineering applications. To make the best use of materials, combinations of FRP and conventional materials have recently been investigated by a number of researchers. The advantages of the combined or hybrid structural systems include the cost-effectiveness and the ability to optimize the structural section based on material properties of each constituent material. The objective of this paper is to present the proposed hybrid concept of composite sandwich panel system for bridge decks. The panel system is composed of the hybrid FRP grid core and steel box tube core. This study is focused on the flexure performance of the proposed system under static loading through an experimental program. Its structural performance under the DB-24 live load (MOCT, 2000) is also analysed by using the ANSYS finite element program.

2. BEHAVIOR AND DESIGN OF HYBRID FRP-STEEL DECK PANELS

The proposed hybrid FRP-steel sandwich panel for highway bridge deck consists of FRP composite top and bottom facings, FRP composite grid and multiple steel box cells core, as shown in Figure1.

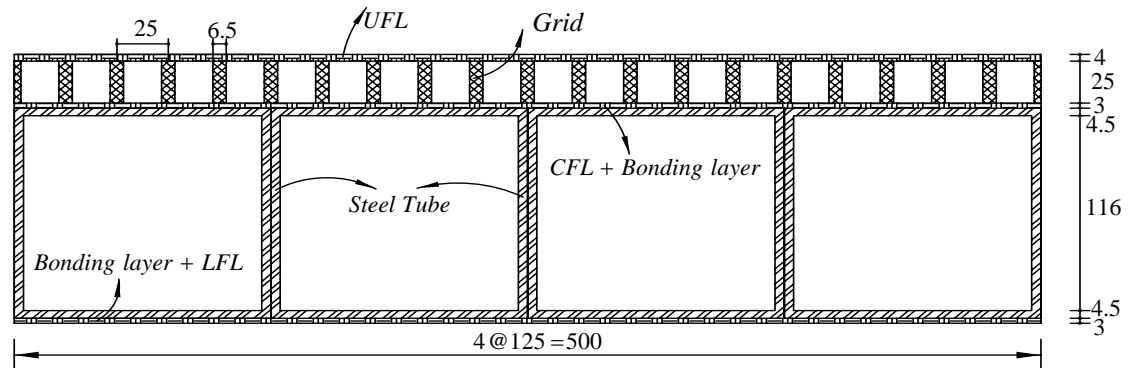


Figure 1: Cross sections of composite sandwich panel (All Dimensions in mm)

In order to consider local effect due to tire contact at the top facing, the upper core was designed as a composite grid. The constituents properties used for the sandwich panel are shown in Table 1.

Table 1: Fiber and matrix constituent material properties

Material	E (GPa)	G (GPa)	ν	ρ (g/cm^3)
E-glass fiber	72.5	27.6	0.22	2.54
Polyester resin	3.38	1.38	0.38	1.24
Vinyl ester resin	3.91	1.43	0.37	1.15

By using a simple rule of mixtures approach, the layer stiffness and properties of the composites can be determined as shown in Table 2.

Table 2: Layer stiffness and properties predicted using micro mechanics model

Ply name	Ply type	Ply thickness (mm)	Plys per layer	V_f	Ply orientation	E_1 (GPa)	E_2 (GPa)	G_{12} (GPa)	ν_{12}
UFL	CSM	3.2	4	0.194	Random	7.99	7.99	1.69	0.349
	Roving	2.4	2	0.234	$0^\circ/90^\circ$	19.55	4.35	1.77	0.343
LFL	CSM	3.2	4	0.194	Random	7.99	7.99	1.69	0.349
CFL	Roving	2.4	2	0.234	$0^\circ/90^\circ$	19.55	4.35	1.77	0.349
Grid core	Roving	25.0	25	0.246	0°	20.38	4.42	1.80	0.341
Steel core	-	125.0	-	-	Isotropic	204	204	76.9	0.300
Bonding layer	CSM	1.6	2	0.183	Random	8.17	8.17	1.73	0.343

Where UFL = upper facing laminate; CFL= core facing laminate; LFL = lower facing laminate; CSM = chopped strand mat; Roving = woven roving; V_f = fiber volume fraction. In general, the polyester resin is used. However, the bonding layers consist of the vinyl ester resin due to the presence of the elongation difference between the steel tube and facing laminate. The stiffness of each ply can be predicted from micromechanics models (Julio et al., 2001) shown in Table 2. To predict the deflection, a preliminary analysis was conducted using the theory of anisotropy sandwich beam. Then, the detailed finite element analysis was used. The composite sandwich panel was modeled and analyzed by the finite element analysis program ANSYS. GFRP laminates were modeled by 8-node

shell elements, while the FRP grid and steel tube were modeled by solid elements. Perfect bonding between FRP grid and steel tube was assumed in all analyses. The boundary conditions were modeled as a pin and a roller for the end supports. Pressure load was applied in the middle of the deck. The FE analysis was conducted for a composite sandwich panel using the material properties in Table 2. The composite sandwich panel deck was fabricated by a hand lay-up method according to the detailed design.

3. EXPERIMENTAL STUDY

The testing setup for the deck is shown in Figure 2. The bending test was conducted in order to evaluate the structural performance of the composite sandwich panel of $1.0m \times 3.0m \times 0.163m$. Two composite sandwich deck specimens were tested. The load was applied at center of the deck onto the tire contact area of $500mm \times 200mm$ by the 500kN-MTS actuator. Figure 3 shows the location of LVDTs (D1, D2, and D4) and strain gauges (TR1, T1, TR4 = top strain; BR1, B1, BR4 = bottom strain).



Figure 2: Experimental setup

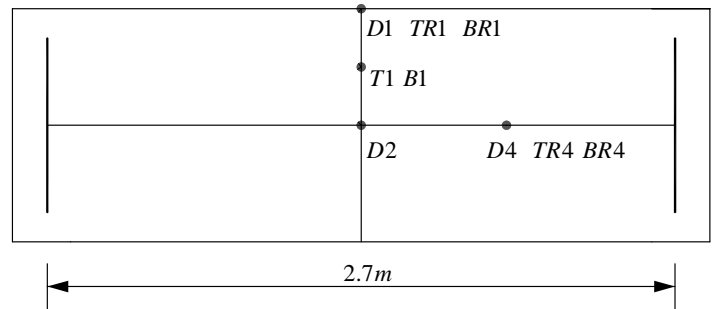


Figure 3: The location of LVDTs and strain gauges

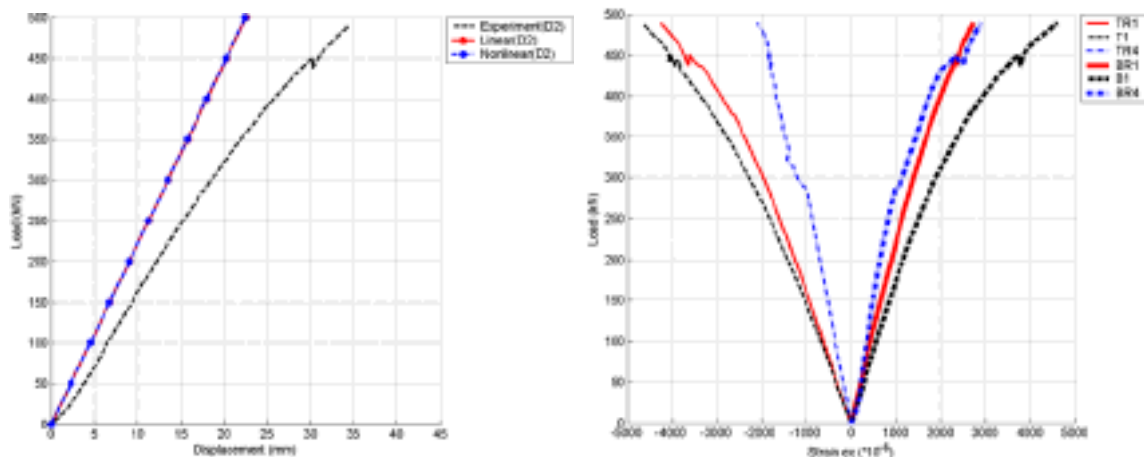


Figure 4: Load-deflection, strains response of composite sandwich panel

The load-deflection curves from testing and analysis and strains curves of the composite sandwich deck are shown in Figure 4. The stiffness was calculated to be $16.7kN/mm$. The comparison of deflection results under a service load for the two specimens is shown in Table 3. The one rear axle load of DB24 (MOCT, 2000) is $94.08kN$. The deflection for this service load, $94.08kN$ was $6.00mm$ (mean value). This is less than the span design limitation of $L/425$ (LRFD, 2004) of $6.35mm$ for the composite sandwich deck.

Table 3: Comparison of results for a composite sandwich deck under $P=94.08 kN$

	Theory of anisotropy beam	ANSYS	Exp.	Remark
Deflections (mm)	4.67	4.35	5.65	6.00 (Mean value)
			6.35	

The maximum load applied was 491kN and lateral deflection was 35.6mm (average). The predicted failure load was under 500kN. However, no visible damage was observed during the testing up to 491kN. The comparison of displacement and strain results under the testing load of 400kN is shown in Table 4.

Table 4: Comparison of displacement and strain under P=400kN

Experiment	Displacement (D4)		Strain (T1)		Strain (B1)	
		25.56mm	25.66mm	-0.00329	-0.00333	0.00298
	25.77mm	(Mean value)	-0.00337	(Mean value)	0.00294	(Mean value)
Analysis (ANSYS)	18.11mm		-0.00288		0.00208	

As the failure mode, the significant de-lamination between the FRP grid and steel tube was observed, but there was no collapse of the deck. It is possible to confirm no collapse because of the flexibility failure of the steel tube by comparing the all GFRP deck. On visual inspection, any local damage failure at the loaded part of the top flange was not observed. The construction costs for traditional small highway bridges are estimated as shown in Table 5.

Table 5 Cost of the bridge decks

Description of cost categories	Cost for a bridge deck with different materials (US \$)		
	Concrete	All GFRP	Proposed Hybrid
Total direct costs	\$200/m ²	\$400/m ²	\$250/m ²
Material cost	120	300	180
Handling	12	63	39
Shipping	4	1	1
Installation	24	7	4
Corporate overhead	40	29	26

Although roughly estimated that of the hybrid FRP are 1.25 higher than those for a concrete bridge deck, these increases are offset by savings on other costs such as maintenance and repair costs. Therefore, the hybrid FRP decks may be able to compete with the concrete ones.

4. CONCLUSIONS

The static testing and analysis of a hybrid FRP-steel composite sandwich panel for highway bridges are briefly discussed in this paper. Based on the study presented in this paper, several conclusions are summarized in the following. It is possible to confirm the efficient use of steel tube core in the core of sandwich panel to increase the system stiffness instead of using GFRP, and to reduce the amount of GFRP composites and initial costs. It was demonstrated that the proposed composite sandwich deck is considered to possess safety factors for strength and serviceability much higher than the Korean Highway Code requirements. The depth of deck may be decreased 20% when comparing with the all GFRP deck so that the same flexural rigidity can be obtained, and the strength can be used more efficiently as well. Roughly estimated cost of this composite sandwich deck is \$250/ m² comparing with an estimated cost of \$400/m² for all GFRP deck. Therefore, the use of the hybrid FRP-steel composite sandwich deck in bridge construction may be very efficient and be able to compete with the conventional and all FRP decks.

5. REFERENCES

- AASHTO LRFD (2004), "AASHTO LRFD Bridge Design Specifications", American Associations of State Highway and Transportation Officials, 3rd Ed., Washington D.C.
- Ministry of Construction and Transportation (MOCT) (2000), "Standards specifications for highway bridge " 2nd Ed., Korea.
- ANSYS. Version. 10.0.
- Julio F. Davalos et al. (2001). "Modeling and characterization of fiber-reinforced plastic honeycomb sandwich panels for highway bridge applications". *Composite Structures*, Vol. 52, pp. 441-452.
- Ji, H.S., Son, B.J., and Chang, S.Y. (2006) "Field Testing and Capacity-Ratings of Advanced Composite Materials Short-span Bridge Superstructure, *Composite Structures*, in press

Part XIII. Masonry Structures

CHARACTERIZATION OF MASONRY WALLETES AND SHEAR TRIPLET SPECIMENS RETROFITTED WITH GFRP COMPOISTES

Prakash, S.S

(Graduate Research Assistant, University of Missouri Rolla, Rolla, Missouri, USA)

Alagusundaramoorthy, P

(Associate Professor, Indian Insitute of Technology Madras., Chennai, Tamil Nadu,India)

ABSTRACT

Masonry is one of the oldest construction materials that is in use around the world for reasons due to its accessibility, functionality and cost. Masonry buildings are the major building stock around the world, fail in earthquakes mainly because of their low tensile and shear resistance. These masonry structures are retrofitted with FRP composites is found to increase its seismic performance. Experimental studies on masonry wallettes and shear triplet specimens with and without retrofitting using GFRP composites were conducted under monotonic loading. The increase in deformation limit and ultimate load resistance of the retrofitted wallettes and triplets were compared to that of control specimens. Finite element (FE) models were created, and the results were verified with experimental data. Macromodeling was adopted for the analysis of masonry wallettes. Shear triplets were analyzed by micromodeling. Parametric studies were conducted to study the changes in the deformation limit and ultimate load resistance for varying thickness of GFRP composites and fiber orientations. It is concluded that GFRP composites retrofitting increases the strength and stiffness of wallettes and strength and ductility of shear triplets.

KEYWORDS

Masonry; Wallettes; Shear triplets; FRP composites; Retrofitting

1. INTRODUCTION

This study focuses on the characterization of the masonry wallettes, shear triplets, and GFRP composite materials to study the effect of retrofitting on the strength and deformational capacity of brick masonry. The behavior of unreinforced masonry is brittle, with little or no ductility, and it suffers form damages ranging from invisible cracking to extensive crushing and that leads to brittle/sudden failure during earthquakes. Earthquakes like Bhuj in India in 2001 have shown that the damage to lives and property are mainly by the failure of unreinforced brick masonry walls. To understand the behavior of retrofitted load bearing and infill walls, the basic material properties of masonry components are essential. In this study, the strength and elastic properties of bricks, cement mortar, brick masonry wallettes and shear triplets, and GFRP composite materials are evaluated. The effect of GFRP retrofitting on the behavior of masonry wallettes and shear triplets are studied by testing the specimens and finite element analysis. Based on the results of finite element analysis and experimental study, a set of conclusions are drawn.

2. EXPERIMENTAL STUDY

Bricks and mortar were tested to determine the elastic properties as per IS: 1905, 1987. The modulus of elasticity of the brick and mortar are found to be 808 N/mm² and 1540 N/mm² respectively. A composite laminate was fabricated using the epoxy resin with hardener in 10:1 ratio and glass fiber woven roving mat with a resin to fiber ratio of 1:1. Tests were conducted on the GFRP composite to find water absorption, hardness, volume fraction of fibers, tensile strength, and flexural strength as per BS 2782, 1996.

2.1 Tests on Masonry Wallettes

Fifteen wallettes were cast with and without retrofitting using GFRP composites (Table 1). Wallettes were cured for fifteen days and tested in the compression testing machine both normal and parallel to bed joints (EN 1052, 1998). The specimens (WNB1 to WNB5) were tested under uniaxial compression normal to bed joint and they failed

through vertical cracking in the middle. When the principal tensile stress reaches the tensile strength of the bricks, crack forms, and failure occurs. The wallettes (WPB6 to WPB9) under compression parallel to bed joint failed by the formation of vertical separation of cracks along the bed joint from differential normal deformation of bricks and the mortar joint. The modulus of elasticity under compression parallel to bed joint is higher than the modulus of elasticity normal to bed joint for the solid brick masonry wallettes (Table 1). Three GFRP retrofitted specimens (RWNB1 to RWNB3) were tested under compression normal to bed joints, and the other three GFRP retrofitted specimens (RWPB4 to RWPB6) were tested under compression parallel to bed joints. Under compression normal to bed joints, the increase in the strength was around 20%. However, the FRP retrofitting reduced the ultimate strain significantly (Up to 40%), which is detrimental to the seismic demand (ductility). The behavior of the retrofitted specimen is stiffer with $E_{avg}=336 \text{ N/mm}^2$, compared to the control specimen with $E_{avg}=168 \text{ N/mm}^2$ (Table 1). The stiffness of the wallettes increased by around 100% by retrofitting. The retrofitted wallettes failed under compression by crushing due to the confining effect of retrofitted laminates. Eventhough, debonding of the laminates was noticed at the initial phase of loading, the overall bond with brick surface was intact throughout the loading. GFRP retrofitting increased the ultimate load under compression parallel to bed joint. The increase in the load resistance was around 3.5%. However, the ultimate strain under compression parallel to the bed joint does not reduce due to GFRP composite retrofitting as in the case of compression normal to bed joint. The behavior of the retrofitted specimen under compression parallel to bed joint is stiffer with $E_{avg}=563 \text{ N/mm}^2$ compared to that of the control specimen $E_{avg}=405 \text{ N/mm}^2$. The increase in the stiffness is about 39%. After reaching the peak load, a bursting sound was heard as a result of separation of the bed joint mortar from the bricks.

Table 1. Ultimate Strength of Control and Retrofitted Wallettes under Compression

Specimen	Direction of Loading	Size (l x b x t) (mm)	Density (kN/m ³)	Ultimate Strength (N/mm ²)	Ultimate Strain	Young's Modulus (N/mm ²)	Axial Secant Stiffness at Failure (kN/mm)
WNB1	Normal to Bed Joint	393 x 410 x 132	19600	3.3	Strain readings were not consistent	Strain readings were not consistent	Strain readings were not consistent
WNB2	„	395 x 410 x 130	19400	2.6	„	„	„
WNB3	„	396 x 405 x 122	19300	3.3	0.01900	176	21.9
WNB4	„	398 x 408 x 126	19600	3.1	0.01920	163	21.1
WNB5	„	390 x 404 x 123	19500	3.0	0.01850	164	20.9
Average		395 x 407 x 126	19520	3.0	0.01890	168	21.3
WPB6	Parallel to Bed Joint	392 x 408 x 123	19900	3.3	0.00775	425	54.4
WPB7	„	396 x 409 x 125	20800	3.2	0.00765	420	54.2
WPB8	„	398 x 406 x 127	19600	3.0	0.00770	393	50.9
WPB9	„	393 x 408 x 128	21200	2.9	0.00775	381	50.6
Average		396 x 407 x 127	20375	3.1	0.00771	405	52.6
RWNB1	Normal to Bed Joint	395 x 408 x 130	20400	3.6	0.01140	316	42.4
RWNB2	„	396 x 406 x 131	20600	3.9	0.01120	348	46.8
RWNB3	„	396 x 405 x 128	20500	4.1	0.01190	345	45.2
Average		396 x 406 x 130	20500	3.9	0.01150	336	44.8
RWPB4	Parallel to Bed Joint	394 x 409 x 130	20300	3.5	0.00580	603	81.4
RWPB5	„	397 x 407 x 129	20800	3.2	0.00570	561	74.2
RWPB6	„	396 x 406 x 128	20200	3.0	0.00570	526	69.1
Average		396 x 406 x 129	20433	3.2	0.00570	563	74.9

2.3 Tests on Shear Triplets

Shear triplet specimens without retrofitting (STS1, STS2, and STS3) and with retrofitting (RSTS1, RSTS2, and RSTS3) were cast for testing. Specimens STS1, STS2, and STS3 were tested to determine the initial shear strength under zero vertical compression. The shear resistance increased with relatively no deformation up to a load of 10 kN. Thereafter, the load resistance linearly increased from 10 kN to 14 kN up to a deformation of 0.01 mm. After the deformation of 0.02 mm the crack started propagating suddenly along the bed joint, and the specimen failed. This result shows that the unretrofitted triplet has failed through slipping mode of brick and bed joint mortar at very low displacement levels. The average shear strength of triplets was found to be 0.29 N/mm^2 (Table 2). The specimens RSTS1, RSTS2, and RSTS3 were retrofitted with one layer of GFRP composite to study the effect of retrofitting on increase in strength and ductility. The test results of shear triplets showed that GFRP retrofitting was

observed to increase the ultimate load from 13.8 kN to 39 kN. The increase in the load resistance was up to 180%. The ultimate displacement has increased dramatically from 0.016 mm to 3.0 mm. Even though initial debonding occurred, the final failure of the triplet is by cracking of the middle brick and this shows that the retrofitting by GFRP composites increases the ductility of the masonry under shear. This failure mode indicates that with good bonding of GFRP laminates on the brick surface, the shear failure can be totally eliminated, and the increase in strength will be governed by the compressive strength of masonry.

Table 2. Ultimate Shear Strength of Control and Retrofitted Triplets

Specimen	Size (L x B x H) (mm)	Failure Load (kN)	Ultimate Shear Strength (N/mm ²)	Maximum Shear Deformation (mm)
STS1	233 x 110 x 230	13.5	0.28	0.020
STS2	232 x 110 x 230	14.2	0.29	0.020
STS3	233 x 110 x 230	13.9	0.29	0.014
Average	233 x 110 x 230	13.8	0.29	0.018
RSTS1	234 x 112 x 230	37.8	0.78	3.200
RSTS2	232 x 112 x 230	39.3	0.81	2.900
RSTS3	232 x 112 x 230	40.0	0.83	2.800
Average	233 x 112 x 230	39.0	0.81	2.967

3. NUMERICAL STUDY

Homogeneous macromodeling with smeared cracking concrete material model for the analysis of masonry wallettes and heterogeneous micromodeling using elastic properties for analysis of shear triplets are adopted. Macromodeling is adopted for the analysis of brick masonry wallettes due to its simplicity and practical significance (Giordano et al 2002). The material properties for macromodeling are obtained from the testing of brick masonry wallettes (Table 1). The modulus of elasticity for the numerical study is obtained from the experimental results as $E_x=168$ N/mm² normal to bed joint and $E_y=405$ N/mm² parallel to bed joint. The Poisson's ratio for the masonry material is normally around 0.15 to 0.2, and it is taken as 0.2. For micromodeling, the average modulus of elasticity of the clay brick masonry unit is found to be 808 N/mm². The modulus of elasticity of the mortar is found to be 505 N/mm². The Poisson's ratio for the brick and mortar is taken as 0.2 (Sahlin, 1971). The friction on the interface between brick and mortar normally varies from 0.45 to 0.80 and is taken as 0.6. The normal stiffness for the contact analysis is given a very high value in order to avoid interpenetration of continuum. FRP material used for retrofitting is a glass fiber woven roving mat with an area density of 360 gsm. It is modeled assuming elastic behavior through the lamina option in ABAQUS (Hibbit et al, 2002). The tensile strength of the laminate was determined as per procedures given in the standard (BS 2782, 1996). The average Young's modulus in tension along the warp and weft directions is found to be $E_x=12984$ N/mm² and $E_y=11500$ N/mm². The Poisson's ratios ν_{xy} and ν_{yx} are found to be 0.126 and 0.112, respectively. Perfect bond is assumed to exist between GFRP composite and the masonry wall surface.

3.1 Macromodeling of Masonry Wallettes

Masonry wallettes are modeled using macromodeling concepts with the smeared crack concrete model. The average Young's modulus and Poisson's ratio from the corresponding wallette results are used for the elastic zone of the model. For the plastic zone, the parameters are taken from the nonlinear part of uniaxial compression stress strain curve (stress and corresponding absolute plastic strain). The "failure surface" option is used to define the shape of the failure surface. The GFRP composite is modeled as an elastic orthotropic material. In the retrofitted and unretrofitted specimens, wallettes are modeled by eight noded linear continuum elements (C3D8R) with reduced integration and hourglass control. The GFRP composite is modeled using 3D shell elements (S4R) with both rotation and translations at each node. The loading is applied at the top surface of the wallette as displacement. The bottom of the wallettes is assumed to be fixed with all the degrees of the freedom arrested. It is assumed that a perfect bond exists between the wallette surface and GFRP composite. The behavior of the FE-model is found to be in close agreement with the experimental data upto the elastic limit in the unretrofitted control wallettes and GFRP composite retrofitted wallettes (Figs. 1a and 1b).

3.2 Micromodeling of Shear Triplets

In micromodeling of shear triplets, the brick as well as mortar are taken as linear elastic materials with appropriate material properties from the experimental data. Both the brick and mortar are modeled using 3D continuum elements (C3D8R). The GFRP composite is modeled using 3D shell elements (S4R) with orthotropic material properties. The interface between brick and mortar was modeled using surface to surface contact algorithm with interface elements.

The brick surface is considered as the master surface and mortar surface is considered as the slave surface. Tangential behavior of the interface between the brick and mortar is modeled using the penalty friction formulation with friction coefficient as 0.6. The normal behavior of the interface is modeled using linear pressure over closure with normal stiffness as 1000 N/mm. Initially, the increase in load resistance was stiffer before cracking of the bed joint up to 10 kN in the case of the control triplet. After the cracking at the bed joint, the GFRP composite started to resist the load. In FE-model, the increase in the load resistance was linear up to the ultimate displacement of 3.0 mm (Fig. 1c). From the analysis of the FE-model, the load resistance was 70 kN compared to the experimental value of 40 kN (Fig. 1c) at the ultimate displacement of 3.0 mm. This result is due to the perfect bond assumption made in the modeling between the triplet surface and the GFRP composite surface.

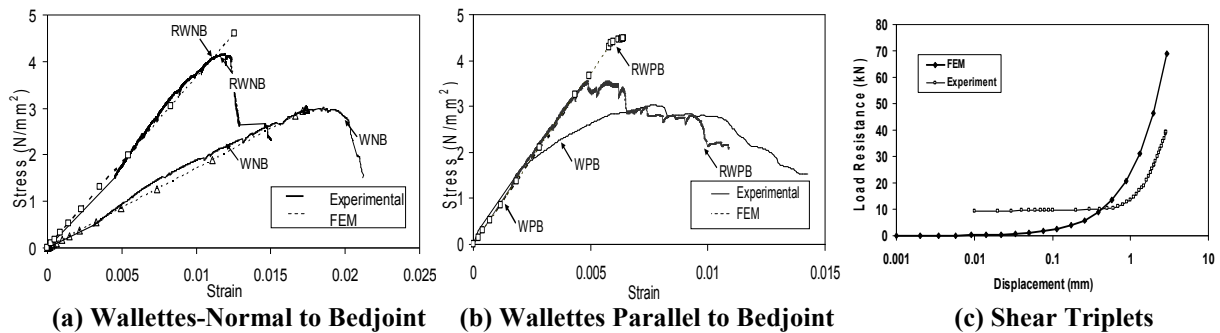


Fig. 1 Comparison of FEM Results with Experiment Data

4. DISCUSSION OF RESULTS

Both the experimental and FE analysis the results showed that the retrofitting of masonry wallettes and shear triplets using GFRP composites increased their load resistance. However, the failure strain of wallettes reduced from 0.0189 to 0.0115 under compression normal to bed joint and under compression parallel to bed joint no reduction in the failure strain is observed. In general, under compression, retrofitting using GFRP composites increased the strength and stiffness of wallettes but reduced the ductility. In the case of shear triplets, retrofitting increased strength and ductility. The increase in the ultimate shear deformation was from 0.018 mm to 3.0 mm. This result shows that the GFRP retrofitting can significantly enhance the seismic performance of the masonry walls under shear, since the forces generated in the earthquake are predominantly shear. The FE model results showed good correlation with the experimental results for the unreinforced and retrofitted specimens.

5. SUMMARY AND CONCLUSIONS

The behavior of masonry wallettes with and without retrofitting using GFRP composites under compression parallel to bed joint, normal to the bed joint, and their failure modes were explained. The behavior of GFRP composite retrofitted shear triplets were compared to that of control shear triplets. FE results were compared to experimental data, and were found to be in good agreement with the test data. The following conclusions were drawn based on the experimental and analytical studies: (i) GFRP composite retrofitting increases the strength and stiffness but reduces the ductility in the case of masonry wallettes under compression normal and parallel to bed joint, (ii) GFRP composite retrofitting increases the strength and ductility in the case of shear triplets, (iii) Smeared crack concrete model is found to predict the behavior of masonry reasonably well under monotonic loading and can be further extended to study the crack pattern, and (iv) Micromodeling is feasible for the analysis of small-scale specimens like triplets, but suitable algorithms have to be developed to improve the convergence in large scale modeling.

6. REFERENCES

1. IS: 1905 (1987). "Indian standard code of practice for structural use of unreinforced masonry," *Bureau of Indian Standards*, New Delhi.
2. EN 1052-1(1998). "Methods of test for masonry - Part 1: Determination of compressive strength", European Standards.
3. BS 2782-10: Method 1006 (1996). "Methods of testing plastics, glass reinforced plastics."
4. Sahlin, S. (1971). *Structural Masonry*, Prentice Hall, Englewood Cliffs, Newjersey.
5. Hibbit, D., Karlson, B., and Sorensen, P. (2002). *ABAQUS/ Standard theory manual*.
6. Giordano, A., Mele, E. and De Luca, A. (2002). "Modeling of historical masonry structures: comparison of different approaches through a case study", *Engineering Structures*, 24(2002), 1057-1069.

FRP COMPOSITE REINFORCEMENTS ON MASONRY VAULTS: EFFECTIVENESS AND RELIABILITY

Alessandro Baratta

(Full professor, University of Naples Federico II, Naples, Italy)

Ottavia Corbi

(Associate professor, University of Naples Federico II, Naples, Italy)

ABSTRACT

In the paper, for treating the problem of FRP reinforcements in barrel masonry vaults, one first presents a theoretical approach for the analysis of this vault typology. Under the basic assumptions of purely membrane state of stress and indefinite length of the vault, the referred model is demonstrated to behave as a series of independent arches; the case of FRP reinforcement is then considered and theoretical and experimental results are shown to be in good agreement, also emphasizing the effectiveness of the adopted reinforcement.

KEYWORDS

Masonry vaults, theoretical setup, FRP reinforcements, experimental validation.

1. INTRODUCTION

Advanced technologies and the identification of innovative materials, such as composites, able to respond in a satisfactory way to needs rarely met by the adoption of traditional materials and methodologies, are acquiring more and more interest for protection of historical buildings. On the other side, the NRT (not-resisting-tension) model for structural analysis of masonry structures proves to be an effective tool for analyzing the behavior of original structures as well as the effectiveness of reinforcements, also with respect to seismic thrust.

In the present paper, this problem is approached by modeling the basic masonry structure by the no-tension pattern, and the FRP reinforcement, working in uni-axial stress state. The behavior of basic masonry vault models reinforced with FRP strips, and subject to vertical and horizontal loads, is analyzed and compared to experimental results.

2. THEORETICAL SETUP OF THE PROBLEM OF BARREL MASONRY VAULTS WITH INDEFINITE LENGTH

As regards to barrel vaults, first of all, one should consider that, since the vault geometrically derives by the translation along a directrix of a generating arch curve, in this case, the meridian lines coincide with the generatrix in their shapes; if one considers a rectilinear directrix, the vault parallels are horizontal and rectilinear as well (Figure 1). The surface of the shell representing the mid-surface of the vault may be defined by the equation $z = f(x)$.

Because of the vault geometry, one has that

$$\theta = 0, \quad \tan \varphi = \frac{\partial z}{\partial x}, \quad \tan \theta = \frac{\partial z}{\partial y} = 0 \quad (1)$$
$$ds_x = \frac{dx}{\cos \varphi}, \quad ds_y = \frac{dy}{\cos \theta} = dy, \quad dA = ds_x ds_y = \frac{dx}{\cos \varphi} \frac{dy}{\cos \theta} = \frac{dx}{\cos \varphi} dy$$

where ds_x and ds_y denote the length of the sides of the generic vault element ABCD of area dA dx and dy the length of the corresponding sides on the element A'B'C'D' projected in the xy -plane, and φ and θ denote the angles formed by the meridian sides AB and DC of the element with the x -axis and by the parallel sides AD and BC with the y -axis, respectively.

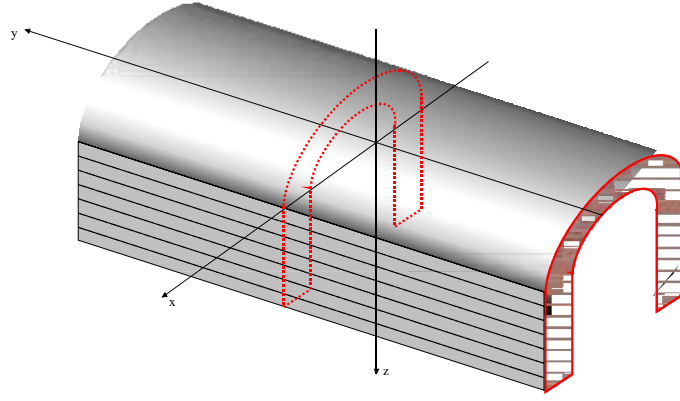


Figure 1: Barrel barrel vault with horizontal directrix.

As concerns equilibrium, hypothesizing that the vault is in a membrane state of stress, a correspondence can be established between forces acting on the element ABCD (stresses $N_x, N_y, N_{xy} = N_{yx}$ and applied load for unit area, p_x, p_y, p_z) and projected forces acting on the associated element A'B'C'D' ($\bar{N}_x, \bar{N}_y, \bar{N}_{xy} = \bar{N}_{yx}$ and $\bar{p}_x, \bar{p}_y, \bar{p}_z$) in the xy-plane [Baratta and Corbi 2006]. In absence of horizontal loads and if the vertical load is not dependent on "y", as it happens when the vault is subject to only vertical loads due to the self-weight (i.e. $\bar{p}_z = \bar{p}_z(x) \geq 0$), and, additionally, assuming that the vault has an indefinite length in the direction y, equilibrium may be expressed in the form

$$\frac{\partial^2 \psi(y)}{\partial y^2} \frac{\partial^2 z}{\partial x^2} = -\bar{p}_z, \quad \frac{\partial^2 \psi(y)}{\partial y^2} = \bar{N}_x \quad (2)$$

which reduces the problem to the determination of stress function $\psi(y)$.

Assuming that the directrix curve of the vault is a circular arch (Figure 2) of radius R, with constant thickness "s" and unit weight γ , and imposing suitable constraint conditions, one yields the final solution [Baratta and Corbi 2006]

$$z(t) = -\gamma s \frac{R^2}{H} \left[\arcsin(t) + \sqrt{1-t^2} + C \right] \quad (3)$$

$$\text{with } C = -\left(1 + \frac{H}{R^2} \frac{z_0}{\gamma s} \right), \quad H = \gamma s \frac{R^2}{(z_1 - z_0)} \left[1 - t_1 \arcsin(t_1) - \sqrt{1-t_1^2} \right] \quad (4)$$

where z_0 and z_1 are arbitrary ordinates, conditioned by the fact that $z(t)$ should be contained in the interior of the profile of the vault.

After this result, it is possible to calculate the internal forces $\bar{N}_x \leq 0, \bar{N}_y = \bar{N}_{xy} = 0$ and $N_x \leq 0, N_y = N_{xy} = 0$

$$N_x = \frac{\bar{N}_x}{\cos \varphi} = \frac{H}{\cos \varphi} \quad (5)$$

It is also possible to realize that the equilibrium solution allows the structure to behave as a sequence of identical independent arches. From this result, in the following one refers to the portal arch model, reinforced or not with some FRP strips, whose analytical problem implementation is shown to give theoretical results in perfect agreement with the produced experimental data, also exhibiting very effective results in the reinforced case.

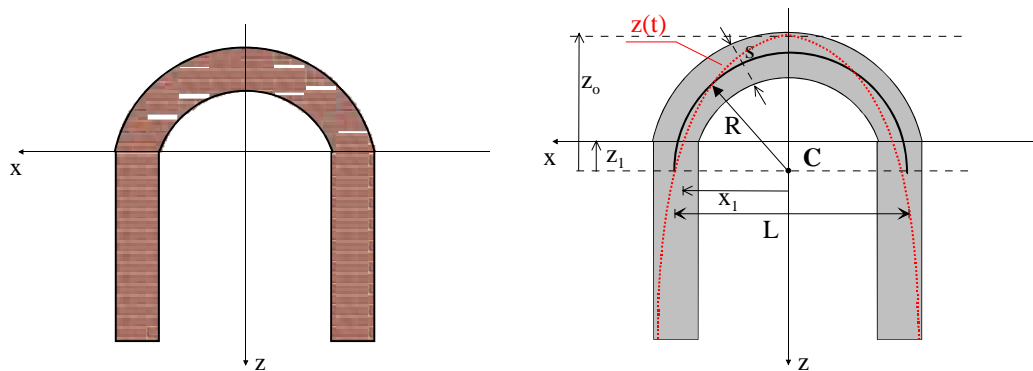


Figure 2: Cross section of a barrel vault with circular arch generatrix.

3. NUMERICAL/EXPERIMENTAL RESULTS FOR FRP REINFORCED OR UNREINFORCED MASONRY MODELS

Results from analytical and experimental investigations [Baratta 1991, Baratta and Corbi 2005] developed on masonry portal arches made of tuff brick with lime mortar, reinforced or not with carbon fibre strips and subject to the self-weight and to an increasing horizontal force, are briefly reported in the following. Actually, as regards to the consolidated case, one refers to the adoption of a continuous mono-directional FRP strips applied on the extrados of the arch.

In both the reinforced and unreinforced cases, the representation of the collapse condition deriving from the theoretical settlement of the problem leads to a situation relevant to the opening of fractures and subsequent collapse mechanism activations which perfectly agrees with the real situation monitored during experiments: this is clear from Figure 3, showing the deformed configurations for the two cases obtained by the codes which have been produced for numerically implementing the problems, whence one can deduce the hinges distribution.

Figures 4 depict the numerical/experimental comparison of the absolute displacement u (mm) of the right abutment versus the horizontal force F (N) for the two cases, showing a perfect agreement of the data and, moreover, a pretty consistent increase in the model loading capacity when adopting the FRP reinforcement.

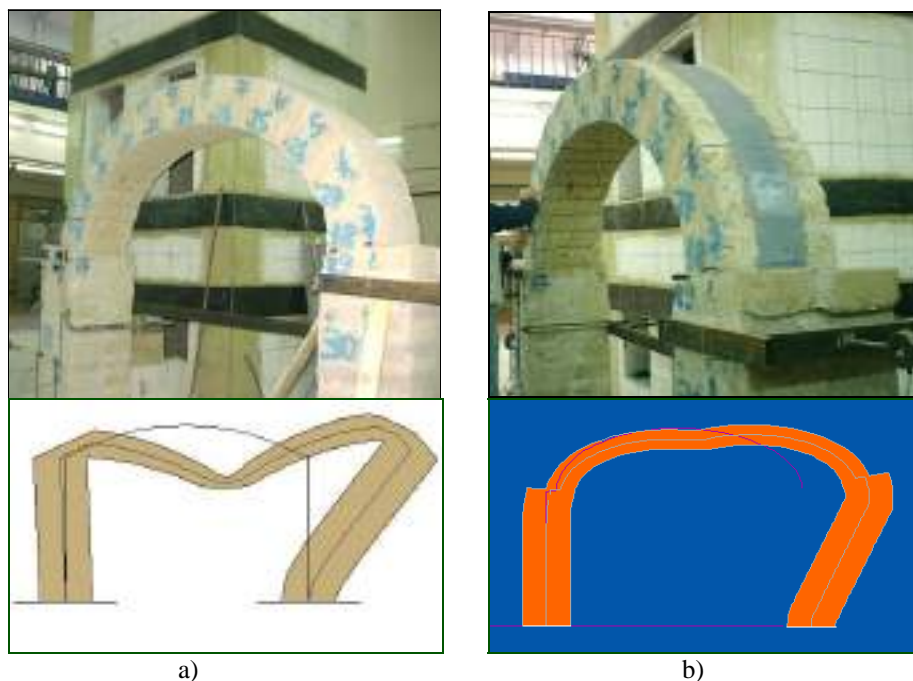


Figure 3. Sketches of the deformed configuration at collapse condition for the a) unreinforced and b) reinforced models as deduced from calculus codes.

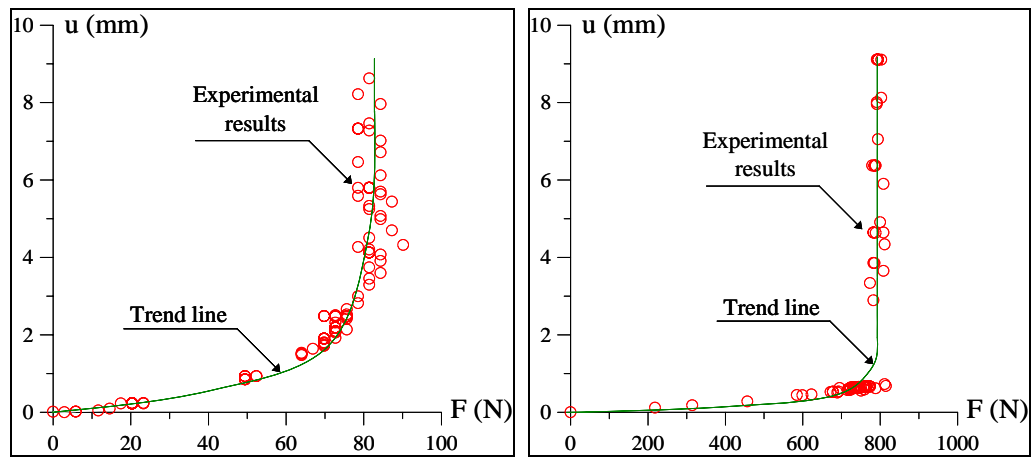


Figure 4. Absolute displacement u (mm) of the right abutment versus the horizontal force F (N): a) unreinforced and b) reinforced model.

4. CONCLUSIONS

The paper focuses on the possibility of proposing a theoretical treatment for the reinforcement with FRP of barrel masonry vaults. To this aim a theoretical approach of the problem of analysis of barrel vaults is presented, leading, under the hypothesis of membrane state of stress, to equilibrium and admissibility conditions. The case of barrel vault with indefinite length is specifically considered and demonstrated to behave according to the model of a series of independent arches. Upon this result, one refers to the portal arch model, reinforced or not with some FRP strips, whose analytical problem implementation is shown to give theoretical results in perfect agreement with the produced experimental data, also exhibiting very effective results in the reinforced case.

5. ACKNOWLEDGEMENTS

The present research has been developed thanks to the financial support by the Dept. of "Protezione Civile" of the Italian Government, through the RELUIS Pool (Convention n. 540 signed 07/11/2005, Research Line n. 8)

REFERENCES

- Baratta, A., (1991). "Statics and reliability of masonry structures", in "Reliability Problems: General Principles and Applications in Mechanics of Solids and Structures", F.Casciati & J.B.Roberts Eds, CISM, Udine, Italy.
- Baratta, A., Corbi, O. (2003) "The No Tension Model for the Analysis of Masonry-Like Structures Strengthened by Fiber Reinforced Polymers". *Intern. Journal of Masonry International*, British Masonry Society. Vol.16, No.3, pp 89-98.
- Baratta, A., Corbi, O. (2005) "On Variational Approaches in NRT Continua". *Intern. Journal of Solids and Structures*, Elsevier Science. Vol. 42, pp 5307-5321.
- Baratta, A., Corbi, O. (2005) "Fibre Reinforced Composites in Civil Engineering. Experimental Validation of C-Fibre Masonry Retrofit". *Intern. Journal of Masonry International*, British Masonry Society. Vol.18, No. 3, pp 115-124.
- Baratta, A., Corbi, O. (2005) "Relationships of L.A. Theorems for NRT Structures by Means of Duality". *Intern. Journal of Theoretical and Applied Fracture Mechanics*, Elsevier Science. 2005, Vol. 44, pp 261-274.
- Baratta, A., Corbi, O. (2006) "Analysis of Masonry Vaulted Systems: the Barrel Vaults". SAHC 2006, the 5th International Conference on Structural Analysis of Historical Constructions. November 6-8, 2006, New Delhi, India
- Heyman, J., (1966). "The stone skeleton". *Journal of Solids and Structures*. Vol.2, pp 269-279.
- Heyman, J., (1977). "Equilibrium of shell structures", Oxford University Press.
- Ugural, A.C., (1999). "Stresses in plates and shells", McGraw-Hill.

ON THE REINFORCEMENT OF MASONRY WALLS BY MEANS OF FRP PROVISIONS

Alessandro Baratta

(Full Professor, University of Naples "Federico II", Naples, Italy)

Ileana Corbi

(University Researcher, University of Naples "Federico II", Naples, Italy)

ABSTRACT

In a much more extended research a computational procedure for solving two-dimensional equilibrium problems, which are representative of the behavior of masonry walls loaded by in-plane forces, has been developed. So in order to test the procedure some laboratory tests concerning masonry panels designed to be similar as the theoretical model are made. The two tested panels have been built: the first panel with tufa bricks not jointed to each other, and the second panel with tufa bricks jointed by a pozzuolana mortar, in order to test the influence in terms of resistance that is conferred to the masonry. After the collapse some reinforcements are directly applied on the panel and a comparison between the behavior of the masonry panel before and after the application of the refurbishments is shown.

KEYWORDS

Structural analysis, Laboratory tests, Masonry panel, Refurbishments technique, FRP reinforcements.

1. INTRODUCTION

This paper represents a part of a more extended research about a procedure for solving two-dimensional equilibrium problems, which are representative of the behavior of masonry walls loaded by in-plane forces. The elaboration of the mechanical model of a structure, e.g. a masonry panel, requires first of all that the characteristics of the masonry texture are formally and qualitatively defined because they strongly condition the behavior and the resistance of the structure. In the case of a structure composed by a regular distribution of masonry square blocks, it can be modeled by assuming that the material has not the capacity to transmit any tensile stress along the joints' direction, but that a low and significant tensile resistance can arise by means of a suitable relative stagger between the blocks. So the panel can be associated to an homogeneous bi-dimensional continuum by considering a very low tensile resistance due to the combined action of the friction and of the stagger of the bricks, in absence of the breaking of the single block. On the other hand, in order to study a masonry having an irregular texture, the Not Resisting Tension (NRT) model can be assumed as reliable, exhibiting a simple linear elastic behavior under compression stress states and no resistance in tension, and, thus, resulting in an overall fragile non-linear behavior. If the loading capacity of NRT structures can be investigated by means of the tools of the Limit Analysis (L.A.) theory, on the other hand, the study of the intermediate crack situation can not be performed by L.A.-techniques, whilst the elastic analysis of the masonry tissue under the assumptions of perfect integrity of the structure and of purely compressive stresses can lead to significant results. In conclusion, some optimization (stress or strain) procedures, deriving from the implementation of the basic variational methods extended to NRT models, can be developed [for the extended procedure see e.g. Baratta and Toscano (1982), Baratta and Voiello (1988), Baratta (1991), Baratta and Corbi (2003), Baratta and Corbi (2004)].

In order to test the developed computational procedure some laboratory tests concerning masonry panels designed to be similar as the theoretical model are made. In the following a comparison between the behavior of a masonry panel made with alone tufa bricks and a masonry panel made with tufa bricks jointed by a light mortar is shown. After being collapsed the two panel have been reinforced by means of some usually reinforcements.

Fiber Reinforced Polymers (FRPs) are a type of composites characterized by a polymeric *matrix* reinforced with continuous *fibers* (see Schwegler, 1994; Traintafillou, 1996), which exhibit desirable features, such as high mechanical properties, lightweight, high resistance to chemical agents and corrosion, increased fatigue resistance, reliability and durability, low thickness, adaptability and easy applicability to complex structural shapes, low invasiveness on the construction. A wide range of amorphous and crystalline materials can be used as the fiber in FRP materials. In the construction industry the most common fiber used are: glass fiber, carbon fiber or aramid fiber. Carbon, glass and aramid fibers can be used separately or in conjunction as a hybrid to increase the stiffness of a structural member or the area within a structure or some the other mechanical characteristics of the FRP fibers (e.g. density, elastic modulus, tensile strength, ultimate elongation, etc). The embedded fiber matrix (polyester, urethane, vinilester or epoxy) is responsible not only for keeping the fibers together but also to protect them against environmental and localized effects. In order to help the application of the FRP reinforcements which are directly laminated on the structure, some fire retardants are usually incorporated in the resin itself or as an applied gel-coat. Fillers and pigments are also used in resins for a variety of purposes, the former principally to improve mechanical properties and the latter for appearance and protective action. In the field of structural rehabilitation the most commonly adopted forms of FRP are strips and tissues; strips, which are given by parallel continuous fibers, exhibit a mono-directional behavior, and are then strongly non-isotropic; tissues, which are obtained by the plait of two series of parallel fibers, are characterized by reduced mechanical characteristics of the final product, but are reduced in their anisotropy as well.

2. LABORATORY TESTS ON THE MASONRY PANEL

Some masonry panels have been realized at the Laboratory of Materials and Structural Testing of the University of Naples “Federico II”, which are symmetrical, with a central hole covered by a steel architrave, and having upper part characterized by a concrete fascia lightly reinforced by steel. The panel geometry is shown in Figure 1(a).

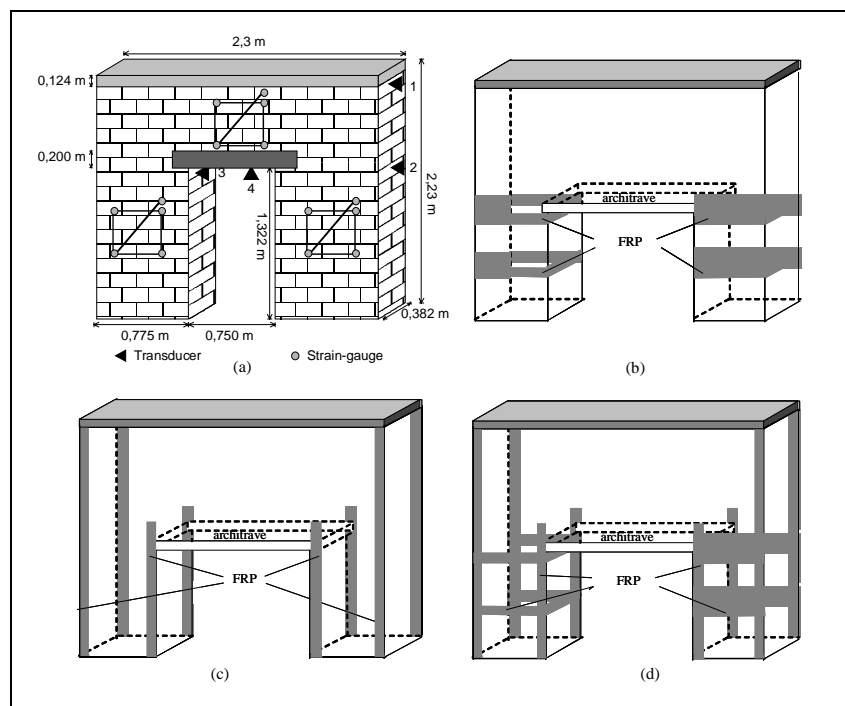


Figure 1: (a) Masonry panel geometry, (b), (c) and (d) different applications of the FRP strips on the panel.

2.1 Masonry panel without mortar

In the first case, the panel is made of tufa bricks (type “yellow tufa of Naples”, Italy) not jointed to each other, in order to do not confer any additional resistance to the masonry; the masonry itself is characterized by unit weight $\gamma=10300$ N/m and Young modulus $E=5.5$ GPa. In correspondence of the concrete fascia on the top of the panel a

varying force has been applied, and some loading/unloading cycles have been made. After the collapse some FRP strips has been directly laminated on the masonry as in Figure 1(b), at the same time with the impregnation of the fibers by means of a special bi-component epoxy resin, and some loading/unloading cycles have been made again. The adopted reinforcement, produced by FTS, is a BETONTEX system GV330 U-HT, made of 12 K carbon fiber, jointed by an ultra light net of thermo-welded glass. The mechanical characteristics of the employed carbon fibers are: tensile limit stress $\sigma_{frp}= 4.89$ GPa, elastic modulus in traction $E_{frp}=244$ GPa, limit elongation $\varepsilon_{frp}=2\%$. The FRP strip is characterized by thickness of 0.177 mm and depth of 200 mm.

The induced displacements at some selected points [1, 2, 3 and 4 in Figure 1(a)] of the panel are recorded by a monitoring equipment consisting of: 4 transducers, placed at different locations of the panel in order to record the absolute displacements, and 15 strain-gauges, arranged in 3 blocks of 5 strain-gauges, each block is devoted to record the related strain situation. In details two transducers are located horizontally at two different heights on the panel right side (transducers 1 and 2), and two in correspondence of the opening, one in horizontal position at the top of the left side of the hole (transducer 3) and the other one under the architrave, which is devoted exclusively to control the panel deflection (transducer 4). A sample of the displacements $s(\text{mm})$ versus the varying force $F(\text{N})$ read by the transducer 1 during the loading/unloading cycles in the not-reinforced case and in the reinforced case with some horizontally applied C-FRP strips is shown in Figure 2(a) and (b).

2.2 Masonry panel with mortar

In the second case, the panel is made of tufa bricks jointed by a pozzuolana mortar in order to confer a light additional resistance to the masonry. The masonry is made with the same type of tufa bricks used in the building of the first panel, and a varying force has been applied in the middle left part of the panel, rather than on the top, in way to mitigate the proneness of the panel to sliding of bricks with respect to each other. The induced displacements at the selected points 1, 2, 3 and 4 have been recorded during some loading/unloading cycles on the alone masonry panel [Figure 2(c)] and after the application of the C-FRP reinforcement. Two applications of the FRP strips have been made: in the first case the C-FRP strips have been laminated along the vertical direction on the panel in order to contrast the principal tensile stresses [Figure 1(c)]; in the second case other horizontal strips have been superimposed on the last intervention [Figure 1(d)]. A sample of the displacements read by the transducer 1 during the loading/unloading cycles in the not-reinforced case and in the two reinforced cases is shown in Figure 2(c), (d) and (e).

2.3 General considerations

By the diagrams in Figure 2, which report the displacements $s(\text{mm})$ versus the varying force $F(\text{N})$ read by the transducer 1, some considerations can be made. In first instance it is evident the effect of the mortar between the bricks in terms of global resistance, so the panel with mortar collapses in correspondence of load value about 5000 N instead of 2500 N in case of the panel without mortar.

Then, with reference to the panel's reinforcement by means of the application of some C-FRP strips, both in the panel with mortar that without mortar, the major effect of the C-FRP intervention is the reduction of the stress in the masonry. In general lower displacements at the locations monitored by the transducers can be recorded in the consolidated case with comparison to the unconsolidated case. Actually one can notice that, with reference to the same load intensity [e.g. in correspondence of the load value 3000 N in Figure 2(c), (d) and (e)], lower displacements can be recorded in case of FRP insertions. Obviously the effect results much more evident in the panel with mortar with respect to the panel without mortar, and is evident still more when the intervention becomes more invasive as in the scheme of Figure 1(d). Moreover, the increase of the overall stiffness of the panel results in a higher loading capacity with respect to not-reinforced masonry wall. In particular the trend of each curve, shows that it is closer to the x-axis (representing the load variable), thus indicating an increase in the stiffness which is also related to an higher collapse value of the load.

3. CONCLUSIONS

In the paper some laboratory tests developed for evaluating the effectiveness of alternative technologies, and based on the adoption of innovative materials for repairing ancient constructions, are reported.

Actually the modern technology of materials offers a wide variety of possibilities for the refurbishment of existing structures: new advanced materials are often preferable to traditional materials for their enhanced characteristics in terms of effectiveness, reliability and flexibility, which always ensure high standard of performance.

In details one focuses on Fibre Reinforced Polymers (FRP), which are special composites currently attracting much attention for refurbishing and/or consolidating masonry structures with effective and low invasive interventions. All the considerations above mentioned give the idea that researchers and technicians before to make any intervention on a structure it should be fundamental to know very well the stresses distribution and its fracture scenario, in order to select the really most appropriate typology of reinforcement and use correctly the innovative materials as the composites.

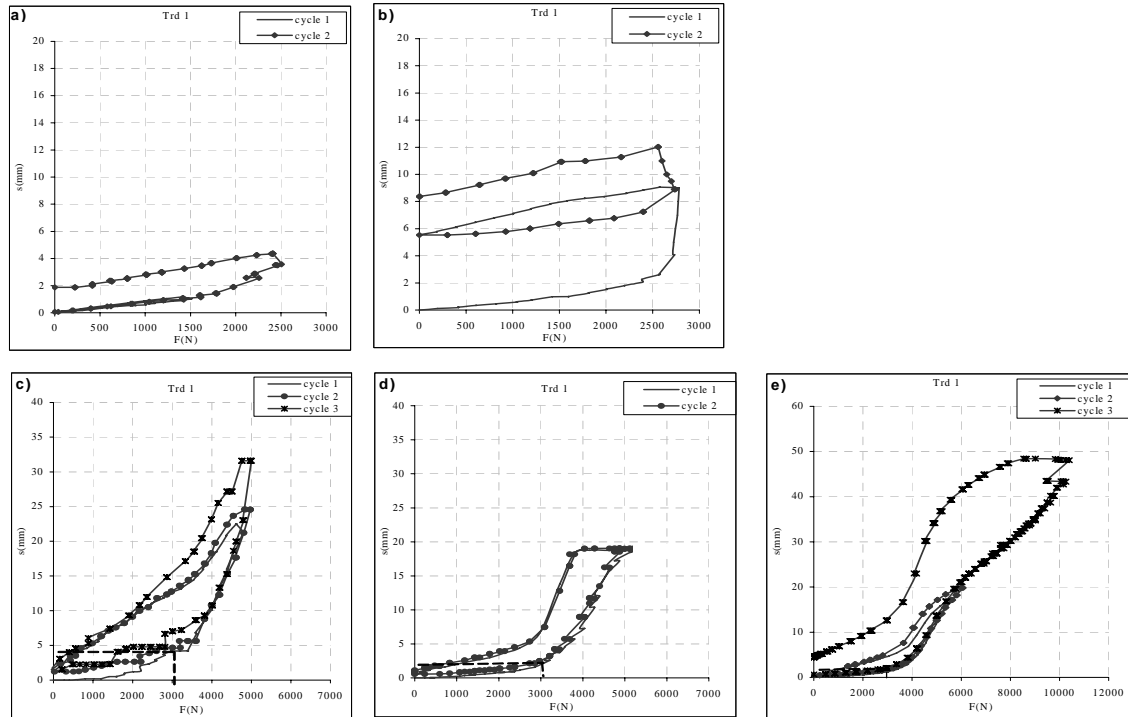


Figure 2: Displacements recorded on the masonry panel without mortar in the not-reinforced case (a) and with FRP strips (b), and on the panel with mortar in the not-reinforced case (c) and in the case with different application of the FRP strips (d) and (e).

ACKNOWLEDGEMENT

The present research has been performed thanks to the financial support by the Department of “Protezione Civile” of the Italian Government, through the RELUIS Pool (Convention n. 540 signed 07/11/2005, Research Line n. 8).

REFERENCES

- Baratta, A. (1991). “Statics and reliability of masonry structures”, In: F.Casciati & J.B.Roberts (Eds), “*Reliability Problems: General Principles and Applications in Mechanics of Solids and Structures*”, CISM, Udine, Italy.
- Baratta, A., and Corbi, I. (2003). “Investigation of FRP consolidated masonry panels”. *Proceedings of Ninth International Conference on Civil and Structural Engineering CC03*, paper n. 99, The Netherlands.
- Baratta, A., and Corbi, I. (2004). “Iterative Procedure in No-Tension 2D Problems: theoretical solution and experimental applications”, In: G.C.Sih & L.Nobile (Eds.), “*Restoration, Recycling and Rejuvenation Technology for Engineering and Architecture Application*”, Aracne Ed, p. 67-75, Bologna, Italy.
- Baratta, A., and Toscano, R. (1982). “Stati Tensionali in Pannelli di Materiale Non Reagente a Trazione”, *Proceedings of Fourth National Congress of AIMETA*, Genova, Italy (in Italian).
- Baratta, A., and Voiello, G. (1988). “Teoria delle pareti in muratura a blocchi: un modello discretizzato di calcolo”, In: *Franco Jossa e la sua opera*, Giannini Ed., Napoli, Italy (in Italian).
- Schwegler, G. (1994). “Masonry Construction Strengthened with Fiber Composites in Seismically Endangered Zones”, *Proceedings of the Tenth European Conference of Earthquake Engineering*, Vienna, Austria.
- Trantafillou, T.C. (1996). “Innovative Strengthening of Masonry Monuments with Composites”, *Proceedings of the Second International Conference Advanced Composite Materials in Bridges and Structures*, Montréal, Canada.

STRENGTHENING MASONRY ARCHES WITH COMPOSITES

Giulio Castori

(Ph.D. Candidate, University of Perugia, Perugia, Italy)

Antonio Borri

(Professor, University of Perugia, Perugia, Italy)

Skip Ebaugh

(Vice President, Hardwire LLC, Pocomoke City, Maryland, USA)

Paolo Casadei

(Lecturer, University of Bath, Bath, United Kingdom)

ABSTRACT

The present research project investigates the application of innovative composite materials, based on fine steel cords embedded in either an epoxy (Steel Reinforced Polymer) or cementitious matrix (Steel Reinforced Grout), to strengthen masonry arches. This application combines, to the traditional advantages proper of Fiber Reinforced Polymers (FRP), the performances of this new family of composite materials, reducing installation and material costs, and inducing an increase of ductility particularly when a cementitious matrix is used. In this way the use of these materials could become extremely interesting in the restoration of masonry arches in historical building, and more particularly, in road, rail, and waterway infrastructures. In the UK, for instance, there are over 40,000 masonry arch bridges, the majority of which, being at least 100 years old, are in need of repair due to natural deterioration or lack of maintenance, or in need of strengthening due to ever increasing traffic volume and vehicle weight. In response to this situation a comprehensive study on the behavior of masonry arches strengthened by composite laminates is here presented. The influence of the type of fibers (steel and carbon), matrix (epoxy and cementitious), their location (intrados and extrados) and boundary conditions are investigated in the laboratory on scaled samples.

KEYWORDS

Arches, Masonry, Fiber reinforced polymers, Steel reinforced polymers, Reinforcement.

1. INTRODUCTION

Thanks to their adaptability to the changes of the geometric configuration, masonry arches are able to distribute the strain along the mortar joints, avoiding the formation of significant cracks. Thus the collapse mechanism doesn't depend by the materials' limit strength, but it is due to the incapability of the structure to fit the horizontal and vertical displacements of the abutments. Consequently it is clear that similar displacements should be considered when strengthening masonry arches, introducing only systems which are able to reinforce the arch without changing its constructive features. Such aims have led researchers to suggest strengthening masonry shells with FRP laminates in the form of bonded surface reinforcements. There are several advantages related to this strengthening technique: very low weight, high tensile strength and low thermal expansion coefficient. On the contrary, their up-to-failure linear elastic behavior, which doesn't allow for any ductility of the system, their lack of fire resistance and their relatively high cost, may represent an obstacle for a widespread use. A new family of composite materials based on high strength twisted steel wires of fine diameter (0.20-0.35mm), that can be impregnated with epoxy resin or cementitious grout is presented in this paper. SRP has the potential to address the three shortcomings mentioned for FRP, in fact: a) steel cords have some inherent ductility (thanks to their manufacturing process) and reduced cost when compared to CFRP; b) impregnation with cementitious paste may overcome the problems of fire endurance and reduce installation costs. The steel cords used in SRP/SRG are obtained from the same manufacturing process used for making the reinforcement of automotive tires, and re-manufactured, to obtain the shape of the fabric tape

prior to impregnation. The twisting of the cords allows some mechanical interlock between the cords and the matrix, and may also induce a ductile behaviour upon stretching. Huang et al. (2002) investigated the mechanical properties of SRP/SRG, testing different kinds of matrix (epoxy and cementitious). Test results showed that the material does not experience a substantial yielding, but rather a similar behaviour to the one experienced by high-strength steel used in prestressed concrete construction, with a slight non-linear range prior to rupture of the cords. Thus, to clarify the behavior of brick masonry arches strengthened by composites, nine arch specimens have been tested under monotonic vertical loads applied to $\frac{1}{4}$ of their span. Such condition is the most severe case of loading for an arch, and can be considered to simulate particular situations of the arches (e.g. bridges, library, etc.). The aim of the study is to compare the behavior up to collapse of arches strengthened by different types of fibers (steel and carbon) and matrix (epoxy and cementitious), and by placing the reinforcement in different positions (intrados or extrados).

2. BEHAVIOR OF THE STRENGTHENED ARCHES

The application of composite laminates, as externally bonded strengthening materials, modifies the static behavior of an arch because the reinforcement can bear the stresses occurring at the tensed edges. Therefore, the brittle failure of such structures, typically caused by the formation of four hinges, can be avoided. Depending on the position of the laminate, in fact, the formation of the forth hinge can be prevented (Foraboschi, 2004). In the case of extrados strengthening the line of thrust can fall outside the lower edge of the arch. As a results, the arch becomes an isostatic structure (three hinges arch) consisting of two curved beams strengthened on their upper sides. Conversely, in the case of a structure strengthened at the intrados, although the outcoming static scheme is similar to the one adopted in the previous case, the distribution of the stress is different: the thrust line falls outside the upper edge of the structure and the fibers prevent the forth hinge formation close to the load point. Consequently, in both cases, the collapse is due to other mechanisms, which are involving the limits of strength of the constituent materials (masonry and reinforcement) and their interactions at the local level. Thus depending on the position and of the amount of the reinforcement, the modified failure mode are: masonry crushing, sliding, debonding, reinforcement rupture.

3. EXPERIMENTAL STUDY

3.1 Characterization of the Materials and their Interaction

The experimental program comprises a series of preliminary tests for the mechanical characterization of the constitutive materials of the arches. Concrete pavours (200x100x50mm) and an hydraulic lime mortar were used for the construction of the arches. The bricks reached a compressive and a flexural stress equal to 43.3 and 10.9 MPa respectively, whereas compressive tests on mortar prisms after 28 days of curing gave 0.8 MPa. The adhesion properties between the masonry and the reinforcement were investigated for loads perpendicular (pull-off tests) to the reinforcement, on sixteen strengthened specimens. In particular, two groups of specimens were cast for this part of research, representing different type of reinforcement (SRP or SRG). The mean value of the tensile bond strength was 1.29 and 1.57 MPa for specimens strengthened with SRG and SRP, respectively. As for the failure mode, while all SRP specimens failed in the substrate, SRG specimens failed or in the overlay. Table 1 resumes some geometrical and mechanical characteristics of the steel and the carbon fibers used as strengthening material.

Table 1: Properties of the fibers

Property	Fibers Type		
	Steel (3X2-4)	Steel (3SX-12)	Carbon (T700 SC)
Tensile strength (MPa)	2479	1657	4900
Elastic Modulus (MPa)	210000	210000	230000
Thickness (mm)	0.89	0.81	0.44
Ultimate strain (%)	1.6	1.2	2.1

3.2 Tests on the Strengthened Arches

A series of nine arch specimens (Figure 1) built by bricks arranged in a single layer (100mm of thickness) have been tested under monotonic vertical loads applied to $\frac{1}{4}$ of their span. Different laminates arrangements and different

types of fibers have been used, namely: a control unreinforced specimen (UN.01), three specimens have been strengthened with steel fibers (3SX) at the extrados by using a cementitious grout (EX.01 and EX.03 tests) and a polymeric matrix (EX.02 test), a specimen have been strengthened at the extrados with carbon fibers (EX.04 test), three specimens have been strengthened with steel fibers (3X2) at the intrados by using a cementitious grout (IN.01 and IN.03 tests) and a polymeric matrix (IN.02 test), whereas steel fibers (3SX and 3X2) and cementitious grout have been used to strengthen the intrados and the extrados (IN+EX.01 test) of the last specimen. A single ply of laminate, 150mm wide, has been applied for each arch, with the exception of the IN.03 specimen, where two plies of laminate have been used; furthermore, in two cases (EX.03 and IN.03 tests), in addition to the reinforcement, steel anchors were adopted: in the first case two angle plates were used to anchor the ply to the abutments, while in the second case flat plates, screwed into the bricks, were used to secure the ply to the arch soffit.

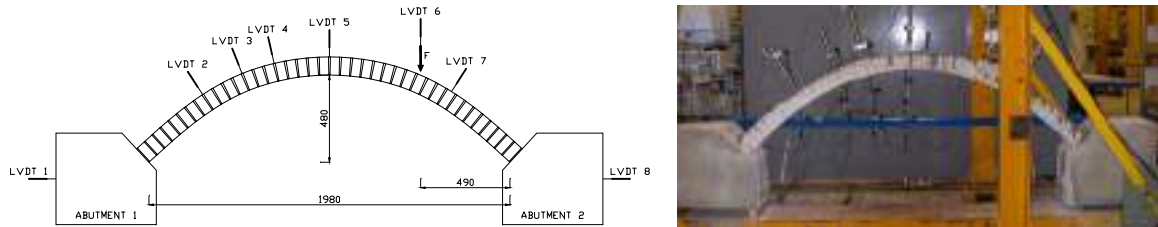


Figure 1: Experimental set-up: dimensions of the specimens and scheme of loading.

The unreinforced arch showed a brittle failure (four hinges mechanism) and a very small load capacity (0.7 kN). The arches strengthened at their extrados with 3SX fibers presented, with the exception of specimen EX.01, the same failure mode (Figure 2a). In particular, while the specimen EX.01 showed, because of a set-up problem, a notable rotation of the abutments, that not allowed any further increment in load, in the other two cases (specimens EX.02 and EX.03) the collapse occurred because of the sliding between brick and mortar in the first joint closest to the springer and to the edge of the steel anchor, respectively; in both cases such collapse occurred without any warning. The ultimate load was 9.2 kN for specimen EX.01, whereas it was 13.3 and 23.5 kN for specimens EX.02 and EX.03, respectively. Conversely, the arch reinforced at its extrados by CFRP (specimen EX.04) showed the same failure mode (sliding in the first joint closest to the springer) and a lower ultimate load capacity (11.5 kN). The arches strengthened by 3X2 fibers at their intrados presented different patterns of collapse: specimens IN.01 and IN.02 showed a brittle failure due to the reinforcement rupture, whereas in specimen IN.03 (where there were two plies of laminate) collapse occurred due to local debonding of the reinforcements under the point of application of the load (Figure 2b). In such case the failure was not brittle because the fibers contributed in holding the bricks together during the last phase. The ultimate load was 16.2 and 14.7 kN for specimens IN.01 and IN.02 respectively, whereas it was 23.0 kN for specimen IN.03. Finally, the arch strengthened both at its extrados and intrados with 3SX and 3X2 laminate, respectively (specimen IN+EX.01), presented a different pattern of collapse (sliding in the joint under the point of application of the load, Figure 2c) and a considerably higher ultimate load (32.8 kN).



Figure 2: Failure mode: a) and c) sliding along a mortar joint (EX.03 and IN+EX.01), b) debonding (IN.03).

4. ANALYSIS OF THE RESULTS

The analysis of the experimental results allowed to evidence some aspects of the behavior of the strengthened arches and propose some suggestions about the use of SRP/SRG in real cases. Figure 3 shows a load vs displacement (measured at the location where load was applied) plot for all specimens. As for the ultimate behavior of the arches,

some important considerations can be drawn. For the arches strengthened at their extrados, despite different fiber types have been used, the results showed that masonry sliding is the prevalent failure mechanism. Such kind of failure takes place only on the arches strengthened at the extrados because the weakest point of the structure is the hinge forming at the abutment. Thus, in the repair phase of real structures, a solution that could increase the ultimate load capacity could be achieved, as done in specimen EX.03, by anchoring the first ply to the abutment by means of steel plate bolted to the support and simply adhered to the reinforcement. For the arches strengthened at their intrados, the reinforcement rupture in proximity of the loaded section has been detected to be the critical one. Thus, in the repair phase of real structures, a solution that could increase the ultimate load capacity could be, as seen with IN.03 test, the use of two plies of laminate, to avoid the reinforcement rupture, and steel anchors, in the form of steel plates screwed in the masonry substrate, able to tie the strip to the arch soffit retarding premature delamination. Finally the application of the reinforcement both at the intrados and at the extrados of the arch is clearly an ideal application, used as well as the unreinforced arch, to evaluate the efficiency of the adopted strengthening method.

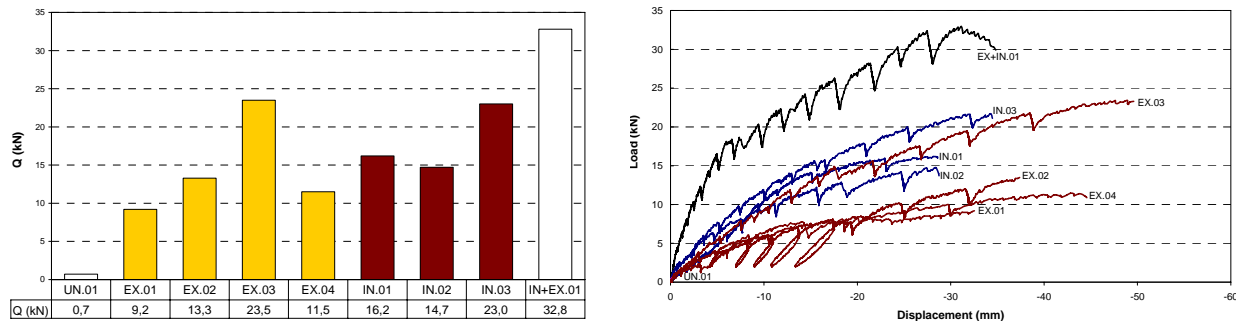


Figure 3: Comparison among the experimental results; load-displacement curves.

5. CONCLUSIONS

The following conclusions may be drawn from this experimental program:

- SRP/SRG composite materials have shown to be effective in increasing the ultimate load capacity of the arches.
- Mechanical anchors, not allowed in standard FRP applications, have shown to allow a substantial increase in the ultimate load both for intrados and extrados applications.
- SRP/SRG are similar to FRP in terms of ease of installation.
- Cementitious grout well behaved in bonding the steel tape to the masonry substrate and provided an overall better performance than the epoxy matrix allowing better redistribution of stresses between the laminate and the substrate.

6. ACKNOWLEDGMENTS

The authors would like to acknowledge Hardwire LLC., Pocomoke City, MD, for providing the steel tapes and the Department of Architecture and Civil Engineering at the University of Bath for hosting this collaborative research.

REFERENCES

- Borri, A., and Castori, G. (2004). "Influence of bonding defects in masonry vaults and arches strengthened at their intrados with FRP", *Proceeding of the 2nd National Conference*, Venice, Italy, pp 7-16.
- Foraboschi, P. (2004). "Strengthening of masonry arches with fiber-reinforced polymer strips". *Journal of Composites for Constructions*, ASCE 8(3), pp 96-104.
- Hardwire LLC. (2002). What is Hardwire. <http://www.hardwirellc.com>. Pocomoke City, MD.
- Heyman, J. (1982). *The masonry arch*, Ellis Horwood – Wiley, West Sussex, UK.
- Huang, X., Birman, V., Nanni, A., and Tunis, G. (2005). "Properties and potential for application of steel reinforced polymer and steel reinforced grout composites". *Composites, Part B*, Vol. 36, pp 73-82.
- Triantafillou, T. C. (1998). "Strengthening of masonry structures using epoxy – bonded FRP laminates". *Journal of Composites for Constructions*, ASCE 2(2), pp 96-104.

PRIORITIZED FRP RESEARCH FOR CONCRETE AND MASONRY STRUCTURES

Max Porter

(Professor, Iowa State University, Ames, IA, USA)

Kent Harries

(Assistant Professor, University of Pittsburgh, Pittsburgh, PA, USA)

ABSTRACT

A workshop was held to determine the prioritized research needs of FRP use as related to concrete and masonry structures, and hybrid structures. The workshop had seven sessions and 48 participants from different countries representing various disciplines of academia, design, government, owner and code officials. Prioritized research needs were established in each of the following topical session areas: internal FRP; external FRP; durability; QC/NDE/SHM; fire and extreme loads; and hybrid structures. A final session of prioritized overall voting determined rank-ordered research needs.

The workshop was sponsored by American Concrete Institute (ACI), ISIS of Canada, and the National Science Foundation (NSF) was organized by ACI Committee 440-D. A final report was published in March 2005 and a final project report was submitted to the NSF in July 2006.

The prioritized outcomes given in this paper are divided into two main categories; namely, those of Highly Recommended Research and those of Recommended Research. The Highly Recommended Research generally fell into the topics of Durability, Performance-Based Areas, New Materials and Systems, Need for Integrated Education, and Research Partnerships. The paper gives a summary of these highly recommended items and references the complete Workshop report.

KEYWORDS

FRP, Reinforcement, Durability, Reinforced Concrete, Reinforced Masonry.

1. INTRODUCTION AND CONDUCT OF THE WORKSHOP

A workshop sponsored by American Concrete Institute (ACI), ISIS of Canada, and the National Science Foundation (NSF) was organized by ACI Committee 440-D. A final report was published in March 2005 and a final project report was submitted to the NSF in June 2006.

The workshop goals were:

- To Identify and Prioritize Research Issues:
 - By industry, practitioners and academia
- To improve our understanding of behavior of
 - FRP materials
 - FRP structural
 - Repair systems.

The detailed objectives of the workshop were as follows:

- Develop a consensus of state-of-the-art in application FRP composites for infrastructure applications
- Identify critical research needs
- Develop a consensus on the priority of these needs.
- Identify emerging and novel applications
- Develop a coordinated plan
- Identify improved mechanisms by which research results may be disseminated

- Provide a brief assessment of research facilities and capabilities in the USA

Session topics were determined based on the consensus of the Workshop steering committee and the topics were largely based on categories identified in a survey of the profession conducted in early 2002 (Harries et al. 2002). Prioritized research needs were established in each of the following topical session areas: internal FRP; external FRP; durability; QC/NDE/SHM; fire and extreme loads; and hybrid structures. A final session of prioritized overall voting determined rank-ordered research needs.

The workshop participants were from various disciplines and countries as shown in Table 1 below:

Table 1: Distribution of Participants

<u>By Discipline</u>	<u>Number of Participants</u>	<u>Percentage of each category</u>
Academia	36	75
FRP Industry	6	13
Consulting/Design Engrg.	2	4
Gov't./Owners/Code Officials	4	8
<u>By Country</u>		
USA	34	71
Canada	10	21
UK	3	6
Belgium	1	2

2. PRIORITIZED OUTCOMES

The prioritized outcomes given in this paper are divided into two main categories; namely, those of Highly Recommended Research and those of Recommended Research. First, the Highly Recommended Research generally fell into the topics of Durability, Performance-Based Areas, New Materials and Systems, Need for Integrated Education, and Research Partnerships. These are summarized below:

- **Durability Topics:**
 - ***Identification of appropriate environments for durability testing*** - The environmental parameters that need to be considered when using FRP materials remains a debatable question. Additionally, the intended use, regional climates and maintenance practices will significantly impact which parameters affect a particular application. Specific environmental exposures and/or durability issues were identified as being critical in the application of FRP materials in concrete infrastructure
 - ***Development of standardized durability/environmental exposure test methods*** - A consensus on accelerated environmental conditioning techniques and subsequent durability test methods is required. Methods are required for both external FRP and internal FRP reinforcement applications.
 - ***Durability studies of externally bonded FRP repair/strengthening measures*** - Identification of time-dependent material properties and their effects on behavior, as well as the associated loading factors (including fatigue) is needed. Clearly, the durability of the adhesive bond and/or substrate-FRP interface is of primary concern.
 - ***Durability studies of internal FRP reinforcement*** – Also, time dependent material properties and effects on behavior and the factors affecting them (including fatigue and sustained loads) is needed for internal reinforcement, as well. The critical issue here is the behavior of FRP embedded in concrete; thus, research must account for the concrete environment in which the FRP is embedded, the expected cracking behavior (which may differ from steel-reinforced concrete), the environmental factors (which also differ somewhat from those of importance for steel-reinforced members), and the impact on the material strength and bond of FRP in a concrete medium.
- **Performance-Based Areas**
 - ***Service life prediction of FRP reinforced or strengthened structures*** - Models are needed to extrapolate short term test results to long term service life models. Models for the degradation processes are needed. Fatigue life of bonded FRP has been shown to be of particular concern and predictive models of this behavior are required.

- **Fire resistance and protection of FRP reinforced or strengthened structures** - The behavior of FRP materials, whether imbedded in concrete or externally applied, subject to fire loading is largely unknown. Modeling techniques must be developed and verified for predicting fire performance of FRP materials and FRP reinforced or strengthened concrete structures.
- **Seismic and Blast Resistance of FRP Systems** - FRP systems are often used for structural retrofit including efforts to mitigate the effects of earthquake or blast loads. Methods of assessing the appropriateness of existing and innovative FRP systems for mitigating the effects of extreme loading need to be developed, which also need to include the strain-rate effects.
- **New materials and systems**
 - **Innovative and hybrid materials** - Research aimed at developing new and hybrid FRP materials having properties better matched to concrete is necessary. Such systems may be as simple as composite CFRP, GFRP and AFRP products or as innovative as polymer-free chemically prestressed systems. More work is needed on hygrothermal behavior.
 - **Innovative reinforcing schemes** - Development FRP materials should involve getting away from the paradigm of “replacing steel with FRP” and toward the development of innovative reinforcing schemes which should make both FRP reinforcement and concrete construction more cost-effective. One role that concrete plays in reinforced concrete systems is to protect the reinforcing system. If FRP systems can be made more robust and durable, this role for concrete becomes obsolete and should result in a savings.
 - **Self-sensing FRP structural health monitoring systems** - FRP materials are unique in terms of their properties and their fabrication which lends itself well to the development of integrated sensor systems. Such systems facilitate improved structural health monitoring and potential feedback to the occupants and owners over time.
- **Need for integrated education** – Although not specifically a research need, the education and training of design professionals and the need for development and integration of student courseware is needed for the following categories:
 - Education in Schools of Engineering and Architecture.
 - Training of design professionals
 - Need for development and integration of student courseware in civil engineering, materials, and architecture
- **Research Partnerships** - For seminal research to be conducted, partnerships are needed for the following:
 - Close collaboration between academe and industry is essential
 - Innovative industry/academe/government partnerships must be developed to facilitate seminal research
 - Interaction between industry and academe should take the highest priority and is likely to yield the most fruitful results
- **Other Recommended topics:**
 - Hybrid – Connections
 - External FRP – Fundamental design philosophies
 - Hybrid – Innovative design approaches
 - Hybrid – Mechanical anchorage, bonded or not
 - Durability – Extrapolate short-term test results to service life
 - Internal FRP – Structural performance issues
 - External FRP – Emerging systems
 - Fire – Residual strength of members

The results of all of these prioritized research topics are tabulated in more detail in the workshop report (Porter and Harries 2005). Recommendations are also given in the report for the topics to include in a plan of organized research involving partnerships and a national laboratory.

3. SUMMARY

The NSF-sponsored Workshop had seven topical sessions and balloting was conducted to determine priority needs for FRP research in the concrete and masonry environments. The Workshop included participants from various engineering professions and from several countries. Those priorities presented in this paper are those deemed to be

of “Highly Recommended” and other “Recommended” topics. A Final Report showing details of the balloted topics and more detailed topics was submitted to NSF (Porter and Harries 2005).

4. ACKNOWLEDGEMENTS

The contributions of all Workshop participants, the steering committee and especially the break-out session leaders and recorders are gratefully acknowledged. The Workshop was sponsored by the National Science Foundation (NSF) through grant number CMS 0338037. Additional support for the Workshop was provided by the American Concrete Institute (ACI) and ISIS Canada.

5. REFERENCES

Harries, K.A., Porter, M. and Busel, J., 2003. FRP Materials and Concrete – Research Needs, *Concrete International*, Vol. 25. No. 10, pp 49-54.

Porter, M.L. and Harries, K.A., 2005. *Workshop on Research in FRP Composites in Concrete Construction – Final Report*. Submitted to the National Science Foundation, March 2005, followed by a complete project final report in July 2006, 40 pp.

A summary ballot was developed and is shown below in Figure 1.

	IIA	IIB	IIIA	IIIB	IVA	IVB
	INTERNAL FRP	EXTERNAL FRP	DURABILITY	QC/NDE/SHM	FIRE/EXTREME	HYBRID
1	Material science 23 issues (durability, ductility, creep, fatigue, fire, new system development)	Time dependent 17 effects and factors affecting them	Develop standard 20 durability test methods and interpretation	Data 7 interpretation and integration	Develop fundamental models for predicting fire resistance (materials and systems)	Connections 14
2	Developing cost 20 effective and innovative schemes for use of FRP	Seismic design 9 gaps	Service life 16 models	Definition of 2 QC/NDE/SHM objectives	Performance of 17 seismic and blast resistance of FRP reinforced and strengthened structural members (concrete and masonry)	2D and 3D grids (fabrication methods of 3D grids)
3	Innovative 17 reinforcement schemes (including 2D and 3D grids, etc.)	Fundamental 14 design philosophies	Extrapolate short- 12 term test results to service life	Identify cost- 2 benefit of QC/NDE/SHM	Residual strength 11 of internally and externally reinforced members (fire or impact)	Innovative design 13 approaches
4	Structural 11 performance issues (shear, bond)	Emerging sys- 11 tems	Standardize test methods and interpretation [covered in IIIA-1]	Self-sensing 16 FRP materials/self-powered sensors	Develop FRP 9 materials and/or systems to ensure ductile failure	Mechanical 13 anchorage, bonded or non (flexural and shear anchors)
5	Fire response of FRP reinforced structures (modeling, test methods, etc.) [covered in IVA]	Material types 8 (thermoset vs. thermoplastics and hydrothermal mechanical mismatches)	Model degradation 8 process	Approaches to 6 define acceptance criteria	External 3 reinforcement – Fireproofing to meet ASTM E119	Industry 1 collaboration
6			Establish minimum 3 performance requirements	Development of new NDE tools/methods (FRP with concrete) 5	Experimental 10 data fire and extreme loading	
7			Synergistic 10 effects		Fire resistant FRP 6	
8	Write in topic (if you feel we have missed anything):				New fireproofing 6 materials – development and understanding	

Figure 1: Comprehensive Ballot (sample)

Part XIV. Modeling

AN ANALYTICAL AND NUMERICAL INVESTIGATION OF DEBONDING PROBLEMS IN BEAMS STRENGTHENED WITH COMPOSITE MATERIALS

Domenico Bruno
(Professor, University of Calabria, Cosenza, Italy)

Fabrizio Greco
(Associate professor, University of Calabria, Cosenza, Italy)

Paolo Lonetti
(Researcher, University of Calabria, Cosenza, Italy)

ABSTRACT

A refined model able to analyze edge debonding problems in beams strengthened with externally bonded composite laminated plates, is presented. The structural system is viewed as composed by three different physical components: the base beam, the adhesive layer and the bonded plate. Each component may be comprised by one or several mathematical layers which adopts the first-order shear deformation laminate theory. Bonding and continuity conditions between different layers are simulated by using the interface modelling technique. According to a fracture mechanics approach, the analysis is carried out by evaluating the total and individual mode components of energy release rate (ERR). Applications for typical strengthened systems, carried out by numerical integration procedures, are proposed. The approximations introduced in the model with respect to the adopted number of mathematical layers are analyzed and comparisons with existent FE models are given. For the simpler two-layer model of the structure, a closed-form solution is obtained. Finally, the effect of different debonding modes on the overall behaviour of the structural system is analyzed. These results show the capability and the accuracy of the proposed approach to predict debonding failure behaviour in strengthened beams.

KEYWORDS

FRP strengthening, Debonding, Interface models, Computational simulation

1. INTRODUCTION

Composite materials, especially in the form of fiber-reinforced plastic (FRP) strips, are widely used for various strengthening, upgrading or retrofitting applications of existing civil concrete or steel structures. A frequent flexural strengthening technique, consists of externally bonding a laminated composite plates to the tension face of a concrete or steel beam, by means of an adhesive layer. Bonding FRP plates to the external surface of structural members leads to several improvements of the structural performance (see, for instance, Ramana et al., 2000; Lau & Zhou, 2001). On the other hand, experimental evidences have shown that the increase in stiffness and strength provided by the reinforcement is accompanied by a decrease of ductility leading often to debonding failure modes in the FRP strengthened system, characterized by a brittle and unstable nature, which may compromise the effectiveness of the reinforcement (see, for instance, Rabinovitch, 2004). In order to analyze debonding problems several models based both on strength theory (see, for instance, Ziraba et al., 1994) and fracture or damage mechanics (see for instance, Lau et al. 2001) have been proposed. On the other hand, despite the notable steps forward made in this research field, additional progress should be achieved in order to reach a better understanding of the mechanics of debonding between external strengthening system and the base structure. For instance, an in dept characterization of the behaviour of interface fracture including the effects of mixed mode propagation is necessary to obtain a realistic prediction of interface crack growth. Moreover, another interesting aspect is the problem of fracture initiation which cannot be predicted by means of Fracture mechanics. The goal of the paper is to

stresses, and is adopted in order to reduce the number of generalized displacement variables. The related constraint equations imposing displacement continuity requirements between any two adjacent layers, i and $i+1$, are:

$$\Delta u_i = 0, \Delta w_i = 0, \text{ where } \Delta u_i = u_i - \frac{t_i}{2}\psi_i - u_{i+1} - \frac{t_{i+1}}{2}\psi_{i+1}, \Delta w_i = w_i - w_{i+1}. \quad (4)$$

In the case when a collapsed interface model is introduced, ERR and its mode decomposition can be evaluated by applying a virtual crack closure type formula in terms of interfacial concentrated forces at the delamination tip arising as reactions to constraint equations (4). It can be shown that results obtained for ERR and mode decomposition are equivalent to those obtained by using the strong interface formulation. As a matter of fact, in the limit of the strong interface procedure stress singularities become equivalent to the above mentioned concentrated forces.

3. RESULTS

For simplicity at this stage and without loss in generality, the analysis is carried out by adopting only two mathematical layers to model the strengthened beam and using a collapsed interface model to simulate adhesion. The upper mathematical layer is denoted with the subscript 2 and the lower one with the subscript 1. The obtained field equations will be used for the computation of closed-form expressions for ERR. In particular one mathematical layer represents the element to be strengthened and the other one the composite system, comprised of the adhesive layer and the FRP layer. Energy release rate and mode partition are evaluated by using the virtual crack closure technique (VCCT) by using a procedure introduced by the authors (see Bruno et al., 2003) in the context of a multi-layer model. According to the VCCT the energy released into individual modes is half the work performed by interfacial concentrated forces at the delamination tip through displacement jumps occurring after the delamination is extended by da . Consequently, the mode I, mode II and the total ERRs are evaluated as

$$G_I = \frac{1}{2} \llbracket T_1 \rrbracket_d \llbracket \gamma_1 - \gamma_2 \rrbracket_d, \quad G_{II} = \frac{1}{2} \llbracket N_1 \rrbracket_d \left\| \left\| \varepsilon_1 - \varepsilon_2 - \kappa_1 \frac{t_1}{2} - \kappa_2 \frac{t_2}{2} \right\| \right\|, \quad G = \sum_{i=1}^2 \left(\frac{1}{2} \llbracket N_i \varepsilon_i + M_i \kappa_i + T_i \gamma_i \rrbracket_d - \llbracket T_i \rrbracket_d \psi_i \right) \quad (5)$$

where the double bracket $\llbracket f \rrbracket_k = f^+ - f^-$ denotes the jump across the delamination tip $x=L_u+L_s-a$ and N_i , M_i , and T_i , are the axial, bending and shear stress resultants, respectively. Closed-form solutions for the quantities in eqs (5) can be obtained by using the equilibrium solution for the two-layer system.

The two-layer model suffices only to obtain an accurate evaluation of the total ERR, whereas individual energy release rates may be computed with a reasonable accuracy only if more than one mathematical layer is used to model each physical layer. However the use of a refined multi-layer model implies that mode partition must be performed numerically rather than analytically, since a general closed form solution of the governing equations is hard to be obtained. Energy release rates are obtained by using the strong interface formulation eqs (3). An iterative collocation method is adopted which starting from an initial guess for the solution and the mesh, at each iteration the method adapts the mesh to obtain a sufficiently accurate numerical solution. Results shown in Figure 2 with reference to a cantilever beam subjected to an edge transverse force evidence that the total energy release rate from the proposed approach converges to that calculated by means of an FE solution of the 2D continuum model of the structural system as the number of mathematical layer increases. The characteristics of the bonded plate are representative of a typical carbon-epoxy unidirectional lamina, whereas those of the beam refers to a typical concrete beam. The numerical finite element analysis has been carried out by modeling the system with 2D plane stress four-noded elements and computing the energy release rate by the aid of the VCCT. In addition in Figure 2 the closed-form solution extracted from equations (5) is plotted for comparison purposes. The structure is here divided into 7 mathematical layers: 2 for the FRP plate; 1 for the adhesive and 4 for the beam. Starting from the lowest one their thicknesses are, respectively, 0.5 tp, 0.5 tp, ta, 0.01 tb, 0.07 tb, 0.32 tb, 0.6 tb. This layer assembly is denoted as (2/1/4). Figure 2 shows that the total energy release rate has an excellent agreement with the FE results with relative errors smaller than 1%. Consequently, the solution provided by the closed form expressions of eqs (5) is refined by using an appropriate layer assembly and the accuracy is improved by increasing the number of layers. The convergence of the total energy release rate and of its individual mode components for a fixed delamination length ($a=400\text{mm}$) is also shown at the right of Figure 2, where it can be observed that individual energy release rate components converge too, but toward asymptotic values different from FE predictions, which are mesh dependent due to the oscillatory singularities. The (1/1/4) assembly adopts the following thickness distribution: tp, ta, 0.017 tb, 0.05 tb, 0.33 tb, 0.6 tb, whereas the (1/1/2) assembly adopts the following thickness distribution: tp, ta, 0.33 tb, 0.67 tb.

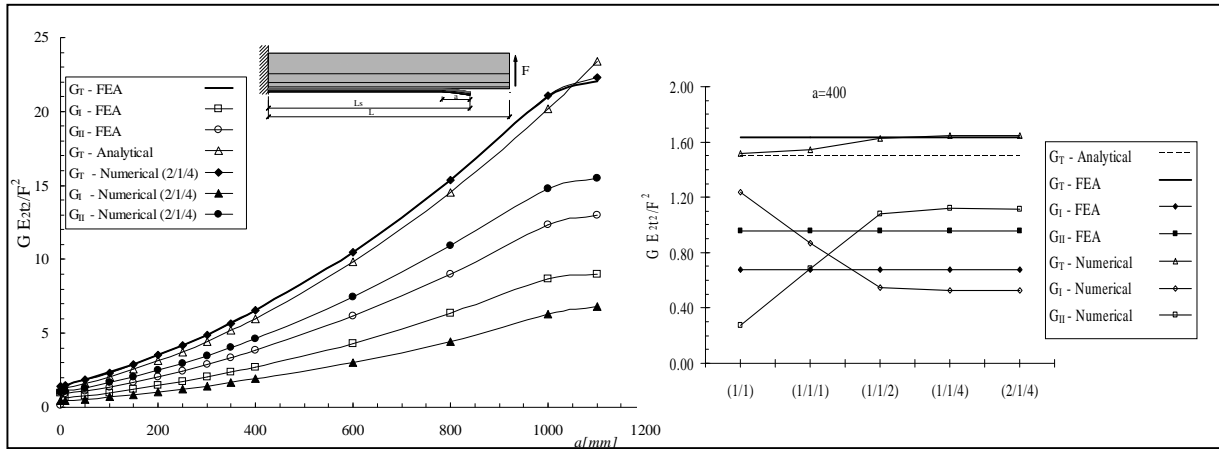


Figure 2. Convergence to the FE results for a cantilever beam configuration under an edge transverse force as a function of the delamination length and for a fixed delamination length ($a=400\text{mm}$).

4. CONCLUSIONS

An improved mechanical model for the analysis of debonding failure starting at the edge of beams strengthened with externally bonded composite plates is proposed, by modelling a strengthened structural system as an assembly of shear deformable mathematical layers. Introducing strong and collapsed interface layers and an appropriate layer assembly based on the structure physical configuration, an accurate description of the problem is obtained. It has been shown that for a two-layer version of the proposed model, closed-form solution for the total energy release rate are available. Unfortunately, the energy release rate mode components predicted by the above analytical solution are not sufficiently accurate and, as a consequence, one has to introduce more than one mathematical layer to model each physical component to capture the local warping of the layers near the crack tip. The energy release rates curves as a function of the crack length for different structural schemes and different debonding failure modes, confirm the brittle and catastrophic unstable behavior which accompanies debonding growth and the observed failure modes pointed out during experiments. Results obtained by numerical integration for typical strengthened systems, compared with predictions from very refined 2D-continuum FE investigations, show the capability and the accuracy of the proposed approach to predict debonding failure behavior. Contrary to the FE methodologies, which involve considerable complexities due to the detailed mesh required to capture edge stress singularities and differences in length scales and in mechanical properties of the single components of the system, the proposed approach is more computationally efficient due to the use of plate variables.

5. REFERENCES

- Bruno, D., Greco, F., (2001). "Mixed mode delamination in plates: a refined approach". *Int. J. Solids Structures* Vol. 38/50–51, pp. 9149–9177.
- Bruno, D., Greco, F., Lonetti, P., (2003). "A coupled interface-multilayer approach for mixed mode delamination and contact analysis in laminated composites". *Int. J. Solids Structures*, Vol. 40, pp. 7245–7268
- Lau K.-T., Zhou L.-M. (2001). "Mechanical performance of composite-strengthened concrete structures". *Composites Part B: Engineering*, Vol. 32, pp. 21-31.
- Lau KT, Dutta PK, Zhou LM, Hui D (2001). "Mechanics of bonds in an FRP bonded concrete beam". *Compos: Part B*; Vol. 32, pp. 491–502.
- Rabinovitch, O. (2004). "Fracture-mechanics failure criteria for RC beams strengthened with FRP strips-a simplified approach", *Composite Structures*, Vol. 64, pp. 479-492.
- Ramana V.P.V., Kant T., Morton S.E., Dutta P.K., Mukherjee A., Desai Y.M., (2000). "Behavior of CFRPC strengthened reinforced concrete beams with varying degrees of strengthening", *Composites Part B*, Vol.31: pp. 461-470.
- Ziraba YN, Baluch MH, Basunbul IA, Sharif AM, Azad AK, Al-Sulaimani GJ (1994). "Guidelines toward the design of reinforced concrete beams with external plates". *ACI Struct* ; Vol. 91(6), pp. 639–46.

NUMERICAL ANALYSIS OF TWO-WAY CONCRETE SLABS WITH OPENINGS STRENGTHENED WITH CFRP

M. Sc. Piotr Rusinowski

*(Ph.D. Student, Technical University of Denmark, Lyngby, Denmark
Norut Technology Ltd., Narvik, Norway)*

Lic. Tech. Ola Enochsson

(Ph.D. Student, Luleå University of Technology, Luleå, Sweden)

Prof. Björn Täljsten

*(Professor, Technical University of Denmark, Lyngby, Denmark
Luleå University of Technology, Luleå, Sweden)*

ABSTRACT

Carbon Fiber Reinforced Polymers, CFRP, offer excellent corrosion resistance to environmental agents as well as the advantages of high stiffness-to-weight and strength-to-weight ratios when compared to conventional construction materials. One common application for CFRP sheets is to strengthen slabs and walls when openings are to be made. In spite of this, there have not been many studies reported on slabs with openings strengthened with CFRP and especially, not with distributed loading. This paper presents numerical analyses of simply supported two-way concrete slabs with openings strengthened with CFRP sheets. The finite element program Abaqus is utilized for the analyses. The analyses are compared with full-scale laboratory tests and show a good agreement.

KEYWORDS

CFRP, FE-analysis, strengthening, slabs, openings

1. INTRODUCTION

Reinforced concrete slabs and shells are commonly used structural elements in building structures. Due to changes in use and new functionality demands, existing constructions often need to be rebuilt and new openings in existing slabs or shells are to be made. The effect of small openings is usually neglected due to ability of the structure to redistribute additional stresses. The problem appears with larger openings when the static system may be altered and strengthening must be applied. External bonded FRP sheets are becoming increasingly used in reconstruction. Despite the growing popularity of FRP strengthening, the existing design guidelines do not normally cover strengthening of openings. The calculation method of FRP strengthening for slabs with openings, applied also in this paper, uses the instructions concerning required amount of steel reinforcement in slabs cast with openings given by the building codes. This method is described in Enochsson (2005) and more generally in Täljsten (2004). The study presented in this paper is a part of the ongoing research on two-way concrete slabs with openings at Luleå University of Technology.

2. OBJECTIVE

The aim of the study presented in this paper was to model the behaviour of CFRP strengthened concrete slabs using Finite Element and to compare the result with experimental tests. The FE-model can then both be used to investigate the influence of different opening-to-slab sizes on the behaviour and how to strengthen a slab most efficient due to a made opening. However, the idea of the entire study and the experiments was to obtain as much information as

possible about the effect of openings in two-way RC slabs and the efficiency of the CFRP strengthening configuration. In order to carry out a necessary comparison the following slab configurations were tested:

- Without opening (Homogeneous)
- With opening (Weakened)
- With opening strengthened with CFRP (Strengthened)
- With an additionally steel reinforced cast opening (Reinforced)

3. EXPERIMENTAL PROGRAM AND DESIGN OF TEST SPECIMEN

All specimens were quadratic with a side length of 2600 mm and a thickness of 100 mm. The openings were also quadratic and located in the center of the slabs. The size of the openings, 850×850 mm, was slightly larger than allowable for the simplified design method according to the Swedish code. Figure 1a shows the types of specimens considered in this paper.

The slabs were manufactured in four concrete batches with a designed 28 days characteristic compressive strength of 40 MPa. All slabs were reinforced with steel bars, Nps 50 ϕ 5, with the nominal characteristic yield strength $f_{yk} = 510$ MPa. The bars were arranged into a welded net with spacing of $s = 150$ mm. The strengthening system was provided by Sto Scandinavia AB with the brand name Sto FRP Sheet S300.

The distributed load was provided by a system of airbags, embedded in a heavy steel structure, see Figure 1b. Since the load was applied from underneath, the specimens had to be placed “upside-down”. The steel frame, made of I-beams, provided line supports along the specimens’ edges. The four load-cells, that connected the supporting frame with the fixture in each corner, measured the magnitude of load.

The homogeneous slab was designed using the Swedish standard method, based on the theory of elasticity and in some extent also on the yield line theory. The method, described in Hilleborg (1990), uses a simple formula for estimating the maximum moment, from which the required amount of reinforcement can be calculated.

The slabs with the openings were designed with the traditional method, which can be described in two phases. In the first phase, the calculation for a homogeneous slab is to be carried out. Afterwards, the moment capacity from the area where the opening is to be made is distributed into the bands around the opening. In principle, with an assumption that moments in this area are constant, the method leads to spreading designed reinforcement around the opening. The procedure is described in Enochsson (2005).

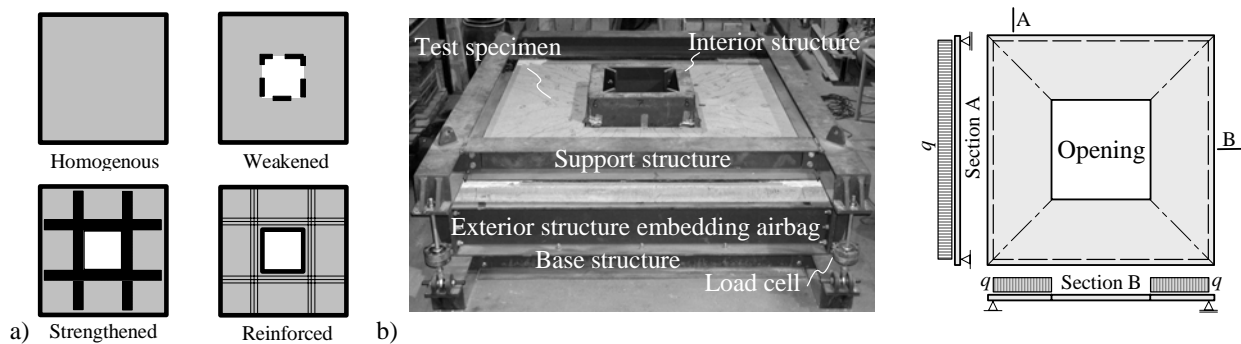


Figure 1: a) Specimens, b) Test set-up and static system

4. NUMERICAL ANALYSIS

Numerical analysis of the slabs considered in this paper included several nonlinear considerations concerning material properties, boundary conditions and geometries. In order to achieve the convergence application of explicit integration had to be used. The finite element mesh was regular for all parts in the model, see Figure 2a. The concrete part of the slab was modeled with eight-node brick elements with reduced integration. The reinforcement grid was represented by discrete truss elements. Support steel plates, which transferred reaction forces by means of contact formulation, were modeled by shell elements with reduced integration. Orthotropic property of CFRP sheets was assigned by using membrane elements with no stiffness in the direction perpendicular to the fibers.

A damaged plasticity constitutive model for concrete was used in the FE-calculations. The post failure behavior in tension was specified in terms of the stress-displacement response described by a bilinear curve, see Figure 2b.

The model for reinforcing steel was ideal elasto-plastic and full bond between reinforcement and concrete was assumed. The CFRP material was considered to be elastic. The interface between the concrete slab and the CFRP was modeled as ideal bonding, i.e. full composite action. This property was obtained by using interaction “tie” between surfaces, which locks the distance between adjacent nodes. The FE-model assumed an ideal line support which cannot be achieved in the field conditions due to imperfections of the test rig and uneven concrete surface. Commonly, some elastic deformations are enabled and the supports can be then modeled as a set of discrete springs, see Rusinowski (2005), or continually by applying simply supported deformable plates along slab edges. The latter method was used for comparison between elastic and stiff supports. Figure 2c presents deflection curves obtained from the experiment and the analyses of CFRP strengthened slab. The analysis with the elastic supports shows good agreement with the experiment until plastic phase but introduces dynamic problem later on which was noticed in the curve before smoothing. This fact cause inaccuracies especially considering concrete damaged plasticity model and for this reason stiff line supports are used in further analyses.

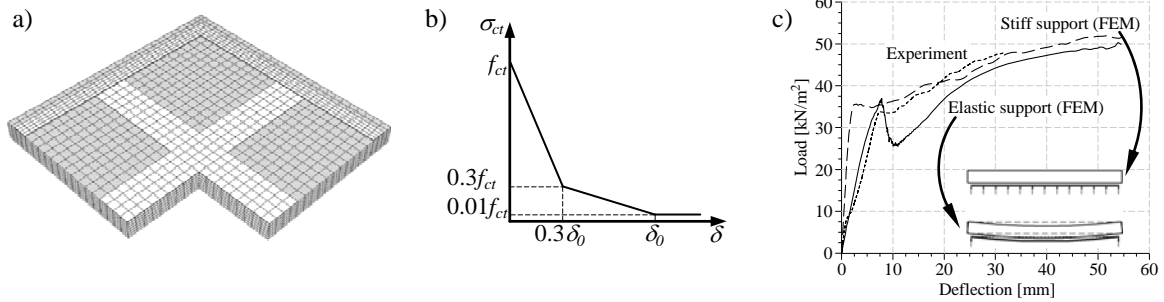


Figure 2: a) FE-mesh, b) Concrete tension behavior, c) Model of elastic support

5. RESULTS

The result from the numerical analysis is compared with the outcome from the experiments. The displacements were measured in the middle of the opening’s edge, where slabs deflect most. Comparison with the load - deflection curve is the easiest way to judge the general behavior and the load capacities of the slabs. Figure 3a presents the load - displacement relationships for all the slabs both for the experiments and the numerical analyses. The shapes of the curves show relatively good agreement between the experiments and the FE analyses. The CFRP-strengthened slab hardens after the plastic phase. The possible reason for this phenomenon might be elastic behavior of carbon fibers and the fact that the CFRP strengthening is distributed, in contrast to steel reinforcement. These two features may delay crack initiation and propagation. The strains were measured in three locations along the openings. Strain distribution along one of the CFRP sheets, see Figure 3b, is compared in three phases called: elastic, cracking and plastic. The “elastic” phase is always set to load 10 kN/m² regardless slab type and represents the state before concrete reaches its tensile strength. The “cracking” phase corresponds the time when a slab begins to crack. The first cracks, which are very narrow, could not be noticed during the experiments and this moment could be detected only in numerical analyses. Finally “plastic” phase represents the moment when slab is fully cracked and begins to deform plastically. This stage has been found individually for the experiments and the numerical analysis.

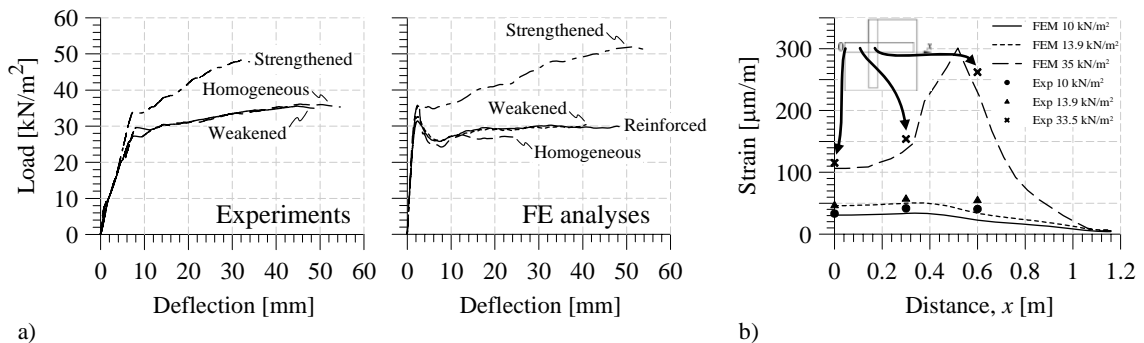


Figure 3: Comparison of results: a) maximum deflection, b) strain distribution along the opening edge

Figure 4 shows similarities in comparison of crack distribution between experiments and numerical analyses. The plastic region in CFRP strengthened slab is more widely spread compared with the other analyzed and tested slabs, which may be the effect of distributed strengthening.

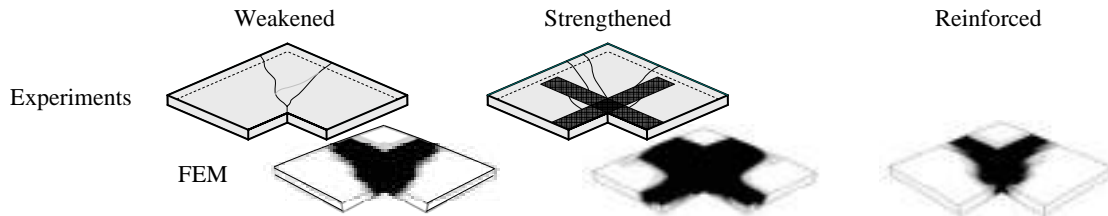


Figure 4: Comparison of crack distribution obtained in experiments with final principal plastic strain distribution in FE analyses

6. CONCLUSIONS

The FE calculations used in this study show good agreement with the experiments although relatively simple model was applied. In opposite to the experiments, however, CFRP failure was not reached in the numerical calculations. In FE analyses, using either smeared cracking or damaged plasticity model of concrete, cracks are distributed over a larger region. In the reality, a few discrete cracks propagate and the stresses are concentrated in the reinforcing steel and CFRP sheets. In these formulations mesh must be much finer to localize failure.

The model of CFRP strengthening assumes an ideal bonding, i.e. possible peeling off at crack cannot be investigated. Furthermore, the stiffness of CFRP is assumed to be equal in compression and tension and this is suitable for cases where CFRP sheets are only stretched. For more complex problems, as two-way concrete slabs or structures subjected to cycle loading, different material properties of CFRP in tension and compression should be assigned.

Apart from these observations, the explicit FE analysis gives more insight to the strengthening effect of the CFRP sheets. It also gives more confidence to the future utilization of the non-linear FE analysis in order to evaluate larger slabs with different opening configurations.

For further investigation of two-way concrete slabs with openings it is necessary to study the bond behavior between the CFRP and the underlying concrete in detail. Furthermore, better models of the crack localization in the concrete are needed to be able to accurately predict the ultimate failure.

7. ACKNOWLEDGEMENT

The research work presented in this paper has mainly been performed at Luleå University of Technology in Sweden, and has been financed by Skanska Teknik AB Sweden and SBUF (The Development Fund of the Swedish Construction Industry) and also partly by the European Union regional funds, Sto Scandinavia AB and the Norwegian Research Council through the strategic institute program RECON at Norut Technology Ltd.

8. REFERENCES

- Enochsson, O. (2005): *CFRP Strengthening of Concrete Slabs, with and without Openings – Experiments, Analysis, Design and Field Application*. Licentiate Thesis 2005:87, Luleå University of Technology, Div. of Structural Engineering, ISSN 1401-1757, p 168.
- Hillerborg, A. (1996): *Strip Method - Design Handbook*. First edition. London, UK: Chapman & Hall. ISBN 0-419-18740-5.
- Rusinowski, P. (2005): *Two-Way Concrete Slabs with Openings – Experiments, Finite Element Analyses and Design*. Master's Thesis 2005:200 CIV, Luleå University of Technology, Div. of Structural Engineering, ISSN 1402-1617. p 126.
- Täljsten, B. (2004): *FRP Strengthening of existing concrete structures - Design Guidelines*. Third edition. Luleå, Sweden: Luleå University printing office, ISBN 91-89580-03-6, 2004, p 230.

NUMERICAL MODELING OF FRP SHEAR STRENGTHENED RC BEAMS USING COMPRESSION FIELD THEORY

Zhe Qu

(Postgraduate, Tsinghua University, Beijing, China)

Xin-Zheng Lu

(Lecturer, Tsinghua University, Beijing, China)

Lie-Ping Ye

(Professor, Tsinghua University, Beijing, China)

Jian-Fei Chen

(Lecturer, Edinburgh University, Edinburgh, UK)

John Michael Rotter

(Professor, Edinburgh University, Edinburgh, UK)

ABSTRACT

The modified compression field theory and an advanced bond-slip model are implemented in a general finite element analysis package to evaluate the shear behaviour of FRP strengthened reinforced concrete beams. The inclination angle of the critical shear crack is estimated and the debonding phenomenon is simulated. A close agreement is achieved between the predicted average FRP strains and those in a test beam reported in the literature. Further research is being conducted to simulate behaviour of FRP shear the interaction between the external FRP shear reinforcement and concrete.

KEYWORDS

Shear, FRP, strengthening, concrete, modified compression field theory (MCFT)

1. INTRODUCTION

The modified compression field theory (MCFT) has been an alternative method for shear design of reinforced concrete members since late 1980s when it was established by Vecchio and Collins (1986). It takes into account the three basic principles of mechanics and is able to calculate the inclination of the diagonal shear crack, which is essential in predicting the shear behaviour of reinforced concrete beams.

With the increasing interest in the technique of strengthening RC members with externally bonded FRP for shear, a number of studies have been carried out to include the contribution of FRP in the MCFT in the last few years. Malek and Saadatmanesh (1998) extended MCFT to include the contribution of FRP sheets with variable concrete crack angles. However, they assumed a uniform distribution of FRP strain throughout the depth of the beam and no slip between the FRP and concrete was taken into account. Lees *et al.* (2002) analysed the development of strain in FRP sheets using MCFT based on similar assumptions. Wong *et al.* (2003) considered the bond-slip behaviour of FRP-concrete interface in the MCFT model by introducing elastic or perfectly elasto-plastic link elements. They concluded that it is necessary and viable to model the interface behaviour between FRP and concrete but a more advanced bond-slip constitutive model must be adopted.

In this paper, the MCFT is implemented in the finite element software MSC. MARC (2003) to simulate the shear behaviour of FRP strengthened concrete beams. An advanced bond-slip relationship is adopted to model the FRP-concrete interface. Numerical predictions are compared with test results from the literature.

2. THE MODEL

The MCFT adopts a smeared crack model. The bond behaviour between the FRP and the concrete plays a crucial role and debonding of FRP from concrete almost always happens prior to the final shear failure of a concrete beam shear strengthened with FRP (Chen and Teng 2003). However, this interfacial bond-slip behaviour cannot be directly incorporated into the MCFT model when the FRP starts to debond. In this study, the reinforced concrete is modelled using a constitutive model based on the MCFT. The FRP strips are modelled separately and linked to the concrete surface by using nonlinear springs based on Lu *et al.*'s (2005) bond-slip relationship (Fig. 1a).

In the MCFT, the reinforced concrete is treated as a continuous material with the reinforcements and cracks smeared in the elements. The rotating-angle crack model is commonly used. The in-plane constitutive model in the MCFT is established based on the uniaxial constitutive models for concrete and steel reinforcement. The widely-used uniaxial stress-strain relationship for concrete proposed by Hognestad (1952) and that for steel reinforcements (Fig. 1b) suggested by T. T. C. Hsu and his colleagues (Belarbi and Hsu 1995) are adopted in this study. To introduce the compression softening effect of concrete, Hognestad's model is modified here by including a softening coefficient ζ which was proposed by Belarbi and Hsu (1995). The concrete compressive stress (σ) strain (ε) relationship (Fig. 1c) is thus given as

$$\sigma = \zeta \sigma_0 \left[\frac{2\varepsilon}{\varepsilon_0} - \left(\frac{\varepsilon}{\varepsilon_0} \right)^2 \right] \quad \varepsilon \leq \varepsilon_0 \quad (1a)$$

$$\sigma = \zeta \sigma_0 \left[1 - 0.15 \left(\frac{\varepsilon - \varepsilon_0}{\varepsilon_u - \varepsilon_0} \right)^2 \right] \quad \varepsilon_0 \leq \varepsilon \leq \varepsilon_u \quad (1b)$$

$$\text{where } \zeta = \frac{0.9}{\sqrt{1 + 400\varepsilon_1}} \quad (1c)$$

where σ_0 is taken as the concrete cylinder compressive strength, ε_0 and ε_u are the peak and ultimate compressive strains respectively, and ε_1 is the current principal tensile strain in the concrete.

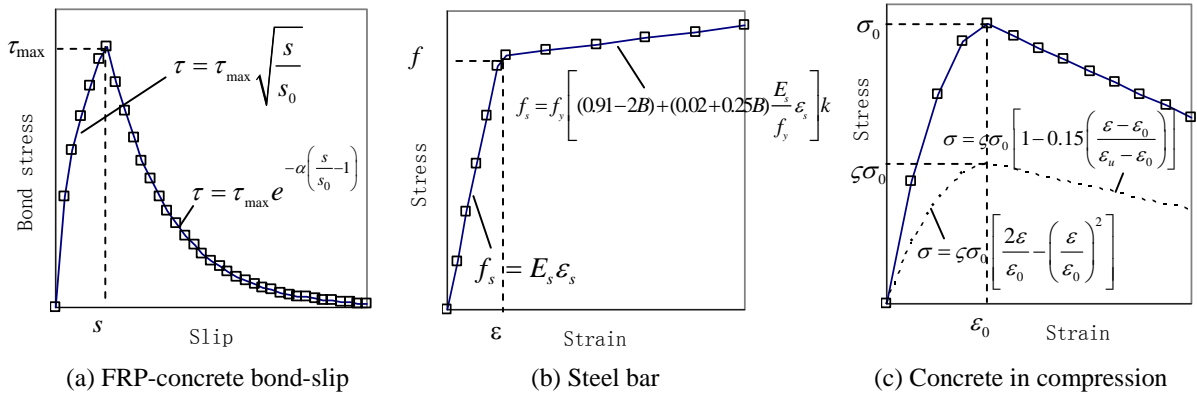


Figure 1: Uniaxial stress-strain relationships

To take into account the effect of the complex stress state of concrete underneath the FRP strips on the FRP-concrete bond-slip behaviour, the biaxial strength model for concrete proposed by Kupfer (1969) is introduced into the FE model to modify the concrete tensile strength:

$$f_t' = \left(1 - 0.8 \frac{\sigma_2}{f_c} \right) f_t \quad (2)$$

where σ_2 is the principal compressive stress in the concrete, and f_c and f_t are the uniaxial compressive and tensile strengths of concrete respectively.

A procedure for determining the stress state from a given strain state and strain increment was derived within the framework of MCFT, which makes use of compatibility and equilibrium conditions and the above constitutive relationships. The procedure was implemented in MARC through the user subroutine HYPELA2.

3. NUMERICAL PREDICTIONS AND COMPARISON WITH TEST RESULTS

RC beam SCU-2-1 shear-strengthened with CFRP U-jackets and its corresponding un-strengthened control beam S0-2-0 as reported in Tan and Ye (2003) were investigated using the aforementioned FE model. Both beams had a shear span-to-depth ratio of 2.155 and were tested under 4-point-bending. The beams had a depth of 260mm and material properties as listed in Table 1. The concrete cylindrical compressive strength f_c was taken to be $0.8f_{cu}$.

Table 1: Material properties of specimens

Specimen ID	Concrete cubic compressive strength f_{cu} (MPa)	Web steel reinforcement		Longitudinal steel reinforcement		FRP strips	
		ρ_v	f_{vy} (MPa)	ρ_s	f_{sy} (MPa)	ρ_f	E_f (GPa)
S0-2-0	31.8	0.19%	377	2.9%	395		
S-CU-2-1	37.6	0.19%	377	2.9%	395	0.074%	235

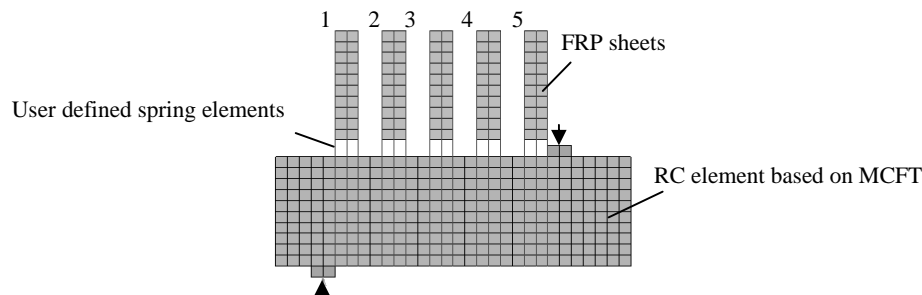


Figure 2: Finite element model for specimen S-CU-2-1

Due to symmetry, only a half span of the beams was modelled (Figure 2). The RC beams were modelled using the user-defined 2D RC material model based on MCFT and the FRP strips were modelled as an orthotropic material. The nodes of the FRP elements were linked to the nodes of the RC element by user-defined nonlinear spring elements with appropriate properties of the adopted bond-slip model. The lowest row of the FRP nodes was rigidly linked to the bottom of the beam because no slip was possible between the beam and the FRP U jackets there.

Figure 3 shows a comparison of the distribution of the predicted principal tensile strain with the test diagonal crack pattern. It is seen that the predicted inclination angle is very close to the test crack angle. Figure 4 shows the simulated failure process where the FRP strain value is proportional to the darkness of the colour. In the test, FRP strip No. 4 was debonded first, followed by the debonding of strip No.3 and then No. 2. The beam eventually failed due to the debonding of FRP strip No. 1. This failure process is closely reproduced as in Figure 4.

The predicted load-deflection curve for the un-strengthened beam specimen S0-2-0 is in good agreement with the test results (Fig. 5), but that for the FRP strengthened specimen SCU-2-1 has some deviation from the test curve. The main cause for this disparity may be the inability of the present FE model to simulate factors such as the enhanced dowel action by the presence of the FRP. Figure 6 shows that the average tensile strain in the FRP strips along the diagonal crack is close to the test value, but the predicted strain distribution is more uniform compared with the test results which may be attributed to the adoption of the smeared crack model.



Figure 3: Predicted principal tensile strain versus test crack pattern when the middle FRP strip debonded

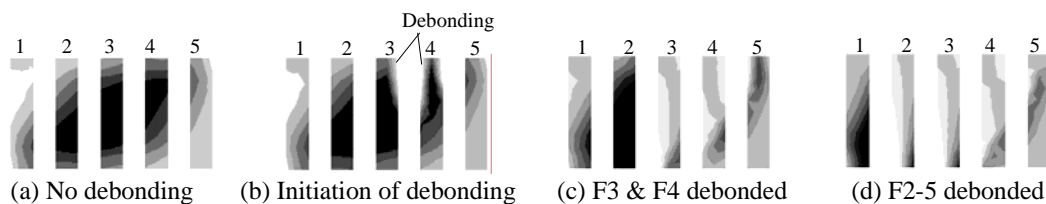


Figure 4: Development of axial strain distribution in FRP strips

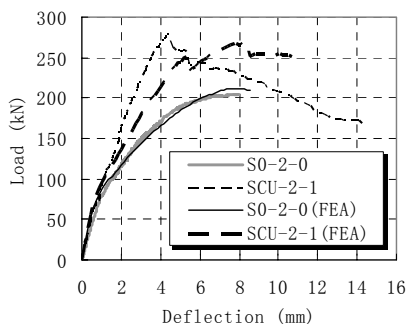


Figure 5 Load-deflection curves

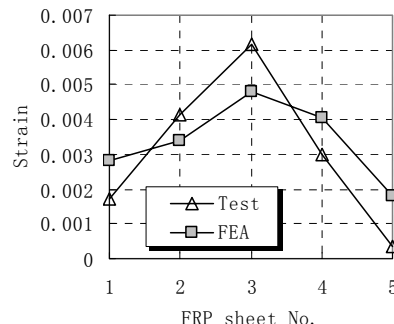


Figure 6 Strain distribution along the diagonal crack

4. CONCLUSIONS

This paper has presented a study on the shear behaviour of FRP strengthened RC beams. The modified compression field theory is built into a general-purpose finite element analysis software package. The bond-slip relationship of FRP-concrete interface is modified by reducing the concrete tensile strength according to the biaxial stress state of concrete underneath the FRP strips. The results show that the model is capable of predicting the inclination angle of critical shear crack as well as the debonding procedure of FRP strips, which are both essential in predicting the shear capacity of FRP strengthened RC beams.

5. ACKNOWLEDGEMENTS

The authors would like to acknowledge the financial support provided by the Royal Society through the Royal Society-NSFC UK-China Joint Project (Grant No. IS 16657) and the National Natural Science Foundation of China through a key project for FRP in construction (Project No. 50238030).

6. REFERENCES

- Belarbi, A. and Hsu, T.T.C. (1995). "Constitutive laws of softened concrete in biaxial tension-compression". *ACI Structure Journal*, Vol. 92, No. 5, pp562-573.
- Chen, J.F. and Teng, J.G. (2003). "Shear capacity of FRP strengthened RC beams: FRP debonding". *Construction and Building Materials*, Vol.17, No.1, pp27 – 41.
- Hognestad, Eivind (1952). "Inelastic behaviour in tests of eccentrically loaded short reinforced concrete columns". *ACI Journal*, Vol. 49, No. 10, pp117-139.
- Kupfer, H., Hilsdorf, H. K., Rush H. (1969). "Behavior of concrete under biaxial stresses". *ACI Journal*, Vol. 66, No. 8, pp656-666
- Lu, X.Z., Teng, J.G., Ye, L.P. and Jiang, J.J. (2005). "Bond-slip models for FRP sheets/plates externally bonded to concrete". *Engineering Structures*. Vol. 27, No. 6, pp938-950.
- Lees, J.M., Winistorfer, A.U., Meier, U. (2002) "External prestressed carbon fiber-reinforced polymer straps for shear enhancement of concrete." *Journal of Composites for Construction*, Vol. 6, No. 4, pp249-256.
- Malek, A.M., Saadatmanesh, H. (1998). "Ultimate shear capacity of reinforced concrete beams strengthened with web-bonded fiber-reinforced plastic plates." *ACI Structure Journal*, Vol. 95, No. 4, p391-399.
- Tan, Z. and Ye, L.P. (2003) "Experimental research on shear capacity of RC beam strengthened with externally bonded FRP sheets". *China Civil Engineering Journal*, Vol. 36, No. 11, pp12-18
- Vecchio, F.J. and Collins, M.P. (1986). "The modified compression-field theory for reinforced concrete elements subjected to shear". *ACI Journal*, Vol. 83, No. 2, pp219-231.
- Wong, Rita S.Y. and Frank J. Vecchio. (2003). "Towards modeling of reinforced concrete members with externally bonded fiber-reinforced polymer composites." *ACI Structure Journal* Vol. 100, No. 1, pp 47-55.

NUMERICAL SIMULATION OF BOND DETERIORATION BETWEEN CFRP PLATE AND CONCRETE IN MOISTURE ENVIRONMENT

Zhenyu Ouyang

(Ph.D. Student, Marquette Universit, Milwaukee, WI, USA)

Baolin Wan

(Assistant Professor, Marquette Universit, Milwaukee, WI, USA)

ABSTRACT

This research investigated the effect of interface region relative humidity (IRRH) on the bond between CFRP and concrete using computer simulation technique. After FRP is peeled off concrete substrate, there is a layer of residue concrete on the detached FRP if the bond is sound. The experimental program related to this research found that the residual thickness of concrete (RTC) was directly related to the IRRH. A constitutive equation, which calculated the RTC from IRRH, was proposed in this research based on the experimental data. The calculated RTCs were used to build a series of finite element models and the virtual crack closure technique (VCCT) was used to calculate the bond fracture energy G_f for debonding. Through the RTC, the bond fracture energy G_f was related to the interface region relative humidity (IRRH). The model and FEM results had excellent agreement with the experimental data. These models can be used to simulate the bond degradation for CFRP bonded concrete specimens suffering from moisture attack.

KEYWORDS

Bond, CFRP, Deterioration, Moisture, Numerical simulation

1. INTRODUCTION

Externally bonding fiber reinforced polymer (FRP) composite materials to concrete beams in order to strengthen or rehabilitate structures is receiving worldwide attention and application. However, many experimental studies (Karbhari et al., 1997; Nguyen et al., 1998; Wan et al., 2006; Ouyang and Wan, 2006) conducted in the past decade show that the water can seriously deteriorate the bond between FRP and concrete. Normally, the fracture mode shifts from cohesive failure in concrete to adhesive failure in interface, where it is the weakest part of bonded structures, in moist environment. Since the vast majority of advanced structural adhesives are epoxy based, they have the propensity to absorb moisture, which can lead to undesirable changes in strength, stiffness and interfacial adhesion. Therefore, the bond durability in moist environment is one of the most important issues for extensive field application of FRP repairing technique in future. Although a lot of experimental researches have been conducted, the mechanism for bond deterioration due to moisture attack is still not clear and how to model such deterioration is still a problem needed to be solved.

Fracture mechanics has been widely used to study the debonding phenomena. The fracture mechanics parameter, fracture energy G_f , includes both crack length and load information for a specimen with crack. Therefore, it is a good criterion to study the bond performance of the FRP bonded concrete members. Besides of the material properties, the critical fracture energy is also considered as an important parameter for modeling FRP debonding from concrete (Coronado and Lopez, 2005). After FRP is peeled off concrete substrate, there is a layer of residue concrete on the detached FRP if the bond is sound. The experimental program related to this research (Ouyang and Wan, 2006) found that the residual thickness of concrete (RTC) remaining on the FRP after it was peeled off concrete substrate was directly related to the interface region relative humidity (IRRH). It was also found that bond fracture energy G_f of FRP-concrete system was directly related to the RTC. This research proposed a constitutive equation and built a series of finite element models to connect IRRH, RTC and G_f .

2. RESEARCH SIGNIFICANCE

A constitutive equation, which calculated the RTC from IRRH, was proposed in this research based on the experimental data. The calculated RTCs were used to build a series of finite element models to calculate the bond fracture energy G_f for debonding. Through the RTC, the bond fracture energy G_f was related to the interface region relative humidity (IRRH).

3. NUMERICAL MODELS

3.1 Constitutive Equation to Calculate RTC from IRRH

As observed in experimental program (Ouyang and Wan, 2006), the fracture energy G_f of control specimens was not significantly affected by the residual thickness of concrete (RTC) in dry environment. After the specimens were submerged in water for different durations, RTC decreased with the increase of interface region relative humidity (IRRH). In this situation, even small change of RTC could cause significant decrease of bond fracture energy due to the moisture at the interface region.

When FRP was peeled off concrete substrate, the crack tip actually located at the place with a distance of RTC from the nominal interface bond line as shown in Figure 1. Since the bond fracture energy G_f is sensitive to RTC after specimens are attacked by moisture, the deviation of crack tip location from nominal bond-line should not be neglected in the debonding analysis models. It is shown in Figure 2 that RTC does not change significantly when the interface is relatively dry. However, it decreases proportionally with the increase of IRRH after IRRH is higher than certain value. Therefore, a bi-linear relation between RTC and IRRH is proposed as Equation 1.

$$RTC = \begin{cases} RTC_c - \left(\frac{IRRH - IRRH_c}{IRRH_0 - IRRH_c} \right) \times RTC_c & \text{For } IRRH \geq IRRH_c \\ RTC_c & \text{For } IRRH < IRRH_c \end{cases} \quad (1)$$

where $IRRH_c$ is the critical value of IRRH to start decreasing the RTC; RTC_c is the constant value of RTC when IRRH is less than the $IRRH_c$; and $IRRH_0$ is the IRRH value when perfect interface adhesive failure happens ($RTC = 0$). This equation assumes that the change of RTC will cause the change of the fracture energy G_f only when IRRH is greater than $IRRH_c$.

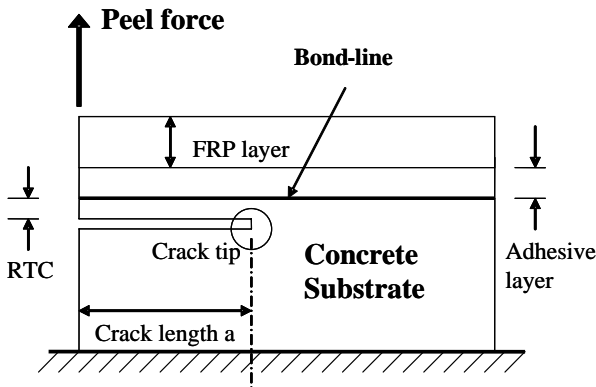


Figure 1: Crack tip location determined by RTC

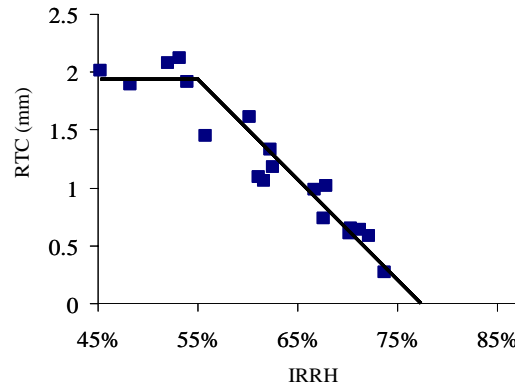


Figure 2: RTC vs. IRRH

The RTC might be different for different loading modes and material properties. All specimens were tested by Mode I (peeling) loading in this study. It is shown in Figure 2 that $IRRH_c$ was 55% and RTC_c was 2.0 mm for the specimens in this research. It can also be found in the figure that IRRH is 77% if the line is extended to intercept with the IRRH axis where the RTC is 0. Thus, $IRRH_0$ was set to be 77% in this study. Equation 2 was used to calculate the RTC for finite element models in this study.

$$RTC = \begin{cases} 2.0 - \left(\frac{IRRH - 0.55}{0.77 - 0.55} \right) \times 2.0 & \text{For } IRRH \geq 55\% \\ 2.0 & \text{For } IRRH < 55\% \end{cases} \quad (2)$$

3.2 Virtual Crack Closure Technique (VCCT)

The virtual crack closure technique (VCCT) is widely used to calculate the interfacial energy release rates from finite element models through a single geometric model for crack propagation. A modified virtual crack closure integral for square-root singularity elements was derived by Sethuraman and Maiti (1988) in order to compute the strain energy release rate by moving the mid-side node position of the isoparametric quadratic element to the quarter location. This method can increase the accuracy of strain energy calculation for linear elastic analysis. The strain energy release rate, G , can be expressed as,

$$G_I = \frac{(u_{yk} - u'_{yk})}{\Delta a} [F_{yj} + (1.5\pi - 4)F_{yi}] \quad (3)$$

$$G_{II} = \frac{(u_{xk} - u'_{xk})}{\Delta a} [F_{xj} + (1.5\pi - 4)F_{xi}] \quad (4)$$

where (F_{xi}, F_{yi}) and (F_{xj}, F_{yj}) represent the nodal forces at nodes I and J, respectively; and (u_{xk}, u_{yk}) and (u'_{xk}, u'_{yk}) represent the nodal displacements behind it as shown in Figure 3. The total energy release rate is the sum of G_I and G_{II} . In this study, the modified virtual crack closure integral was used to calculate the bond fracture energy G_f of FRP bonded concrete specimen.

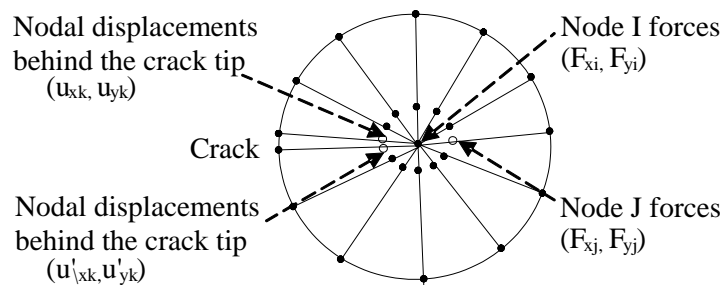


Figure 3: Nodes and elements generated around the crack tip in FE model for energy release rate analysis.

Figure 1 was used to build the geometric model in FE analysis. The dimension of the concrete specimen was 76 x 76 x 191 mm. The width of CFRP plate was 51 mm and the thickness of it was 2 mm. The ultimate tensile strength and tensile modulus in the principal fiber direction were 2.02 GPa and 139 GPa, respectively. The tensile modulus and tensile strength of the epoxy adhesive used in the study were 3.18 GPa and 72.4 MPa respectively. The crack length was set as 33 mm which was the typical first crack length in the tests. The load recorded in the test was applied to the FE model. The RTC, which is the distance from nominal bond line to the crack in FE models, was calculated by Equation 2 for different IRRH values. Ansys 10.0 was used to do finite element analysis and Plane 183 element was selected to mesh the geometric model. All materials were assumed to be linear elastic. It was found that materials' moduli did not have significant effect on G_f for linear elastic analysis (Wan and Ouyang, 2006). Therefore, the material properties change due to moisture attack was not considered in this research.

4. NUMERICAL RESULTS AND DISCUSS

The FEM and experimental results of bond fracture energy G_f is plotted versus residual thickness of concrete as shown in Figure 4. It is shown that the FEM results had excellent agreement with the experimental data. The G_f value decreased with the decrease of RTC value. When the fracture location was moved closer to the bond line (RTC = 0), G_f was significantly lower than that of control specimens. This phenomenon is consistent with the common experimental result that adhesive failure has lower bond strength than cohesive failure. It can also be seen in Figure 4 that slope of the trend line changed around the RTC value of 1.5 mm. When RTC was less than 1.5 mm, the G_f value was very sensitive to the change of RTC value. However, the increase of RTC did not result the significant increase of G_f when RTC was greater than 2 mm.

The relation between bond fracture energy and interface region relative humidity is shown in Figure 5. When IRRH was smaller than 55%, there was no significant change in fracture energy. The FEM result with RTC value of 2.0 mm showed good approximation for this stage. When IRRH was larger than 55%, the reduction of fracture energy

with the increase of IRRH was very obvious. As shown in Figure 5, the FEM results agreed well with the experimental data although the G_f values calculated from FEM were slightly larger than the corresponding experimental results. This was due to the local nonlinearity at the crack tip while the finite element model was based on linear elastic fracture mechanics. Figure 5 shows a nonlinear relation between RTC and fracture energy although the linear relation was assumed between RTC and IRRH in Equations 1 and 2. When the interface was relatively dry (IRRH < 55%), the G_f kept relatively constant. G_f value decreased significantly with the increase of IRRH when it was higher than 55%.

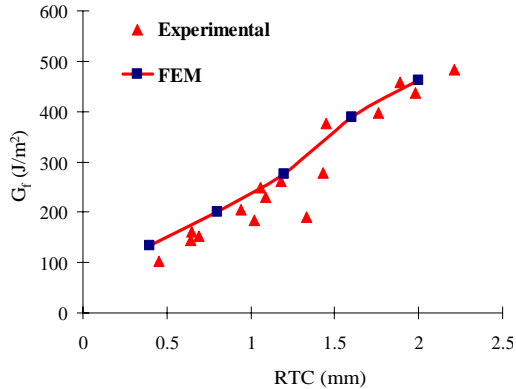


Figure 4: G_f vs. RTC

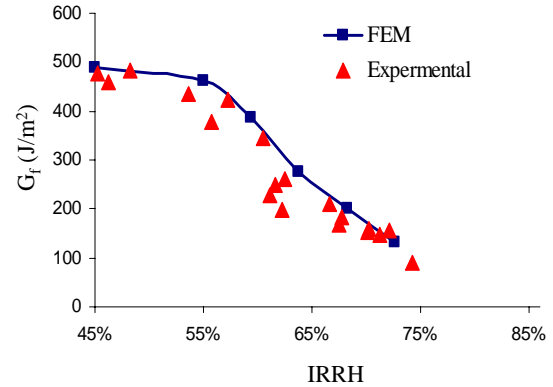


Figure 5: G_f vs. IRRH

5. CONCLUSION

A constitutive equation was proposed in this research to calculate the residual thickness of concrete (RTC) from the value of interface region relative humidity (IRRH). Using this equation and finite element models, the relation between bond fracture energy and the IRRH of the FRP bonded concrete specimens was successfully established.

6. REFERENCE

- Coronado, C.A. and Lopez, M.M. (2005). "Modeling of FRP-concrete bond using nonlinear damage mechanics", *Proceedings of the 7th Conference on Fiber Reinforced Polymers for Reinforced Concrete Construction (FRPRCS7)*, Kansas City, U.S., pp 411-426.
- Karbhari, V.M., Engineer, M. and Eckel II, D.A. (1997). "On the Durability of composite rehabilitation schemes for concrete: use of a peel test", *Journal of Material Science*, Vol. 32, 1997, pp147-156.
- Kinloch, A.J. (1987). *Adhesion and Adhesives - Science and Technology*, Springer, Germany.
- Nguyen, T., Byrd, W. E., Alsheh, D., Aouadi, K., Chin, J. W. (1998). "Water at the polymer/substrate interface and its role in the durability of polymer/glass fiber composites", *Durability of Fibre Reinforced Polymer (FRP) Composites for Construction (CDCC'98), 1st International Conference*, Canada, pp451-462.
- Ouyang Z. and Wan. B. (2006). "Deterioration mechanism of bond between CFRP plate and concrete in moisture environment", *Third International Conference on FRP Composites in Civil Engineering (CICE 2006)*, Miami, Florida, USA.
- Sethuraman, R. and Maiti, S.K. (1988). "Finite element based computation of strain energy release rates by modified crack closure integral," *Engineering Fracture Mechanics*, Vol. 30, pp 227–231.
- Wan, B., Petrou, M.F. and Harries, K.A. (2006). "Effect of the presence of water on the durability of bond between CFRP and concrete", *Journal of Reinforced Plastics and Composites*, Vol. 25, No. 8, pp875-890.
- Wan. B. and Ouyang Z. (2006). "Finite element analysis of FRP debonding from concrete undergoing global mixed mode I/II loading", *Third International Conference on FRP Composites in Civil Engineering (CICE 2006)*, Miami, Florida, USA.

NUMERICAL STUDY ON MASONRY LOAD BEARING WALLS RETROFITTED WITH GFRP COMPOSITES

Prakash, S.S

(Graduate Research Assistant, University of Missouri Rolla, Rolla, Missouri, USA)

Alagusundaramoorthy, P

(Associate Professor, Indian Institute of Technology Madras, Chennai, Tamil Nadu, India)

ABSTRACT

The failure of masonry buildings due to earthquakes is because of its low tensile and shear resistance. To improve the strength and enhance the seismic performance of masonry structures, retrofitting using fiber reinforced polymer (FRP) composites is explored in this study. Characterization of materials and finite element analysis (FEA) are carried out. Homogeneous macromodeling using the smeared crack concrete model is adopted for the analysis of load bearing brick masonry walls under inplane loading. The resistance of the masonry walls is studied for a shear specimen with an aspect ratio (*length/height*) of one and a flexure specimen with an aspect ratio of two. Effects of different strengthening techniques like X-bracing, full-surface-bonding, and two-end-strap coating using FRP composites are studied using the developed model based on the failure pattern of control specimens. Parametric studies are also carried out to study the effect of vertical compression, and the results are discussed. It is concluded that the effectiveness of FRP in increasing the lateral strength of masonry is based on the compressive strength of masonry.

KEYWORDS

Masonry, load bearing walls, FRP composites, retrofitting, finite element modeling

1. INTRODUCTION

Brick masonry is a heterogeneous material with orthotropic mechanical characteristics that depend not only on the properties of the brick unit and mortar but also on their interaction (Lourenco, 1996). In general, models for masonry are categorized into homogeneous models and heterogeneous models. In a homogeneous material model, the behavior of masonry is modeled by a fictitious material having properties that are equivalent to the material behavior of brick masonry. In the heterogeneous model, the bricks and mortar are modeled through their respective constitutive laws with the interaction in between them (Page, 1978). Both homogeneous and heterogeneous models can be based on either smeared crack or discrete crack approaches (Lofti and Shing, 1991). However, the latter involves large computational effort. Giordano et al (2002) studied the behavior of masonry with macromodeling techniques using a smeared crack concrete model and found good correlation with the experimental results. In this study, macro modeling is adopted for the analysis of load-bearing masonry due to its simplicity and practical significance. The effect of different strengthening techniques like X-bracing, full-surface-bonding, and two-end-strap coating using FRP composites on the behavior of masonry load bearing specimens are studied, and the results are discussed.

2. CHARACTERIZATION OF MATERIALS

Tests were conducted to determine the strength and elastic properties of bricks, cement mortar cubes, brick masonry wallets, and shear triplets. The material parameters for FRP composites were found through testing of coupons for tension, shear, and flexure. A FE model of a masonry load bearing wall is developed and calibrated with the experimental test data of a load bearing wall subjected to a vertical compression of 0.55 N/mm^2 .

3. NUMERICAL STUDY

The smeared crack concrete model available in ABAQUS/Standard uses the concepts of oriented damaged elasticity (smeared cracking) and isotropic compressive plasticity to represent the inelastic behavior of concrete. The model is

defined by using the uniaxial stress-strain relations, tension stiffening data from the uniaxial tension test results, and optionally by defining the shear retention and the failure ratios options. This model can be used for plain concrete or masonry, even though it is intended primarily for the analysis of reinforced concrete structures.

3.1 Material Properties for Modeling

Material properties of brick masonry are obtained from the testing of brick masonry wallettes of size 400 mm x 400 mm under compression. The modulus of elasticity for the numerical study is calculated from the test data as 168 N/mm^2 in the direction normal to the bed joints and 405 N/mm^2 parallel to the bed joints. The Poisson's ratio for the masonry material is normally around 0.15 to 0.2, and it is taken as 0.2. For the plastic part of the model, the parameters are taken from the nonlinear part of the uniaxial compression stress-strain curve (stress and corresponding absolute plastic strain). Tension stiffening data is the post cracking behavior under uniaxial tension, and the parameters for input are a fraction of the remaining stress to stress at cracking and the corresponding absolute value of the direct strain minus the direct strain at cracking. FRP material used for retrofitting is glass fiber woven roving mat (WRM) with an area density of 360 gsm. FRP composite is modeled assuming elastic behavior through lamina option (Hibbit et al, 2002). The tensile strength of the laminate was determined as per procedures given in BS 2782 (1996). The average modulus of elasticity in tension is found to be $E_x=12984 \text{ N/mm}^2$ in the warp direction and $E_y=11500 \text{ N/mm}^2$ in the weft direction. The Poisson's ratios ν_{xy} and ν_{yx} are found to be 0.126 and 0.112 respectively. Perfect bond is assumed to exist between the FRP material and the masonry wall surface. FE studies assume no debonding of the FRP from masonry. It is assumed that premature debonding failure of FRP will be prevented by suitable anchorage of FRP composites with masonry walls.

3.2 Description of Finite Element Model

In the test setup, the wall is placed on a rigid concrete foundation beam, which is connected to the laboratory floor by high strength steel anchored bolts. The vertical compression is applied through pretensioned high strength steel strands. The cyclic or monotonic lateral load is applied to the side of the loading beam by an actuator anchored against a strong wall. Brick masonry wall panels of sizes 2500 mm x 2500 mm x 230 mm and 1250 mm x 2500 mm x 230 mm are used as shear and flexural specimens in FE study. The shear specimen is supported on a concrete beam foundation of size 2700 mm x 230 mm x 200mm. The vertical and horizontal loading is applied on the top face of the wall. The flexural specimen is supported on a concrete foundation of size 1450 mm x 2500 mm x 240 mm. In the retrofitted and unretrofitted specimens, the concrete beams and the wall are modeled by eight noded linear continuum elements (C3D8R) with reduced integration and hourglass control. The FRP material is modeled using 3D shell elements (S4R) with both rotation and translations at each node. All specimens are loaded laterally on the top face of masonry wall by giving linearly increasing displacements. The vertical compression load is applied through different pressure loading of magnitudes 0.3 N/mm^2 , 0.55 N/mm^2 , 1.0 N/mm^2 and 2.0 N/mm^2 on the top face of the wall. The interface between the bottom foundation beam and the wall surface is modeled using surface-based tie constraints. The bottom of the foundation beam is given a fixed-end condition by arresting all the degrees of the freedom.

4. RESULTS AND DISCUSSION

The smeared crack concrete model adopted is verified with experimental data of a load bearing wall subjected to a vertical compression of 0.55 N/mm^2 . The prediction using the macromodel was found to be accurate enough when the uncertainties associated with the derived material properties and the advantages of reduction in the computational cost compared to a detailed micromodel are taken into account. The FE result underestimated the stiffness of the test specimen but the maximum load resistance predicted is in close agreement (Fig. 1). The failure of the test specimen was by diagonal cracking, and the same was observed in FE analysis. After the validation of the FE-model, as a parametric study, two types of load bearing walls (namely, flexure and shear specimens) are analyzed for different constant vertical compressions with monotonic lateral loading. Based on the results of the FE analysis, two types of retrofitting strategies are suggested for both the specimens (Fig. 2). The shear specimen is retrofitted using (i) X-bracing of FRP strips and (ii) a full-surface bonding of FRP composites. The flexural specimen is retrofitted using (i) two-end-strap coating and (ii) a full-surface bonding of FRP composites. After the retrofitting, the increases in load resistance and displacement levels are calculated and compared with the behavior of the control specimen. The effect of vertical compression with lateral loading on the load resistance is also studied.

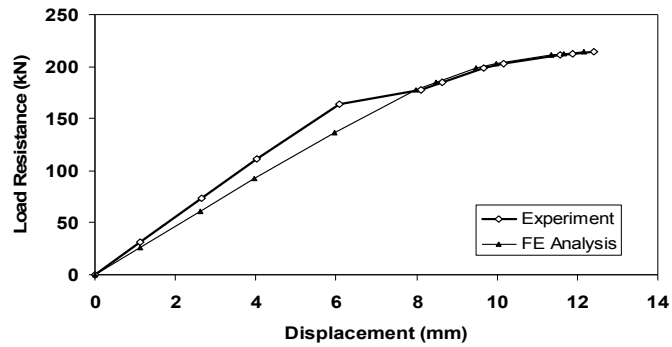


Fig. 1 Comparison of FE Results of a Load Bearing Wall with Experimental Data

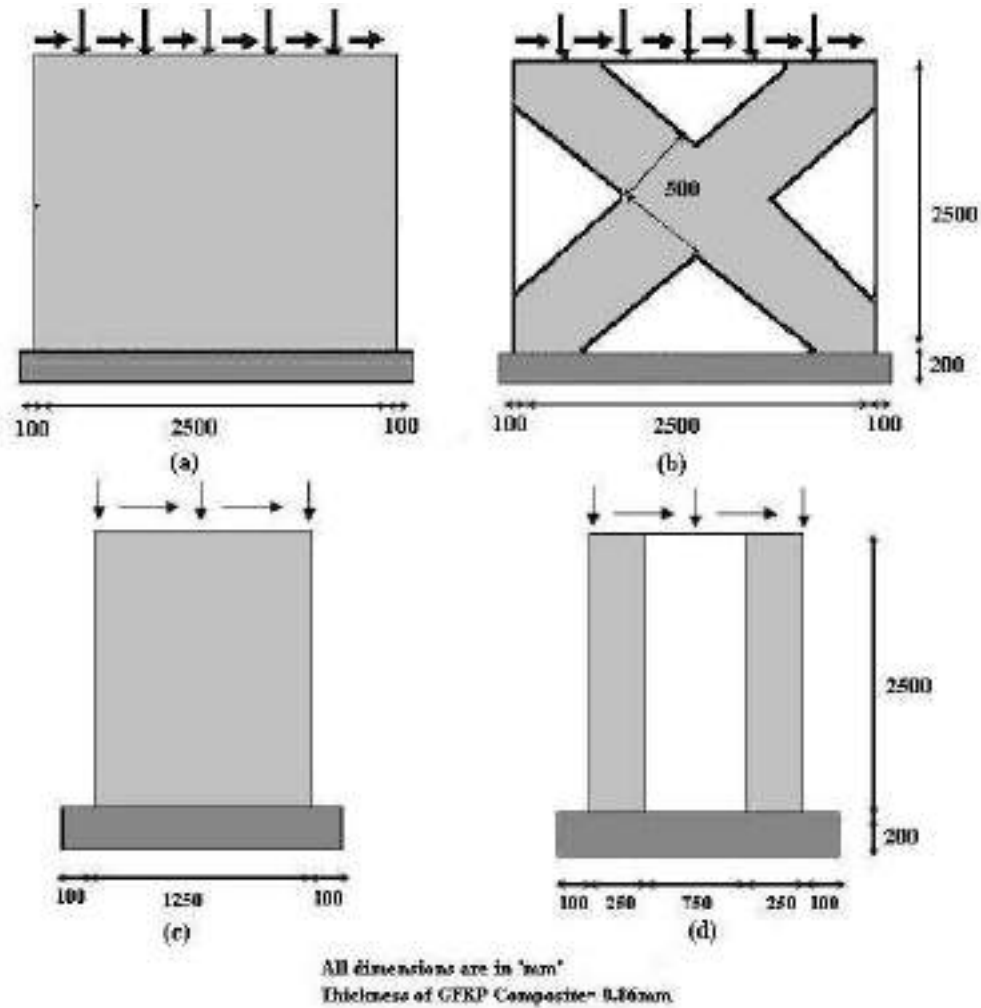


Fig. 2 (a) Full Surface Bonding for Shear Specimen (b) X-Bracing for Shear Specimen (c) Full-Surface Bonding for Flexure Specimen (d) Two-End-Strapping for Flexure Specimen

4.1 Shear Specimen

In the shear specimen, strut action along the compression diagonal is observed. The load resistance increases linearly up to 26.8 kN (Fig. 3a). Thereafter, the load shedding is observed. With increase in the vertical compression, the ultimate load resistance also significantly increases. In the case of vertical compression of 1.0 N/mm², the load resistance increased from 26.8 kN to 160 kN. At vertical compression of 2.0 N/mm², the ultimate load resistance observed is 128 kN because of the compression failure of masonry. The ultimate load resistance in retrofitted shear specimen with X-bracing, increased from 26.8 kN to 94 kN (Fig. 3d). The first cracking load also increased from 25 kN to 44 kN. Significant increase exists in the load resistance for the X-

Bracing under vertical compression (Fig. 3b). For the vertical compression of 2.0 N/mm^2 , the increase in the load resistance is linear up to the final compression failure of the masonry. The ultimate load resistance increased from 26.8 kN to 271 kN (Fig. 3d). A gradual increase happens in the load resistance in the case of full-surface bonding due to the presence of vertical compression, unlike retrofitting with X-Bracing (Fig. 3c). In the case of a vertical compression of 2.0 N/mm^2 , the full-surface bonding of FRP prevented the compression failure of masonry and increased the ultimate deformation of masonry up to 60 mm , unlike in X-Bracing.

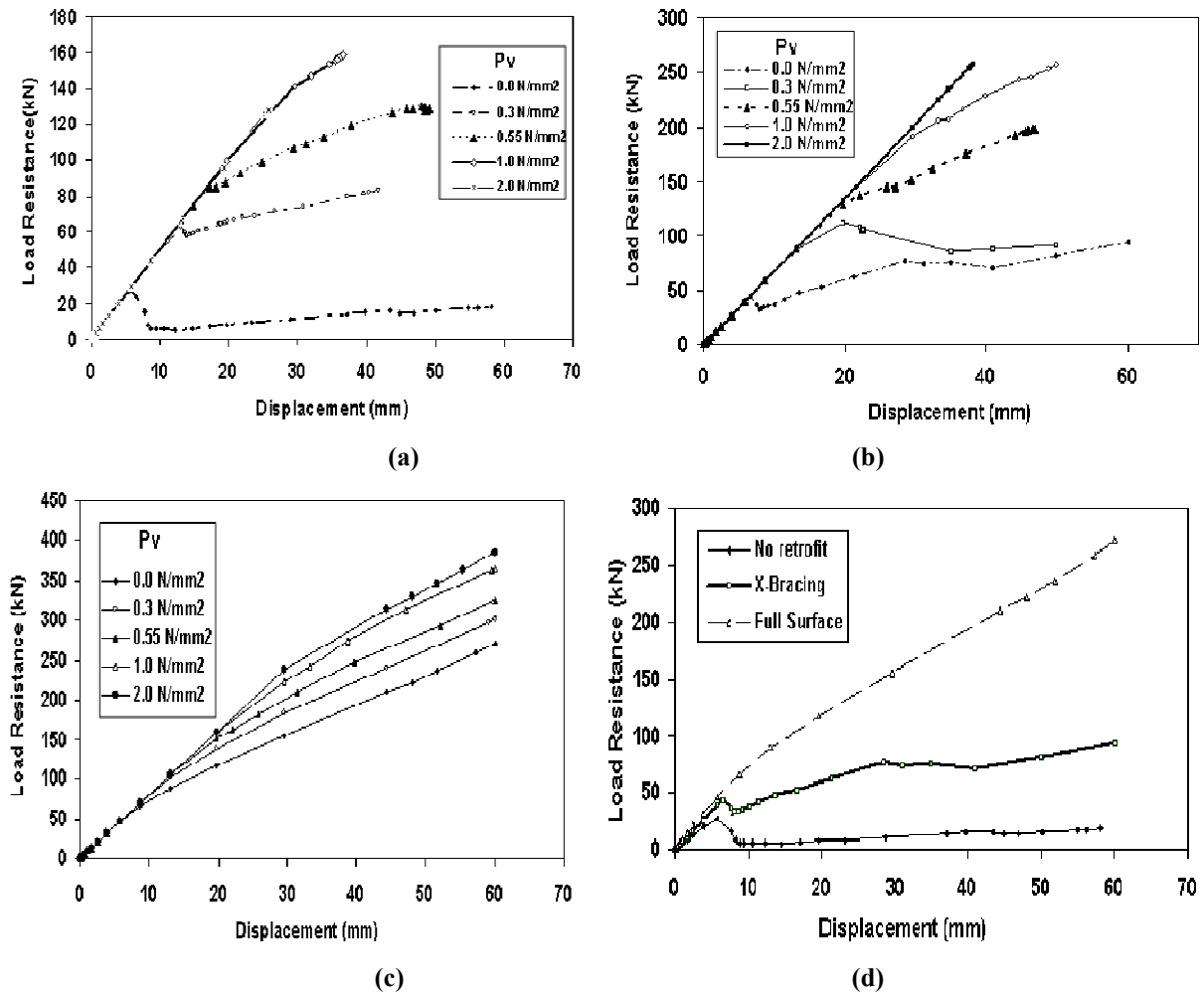


Fig. 3 Load Displacement Curves for (a) Control Shear Specimen (b) Retrofitted Specimen with X-Bracing (c) Retrofitted Specimen with Full-Surface Bonding and (d) Comparison of X-Bracing and Full-Surface Bonding with Control Shear Specimen

4.2 Flexure Specimen

The flexural specimen is retrofitted using (i) two end strap coating and (ii) a full surface bonding of FRP composites. For the flexural specimen without vertical compression the load resistance linearly increased up to 8 kN with corresponding displacement of 10 mm (Fig. 4a). Load shedding is observed after this load. The ultimate load resistance increased from 8 kN to 40 kN for the increase in vertical compression from 0 to 1.0 N/mm^2 . In the case of retrofitted flexural specimens with two end straps, the load resistance increased linearly up to a load of 18 kN with the corresponding displacement of 10 mm (Fig. 4b). Due to retrofitting with end straps the ultimate resistance increased from 18 kN to 36 kN , corresponding to the ultimate displacement of 48 mm for the unretrofitted specimen (Fig. 4d). For two-end strapping, due to vertical compression, a gradual increase happens in the load resistance as well as in the cracking displacement. In the case of the retrofitted flexural specimen with full-surface bonding of FRP, the load displacement response is stiffer compared to the control specimen, and the ultimate load resistance increased from 8 kN to 58 kN (Fig. 4d). Due to vertical compression, a gradual increase happens in the load resistance as well as in the cracking displacement (Fig. 4c). The increase in the ultimate displacement (60 mm) was higher compared to that of the control flexure specimen, which had ultimate displacement of 46 mm . This result shows that full-surface retrofitting with FRP increases the ductile behavior of the flexure specimen.

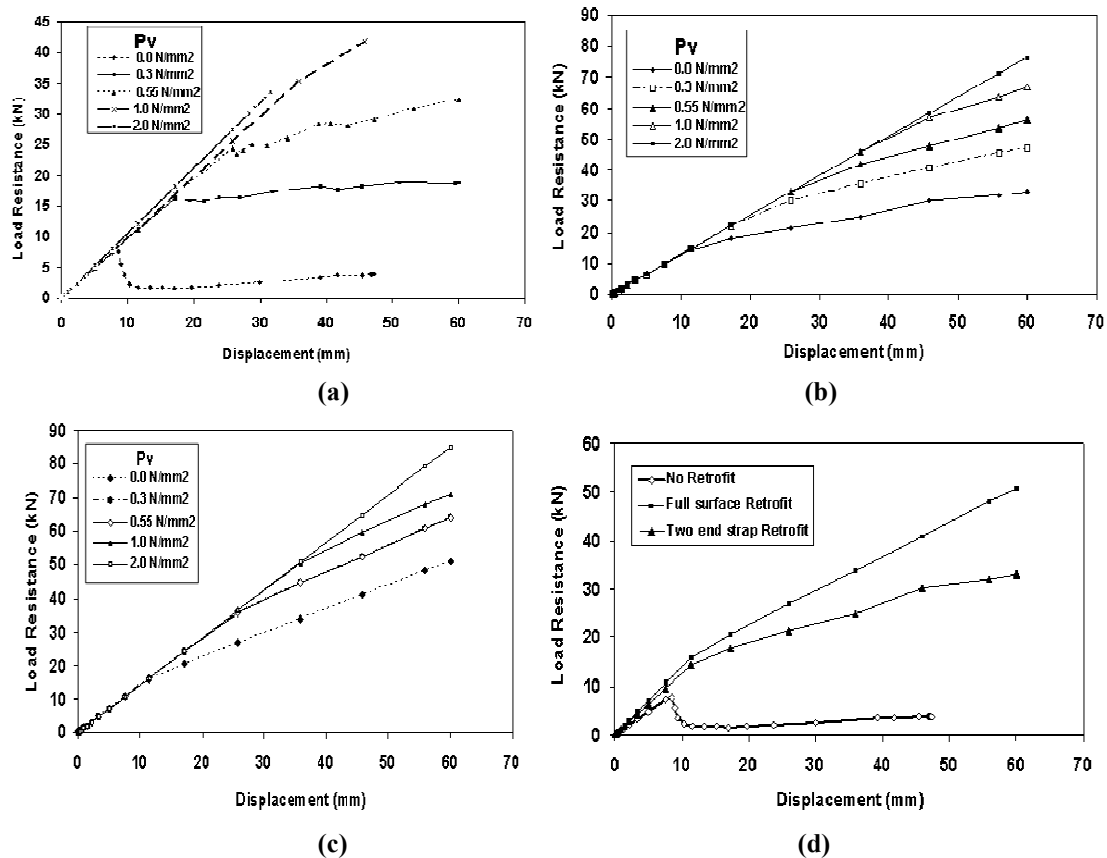


Fig. 4 Load Displacement Curves for (a) Control Flexure Specimen (b) Retrofitted Specimen with Two-End Straps (c) Retrofitted Specimen with Full-Surface Bonding and (d) Comparison of Two-End Strapping and Full-Surface Bonding with Control Flexure Specimen

5. SUMMARY AND CONCLUSIONS

Two types of load bearing wall specimens (namely, flexure and shear) were analyzed for different constant vertical compressions with monotonic lateral loading. Based on the analysis, two types of retrofitting strategies were suggested for both the specimens. The flexural specimen was retrofitted using (i) two-end strap coating and (ii) a full-surface bonding of FRP composites. The shear specimen was retrofitted using (i) X-bracing and (ii) a full surface bonding of FRP composites. Retrofitting using FRP composites was observed to increase the load at first crack and the ultimate load. For the flexure specimen, a significant change was noticed in ultimate load resistance when retrofitted with two-end straps and full-surface bonding. However, the increase in ultimate displacement was high in case of full-surface bonding, thereby increasing the ductile behavior of the specimen. For shear specimen, the ultimate load resistance increased from 26.8 kN to 271 kN, and the increase in ultimate displacement was from 50 mm to 60 mm for the shear specimen retrofitted with full surface bonding. Based on the results, the following major conclusions are drawn: (i) FRP composites significantly increase the load at first crack, ultimate load and deformational capacity, (ii) The effectiveness of FRP in increasing the lateral strength of masonry depends on compressive strength of masonry, and (iii) Small amounts of vertical compression significantly increase the load at first crack and ultimate load.

6. REFERENCES

1. Lourenco, P.B. (1996). "Computational strategies for masonry structures." TU-Delft, ISBN 90-407-1221-2.
2. Page, A.W. (1978). "Finite element model for masonry." *Journal of structural division*, 104(8), 1267-1285.
3. Lofti, H.R., Shing, P.B. (1991). "An appraisal of smeared crack models for masonry shear wall analysis", *Computers and Structures* 41(3), 413-425.
4. Giordano, A., Mele, E. and De Luca, A. (2002). "Modeling of historical masonry structures: comparison of different approaches through a case study", *Engineering structures*, 24(2002), 1057-1069.
5. Hibbit, D., Karlson, B. and Sorensen, P. (2002). ABAQUS/ Standard theory manual.
6. BS 2782-10: Method 1006. Methods of testing plastics, glass reinforced plastics: determination of tensile properties, 1996".

MODELLING OF RC SQUARE HOLLOW PIERS WRAPPED WITH CFRP

Gian Piero Lignola, Andrea Prota, Gaetano Manfredi and Edoardo Cosenza

(Dept. of Structural Analysis and Design, University of Naples Federico II, Naples, ITALY)

ABSTRACT

A large number of concrete bridges built in Europe were characterized by Reinforced Concrete (RC) hollow piers; many of them are now in need of a seismic upgrade to improve their response under severe earthquakes. Researchers have mainly focused their attention on solid piers; few studies have been done about hollow cross sections. To study the behaviour of rectangular hollow piers subjected to combined axial load and bending, a total of 7 specimens have been tested. The strengthening was performed by Carbon Fiber Reinforced Polymers (FRP) wrapping. Planned tests have allowed to improve the knowledge of unstrengthened hollow rectangular piers and to provide a contribution towards the comprehension of the resistant mechanisms of hollow piers in presence of FRP confinement. The experimental results and the related database has been used for validation of CFRP strengthening design methods for hollow cross sections and for assessment of potential extension of the current models available for solid sections to non-circular hollow sections. Strengthened and unstrengthened members have been numerically modelled. The results of the present work suggest that a reliable numerical procedure to predict hollow cross section behaviour under combination of flexure and compression should include appropriate models for compressed bars buckling and concrete cover spalling.

KEYWORDS

Concrete columns, Buckling, FRP confinement, Hollow sections, Modelling

1. INTRODUCTION

To maximize structural efficiency of the strength-mass and stiffness-mass ratios and to reduce the mass contribution of the pier to seismic response and high carrying demand on foundations, it is desirable to use hollow cross sections. However modern codes of practice oriented to new design do not recognize any specific problem related to hollow sections. A large number of existing bridges have hollow piers. Many of them are now in need of a seismic upgrade but few researches have been done on hollow columns strengthened with Fiber Reinforced Polymers (FRP). Hollow reinforced piers may be required to dissipate energy by forming ductile plastic hinges when they are subjected to seismic forces while, due to its brittle nature, failure in shear of Reinforced Concrete (RC) bridge piers has in any case to be avoided. Research programs have mainly addressed the behaviour of solid columns with either rectangular or circular cross sections and have shown how FRP confinement can play a significant role in constraining the concrete core and consequently improving flexural strength and ductility and adding additional reinforcement in the hoop directions, increasing also shear strength, such reducing seismic vulnerability. It can be seen that jacket thicknesses for shear, bar buckling restraint and lap splice clamping are driven by the modulus of the jacket in the hoop direction, which favours higher modulus materials, whereas the flexural plastic hinge confinement can also efficiently be achieved with a lower modulus material. Simple calculations procedures for the assessment of strength and deformations capacity of existing bridge have been proposed in last years, but their reliability has been checked mainly on columns with solid sections; their extension to those hollow (Fam and Rizkalla 2001), especially rectangular, has been much less investigated.

Fam et al. (2005) tested under flexure rectangular concrete-filled FRP tubes with inner void and fibers oriented in several directions (not only transverse). No reinforcement was provided other than the outer FRP shell. Buckling of the FRP not only reduced the effectiveness in carrying compression forces, but eliminated any partial confinement effect on the thin compression concrete inward buckling and cracking.

2. RESEARCH OBJECTIVES

This paper focuses on the upgrade and retrofit of existing RC piers with rectangular hollow cross section using FRP composite materials applied in the transverse direction (only confinement) to enhance flexural strength and ductility. The research aimed at investigating the behaviour of unstrengthened and FRP jacketed square hollow piers subjected to combined axial load and bending un-coupled from shear; therefore, slender specimens were investigated. The capability of external wrapping using FRP materials to change the failure mode was checked and modelled.

3. SUMMARY OF THE EXPERIMENTAL PROGRAM

A total of 7 hollow square cross section concrete columns were tested. Test specimens reproduce in scale 1:5 typical bridge piers (Fig. 1a). The test matrix was designed in order to assess the FRP wrapping effectiveness in correspondence of three P/M ratios. Accordingly three unstrengthened specimens (U1, U2 and U3) and other three strengthened with CFRP laminates (S1, S2 and S3) were tested with a load eccentricity and kept constant during each test. A total of 2 plies of CFRP wet lay-up unidirectional fabric (600 gr/m^2) have been applied in the transverse direction in all strengthened specimens for the entire specimen height. The number of installed plies was considered an upper limit that could be derived from an economical and technical analysis, also accounting for the scale reduction. However jacket thickness modestly affects the response of non-circular sections (Fam et al. 2005). One unstrengthened specimen under pure axial load was also tested. Details on the experimental program and outcomes can be found in (Lignola et al. 2006), herein only results relevant for the numerical comparison will be summarized.

4. REFINED ANALYSIS OF THE CROSS SECTION BEHAVIOUR

Through the use of a fiber model that meshes the concrete cross-sectional geometry into a series of discrete strips, sections of completely arbitrary cross-sectional shape (including hollow prismatic cross sections) can be modeled. Each discrete strip is assumed to have a constant stress. For a specified neutral axis location and a specified section curvature (given a reference strain in a given point of the cross section and with neutral axis known) internal section forces are computed (Fig. 1b).

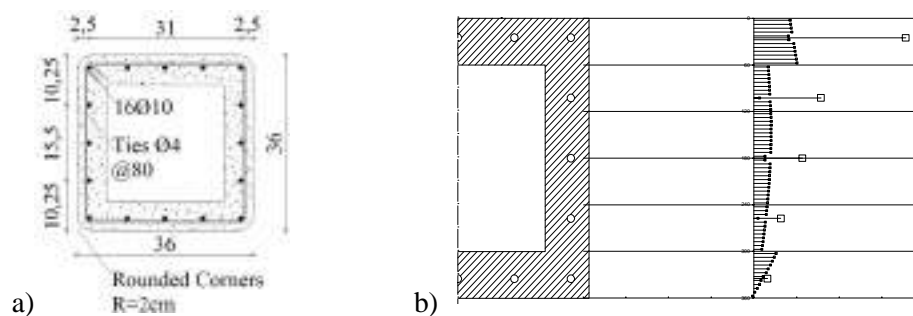


Figure 1: Cross Section Geometry (a), Cross Section meshing and forces equilibrium (b)

The neutral axis position is changed until the net internal axial force in the section is in equilibrium with the externally applied axial load acting on the section, then the internal section flexural moment is computed and the corresponding moment curvature diagram is plotted. Perfect bond is assumed at the interfaces between concrete and steel reinforcing bars; plate buckling (as local buckling of a thin compression flange) is not accounted, so that the ultimate strength is generated by material failure and/or steel reinforcement bar buckling. Tension stiffening effect, compressed bars buckling, concrete cover spalling and FRP confinement of concrete are included in the model.

When steel reinforcement reaches in compression the buckling stress, as it pushes outward surrounding concrete, the concrete cover spalls out. The spalling of concrete cover and the buckling of the reinforcement is taken into account by not considering a portion of the concrete cover area in the equilibrium. In the case of member wrapped with CFRP the steel bars push internal concrete cover in the inward direction (in the hollow part) when they start buckling and in the numerical model concrete cover spalling has been simulated by discarding a portion of the internal concrete cover area.

4.1 Material Constitutive Laws

The numerical method uses nonlinear stress-strain relationships for concrete and steel. A reliable stress-strain behaviour of concrete is necessary particularly when a member is subjected to combined bending and axial load. The theoretical analyses have been carried considering four constitutive models for concrete. For the unstrengthened members the Mander model (1988) and the Model Code (1990) were adopted for concrete combined with the size effect theory after Hillerborg (1989). To simulate the effect of the FRP confinement a simplified approach was used to obtain a preliminary assessment of the behaviour of the FRP confined members. Spoelstra-Monti model (1999) and the model recommended by the CNR Italian Guidelines (2004) have been considered. The numerical stress-strain model (after Cosenza and Prota 2006) was used for the reinforcing steel bars under compression. Analyzing the failure mode of eccentrically loaded columns, the more compressed wall is considered confined by FRP. The transverse dilation of the compressive concrete walls stretches the confining device, which along with the other restrained walls applies an inward confining pressure. The effective pressure f'_1 is reduced by a reduction factor k_{eff} due to the so-called arching effect in the wall. The reduction factor is given by the ratio of the effective confinement area, the core of the walls, to the total area of concrete enclosed by the FRP jacket; in the present case is $k_{eff}=0.69$ and confinement is evaluated on an equivalent circular column of a diameter D equal to the average (longer) side length ($D \approx 300\text{mm}$). The ultimate compressive axial strain of FRP-confined concrete is considered to be attained when lateral strain is equal to FRP ultimate strain; however experimental evidence shows that FRP failure did not occur. It is noted that the Spoelstra-Monti model is rather more conservative than CNR. This algorithm allowed to draw the theoretical P-M interaction diagram (Fig. 2a), moment-curvature diagrams (Fig. 2b) and theoretical strain development during load history.

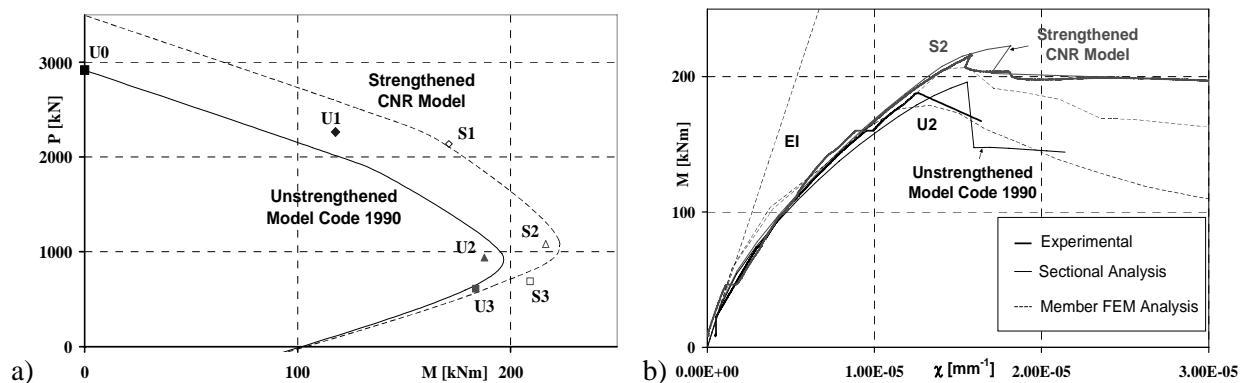


Figure 2: P-M interaction diagram and experimental outcomes (a), Flexural Moment vs. Curvature Diagram (experimental U2/S2 and theoretical $e=200\text{mm}$) (b)

4.2 Experimental-Theoretical Comparison

The developed refined methodology with the selected material models and the assumptions made seems to predict both the sectional strength and deformability of the hollow columns. The strength increase of FRP confined columns with respect to the unstrengthened columns is about 15%. Wrapping has delayed buckling of steel longitudinal reinforcement and concrete cover spalling, allowing for the full development of the load capacity of the concrete. The beneficial effect of confinement increases as the compressed part of the cross-section increases. The strength increase is about 7% in the case of larger eccentricity and 19% in the case of smaller eccentricity (see also P-M diagram in Fig. 2a), while a gradually more ductile behaviour when increasing the eccentricity has been observed. The bar buckling brittle mechanism acting together with internal concrete cover spalling has been modelled and the predicted post peak behaviour is consistent with the experimental observation. The ascending branch is very well predicted by numerical model, and curve drop was generally attained (in the numerical analysis the concrete cover spalls and pier response deteriorates when compressed steel reinforcement reaches buckling strain).

5. FEM ANALYSIS OF THE MEMBER BEHAVIOUR

One of the aims of this study was to develop finite-element models (FEM) that could simulate the behaviour of tested specimens, evaluate and confirm the FRP confinement effect. An accurate analysis has been performed using

the multipurpose finite-element analysis software DIANA v9.1, which can handle non-linear concrete behaviour. The columns were modelled by 15520 eight-node, three-dimensional solid brick element, and the steel embedded reinforcement by 1568 two-node truss elements, while the FRP confinement by 6531 three-node plane bonded elements (Fig. 3a). In the FEM the concrete is modelled according to a Total Strain Rotating crack model with linear softening in tension and Thorenfeldt curve in compression. Steel reinforcement is ideally elasto-plastic, while FRP is modelled as an elastic material. It is remarked that at date the FEM analysis does not take into account reinforcement buckling and concrete cover spalling, but only concrete cracking and plasticity. A comparison of FEM results and refined section modeling with experimental outcomes for both U2 and S2 is plotted in Fig. 2b. Fig. 3b shows the crack pattern at peak load for U2 specimen that is consistent to the experimental data. Fig. 3c depicts the FRP strain ascending branch evolution for S2 specimen compared to experimental.

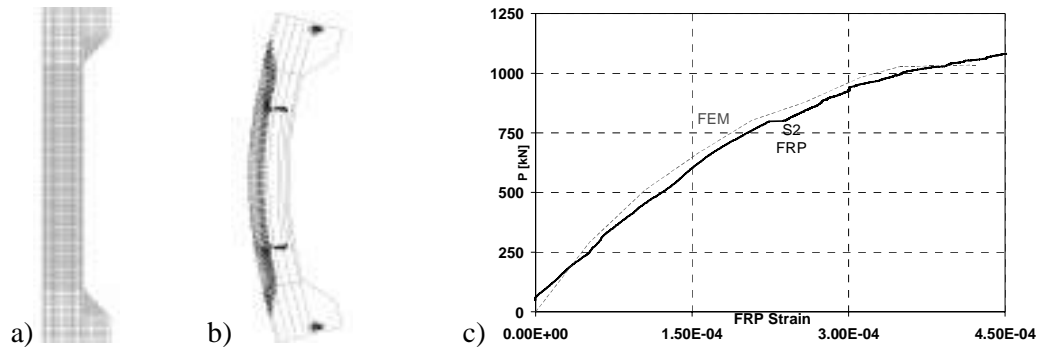


Figure 3: F.E.M. model (a), Crack pattern at peak load U2 (b), S2 FRP strain development (exp. vs. FEM) (c)

6. CONCLUSIONS

The present work is included into a wider activity that aims to improve the knowledge and develop an effective design method for fast strengthening of hollow bridge columns so that bridge function can be quickly restored. The presented numerical procedure to predict hollow cross section behaviour under combination of flexure and compression included appropriate models for compressed bars buckling and concrete cover spalling, because the failure of unstrengthened members is strongly affected by the occurrence of these premature mechanisms; the FRP confinement allows delaying these mechanisms thus resulting in both strength and ductility increases of members even under large eccentricities. The occurrence of these mechanisms has been modelled and the results of experiments and theoretical and FEM analyses show that a good agreement was achieved between the experimental outcomes and the analytical calculated results.

7. REFERENCES

- CEB-FIP Model Code 1990, "Design Code". *Comité Euro-International du Béton*, Lausanne, Switzerland, Telford.
- CNR-DT 200 (2004) "Guide for the Design and Construction of Externally Bonded FRP Systems for Strengthening Existing Structures". *Roma – CNR*
- Cosenza E and Prota A (2006) "Experimental Behavior and Numerical Modelling of Smooth Steel Bars under Compression", *Journal of Earthquake Engineering*. In press.
- Fam, Amir Z. and Rizkalla, Sami H. (2001) "Confinement Model for Axially Loaded Concrete Confined by FRP Tubes," *ACI Structural Journal*, 98(4):251-461.
- Fam, A., Schnerch, D. and Rizkalla, S. (2005) "Rectangular Filament-Wound GFRP Tubes Filled with Concrete under Flexural and Axial Loading: Experimental Investigation", *Journal of Composites for Construction*, 9(1):25-33.
- Hillborg A. (1989) "The compression stress-strain curve for design of reinforced concrete beams". *Fracture Mechanics: Application to Concrete*, ACI SP-118:281-294.
- Lignola GP, Prota A, Manfredi G and Cosenza E. (2006) "Experimental performance of RC hollow columns confined with CFRP". *ASCE Journal of Composites for Construction*. In press.
- Mander JB, Priestley MJN and Park R. (1988) "Theoretical stress-strain model for confined concrete" *ASCE Journal of Structural Engineering*, 114(8):1804-1826.
- Spoelstra MR, Monti G. (1999) "FRP-confined concrete model". *ASCE Journal of Composites for Construction*, 3(3):143-150.

PREDICTION OF FAILURE LOADS OF FRP PULTRUDED PROFILES USING CLOSED-FORM EQUATIONS

Linda M. Vanevenhoven

*(Graduate Research Assistant, Dept. of Civil and Environmental Engineering, University of Wisconsin, Madison,
WI 53706, USA)*

Carol K. Shield

(Professor, Dept. of Civil Engineering, University of Minnesota, Minneapolis, MN 55455, USA)

Lawrence C. Bank

(Professor, Dept. of Civil and Environmental Engineering, University of Wisconsin, Madison, WI 53706, USA)

ABSTRACT

FRP pultruded profiles having I-shaped sections are used as load bearing compression and flexural members in truss and frame structures. For design purposes closed form expressions are desired for predicting both global and local failure loads due to buckling or material rupture. A set of closed-form equations has been assembled from the technical literature for the prediction of the critical local and global failure modes of pultruded columns needed for design. A database of tests on pultruded columns conducted over the last 15 years and reported in the technical literature was used to verify the accuracy of the proposed theoretical equations. Only those test data for which the measured orthotropic material properties of the profiles tested were reported were considered. This paper presents comparisons between the theoretical equations and test data for wide-flange pultruded columns for two failure modes, local-flange buckling and global-flexural buckling. Insufficient test data exist in the literature on other profiles (such as narrow flange I beams or box sections) or for failure modes other than those noted. However, since most pultruded columns used are of the wide-flange profile type and have been shown to fail either in local or global buckling modes, the results presented are of practical importance. The paper also addresses the phenomenon of the interaction of local and global buckling modes for intermediate length columns. Ultimately, the results of this investigation will be used to develop resistance factors for a load and resistance factor design (LRFD) basis for pultruded columns.

KEYWORDS

Columns, Global buckling, Local buckling, Pultrusion, Wide-flange profiles.

INTRODUCTION

Wide-flange, pultruded, glass-reinforced FRP profiles are produced by a number of manufacturers in the US. They have geometries, ranging from depths of 4 inches to 12 inches and wall thickness of $\frac{1}{4}$ inch to $\frac{1}{2}$ inch. In these commonly produced profiles the height of the section, h , is equal to the breadth, b , and the wall thickness, t , is the same in the web and the flanges of the profile. The walls of these pultruded profiles typically contain alternating layers of E-glass rovings and continuous filament mats (CFMs). Profiles of polyester and vinylester resin systems are generally produced. Due to the proprietary fiber architectures used by different manufacturers, the profiles generally have different mechanical properties from manufacturer to manufacturer even though their geometric dimensions are nominally identical.

Over the last 15 years, a number of studies have been conducted to determine the failure modes of wide-flange pultruded columns. Concurrently, studies have been conducted to develop theoretical equations to predict the observed failure modes and loads. Recently, a set of these theoretical equations has been assembled and recommended for use for the design of pultruded columns (Bank, 2006). The equations are based on orthotropic plate theory and include the failure modes of local in-plane and shear buckling, global buckling, and material rupture. In this paper the equations presented in Bank (2006) for local flange buckling, global flexural buckling,

and their interaction are presented and comparisons are made with test data presented in the literature to verify the accuracy of these equations. The effect on the variability in the reported measured material properties of the profiles tested is also discussed. In order to judge the validity of the proposed expressions for global and local buckling of open pultruded sections, test results that did not include any measured material properties were discarded. Ultimately, 75 buckling tests meeting the criteria on sections including W12×12×½, W10×10×½, W10×10×¾, W8×8×½, W8×8×¾, W6×6×¾, and W4×4×¼ were identified (Mottram et al., 2003; Lane and Mottram, 2002; Scott, 1997; and Yoon, 1993).

To predict the global flexural buckling of pultruded columns the Euler buckling equation with a correction for shear deformation is recommended (Bank, 2006). Numerous investigators have proposed this equation to predict the global buckling load of “long” columns (Barbero and Tomblin, 1993; Zureick and Scott, 1997; Mottram et al., 2003). For global buckling about the minor axis of the wide-flange section, the following equations are used:

$$P_{global} = \frac{P_{euler}}{1 + \frac{P_{euler}}{k_s A_g G_{LT}}}; \quad P_{euler} = \frac{\pi^2 E_L I_{min}}{(kL)^2}; \quad k_s = \frac{A_f}{1.2 A_g}$$

where, P_{euler} is the Euler buckling load, k_s the shear coefficient (Scott, 1997), A_g the gross area of the cross section, G_{LT} the in-plane shear modulus of the pultruded material in the flanges, E_L the longitudinal modulus of the pultruded material in the flanges, I_{min} the second moment about the minor axis of the profile, k the end-restraint coefficient, and A_f the area of both flanges of the profile.

In recent years, numerous numerical and approximate equations have been proposed to predict local flange buckling in pultruded profiles (Mottram, 2004). The equation proposed by Kollár (2003) is recommended by Bank (2006). This closed-form equation is based on classical orthotropic laminated plate theory and includes an explicit method to determine the coefficient of restraint at the web-flange junction in the profile:

$$P_{local} = \sigma_{local} A_g; \quad \sigma_{local} = \frac{7}{(b_f/2)^2 t_f} \sqrt{\frac{D_L^f D_T^f}{1 + 4.12 \zeta_I} + 12 D_S^f}; \quad \zeta_I = \frac{D_T^f}{k_I (b_f/2)}$$

$$k_I = \frac{D_T^w}{d_w} \left(1 - \frac{(\sigma_{free}^{ss})_f E_L^w}{(\sigma_{ss}^{ss})_w E_L^f} \right); \quad (\sigma_{ss}^{ss})_w = \frac{2\pi^2}{t_w d_w^2} \left(\sqrt{D_L^w D_T^w} + D_{LT}^w + 2 D_S^w \right); \quad (\sigma_{free}^{ss})_f = \frac{4 t_f^2}{b_f^2} G_{LT}^f$$

where, σ_{local} is the in-plane buckling stress of one outstanding flange, b_f is the breadth of the profile (twice the flange breadth), t_f or t_w is the thickness of the flange or web, ζ_I is the flange coefficient of restraint, k_I is the web-flange junction rotational stiffness, d_w is the depth of the profile, σ_{free}^{ss} is the in-plane buckling stress of the flange

assuming no restraint at the web-flange junction, σ_{ss}^{ss} is the in-plane buckling stress of the web assuming it is simply supported at the web-flange junction. The wall flexural rigidities, D_L , D_T , D_{LT} , and D_S are given in terms of the orthotropic material properties, E_L , E_T , G_{LT} , ν_L , and ν_T , of either the web or the flange as,

$$D_L = \frac{E_L t^3}{12(1 - \nu_L \nu_T)}; \quad D_T = \frac{E_T t^3}{12(1 - \nu_L \nu_T)}; \quad D_{LT} = \nu_T D_L; \quad D_S = \frac{G_{LT} t^3}{12}$$

For columns of intermediate length, interaction between the local and global buckling modes (termed “combined buckling”) is thought to occur and has been observed in a small number of the tests considered in this paper (Mottram et al., 2003). To account for the interaction between local and global buckling, an equation has been proposed by Barbero and Tomblin (1994) as follows,

$$P_{cr} = k_i P_{local}; \quad \lambda = \sqrt{\frac{P_{local}}{P_{global}}}; \quad k_\lambda = \left(1 + (1/\lambda)^2 \right) / 2c; \quad k_i = k_\lambda - \sqrt{k_\lambda^2 - \frac{1}{c\lambda^2}}$$

where, P_{cr} is the critical buckling load, λ is a non-dimensional column length, and c is a curve-fitting parameter that is used to calibrate the interaction equation with experimental data. When $\lambda = 1$ the critical length is obtained where local and global buckling are predicted to occur at the same critical load. When $c = 1$ the second-order interaction equation reduces back to the two separate equations, one for local buckling ($P_{cr} = P_{local}$ which is length independent) and one for global buckling ($P_{cr} = P_{global} = P_{local} \lambda^2$).

DATA ANALYSIS

Three different failures were identified in the tests found in the literature: global buckling about the minor axis, local buckling, and “combined” buckling. Predictions for global buckling depend on both E_L and G_{LT} . Predictions

for local buckling depend on these two material properties, as well as E_T and ν_L . Because some of these tests were performed mainly to investigate global buckling, not every researcher measured every material property. Table 1 indicates which properties and dimensions were measured and reported by each researcher.

Table 1 Values measured through experimental investigation

Publication	E_L	E_T	ν_L	G_{LT}	t	d	b
Yoon (1993)	x	x	x	x	x	x	x
Scott (1997)	x	-	-	x	x	x	x
Lane & Mottram (2002)	x	-	-	-	x	x	x
Mottram et al (2003)	x	-	-	-	-	-	-

Material properties of pultruded sections vary among size and manufacturer, so different methods were used to estimate the missing data from each of the studies (Vanevenhoven, 2006). The tests done by Yoon (1993) and Scott (1997) were both performed at Georgia Institute of Technology, so it was assumed that the specimens were reasonably similar. Therefore, the Yoon data was used to help estimate reasonable E_T and ν_L for the Scott data.

Scott tested $W6 \times 6 \times \frac{3}{8}$ sections and $W4 \times 4 \times \frac{1}{4}$ sections. Yoon also tested $W6 \times 6 \times \frac{3}{8}$ sections; material properties for the Yoon section that best matched Scott's measured E_L were used for Scott's $W6 \times 6 \times \frac{3}{8}$. The values for the $W4 \times 4 \times \frac{1}{4}$ sections that Scott tested were estimated using the Yoon data assuming that the ratios between the needed properties and E_L were constant for the same manufacturer. Estimates for the non-measured properties for Lane & Mottram (2002) and Mottram et al. (2003) were determined by using other data from the literature on tests of similar sections (Bank et al., 1996) from the same manufacturer at approximately the same time period.

Figure 1 shows a plot of the experimental buckling load normalized by the predicted local buckling load as a function of λ with the theoretical curves using values of $c = 1$ (no interaction between local and global buckling), $c = 0.8$ as recommended by Bank (2006) and $c = 0.99$. In general, the tests that failed in global buckling (solid points) follow the curve predicted using $c = 1$ well, with the tests from Lane and Mottram, and Mottram et al. lying closer to the theoretical curve than those from Scott. Test-to-predicted ratios based on $c = 1$ for each reference are given in Table 2. The tests failing in local buckling (open symbols) show significantly more scatter than those that failed in global buckling. For small λ , a small number of half wavelengths was observed in the tests (typically 3 for the smallest λ and up to 7 for λ close to 1). When there are few half wavelengths, the effect of unwanted test end restraint could increase the measured local buckling load. The local buckle failures also have a higher test-to-predicted ratio. The other two tests, identified as "combined" failure, occurred at $\lambda \approx 1$ at a load close to the predicted local buckling load. These two tests have a lower test-to-predicted ratio than the tests that failed in local buckling, thus it may be possible that an interaction between global and local buckling caused the tests with the combined failures to fail prematurely. It also appears that the interaction between these buckling modes is limited to λ very close to 1, so using values of c around 0.99 would limit the affect of interaction on the theoretical predictions to λ very close to 1, as opposed to $c = 0.8$, which affects the curve between $0.2 < \lambda < 2$.

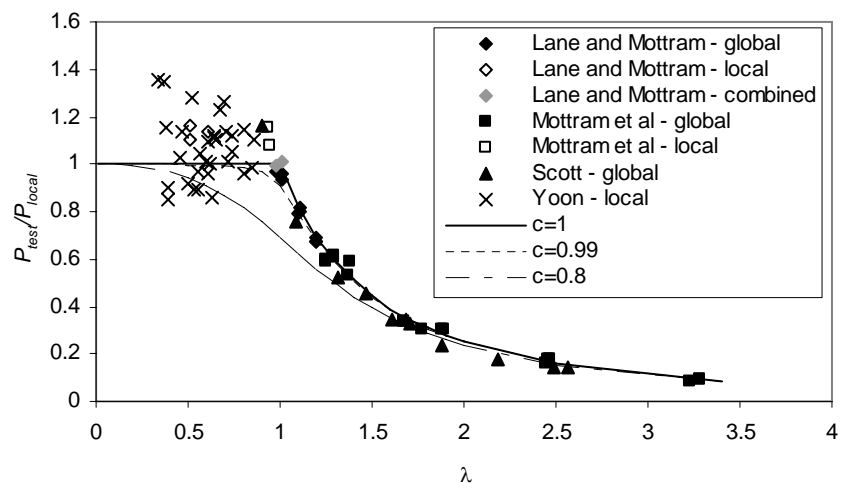


Figure 1 Nondimensional buckling load versus length

Table 2 Test-to-Predicted Ratios

	Global			Local			Combined		
	ave	COV	n	ave	COV	n	ave	COV	n
Lane&Mottram	0.97	2.0%	9	1.13	2.5%	3	0.98	4.1%	2
Mottram et al	1.01	6.2%	17	1.11	5.0%	2	---	---	
Scott	0.92	4.9%	11	---	---		---	---	
Yoon	---	---		1.07	12.9%	31	---	---	

Because measured material data from the exact columns tested was not available for all the tests, a sensitivity study was conducted using the column test data from Lane and Mottram to determine the sensitivity of the results to the non-measured material properties. Yoon (1993) found coefficients of variations (COVs) of 12.5% for E_T , 3.6% for ν_L and 12.7% for G_{LT} based on coupon tests. Using these COVs, the Lane and Mottram data was re-evaluated using transverse material properties two standard deviations higher and lower than the estimated mean. The results of this study are shown in Table 3. For the tests that failed by local buckling, changing the transverse material properties had a large impact on the predicted buckling loads. Increasing the E_T , G_{LT} , and ν_L by 2 standard deviations caused the predictions to go from conservative to unconservative. As expected, the effect of changing E_T , ν_L and G_{LT} on the predictions for the global buckling tests was much less significant, as the global buckling load is only slightly dependent on G_{LT} and not at all dependent on the other two properties. Because of the large impact of transverse material properties on local buckling, it may be possible to attribute the large variation in the Yoon data in Figure 1 to the variation in measured material properties that Yoon found, even within a single profile series.

Table 3 Test-to-Predicted Ratios for Lane and Mottram Data

E_T, ν_L, G_{LT}	Local		Global	
	ave	COV	ave	COV
-2 std dev	1.42	2.5%	0.98	1.9%
mean	1.13	2.5%	0.97	2.0%
+2 std dev	0.94	2.5%	0.97	2.0%

CONCLUSIONS

In general, the presented design equations yield good agreement with the available test data for the global and local buckling of pultruded GFRP columns, although very few complete sets of data exist. In the past, adequacy of the proposed theoretical equations for global and local buckling and their interaction have been investigated using measured buckling loads paired with nominal design material properties, or in some cases unspecified material properties. In order to determine the professional factor for a reliability based calibration of the design equations, the adequacy of the theoretical predictions must be evaluated using measured material properties. Different approaches to achieving safety in the design equations are also possible. Some have suggested adjusting the value of c in the interaction equation to achieve a lower bound design equation over the entire range of slendernesses (Barbero and Tomblin, 1994). An alternative approach would be to select a large value of c to account only for interaction between local and global buckling over a small range of slenderness ($0.9 < \lambda < 1.1$), and use a reliability based calibration of a resistance factor to provide the required safety.

ACKNOWLEDGEMENTS

Support for the first author from Universities of Wisconsin-Madison and Minnesota is gratefully acknowledged.

REFERENCES

- Bank, L.C. (2006). Composites for Construction: Structural Design with FRP Materials, Wiley, NY, Chapter 14
- Bank, L.C, Gentry, T.R., and Nadipelli, M., (1996) "Local Buckling of Pultruded FRP Beams - Analysis and Design," *Journal of Reinforced Plastics and Composites*, V15, No. 3, pp. 283-294.
- Barbero E.J. and Tomblin J. (1993) "Euler buckling of thin-walled composite columns," *Thin-Walled Structures*. V17, 237-258.
- Barbero E.J. and Tomblin J. (1994) "A phenomenological design equation for FRP columns with interaction between local and global buckling," *Thin-Walled Structures*. V18, 117-131.
- Kollár, L.P. (2003) "Local buckling of fiber reinforced plastic composite structural members with open and closed cross sections," *Journal of Structural Engineering*, V129, No. 11, 1503-1513.
- Lane A. and Mottram J.T. (2002) "Influence of modal coupling on the buckling of concentrically loaded pultruded fibre-reinforced plastic columns," *Proc Inst Mech Engrs Part L: J Materials: Design and Applications*, V216, 133-144.
- Mottram, J.T. (2004) "Determination of critical load for flange buckling in concentrically loaded pultruded columns," *Composites Part B: Engineering*, V35, N1, 35-47.
- Mottram J.T., Brown N.D. and Anderson D. (2003) "Physical testing for concentrically loaded columns of pultruded glass fibre reinforced plastic profile," *Structures & Buildings* 156 Issue 2, 205-219.
- Scott D.W. (1997) Short- and Long-Term Behavior of Axially Compressed Slender Doubly Symmetric Fiber-Reinforced Polymeric Composite Members, PhD Thesis, Georgia Institute of Technology.
- Vanevenhoven, L. (2006) "Closed-form Equations for Predicting Failure Loads of Pultruded Profiles," Independent Study Report. University of Wisconsin-Madison.
- Yoon S.J. (1993) Local Buckling of Pultruded I-Shape Columns, PhD Thesis, Georgia Institute of Technology.
- Zureick, A. and Scott, D., (1997), "Short-term Behavior and Design of Fiber-reinforced Polymeric Slender Members Under Axial Compression," *Journal of Composites for Construction*, V1, pp. 140-149.

THEORETICAL STUDY ON SPALLING RESISTANCE OF FRP SHEETS BONDED TO BENT CONCRETE SURFACE

Hong YUAN

(Professor, Department of Mechanics and Civil Engineering, Jinan University, Guangzhou 510632, P R China)

Ren-huai LIU

(Professor, Department of Mechanics and Civil Engineering, Jinan University, Guangzhou 510632, P R China)

ABSTRACT

In this paper, the peeling behavior and the spalling resistance effect of fiber reinforced polymer (FRP) sheets externally bonded to bent concrete surface are firstly investigated theoretically. A peeling load is applied on the FRP sheet by loading a circular rod placed into the central notch of beam, and the theoretical analysis is conducted for the specimens. Load is expressed as the function of peel angle by geometry analysis and equilibrium of forces between FRP sheets and circular rod. Interfacial fracture energy is calculated analytically using membrane peeling method. Both initial loading and debonding propagation stages are explored. It is realized that only two material parameters, the interfacial fracture energy of FRP-concrete interface and the tensile stiffness of FRP sheets, are necessary to represent the interfacial spalling behavior. Finally, the peeling load – deflection curves for various radii of curvature of concrete surface are demonstrated by means of a numerical example. It is found that radius of curvature has remarkable influence on peeling load.

KEYWORDS

FRP sheet, interfacial fracture energy, debonding, spalling resistance, bent concrete surface

1. INTRODUCTION

Acceptance of high performance composites in the construction industry has grown at a rapid pace during the last decade. One of the areas where composites are preferable is the rehabilitation of existing structures against spalling failure. When FRP sheet is applied to a concrete surface to prevent pieces of the concrete from peeling and spalling, acting force on FRP sheet is similar with the usual peel test to peel a sheet from a substrate. Nevertheless, there exists an important difference between peel and spalling resistance test. In peel test, the peel angle can be adjusted according the experimental need, and can be varied independently. But in the spalling resistance test, peel angle is determined by the interfacial geometric and material properties, and is not an independent variable.

Kimpara et al. (1998) proposed firstly a spalling resistance test method of FRP sheets bonded to mortar and concrete to characterize the peeling strength and also to examine the effects of different surface treatment and primer. Wu et al. (2005a,b) studied experimentally and analytically the peeling behavior and spalling resistance effect of unidirectional and bi-directional FRP sheets externally bonded to plane concrete surface. Simple expressions among peeling load, interfacial energy and FRP sheet stiffness were obtained. The theoretical results were validated by comparing with experimental results. In this paper, the peeling behavior and the spalling resistance effect of FRP sheets externally bonded to bent concrete surface are investigated theoretically.

2. THEORETICAL ANALYSIS

Theoretical analysis is carried out on specimens representing the spalling resistance effect of unidirectional FRP sheets externally bonded to bent concrete surface. A notch of $2a_0 \times 2a_0$ is made in the mid-span at the bottom side of the beam specimens, where loading pin is situated. Figure 1 shows the detail dimensions of the specimen and the

loading arrangement. Both initial loading stage before debonding and debonding propagation stage are explored. The bending energy of the FRP sheets is neglected to simplify the analysis.

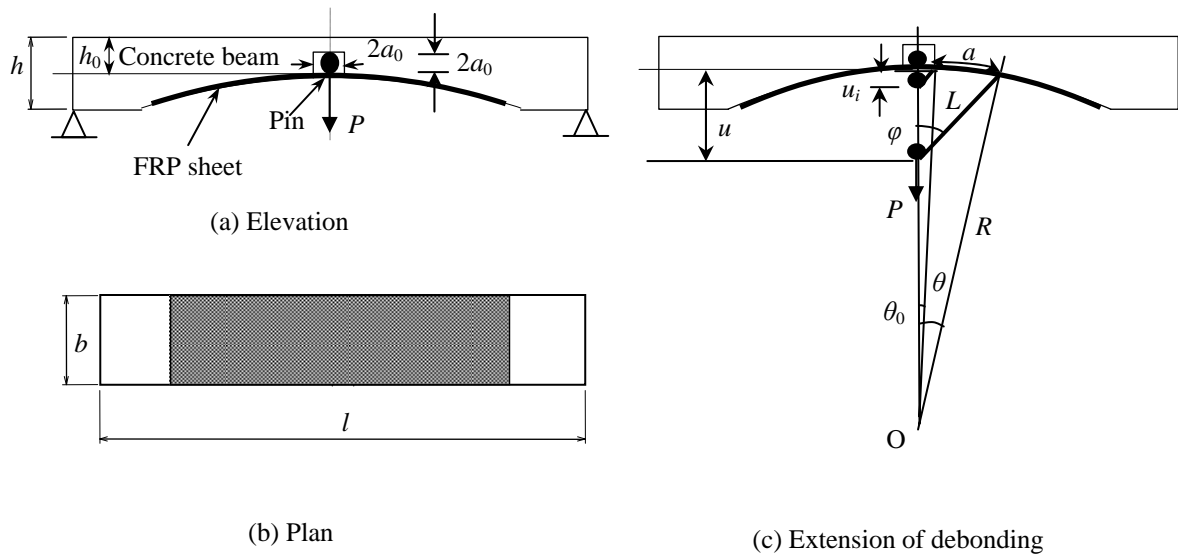


Figure 1: Specimen Details and Loading Arrangement

Refer to Figure 1, where l is span of the beam, h is height of the beam, h_0 is height of the beam at middle span, b is width of FRP sheet, whereas t is the thickness of FRP sheet. φ is the angle between vertical line and FRP sheet. u is the deflection of the loading pin. a is debonding length, whereas a_0 is the initial debonding length. T is peel force per unit width of FRP sheet. P is the load on the circular pin and applied through the loading device. a_0+a is total debonding length. L is the deformed length of original FRP length $L_0=a_0+a$. R is curvature radius of bent surface, and stands for the instant FRP debonding location. O is curvature center. θ_0 is angle between vertical line and R at initial debonding location. θ is angle between vertical line and R at instant debonding location.

2.1 Initial Loading Stage Before Debonding

When load is acted on the pin, the FRP sheet of length $2a_0$ is firstly subjected to deformation because of the existence of initial debonding length a_0 as shown in Fig. 1. Peel angle increases from zero to the maximum value with the increase of loading. By assuming the diameter of pin is small compared to the debonding length, equilibrium of the pin gives

$$P = 2Tb \cos \varphi \quad (1)$$

According to the geometrical deformation, normal strain in FRP sheet ε is obtained as

$$\varepsilon = \frac{1}{\sin \varphi} - 1 \quad (2)$$

Assume that FRP sheet is linear elastic and obey Hook's law, the peel force per unit width of FRP sheet is

$$T = Et\varepsilon \quad (3)$$

where E is Young's modulus of FRP sheet. Substituting (3) and (2) into (1) yields

$$P = 2Etbx \left(1 - \frac{1}{\sqrt{1+x^2}} \right), \quad x = \cot \varphi = \frac{1}{\tan \varphi} = \frac{u}{a_0}, \quad \text{for } 0 \leq u \leq u_m = a_0 \cot \varphi_m \quad (4)$$

where u_i is the deflection of the loading pin before debonding and u_m is the maximum deflection of the loading pin before debonding. φ_m is value of φ when debonding appears and begin extend.

2.2 Debonding Propagation Stage

When interfacial debonding between FRP sheet and concrete beam occurs, debonding length can be calculated as

$$a = R(\theta - \theta_0), \text{ for } \theta \geq \theta_0 \quad (5)$$

Original length of FRP sheet is

$$L_0 = a_0 + a = a_0 + R(\theta - \theta_0) \quad (6)$$

The deformed length of original length L_0 is

$$L = \sqrt{R^2 + (R \cos \theta_0 - u)^2 - 2R(R \cos \theta_0 - u) \cos \theta} = \sqrt{[u - R(\cos \theta_0 - \cos \theta)]^2 + R^2 \sin^2 \theta} \quad (7)$$

Angle φ is obtained by geometrical analysis

$$\cos \varphi = \frac{u - R(\cos \theta_0 - \cos \theta)}{L} \quad (8)$$

and normal strain in FRP sheet is

$$\varepsilon = \frac{L - L_0}{L_0} = \frac{\sqrt{R^2 + (R \cos \theta_0 - u)^2 - 2R(R \cos \theta_0 - u) \cos \theta}}{a_0 + R(\theta - \theta_0)} - 1 \quad (9)$$

Similar derivation with Eq. (4) gives

$$P = 2Et b \varepsilon \cos \varphi = 2Et b \left(\frac{L}{L_0} - 1 \right) \frac{u - R(\cos \theta_0 - \cos \theta)}{L} \quad (10)$$

Namely

$$P = 2Et b \left[\frac{u - R(\cos \theta_0 - \cos \theta)}{L_0} - \frac{u - R(\cos \theta_0 - \cos \theta)}{L} \right] \quad (11)$$

As the observed load-deflection curve is not linear, the conventional compliance method is not appropriate to be applied to evaluate the energy release rate. To evaluate the energy release rate, a modification of the compliance method was proposed by Kimpara et al. (1998). Elastic strain energy U can be obtained by integrating equation (11) with respect to u under the condition that debonding length a is constant.

$$U = 2Et b \left[\frac{0.5u^2 - Ru(\cos \theta_0 - \cos \theta)}{L_0} - L + \sqrt{R^2(1 + \cos^2 \theta_0) - 2R^2 \cos \theta \cos \theta_0} \right] \quad (12)$$

Finally, energy release rate G is derived by differentiating strain energy with respect to a under the condition that u of FRP sheet is constant.

$$G = -\frac{\partial U}{2bR\partial \theta} = Et \left[\frac{0.5u^2 - Ru(\cos \theta_0 - \cos \theta)}{L_0^2} + \frac{u \sin \theta}{L_0} + \frac{(R \cos \theta_0 - u) \sin \theta}{L} - \frac{\sin \theta \cos \theta_0}{\sqrt{(1 + \cos^2 \theta_0) - 2 \cos \theta \cos \theta_0}} \right] \quad (13)$$

Letting $\theta = \theta_0$, $L_0 = a_0$, $L = \sqrt{u_m^2 + a_0^2}$, $G = G_f$ obtains deflection u_m when debonding initiates.

$$G_f = Et \left[\frac{u_m^2}{2a_0^2} + \frac{u_m}{R} + \frac{\cos \theta_0 - \frac{u_m}{R}}{\sqrt{\frac{u_m^2}{a_0^2} + 1}} - \cos \theta_0 \right] \quad (14)$$

where G_f is interfacial fracture energy. Initial debonding load is given by equation (4) as

$$P_m = 2Et b x_m \left(1 - \frac{1}{\sqrt{1 + x_m^2}} \right), \quad x_m = \frac{u_m}{a_0} \quad (15)$$

Setting $G = G_f$ in equation (13) yields a relation between deflection u and θ . Finally, (11) gives load-deflection curves at debonding propagation stage. Obviously, only two material parameters, the interfacial fracture energy of FRP-concrete interface G_f and the tensile stiffness of FRP sheets Et , are necessary to represent the interfacial spalling behavior.

3. NUMERICAL SIMULATIONS

The peeling load – deflection curves for various radii of curvature of concrete surface are shown in Figure 2. The following parameters are used in the examples: $t=0.111\text{mm}$, $b=120\text{mm}$, $a_0=15\text{mm}$, $E=230\text{GPa}$, $G_f=0.40\text{N/mm}$, and R varies between 2000mm and ∞ . It can be concluded that radius of curvature has remarkable influence on peeling load. At initial loading stages before debonding, peeling load – deflection curves are the same linear lines. When initial debonding occurs, peeling load decreases with increasing deflection. Peeling load decreases more rapidly with deflection for small radii of curvature.

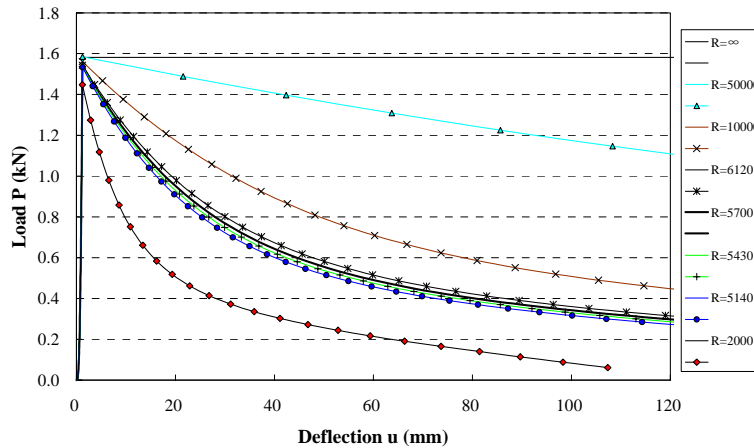


Figure 2: Peeling Load-Deflection Curves for Different Radii of Curvature

4. CONCLUSIONS

The peeling behavior and the spalling resistance effect of fiber reinforced polymer (FRP) sheets externally bonded to bent concrete surface are firstly investigated theoretically. It is realized that only two material parameters, the interfacial fracture energy of FRP-concrete interface G_f and the tensile stiffness of FRP sheets Et , are necessary to represent the interfacial spalling behavior. It is found that radius of curvature and interfacial fracture energy have remarkable influence on peeling load – deflection curves.

ACKNOWLEDGMENTS

The authors gratefully acknowledge the financial support provided by the Scheme of Science and Technology of Guangdong Province (2005B32801002), Ministry of Construction (No. 05-K4-45), Guangzhou City (2005J1-C0251) and Jinan University, China.

REFERENCES

- Kimpara, I., Kageyama, K., Suzuki, T., Ohsawa, I. and Yamaguchi, K. (1998). “Characterization of peeling strength of FRP sheets bonded on mortar and concrete”, *Proceedings of the Eighth JAPAN-U.S. Conference on Composite Materials*, pp 1010-1019.
- Wu, Z. S., Yuan, H., Kojima, Y., and Ahmed, E. (2005a). Experimental and analytical studies on peeling and spalling resistance of unidirectional FRP sheets bonded to concrete, *Composites Science and Technology*, Vol. 65, No. 7-8, pp. 1088-1097.
- Wu, Z. S., Yuan, H., Asakura, T., Yoshizawa, H., Kobayashi, A., Kojima, Y., and Ahmed, E. (2005b). Peeling behavior and spalling resistance of bonded bi-directional fiber reinforced polymer sheets, *Journal of Composites for Construction*, Vol. 9, No. 3, pp. 214-226.

THEORY OF A NEW METHOD FOR EXTERNALLY ANCHORED FRP BAND PRE-STRESSED REINFORCEMENT

Zhuo Jing

(Chongqing Communications Research & Design Institute, Chongqing, China 400067)

Li Tangning

(School of Civil Engineering, Chongqing University, Chongqing, China 400045)

ABSTRACT

After several years of development, FRP sheet pre-stress technology still remains in lab stage. The reason is that no FRP sheet grips or anchors suitable for easy application on a reinforcement site, the most critical aspect of pre-stress reinforcement technology, have been developed from previous experiments and researches. The invention of WSGG (a new type anchorage of FRP, which is made of two or more wave shaped gear plates) anchor resolves the problem of FRP sheet anchoring. After a series of researches, a brand-new method for externally anchored FRP sheet pre-stress reinforcement (invention patent No. 02128047.9) is conceived, which makes full use of the features of WSGG anchors by fixing both ends and then fastening in the middle to force FRP sheets to elongate geometrically and generate a pre-tension. Worn bridge members (solid RC plates of 8m long) removed from Cheng-Yu Expressway is used to take an experiment of externally anchored carbon fiber fabric pre-stress reinforcement. Results of the experiment demonstrates that application of pre-stress by the method is very simple, easy, and technically practicable, requires no special straining devices, and remarkably enhances effects of reinforcement, showing quite broad prospects of generalization and application.

KEYWORDS

pre-stressed, carbon fiber fabric, reinforcement, WSGG anchor

1. INTRODUCTION

If an FRP sheet is simply bonded to the surface of a structural member for reinforcement, tensile stress in the FRP sheet remains low until the member is damaged under a load; therefore, material strength cannot function well. Especially in actual reinforcement engineering cases, where an initial load usually exists on the members to be reinforced, strain in the FRP sheet will lag much behind that in steel bars in the beam under secondary load and makes economic effect of reinforcement less evident if an ordinary method for FRP sheet reinforcement is used. For the purpose of making more adequate and more effective use of the feature of high strength of FRP sheets and achieving better effects of reinforcement, the technology of pre-tensioned FRP sheet reinforcement has significant application value. Initial pre-stress generated by pre-tensioning of FRP sheets can be used to balance part of the dead weight of or the load on the structure so that FRP sheets can fully exert its effects of reinforcement, such as considerable deferment of crack development and reduction of crack width, effective enhancement of structural rigidity, reduction of structural member deflection, mitigation of internal bar strain, and enhancement of bar yield load and of ultimate bearing capacity of the structure (Stöcklin and Meier, 2001) (Triantafillou et al., 1992).

After several years of development, however, FRP sheet pre-stress technology remains in lab stage as there exist this and that problems that prevent it from being utilized (Wu and Matsuzaki, 1998). One of the problems is the complex arrangement, complicated operational procedure, and small tonnage of tensioning implements. To resolve existing technical problems in relation to FRP sheet pre-tensioning and anchoring, WSGG anchorage is developed specifically for FRP sheets (Zhuo and Li, 2004). The reliability of FRP sheets gripped and anchored with WSGG anchors has been verified by a number of experiments which show their anchoring performance much superior to U-shaped FRP sheets or bolts (Zhuo and Li, 2005). Based on the features of WSGG anchors, we specially conceive a brand-new method for externally anchored carbon fiber band pre-stress reinforcement (invention patent No.:

02128047.9), which has very simple operating procedure and requires no special equipment but fastening operations on bolts to perform pre-tensioning and anchoring of FRP sheets. The following is our study on the pre-stress theory of the method as well as experimental verification by actual bridge members.

2. THEORY OF THE METHOD FOR EXTERNALLY ANCHORED FRP SHEET PRE-STRESS REINFORCEMENT

2.1 Basic theory of the occurrence of pre-stress from gripping and anchoring of FRP sheets with WSGG anchors

As shown in Fig 1 (a), an FRP sheet with straight length l is fixed and restrained at both ends. When a WSGG anchor is used to grip the middle of the FRP sheet, the FRP sheet will be forced to elongate. Since there is difference δ between the stretched length of the camber line of WSGG anchor's wave-shaped gear faces and the projected length of its plane, the FRP sheet will elongate by δ when upper and lower wave-shaped gear faces of the WSGG anchor get fully held down in perfect fitness, as shown in Fig 1 (b). The value of such forced elongation causes the occurrence of pre-stress in the FRP sheet:

$$F = EA \times \frac{d}{l} \quad (1)$$

F : Built-up pre-tension in the FRP sheet;

E : Tensile elastic modulus of the FRP sheet;

A : Sectional area of the FRP sheet;

l : Net length of the FRP sheet between two fixed ends;

d : Difference between the stretched length of the camber line of WSGG anchor's wave-shaped gear faces and its horizontally projected length

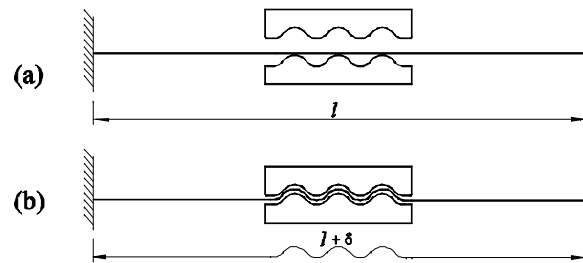


Fig 1 Schematic of the pre-stress applied to the FRP sheet by a WSGG anchor

During actual reinforcement of a structure, fixing restraint on both ends of an FRP sheet can be implemented by WSGG anchors fixed to the structure. To achieve pre-stress tensioning and anchoring of said FRP sheet, therefore, just 3 or more WSGG anchors will do. To be specific, both ends of the FRP sheet are anchored with fixed WSGG anchors to form two anchor points before gripping and anchoring the middle of two anchor points with WSGG anchors, so as to generate a pre-tension in the FRP sheet.

2.2 Theory of pre-stress in a multipoint anchored FRP band

Where multipoint anchoring of an FRP sheet is required for reinforcement of a longer structure, the basic pre-stress theory detailed in Section 1.1 is still applicable to multipoint gripping and anchoring of the FRP sheet. For example, the following technical program for pre-stress reinforcement can be used when 5 WSGG anchors are used for pre-stress tensioning and anchoring of an FRP sheet, as shown in Fig 2:

Step 1: Fix in advance lower wave-shaped gear plates of 5 WSGG anchors to the structure to be reinforced and then anchor both ends of the FRP sheet at WSGG anchors A and E to form two anchor points, as shown in Fig 2(a).

Step 2: Close upper wave-shaped gear plates of WSGG anchors B and D simultaneously and screw up the bolts synchronously and uniformly such that upper and lower wave-shaped gear faces of WSGG anchors B and D get completely held down in perfect fitness, as shown in Fig 2(b). For the purpose of simplicity, it's assumed that all pre-stress losses in the FRP sheet are ignored, including the assumption that the reinforced structure maintains its

rigidity or, in other words, the reinforced structure will not suffer any loss arising from deformation (bending and compression) under eccentric load of FRP sheet pre-stress. Under such ideal conditions, then, the FRP sheet between two anchor points of WSGG anchors A and E can be considered to be stretched forcibly by 2δ when upper and lower wave-shaped gear faces of WSGG anchors B and D get completely held down in perfect fitness, giving rise to the pre-tension shown in Formula (2):

$$F_1 = EA \times \frac{2d}{l_{AE}} \quad (2)$$

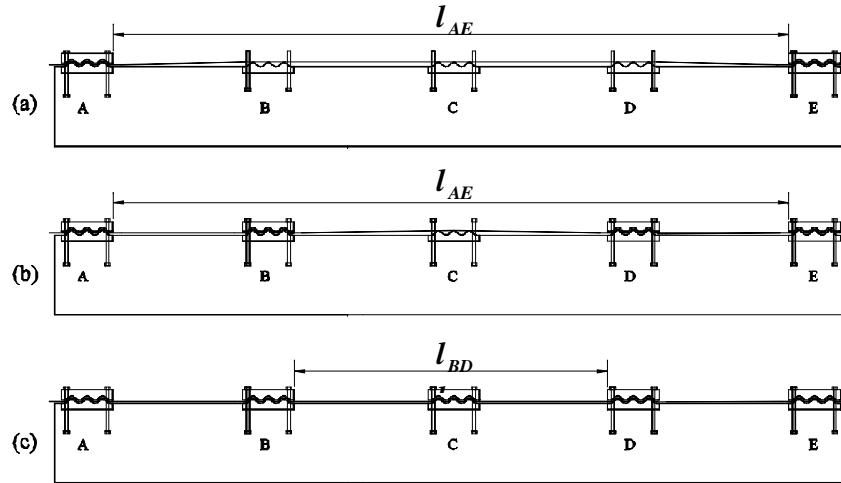


Fig 2 Schematic of the pre-stress applied to an FRP sheet by WSGG anchors in series

Under said conditions, pre-tension in the FRP sheet applies an eccentric pre-stress of magnitude F_1 to the reinforced structure via WSGG anchors A and E. Since the action of the FRP sheet on WSGG anchor B or D is vertical during fastening with WSGG anchors B and D, longitudinal eccentric pre-stress of both WSGG anchors B and D on the reinforced structure is 0.

Step 3: Next, close upper wave-shaped gear plate of WSGG anchor C and screw up the bolts uniformly such that upper and lower wave-shaped gear faces of WSGG anchor C get completely held down in perfect fitness, as shown in Fig 2(c). For the purpose of simplicity, the same assumptions as in Step 2 are made, plus further assumption that the FRP sheet is completely anchored at WSGG anchors B and D or, in other words, that no slippage will arise to the FRP sheet in WSGG anchor B or D. Under ideal conditions, then, the FRP sheet between two anchor points of WSGG anchors B and D can be considered to be stretched forcibly by δ when upper and lower wave-shaped gear faces of WSGG anchor C get completely held down in perfect fitness, giving rise to the pre-tension increment shown in Formula (3):

$$\Delta F_2 = EA \times \frac{d}{l_{BD}} \quad (3)$$

Under said ideal assumptions, various pre-stressing losses are ignored and Formula (2) is added to Formula (3) to get the pre-tension in the FRP sheet between two anchor points of WSGG anchors B and D:

$$F_2 = F_1 + \Delta F_2 = EA \times \frac{2\delta}{l_{AE}} + \frac{\delta}{l_{BD}} \quad (4)$$

Similarly under said conditions, pre-tension increment in the FRP sheet between WSGG anchors B and D applies longitudinal eccentric pre-stress of magnitude ΔF_2 to the reinforced structure via WSGG anchors B and D. WSGG anchors A and E maintain application of longitudinal eccentric pre-stress of magnitude F_1 to the reinforced structure and longitudinal eccentric pre-stress of WSGG anchor C on the reinforced structure is 0.

or multipoint FRP sheet gripping and anchoring, different operational sequence corresponds to different pre-tension arising to each section of the FRP sheet; therefore, reasonable pre-stressing construction program can be arranged depending on actual case of reinforcement.

Of course, it's taken into account that there will be a variety of pre-stressing losses during actual operation, such as loss caused by eccentric pressure on a member, loss arising from possible slippage of a sheet between anchors at both fixed ends, and loss arising from incomplete fitness of intermediate anchors. Research activities in such aspect need to be further carried out.

3 DISCUSSION OF EXTERNALLY ANCHORED FRP BAND PRE-STRESS REINFORCEMENT TECHNOLOGY

(1) An FRP sheet achieves effective multipoint anchorage on a reinforced structure and ensures reliable transfer of FRP sheet pre-tension. Especially for greater pre-tensioning tonnage, ordinary U-shaped FRP sheet anchoring or bolt anchoring cannot achieve this at all, whereas reliable multipoint anchorage can bear not only pre-tension but also tension increment caused by later load.

(2) The technology provides simple, convenient FRP sheet pre-tensioning operations and requires no special equipment but fastening operations on bolts to perform pre-stress tensioning and anchoring of an FRP sheet. This feature makes the method easy to be applied to engineering practice.

(3) Pre-tension in an FRP sheet is allocated between several anchor points in operational sequence; each of the anchor points bears part of FRP sheet pre-tension only. This feature is helpful in that anchor zone design for anchor points becomes simpler; especially for reinforcement of an existing structure, the smaller the anchor point tonnage is, the easier it is to accomplish anchor zone design and construction.

(4) Distribution of FRP sheet pre-tension is different for different anchor sections and different operational sequences. This feature is significant for reinforcement of a bridge structure with larger span. For example, a simply supported beam with larger span requires larger pre-stress for the middle section of its span and requires gradually decreasing pre-stress towards its two sides; distribution of FRP sheet pre-stress after construction by the technology can meet the requirement.

(5) When pre-stress reinforcement is carried out with the technology, it's unnecessary for an FRP sheet to perform bonding operations on the surface of the reinforced structure. This is mainly because WSGG anchors perform concentrated anchoring of an FRP sheet, which has smaller width and usually larger thickness, and the function exerted by bonding force of the bonded surface has gone down to a minor place on account of the influence of various factors; in other words, there will be no significant influence on the effects of reinforcement even if the FRP sheet is not bonded to the reinforced structure.

(6) Since an FRP sheet is pre-tensioned and anchored by section, its pre-stress reinforcement calculation is relatively more complicated.

REFERENCES

- Wu zhishen, Tanabe K, Matsuzaki T, et al (1998). A retrofitting method for concrete structures with externally prestressed carbon fiber sheets[J]. *Journal of Structural Engineering*, 1998, 44A:1299-1308
- Stöcklin I, Meier U (2001). Strengthening of concrete structures with prestressed and gradually anchored CFRP strips[A]. *Proceedings of the Fifth International Conference on Fiber-reinforced Plastics for reinforced concrete Structures(FRPRCS-5)* [C], Cambridge, UK, 16-18 July, 2001. 291-296
- Triantafillou T C, Deskovic N, Deuring M (1992). Strengthening of concrete structures with prestressed fiber reinforced plastic sheets[J]. *ACI Structural Journal*, 1992, 89(3):235-244
- Zhuo Jing, Li Tang-ning (2004). An innovative WSGG anchor of FRP sheet[A], *ACMBS-IV*, 2004.8:86
- Zhuo Jing, Li Tang-ning (2004). The mechanism of an innovative WSGG anchor of FRP laminations[A], *ISSEYE-8*, 2004.7:805-811
- Zhuo Jing, Li Tang-ning (2005). The mechanics of an innovative wave-shape-teeth-grip anchor of FRP laminations or sheets[J], *China Civil Engineering Journal*, 2005(10):49-53
- Zhuo Jing, Li Tang-ning (2005). The Experimental Research of RC Beam Strengthened with Carbon Fiber Sheet Which End Anchored by Wave-shaped-teeth-grip anchorage[J], *Building Structure*, 2005(7):63-66

POST-BUCKLING BEHAVIOR OF FRP COMPOSITE THIN-WALLED MEMBERS

Nuno Freitas Silva¹, Nuno Silvestre², Dinar Camotim³

¹Ph.D. Student, ²Assistant Professor, ³Associate Professor

Dept. of Civil Engineering, ICIST/IST, Technical University of Lisbon, Av. Rovisco Pais, 1049-001 Lisboa, Portugal

ABSTRACT

This paper (i) provides a brief account of the steps and procedures involved in deriving and implementing a geometrically non-linear orthotropic formulation based on Generalized Beam Theory (GBT) and (ii) illustrates its application and capabilities by presenting and discussing numerical results concerning the distortional post-buckling behavior of lipped channel FRP composite columns. Taking advantage of the GBT modal features, it is possible to provide fresh insight on the member post-buckling behavior, namely to obtain (i) accurate “exact” and approximate (but with a “controlled approximation”, achieved by including just a few selected deformation modes) post-buckling equilibrium paths, as well as (ii) the evolution, along those paths, of the most relevant displacements and stresses. For validation purposes, some GBT-based results are compared with values yielded by finite element analyses, performed in the code ABAQUS and adopting shell elements to discretize the thin-walled members.

KEYWORDS

Thin-walled members; FRP composites; Local buckling; Distortional post-buckling; Generalized Beam Theory (GBT)

1. INTRODUCTION

The use of composite material in civil engineering became significant in the last decade, as their well known structural efficiency and excellent behavior in aggressive environments conditions were joined by sufficiently low fabrication costs. In particular, these three features are responsible for the growing demand for thin-walled composite structural members in the construction industry, namely in off-shore structures and chemical plants. On the other hand, most composite materials exhibit linear elastic stress-strain relations (with fairly low moduli), almost no ductility (*i.e.*, they remain elastic up to collapse) and different types of orthotropy – these material properties clearly point towards a high susceptibility to (i) local and/or global instability phenomena and (ii) brittle collapse modes. Since mastering these two aspects is very important to achieve efficient (safe and economic) designs, engineers must have analytical/numerical tools to model them accurately, so that their effect on the member structural response may be properly assessed. In order to illustrate the capabilities of Generalized Beam Theory (GBT), concerning the first aspect, one studies the post-buckling behavior and strength of lipped channel FRP composite columns.

2. GBT POST-BUCKLING ANALYSIS

GBT may be viewed as either (i) a *bar theory* incorporating cross-section in-plane deformation or (ii) a *folded-plate theory* including plate rigid-body motions. By (i) decomposing the member deformed configuration or buckling mode shape into a linear combination of cross-section *deformation modes* and (ii) assessing their individual contributions, GBT provides a general approach to obtain accurate, elegant and clarifying solutions for several structural problems. A GBT post-buckling analysis comprises two main tasks: (i) a *cross-section analysis* and (ii) a *member analysis*. Next, one briefly addresses the most relevant concepts and procedures involved in performing and numerically implementing these tasks – their application is subsequently illustrated through the investigation of the post-buckling behavior of FRP composite lipped channel columns.

Take a reference system where x, s, z (u, v, w) are coordinates (displacement components) along the member length, cross-section mid-line and wall thickness. For a displacement representation compatible with a classical beam theory, one considers

$$u(x, s) = u_k(s) \phi_{k,x}(x) \quad v(x, s) = v_k(s) \phi_k(x) \quad w(x, s) = w_k(s) \phi_k(x) \quad , \quad (1)$$

a variable separation where (i) $(\cdot)_{,x} \equiv d(\cdot)/dx$, (ii) the summation convention applies to subscript k , (iii) $\phi(x)$ is a “mode

displacement amplitude function”, defined along the member length, and (iv) $u_k(s)$, $v_k(s)$ and $w_k(s)$ are the displacement profiles associated with deformation mode k . The whole set of GBT deformation modes can be divided into three families: (i) *conventional*, (ii) *shear* and (iii) *transverse extension* modes (Silvestre and Camotim 2003, Silvestre 2005). The *conventional* modes constitute the original core of GBT, were developed by Schardt (1989) and are based on Vlasov’s null membrane shear strain ($\gamma_{xs}^M=0$) and transverse extension ($\epsilon_{ss}^M=0$) assumption – they exhibit warping displacements varying linearly within each wall mid-line and comprise global (extension, major and minor axis bending, torsion), distortional and local-plate modes – the last ones are obviously associated with null warping displacements. The *shear* modes deal exclusively with the *non-linear* variation of the warping displacements along the various cross-section wall mid-lines and involve no cross-section in-plane deformation – since the membrane shear strains are *non-null* in each wall mid-line ($\gamma_{xs}^M=\partial u/\partial s \neq 0$), the shear modes do not comply with Vlasov’s first assumption. Because they are included in a GBT analysis *independently* from the *conventional* modes (all shear undeformable), their joint participation in the deformed configuration provides a very clear assessment of the influence of shear deformation on the member post-buckling behavior. The *transverse extension* modes involve only in-plane displacements (*i.e.*, have null warping) and exhibit non-null membrane transverse extensions ($\epsilon_{ss}^M=\partial v/\partial s \neq 0$) – these deformation modes are coupled with the conventional ones and their joint participation accounts for the “bowing effect” due to wall transverse bending, a phenomenon linked to the in-plane (local) cross-section deformation and only relevant in the advanced post-buckling stages. For illustration, consider the cross-section discretization shown in figure 1(b) (6 *natural* and 7 *intermediate* nodes: $n=6$ and $m=7$), later adopted to analyze the post-buckling behavior of “cross-ply orthotropic” lipped channel members dealt with in this work (see figure 1(a)) – it leads to (i) 13 *conventional* (4 global, 2 distortional, 7 local-plate), (ii) 10 *shear* and (iii) 15 *transverse extension* deformation modes – their most important features are displayed in figures 2-4.

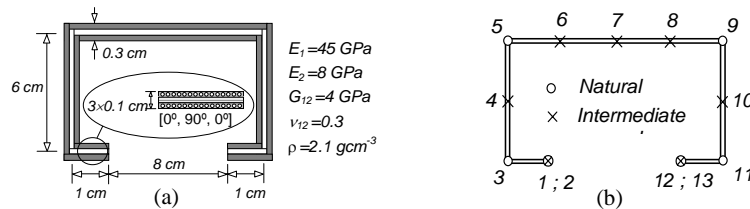


Figure 1: Orthotropic lipped channel members: cross-section (a) geometry and (b) GBT discretization

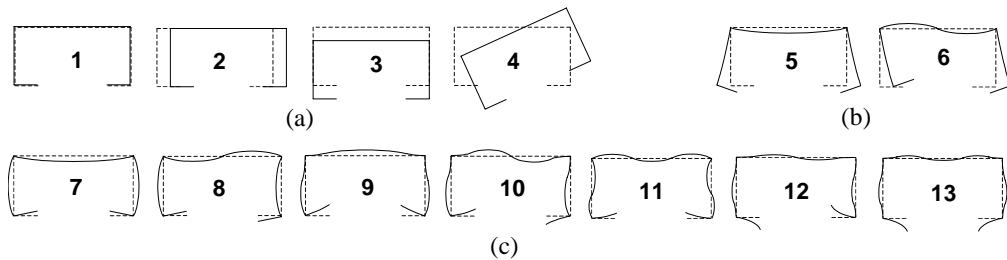


Figure 2: Conventional mode in-plane shapes: (a) global, (b) distortional and (c) local-plate

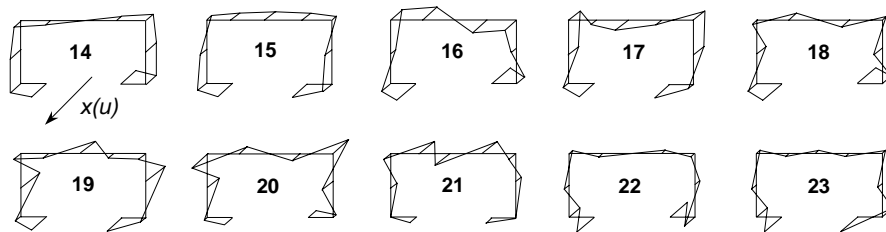


Figure 3: Warping displacement profiles of the shear deformation modes

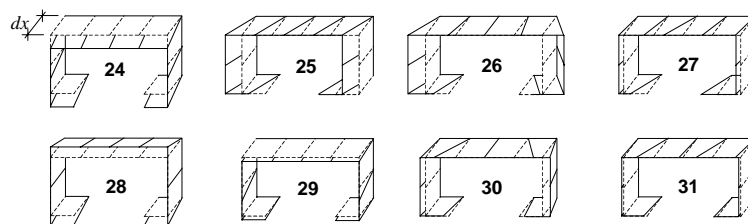


Figure 4: In-plane shapes of the first 8 (out of 15) transverse extension deformation modes

After completing the cross-section discretization procedure (*i.e.*, knowing the deformation mode displacements), determining the member post-buckling behavior involves the solution of the *one-dimensional* problem defined by the non-linear system

$$C_{kh}(\phi_k - \bar{\phi}_k)_{,xxxx} + H_{kh}(\phi_k - \bar{\phi}_k)_{,xxx} - D_{kh}(\phi_k - \bar{\phi}_k)_{,xx} + F_{kh}(\phi_k - \bar{\phi}_k)_{,x} + B_{kh}(\phi_k - \bar{\phi}_k) - C_{kjh}(\phi_{k,xx}\phi_{j,x} - \bar{\phi}_{k,xx}\bar{\phi}_{j,x})_{,x} + \frac{1}{2}C_{hjk}(\phi_{k,x}\phi_{j,x} - \bar{\phi}_{k,x}\bar{\phi}_{j,x})_{,xx} + \frac{1}{2}C_{kijh}(\phi_{k,x}\phi_{i,x}\phi_{j,x} - \bar{\phi}_{k,x}\bar{\phi}_{i,x}\bar{\phi}_{j,x})_{,x} + h.o.t. = 0 \quad (2)$$

where $\bar{\phi}_k$ are modal amplitude functions describing the member initial geometrical imperfections – similarly to eq. (1), any initial imperfection shape can be expressed as a linear combination of products involving deformation mode displacements one-dimensional amplitude functions. For example, the components of the 2nd, 3rd and 4th-order C tensors appearing in (2) read

$$C_{kh} = \int_b \int_t Q_{11}(u_k u_h - z(w_k u_h + w_h u_k) + z^2 w_k w_h) dz ds \quad C_{kjh} = \int_b \int_t Q_{11}(u_k - z w_k)(v_j v_h + w_j w_h) dz ds$$

$$C_{kijh} = \int_b \int_t Q_{11}(v_k v_i + w_k w_i)(v_j v_h + w_j w_h) dz ds \quad (3)$$

and are obtained through the integration, along the cross-section mid-line and thickness, of terms involving material constants and deformation mode displacements and/or their derivatives. While the 2nd-order quantities (C_{kh} , H_{kh} , D_{kh} , F_{kh} , B_{kh}) are *modal mechanical properties* characterizing the cross-section linear behavior, the 3rd and 4th-order ones (C_{kjh} , C_{kijh}), as well as additional ones related to higher order terms (not explicitly shown in eqs. (2)), are associated with its geometrically non-linear behavior. After establishing the system (2), which includes information about (i) the cross-section modal mechanical properties, (ii) the member length and end support conditions and (iii) the applied load nature and values, one solves it numerically by means of the finite element method – a non-linear beam finite element has been formulated, following the work of Silvestre and Camotim (2003) developed in the context of cold-formed steel members, which adopts Hermite and Lagrange polynomials to approximate the modal amplitude functions. The solution of the ensuing system of non-linear algebraic equations is obtained through an incremental-iterative technique based on (i) the well-known Newton-Raphson method and (ii) an arc-length control strategy. The *post-buckling* results include equilibrium paths describing the evolution of the member deformed configuration (amplitude functions $\phi_k(x)$) with the applied load parameter λ . A detailed account on the (beam finite element) numerical implementation of the non-linear GBT formulation can be found in the recent work of Silvestre (2005).

3. ILLUSTRATIVE EXAMPLE

In order to illustrate the application and capabilities of the proposed GBT formulation, some numerical results are presented and briefly discussed next. They concern the distortional post-buckling behavior of two identical FRP laminated plate lipped channel members (i) length $L=40\text{ cm}$, (ii) submitted to uniform axial compression, (iii) having locally/globally pinned and free-to-warp end sections, (iv) with the material properties and cross-section dimensions given in figure 1(a), (v) containing critical-mode initial geometrical imperfections with amplitudes $v_0 = \pm 0.15t$ (t is the wall thickness and v_0 is the outward or inward motion of the mid-span flange-lip corners), and (vi) discretized into 8 beam finite elements (the cross-section discretization was already shown in figure 1(b)). It is worth noting that the column geometry selected ensures that (i) buckling occurs in a single-wave distortional mode and that (ii) local-plate/distortional mode interaction effects are not relevant – the ratio between the minimum local-plate and distortional buckling loads is 1.6.

Figure 5(a) shows the post-buckling equilibrium paths $\sigma/\sigma_{cr,D}$ vs. v/t of the two columns ($\sigma_{cr,D}=38.6\text{ MPa}$ is the critical buckling stress and v is the *additional* outward/inward mid-span flange-lip corner motion – *i.e.*, it does not include the initial value), hereafter identified by the terms “outward” and “inward” – also included, for comparison purposes, are the results yielded by shell finite element analyses performed in ABAQUS (HKS 2002). Figure 5(b), on the other hand, displays modal participation diagrams providing the contributions of the various GBT deformations modes (depicted in figures 2-3 and 4) to various column deformed configurations located along the post-buckling equilibrium paths. Finally, figure 5(c) provides the post-buckling evolution of the mid-span normal stress distribution along the mid-lines of the outward and inward column outer layers (longitudinally aligned fibers). A close observation of the above figures leads to the following conclusions:

- (i) First of all, one instantly recognises the important role played by the initial imperfection “sign” – indeed, the inward column post-buckling stiffness and strength are larger than their outward column counterparts by a non-negligible amount. Like in isotropic members (Silvestre and Camotim 2003), these distortional post-buckling *asymmetry* stems mostly from the different contributions of the shear modes **15+19+23** to the outward and inward column deformed configurations.
- (ii) Then, one also notices the virtual coincidence between the GBT-based equilibrium paths and the post-buckling results yielded by the ABAQUS analyses. Moreover, the fact that the GBT analyses never involved more than 450 degrees of freedom provides clear evidence of the high computational efficiency of the GBT-based approach – the corresponding (and similarly accurate) shell FEM results required column discretization into very refined shell element meshes.

- (iii) In the initial pre-buckling stages, the normal stress distribution is uniform (*i.e.*, mode 1 fully dominates). As post-buckling progresses, and regardless of the v_0 sign (outward or inward motions), the normal stress distribution becomes non-linear in the web and flanges, mostly due to the influence of the shear modes 15+19+23.
- (iv) In the outward column post-buckling stages, the contributions of modes 5 and 15 account for the fact that the compressive stresses (iv_1) increase near the web-flange corners and (iv_2) decrease in the vicinity of the flange-lip corners. Moreover, for $\sigma/\sigma_{cr,D} \geq 1.0$ tensile stresses start to develop around the flange-lip corners and rather high compressive stresses appear close to the lip free ends. Conversely, the inward column exhibits a compressive stress increase near the flange-lip corners (the whole flanges are under compression) and high tensile stresses develop in the neighbourhood of the lip free ends – however, these tensile stresses are lower than the compressive ones appearing in the outward column. This last fact is due to the relevant participation of mode 19, which reinforces mode 5 in the outward column and opposes it in the inward one.

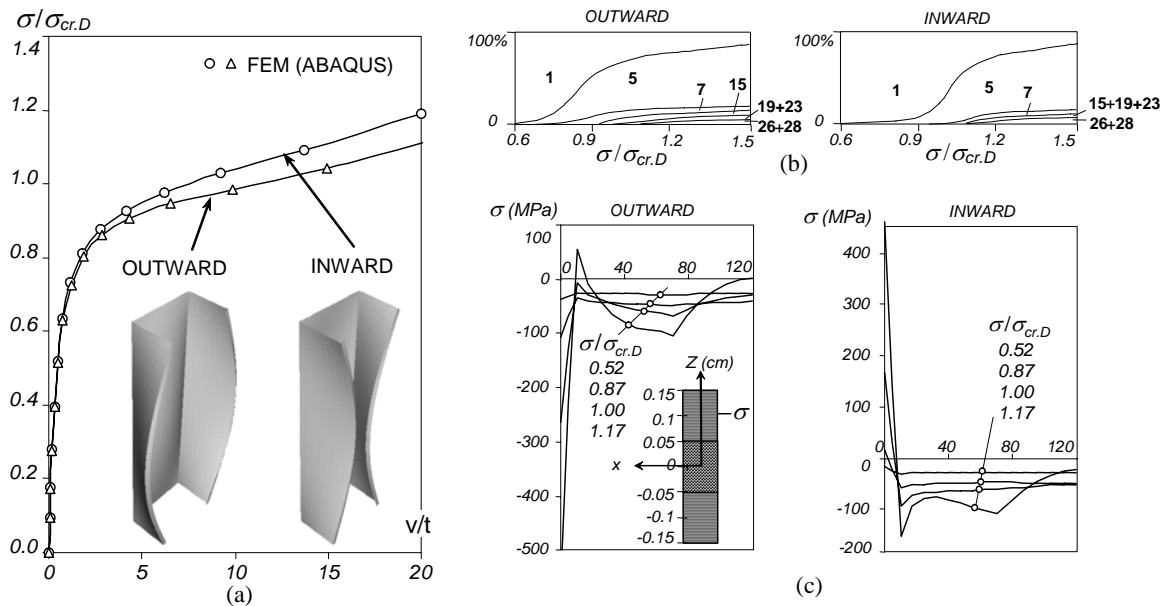


Figure 5: Outward and inward column (a) distortional post-buckling equilibrium paths $\sigma/\sigma_{cr,D}$ vs. v/t , (b) modal participation diagrams providing the evolution of the deformed configurations and (c) evolution of the mid-span normal stress distribution along the outer layer mid-line $\sigma(x=20\text{cm}; z=0.1\text{cm}; s)$

4. CONCLUDING REMARKS

The main steps and procedures involved in deriving and numerical implementing (beam finite elements) a geometrically non-linear orthotropic formulation based on Generalized Beam Theory were briefly described. In order to illustrate its application and capabilities, numerical results concerning the distortional post-buckling behavior of lipped channel FRP composite columns were presented and discussed. For validation purposes, some GBT-based results were compared with values yielded by ABAQUS shell finite element analyses (involving many more d.o.f.) – a virtually perfect match was found in all instances.

5. ACKNOWLEDGEMENTS

The first author gratefully acknowledges the financial support provided by *FCT – Fundação para a Ciência e Tecnologia* (Portugal), through scholarship n° SFRH/BD/21439/2005.

6. REFERENCES

- Hibbit, Karlsson and Sorensen Inc. (HKS) (2002). *ABAQUS Standard* (version 6.3-1).
- Schardt, R. (1989). *Verallgemeinerte Technische Biegetheorie*, Springer Verlag, Berlin. (German)
- Silvestre, N. (2005). *Generalized Beam Theory: New Formulations, Numerical Implementation and Applications*, Ph.D. Thesis, Civil Engineering Department, IST, Technical University of Lisbon. (Portuguese)
- Silvestre, N. and Camotim, D. (2003). “Non-linear generalised beam theory for cold-formed steel members”, *International Journal of Structural Stability and Dynamics*, Vol. 3, No. 4, pp. 461-490.

FATIGUE CRACK GROWTH SIMULATION FOR CFRP BONDED STEEL PLATES USING BOUNDARY ELEMENT METHOD

Hongbo Liu, Xiao-Ling Zhao, Riadh Al-Mahaidi
(Department of Civil Engineering, Monash University, Victoria 3800, Australia)

ABSTRACT

Composite repair has been verified to be an efficient and economical method to extend the service life of cracked steel components. There is a need to develop an accurate tool for investigating the stress intensity factor in the cracked steel structure after repair. In this paper the crack propagation of steel plates bonded with CFRP sheets is studied numerically using the boundary element method. The composite patch and the cracked steel plate are simulated using surface elements, whereas the adhesive layer is simulated as interface elements to connect the patch and steel plate. The numerical results are compared with the experimental results from previous research. The influences of the boundary conditions, CFRP modulus and the spring stiffness on the results are discussed.

KEYWORDS

CFRP (Carbon Fibre Reinforced Polymer), Crack Propagation, Fatigue Life, Boundary Element (BE) Method.

1. INTRODUCTION

Adhesively bonded composite repair has proved to be an efficient and cost-effective method to prevent or retard the crack re-initiation or crack propagation in civil engineering structures (Domazet, 1996; Bassetti *et al.*, 1998; Jones and Civjan, 2003; Tavakkolizadeh and Saadatmanesh, 2003). Carbon fiber reinforced polymer (CFRP) materials have a very high directional stiffness, high strength, low density, high failure strain and durability under cyclic loading. These advantages make CFRP very effective in prolonging the fatigue life of structures. In Bassetti's study (2000), the CFRP patches could increase the fatigue life of the un-reinforced steel plate by three times. With the wide application of composites there is a need for research towards a better understanding of repair effectiveness and improvement of repair design. To reduce the high costs involved in experimental methods, investigations based on numerical analysis, utilising the increase in computational power, can be used together with experimental calibration. In this paper the BEM was used to analyse cracked steel plates repaired with CFRP patches and its accuracy was assessed by comparing the results with experimental findings from previous research by Colombi *et al.* (2005). A parametric study was also performed to investigate the sensitivity of the stress intensity factor at the crack tip to variations in the patch modulus, adhesive stiffness and boundary conditions.

2. BOUNDARY ELEMENT MODEL

A schematic view of the specimens' geometry reported in Colombi *et al.* (2005) is shown in Figure 1(a). The base plate is of grade FeE 235-C steel, with a yield stress of 292MPa and an ultimate tensile strength of 374MPa. In the centre of the plate there is a notch consisting of a 10mm hole and two 5mm long initial transverse cracks. Four 1.2mm thick CFRP strips were bonded on both sides of the plates. The carbon fibre used was Sika CarboDur S512, which has a Young's modulus of 174GPa in the fibre direction. Structural adhesive was used to bond the composites to the steel plates. The adhesive is a two-component epoxy, with an elastic modulus E_a of 714MPa and thickness T_a of 0.3mm. For this kind of structural adhesive, its shear modulus is about 1000MPa. All the specimens were tested to failure by constant amplitude tensile loading with a stress range of 80MPa and stress ratio of 0.4 (Colombi *et al.* 2005).

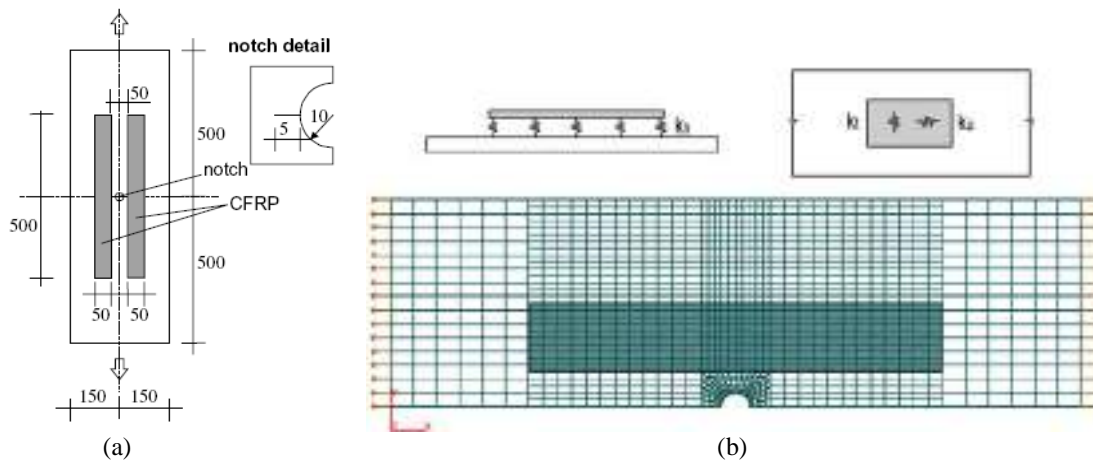


**Figure 1: (a) Crack emanating from a centre hole reinforced by composite patch (lengths in [mm])
(b) Boundary element model of cracked steel plates with repair patches**

The numerical study was undertaken by using BEASY Fatigue and Crack Growth software, which was developed on the basis of boundary element theory and proved well suited for simulating fracture and crack propagation (Beasy, 2005). The specimen was modelled three-dimensionally and due to symmetry only half of the specimen was meshed, as shown in Figure 1(b). The steel plate and each CFRP strips were modelled as continuous plates composed of several zones. Quadrilateral elements were placed on all external boundaries and interface surfaces. The centre hole in the steel plate was meshed and the 0.1mm wide slot was defined as the initial crack using BEASY fracture wizard. It provides a simple method of adding the crack into the model by simply selecting a crack type from the library and supplying orientation data. Material properties used in the modelling were as reported previously for the test specimens. According to the method introduced by BEASY, the structural adhesive used to bond the composites to the steel plates was simulated as interface elements providing both in-plane and out-of-plane stiffness, as illustrated in Figure 1(b). They were represented as zone interfaces with internal spring boundary conditions. The stiffnesses are defined as follows:

$$K_t = \frac{G_a}{T_a}, \quad K_u = \frac{G_a}{T_a}, \quad K_n = \frac{E_a}{T_a}$$

where G_a is the adhesive shear modulus, T_a is the bond line thickness, E_a is the Young's modulus of the adhesive. In practice the adhesive materials are critical to performance and a lot of failures are caused by the interface debonding. Therefore it is essential to define the shear stiffness to realise the patch effectiveness.

3. ANALYSIS

To simulate the notched steel plate without CFRP composites Model 0 was designed. It was shown in Figure 2 that good agreement was achieved between the numerical and experimental results. Therefore the validity of the boundary element method was established. In the parametric study the effect of the spring stiffness representing the adhesive, the CFRP modulus and the boundary conditions were considered. In total, eight different models were analysed. Models 1, 2, 3 were designed to analyse the influence of in-plane spring stiffness. Compared to Model 1, Models 2 and 3 have in-plane stiffness two and three times that of Model 1. The elastic modulus of CFRP and boundary conditions in Models 1, 2, 3 are the same as shown in Table 1. Model 4 is identical to Model 2 except that the CFRP elastic modulus was doubled. In this study all the models were subjected to uniform cyclic loads (representing the constant amplitude fatigue loading) applied over the cross section at two ends. Three models, 5, 6 and 7, were used to study the influence of boundary conditions. Models 5 and 6 were developed on the basis of Model 1. In addition to the tractions in the x-direction, representing the cyclic loads, displacements restrains in the y- and z- directions were applied at the end patches of Models 5 and 6. Models 6 and 7 were compared with Models 5 and 2 in order to investigate the effect of boundary conditions on the symmetry plane. There are two methods to define the symmetrical condition. One is to use the symmetry command available in BESAY. The other is to define a set of elements on the symmetry plane and enforce the symmetry by the use of displacement restrains in the y-direction and springs in the z- direction. All the variables of the models are detailed in Table 1, in which x y and z represent the longitudinal, transverse and thickness directions, respectively.

Table 1: Variables of the Parametric Studies

Model No.	Spring Stiffness		CFRP Modulus	Boundary Condition	
	Kt, Ku	Kn		On Symmetry Plane	At the end patches
Model 0	-	-	-	Symmetry command used	Traction of 133.3MPa in x
Model 1	3333MPa	2380MPa	174GPa	Zero displacements in y and spring of 5000MPa in z	Traction of 133.3MPa in x
Model 2	6666MPa	2380MPa	174GPa	As above	Traction of 133.3MPa in x
Model 3	13332MPa	2380MPa	174GPa	As above	Traction of 133.3MPa in x
Model 4	6666MPa	2380MPa	350GPa	As above	Traction of 133.3MPa in x
Model 5	3333MPa	2380MPa	174GPa	As above	Traction of 133.3MPa in x, 0 displacement in y and z
Model 6	3333MPa	2380MPa	174GPa	Symmetry command used	As above
Model 7	6666MPa	2380MPa	174GPa	Symmetry command used	Traction of 133.3MPa in x

4. RESULTS AND DISCUSSION

The curves of crack propagation versus fatigue cycle numbers are plotted in Figure 2. The curves without any notations represent the experimental results. It can be concluded that the application of CFRP strips is effective in prolonging the fatigue life of the notched steel plates and the results of boundary element analysis (Models 0, 1, 2, 3, 5, 7) match well with the experimental results.

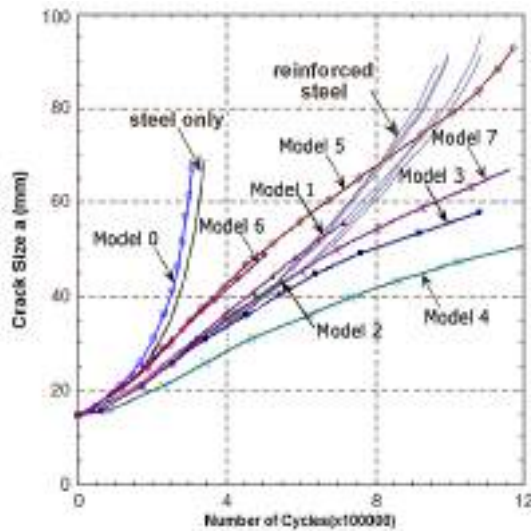


Figure 2: Comparison of numerical and experimental results

Figure 2 shows that for the steel only model, the numerical curve is very close to the experimental one. The boundary element method predicted its crack growth and fatigue life accurately. For the CFRP repaired steels, at the initial stage of the crack growth, Models 1, 2, 3 and 7 provided very accurate predictions. With the crack propagating, the curve of Model 5 closely follows the experimental results.

As mentioned previously, Model 5 was developed on the basis of Model 1. It had additionally applied displacement restrains in the y- and z- directions. Their curves in Figure 2 showed that Model 5 has a much steeper curve than Model 1. When the traction acts in the longitudinal direction of the model, the entire volume had a tendency of contracting in the transverse direction, which was held back by the displacement restrains. Therefore more energy was needed to get the same crack propagation. The stress intensity factor was increased and the crack grew faster when there were displacement restrains. In Figure 2, Models 6 and 7 was designed to compare with Models 5 and 2 respectively. The slight difference in results revealed that the methods to apply the boundary conditions on

symmetry plane had no effect on the results. So in BEASY the displacement restrains was recommended to be applied at the end patches and the symmetry command was proved to be a convenient way in setting up the model.

Comparing the curves of Model 1, 2 and 3, it was shown that as the in-plane stiffness of the spring increased more energy was required for crack growth. This caused a reduction in crack growth rate. For the CFRP repaired steel plates, the stresses were carried by both the CFRP and steel. The load transfer between them occurred through the interface spring, representing the adhesive. As the stiffness value increased, the spring performed more efficiently and thus additional loads were potentially transferred to the CFRP from the steel plate. Therefore the stresses in the steel were reduced, which lead to a small value of stress intensity factor at the crack tip. As a consequence, the crack growth rate was slowed down. For this application of structural adhesive, the in-plane spring stiffness of 6666, two times the value of shear modulus divided by the bond line thickness, showed the best agreement with the experimental curves.

From the comparison between Model 4 and Model 2, it was concluded that the model with higher elastic modulus of CFRP materials had a slower growth rate. In general, when the loads are applied on the composites, both the fibres and epoxy are subjected to the same strain while the stresses in the two phases differ depending on their volume fraction and the elastic moduli. The high modulus CFRP reflects high stiffness. When the same strain was introduced in the structural adhesive, high stiffness fibers carried more stress compared with low stiffness CFRP. Therefore the steel plates repaired with high modulus CFRP can carry more loads without increasing the stress level in the steel plate. Thus the stress intensity factor on the crack tip is effectively reduced and the crack growth rate is slowed down.

5. CONCLUSIONS

Three-dimensional boundary element analyses of composite patch repaired steel plates were performed. The variables that affect the fatigue life of the numerical models were also discussed. From the results the following conclusions are made:

- The boundary element analysis could be used to simulate the crack propagation of the adhesive bonded steel plates and its results agree well with the experimental results.
- Interface elements can simulate the action of structural adhesive efficiently. Different in-plane stiffness for the interface elements results in different crack growth rates. The spring constants in the interface elements evaluated in this study are limited to one type of adhesive and one thickness. Their properties were provided in Colombi *et al.* (2005).
- When CFRP is used to repair the cracked steel plates, a higher value of elastic modulus of CFRP seems much more efficient.
- Displacement restrains are recommended to be applied at the end patches when using the Boundary Element Method.

6. REFERENCES

- Bassetti, A., Liechti, P. and Nussbaumer, A. (1998). "Fatigue Resistance and Repairs of Riveted Bridge Members", *Fatigue Design 1998*, Espoo, Finland, pp 535-546.
- Bassetti, A., Nussbaumer, A. and Manfred, A. (2000). "Crack Repair and Fatigue Life Extension of Riveted Bridge Members Using Composite Materials", *Bridge Engineering Conference ESE-IABSE-FIB*, pp 227-238.
- Beasy (2005). Crack Growth Guide, Acoustic Guide, Corrosion and CP Guide, Computational Mechanics BEASY, Ashurst, Southampton.
- Colombi, P. (2005). "Plasticity induced fatigue crack growth retardation model for steel elements reinforced by composite patch". *Theoretical and Applied Fracture Mechanics*, Vol. 43, No. 1, pp. 63-76.
- Domazet, Z. (1996). "Comparison of Fatigue Crack Retardation Methods". *Engineering Failure Analysis*, Vol. 3, pp 137-147.
- Jones, S.C. and Civjan, S.A. (2003). "Application of Fiber Reinforced Polymer Overlays to Extend Steel Fatigue Life". *Journal of Composites for Construction*, Vol. 7, pp 331-338.
- Tavakkolizadeh, M. and Saadatmanesh, H. (2003). "Fatigue Strength of Steel Girders Strengthened with Carbon Fiber Reinforced Polymer Patch". *Journal of Structural Engineering, ASCE*, Vol. 129, pp 186-196.

NONLINEAR FINITE ELEMENT MODELING OF RC BEAMS STRENGTHENED WITH DIFFERENT CFRP SCHEMES

Rajai Z. Alrousan

(Ph.D. Student, University of Illinois at Chicago, Chicago, IL, USA)

Mohammad A. Alhassan

(Ph.D. Student, University of Illinois at Chicago, Chicago, IL, USA)

Mohsen A. Issa

(Professor of Structural and Materials Engineering, University of Illinois at Chicago, Chicago, IL, USA)

ABSTRACT

This paper presents the effect of the number and configuration of CFRP sheets on the flexural strength and ductility of RC beams and provides useful relationships that can be effectively utilized to determine the required number of CFRP sheets for a certain necessary increase in the beam flexural strength without a major loss in its ductility. The reinforced concrete beams are identical in the geometric and reinforcement details. The variables in this paper are the number and configuration of CFRP sheets. The RC beams were modeled and analyzed using the nonlinear finite element ANSYS (Version 9) software package. The FEA results were validated with the experimental test results of identical RC beams. The validation of the FEA results with the experimental test results concludes that the nonlinear FEA modeling could predict accurately the ultimate load capacity, deflections, concrete strains, steel strains, and CFRP strains of the CFRP strengthened slabs. Analysis of the FEA shows that the normalized flexural moment capacity (M/M_0) of the beams strengthened with 1 layer ($t/d = 0.00081$) and 5 layers ($t/d = 0.00406$) of the U-wrap scheme were 1.7 and 2.7 times that of the control beam, respectively. For the corresponding beams strengthened with the tension face scheme, the M/M_0 was 1.25 and 1.8 times that of the control beam, respectively. Approximately 5 layers of the tension face scheme are equivalent to 1 layer of the U-wrap scheme. In both schemes, it was confirmed that after a certain t/d value, there would be no further noticeable increase in the flexural strength of the beam, while significant reduction in its ductility continues to occur.

KEYWORDS

CFRP, Strengthening, FEA, t/d ratio, RC beams, Flexural Strength Capacity, Ductility.

1. INTRODUCTION AND OBJECTIVES

Carbon fiber reinforced polymer (CFRP) composites are one of the most economical and reliable methods of strengthening deficient structural members with high corrosion and fatigue resistant, high strength/weight ratio, and ease of application. The critical factor for commercial applications of CFRP composites is the cost. Various studies have been conducted to investigate the static and fatigue behaviors of CFRP-strengthened reinforced concrete members (Issa et al., 2003, Shahway et al., 2001, and Kachlakev et al., 2000). The use of the finite element analysis (FEA) to simulate the response of RC members provides substantial advantages mainly in terms of reduction in the cost and time as well as the ability to model any strengthening scheme and sophisticated geometry. This paper reports on nonlinear finite element analysis (FEA) of reinforced concrete (RC) beams strengthened with different number and configurations of CFRP sheets. The main objectives were to assess the effect of the number and configuration of CFRP sheets on the flexural strength and ductility of RC beams and to provide useful relationships that can be effectively utilized to determine the required number of CFRP sheets for a necessary increase in the beam flexural strength without major loss in its ductility. The FEA results were validated with experimental test results of identical specimens. Detailed modeling methodology and practical results are provided in the following sections.

2. FINITE ELEMENT ANALYSIS METHODOLOGY

2.1 Geometric and Reinforcement Details of the Beams

In this study, nonlinear finite element modeling and analysis was carried out using ANSYS software for eleven RC beams identical in the geometric and reinforcement details while having different number and configuration of CFRP sheets. The beams are 2.44 m (8 ft) long with a cross section of 150x230 mm (6x9 in.), and reinforced with 3 #4 steel bars at the bottom, 2-3/16" in diameter bars at the top, and 3/16" in diameter stirrups spaced at 75 mm (3 in.). This reinforcement design ensures flexural failure mode. The beams included a control beam (without CFRP) and 2 groups of strengthened beams, each included 5 beams strengthened with 1, 2, 3, 4, and 5 layers of CFRP sheets. The first group (CFRP applied on the entire tension face) was designated as tension face strengthening scheme, while the second group (CFRP applied on the entire tension face and both sides) was designated as U-wrap strengthening scheme. The exact geometric and reinforcement details of the beams were employed in the FEA modeling.

2.2 Element Types and Material Properties

SOLID65 element was used to model the concrete. This element is typical for the 3-D modeling of solids with or without reinforcing steel bars. The most important aspects of the SOLID65 are the treatment of nonlinear material properties and the capability of cracking in 3 orthogonal directions, crushing, plastic deformation, and creep. The ultimate tensile and compressive strengths are required to define a failure criterion for the concrete. The shear transfer coefficient (β_t) represents the condition of the crack face. The available literature showed a range of values for β_t (0.05-0.25), and the most common value of 0.2 was used in this study. The 28-day compressive strength of concrete (f'_c) of 55 MPa (8000 psi), young's modulus (E_c) of 35063 MPa (5100 ksi), and Poisson's ratio of 0.2 were used. The steel reinforcement was assumed to be an elastic-perfectly plastic material identical in tension and compression. The 3-D LINK8 element was used to model the steel reinforcement with Poisson's ratio, elastic modulus, and yield stress of 0.3, 200 GPa (29,000 ksi), and 413 MPa (60 ksi), respectively. The SOLID45 element was used to model the supports and loading steel plates (75x50x25 mm). The layered SOLID46 element was used to model the CFRP sheets (0.165 mm thick) and the epoxy (0.835 mm thick) materials. The SOLID46 element allows up to 250 different layers of orthotropic materials with different orientations. The CFRP was assumed to be an orthotropic material having a tensile strength of 4272 MPa (620 ksi), an elastic modulus of 228 GPa (33,000 ksi), and an ultimate tensile strain of 0.0167 in the fibers direction. In the directions perpendicular to the fiber direction, the elastic modulus of CFRP was assumed to be 10^{-6} times that of the main direction. The ultimate tensile strength of the epoxy was 55 MPa (8000 psi), elastic modulus of 30 GPa (440 ksi), and ultimate tensile strain of 0.03. Linear elastic properties for the CFRP and epoxy were assumed. The SOLID65, SOLID45, SOLID46 are defined by 8 nodes, while LINK8 is defined by 2 nodes, and all of the four elements have 3 degrees of freedom at each node (translations in the nodal x, y, and z directions). Real constant set 1 was used for the SOLID65 element. It requires material number (type of the reinforcing rebars), volume ratio (steel/concrete ratio in the element), and orientation angles (orientation of the reinforcement). In this paper, the beams were modeled using discrete reinforcement, i.e. a value of zero was entered for all of the real constants of SOLID65, which turned the reinforcement capability of the SOLID65 element off. The cross sectional areas of the main steel and stirrups were entered for the LINK8 element as real constant sets 2 and 3, respectively. Real constant sets 4 and 5 were used for the epoxy and the CFRP materials, respectively.

2.3 Meshing and Boundary Conditions

Square and rectangular elements were created for the rectangular volumes (concrete, CFRP, epoxy, and steel plates) using the volume-mapped command. This properly sets the width and length of the steel reinforcement elements to be consistent with the elements and nodes of the concrete. A convergence study was carried out to determine the appropriate mesh density as shown in Fig. 1. The meshing of the reinforcement was a special case and the individual elements were created in the modeling process as shown in Fig. 1. However, the necessary mesh attributes for the concrete were set before each section of the reinforcement was created. The SOLID46 elements for epoxy and CFRP layers have the same meshing as SOLID65 elements for concrete to allocate the node over the node of each element. The command merge item was used to merge separate entities that have the same location into single entities. To reduce the computation time and disk space requirements and since there are symmetries in the cross-section of the RC beams and in the applied load about 2 planes, a quarter of each beam was modeled with proper boundary conditions. The models were 1.22 m (48 in.) long having a cross-section of 75x230 mm (3x9 in.).

To ensure proper modeling, displacement boundary conditions were applied at the planes of symmetry. The symmetry boundary conditions were set first. Nodes defining a plane through the beam cross-section at the center of the beam define one plane of symmetry. The nodes on this plane were constrained in the perpendicular direction. These nodes, therefore, have a degree of freedom constraint $UX = 0$. Second, all nodes selected at $Z = 0$ define another plane of symmetry. These nodes were given the constraint $UZ = 0$. The support was modeled as a roller that allows the beam to rotate at the support. The applied force was applied across the entire centerline of the steel plate. The beams were analyzed simulating 4-point loading case with the distance between the 2-point of loading is 610 mm (24 in.). The total applied load was divided into a series of small load increments, each 0.45 kN (0.1 kip). The Modified Newton–Raphson equilibrium iterations were used to check the convergence at the end of each load increment within a tolerance value of 0.001. The static analysis type was utilized to obtain the response of the beams. The model failure was identified when the solution of 0.0045 kN (0.001kips) load increment was not converging.

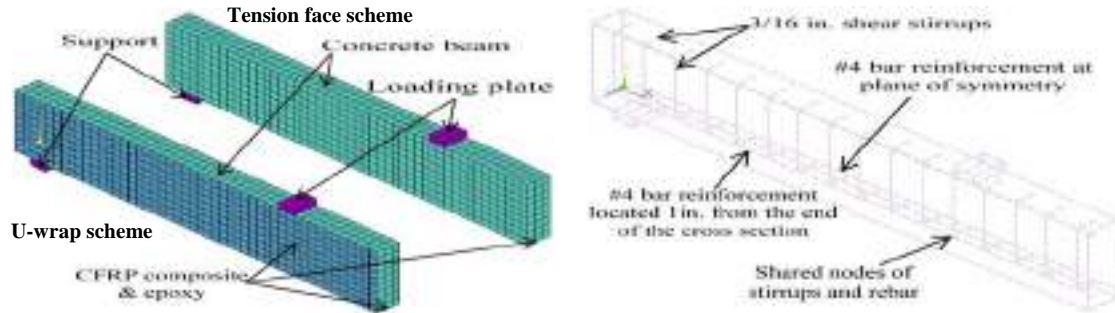


Figure 1: Meshing and Reinforcement Configuration for Quarter of the Beam

3. FINITE ELEMENT ANALYSIS RESULTS

The FEA results were validated with experimental test results of identical beams as shown in Fig. 2. The load deflection curves, load strain curves, ultimate flexural strengths, and ultimate displacements obtained from the FEA were in good agreement with the experimental test results. Fig. 2 shows typical load deflection curves for control beams and CFRP-strengthened beams with 1, 2, 3, 4, and 5 layers on the tension face and U-wrap strengthening schemes. Additional tables and figures that confirm the good agreement between the FEA and the experimental results will be presented at the conference. Fig. 2 reveals that for both strengthening schemes, increasing the number of CFRP layers leads to a non-proportional increase in the flexural strength capacity of the beam and to a reduction in the ultimate displacement.

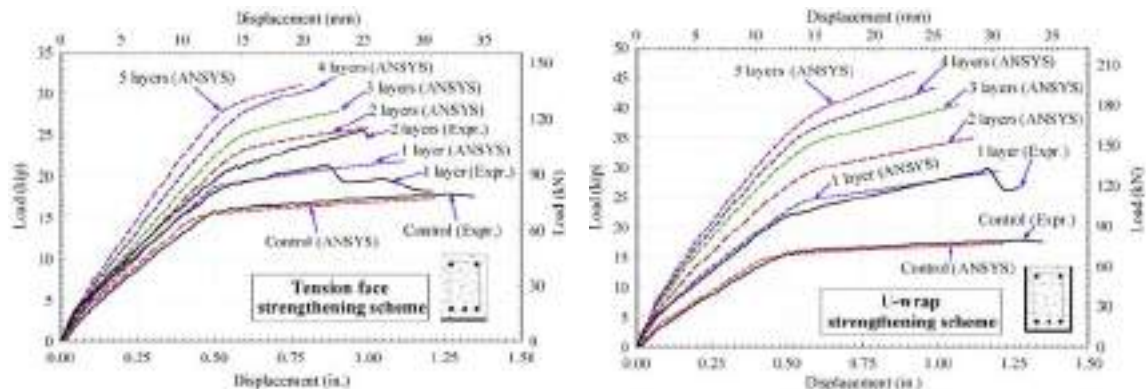


Figure 2: Load-Deflection Curves for the Control and Strengthened RC Beams

For further illustration, the normalized thickness of the CFRP sheet layers/effective beam depth ratio (t/d) was plotted versus the normalized flexural moment capacity (M/M_0) and versus the normalized ultimate displacement (Δ/Δ_0) as shown in Fig. 3. Logarithmic relationships were observed with high correlation coefficients as shown in Eqs. 1 and 2 below:

$$\frac{M}{M_o} = 0.6078 \ln\left(\frac{t}{d}\right) + 5.985 \quad (R^2 = 0.9894) \quad (1)$$

$$\frac{M}{M_o} = 0.3493 \ln\left(\frac{t}{d}\right) + 3.7398 \quad (R^2 = 0.9862) \quad (2)$$

Depending on the effective depth (d) of a RC beam having similar materials properties, these relationships can be utilized to predict the required thickness of CFRP sheet layers (t) for a required increase in the flexural moment capacity (M/M_o). The M/M_o of the beams strengthened with 1 layer ($t/d = 0.00081$) and 5 layers ($t/d = 0.00406$) of the U-wrap scheme were 1.7 and 2.7 times that of the control beam, respectively. For the corresponding beams strengthened with the tension face scheme, the M/M_o values were 1.25 and 1.8 times that of the control beam, respectively. The FEA results show that 5 layers of the tension face scheme are equivalent to 1 layer of the U-wrap scheme in terms of the improvement in the flexural moment capacity. Also, the reduction in the ultimate displacement is smaller and more stabilized for the beams strengthened with the U-wrap scheme than the beams strengthened with the tension face scheme. For $t/d = 0.00081$, the ultimate displacement of the beam strengthened using the U-wrap scheme was similar to the control beam, while it was about 90% of the ultimate displacement of the control beam for the beam strengthened using the tension face scheme. Using $t/d = 0.00406$, the reduction in the ultimate displacement was about 20% using the U-wrap scheme, while 35% using the tension face scheme. After a certain t/d ratio, there would be no further significant increase in the flexural moment capacity of the beam, while significant reduction in its ductility continues to occur.

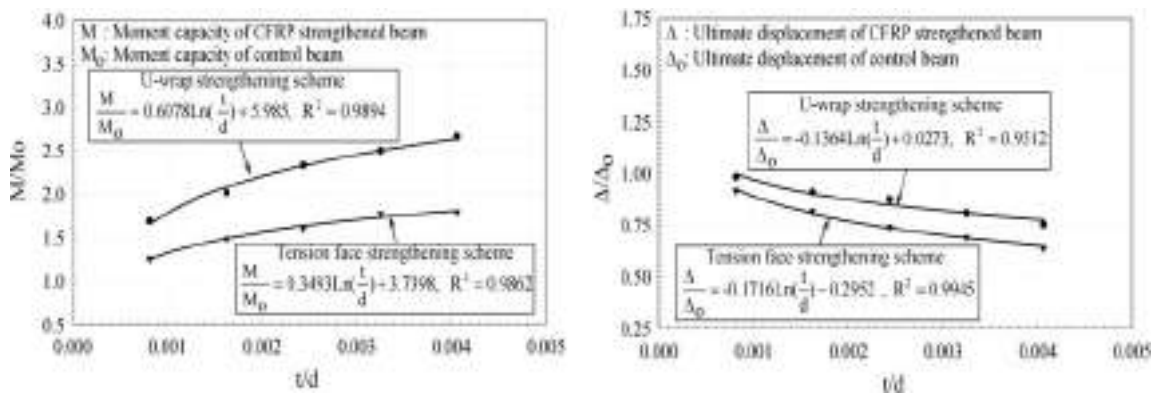


Figure 3: Normalized Ultimate Flexural Moments and Ultimate Displacements

4. CONCLUSIONS

A good agreement was observed between the FEA and the experimental test results. This concludes that FEA modeling could accurately predict the ultimate load capacity and deformation of CFRP strengthened slabs. The U-wrap CFRP-strengthening scheme improves the flexural strength of RC beams while maintaining acceptable ductility much better than the tension face scheme. After a certain t/d ratio, there would be no noticeable increase in the flexural strength of the beam, while significant reduction in its ductility continues to occur.

5. REFERENCES

- ANSYS (2005), ANSYS User's Manual Revision 9.0, ANSYS, Inc.
- Issa, M.I., Shabila, H., and Issa, Moussa A. (2003). "Structural behavior of reinforced concrete beams strengthened with CFRP subjected to static and fatigue loading". *Advanced Composites for Concrete Repair-1, Proceedings of the Structural Faults and Repair Conference*, Commonwealth Institute, Kensington, London, UK.
- Kachlakev, D.I., Miller, T.H., Yim, S., Chansawat, K., and Potisuk, T. (2000). "Linear and nonlinear finite element modeling of reinforced concrete structures strengthened with FRP laminates," *United States Department of Transportation, Federal Highway Administration*.
- Shahway, M., Beitelman, T., Arockiasamy, M., and Sowrirajan, R. (2001). "Flexural strengthening with carbon fiber-reinforced polymer composites of preloaded full-scale girders". *ACI Structural Journal*, pp. 735-742.

FINITE ELEMENT ANALYSIS OF FRP DEBONDING FROM CONCRETE UNDERGOING GLOBAL MIXED MODE I/II LOADING

Baolin Wan

(Assistant Professor, Marquette Universit, Milwaukee, WI, USA)

Zhenyu Ouyang

(Ph.D. Student, Marquette Universit, Milwaukee, WI, USA)

ABSTRACT

This research studies FRP debonding from concrete substrate of Modified Double Cantilever Beam (MDCB) specimen undergoing global mixed mode I/II loading. A series of 2D finite element models were built using ANSYS 10.0 software package to simulate the MDCB test. A modified virtual crack closure technique (VCCT) was used to extract the mode I and mode II interfacial energy release rates from the models. The finite element model was validated and calibrated by experimental data. The relationship between loading angle and critical interfacial energy release rate was obtained by a series of FEM analysis with different loading angles. Parametric studies were conducted to investigate the characteristics of FRP bonded concrete system. Seven parameters were considered: Young's modulus of concrete strength, Young's modulus and thickness of primer concrete layer, Young's modulus and thickness of adhesive layer and Young's modulus and thickness of FRP. It was found that Young's moduli of the materials had relatively small effects, while the thicknesses of primer concrete, adhesive layer and FRP had significant effects on the interfacial energy release rate while FRP debonding failure happened.

KEYWORDS

Bond, FRP, concrete, finite element, modified virtual crack closure (VCCT)

1. INTRODUCTION

One of major failure modes of the fiber reinforced polymer (FRP) composite materials repaired reinforced concrete beams is the FRP debonding failure from concrete substrates. This debonding failure limits the strength contribution from the FRP. There are five debonding mechanism (Oehlers, 2005) including plate end (PE), critical diagonal crack (CDC), flexural intermediate crack (FIC), shear intermediate crack (SIC) and axial intermediate crack (AIC). PE is concrete cover delamination starting from the end of FRP due to peeling force normal to the FRP. Such peeling force can be considered as Mode I loading based on the fracture mechanics definition. FIC and SIC propagate due to both shear and opening forces after concrete crack. Therefore, they are under mixed Mode I and II loading. AIC happens under pure shear loading condition which can be considered as Mode II loading. Modified Double Cantilever Beam (MDCB) test can be used to determine the energy release rate of FRP debonding from a concrete or masonry substrate under pure Mode I, mixed modes and pure Mode II loadings (Wan, 2002; Wan et al., 2004). Therefore, using MDCB test can simulate PE, FIC, SIC and AIC debonding.

The virtual crack closure technique (VCCT) has been widely used to extract the Mode I and Mode II interfacial energy release rates from finite element models (Krueger, 2002). The advantage of VCCT is that energy release rates can be calculated in a single geometric model instead of two complete analyses. Sethuraman and Maiti (1988) derived a modified virtual crack closure integral for square-root singularity elements in order to compute the strain energy release rate by moving the mid-side node position of the isoparametric quadratic element to the quarter location. This method can increase the accuracy of strain energy calculation for linear elastic analysis. In this study, the modified virtual crack closure integral was successfully used to model FRP debonding from concrete substrate under mixed mode loading conditions of MDCB tests. A series of FE models were built to study the effect of different parameters on the FRP debonding behaviors.

2. FINITE ELEMENT MODEL

Using the modified virtual crack closure integral, the strain energy release rate, G , can be expressed in terms of the nodal forces ahead of the crack tip and the opening displacements behind it (Sethuraman and Maiti, 1988).

$$G_I = \frac{(u_{yk} - u'_{yk})}{\Delta a} [F_{yj} + (1.5\pi - 4)F_{yi}] \quad (1)$$

$$G_{II} = \frac{(u_{xk} - u'_{xk})}{\Delta a} [F_{xj} + (1.5\pi - 4)F_{xi}] \quad (2)$$

where (F_{xi}, F_{yi}) and (F_{xj}, F_{yj}) represent the nodal forces at the node of crack tip and the node ahead of it, respectively; and (u_{xk}, u_{yk}) and (u'_{xk}, u'_{yk}) represent the nodal displacements behind it as shown in Figure 1.

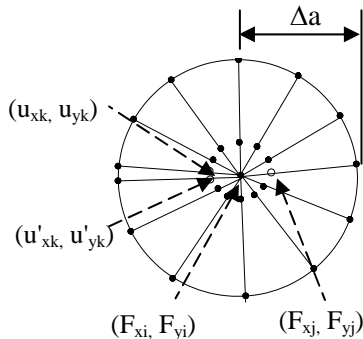


Figure 1: Elements and nodes around crack tip.

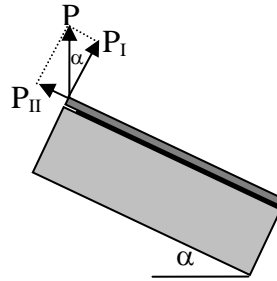


Figure 2: MDCB test under mixed modes loading

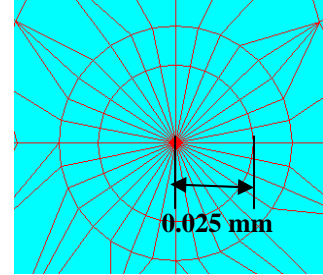


Figure 3: Elements around the crack tip

Wan et al. (2004) used MDCB test frame to study the bond between CFRP and concrete undergoing global mixed mode I/II loading. Three loading angles were used in the test program and corresponding energy release rates, G_I and G_{II} were calculated. The loading angle was defined as the angle between the bonding line and the horizontal plane as shown in Figure 2. It was reported (Wan, 2002) that a layer of concrete residue remaining on the fracture surface of the detached CFRP after MDCB test. Such layer of concrete contains the primer which penetrated into concrete through the microcracks, void and capillary pores on the superficial concrete. It was defined as primer-concrete in this research. The typical Young's modulus of polymer modified concrete is 4.2×10^4 MPa (Blaga and Beaudoin, 1985) and this value was used in the models in this research. ANSYS 10.0 was used to generate 2D finite element models and perform parametric studies in this research. The geometric and material properties used in experimental test (Wan, 2002; Wan et al., 2004) were adopted. All materials were assumed to be linear elastic. The crack was assumed to locate between primer-concrete and concrete substrate. The element length of the first group of elements around crack tip was 0.025 mm as shown in Figure 3. The critical energy release rates G_{IC} and G_{IIC} obtained in the experimental test with its linear least-squares best fit are shown in Figure 4. The loads used in FE models were calibrated by referring the experimental results in order to calculate the critical energy release rates. It is shown in Figure 4 that the FE results had excellent agreement with the experimental data.

3. COMPUTER SIMULATIONS

The validated FE model presented in previous section was used as control model. The calibrated load values were applied in the models for parametric studies. Seven parameters were selected, i.e., (a) Young's modulus of concrete, E_c , (b) Young's modulus of primer concrete, E_{pc} , (c) thickness of primer concrete, t_{pc} , (d) Young's modulus of adhesive, E_a , (e) thickness of adhesive, t_a , (f) Young's modulus of FRP, E_{frp} and (g) thickness of FRP, t_{frp} . The following paragraphs introduce each study and discuss the findings. In Figures 5 to 11, the solid line represents the critical G values for FRP debonding from concrete substrate in control specimen. If the calculated G values fall in the left of and below the line, it means FRP will not debond under the calibrated loads and larger loads are needed to debond for such cases.

The Young's modulus of concrete, E_c , was modified by $\pm 10\%$ and $\pm 20\%$ to study its effect on FRP debonding. It is shown in Figure 5 that total energy release rate increased slightly with the decrease of E_c . However, such change was very small. The change of total G value was less than 1% when E_c was changed up to 20%.

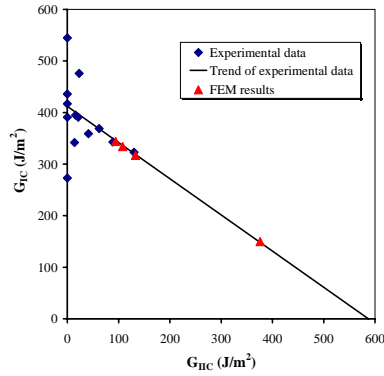


Figure 4: Critical G values

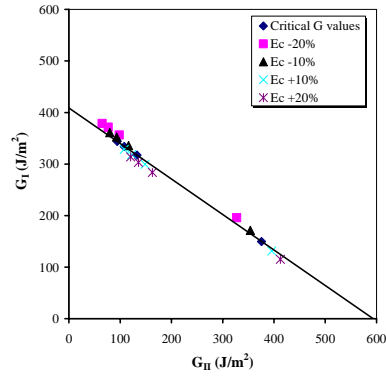


Figure 5: Effect of E_c

The Young's modulus of primer-concrete, E_{pc} , was modified by $\pm 10\%$ and $\pm 20\%$. When E_{pc} decreased, G_{II} component increased while G_I component kept almost same as control specimen as shown in Figure 6. Total G value increased with the decrease of E_{pc} . It indicated that the specimen with lower value of E_{pc} would be easier to debond. The average thickness of primer-concrete in experimental test was 2 mm. Four different primer-concrete thicknesses were selected for the parametric study: 0, 1, 3 and 4 mm. When primer-concrete thickness decreased, the energy release rate values increased significantly if the load was kept same as control model (Figure 7). It means that actual fracture load with thinner primer-concrete would be significantly lower.

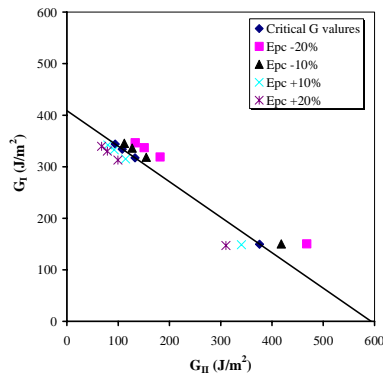


Figure 6: Effect of E_{pc}

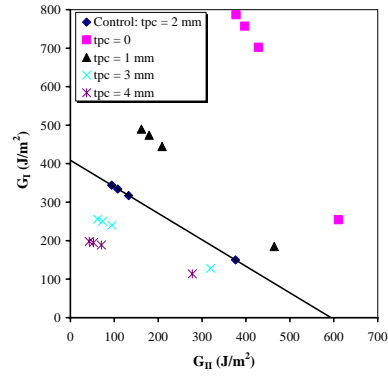


Figure 7: Effect of t_{pc}

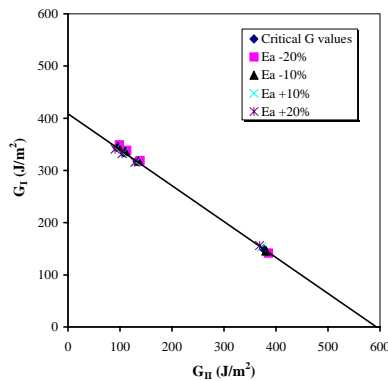


Figure 8: Effect of E_a

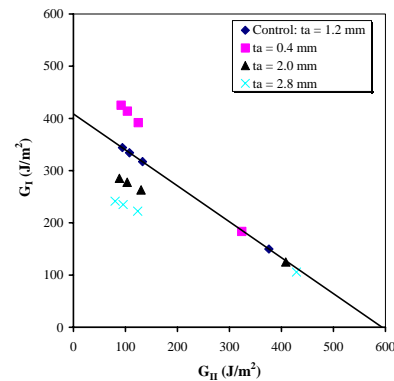


Figure 9: Effect of t_a

The Young's modulus of adhesive, E_a , was modified by $\pm 10\%$ and $\pm 20\%$. It is shown in Figure 8 that there was almost no change of G values for the $\pm 20\%$ change of E_a values. Therefore, Young's modulus of adhesive did not have significant effect on the FRP debonding phenomenon in the scope of this study. The average thickness of adhesive in experimental tests was 1.2 mm. Three different primer-concrete thicknesses were selected for parametric study: 0.4, 2.0 and 2.8 mm. The adhesive thickness effect is shown in Figure 9. In the region where G_I

value was dominant, calculated G value increased with the decrease of t_a value. It indicated that the specimen with thinner adhesive layer was easier to fracture when Mode I component was dominant. In the region where Mode II loading was dominant, thinner adhesive layer would result lower G_{II} value but higher G_I value. However, the total G value located on the critical line for all selected thickness in this situation. It indicated that the fracture loads for them would be same as those for control specimen.

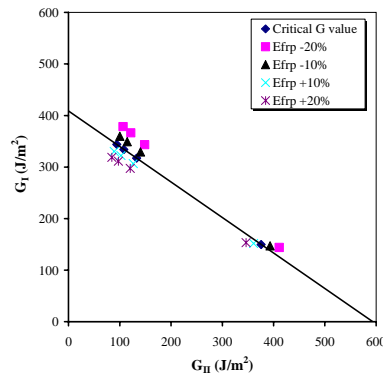


Figure 10: Effect of E_{frp}

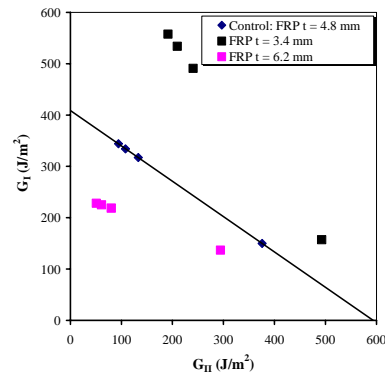


Figure 11: Effect of t_{frp}

The Young's modulus of FRP, E_{frp} , was modified by $\pm 10\%$ and $\pm 20\%$. It is shown in Figure 10 that G values increased with the decrease of E_{frp} . Therefore, the FRP with lower Young's modulus would be easier to debond. The average thickness of FRP in experimental tests was 4.8 mm. The FRP thicknesses of 3.4 and 6.2 mm were selected for parametric study: 3.4 and 6.2 mm, which were $\pm 30\%$ of the control specimen. It is shown in Figure 11 that thinner FRP would be easier to debond if the stress in FRP itself did not reach its ultimate strength.

4. CONCLUSIONS

This research modeled the MDCB tests using finite element method and parametric study was performed. The following conclusions can be drawn from this study:

1. Concrete Young's modulus did not have significant effect on the energy release rate when FRP was debonding.
2. The specimen with lower value of E_{pc} and thinner primer-concrete would be easier to debond.
3. Young's modulus of adhesive did not have significant effect on the FRP debonding phenomenon in the scope of this study. The specimen with thinner adhesive layer was easier to fracture when Mode I component was dominant. When there was significant Mode II loading component, the fracture loads for the specimens with different thickness of adhesive layer were same as those for control specimen.
4. If FRP had lower Young's modulus and smaller thickness, the specimen would be easier to debond.

5. REFERENCES

- Blaga, A. and Beaudoin, J.J. (1985). "Polymer Modified Concrete", Canadian Building Digests, CBD-241, http://irc.nrc-cnrc.gc.ca/pubs/cbd/cbd241_e.html, 04/03/06.
- Krueger, R. (2002). "The virtual crack closure technique: history, approach and applications", NASA/CR-2002-211628, ICASE Report No. 2002-10, Hampton, Virginia, 64 pp.
- Oehlers, D.J. (2005). "Generic debonding mechanisms in FRP plated beams and slabs", *Proceedings of the International Symposium on Bond Behaviour of FRP in Structures*, December 7-9, 2005, Hong Kong. pp 35-44.
- Sethuraman, R. and Maiti, S.K. (1988). "Finite element based computation of strain energy release rates by modified crack closure integral," *Engineering Fracture Mechanics*, Vol. 30, pp 227-231.
- Wan, B. (2002). *Study of the Bond Between FRP Composites and Concrete*, Ph.D. Dissertation, Department of Civil and Environmental Engineering, University of South Carolina, 205 pp.
- Wan, B., Sutton, M., Petrou, M.F., Harries, K.A., and Li, N. (2004). "Investigation of bond between FRP and concrete undergoing global mixed mode I/II loading", *ASCE Journal of Engineering Mechanics*. Vol. 130 No. 12, pp 1467-1475.

FINITE ELEMENT MODELLING OF FRP SHEAR-STRENGTHENED RC BEAMS

O.F.A. Otoom

(PhD Candidate, Centre for Built Infrastructure Research, University of Technology Sydney, Australia)

S.T. Smith

(Senior Lecturer, Centre for Built Infrastructure Research, University of Technology Sydney, Australia)

S.J. Foster

*(Associate Professor, School of Civil and Environmental Engineering,
The University of New South Wales, Australia)*

ABSTRACT

Reinforced concrete (RC) beams can be strengthened in shear with externally bonded fibre reinforced polymer (FRP) composite strips. Despite the relatively large body of research available, there remains uncertainty regarding the distribution and magnitude of strains and stresses in the concrete, and in the externally bonded FRP. Of particular importance is the contribution of the FRP reinforcement to the shear strength at ultimate. In this paper, a finite element (FE) investigation on RC beams strengthened in shear with epoxy bonded FRP strips is undertaken and the results compared with test data. The study shows that the FE approach is able to capture the overall behaviour of the test specimens, including debonding of the FRP strips.

KEYWORDS

FRP, Reinforced Concrete, Strengthening, Shear, Finite Element Modelling, External Bonding

1. INTRODUCTION

The shear capacity of a reinforced concrete (RC) beam can be enhanced with the addition of externally bonded fibre reinforced polymer (FRP) strips or sheets as has been reported from numerous experimental studies (e.g. Khalifa and Nanni 2002, Bousselham and Chaallal 2006). Tests have found anchored FRP strengthening to predominantly fail by rupture of the FRP, while debonding was found to occur for unanchored strips. Only a handful of papers (e.g. Khalifa and Nanni 2002) describing tests on FRP shear-strengthened RC beams have reported the geometrical and material properties of the concrete, steel reinforcement and FRP strengthening, as well as the failure mode, in enough detail for the results to be meaningfully computationally analysed.

A limited number of finite element (FE) studies are reported on the modelling of shear-strengthened RC beams with the study by Wong and Vecchio (2003) being one of the more comprehensive. Wong and Vecchio compared FE predictions with tests on RC beams, without steel shear stirrups, strengthened with side bonded FRP. All beams failed by debonding and the bond-slip behaviour of the FRP-to-concrete was a key component in the modelling of debonding failures. More recently, Smith et al. (2006) used FE to analyse the distribution and magnitude of strains and stresses in RC beam containing internal steel stirrups and strengthened in shear with FRP strips. Tests are urgently required in order to overcome the lack of reliable experimental data that is prohibiting further comparison with FE predictions. In such tests, it is imperative that all control and material data needed as input into an analytical or numerical model be collected.

In this paper the results of a FE investigation are reported on RC beams, without steel shear stirrups, strengthened in shear with FRP U-jackets. The FE predictions are compared with experimental results of Khalifa and Nanni (2002) of a FRP U-strip shear-strengthened RC beam failing by FRP debonding.

2. FINITE ELEMENT MODELLING OF FRP-STRENGTHENED RC BEAMS

The non-linear reinforced concrete FE program RECAP (Foster and Gilbert 1990), updated to account for externally bonded FRP, is used in this study. A brief description of the elements used for modelling of FRP strengthened members is given below with a full implementation of the model in Khomwan and Foster (2004a, 2004b).

Modelling of repaired concrete beams where the repair is on the sides of the beam can be undertaken by attaching a layer of repair elements to the beam via a layer of interface elements (Figure 1a). Side face repaired beams can be modelled using either a 2D element formulation, e.g. as presented by Khomwan and Foster (2004a, 2004b), or using 1D discrete bar elements with an area equal to the thickness of the FRP times the width over which it acts.

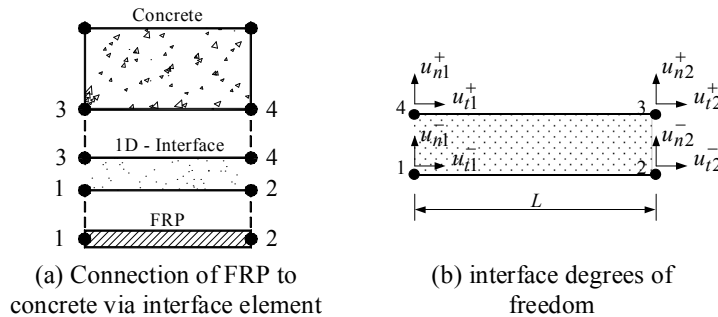


Figure 1. Concrete, steel and interface elements

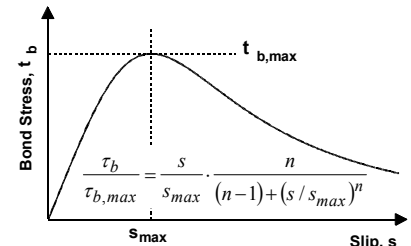


Figure 2. Bond stress-slip model

Bar elements are used to model the FRP and a 4-node interface element, shown in Figure 1b, is used to model slip between the FRP and the concrete. To maintain compatibility between the FRP and the concrete in the normal direction, a stiff elastic modulus is used. In the tangential direction Popovics (1973) equation, as shown in Figure 2, is used to represent the local bond stress τ_b versus slip s relationship where $\tau_{b,max}$ is the maximum local bond stress; s_{max} is the slip at $\tau_{b,max}$; and n is a constant. The parameters $\tau_{b,max}$, s_{max} and n in the current study were matched to the ascending portion of Lu et al.'s (2005) generic bond-slip relationship using concrete and FRP properties of the test beam described in Section 3. The results of the FE model were not found to be overly sensitive to the shape of the descending curve. For stability of the solution process, the bond stiffness (in the tangential direction) is taken as the secant stiffness in a modified Newton-Raphson solution procedure with more details in Chong et al. (2004). The cracked membrane model finite element (CMM-FE) formulation of Foster and Marti (2003) was used for the RC.

3. COMPARISON OF FE RESULTS WITH TEST DATA

The FE model is compared with tests undertaken by Khalifa and Nanni (2002) on RC beams strengthened with externally bonded FRP U-jackets strips that failed by debonding of the FRP.

3.1. Test Beams and FE Mesh

Khalifa and Nanni (2002) tested 12 RC beams of which four were unstrengthened reference beams and seven were strengthened in shear with different arrangements of externally bonded FRP U-jacket strips or continuous U-jacket sheets. Other variables investigated were of different amounts of internal shear reinforcement (i.e. two with stirrups and two without stirrups in the critical shear span) and different shear span-to-effective depth ratios. Two of these beams have been selected for analysis; reference beam S03-1 which was unreinforced in shear in one shear span and beam S03-2 which was also unreinforced for shear but externally strengthened using CFRP U-jackets (Figure 3).

The mean cylinder compressive strength of both beams was $f_{cm} = 28$ MPa, and the concrete tensile strength in the present paper was taken as 1.7 MPa ($0.33\sqrt{f_{cm}}$). The yield and fracture strengths of the 10 mm diameter stirrups were 350 MPa and 530 MPa, respectively, with corresponding yield and fracture strains of 1750 $\mu\epsilon$ and 2650 $\mu\epsilon$ respectively. The yield strength and elastic modulus of the longitudinal bars were 460 MPa and 200 GPa respectively. The effective depth of the longitudinal tension steel bars was taken as 260 mm with clear cover assumed to be 20 mm. Each FRP strip was 50 mm wide and 0.165 mm thick and was applied using a wet lay-up procedure. The ultimate tensile strength and corresponding fracture strain of the FRP were 3,790 MPa and 16,620 $\mu\epsilon$ respectively. Based on the concrete strength and geometric properties of the FRP and concrete for beam S03-2, the values of parameters $\tau_{b,max}$, s_{max} and n for use in Popovics equation were 4.5 MPa, 0.06 mm and 2.5, respectively.

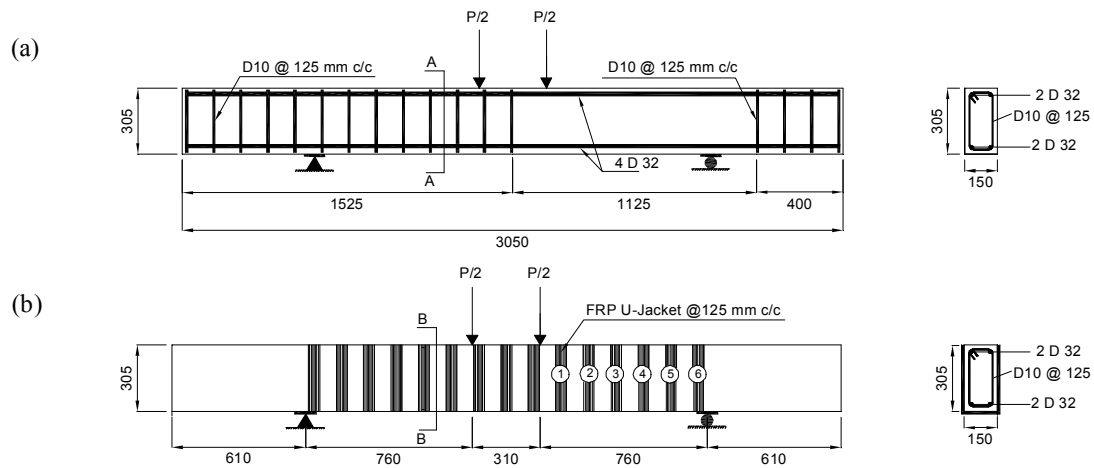


Figure 3. Khalifa and Nanni (2002) specimens: (a) beam S03-1, and (b) beam S03-2.

The FE model used in the study was based on a 25 mm square mesh using 4-node isoparametric elements. Cracking was modelled using a crack band approach (Bazant and Oh 1983) with the tensile fracture energy taken as 75 N/m. The longitudinal reinforcing steel was smeared within the concrete element and shear reinforcing steel was modelled using bar elements overlayed on the concrete mesh. In mesh sensitivity studies by Khomwan and Foster (2004a), the solution involving debonding failure, using the elements described, was shown to be mesh size independent.

3.2. FE and Test Results

3.2.1 Reference Beam, S03-1

The load versus midspan deflection response for the reference beam is given in Fig. 4a. A reasonable correlation exists between the experimental results (denoted as S03-1 (Exp)) and the FE calculation (denoted as S03-1 (FE)). Although the FE model gave a higher failure load, the results were found to be sensitive to the concrete tensile strength adopted. The FE model correctly predicted the beam to fail in a shear mode.

3.2.2 FRP-Strengthened Beam, S03-2

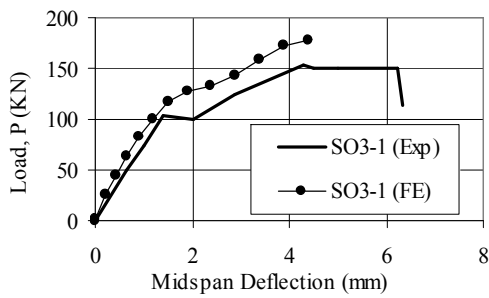
The load versus midspan deflection response for beam S03-2 is given in Figure 4b. Good correlation is observed between the experimental results and FE calculations. Figure 5a shows the variation of slip along the length of the FRP strips at the maximum applied shear ($P = 265\text{kN}$). The greatest slip is recorded in strips labelled 3 and 4 in Figures 5b and 3b. These two strips correspond to the debonded strips in Figure 5b from Khalifa and Nanni (2002). Strips 2 and 5 also debonded as can be seen in Figure 5b and their slips also slightly exceeded the peak slip in Figure 5a. It is likely the debonding of strip 5 in Khalifa and Nanni's (2002) experiment occurred from a sudden shift of load from debonding of strips 3 and 4. Strip 2, which debonded near its free end, may have debonded at quite a low load but it did not affect the load carrying capacity of the system

4. CONCLUSIONS

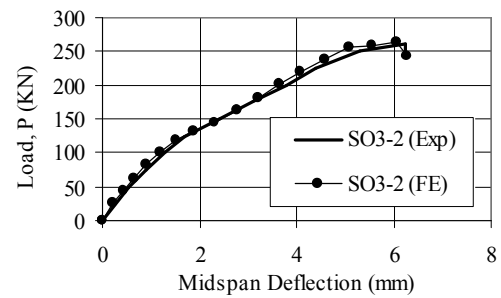
The behaviour of FRP-strengthened RC beams has been determined by FE modelling with the epoxy bond interface included in the model. The computed load versus displacement response compared well with that measured in the test. The numerical model accurately predicted a shear failure mechanism for the reference beam and FRP debonding for the strengthened beam.

5. ACKNOWLEDGEMENTS

This project was funded by Australian Research Council (ARC) Discovery Grant DP0453096. The financial assistance of the ARC is gratefully acknowledged.

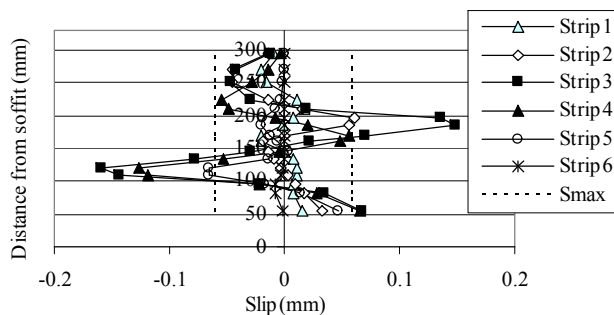


(a) Reference Beam – S03-1



(b) Strengthened beam – S03-2

Figure 4. FE and experimental results: load versus deflection



(a) Distance from soffit versus FRP slip at maximum applied shear



(b) Test beam (Khalifa and Nanni 2002)

Figure 5. FE and experimental results, and behaviour of FRP

6. REFERENCES

- Bazant, Z.P. and Oh, B.H. (1983). "Crack band theory for fracture of concrete". *Materials and Structures*, Vol. 16, No. 93, pp. 155-177.
- Bousselham, A. and Chaallal, O. (2006). "Effect of transverse steel and shear span on the performance of RC beams strengthened in shear with CFRP". *Composites: Part B*, Vol. 37, pp. 37-46.
- Chong, K.T., Gilbert, R.I. and Foster, S.J. (2004). "Modelling time-dependent cracking in reinforced concrete using bond-slip interface elements". *Computers and Concrete*, Vol. 1, No. 2, pp. 151-168.
- Foster, S.J. and Gilbert, R.I. (1990). *Non-linear Finite Element Model for Reinforced Concrete Deep Beams and Panels*. UNICIV Report No. R-275, School of Civil Engineering, University of New South Wales, Australia, December, 113 pp.
- Foster, S.J. and Marti, P. (2003). "Cracked Membrane Model: FE Implementation". *Journal of Structural Engineering, ASCE*, Vol. 129, No. 9, pp. 1155-1163.
- Khalifa, A. and Nanni, A. (2002). "Rehabilitation of rectangular simply supported RC beams with shear deficiencies using CFRP composites". *Construction and Building Materials*, Vol. 16, pp. 135-146.
- Khomwan, N. and Foster, S.J., (2004a) *Finite Element Modelling of FRP Strengthened Walls*, UNICIV Report R-432, The University of New South Wales, School of Civil and Environmental Engineering, Kensington, Sydney, Australia, November 2004, ISBN: 85841 399 X, 68 pp.
- Khomwan, N. and Foster, S.J. (2004b). "FE Modelling of Bond in FRP-Repaired Plane Stress Members". *Proc., 18th Australasian Conf. on the Mech. of Struct. and Mat., ACMSM 18*, 1-3 December, Perth, Australia, pp. 113-118.
- Lu, X.Z., Teng, J.G., Ye, L.P. and Jiang, J. (2005). "Bond-slip models for FRP sheets/plates bonded to concrete". *Engineering Structures*, Vol. 27, pp. 920-937.
- Popovics, S. (1973). "A numerical approach to complete stress-strain curve of concrete". *Cement and Concrete Research*, Vol. 3, pp. 583-559.
- Smith, S.T., Ootom, O.F.A. and Foster, S.J. (2006). "Finite element modelling of RC beams strengthened in shear with FRP composites". *Proc. (CD Rom), 2nd International fib Congress*, Naples, Italy, 5-8 June.
- Wong, R.S.Y. and Vecchio, F.J. (2003). "Towards modelling of reinforced concrete members with externally bonded fiber-reinforced polymer composites". *ACI Structural Journal*, Vol. 100, No. 1, pp. 47-55.

A FINITE ELEMENT ANALYSIS ON SHEAR AND NORMAL STRESSES IN ADHESIVELY-BONDED JOINTS OF COMPOSITE STRUCTURES

Luciano Feo

(Associate Professor, Department of Civil Engineering, University of Salerno, Fisciano (Sa), Italy)

Francesco Ascione

(PhD Student, Department of Civil Engineering, University of Rome "Tor Vergata", Rome, Italy)

ABSTRACT

A two-dimensional finite element analysis is developed in this paper to study the effect of adherends transverse moduli on the distributions of shear and normal stresses in adhesively double-lap joints of composite structures. The numerical results are compared with those of analytical solutions.

KEYWORDS

Adhesion, Bonded joints, Pultrusion, Composite structures, FEA.

1. INTRODUCTION

Fiber-reinforced composite (FRP) materials are being used more and more in civil engineering structures due to their positive mechanical properties such as elevated rigidity/weight and resistance/weight ratios, high corrosion resistance and rapid installation of components. The advances in pultrusion technology allow large-scale structural profiles with acceptable cost for civil infrastructure applications [Barbero, 1998, Head, 1996, Keller, 2001] to be produced.

As well-known, structural FRP components are still difficult to connect due to the brittle fibrous and anisotropic nature of the materials. The current practice of bolting leads, in most cases, to an over-sizing of the components. Adhesive bonding is therefore more appropriate for FRP composites. Adhesive joints show higher joint efficiencies and are much stiffer compared to bolted joints. Furthermore, the load transfer in adhesive joints is more uniform with fewer stress concentrations when compared to bolted joints.

Joint strength must be predictable as a function of the material properties, the joint geometry and the type of loading, for adhesive bonding to be used in the design of FRP structures. The understanding of the stress-strain state in the joint is a prerequisite for the successful prediction of joint strength. Stress analyses are readily performed through numerical analyses such as finite element method. In literature one of the first theories about adhesive joints was proposed by [Volkersen, 1938] who studied a simple shear lag model based on the assumption of one dimensional bar-like adherends with only shear deformation in the adhesive layer. Over the years, this theory has been modified by incorporating with adherend shear deformation [Hart-Smith, 1987, Hart-Smith, 2002, Tsai, Oplinger and Morton, 1998].

The aim of this paper is to evaluate the effect of adherends shear deformation on the shear and normal stress distributions along the overlap of double-lap joints made from FRP.

2. DOUBLE-LAP JOINT

The geometric profile of a double-lap joint is shown in Fig.1, where: $2c$ is the length of the overlap, t_o and t_i are the thicknesses of the outer and inner adherends, respectively, E_o and G_o are the elastic modulus (in the longitudinal direction) and the shear modulus (in the transverse direction) for the outer adherends, respectively, E_i and G_i are the corresponding properties of the inner adherend, G_c and η are the adhesive shear modulus and the corresponding thickness, T is an applied force per unit width.

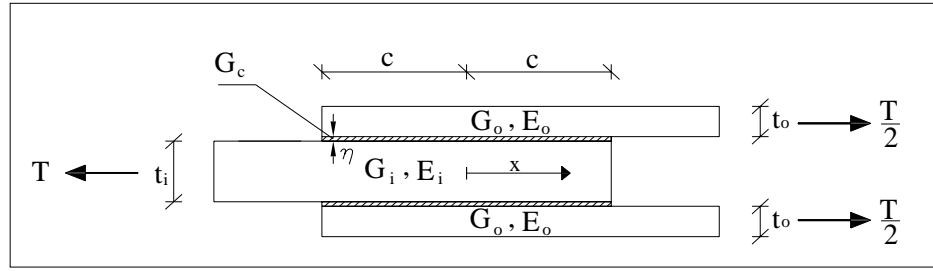


Figure 1: Geometric profile of a double-lap joint

In [Tsai, Oplinger and Morton, 1998] it is possible to find the integral version of the double-lap joint (TOM theory). The shear stresses, τ_c , in the adhesive layer can be expressed as the following form:

$$\tau_c = A \sinh(\beta x) + B \cosh(\beta x). \quad (1)$$

The expressions of the constant coefficients A and B are:

$$A = \frac{\beta T}{4 \cosh(\beta c)} \left[\frac{1 - \frac{E_i t_i}{2E_o t_o}}{1 + \frac{E_i t_i}{2E_o t_o}} \right], \quad B = \frac{\beta T}{4 \sinh(\beta c)}, \quad (2)$$

where the parameter β is defined as:

$$\beta^2 = \lambda^2 \alpha^2, \quad (3)$$

λ and α being, respectively, the *elongation parameter* and the *shear deformation parameter*:

$$\lambda^2 = \frac{G_c}{\eta} \left(\frac{2}{E_i t_i} + \frac{1}{E_o t_o} \right), \quad (4)$$

$$\alpha^2 = \left[1 + \frac{G_c}{\eta} \left(\frac{t_i}{6G_i} + \frac{t_o}{3G_o} \right) \right]^{-1}. \quad (5)$$

The closed form solution proposed by [Volkersen, 1938] can be recovered by assuming that adherends shear deformations are zero, or that adherends shear moduli, G_i and G_o , are infinitely large, therefore $\alpha = 1$.

3. THE FINITE ELEMENT ANALYSIS

A balanced double-lap joint, with graphite-epoxy laminated adherends, has been considered in this study. The 2D finite element analysis has been performed by using the commercial program Straus7. Fig.2 shows the finite element mesh, where the six-node triangle is employed. In Table 1 the values of the used geometrical and mechanical parameters are summarized.

Fig.3 shows the comparison between FEM results and those of the analytical solutions, both TOM theory ($\alpha < 1$) as well as Volkersen (VT) ($\alpha = 1$), in terms of shear stress distribution in the adhesive layer.

As it can be seen, the shear stress distribution, obtained by FEM, is characterized by higher values than the analytical ones in the central part of the overlap region. Moreover, it can be observed that in the finite element analysis the maximum shear stress does not occur on both ends simultaneously in contrast to the analytical solutions. Furthermore, the maximum values of shear stress, at the ends, are also lower.

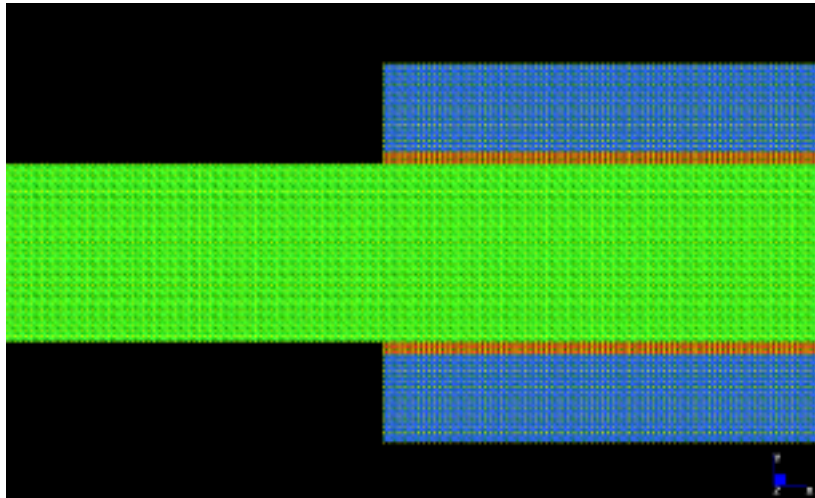


Figure 2: Finite element mesh of the double-lap joint.

Table 1: Geometrical and mechanical parameters.

Parameters	Length [mm]	Thickness [mm]	Shear Mod. [GPa]	Young Mod. [GPa]
Adhesive	12.7	0.15	0.910	2.51
Outer adherend	12.7	1.00	137.0	4.83
Inner adherend	12.7	2.00	137.0	4.83

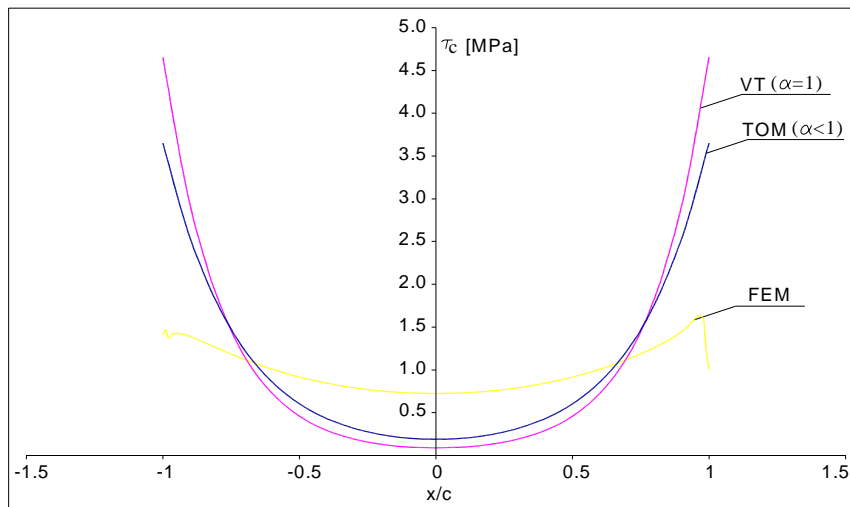


Figure 3: Comparison between FEM results and analytical solutions: VT ($\alpha=1$), TOM ($\alpha<1$).

4. PARAMETRIC STUDY

In the classical theory [Volkersen, 1938], adherend shear deformations are ignored, either possibly due to the relatively small values compared to longitudinal normal deformations in some cases, or to the complexity of formulations.

The maximum shear distribution in the adhesive is over-estimated if adherend shear modulus is neglected, as highlighted in [Tsai, Oplinger and Morton, 1998]. This effect is more accentuated especially for adherends with relatively low transverse shear modulus as in the case of laminate composite adherends.

In order to investigate the effect of shear adherends modulus on the adhesive shear and normal stress distributions, a parametric study, with respect to the below parameter, has been developed in this work:

$$\frac{k G}{G_c}, (G = G_o = G_i) . \quad (6)$$

Figs. 4,5 show, respectively, the influence of shear adherends modulus on the adhesive shear and normal stress distributions along the overlap length. It can be observed, in particular, that as k increases the adhesive shear stress belongs to VT solution ($\alpha=1$).

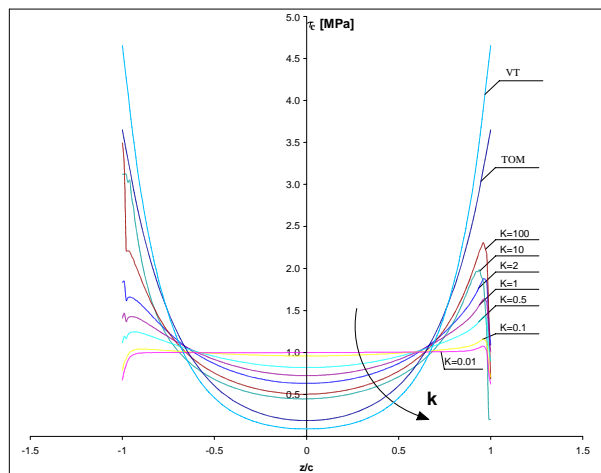


Figure 4: Shear stress distributions.

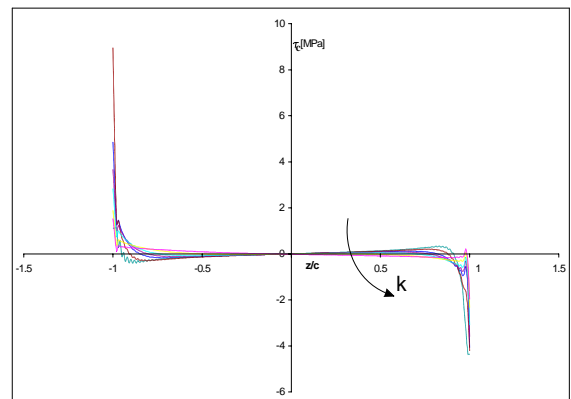


Figure 5: Normal stress distributions.

5. CONCLUSIONS

A two-dimensional finite element analysis has been developed to study adhesive bonding for double-lap joints of FRP materials. The effect of shear adherend modulus on the shear and normal stress adhesive distributions has been investigated, showing that such stresses depend on the adherend shear modulus, in particular for laminated composites with low shear modulus. When comparing FEM results to classical theory it is possible to note that the latter over-estimates them.

6. REFERENCES

- Barbero E , 1998, "Introduction to composite material design", Taylor & Francis.
- Hart-Smith LJ. , 1987, in: Matthews FL Editor., "Design of adhesively bonded joints. Joining fiber-reinforced plastics". Elsevier Applied Science; 271–311.
- Hart-Smith LJ., 2002, "Adhesive bonding of composite structures—progress to date and some remaining challenges". J Compos Technol Res; 24(3):133–53.
- Head P. R., 1996, "Advanced composites in civil engineering - A critical overview at this high interest, low use stage of development", II International conference on advanced composite materials in bridges and structures, Montréal, Québec, Canada; 3-15.
- Keller T. , 2001, "Recent all-composite and hybrid fiber reinforced polymer bridges and buildings". Progress Struct Eng Mater; 3/2:132–40.
- Tsai MY, Oplinger DW, Morton J., 1998, "Improved theoretical solutions for adhesive lap joints". Int J of Solids Struct; 35(12):1163–85.
- Volkersen O., Die Nietkraftverteilung, 1938, in "Zugbeanspruchten" Konstanten Laschenquerschnitten. Luftfahrtforschung; 15:41–7.

FINIT ELEMENT MODELING OF FRP-FILAMENT WINDED POLES

R.Masmoudi

(Professor, University of Sherbrooke, Sherbrooke, QC, Canada)

H. Mohamed

(Ph.D Student, University of Sherbrooke, Sherbrooke, QC, Canada)

ABSTRACT

A large-scale research program is currently undertaken at the Department of Civil Engineering, University of Sherbrooke, Canada, to assess the general behaviour of light weight, glass fibre reinforced polymer (GFRP), pole structures. A finite element (FE) program was used to perform a nonlinear numerical analysis to model the static flexural behaviour of GFRP poles. The results of the FE analysis are compared to the experimental results conducted on full scale identical GFRP poles. A parametric study on 12 m (40 ft) GFRP poles was carried out to show the effect of fibre orientation and the number of circumferential layers on the load carrying capacity and deflection behaviour. The results show a good agreement between the FE analysis and the experimental data. The theoretical model is used to evaluate the performance of a GFRP pole and to determine the optimum cross section dimensions at three different zones along the height of the GFRP pole structure.

KEYWORDS

Fibre Reinforced Polymers, FRP Structural Shapes, FRP poles, Flexural behaviour, Filament Winding.

1. INTRODUCTION

The GFRP poles technology has been used for over thirty years in the application of the light poles and electrical transmission tower element, as a replacement for the conventional materials, due to their high strength-to-weight ratio and corrosion resistance (Ibrahim et al 2000 and Ibrahim et al., 1999). High quality surface coating and the ultraviolet radiation resistance treatment give the FRP pole a long service life, beyond eighty (80) years (Miller et al., 1995). A limited number of experimental and theoretical studies have been conducted on the behaviour of the tapered GFRP poles structure under lateral load (Lin 1995, Crozier et al., 1995, Derrick 1996). Due to the existence of a service opening at 2.7 m from the bottom of the FRP pole, and also due to small thickness-to-radius ratio, local buckling failure can reduce significantly the load carrying capacity. Therefore the part which includes this service opening must be addressed. It is important to find the optimum geometrical details for the region of the service opening, in order to be compatible with the upper and lower zones over the length of the pole. t

In this paper, a finite element program with a nonlinear numerical analysis was used to optimize the design of a 12 m (40ft), GFRP poles having a service opening.

2. FINITE ELEMENT ANALYSIS

A nonlinear finite element model was developed using the software ADINA finite element program. The finite element analysis was verified through comparison with the experimental data obtained from the static testing of full-scale GFRP poles, according to the recommendations described in ASTM and ANSI standard (Masmoudi and Metiche, 2006). The specimens were tapered hollow sections, and divided through the height into three zones, I, II and III. The 101.6 x 304.8mm-(width x length) service opening is located at the center of the middle zone II and was in the compression side, when loaded. The typical specimen dimensions and details of the three zones are shown in Figure 1. GFRP poles are fabricated using the filament winding technique. E-glass fibres and Epoxy resin were used for these poles. The pole modeled with a total number of elements equal to 2288 (16 and 143 in the

circumference and longitudinal direction, respectively). The mesh layout was fine for zones I and II, where maximum stresses and failure are expected to occur, and gradually becomes coarse at the top. This was made by the automatic mesh density option of the program. The general layout of the mesh distribution and the used finite element models are shown in Figure 1.

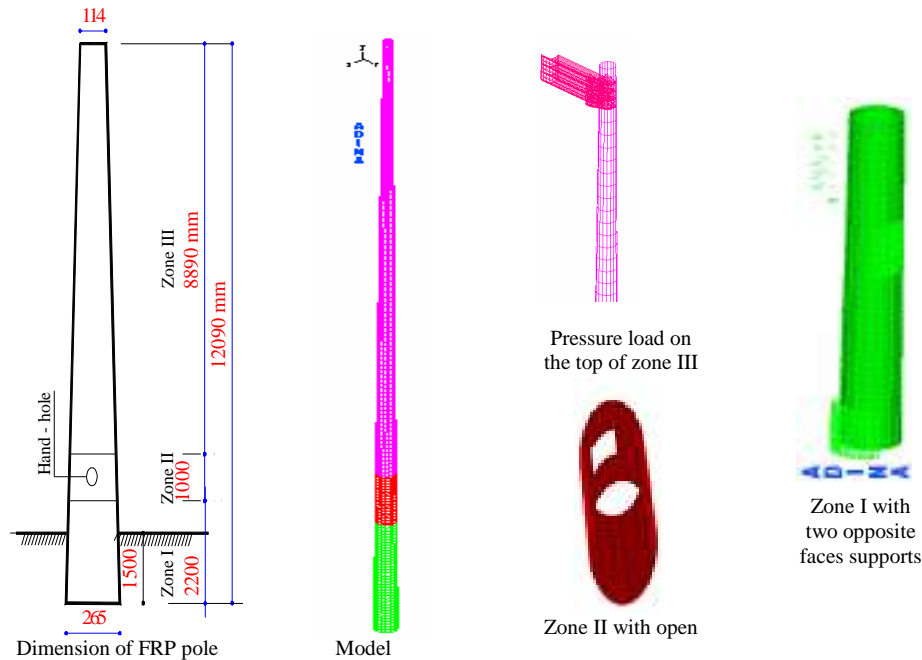


Fig. 1: The typical specimen dimensions and the details of the finite element model.

The under ground length of the GFRP poles were restraint along two opposite half circumference area, the first area at the end of the base and the second area at the ground line. This Configuration of restraints was to simulate the support condition described in standards ASTM D 4923-01 and ANSI C 136.20-2005. The GFRP pole was subjected to a horizontal pressure load (W) from the top of the pole edge by 300mm according to the ANSI C 136.20-2005 recommendations. The pole was incrementally loaded using 100-200 time steps. To avoid local failure under the applied load, a pressure-load has been used to simulate the same effect as in the experimental testing.

An eight-node quadrilateral multilayered shell element is used in the model; each node has six degrees of freedom, three translations (U_x , U_y , and U_z) and three rotations (R_x , R_y , and R_z). The composite shell elements are kinematically formulated in the same way as the single layer shell elements, but an arbitrary N number of layers can be used to make up the total thickness of the shell. The basic equations used in the formulation of the Multilayered Shell Element are given in the reference Bathe 1996. The material model used with the shell element is elastic-orthotropic with large displacement /small strain. The mechanical properties of the FRP laminate were obtained from the material properties of the E-glass fibre and the epoxy resin. Orthotropic material properties in the fibre and transverse to the fibre direction were defined. Fibre orientation for each layer was specified by defining the fibre angle with respect to the element axes. The effective materials properties were taken as follows: $E_1 = 45.5$ GPa, $E_2 = 10.5$ GPa, $G_{12} = 4.875$ GPa, $\nu_{12} = 0.31$, where, E_1 , E_2 , G_{12} and ν_{12} are the Young's modulus in the fibre direction, the Young's modulus in the transverse direction, the shear modulus, and the Poisson's ratio, respectively. Table 1 presents the fiber orientations and the stacking sequences for the actual and new designs.

Table 1. Stacking sequences for the tested poles and proposed new designs

Zone	Masmoudi and al. (2006)		New design
	Fibre orientation θ (Degrees)	Thickness (mm)	Fibre orientation θ (Degrees)
I	$[\pm 70, \pm 30, \pm 90]$	5.56	$[90, (\pm 10)_5, 90]$
II	$[90, \pm 20, \pm 70]$	13.62	$\{90, \pm 45, [90, (\pm 10)_5, 90] \pm 45, 90\}$
III	$[\pm 70, \pm 10, \pm 70]$	6.3	$[90, (\pm 10)_5, 90]$

3. RESULTS AND DISCUSSION

Failure of the modeled FRP poles was determined when the divergence of the solution was achieved or when the Tsai-Wu failure criterion value reached unity. A comparison between the finite element analysis and the results obtained from experimental testing of full-scale prototypes obtained by Masmoudi and al., 2006, was in terms of the load-deflection relationship and the ultimate load carrying capacity. Figure 2 represents the load deflection relationship for the experimental and finite element analysis. It is evident from this figure that there is a strong correlation between the results obtained from the finite element analysis and the experimental results.

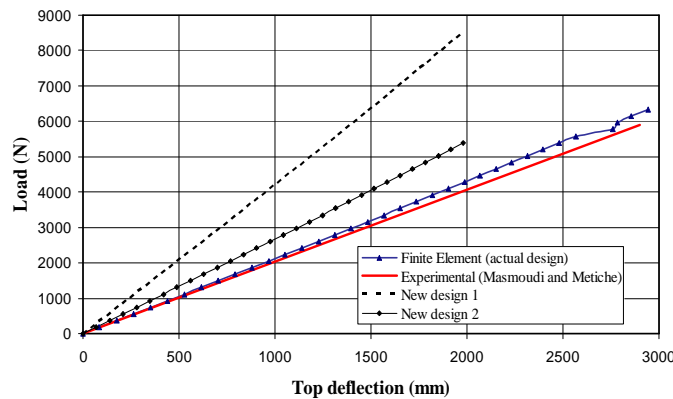


Figure 2: Comparison between experimental and FE analysis Load-deflection behaviour

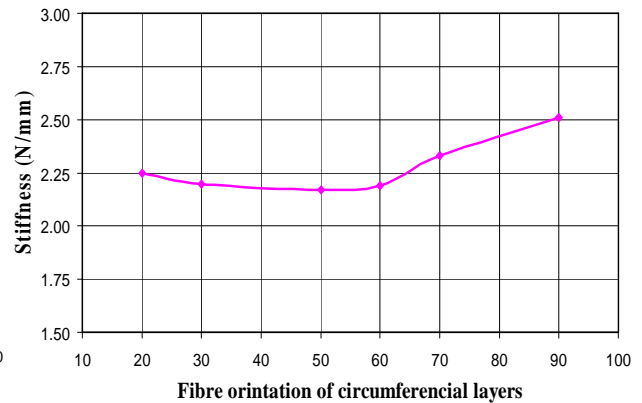


Figure 3: Effect of fibre orientations of circumferential layers on the stiffness of GFRP pole

Because of this agreement, the same finite element analysis was used to extend the study and examine the effect of fibre orientation of circumferential layers on the flexural behaviour of GFRP poles. To study this parameter the circumferential layers with fiber orientation of 70 degree were changed to 90, 60, 50 and 30 degree, with the same details of wall thickness, dimension of the GFRP pole and material properties. Figure 3 shows the relation between fibre orientations of circumferential layers and stiffness of GFRP pole for different models. It is clear that 90 degree of the fiber orientation gives the highest stiffness.

Description of the proposed GFRP pole design to reach an equivalent performance of classes 2 and 4 of wooden pole

The design criteria to satisfy the requirement strength criteria as given in the ASTM D 4923-01, AASHTO, and the general standard specifications of ANSI C 136.20-2005 for maximum deflection, ultimate load capacity and minimum embedment depth. The different combinations of parameters such as fibre orientation, number of longitudinal and circumferential layers and layer thickness are considered. It was also assumed that the total number of layers to be constant equal to 12 layers, (10 longitudinal and two circumferential layers in zone I, II, III). However, in order to reinforce zone II (service opening), 6 additional layers are used (3 inside the 12 previous layers and 3 outside the 12 previous layers), which make the total layers of this zone equal 18. The fibre angles assumed to be $+10^{\circ}/-10^{\circ}$ for longitudinal layers and 90° for circumferential layers. The $(90^{\circ}, +45^{\circ}/-45^{\circ})$ orientation are used for the 6 additional layers. The thickness of each layer was varied from 0.40 mm to 0.8 mm and for the thickness of each additional was assumed to be twice the previous thickness.

The finite element analysis was employed to optimize the design of the 12 m (40 ft) FRP pole to achieve an equivalent ultimate load capacity required for class 4 and class 2 wooden poles. After several FE simulations with different thickness, the results indicate that; the requirements for the FRP pole class 2 and class 4 achieved when the thickness of each layer were to be equal 0.5 mm and 0.75 mm, respectively. Thus, the total thickness of the laminate in zone I and zone III for class 4 and class 2 equal 6 mm and 9 mm, respectively, where the total thickness in zone II will be over by the thickness of the 6 additional layers which is equal to 12 mm and 18 mm for FRP class 4 and class 2, respectively. The mode of failure for these model occurred at the ground level due to the local buckling. Figure 2

shows the load deflection relationships for GFRP poles equivalent to class 2 (New design 1) and class 4 (New design 2) wooden poles.

4. CONCLUSION

The finite element program ADINA (version 8.2) was used to perform a nonlinear numerical analysis of tapered GFRP poles. Layered composite shell elements were used in this finite element analysis. The program accounts for the nonlinear behaviour of the poles and includes a strength failure check by applying the Tsai-Wu failure criterion. The results were in an excellent agreement with the experimental results. The finite element method used in this investigation provided an excellent prediction of the critical buckling and material failure loads, as well as the corresponding modes of failure for thin-walled GFRP poles. The load-deflection curve of GFRP poles under lateral loading can be considered linear up to failure. The fibre orientation of circumferential layer with 90 degree for the tapered GFRP poles gives the higher load capacity and stiffness. The internal and external additional three layers (90, ± 45) for the laminate at the middle zone II, improved the flexural behaviour due to the existed hand-service opening. The proposed models with 12 layers with two circumferential with 90 degree and ten with 10 degree give excellent result. Optimum designs for 12 m (40 ft) GFRP poles equivalent to class 4 and class 2 wood poles were obtained using the finite element model, to satisfy the requirement strength criteria as specified in the ASTM, AASHTO and ANSI standards for the maximum deflection and ultimate load capacity.

5. REFERENCES

- ADINA (2004), *Theory and Modeling Guide*, Volume I, Chapter 3, Version 8.2. ADINA R&D Inc., Watertown, MA, USA.
- American Association of State Highway and Transportation Officials, AASHTO (2001), "Standard Specifications for Structural Supports for Highway Signs, Luminaires and Traffic signals".
- American National Standard Institute. (2005). "Fiber-Reinforced Plastic (FRP) Lighting Poles, American National Standard for Roadway Lighting Equipment", USA, ANSI C 136.
- American Society for Testing and Materials. (2001). "Standard Specification for Reinforced Thermosetting Plastic Poles", Annual book of ASTM Standards, D 4923 – 01, USA.
- Bathe, K.J. (1996). *Finite Element Procedures*. Prentice-Hall.
- Crozier, W., Dussel, J.P., Bushey, R., West, J. (1995). "Evaluation of deflection and bending strength characteristics of fibre-reinforced plastic lighting standards". Department of Transportation, New York, State of California, USA.
- Derrick, G. L. (1996). "Fiberglass Composite Distribution and Transmission Poles", Manufactured Distribution and Transmission Pole Structures Workshop Proceeding, July 25-26, Eclectic Power Research Institute, pp. 55-61.
- Ibrahim, S., and Polyzois, D., and Hassan, S. (2000). "Development of glass fiber reinforced plastic poles for transmission and distribution lines". *Can. J. Civ. Eng.* Vol. 27, pp. 850-858.
- Ibrahim, S., and Polyzois, D. (1999). "Ovalization analysis of fiber reinforced plastic poles". *Composite Structures*, Vol.45, pp 7–12.
- Lin ZM. (1995). "Analysis of pole-type structures of fibre-reinforced Plastics by finite element method", Ph.D. Thesis, University of Manitoba, Winnipeg, Manitoba, Canada.
- Masmoudi, R., Metiche, S., (2006). "Experimental and Theoretical Evaluation of the Flexural Behaviour of Fibre-Reinforced Polymer (FRP) Poles", Accepted for publication in the *Journal of Composite Materials*, 26p.
- Miller, M. F., Hosford, G.S. and Boozer III, J.F. (1995). "Fiberglass Distribution Poles: A Case of Study" IEEE transactions on Power delivery, Vol. 10, No. 1, pp. 497-503.
- Tsai, S. W., and Wu, E. M. (1971). "A General Theory of Strength for Anisotropic Materials" *Journal of Composites materials*, Vol. 5, pp. 58-80.

Part XV. Novel Applications

ADVANCED GRID STIFFENED FRP TUBE ENCASED CONCRETE CYLINDERS

Guoqiang Li

*Assistant Professor, Department of Mechanical Engineering, Louisiana State University, Baton Rouge, Louisiana,
USA-70803*

Dinesh Maricherla

*Graduate Student, Department of Mechanical Engineering, Louisiana State University, Baton Rouge, Louisiana,
USA-70803*

ABSTRACT

In this study, an advanced grid stiffened (AGS) composite tube, which was made of a lattice of interlaced fiber reinforced polymer (FRP) ribs that was wrapped by a FRP skin, was used to encase concrete cylinders. Two types of cylinders were prepared. One was a circular cylinder and the other was a square cylinder. For the circular cylinders, a uniaxial compression test was conducted; for the square cylinders, both uniaxial compression test and four-point bending test were conducted. The test results showed that the AGS tube confined concrete cylinders displayed a considerable positive composite action due to the mechanical interlocking. The AGS tube provided an “active” confinement to the concrete core. The elastic range and the specific axial strength of the circular AGS cylinders, and the specific bending strength of the square AGS beams were higher than those encased by solid FRP tubes, solid steel tubes, or steel grid tubes. The square AGS tubes were not as effective as the circular AGS tubes in confining concrete.

KEYWORDS

Grid, stiffener, rib, FRP, concrete, cylinder, beam, confinement.

1. INTRODUCTION

In recent years, an ever-increasing attention has been paid to use fiber reinforced polymer (FRP) tube-encased concrete columns for new construction and rebuilding of engineering structures [1,2]. The mechanism in FRP tube-encased concrete columns is to replace the steel rebar by a corrosion-resistant laminated FRP shell. The FRP tube serves as a stay-in-place formwork during construction; during service, the tube confines the lateral expansion of the concrete core and transfers the core to a triaxial compressive stress condition. As a result, the compressive strength and ductility of the column are enhanced significantly.

Subjected to an axial compressive load, sufficiently confined concrete cylinders behave bi-linearly [3-6]. The confinement provided by the FRP tube is passive. The FRP tube cannot confine the concrete core until the concrete has sufficient lateral expansion, i.e., when the concrete is cracked or crushed. The higher ultimate compressive strength of the confined concrete cannot be realized unless the concrete is damaged and there is an excessive axial strain (an axial strain in the order of 0.02 or higher), which is much larger than the currently accepted design strain of 0.003, as specified by the American Concrete Institute (ACI318-99). Since confined concrete cylinders are designed to work in the elastic region, i.e., the first linear region in the axial stress-axial strain curve, the strengthening potential of the FRP tube cannot be realized and utilized in practice. In order to utilize the strengthening potential of the FRP, the first region must be enlarged.

The reasons for this have been summarized in [7]. They include (1) a FRP tube usually has a much larger radial (out-of-plane) Poisson's ratio than that of concrete core before the concrete cracks and (2) For most FRP tubes, fibers are aligned towards the hoop direction in order to provide higher confinement. As a result, the axial stiffness of the FRP tube may be lower than that of the concrete core. These result in a transverse expansion of the FRP tube larger than that of the concrete core before the concrete cracks or crushes. Since these are intrinsic properties to FRP and concrete, innovative ways must be found to solve this problem.

A viable way of solving this problem is to use grid stiffened composite tube. It was proved that, by using a hybrid tube – a lattice of steel grids that were wrapped by a FRP skin, a mechanical interlocking between the tube and the core was developed [8,9]. This insured that any additional transverse expansion by the concrete core be resisted by the confining tube, leading to early activation or engagement of the tube in confining the concrete core. As a result, the confined concrete cylinders had a higher elastic region than the solid FRP tube confined counterparts. Because FRPs behave linearly elastic while steel behaves elastic-perfectly plastic, it is interesting to find how FRP grid tube encased concrete cylinders behave. The purpose of this study is thus to use advanced grid stiffened (AGS) tubes to encase concrete cylinders. Both column and beam behaviors will be investigated.

2. SPECIMENS PREPARATION AND TESTING

2.1 Raw Materials

Type I Portland cement, gravel, natural sand, water, and a superplasticizer DAVA 170 were used to prepare the concrete. The mix design followed ACI Standard 211.1 (“Standard” 1991). The mix ratio by weight was cement : water : coarse aggregate : fine aggregate : admixture = 1 : 0.56 : 3.80 : 2.19 : 0.001. The maximum coarse aggregate diameter was 25.4mm. The slump was 140.2mm; the air content was 6.8%; and the 28-day cylinder compressive strength was 30 MPa. The same concrete has been used previously [8]. The AGS composite tubes were fabricated using a Fibrex 503 E-glass fiber roving and a Sunrez UV curing vinyl ester resin. The same fiber and resin were used to manufacture circular AGS tubes and square AGS tubes. For the FRP skin, the same resin was used. The fiber was a unidirectional E-glass 7715 style plain woven fabric.

2.2 AGS Tube Fabrication

While a number of manufacturing methods have been explored in the literature [10,11], a hand lay-up process based on a mandrel-pin system, which simulated the filament winding technology, was used to fabricate circular grid tubes. The fiber rovings with resin were first wound along the pin-guidance to form the grid skeleton. Once the designed thickness was achieved, the fiber was cut and the specimen was exposed to an UV-A light source (or sunlight) for curing. Typical curing time was about half an hour for each specimen. Once the specimen was fully cured, the pins were removed and the mold was pushed out of the cured grid. The plain woven fabric with resin was then wrapped around the skeleton to form the skin. The cured circular grid tube had an inner radius 50.8mm and height 304.8mm; the ribs had a thickness 6.25mm and width 5.08mm. The bays were squares with a side length 25.4mm. Two types of square AGS tubes were fabricated. The first type had a height 304.8mm and the second type had a height 558.8mm. Both types had the same square cross-section with a side length 114.3mm. Each bay was again a square with a side length 25.4mm. A total of three circular AGS tubes, three shorter square AGS tubes with a height 304.8mm, and three taller square AGS tubes with a height 558.8mm were prepared. The average weight of the circular tubes was 0.58kg; it was 0.64kg for the shorter square AGS tubes and 1.31kg for the taller square AGS tubes. A burn-off test per ASTM D2584 was used to determine the fiber volume fraction in the grids. It was found that the fiber volume fraction was about 30%. The cured thickness of the skin was 0.738mm.

2.3 Instrumentation and Testing

2.3.1 Compression test

Two pairs of strain gages were used for each specimen. Each pair contained two strain gages mounted at the mid-height of the cylinder aligned in the hoop and axial directions, respectively. The two pairs were spaced at 180° in the hoop direction. The strain gages were mounted on the surface of the FRP skin above the ribs. During the axial compression test, each specimen was loaded uniaxially to about 40% of the compressive strength of the unconfined concrete (30.0MPa) and unloaded to guarantee close contact between each component. Then, the specimen was reloaded until failure. The compression testing was conducted using a FORNEY machine, with a capacity of 2,688kN. The assembled computer data acquisition system can directly record the load-displacement curves. The strain was recorded using a Yokogawa DC100 Data Acquisition Unit. Compression testing was conducted per ASTM C 39. The loading rate was 0.23MPa/s.

2.3.2 Four-point bending test

Four-point bending tests were conducted on each second-type square specimen. This was a simply supported bending test with a span length 457.0mm. Each specimen was first loaded with a preload of 20kN to guarantee close

contact between each component. The specimen was then unloaded and reloaded until failure. The tests were conducted using the same FORNEY machine. The test was conducted per ASTM C 78. The loading rate was 230N/s.

3. RESULTS AND DISCUSSION

3.1 Axial stress-axial strain behavior

Typical axial stress-axial strain behaviors of an AGS circular tube encased cylinder, an AGS square tube encased cylinder, a solid FRP tube encased cylinder, a solid steel tube encased cylinder, and an axial steel grid tube encased cylinder are shown in Fig. 1. The test results of the solid FRP tube, solid steel tube, and axial steel grid tube encased cylinders are obtained from [8] by dividing the axial stress by their respective tube weight of 1.32kg, 5.08kg, and 2.52kg. It is seen that the circular AGS tube behaves differently from the solid FRP tube. The axial stress-axial strain curve before the peak stress can be represented by a linear section followed by a non-linear section, instead of the typical bi-linear curve connected by a transition zone. The specific stress at the end of the linear section (about 75MPa/kg) for the circular AGS cylinder is much higher than that at the end of the first linear section (about 30MPa/kg) for the solid FRP cylinder. This suggests that the elastic region of the AGS tube encased concrete cylinder is enlarged. The square AGS tube and the axial steel grid tube behaved similarly to that of the circular AGS tube. The difference is that the axial steel grid cylinder has a higher stiffness in the elastic region probably due to the higher axial stiffness of steel than that of FRP. The axial stiffness of the square AGS cylinder is the lowest due to the larger lateral and thus axial deformation of the AGS tube caused by the stress concentration at the four sharp corners of the tube. For the solid steel tube confined cylinders, the specific strength is the lowest among all the encasing devices. This is due to the larger density of steel and the lack of mechanical interlocking between the tube and the concrete core.

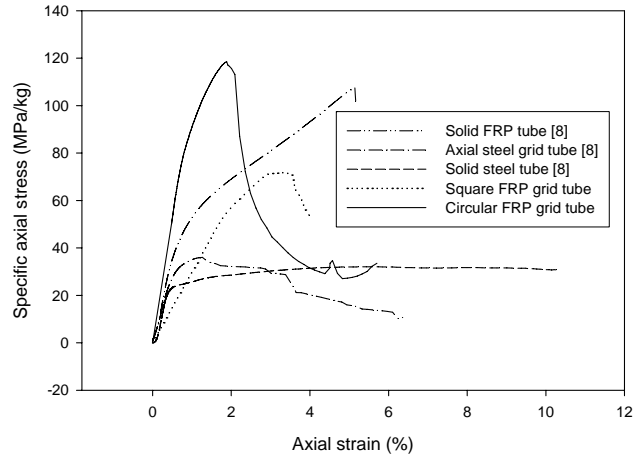


Fig. 1 Comparison of specific axial stress-axial strain behavior of various types of tubes encased concrete cylinders

3.2 Specific compressive strength

From Fig. 1, the specific compressive strength is the highest for the cylinder encased by the circular AGS tube, followed by the solid FRP tube, square AGS tube, axial steel grid tube, and solid steel tube. This means that, for an ideal case, i.e., assuming linear relationship between the tube weight and the confinement strength, the circular AGS tube encased concrete cylinder would have the highest compressive strength if the same amount of materials is used. Therefore, the circular AGS tube not only has a larger elastic region, but also has a higher ultimate specific strength. Comparing the circular AGS tube with the square AGS tube, the square AGS tube shows a much smaller specific strength and ductility due to the stress concentrations at the four sharp corners.

3.3 Bending strength

Figure 2 shows the transverse bending load-deflection curves from the four-point bending test. One was encased by the taller square AGS tube and the other was encased by the same size steel grid tube from [9]. Three observations can be made. (1) The AGS tube encased beam shows a linear elastic behavior up to the peak load, while the steel grid tube encased beam shows a linear section followed by a non-linear section with a continuous reduction in stiffness. (2) The specific load and deflection of the AGS beam is higher than those of the steel grid beam. Together with the higher specific compressive strength, it is concluded that, using the same amount of materials, AGS tube encased cylinders would have a higher load carrying capacity than the steel grid tube

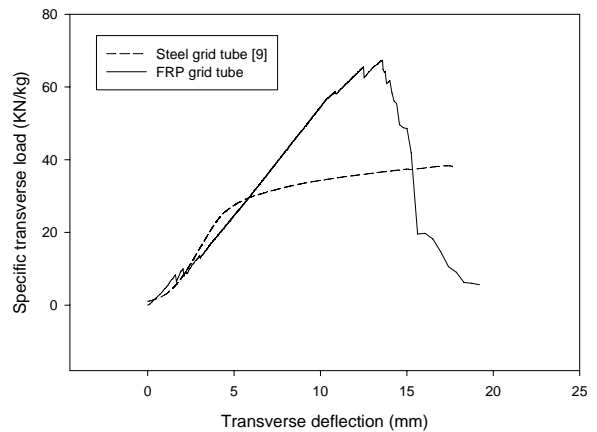


Fig. 1 Comparison of steel grid tube confined concrete beam with FRP grid tube confined concrete beam under bending

encased concrete counterparts. (3) Both before and after the peak load, the AGS beam shows some fluctuations of load. This is because of the load redistribution through the network once the skin or some ribs fail.

3.4 Failure mode

The failure modes of the circular AGS cylinder, the square AGS cylinder, and the square AGS beam are shown respectively in Fig. 3 (a) – (c). From Fig. 3 (a), both the axial ribs and hoop ribs have fractured, close to the nodal area. The very even fractured surface suggests that the failure is due to shear stress. For the square AGS cylinder, the failure is primarily due to the fracture of the hoop ribs at the corner, as shown in Fig. 3 (b). This is due to the stress concentration at the sharp corner of the square AGS tube. For the AGS beam, Fig. 3 (c), the failure is due to the fracture of the longitudinal ribs.



(a) (b) (c)

Fig. 3 Failure modes

4. CONCLUSIONS

An innovative FRP grid tube confined concrete cylinders have been developed and experimentally tested subjected to both compression and bending. It is found that the AGS tube confined concrete cylinders or beams have the highest specific strength than counterparts confined by steel tubes, FRP tubes, and steel grid tubes.

ACKNOWLEDGMENT

This study was partially sponsored by the Louisiana Board of Regents and EDO Fiber Science under contract number LEQSF(2004-07)-RD-B-05. The encased concrete cylinders and beams were prepared and the tests were conducted in the Concrete Laboratory at the Louisiana Transportation Research Center (LTRC). The support by Mr. Randy Young, Mr. John Eggers, Mr. Sadi Torres, and Mr. Walid Alaywan from LTRC is greatly appreciated.

REFERENCES

1. L.C. Hollaway, "The evolution of and the way forward for advanced polymer composites in civil infrastructures," *Construction and Building Materials*, 17, pp. 365-378, (2003).
2. A. Mirmiran, L. C. Bank, K. W. Neale, J. T. Mottram, T. Ueda, and J. F. Davalos, "World Survey of Civil Engineering Programs on Fiber Reinforced Polymer Composites for Construction," *Journal of Professional Issues in Engineering Education and Practice*, 129, pp. 155-160, (2003).
3. F. Seible, A. Davol, R. Burgueno, R.J. Nuismer, and M.G. Abdallah, "Structural behavior of concrete filled carbon fiber composite tubular columns," *Proceedings of 28th International SAMPE Conference*, Seattle, WA, pp. 1258-1269, (1996).
4. A. Mirmiran and M. Shahawy, "A new concrete-filled hollow FRP composite column," *Composite Part B: Engineering*, 27B, pp. 263-68, (1996).
5. A.Z. Fam and S.H. Rizkalla, "Behavior of axially loaded concrete-filled circular fiber-reinforced polymer tubes," *ACI Structural Journal*, 98, pp.280-289, (2001).
6. G. Li, S. Torres, W. Alaywan, and C. Abadie, "Experimental Study of FRP Tube-Encased Concrete Columns," *Journal of Composite Materials*, 39, pp. 1131-1145, (2005).
7. G. Li, "Experimental Study of FRP Confined Concrete Cylinders," *Engineering Structures*, 28, pp. 1001-1008, (2006).
8. G. Li, "Experimental Study of Hybrid Composite Cylinders," *Composite Structures*, (2005), (in press) [doi:10.1016/j.compstruct.2005.08.028](https://doi.org/10.1016/j.compstruct.2005.08.028).
9. G. Li, M. John, and D. Maricherla, "Experimental Study of Hybrid Composite Beams," *Construction and Building Materials*, 2005 (in press) [doi:10.1016/j.conbuildmat.2005.11.003](https://doi.org/10.1016/j.conbuildmat.2005.11.003).
10. S.M. Huybrechts, T.E. Meink, P.M. Wegner, G.M. Ganley, "Manufacturing theory for advanced grid stiffened structures," *Composite Part A: Applied Science & Manufacturing*, 33, pp. 155-161, (2002).
11. DY Han and SW Tsai, "Interlocked composite grids design and manufacturing," *Journal of Composite Materials*, 37, pp. 287-316, (2003).

APPLICABILITY OF FIBER REINFORCED PLASTICS TO HYDRAULIC GATES

Tomonori TOMIYAMA

(Research Staff, Public Works Research Institute, Tsukuba, Ibaraki, Japan)

Itaru NISHIZAKI

(Team Leader, Public Works Research Institute, Tsukuba, Ibaraki, Japan)

ABSTRACT

Following the results of surveys targeting related government ministries and agencies, industry organizations, local governments, etc., it has become clear that Fiber Reinforced Plastics (FRP) have been applied to members of hydraulic gates since the 1960s with over 400 structures now existing in Japan. Fifty FRP gates were visually inspected. Though they have been only lightly maintained over 30 years, little deterioration is evident. Results of durability tests with FRP specimens in the laboratory indicate that FRP for hydraulic gates has satisfactory water and corrosion resistance, though appearance gradually deteriorates from exposure to ultraviolet light.

KEYWORDS

Fiber Reinforced Plastics (FRP), Hydraulic Gate, Durability, Weather Resistance, Corrosion Resistance

1. INTRODUCTION

Hydraulic gate facilities are main structures in river-ways and play key roles in flood control and water utilization works. At present, mainly steel materials have been used for these facilities. Though these structures are always exposed to severely corrosive environmental elements, there are few effective anticorrosion engineering options. Hence, it is desirable to develop advanced materials having excellent corrosion resistance in order to reduce the labor and cost for maintaining hydraulic gates. In this paper, present situations of FRP that have been utilized as hydraulic gates in Japan were investigated and problems for bringing FRP to market were clarified in order to promote the application of FRP for hydraulic gates. In addition, field studies were carried out on 53 in-service FRP hydraulic gates in order to understand their actual conditions and performance. Furthermore, long-term durability of FRP for hydraulic gates was examined by accelerated weathering and water immersion tests.

2. MARKET RESEARCH OF FRP HYDRAULIC GATES IN JAPAN

In association with the main Japanese manufacturer, construction results of FRP hydraulic gates in Japan were investigated. Results of these investigations showed that 438 FRP gates were initiated from 1961 to 2002 in Japan but of these, the existence of only 59 FRP gates was confirmed. The reason for this low number of verified FRP gates is because many of them were delivered to general contractors and are therefore now impossible to track. Figure 1 shows initial construction data of FRP hydraulic gates arranged by construction year. This data shows that more than 80% of total FRP gates were constructed before 1990, whereas construction in recent years has significantly declined. The styles of FRP gate adopted in Japan are slide gate, flap gate, roller gate, swing gate, miter gate, sliding gate and angle chute; most gates are compact in size. The area is smaller than 4.0 m² on almost 90% of adopted FRP door bodies. It is assumed that FRP was difficult to apply to large door bodies because FRP has low elastic modulus and is flexible. In the present state, it may be effective to promote the advantages of FRP by limiting targets to comparatively small-scale (such as 10 m² or less) hydraulic gate facilities.

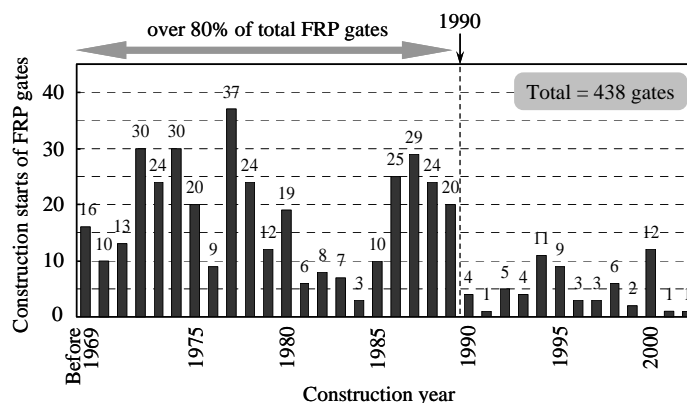


Figure 1: Construction Starts of FRP Hydraulic Gates in Japan

In order to examine the marketability of FRP hydraulic gates, questionnaire surveys were carried out targeting related government ministries and agencies, industry organizations, local governments, and so on. The questionnaires consisted of questions about durability, abrasion resistance, ease of installation, maintenance, weather resistance, strength, corrosion resistance, initial cost, and running cost for FRP hydraulic gates. The results of the questionnaire showed that low visibility of FRP within the FRP hydraulic gates market has been one of the obstacles against its increased use.

3. LONG-TERM DURABILITY OF FRP IN RIVER ENVIRONMENTS

In order to confirm the applicability of FRP to members of hydraulic gate facilities, age deterioration of in-service FRP gates was investigated.

3.1 Field Studies on Existing FRP Hydraulic Gates

Field studies were carried out on 53 FRP hydraulic gates which were in service. Material degradations of FRP members caused by river water or ultraviolet rays were evaluated visually. Results of the visual inspections show all FRP gates had no major deterioration except for slight discoloration and water stain despite the fact that they were hardly maintained for 30 years. Thus, FRP gates seem to be more durable than steel gates after an equivalent period of time.

3.2 Disassembling Investigations on an FRP Door Body

An FRP door body which had been used as a sluice gate on an agricultural waterway was selected and examined (see Table 1).

Table 1: Overview of FRP Hydraulic Gate Selected for Strength Tests

Construction Year	before 1969	 <p>Panoramic View</p>
In-service Period	more than 35 years	
Gate Style	slide gate	
Dimensions	1.15m x 1.00m	
Applied FRP	door body, door stop	
Forming Method	hand lay-up	
Operating Situation	full-time operating	
Transformation by Water Absorption	N/A	
Erosion Damage	N/A	
Degradation	water stain discoloration	

Tensile tests were carried out by using a main girder channel and a skin plate of a dismantled door body. From the channel and sections of both the submerged area and non-submerged area of the skin plate, five test specimens were

cut into pieces 8 mm thick, 25 mm wide, and 250 mm long respectively. For comparison, tensile tests were also similarly carried out on another FRP channel and laminate that were newly fabricated with exactly the same laminate composition as that of the obtained old door body. The sampling method of the FRP door body for the tensile test is shown in Figure 2. After testing, specimens were examined by scanning electron microscope (SEM), energy dispersive X-ray spectrometer (EDS), Fourier transform infrared spectrophotometer (FT-IR), and so on.



Figure 2: Sampling Methods of FRP Door Body for Tensile Test

Table 2 shows a part of the results. Some data spread on tensile strength, which is a weakness of FRP material, was recognized. A future challenge is to reduce such data spread. In any case, it was confirmed that the mean values of tensile strength and modulus were almost the same between the two FRP laminates. Results of instrumental analyses for specimens after tensile tests did not indicate significant deterioration of the FRP door body.

Table 2: Comparison of Tensile Properties between FRP Skin Plate after Use for 35 Years and Newly Fabricated Laminate

Specimen No.	After Use for 35 Years				Newly Fabricated	
	Non-Submerged Area		Submerged Area		Tensile Strength [MPa]	Tensile Modulus [GPa]
	Tensile Strength [MPa]	Tensile Modulus [GPa]	Tensile Strength [MPa]	Tensile Modulus [GPa]		
1	168.49	17.10	152.35	15.62	161.69	15.04
2	156.71	15.25	149.60	15.31	168.82	15.08
3	144.87	15.57	149.91	23.61	162.90	17.66
4	135.63	16.49	148.65	15.25	167.19	16.43
5	135.63	15.83	149.72	15.55	173.62	15.86
Average	148.27	16.05	150.04	17.07	166.84	16.02

4. DURABILITY TESTS OF FRP FOR HYDRAULIC GATES

Generally, FRP for hydraulic gate members is produced using the hand lay-up, resin injection, or pultrusion molding methods. Matrix resins of those FRP are epoxy resins, unsaturated polyester resins, or vinylester resins, with glass fibers used as reinforcement. General characteristics of FRP for hydraulic gate members are shown in Table 3. In order to obtain basic knowledge about the long-term durability of FRP, accelerated weathering tests and water immersion tests were carried out. FRP laminates manufactured by hand lay-up, resin injection, and pultrusion were used as testing samples. Dimensions of test specimens were 4–10 mm thick, 15 mm wide, and 200 mm long. In accelerated weathering tests, specimens were put into an accelerated weathering tester in the laboratory and exposed to xenon-arc sources. Changes of properties with UV irradiation were evaluated by glossiness and color difference on specimen surface, flexural strength, and flexural modulus. In water immersion tests, the same specimens as the accelerated weathering tests were immersed in water at 20–25°C. Changes of properties with penetration of water were evaluated by weight change, flexural strength, and flexural modulus.

In Figure 3 (a), gloss retentions in all cases were significantly reduced from the beginning of exposure and then decreased to less than 20% of the original glossiness at about 2500 hours exposure. On the other hand, Figure 3 (b) shows that the flexural strength of each FRP sample barely changed from before and after exposure to ultraviolet light for 2500 hours, though pultrusion FRP strength showed some loss. From these results, it was determined that degradation of FRP by ultraviolet rays had occurred only at the surface after 2500 hours exposure, indicating that FRP's strength remained virtually intact. It is supposed that such degradation in FRP surface by ultraviolet light can

be chemically improved by coating the FRP surface with, for example, a gel coating with high resistance to UV radiation.

Table 3: General Characteristics of FRP* for Hydraulic Gate Members

Molding Method	V _r [%]	Mechanical Properties					Thermal Properties		
		Tensile Strength [MPa]	Tensile Modulus [GPa]	Flexural Strength [MPa]	Flexural Modulus [GPa]	Compression Strength [MPa]	Coefficient of Linear Expansion [10 ⁻⁵ /°C]	Thermal Conductivity [W/mK]	Specific Heat [J/gK]
Hand Lay-up	25 - 40	80 - 120	7 - 10	120 - 180	7 - 9	120 - 170	3 - 4	0.17 - 0.23	1.38
Resin Injection	25 - 40	80 - 120	7 - 10	120 - 180	7 - 9	120 - 170	3 - 4	0.17 - 0.23	1.38
Pultrusion	55 - 85	500 - 900	20 - 40	590 - 900	20 - 35	250 - 500	0.6 - 0.8	0.29 - 0.52	1.05 - 1.26

*matrix: unsaturated polyester resin, reinforcement: glass fiber

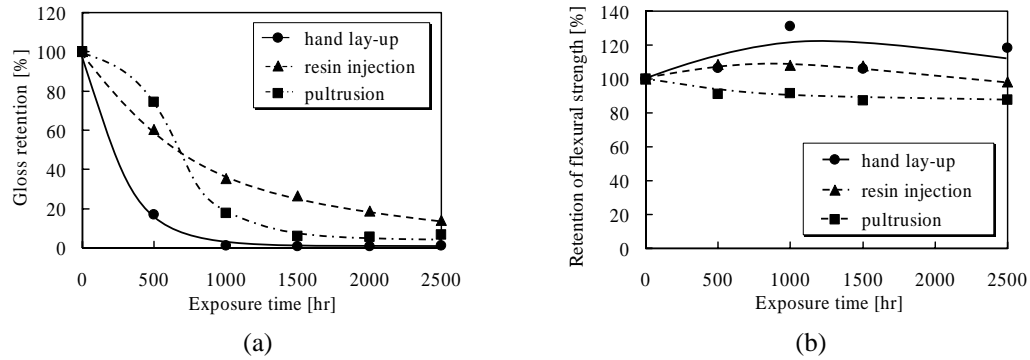


Figure 3: Results of Accelerated Weathering Test; Gloss Retention (a) and Retention of Flexural Strength (b) of FRP Exposed to Laboratory Xenon-arc Sources

In the immersion tests for 2500 hours, the largest value of material swelling rates was +0.61% and that of weight changes was about +1.4%. In three-point bending tests, the flexural strength of FRP decreased slightly. It seemed that the strength degradation of FRP was caused by swelling due to water absorption. In this immersion test, swelling and strength degradation of FRP did not exceed the permissible limit, since water absorption of FRP was very small.

The results of durability tests clarified that FRP for hydraulic gates has satisfactory water resistance and corrosion resistance, while appearance gradually deteriorates from exposure to ultraviolet light. Therefore, it seems that FRP is especially suitable for hydraulic gates which are usually submerged in water.

5. CONCLUSION

The present study revealed that FRP is especially suitable for hydraulic gates usually submerged in water since they have excellent durability and water or corrosion resistance. For the future, it will be necessary to formulate guidelines for the application of FRP to hydraulic gate members in order to improve the visibility of FRP and promote its utilization in the hydraulic gates industry.

REFERENCES

- Chowdhury, M., Hall, R. (1998): "Performance Evaluation of Full-Scale Composite and Steel Wickets for Use at Olmsted Locks & Dam", *Proceedings of the 2nd International Conference on Composites in Infrastructure (ICCI'98)*, Vol. 1, pp. 667-681
- Xue, X., Jiang, S., Fang, X. (1990): "Application of resin coating on hydraulic construction", *Proceedings of the 6th International Congress on Polymers in Concrete*, pp. 634-641
- Yoshida, M., Gocho, M., Noguchi, T., Hoshino, J., Momojima, H., Saeki, N. (1990): "Development of slide sluice gate by carbon hybrid FRP (In Japanese)", *Reinforced Plastics*, JRPS, Vol. 36, No. 5, pp. 159-162

STRESSED ARCH MODULAR DEPLOYABLE COMPOSITE SHELTERS CONCEPT AND DEVELOPMENT

T Omar

(PhD Candidate, Fibre Composites Design and Development, University of Southern Queensland, Toowoomba, Australia)

G Van Erp

(Professor Fibre Composites Design and Development, University of Southern Queensland, Toowoomba, Australia)

P W Key

(Manager & Engineering director, Kencana Strarch Asia Pacific, Kuala Lumpur, Malaysia)

ABSTRACT

Deployable shelters of various forms have been utilised since ancient civilisation. The need for these systems has not diminished over time and development continues for military forces, civilian humanitarian aid, and post-natural disaster scenarios. Recent developments have focussed mainly on tent type structures, air beam technology and steel frames supporting soft fabric, yet none of these systems have fully satisfied the deployability requirements.

The Military Modular Shelter System (M²S²) initiative is a research project that aims to develop a fibre composite re-deployable arched shelter system with rigid or fabric cladding. The main frames are formed from modular fibre composite panels that are connected and stressed in position by prestressing cables. Different geometries can be obtained using this system by changing the number of panels per frame and the packer sizes between panels.

This paper presents the concept of M²S² with background about existing systems followed by the development and testing of an innovative, simple to manufacture, truss module that was investigated as part of this project. The test results showed good characteristics. These include having alternate load paths and failure initiated and propagated in the web with no, undesirable, failure observed in the adhesive layers.

KEYWORDS

Shelters, Composites, Deployable, Hanger, Strarch, Truss.

1. INTRODUCTION

The need for deployable structures has existed since ancient times. Deployable structures are similar to normal structures in that they have to be stable and able to carry designated loads in their deployed status (Gantes, 2001). In addition, they should satisfy the deployability requirements of being able to be dismantled, stored and transported in a compact form. They should also have an inherent deploying mechanism that allows the transition between the deployed status and the dismantled status and vice versa. Deployable shelters are an important application of deployable structures. They are needed for military applications, aircraft maintenance hangers, aid relief and temporary and/or remote structures.

Over time, the performance requirements of modern deployable shelters have become more demanding, which has driven the development of more sophisticated structural forms and solutions. The basic components of deployable shelters are the structural system (primary load transfer) and the cladding system. The cladding system can have different functions depending on its inherent properties and those of the structural system used. For example, cladding systems can be used to stabilize the structural system, assist in carrying primary loads, or can be integrated with the overall load carrying system. Consequently the two sub-systems are generally dependent on each other. The recent developments of deployable shelter technology can be categorized as air-inflated shelters; rigid frames supporting soft fabric shelters and stressed arch systems. These developments were reviewed by Verge

(www.natick.army.mil) and Omar et. al. (2006). These reviews showed that the currently used deployable shelter systems do not fully satisfy the shelter deployability requirements. Air beam technology has not satisfied the needs for deployable shelters in spite of being under development for a significant period. Low pressure air beams can only be used for short spans. High pressure air beams store significant amounts of energy and still can not be used for large spans. The state-of-the-art deployable shelter system may well be the Widespan by Weatherhaven. The system can be used for large free spans. However, steel frames are used for the main panels with a dimension of 3.66m in length and a weight of 68kg (<http://www.weatherhaven.com/>). Both the size and the weight of these panels are more than the legal carrying capacity of two persons, in Australia. This may necessitate using some form of crane to erect this system. The Weatherhaven systems use soft fabric for the cladding which creates the impression of a temporary structure that accommodates large deformations.

The M²S² research project aims to investigate the behavior of a composite arch deployable shelter system that uses the post-tensioning prestressed technology as a deploying mechanism. One of the core components of this system was its modular panel. An innovative, simple to manufacture, adhesively bonded truss panel system was developed for this purpose. In this paper, the M²S² concept is presented followed by the development and testing of its panel.

2. M²S² CONCEPT

The concept of the prestressed arch technique has been implemented successfully in Strach steel frames (Strach 1999). The continuous nature of the top chord, the plastic deformation during stress erection and the strength to weight ratio associated with the steel trusses all provide challenges to the deployable functionality of conventional Strach frame systems.

The M²S² concept is similarly based on the stressed arch concept. However, it is adapted to the requirements of deployability by using more manageable (approx. 1500mm square), light-weight truss panels that do not require plastic deformation. The top chord deformation is concentrated at discrete joints (Figure 1). The concept of M²S² can be summarized as follows:

1. Frames are manufactured, mostly, from identical standard panels;
2. Standard panels are stacked to form each frame on the ground;
3. Panels are then connected by inter-panel top hinged joints. The difference in dimension between the top chord and the bottom chord allows having initial gaps at the bottom chord;
4. One side of the frames is fixed to the foundation, while the other is free to move horizontally during erection. The prestressing cables are threaded through the bottom chord;
5. Roof sheeting (rigid type) and other services are assembled while the frames are still on the ground, prior to carrying out any prestressing (Assembly stage);
6. Finishing the installation of services; frames are stressed using prestressing cables. The bottom chord gaps allow the geometry to change to an arch shape during the prestressing process (Erection stage);
7. The prestressing cables are stressed to the level that allows for losses and/or relaxation in addition to ensuring that the bottom chord will be in compression under any serviceability loads. The cables are then blocked and the moveable frame support is fixed. The shelter is complete and ready to use (Deployed stage).

The concept of M²S² is quite flexible. The number of panels per frame and the packer sizes define the frame span and height in the deployed position. Table 1 shows the effect of increasing the packer sizes from 200mm to 220mm on the frame geometry (frames are based on 32 standard panels). Increasing the packer size increases the frame span, reduces the rise/span ratio and the subtended angle. This flexibility should be accounted for when investigating the behavior of such frames.

Table 1 Effect of packer size on frame geometry

Frame Alternative	A1	A2	A3
Packer Size(mm)	200	210	220
Rise/Span – Radius(m)	12.1/36.7– 19.9	11.1/38.4– 22.1	10.1/40.0– 24.8
Rise/Span Ratio	0.330	0.289	0.252
Subtended Angle (deg)	133.3	120.3	107.2

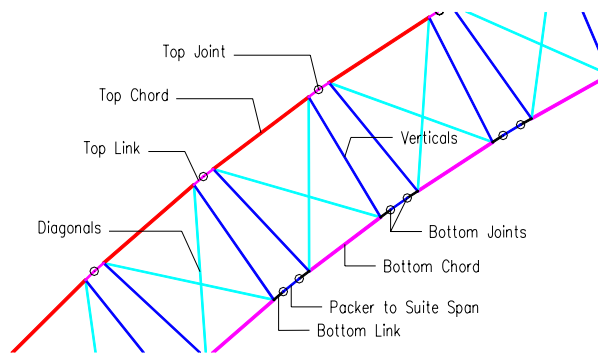


Figure 1 M²S² system – main components

3. THE M²S² MODULAR PANEL

The panel system is the core of the M²S² concept. Accordingly, it was the first investigated component. As per the requirement of the system, the panel should have hollow sections for the chords to accommodate the prestressing cables. Previous investigations showed that it is recommended to have panels with flat-sided standard components; extended joint area and alternate load path after failure (Omar et al, 2006). Using a multi-pultruded panel with diaphragm bracing system satisfied these requirements. In addition, it was simple to manufacture and allows the use of multi-cables for prestressing.

Due to the arch geometry, the shelter frames are mainly subjected to axial forces. In addition, shear and bending moments are generated due to the un-symmetric loading of wind and live loads. In using standard pultrusion sections for the chords and vertical members, the member capacity under axial loads can be predicted using design codes. However, the diagonal skins and connections to the chord and vertical members need further investigations. These necessitated conducting prototype panel testing by applying shear forces on the panel to investigate its behavior. The panel was tested in beam mode with loads applied at mid span. The tested configuration had two panels of 650mm centerline dimension, with 50mm gap at the centre (Figure 2). The overall structure consists of three identical frames of 50mmx50mmx5mm hollow square pultrusions which were adhesively bonded to the two web laminates using a toughened epoxy adhesive. Load, deflection and strains were recorded at locations shown in Figure 2. Strain gauges located across the panel thickness were used to locate any differential stress and strain distributions. Gauges located on the laminated web were used to measure the tensile and compressive strains in the ± 45 deg direction. Loads were applied using an Instron loading ram with a 500kN capacity. The structure was loaded using a displacement controlled loading rate of 2mm/min.

4. PANEL TEST RESULTS

The tested panel showed good performance with a load-deflection curve shown in Figure 3. The load-deflection curve indicates that the panel still reserves partial load carrying capacity (about 50% of its ultimate capacity) after failure in spite of continuous increase in the applied displacement. Failure initiated at the top corner of the diaphragm, due to the combined tension in the diagonal direction and compression in the perpendicular direction. Compressive forces were due to the confinement of the web with the tendency of the angle between the vertical and top chord members to reduce under the applied loads. Failure propagated along the inner faces of the vertical and top chord following the pattern of the formed wave of the buckled web (Figure 3). No failure was observed in the adhesive layers. This was another desirable feature as adhesive failure is inherently brittle. In releasing the applied load, the panel restored most of its deflection (in spite of rupturing of the web). More detailed behavioral investigation of this panel will be the subject of future publication where a finite element model was developed at the micro level to provide an insight of the panel is good attributes.

5. CONCLUSIONS

Combining the effectiveness of the arch as a structural form, the post tensioning prestressing technology and composite light weight materials has significant potential for developing effective deployable shelter systems. The M²S² concept seems able to deliver a flexible deployable shelter system that satisfies the deployment requirements

and the flexibility needed by the end users. The flexibility is achieved by using modular panels of manageable size and weight which are within the carrying capacity of two persons. In using packers at the bottom chord, different structural configurations can be obtained with different span to height ratio.

Using a multi-pultrusion panel system with diaphragm web showed good characteristics with the advantages of having alternate load paths, simplicity of manufacturing and allowing the usage of multi-prestressing cables. For the panel tested, failure initiated and propagated in the laminated web with no failure observed in the adhesive layers. The laminated web was able to restore the panel original geometry after releasing the applied loads.

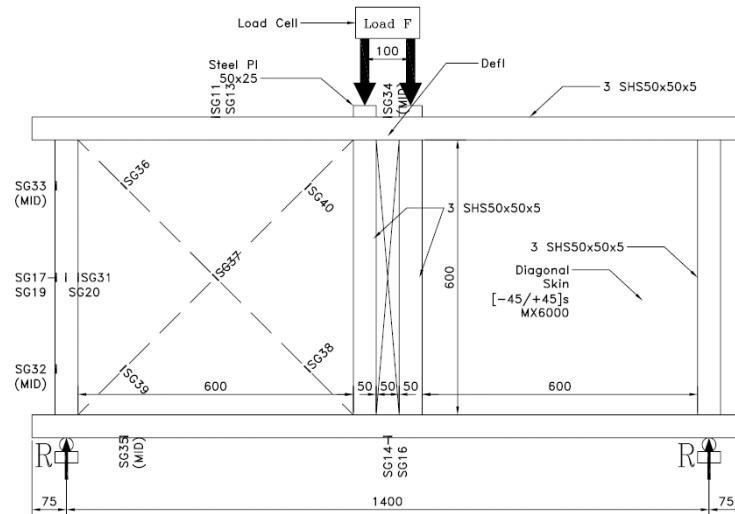


Figure 2 Test panel geometry and strain gauge positions

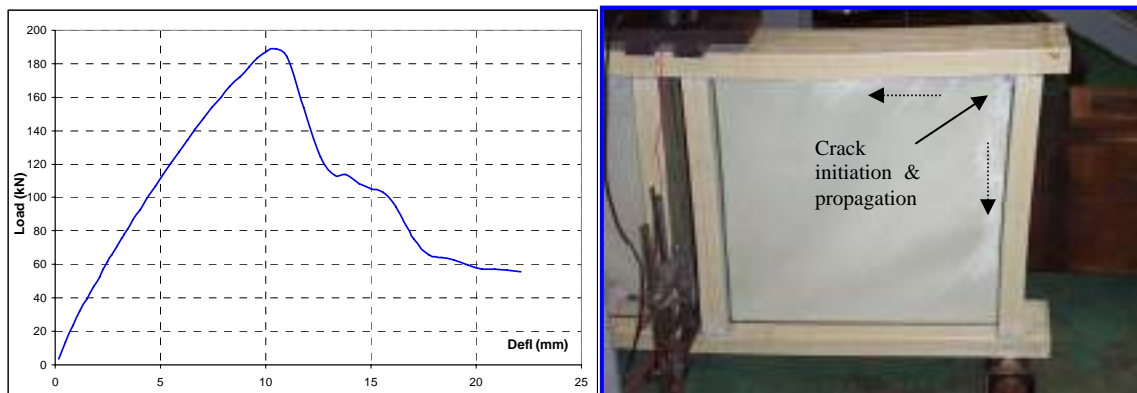


Figure 3 MK III load deflection curve and failure mode

5. References

- Clarke, M. J. and Hancock, G. J. (1994). Behavior and design of stressed-arch (Strarch) frames. IASS-ASCE International Symposium 1994 on spatial, lattice and tension structures, Atlanta, ASCE.
- Gantes, C. J. (2001). Deployable structures: Analysis and design. Southampton, WIT Press, UK.
- Omar, T., Heldt, T., and al, e. (2006). "M²S² Modular Deployable Composite Shelters - Concept and loading criteria." Australian J of Structural Engineering, 6(3), 217-226.
- Strarch (1991). Analysis of US military requirements for large deployable shelters, Sydney, Australia.
- Strarch (1999). The Strarch building system – Technical discussion. Sydney, Australia.
- Verge, A. S. "Rapidly deployable structures in collective protection systems", Massachusetts, U.S. Army Natick Soldier Center: (www.natick.army.mil).
- Weatherhaven Home page, (<http://www.weatherhaven.com/>)

EVALUATION OF EPOXY ENCAPSULATED TIMBER PILES

Nakin Suksawang

(Assistant Professor, Florida International University, Miami, FL, USA)

Hani Nassif

(Associate Professor, Rutgers, The State University of New Jersey, Piscataway, NJ, USA)

Ozgul Ozkul

(Structural Engineer, Leslie E. Robertson Associates, New York, NY, USA)

Ali Maher

(Professor, Rutgers, The State University of New Jersey, Piscataway, NJ, USA)

Abbas Sarmad

(Vice President, DMJM+Harris, New York, New York, USA)

ABSTRACT

Many bridges are supported on timber piles that have significant deterioration due to fungal decay of the wood. A method of repair is proposed to encase the damaged timber pile in Glass Fiber Reinforced Polymer (GFRP) wraps that are injected with special epoxy mortar. The composite repaired piles need to be tested to determine their ultimate load capacity under combined shear and flexure. This paper evaluates the behavior of extracted repaired timber piles under lateral loads. Sixteen repaired timber piles are extracted from actual conditions and tested as cantilever beams. Special experimental setup is designed to test the piles under flexure and shear. Various types of measurements such as deflections and strains are measured at different locations of the pile. Results show that all repairing systems increase the stiffness and lateral load capacity of existing timber piles (Douglas fir) regardless of the dimensions of the cross section. The stiffness and lateral load capacity of the repaired timber pile could be as high as that of the Greenheart but requires more epoxy mortar thickness.

KEYWORDS

Glass Fiber Reinforced Polymer, Timber Pile, Epoxy Mortar, Repairing Techniques.

1. INTRODUCTION

Timber piles are one of the oldest and most frequently used pile foundations in North America. They still remain one of the most cost-effective solutions for foundation. However, one of the problems with timber piles is the deterioration above ground water table where the pile is liable to attack by marine organisms, fungi, and wood eating insects (Chellis, 1961, Lopez et al., 2004). Overtime, the deterioration is severe enough that the pile loses its bearing capacity, and it could eventually lead to foundation failure. A strong commitment by the New York City Economic Development Corporation (NYCEDC) is now underway to prevent further losses. A new repairing technique using epoxy encapsulation to provide protection and preservation is proposed by DMJM+Harris, New York and conducted by Trevcon Construction Co. Since, this technique is relatively new; its performance needs to be evaluated (Menzel et al., 2004).

A total of sixteen timber piles were tested laterally using a 1780 kN loading frame at the Rutgers University Structural Engineering Laboratory (Nassif et al., 2005). The project compares the lateral load carrying capacity of repaired timber piles using glass fiber reinforced polymer (GFRP) jacket and epoxy mortar obtained from three manufacturers (i.e., Sika Corp./MFG Construction Products, Master Builders/Watson Bowman, and Fox Industry, Inc.) to existing timber piles (Douglas fir), and replacement alternative (Greenheart). In addition, the long-term performance is also investigated. Figure 1a and 1b illustrate the cross section of the repaired timber pile and test

setup, respectively. The epoxy mortar is a mixture of sand and epoxy that is injected through an access port at the bottom of the GFRP jacket to fill the space between the wood and the GFRP, as well as the burrows.

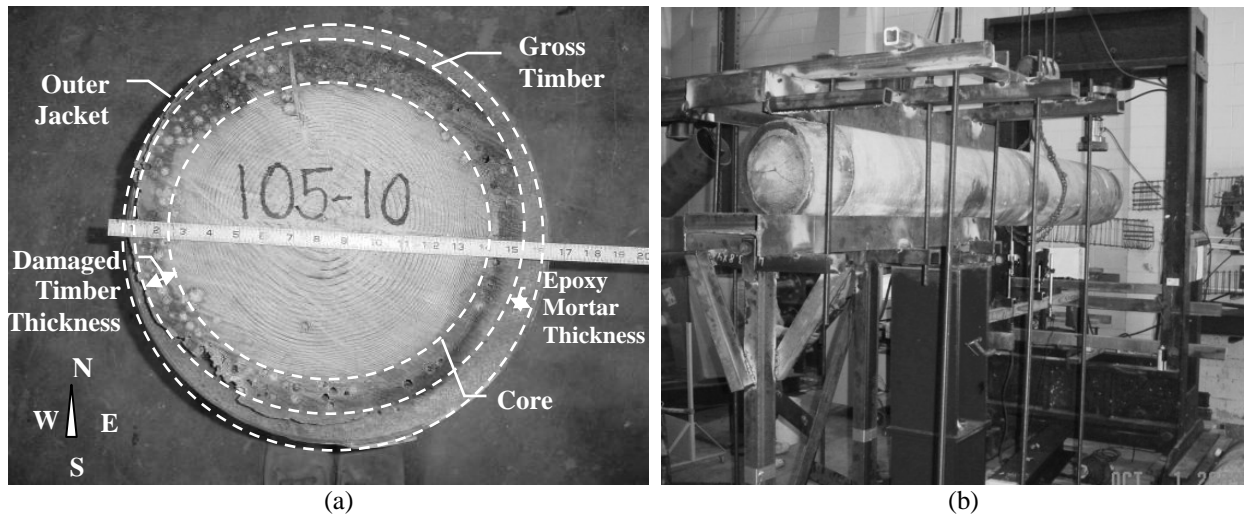


Figure 1: (a) Typical Cross Section of a Pile Specimen and (b) Test Setup

2. EXPERIMENTAL PROGRAM

The sixteen timber piles consisted of twelve GFRP encapsulated Douglas fir timber piles, two deteriorate Douglas fir timber pile, and two new Greenheart timber pile. The twelve timber piles were encapsulated using GFRP and epoxy mortar from different manufacturer. Three manufacturer combinations were used: (1) Sika epoxy mortar and MFG Construction Product GFRP (Sika), (2) Watson Bowman epoxy mortar and GFRP (WB), and (3) Fox Industries epoxy mortar and GFRP (Fox). Table 1 summarizes the cross section of each timber pile specimen used in this study.

Table 1—Cross Section at failure location of the Tested Timber Piles

Test No	Manuf.	Undamaged Timber Diameter (mm)			Gross Wood Diameter (mm)			Outer Jacket Diameter (mm)			Ave. Epoxy Thickness (mm)
		E-W	N-S	Ave.	E-W	N-S	Ave.	E-W	N-S	Ave.	
1 (S1)	Sika	292	279	286	394	375	384	438	445	441	25
2 (S2)	Sika	349	330	340	349	330	340	445	445	445	49
3 (F1)	Fox	241	229	235	343	324	334	445	445	445	52
4 (S3)	Sika	298	305	302	368	375	372	432	438	435	29
5 (W1)	WB	279	279	279	394	394	394	438	445	441	21
6 (S4)	Sika	337	324	330	362	387	375	438	438	438	29
7 (W2)	WB	248	241	245	343	362	349	419	432	425	35
8 (W3)	WB	279	248	264	356	330	343	432	432	432	41
9 (F2)	Fox	279	279	279	343	356	349	470	470	470	57
10 (W4)	WB	298	279	289	381	375	378	445	438	441	29
11 (D2)	N/A	273	292	283	311	318	314	N/A			
12 (F3)	Fox	254	248	251	343	356	349	445	445	445	44
13 (S5)	Sika	305	279	292	381	368	375	432	425	429	24
14 (G1)	N/A	305	305	305	305	305	305	N/A			
15 (G2)		330	330	330	330	330	330				
16 (D1)		356	356	356	356	356	356				

Notes: S, F, W, D, and G denotes Sika, Fox, Watson Bowman, deteriorated Douglas fir, and new Greenheart timber piles.

3. RESULTS

Table 2 summarizes the results from tests performed on the pile specimens. The cracking load is the load when a crack is initiated, as observed during the tests, on either the tension or compression side of the GFRP jacket. The ultimate load is the peak load, whereas the failure load is the instantaneous load before the specimen completely fails. If the failure of the timber pile is brittle, then the cracking, ultimate, and failure loads are very close.

A summary of the failure modes of each timber piles is also reported. Majority of repaired timber pile specimens failed in a similar failure mode: first by having a local cracking of the GFRP jacket near the support and compressive failure of the epoxy mortar, leading to a tensile cracking of the GFRP jacket, denoted as “A” on the table. Figure 2 illustrates typical failure mode “A”. The other failure modes consisted of tensile failure, denoted as “B”, where GFRP jacket fail in tension first followed by compression failure of the epoxy mortar. This failure mode is more desirable since it yield higher ultimate strength and provide more toughness to the repaired timber piles. The other two failure modes, denoted as “C” and “D”, are also compression failure similar to “A” but the failure is located not at the position of maximum moment but at the weakest location along the repaired timber piles, i.e., GFRP splice and injection port, respectively.

Table 2—Timber Pile Loading Capacity at Ultimate, Failure, and Cracking

Test No	Months In Place	Load (kN)			Deflection (mm)			Failure Mode
		Cracking	Ultimate	Failure	Cracking	Ultimate	Failure	
1 (S1)	15	62.3	81.6	75.9	102	208	230	A
2 (S2)	4	111.2	112.2	100.9	152	152	207	B
3 (F1)	23	75.6	84.9	57.1	137	229	291	C
4 (S3)	15	71.2	116.0	--	64	171	--	A
5 (W1)	31	86.8	--	--	224	--	--	D
6 (S4)	18	111.2	115.5	--	127	5.20	--	A
7 (W2)	31	53.4	49.5	127	184	212	212	A
8 (W3)	31	106.8	83.9	140	189	264	264	B
9 (F2)	23	115.7	133.0	127	187	212	212	A
10 (W4)	31	106.8	84.4	119	120	213	213	A
11 (D2)	>25	21.7	--	--	132	--	--	A
12 (F3)	23	71.2	96.7	93.9	102	213	237	A
13 (S5)	15	75.6	77.8	--	254	258	--	A
14 (G1)	0	115.7	145.7	--	157	210	--	A
15 (G2)	0	124.6	159.1	--	135	180	--	A
16 (D1)	>25	80.1	91.2	--	178	261	--	A

Note:

The following are the description of the failure mode:

A = Compressive failure in the GFRP jacket and epoxy mortar, followed by a tensile failure in the GFRP jacket.

B = Tensile failure in the GFRP jacket, followed by compressive failure in the GFPR jacket and epoxy mortar.

C = Failure mode similar to A but the tensile failure is located at the splice of the GFRP jackets.

D = Failure mode similar to A, but the tensile failure is located at injection port.

In order to perform a comparison between the three repairing systems, an attempt to normalize the applied load to the corresponding cross section is made. The normalization is achieved by dividing the applied load by the moment of inertia of the pile specimens. The moment of inertia is based on intact specimen using the secant modulus of elasticity and Hook’s Law. The reason for using the moment of inertia is to incorporate the cross section properties, which are highly variable in each group, as a factor in deciding the efficiency of each system.

Figure 3 illustrates the relationship between the load-section efficiency factors (i.e., the ratio of the load capacity to the elastic moment of inertia of the composite section) versus the tip deflection of the pile. As expected, the new Greenheart specimens outperformed the repaired timber piles. However, all the repaired timber piles outperformed the existing deteriorated timber piles (Douglas fir). This shows that, in general, the repair techniques used in this

study are highly effective in adding to the capacity of the existing Douglass fir timber piles. Moreover, comparing the absolute load carrying capacities without considering the section properties shows that Sika has outperformed all other specimens. However, the best performing specimens among all groups, the WB specimen (W3) has shown comparable performance as the Sika specimen (S3). Thus, all epoxy and GFRP jacket manufacturers provide a good protective system with an added benefit of increasing the lateral load carrying capacity of the existing deteriorated timber piles.

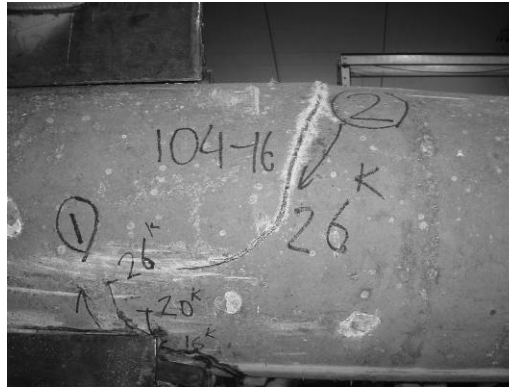


Figure 2: Typical Failure Mode (Mode A)

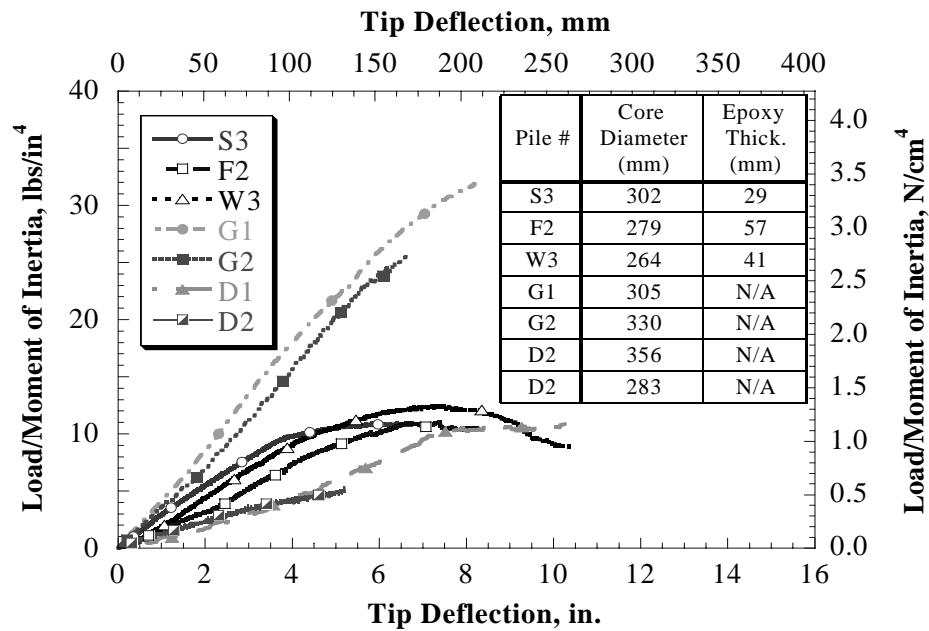


Figure 3: Relationships of Load and Moment of Inertia of Composite Section on Pile Specimens

4. CONCLUSIONS

The following conclusions can be made from the testing program:

1. Overall, all repairing systems increase the stiffness and lateral load capacity of existing timber piles (Douglas fir) regardless of the dimensions of the cross section. The stiffness and lateral load capacity of the repaired timber pile could be as high as that of the Greenheart but requires more epoxy mortar thickness. However, it should be noted that the repaired timber will generally have larger diameters than the Greenheart timber pile.

2. The cracking and ultimate load carrying capacities of the piles are highly dependant on the undamaged timber radius as well as the damaged timber thickness. Repaired timber piles with larger undamaged timber radius have exhibited higher cracking and ultimate load carrying capacities. However, since the cross section of the existing pile is uncontrollable, it is recommended that thicker epoxy mortar be used.
3. Quality control process, especially with the production of epoxy mortar, plays a significant role in the pile lateral load capacity.

5. ACKNOWLEDGEMENTS

The authors would like to thank Paul Menzel from DMJM+Harris inc., New York, Keith Neuscheler from Turner Construction Co., New York, and Dmitri Konon and Patrick Askew from New York City Economic Development Corporation (NYCEDC) for their help and assistance during the period of the project. Also, the assistance of laboratory technician, Edward Wass, for fabricating the testing setup, is thankfully acknowledged.

6. REFERENCES

- Chellis, R. D. 1961. "Deterioration and Preservation of Piles, Pile Foundations", McGraw-Hill, New York: 339-372.
- Lopez-Anido, R., Michael, A.P., Goodell, B. & Sanford, T.C. 2004. "Assessment of Wood Pile Deterioration due to Marine Organisms", *Journal of waterway, port, coastal and ocean engineering, ASCE*, March-April: 70-76.
- Menzel, P., Sarmad, A., and Carel, J. 2004 "Epoxy Encapsulation Systems & Construction Methods for Timber Repairs," Ports 2004, Houston, TX, May 23-26.
- Nassif, H., Suksawang, N. & Ozkul, O., Maher, A. 2004. "Test Evaluation of Repair Techniques for Timber Piles-Final Report". *Department of Civil and Environmental Engineering, Rutgers University*, RU-CEE-No. 2004-02, p.30.

Part XVI. Prestressing Applications

CFRP PRESTRESSING TENDONS: SOLUTION UPTAKE AND SWELLING EFFECTS

Paul Scott

(PhD Candidate, University of Cambridge, Cambridge, United Kingdom)

Dr Janet Lees

(Senior Lecturer, University of Cambridge, Cambridge, United Kingdom)

ABSTRACT

Experimental work has been undertaken to assess the nature of water, salt water and concrete pore solution uptake, and corresponding swelling effects, in Carbon Fibre Reinforced Polymer tendons. A method is presented to predict the long-term diffusion behaviour of aqueous solutions in CFRP tendons using short-term tests and Fickian models. Year long uptake tests have shown Fickian diffusive behaviour that is insensitive to the solution types considered. After one year, tendon mass and volume increases in the order of 0.3 % and 0.5 % respectively have been observed and the two phenomena appear to increase proportionally with respect to each other. Compared to thermal expansion effects, such swelling may be significant: potentially affecting the integrity of prestressed concrete structures.

KEYWORDS

CFRP, Prestressing Tendons, Durability, Solution Uptake, Swelling

1. INTRODUCTION

Carbon Fibre Reinforced Polymer (CFRP) materials are permeable to aqueous solutions which have been shown, in epoxy matrices, to affect their chemical and mechanical properties (Springer, 1988). The modelling of phenomena such as the diffusion of solutions into CFRP tendons and associated swelling effects have yet to be fully addressed but are of significance when designing CFRP prestressed concrete for durability in aggressive environments. This paper characterizes the possible behaviour of CFRP tendons in the marine environment through studying the diffusion of water, salt water and synthetic concrete pore solution (CPS) in tendon samples.

2. CFRP TENDONS: THEORETICAL DIFFUSIVE BEHAVIOUR AND SWELLING

Space between molecular chains in epoxies makes them permeable to aqueous solutions. Solution uptake into CFRP tendons with epoxy matrices is a dual mode process: whilst the solution diffuses into the tendon, it also interacts chemically with the epoxy. Models proposed to characterize diffusion into polymers include Fickian, Dual Mode Sorption (considering both diffusion and chemical interaction) (Barrer, 1984) and Langmuir (for anomalous moisture diffusion) (Carter and Kibler, 1978). This paper considers Fickian diffusion only, given its robustness and reported suitability for use when considering diffusion in both matrix and composite materials (Springer, 1988).

Fick's first and second laws, equations (1) and (2), relate the rate of transfer of diffusing substance per unit area, F , to its concentration, C , in the direction of diffusion, x , perpendicular to the unit area considered. The diffusion coefficient, D , is a function of how permeable a given material is to a given solution over time, t . Diffusion behaviour in materials can be measured using gravimetric sorption: periodically weighing samples exposed to solutions to assess the rate of uptake. Equation (3) is used to calculate the percentage increase in mass of a sample (mass increase), M_t , based on its mass at time t , m_t , compared to its initial dry mass, m_o , prior to solution uptake.

$$F = -D \frac{\partial C}{\partial x} \quad (1)$$

$$\frac{\partial C}{\partial t} = D \frac{\partial^2 C}{\partial x^2} \quad (2)$$

$$M_t = 100 \left[\frac{m_t - m_o}{m_o} \right] \quad (3)$$

Fickian diffusion can be used to model aqueous solution uptake in CFRP in the absence of matrix cracking, moisture propagation along the fibre/matrix interface, voids or non-Fickian matrix behaviour due to, for example, significant relaxation as a result of solution uptake (Springer, 1988). When studying the diffusion of solutions into materials, the diffusion coefficient and the mass increase at saturation, M_{∞} , are key parameters. For CFRP, suitable diffusion parameters must be calculated bearing in mind the heterogeneous nature of the material. The permeability of carbon fibres is insignificant compared to that of the surrounding epoxy matrix so the mass increase in a saturated composite, $M_{c\infty}$, is a function of the volume fraction, V_f , and the mass increase in the saturated neat resin, $M_{e\infty}$, as shown in equation (4) (Springer, 1988). Similarly, the fibres act as geometric barriers to diffusion, so the diffusion coefficient for a solution to pass through CFRP perpendicular to the fibre direction, D_c , is a function of the diffusion coefficient of the epoxy, D_e , and the volume fraction as shown in equation (5) (Springer, 1988). Crank (1975) derived equation (6) that shows how data from solution uptake experiments measuring the mass increase at time t , M_{et} , and at time of saturation in thin films of epoxy material of thickness l , could be used to calculate the Fickian diffusion coefficient for the respective solution-epoxy interaction.

$$M_{c\infty} = (1 - V_f)M_{e\infty} \quad (4)$$

$$D_c = \left(1 - 2\sqrt{\frac{V_f}{\pi}}\right)D_e \quad (5)$$

$$\frac{M_{et}}{M_{e\infty}} = \frac{4}{l} \sqrt{\frac{D_e t}{\pi}} \quad (6)$$

It is possible to predict solution uptake in prestressing tendons, considered as long cylinders, using a Fickian radial diffusion model. From equations (1) and (2), using suitable boundary conditions, Crank (1975) derived equation (7) that calculates the mass increase of an isotropic cylinder of constant radius, r , when submerged in solution by summing n roots, $\alpha_n r$, of a Bessel function of the first kind, of order zero. As the number of summation terms evaluated in equation (7) approaches infinity, the solution tends to a linear relationship between mass increase and the square root of time, which tails off as uptake reaches 80 % saturation. By reasonably assuming that the models leading to equations (4) and (5) are valid when considering radial diffusion in CFRP tendons, mass increase at time t , M_{ct} , can therefore be predicted by specifying suitable parameters for the composite, as shown by equation (8).

$$\frac{M_t}{M_{\infty}} = 1 - \sum_{n=1}^{\infty} \left(\frac{4}{r^2 \alpha_n^2} \exp(-D \alpha_n^2 t) \right) \quad (7)$$

$$\frac{M_{ct}}{M_{c\infty}} = 1 - \sum_{n=1}^{\infty} \left(\frac{4}{r^2 \alpha_n^2} \exp(-D_c \alpha_n^2 t) \right) \quad (8)$$

Uptake of aqueous solutions into epoxies causes swelling due to the formation of hydrogen bonds between the solutions and polar groups on the polymer chains. These bonds cause water molecules to be adsorbed onto the polymer chains, causing the physical structure of the polymer to open up and swell. Wright (1981) reports a number of studies that have shown linear relationships between mass increase and volume change of CFRP laminates.

3. EXPERIMENTAL WORK

Experiments were carried out to measure the rate of radial solution uptake and diameter increase of CFRP tendons immersed in water, salt water and CPS. The tendons were made of Tenax UTS 5131 fibres, volume fraction 0.63, in a Bakelite EPR 4539 epoxy matrix. In each experiment, five specimens were prepared for testing in each solution. The silica coating was removed from the tendons, which were then manually sanded smooth to a diameter of 4.2 mm. The solutions were formulated as described by Chin *et al.* (1999), using deionised water in all cases. The salt water solution was of 3.5 % by mass sodium chloride in deionised water. The CPS was of 1.8 % by mass potassium hydroxide, 0.68 % by mass sodium hydroxide and 0.5 % by mass calcium hydroxide in deionised water. All solutions were maintained at 22 °C in airtight polypropylene flasks throughout the experiments.

In the uptake experiment, samples were cut to 150 mm length, dry weighed then submerged. Given the large ratio of tendon length to diameter, axial solution uptake in the tendons can be considered negligible (Broughton and Lodeiro, 2000). Gravimetric sorption was used to measure the solution uptake: the tendons were removed from solution, rinsed in deionised water, blotted dry, then weighed before being returned into solution. Readings were taken using a Mettler AE160 balance of 0.1 mg resolution and the mass increase was calculated periodically using equation (3).

In the swelling experiment, samples were cut to 50 mm length. For each reading, three diameter measurements were made of each tendon at distinct positions about the centre of the tendon length using a Universal Horizontal Microscope of 100 nm resolution. Dry readings were taken before submerging five tendons in each solution. Tendons were rinsed in deionised water and blotted dry prior to taking each set of subsequent measurements.

4. EXPERIMENTAL AND MODELLING RESULTS

Experimental and modelling results are shown in Figures 1 to 6, where each data point represents the mean of five readings. Error bars where shown give 95 % confidence limits based on the standard error of the mean, assuming a normal distribution of data. Water, salt water and concrete pore solution are abbreviated to W, SW and CPS respectively in all figures. Diameter increase, Δ_{ct} , and volume increase assuming constant length, V_{ct} , of the tendons were calculated in the same way as mass increase. Figures 1 and 4 show observed increases in tendon mass and diameter respectively over time. Figures 2 and 5 take logarithms of positive experimental data values, facilitating the hypothesis of relevant relationships by considering lines of best fit. Increases in tendon mass and volume are directly compared using lines of best fit in Figure 6. By summing the terms of equation (8) until the solutions converged, curves predicting mass increase over the test period and up to saturation are shown in Figures 1 and 3 respectively. Without data specific to the epoxy used; data for water, salt water and CPS uptake into epoxies at room temperature studied by Chin *et al.* (1999) was modified using equations (4) and (5). Values of $M_{c\infty}$ used were 0.525, 0.662 and 0.607 % respectively. Values of D_c used were 55.3×10^{-12} , 109×10^{-12} and 69.9×10^{-12} cm²/s respectively.

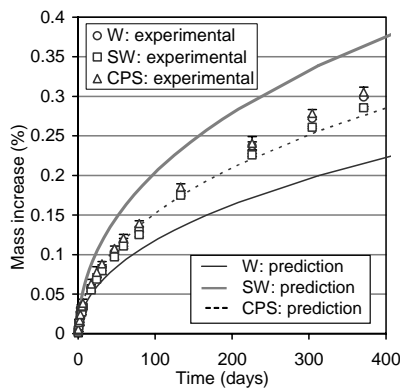


Fig. 1. Tendon mass increase with time

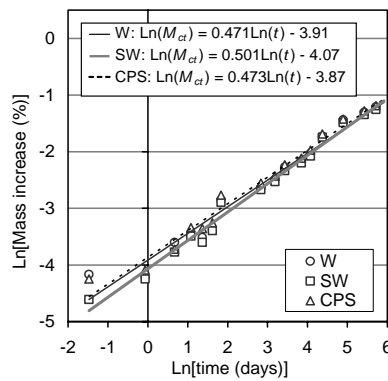


Fig. 2. Log-log plot of tendon mass increase with time

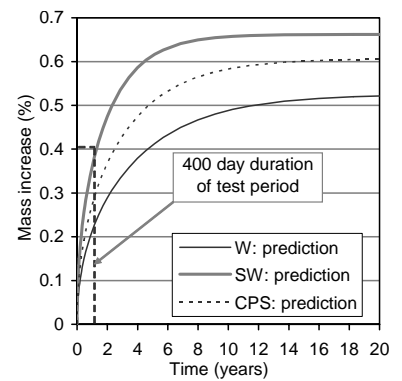


Fig. 3. Predicted long-term tendon mass increase with time

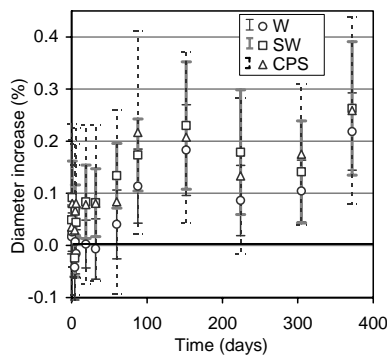


Fig. 4. Tendon diameter increase with time

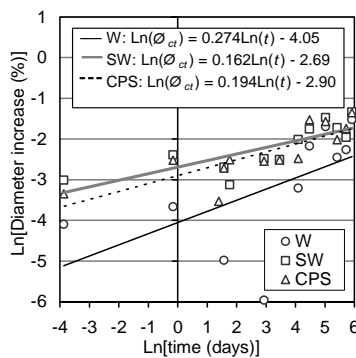


Fig. 5. Log-log plot of tendon diameter increase with time

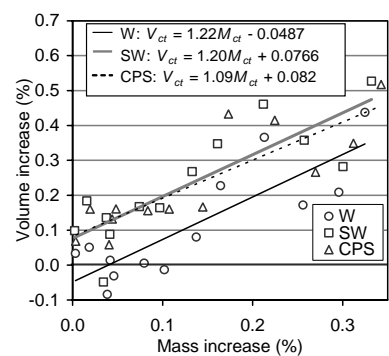


Fig. 6. Tendon volume increase with mass increase

5. DISCUSSION

The precise and repeatable results from the uptake experiment, shown in Figure 1, indicate relatively small increases in tendon mass, in the order of 0.3 %, over a one year period. Figure 2 shows mass increase is proportional to the square root of time in all cases: an indication of Fickian diffusion as predicted by equation (8). The predicted diffusion behaviour shown in Figures 1 and 3 differs from the observed experimental results. This discrepancy is due to the fact that different epoxies may have significantly different values of diffusion coefficient and mass increase at saturation (Wright, 1981). Given that the modelling predictions were made based on data for a different epoxy to the one used in this study, these discrepancies are to be expected. The difference in diffusion behaviour due to the type of aqueous solution used are most likely attributable to the difference in specific chemical composition of each

epoxy. Whereas solutions containing greater concentrations of polar molecules diffused more favourably through the material studied by Chin *et al.* (1999), the solution type made little difference to the diffusion behaviour in this study. Despite the discrepancies between the sets of data in Figure 1; given their similar behaviour, the model shows it is possible to predict the rate of solution uptake in CFRP tendons, and hence corresponding effects, using diffusion models and data that can be calculated from short-term thin film tests. When saturation of such tendons could take over ten years to occur, as shown in Figure 3, this method facilitates the prediction of long-term behaviour by using equations (4), (5), (6) and (8) to manipulate thin film diffusion data that can be obtained in less than one month.

In the swelling experiment, limited repeatability when locating tendons in the Metroscope, combined with deviations in tendon roundness resulted in considerable data scatter. Best fit lines and equations in Figures 5 and 6 are therefore indicative rather than absolute. Figure 5 shows diameter increases occurring between rates proportional to $t^{0.16}$ and $t^{0.27}$. A rate proportional to $t^{0.25}$, within the bounds of results obtained, indicates a proportional relationship between solution uptake and volume change: as suggested in Figure 6 and reported in the literature for laminate behaviour (Wright, 1981). The type of aqueous solution made little difference to the rates of swelling observed. Figure 6 shows volume increases in the order of 0.5 % over one year. If the tendons proceed to absorb solution as predicted in Figures 1 and 3, and the relationship between volume and mass increase is linear, they may ultimately swell in volume by 1 %. The significance of this swelling can be assessed in comparison with thermal effects. Transverse coefficients of thermal expansion of CFRP tendons are in the order of $50 \times 10^{-6} / ^\circ\text{C}$ (ACI Committee 440, 2003). A temperature change of 50°C , a theoretical seasonal variation, would cause a tendon volume change of 0.51 %. Thus, swelling effects due to solution uptake may ultimately be greater than due to thermal effects: potentially affecting the micromechanics of tendon failure, the tendon-concrete bond integrity, and placing a lower bound on feasible thicknesses of concrete cover.

6. CONCLUSIONS

1. Solution uptake into CFRP tendons studied has been observed to behave according to Fickian diffusion models
2. A method has been presented to predict the long-term diffusion behaviour of solutions into CFRP tendons using short-term thin film tests and Fickian diffusion models
3. Tendon volume appears to increase linearly with solution uptake in the CFRP tendons considered
4. The specific nature of the aqueous solutions considered had little effect on the diffusion or swelling behaviour
5. Tendon volume increases of approximately 0.5 % have been observed over one year and may ultimately be greater than thermal effects, potentially compromising the integrity of prestressed concrete structures

ACKNOWLEDGEMENTS

The authors wish to thank Dr Michael Sutcliffe, University of Cambridge, for guidance given to the research project. The support of Dr Giovanni Terrasi and SACAC, Switzerland, is much appreciated. The UK Engineering and Physical Sciences Research Council (EPSRC) is gratefully acknowledged for sponsoring the work undertaken.

REFERENCES

- ACI Committee 440 (2003). *Guide for the Design and Construction of Concrete Reinforced with FRP bars*, ACI, Farmington Hills.
- Barrer, R.M. (1984). "Diffusivities in glassy polymers for the dual mode sorption model". *Journal of Membrane Science*, Vol. 18, pp 25-35.
- Broughton, W.R. and Lodeiro, M.J. (2000). *Techniques for Monitoring Water Absorption in Fibre-Reinforced Polymer Composites*, HMSO, London.
- Carter, H.G. and Kibler, K.G. (1978). "Langmuir-type model for anomalous moisture diffusion in composite resins". *Journal of Composite Materials*, Vol. 12, pp 118-131.
- Chin, J.W., Nguyen, T. and Aouadi, K. (1999). "Sorption and diffusion of water, salt water and concrete pore solution in composite matrices". *Journal of Applied Polymer Science*, Vol. 71, No. 3, pp 483-492.
- Crank, J. (1975). *The Mathematics of Diffusion*, Oxford University Press, New York.
- Springer, G.S. (1988). *Environmental Effects on Composite Materials*, Technomic Publishing co., Westport.
- Wright, W.W. (1981). "The effect of diffusion of water into epoxy resins and their carbon-fibre reinforced composites". *Composites*, Vol. 12, No. 3, pp. 201-205.

EXPERIMENTAL STUDY ON BEHAVIORS OF CONCRETE BEAMS STRENGTHENED WITH EXTERNAL PRESTRESSING CFRP TENDONS

Zhi Fang

(Professor, Hunan University, Changsha, Hunan, China)

Hongfang Li

(PhD candidate, Hunan University, Changsha, Hunan, China)

ABSTRACT

The purpose of present paper was to study the flexural behaviors of concrete T-beams prestressed with external carbon fiber reinforced polymer(CFRP) tendons. Tests were carried out on 5 beams under four-point load, in which four beams were reinforced with hybrid external CFRP tendons and steel rebar and another one only reinforced with steel rebar. Such parameters as the different initial loading states at external CFRP tendon jacking and different jacking stress in tendon were considered. Based on the test results, the loading capacity, deformation, ductility index, cracking pattern, failure mode of those beams were studied. It was showed that the initial loading state on the beam at tendon jacking is insignificant to the ultimate behaviors of the beams. Non-prestressing reinforcement can improve the flexural behaviors effectively since it can lead to a more rational crack distribution and better ductility. The ductility index of those beams prestressed with external CFRP tendons can reach about 2.5, which can meet the requirement of engineering application.

KEYWORDS

prestressed concrete, beam, strengthen, Carbon Fiber Reinforced Polymer/Plastic(CFRP), externally prestressed, flexural behavior

1. INTRODUCTION

The external prestressing is a post-tensioning technique which is becoming more popular both in new construction and in strengthening of existing structures. The stress lag in external tendons can be prevented and material benefits can be maximized using the technique to strengthen the existing structures. Corrosion free, high strength-to-weight ratio enable CFRP composites to be a potential replacement for ordinary steel external tendons in engineering applications. In contrast to the wide investigation on behaviors of concrete beams externally prestressed with steel tendon(Tan and Ng, 1997; Ng, 2003; Tan and Tiandra, 2003; Wollmann et al., 2005), even though a number of studies on flexural behaviors of concrete beams with external CFRP tendons have been carried out in recent years(Mutsuyoshi and Machida, 1993; Grace and Sayed, 1998; Grace, 1999), it is insufficient to fully understand the performance of the structures. The objective of this paper focus on the flexural behaviors of concrete beams strengthened with external prestressing CFRP tendons.

2. EXPERIMENTAL PROGRAM

The test specimens included one ordinary reinforced concrete beam and four prestressed concrete beams with external CFRP tendons. All beams were 4.2m in length and 3.9m in span. The rising angle of external tendon to base line of the beam at deviators was 2° . 2 deviators with 5cm wide, 31cm deep for each tendon were located at the one-third span separately and a stainless steel plate was placed at a saddle-like interface between the tendon and deviator to reduce the friction. The jacking stress in tendons was about $0.30\sim 0.45 f_p$, here f_p referred to the guaranteed tensile strength of tendon. Of 4 prestressed beams, the two of EB-45-N and EB-30-N were jacked at 0 applied load and called new beams hereafter; another two of EB-35-S and EB-30-S jacked at 40kN applied load and called strengthened beam hereafter. Because those strengthened reinforced concrete beams with short or middle span are

usually cracking and under dead load of about 50% total action effect, a 40kN pre-load of about 50% ultimate capacity of beam RCB was applied on those strengthened beam EB-35-S and EB-30-S to simulate the initial loading state of the beam at strengthening . All beams were tested under four-piont load. The details about cross section and reinforcement were shown in Fig.1, test set-up and external tendon profile were shown in Fig.2, material properties and effective prestress in tendons were listed in table 1.

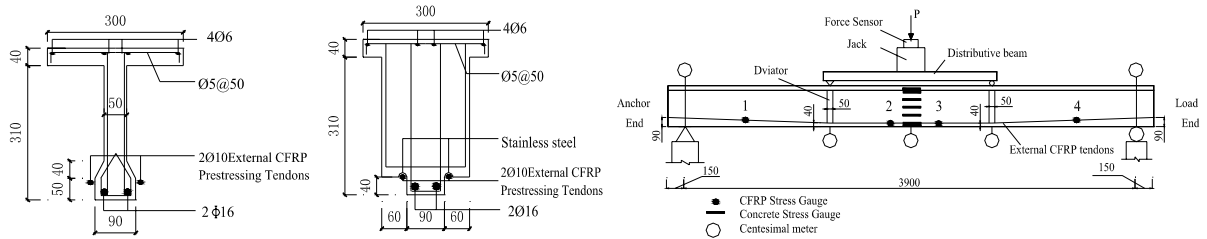


Fig.1 Reinforcement and Cross Section of Beams and Deviators

Fig.2 Test set-up

Table 1 Material Properties and Effective Prestress in Tendons

Beam No.	con/f_p %	PPR %	f_e MPa	CFRP tendon			Reinforcement		Concrete	
				A_p/mm^2	E_p/GPa	f_p/MPa	f_y/MPa	E_s/GPa	f_{cu}/MPa	E_c/GPa
RCB	/	/	/	/	/	/	347.3	201.3	53.5	35.1
EB-45-N	44.9	70.3	919.9	157.1	120	2100	347.3	201.3	62.5	36.3
EB-35-S	32.3	72.1	673.5	143.6	147	2550	347.3	201.3	62.5	36.3
EB-30-N	29.5	72.1	747.9	143.6	147	2550	347.3	201.3	56.6	35.5
EB-30-S	29.6	72.1	754.1	143.6	147	2550	347.3	201.3	54.8	35.3

Note : RCB is a reinforced concrete beam, EB-45-N and EB-30-N are prestressed concrete beams jacked at 0 applied loaded, EB-35-S and EB-30-S are prestressed concrete beams jacked at 40kN applied load; partial prestress ratio $PPR = A_p f_p / (A_p f_p + A_s f_s)$, A_p and A_s are the area of two CFRP tendons and reinforcement respectively, f_p and f_s are the strength of CFRP tendon and reinforcement; con is jacking stress in CFRP tendon; f_e is effective stress; E_p , E_s and E_c are the modulus of elasticity of CFRP tendon, reinforcement and concrete respectively; f_{cu} is the cube strength of concrete.

3. TEST RESULTS AND DISCUSSION

3.1 Load-deflection and load-prestress increment response and failure mode in the beams

The measured load-mid-span deflection and load-prestress increment curves of the beams were shown in Fig.3, and crack distribution on the beams at ultimate shown in Fig. 4, some results were listed in table 2.

The typical load-deflection curves of new beams were of nearly tri-linear type, The point A, B and C on the curves were corresponding to the concrete cracking, steel yielding and concrete crushing or tendon rupturing, respectively. The typical load-deflection curves of those strengthened beams demonstrated bi-linear nearly for they had cracked at jacking. The mid-span deflection both at loading and after unloading was relative small before reinforcement yielding since reinforcement and CFRP tendons were at linearly elastic state in this stage. After steel yielding, the deflection increased rapidly with applied load increasing and the residual deflection also became larger. The load-prestress increment curves were in the similar manner to those load-deflection relationships. The prestress increment in external CFRP tendon was nearly proportional to the mid-span deflection, which also could be found in those beams internally prestressed with unbounded steel strands (Burns et al., 1978).

It also could be seen from fig.3 there almost existed an identical post cracking manner both in new and strengthened beams, which indicated that the initial load state at the tendon jacking was insignificant to the flexural behaviors of the beams if only those beams were not beyond yielding at the initial applied load.

All beams failed with concrete crushing except for beam EB-45-N failed suddenly with CFRP tendon rupture near the deviator since the CFRP tendon in the latter was of lower strength, higher effective stress and worse quality. It is expected that failure mode of the beams is concrete crushing rather than tendon rupturing for engineering safety.

The crack distribution in fig.4 showed that the crack space in the beams prestressed with external CFRP tendons was larger than that in reinforced concrete beam. Compared with the crack distribution in new beam EB-30-N, the crack space in strengthened beam EB-30-S was smaller and similar to that in reinforced concrete beam RCB, which resulted from the strengthened beam cracked at initial applied load before external tendon jacking. Non-prestressing reinforcement could lead to a more rational crack distribution in externally prestressed concrete beams.

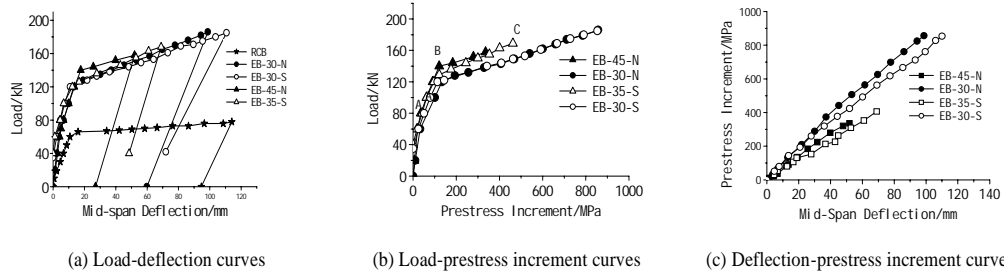


Fig.3 Relationship of deflection, load and prestress increment

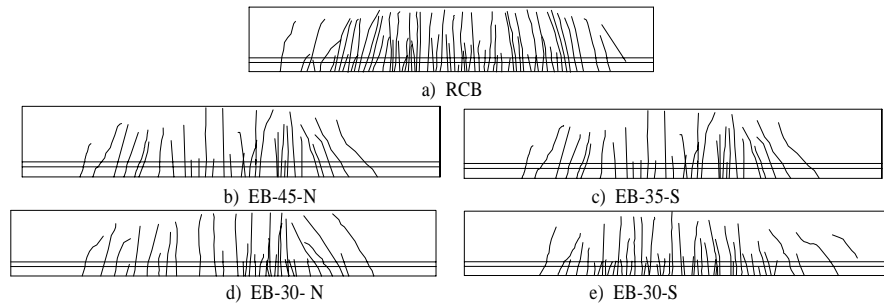


Fig 4 Crack Distribution of Beams at Ultimate

Table 2 Comparison between test and computed values

Beam	Concrete Cracking			Reinforcement Yielding			Ultimate State		
	Load /kN	Deflection /mm	Prestress increment /MPa	Load /kN	Deflection /mm	Prestress increment /MPa	Load /kN	Deflection /mm	Prestress increment /MPa
RCB	19	2.23	-	65	11.06	-	82	146.2	-
EB-45-N	68	4.32	28.27	140	17.62	120.86	(158)	(51.9)	(335.86)
EB-35-S	-	-	-	127	17.50	109.25	168	168	461.99
EB-30-N	60	3.63	32.00	120	13.15	133.31	186	98.70	886.00
EB-30-S	-	-	-	120	10.82	113.00	185	110.68	854.00

Not: 1. EB-45-N failed accidentally with CFRP tendon rupture near the deviator, the data in bracket was measured at the test terminating state.

2. EB-35-S and EB-30-S were strengthened after cracking, so there was no data at cracking state.

3.2 Ductility of the beams

The ductility index μ of beams prestressed with external CFRP tendons is defined on the energy concept as (NAAMAN and JEONG, 1995):

$$\mu = (E_{tot} / E_{el} + 1) / 2 \quad (1)$$

Where $E_{tot} = E_{pl} + E_{el}$, E_{tot} refers to the total energy, E_{pl} to the plastic energy, E_{el} to the elastic energy, and they are shown schematically in Fig.5. The ductility indexes of the beam RCB, EB-45-N, EB-35-S, EB-30-N and EB-30-S are 5.86, 2.19, 2.54, 2.45 and 2.25, respectively. The index of EB-45-N is smaller than those of other beams for beam EB-45-N failed suddenly with CFRP tendon rupture near the deviator. It could be seen that the ductility index for beams prestressed with external CFRP tendons would be larger than that for the beams prestressed with internal CFRP tendons which was less than 2 generally (Fang and Yang, 2005). So the ductility of the beams prestressed with

external CFRP tendons can meet the requirement of engineering application if only appropriate non-prestressing reinforcement is placed in the beams.

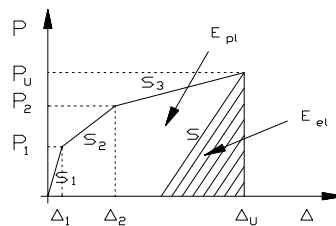


Fig.5 Sketch of load-deflection curve and energy component

4. CONCLUSIONS

The following conclusions can be drawn from the above investigations on the flexural behaviors of concrete beams prestressed with external CFRP tendons:

(1) There almost existed an identical post cracking manner both in new and strengthened beams, which indicated that the initial load state at the tendon jacking was insignificant to the flexural behaviors of the beams if only those beams were not beyond yielding at the initial applied load.

(2) The load-prestress increment in tendon curves were in the similar manner to those load-deflection relationships, and the prestress increment in external CFRP tendon was nearly proportional to the mid-span deflection, which also could be found in those beams internally prestressed with unbonded tendons

(3) The appropriate non-prestressing reinforcement can improve the flexural behaviors of beams prestressed with external CFRP tendons effectively since it can lead to a more rational crack distribution and better ductility.

(4) The ductility index of those beams prestressed with external CFRP tendons can reach about 2.5, which can meet the requirement of engineering application.

REFERENCES

- Burns, N.H., Charney, F.A. and Vines, W.R.(1978). "Tests of One-Way Post-Tensioned Slabs With Unbonded Tendons". *PCI JOURNAL*, Vo. 23, No. 5, pp. 66-83.
- Fang, Z and Yang, J (2005). "Behaviors of Concrete T-beams Prestressed with Partially Bonded CFRP Tendons", *11th International Conference on Fracture*, Editors: Alberto Carpinteri, Turin [Italy], pp. 448.
- Grace, N.F. and Sayed, G.A.(1998). "Ductility of Prestressed Bridges Using CFRP Strands". *Concrete International*, Vo.20, No. 6, pp.25-30.
- Grace, N.F. and Sayed, G.A.(1998). "Behavior of Externally Draped CFRP Tendons in Prestressed Concrete Bridges". *PCI JOURNAL*, V. 43, N. 5, pp. 88-101.
- Grace, N.F. (1999). "CONTINUOUS CFRP PRESTRESSED CONCRETE BRIDGES". *Concrete International*, Vo.21, No. 10, pp.42-48.
- Mutsuyoshi, H. and Machida, A. (1993). "Behavior of Prestressed Concrete Beams using FRP as External Cable". *SP-138, American Concrete Institute*, 401- 418.
- Ng, C.K.(2003). "Tendon Stress and Flexural Strength of Externally Prestressed Beams". *ACI Structural Journal*, V.100, N.5, pp. 644-653.
- Tan, K.H. and Ng, C.K.(1997). "Effects of Deviators and Tendon Configuration on Behavior of Externally Prestressed Beams". *ACI Structural Journal*, Vol. 94, No. 8, pp. 13-22.
- Tan, K.H. and Tjandra, R.A.(2003). "Shear Deficiency in Reinforced Concrete Continuous Beams Strengthened with External Tendons". *ACI Structural Journal*, V.100, N. 5, pp. 565-572.
- Wollmann, C.L.R., Kreger, M.E., Rogowsky, D.M. and Breen, J.E. (2005). "Stresses in External Tendons at Ultimate". *ACI STRUCTURAL JOURNAL*, V.102, No.2, pp. 206-213.
- NAAMAN, A. E. and JEONG, S. M. (1995). "Structural ductility of concrete beams prestressed with FRP tendons". Non-metallic (FRP) reinforcement for concretes structures, Proceeding of the 2th international RILEM symposium (FRPRCS-2)], Editor: Taerwe, E& FN Spon, London, pp. 379 –386.

POST-STRENGTHENING OF PRESTRESSED CONCRETE BEAMS USING UNSTRESSED AND PRESTRESSED CFRP STRIPS

Mohammad Reza Aram

(PhD student, Faculty of Civil Engineering, University of Tehran, Tehran, Iran)

Masoud Motavalli

(Assistant Professor, University of Tehran and Empa, Swiss Federal Laboratories for Materials Testing and Research, Dübendorf, Zürich, Switzerland)

Christoph Czaderski

(Project leader, Empa, Swiss Federal Laboratories for Materials Testing and Research, Dübendorf, Zürich, Switzerland)

ABSTRACT

Four prestressed concrete beams were constructed and tested to investigate the effectiveness of flexural post-strengthening with prestressed CFRP strips. One of the beams served as reference beam, another was bonded with unstressed CFRP strip, and two specimens were strengthened with prestressed CFRP strips in two prestressing levels. Gradient method was used for the anchorage of the prestressed CFRP strips. Experimental results and failure modes are explained in this paper.

KEYWORDS

Strengthening, Prestressed CFRP, Prestressed concrete beams, Gradient method

1. INTRODUCTION

Today there is a great demand on post-strengthening of concrete structures. A well-known material for post-strengthening is CFRP, Carbon Fiber Reinforced Polymer. To take full advantage of the material, it is beneficial to apply prestressed strips. Relatively little work has been carried out on the strengthening of internally prestressed concrete structures using prestressed CFRP strips (e.g. El-Hacha et al., 2004). Most of references investigated the application of prestressed CFRP strips by mechanical anchorage system. An anchorage system was developed at Swiss Federal Laboratories for Materials Research (Empa) without using any mechanical devices for anchoring of the end parts of the CFRP strips (Stöcklin and Meier, 2003). The prestressing force is gradually reduced to zero at the end parts of the strips. At Empa a project for strengthening of large-scale concrete bridge girders with prestressed CFRP strips anchored using gradient method (Czaderski and Motavalli, 2005) was performed. The project was the motivation to carry out a new set of small scale tests which aims at investigation of debonding of prestressed CFRP strips anchored with gradient method. In this paper, results of this small scale tests are presented.

2. EXPERIMENTS

Test specimens

Four 2.4m-long prestressed RC beams were constructed with the dimensions shown in Figure 1. All the beams were loaded in a four-point bending test scheme with a span of 2.0m. In attempt to examine the effect of prestressed CFRP strips, one beam was not strengthened and served as a control to the other three beams, which were strengthened with either unstressed or prestressed (two different stress levels) CFRP strips. A short description of each beam appears in Table 1. The concrete compressive and tensile strength tests were conducted using cylindrical

and cubic samples respectively at the ages of 28 days and at the time of the experiments. Steel bars with a nominal yield strength of 500 MPa and elastic modulus of 205 GPa were used for the longitudinal and shear reinforcement. Prestressing strands had a yield strength of 1618 MPa and an ultimate strength of 1869 MPa with an assumed elastic modulus of 195 GPa.

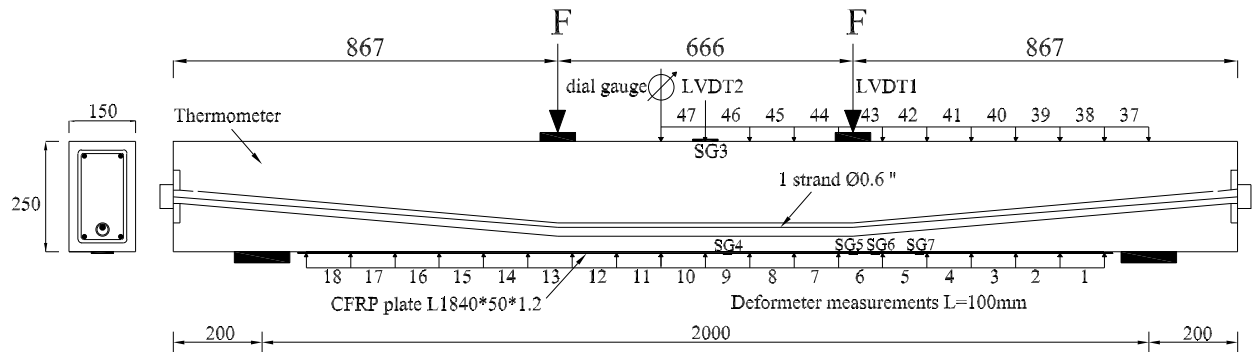


Figure 1: Dimensions, test setup and monitoring devices of the tested beams

Sika CarboDur unidirectional carbon/epoxy strips with a nominal width of 50 mm and thickness of 1.2 mm were used for strengthening. The flexural elastic modulus, E_a , and the flexural tensile strength, f_{ta} , of the epoxy adhesive were determined through tests of adhesive samples at the ages of 7 days. The compressive strength of the adhesive, f_{ca} , was evaluated through cubic compression tests. The mechanical properties of the CFRP composite strips, the adhesive and the concrete are summarized in Table 1.

Table 1. Material properties of test beams

Beam	Concrete			Adhesive			Strip	
	f_c^+ (MPa)	f_t^+ (MPa)	E_c^+ (MPa)	E_a (MPa)	f_{ta} (MPa)	f_{ca} (MPa)	E_f^* (GPa)	f_f^* (MPa)
Pb1 (reference beam)	48.9	3.1	33400	---	---	---	---	---
Pb2 (strengthened with unstressed CFRP)	48.1	3.3	33400	12600	42.6	105.6	165	>2800
Pb3 (strengthened with prestressed CFRP, 32% of f_f)	51.5	2.8	37450	12200	41.8	128.9	165	>2800
Pb4 (strengthened with prestressed CFRP, 16% of f_f)	47.1	2.3	34400	12200	41.8	128.9	165	>2800

+ at the time of the experiments, * specified by Sika[®] (E_f : mean value of tensile elastic modulus, f_f : minimum value of tensile strength)

Prestressing technique

To prevent premature failure of prestressed CFRP strips due to high shear stresses at the ends, the strips have to be anchored with special devices. This mechanical anchorage is expensive, difficult to install and often subjected to corrosion. To overcome these anchorage problems, the prestressing force can be anchored using gradient method developed at Empa (Stöcklin and Meier, 2003). In this method the prestressing force is reduced gradually towards both ends of the strip in steps. The CFRP strips were bonded to the concrete by using an epoxy based adhesive (Sikadur-30 LP) which cures faster at elevated temperatures (80°C). A special computer controlled device was used to control the prestressing and heating process. After heating of the strip and therefore curing of the adhesive in sector 1, the prestress force was reduced. Then, sector 2 was cured, followed by a reduction in prestress force and so on. Approximately 3½ hours were required to finish the gradient and the strip was then cut at the end. Lastly, the free length of the strip between the gradients was also cured by resistance heating, to ensure good adhesive quality. Each strip with a cross-section of 60 mm² was prestressed to approximately 60 kN (Beam Pb3) and 30 kN (Beam Pb4) in the same gradient length and number of steps. These prestressing forces correspond to two prestress levels of 32% (Beam Pb3) and 16% (Beam Pb4) of the nominal tensile strength of the strip (2800 MPa).

Test setup

The test setup, the various monitoring devices and their locations along the beams are shown in Figure 1. The beams were loaded mid-span displacement controlled using a testing machine with two 150 kN hydraulic actuators. The loading rate was 0.02 mm/s. The monitoring devices include linear voltage displacement transducer (LVDT), dial gauge, thermometer, strain gauges (SG) and *mechanical strain gauges* on CFRP and concrete. Slippage between CFRP and concrete is obtained from difference between mechanical strain gauge measurements on CFRP and concrete. The manual mechanical strain gauge measurements were performed during load steps where the deformation at mid-span kept constant and the load was adapted. From mechanical strain gauge measurements length of 100mm, the mean value strain along each 100mm length of CFRP can be determined. Cracks width were also measured in some load steps.

Results

The load versus midspan deflection curves for the beams are illustrated in Figure 2. These curves include a linear response up to the cracking, a cracked behaviour up to the yielding of the internal unstressed rebars and an inelastic response up to ultimate load. The curves reveal that the strengthening process has increased the load resistance capacity of the beam up to 17% for unstressed CFRP application (Pb2). For Pb3 and Pb4, in spite of compression effect of externally prestressing force on the concrete cross section, the load capacity increase is less than unstressed case due to premature debonding of strips. It can also be found that beams strengthened with prestressed strip have lower deflections at the service load and at failure (ductility). Another effect of prestressing was that cracks width decreased enormously in comparison to the unstressed beam.

Failure of control beam, Pb1, occurred due to crushing of the concrete in compression. The maximum compressive strain measured on the top of midspan was 0.00296. The cracking pattern, as shown in Figure 3, includes vertical flexural cracks around midspan and diagonal shear-flexure cracks in the shear spans.

The failure of beam Pb2 was associated with a rapid and unstable debonding of the CFRP strip followed by concrete crushing at top. This debonding was initiated at a large flexural crack in the midspan which is named C in Figure 3.

The failure of beam Pb3 was a sudden failure due to delamination of the CFRP strip along with the concrete cover beneath the internal reinforcement in the midspan (Figure 3). Additional CFRP strain from loading was 3 ‰ (SG4) at failure added to the initial prestressing strain results in a total CFRP strain of 9 ‰.

The failure of beam Pb4 was a rapid, sudden separation of the CFRP strip. The separation started at a shear crack in the midspan which was formed suddenly near crack M (Figure 3). Maximum measured slip is for this shear crack. Such a crack is usually associated with discontinuity in the vertical deflections and yields different deflections left and right of the cracked section. In most cases, the thin adhesive layer cannot accommodate such vertical displacements and cannot resist the corresponding vertical normal stresses developed. The beam after failure appears in Figure 3, which clearly shows the discontinuous vertical deflections at the lower face of the beam and the delamination of the CFRP strip. For Pb4, additional CFRP strain from loading was 4.9 ‰ at failure which results in a total CFRP strain of 7.9 ‰ including the prestressing strain. Based on the strain gauges SG1, SG4, it appears that the concrete didn't exceed its crushing strain and the CFRP strip didn't reach its rupture strain. It means that beams Pb3 and Pb4 didn't exceed its potential flexural capacity due to the premature debonding failure.

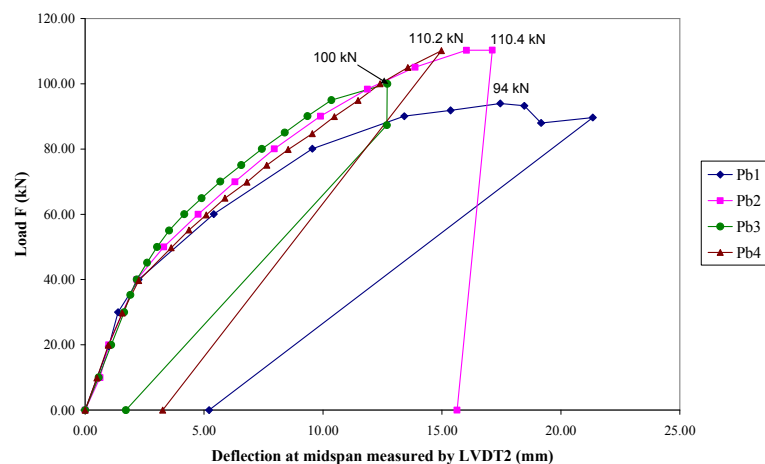


Figure 2: Experimental load deflection diagrams; Pb1: control beam, Pb2: strengthened with unstressed CFRP, Pb3 and Pb4: strengthened with prestressed CFRP

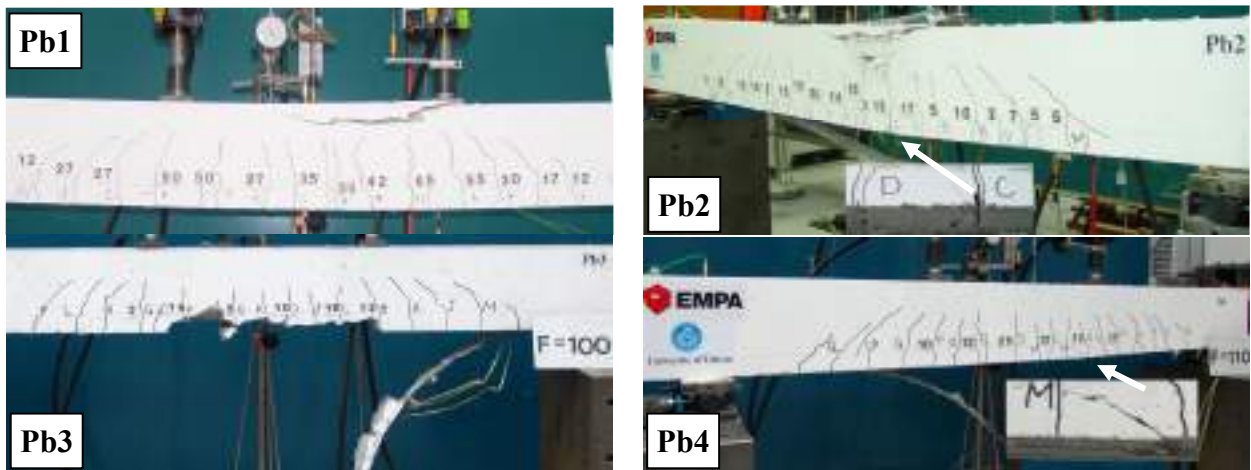


Figure 3: Test beams after failure

A summary of measured results can be found in Table 2. This table shows that for unstressed strip, 6 ‰ strain and 3 MPa bond shear stress were critical values for CFRP. For prestressed strips anchored with gradient method, the maximum achievable CFRP strain depends on prestress level and anchorage length on uncracked region. The gradient anchorage part of these small beams was in cracked region with high shear stresses and total CFRP strain was limited to 9 ‰ for Pb3 and 7.9 for Pb4. Maximum additional slip generated from loading was 0.165 mm and 0.193 for Pb3 and Pb4 respectively. Gradient force of strip at the anchorage zone produces an initial shear stress between CFRP and concrete. In Table 2 total maximum bond shear stress including this initial stress is presented.

Table 2: Maximum measured values

Beam	Failure load (kN)	Max. CFRP strain (‰)	Max. slip (mm)	Max. bond shear stress (MPa)
Pb1	94	---	---	---
Pb2	110.4	6.7	not measured	3.1
Pb3	100	9.0	0.165	4.3
Pb4	110.2	7.9	0.193	3.2

3. Conclusion

An experimental investigation of four prestressed concrete beams strengthened using unstressed and prestressed CFRP strips was presented. Prestressing the strip caused decrease in beam deflection and crack width if compared to the unstressed strips. However, the failure load could not be increased, it was even smaller. Furthermore, the ductility was clearly smaller. The results of the experiments point out that gradient anchorage method was not effective because the gradient anchorage was in the region of high shear stresses. The short beams provided not enough anchorage length on uncracked regions. This method would be more effective for large span beams like bridge girders. Strengthening using prestressed strips or plates has to be planned very carefully and the gradient anchorage should not be in regions with high shear stress. More research is needed in order to determine appropriate anchorage length as well as minimum beam length for applying this novel prestressing technique more efficiently.

4. References

- El-Hacha, R., Wight, R.G., and Green, M.F. (2004). "Prestressed carbon fiber reinforced polymer sheets for strengthening concrete beams at room and low temperatures". *Journal of Composites for Construction*, Vol. 8, No. 1, pp 3-13.
- Stöcklin, I., and Meier, U. (2003). "Strengthening of concrete structures with prestressed and gradually anchored CFRP strips". *Proceeding of FRPRCS-6*, Singapore.
- Czaderski, C., and Motavalli, M. (2005). "Large-scale concrete bridge girder strengthened with prestressed CFRP plates anchored using gradient method". *Composites Part B: engineering*, submitted for consideration for publication.

REINFORCEMENT TECHNOLOGY BY PRESTRESSED CARBON FIBER REINFORCED PLASTICS (CFRP)

Shouping Shang, Yongjun Jin, Hui Peng, Ming Wang, Qiaojuan Leng
(*College of Civil Engineering, Hunan University, Changsha, PR China*)

ABSTRACT

The carbon fiber reinforced plastics (CFRP), which has the great characteristics of inoxidizability, durability as well as high specific tenacity (unit quality intensity), is among the most ideal reinforcement materials. However, If CFRP is used directly in strengthening building and bridge structures; it can make certain enhancement to the load, but seldom enhance the rigidity distinctly. Moreover, this way cannot fully develop the CFRP's superiority of high strength, and may lead to component's debonding failures.

It is indicated by some related experiments that using prestressed carbon fiber reinforced plastics (CFRP) technique not only can effectively improve the rigidity of the reinforced concrete component, but also can greatly restrain crack development. The reinforced concrete structure which is reinforced by prestressed CFRP is not easy to appear debonding failures, and can fully reach its high intensity. It takes less expenditure compared to other reinforcement techniques also.

In conclusion, Reinforcement technology by prestressed CFRP has wide applicable prospect.

KEYWORDS

Prestressing force, CFRP, Strengthening, Stretching

1. INTRODUCTION

As compared to conventional strengthening technology, carbon fiber strengthening technology possesses obviously synthetic advantages. For example, it has extensive applicability, facilitative construction, swift construction velocity, small disturbance, high reinforcement efficiency, easily guaranteed quality, long service time, low synthetic construction cost and it doesn't increase the deadweight and volume of the structural component and so on.

With the continual development of the research work and the practical engineering applications, researcher found its shortcomings at the same time of taking cognizance of its advantages. The high-intensity predominance of CFRP can not exert fully and that will cause the material strength waste. The bonded amount of CFRP is limited restricted by the adhesion agent and destruction of bond easily occurs. In addition, the rigidity reinforcement effort of CFRP is indistinct and the deformation of the structural member can't be restrained availably.

The application of prestressing force in CFRP for strengthening concrete structure members is strengthening method which has emerged in the last few years. Compared with the common concrete strengthening technology, its technologic advantage is very obvious. Besides the merit of the common CFRP strengthening technology, it improves the deficiency of the common CFRP strengthening technology.

1.1 Utilize the characteristic of the CFRP effectively and give full play to the high-intensity advantage of CFRP.

Imposing prestressing force on CFRP will raise the starting point of bearing load. The CFRP can participate in working immediately and play a greater role at the beginning of the strengthening member carrying load. Compared with the non-prestressed CFRP reinforcement member, the high-intensity advantage of CFRP can be exerted ahead of time. Moreover, bonding a layer of CFRP cloth with high level initial stress is equivalent to bonding several layers of non-prestressed CFRP and makes the reinforcement technology with CFRP have preferable economic benefit.

1.2 The obvious effect of the rigidity strengthening restrains the structural member deformation and the

appearance and development of the cracks.

The prestressing force can restrain the appearance and the development of the crack of the structure member, and so improve the sectional rigidity remarkably. Prestressing force can also improve and adjust the stress of the original structure, eliminate the phenomenon of stress stain lagging which is caused by the initial load of the structure and reduce the deflection of the flexural member obviously though allowance for camber.

1.3 Seldom emergence of destruction of bond and desquamation destroy

First of all, because the increment of the stress and strain in the CFRP of the prestressed member is less than that in the CFRP of the non-prestressed member, the shear deformation the of epoxy resin layer and the shear stress transmitted by the epoxy resin layer is smaller than these of the non-prestressed member and the prestressed member is not apt to appear destruction of bond. Secondly, because the CFRP has been stretched while making prestressed test piece, it is extraordinary flat while being bonded. The CFRP will not deform with the test specimen surface, and not follow the surface undulation of structural member, which reduce the peel stress caused by curvature under combined tension and bending condition.

2. THE DIFFICULT AND THE KEY TECHNOLOGY OF STRENGTHENING TECHNOLOGY WITH PRESTRESSED CFRP.

2.1 Technical difficulty

CFRP is one kind of material with high tensile strength and low shear strength. Because of that special character of the CFRP, it is usually to paste the CFRP and jig together though adhesion agent, and the CFRP is anchored by the cohesive force of the adhesion agent. There are a lot of problems in this stretching mode.

First of all, it can't guarantee uniformly stretching. The CFRP is very apt to tearing failure during the stretching process. In addition, because the shearing strength of the adhesion agent is limited, the prestressing force value applied can't be too high. Though the CFRP is stretched successfully and pasted to the surface of concrete, there will be some CFRP silk which reach high stress value in advance and be destroyed, thereby influence the effective exertion of the material strength. Secondly, the adhesion agent can't function without solidification, thus it adds a solidification cycle in the whole process, and prolong the construction cycle. Furthermore, if we use one-off anchorage to apply prestressing force, the cost of reinforcement will increase.

The application of prestressing force to the CFRP will make the inherent advantages of the CFRP strengthening technology lost, including simple process and convenient construction. Therefore, how to ensure the whole rang of process of stretching and plastering simple and practical enough while exerting prestressing force to the CFRP uniformly and effectively has become the difficulty of the study of this technology.

Strengthening concrete flexural member with prestressed CFRP technology differed widely from the traditional CFRP strengthening concrete flexural member technology, and the flexural performance of reinforcement member will inevitably have great difference, so the traditional design calculation theory of the concrete beam strengthening with CFRP can't supervise the design of concrete beam strengthening with prestressed CFRP. In order to make strengthening concrete flexural member with prestressed CFRP to be a practical engineering technology, we must study and grasp the flexural performance of the concrete beam strengthening with CFRP, then bring forward corresponding design calculation theory and practical formula. This is another difficulty of the strengthening technology with prestressed CFRP.

2.2 Key technology

In order to solve the difficulty above-mentioned, though iterative experimental study, we have developed the prestressing force strengthening construction machinery which is suitable for prestressed CFRP cloth and plate materials

The stretching rig of the CFRP cloth adopts friction self-lock mechanism. The hardcore is a jig composed of two semi-cylinders. The CFRP cloth enwind on the semi-cylindrical jig, such design make the CFRP cloth could self-regulate the stress distribution under the function of the tensile force. The actuation force in the tensioner of CFRP cloth is induced by the handle. The impetus of transmission system guide screw rotation, which causes the nut to move. When the nut moves along the steering bar to the limiting position, the carbon fiber cloth material starts to be pulled. When the carbon fiber cloth material is stretched to predetermined condition, stop inputting actuation external force. The implement is promoted by the equipment, then the carbon fiber cloth materialist glued strictly onto the member which will be reinforced. The practices indicate that the design make the CFRP cloth could reach a higher prestressing level

when being stretched.

The stretching rig of the CFRP plate is different from the stretching rig of CFRP cloth, because of the special physical property of the CFRP plate compared with cloth material. The construction machinery is composed of tensioner and jig. The tensioner consists of a fixed end with mobile rod and a movable clamp which could move along the mobile rod. And the jig consists of a piece of soleplate with tooth shape grain and four pieces of clamp splice. When the CFRP plate is being stretched by the implement. The plate and the member, the rubber, and the bottom surface must be the strictly contacted. And that is realized by the making slope on the member surface and gelatinizing satiety. The partial tiny slit may be improved by the external angle steel.

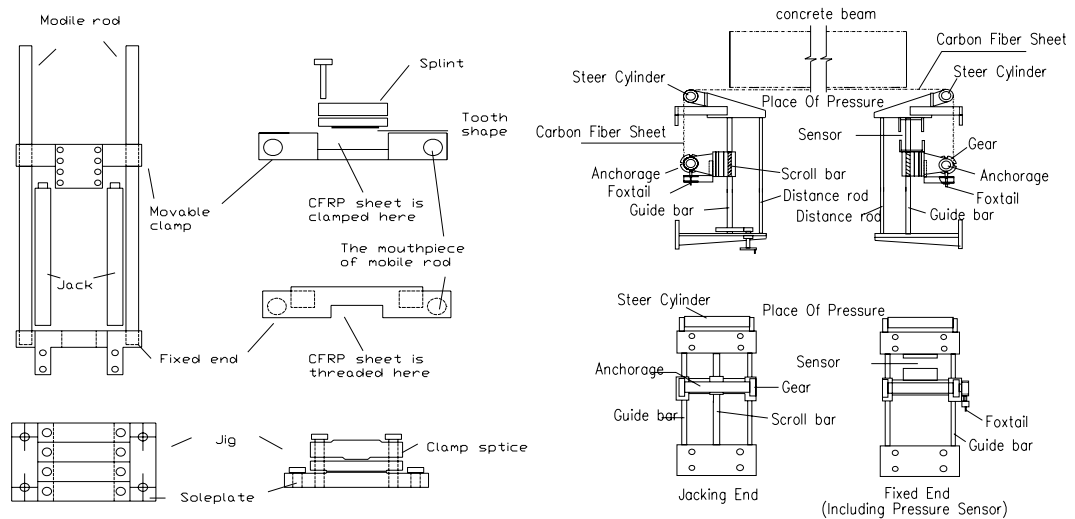


Figure 1: The schematic diagram of CFRP sheets rig and CFRP cloth machine

The prestressed CFRP strengthening construction process only add two links compared with the traditional CFRP strengthening process, including fixing construction machinery and stretching, and is convenient as traditional CFRP strengthening process. The actual engineering application proves that the construction process is advanced and simple and can obtain favorable effect.

In addition, in order to put forward the design theories to guide the application of the prestressed CFRP strengthening technology to practice in the engineering, it is necessary to study and grasp the stressing performance of the concrete flexural member strengthened with prestressed CFRP. According to experiment result and the mechanics model built up, we put forward a design method of the strengthen technology with prestressed CFRP.

3. THE MAIN TEST RESULTS

In order to ascertain the performance of flexural member strengthened with the CFRP(Carbon Fiber Reinforced Plastic) sheet material nine piece of small flexural member (100×150×2000mm) strengthened with the CFRP cloth material are tested . The primary test result is showed in table 3-1.

According to the test result, the cracking load of concrete and the yield load of steel bar will increase remarkably in the member strengthened by prestressed CFRP material, which will make the flexural rigidity of the member increase according to the prestressing force level of test piece. However, the using of prestressed CFRP material has on effect on the ultimate bearing resistance of structural member. The different midspan flexural deflections of two kinds of test pieces subjected to the yield load of the standard test piece reflect the influence of the prestressing force level on the flexural rigidity of test pieces. According to the data display, the strengthen technology with prestressed CFRP adequately bodied forth the predominance on rigidity strengthening.

It can be observed from the table that the tensile deformation of CFRP material in non-prestressed CFRP cloth reinforced member is restricted to 10.6% of its theoretical limits deformation (0.018) when the tension reinforcement yield. After stressing, but the tensile deformation of CFRP with maximal initial stress level reaches 60% of the theoretical limits deformation when the tension reinforcement yield, the increase degree is five times of non-prestressing force CFRP , it is observed that prestressing force cause the high performance of CFRP bring into full play.

Experimental study on the performance of flexural members reinforced by CFRP plates has started recently. In

the previous period, we have developed a stretching rig and jig which are applicable to prestressed CFRP plates strengthening, judged from the test result, the effect was beyond compare. In the next step, we should take the study on fatigue performance of CFRP reinforcement member.

Test Result of Prestressed CFRP Reinforcement Member 3-1

Serial Number	Initial Strain ϵ_{pi} ($\times 10^{-6}$)	Cracking Load /KN	Percentage Of Increase	Yield Load /KN	Percentage Of Increase	Ultimate Load /KN	Ratio	Midspan Deflection In Force Of 12.3KN /mm	Ratio
B _{1~4}	0	3.5	-	12.25	-	22.1	100%	7.5	100%
B ₅	6000	-	-	16.0	30.6%	18.0	81.1%	4.01	53.5%
B ₆	6000	9	157%	17.0	38.8%	28.0	126.1%	3.81	50.8%
B ₇	6000	8	129%	20.0	63.3%	26.0	117.1%	4.23	56.3%
B ₈	3300	5	43%	14.0	14.3%	21.5	96.8%	4.16	55.4%
B ₉	8400	11	214%	20.0	63.3%	25.0	112.6%	2.24	29.8%

Notes: B₅ (prestressing test piece) have loading history before strengthening, so have no cracking load indices.

4. EXAMPLE OF ENGINEERING APPLICATION (PHOTOGRAPHS)

Not long ago, bridge strengthening apply these strengthening technology in Liuyang County, Hunan province, China. Because of long service time of this bridge, the traffic capacity and traffic loads exceed the, design index. The main girder emerge quite a lot and wide cracks, some cracks already exceed the standard of governing code. According to the appraisal of related department, the bridge was in danger. Owing to better quality of concrete and well condition of foundation works, strengthening this bridge is greatly fit for applying ,prestressed CFRP. Strengthening 10 pieces of T-section beam rib which the length is 19.5m, the height is 1.245m, and the width is 0.175m, the practical engineering time was about 20 days, not including the time of preparing material and corollary equipment. As seen from the detection result of static test, the strengthening effect was beyond compare.

5. CONCLUSIONS

As seen from ongoing experimental study and practical engineering application, the performance of prestressing force CFRP strengthening technology greatly superior. but we do not know well of this strengthening technology, at the same time, for the sake of preferably exerting the predominance of this strengthening technology, it remains to require the researchers to take the study about durability, fatigue performance, interfacial blocking property and the influence of prestressing force, concrete creep, stress loss, and so on to reinforcement member performance, and so on.

6. REFERENCES

- Technical Specification for Strengthening Concrete Structure with Carbon Fiber Reinforced polymer Laminate(CECS146:2003). Beijing: China Planning Press. 2003
- Feiwei, Jiang shiyong, Peng feifei, et al. (2003). The experimental study of prestressing carbon cloth strengthening concrete flexural member. *Sichuan Building Research*, Vol. 29, No.2.
- Shang shouping, Peng hui, Tong hua, et al. (2003). The flexing resistance study of the prestressing carbon cloth material strengthening concrete flexural member. *Architecture Structures Journal*, Vol. 24, No. 5.
- Zhang tanxian, Lv xilin, Xiao dan, et al. (2005). Experimental study on primary and secondary load for RC beam strengthened with Prestressed CFRP sheet. *Structural Engineer*, Vol. 21, No.2.

WEDGE ANCHORAGE FOR LOADED OR PRESTRESSED FRP

Stefan L. Burtscher

Research Associate, Vienna University of Technology, Vienna, Austria

ABSTRACT

Wedge systems are used for steel tendons since many years with great success. The application of conventional wedge anchorages for CFRP tendons leads to a high lateral stress peak at the tip of the wedge that destroys the tensile element before the tensile strength is reached. In the paper the patented "Composite Wedge anchorage" (Burtscher, 2004) is described. The idea is that the wedge is formed of two materials with high and low modulus of elasticity. The material with low modulus of elasticity is arranged parallel to the tensile element and the thickness increases from the rear to the tip of the wedge. This influences the wedge stiffness normal to the CFRP element and distributes the pressure and shear stresses in the CFRP-wedge interface. The pressure and shear stress distributions determined by numerical simulations are continuous without stress peaks. The experimental results clearly show that the anchorage is very efficient and is able to anchor CFRP strips with thicknesses of 1.2 mm with an efficiency of more than 100 %. All 1.2 mm strips failed by exceeding the tensile strength of the strip and the failure did not occur in the anchor region. The tests on 2.5 mm thick CFRP that were bonded to the wedge reached efficiencies of 84 and 87 %. Tests on the same CFRP strips, but with a friction interface even gave an efficiency of 93 %: The failure in all tests occurred by slipping of the strips and not due to exceeding the transversal strength. The improved friction surface of the next generation of wedges will allow an even higher efficiency of the anchoring system.

KEYWORDS

Wedge anchorage, composite wedge, prestressing, CFRP

1. INTRODUCTION

In recent years strengthening of concrete structures has become a large application field for carbon fiber reinforced plastics (CFRP). The structures are strengthened by bonding or prestressing the strips on the tensed surface. Bonded strips increase the load bearing capacity of the structure. When the strips or rods will be prestressed an additional benefit is that the deflections under load can be reduced and less CFRP strips are often necessary. In some cases it is also possible to increase the durability of the structure. Anchorages developed for steel tendons cannot be applied for FRP tendons because of the sensitivity to transversal pressures. Therefore, special anchorages are necessary. In the passed decades investigations on cast anchors with resin or grout, anchors with expansive material, spike anchors, wedge anchors, other clamping mechanisms and various combinations were found in literature, see e.g. Nanni et al. (1996), Pincheira et al. (2001), Stresshead (2005), Horvatits et al (2003), Meier (1996), Andrä (2005). High anchoring loads were found for cast anchorages and other systems, where the CFRP tendons are fixed by bonding using resin. For easily installable wedge anchors the transferable loads were low.

For economic purposes it is important that the anchorage is able to anchor high loads, easy to apply, produced at low cost, easy to handle on the construction site and necessitates only a short time for the anchoring process. These requirements can be met by applying the Composite Wedge System (Burtscher, 2004), which is presented in this paper. The anchorage combines the advantages of the wedge anchors used for prestressing high strength steel tendons, with the ability to anchor high loads coming from CFRP strips or rods.

First numerical simulations on conventional wedge anchors and the composite wedge anchor are presented to explain the working principle of the Composite Wedge anchorage. Next, experiments on 1.2 mm and 2.5 mm thick CFRP strips are presented, that confirm the high efficiency of the anchorage system. In the experiments the interface between wedge and CFRP strip was established by bonding using an epoxy adhesive, but also by a simple friction interface. Several tests with the friction interface were performed. Here only one test on a 2.5 mm thick CFRP strip is presented. Finally, some further economic designs that will be investigated in the future will be presented.

2. STRESS DISTRIBUTION FOR THE CONVENTIONAL AND THE COMPOSITE WEDGE ANCHORAGE

The load applied to a tensile element (rod or strip) has to be transferred first to the wedges and then to the anchor body. The wedges and the anchor body are sliding along each other on an inclined plane. When a tensile force F is applied to the rod or to the strip the wedges are pressed to the tensile element. Figure 1 shows the composite wedge system, the wedges are made of two components, epoxy and steel. The epoxy component is in parallel to the CFRP strip and its thickness decreases from the wedge tip to the rear part of the wedge. The epoxy component has a much lower elastic modulus than the steel component. Therefore, the stiffness of the Composite Wedge is primarily determined by the thickness and elastic modulus of the epoxy component. Due to the higher epoxy thickness at the wedge tip than in the rear part, the transversal stiffness increases from the wedge tip to the rear part.

A traditional wedge is made of one material only. The transversal stiffness of a traditional wedge is therefore increasing in opposite direction, from rear part to wedge tip. In figure 1 the transversal pressure and shear stress distribution determined by finite element simulation at mean ultimate load ($f_t = 3100 \text{ N/mm}^2$) of a 1.2 mm thick CFRP strip are shown for a traditional wedge (dashed line) and the Composite Wedge System (solid line). The traditional wedge design leads to a high value of transversal pressure and a high gradient at the wedge tip, therefore the CFRP strip fails by exceeding the transversal compression strength, before the ultimate tensile load will be reached.

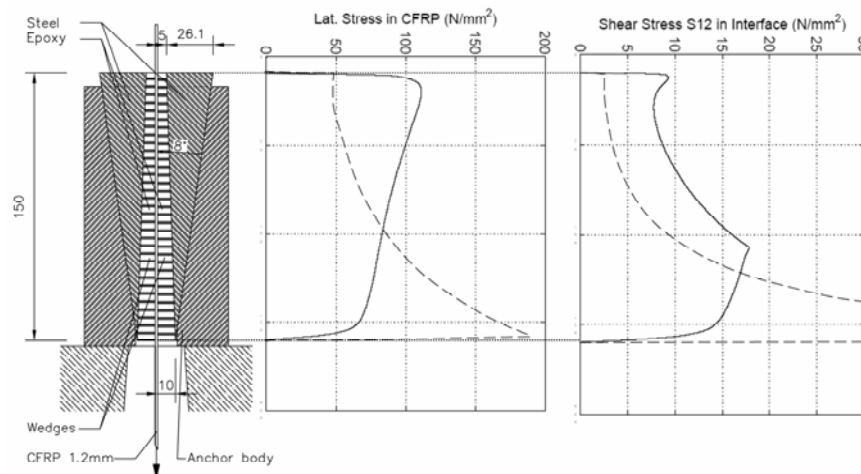


Figure 1: Transversal stresses on CFRP element and shear stresses in the wedge-CFRP interface determined by elastic finite element simulation. The dashed line is for traditional wedges and solid line for the Composite Wedge System.

The Composite Wedge System distributes the transversal pressure uniformly, no high gradients occur and the ultimate load of the CFRP strip can be exploited, see figure 1. The same holds for the shear stresses. With the Composite Wedge System it is possible to adapt the pressure and shear stress distributions on the CFRP tendon as required. The geometric parameters are the angle of the wedge (angle between axis of the tensile element and the sliding surface) and the thickness ratio of the epoxy component in the rear region and wedge tip. With the variation of the angle, the total lateral force acting on the CFRP tendon can be changed. The total lateral force corresponds to the area below the pressure curve in figure 1. The smaller the wedge angle the higher is the total lateral force and the area under the pressure curve. The stress distribution can be adjusted by changing the thickness ratio of the epoxy component in the rear region and the wedge tip. The pressure stress can be constant from the wedge tip to the rear region or increasing with a desired gradient. Due to this smooth transitions, low gradients and low maximum values it is possible to activate the whole wedge length, which leads to high ultimate anchoring loads.

4. EXPERIMENTAL VERIFICATION

In this experimental series the components of the Composite Wedges were of steel and epoxy resin. The length of the wedge was 150 mm, the width 60 mm and the angle to the axis of the strip 8° , see drawing in figure 1. The steel

component of the Composite Wedge was made with smooth sliding surfaces and a structured surface that will be in connection with the epoxy layer. For the tests with the friction interface the wedges were produced with a surface that was rough. The load was applied using a hydraulic jack with a hollow piston. Identical anchor bodies and Composite Wedges were used on both tendon ends. The load was monotonically increased and measured with load cells arranged between the hydraulic jack and an additional loading plate. The displacement was measured as the stroke of the hydraulic jack. For the tests on the CFRP strip with thickness 1.2 mm (T12V1 to T12V4) and 2.5 mm (T25V1, T25V2) the wedges were bonded to the strip before testing. The adhesive used was Sikadur 30, see Table 1 for details. Several tests with a friction surface (Type FT1), without adhesive, were performed successfully with different test configurations and strips. Here only one test on 2.5 mm thick CFRP strips (T25FT1) is presented.

4.1 Experiments on 1.2 mm thick CFRP Strips

The tests on 1.2 mm thick strips showed the same failure load, which was equal to the mean tensile stress ($f_t=3100$ N/mm²) times the area. In Table 1 F_{calc} and the efficiency are determined with the guaranteed tensile strength of $f_t=2800$ N/mm² (Sika, 2003). The efficiency was between 110 to 114 %. The failure occurred due to failure of the CFRP strip. Figure 2 shows an image of one test series after removal from the testing machine. The wedges were still bonded together and no indication of slippage or failure due to high transversal pressure occurred. The conclusion is that the wedge anchorage system in this configuration is able to anchor higher loads.



Figure 2. Two Composite Wedges after failure test.

Table 1: Test specimens and experimental results.

	F_{test} (kN)	bxt (mm)	F_{calc} (kN)	Efficiency (%)	Interface
T12V1	186.3	50x1.2	168	111	Adhesive
T12V2	186.5	50x1.2	168	111	Adhesive
T12V3	184.3	50x1.2	168	110	Adhesive
T12V4	191.5	50x1.2	168	114	Adhesive
T25V1	152.9	24.8x2.5	181	84	Adhesive
T25V2	149.2	23.7x2.5	171	87	Adhesive
T25F1	160.7	24.1x2.5	173	93	Friction

4.2 Experiments on 2.5 mm thick strips using bond and friction interfaces

To determine the limits of this anchorage tests on 2.5 mm thick CFRP strips were prepared. The strips were cut to a width of approximately 25 mm, see Table 1. Although the width of the 2.5 mm thick CFRP strip is smaller than the width of the 1.2 mm one, the transversal and shear stress in the interface are the same for different width of strips, but increase strongly with higher strip thickness. The reason for that is that the whole anchorage including strip is a plain stress problem. Therefore, for strips with the same thickness it is possible to reduce the width of the strip and end up with the same shear stress and pressure normal to the strip axis.

For the 2.5 mm thick CFRP strip the manufacturer guarantees 2800 N/mm². The efficiency reached in the tests with adhesive in the interface was 84 and 87 %. The observation of the specimens after testing showed that the CFRP strips slipped in the anchor region, without causing any damage due to transversal stress.

The tests with the friction interface were performed on the same CFRP strips, but the wedges were prepared with a rough surface and sandpaper was used in the interface. Again the failure was initiated by slipping in the wedge CFRP strip interface. As before no damage due to excessive transversal pressure was observed. The results are given in Table 1. By comparing the efficiencies of the tests on 2.5 mm thick strips it can be observed that the friction interface showed the best performance with an efficiency of 93 %.

4. SPECIAL LAYOUTS OF THE COMPOSITE WEDGE SYSTEM FOR STRIPS

The standard layout of the Composite Wedge System is shown in figure 1. An advanced system that exploits symmetry conditions leads to an anchorage for near surface mounted prestressing strips, see figure 3 (left). Here only one wedge is necessary. The short distance from the structure surface reduces the requirements for bonding and bolting. One important application of this special Composite Wedge layout could be for the strengthening of bridges. In figure 3 (right) two strips are anchored in one anchor body. This reduces the size of the anchor body and the number of wedges necessary. Another advantage is that two strips can be prestressed in one step.

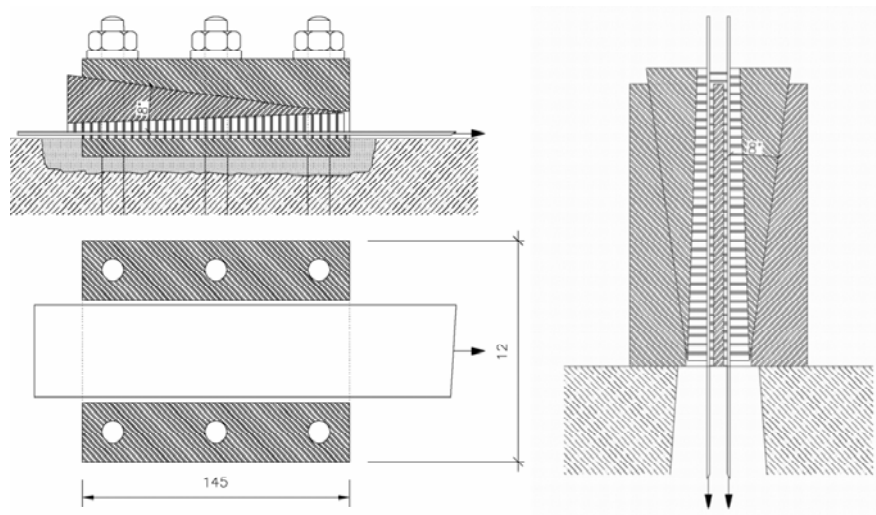


Figure 3: Asymmetric Composite Wedge System for near surface mounted strips and anchorage for two strips.

2. REFERENCES

- Andrä H.-P., Maier M. (2005). "Instandsetzung von Brücken mit einer neuen Generation von Spanngliedern auf Basis von CFK-Bändern", *Bauingenieur*, Vol. 80, pp. 7-15.
- Burtscher, S.L. (2004). "Keilverankerung für vorgespannte und/oder belastete Zugelemente (Wedge anchorage for prestressed and/or loaded tensile elements)", Austrian Patent.
- Harper, C.A. (2002). "Handbook of Plastic, Elastomers & Composites", MacGraw-Hill, New York.
- Horvatits J., Kollegger J. (2003). "Anchorage Advances", *Bridge Design & Engineering*, Vol. 33, No. 4, pp. 69-71.
- Meier U. (1996). "Zwei CFK-Kabel für die Storchenbrücke", *Schweizer Ingenieur und Architekt*, Vol. 44, pp. 980-985.
- Nanni A., Bakis C.E., O'Neil E.F., Dixon T.O. (1996). "Performance of FRP Tendon-Anchor Systems for Prestressed Concrete Structures", *PCI Journal*, January-February, pp. 34-44.
- Pincheira J.A. (2001). "Anchorage of Carbon Fiber Reinforced Polymer (CFRP) Tendons using Cold-Swaged Sleeves", *PCI Journal*, November-December, pp. 100-111.
- SIKA (2003). "Construction: Sicher bauen mit System", Technische Merkblätter, Ausgabe 5.
- Stresshead (2005). *Technische Dokumentation*.

Part XVII. Repair of Columns

EVALUATION OF THE CARRYING CAPACITY OF RC COLUMNS STRENGTHENED WITH COMPOSITE MATERIALS

E. Ferrier

(Assistant professor, University Lyon 1, Lyon, France)

M. Quiertant

(Researcher, Structural Engineering Unit - French Public Works Research Laboratory - LCPC, Paris, France)

P. Hamelin

(Professor, University Lyon 1, Lyon, France)

ABSTRACT

This paper presents a simple evaluation procedure of the ultimate capacity of RC columns strengthened with composite materials. This method, which is based on the French design guidelines (BAEL) permits to take into account the influence of the CFRP confinement on the mechanical behavior of columns. The procedure is a quite general frame that allows the evaluation of different combinations of reinforcement with continuous or discontinuous confinement associated or not with flexural reinforcement using FRP laminates or sheets. After a detailed presentation, results obtained by the proposed relations are compared to experimental data.

KEYWORDS

Reinforcement, CFRP, RC columns, Confinement, Design.

1. INTRODUCTION

The confinement of RC columns is an application where the external wrapping by fiber-reinforced polymer (FRP) sheets is particularly effective and offer numerous advantages as related to speed and easiness of application, high strength-to-weight ratio, durability and corrosion resistance. This technique, which is applied either to the repair of damaged columns or to the rehabilitation of healthy structures, is increasingly used in USA, Canada and Japan. It permits to extend the life expectancy of ageing structures as well as to answer seismic requirements. The purpose of this work is to propose a design method with simple calculation procedure of the ultimate capacity of RC columns externally strengthened with bonded composite materials.

2. DESIGN METHOD

1.1 Evaluation of the carrying capacity of a confined column

In the proposed study, four combinations of external reinforcement of columns are considered: continuous or discontinuous rings for the confinement, associated or not with flexural reinforcement using FRP laminates or sheets. External reinforcement has to be carried out according to the recommendations of the French Civil Engineering Association (AFGC, 2003). The proposed calculation take into account the confinement effect and the axial reinforcement on the carrying capacity of columns, but the procedure is restricted to the following conditions related to:

➤ Slenderness ratio (λ): Only short columns, with slenderness ratio limited to fifty are considered ($\lambda \leq 50$). Sections can be circular rectangular or square.

- Loading condition: The applied compressive load must be applied with an eccentricity lower or equal to e_{max} , where e_{max} is the upper value comparing 2 cm (this absolute value is referred to acceptable construction deviation) to 10% of the smallest side of the cross section (or 10% of the diameter in case of circular section). Columns with the smallest side of the cross section smaller than 200 mm are not considered here (at date this point is still debated in the task group).
- Conditions of continuity: Columns have to respect the constructive dispositions proposed by AFGC (AFGC, 2003), in particular the conditions on the covering lengths and the curvature radius of the corners. For square or rectangular section, it is necessary to round off angles, to prevent a premature local failure of the composite. Indeed, the tensile strength of the composite significantly decreases for low corner radius (Yang et al., 2001).

1.2 Calculation procedure for confined columns

The compressive strength (f'_{cc}) of the confined concrete is evaluated using the following general form:

$$f'_{cc} = f'_c + k_1(\psi_f k_c k_h f_{pu} + k_e f_{pa}) \quad (1)$$

The performance coefficient ψ_f depends on the strengthening technique, the kind of reinforcement and the curvature radius of the composite. We consider in a first approach:

$$\psi_f = 0.8 \quad \text{Circular section} \quad \psi_f = 0.6 \quad \text{Square section (with } r_c \geq 35 \text{ mm)}$$

This coefficient can be corrected from tests on composites adopting the specified curvature radius (Yang et al., 2001). The confinement pressure f_{pu} resulting from the composite is expressed as follows:

$$f_{pu} = E_p \cdot \varepsilon_{fu} \quad (2)$$

With the ultimate strain of the composite ε_{fu} (measured from a tensile test on a composite) and the confinement modulus E_p , which traduces the confinement stiffness and given as follows:

$$E_p = \frac{t_f \cdot n_p}{r} \cdot E_f \quad \text{For circular section} \quad (3) \quad E_p = \frac{2t_f \cdot n_p}{b} \cdot E_f \quad \text{For rectangular section (3')}$$

With E_f the tensile modulus of the composite, t_f the thickness of one layer and n_p the number of layers. b and r are respectively the biggest side (in the case of square or rectangular section) and the radius of the concrete core for a circular section. Many studies show that FRP-confinement can significantly enhance the ultimate strength and strain of the concrete. Ultimate compressive strength directly depends on confinement ratio (fig. 1).

Depending on the concrete strength, the coefficient k_1 is given by (Berthet et al., 2005a, b):

$$k_1 = 3.45 \quad \text{With } f'_c \leq 50 \text{ MPa} \quad (4)$$

In circular sections, the confinement pressure is uniform in the concrete core whereas in rectangular columns, the distribution of the confinement pressure is not homogeneous (fig. 1). In these cases, only a part of the concrete core is effectively confined, that considerably reduces the confinement efficiency. Square sections generate parabolic distribution for confinement pressure with an initial angle of 45° with the jacket, depending only on the geometry of the section (Mander et al., 1988).

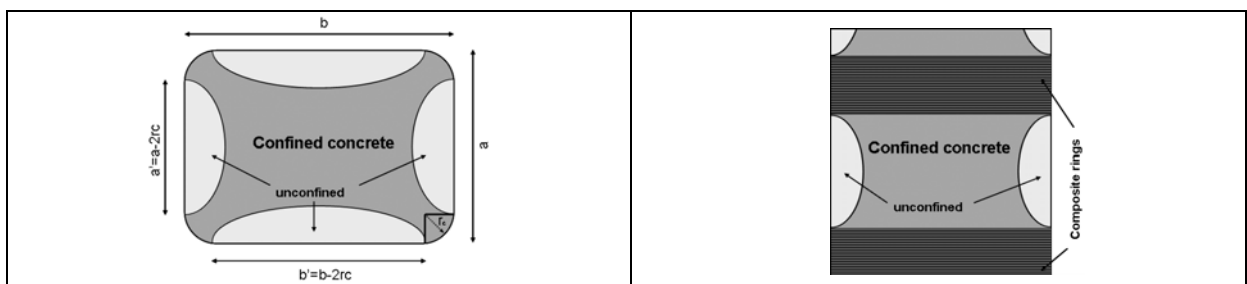


Figure 1: Confinement pressure on a cross section

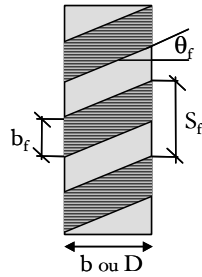
Figure 2: Confinement pressure between two rings

For the calculation, we shall consider an effective confinement pressure. So, the nominal confinement pressure is corrected using a coefficient k_c , which takes into account the geometry of the columns (CSTB-Freyssinet, 2001):

$$k_c = 1 - \frac{a^2 + b^2}{3A_b} \quad \text{for square section} \quad (5) \quad k_c = 1 \quad \text{for circular section} \quad (5')$$

For a discontinuous confinement, the distribution of the confinement pressure is not homogeneous on the height of the column (fig. 2). f_{pu} is then combined with a coefficient k_h which integrates the width of the composites rings b_f , their spacing S_f and their orientation θ_f , k_h is given by the produce of two coefficients η_1 and η_2 , which traduce respectively the influences of the orientation and the spacing of the composite rings and defined using:

$$k_h = \eta_1 \eta_2 \quad (6)$$



Rectangular section:

$$\eta_1 = 1 \quad (7')$$

$$\eta_2 = \frac{\left(1 - \frac{S_f - b_f}{2D}\right)^2}{1 - \rho_l} \quad (8)$$

Circular section:

$$\eta_1 = \frac{1}{1 + \frac{\theta_f}{\pi D}} \quad (7)$$

$$k_h = \left(1 - \frac{(a - 2 \cdot r_c)^2 + (b - 2 \cdot r_c)^2}{3 \cdot a \cdot b \cdot (1 - \rho_l)}\right) \cdot \left(1 - \frac{(a + b)(S_f - b_f)}{3 \cdot a \cdot b \cdot (1 - \rho_l)}\right)$$

With ρ_l longitudinal steel ratio (A_s/B), θ_f winding angle of the reinforcement (between fibers axis and transverse direction of the column), a and b , the straight lengths of the sides ($a' = a - 2r_c$ and $b' = b - 2r_c$).

The confinement pressure f_{pa} generated by the steel stirrups is estimated (Mander et al., 1988) using:

$$f_{pa} = \frac{A_{st}}{s_t d} f_y \quad \text{for circular section} \quad (9) \quad f_{pa} = \frac{A_{st}}{s_t b_t} f_y \quad \text{for square section} \quad (9')$$

The effective confinement pressure induced by the stirrups is estimated by associating to the nominal confinement pressure a coefficient k_e which takes into account the geometry of the section and stirrups spacing (Mander et al., 1988):

$$k_e = \frac{\left(1 - \frac{s_t}{2D_t}\right)^2}{1 - \rho_l} \quad \text{(Circular section)} \quad (10) \quad k_e = \frac{\left(1 - \frac{a_t^2 + b_t^2}{3A_{bt}}\right) \left(1 - \frac{s_t}{2a_t}\right) \left(1 - \frac{s_t}{2b_t}\right)}{1 - \rho_l} \quad \text{(Square section)} \quad (10')$$

1.3 New carrying capacity for strengthened columns

Developed method is an extension of the French design guidelines (BAEL) and takes into account the influence of the confinement effect on the mechanical behavior of the concrete. In these relations, confined concrete strength f'_{cc} is substituted to plain concrete strength f'_c . A significant reduction of the confinement efficiency in slender column was demonstrated from experimental studies (Mirmiran et al., 2001; Thériault, et al., 2001) and this effect is integrated in the parameter α .

The maximum axial load for a confined column is given by:

$$N_u \leq \alpha [A_b f'_{cc} + A_s f_a] \quad (10)$$

With α , a coefficient depending on the slenderness ratio and given under the following form:

$$\alpha = \frac{0.85}{1 + 0.2 \left(\frac{\lambda'}{35}\right)^2} \quad \text{for } \lambda' \leq 50 \quad \text{with } \lambda' \text{ slenderness ratio} \quad (11)$$

3. COMPARISON WITH EXPERIMENTAL RESULTS

Comparison of predicted results and those experimentally obtained by others authors (Quiertant et al., 2004) is reported in table 1. The experimental program was based on tests on twenty columns with a 200 x 200 mm² square cross section and an overall height of 2,500 mm. Two series of specimens were cast, with two different concrete (40 and 55 MPa strength) and two different internal reinforcements (low and medium). Finally columns were externally strengthened with different combinations of longitudinal and transverse CFRP layers. From table 1, it can be seen, that the model slightly underestimates the ultimate capacity of the reinforced columns. Indeed, the average differences between experimental values and those calculated from the model are inferior to 10 %.

Table 1: Comparison between calculated and experimental data

CFRP for Flexural reinforcement t_f/E_f	CFRP wrapping confinement t_f/E_f	Columns with low internal reinforcement		Columns with medium internal reinforcement	
		Ultimate load	Predicted	Ultimate load	Predicted
None	None	1215* kN	1088 kN	1254* kN	1295 kN
6 CFRP plates (2cm width) 1.2 mm/180 GPa	1 layer of CFRP 0.43 mm /105 GPa	1578* kN	1407 kN	1711* kN	1594 kN
1 layer of CFRP 0.117 mm /240GPa	1 layer of CFRP 0.117 mm /240 GPa	1194* kN	1326 kN	1653* kN	1540 kN
2 CFRP plates (2cm width) 1.2 mm /165 GPa	1 layer of CFRP 0.13 mm /230 GPa	1422* kN	1334 kN	1689* kN	1545 kN
1 layer of CFRP 1 mm /62-70 GPa	1 layer of CFRP (angle of 20°) 1 mm /62-70 GPa	1462* kN	1493 kN	1628* kN	1654 kN

(*) Mean value of two tests

4. CONCLUSION

A design method, based on an extension of the French design guidelines (BAEL) and modified from experimental study, is presented. This method take into account different parameters such as confinement level, steel bars and stirrups ratio, longitudinal reinforcement ratio and concrete core strength,. Based on comparison with experimental results, it can be concluded that the developed approach provides a good estimate of the carrying capacity of RC columns strengthened with composite materials.

5. REFERENCES

- AFGC. (2003) Documents scientifiques et techniques, fascicule « Réparation et renforcement des structures en béton au moyen des matériaux composites ».
- Berthet J.F., Ferrier E., Hamelin P. (2005a). “Compressive behavior of concrete externally confined by composite jackets. Part A: experimental study” *Construction & building materials*, Elsevier ed. Vol. 19, Issue 3, pp. 223-232.
- Berthet J.F., Ferrier E., Hamelin P. (2005b). “Compressive behavior of concrete externally confined by composite jackets. Part B: modeling” *Construction & building materials*, Elsevier ed. On line.
- CSTB-Freyssinet (2001). « Éléments de structure renforcés par un procédé de collage de fibres de carbone », Avis technique 3/04-424.
- Mander J.B., Priestley M.J.N. and Park R. (1988). “Theoretical stress-strain model for confined concrete”. *Journal of structural engineering*, Vol 114, n° 8, pp. 1804-1849.
- Mirmiran A., Shahawy M. and Beitleman T.(2001) “Slenderness limit for hybrid FRP-concrete columns”. *Journal of composites for construction*, vol. 5 N°1, pp. 26-34.
- Quiertant M., Toutlemonde F., Clément J.-L. (2004) “Combined flexure-compression loading for RC columns externally strengthened with longitudinal and transverse CFRP retrofitting” *Proceeding of the fib Symposium 2004 – April 26-28 – Avignon, France*.
- Thériault, M., Claude, S. & Neale, K.W. (2001). “Effect of size and slenderness ratio on the behaviour of FRP-wrapped columns”. *Fibre-reinforced plastics for reinforced concrete structures*, ed by C.J. Burgoyne, London, pp. 765-771.

LARGE-SIZE REINFORCED CONCRETE COLUMNS STRENGTHENED WITH CARBON FRP: EXPERIMENTAL EVALUATION

Silvia Rocca

(Ph D. Candidate in Civil Engineering, University of Missouri - Rolla, Rolla, Missouri, USA)

Nestore Galati

(Research Engineer, University of Missouri - Rolla, Rolla, Missouri, USA)

Antonio Nanni

(Chair & Professor of Civil Engineering, University of Miami – Coral Gables, Coral Gables, Florida, USA)

ABSTRACT

The use of Fiber Reinforced Polymer wrapping technique has been extensively studied; in particular, the behavior of confined elements of circular cross-sections subjected to pure axial loads has been studied. However, the available models are based on small-scale specimens. Limited studies are found for the cases of prismatic members, especially on large-size ones.

To analyze the behavior of axially loaded large-size Reinforced Concrete (RC) columns confined by means of Carbon FRP (CFRP) wrapping, a test matrix was designed to investigate the effect of different variables, such as the geometry of the specimen (circular, square, and rectangular), the area aspect ratio, the side aspect ratio, and a height-to-width aspect ratio. A total of 22 specimens were divided into six series of three specimens each and two series of two specimens. The largest column tested had a cross-sectional area of 0.8 m^2 (9 ft^2) and the smallest one an area of 0.1 m^2 (1 ft^2). The experimental results are compared and contrasted with current available data on reinforced concrete specimens with one minimum dimension of the cross-section of 300 mm (12 in). This evaluation allowed concluding and confirming that among circular and square specimens of the same cross-sectional area, the confinement effect of the FRP is less effective for the latter. It was observed that within specimens of circular and prismatic cross-sections with size-aspect-ratio less or equal than 2.0, the size effect could be negligible.

KEYWORDS

Confinement, Ductility, FRP-Strengthening, Prismatic Columns, Reinforced Concrete.

1. INTRODUCTION

Confinement of Reinforced Concrete (RC) columns by means of Fiber Reinforced Polymer (FRP) jackets is a technique being used with growing frequency to seek the increment of load carrying capacity and/or ductility of such compression members.

The confinement of prismatic columns is generally acknowledged to be less efficient than the confinement of circular columns, since in the latter case, the wrapping provides circumferentially uniform confining pressure to the radial expansion of the compression member. In prismatic columns, the confinement is concentrated at the corners rather than over the entire perimeter.

Extensive work in both the experimental and analytical areas has been conducted on RC columns of circular cross-sections confined with FRP and subjected to pure axial compressive loading. Studies focused on RC columns of non-circular cross-sections have also been conducted; however, such work is limited because the experimental research has primarily been on small specimens of plain concrete due to high cost and lack of high-capacity testing equipment. This situation has been the main reason for overlooking the following important effects on the element performance that are not accounted for in most of the available models: (a) the size of the cross-sectional area, (b) the dimensional aspect ratio of the cross-sectional area, (c) the presence and possible detrimental effect of longitudinal steel reinforcement instability, (d) the concrete dilation dependant on a pseudo-Poisson ratio, and (e) the

contribution of the internal transverse steel reinforcement. In spite of these obstacles, several models have been proposed (Wang and Restrepo 2001, Lam and Teng 2003, Maalej et al. 2003) and have become the basis for design provisions.

2. EXPERIMENTAL PROGRAM

2.1. Test Matrix

The test matrix (Table 1) was designed to investigate the influence of different variables: side aspect ratio (h/b), area aspect ratio (based on an area of 457 x 457 mm [18 x 18 in]), and height-to-side aspect ratio (H/h). The experimental program was divided into two sub-matrices based on the laboratories where the experiments were carried out: CALTRANS Seismic Response Modification Device Testing Laboratory (SRMD) at the University of California San Diego (UCSD) with 18 specimens (six series of three specimens each: A, B, C, D, E, and F), and the Building and Fire Research Laboratory at the National Institute of Standards and Technology (NIST) with four specimens (two series of two specimens each: G and H). Table 1 presents the characteristics of the test units in the following order: specimens acronym, diameter D of the circular columns (Series A), side dimensions of the prismatic columns (b , h), side-aspect-ratio h/b , overall specimens height H , height-to-side-aspect ratio (H/h), gross section area A_g , area-aspect-ratio $A_g/A_{g(C)}$ ($A_{g(C)}$ is the gross area of specimens series C), longitudinal steel reinforcement ratio ρ_l , yield strength of longitudinal steel reinforcement f_y , FRP volumetric ratio ρ_f , and average characteristic concrete compressive strength at the corresponding age of testing of each column f'_c .

Table 1: Test Matrix

Test Unit	D (mm)	b (mm)	h (mm)	$\frac{h}{b}$	H (m)	$\frac{H}{h}$	A_g (cm ²)	$\frac{A_g}{A_{g(C)}}$	ρ_l (%)	f_y (MPa)	ρ_f (%)	f'_c (MPa)
A1	508	NA		NA	1.1	NA	2027	NA	1.53	446	0.00	31.7
A2											0.26	31.9
A3											0.33	31.9
B1	NA	313	635	2.0	1.4	2.2	1984	1	1.56	447	0.00	30.2
B2											1.12	30.4
B3											0.32	30.4
C1	NA	457	457	1.0	1.0	2.2	2090	1	1.48	446	0.00	32.1
C2											0.58	32.3
C3											0.29	32.1
D1	NA	648	648	1.0	1.4	2.1	4195	2	1.48	446	0.00	30.7
D2											0.52	30.9
D3											0.21	30.7
E1	NA	324	324	1.0	0.7	2.1	1049	1	1.53	447	0.00	32.3
E2											0.41	33.0
E3											0.53	33.2
F1	NA	324	324	1.0	1.4	4.2	1049	1	1.53	447	0.00	31.5
F2											0.41	31.5
F3											0.53	31.7
G1	NA	914	914	1.0	2.0	2.2	8361	4	1.50	690	0.00	31.6
G2											0.58	31.6
H1	NA	635	1270	2.0	2.7	2.2	8065	4	1.52	690	0.00	30.3
H2											1.50	30.3

Series A, B, C, D, E, and F consist of three specimens each: one control unit (A1, B1, C1, D1, E1, and F1), one unit strengthened to achieve an increment of 30 percent of load carrying capacity featuring a full wrapping scheme (A2, B2, C2, D2, E2, and F2), and a third unit whose thickness of FRP jacket matched the same number of plies used in the specimen A2 (B3, C3, and D3). Specimens A3, E3, and F3 were partially strengthened to attain 30 percent

increment of carrying capacity as well. Series G and H were composed of two test units each: one control (G1 and H1), and one strengthened to gain the same level of increase in axial capacity (G2 and H2). Regarding the wrapping scheme of all the strengthened specimens, a gap of about 7-13 mm (0.25-0.5 in) was left at the top and bottom ends between the edge itself and the fabric to avoid axial compressive loading of the FRP jacket. The partially wrapped specimens featured strips of 133 mm (5.25 in) wide and a pitch of 76 mm (8.25 in).

All the specimens featured a clear concrete cover of 38 mm (1.5 in), and the prismatic specimens were designed with a corner radius of 30 mm (1.2 in). Further details on the construction and strengthening of the specimens can be found in Rocca et al. (2006).

2.2. Material Properties

All the specimens were designed with a nominal concrete compressive strength of 28 MPa (4,000 psi) and steel Grade 60 (420 MPa). The concrete and steel characteristics strengths (f_y and f'_c) shown in Table 1 were determined according to ASTM C39-04 and ASTM A370, respectively.

Unidirectional Carbon FRP (CFRP) of ply nominal thickness (t_f) of 0.167 mm (0.0066 in) was the wrapping material used for the entire research project. Tensile coupon tests were performed to determine the mechanical properties of the CFRP material used in the evaluation of the test results. For the preliminary design, the mechanical properties provided by the manufacturer were used. This characterization was conducted according to ASTM D3039-00 and yielded an ultimate tensile strain ϵ_{fu} of 0.93 percent, an ultimate tensile strength f_{fu} of 2668 MPa (387 ksi), and a modulus of elasticity E_f of 291 GPa (42,200 ksi).

2.3. Instrumentation and Test Setup

The instrumentation consisted of internal sensors (strain gages) located on both longitudinal and transverse steel reinforcement and external sensors to measure axial deformation (linear potentiometers in UCSD specimens and LVDTs in NIST specimens), fixed to the faces of the columns at about mid-height. Additionally, strain gages were installed on the FRP jacket at critical locations (corner areas and middle distance on each side) along the perimeter of the cross-section on the central region of the strengthened specimens.

The equipment at both UCSD and NIST laboratories is capable of applying an axial compressive force of 53 MN. However, because of the height limitation of the former (1.5 m [5 ft]), the larger specimens (groups G and H) were tested at NIST.

3. TEST RESULTS

The results from this experimental program are presented along with collected relevant available data on RC columns of circular and prismatic cross-sections ($h/b \leq 2$) in terms of trends of the strengthening ratio f'_{cc}/f'_{co} versus the parameter $\rho_f E_f / E_c$ (See Figure 1). f'_{cc} and f'_{co} represent the peak concrete strengths corresponding to the maximum load carried by the RC column for confined and unconfined cases, respectively. In $\rho_f E_f / E_c$, the FRP volumetric ratio ρ_f considers the thickness of the FRP jacket and the geometry of the cross-section, and the relative stiffness of the confining FRP to the axial stiffness of the concrete is represented by the ratio E_f / E_c . Figure 1(a), (b), (c) refer to cases of specimens of circular, square and rectangular cross-sections, respectively. Figure 1(d) presents the linear trends of the types of cross-sections and their reliability indexes obtained by regression analysis corresponding to each dataset. The specimens' acronyms correspond to the following references: CH to Carey and Harries (2003), DN to Demers and Neale (1999), KE to Kestner et al. (1997), MA to Matthys et al. (2005), RO to specimens of the presented study (Rocca et al., 2006), and WR to Wang and Restrepo (2001). Each acronym is followed by a number(s), which in Figure 1(a) indicates the diameter of the cross-section, and in Figure 1(b) and (c) indicate the dimensions of the cross-sections. With respect to Figure 1(a), circular cross-section dataset, note the uniformity of the trend and minor scattering. No pattern reflecting the effect of cross-sectional area size is identified leading to the establishment of the lack of such effect on this type of cross-section. Regarding Figure 1(b), square cross-section dataset, the scatter of data is more pronounced. Concerning the specimens of rectangular cross-sections (Figure 1(c)), no definite observation can be concluded because of the high level of scatter of the data and the limited number of data points. The linear trends of the three datasets presented in Figure 1(d) reflect the level of effectiveness of the FRP confinement in the axial strengthening. The slopes of the trends corresponding to the prismatic specimens are similar, and their strengthening performance is less effective than in the case of specimens of circular cross-sections, which confirms the generally accepted notion of confinement of different cross-section shapes.

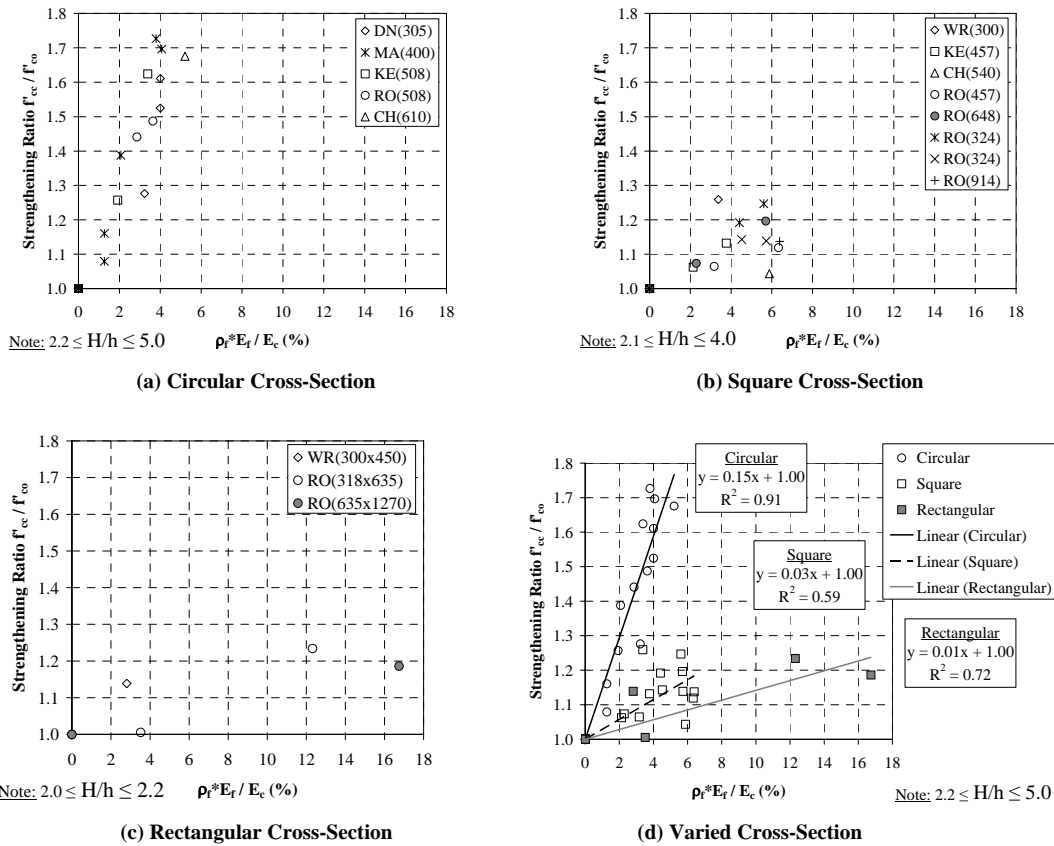


Figure 1: Strengthening Performance of FRP-Confined RC Columns

4. CONCLUSIONS

Based on experimental observations on RC specimens of varied circular cross-section areas it can be concluded the lack of size effect. However, for the case of RC prismatic specimens, the high scattering and limitation of data-points does not allow at the present time to draw a definite concluding remark with respect to the size effect.

5. REFERENCES

Carey, S. and Harries, K. (2003). "The Effects of Shape, 'Gap', and Scale on the Behavior and Modeling of Variably Confined Concrete," Report No. ST03-05, University of South Carolina, Columbia, SC.

Demers, M. and Neale, K. (1999). "Confinement of Reinforced Concrete Columns with Fibre Reinforced Composites Sheets - An Experimental Study," *Canadian Journal of Civil Engineering*, No. 26, pp. 226-241

Kestner, J. T., Harries, K. A., Pessiki, S. P., Sause, R., and Ricles, J. M. (1997). "Rehabilitation of Reinforced Concrete Columns using Fiber Reinforced Polymer Composite Jackets," ATLSS Report No. 97-07, Lehigh University, Bethlehem, PA.

Lam, L., and Teng, J. (2003). "Design-oriented Stress-Strain Model for FRP-confined Concrete in Rectangular Columns," *Journal of Reinforced Plastics and Composites*, Vol. 22, No. 13, pp. 1149-1186.

Maalej, M., Tanwongval, S., and Paramasivam, P. (2003). "Modeling of Rectangular RC Columns Strengthened with FRP," *Cement & Concrete Composites*, Vol. 25, pp. 263-276.

Matthys, S., Toutanji, H., Audenaert, K., and Taerwe, L. (2005). "Axial Load Behavior of Large-Scale Columns Confined with Fiber-Reinforced Polymer Composites," *ACI Structural Journal*, Vol. 102, No. 2, pp. 258-267.

Rocca, S., Galati, N., and Nanni, A. (2006). "Experimental Evaluation of FRP Strengthening of Large-Size Reinforced Concrete Columns," CIES Report No. 06-63, University of Missouri – Rolla, Rolla, MO.

Wang, Y. C., and Restrepo, J. I. (2001). "Investigation of Centrally Loaded Reinforced Concrete Columns Confined with Glass Fiber-Reinforced Polymer Jackets," *ACI Structural Journal*, V. 98, No. 3, pp. 377-385.

PARAMETRIC ANALYSIS OF SHAPE EFFECTS IN CONCRETE COLUMNS CONFINED WITH FRP

Ricardo Carrazedo

(PhD in Structural Engineering, São Carlos School of Engineering / University of São Paulo, São Paulo, SP, Brazil)

João Bento de Hanai

(Professor of Civil Engineering, São Carlos School of Engineering / University of São Paulo, São Carlos, SP, Brazil)

ABSTRACT

This work presents the results of a parametric study on shape effects in concrete columns confined with FRP. The study was developed through numerical simulation with the Finite Element Method (FEM) and experimental analysis. Parametric input files were used to model square columns with different corner radius wrapped by Carbon Fiber Reinforced Polymers. A 3D non-associated plasticity model was used to model concrete behavior. Comparison of numerical x experimental results showed a good correspondence. The results showed that the variable $2r/D$ (where r is the corner radius and D is the column cross section size) can be used as an effectiveness coefficient to reduce the nominal lateral pressure and estimate strength gains.

KEYWORDS

Concrete, confinement, FRP, plasticity.

1. INTRODUCTION

It is well known that the cross section geometry plays a main role in defining the stress x strain behavior of concrete columns confined with FRP. Rochette (1996) showed that the ratio $2r/D$ can be used to evaluate the confinement effectiveness.

Alternatively, FIB (2001) suggested the use of an effectiveness parameter based on the shape of the effectively confined core. The effectively confined core was defined by subtracting the unconfined areas near to the flat sides of the column. These areas were defined by parabolas with initial and final slope of 45 degrees. For a square column with an external dimension (D) and a corner radius (r) this effectiveness coefficient (A_{cc}/A_c) is given by equation 1:

$$\frac{A_{cc}}{A_c} = 1 - \frac{2}{3A_c} \cdot (D - 2r)^2 \quad \text{Equation 1}$$

where A_c is the gross cross-sectional area and A_{cc} is the effectively confined area.

In order to evaluate the performance of the existing equations to predict the strength increase of concrete columns wrapped by CFRP with different cross section geometries, a parametric analysis was developed using the Finite Element Method. This approach was based in the fact that the constitutive model used for concrete showed a very good match to experimental behavior in uniaxial compression and confinement tests. Consequently, in addition to some test results of concrete columns confined by CFRP wraps, in this study several columns were numerically modeled, expanding the range of results for analysis.

2. EXPERIMENTAL ANALYSIS

Nine concrete columns were tested under uniaxial compression loading. Three different geometries were used: a circular cross section column with 150 mm of diameter, a square cross section (150 mm x 150 mm) column with

rounded corners of 30 mm of radius and a square cross section column with rounded corners of 10 mm of radius. All columns had a length of 450 mm. Three columns of each geometry were tested wrapped by 0, 1 and 2 CFRP layers.

The concrete compressive strength determined by testing of 100 mm x 200 mm cylindrical specimens was of 42.5 MPa and the elastic modulus was of 28.5 GPa. The mechanical properties of the composite (CFRP) in the direction of the fibers were tensile strength of 872 MPa and modulus of elasticity of 71 GPa, respectively. These properties were evaluated with a thickness per layer of the composite equal to 0.5 mm.

3. NUMERICAL ANALYSIS

The numerical models were developed using the software ABAQUS release 6.2 and parametric input files which allowed creating a parametric mesh, using some variables whose values were defined in the parametric study. These variables were the cross section sides length h_x and h_y (which assumed constant values of 150 mm in this study) and the corner radius r , as shown in Figure 1.

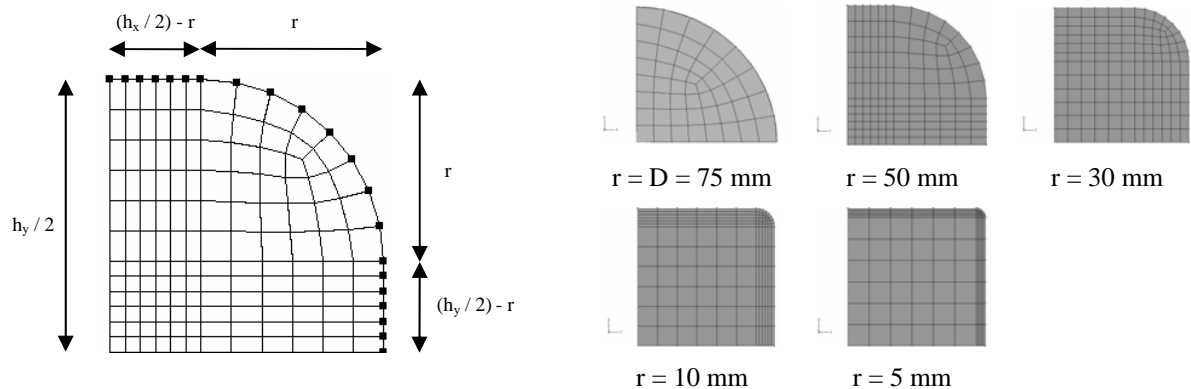


Figure 1: Parametric shape variation

Concrete behavior was modeled using an Umat subroutine based on Grassl *et al.* (2002) model. Some new equations were added to this 3D non-associated plasticity constitutive model, and the complete code of the subroutine was presented in Carrazedo (2005). CFRP was modeled using orthotropic material properties for which the maximum strain criterion was used, with a value of 0.0106 for the ultimate strain in fibers direction.

4. RESULTS AND DISCUSSION

As shown in Figure 1, the numerical and experimental stress x strain curves generated were similar. As expected, the confinement effects were higher as the cross section shape was closer to circular. For $r = 10$ mm the confined specimens showed a descending stress x strain diagram after a small strength increase was obtained. The columns with $r = 30$ mm showed a higher strength increase with an almost horizontal second branch. The circular columns showed a second branch with a positive slope, resulting in high strength and ultimate strain increases.

Both experimental and numerical failures were caused by FRP rupture. However, the numerical response in the stress x strain curve continued further than the experimental one. This occurred mainly due to three factors: the ultimate strains measured during the experiments, through strain gages attached to the perimeter of the square columns, were in some cases smaller than the adopted in the simulations (0.0106); the experiments showed an important concentration of stresses in the limit between the flat sides and the rounded corners, not captured properly by the numerical model; the dilation of concrete in the numerical model during the descending branch was lower than the experimental. However, as can be noticed in Fig. 2, the shapes of the numerical and experimental curves were very similar, indicating that a proper representation of the problem was obtained in the numerical modeling.

In addition to the columns whose results are shown in Figure 2, the numerical parametric study included columns wrapped by four CFRP layers and with different round off radius. The description of columns characteristics and main results are shown in Table 1. Complete axial stress (σ_3) x strain (ϵ_3) curves are shown in Figure 3.

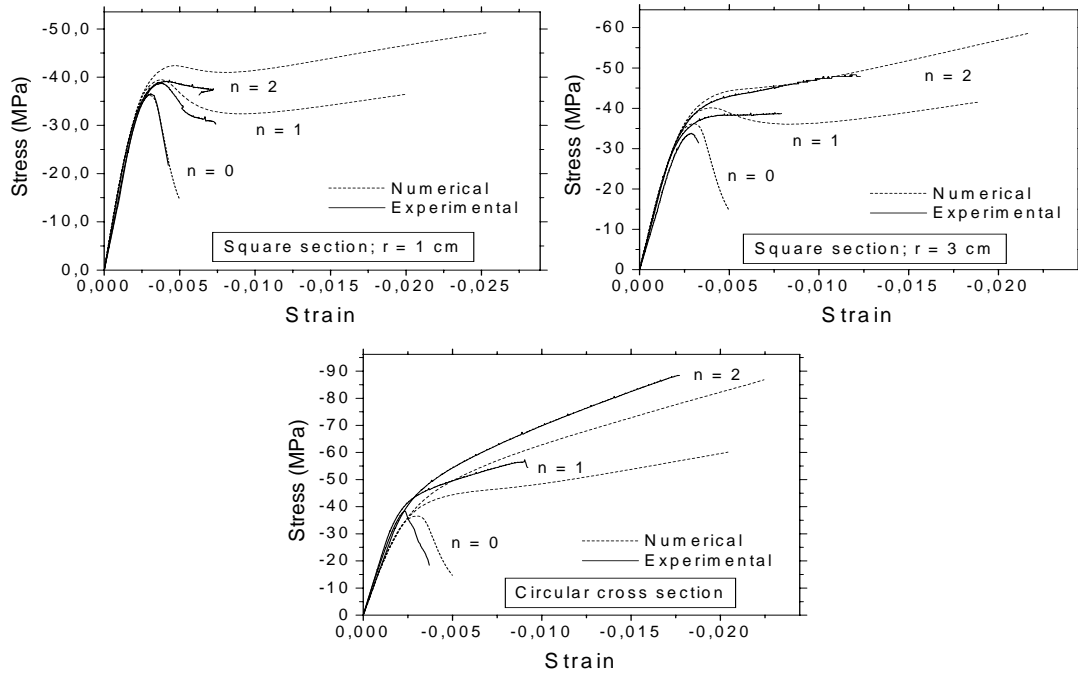


Figure 2: Comparison of experimental x numerical stress x strain diagrams

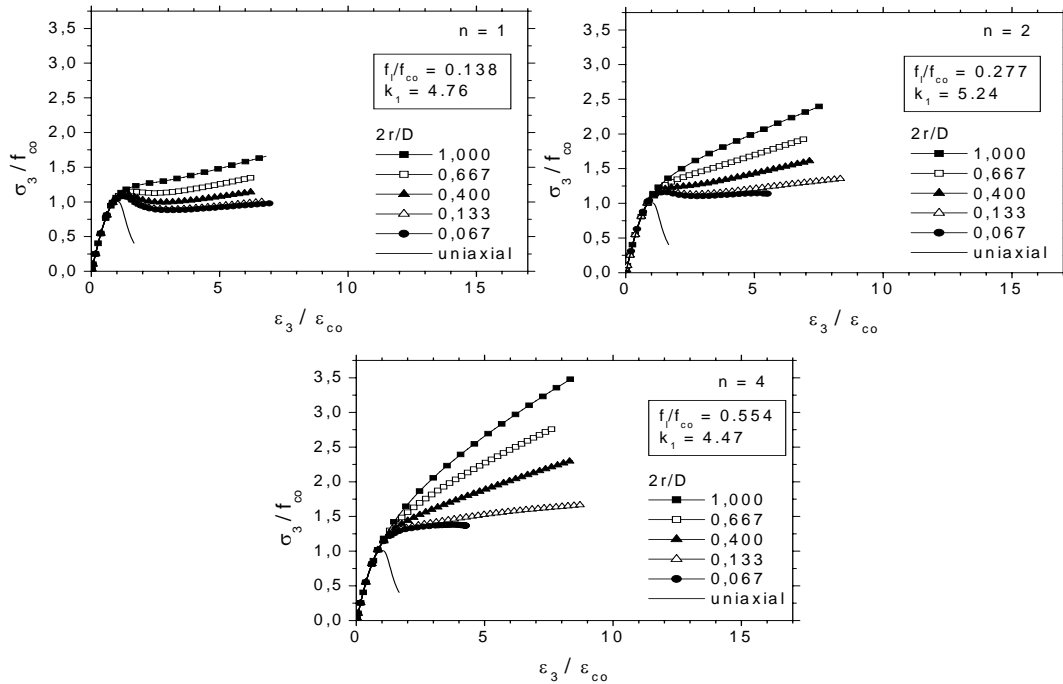


Figure 3: Stress x strain diagrams generated in the numerical parametric study

The shape effectiveness coefficient (k_e) from the tests and numerical simulations was isolated using Equation 2. As for circular columns $k_e=1$ by definition, the coefficient k_1 was determined from the results of these columns. As k_1 is a concrete property also dependent on the variable f_1/f_{co} , one value of k_1 was evaluated for each number of applied CFRP layers. The obtained results are shown in Table 1 and graphically in Figure 4. In Figure 4 it is possible to notice that the variable $2r/D$ has a closer match to k_e than A_{cc}/A_c . Consequently $2r/D$ or a function of this variable can be used to evaluate the effective lateral pressure $f_{le}=k_e \cdot f_1$ in non-circular concrete columns wrapped by CFRP. Finally the increase on the ultimate stress of confined concrete can be estimated as $k_1 \cdot f_{le}$.

$$\frac{f_{cc}}{f_{co}} = 1 + k_1 \cdot k_e \cdot \frac{f_l}{f_{co}}$$

Equation 3

Table 1: Columns characteristics and main results

Numerical						Numerical						Experimental							
Column	n	2r/D	A _{cc} /A _c	k _e	f _{cc} /f _{co}	Column	n	2r/D	A _{cc} /A _c	k _e	f _{cc} /f _{co}	Column	n	2r/D	A _{cc} /A _c	k _e	f _{cc} /f _{co}		
P1	1	0,667	0,918	0,539	1,355	P9	4	0,667	0,918	0,719	2,780	S10r3	1	0,400	0,751	0,321	1,150		
P2	1	0,400	0,751	0,225	1,148	P10	4	0,400	0,751	0,528	2,308	S10r1	1	0,133	0,497	0,132	1,062		
P3	1	0,133	0,497	0,135	1,089	P11	4	0,133	0,497	0,270	1,668	S20r3	2	0,400	0,751	0,333	1,430		
P4	1	0,067	0,419	0,131	1,086	P12	4	0,067	0,419	0,153	1,380	S20r1	2	0,133	0,497	0,057	1,074		
P5	2	0,667	0,918	0,661	1,922	P13	1	1,000	1,000	0,999	1,658	C10	1	1,000	1,000	1,000	1,468		
P6	2	0,400	0,751	0,443	1,618	P14	2	1,000	1,000	1,000	2,395	C20	2	1,000	1,000	1,000	2,290		
P7	2	0,133	0,497	0,256	1,357	P15	4	1,000	1,000	1,000	3,477								
P8	2	0,067	0,419	0,115	1,161														

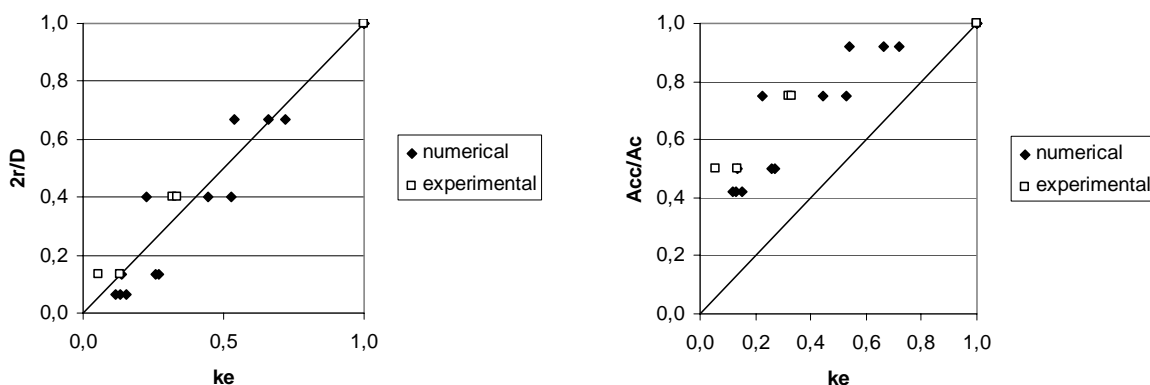


Figure 4: Comparison of $k_e \times 2r/D$ and A_{cc}/A_c

5. CONCLUSIONS

This paper showed the results of numerical and experimental investigations on shape effects in confinement of concrete with CFRP. A parametric study was developed using a 3D non-associated plasticity model through an Umat subroutine, obtaining a good match to experimental results. The numerical and experimental results were used to evaluate the influence of $2r/D$ and A_{cc}/A_c on strength gains of confined concrete, where r is the round off corner radius; D is the side of a square column; A_{cc} is the effectively confined area and A_c is the gross cross section area. The investigation showed that the variable $2r/D$ is more adequate to estimate the shape effectiveness coefficient (k_e) and consequently the effective lateral confinement pressure f_{le} .

6. ACKNOWLEDGEMENTS

The authors express their gratitude to FAPESP (São Paulo State Foundation for Research) for the financial support and scholarship.

7. REFERENCES

- Carrazedo, R. (2005). *Confinement mechanisms in concrete columns wrapped by carbon fiber reinforced polymers subjected to flexural compression*. Ph.D. Thesis – São Carlos School of Eng. / Univ. of São Paulo, São Carlos, 2005.
- Fédération Internationale du Béton (2001). *FIB – Externally bonded FRP reinforcement for RC structures*. Bulletin 14, July, 2001.
- Grassl, P.; Lundgren, K.; Gylltoft, K. (2002). “Concrete in compression: a plasticity theory with a novel hardening law”. *International Journal of Solids and Structures*. v. 39, p. 5205–5223.
- Rochette, P. (1996). *Confinement of short square and rectangular columns with composite materials*, MS Thesis, Univ. of Sherbrooke, Quebec, Canada.

SLENDERNESS EFFECTS ON CIRCULAR FRP-WRAPPED REINFORCED CONCRETE COLUMNS

Jason Fitzwilliam

(M.Sc. Student, Queen's University, Kingston, Ontario, Canada)

Luke Bisby, Ph.D., P.Eng.

(Assistant Professor, Queen's University, Kingston, Ontario, Canada)

ABSTRACT

Externally-applied circumferential FRP wraps have proven to be an efficient and effective technique to repair and strengthen structurally deficient reinforced concrete columns. Guidelines for the design of FRP-wrapped concrete members are currently available and field applications of this technique have been implemented around the world. However, two specific and related issues that require research attention are eccentric loading and slenderness effects on FRP-wrapped concrete columns. To date, the vast majority of tests on FRP-confined concrete have been performed on short, un-reinforced, small-scale concrete cylinders with height-to-diameter ratios of less than 3, and tested under concentric, monotonic axial load. These tests have been useful as a means of accurately characterizing the stress-strain behaviour of FRP-confined concrete such that it is now reasonably well understood. In practice however, most columns are subjected to eccentric loads and have considerably larger height-to-diameter ratios. The potential for increased susceptibility of FRP-wrapped columns to slenderness effects has received relatively little research attention, both for columns that become slender as a consequence of wrapping and increased service loads, and for strengthening of pre-existing slender members. This paper presents the results of an experimental program to investigate the effects of slenderness on FRP-wrapped circular reinforced concrete columns.

KEYWORDS

Fibre reinforced polymers, FRP wraps, reinforced concrete columns, confinement, slenderness, eccentric loads.

1. INTRODUCTION AND BACKGROUND

FRP-wraps for axial strengthening of reinforced concrete columns are an effective and efficient application of FRP materials in Civil Engineering (Bisby et al., 2005). However, most existing design guidelines are applicable only to short columns under concentric axial loads. In reality, concrete columns are often subjected to eccentric loads and may be susceptible to increased instability resulting from their slenderness. Furthermore, FRP-wrapping of short columns has the potential to change the behaviour of from "short", under existing loads, to "slender" under increased (strengthened) loads. To date, relatively few studies have investigated the behaviour of slender FRP-confined concrete members under eccentric axial loading (Fam et al., 2003; Hadi, 2006; Mirmiran et al., 2001; Tao et al., 2004). In reinforced concrete column wrapping applications, FRP wraps are typically applied in the hoop direction and thus provide confining reinforcement only – they cannot be relied upon for additional bending or buckling strength. Furthermore, while several theoretical studies have been performed to develop axial load-moment (M-N) interaction diagrams for FRP-confined concrete columns (Teng et al., 2002), these have not generally been validated through comparison with test data. Since current design recommendations for FRP-wraps are limited to the design of short concentrically loaded columns (ACI, 2002; ISIS, 2001), they cannot be used in cases where slenderness or load eccentricity are concerns, and additional experimental data and analysis are therefore required.

With the above points in mind, the objectives of the research program are: (1) to experimentally evaluate the performance and effectiveness of circumferential FRP-wraps for circular concrete columns of increasing slenderness; (2) to study the effectiveness of longitudinal FRP wraps in reducing the susceptibility FRP-wrapped circular concrete columns to slenderness effects; (3) to develop and validate procedures for the

development of theoretical bending moment-axial load interaction diagrams for circular FRP-wrapped reinforced concrete columns and subsequently conduct parametric studies; and (4) to suggest rational procedures for the design of FRP-wrapped circular columns that account for the effects of slenderness and/or load eccentricities.

2. EXPERIMENTAL PROGRAM

As outlined in Table 1, eighteen small-scale circular reinforced concrete columns of varying slenderness were tested to failure in monotonic, eccentric axial compression. All columns were 152 mm in diameter and were reinforced with four 6.4 mm diameter bars longitudinally and with 6.4 mm diameter circular ties spaced at 100 mm center-to-center in the transverse direction with a cover of 25 mm to the longitudinal reinforcement. Parameters varied among the specimens included the length (i.e., slenderness), number of hoop wraps (i.e., level of confinement), and number of longitudinal wraps (i.e., level of increase in flexural rigidity). The reader should note that kL/r in Table 1 has been calculated based on a transformation of the initial tangent elastic moduli of the component materials. Clearly, at high levels of axial load, the elastic modulus of the concrete is significantly decreased and the effects of the longitudinal FRP wraps on the effective kL/r values are much more significant than implied by the data in Table 1. The SikaWrap® Hex 230C carbon/epoxy FRP strengthening system was used for all wraps and in all cases the longitudinal wraps were installed before the hoop wraps. The FRP system has a manufacturer specified design thickness of 0.381 mm, and ultimate strength and strain of 894 MPa and 1.33 % respectively. The columns were tested using end conditions that were pinned-pinned about one horizontal axis and effectively fixed-fixed about the other. All columns were tested under a constant load eccentricity of 20 mm to simulate inevitable field eccentricities and to promote bending in the desired direction. All columns were instrumented with four Pi-type strain gauges in the axial direction and eight electrical resistance strain gauges in the hoop direction at mid-height. Lateral deflection was monitored using three linear potentiometers.

Table 1: Overview of Experimental Program and Summary of Test Results

Name ^a	kL/r	No. hoop wraps	No. long. wraps	Ult. load (kN)	Ave. axial strain @ ultimate (%)	Peak axial strain @ ultimate (%)	Ave. hoop strain @ ultimate (%)	Peak hoop strain @ ultimate (%)	Lateral defl. @ ultimate (mm)
300U-A	9.74	0	0	471	0.149	0.495	-	-	0.0
300U-B	9.74	0	0	462	0.135	0.480	-	-	0.4
300C-1-0-A	9.74	1	0	675	0.292	1.930	0.660	1.20	1.9
300C-1-0-B	9.74	1	0	679	0.300	1.660	0.810	1.67	1.4
300C-1-2-A	9.51	1	2	681	0.601	2.000	0.464	0.734	0.6
300C-2-0-A ^b	9.74	2	0	671	0.566	1.820	0.476	0.981	0.0
300C-2-0-B	9.74	2	0	911	0.858	3.140	N/A ^c	1.37	N/A ^c
600U-A	17.63	0	0	428	0.217	0.611	-	-	1.4
600C-1-0-A	17.63	1	0	563	0.309	1.210	0.235	0.373	5.3
900U-A	25.53	0	0	398	0.100	0.199	-	-	2.1
900C-1-0-A	25.53	1	0	549	0.198	1.280	0.483	0.939	9.7
1200U-A	33.42	0	0	389	0.113	0.267	-	-	2.7
1200U-B	33.42	0	0	411	0.102	0.315	-	-	6.2
1200C-1-0-A	33.42	1	0	451	0.152	2.420	0.326	0.781	27.4
1200C-1-0-B	33.42	1	0	481	0.125	1.630	0.263	0.627	23.3
1200C-1-2-A	32.65	1	2	584	0.463	2.010	0.413	0.820	20.3
1200C-1-4-A	31.91	1	4	673	0.975	2.540	0.419	0.847	19.1
1200C-2-0-A	33.42	2	0	539	0.175	3.100	0.572	1.51	45.7

^a For example, 1200C-1-4-A is 1200mm long, wrapped with carbon, 1 layer hoop FRP, 4 layers longitudinal FRP

^b Failure of restraining collar caused premature failure of specimen at lower loads than expected

^c Some data unavailable due to malfunctioning of lateral displacement and hoop strain instrumentation

3. EXPERIMENTAL RESULTS AND DISCUSSION

The test data provided in Table 1 show the observed trends in ultimate load capacity, average and peak axial strain, and average and peak hoop strain for all of the columns. As expected, column strength increases with increasing numbers of hoop wraps and with decreasing slenderness. Also as expected, the effects of hoop wraps appear more significant for shorter columns, whereas the effect of longitudinal wraps is more significant for slender columns. In fact, the data indicate that the addition of four longitudinal wraps allowed slender column 1200C-1-4-A to achieve the same strength level as columns 300C-1-0-A and 300C-1-0-B, whereas without the longitudinal wraps the slender columns experienced strength reductions in the order of 31% due to slenderness effects. For columns of the same slenderness, the data of Table 1 also show that the lateral deflection at failure is increased by increasing levels of confinement (which tends to increase the failure strain of the concrete in compression), and decreased by the addition of longitudinal wraps (which tend to increase the columns' flexural rigidity, as expected). In all cases, confinement with FRP hoop wraps drastically increased the columns' deformation capacity.

Figure 1(a) gives applied load versus mid-height deflection plots for all single-wrapped columns, and clearly shows the effects of increasing slenderness on load carrying capacity and lateral deformation of the FRP-wrapped columns. Figure 1(b) also shows the effect of increasing slenderness on the ultimate strength of both wrapped and unwrapped columns (including least-squares regression trends), where it appears that slenderness effects are more significant for FRP-wrapped columns. Of course, this is due to the flexure-dominated behaviour of the slender columns and the fact that circumferential FRP wraps' effects on the strength of confined concrete are more significant than their effects on stiffness. Again, it appears that the addition of longitudinal wraps (increasing flexural rigidity) significantly improves the behaviour of the slender FRP-wrapped columns (but has no significant effect on short columns).

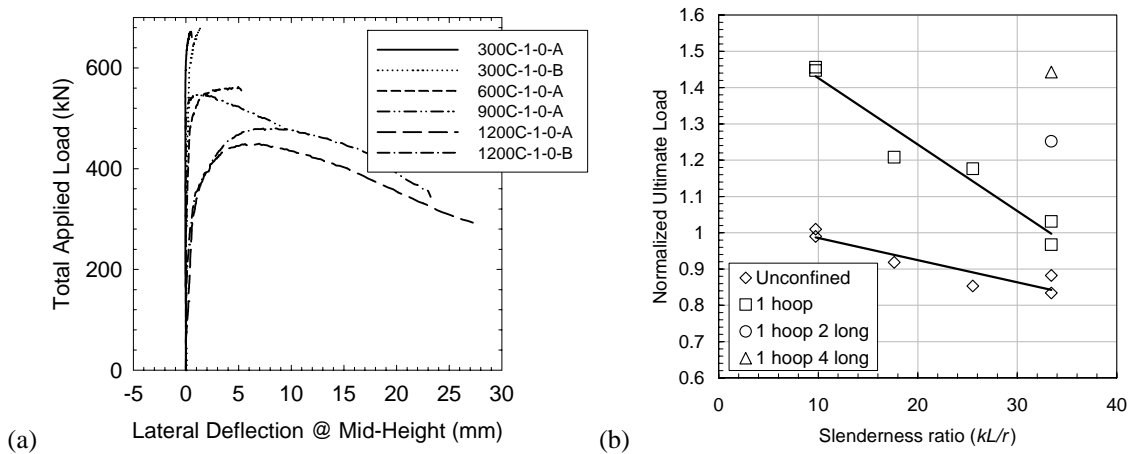


Figure 1: (a) Experimental Load versus Mid-Height Deflection Curves for all Single Wrapped Columns and (b) Effect of Slenderness on Ultimate Load Capacity

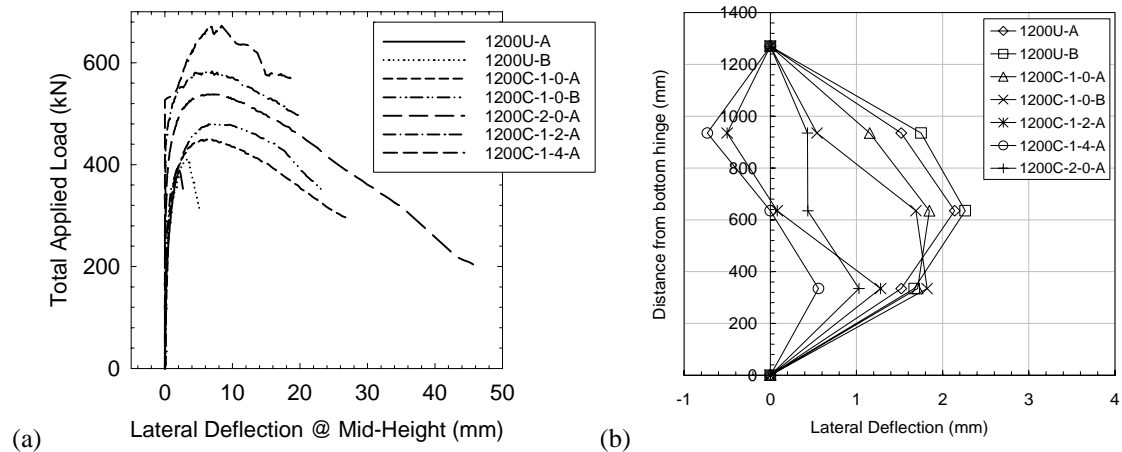


Figure 2: (a) Experimental Load versus Mid-Height Deflection Curves for all 1200mm-Long Columns and (b) Deflected Shapes of all 1200mm-Long Columns at 390kN Applied Load

Figure 2(a) provides a plot of applied load versus mid-height deflection for all 1200 mm long columns with various wrapping schemes. This figure shows the beneficial effects of both increasing levels of confinement and addition of longitudinal FRP wraps on the load carrying capacity and deformation response of slender FRP-wrapped concrete columns. Indeed, adding four longitudinal wraps allows the slender FRP-wrapped column to achieve the same strength as the short wrapped columns. Figure 2(b) shows deflected shapes recorded for all of the 1200 mm long columns at 391 kN (the ultimate load for the unwrapped 1200 mm long columns) and clearly illustrates the stiffening effect of both longitudinal FRP wraps and increasing levels of confinement on slender FRP-wrapped circular concrete members.

5. CONCLUSIONS

This paper has very briefly presented and discussed the results of a series of tests on small-scale FRP-wrapped reinforced concrete columns, conducted to study the effects of both circumferential and longitudinal FRP wraps on the performance of circular reinforced concrete columns of increasing slenderness under a constant eccentric axial load. On the basis of the test observations presented in this paper, the following conclusions can be drawn:

- Circumferential FRP wraps increase strength and deformation capacity of both short and slender circular concrete columns, although the effects on strength are more significant for short columns.
- Column strength increases with increasing numbers of hoop wraps (i.e., increasing levels of confinement) and with decreasing slenderness.
- Adding longitudinal FRP wraps to slender FRP-wrapped circular concrete columns can improve their behaviour and allow them to achieve strengths similar to equivalent short FRP-wrapped columns. The longitudinal FRP wraps had no significant effect on the strength or deformation capacity of short columns.

Research is ongoing in this area to better understand the mechanics of confinement for slender and eccentrically-loaded FRP-wrapped circular concrete columns. Procedures are also being developed for prediction of theoretical axial load-moment interaction diagrams and appropriate slenderness limits for FRP-wrapped columns. It is hoped that experimental data obtained in this study can be used to at least partially validate theoretical and design calculations for these types of members.

6. ACKNOWLEDGEMENTS

The authors are members of the Intelligent Sensing for Innovative Structures Network (ISIS Canada) and wish to acknowledge the support of the Networks of Centres of Excellence Program of the Government of Canada and the Natural Sciences and Engineering Research Council of Canada. We would also like to thank Queen's University and Sika Canada Inc.

7. REFERENCES

- ACI (2002). *ACI 440.2R-02*, American Concrete Institute, Farmington Hills, USA.
- Bisby, L.A., Dent, A.J.S., and Green, M.F. (2005). "Comparison of confinement models for fiber-reinforced-polymer-wrapped concrete". *ACI Structural Journal*, Vol. 102, No. 1, pp. 62-72.
- Fam, A., Flisak, B., and Rizkalla, S. (2003). "Experimental and analytical modeling of concrete-filled fiber-reinforced polymer tubes subjected to combined bending and axial loads". *ACI Structural Journal*, Vol. 100, No. 4, pp. 499-509.
- Hadi, M.N.S. (2006). "Comparative study of eccentrically loaded FRP wrapped columns". *Composite Structures*, Vol. 74, pp. 127-135.
- ISIS (2001). *Design Manual No. 4*, ISIS Canada, Winnipeg, Canada.
- Mirmiran, A., Shahawy, M., and Beitleman, T. (2001). "Slenderness limit for hybrid FRP-concrete columns". *Journal of Composites for Construction*, Vol. 5, No. 1, pp. 26-34.
- Tao, Z., Teng, J.G., Han, L-H., and Lam, L. (2004). "Experimental behaviour of FRP-confined slender RC columns under eccentric loading". *Proceedings of the Second International Conference on Advanced Polymer Composites for Structural Applications in Construction*, Editors: L.C. Hollaway, M.K. Chryssanthopoulos, and S.S.J. Moy, University of Surrey, Guildford, UK, pp. 203-212.
- Teng, J., Chen, J., Smith, S., and Lam, L. (2002). *FRP Strengthened RC Structures*, Wiley, UK.

THEORETICAL MODEL FOR FRP-CONFINED CIRCULAR CONCRETE-FILLED STEEL TUBES UNDER AXIAL COMPRESSION

J. G. Teng

*(Chair Professor of Structural Engineering, Department of Civil and Structural Engineering,
The Hong Kong Polytechnic University, Hong Kong, China)*

Y. M. Hu

*(PhD Student, Department of Civil and Structural Engineering,
The Hong Kong Polytechnic University, Hong Kong, China)*

ABSTRACT

Fibre-reinforced polymer (FRP) jackets have been widely used to confine reinforced concrete (RC) columns for enhancement in both strength and ductility. More recently, the benefit of FRP confinement of concrete-filled steel tubes has been explored by researchers. The main aim of this paper is to present and verify a theoretical model for FRP-confined concrete-filled steel tubes based on a recent analysis-oriented model for FRP-confined concrete. To this end, results of a series of tests on FRP-confined concrete-filled steel tubes are first presented. The theoretical model is next presented and verified using these test results. Both the test and the theoretical results show that FRP jacketing can significantly enhance the ultimate load but may reduce the ductility of concrete-filled FRP columns.

KEYWORDS

Fibre-reinforced polymer (FRP), concrete-filled steel tubes, confinement, theoretical model, tests

1. INTRODUCTION

In concrete-filled steel tubes, the concrete and the steel tube interact in a beneficial manner: the steel tube confines the concrete and the concrete delays the occurrence of local buckling in the steel tube. Concrete-filled steel tubes are thus an economic form of structural members. Although inward buckling deformations are now prevented, degradation in steel confinement, strength and ductility can result from inelastic outward local buckling. Xiao (2004) and Xiao et al. (2005) recently explored the use of FRP jackets for the confinement of the critical regions of concrete-filled steel tubes. Although his work was directed at new construction, the same concept can be employed in the retrofit of columns. In such concrete-filled steel tubular columns, the inward buckling deformation of the steel tube is prevented by the concrete core while the outward buckling deformation is prevented by the FRP jacket. FRP jacketing therefore provides an effective means of suppressing local buckling failures at the column ends. Teng and Hu (2005) confirmed the effectiveness of this technique.

The main aim of this paper is to present and verify a theoretical model for FRP-confined concrete-filled steel tubes based on a recent analysis-oriented model for FRP-confined concrete developed by Teng et al. (2006). To this end, results of a series of tests on FRP-confined concrete-filled steel tubes are first presented. The theoretical model is next presented and verified using these test results. Both the test and the theoretical results show that FRP jacketing can significantly enhance the ultimate load but may reduce the ductility of concrete-filled FRP columns.

2. EXPERIMENTS

2.1 Test Specimens and Procedure

The existing test data of FRP-confined concrete-filled steel tubes is very limited (Xiao 2004; Xiao et al. 2005). Several series of tests have therefore been conducted at The Hong Kong Polytechnic University to supplement the

existing test data, to provide further insight into the experimental behavior, and provide test data for the verification of theoretical models in the future. Only the first series (series I) of tests are presented here. This series consisted of four specimens: I-F0, I-F1, I-F2, and I-F3, where “I” indicates the series they belong to, “F” represents the FRP jacket with the number that follows representing the number of plies of the FRP jacket. The steel tubes all had an outer diameter of 165 mm, a thickness of 2.75 mm (i.e. a D/t ratio of 60), and a length of 450 mm and were filled with concrete with a cube compressive strength of 56 MPa determined from three cube tests. The average values of the elastic modulus, yield stress and ultimate strength of the steel from tensile tests of three coupons taken from the same long tube which provided the four steel tubes in the test specimens were 201.3 GPa, 385.9 MPa, and 486.8 MPa respectively. The average values of the elastic modulus and tensile strength from five coupon tests for the GFRP, calculated on the basis of the nominal ply thickness of 0.17 mm, were 80.1 GPa and 1,825.5 MPa respectively, leading to an ultimate tensile strain of 0.0228.

The compression tests were all conducted using an MTS machine with displacement control at a constant rate of 0.5mm/min until failure. Four bidirectional strain gauges with a gauge length of 20mm were installed evenly at 90° apart at the mid-height to measure the axial and hoop strains of the FRP jacket. The total axial shortening was measured by using three transducers at approximately 120° apart.

2.2 Test Results

Specimen I-F0 (concrete filled steel tube without FRP jacketing) failed by local outward buckling, as has been observed in many tests by other researchers. Specimens I-F1, I-F2 and I-F3 (FRP-confined concrete-filled steel tubes) all failed by the rupture of the FRP jacket due to hoop tension (Figure 1). Once rupture of the FRP jacket occurred, the confinement effect of the FRP jacket disappeared and the load carried by the tube reduced immediately and rapidly. With further loading, local buckling occurred where FRP ruptured. The axial load-axial shortening curves of these four specimens are shown in Figure 2, where the axial shortening was the mean reading of the three transducers located on the loading platens. The curve of the concrete-filled steel tube without FRP confinement features a slowly descending branch after reaching the peak load, while those of the FRP-confined tubes all exhibit a monotonically increasing bilinear shape before the rupture of the FRP at peak load. Following the rupture of the FRP jacket, the load reduced immediately and rapidly and the specimen then was able to follow a ductile path at a lower load level. The results from these tests illustrate two important points: (a) the FRP jacket can effectively enhance the strength of the column but the strain capacity is not always enhanced; (b) if ductility enhancement is the aim, then a suitable gap between the steel tube and the FRP jacket should be provided as has been explored by Xiao et al. (2005).



Figure 1: Failure modes of test specimens

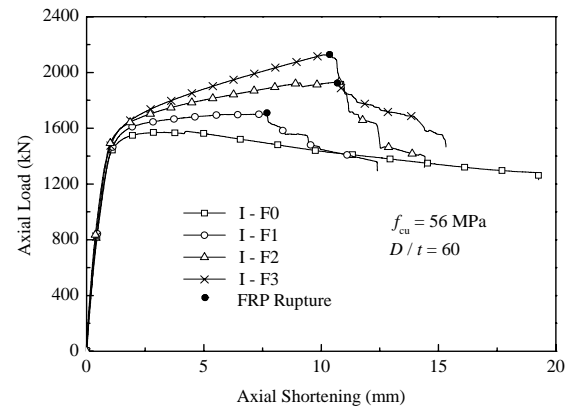


Figure 2: Experimental load-axial shortening curves of all four specimens

3. THEORETICAL MODEL

3.1 General

Teng et al. (2006) proposed a theoretical model for FRP-confined concrete for which the confining pressure is related to the hoop strain in the FRP jacket by the following simple expression:

$$\sigma_l = \frac{2E_{frp}t_{frp}\epsilon_{\theta,frp}}{D} \quad (1)$$

where σ_l is the lateral confining pressure, D is the diameter of the concrete core, and E_{frp} , t_{frp} and $\varepsilon_{\theta, frp}$ are the elastic modulus, thickness and hoop strain (equal to the lateral strain in magnitude) of the FRP jacket. Teng et al. (2006) showed that their model can also be used to concrete confined with any other material, provided an equation equivalent to Eq. 1 to predict the confining pressure-hoop strain relationship can be established for the confining material. Teng et al. (2006) has shown that their model provides close predictions of test results. It is easy to see that if the confining pressure-hoop strain equation (Eq. 1) is modified to reflect the combination of confinement provided by the steel tube and the FRP jacket, this model can be expected to be capable of predicting the behavior of the present tests.

3.2 Evaluation of the Stress-Strain Curve

The evaluation of confining pressure is based on the assumption that the steel tube does not experience any bending or buckling deformations. This assumption is later shown to be reasonable for FRP-confined steel tubes before the rupture failure of the FRP jacket. The total confining pressure is equal to the sum of that from the steel tube and that from the FRP jacket. The confining pressure from the FRP jacket can be easily found using Eq. 1, but the evaluation of the confining pressure from the steel tube is slightly more involved.

Based on the assumption mentioned above, the steel tube is subjected to membrane stresses only. As strain hardening of the steel is generally insignificant before the tensile rupture of the FRP jacket, the stress-strain curves of the steel are assumed to be elastic-perfectly plastic, which approximate the test stress-strain curves closely. The concrete, the steel tube and the FRP jacket are all assumed to be perfectly bonded at the interfaces in the analysis. The effect of permitting separations to occur between the steel tube and the concrete in the initial stage of loading on the predicted axial stress-strain response was investigated and was found to be small, so this assumption is acceptable. The evaluation of the axial stress-axial strain curve of the concrete in an FRP-confined steel tube involves an incremental process.

In each increment, a small increment of hoop strain is specified first, from which the total lateral strain, the hoop stress in the FRP jacket and the confining pressure supplied by the FRP jacket can be calculated. The total axial strain that satisfies the lateral-axial strain equation of Teng et al. (2006) corresponding to the total lateral strain is then determined using the bi-section method, starting with suitable lower and upper bounds. The axial strain increment can then be easily deduced. In this iterative process, the J_2 flow theory of plasticity for a plane stress condition is employed to determine the axial and hoop stress increments for known hoop (lateral) and axial strain increments. A tolerance of 0.1% of the axial strain was used in obtaining the numerical results presented later in this paper. Once this tolerance is satisfied, the hoop strain, the axial strain and the confining pressure are employed in Teng et al.'s (2006) model to generate a point on the stress-strain curve for the concrete in the steel tube and the analysis process moves to the next lateral increment. The evaluation of the stress-strain curve for concrete in FRP-confined steel tubes is therefore an incremental iterative process.

3.3 Comparison with Test Data

In Figure 3, the test axial load-axial strain curves are compared with the predictions of the theoretical model. In these comparisons, the nominal axial strain was obtained from the transducer readings as the average shortening divided by the length of the specimen, and the concrete cylinder compressive strength f'_c was taken as 0.8 times the cube compressive strength f_{cu} . The theoretical axial load resisted by the specimen is a sum of that resisted by the steel tube and that resisted by the confined concrete. It is seen that for specimens I-F2 and I-F3, which had a two-ply FRP jacket and a three-ply FRP jacket respectively, the test results are in close agreement with the theoretical predictions. However, for specimen I-F0 which had no FRP jacket and specimen I-F1 which had a one-ply jacket, the

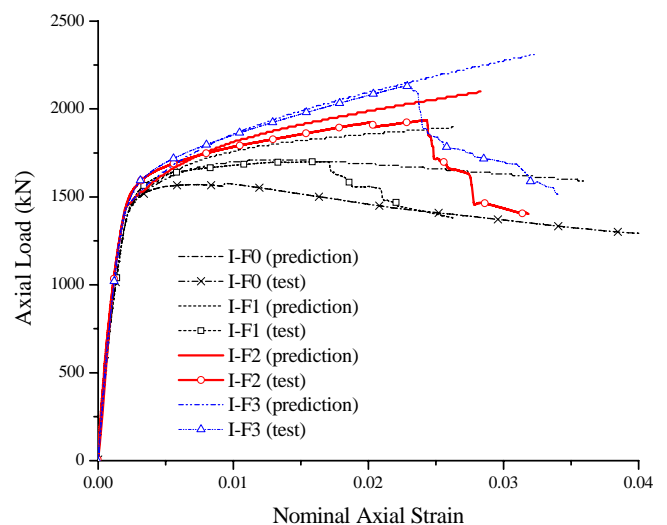


Figure 3: Comparison of load-strain curves between test results and theoretical predictions

theoretical predictions significantly overestimate the resistance of the specimens. These comparisons clearly show that the model is limited by its assumption of no bending or buckling deformations in the steel tube and provides accurate predictions of test results only before significant buckling deformations develop in the steel tube. If a thick steel tube is used so that local buckling does not occur or if a sufficiently strong FRP jacket is employed to suppress buckling deformations in the steel tube, then the theoretical model can be expected to deliver accurate predictions. In specimen I-F0, no FRP jacket was provided and local buckling of the steel tube was obvious during the test. In specimen I-F1, the comparison given in Fig. 3 indicates that the one-ply FRP jacket was insufficient to suppress the local buckling deformations in the steel tube.

As most of the strain gauges had been damaged before the FRP jacket ruptured, in making the theoretical predictions, the hoop rupture strain of the jacket was assumed to be equal to that obtained from flat coupon tensile tests (ie 0.0228). The resulting theoretical stress-strain curves show rupture failures of the FRP jackets at significantly higher axial strain levels than observed in the tests. This observation indicates that the FRP jackets in the tests ruptured at hoop strains lower than the rupture strain from tensile coupon tests. This phenomenon of premature hoop rupture failure has been widely observed in FRP-confined concrete cylinders (Teng and Lam 2004; Lam and Teng 2004). Further research is needed to evaluate the extent of reduction in the ultimate strain of the FRP jacket when used to confine a steel tube.

4. CONCLUSIONS

This paper has been concerned with the modeling of the axial compressive behavior of FRP-confined concrete-filled steel tubes. Results of a series of axial compression tests on FRP-confined circular concrete-filled steel tubes were first presented. A theoretical model for FRP-confined concrete-filled circular steel tubes modified from the recent analysis-oriented model for FRP-confined concrete proposed by Teng et al.'s (2006) was next presented and compared with these test results. It can be concluded that the theoretical model, based on the assumption of no bending/buckling deformations in the steel tube, provides close predictions of test results if the steel tubes does not buckle. This condition is satisfied when the steel tube is sufficiently thick or the FRP jacket is sufficiently strong to suppress local buckling deformations. The comparisons also indicate that FRP jackets confining a concrete-filled circular steel tube rupture at a hoop strain lower than the ultimate tensile strain from flat coupon tensile tests, similar to what has been widely observed in tests on FRP-confined plain concrete cylinders. The success of the proposed theoretical model lends further support to Teng et al.'s (2006) model as an accurate analysis-oriented model for concrete confined by different materials. The proposed model can be deployed to again further insights into the effect of various parameters, such as the inclusion of a gap between the steel tube and the FRP jacket to increase the ductility of the FRP-confined tube (Xiao et al. 2005). The authors will report their research on the effect of such a gap in a future paper.

5. ACKNOWLEDGEMENTS

The authors are grateful to the Research Grants Council of the Hong Kong Special Administrative Region (Project No: PolyU 5269/05E) and The Hong Kong Polytechnic University (Project Code: RGU4) for their financial support.

6. REFERENCES

- Lam, L. and Teng, J.G. (2004). "Ultimate condition of fiber reinforced polymer-confined concrete". *Journal of Composites for Construction*, ASCE, Vol. 8, No. 6, pp. 539-548.
- Teng, J.G. and Lam, L. (2004). "Behavior and modeling of fiber reinforced polymer-confined concrete". *Journal of Structural Engineering*, ASCE, Vol. 130, No. 11, pp. 1713-1723.
- Teng, J.G. and Hu, Y.M. (2005). "Enhancement of seismic resistance of steel tubular columns by FRP jacketing". *Proceedings, 3rd International Conference on Composites in Construction*, 11-13 July, Lyon, France, pp. 307-314.
- Teng J.G., Huang Y. L., Lam L., Ye L.P. (2006). "Theoretical model for fiber reinforced polymer-confined concrete". *Journal of Composites for Construction*, ASCE, accepted for publication.
- Xiao, Y. (2004). "Application of FRP composites in concrete columns". *Advances in Structural Engineering*, Vol. 7, No. 4, pp. 335-341.
- Xiao, Y., He, W.H. and Choi, K.K. (2005). "Confined concrete-filled tubular columns". *Journal of Structural Engineering*, ASCE, Vol. 131, No. 3, pp. 488-497.

Part XVIII. Repair Techniques

METHODOLOGICAL CONSIDERATIONS FOR REINFORCED CONCRETE STRUCTURES REPAIR USING POSTENSIONED CFRP STRIPS.

José Antonio Bellido de Luna del Rosario
(Researcher, Universidad Central de Chile, Santiago de Chile, Chile,)

ABSTRACT

Fiber Bond composites (Carbon Fiber Reinforced Polymer) **CFRP**, are used like an external reinforcing of structural elements. This system is completely studied and has been applied with much success to a great number of structures with problems of resistance and camber

The paper shows a methodologic study conducted to determine the CFRP area and the tension to which it will have to be submitted to resist the additional ultimate state loads to which the analyzed structure will be exposed, or for the deflection decrease and the excessive cracks limiting the demanded minimum level.

KEYWORDS

Reinforced, concrete, carbon, postensioned

1. INTRODUCTION

Fiber Bond composites (Carbon Fiber Reinforced Polymer) **CFRP**, are used like an external reinforcing of structural elements. This system is completely studied and has been applied with much success to a great number of structures with problems of resistance and camber

The paper shows a methodology study conducted to determine the CFRP area and the tension to which it will have to be submitted to resist the additional ultimate state loads to which the analyzed structure will be exposed, or for the deflection decrease and the excessive cracks limiting the demanded minimum level.

2. MINIMAL REINFORCEMENT CRITERIA.

It is important, in case of FRP use, to take into account different considerations of the internal characteristics of materials that could determine certain limits in reinforcement. Reinforcement limits are imposed to protect against structure collapse and also in case of bond failure or other FRP failures due to fire vandalism or other causes. This criterion tries to avoid a surprising collapse of the structure.

If this condition is not fulfilled, FRP reinforcement is not recommendable and other type of reinforcement should be selected.

3. MAXIMUM REINFORCEMENT CRITERIA.

Maximum reinforcement criterion is focused in keeping a ductile behavior of CFRP reinforced element. Limit amount of reinforcement should be taken, the reinforced element would have a ductile behavior at the moment of failure.

4. CONFIGURATION AT ULTIMATE LIMIT STATE.

Figure 1 represents the equilibrium condition for ultimate limit state of a beam at flexure with ordinary and CFRP reinforcement.

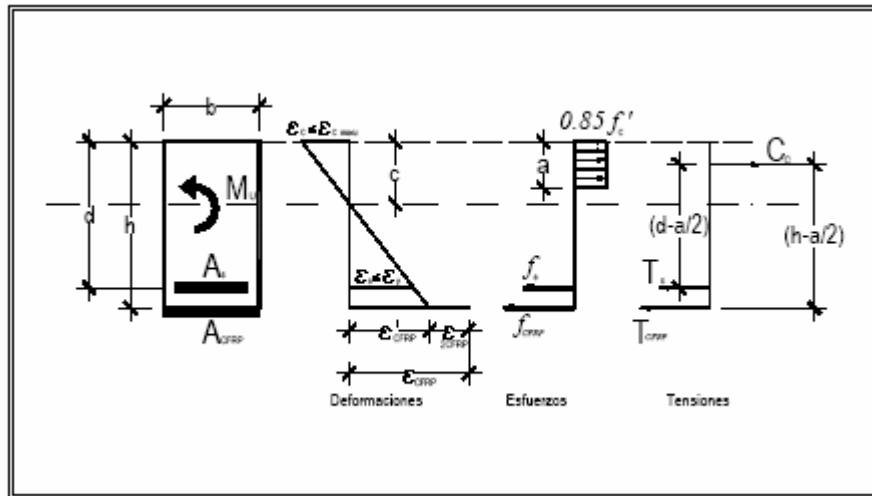


Figure 1 : Force, stress and strain diagram for a rectangular section reinforced with ordinary and CFRP reinforcement.

From equilibrium diagram shown in Fig. 1, the value of the force acting on CFRP is obtained as:

$$T_{CFRP} = 0,85 \cdot f'_c \cdot b \cdot a - T_s \quad (3)$$

From moment equilibrium represented in Fig. 1 is seen:

$$\frac{M_u}{\phi \cdot \psi_{CFRP}} = T_s \cdot \left(d - \frac{a}{2} \right) + T_{CFRP} \cdot \left(h - \frac{a}{2} \right) \quad (4)$$

Where ψ_{CFRP} is a CFRP strength reduction factor depending on the exposition conditions, being $\psi_{CFRP} = 0,85$ for exterior and aggressive environments and $\psi_{CFRP} = 0,95$ for exposition in interior locals.

Values of compressions block “a” and force T_{CFRP} can be obtained combining adequately equations (3) and (4).

5. DETERMINATION OF THE REQUIRED PRESTRESSING FORCE.

Existing section at the time of prestressing is strained and cracked, loads acting on the element at the moment of repair should be determined. What is normal is to have the solely action of permanent load; thus the required prestressing force to nullify tension in the ordinary reinforcement should be determined for the time of rehabilitation.

To achieve the above mentioned condition, it is necessary to determine the initial strain on the steel due to permanent loads at the instant just before putting the reinforcement. With this strain, it is possible to obtain the stress on the steel to be counteracted with the prestressing force, achieving the closure of cracks in the element to be reinforced and that the beginning of flexure development of steel and CFRP from a known point for the steel, $\epsilon_{s0} = 0$.

From the compatibility of deflections, the following equation for ordinary deflection for steel under permanent loads:

$$\varepsilon_{1a} = \frac{[(M_{CP}) \cdot 10^{-5} (d - k_1 d)]}{E_c \cdot I_{cr1}} \quad (5)$$

Where M_{cp} ; is the moment due to permanent loads at the cross section at the time of reinforcement.

I_{cr1} ; is the cracked moment of inertia at the cross section according to Chapter 9 of ACI 318-2002.

k_1 ; coefficient defining the depth of compression block, obtained as:

$$k_1 = \sqrt{(\rho_s \cdot n_s)^2 + 2 \cdot (\rho_s \cdot n_s)} - \rho_s \cdot n_s \quad (6)$$

Being: ρ_s : Ordinary reinforcing ratio.

n_s : Elasticity modulus ratio; $n_s = \frac{E_s}{E_c}$

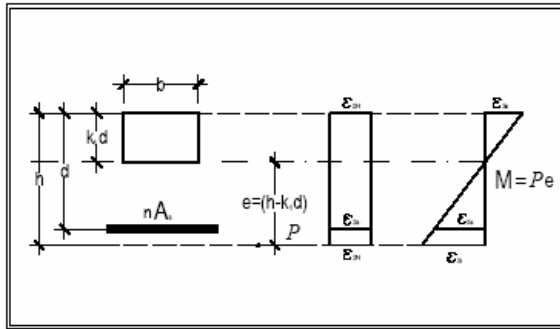


Figure 2 : Strain configuration due to prestressing force.

Strain diagram when the prestressing force acts is shown in Fig. 2, obtaining this force as:

$$P = \frac{\varepsilon_{1a} \cdot E_s}{\left(\frac{1}{A_s}\right) + \frac{[(h - k_1 \cdot d)(d - k_1 \cdot d)]}{I_{cr1}}} \quad (7)$$

When the element is tensioned and the load are acting, there will be generated on the CFRP strip two kinds of deformations: the first one induced by the strip prestressing itself, and the second due to loads action, producing the deflection diagram indicated in Fig. 3, from which the required CFRP area can be obtained with the following analysis:

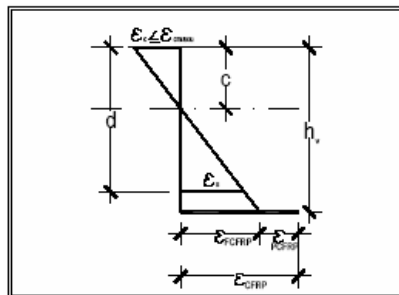


Figure 3 : Tension diagram at ultimate limit state.

$$\varepsilon_{CFRP} = \varepsilon_{fCFRP} + \varepsilon_{pCFRP} \quad (8)$$

Where: ε_{fCFRP} ; is the CFRP strip deflection due to load action, ε_{pCFRP} ; is the CFRP strip deflection due to prestressing action.

The required CFRP strip area can be obtained as:

$$A_{CFRP} = \frac{(T_{CFRP} - P)}{\varepsilon_{fCFRP} \cdot E_{CFRP}} \quad (12)$$

This area should be brought to a discrete amount of strips and then determine the CFRP ratio according to:

$$\rho_{CFRP} = \frac{A_{disCFRP}}{b \cdot d} \quad (13)$$

6. PRESTRESSING FORCE LOSSES.

In CFRP tension there are also some losses, some of them by the same causes as in a normal prestressed element. Each one of these losses should be evaluated to determine the effective prestressing force to provide to the strips, obtained as:

$$P_{efec} = P + \Delta P \quad (14)$$

Being ΔP the value of losses.

7. VERIFICATION OF MAXIMUM CFRP DEFLECTIONS.

After obtaining the effective prestressing force to apply to the CFRP area, it is possible to determine and control the limit of maximum deflection due to prestressing and the ultimate deformation of CFRP strips.

8. CONCLUSIONS.

An important condition at the time of structural reinforcement design with post-tensioned CFRP strips is “existing reinforcement limit”, which conditions the reinforced concrete element to have a minimum bearing capacity for the new loads to which it is going to be submitted.

Though post-tensioned CFRP strips have mechanical properties, regarding stress and strain, quite high in comparison to those of the steel, the previously mentioned “ductility” and “minimum reinforcement criteria”, allows a greater design factor with the application of this new technology. Remember that the study of composite materials and their applications is relatively new; therefore these criteria are valid in this methodology.

The methodology developed here is focused on the application of post-tensioned CFRP strips; however, it could be applicable to any kind of material susceptible of being used as an active external reinforcement. This is due to the fact that this theory is based on basic theories of structural design.

This methodology still requires multiple tests that allow corroborating its theoretical components.

9. REFERENCES

- Aparicio, C. y Ramos, G. (1993) “Estado actual de la técnica del pretensado exterior aplicado a puentes de carretera”, MOPT MA, Madrid.
- Bellido de Luna, J.A. (2002) “Elementos Pre y Post tensados de Hormigón, Bases de Diseño. Control de Obra”. 4 edición, Universidad de Santiago de Chile, Santiago 2002.
- Bellido de Luna, J.A. (1997) “La tecnología del Pretensado Parcial en Elementos de Hormigón”. Calculo y Diseño. Universidad de Santiago de Chile. Santiago.
- Brito, M.(1997) “Caracterização do comportamento dos plásticos reforçados com vista a aplicações estruturais”, LNEC, Departamento de materiais de construção, núcleo de cerâmica e plásticos, Lisboa, Outubro.
- Monteiro, L. y Gomes A. (1996) “Reforço à flexão de vigas de betão armado- modelos de dimensionamiento e verificação de segurança, betão estrutural”, 6º encuentro Nacional de la asociación de preesfrozado Portugues, LNEC Noviembre,.
- Sika Colombia S.A.(2003) “Guía de Diseño e Instalación Platinas Sika CarboDur, Tejidos SikaWrap, Platinas en forma de L Sika CarboShear Platinas Preesforzadas Sika Leoba CarboDur y Sika StressHead”, Bogotá D.C., Colombia, Enero.

Physico-chemical and mechanical behaviors of fiber reinforced repair mortars

Amjad Mallat

(PhD student, MSSMAT Laboratory, Ecole Centrale Paris, Châtenay-Malabry, France)

Abdenour Alliche

(Professor, LM2S Laboratory, Université Pierre et Marie Curie, Paris, France)

ABSTRACT

We have investigated the mechanical behavior of two fiber reinforced repair mortars. A lime-based mortar and a cement-based mortar containing a small quantity of silica fume. Physico-chemical characterization of the materials is carried out by measurements of porosity and shrinkage strains, and by Infra-red spectrometry and X-ray diffraction analysis. The microstructure of the mortars is investigated by microscopic observations. Mechanical characterization is based on compression, three-point bending and tensile tests. For that, we propose a new post-peak tensile testing configuration to study the damaged behavior of the materials. The evolution of the mechanical properties and the influence of the cure conditions of the mortars are also investigated in this study. The bond between the repair mortars and substrate is studied by slant shear and three points bending tests. Results obtained have demonstrated the influence of the surface roughness and moisture conditions on the bond strength. Finally, SEM observations show the morphology of the substrate-to-repair mortar interfacial zone. They allow us to observe and understand the phenomena occurred at the interface, affecting the bond between substrate and repair mortar.

KEYWORDS

Fiber reinforced repair mortars, physico-chemical characterization, mechanical characterization, bond strength.

1. INTRODUCTION

In recent years, repair, refurbishment and maintenance of concrete structures have become a significant part of the total cost of construction worldwide (Mangat and Limbachiya, 1997). Various repair methods and materials are currently used to overcome damage in deteriorated structures. Fiber-reinforced mortar (FRM) is one of materials widely used to repair old concrete. Under current practice, there are no standard procedures for the design of patch repairs. Design is usually based on the experience of specialist contractors and when selection of repair materials is made, emphasis is normally given to their relative short-term properties such as strength, bond and early age plastic shrinkage/expansion etc. Although these properties indicate the immediate performance of the repair, they give little information on its long-term performance. Therefore, there is an important need for recognizing and understanding the properties of repair materials, which are of significance to the subsequent structural behaviors of repaired concrete members. The present study presents an experimental method to investigate the mechanical behavior of two fiber-reinforced repair mortars, both in elastic and damaging regime.

2. MATERIALS AND EXPERIMENTAL TESTS

Two repair mortars (FLM and FOM) reinforced with polyacrylonitrile fibers were used, together with an ordinary mortar (OM), which it was used to provide control specimens for comparison and to replace the substrate for bond tests. FLM is a lime-based mortar containing thickening agent, limestone and additives. FOM is a non-shrinkable cement-based mortar containing silica fume and additives. OM is prepared using CEMII cement. The mix proportions (by weight) were 1:3.68:0.48 (cement:sand:water), to achieve 28 days strength of 25 MPa and of 20 GPa Young's modulus. All samples were cured and stocked at 23°C and 50% RH. Physico-chemical characterization of the materials is carried out by measurements of porosity and shrinkage strains, XRD and FT-IR analysis, and by SEM exams. Mechanical characterization was carried out by compression, tensile and three-point bending tests. The

bond strength is tested by slant-shear and three-point bending tests. For that a range of surface roughnesses with various substrate moisture contents was used. Table 1 summarizes some physical properties of the mortars.

Table 1: Some physical properties of the mortars.

Mortar	Grain size	slump	pH	Porosity	Density	Fiber length	Fiber content
FOM	0 – 2 mm	1-5 cm	12.5	23%	2.08	8 mm	0.2
FLM	0 - 1.25 mm	2 cm	12.5	31%	1.82	4 mm	0.3
OM	0 - 0.8 mm	–	12.5	24%	2	No fiber	No fiber

3. RESULTS

Shrinkage strains measurements show that the repair mortars exhibit greater shrinkage compared with the OM. Although the FOM was designed to be non-shrink, however it displays higher shrinkage than the OM. The highest shrinkage is accorded to the FLM. The shrinkage is fast during the first two weeks then it becomes relatively slow with time. SEM observations of the FOM did not reveal the presence of added silica fume in the hardened paste, which is probably due to a possible pozzolanic effect. The morphology of thickening agent within the FLM was not observed by the SEM. Infra-red spectrometry and X-ray diffraction analyses of the anhydrous and hydrated materials showed that the synthetic fibers and thickening agent would not modify the nature of the cement hydration products even if the thickening agent seems to slow down the kinetic of the reaction. Fig. 1 presents the variation in Young's moduli and compression strengths of the repair mortars according to the age of materials. It is obvious that both Young's modulus and compression strength of the FLM increase almost linearly with time. This evolution may be due to: (1) the reduction of the hydration rate due to the water retention by the thickening agent and, (2) the slow carbonation of the portlandite in the lime-based mortar. FOM modulus increases slightly with time. Its compressive strength increases strongly at early age until 28 days, and hardly evolves beyond this age, what indicates that the mortar has achieved most of its hydration during the first month.

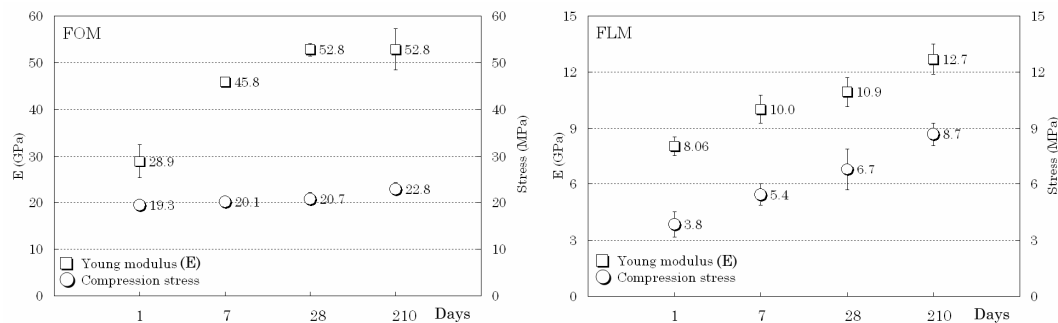


Figure 1: Evolution of compression strengths and Young moduli of the repair mortars.

FLM flexural load increases with time, however the mortar becomes more brittle; at 210 days mortar age, FLM samples fail brutally by three-point bending test. FOM flexural strength increases until 28 days. Then, a decrease of strength has been noted. Three reasons can explain the evolution of the flexural strength of the materials: (1) the porosity, (2) a possible difference in cement hydration, and (3) the percolation of the thickening agent over the FLM samples, which may limit these samples from drying out and, therefore, from surface micro-cracking (Mallat, 2006). The flexural strength is strongly influenced by the cure conditions. FLM strength increases with humid cure (100% HR), contrary to the FLM whose the strength decreases with humidity. Both FOM and FLM flexural strengths decrease when the samples were exposed to UV light which seem to degrade synthetic fibers.

Two testing configurations (Mallat and Alliche, 2006) were used to study tensile behavior (Fig. 3): (1) *Direct tensile test* showing a linear behavior of the mortars until failure which occurs by an unstable way and, (2) *Post-peak tensile test* giving complete tensile response. The highest tensile strength is accorded to the FOM containing silica fume. Also, silica fume has increased the tensile strain capacity of the FOM compared with the OM having similar Young's modulus. FLM shows the highest tensile strain capacity which may be due to the thickening agent and the microstructure. The Young's moduli and tensile strengths of the repair materials increase with time. The FLM Young's modulus evolves very slowly at early age and increases significantly at 210 days.

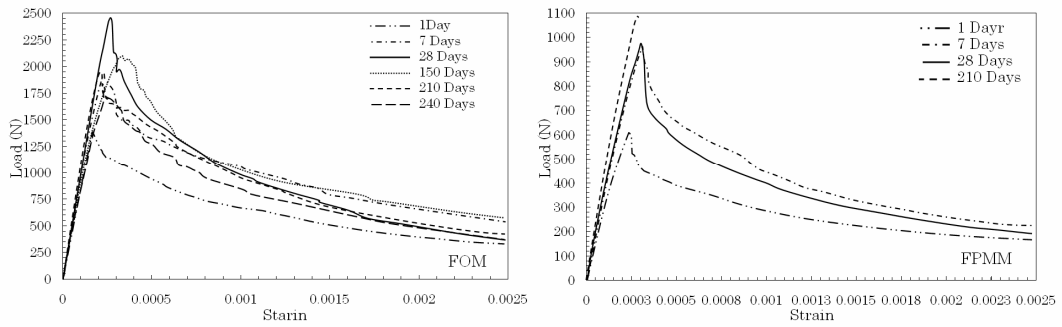


Figure 2: Envelope of load – strain curves in three-point bending test of the repair mortars.

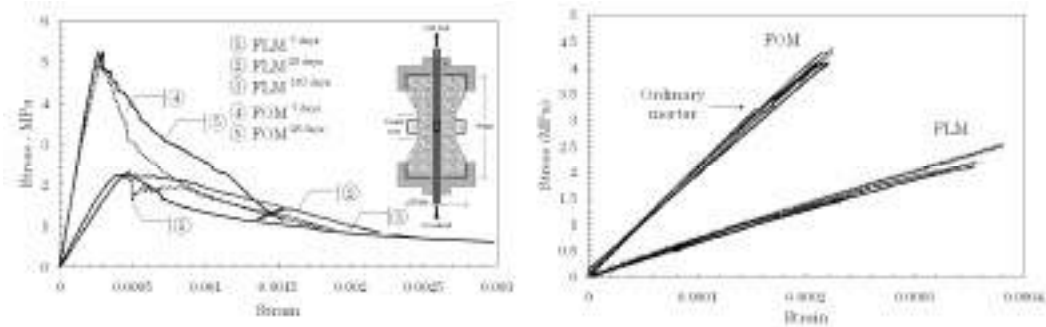


Figure 3: Tensile tests of the repair mortars

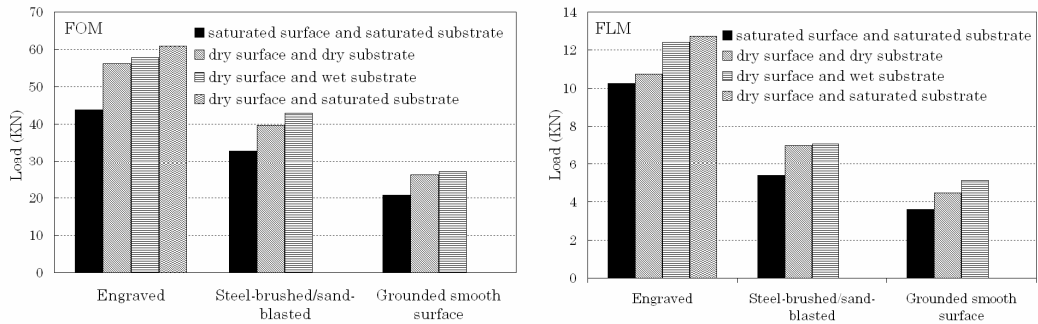


Figure 4: Bond strength vs. surface roughness and moisture content of the substrate by slant-shear tests

FOM shows the highest bond strength, in both slant shear and three points bending tests. Slant shear test results show that wet substrates with dry surfaces gave the highest bond strengths compared with the other moisture conditions. All FOM-to-substrate specimens underwent a monolithic behavior. However, debonding was occurred for all FLM-to-substrate specimens. Three points bending tests show (Fig. 2) that the bond strengths of FOM-to-substrate specimens were between the flexural strengths of the two basic mortars (FOM and substrate). This is not true for FLM-to-substrate specimens, where the bond strengths were lower than the flexural strengths of the basic mortars. All FOM-to-substrate samples have undergone failure in the substrate or in the repair mortar (cohesive failure), contrary to FLM-to-substrate samples where only debonding (adhesive failure) was occurred.

SEM observations of the repair mortars-to-substrate interfacial zones highlight a high micro-cracking in the FLM, probably due to differential shrinkage between the hardened substrate and the freshly laid plastic overlay. Under an applied load, these flaws cause stress concentrations and weakens the interface. Low bond strength of the FLM may also be related to the presence of a film of thickening agent at the interface and the bond depends mainly on glutinous nature of the thickening agent (molecular force). FOM-to-substrate interfacial zone is more compact and uniform. Chemically, the silica fume reacts pozzolanically with portlandite to produce a greater solids volume of

CSH gel, leading to an additional reduction in capillary porosity. Physically, the silica fume particles fill the weak spaces of interfacial and transition zones making them denser and more homogeneous. C-S-H type IV (clear gray crown, Fig. 6) was also observed around the clinker grains in the FLM hardened paste. These hydrates or “inner-products” appear tardily during the hydration, which indicates that the hydration process will continue longer.

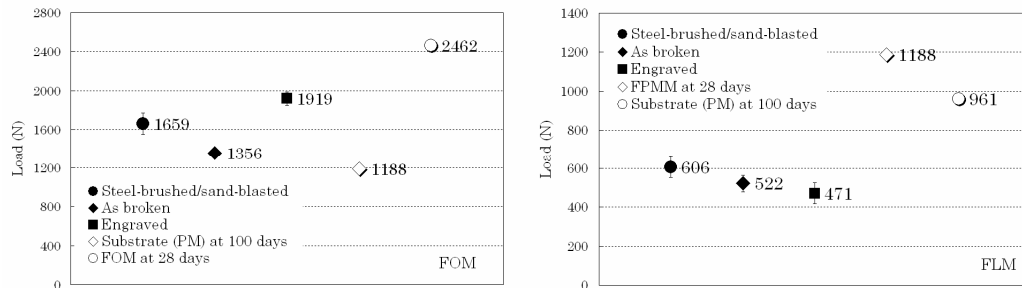


Figure 5: Bond strength according to the surface roughness of the substrate by three points bending tests.

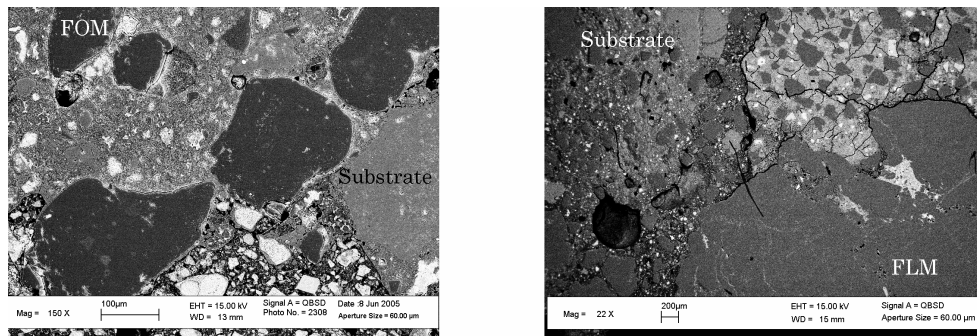


Figure 6: SEM exams of the repair mortars-to-substrate interfacial zone.

4. CONCLUSION

Synthetic fibers and thickening agent would not modify the nature of the cement hydration products. The slow carbonation of portlandite and the thickening agent slow down the evolution of the FLM mechanical properties. FOM flexural strength increases until 28 days and decreases after. FLM flexural strength remains increasing with time. Since the influence of porosity is difficult to verify and a difference in cement hydration cannot explain the evolution of the materials, it is suggested that the percolation of the thickening agent over the sample increases its flexural strength. Tensile tests show that fibers and silica fume enhance the tensile strength and strain capacity of mortars. The tensile strain capacity seems also to be increasing with the thickening agent. Silica fume increases the mechanical properties of the repair mortars-to-substrate interfacial zone and interfacial transition zones, leading thus to a better bond. Cracking due to differential shrinkage between the substrate and the FLM weakens the bond strongly influenced by the moisture content and the surface roughness of the substrate. The bond may also be dependent on the glutinous nature of the thickening agent. Finally, a repair mortar with Young's modulus close to that of the substrate is recommended.

4. REFERENCES

- Mangat, P.S. and Limbachiya, M.C. (1997), “Repair material properties for effective structural application”, *Cement and Concrete Research*, Vol. 27, No. 4, pp 601-617.
- Mallat, A. (2006). “Etude des phénomènes de dégradation des monuments anciens. Techniques et matériaux de réhabilitation”, Ph.D. thesis, Ecole Centrale Paris, Châtenay-Malabry, France.
- Mallat, A. and Alliche, A. (2006). “Mechanical behavior and bond characterization of fiber-reinforced repair mortars”, *Concrete Solutions 2006, Proceedings of the Second International Conference on Concrete Repair*, Editors: M. G. Grantham, GR Technologie Ltd. London, UK, pp. 568-580.

SEVERELY DAMAGED URM WALLS RETROFITTED WITH FRP STRIPS SUBJECTED TO OUT-OF-PLANE LOADING

C. R. Willis

(Postdoctoral Fellow, School of Civil and Environmental Engineering, The University of Adelaide, S.A., Australia)

Q. Yang

(Masters Candidate, School of Civil and Environmental Engineering, The University of Adelaide, S.A., Australia)

R. Seracino

(Senior Lecturer, School of Civil and Environmental Engineering, The University of Adelaide, S.A., Australia)

S. H. Xia

(Lecturer, School of Civil and Environmental Engineering, The University of Adelaide, S.A., Australia)

M. C. Griffith

(Associate Professor, School of Civil and Environmental Engineering, The University of Adelaide, S.A., Australia)

ABSTRACT

Unreinforced masonry (URM) structures comprise a significant proportion of the building stock in many countries worldwide. However, URM walls do not behave well when subjected to out-of-plane loading, such as that experienced under seismic events. Consequently, many existing URM structures require some form of retrofit to comply with existing codes. As part of ongoing research at The University of Adelaide on the behaviour of URM walls subject to out-of-plane loading, three full-scale walls (with window openings) were tested under reversed-cyclic loading. The severely damaged walls were subsequently retrofitted using externally bonded fibre-reinforced polymer (FRP) strips to quantify the increase in strength and ductility relative to the original capacities. This paper presents the results of the wall tests and observations leading to future work. It was observed that the FRP strips may act as boundaries such that failure of the wall is governed by the capacity of sub-panels bound by the strips.

KEYWORDS

Fibre-Reinforced Polymer, Externally Bonded, Masonry Walls, Out-of-plane Loading.

1. INTRODUCTION

Recent catastrophic failures of unreinforced masonry (URM) walls during seismic events worldwide (e.g. Newcastle, Australia in 1989 and Kocaeli, Turkey in 1999) have driven the development of new techniques for strengthening URM structures. Externally bonded (EB) and near surface mounted (NSM) fibre-reinforced polymer (FRP) strips have been successfully used to increase the flexural capacity of reinforced concrete structures (Oehlers and Seracino, 2004). Due to the brittle nature of both masonry and concrete, the debonding mechanisms for retrofitted URM are expected to be similar to those characteristic of retrofitted RC behaviour. As a result, the use of FRP retrofitting techniques has been extended to URM in recent times.

Test results reported in the literature have demonstrated the effectiveness of using FRP to strengthen URM walls by improving the flexural capacity and ductility under out-of-plane loading (Triantafillou, 1998; Velazquez-Dimas and Ehsani, 2000; Albert et al., 2001; Hamoush et al., 2001; Kuzik et al., 2003; Ghobarah and Galal, 2005). The current Australian Masonry Code (Standards Australia, 2001) uses the virtual work method for the design and analysis of URM walls subjected to out-of-plane loading. This design procedure assumes that the initial horizontal crack at wall mid-height would develop at a low level of applied loading such that the vertical bending moment capacity does not

contribute to the ultimate wall capacity. This can lead to overly conservative estimations of strength for walls with high levels of axial loading. However, the consideration that vertical bending is the weak link in the two-way bending of URM walls has provided the impetus for the application of vertical FRP strips to strengthen such walls, which is anticipated to improve the vertical bending capacity and thus the ultimate wall capacity.

2. WALL TESTS

2.1 URM Wall Specimens

As part of ongoing research at The University of Adelaide investigating the out-of-plane behaviour of URM walls, three full-scale walls (with window openings) were tested under two-way reversed-cyclic loading (Griffith and Vaculik, 2005). The walls (height, $H = 2.5$ m and length, $L = 4.0$ m) each had a 1.0 m \times 1.2 m window opening and two 480 mm long return walls. The failure modes for the wall tests are shown in Figure 1. The severely damaged walls were subsequently retrofitted with vertical EB CFRP and GFRP strips (of cross-sectional dimensions 1.2 mm \times 77 mm and 2.0 mm \times 154 mm, respectively) and tested under two-way monotonic static out-of-plane loading to determine the increase in strength and ductility compared to the original capacities. A fourth wall ($H = 2.5$ m \times $L = 2.5$ m) was also tested and strengthened using vertical NSM CFRP strips (of cross-sectional dimensions 1.4 mm \times 20 mm). For completeness, the failure pattern is presented in Figure 1 (iv), however due to space limitations, discussion of this test is beyond the scope of this paper.

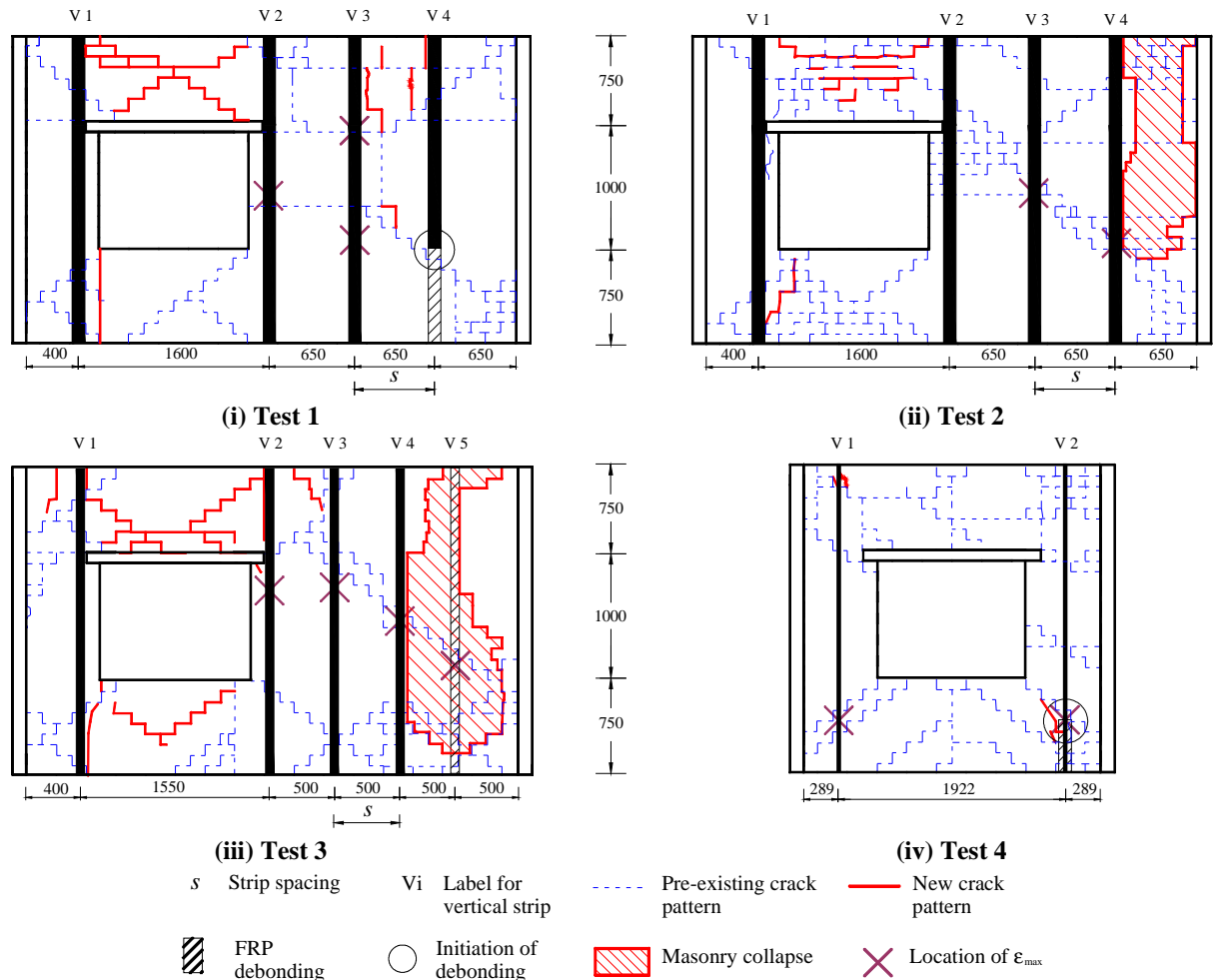


Figure 1: Failure Patterns For Wall Tests

2.2 Material Properties

Tests were conducted to determine the material properties of the masonry. The mean values of the compressive strength, f_{mc} , flexural tensile strength of the masonry, f_{mt} , modulus of elasticity of the masonry, E_m , and lateral modulus of rupture of the brick unit, f_{ut} , were 16 MPa, 0.61 MPa, 3539 MPa and 3.55 MPa with coefficients of variation of 0.14, 0.19, 0.41 and 0.27, respectively. The FRP material properties were provided by the manufacturer (corresponding experimental data is given in brackets). For the CFRP, the modulus of elasticity, E , ultimate strain at failure, ϵ_{ult} , and ultimate stress at failure, f_t , were 165 (162) GPa, 1.4 (1.7)% and 2700 (2799) MPa. For the GFRP plate, the corresponding values were (16) GPa, (1.4)% and (202) MPa. For the adhesive, $E = (6.7)$ GPa and $f_t = (13.9)$ MPa.

2.3 Test Set-up And Instrumentation

All but one of the walls tested were left unrepaired before strengthening. The damaged mortar joints of wall 3 were repaired to compare the initial stiffness of the strengthened wall and the impact of pre-existing cracks. Prior to application of the FRP strips, the wall surfaces were prepared by sanding. The FRP strips were applied vertically to the tension side of each wall as indicated in Figure 1. The walls were simply supported on four sides and out-of-plane loading was applied using air bags. A displacement transducer was placed at the centre of each wall to measure the out-of-plane displacement. Several strain gauges were attached along the FRP strips to provide a strain distribution profile.

For walls 1 to 3, the FRP material type (carbon or glass) and strip spacing, s , were varied while the theoretical value of the maximum tensile force that can be developed in an FRP strip, $F_T = A_{FRP} \cdot E_{FRP} \cdot \epsilon_{db}$, was kept constant (where A_{FRP} is the cross-sectional area of the strip, E_{FRP} is the modulus of elasticity of the strip and ϵ_{db} is the strain at debonding). The value of F_T required for equilibrium was determined by cross-sectional analysis at the position of maximum moment, assuming masonry crushing and FRP debonding, i.e. a balanced section. The intermediate crack (IC) debonding strain of the FRP used in the analysis was based on push-pull tests (Yang et al., 2006). From this, the geometry of the strip was calculated. The values of A_{FRP} , E_{FRP} and ϵ_{db} for the CFRP were 92.4 mm^2 (i.e. $1.2 \text{ mm} \times 77 \text{ mm}$), 160 GPa and $5000 \mu\epsilon$ respectively, while for the GFRP the values were 308 mm^2 (i.e. $2.0 \text{ mm} \times 154 \text{ mm}$), 20 GPa and $12000 \mu\epsilon$. For these combinations of parameters, the corresponding value of F_T was 73.92 kN for both CFRP and GFRP.

3. RESULTS AND CONCLUSIONS

Results of the wall tests are given in Table 1. Two main types of failure occurred, i.e. FRP debonding and masonry collapse. For wall 3, the ultimate displacement, Δ_u , did not occur at the ultimate load, P_u . Figure 2 shows the typical static load-displacement behaviour of the original unreinforced wall (wall 1), the envelope of its cyclic behaviour after damage and the static behaviour of the retrofitted wall. The application of vertical FRP strips allowed the formation of new vertical cracks in the wall segments and as a result, the cracking patterns and failure modes changed compared to the unreinforced walls (Figure 1) leading to increased load-carrying capacity and a more ductile response. For example, comparison of the cyclic envelope and the retrofitted wall behaviour at a level of displacement of approximately 50 mm (Figure 2) indicates that the retrofitted wall has a corresponding lateral load carrying capacity approximately 2.5 times that of the damaged wall.

Table 1: Test Results

Test	H (m)	L (m)	Retrofitting Technique	s (mm)	P_u (kPa)	Δ_u (mm)	ϵ_{max} ($\mu\epsilon$)	Failure Mode
Control A	2.5	4.0	-	-	5.1	25.2	-	-
Wall 1	2.5	4.0	CFRP / EB	650	9.7	72.7	4729	Debonding V4
Wall 2	2.5	4.0	GFRP / EB	650	10.5	143.5	12412	Collapse (No FRP Failure)
Wall 3	2.5	4.0	GFRP / EB	500	12.1	119.4	10117	Debonding V5 + Collapse
Control B	2.5	2.5	-	-	8.7	26.5	-	-
Wall 4	2.5	2.5	CFRP / NSM	-	8.2	101.7	5897	Debonding V2

For the retrofitted wall tests compared to the unreinforced wall response, the results may be summarised as follows:

- Ultimate load, P_u , increased by 90 to 137% (average of 111%); and,
- Ultimate displacement, Δ_u , increased by 188 to 469% (average of 344%).

For the retrofitted wall tests, the following outcomes were observed:

- GFRP is less stiff than CFRP, hence the maximum strain, ϵ_{max} , and thus the ultimate displacement, Δ_u , is greater (i.e. comparison of tests 1 and 2) which increases the level of energy absorption;
- By increasing the number of strips (i.e. comparison of tests 2 and 3) and thus reducing the strip spacing, s , by 23% while keeping the FRP material type constant, the ultimate load, P_u , increased by 15% and as the rigidity of the wall was increased, the ultimate deflection, Δ_u , decreased by 16%;
- As expected, the maximum strain, ϵ_{max} , generally occurred at the locations of cracks; and,
- The values of ϵ_{max} (Table 1) approached ϵ_{db} , but IC debonding did not appear to be the form of debonding observed. As this was the basis for the design of the strengthening scheme further work is required.

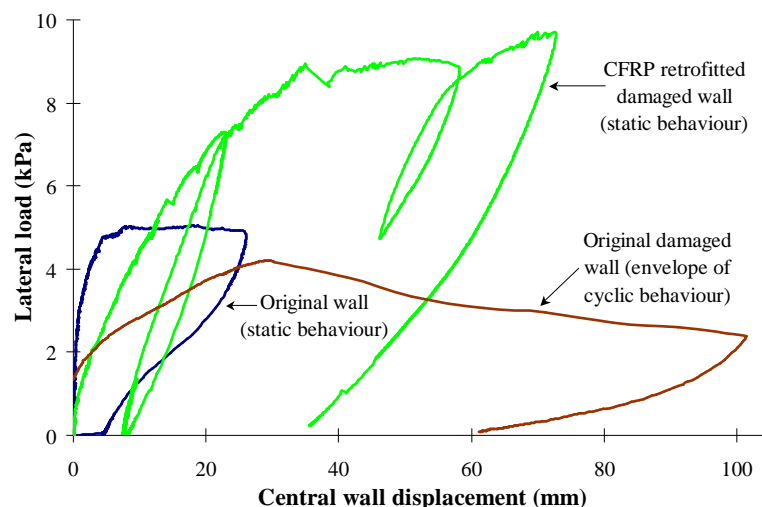


Figure 2: Typical Load-Displacement Behaviour

4. REFERENCES

- Albert, M.L., Elwi, A.E., and Cheng, J.J.R. (2001). "Strengthening of unreinforced masonry walls using FRPs." *Journal of Composites for Construction*, Vol. 5, No. 2, pp. 76-84.
- Ghobarah, A., and Galal, K.E.M. (2004). "Out-of-plane strengthening of unreinforced masonry walls with openings." *Journal of Composites for Construction*, Vol. 8, No. 4, pp. 298-305.
- Griffith, M.C., and Vaculik, J. (2005). "Flexural strength of unreinforced clay brick masonry walls", *Proceedings of the 10th Canadian Masonry Symposium*, Banff, Alberta.
- Hamoush, S.A., McGinley, M.W., Mlakar, P., Scott, D., and Murray, K. (2001). "Out-of-plane strengthening of masonry walls with reinforced composites." *Journal of Composites for Construction*, Vol. 5, No. 3, pp. 139-145.
- Kuzik, M.D., Elwi, A.E., and Cheng, J.J.R. (2003). "Cyclic flexure tests of masonry walls reinforced with glass fiber reinforced polymer sheets." *Journal of Composites for Construction*, Vol. 7, No. 1, pp. 20-30.
- Oehlers, D.J., and Seracino, R. (2004). *Design of FRP and Steel Plated RC Structures: Retrofitting of Beams and Slabs for Strength, Stiffness and Ductility*, Elsevier, Kidlington, Oxford, UK.
- Standards Australia (2001). *AS 3700-2001: Masonry Structures*, Standards Australia, Sydney.
- Triantafillou, T.C. (1998). "Strengthening of masonry structures using epoxy-bonded FRP laminates." *Journal of Composites for Construction*, Vol. 2, No. 2, pp. 96-104.
- Velazquez-Dimas, J.I., and Ehsani, M.R. (2000). "Modeling out-of-plane behavior of URM walls retrofitted with fiber composites." *Journal of Composites for Construction*, Vol. 4, No. 4, pp. 172-181.
- Yang, Q., Willis, C.R., Seracino, R., Xia, S. H., and Griffith, M. C. (2006). "Push-pull tests on FRP retrofitted URM units." *Proceedings of the 19th Annual Conference on the Mechanics of Structures and Materials*, Christchurch, New Zealand (under review).

SUPPORTING CONDITIONS EFFECTS IN THE OUT-OF-PLANE BEHAVIOR OF URM WALLS STRENGTHENED WITH EXTERNALLY BONDED FRP STRIPS

Ehab Hamed

(Ph.D Student, Technion-Israel Institute of Technology, Haifa, Israel)

Oded Rabinovitch

(Senior Lecturer, Technion-Israel Institute of Technology, Haifa, Israel)

ABSTRACT

The effect of the supporting conditions on the overall and the localized out-of-plane behavior of un-reinforced masonry (URM) walls strengthened with externally bonded composite materials is analytically investigated. Four combinations of supporting conditions with different restrictions of the longitudinal elongation and rotation are examined. These cases reflect some of the possible realistic supporting conditions that may exist in practical applications. A theoretical model that is based on variational principles, equilibrium equations, and compatibility requirements between the structural components (masonry, mortar, FRP, adhesive) is used for the investigation. The effect of cracking of the mortar joints and the interaction of the existing wall with the composite strengthening system through the adhesive layer are considered. The results reveal the critical influence of the various supporting conditions on the response of the strengthened wall and shed some light on aspects of the design of the externally bonded strengthening system.

KEYWORDS

Bonding, FRP, Masonry, Strengthening, Supporting conditions.

1. INTRODUCTION

Externally bonded fiber reinforced polymers (FRP) provide an excellent solution for strengthening and upgrading of existing unreinforced masonry (URM) walls. The results of experimental investigations conducted on FRP strengthened URM walls and subjected to out-of-plane loading indicate that the externally bonded strips allow an increase of up to 10-50 times in the strength of the URM wall, enhance its stiffness, and provide the URM wall with the ability to resist bending moments beyond the cracking point (Hamilton and Dolan 2001; Albert et al. 2001). However, while most of the laboratory tests have focused on simply supported masonry walls that are free to rotate and longitudinally elongate at their edges, in practice, masonry walls are usually built within a surrounding rigid frame. The realistic supporting conditions provided by the supporting frame partially or totally restrict the rotations and the longitudinal deformations at the edges of the wall and allow the arching effects to develop (McDowell et al. 1956). These effects significantly increase the stiffness of the wall, give rise to stability issues, and affect the structural role of the strengthening system. Field applications of the strengthening technique indicated that the increase in the strength of the wall due to the externally bonded FRP reinforcement is limited to a factor of about 1.4 (compared to a factor of about 10-50 in simply supported laboratory specimens) (Tumialan et al. 2003; Davidson et al. 2005). A dominant contributor to the large differences between the laboratory and the field results is the influence of the supporting conditions on the structural behavior of the strengthened wall. Another aspect of the strengthening and upgrading task is the uncertainty regarding the condition of the existing structure at hand. In particular, strengthening of masonry walls is conducted under some level of uncertainty with regards to the supporting conditions of the existing wall. In these cases, the assessment of the influence of the range of possible supporting conditions is essential for the design of the strengthening system.

In this paper, the effect of the supporting conditions on the out-of-plane bending behavior of URM walls strengthened with bonded FRP strips is studied. The goals of the paper are to examine the role of the supporting

conditions in the structural response of the strengthened wall and to shed some light on the influence of the uncertainty regarding these conditions on the design of the strengthening system. To achieve this goal, four types of supporting conditions with different restrictions of the longitudinal elongation and the rotation are investigated. The investigation uses the theoretical model developed by Hamed and Rabinovitch 2006. This model is based on a one-way flexural response of the strengthened wall; the first order shear deformations theory for the modeling of the masonry units, the mortar joints, and the FRP strips; and the 2D elasticity theory for the modeling of the adhesive layer. The cracking of the mortar joints and the debonding of the FRP strips near the cracked joint are considered. The four cases are investigated in the numerical study presented next. A summary and conclusions close the paper.

2. NUMERICAL STUDY

Four URM walls strengthened with GFRP strips and subjected to out-of-plane loading are examined. The walls differ only in their supporting conditions. The geometry of the walls, the strengthening system, the material properties, the loads, and the four supporting conditions appear in Fig. 1. It is assumed that the FRP reinforcement is fully bonded through the height of the masonry wall. However, due to the inability of the cracked joints to transfer shear stresses, it is assumed that debonded regions are formed near the cracked joints. The length of the debonded regions is estimated as the height of the mortar joint plus twice the thickness of the adhesive layer (see Fig. 1b). It is also assumed that the debonded interfaces are free of shear stresses. However, in case the debonded interfaces are in contact, they can transfer compressive out-of-plane normal stresses. The supporting conditions (Fig. 1e) include two types of simply supported conditions with and without restriction of the longitudinal elongation (cases II and I respectively), and two types of clamped conditions with and without restriction of the longitudinal elongation (cases IV and III respectively).

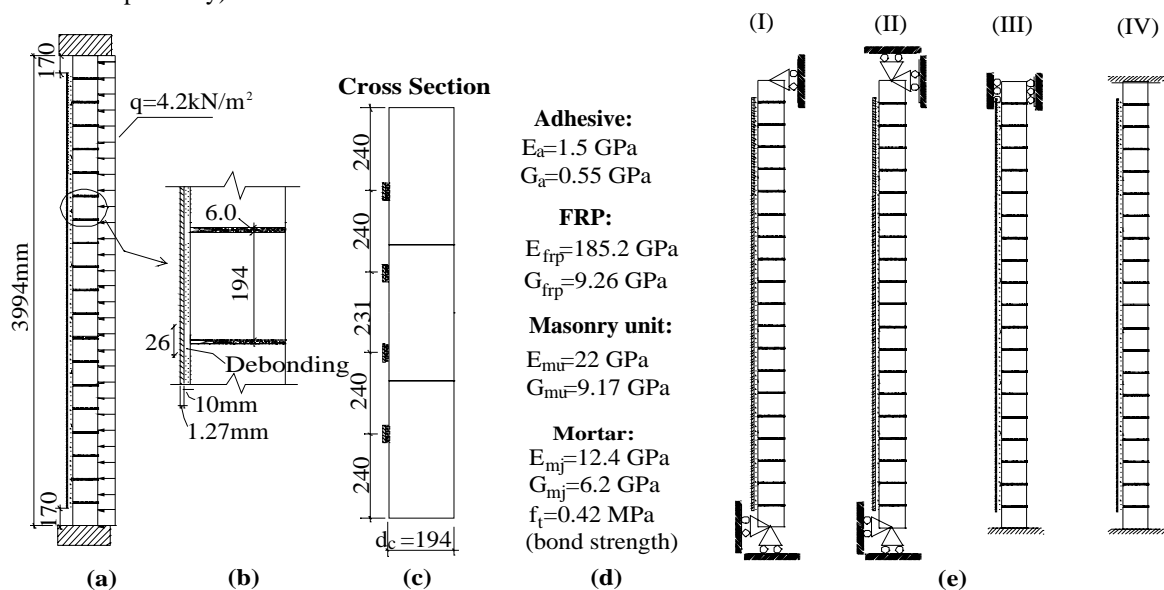


Figure 1: Geometry, material properties, and loads: (a) Geometry and loads; (b) Cracked mortar joint and debonded regions; (c) Cross section; (d) Mechanical properties; (e) Supporting conditions.

The distributions of the out-of-plane deflections, the bending moments, and the axial forces in the masonry walls and the FRP reinforcement under the different supporting conditions appear in Fig. 2. The comparison between the two simply supported cases (I and II) reveals that the restraint of the longitudinal elongation significantly decreases the out-of-plane deflection (Fig. 2a). This is due to the development of compressive "arching" forces that increase the cracking load and provide the wall with the ability to resist bending moment by means of eccentric thrust forces forming an "arching action" (Fig. 2b). The results also show that the variation of the flexural rigidity of the masonry wall between the masonry unit section and the cracked joint section influences the distributions of the bending moments and the axial forces through the height of the wall (see Hamed and Rabinovitch 2006). Note that under supporting condition (I), almost all mortar joints are cracked. On the other hand, under supporting condition (II), only the critical joints at midspan are cracked. Due to the inability of the longitudinally free wall to resist bending moments by means of the arching action, the tensile forces in the FRP and thus the portion of the moment that is

carried by means of a tension-compression couple ("composite action") are much higher under condition (I) than under condition (II) (Fig. 2d). These observations indicate that rupture failure of the FRP reinforcement is more likely to occur in walls with free elongation edges (Hamilton and Dolan 2001). However, due to the magnified compressive axial forces in the longitudinally restrained walls, crushing failure of the masonry may control the behavior of these walls (Tumialan et al. 2003). In slender walls, the thrust forces may also lead to loss of stability and a snap-through type of failure (Carney and Myers 2005). The notable differences between the behavior of the wall under conditions (I) and (II) and the uncertainty regarding the ability of the adjacent components to restrain the longitudinal deformation of the wall imply that the design of the strengthening system has to take into account both supporting conditions.

The comparison between supporting conditions (III) and (IV) further highlights the influences of the arching action and the associated cracking pattern on the behavior of the strengthened wall. Fig. 2e shows that the ratio between the negative moment at the edges and the positive one at midspan is highly affected by the longitudinal supporting conditions. Under conditions (III), the peak negative moment is smaller than the positive one (in absolute value) due to cracking of almost all joints. In the fully constrained wall (conditions (IV)), the ratio equals about 2. This is attributed to the stiffening effect of the arching forces and to the restrained cracking of the joints in conditions (IV) (see Figs. 2b,c). As a result, the negative moment zone is much smaller in conditions (III) than (IV) (Fig. 2c). This observation is critical for the design of the strengthening system and implies that strengthening on both sides of the wall may be needed. Fig. 2d shows that the restriction of the longitudinal elongation yield compressive stresses in the bonded FRP strips. This effect may lead to buckling/wrinkling of the FRP reinforcement and to total debonding failure of the strengthening system (Hamed and Rabinovitch 2006).

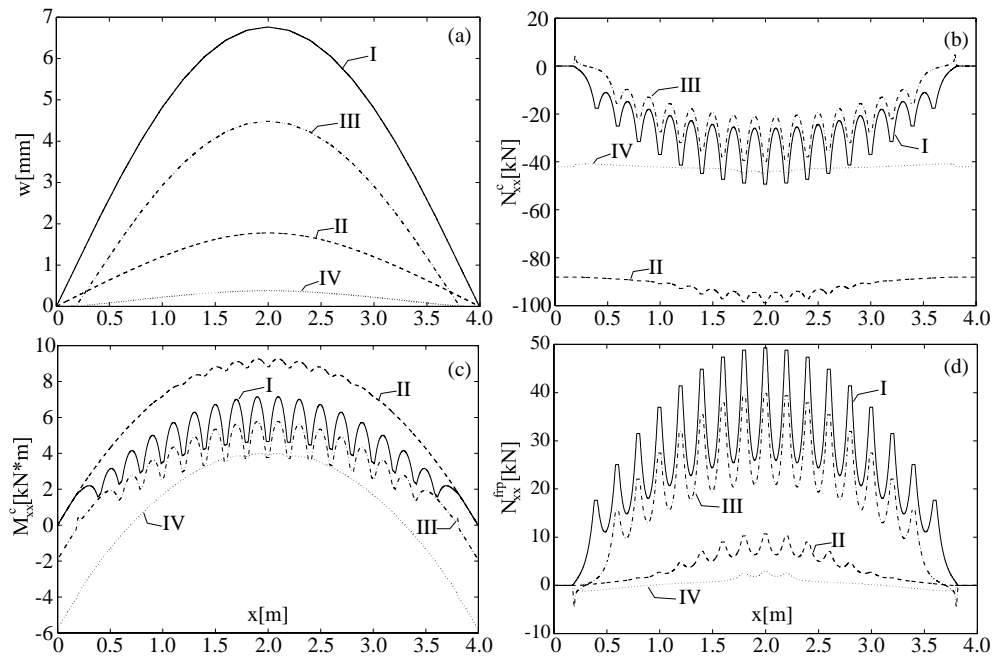


Figure 2: Response of the strengthened wall with different supporting conditions: (a) Out-of-plane deflections; (b) Axial forces in the masonry; (c) Moments in the masonry; (d) Axial forces in the FRP.

The comparison between all four conditions reveals that the restriction of the elongation plays a more critical role than the restriction of the rotations. Note that the deflections observed in the longitudinally constrained simply supported wall (conditions II) are smaller than the ones observed in the longitudinally free clamped wall (conditions III) (Fig. 2a). Also, due to the cracking of almost all joints in the longitudinally free walls (conditions (I), (III)), the behavior of these two walls in terms of the bending moments and axial forces is qualitatively similar and not affected by the restriction of the rotation in case (III) (Figs. 2b-d). These results also imply that the ability to restrict the elongation of the wall may affect the design and the detailing of the FRP strengthening system.

The use of externally bonded strengthening system is usually characterized by local effects in the form of shear and normal out-of-plane (peeling) stresses within the adhesive layer. The distribution of the shear stresses through the height of the wall and the distribution of the peeling stresses near midspan under supporting conditions (I) and (II)

appear in Fig. 3 and reveal the development of the stress concentrations near the cracked mortar joints. Due to the absence of the arching action under supporting conditions (I), the contribution of the strengthening system to the global moment resistance mechanism is much larger than under supporting conditions (II) (see Fig. 2d). As a result, the shear and peeling stresses that develop under supporting condition (I) are much higher than the ones observed under conditions (II). This observation implies that debonding mechanisms of the strengthening system as well as localized diagonal shear cracks at the edges of the masonry units (Albert et al. 2001), which are both governed by the stress concentration near the joints, are more likely to occur in walls that are free to elongate.

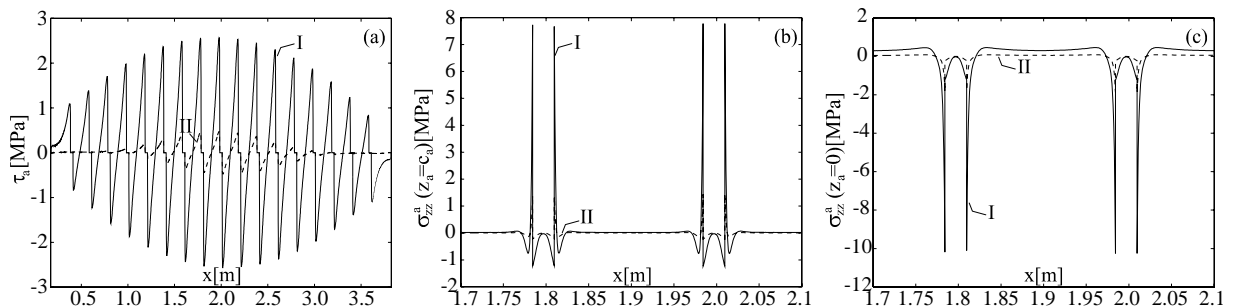


Fig. 3: Stresses in the adhesive under supporting conditions (I) and (II): (a) Shear stresses; (b) Peeling stresses at the adhesive-FRP interface; (c) Peeling stresses at the adhesive-masonry interface.

3. SUMMARY AND CONCLUSIONS

The influence of the supporting conditions on the flexural response of masonry walls strengthened with composite materials has been investigated. It has been shown that the potential restriction of the longitudinal deformation and thus the development of the arching action significantly affect the local and global behavior of the wall. As a result, it plays a major role in the detailing of the strengthening system and in the expected failure mode of the strengthened wall. These observations imply that in cases of uncertainty regarding the actual supporting conditions of the existing wall, the design must account for a response envelope obtained using different supporting conditions rather than be limited to a single characteristic case.

4. ACKNOWLEDGMENT

The financial support for this study by the Ministry of Construction and Housing is gratefully acknowledged.

5. REFERENCES

- Albert, M.L., Elwi, A.E. and Roger Cheng, J.J. (2001). "Strengthening of Unreinforced Masonry Walls using FRPs". *Journal of Composite for Construction*, **5**(2): 76-84.
- Carney, P. and Myers, J.J. (2005). "Out-of-Plane Static and Blast Resistance of Unreinforced Masonry Walls Connections Strengthened with FRP". *7th International Symposium on Fiber Reinforced Polymer (FRP) Reinforcement for Concrete Structures (FRPRCS-7)*, Carol K. Shield, John P. Busel, Stephanie L. Walkup, Doug D. Gremel, pp: 229-248, Kansas, MI.
- Davidson, J.S., Fisher, J.W., Hammons, M.I., Porter, J.R., and Dinan, R.J. (2005). "Failure Mechanisms of Polymer-Reinforced Concrete Masonry Walls Subjected to Blast". *Journal of Structural Engineering*, **131**(8): 1194-1205.
- Hamed, E. and Rabinovitch, O. (2006). "Out-of-Plane Behavior of Unreinforced Masonry Walls Strengthened with FRP Strips ". Accepted for publication in *Composites Science and Technology*
- Hamilton, H.R. and Dolan, C.W. (2001). "Flexural Capacity of Glass FRP Strengthened Concrete Masonry Walls". *Journal of Composites for Construction*, **5**(3): 170-178.
- McDowell, E.L., Mckee, K.E. and Sevin, E. (1956), "Arching Action Theory of Masonry Walls". *Journal of Structural Division*, **82**(ST2): 915-1: 915-18.
- Tumialan, J.G., Galati, N. and Nanni, A. (2003). "Field Assessment of Unreinforced Masonry Walls Strengthened with Fiber Reinforced Polymer Laminates". *Journal of Structural Engineering*, **129**(8): 1047-1056.

TWO DIMENSIONAL EVALUATION OF PATCH REPAIRS OF STRUCTURAL ELEMENTS

Dr. Sameer Hamoush

(Professor, North Carolina A&T State University, Greensboro NC, USA)

Maurice McNeal

(Student, North Carolina A&T State University, Greensboro NC, USA)

Hisham Abdul-Fattah

(Assistant Professor, University of Sharjah, P. O. Box 27272, Sharjah, United Arab Emirates)

ABSTRACT

The recent advances in the field of composite materials make the use of Fiber Reinforced Plastic (FRP) an effective solution to upgrade and retrofit of deficient structural members. Due to the wide range of bonding process of the patch to the structural elements, there is a need to evaluate performance of the patch under load application especially if imperfection occurs during the bonding process. A two dimensional evaluation of both good and defective patch repairs of structural elements was performed in this paper. The analysis is carried out on 0.6-inch wide strips extracted from a full scale panel repaired in accordance with an approved structural engineering standard. The experimental program was extended to evaluate elements with a perfect bond patch and to patch with internal defect between the patch and the parent materials. The considered defects were 1-inch wide flaw between the sixth ply and the parent material. A finite element model was developed to evaluate the stress field within and adjacent to the patch area. Due to the thin nature of the patch, the developed model is based on a geometric nonlinear formulation. Experimental results are being used to validate and guide the analytical approach. Results of the program will be presented to quantify the effectiveness of the patch repair in structural upgrading applications.

KEYWORDS

Scarf, Two-dimensional, Repair, Tensile, Disbond

1. INTRODUCTION

There are numerous studies related to the field of composite materials and their investigation, maintenance, and repair. In 1973, Findik et al., [1] reported that engineers proposed the repair of aircraft structures using composite material patches which would be adhesively bonded over cracks in the metal of the aircraft structures. Analytical and numerical studies of an isotropic cracked plate repaired with bonded composite patches were conducted by Tsamasphyros et al., [2]. An investigation into the tensile failure of sandwich joints was carried out by Qian and Akisanya [3], who established that for a given scarf joint the failure was initiated along the edge of the repair and was regulated by the free edge fracture toughness. One of the typical failure modes of composite plates is the interlayer crack and delamination which are investigated by Luo and Hanagud [4]. Schipperen and Lingen [5] investigated free edge delamination through two-dimensional calculations. Odi and Friend [6] improved upon the two-dimensional model for composite joints. Found and Friend [7] evaluated two wet lay-up and one prepreg repair systems. Their investigation was focused on the improvement of repairs which would take place on the structure and the problems associated with in situ repairs. Ahn and Springer [8] also showed that the prepreg load at failure was higher than that of wet lay-up repairs in both scarf repairs and stepped lap repairs. Baker et al., [9] demonstrated that scarf repairs can be used to mend highly strained graphite/epoxy structures by repairing the stabilator of an F/A-18

Hornet fighter aircraft. Oztelcan et al., [10] also demonstrated the effectiveness of scarf repair by designing test coupons for the scarf repair of composite helicopter blades. Hamoush, et al., [11] experimented with the evaluation of scarf repair of solid ((-60/60/0)s) composites.

2. MATERIALS SELECTION AND SPECIMEN FABRICATION

The material used to construct the panels consists of carbon fibers which are pre-impregnated (prepreg) with epoxy resin. The Hexcell AS4/3501-6 prepreg is composed of continuous AS4C carbon (graphite) fibers and an amine-cured epoxy resin system. The orientation in which the pieces of prepreg are cut must match the desired fiber orientation (-60/60/0/0/60/-60) of the stacked panels.

After curing and trimming the panel the defect area is made using a drill press with a 1" hole cutting saw. A 7" slot was removed along the bottom two thirds of the panel. This circular drilling is a rough cut which will obviously not leave the investigator with a straight edge. The edges of the slot are smoothed by hand by filing the extruding corners away carefully until the edge of the 1" boundaries is reached. The ends of the slot are also filed in order to produce a rectangular (1x 7 inch) slot. Each side of this slot will be scarfed to reveal 0.5" of each successive layer. A 22,500 revolution per minute (RPM) Chicago Pneumatic die grinder (CP875) is the scarfing tool used for this process. The first scarfing or sanding disk used is a 1" Powerlock 80 grit sanding disk. This disk is used at an angle along the cut edge of the slot to carefully expose all six layers. After all layers have been exposed they are scarfed away from the opening to expose 0.5" of each layer. After the initial exposure with the 80 grit disk, the disk is changed to a finer 120 grit 1" disk to continue the operation. The bottom -60° ply will be exposed 0.5" from the edge of the slot. This layer is very thin and a very fine 240 grit 1" disk is used to remove the fifth ply material from this bottommost ply. The lines previously marked along the perpendicular tape are extended by pencil over the scarf area to ensure that the proper 0.5" area of each ply is removed. After the scarf was completed the sample was cleaned and oven dried for the patching process. The patch material is AS4/3501-6 in the same prepreg form as the scarfed laminate. The patch layers must match the fiber orientations of the layer that it is adhered to. The first layer of the patch is the Spec BMS 5-154C structural adhesive film which was manufactured by Critical Materials Incorporated. A 1" 90° filler ply follow the adhesive film and the remaining six layers of prepreg are laid to cover the 0.5" exposed ply and the fiber angles. The panel is debulked after application of each layer of the patch. Once the patch has been cured, the panel is ready to be cut into fifteen, 0.6" wide strips which serve as the specimens used for testing.

3. TESTING

The specimens will be subjected to axial tensile loading using an Instron testing machine. The test is performed under displacement control of 0.5in/min. The strain values are recorded from the five pristine strips through the use of an Instron extensometer. This device is designed to be spring attached to a specimen that is to undergo testing. The extensometer calculates how long the material has stretched relative to its original position of 1" between the leads. The values for strain and load are imputed into a data recovery computer system. The extensometer system was sufficient for the pristine strips which were expected to experience a constant strain throughout the length. According to the raw data collected however, there is evidence that the leads on these strain gages may have begun to slip as the material reached closer the ultimate failure load.

The repaired strips would have to have strain gages attached to the specimen in order to monitor strains along their axis since the strains for this repaired system are not the same throughout the length. For the good repair strips, strain gages were adhered to the specimen over the same area which has a through width delamination in the defective repair strips to enable the comparison of the strain values. A total of two strain gages were used for each good repair strip; one in the center on the top side of the patch which would be numbered as gage 1 for data collection and one over the area which corresponds to the area which would have the defect in the defective repair.

In order to perform stress calculations from the strain data collected, the areas of the samples were taken by measuring the width and thickness of the strips in four areas. The patch area or the middle of the strips, each end, and the mid distance between the center of the strip and the end of the strips were measured and recorded. The defective repair strips used a minimum of three strain gages to record the strain values along the length of the sample. One gage was placed in the center of the top surface of the patch area and two others were placed along the rear of the engineered defect area. For one strip of the defective repair samples, an additional strain gage was placed in the pristine area of the sample in order to make a comparison with the pristine strips. The load values at failure were recorded and the broken strips were inspected to search for similarities in the failure modes. The pristine strips

failed explosively with much of the material destroyed during the failure stage. Both types of repair strips failed similarly with the defective repair strips failing at both through width delamination areas leaving much of the center of the patch intact. The good repair strips failed at varying locations within the patch area with greater size of broken pieces than the good repair.

The load values recorded were in accordance with expected failure levels as calculated from the testing data for the previous test [11] of whole panels and dividing the failure loads recorded there by the cross sectional area of the 0.6" strips. Examination of the results shows that the pristine strips carried loads closest to the 2000lb. expected failure load. The highest ultimate load recorded of 2231lb. belonged to pristine strip 4 which also had the largest cross sectional area of the pristine strips. The width of the pristine strip which had the lowest ultimate load of 1802lb. was also the smallest width of the fifteen tested strips.

The two scarf repaired samples indicate that the repair was a successful process due to the capability of the repairs to carry over 95% of the pristine failure load. This ability to carry loading is promising to the repair industry. These static loading conditions may not accurately represent service loading conditions and fatigue loading or hot/wet loading conditions may be needed to better evaluate the performance of the repair. The engineered defect's impact upon the static tension load characteristics of the repairs was minimal due to the location and orientation of the plies in which it was inserted. The break in the top -60° ply caused a stress concentration in the plies below it since the same load was supported by a smaller cross section. The 0° fiber orientation plies carry the greatest tensile force due to the increased stiffness of these two layers. The loss of one -60° ply from the delamination caused a slight drop in the ultimate load, but the amount of load which would typically be carried by this layer is smaller than the load carried by the center plies and could be more easily distributed to the other layers. These scarf repairs with imbedded defects were still able to carry an average load of 1998lb. which is still over 95% of the average failure load of the pristine samples. The failure load was reduced in the scarf repair specimens and further reduced for the engineered defect repairs.

4. NUMERICAL EVALUATION

The repaired panel was modeled by 8 node elements (see Figure 1). Because of symmetry, one half of the panel with the appropriate boundary conditions was modeled. All layers of the patch and parent panels and the adhesive layer were modeled as 2-D elements with their respective material properties. A commercial FE software ANSYS was used to perform the analysis. Due to the geometric nature of the panel, the geometric nonlinearity was used in the analysis. The model considers each ply separately with the appropriate fiber orientations. The material properties used is listed in Table 1. A reduction of 5 percent was implemented for the patch properties for both the strength and stiffness to account for the difference in fabrication process between the parent materials and the patch. The parent material was fabricated by autoclave while the patch was added with the assistance of the vacuum bag.

Systematic convergence study was made to confirm the convergence of the mesh and results. Analysis was conducted by incrementing the displacements till the overall panel strain in the x-direction reaches one percent. The complete displacements, strains, and stresses in the model at various load levels were analyzed. The peel and shear stresses in the resin layer are shown in Figures 2 and 3.

Table 1: The Used Materials Properties.

AS4/3501-6

$E_{11} = 142$ GPa, $E_{22} = E_{33} = 8.27$ GPa, $G_{12} = G_{13} = 4.82$ GPa, $G_{23} = 2.27$ GPa, Poisson's Ratio in the direction 1-2 = $\nu_{12} = 0.33$, and Poisson's Ratio in the direction 2-3 = $\nu_{23} = 0.33$

Adhesive Properties $E_{xx} = 4.24$ GPa and $\nu_{xy} = 0.3650$

5. CONCLUSIONS AND RECOMMENDATIONS

The objectives of the present paper are to evaluate the response of the patch repair to tension static loading conditions and to investigate the performance of defectively repaired panels under unidirectional tensile load. Based on the test performed in this study, the following can be concluded:

1. It appears that stress concentration is experienced at the connection of the patch and the parent materials.
2. Scarf repairs are an effective retrofitting technique of defected members. It restores 85 to 95 percent original strength.

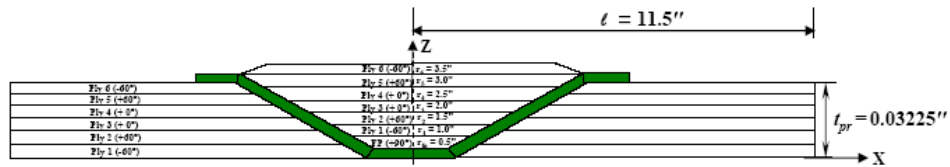


Figure 1: Finite Element Model

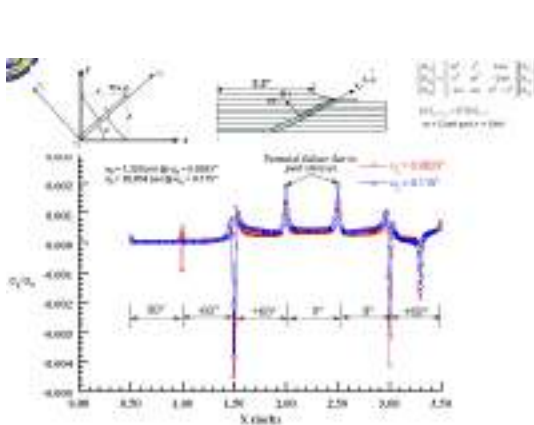


Figure 2: The Peel Stress at Resin Line

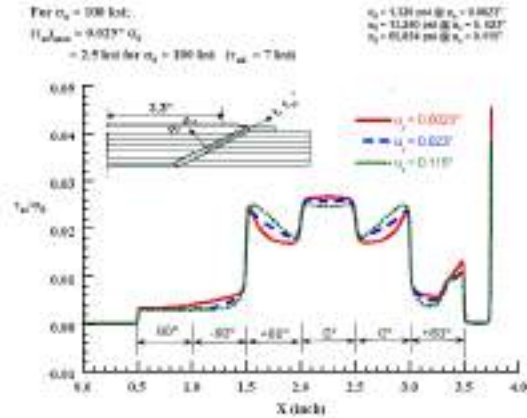


Figure 3: The Shear Stress at Resin Line

Acknowledgements

The work in this research is supported by FAA through the Air awareness center of excellence Iowa State university grant number 4-48453.

4 REFERENCES

- Findik F., Mrad N., Johnson A., "Strain Monitoring in Composite Patched Structures", The Journal of Composite Structures, Vol. 49, 2000.
- Tsamasphyros G. J., Kanderakas G. N., Karalekas D., Rapti D., Gdoutos E. E., D. Zacharopoulos, and Z. P. Marioli-Riga, "Study of Composite Patch Repair by Analytical and Numerical Methods", Fatigue Fracture Engineering Material Structures, Vol. 24, 2001.
- Qain Z. and Akisanya A. R., "An Experimental Investigation of Failure Initiation in Bonded Joints", Acta Materials, Vol. 46, 1998.
- Luo H., and Hanagud S., "Delamination Modes in Composite Plates", Journal of Aerospace Engineering, Vol. 9, 1997.
- Schipperen J. H. A. and Lingen F. J., "Validation of Two-dimensional Calculations of Free Edge Delamination in Laminated Composites", The Journal of Composite Structures, Vol. 45, 1999.
- Odi R. A. and Friend C. M., "An Improved 2D Model for Bonded Composite Joints", International Journal of Adhesion and Adhesives, Vol. 24, 2004.
- Found M. S. and Friend M. J., "Evaluation of CFRP Panels with Scarf Repair Patches", Journal of Composite Structures, Vol. 32, 1995.
- Sung-Hoon A. and Springer G., "Repair of Composite Laminates-I: Test Results", Stanford University Department of Aeronautics and Astronautics.
- Baker A. A., Chester R. J., Hugo G. R., and Radtke T. C., "Scarf Repairs to Highly Strained Graphite/epoxy Structure", International Journal of Adhesion and Adhesives, Vol. 19, 1999.
- Oztelcan C., Ochoa O. O., Martin J., and K. Sem, "Design and Analysis of Test Coupons for Composite Blade Repairs", Journal of Composite Structures, Vol. 37, 1997.
- Hamoush S., Shivakumar K., Darwish F. H. and Sharpe M., "Defective Repairs of Laminated Solid Composites", Department of Civil and Arch Engineering, Department of Mechanical Engineering, Center for Composite Materials Research, North Carolina A&T State University

Part XIX. Retrofit of Slabs

ANALYSIS OF DEBONDING FAILURES IN FRP-STRENGTHENED CONCRETE BEAMS AND SLABS

K.W. Neale

(Professor, University of Sherbrooke, Sherbrooke, QC, Canada)

U.A. Ebead

(Research Associate, University of Sherbrooke, Sherbrooke, QC, Canada)

W. Elsayed, H. Abdel Baky, and A. Godat

(PhD Students, University of Sherbrooke, Sherbrooke, QC, Canada)

ABSTRACT

This paper deals with the nonlinear finite element analysis of the load–deformation behaviour of reinforced concrete beams and slabs strengthened with externally bonded fibre reinforced polymers (FRPs). The particular focus is on the implementation of appropriate constitutive models for the FRP/concrete interface that are capable of properly simulating interfacial stresses and strains, as well as characterizing possible debonding failures. Various applications are considered including the flexural and shear strengthening of beams and slabs. The proposed numerical models are validated against experimental data. The numerical analyses are shown to provide useful insight into phenomena that are virtually impossible to observe experimentally.

KEYWORDS

FRP, Strengthening, Reinforced concrete, Slabs, Beams, Flexure, Shear

1. INTRODUCTION

In this paper, we review some of our research work on the finite element simulations of FRP strengthened concrete beams and slabs in Neale et al. (2006), Abdel Baky et al. (2006), Godat et al. (2006), and Elsayed et al. (2006). For the beam applications, the finite element models address the FRP/concrete interfacial responses and are capable of simulating the various failure modes, including FRP debonding at either the plate end or at intermediate cracks. With regard to slab applications, various FRP configurations, with both passive as well as prestressed FRP strengthening, are considered. We present typical results in terms of load–deflection relationships, ultimate load capacities, and interfacial slip and stress distributions. To accurately predict the ultimate load carrying capacities and capture the debonding failures, it is necessary to properly model the bond behaviour at the FRP/concrete interface. For this purpose, interface elements that are able to properly represent the local shear–slip characteristics and failure are utilized.

2. NONLINEAR FINITE ELEMENT MODELS

The numerical analyses are carried out using the finite element software package ADINA (2004a). This allows us to simulate the entire nonlinear load–deformation behaviour of the structure under displacement-controlled loading conditions. In the analyses, the software formulations for the concrete, steel and FRP are employed. These are described in detail in the ADINA theory and modelling guide (ADINA, 2004b), and are briefly summarized below. To model the FRP/concrete interface, we introduce appropriate bond stress–slip relations via truss elements for the direct shear and flexurally-strengthened beam applications, and spring elements for the slabs and shear-strengthened beam applications. Both truss and spring elements are used to link the FRP laminates to the concrete.

The constitutive law used to model the concrete has the following features (ADINA, 2004b): (i) a nonlinear stress–strain relation to allow for the weakening of the material under increasing compressive stresses, (ii) failure envelopes that define both failure in tension and crushing in compression, and (iii) a strategy to model the post-cracking and post-crushing behaviour of the material. The general multiaxial stress–strain relations are derived from a nonlinear uniaxial stress–strain relation. The cracked concrete is assumed to be orthotropic, with the directions of orthotropy being defined by the principal stress directions. Failure envelopes are used to establish the uniaxial stress–strain law accounting for multiaxial stress conditions, and to identify whether tensile or crushing failure of the concrete has occurred. The post failure material behaviours account for post-tensile cracking, post-compression crushing, and strain softening.

For the steel reinforcement, a uniaxial elastic–plastic stress–strain law is employed. A linear elastic orthotropic constitutive relation is adopted for the FRP composites. The mechanical behaviour of the FRP/concrete interface is represented by a relationship between the local shear stress, τ , and the relative displacement, s , between the FRP laminate and the concrete. The area under the τ – s curve represents the interfacial fracture energy, G_f , which corresponds to the energy per unit bond area required for complete debonding of the laminate. The details of the formulations of the bond–slip model can be found in (Lu et al., 2005; Neale et al., 2006).

In the characterization of the interfacial behaviour, the FRP nodes are connected to the concrete nodes using nonlinear translational interface elements, as shown in Figure 1. It is necessary to emphasize that these elements represent the overall interfacial behaviour between the concrete and the FRP, and not the adhesive as such. The aforementioned constitutive model (the bond–slip model) thus represents the overall contribution of the FRP composites, adhesive and concrete. The relative displacement between Point 1 and Point 2 of the interface element (Figure 1) represents the interfacial slip, and the stress in the two-node interface element represents the interfacial shear stress. Full strain compatibility is assumed between the FRP nodes and the concrete nodes in the peeling-off direction by enforcing suitable constraint equations.

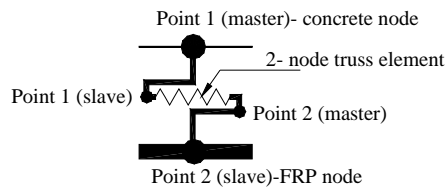


Figure 1: Interface element

For the flexurally-strengthened beam application, plane stress elements are used to simulate the concrete. For the shear-strengthened beams and the strengthened slabs, 3-D analyses are employed. Due to the geometrical and the loading symmetry; only one half of the beam or one quarter of the slab is modelled. Detailed descriptions of the geometrical parameters of the beams and the slabs are given in Neale et al. (2006), Abdel Baky et al. (2006), Godat et al. (2006), and Elsayed et al. (2006).

3. NUMERICAL RESULTS AND DISCUSSION

Typical results are presented in the subsequent sections in terms of the ultimate load carrying capacities and load–deflection relationships for the different applications simulated in this study. Special emphasis is placed on the results of the interfacial behaviour between the FRP laminates and the concrete in terms of the interfacial stress distributions and slip profiles. The specimen notations here correspond to those employed in the original references.

Ultimate load carrying capacities and load–deflection relationship

The experimental results of 25 flexurally-strengthened beams were used to assess the validity of the finite element model (Abdel Baky, et al., 2006). In addition, 15 shear-strengthened beams are considered (Godat et al., 2006). There is a very good agreement between the numerical predictions of the ultimate load capacities and the experimental data. The average numerical-to-experimental load capacity ratio for the flexurally-strengthened beam applications is 100.3% with a standard deviation of 6.5%. The corresponding values of the average and the standard

deviation in the case of the shear-strengthened beams are 102% and 2.31%, respectively, thus indicating an excellent agreement. With regard to the slab application, we obtained a very good agreement when comparing the numerical results with the experimental data of 12 different specimens with an average numerical-to-experimental load capacity ratio of 97% with a standard deviation of 7.3% (Elsayed, et al., 2006). Detailed numerical-to-experimental comparisons can be found in Abdel Baky et al. (2006), Godat, et al. (2006), and Elsayed et al. (2006).

The proposed models are able to simulate the entire load–deflection relationships, including the descending and post failure profiles, in view of the displacement-controlled solution adopted in these analyses. Figures 2a and 2b show typical numerical versus experimental comparisons in terms of the load–deflection relationships for beam and slab specimens (M’Bazaa, 1995; Longworth et al., 2004). As seen here, we were able not only to capture the debonding load, but also the complete post-debonding plateau until complete failure.

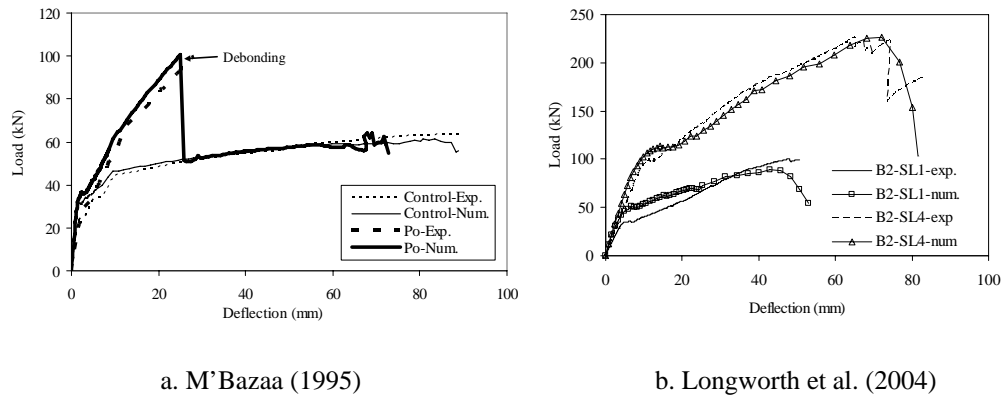


Figure 2: Typical load–deflection relationships for selected specimens

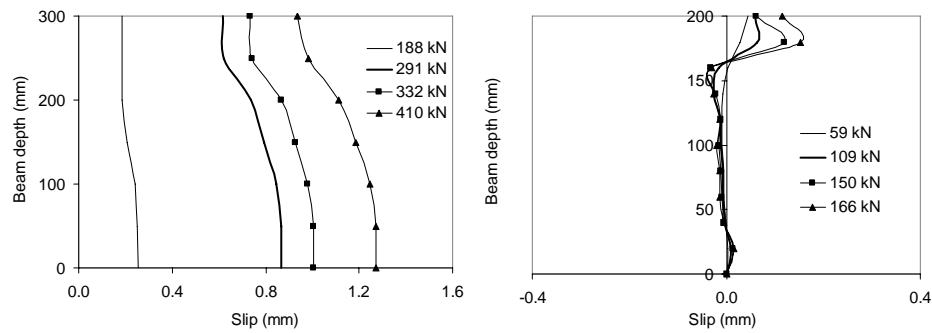
Interfacial shear stresses and slip profiles

A distinct advantage of having reliable numerical tools is that they can provide valuable insight into phenomena that are very difficult to assess experimentally. For example, knowing the values of the interfacial stresses and slips between the bonded FRPs and concrete can be very helpful for a better understanding of the FRP/concrete interfacial behaviour and bond performance. These observations are virtually impossible to detect in experiments. The numerical results shown in Figures 3a and 3b represent the slip profiles along the beam depth for an FRP side-bonded beam tested by Pellegrino and Modena (2002) and a U-shaped bonded beam tested by Adhikary and Mutsuyoshi (2004). The slip profiles depicted in these figures correspond to load increments up to failure for a section midway the shear span. As seen in Figure 3a for the side-bonded beam, the predicted slip values are significantly higher at the bottom of the beam than those at the top; this is due to the tensile stresses in this region. This suggests that this specimen should experience debonding of the FRP laminate at the bottom edge of the beam, which is in accordance with the experimental results. For the specimen strengthened using U-shaped FRP wraps the interfacial slips are higher at the top edge and shift to negative values around the mid-depth. With an increase of the applied shear force up to failure, the interfacial positive and negative values of slip are increased. It is thus obvious that using U-shaped FRP wraps rather than side-bonded laminates is more efficient in mitigating debonding, as seen from comparing the corresponding slip values.

4. CONCLUSION

A review has been presented on finite element analyses to address the interfacial behaviour of FRP-strengthened reinforced concrete structures. A nonlinear constitutive model was incorporated to represent the interfacial behaviour between the bonded FRP laminates and concrete substrate. In order to investigate the validity of the numerical models, theoretical predictions have been calibrated against published experimental data. The comparisons between the numerical and experimental results showed very good correlations in terms of the ultimate carrying capacities and load–deflection relationships. Our studies have shown the importance of appropriately modelling the FRP/concrete interface if accurate predictions of the behaviour of externally FRP-strengthened

members are to be obtained. These studies has also demonstrated that reliable numerical models represent very valuable tools for gaining insight into phenomena that are extremely difficult to assess experimentally.



a. Side-bonded (Pellegrino and Modena 2002) b. U-wraps (Adhikary and Mutsuyoshi 2004)

Figure 3: Typical slip profiles for FRP shear-strengthened beams

5. ACKNOWLEDGEMENTS

This research was funded by the Natural Sciences and Engineering Research Council of Canada (NSERC), and the Canadian Network of Centres of Excellence on Intelligent Sensing for Innovative Structures (ISIS Canada). KWN is Canada Research Chair in Advanced Engineered Material Systems and the support of this program is gratefully acknowledged.

6. REFERENCES

- Abdel Baky, H., Ebead, U.A. and Neale, K.W. (2006). "Flexural and interfacial behaviour of FRP-strengthened reinforced concrete beams". *Journal of Composites for Construction, ASCE*, submitted.
- Adhikary, B. and Mutsuyoshi, H. (2004). "Behaviour of concrete beams strengthened in shear with carbon-fibre sheets". *Journal of Composites for Construction, ASCE*, Vol. 8, No. 3, pp. 258-264.
- ADINA (2004a). *Automatic Dynamic Incremental Nonlinear Analysis*, Finite Element Software, Version 8.2. ADINA R&D Inc., Watertown, MA, USA.
- ADINA (2004b). *Theory and Modeling Guide*, Volume I, Chapter 3, Version 8.2. ADINA R&D Inc., Watertown, MA, USA.
- Elsayed, W., Ebead, U.A. and Neale, K.W. (2006). "Interfacial behaviour and debonding failures in FRP-strengthened concrete slabs". *Journal of Composites for Construction, ASCE*, submitted.
- Godat, A., Neale, K.W., and Labossière, P. (2006) "Numerical modelling of FRP shear-strengthened reinforced concrete beams". *Journal of Composites for Construction, ASCE*, submitted.
- Longworth, J., Bizindavyi, L., Wight, R.G. and Erki, A. (2004). "Prestressed CFRP sheets for strengthening two-way slabs in flexure". *Advanced Composite Materials in Bridges and Structures*, El-Badry, M. and Dunaszegi, L., Eds., Canadian Society for Civil Engineering, 8 p.
- Lu, X. Z., Teng, J. G., Ye, L. P. and Jiang, J. J. (2005). "Bond-slip models for sheets/plates bonded to concrete". *Engineering Structures*, Vol. 27, pp. 920-937.
- M'Bazaa, I. (1995). "Renforcement en flexion de poutres en béton armé à l'aide de lamelles en matériaux composites: optimisation de la longueur des lamelles". *Mémoire de maîtrise*, Département de génie civil, Université de Sherbrooke, Canada.
- Neale, K.W., Ebead, U.A., Abdel Baky, H., Elsayed, W., Godat, A. (2006). "Towards understanding the load-deformation behaviour and debonding for FRP-strengthened concrete structures". *Advances in Structural Engineering*, Special Issue, submitted.
- Pellegrino, C. and Modena, C. (2002). "Fibre reinforced polymer shear strengthening of reinforced concrete beams with transverse steel reinforcement". *Journal of Composites for Construction*, 6(2), 104-111.

AUSTRALIAN GENERIC RETROFITTING GUIDELINE FOR PLATING RC BEAMS and SLABS

Deric John Oehlers

(Associate Professor, The University of Adelaide, Adelaide, South Australia, Australia)

ABSTRACT

Strengthening reinforced concrete beams and slabs using adhesively bonded or bolted plates is well established because the fundamental plate debonding and failure mechanisms are now generally understood and recognised in most published guidelines. Furthermore, research is well advanced in quantifying these failure mechanisms, so that plating for strength can be applied in practice and generally with confidence. The aim of the Australian guideline, as with established generic national standards such as those for reinforced concrete design, is to provide engineers with comprehensive and, in particular, generic design tools that cover all forms of plating, that will allow them to find their own best solutions, to develop their own plating techniques and to encourage current and future developments in this new and rapidly developing retrofitting technique. The generic nature of this guideline and philosophy behind this guideline is described in this paper as it is felt that a generic approach is needed if FRP plating is to reach the same status and application as other structural forms.

KEYWORDS

FRP Guideline, FRP, retrofitting, reinforced concrete, adhesive bonding, bolting.

1. INTRODUCTION AND SCOPE OF GUIDELINE

The philosophy behind the Australian Guideline (Oehlers et al 2006) is to provide the choice of a wide variety of plating techniques, and their associate design rules, that covers all forms of failure, in order to allow engineers the freedom to find their own solutions; furthermore, to develop a generic approach to encourage the development of new plating techniques. For example, the Australian Guideline covers externally bonded (EB) plates that can be adhesively bonded to any surface of an RC member as in Fig.1. This form of retrofitting is now well established, however, it is known to be prone to brittle failure at low strains and, hence has a limited application even though cost effective. If this approach is found by the engineer to be unsuitable, then design rules for near surface mounted (NSM) plates are provided where the plate is adhesively bonded within the concrete cover as it is now known that much larger strains can be developed, hence, greater ductility. Finally if this approach is also found to be unsuitable, then FRP plates can be bolted to the RC beam and the bolt extended well beyond the cover into the confined region of the concrete to form a strong and ductile plating technique, although, this approach can be expensive.

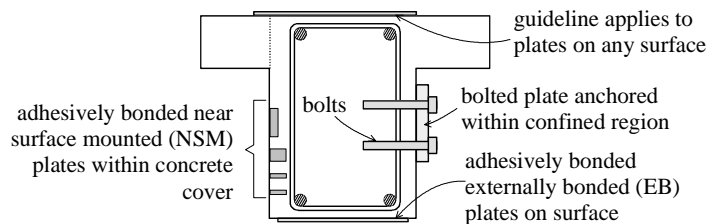


Figure 1: Forms of plating

The Australian plating guideline “Design Guideline for RC Structures Retrofitted with FRP and Metal Plates: beams and slabs”: first identifies the generic deformations and stress resultants that can induce failure and which are applicable to all forms of plating; then generic failure mechanisms are developed from these generic stress resultants; and then, where possible, generic design rules are given. Hence, much of the Guideline is applicable to new techniques and not just the established techniques in Fig.1 It is hoped that this approach will encourage the

development of new techniques and, hence, further increase the application of FRP plating. In summary, the Australian Guideline covers: the techniques of either adhesive bonding or bolting plates; any type of plate material; prestressed or unprestressed beams; plates on any surface of the structural member; generic stress resultants and capacities that have to be designed for; generic debonding mechanisms in adhesively bonded EB and NSM plates; generic debonding mechanisms in mechanically fastened that is bolted plates; longitudinal shear capacities; plate buckling; strength design philosophies for longitudinal plates; and generic ductility principles.

2. GENERIC STRESS RESULTANTS

Of fundamental importance to the Australian Guideline is the identification of the stress resultants within a plated beam as it is these stress resultants that cause the design failure or premature failure. The flexural analysis of a side plate beam is shown in Fig.2 where full details are given elsewhere (Oehlers and Seracino 2004). Of importance are: the various failure strains shown in Fig.2(b) that have to be catered for; the fact that part of the concrete may remain elastic at failure as in Fig.2(c); and, very importantly, that the plate is subject to a moment and axial force in Fig.2(d). Hence, all longitudinal plates are subjected to an axial force P_{plate} and moment M_{plate} , no matter what the position of the longitudinal plate, that have to be resisted by the bond between the plate and the RC beam. For example, M_{plate} is resisted by transverse forces in the bond, V_{plate} in Fig.3, which applies to both adhesive bonds and bolted bonds and which should not be ignored in a generic design approach even though they may be shown to be minor under certain circumstances such as for thin FRP plates on the tension face.

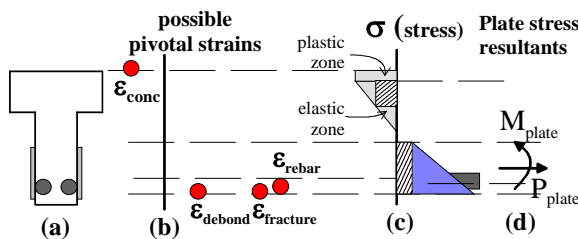


Figure 2: Flexural Analysis of Side Plated Beam

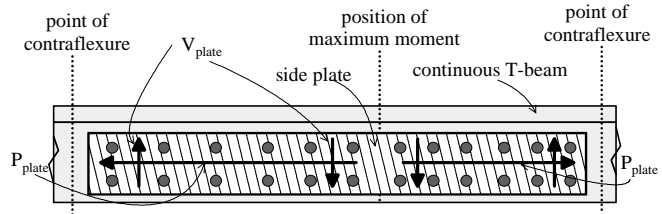


Figure 3: Plate Debonding Forces

The shear deformation that causes failure in an RC beam is the formation of a critical diagonal crack (CDC) in Fig.4. Shear is transferred by aggregate interlock across the CDC, that requires normal forces to the CDC provided by the reinforcement. It is the rigid body deformation across the CDC that controls the concrete component V_c of the shear capacity of the RC beam and this form of crack and deformation should not be confused with inclined flexural/shear cracks. It is common practice in RC design to assume that the longitudinal reinforcing bars contribute to V_c , hence for this reason it can be assumed that longitudinal plates as in Figs.1 and 3 affect V_c and that the horizontal component of the plate force $(P_{plate})_h$ in Fig.4 also contributes to V_c . Furthermore, it is common practice to assume that the internal steel stirrups resist the shear force directly V_s and, hence, transverse plates resist the shear directly or the vertical component $(P_{plate})_v$ of inclined plates.

3. GENERIC DEBONDING MECHANISMS IN ADHESIVELY BONDED PLATES

The generic deformations and associated stress resultants described previously have to be resisted by the adhesive bond (CNR 2005). Any crack of width w as in Fig.5 that intercepts a plate induces additional interface shear due to the stress concentration about the crack. This is often referred to as IC debonding and the shear/slip (τ/δ) of this partial-interaction interface bond has been well researched (Teng et al 2002). When the crack w in Fig.5 is induced and widened by flexure, then the flexural IC debonding resistance (FIC) of the plate must be able to resist P_{plate} in Figs.2 and 3. When the crack width w in Fig.6 is widened through shear deformations and aggregate interlock, then the force in the plate is still controlled by the IC debonding resistance but in this case it is referred to as CDC debonding as it affects V_c . For vertical plates crossing a CDC crack, the force in the plate is also controlled by the IC debonding resistance and this is referred to as SIC in the Australian Guideline. It can be seen that three distinct debonding failures (CNR 2005) that depend on the IC debonding resistance, that is FIC, CDC and SIC, have been identified.

The transverse forces V_{plate} in Fig.3 induce debonding from the stress concentration at the plate end as in Fig.7 and this is referred to as plate end (PE) debonding. This form of debonding starts at the plate end and propagates inwards

in contrast to IC debonding and, hence, is totally different from IC debonding and is not dependent on the τ/δ characteristics but on the tensile strength of the concrete. This form of debonding should not be confused with the IC debonding of short plates where debonding starts at the position of maximum plate strain and not at the position of zero plate strain as occurs in PE debonding. The Australian Guideline also recognises that away from stress concentrations the elementary interface shear VAY/lb still exists and depends on the tensile strength of the concrete.

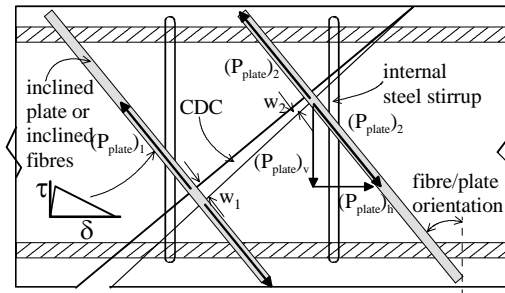


Figure 4: Shear contribution from inclined plates

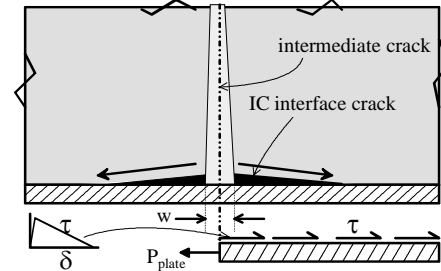


Figure 5: Intermediate Crack Debonding

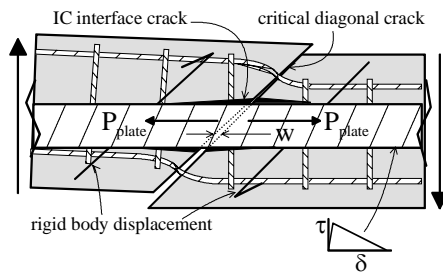


Figure 6: Critical Diagonal Crack Debonding

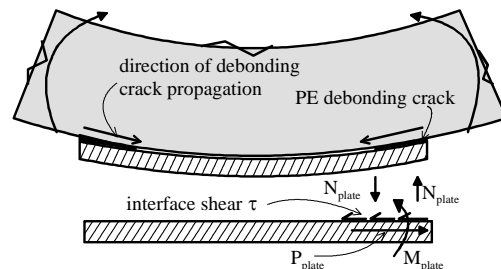


Figure 7: Plate End Debonding

4. GENERIC DEBONDING MECHANISMS IN BOLTED PLATES

The Australian Guideline gives comprehensive design rules for the bolt shear connectors that are based on extensive research on the behaviour of stud shear connectors in composite steel and concrete beams (Oehlers and Bradford 1995). The transverse forces V_{plate} and axial forces P_{plate} in Fig.3 are resisted directly by the bolts either through their dowel or shear resistance or through their axial or embedment resistance depending on the configuration of the plate being bolted. The bolt dowel forces, that resist the longitudinal force P_{plate} in Fig.3, apply concentrated forces to the plate as well as to the concrete beam shown as D in Fig.8. The dispersal of these concentrated forces induce both lateral tensile and compressive forces P. These stresses can cause the plate or concrete elements to split and have to be designed against. Furthermore, the lateral force V_{plate} in Fig.3 may be resisted by the RC beam in regions where there are already flexural cracks as in Fig.9, in which case design rules are given for the post-splitting resistance.

5. LONGITUDINAL SHEAR PLANE CAPACITIES AND PLATE BUCKLING

Combinations of shear connections can also cause the concrete element to fail along shear planes that surround the shear connection and this applies to both adhesively bonded plates as well as bolted plates as in Fig.10. Failure can occur along shear planes that surround individual or groups of shear connectors as shown and it is necessary to find the weakest failure plane by considering all possible failure planes. This form of failure also occurs in beams with transverse plates. Adhesively bonded plates and bolted plates can also buckle as in Fig.11 and design rules are given in the Australian Standard for the buckling resistances for both FRP and steel plates that are either adhesively bonded or bolted.

6. PHILOSOPHY BEHIND GUIDELINE

Plated RC structures are a new and unique form of structure which has similar failure mechanisms or behaviours as in both RC structures and composite steel and concrete structures. However plated structures also have many new

failure mechanisms that are not covered in RC and composite design manuals. As with all new forms of structures and because plating is a very efficient retrofitting technique, plating is being applied concurrently with the development of design rules. Hence, it is not possible at this stage of development of this new and unique technique to formulate prescriptive design rules that cover all situations. This should not hinder the application of plating but it does require a deep understanding of the behaviour of plated structures to ensure a safe design which consequently requires a deep understanding of the behaviour of both RC structures and composite steel and concrete structures. The *Australian Guideline* consists of a *Guideline* and a *Commentary*. The *Guideline* covers the generic and fundamental behaviour of both plated beams and plated slabs and it is these behaviours that have to be designed for. The more advanced design rules that quantify the generic fundamental behaviours in the *Guideline* are given in the *Commentary*. Hence the designer needs to be aware and design for the generic behaviours described in the *Guideline*. However, the *Commentary* is only meant to assist in the design and the designer is free to use any approach that satisfies the *Guideline*. It is recognised that these rules are improving and developing rapidly. In the long run, it is the intention of the committee to gradually transfer information from the *Commentary* to the *Guideline* as design rules not only become established but more importantly are proven to be correct and safe under all design circumstances. The *Guideline* requires fundamental structural mechanics principles to be adhered to. It is recognised that design rules are improving and developing rapidly. In the long run, it is the intention to gradually transfer information from the *Commentary* to the *Guideline* as design rules become established.

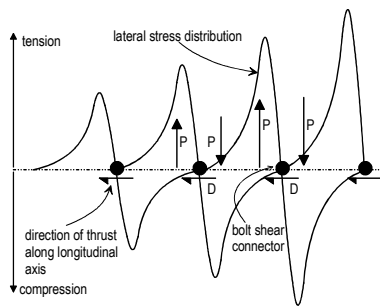


Figure 8: Longitudinal Splitting

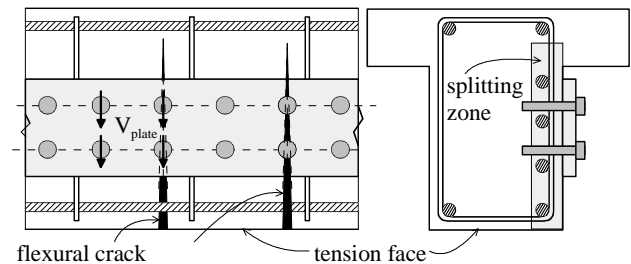


Figure 9: Transverse Post-Splitting Resistance

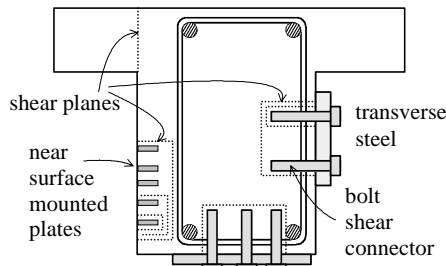


Figure 10: Shear Plane Perimeters



Figure 11: Plate Buckling

7. REFERENCES

- CNR (2005) *Instructions for the design, execution and control of strengthening measures through fibre-reinforced composites*. CNR-DT 200/04, Italian Research Council, Rome, Italy
- Teng, J.G., Chen, J.F., Smith, S.T. and Lam, L. (2002). *FRP Strengthened RC Structures*. John Wiley and Sons Ltd. England.
- Oehlers, D.J., Seracino, R., and Smith, S (2006) *Design Guideline for RC structures retrofitted with FRP and metal plates: beams and slabs*. SAI Global Limited Australia, Standards Australia, In press.
- Oehlers, D.J. and Seracino, R. (2004) *Design of FRP and Steel Plated RC Structures: retrofitting beams and slabs for strength, stiffness and ductility*. Elsevier England.
- Oehlers, D. J. and Bradford, M. A. (1995) *Composite Steel and Concrete Structural Members: Fundamental Behaviour*. Pergamon Press, England

INDIRECT CRACK CONTROL PROCEDURE FOR FRP-REINFORCED CONCRETE BEAMS AND ONE-WAY SLABS

Carlos E. Ospina

(Project Engineer, Berger/ABAM Engineers Inc., Federal Way, WA, USA)

Charles E. Bakis

(Professor, Dept. of Engineering Science and Mechanics, Pennsylvania State University, University Park, PA, USA)

ABSTRACT

This paper reports an alternative model for flexural crack control of FRP-reinforced members in which, consistently with current ACI 318 recommendations for steel-reinforced members, cracks are controlled indirectly through a maximum bar spacing requirement instead of being calculated directly. The proposed procedure results from the impracticalities associated with direct crack width measurement in concrete structures due to the high variability of both concrete cracking and crack width measurements. The proposed model explicitly accounts for the dominant effects that bar cover, FRP reinforcement stress, stiffness and bond properties have on cracking of FRP-reinforced concrete beams and one-way slabs. The procedure is seen as a simplification of the existing ACI 440.1R-06 direct crack control recommendations for serviceability design of FRP-reinforced members, rather than a modification.

KEYWORDS

Cracking, Crack widths, FRP Reinforcement, Serviceability, Slabs.

1. INTRODUCTION

1.1 Flexural Crack Control in Steel-reinforced Concrete Members

According to Frosch (1999), the maximum crack width at the tension face of a reinforced concrete beam or one-way slab can be calculated as:

$$w = 2 \frac{f_r}{E_r} \beta k_b \sqrt{d_c^2 + \left(\frac{s}{2}\right)^2} \quad (1)$$

where f_r is the reinforcing bar stress, calculated assuming elastic-cracked conditions, E_r is the modulus of elasticity of the reinforcement, β is the ratio of the distance from the neutral axis to the tension face of the member to the distance from the neutral axis to the centroid of the tensile reinforcement, d_c is the cover thickness from the tension face to the center of the closest rebar, s is the bar spacing (taken as the member width for a single bar case) and k_b is a coefficient that accounts for the bond characteristics of the bars. For steel-reinforced concrete members, β can be taken as $1 + 0.0031 d_c$, with d_c in mm (Frosch, 1999). Equation 1 is expressed herein in generic form because it is valid regardless of the type of reinforcement.

Based on Frosch's work, ACI 318 introduced in 1999 changes to the crack control rules in which a maximum bar spacing, rather than a z-factor (related to crack width), is prescribed. The exposure condition dependence was also eliminated. These changes resulted from the high variability of concrete cracking and crack width measurements, unacceptable results with the traditional Gergely-Lutz model for large bar covers, and research showing no direct relationship between bar corrosion and crack width. The crack control equation in ACI 318M-05 is defined as

$$s = 380 \left(\frac{280}{f_s} \right) - 2.5 c_c \leq 300 \left(\frac{280}{f_s} \right) \quad (f_s \text{ in MPa}) \quad (2)$$

where f_s is the steel reinforcement stress at service level and c_c is the clear cover. This approach is “indirect” because if Eq. 1 (which is the basis for Eq. 2) were to be solved for the maximum bar spacing, the resulting equation (Eq. 3) becomes constrained by a crack width limit, w .

$$s = 2 \sqrt{\left(\frac{w E_r}{2 f_r \beta k_b} \right)^2 - d_c^2} \quad (3)$$

Although ACI 318M-05 does not explicitly link Eq. 2 to a particular crack width, Frosch (1999) showed that Eq. 2 is indirectly tied to a crack width that varies between 0.4 mm (0.016 in.) to about 0.52 mm (0.02 in.). The latter is just a 30% variation from the former. In lieu of more precise calculations, f_s can be taken as $0.67 f_y$ which exceeds the $0.6 f_y$ value assumed in earlier ACI 318 code versions. This is because of the new load factors in ACI 318. The higher stress level leads to a control crack width lower bound of $(0.4 \text{ mm})(0.67/0.6) = 0.44 \text{ mm}$ (0.018 in.).

Figure 1 shows Eq. 3 predictions in terms of concrete cover for crack widths between 0.44 mm and 0.58 mm. The figure shows that Eq. 2 is a discontinuous representation of Eq. 3 for this crack width range.

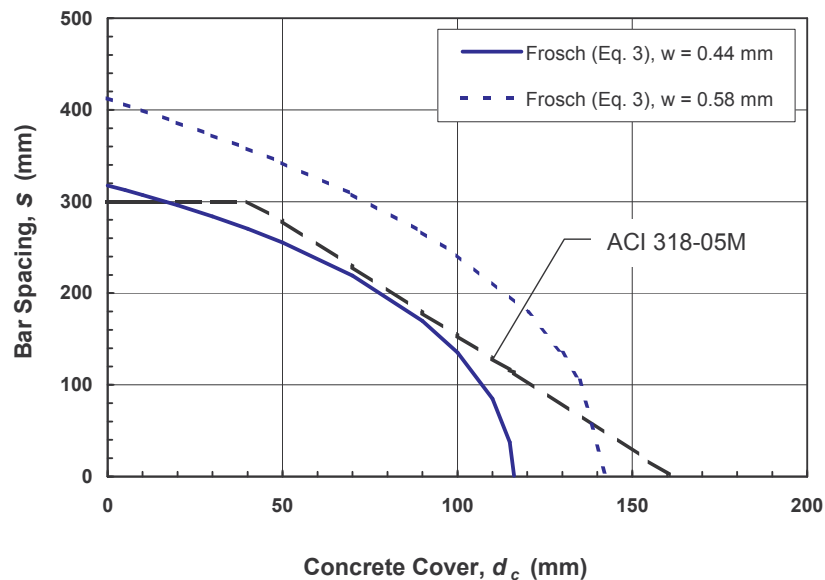


Figure 1: ACI 318M-05 Crack Control Provisions

1.2 Flexural Crack Control in FRP-reinforced Concrete Members

In ACI 440.1R-06, cracks are controlled directly by comparing maximum crack widths per Eq. 1 with crack width limits equal to 0.5 mm (0.020 in.) and 0.7 mm (0.028 in.), for exterior and interior exposure conditions, respectively. For FRP bars with bond similar to that of black steel bars, k_b is equal to one. For FRP bars with better bond, k_b is less than one. For FRP bars with inferior bond, k_b is greater than one. If k_b is unknown, it shall be taken as 1.4 for non-smooth bars. The crack width limits in ACI 440.1R-06 are taken from the Canadian Highway Bridge Design Code (2000). These limits are more relaxed than those associated with conventional reinforced concrete design due to the corrosion-free nature of FRP.

The main objective of this paper is to propose an indirect crack control model for FRP-reinforced concrete beams and one-way slabs in which a maximum bar spacing is prescribed in lieu of direct calculation of crack widths. The

goal is to keep the format of Eq. 2, including the dominant variables already identified by ACI 318M-05, together with the relevant mechanical properties of FRP that influence cracking in FRP-reinforced concrete members.

2. PROPOSED MODEL

Using Eq. 2 as a starting point, the maximum spacing of FRP bars in FRP-reinforced concrete beams and one-way slabs can be expressed as:

$$s = 380 \left(\frac{280}{f_r} \right) \left(\frac{E_r}{200,000} \right) \left(\frac{w}{0.44} \right) \frac{1}{k_b} - 2.5 c_c \leq 300 \left(\frac{280}{f_r} \right) \left(\frac{E_r}{200,000} \right) \left(\frac{w}{0.44} \right) \frac{1}{k_b} \quad (4)$$

with f_r and E_r in MPa. The terms E_r and w have been normalized by 200,000 MPa and 0.44 mm, respectively, to enable the calculation of the maximum bar spacing in members reinforced with FRP bars. In turn, Eq. 4 leads to

$$s = 1.2 \frac{E_r w}{f_r k_b} - 2.5 c_c \leq 0.95 \frac{E_r w}{f_r k_b} \quad (f_r \text{ and } E_r \text{ in MPa}) \quad (5)$$

which is conceptually consistent with the approach recommended by Frosch (2001) and suitable to comply with any target crack width limit. For instance, substituting $w = 0.7$ mm into Eq. 5, and simplifying, renders

$$s = 0.8 \frac{E_r}{f_r k_b} - 2.5 c_c \leq 0.7 \frac{E_r}{f_r k_b} \quad (f_r \text{ and } E_r \text{ in MPa}) \quad (6)$$

Figure 2 shows maximum bar spacing predictions from Eqs. 3 and 5 as a function of d_c for a member with GFRP bars with $E_r = 40$ GPa, $f_r = 80$ MPa, and $k_b = 1.4$, for limiting crack widths of 0.7 and 0.91 mm. In the bar spacing predictions for $w = 0.7$ mm, three β expressions are examined: $\beta = 1 + 0.0063 d_c$ (shallow members, $d = 230$ mm), $\beta = 1 + 0.0031 d_c$ (deeper members, $d = 1800$ mm), and $\beta = 1 + 0.0008 d_c$, as assumed by Frosch for steel-reinforced members. These β values were derived using Eq. 7, assuming $k = 0.3$.

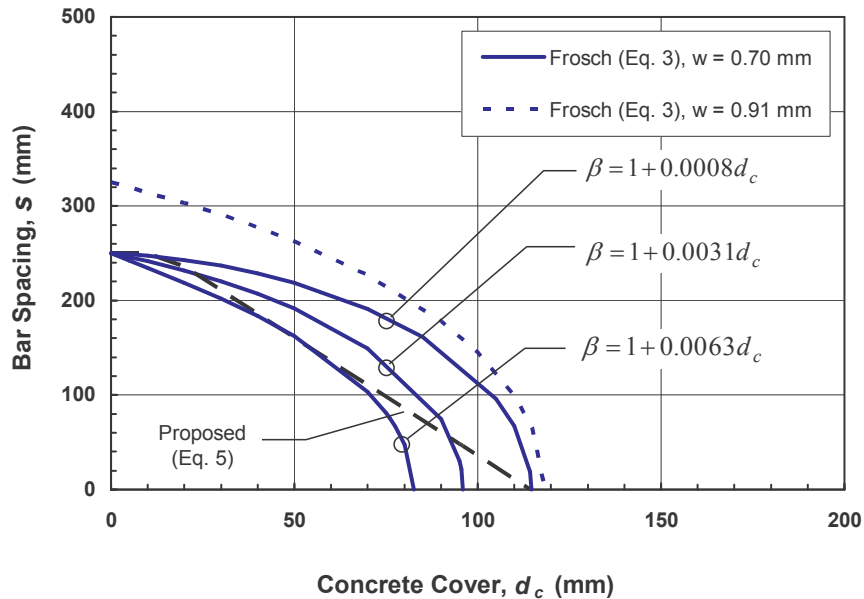


Figure 2: Proposed Crack Control Provisions for GFRP-reinforced Concrete Members

$$\beta = 1 + \frac{d_c}{d(1-k)} \quad (7)$$

The evaluation of the β effect is necessary because the flexural depth, d , can vary significantly in concrete construction. The bar spacing predictions for $w = 0.91$ mm are based on $\beta = 1 + 0.0031 d_c$ only.

Figure 2 shows that, in theory, it is possible to explicitly account for the β effect in the maximum bar spacing calculation. However, for reasons of simplicity, Frosch's assumption for β looks appropriate as a balance between shallow and deep FRP-reinforced concrete members. It is worth noting that the proposed indirect crack control procedure implicitly uses $\beta = 1 + 0.0031 d_c$. Figure 2 also shows that Eq. 5 provides a reasonable representation of Eq. 3 for crack control of FRP-reinforced concrete members for the specific conditions assumed.

3. DISCUSSION

Because of its general nature, Eq. 5 can be applied to both steel- and FRP-reinforced concrete beams and one-way slabs, provided k_b is defined accordingly. In addition to the clear cover, the model accounts for the elastic stiffness and bond characteristics of FRP, which are key parameters for serviceability design of FRP-reinforced members.

The model is meant for use in conjunction with allowable crack width values that are considered satisfactory for the designated function of the structure. Equation 5 can be used to ensure compliance with any crack width value to be controlled. For steel-reinforced concrete members, the indirect crack control equation of ACI 318M-05 may not be readily used in situations in which crack widths much smaller than 0.4 mm are to be controlled, as is the case of structures where water tightness control is essential and structures subject to the use of deicing chemicals. Equation 5 also gives freedom to designers to select a target FRP strain to ensure compliance with both the serviceability and ultimate limit states, especially in those cases where either excessive deflections or brittle failure due to GFRP reinforcement creep rupture may be caused by allowing cracks that are too wide.

Rather than being a drastic departure from the ACI 440.1R-06 model, Eq. 5 provides a discontinuous representation of Eq. 3. The procedure is simpler because the impracticalities associated with crack width measurements are avoided. Using indirect procedures for serviceability design of FRP-reinforced members is not new. In fact, ACI 440.1R-06 provides an indirect procedure for deflection control of beams and one-way slabs with FRP bars.

4. CONCLUSION

This paper presents an indirect procedure to control cracking in FRP-reinforced concrete beams and one-way slabs in which a maximum bar spacing is prescribed instead of a maximum crack width. The procedure is indirect because the maximum bar spacing requirement is indirectly linked to a target crack width value that is to be complied with. The proposed procedure can also be applied to steel-reinforced concrete beams and one-way slabs.

5. REFERENCES

- ACI Committee 318, (2005), "Metric Building Code Requirements for Reinforced Concrete and Commentary (ACI 318M-05)," American Concrete Institute, Farmington Hills, Mich., 436 p.
- ACI Committee 440, (2006), "Guide for the Design and Construction of Structural Concrete Reinforced with FRP Bars (ACI 440.1R-06)," American Concrete Institute, Farmington Hills, Mich., 44 p.
- Canadian Standards Association, (2000), "Canadian Highway Bridge Design Code (CAN/CSA-S6-00)," CSA International, Toronto, Ontario.
- Frosch, R.J., (1999), "Another Look at Cracking and Crack Control in Reinforced Concrete," *ACI Structural Journal*, V. 96, No. 3, May-June, pp. 437-442.
- Frosch, R.J., (2001). "Flexural Crack Control in Reinforced Concrete," *Design and Construction Practices to Mitigate Cracking*, SP 204, American Concrete Institute, Farmington Hills, Mich., pp. 135-154.

STRENGTHENING OF PRECAST PRESTRESSED HOLLOW CORE SLABS WITH CFRP SHEETS

M. Kalimur Rahman

(Research Engineer, Research Institute, K.F.U.P.M, Dhahran, Saudi Arabia)

A. H. Al-Gadhib

(Associate Professor, Civil Engineering, K.F.U.P.M, Dhahran, Saudi Arabia)

Jaffer Mohiuddin

(Graduate Student, K.F.U.P.M, Dhahran, Saudi Arabia)

M. H. Baluch

(Professor, Civil Engineering, K.F.U.P.M, Dhahran, Saudi Arabia)

ABSTRACT

Precast prestressed hollow core slabs are very commonly used as floor system in Saudi Arabia in the booming precast concrete construction industry. Strengthening of these slabs may be required for several reasons including increased load due to higher dead or live loads, architectural modifications in locations of walls, damage due to corrosion, installation of heavy machinery, opening cut through slabs and errors in planning, construction and design. This paper presents the results of flexural strengthening of hollow core slabs using CFRP sheets. Seven full-scale hollow core slabs (5.0 m span, 1.2 m width and 0.2 m thickness) were tested under flexure using four point loading up to failure, with one slab being tested as control specimen and the remaining six slabs strengthened with CFRP. Experimental results show that the flexural load carrying capacity of precast prestressed hollow core slabs increased in the range of 14 to 40% depending on the width/layers of CFRP sheets used. Interesting transition in the behavior of the hollow core panels from flexure to shear failure was noted as the number of layers of CFRP sheets was increased. A good correlation was observed between the experimental and the predicted values obtained using a strain compatibility approach.

KEYWORDS

Strengthening, CFRP sheets, prestressed slab, hollow core slab, full-scale test

1. INTRODUCTION

There has been a surge in the precast concrete construction of commercial and residential structures in the recent years in Saudi Arabia. Precast prestressed hollow core (PPHC) slabs are primarily used as floor or roof system in the precast construction. Prestressed hollow core slabs also have application as spandrel members and bridge deck units and as wall panels. Strengthening of PPHC slabs may be needed to upgrade the load-carrying capacity, changes in locations of walls, damage due to corrosion, installation of heavy machinery, opening a cut through slabs for heating/ventilation units and errors due to insufficient design and prestressing steel.

CFRP composite sheets are now being used for strengthening, repair and extension of service life of reinforced concrete elements including beams, columns, one-way and two-way slabs and wall panels (Bakis et. al. 2002, Nanni, 1995, El-Maaddawy et al., 2005). CFRP has excellent properties of high tensile strength, lightweight, and corrosion resistance which make it amenable for retrofitting of structures. The ultimate flexural strength of reinforced concrete beams can be increased significantly by application of CFRP sheets on the tension face of these elements (Arduini and Nanni, 1997). CFRP sheet has also been used to strengthen beams in shear, by placing CFRP sheets in high shear stress zones (Li et al., 2001). Some research has been conducted on the strengthening of one and two-way

reinforced concrete slabs using CFRP laminates and sheets (Arduini et al., 2004, Mosallam and Mosallam, 2002) but research on prestressed and hollow core slabs is limited (Hosny et al., 2003). This paper presents the results of full-scale load test on PPHC slabs strengthened by CFRP sheets in flexure and comparison made with the predicted flexural load capacity using a mechanistic model.

2. EXPERIMENTAL DESIGN

A series of seven full scale hollow core concrete slabs (Table 1: Designated as S1 to S7) having a 5.0 m span, 1.2 m width and 0.2 m thickness and made from concrete having a compressive strength of 45 MPa, were procured from a commercial precast factory. Each PPHC slab has 44% voids and is reinforced with four 7-wire pretensioned steel strands of 12.7 mm diameter.

The PPHC slabs were strengthened with CFRP sheets (SIKA wrap hex 230C with unidirectional carbon fiber fabric) applied at the bottom of the slabs using Sikadur 330 epoxy resins. The CFRP sheets, 0.3 m in width and 0.13 mm thickness, has a tensile strength of 3.45 GPa, tensile modulus of 230 GPa and an ultimate strain of 1.5%. The simply supported PPHC slabs were tested in flexure using four point loading up to failure. An array of five LVDT's was used at different points on the slab to measure the deflection. Strain gauges were applied on concrete and CFRP sheets and all data was captured using a data logger. The testing arrangement is shown schematically in Figure 1.

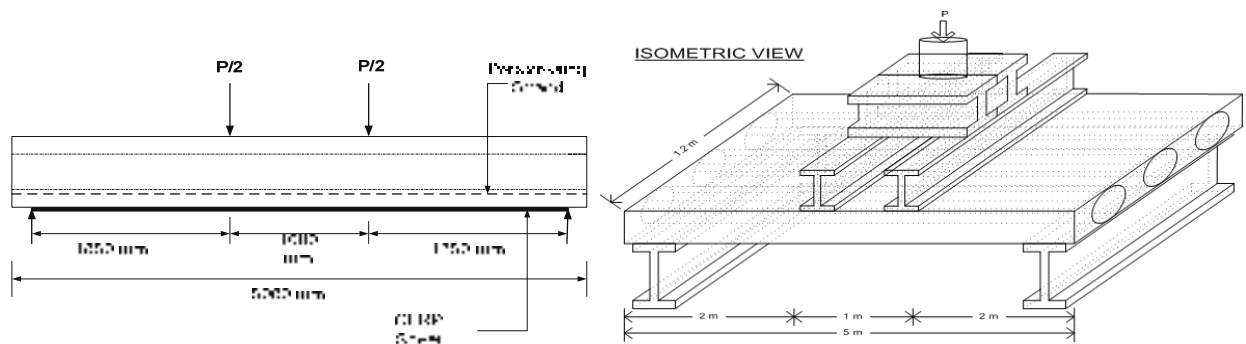


Figure 1: Details and Isometric View of Experimental Setup

Table 1: Designation and Description of Strengthening for Hollow Core Slabs

S. No	Slab Specimens ID	Description
1	S1	Control specimen
2	S2	Single layer CFRP sheet on 300 mm width
3	S3	Single layer CFRP sheet of 300 mm width (Identical to S2)
4	S4	Single layer CFRP sheet of 600 mm width
5	S5	Single layer CFRP sheet of 900 mm width
6	S6	Two Layers CFRP sheet of 600 mm width
7	S7	Damaged slab strengthened with single layer CFRP sheet of 300 mm width

3. RESULTS AND DISCUSSIONS

The cracking load, ultimate load, deflection at maximum load and failure mode of all the slabs are summarized in Table 2. The virgin slabs strengthened using various widths of CFRP strips (S2 to S5) showed a brittle rupture of the CFRP sheet at failure (Figure 2). The Slab S6 which was strengthened with two layers of CFRP sheets showed a sudden failure in shear with diagonal crack emanating from outside the point of load application as shown in Figure 3. The flexural strength enhancement of PPHC slabs is limited by shear strength of these slabs. There is a transition in the failure mode from flexural to shear failure once the shear capacity of these slabs is exceeded. It is therefore important to strengthen these slabs in shear if the flexural capacity needs to be increased further. The load deflection curves for the virgin slabs strengthened by CFRP sheets are shown in Figure 4. This figure shows identical linear

behavior of all specimens until cracking occurred at a load of about 65-70 kN. A non-linear behavior ensues subsequently till the brittle failure of CFRP. The flexural capacity of the PPHC slab increases by 14-36% depending on the cross sectional area of the sheets applied. Slab damaged by loading up to cracking load and subsequently strengthened by CFRP showed 18% increase in ultimate moment capacity (Figure 5).



Figure 2: Brittle Rupture of CFRP Strip



Figure 3: Shear Failure of Slab S6

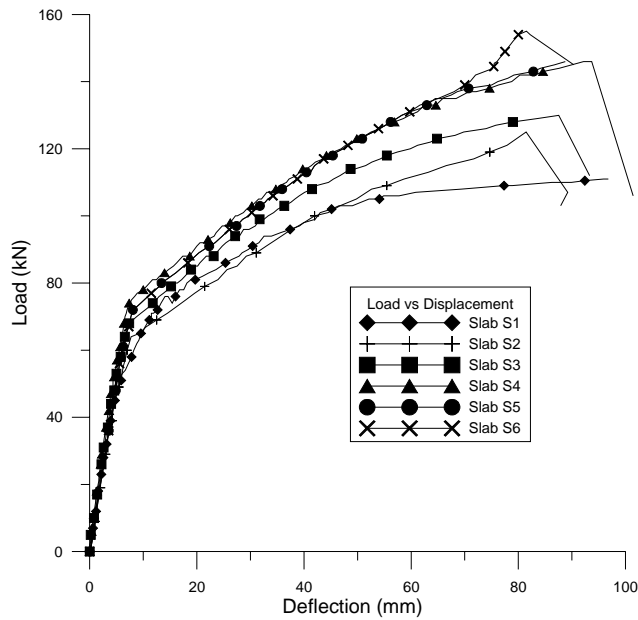


Figure 4: Load vs. Deflection of Virgin Strengthened Slabs

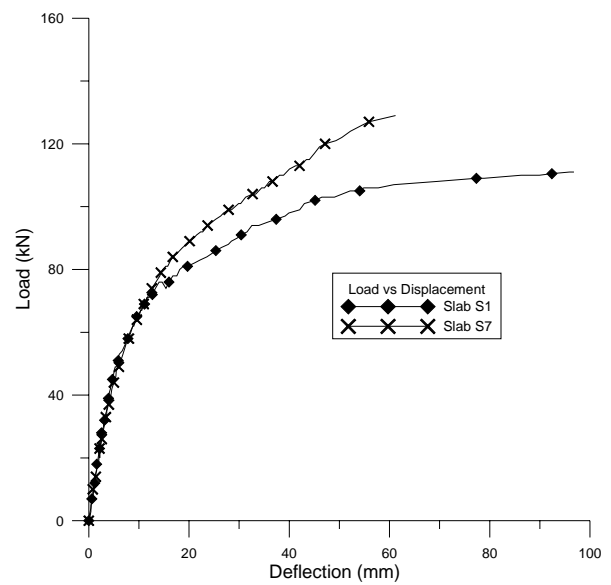


Figure 5: Load vs. Deflection of Cracked Slab

Table 2: Experimental Results for Flexural Strengthening of PPHC Slabs with CFRP sheets

Slab	Cracking Load (kN)	Maximum Load (kN)	% Increase	Deflection at Max Load (mm)	Failure Mode
S1 (control)	65	110	-	97	Flexural Failure
S2	64	125	14%	89	Rupture of CFRP
S3	68	130	18%	87	Rupture of CFRP
S4	69	145	32%	84	Rupture of CFRP
S5	67	148	36%	83	Rupture of CFRP
S6	66	154	40%	79	Shear failure,
S7	64	130	18%	61	Flexural and Shear Cracks

Cracking load of PPHC slabs was calculated using the method outlined in the PCI manual for the design of hollow core slabs (PCI, 1998). Strain compatibility approach (ISIS M05-00, 2001) was used to predict the flexural failure loads of PPHC slabs strengthened with CFRP sheets. A good correlation between the experimental and predicted values was obtained for slabs S1 to S4 (Percent variation 2 % to 5 % - Table 3). For slabs S5 and S6 as the percentage of CFRP sheet was increased beyond the balanced level, the experimental value of ultimate flexural load was found to be significantly smaller than the predicted capacity. The pattern of cracking especially in Slab S6 was predominantly diagonal, showing shear failure rather than flexural failure in the slabs.

Table 3: Comparison of Cracking Load and Ultimate Load

Slab	Cracking Load (kN)		Ultimate Flexural Load (kN)	
	Experimental	Predicted	Experimental	Predicted
S1	65	75	110	105
S2	64	75	125	123
S3	68	75	130	123
S4	69	75	145	143
S5	67	75	148	162
S6	66	75	154	180

4. CONCLUSIONS

The present study showed that CFRP sheets can be successfully used for flexural strengthening of virgin PPHC with an increase in flexural capacity ranging from 14 % to 36% depending on the cross-sectional area of CFRP used. Slabs with initial damage, repaired and strengthened with CFRP sheet, showed a significant increase in ultimate flexural capacity. A good correlation was obtained between the experimental and predicted values of failure loads using strain compatibility approach for under-reinforced slabs. Over-reinforced slabs showed a transition to shear failure (in contrast to flexural failure) due to the limited shear capacity of the hollow core slabs. As an engineering guideline, it is recommended to ensure that $\rho_{cfpr} < 0.75\rho_{(cfpr) bal}$ in strengthening hollow core slabs.

5. ACKNOWLEDGEMENTS

The support of Civil Engineering Department and Research Institute at King Fahd University of Petroleum & Minerals (KFUPM) is deeply acknowledged. Thanks to INCO Precast Company and SIKA for providing materials.

6. REFERENCES

- Bakis, C. E. et al. (2002). "Fibre-Reinforced Polymer Composites for Construction-State of the Art Review," *Journal of Composites for Construction, ASCE*, Vol. 6, No. 2, pp. 73-87.
- Nanni, A.(1995). "Concrete Repair with Externally Bonded FRP Reinforcement," *Concrete International*, Vol. 17, No. 6, pp. 22-26.
- El Maaddawy, T. and Soudki, K. (2005). "Carbon-Fiber-Reinforced Polymer Repair to Extend Service Life of Corroded Reinforced Concrete Beams", *Journal of Composites for Construction, ASCE*, Vol. 9, No. 2, pp. 187-194.
- Arduini, M. and Nanni, A. (1997). "Behavior of Precracked RC Beams Strengthened with Carbon FRP Sheets", *Journal of Composites for Construction, ASCE*, Vol. 1, No. 2, pp 63-70.
- Li, A., Assih, J, and Delmas, Y. (2001). "Shear Strengthening of RC Beams with Externally Bonded CFRP Sheets", *Journal of Structural Engineering*, Vol. 127, No. 4, 2001, pp. 374-380.
- Arduini, M., Nanni, A., and Ramagnolo, M. (2004) "Performance of One-Way Reinforced Concrete Slabs with Externally Bonded Fiber-reinforced Polymer Strengthening", *ACI Structural Journal*, Vol. 101, No. 2, pp. 193-201.
- Mosallam, A.S., and Mosallam, K.M. (2002). "Strengthening of Two-way Slabs with FRP Composite Laminates." *Construction and Building Materials*, Vol. 17, pp. 43-54.
- Hosny, A., Abdelrahman, A. and Elarabi, A. (2003) "Strengthening of Prestressed Concrete Slabs Using CFRP", *Proceedings International Conference on Composites in Construction CCC2003*, Cosenza, Italy, pp. 355-359.
- PCI. (1998) "Manual for the Design of Hollow Core Slabs" Second Edition, *Precast Concrete Institute*.
- ISIS M05-00 (2001). "Strengthening Reinforced Concrete Structures with Externally Bonded Fiber Reinforced Polymers", *ISIS Canada*, University of Manitoba, Winnipeg, Manitoba, Canada.

USE OF CARBON-FIBER REINFORCED POLYMERS IN SLAB-COLUMN CONNECTION REPAIRS

Widianto

(Structural Engineer, Bechtel Corporation, Houston, TX 77056, USA)

Ying Tian

(Graduate Research Assistant, University of Texas at Austin, Austin, Texas 78712, USA)

Jaime Argudo

(Project Manager, Engineering Diagnostics, Inc., Austin, Texas 78701, USA)

Prof. Oguzhan Bayrak

(Professor, Dept. of Civil Engineering, University of Texas at Austin, Austin, Texas 78712, USA)

Prof. James O. Jirsa

(Professor, Dept. of Civil Engineering, University of Texas at Austin, Austin, Texas 78712, USA)

ABSTRACT

Five 2/3-scale slab-column connections were tested to compare the efficiency of different rehabilitation techniques for repair and strengthening earthquake-damaged connections. Two strengthening and repair techniques using CFRP were studied: (i) externally installed CFRP stirrups, (ii) externally installed CFRP sheets on the tension surface and anchored into the slab using CFRP anchors. Both techniques increased the connection strength and improved the residual capacity after punching failure.

KEYWORDS

Repair, strengthening, slab-column connection, two-way shear, carbon-fiber reinforced polymers sheets.

1. INTRODUCTION

Flat-plate structural systems may be prone to shear failure at slab-column connections during or after strong ground motions. Such failures may result in a progressive collapse of a building. Therefore, slab-column connections with insufficient punching shear strength or connections damaged during strong ground motions may require rehabilitation. This paper focuses on rehabilitation of typical flat-plate structures, built in the mid 1900s, that have been subjected to an earthquake.

Typical flat-plate structures do not have a concentration of the slab top steel near the column as required by the current building code (ACI 318-05). Structural drawings of several flat-plate structures located in Western US show that those structures have roughly 0.5% reinforcement ratio in the column strip and no shear reinforcement. Since low percentage of longitudinal reinforcement in the column strip results in low two-way shear strength (Marzouk and Hussein, 1991), the rehabilitation of the earthquake-damaged connections in the existing structures usually involves strengthening for flexure and punching shear. In order to preserve the advantage of flat-plate system (i.e. maximizing clear space for given story heights), Carbon-Fiber Reinforced Polymer (CFRP) materials were used in rehabilitation because the CFRP materials do not change the useable space in the building.

ACI 318-05 states that the nominal two-way shear strength V_c of an interior slab-column connection with a square column is the lesser of Eqs. 1 and 2: $V_c = (40 \times d/b_o + 2) \times \sqrt{f_c'} \times b_o \times d$ (Eq.(1)) ; $V_c = 4 \times \sqrt{f_c'} \times b_o \times d$ (Eq.(2)), where d is the average depth of slab reinforcement, b_o is the critical shear perimeter located at a distance $d/2$ away from the edge of the column or from the outermost shear reinforcement, and f_c' is the concrete compressive strength.

2. TEST PROGRAM, MATERIAL PROPERTIES, AND TEST SETUP

Five two-third-scale specimens representing interior slab-column connections were tested (Table 1). The prototype structure for all specimens, except G1.0, was assumed to have office occupancy, a live load of 50 psf, partition and additional dead load of 20 psf, 21' span length, 24" square column, and 9" slab thickness. All slabs, except G1.0, had 0.5% top reinforcement in the column strip, 0.25% reinforcement elsewhere, and no shear reinforcement. G1.0 had 1.0% top reinforcement between lines that are $1.5 \times (\text{slab thickness})$ outside opposite faces of the column (a width of $(c+3h)$), which is typical in the flat-plate structures designed using ACI 318-05. All slabs had the same bottom reinforcement.

Grade 60 deformed reinforcement satisfying ASTM A 706-06 requirements and 4000-psi concrete were used in the experimental program. The actual concrete compressive strengths for all specimens are shown in Table 1. The details of slab reinforcement are given elsewhere (Widiyanto et al., 2006). 0.04" thick, unidirectional CFRP sheet with aramid cross fibers (Tyfo SCH-41S) was used. The specified elastic modulus, ultimate tensile stress, and ultimate tensile strain of the CFRP sheet are 10500 ksi, 127 ksi, and 0.012, respectively.

Table 1. Test program, specimens, and results

Specimen	Test program	f_c' (psi)	ρ_{top} within $(c+3h)^*$	V (kip)	ACI b_o (in)	$v = V / (b_o d)$
G0.5	Punching shear loading only	4550	0.5	69.9	84	$2.47 \sqrt{f_c'}$
G1.0	Punching shear loading only	4070	1.0	90.2	84	$3.37 \sqrt{f_c'}$
LG0.5	Lateral loading up to 1.25%, then punched	4860	0.5	72.7	84	$2.48 \sqrt{f_c'}$
LRstG0.5	Lateral loading up to 1.25%, rehabilitated by external CFRP stirrups, then punched	4930	0.5	86.5	84** / 135***	$2.93 \sqrt{f_c'}$ / $1.83 \sqrt{f_c'}$
LRshG0.5	Lateral loading up to 1.25%, rehabilitated by CFRP sheet, then punched	4630	0.5	97.5	84	$3.41 \sqrt{f_c'}$

Specimen notation: **G**: Gravity load up to failure (concentric punching shear test)

L: Reverse cyclic lateral load up to 1.25% drift

Rst: Rehabilitation using externally installed CFRP stirrups

Rsh: Rehabilitation using externally installed CFRP sheets

0.5: 0.5% slab top steel within $(c+3h)$

1.0: 1.0% slab top steel within $(c+3h)$

* $c=16"$ (column dimension of the specimen), $h=6"$ (slab thickness of the specimen)

ρ_{top} : % slab top steel

** $b_o=84"$ was calculated for the critical perimeter $d/2$ away from the column face ($d=5"$).

V : Punching load

*** $b_o=135"$ was calculated for the critical perimeter $d/2$ away from the outermost CFRP stirrup ($d=5"$).

v : Failure shear stress

Specimens G0.5 and G1.0 served as control specimens to provide information on punching shear strength of undamaged and unstrengthened specimens. Specimens LG0.5, LRstG0.5, and LRshG0.5 were first subjected to reversed cyclic lateral displacements up to 1.25% to produce damage in the slab-column connection, and then the slab was subjected to a concentric punching shear loading up to failure. At the end of the simulated seismic loading, specimens LRstG0.5 and LRshG0.5 were rehabilitated. In order to mimic the rehabilitation process in a flat-plate building that is unshored, the column axial load producing a shear force of $0.23V_c$ (representing dead load plus 25% of live load on the prototype structure) on the critical shear perimeter was maintained during rehabilitation.

Figure 1 shows the test setup for simulated seismic loading and for concentric punching shear loading. The positions of the struts were selected to reflect results of finite element analyses conducted on the prototype structure subjected to lateral and gravity loads. More details of test setup are given elsewhere (Widiyanto et al., 2006).

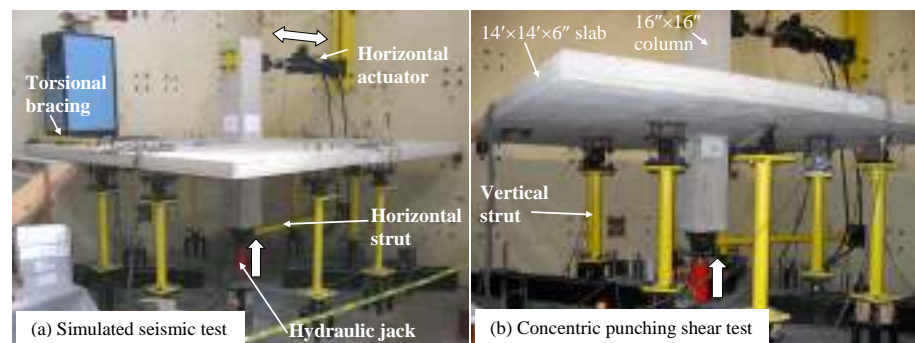


Figure 1: Test setup

3. REHABILITATION PROCESS

3.1 Installation of CFRP Stirrups

LRstG0.5 was repaired by installing external CFRP stirrups around the column (Figure 2). This rehabilitation technique was previously studied by Binici (2003). Surface preparation involved (i) locating the slab reinforcement using non destructive testing, (ii) drilling 3/4-inch holes, (iii) grinding the slab surface, and (iv) chamfering the edge of the hole to minimize stress concentrations. 3/4-inch wide CFRP strips were cut from a roll of CFRP fabric. The first row of CFRP stirrups were located as close to the column face as possible ($d/4$ away from column face) in order to intercept the shear crack. The other rows of CFRP stirrups were spaced at about $d/2$. After being impregnated with epoxy and passed through a saturator to remove excessive epoxy, the CFRP strips were stitched (once or twice) through the holes and wrapped to form closed stirrups. After the completion of CFRP stirrup placement, the bottom of the vertical holes were plugged and the holes were filled with epoxy.

3.2 Installation of Well-anchored CFRP Sheets

LRshG0.5 was repaired by applying 12"-wide CFRP sheets around the column (Figure 2), on the tension surface of the slab to increase the flexural capacity of the slab that had only 0.5% steel within ($c+3h$) critical section. The amount of CFRP reinforcement was selected to produce the same flexural capacity as that of the connection with 1.0% steel. The installation of CFRP sheets involved drilling four holes (3/4-inch diameter and 4 1/2-inch deep) at each corner of the column so that CFRP anchors could be inserted. The edges of the holes were chamfered and the concrete surface was ground smooth and cleaned. The CFRP placement was done as follows: (i) Epoxy was poured into cracks and holes, (ii) concrete surface was coated with the epoxy, (iii) an epoxy-impregnated CFRP sheet was inserted into a saturator to remove excessive epoxy, (iv) the sheet was placed on the concrete surface and a paint roller was used to remove air pockets below the sheet, (v) CFRP anchors were inserted into the holes, and (vi) the protruding ends of the anchors were splayed over the CFRP sheet.

4. TEST RESULTS AND DISCUSSIONS

Figure 2 shows the gravity load versus vertical displacement (at the column) curves for a punching shear test. The gravity load capacity and the shear stress at the critical shear perimeter v_c are summarized in Table 1. For the connections tested in this study (all specimens except LRstG0.5), Eq. 2 governs the design. The critical shear perimeter of LRstG0.5, which is at $d/2$ away from the outermost CFRP stirrup, is larger than that of the other specimens. Thus, Eq. 1 governs and gives v_c of $3.48\sqrt{f'_c}$ for LRstG0.5. The measured v_c of LRstG0.5 was $1.83\sqrt{f'_c}$.

Table 1 shows that all of the specimens tested in this study failed at shear stress levels that were lower than $4\sqrt{f'_c}$, the value used in most designs. Punching shear failure was initiated by large flexural cracks that reduced concrete contribution to shear strength and caused early punching shear failure. At failure, the v_c inferred from the measurements of specimens G0.5 and G1.0 were $2.47\sqrt{f'_c}$ and $3.37\sqrt{f'_c}$, respectively. The measured strengths were only 63% and 85% of the strength estimated using ACI 318-05 expression (Eq. 2). This observation is consistent with the test results of a 45-foot square flat-plate structure (Guralnick and LaFraugh, 1963).

4.1 Effect of Externally Installed CFRP Stirrups

Comparing the behavior of LRstG0.5 with that of LG0.5 shows that the externally installed CFRP stirrups improved the punching shear strength and deformation capacity of an earthquake-damaged connection. A tightly knit array of CFRP stirrups shifted the failure surface away from the column (increased the critical shear perimeter) and also engaged more flexural reinforcement into the punching cone for improved dowel resistance following a punching shear failure. Therefore, the CFRP stirrups increased the punching shear capacity and residual capacity after punching shear failure. A peak shear stress of $2.93\sqrt{f'_c}$ on the critical perimeter $d/2$ away from the column face was inferred from measurements. On the critical section $d/2$ away from the CFRP-reinforced zone, the shear strength of concrete was equal to $1.83\sqrt{f'_c}$, which is equivalent to 53% of the capacity calculated using Eq. 1.

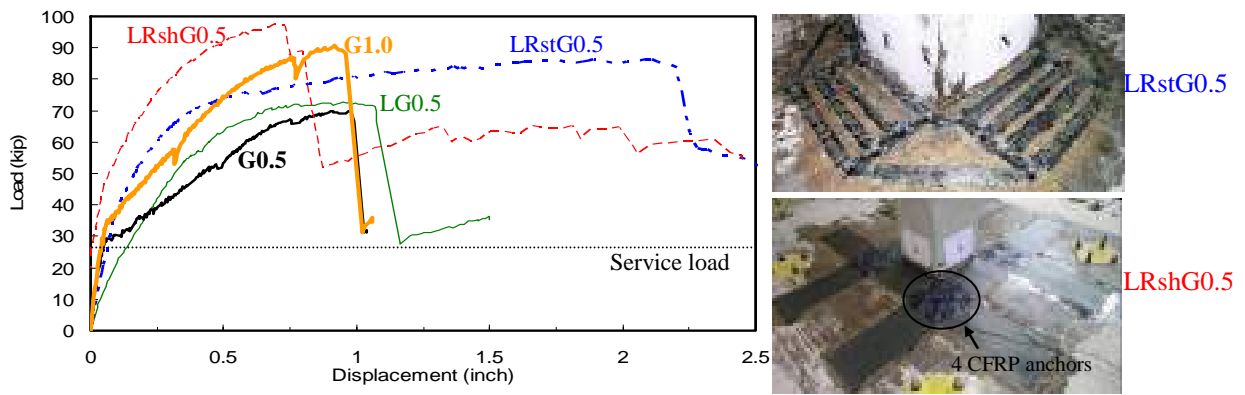


Figure 2: Test results

4.2 Effect of Well-anchored CFRP Sheets

Comparing the behavior of LRshG0.5 with that of LG0.5 shows that the installation of well-anchored CFRP sheets on the tension side of the slab improved the punching shear strength of an earthquake-damaged connection. Table 1 shows that the CFRP installation improved the punching shear strength of the connection by 38% (from $2.47\sqrt{f'_c}$ to $3.41\sqrt{f'_c}$). The area of the CFRP sheets was selected to match the flexural capacity of a connection with 1.0% steel within $(c+3h)$ region. Figure 2 shows that the ultimate capacity of LRshG0.5 was about the same as that of G1.0, implying that external CFRP sheets were just as effective as the steel reinforcement. Four CFRP anchors per column corner (Figure 2) were very effective in preventing early delamination. At failure, the CFRP sheets close to the middle of the column face ruptured (causing significant decrease in load-carrying capacity as shown in Figure 2), whereas the sheets elsewhere were still attached to the slab. After punching shear failure occurred, the well-anchored CFRP sheets acted as tension bands and allowed the slab to carry substantial shear force through larger deformations. The CFRP sheets did not change the location of the failure surface but limited the width of flexural cracks (that occurred due to simulated seismic displacements) so that the area of concrete resisting shear was maintained and the connection was able to carry more load before a punching shear failure occurred.

5. CONCLUSIONS

Two-way shear strength was sensitive to the slab top reinforcement ratio within $(c+3h)$. Two-way shear strength of the undamaged control specimens with 0.5% and 1.0% top reinforcement ratio was only 63% and 85% of that estimated using ACI 318-05 expression ($V_c = 4 \times \sqrt{f'_c} \times b_o \times d$). Both the installation of the external CFRP stirrups and the application of the well-anchored CFRP sheets on the tension surface of the slab increased the two-way shear strength of the earthquake-damaged slab-column connections and improved the residual capacity after punching shear failure. CFRP anchors were very effective in preventing early delamination of CFRP sheets.

6. REFERENCES

- Binici, B. (2003). "Punching shear strengthening of reinforced concrete slabs using fiber reinforced polymers", Ph.D. dissertation, University of Texas at Austin, Texas, USA.
- Guralnick, S.A., and LaFraugh, R.W. (1963). "Laboratory study of a 45-foot square flat plate structure", *Journal of the American Concrete Institute*, Vol. 60, pp 1107-1185.
- Marzouk, H., and Hussein, A. (1991). "Experimental investigation on the behavior of high-strength concrete slabs", *ACI Structural Journal*, Vol. 88, No. 6, pp 701-713.
- Widianto, Tian, Y., Argudo, J., Bayrak, O., and Jirsa, J.O. (2006). "Rehabilitation of earthquake-damaged reinforced concrete flat-plate slab-column connections for two-way shear", *8th US National Conference on Earthquake Engineering*, San Francisco, California, April 18-22, 2006.

Part XX. Seismic Applications

SEISMIC RETROFIT OF LARGE SCALE CIRCULAR RC COLUMNS WRAPPED WITH CFRP SHEETS

G. Wu

Associate professor, College of Civil Engineering, Southeast University, Nan Jing, China

Z.S. Wu

*Professor, Department of Urban & Civil Engineering, Ibaraki University, Hitachi, Japan
Cheung Kong Scholar, College of Civil Engineering, Southeast University, Nan Jing, China*

Z.T. Lü

Professor, College of Civil Engineering, Southeast University, Nan Jing, China

D.S. Gu

Doctoral Candidate, College of Civil Engineering, Southeast University, Nan Jing, China

ABSTRACT

An experimental investigation was conducted to study the seismic behavior of large scale circular reinforced concrete columns strengthened with carbon fiber reinforced polymer (CFRP). Results from the experimental program are presented in which five 360mm diameter and 1000mm long columns were tested under constant axial load and reversed cyclic lateral load that simulated forces from an earthquake. Each specimen consisted of a column cast integrally with a 1550mm×600mm×700mm stub that represented a beam-column joint area or a footing. The results indicate that the failure models of FRP-wrapped circular RC columns may be shear failure or flexural failure and the cyclic behavior progressively improved as the number of CFRP layers increased. New methods for predicting shear and flexural capacities of FRP-wrapped circular RC columns under seismic loading were proposed.

KEYWORDS

Columns, Concrete, CFRP, Seismic loading, Strength

INTRODUCTION

It is well known that column performance in the inelastic mode is of utmost importance for the safety of a structure during an earthquake. FRP composites has a lot of advantages and has already been widely used for improving the seismic performance of circular reinforced concrete columns. As a result, numerous papers on various aspects related to the subject have been published recently. Most of the work on FRP-wrapped columns was undertaken on small cylinders or columns mainly subjected to axial loading. A very limited amount of experimental data exists on the seismic behavior of realistically sized circular concrete columns confined with CFRP wraps. This research investigates the seismic performance of near full-scale CFRP-retrofitted columns typical of existing buildings and highways. The main variable of the study was the layers of CFRP. New methods for predicting shear and flexural capacities of FRP-wrapped circular RC columns under seismic loading are proposed.

EXPERIMENTAL PROGRAM

Specimens

Five large-scale circular reinforced concrete columns were constructed. Each specimen consisted of a circular column of 360mm diameters cast integrally with a stub of dimensions 1550mm×600mm×700mm. All columns contained fourteen D25mm longitudinal bars uniformly distributed around the core. The D6mm ties were placed at a spacing of 150 mm within the test region. Reinforcement of columns is shown in Fig.1. Properties of steel bars are given in Table 1. One unwrapped column was used as control specimen to evaluate the effects of FRP retrofitting.

Four of these columns were strengthened with CFRP wraps. The main variable of the study was the number of CFRP layers. The region of 100mm from the stub face was strengthened with additional eight D25mm bars, and the D10mm ties were placed at a spacing of 30 mm within this region to minimize the chances of failure at the section of the stub face. All the specimens were tested under constant axial load and cyclic lateral excursions simulating seismic loading conditions. A commercially available CFRP wrap system was used to retrofit the designated specimens. The thickness of one layer of CFRP sheet was 0.167 mm, the average tensile strength, the modulus of elasticity and the tensile rupture strain were 3945MPa, 249.6GPa and 1.52% respectively.

Table 1 Details of test specimens

Specimen	f'_c (MPa)	CFRP treatment	Axial load (kN)	Longitudinal steel				Transver steel				ρ_f (%)
				No.	D_s (mm)	F_y (MPa)	F_{ult} (MPa)	D_s (mm)	S (mm)	F_y (MPa)	F_{ult} (MPa)	
CL0	34.9	Control	1200	12	25	382.4	571.1	6	150	319.8	474.4	0
CL1	34.9	1.0 layer	1200	12	25	382.4	571.1	6	150	319.8	474.4	0.093
CL2	34.9	2.5layers	1200	12	25	382.4	571.1	6	150	319.8	474.4	0.2325
CL3	34.9	3.5layers	1200	12	25	382.4	571.1	6	150	319.8	474.4	0.3255
CL4	34.9	4.5layers	1200	12	25	382.4	571.1	6	150	319.8	474.4	0.4185

Testing

The specimens were tested as shown in Fig. 2. The axial load was applied through a hydraulic jack having the capacity of 3000 kN and was measured using a load cell of similar capacity. To apply reverse lateral load, an actuator with a load capacity of 1000 kN and a stroke capacity of ± 150 mm was used. The load cycles were divided into two phases: load control and displacement control. Load control phase was used up to yielding of the longitudinal bars, beyond that point, a displacement control sequence was used.

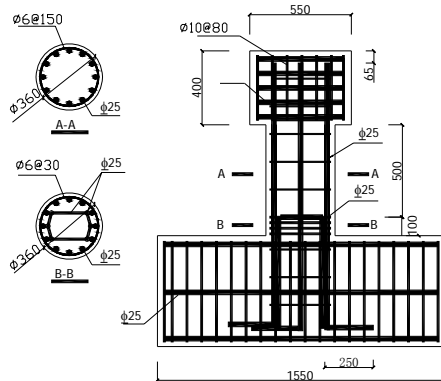


Fig.1 Reinforcement of columns

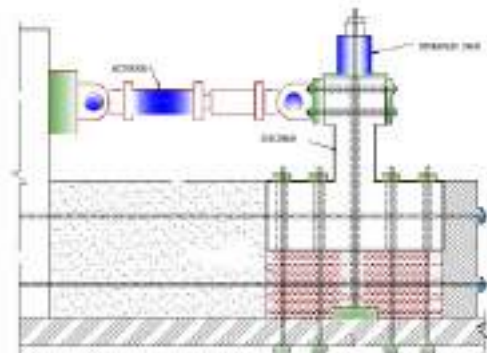


Fig.2 Test setup

Table 2 Test results

Specimen	CFRP treatment	F_y (kN)	Δ_y (mm)	F_{max} (kN)	Δ_u (mm)	Δ_u / Δ_y	Failure modes
CL0	Control column	380	-	424.9	6.0	-	Shear failure
CL1	1 layer CFRP	400	5.6	569.1	24.0	4.3	Shear failure, FRP rupture
CL2	2.5 layers CFRP	360	6.5	634.4	48.0	7.4	Flexural failure, FRP rupture
CL3	3.5 layers CFRP	400	6.2	664.8	48.0	7.7	Flexural failure, FRP rupture
CL4	4.5 layers CFRP	400	7.1	679.8	48.0	6.8	Flexural failure, FRP rupture

Analysis of results

The test results are shown in Table 2. The curves of applied lateral load versus displacement are shown in Fig.3. The maximum lateral load of the control column was 424.9kN, and it was controlled by shear failure. The Column CL1

strengthened with one layer CFRP, the maximum lateral load of the Column CL1 strengthened with one layer CFRP sheet was 569.1kN, 33.9% higher than the control column. Examination of lateral load indicates that columns strengthened with more than 2.5 layers CFRP attained F_{max} that were 49.3% to 60% higher than the F_{max} for the control column. And all these columns had good ductility and failed by flexure. The results also showed that the maximum lateral loads were improved with the increase the layers of CFRP, while the ultimate lateral displacements were almost the same for the Columns CL2, Column CL3 and Column CL4 due to flexural capacities of specimens. It is worth being researched further.

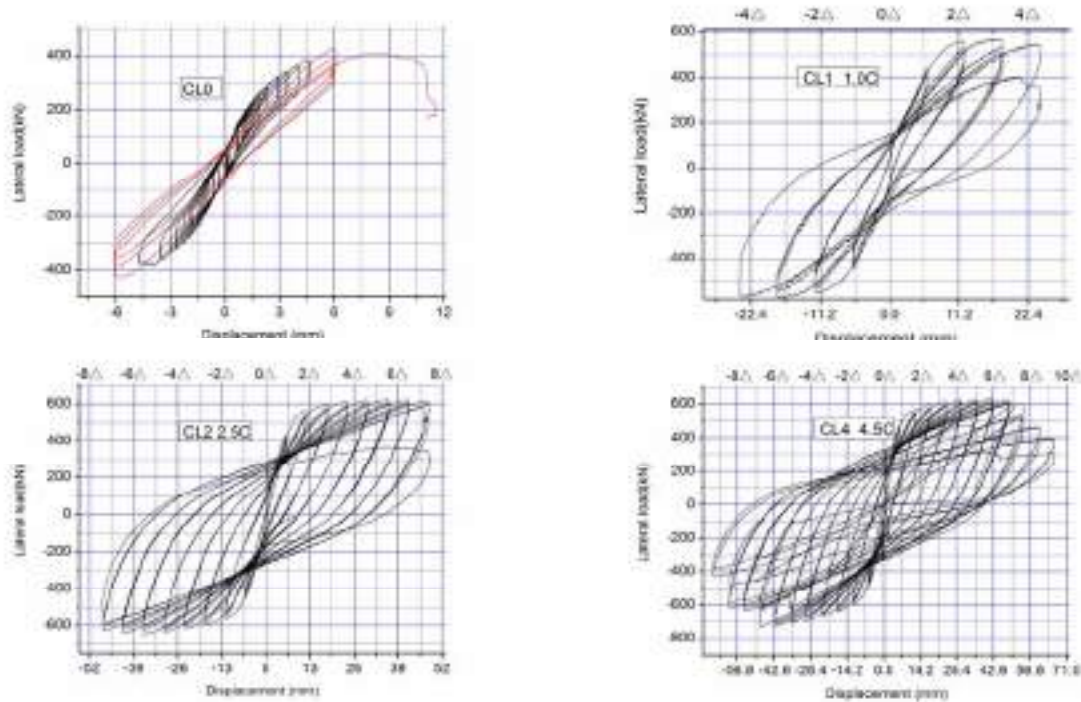


Fig. 3 Lateral load-displacement responses

SHEAR CAPACITY OF CFRP-WRAPPED COLUMNS

Existing researches show that it is difficult to accurately estimate the contribution of FRP sheets to the shear capacity V_f of beams. Detailed investigations on the strengthening of RC members against shear using externally bonded FRP sheets have been relatively limited and, to a certain degree, controversial. Due to the lack of adequate test data, it is difficult to standardize a design equation that takes into account all of the factors affecting V_f .

Many parameter were not considered by the existing models(Nanni 2002; Triantafillou 2000; Chaallah 2004): (1) most of existing models for predicting V_f were suggested based on the test data of concrete beams; (2) the influence of axial load on the ultimate effective strain of FRP sheet was not analogized; (3) some methods were suggested to estimate the contribution of FRP sheets to the shear capacity of rectangular columns, while few on circular RC columns; and (4) the improvement of the confinement of FRP on concrete strength was not considered on the contribution of concrete to the shear capacity.

The following assumptions are made: (1) if the stress-strain curve of FRP-confined concrete circular columns has no strain-softening response, the influence of the confinement of FRP on concrete strength will be considered on the contribution of concrete to the shear capacity; (2) the nominal shear strength of RC columns strengthened using externally bonded FRP sheets can be computed accumulating the contribution of concrete, steel stirrup and CFRP composites; (3) the shear contribution of concrete and steel stirrup can be predicted by the model suggested by Ghae et al.(1989); and (4) the efficiency factor of the ultimate effective strain of CFRP sheet can be temporarily taken as 0.58 according to the Lam&Teng (2003)'s research based on the analysis of CFRP-wrapped circular columns.

Table 3 shows that calculated shear forces of V_{cv} predicted by this paper compare well with the test results.

Table 3 Predicted and experimental values of columns (Unit: kN)

Spec.	CFRP Treatment	V_c	V_s	V_f	$V_{max,t}$	V_{cv}	$V_{cv}/V_{max,t}$	Failure modes
CL0	No CFRP	357.6	31.7	0	424.9	389.3	0.92	Shear failure
CL1	1.0 layers	359.5	31.7	169.9	569.1	561.1	0.99	Shear failure, FRP rupture

FLEXURAL CAPACITY OF CFRP-WRAPPED COLUMNS

A finite element model is developed for the sectional analysis of CFRP-confined columns. The model satisfies force equilibrium and strain compatibility, and utilizes uniaxial constitutive models of concrete and FRP. The following assumptions are made: (1) plane sections remain plane after bending; (2) perfect bond exists between concrete and FRP tube; (3) FRP only provides lateral confinement, without any stiffness in the longitudinal direction; (4) the stress-strain relationship of concrete in compression is defined by Wu et al. (2003; 2006) models; (5) the tensile strength of concrete is ignored; (6) the steel reinforcing bars are elastic-perfectly plastic; (7) any confinement effect of steel hoop reinforcement is ignored; and (8) the ultimate limit state is reached when the strain of the extreme compression fiber of concrete attains the ultimate strain.

Table 4 shows the calculated flexural capacities of V_{cf} predicted by this paper compare well with the test results.

Table 4 Predicted and experimental values of columns

Specimen	CFRP treatment	$V_{max,t}$	V_{cf}	$V_{cf}/V_{max,t}$	Failure modes
CL2	2.5 layers	634.4	536	0.85	Flexural failure, FRP rupture
CL3	3.5 layers	664.8	546	0.82	Flexural failure, FRP rupture
CL4	4.5 layers	679.8	557	0.82	Flexural failure, FRP rupture

SUMMARY AND CONCLUSIONS

The effectiveness of CFRP confined large scale circular column was verified. The seismic behavior of columns progressively improved as the number of CFRP layers increased. The new design methods suggested by this paper can be used to predict the shear and flexural capacities of FRP-wrapped circular RC columns under seismic loading well.

ACKNOWLEDGMENTS

The project sponsored by the Scientific Research Foundation for the Returned Overseas Chinese Scholars, State Education Ministry. The authors also would like to thank the support from Scientific Research Foundation from Qing Hai Science & Technology Department of China (2005G155) and Nanjing Construction Committee of China.

REFERENCES

- A. Khalifa and A. Nanni (2002). "Rehabilitation of rectangular simply supported RC beams with shear deficiencies using CFRP". *Construction and Building Materials*, Vol.16 : 135 -146.
- T.C. Triantafillou and C.P. Antonopoulos (2000) .“Design of Concrete Flexural Members Strengthened in Shear with FRP”. *Journal of Composites Construction*, ASCE, Vol.(4), No. 4, pp. 198-205.
- A.Bousselham and O. Chaallal (2004). "Shear Strengthening Reinforced Concrete Beams with Fiber-Reinforced Polymer: Assessment of Influencing Parameters and Required Research", *ACI Structural Journal* , Vol.(101), No .2, pp.219 - 227.
- G. Wu, Z.T. Lu" and Z.S. Wu, (2006). "Strength and ductility of concrete cylinders confined with FRP composites", *Construction and Building Materials* ,Vol,20, pp.134–148.
- G. Wu, Z.T. Lu and Z.S. Wu, (2003). "Stres-strain relationship for FRP-confined Concrete Cylinders".*Proceedings of the sixth International Symposium on FRPRCS*, pp.552-560.
- L. Lam and J.G. Teng, (2003). "Hoop rupture strains of FRP Jackets in FRP Confined Concrete".*Proceedings of the sixth International Symposium on FRPRCS*, pp. 601-612.
- S.A. Sheikh and G. Yau, (2002). "Seismic Behavior of Concrete Columns Confined with Steel and Fiber-Reinforced Polymers". *ACI Structural Journal*, Vol.99, No.1, pp.72-80.
- J.B.Mander, M.J.N. Priestley, and R.Park.(1988).“Theoretical Stress-strain Model for Confined Concrete ”. *Journal of Structural Engineering*, ASCE, Vol.114, No.8, pp.1804-1826.
- A.B. Ghae, M.J.N. Priestley and T. Paulay.(1989). "Seismic Shear Strength of Circular Reinforced Concrete Columns". *ACI structural Journal*, Vol.(86),No.1, pp. 45-59.

SEISMIC RETROFITTING OF REINFORCED CONCRETE COLUMNS BY CONTINUOUS FIBER ROPE WITH CONCRETE JACKET

Takumi Shimomura

(Associate Professor, Nagaoka University of Technology, Nagaoka, Niigata, Japan)

Nguyen Hung Phong

(Former Graduate Student, Nagaoka University of Technology, Nagaoka, Niigata, Japan)

Akihiro Matsumoto

(Former Graduate Student, Nagaoka University of Technology, Nagaoka, Niigata, Japan)

Kenzo Sekijima

(Tokyo Branch, Kurasoku Kensetsu Consultant Co.Ltd., Tokyo, Japan)

Kyuichi Maruyama

(Vice President, Nagaoka University of Technology, Nagaoka, Niigata, Japan)

ABSTRACT

A new seismic retrofitting method for existing reinforced concrete columns using continuous fiber rope, CF rope, coupled with concrete jacket is developed. CF rope is enough flexible to be easily arranged in structural members by hand and, apart from other FRP materials for concrete such as FRP rod, grid and sheet, CF rope is applied without epoxy resin. This paper presents tests of reinforced concrete column specimens retrofitted with CF rope. Aramid and vinylon CF rope was wound continuously around the column periphery. Instead of epoxy resin, concrete jacket was cast to bond CF rope with the original member and to protect CF rope from environmental attacks. The column specimens were tested under reversed cyclic load. It was experimentally verified that the proposed retrofitting method can successfully increase seismic resistance of the member.

KEYWORDS

continuous fiber rope, seismic retrofitting, ductility, concrete jacketing

1. INTRODUCTION

Continuous fiber materials, such as carbon fiber sheet, are often used in strengthening existing concrete structures. This paper introduces a new seismic retrofitting method for existing reinforced concrete piers and columns using continuous fiber material made in the form of rope. This retrofitting method is a very simple handling method since it makes use of continuous fiber rope, CF rope. CF rope is distinguished from other types of continuous fiber reinforcement for concrete, such as rod, grid and sheet, by its non-epoxy usage. In the previous research, the authors have verified that CF rope can be used as shear reinforcement initially embedded in concrete (Phong et al., 2005). In the present study, CF rope is applied on the surface of existing RC column with concrete jacket. A series of reinforced concrete column specimens are strengthened by this method and tested under reversed cyclic load. Based on the experimental results, load-carrying characteristics and failure behavior of the column specimens are investigated and the effectiveness of CF rope in ductility improvement is verified. Test results are compared with those of RC columns retrofitted with CF sheet that had been done by the authors (Maruyama et al., 2003).

2. CONTINUOUS FIBER ROPE

Two types of CF rope made of aramid and vinylon fiber are used in this study. The CF ropes consist of several bundles of fiber twisted together. Without epoxy resin, CF rope is enough flexible to be easily arranged and adapted to various shapes of existing structural RC members. Tensile properties of the CF ropes were determined based on the uniaxial tensile test that had been developed for this material (Phong et al., 2005). Five test pieces were tested in total for each type of CF rope. Test results are presented in Table 1. The nominal cross sectional area of CF rope was determined by dividing the weight of 1m long of rope by the density of fiber.



Figure 1: Continuous Fiber Rope

Table 1: Tensile Properties of CF ropes

Name of CF rope	Type of fiber	Cross sectional area (mm ²)	Tensile strength (MPa)	Elastic modulus (MPa)	Ultimate strain (%)
CF rope 1	aramid	17.19	1660	53300	3.1
CF rope 2	vinylon	12.66	734	15857	4.6

3. RETROFITTING METHOD FOR EXISTING RC COLUMNS

3.1 The Original Column Specimens

The series of test specimens consists of four identical RC columns. Specimen No.0 is a control specimen without being retrofitted, while three other specimens were to be retrofitted with CF rope and concrete jacket. The column specimens were designed to fail in shear mode. Details of the original column specimens before retrofitting are shown in Figure 2. Compressive strength of concrete and yielding strength of steel reinforcement were 26 MPa and 384 MPa, respectively.

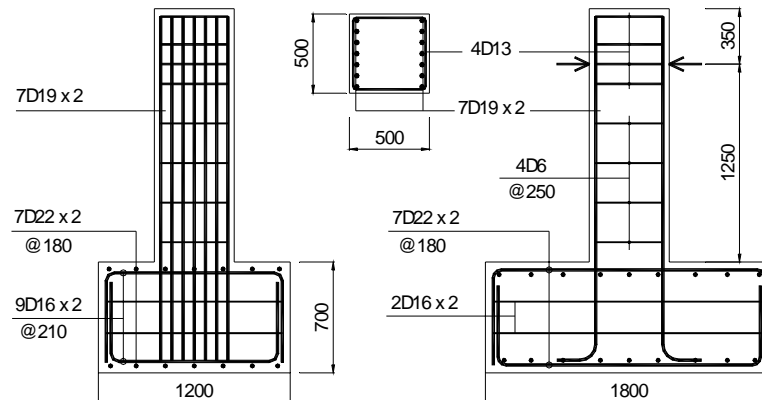


Figure 2: Details of the Original Column Specimens

3.2 Retrofitting Procedure

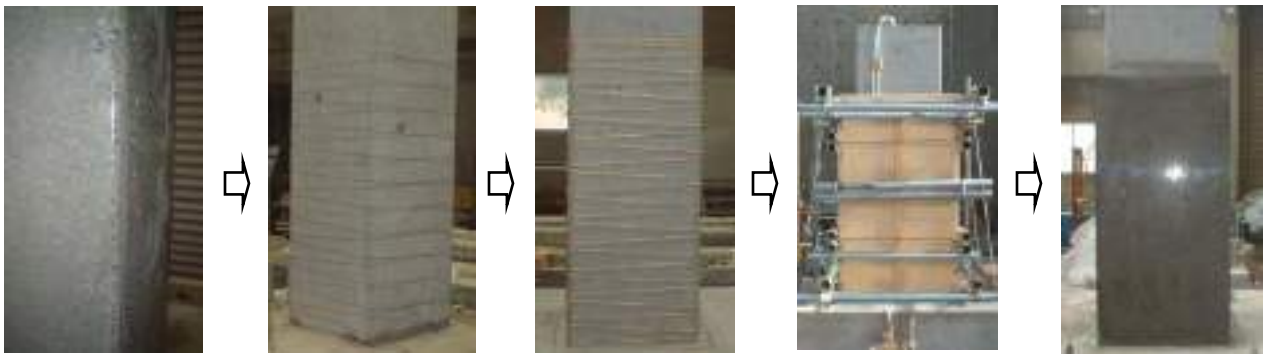
Winding CF rope

Before winding rope, surface of the columns was ground by a grinding machine to ensure bonding between the original concrete in column and the concrete jacket. The corners of the columns were rounded also by a grinding machine to prevent stress concentration in CF rope. Then, CF rope was wound by hand around the outside periphery of the columns. The rope was wound in a closed line: firstly from top to bottom of column and then back from bottom to top. The ends of rope were anchored simply by making a knot. No epoxy resin was used to bond or anchor CF rope on the concrete surface.

Concrete jacketing

After winding rope, formworks were set around the column and concrete whose maximum aggregate size was 13 mm was cast between the column and the formwork as a concrete jacket of 40 mm thickness. Concrete jacket was

cast from the footing up to the height close to the loading point of the column. Retrofitting procedure is shown in Figure 3. Concrete jacket is expected to have multi functions, which are to assure bonding between original concrete and CF rope, to protect CF rope from collision and environmental attack under service, and to make exterior of the member beautiful. Details of the retrofitted column specimens are presented in Table 2. Compressive strength of concrete used in jacket was examined on the day of the loading test of the column specimen.



Grinding Surface → Marking Rope Positions → Winding Rope → Setting Formworks → Jacketing

Figure 3: Retrofitting Procedure

Table 2: Details of the Retrofitted Column Specimens

Specimen	No.1	No.2	No.3
Type of CF rope	CF rope 1	CF rope 1	CF rope 2
Spacing of CF rope (mm)	100 x 2	200 x 2	60 x 2
Strength of concrete jacket (MPa)	26	22	25

4. REVERSED CYCLIC LOADING TEST

4.1 Test Setup and Method

The column specimens were tested under reversed cyclic load to examine their seismic resistance. Firstly, they were loaded until the yielding of the longitudinal reinforcement was observed. The displacement of the column at the loading point at this stage was defined as the yield displacement (δ_y). Then, reversed cyclic load was applied incrementally under deformation control, such as $+1\delta_y$, $-1\delta_y$, $+2\delta_y$, $-2\delta_y$, $+3\delta_y$, $-3\delta_y$. At each deformation step, three cycles of loading were repeated. Failure of the member is defined when its bearing capacity is reduced to 80% of the maximum load.

4.2 Test Results and Discussions

Load – deflection characteristics

Test results of the four column specimens are shown in the first four columns in Table 3. The second row of the table indicates retrofitting ratio of rope or sheet, taking into account their tensile strength. In the last row, ductility ratio of column is defined as the ratio of the maximum displacement and the yield one. An example of the load-deflection curve of the column is shown in Figure 4. For comparison, test results of RC column specimens retrofitted with CF sheet in the previous research by the authors (Maruyama et al., 2003) are also shown in Table 3. These specimens, having the same dimensions and concrete strength with the specimens in this study, were wrapped by CF sheet bonded to concrete surface by epoxy resin.

The maximum load of the column specimens in this study is governed by the yielding of longitudinal reinforcement in spite of retrofitting of CF rope. On the other hand, the maximum displacements are significantly different for the four specimens; the member ductility is improved by retrofitting of CF rope and concrete jacket. The obtained ductility ratio depends on the amount of CF rope retrofitted. Comparing the specimens with approximately the same CF ratio, Column No.2 and No.3, the specimen with smaller rope spacing, Column No.3, had higher ductility ratio.

Table 3: Test results of RC columns retrofitted with CF rope and CF Sheet

Retrofitting method	none	CF rope			CF Sheet	
	No.0	No.1	No.2	No.3	n5	n6
Type of fiber	–	aramid	Aramid	vinylon	aramid	aramid
CF ratio x tensile strength (MPa)	–	228	114	124	64.0	129
Maximum load (kN)	304	309	315	315	297	294
	-263	-300	-296	-300	-287	-303
Maximum displacement (mm)	13.0	55.2	15.9	32.1	20.7	44.0
	-13.3	-25.8	-15.9	-32.1	-21.2	-38.5
Ductility ratio	2	3.3-7	2	5	4	7

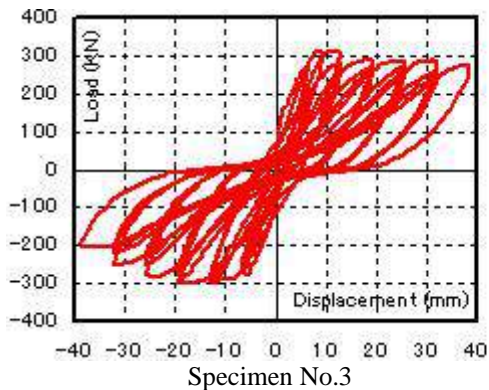


Figure 4: Load-Displacement Curves

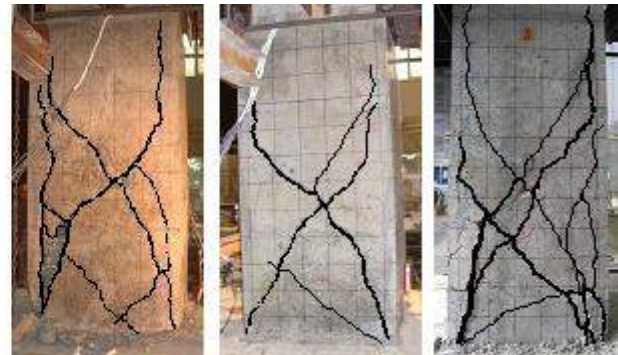


Figure 5: Crack Patterns at failure stage

Failure mode

Under the reversed cyclic load, cracks were formed in concrete jacket and bonding was lost gradually. The crack patterns of the specimens at failure state are shown in Figure 5. At the failure stage, most part of the jacket on the loading surfaces lost bonding with the original column concrete as well as CF rope and could easily be removed from the column. However, CF rope was not ruptured even at the failure stage in all the specimens with CF rope.

Similar to the case of the specimens retrofitted with CF sheet (Maruyama et al., 2003), it was also observed in this study that the specimens having more distributed cracks, specimen No.1 and No.3, show greater deformation capability or ductility. The difference between the case of CF sheet and CF rope lies in the fact that CF sheet was bonded to concrete surface by epoxy resin, while CF rope was covered with concrete jacket instead of epoxy resin. In the case of CF rope, bonding between rope and concrete was lost at the earlier stage than in the case of CF sheet. This is why strain of CF rope was uniformly distributed and CF rope was not ruptured at the failure stage of the specimen, whereas crush of concrete in compressive zone was observed.

6. CONCLUSIONS

A new seismic retrofitting method for existing RC columns using CF rope coupled with concrete jacket was developed. It was experimentally verified that seismic resistance of RC columns could be improved by this retrofitting method as effectively as CF sheet.

7. REFERENCES

- Maruyama, K. et al. (2003). “Ductility Improvement Mechanism of Concrete Columns by Wrapping of FRP Sheets”. Proceedings of the International Conference on Advances in Structures, Sydney, Australia, pp.1391-1397.
- Phong, N.H. et al. (2005). “Shear Strengthening Effectiveness of Continuous Fiber Rope in RC Members”. Proceeding of the Third International Structural Engineering and Construction Conference, Shunan, Japan, pp.57-64.

SEISMIC PERFORMANCE OF HYBRID FRP-CONCRETE PIER COLUMNS

Yilei Shi

(Ph.D. Student, Florida International University, Miami, FL, USA)

Bin Li

(Ph.D. Student, Florida International University, Miami, FL, USA)

Amir Mirmiran

(Professor and Chair, Florida International University, Miami, FL, USA)

M. Saiid Saiidi

(Professor, University of Nevada, Reno, NV, USA)

ABSTRACT

One of the most cost-effective applications of fiber reinforced polymers (FRPs) is in hybrid construction with concrete, where FRP provides the pour form, protective jacket, and shear and flexural reinforcement for concrete. Seismic performance of concrete-filled FRP tubes (CFFT) is the subject of this study. While previous studies have shown the feasibility of the proposed system both at the member level and at the connection level, especially under reverse cyclic loading, this study focuses on the following issues that have not been addressed before: (a) effect of the type of fibers and hybrid lay-up of the tube on the performance of the system, (b) effect of combined shear and moment, especially for shorter columns, (c) lateral performance of two-column bent systems, and (d) holistic performance of the entire bridge structure on shake tables. This paper reports on an on-going project to design the next generation of seismic-resistant bridge substructure, as part of a multi-university project, which is funded by the NSF-Network of Earthquake Engineering Simulation Research (NEESR) program.

KEYWORDS

Cyclic Loading, Fiber Reinforced Polymers, Hybrid Columns, Reinforced Concrete

1. INTRODUCTION

One of the most cost-effective applications of fiber reinforced polymers (FRPs) is in hybrid construction with concrete, where FRP provides the pour form, protective jacket, and shear and flexural reinforcement for concrete. Concrete-filled FRP tubes (CFFT) have been used in Virginia, California, and Florida (Zhu et al. 2006). Seible et al. (1996) studied the feasibility of carbon CFFT columns under simulated seismic actions, and concluded that CFFT without any starter bars would fail prematurely under combined compressive and inter-laminar shear stresses. On the other hand, when carbon tubes are augmented with ample number of starter bars, ductility of the column is increased significantly. A number of more recent studies (as cited in Zhu et al. 2006) have provided evidence as to the advantages of glass over carbon in providing additional ductility for the column. This may be attributed to the lower modulus of elasticity of glass FRP. Most recently, Zhu et al. (2006) showed construction feasibility and superior performance of cast-in-place or precast CFFT columns with reinforced or prestressed connections.

This paper describes an on-going project on the use of FRP tube to enhance seismic performance of reinforced concrete bridge substructure, as part of a multi-university project, which is funded by the NSF-Network of Earthquake Engineering Simulation Research (NEESR) program. The FRP component of the project includes three phases: (1) Single-column tests; (2) Two-column bent tests; and (3) Large-scale four-span bridge tests on shake tables. The focus of this study is to (a) compare the performance of glass, carbon, and hybrid FRP tubes, (b)

compare flexure-dominant versus shear-dominant behavior of CFFT columns, (c) lateral performance of two-column bent systems, and (d) holistic performance of the entire system on shake tables.

2. SINGLE COLUMN TEST PROGRAM

A total of six specimens are prepared in this stage with five CFFT columns and one control RC column. The formwork for the RC control specimen consisted of a 305 mm (12 in.) diameter sonotube, while the other five CFFT columns used FRP tubes as the cast-in-place formwork. One of the tubes was made by the industry using filament-winding of 17 layers of $\pm 55^\circ$ E-glass fibers and epoxy resin, with an inside diameter of 315 mm (12.4 in.) and a wall thickness of 5.1 mm (0.2 in.). The other four FRP tubes were prepared in the Structures and Construction Lab (SCL) at the Florida International University (FIU), by wrapping saturated FRP fabric around sonotubes of the same diameter as that used for the control RC specimen. The sonotubes were first covered with a layer of wax paper, so that the FRP can be easily detached later. All FRP tubes consisted of 152 mm (6 in.) overlaps in the hoop direction and 305 mm (12 in.) overlap in the longitudinal direction. Figure 1 illustrates the preparation of one carbon FRP tube.

Among the four FRP tubes made in SCL, one glass FRP tube was made with 3 layers of bi-directional glass fiber sheets. The cured laminate thickness per layer is 0.33 mm (0.013 in.). Two carbon FRP tubes with shear spans of 1,295 mm (51 in.) and 2,210 mm (87 in.), respectively, were made with 2 layers of bi-directional carbon fiber sheets. The cured laminate thickness per layer is 0.25 mm (0.01 in.). In the hybrid FRP tube, 3 layers of unidirectional glass fiber sheets were wrapped in the transverse direction over the two layers of unidirectional carbon fabric. It may be of interest to note that the layer numbers were designed based on equivalence comparison of the tensile, compressive and shear strengths of cured laminate properties of glass and carbon fabrics. Apart from the CFFT with carbon tube of 2,210 mm (51 in.) shear span (hence long column), all the other five columns have the same 1,295 mm (51 in.) shear spans (hence short columns). Figure 2 shows the five short specimens. Table 1 shows the test matrix of single column experiments.



Figure 1: Preparation of Carbon FRP Tube



Figure 2: Five Short Column Specimens

All six columns had the same longitudinal reinforcement of sixteen 10 mm (No. 3) steel bars of Grade 414 MPa (60 ksi) along the entire length of the columns, with adequate embedment into the footing and the column head. This corresponded to a 1.5% of reinforcement ratio. The RC column additionally featured a spiral reinforcement with 5.3 mm (0.207 in.) steel wire of Grade 414 MPa (60 ksi) with 279 mm (11 in.) outside diameter placed at a pitch of 32 mm (1.25 in.). CFFT columns had no transverse steel reinforcement, except for four or five 279 mm (11 in.) diameter hoops placed at a spacing of 305 mm (12 in.) only to hold the longitudinal reinforcement cage together before casting concrete. Figure 3 shows the column reinforcements of the RC and the long carbon column.

The FRP tubes were embedded 305 mm (12 in.) into the footings to provide sufficient development length, while the embedment into the column heads was only 152 mm (6 in.). Considering the horizontal testing configuration of the columns, the specimens were cast horizontally in two batches with 44.8 MPa (6.5 ksi) and 31.0 MPa (4.5 ksi) 28-day compressive strength. The ready-mix concrete achieved a slump of 254 mm (10 in.), equivalent of a pump mix, to ensure proper placement of concrete along the entire length of the tubes.

A pedestal was designed to accommodate the height of the reaction frame and the actuator, and also to span over the tie-down pattern. Each specimen is placed on top of the pedestal, and post-tensioned with eight threaded rods to the

strong floor through the pedestal and four threaded rods in the middle to the pedestal. All threaded rods are 25.4 mm (1 in.) diameter. Figure 4 depicts the test set-up of specimen CL, i.e., the long column with carbon FRP tube. Tests are currently in progress at FIU.

Table 1: Test Matrix of Single Column Experiments

Specimen Name	Shear Span mm (in.)	Core Diameter mm (in.)	f'_c MPa (ksi)	Longitudinal FRP	Transverse FRP
RC (Control)	1,295 (51)	310 (12.2)	44.8 (6.5)	None	
Y (Yellow tube)	1,295 (51)	315 (12.4)	44.8 (6.5)	17 Layers of $\pm 55^\circ$ E-Glass	
G (Glass)	1,295 (51)	318 (12.5)	44.8 (6.5)	3 Layers of Bi-directional Glass	
CS (Carbon, Short Column)	1,295 (51)	318 (12.5)	31.0 (4.5)	2 Layers of Bi-directional Carbon	
H (Hybrid)	1,295 (51)	318 (12.5)	31.0 (4.5)	2 Layers of Unidirectional Carbon	3 Layers of Unidirectional Glass
CL (Carbon, Long Column)	2,210 (87)	318 (12.5)	31.0 (4.5)	2 Layers of Bi-directional Carbon	

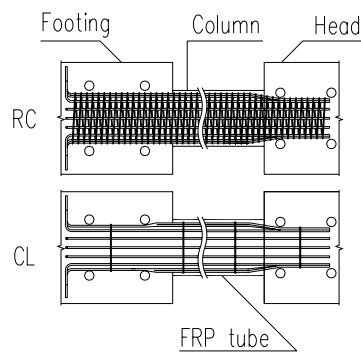


Figure 3: Column Reinforcement for RC and CL



Figure 4: Test Set-up for Carbon Long Column

3. TWO-COLUMN BENT TEST PROGRAM

A total of four (4) bent specimens are being prepared with three CFFT and one control RC (see Table 2). The three CFFT bents are made of yellow tube, carbon and hybrid FRP, which are the same as those described in the single column test program. In the bent specimens, the columns are 203 mm (8 in.) diameter, while the reinforcement is scaled down accordingly. The FRP tubes are made using the same technique as that described for the single column test program. The pier cap beams for all CFFT bents are cast into carbon FRP formwork, which in turn is made by wrapping bi-directional carbon FRP fabric onto a wooden mold. Figure 5 shows the bent specimen design. Figure 6 shows the test layout for the two-column bent specimens. The lateral load is transferred to the pier cap beam through an adapter and four rods outside of the pier cap beam. This phase is currently at the stage of specimen preparation.

Table 2: Test Matrix of Two-Column Bent Experiments

Specimens	Columns	Pier Cap Beam
RCF (Reinforced Concrete Frame)	RC	RC
CFF (Carbon FRP-Concrete Frame)	Carbon FRP	Carbon FRP
GFF (Glass FRP-Concrete Frame)	Glass FRP	Carbon FRP
HFF (Hybrid FRP-Concrete Frame)	Hybrid FRP	Carbon FRP

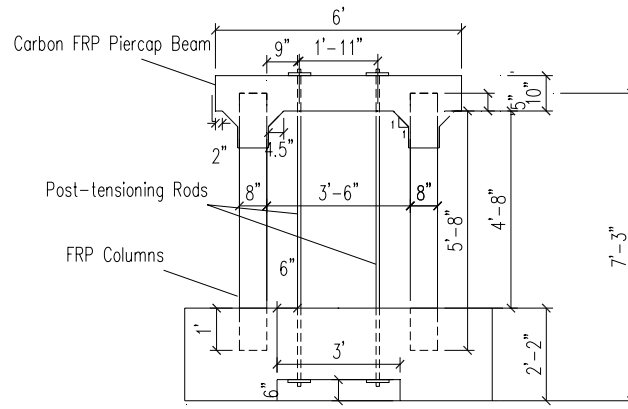


Figure 5: Two-Column Bent Specimen Configuration

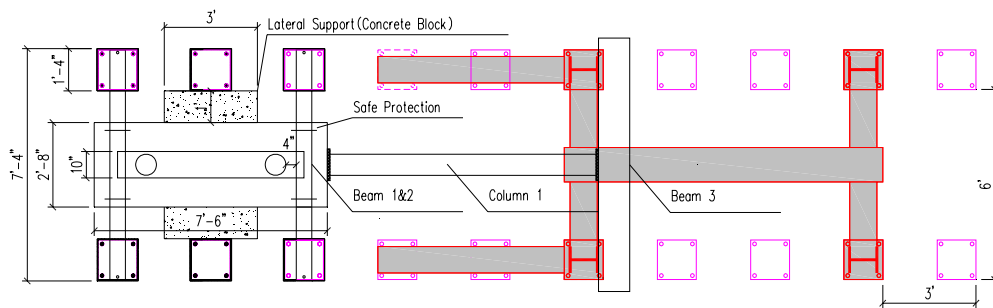


Figure 6: Plan View of Test Layout of Two-Column Bent Specimens

4. FOUR-SPAN BRIDGE MODEL TEST PROGRAM

A large-scaled four-span bridge model will be tested on three bi-directional shake tables at the University of Nevada, Reno to assess the holistic performance of the proposed system. Figure 7 shows the tentative layout of the shake table test of the bridge model.

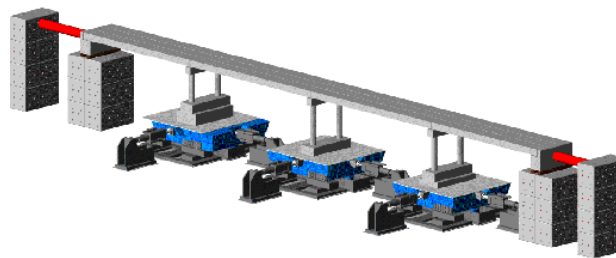


Figure 7: Tentative Layout of Shake Table Test of the Bridge Model

5. REFERENCES

- Seible, F., Burgueño, R., Abdallah, M. G., and Nuismer, R. (1996). "Development of advanced composite carbon shell systems for concrete columns in seismic zones", *Proceedings of the 11th World Conference on Earthquake Engineering*, Pergamon, Elsevier Science Ltd. Oxford, England, Paper No. 1375.
- Zhu, Z., Ahmad, I., Mirmiran, A. (2006). "Seismic Performance of Concrete-Filled FRP Tube Columns for Bridge Substructure", *Journal of Bridge Engineering*, ASCE, Vol. 11, No. 3, pp 359-370.

Experimental study of FRP wrapping for RC bridge under seismic loads

Éric St-Georges

(Teknika-HBA, Granby, Québec, Canada)

Nathalie Roy

(Ph.D. candidate, Université de Sherbrooke, Sherbrooke, Québec, Canada)

Pierre Labossière

(Professor, Université de Sherbrooke, Sherbrooke, Québec, Canada)

Jean Proulx

(Professor, Université de Sherbrooke, Sherbrooke, Québec, Canada)

Patrick Paultre

(Professor, Université de Sherbrooke, Sherbrooke, Québec, Canada)

ABSTRACT

An ongoing research project at Université de Sherbrooke has shown that fibre reinforced polymers (FRPs) enhance ductility as well as flexural capacity and shear resistance. An experimental program was completed on six 2.15-m high column specimens which were tested under combined axial and cyclic lateral loads. The objective of the experimental project presented herein was to test a new strengthening configuration of reinforced-concrete bridge columns using FRP wrapping. The retrofitted columns were subjected to cyclic lateral loads with two varying axial load levels representative of service conditions for bridges and for building, respectively, as well as two wrapping configurations, one based on “conventional” design and the other on displacement-based design. The results are analysed in this paper in order to: (i) evaluate the extent of seismic-related damages in FRP retrofitted bridge columns; (ii) compare the resistance and ductility of each column, before and after the retrofit; and (iii) compare the efficiency of conventional and performance-based wrapping configurations. The paper provides a description of the specimens, rehabilitation techniques, and testing apparatus. Results for three of the six columns under service axial load conditions representative of bridge piers are presented and discussed.

KEYWORDS

CFRP, reinforced concrete bridge column, cyclic loading, performance-based design, seismic retrofit

1. INTRODUCTION

This study is part of a bridge pier seismic retrofit project currently underway at the Earthquake Engineering and Structural Dynamics Research Centre (CRGP) of the Université de Sherbrooke. The objectives are to optimize a retrofitting methodology of bridge columns with carbon fiber reinforced polymers and to evaluate the increase in earthquake resistance by means of reverse-cyclic testing.

2. EXPERIMENTAL PROGRAM

Cyclic tests were performed on six large scale circular columns with properties similar to typical piers of short-span bridge located in eastern Canada. The 2.15-m high columns have a 300-mm diameter and are embedded in a massive stub that was anchored to a strong floor for the tests. The columns were cast vertically with a 30-MPa compressive strength concrete. The specified steel yield strength for the longitudinal reinforcement and the

transverse reinforcement is 400 MPa. The longitudinal reinforcement volumetric ratio, $\rho_l=2.5\%$, and the transverse reinforcement volumetric ratio, $\rho_h=0.8\%$, are typical of columns that were designed and constructed before recent modifications to code requirements for minimum transverse reinforcement. The columns are thus expected to dissipate very little energy during seismic events. The axial force (corresponding to $0.1A_g f'_c$ and $0.35A_g f'_c$) was applied by means of 2 hydraulic actuators (see test setup on figure 1) and was maintained constant during the test. Prescribed displacement histories were imposed on the column by means of a 500-kN double-acting displacement-controlled dynamic-rated servo-hydraulic actuator reacting on a large-capacity vertical reaction wall. For the first cycle, whose purpose was to crack the member and obtain elastic characteristics, the horizontal load reached 75% of the expected yield load. The second cycle reached the yield load and the yield displacement. Each subsequent cycle was repeated twice with a maximum displacement equal to 1.5, 2, 3, ..., times the measured yield displacement up to failure. The columns were fully instrumented with strain gauges. One set of four linear variable displacement transducers (LVDTs) and two sets of four potentiometers were placed in the plastic hinge region on steel rings at respectively 25 mm, 325 mm and 625 mm from the bottom of the column.

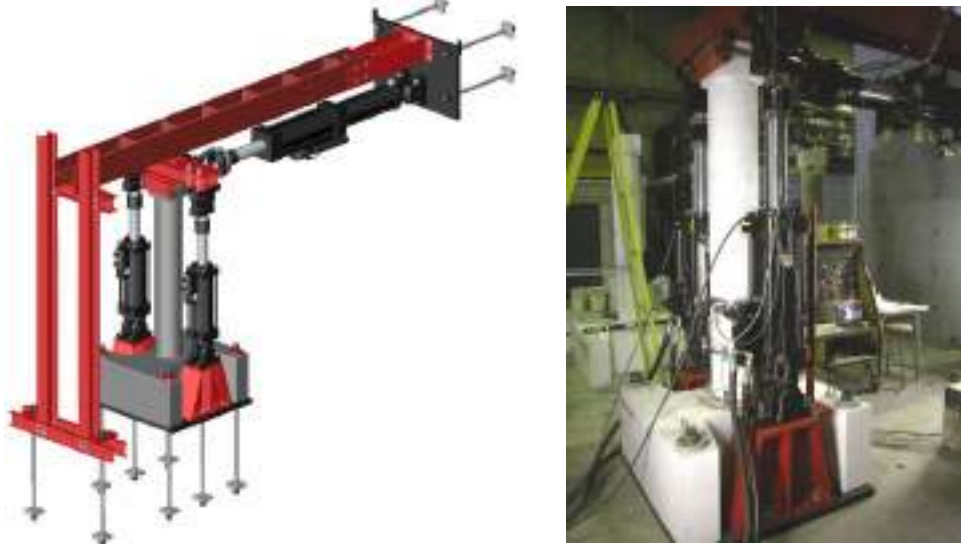


Figure 1: Test Setup

2.1 Performance Based vs Conventional Confinement

The performance-based retrofitting methodology of bridge columns with CFRP optimized in this project was reported by Tian and Chaturvedi, 2004 and is based on performance criteria. In this project, the performance criteria were the following: the retrofitted structure must meet prescribed ductility and drift requirements corresponding to given seismic events having respectively low (1/2500 p.a.), medium (1/475 p.a.) and high (1/100 p.a) probability of exceedance. The capacity spectrum method was utilized for this approach and the non-linear behavior of the columns was accounted for. The conventional methodology consisted of a simplified relationship between ductility capacity and column aspect ratio suitable for force-based design of simple structures proposed by Priestley et al., 1996. The calculations to meet the required ductility level in each case led to two levels of confinement that corresponds to: a) 2 layers of CFRP for the performance-based approach ($\mu_\Delta = 3.5$), and b) 4 layers of CFRP for the conventional approach ($\mu_\Delta = 5.0$). The confinement was limited to a 635-mm length corresponding to twice the estimated plastic hinge length. Table 1 contains the details of the experimental program for the three columns tested under an axial load of $0.1A_g f'_c$ which corresponds to typical service load for bridge piers.

Table 1: Description of Specimens

Specimen	Axial load ($\% A_g f'_c$)	# layers of CFRP
S1	10	0
S2	10	2
S3	10	4

3. TEST RESULTS

The left column of figure 2 shows the appearance of the specimens at the end of the test and the lateral load-tip deflection responses are presented in the column on the right.

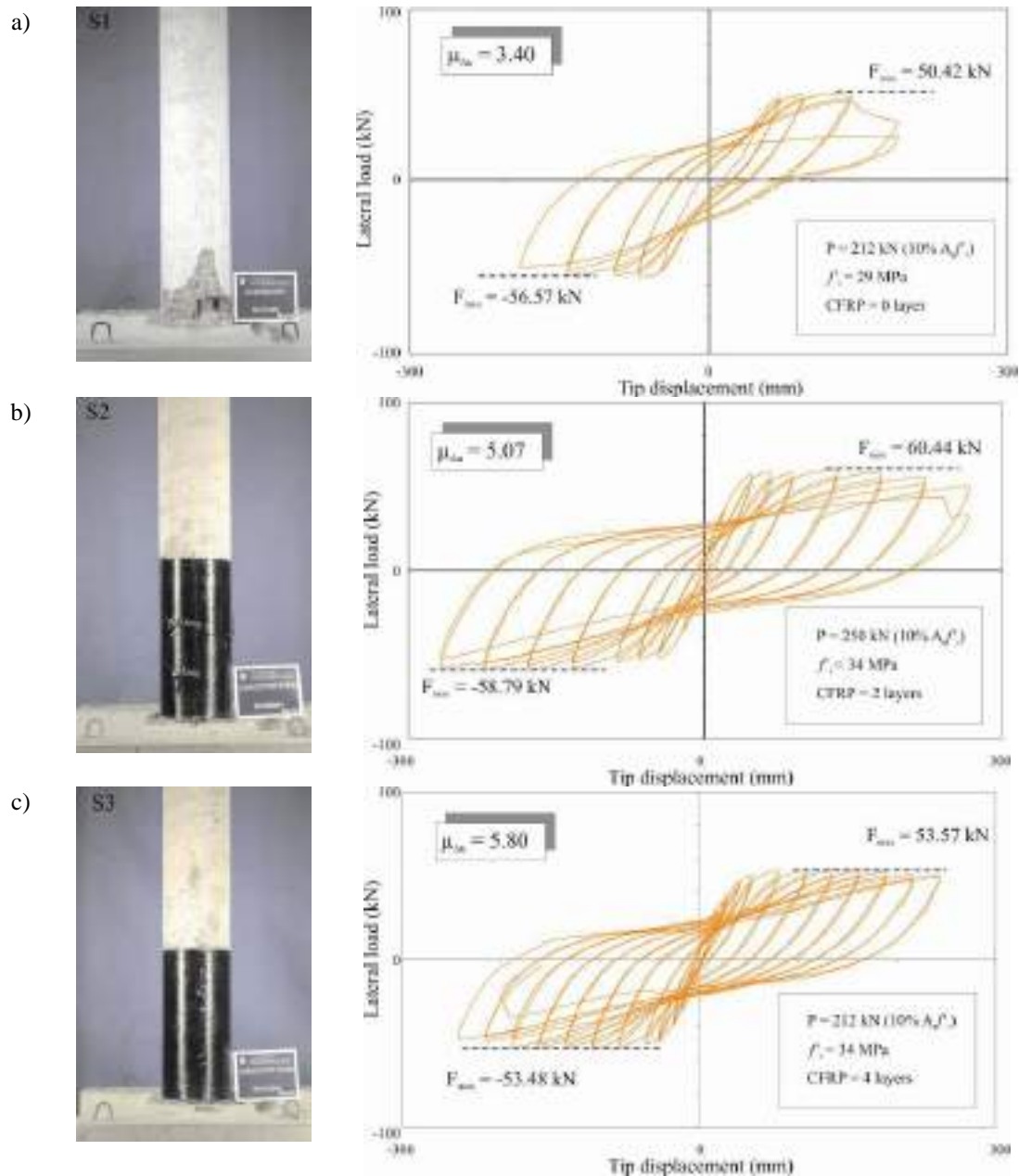


Figure 2: Specimen after testing and lateral load-tip displacement diagram for columns with axial load corresponding to $10\% A_s f_c$ and: a) 0 layer of CFRP (S1), b) 2 layers of CFRP (S2) c) 4 layers of CFRP (S3)

As defined in Paultre et al., 2001, seismic response indicators are generally quantified by curvature and structural ductility and by energy-dissipation capacity. The indicators - namely the ultimate displacement ductility μ_{du} , the ultimate curvature ductility μ_{cu} , the maximum drift ratio δ_{du} , the normalized dissipated energy E_N and the work index I_w proposed by Gosain et al., 1977 - are presented in Table 2 enabling a rational comparison of the columns behavior.

$$E_N = \frac{1}{F_{\max} \Delta_{yI}} \sum_{i=1}^n E_i$$

$$I_w = \sum_{i=1}^n \frac{F_i \Delta_i}{F_{\max} \Delta_{yI}}$$

F is the applied horizontal load, Δ is the tip displacement of the column, Δ_{yI} is the ideal yield displacement, E_i is the energy dissipated for cycle i and n is the number of cycles before conventional failure. Results show that structural ductility criteria were exceeded in both the performance-based and the conventional design. While the sectional ductility is almost the same for the three columns, a significant increase in structural ductility and energy dissipation for the confined columns is observed and this phenomenon is more pronounced between the columns having 0 and 2 layers of CFRP.

Table 2: Summary of Results

Specimen	$\mu_{\Delta u}$	$\mu_{\phi u}$	$\delta_{\theta u}$ (%)	E_N	I_w
S1	3.5	7.7 ¹	8.89	13.56	11.90
S2	5.1	8.0	12.88	34.18	25.05
S3	5.8	7.6	11.72	37.69	31.98

¹calculated at 325 mm from column's base

4. CONCLUSION

Six large-scale reinforced concrete circular columns were tested under cyclic loading. The confinement varied from 0 to 2 and 4 layers of CFRP. The columns were subjected to constant axial loads corresponding to 10 and 35 % of the columns' axial load capacity and to a cyclic bending moment. It is shown that, at constant level of axial compression of 10% of the column capacity, the confinement influences the flexural behavior of the columns and significantly improves the seismic behavior. It is of interest to mention that, in a next phase of the project, the test results will be used to validate a new confinement model that was developed by Eid et al., 2006. This new model features a unique prediction of the confinement effect due to both the transverse steel reinforcement and the FRP.

5. ACKNOWLEDGEMENTS

The authors would like to acknowledge the financial support of ISIS Canada, the Natural Sciences and Engineering Research Council of Canada (NSERC), the Quebec Fonds pour la recherche sur la nature et les technologies (FQRNT) and Sika-Canada. They would also like to thank Marc Demers, Claude Aubé, Sébastien Gauthier and Laurent Thibodeau at the Université de Sherbrooke for their collaboration.

6. REFERENCES

- Eid, R., Roy, N. and Paultre, P. (2006). "Behaviour of Circular Reinforced Concrete Columns Confined with Transverse Steel Reinforcement and Fiber-Reinforced Composite Sheets", *Proceedings of the 2nd Intl FIB Congress*.
- Gosain N.K., Brown, R.H. and Jirsa, J.O. (1977). "Shear Requirements for Load Reversals on RC Members". *Journal of the Structural Division, Proceedings of the ASCE*, Vol. 103, No. ST7, pp. 1461-1475.
- Paultre, P., Légeron, F. and Mongeau, D. (2001). "Influence of Concrete Strength and Transverse Reinforcement Yield Strength on Behavior of High-Strength Concrete Columns". *ACI Structural Journal*, Vol. 98, No. 4, pp. 490-501.
- Priestley, M.J.N., Seible, F. and Calvi G.M. (1996). "Seismic Design and Retrofit of Bridges". John Wiley & Sons, New York, 686 p.
- Tian, Y. and Chaturvedi, S.K. (2004). "A Seismic Retrofit Design Methodology for R/C Bridge Columns Using Fiber Composites". *Earthquake Spectra*, Vol. 20, No. 2, pp 483-502.

USE OF CFRP TO STRENGTHEN POORLY DETAILED REINFORCED CONCRETE BEAMS

InSung Kim
(Graduate Research Assistant, The University of Texas at Austin, USA)

James O. Jirsa
(Professor, The University of Texas at Austin, USA)

Oguzhan Bayrak
(Assistant Professor, The University of Texas at Austin, USA)

ABSTRACT

In many reinforced concrete structures built in the 1970's and earlier, bottom beam reinforcement is not continuous and if a column support is lost due to terrorist attack or other unexpected action, the structure could be vulnerable to progressive collapse. The beams may not develop catenary action if the reinforcement is not continuous. The use of CFRP material may provide a solution for rehabilitating such structures. CFRP materials can not develop full tensile capacity unless they are properly anchored to the reinforced concrete structure. The intent of this study is to find an effective method of anchoring CFRP material to a reinforced concrete beam so that the ultimate tensile strength of the CFRP is realized. In this study, four reinforced concrete beams rehabilitated using different configurations of anchors were tested to assess the effectiveness of the anchors. All the beams were undamaged before they were rehabilitated. Both CFRP anchors and CFRP U-wraps were investigated. The rehabilitated beams were loaded until failure of the CFRP material or anchor occurred. Different failure modes, strengths and deformation capacities of the rehabilitated beams were observed depending on the configurations of anchors. The maximum capacity was obtained using a combination of CFRP anchors and U-wraps.

KEYWORDS

CFRP sheets, CFRP anchors, reinforced concrete, rehabilitation

1. INTRODUCTION

The basic rehabilitation technique for this program was installation of CFRP materials on the sides of the beam to provide continuity to bottom reinforcement (Figure 1). A CFRP sheet was attached to the concrete surface by epoxy resin and through the use of CFRP anchors and CFRP U-wraps in order to develop full tensile capacity of CFRP sheet after delamination of CFRP sheet occurs. This work was supported under a grant from the NSF.

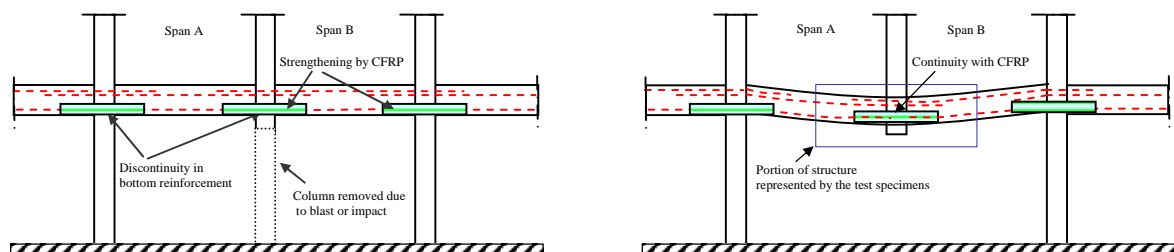


Figure 1: Rehabilitation Technique

2. TEST SPECIMENS

The dimensions of the beams tested are shown below. The length of specimen corresponded to the distance between inflection points. The 12 in. long deepened section at mid span represented a portion of the supporting column. Bottom beam reinforcement extended 4.5 in. from column face with a 3 in. discontinuity existed at the middle of the column (Figure 2).

All specimens were loaded at “mid span” to represent the loading when the column below is removed (Figure 2). The target strength was $P=32$ kip which corresponded to nominal strength of the beam with two #6 continuous bottom bars. If full tensile capacity of the CFRP sheet can be developed, the target strength will be achieved. Applied load and deflection of the column (center of the specimen) were measured.

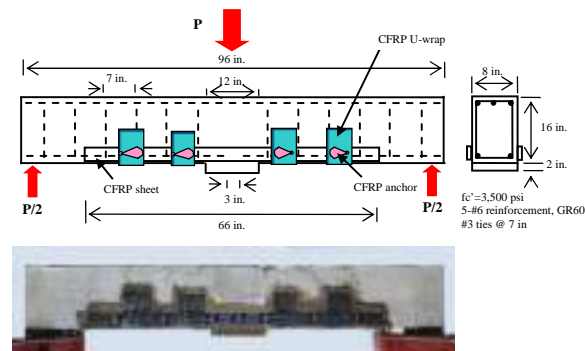


Figure 2: Test Specimen (Specimen No. 4)

3. APPLICATIONS OF CFRP MATERIALS

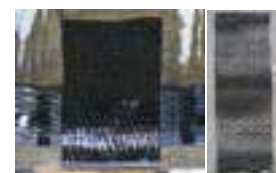
A CFRP sheet was used as a tensile element to provide continuity to the bottom reinforcement (Figure 3-(a)). CFRP anchors are shown in Figure 3-(b) and consist of a roll of CFRP sheet inserted into the concrete and splayed out over the CFRP sheet on the side face of beam. CFRP U-wraps were sheets of CFRP attached transverse to the main sheet as shown in Figure 3-(c).



(a) CFRP sheet



(b) CFRP anchor



(c) CFRP U-wrap

Figure 3: Applications of CFRP Material

4. MATERIAL PROPERTIES

Compressive strength of concrete was 3,500 psi, and GR60 reinforcements are used for the tests. Material properties of CFRP are shown in Table 1.

Table 1: Material Properties of CFRP

Properties	Ultimate Tensile Strength	Elongation at Break	Tensile modulus	Laminate thickness
Typical Test Value	143,700 psi	1.26 %	11.4×10^6 psi	0.035 in.

* Tyfo[®] SCH-35 composites with Tyfo[®] S Epoxy

5. REHABILITATION METHODS USING CFRP MATERIALS

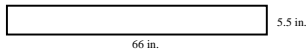
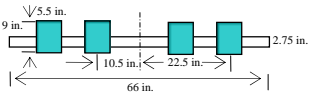
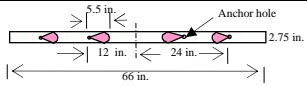
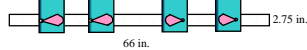
All CFRP materials were installed in symmetric way on both sides of the beams. The CFRP was attached using two different sheet arrangements. In one case, a CFRP sheet 5.5 in. wide x 66 in. long was attached on the both sides of the beam. In the other case, two CFRP sheets 2.75 x 66 in. were placed on top of one another. The area of CFRP materials in both cases was the same, and was selected to provide an ultimate tensile force the same as that at yield using two #6 bottom bars. For the specimen with one CFRP sheet, only epoxy resin was used to attach it to the beam. Two layers of CFRP were used in the other three specimens.

A CFRP anchor was made using the same width of CFRP, 5.5 in., sheet that was attached to the beam. The length of the anchor was 9.5 in. with 4 in. of the anchor inserted into a 5/8 in. hole drilled into the concrete, and the rest of the anchor was spread out in a fan shape on the CFRP sheet. Eight anchor holes were installed in each beam, four located at 12 in., and the other four located at 24 in. from the center of the column.

CFRP U-wrap was also made of the same 5.5 in. width of CFRP sheet, and a total length of 26 in.. The CFRP U-wrap was attached on each side of the beam over the CFRP sheet, and extended 9 in. from the bottom face of the beam. Four CFRP U-wraps were installed in a specimen, and two of them were located 10.5 in. and the others were located 22.5 in. from center of the specimen.

Four different rehabilitation methods using CFRP sheet, CFRP anchor and CFRP U-wrap are shown in Table 2.

Table 2: Rehabilitation Methods

No.	Configuration of CFRP Materials	Number of Layers of CFRP sheet	Type of Anchorage	Failure Mode	Maximum Applied Load
1		1 layer	None	Delamination of CFRP sheet	14.57 kip
2		2 layers	CFRP U-wrap	Delamination of CFRP U-wrap	15.38 kip
3		2 layers	CFRP Anchor	Concrete Failure around Anchor Holes	25.78 kip
4	 <small>* Location of the anchors and U-wraps are the same as specimen No. 2 and No. 3</small>	2 layers	CFRP Anchor & CFRP U-wrap	Fracture of CFRP Sheet	31.94 kip



(a) Specimen No.1



(b) Specimen No.2



(c) Specimen No.3



(d) Specimen No.4

Figure 4: Failure Modes of Specimens

6. TEST RESULTS: FAILURE MODES

Failure mode of each specimen is shown in Table 2 and Figure 4. The most desirable failure mode is fracture of the CFRP sheet after developing full tensile capacity. However, failure of the anchorage system occurred prior to failure of CFRP sheet in all the specimens except No. 4 which had both CFRP anchors and CFRP U-wraps.

One layer of CFRP sheet was only used in specimen No.1 in order to maximize surface area of CFRP sheet attached to the concrete because it did not have anchors, so the area is a critical factor for bonding capacity of CFRP sheet to concrete. Delamination of CFRP sheet was the failure mode of specimen No.1 (Figure 4-(a)). Although CFRP U-wraps were installed in specimen No.2 to provide anchorage to the CFRP sheet, they did not hold the CFRP sheet effectively after delamination of the sheet occurred. CFRP U-wraps delaminated right after delamination of CFRP sheet (Figure 4-(b)). CFRP anchors in specimen No.3 held CFRP sheet to concrete effectively after delamination of CFRP sheet occurred. However, concrete cover around anchor hole crushed before any material failure of CFRP materials (Figure 4-(c)). In specimen No. 4, CFRP U-wrap was installed on CFRP sheet before CFRP anchors were applied to prevent concrete crushing around the anchor hole by confining concrete around anchor hole. Full tensile strength of the CFRP sheet was developed in specimen No. 4, and material failure of the CFRP sheet was observed in specimen No. 4 (Figure 4-(d)).

7. TEST RESULTS: LOAD-DEFLECTION RELATIONSHIPS

As shown in Figure 5, not only strength but also deformation capacity increased as anchorage improved. Strength of specimen No. 4 was 31.94 kip (target strength). The CFRP sheet developed its full tensile capacity with a combination of CFRP anchor and U-wrap.

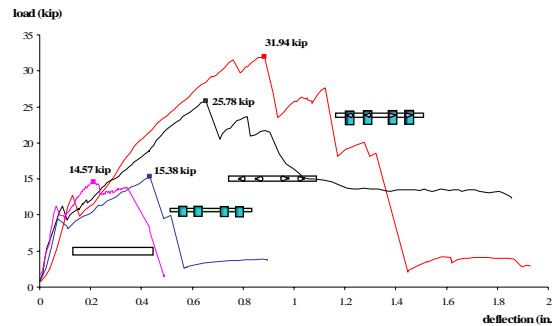


Figure 5: Load-Deflection Relationships

8. CONCLUSION

Rehabilitation using CFRP materials to correct poor details was successful only if proper anchorage was provided. It was necessary to use both CFRP anchors and CFRP U-wraps to achieve full strength of the CFRP sheet. If either CFRP anchors or CFRP U-wraps were used alone, delamination of the sheet leads to failure of anchor or U-wrap.

Further research into various geometries and quantities of CFRP anchors and U-wraps are required before design guidelines can be developed. Moreover, application may be limited because the method requires flat side surfaces and many beam-column connections consist of columns that are wider than the beams. However, it is possible to use the method in other applications in which CFRP sheets are used to provide continuity in the same plane.

9. References

- ACI committee 440. (2002). "Guide for the Design and Construction of Externally bonded FRP Systems for Strengthening Concrete Structures", American Concrete Institute, Farmington Hills, Michigan.
- Brena, S. (2000), "Strengthening Reinforced Concrete Bridges Using Carbon Fiber Reinforced Polymer Composite", Ph.D. dissertation, University of Texas at Austin, Texas, USA
- Kobayashi, K., et al., (2001). "Advanced Wrapping System with CF-Anchor", *Proceedings of the 5th International Conference on Fibre Reinforced Plastics for Reinforced Concrete Structures*, Volume 1, pages 379-388
- Ozdemir, G., Akyuz, U. (2006) "Tensile Capacities of CFRP Anchors", *Advances in Earthquake Engineering for Urban Risk Reduction(Proceedings of the NATO Science for Peace Workshop on Advances in Earthquake Engineering for Urban Risk Reduction, Istanbul, Turkey)*, Springer, pages 471-488
- Teng, J.G., et al., (2002). *FRP-strengthened RC Structures*, Wiley, New York

RESIDUAL BEHAVIOR OF FRP RETROFITTED RC COLUMNS AFTER BEING SUBJECTED TO EARTHQUAKE DAMAGE

Shan, Bo

(Research Assistant, Civil Engineering College of Hunan University, Changsha, Hunan Province, China)

Xiao, Yan

(Associate Professor, University of Southern California, Los Angeles, California, USA)

(Cheung Kong Scholar, Civil Engineering College of Hunan University, Changsha, Hunan Province, China)

Huang, Zhengyu

(Professor, Civil Engineering College of Hunan University, Changsha, Hunan Province, China)

ABSTRACT

Despite the significant importance, residual seismic behavior of reinforced concrete (RC) columns retrofitted with fiber-reinforced plastic (FRP) has received little attention. In this paper, the residual performance of FRP retrofitted columns damaged after simulated seismic loading is studied. Eight model columns with a shear aspect ratio of 5.0 were tested first under cyclic lateral force and a constant load equal to 20% of the column gross axial load capacity. The main parameters considered were the type of FRP jacket and peak drift ratio where the lateral loading was interrupted. Five of the model columns were subjected to long-term axial loading after subjected to limited damage by lateral cyclic loading. The deformation of retrofitted columns under long-term axial loading related to the previous damage intensity and the modulus of FRP. The post damage long-term axial strain corresponding to time increment can be simply estimated using the ACI 209 creep model. The effective creep Poisson's ratios of the retrofitted columns were much smaller than the as-built column but identical for GFRP and CFRP retrofitted columns. Under the testing condition of this study, the long-term axial deformation of retrofitted column tends to be stable, despite subjected simulated earthquake damage.

KEYWORDS

Seismic retrofit; FRP; Earthquake damage; Residual performance; Creep

1. INTRODUCTION

Performance of bridges and buildings during past earthquakes such as Loma Prieta (1989), Northridge (1994) and Kobe (1995) repeatedly demonstrated the vulnerabilities of older reinforced concrete structures. For reinforced concrete buildings and bridges, a significant majority of the structural failure could be attributed to inadequate seismic design of the columns, such as the lack of transverse reinforcement and the poor splicing details of longitudinal reinforcement in potential plastic hinge regions. Recently, fiber reinforced plastics (FRP) have been widely studied and found growing applications, due to the expectation of its high-strength, light-weight, quick and easy installation on site, high resistance against corrosion and easy fabrication.

Numerous existing structures, particularly bridges in California and elsewhere, have been seismically upgraded. Retrofit design is based on the philosophy of enabling the structures to survive essentially one extreme seismic event. However, several questions related to the post-earthquake health of the structure in relation to the residual behavior of the retrofitted bridge columns remain unanswered. These issues are of significant importance. It has been suspected that the rupture of several GFRP jackets installed on the columns of the I-5 and Freeway 2 interchange in Los Angeles was due to the insufficient residual capacity after the columns were subjected to the shaking of the 1994 Northridge earthquake. In this case, prestressing the FRP for active confinement of the concrete also compounded the problem (Hippley 2004). The primary focus of this paper is on the sustained long-term axial loading behavior of FRP retrofitted columns after being subjected to limited damage by simulated earthquake loading.

Research on the long-term performance of FRP retrofitted columns is rare. Naguib and Mirmiran (2002) studied the time-dependence behavior of concrete column retrofitted with FRP jacket under axial load. It should be indicated that while the long-term loading used in this study is similar to that used by Naguib and Mirmiran (2002), the research objectives are distinctly different. The test of Naguib and Mirmiran (2002) mainly studied the creep of FRP confined concrete columns. But the main objective in this paper is emphasis on the residual performance of retrofitted columns with earthquake damage.

2. EXPERIMENTAL PROGRAM

Eight RC model columns were designed to simulate the 1970's design and detailing practice according to the specifications for RC bridges in China. Similar details are also seen in older bridges in the United States and elsewhere. The typical specimen was designed as a vertical cantilever column with a strong footing, as shown in Figure 1. The testing matrix is shown in Table 1. FRP jackets were wrapped for a 400mm long segment near the column bottom end. The FRP retrofit together with the existing transverse reinforcement provides the columns with an equivalent transverse reinforcement slightly exceeding the current ACI 318 code requirement.

Table 1: Testing Matrix

Specimen	f'_c (MPa)	Retrofit	Lateral Displacement Ratio	Testing Condition
CA-1	34.0	—	6%	Lateral Loading Only
CA-2L	35.0	—	3%	Lateral Loading and Long-term Test
CCR-1	30.9	4-layer CFRP	8%	Lateral Loading Only
CCR-2L	38.6	4-layer CFRP	3%	Lateral Loading and Long-term Test
CCR-3L	41.4	4-layer CFRP	6%	Lateral Loading and Long-term Test
CGR-1	38.7	5-layer GFRP	10%	Lateral Loading Only
CGR-2L	34.9	5-layer GFRP	3%	Lateral Loading and Long-term Test
CGR-3L	37.9	5-layer GFRP	6%	Lateral Loading and Long-term Test

During pseudo-static test, a constant axial load, equal to 20% of the static capacity $A_g f'_c$, was applied to the column. The lateral force was cycled under a lateral displacement control condition. Lateral loading program is shown in Figure 2. Three model columns, representing the as built condition, GFRP and CFRP retrofits, respectively, were first tested to failure to establish the benchmark testing data.

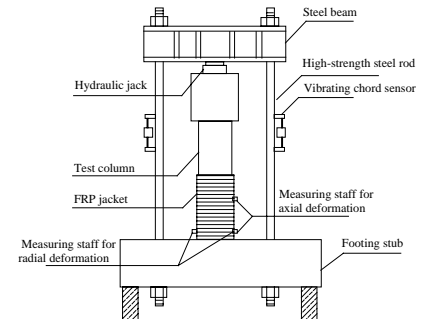
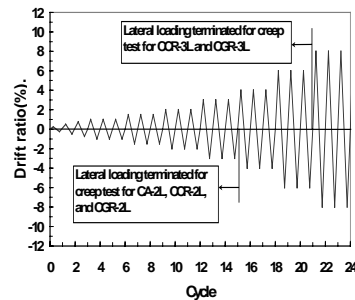
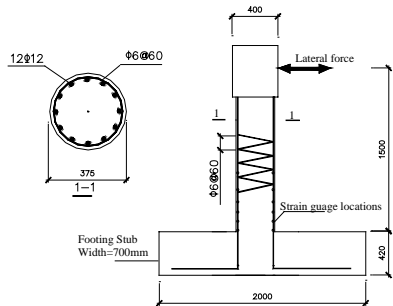


Figure 1:Details of Test Column Figure2: Lateral Loading Program Figure 3:Long-term Test Setup

Five sets of long-term axial loading setups as shown in Figure 3 were manufactured for such testing purpose. The test setup included a 2000kN hydraulic jack, a cross beam and two high-strength steel rods with a diameter of 50mm. The fluctuation of the load application was monitored using vibrating wire gauges, which were mounted on the high-strength steel rods. Several measurement target staffs were fixed on the test columns as shown in Figure 3. Through measuring the varying distance of the measuring staffs on test column using a manual dial gauge, the radial deformation and axial deformation of the test column can be obtained. All the specimens were initially loaded at an axial load level equal to $0.2 A_g f'_c$, and observed for 30 days when the deformation became sufficiently stable. The axial load was then removed and reapplied at a higher axial load level of $0.4 A_g f'_c$, for a period of 60 days. This

adjustment of axial load level was for an attempt to intensify the effects of axial loading, and did not necessarily reflect any actual loading condition.

3. EXPERIMENTAL RESULTS

3.1 Presentation of Data of Long-Term Axial Loading Tests

The characteristic points of Figure 4 and Figure 5 such as A, B, C, D, E, F, G and H denote the strain value after applying axial load, the strain value at the end of pseudo-static test, the strain value removal at axial load, the strain value at the start of long-term loading test, the strain value at the 30th day, the strain value at the end of empty load, the strain value after applying 0.4 axial load ratio and the strain value at the 100th day, respectively.

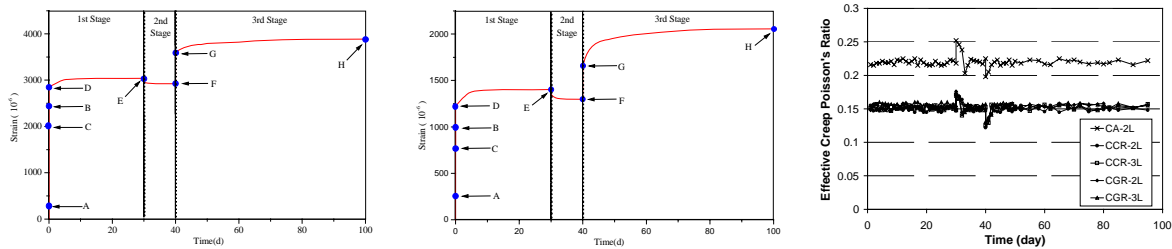


Figure 4: Axial Strain of CA-2L Figure 5: Axial Strain of CCR-3L Figure 6: Effective Creep Poisson's Ratio

3.2 Effective Creep Poisson's Ratio

From circumferential strain and axial strain, the effective creep Poisson's ratio over time can be obtained and shown in Figure 6. Note that the effective creep Poisson's ratios are calculated based on the net creep. It is interesting to note that the trends of the effective creep Poisson's ratios for all model columns are very stable during the entire period of long-term axial loading, except for the interruption for changing the axial load level. There is little difference among the effective creep Poisson's ratios of the retrofitted columns using CFRP or GFRP jacketing. This is considered as the consequence of an equal target strength design with different jackets. The average value of the effective creep Poisson's ratios of the as built model CA-2L is approximately 0.23, which is higher than the average value 0.15 for the FRP retrofitted columns. This reflects the confinement effect of FRP jacketing. Moreover, the test results also indicate that despite having experienced different levels of lateral loading damage, the effective creep Poisson's ratios are identical.

3.3 Axial Deformation under Post-damage Long-term Loading

The axial strain developments of CA-2L and CCR-3L are shown in Figure 4 and Figure 5, respectively. The axial strain stabilized after approximately 7 days during the first 30 days of axial loading. However, the axial strains took a longer period of about 20 to 30 days to cease the increase and stabilize under the higher axial load level of $0.4 A_g f_c'$. Thereafter, because there was no significantly meaningful time dependant augmentation, the loading was terminated after 60 days.

Behaviors during the first 30 days for all the CFRP retrofitted columns, GFRP retrofitted columns and the as built column are shown by the solid curves in from Figure 7 to Figure 11, respectively, along with the creep models based on ACI 209. Comparing Figure 8 with Figure 7, it can be seen that the axial strain of CCR-3L, which experienced the lateral cyclic loading up to a drift ratio of 6%, was about 15% higher than its counterpart model CCR-2L which experienced lateral loading up to a drift ratio of 3%. This indicated that post damage long-term deformation was influenced by the damage level. On the other hand, by comparing the axial deformations of CFRP retrofitted columns shown in Figure 8 with the results of GFRP retrofitted columns shown in Figure 10, it can be observed that the long-term deformation was also affected by the type of FRP jacket, essentially meaning the modulus of elasticity of the FRP jacket. Despite having experienced identical level of lateral loading, the GFRP retrofitted column developed larger strain compared with the counterpart CFRP retrofitted column.

From Figure 11, the lower limit curve based on the ACI 209 creep model approaches the experimental curve for the as-build column. The experimental curves of retrofitted columns are included in the range between lower limit and the upper limit of creep coefficient C_u , and reasonably close to the curves using the average value, $C_u = 2.35$, as shown in from Figure 7 to Figure 10. However, the predicted curves using average value of C_u tend to over-estimate the test results for later loading stages beyond 15 days.

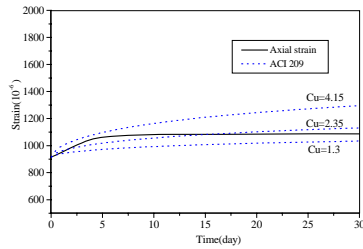


Figure 7: CCR-2L vs. ACI 209

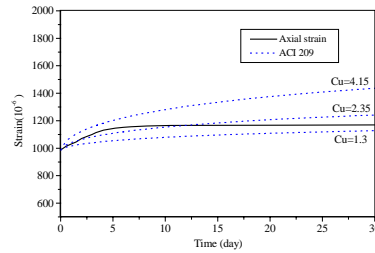


Figure 8: CCR-3L vs. ACI 209

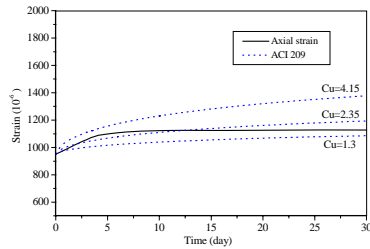


Figure 9: CGR-2L vs. ACI 209

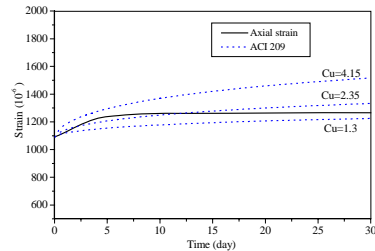


Figure 10: CGR-3L vs. ACI 209

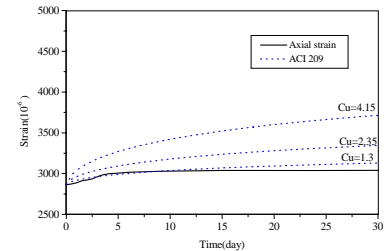


Figure 11: CA-2L vs. ACI 209

4. CONCLUSIONS

During long-term axial loading test after being subjected to some degree of lateral loading damage, the deformation of the FRP retrofitted columns was lower when compared with the non-retrofitted column subjected to similar loading condition. The development of long-term loading deformation of retrofitted column was found to relate to the previous damage level and the modulus of elasticity of the FRP. The post damage long-term axial strain corresponding to time increment can be simply estimated using the simple creep model recommended by ACI Committee 209 committee. The effective creep Poisson's ratio for the retrofitted columns with various testing conditions has an average value of about 0.15. The study essentially confirmed that within the testing range of the axial load ratios between $0.2 \sim 0.4 A_g f'_c$, the post damage long-term axial loading would not cause any significant creep effects to the FRP retrofitted columns.

REFERENCES

- ACI Committee 209, (1992). "Prediction of Creep, Shrinkage and Temperature Effects in Concrete Structures (ACI 209R-92)". American Concrete Institute, Farmington Hills, Mich., 47pp.
- ACI Committee 318 (2002). "Building Code Requirements for Reinforced Concrete and Commentary (ACI 318-02/ACI 418R-02)". American Concrete Institute, Farmington Hill.
- Hipley, P. (2004). "Seismic Retrofit for Columns/Piers Composite Bridge Column Retrofitting in California". Federal Highway Administration, FHWA, Bridge Technology, June, <http://www.fhwa.dot.gov/bridge/frp/frpdatar.htm>
- Naguib, W. and Mirmiran, A. (2002). "Time-dependent behavior of Fiber-Reinforced Polymer confined columns under axial loads". *ACI Structural Journal*, V.99, No.2, pp.142-148.
- Saadatmanesh, h.; and Ehsani, M.R., (1994), "Strength and ductility of concrete columns reinforced with fiber composite straps," *ACI Structural Journal*, Vol.91, No.4, pp.434-447.
- Xiao, Y.(1997). "Seismic retrofit of RC circular columns using prefabricated composite jacking". *ASCE, Journal of Structural Engineering*, Vol.123, No.10, pp.1357-1364.
- Xiao, Y. and Wu, H. (2000). "Compressive Behavior of Concrete Cylinders Confined by Carbon Fiber Composite Jackets". *ASCE, Journal of Materials in Civil Engineering*, Vol. 12, No. 2, May, pp. 139-146.
- Xiao, Y.; Sheikh, S.A.; and Li, Z.X. (2001), "Applications of FRP composites in concrete columns," *Proceedings FRP Composites in Civil Engineering*, Hong Kong, China, December, pp.731-740.
- Xiao, Y. (2004). "Applications of FRP Composites in Concrete Columns". *International Journal of Advances in Structural Engineering*, A Multi-Science Publication, UK, Vol.7, No.4, August, pp.335-344.

ESTIMATION OF THE DUCTILITY OF WEB-BONDED FRP BEAMS FOR ASSESSMENT OF STRENGTHENED RC EXTERIOR JOINTS

S. S. Mahini

(Asst. Professor, Department of Civil Engineering, Yazd University, Yazd, Iran)

H.R. Ronagh

*(Senior Lecturer, Division of Civil Eng. School of Engineering, The University of Queensland,
Brisbane, QLD 4072, Australia)*

ABSTRACT

Beam-column joints in Reinforced Concrete (RC) moment resisting frame (MRF) subjected to lateral loads can be critical regions. They must therefore be designed adequately in order to dissipate large amounts of energy without a significant loss of strength and ductility. When the joint are inadequately designed or damaged under unanticipated loads, web-bonded FRP is one of the possible strengthening methods that can be used. In this paper, a computer model is presented in order to estimate the ductility of strengthened beams and a range of possible design charts is produced to select the type and amount of FRP required for upgrading exterior beam-column joints. Finally, displacement ductility of a subassembly is assessed using these design charts and the result is compared with experiment. The comparison proves the model is acceptable.

KEYWORDS

Ductility, web-bonded, RC, joint, FRP

1. INTRODUCTION

Since 1970s, a significant amount of research studies are carried out studying various aspects of the behaviour of beam-column joints in moment resisting frames (MRF) subjected to severe lateral loads. Shear and flexural failure and penetration of cracks into the joints core have been identified as failure mechanisms resulted from inadequately designed joints (Paulay and Priestley, 1992). Rehabilitation may become necessary when members and joints lack sufficient strength, or ductility. Strengthening the beam end of the joints to improve the joint strength is an area of research that has been over looked. Traiantafillou and Plevris (1992) studied the strengthening of RC beams with epoxy-bonded fibre-composite materials including CFRP and GFRP sheets. They considered several failure mechanisms such as FRP rupture, steel yield, concrete crushing and de-bonding using an analytical model. Traiantafillou and Plevris produced diagrams showing the beam design for which each failure mechanism is dominant and examined the effect of FRP sheets on the ductility of strengthened components. They confirmed their analysis with testing beams under four-point bending. Traiantafillou and Plevris concluded that unless failure is governed by FRP rupture, the results by no means indicate that GFRP should be preferred to CFRP for ductility considerations due to the fact that the GFRP ratio needed to achieve a given moment capacity is much higher than when CFRP composite is used. Duthinh and Starnes (2001) conducted an experimental study on seven pre-cracked concrete beams reinforced internally with steel and externally with an FRP laminate under four-point bending. Duthinh and Starnes concluded that in comparison with a beam reinforced heavily with steel only, CFRP-strengthened RC beams have adequate deformation capacity in spite of their brittle failure.

In this paper, computer models are presented in order to estimate curvature ductility of web-bonded FRP beams. This model can be used to assess the ductility of the strengthened exterior beam-column joints. Design charts are also obtained to facilitate the calculations. Displacement ductility of a beam-column subassembly retrofitted by web bonded FRP, tested by Mahini et al. (2004), is then obtained and the result is compared with the design charts in order to show their reliability.

2. COMPUTER MODELS

The cross-section of a typical rectangular RC beam strengthened with web-bonded FRP is shown in Fig. 1. As is seen, the section has a width b and a height h . The fibre composite has a thickness t_f ; the tensile reinforcement has an area, A_s and compressive reinforcement an area, A'_s . d and d' are distances from the extreme compression fibre to the centroid of tension and compression reinforcements respectively. Modulus of elasticity of steel, concrete and FRP are denoted as E_s , E_c and E_f respectively. Steel bars have a yield stress and strain of f_y and ε_y respectively. The concrete has a compressive strength, f'_c and an ultimate compressive strain ε_{cu} . The ultimate stress and strain of fibre composite at rupture are f_{fr} and ε_{fr} respectively.

This method of strengthening (web-bonded FRP sheets) can be used: 1) for controlling the location of plastic hinge by upgrading the strength of the beam close to the column which may help in moving the plastic hinge away from the edge of the column and 2) for repair of moderately damaged rectangular RC beams in moment resisting frames. There, the best way to repair the damaged beam is by web-bonded FRP, since wrapping the top of the beams in existing buildings is hard to apply due to the presence of the floor slab.

Usually, one of three major flexural failure modes may be observed in reinforced concrete beams strengthened with web-bonded FRP reinforcement. These are: 1) Yielding of reinforcing steel in tension followed by the rupture of FRP (FRP rupture); 2) Yielding of reinforcing steel in tension followed by concrete crushing (tension failure) and 3) Crushing of concrete in compression before yielding of the reinforcing steel (compression failure). In these modes, the quantity of energy absorbance of the web-bonded FRP beam can be evaluated through its curvature ductility.

In order to simplify the analysis of web-bonded FRP beams in different failure modes and to calculate the first yield neutral axes of the beam, a computer procedure has been developed that is presented in the following. The procedure for calculating the depth of neutral axis of the beam section (when first yield occurs, c_y and also at ultimate moment, c) starts with the estimation of the neutral axis depth and ends with a calculated value for c_y and c based on the force equilibrium using the constitutive laws of the materials and the strain compatibility in the section. If the difference between the estimated and calculated values is small, the estimated values are accepted otherwise modified using the bisection method until convergence occurs. For the first yield calculations, compatibility of the strain and stress as is shown in Fig. 1 is used. Based on the yield strain of steel reinforcement ε_y , the strain in the concrete, FRP and the compressive steel reinforcements can be determined. The maximum curvature ductility is expressed as $\mu_\phi = \phi_u / \phi_y$, where ϕ_u the maximum curvature is expected to be attained or relied on and ϕ_y is the yield curvature and can be calculated from strain distribution as shown in Fig. 1.

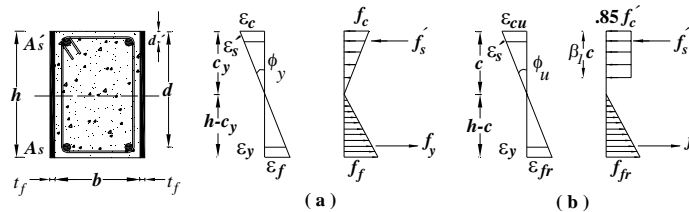


Figure 1: Strain and stress distributions of web-bonded FRP beams (a) at first yield (b) at ultimate

The stresses in the concrete, FRP and the compressive steel reinforcements are $f_c = E_c \varepsilon_c$, $f_f = E_f \varepsilon_f$ and $f'_s = E_s \varepsilon'_s$ respectively, where ε_c and ε_f are the strains in the extreme fibre of concrete and FRP respectively and the ε'_s , is the strain at compressive steel level.

Applying the force equilibrium in the section leads to:

$$c_y = (A_s f_y - A'_s f'_s + f_f (h - c_y) t_f) / 0.5 f_c b \quad (1)$$

In order to calculate the neutral axes at ultimate, the strain distributions shown in Fig. 1 is used. The following criteria are then checked in order to obtain the mechanism governing the failure. If $\varepsilon_{fr} + \varepsilon_{f_0} < \varepsilon_{cu}(h-c)/c$ then the failure is governed by “FRP rupture”. Otherwise the failure is governed by “tension failure”. In that, ε_{fr} and ε_{f_0} are the ultimate strain of FRP and initial strain of unstrengthened beam at the extreme tensile level of the RC section respectively and ε_{cu} is the compressive strain of concrete at ultimate. When failure is governed by “FRP rupture”, the strain in the FRP at failure is equal to the maximum ultimate strain, ε_{fr} and therefore the strain values at the compressive concrete, tensile and compressive steel reinforcements can be determined based on this strain level. The stresses in the steel reinforcements may be calculated assuming an elastic perfectly plastic condition and the stress in the FRP, f_f may be taken as the ultimate tensile strength, f_{fr} . The process when the failure is governed by “tension failure” is similar to FRP rupture mode. In that, the maximum strain of concrete is equal to ε_{cu} . Based on the concrete strain level and the assumed value of c , the strains in the tension and compression steel reinforcements can then be determined. The stresses in the steel reinforcements can be calculated similar to the FRP rupture mode. The FRP behaves linearly to failure, therefore $f_f = E_f \varepsilon_f$. Using force equilibrium into the section leads to the following equation:

$$c = (A_s f_y - A'_s f'_s + f_f (h-c) t_f) / 0.85 f'_c \beta_1 b \quad (2)$$

3. SAMPLE DESIGN CHARTS

Based on the presented computer model and the trail and error procedure, design charts are developed using a computer program. The concrete had a compressive strength around 48.20 MPa and a modulus of elasticity around 35.16 GPa. Yield strength of the main steel reinforcements was around 500MPa and the modulus of elasticity was equal to 200 GPa. CFRP and GFRP possessed a tensile strength of about 3900 MPa and 1700 MPa, a modulus of elasticity of 240GPa and 65 GPa, and an ultimate tensile elongation of 1.55% and 2.80% respectively. The maximum dependable concrete compression strain in the extreme fibre of unconfined beam sections is assumed to be 0.003, when normal strength concrete ($f'_c < 45$ MPa) is used.

The effect of the FRP reinforcement ratio, $\rho_f = t_f h / bd$, on the curvature ductility of the member is shown in Fig. 2 for a wide range of tensile steel reinforcement ratios, $\rho_s = A_s / bd$ and the compressive steel ratio, $\rho'_s = A'_s / bd = 0.0067$. As is seen, when CFRP sheet is used, the ductility increases as ρ_f decreases, unless ρ_f becomes small enough so that failure is caused by FRP rupture. In the case of GFRP-strengthening, the tension failure is governed for any amount of FRP ratios, ρ_f .

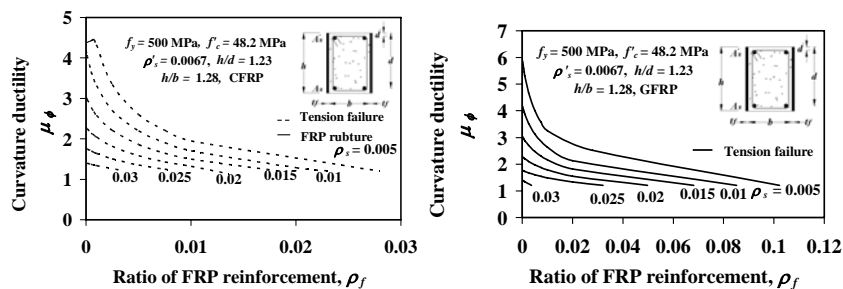


Figure 2: Curvature ductility values

4. DESIGN EXAMPLE

As an example, it is intended to calculate the displacement ductility of an exterior beam-column subassembly strengthened with CFRP web-bonded system shown in Fig. 3 reported by Mahini et al. (2004). Their results showed that the failure is a flexural one which is mainly concentrated in the beam, therefore the ultimate capacity of the subassembly is close to the ultimate capacity of the strengthened beam. The beam-tip and displacement curve of this specimen is shown in Fig. 3. The most convenient quantity to evaluate the structure’s capacity to develop ductility

μ_{Δ} is displacement as define $\mu_{\Delta} = \Delta_u / \Delta_y$, where Δ_u and Δ_y are the lateral tip displacements at ultimate and at yield respectively. As post peak response is often accompanied by strength degradation, a specified limit to this can be considered for the ductility to be calculated. A percentage reduction from the peak load P_u is often assumed (Park, 1989). As a conservative estimate, a 10% reduction in the load can be considered. Consequently from Fig. 3, the experimental displacement ductility can be calculated as $\mu_{\Delta,exp} = 3.3$. The curvature ductility of web-bonded and the plain section can be found directly from Fig. 2 as $\mu_{\phi} = 3.15$ and $\mu_{\phi} = 4.3$ respectively. In order to calculate the displacement ductility factor of the subassembly from curvature ductility, the following relationship presented by Paulay and Priestley (1992), can be used:

$$\mu_{\phi} = 1 + (\mu_{\Delta} - 1) / [3(l_p / l)[1 - 0.5(l_p / l)]] \quad (3)$$

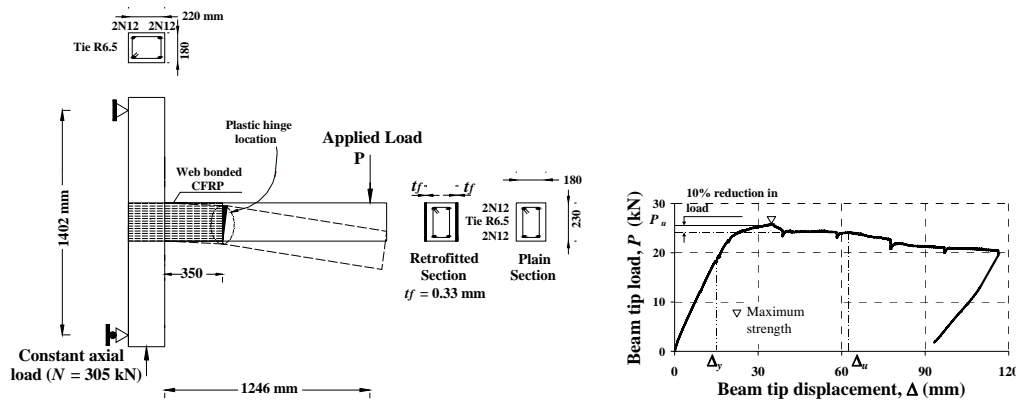


Figure 3: Failure mechanism and load vs. displacement of subassembly tested by Mahini et al. (2004)

where l_p is the plastic hinge length of the beam and l is the cantilever length both in m. Due to the fact that the failure occurs at the cut-off point of FRP, curvature ductility of this plain section is calculated and the displacement ductility of the subassembly is estimated using Eq. 3. Applying $l = 0.896$ m, $\mu_{\phi} = 4.3$ and $l_p = 0.204$ m in that, the analytical value of the displacement ductility for this subassembly is obtained as $\mu_{\Delta,ana} = 2.99$.

5. CONCLUSION

Computer models for calculating the neutral axis of the strengthened section at ultimate and yield conditions leading to the calculation of the curvature were presented and the design charts were then extracted from these models using a computer program. The displacement ductility of a web-bonded CFRP beam-column subassembly using the design charts was calculated and the results were compared with the test. Closeness of these results proved that the presented charts can be used by design engineers with confidence.

6. REFERENCES

- Paulay, T. and Priestley, M. J. N. (1992). *Seismic Design of Reinforced Concrete and Masonry Buildings*, John Wiley and Sons, INC.
- Triantafillou, T. C. and Plevris, N. (1992). "Strengthening of RC beams with Epoxy-Bonded Fibre-Composite Materials". *Materials and Structures*, Vol. 25, pp 201-211
- Duthinh, D., and Starnes, M. (2001). *Strength and Ductility of Concrete Beams Reinforced with Carbon FRP and Steel*, National Institute of Standards and Technology, Technology Administration U.S. Department of Commerce.

Mahini, S.S., Ronagh, H.R. and Dux P.F. (2004). "Flexural Repair of RC Exterior Beam-Column Joints Using CFRP Sheets", *Proc. of the Second International Conference on FRP Composites in Civil Engineering*, CICE 2004, 8-10 Dec. Adelaide, Australia, pp 653-658.

Park, R. (1989) "Evaluation of Ductility of Structures and Structural Assemblages from Laboratory Testing", *Bulletin of the New Zealand National Society for Earthquake Engineering*, Vol. 22, No.3, pp 155-166.

Part XXI. Shear Retrofit

PARAMETERS INFLUENCING THE BEHAVIOR OF RC BEAMS STRENGTHENED IN SHEAR WITH EXTERNALLY BONDED FRP

Omar CHAALLAL

(Professor, Université du Québec, ETS, Montreal, Canada)

Abdelhak BOUSSELHAM

(Research Fellow, Université du Québec, ETS, Montreal, Canada)

ABSTRACT

The identification of parameters and criteria that influence shear resistance mechanisms is conducted using in-depth analysis of experimental data reported in the literature on shear strengthening with FRP. This identification is based on knowledge of the shear behavior of conventional RC structures on the one hand, and on the state of the art regarding the behavior of RC elements retrofitted in shear with FRP on the other.

KEYWORDS

RC beams, strengthening, shear, FRP sheet, parameters, behavior, static loads, research need.

1. INTRODUCTION

The following parameters and criteria are successively assessed and discussed: (a) the influence of mechanical and geometric properties of FRP, (b) the effect of transverse steel ratio, (c) the effect of longitudinal steel, (d) the effect of shear span ratio or type of beams (slender or regular versus deep), and (e) the scale factor effect or size of the specimens. Additionally, other parameters and criteria which are not sufficiently documented, but which may be important, are also discussed in light of the few research studies available in the literature. These include the effect of concrete strength, the effect of fatigue, the effect of pre-cracking, and the effect of prestress.

2. INFLUENCE OF FRP PROPERTIES

Figure 1 shows, for slender beams ($a/d \geq 2.5$) without transverse steel reinforcement, the variation of effective FRP strain ($\varepsilon_{f,e}$) as a function of FRP rigidity, expressed with respect to the compressive strength of concrete ($E_f \rho_f / f_c'^{2/3}$). Figure 1 illustrates the behavior of beams that have failed by debonding. The same trend was observed for those that have failed in shear by modes other than debonding. From Figure 1, it can be observed that the effective FRP strain decreases as FRP rigidity increases. This confirms the results reported by other researchers (e.g. Boussselham and Chaallal 2004; Triantafillou et al. 2000). In addition, results reveal that the average effective strains attained by the FRP are generally smaller when failure occurs by debonding, compared to other modes of shear failure. However, in all cases, these strains represent only a modest fraction of the ultimate FRP strain capacity: the ratio ($\varepsilon_{f,e} / \varepsilon_{f,u}$) is generally less than 0.30 for failure by debonding and approximately 0.40 for other modes of shear failure. This tendency also holds true for the case of slender beams with transverse steel. In addition, in the presence of transverse steel reinforcement, the FRP tends to attain higher strain values compared to those attained in the absence of transverse steel. However, this does not mean that the gain in shear resistance due to FRP is greater, a conclusion confirmed by numerous studies (Boussselham and Chaallal 2006-a; 2006-b; Chaallal et al. 2002; Pellegrino et al. 2002; Li et al. 2001).

3. EFFECT OF INTERNAL TRANSVERSE STEEL REINFORCEMENT

The influence of transverse steel on the contribution of FRP to shear resistance has been documented by many research studies (Boussselham and Chaallal 2004; Pellegrino et al. 2002; Chaallal et al. 2002; Czaderski 2002; Li et al. 2001). More recently, this influence has been further demonstrated through monitoring of the variation of strains in FRP and in transverse steel under increasing load (Boussselham and Chaallal 2006-a; 2006-b). This influence is

confirmed, at a much larger scale, in the present study which encompasses the data from all research studies reported in the literature. Figure 2 presents, for slender beams, the variation of the gain due to FRP as a function of the ratio $(\rho_{s,t} f_{s,t} / \rho_f f_{f,e})$, where $\rho_{s,t}$ and ρ_f represent the transverse steel and the FRP ratios respectively, and $f_{s,t}$ and $f_{f,e}$ the yield stress of the transverse steel and the effective stress of FRP respectively. Figure 2, which refers to beams that have failed by debonding, clearly indicates that the gain in shear resistance due to FRP decreases as the ratio $(\rho_{s,t} f_{s,t} / \rho_f f_{f,e})$ increases. The same tendency was observed for deep beams ($a/d < 2.5$) that have failed by debonding and those that have ruptured by other modes of shear failure. However, the gains in shear resistance due to FRP which were recorded for beams with transverse steel reinforcement are substantially greater in slender beams (more than 90% gain in shear resistance) than in deep beams (less than 30%). The influence of transverse steel on the contribution of FRP to shear resistance is now an accepted fact well-documented by experimental evidence. However, the resistance mechanisms associated with the phenomenon remain to be explained.

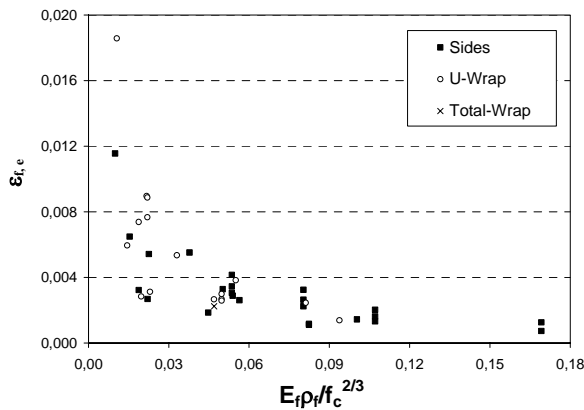


Figure 1: Effective strain of FRP in terms of $E_f \rho_f / f_c^{2/3}$

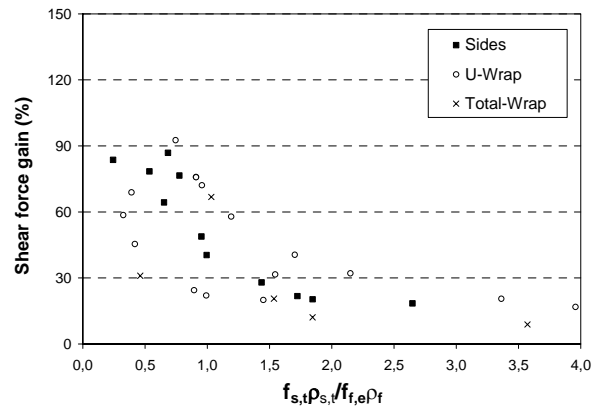


Figure 2: Shear Force Gain in terms of $f_{s,t} \rho_{s,t} / f_{f,e} \rho_f$

4. EFFECT OF SHEAR SPAN TO DEPTH RATIO (SLENDER VS. DEEP BEAM)

Figure 3 typically shows the variation of the gain in shear resistance due to FRP as a function of the so-called a/d ratio involving the shear length (a) and the effective beam depth (d). This figure refers to beams without transverse steel that have failed by debonding. The tendency that is apparent in this figure is the same as that reported in the literature (Bousselham and Chaallal 2004; 2006-b): the gain in shear resistance due to FRP seems in general to be greater in slender beams ($a/d \leq 2.5$) than in deep beams. This is attributed to the strut-and-tie behavior exhibited by the deep beams. It follows that the contribution of external FRP, like that of internal transverse steel, is less significant in deep beams than in slender beams. However, a possible effect of enhanced confinement of concrete in compression due to FRP wrap cannot be excluded (Chaallal et al. 2002). Also, results revealed that failure by debonding of FRP occurs more in slender beams than in deep beams.

5. SCALE FACTOR EFFECT

Figure 4 typically presents the variation of the gain in shear resistance due to FRP as a function of the effective depth of beam section, d . This figure refers to slender beams without transverse steel that have failed by debonding. Figure 4 shows a very clear tendency for gain due to FRP to decrease with increasing effective beam section depth. This confirms the result of a very recent experimental study by Bousselham and Chaallal (2006-c). It must be remembered that the relevance of this result stems from the fact that the experimental data used in this study are derived largely from tests performed on beams of relatively small size, particularly in comparison to bridge girders.

6. EFFECT OF LONGITUDINAL STEEL REINFORCEMENT

Examination of results from the database seems to indicate that the gain due to FRP decreases as the longitudinal steel reinforcement ratio increases. This leads one to suspect the existence of an interaction between the FRP and the longitudinal steel reinforcement. The state of knowledge regarding shear behavior of conventional RC beams indicates that beams with a small longitudinal reinforcement ratio exhibit lower shear resistance than beams with a

larger ratio (ASCE-ACI, 1998). Indeed, the flexural cracks that develop in the latter case are wider and progress at a greater rate towards the compression zone of the beam. In addition, the formation of diagonal cracks occurs earlier (MacGregor and Bartlett, 2000). This affects the shear stress in uncracked concrete, and consequently the contribution of concrete to the shear resistance. Increasing the longitudinal steel reinforcement ratio will translate into a greater contribution of concrete to the shear resistance. Will this increase also translate into a decrease in the gain due to FRP? Clarification of this type of questions may require further experimental and theoretical investigations.

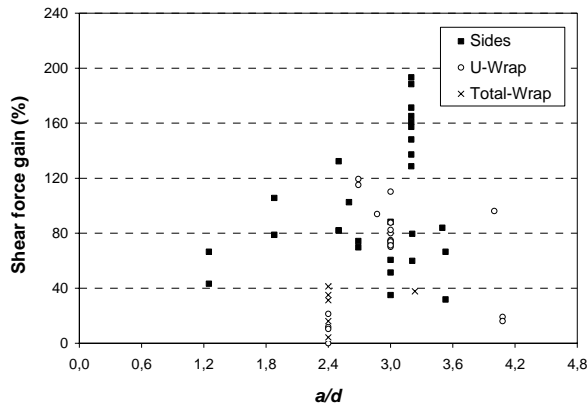


Figure 3: Shear Force Gain in terms of a/d

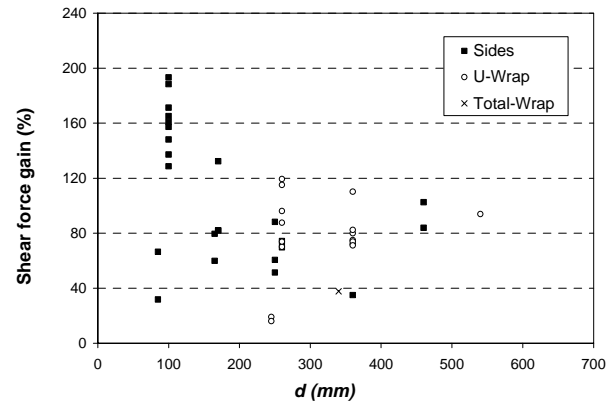


Figure 4: Shear force gain in terms of d

7. EFFECT OF OTHER PARAMETERS AND RESEARCH NEED

Concrete strength has an influence on the performance of shear strengthening with FRP from both the local and the global point of view. From the local point of view, this influence impacts the bonding performance at the FRP-concrete interface. A higher concrete strength will delay, if not inhibit altogether, failure by debonding. From the global point of view, this influence is linked to the failure scenarios proposed, that can differ depending on the level of concrete strength. A high concrete strength (relative to the transverse steel ratio if any, or to the FRP ratio) will inhibit premature crushing of concrete in the compression zone or in the web. Additionally, it will enhance bonding characteristics at the FRP-concrete interface (Bousselham and Chaallal 2006-a). However, despite its importance with regards to the performance of shear strengthening with FRP, the effect of concrete strength has not been systematically studied. It is interesting to note, though, that the guidelines for the design of RC structures strengthened with externally applied FRP take into account the concrete strength when calculating the contribution of FRP to shear resistance (ACI-440.2R 2002; *fib* TG 9.3 2001), either for the determination of the effective FRP or to prevent premature crushing of concrete. Therefore, it may be useful to document this influence analytically and experimentally.

The ACI-215R-05 (2005) Committee has written: “Special attention should be given to the **shear fatigue** strength of beams subjected to high nominal shearing stresses”. This is in accordance with the recommendations formulated by Regan (1993), who, in an exhaustive state-of-the-art report on the shear behavior of RC beams, clearly underlined the need to study this aspect. However, compared to retrofitted RC beams subjected to static loading, the behavior of RC beams retrofitted in shear with FRP and subjected to cyclic loading is much less well-documented. In addition, all the studies on the behavior of strengthened beams under fatigue loading are related either to strengthening of beams in flexure or to the FRP-concrete interface. In contrast, shear strengthening under fatigue is yet to be investigated, since so far there are only two very recent studies reported in the literature dealing with this specific subject (Czaderski 2002; Carolin et al. 2005). It is noted in particular, in the latter study: “There is a tendency for fatigue-loaded beams to have a higher load-bearing capacity when tested to failure compared to beams without a fatigue history.” Nevertheless, additional investigations appear to be necessary, with particular emphasis on the fatigue performance of bonds in the anchorage zone.

Almost all of the experimental investigations conducted so far are related to the shear performance of strengthened RC beams that had not been **pre-loaded (pre-cracked)** prior to their retrofit. However, external strengthening with FRP is most suitable for existing in-service structures that often are pre-cracked, if not pre-damaged. The few investigations carried out so far on RC beams that were pre-cracked prior to their strengthening indicate that pre-

loading does not affect the shear performance of retrofitted beams (Czaderski 2002, Carolin et al. 2005, Hassan Dirar et al. 2006).

According to *fib* T.G 9.3 (2001), “less than 10% of the bridges that have been FRP-strengthened so far are **pre-stressed**”. This seems rather surprising given the number of bridge superstructures made of pre-stressed concrete (PC). To our knowledge, the only study dealing with PC beams strengthened in shear with FRP was performed by Hutchinson and Rizkalla (1999). The latter reported that the prediction by the shear equation in ACI-318 was in good agreement with the test results of seven pre-stressed concrete beams strengthened with CFRP strips. However, there is not a single study in the existing literature dedicated specifically to the effect of pre-stressing on the performance of shear strengthening with externally bonded FRP. It must be borne in mind that this is a very complex problem, because on the one hand, the behavior of PC structures is mostly characterized by long-term phenomena, and on the other hand, strengthening is often applied to structures that have already been subjected to long-term effects such as creep, relaxation, and shrinkage. Therefore, the impact of such effects on the state of deformation of the retrofitted structure remains to be understood and adequately evaluated through simulations or targeted tests.

8. REFERENCES

- ASCE-ACI Task Committee 445. (1998). Recent Approaches to Shear Design of Structural Concrete. *J. of Structural Engineering*, ASCE, 124(12), pp. 1375-1417.
- Bousselham, A., Chaallal, O. (2006-a). Behavior of RC T-Beams Strengthened in Shear with CFRP: An Experimental Study. *ACI Structural Journal*, Vol. 103, No.3, May-June, pp. 339-347.
- Bousselham, A., Chaallal, O. (2006-b). Effect of Transverse Steel and Shear Span on the Performance of RC Beams Strengthened in Shear with CFRP. *Composites: Part B*, Elsevier, Vol. 37, pp 37-46.
- Bousselham, A., Chaallal, O. (2006-c). Influence of the Beam Size on the Shear Strength of RC T-Beams Retrofitted in Shear with CFRP fabrics. To appear in *ACI Structural Journal*, 40 p.
- Bousselham, A., Chaallal, O. (2004). Shear Strengthening Reinforced Concrete Beams with Fiber-Reinforced Polymer: Assessment of Influencing Parameters and Required Research. *ACI Str. J.*, Vol. 101, No.2, pp. 219-227.
- Chaallal, O., Shahawy, M., Hassan, M. (2002). Performance of Reinforced Concrete T-Girders Strengthened in Shear with CFRP Fabrics. *ACI Structural Journal*, 99(3), pp. 335-343.
- Czaderski, C. (2002). Shear Strengthening with Prefabricated CFRP L-Shaped plates. Test Beams S1 to S6, EMPA. Report No. 116/7, Switzerland, 78 p.
- Carolin, A., Taljsten, B. (2005). Experimental Study of Strengthening for Increased Shear Bearing Capacity. *Journal of Composites for Construction*, 9(6), pp. 488-496.
- fib*-TG9.3. (2001). Design and Use of Externally Bonded Fiber Polymer Reinforcement (FRP EBR) for Reinforced Concrete Structures. Technical Report Prepared by EBR Task Group 9.3, Bulletin 14.
- Hassan Dirar, S.M.O., Hoult, N.A., Morley, C.T., Lees, J.M. (2006). Shear Strengthening of Pre-cracked Reinforced Concrete Beams Using CFRP Straps. *Fédération Internationale de Béton (FIB)*, Proceedings of the 2nd International Congress, Naples, Italy, June 5-8, ID 10-70
- Li, A., Assih, J., Delmas, Y. (2001). Shear Strengthening of RC Beams with Externally Bonded CFRP Sheets. *J. of Structural Engineering*, ASCE, 27(4), pp. 374-380.
- Pellegrino, C., Modena, C. (2002). Fiber Reinforced Polymer Shear Stengthening of RC Beams with Transverse Steel Reinforcement. *J. of Composites for Construction*, ASCE, 6(2), pp. 104-111.
- Regan, P.E. (1993). Research on Shear: A Benefit to Humanity or a Waste of Time? *The Structural Engineer*, 71(19), pp. 337-347.
- Rizkalla, S., Hassan, T., Hassan, N. (2003). Design Recommendations for the Use of FRP for Reinforcement and Strengthening of Concrete Structures. *Prog. Struct. Engng. Mater.* Wiley, 5, pp. 16-28.

Calculating the Thickness of FRP Jacket for Shear and Torsion Strengthening of RC T-Girders



A. Deifalla

(Ph.D Candidate, McMaster University, Hamilton, ON, Canada)

A. Ghobarah

(Professor, United Arab Emirates University, Al-Ein, UAE)

ABSTRACT

Failure of a structural element under diagonal compression is brittle in nature and could compromise the structure ductility in seismic design. In many cases, strengthening using FRP Jackets might be the optimum solution to prevent such failures. A procedure for calculating the thickness of the FRP jacket required to resist combined shear and torsion is proposed. The proposed procedure was used to calculate the FRP thickness required for the strengthening of three T-girders subjected to combined shear and torsion. The girders were constructed and tested using a test setup designed to subject the specimen to combined shear and torsion with relatively low moment up to failure. Three strengthening techniques namely; U-jacket, extended U-jacket and full jacket were implemented using $\pm 45^\circ$ carbon fiber reinforced polymers (CFRP). The theoretical predications were compared to the experimental results. The procedure was found to provide reasonable conservative estimates.

KEYWORDS

T-girders, shear, torsion, strengthening, FRP experimental

1. INTRODUCTION

In elevated expressways and bridges, girders are often subjected to significant torsion which could result from eccentricity of lane loading, torsionally restrained joints and supports and curved alignments in plan. The complexity and disadvantages of strengthening using materials such as steel and concrete jackets and the high cost of structures replacement have prompted the research into the area of strengthening structures using composite materials. Fiber reinforced polymers (FRP) laminates and fabrics have been used successfully in various applications. Due to the properties of the FRP such as high strength and low weight as well as ease of installation, these materials are becoming of interest in the civil engineering applications. Research efforts were directed towards strengthening rectangular beams using fully wrapped jackets. In this paper, a simple procedure was proposed to calculate the thickness of FRP jacket required to provide additional combined shear and torsion strength for the RC T-girders. The procedure is an extension of the simplified methodology developed by Deifalla and Ghobarah (2005) for torsion strengthening. The procedure is verified using the results of a pilot experimental program that is conducted to evaluate the influence of externally applied FRP fabrics on the behavior of the strengthened reinforced concrete (RC) T-girders subjected to combined shear and torsion (Deifalla and Ghobarah 2006). Where four T-girders TG1, TG2, TG3 and TG4 were tested under a constant torque to shear ratio of 0.5 m which was chosen as to represent the case of significant torsion combined with shear. TG1 is the control girder while TG2 to TG4 are the strengthened girder.

3. CALCULATION OF THE FRP JACKET THICKNESS

The proposed procedure calculates the thickness required at the critical section where it is reasonable to assume that the effect of the torsion and shear can be added together. The FRP thickness required to resist torsion (t_t) is calculated using the hollow tube analogy, space truss theory such that:

$$t_t = \frac{T - T_o}{2E_f \varepsilon_f A_o [\cos \beta + \sin \beta]} \quad (1)$$

where T is the total torsion capacity of the strengthened girder and T_o is the total torsion capacity of the un-strengthened girder, E_f is Young's modulus of FRP sheets, ε_f is the effective strain in the FRP sheet, β is angle of fiber orientation for the FRP sheets and A_o is the area enclosed inside the critical shear flow path. The threaded anchors were used and were to resist torsion by creating a closed loop for shear flow path. Based on the design provisions CSA-S806-02 (2002), the FRP thickness required to resist the additional shear (t_v) may be computed as:

$$t_v = \frac{V - V_o}{2E_f \varepsilon_f d [\sin \beta + \cos \beta]} \quad (2)$$

where V is the total shear resistance of the strengthened girder, V_o is the total shear resistance of the un-strengthened girder and d is the depth of the FRP sheet resisting shear. Assuming linear interaction between the FRP torsion and shear contribution, the FRP area per unit length required to resist both shear and torsion (t_f) will be taken as the summation of the FRP area per unit length required to resist shear (t_v) and the FRP thickness required to resist the torsion (t_t). Thus, the total FRP thickness required to resist the applied combined torsion and shear (t_f) can be calculated as:

$$t_f = t_v + t_t \quad (3)$$

The procedure requires that the value of the FRP strain at failure is known which is dependent on several parameters including the strengthening scheme used, the concrete, FRP dimensions and properties. No previous studies were conducted on the area of combined shear and torsion strengthening. However, Very limited number of investigations were conducted on the area of torsion strengthening. Deifalla and Ghobarah (2005) proposed three different formulas for calculating the strain for torsion strengthening which were verified using an extensive database gathered from various sources. Although these formulas were developed for torsion strengthening, the T-girders were tested under significant torsion. Hence these formulas can be adopted in the analysis.

2. EXPERIMENTAL RESULTS

The proposed procedure was verified using the results of an experimental investigation conducted for the purpose of investigating the behavior and strengthening of RC T-girders under combined actions. A brief summary of the program and the results is provided. Four T-girders TG1, TG2, TG3 and TG4 were constructed and tested. The compressive strength of 25.6 MPa was obtained from the compression testing of three standard concrete cylinders at 28 days. The CFRP used in this experimental program is Tyfo BCC composite, which includes Tyfo BCC reinforcing fabric and Tyfo S Epoxy (Fyfe Co. 2002). The primary fibers are continuous in the ± 45 directions and the composites provide ultimate strength in the direction of the fibers. The properties of the CFRP as provided by the supplier were a tensile strength of 609 MPa, modulus of elasticity of 63.3 GPa, maximum elongation of 9.6 mm/m, and thickness of 0.86 mm.

The T-girders were tested under significant torsion, shear with a ratio of 0.5 m. The applied bending moment is considered small. The typical cross section of the T-girders is shown in figure 1. The girders were heavily reinforced in the longitudinal direction within the test zone to minimize the effect of the flexure focusing on the shear and torsion behavior. To insure failure occurring within the test zone, the girders were heavily reinforced in the longitudinal direction as well as in the transverse direction. Fig. 2 shows a schematic of the applied loads (L1, L2 and L3) and restraint reactions (R1, R2 and R3) in the test setup.

During the strengthening procedure, special attention was paid to insure the bond between the concrete surface and the CFRP sheets. In addition, the concrete edges were rounded in order to minimize the stress concentration in the fibers at the edges. The strengthening techniques implemented covered most of the different situations. The first technique used consisted of one FRP sheet bonded to the web and anchored below the inner intersection of the web and the flange as shown in Fig. 3.a. The second technique shown in Fig. 3.b consisted of FRP sheet bonded to the web and extended to the bottom of the flange. The FRP sheet was prevented from pulling out at the inner intersection of the web and the flange by a steel angle. The third technique consisted of two FRP sheets, the first piece was similar to the second technique and the second sheet was bonded to the flange. The two sheets overlapped to insure continuation of the forces resisting torsion. A steel angle as well as anchor rod was provided.

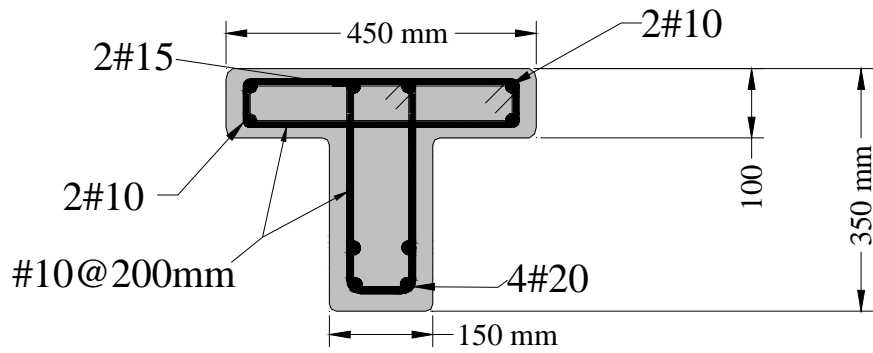


Figure 1: Typical T-girder cross section

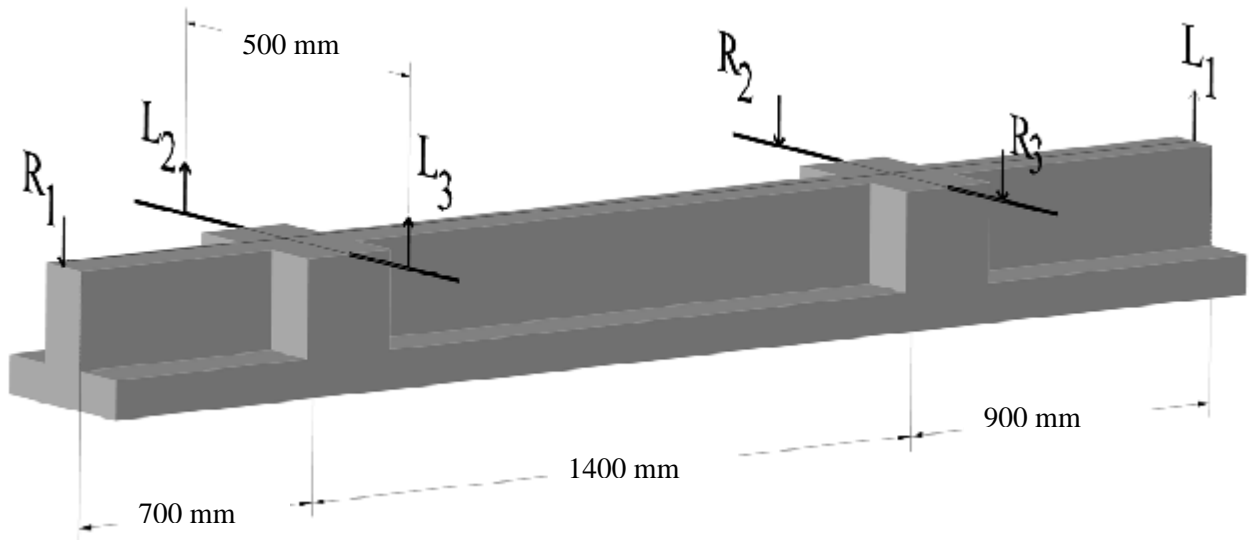


Figure 2: Test Setup

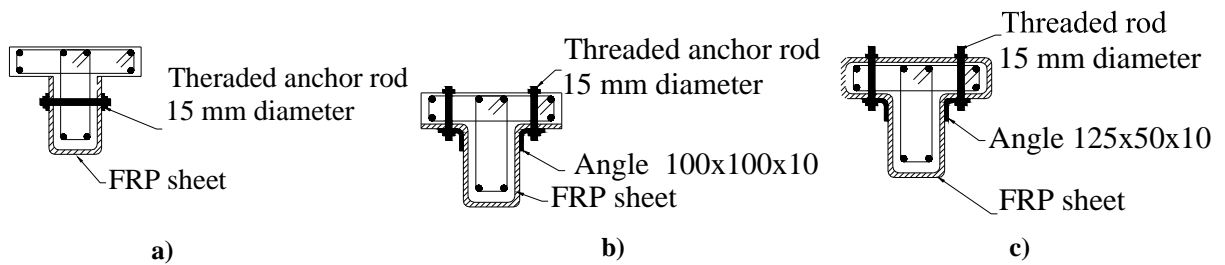


Figure 3: Strengthening Schemes a) U-Jacket, TG2, b) Extended U-Jacket, TG3 and c) Full wrapping, TG4

Table 1 Summary of the experimental results

Girder	Shear* (kN)	Mode of failure
TG1	46	Steel stirrup yield followed by concrete crushing
TG2	68	FRP intermediate debonding followed by flange concrete crushing
TG3	76	FRP intermediate debonding
TG4	80	FRP intermediate debonding

* Torsion to shear ratio is 0.5 m.

Table 1 shows a summary of the maximum shear resistance and the failure mode for the tested girders TG1, TG2, TG3 and TG4. The corresponding torsion resistance can be calculated as 0.5 m multiplied by the maximum shear resistance. All strengthened girders failed due to FRP intermediated diagonal debonding similar to the concrete diagonal cracks due to diagonal tension resulting from applied torsion and shear.

4. VERIFICATION OF THE PROCEDURE

The FRP thickness was predicted using equations 1, 2 and 3. The strain was calculated by the formula developed by Deifalla and Ghobarah (2005) for the FRP intermediate debonding due to concrete cracking. The FRP strain is calculated as follows:

$$\varepsilon_f = \frac{0.33 w_f}{L_e s_f} \quad (4)$$

where w_f is the width of the FRP strips and s_f is the spacing between the centerline of the FRP strips. For the case of continuous FRP sheets $w_f = s_f$ and L_e is calculated using the formula:

$$L_e = \sqrt{\frac{E_f t_f}{\sqrt{f_c}}} \quad (5)$$

Where E_f is the FRP Young's modulus and t_f is the thickness of the FRP sheets and f_c is the compressive strength of the concrete. The values of V_o and T_o are taken the same as the strength of TG1. Table 2 shows the comparison between the predicted and the actual FRP thickness. The thicknesses calculated from the proposed procedure are in a good agreement with the experimentally used thicknesses.

Table 2 Comparison between actual and the calculated FRP thickness

Beam	Strengthening Technique	Ratio between Calculated and Actual FRP thickness
TG2	Anchored U-jacket	0.74
TG3	Anchored Extended U-Jacket	0.85
TG4	Anchored Full wrapping	0.91
	Average	0.83
	Standard deviation	0.09

5. CONCLUSIONS

A procedure for calculating the thickness of the FRP jacket for shear and torsion strengthening of RC T-girders was proposed and verified against the results of an experimental program. The proposed procedure provides conservative estimates for the FRP thickness required to resist the applied torsion and shear. Further experimental testing is required to generalize the procedure, in particular, the predication of the effective FRP strain.

6. REFERENCES

- CSA-S806-02. (2002). "Design and Construction of Building Components with Fiber-Reinforced Polymers", Canadian Standards Association, Rexdale, Canada, 206 pages.
- Fyfe Co. (2002). "<http://www.Fyfeco.com/products/compositesystems/Bcc.html>", accessed January 2002.
- Ghobarah, A., Ghorbel, M., and Chidiac, S. (2002). "Upgrading Torsional Resistance of RC Beams Using FRP", *Journal of Composites for Construction*, ASCE, Vol. 6, No. 4, pp. 257-263.
- Deifalla, A., Ghobarah, A. (2005). "Simplified Analysis of RC Beams Torsionally strengthened Using FRP", *Proceedings of International Symposium on Bond Behavior of FRP in Structures (BBFS 2005)*, Hong Kong, China, edited by Chen and Teng, December 7-9, pp. 381-386.
- Deifalla, A., Ghobarah, A. (2006). "Shear and torsion strengthening of RC T-beams", Submitted, *Composite structures*, Elsevier.

CALIBRATION OF EUROCODE-LIKE EQUATION FOR THE CONCRETE CONTRIBUTION TO THE SHEAR CAPACITY OF FRP RC MEMBERS

Raffaello Fico, Andrea Prota, Renato Parretti, Gaetano Manfredi and Antonio Nanni

(Department of Structural Analysis and Design, University of Naples "Federico II", Naples, Italy)

ABSTRACT

Fiber Reinforced Polymer (FRP) bars represent an interesting alternative to conventional steel as internal reinforcement of Reinforced Concrete (RC) members where some properties such as durability, magnetic transparency, insulation, are of primary concern. Critical aspects of the design of FRP RC members are serviceability issues, bond, and the reduced concrete contribution to the shear capacity compared to equivalent steel reinforced members. The present paper focuses on the calibration of Eurocode-like equation for the evaluation of the shear strength of FRP RC members without shear reinforcement. The calibration is based on an extensive database of experimental data available in the literature. The concrete contribution to shear capacity is analyzed considering tested members without shear reinforcement and, with reference to Eurocode equation for shear capacity of steel RC members, a modified equation is proposed. A parametric analysis is presented comparing the results of the proposed equation with those given by both CSA and ACI guidelines.

KEYWORDS

Design, FRP, Reinforced Concrete, Shear.

1 INTRODUCTION

FRP has much potential as longitudinal reinforcement in concrete structures exposed to reinforcement corrosion and stressed primarily in bending. Bridge decks, footings, floor slabs, soft eyes applications and wall type structures are some examples of such structural components. In these elements, flexural strength is mainly provided by the longitudinal reinforcement, and the shear strength is provided by the concrete alone because of the lack of transverse reinforcement. Hence, it is critical that an accurate assessment of concrete contribution to the shear strength of members reinforced with FRP bars as flexural reinforcement, $V_{c,f}$, is performed. Test results have shown that the shear strength of FRP RC beams is significantly lower than that predicted using equations developed for steel reinforcement. Nevertheless, it is definitely recognized that the shear strength due to concrete, $V_{c,f}$, can be calculated according to the same principles as for steel reinforced concrete after accounting for the different mechanical properties between FRP and steel reinforcement. This is the approach taken herein to calibrate the equation given by Eurocode 2 for the calculation of the concrete contribution to shear capacity of steel RC members. Based on this equation, a new formula accounting for the concrete contribution to shear capacity of FRP RC elements was derived; this expression has been included in the lately issued guidelines of the Italian Research Council CNR-DT 203/2006.

2 REVIEW OF CURRENT DESIGN PROVISIONS

Findings from experimental investigations on concrete beams without stirrups and longitudinally reinforced with carbon and glass FRP bars show that the shear strength reduction experienced by such members when compared to the shear strength of those reinforced with the same amount of steel reinforcement, is mainly due to the relatively lower modulus of elasticity. Such investigations also reveal that the axial stiffness of the reinforcing bars is a key

parameter when evaluating the concrete shear strength of flexural members reinforced with FRP bars. Most of the current international Standard Codes developed methods to compute $V_{c,f}$ that are based on these assumptions. This section summarizes the design equations to compute $V_{c,f}$, as recommended by the American Concrete Institute (ACI 440.1R-03 2003), the Canadian Standard Association (CAN/CSA-S806_02 – 2002) and by Tureyen and Frosh (Tureyen and Frosh, 2003).

2.1 ACI 440.1R-03 Design Guidelines

ACI Committee 440 recommends the following equation for calculating $V_{c,f}$:

$$V_{c,f} = \frac{\rho_f E_f}{\rho_s E_s} V_c \quad (1)$$

where ρ_f and ρ_s are the flexural FRP and steel reinforcement ratio, respectively, E_f and E_s are the modulus of elasticity of FRP and steel reinforcement, respectively, and V_c is the design shear resistance provided by concrete when steel reinforcement is used. It is clear that such equation accounts for the axial stiffness of the FRP reinforcement ($A_f E_f$) as compared to that of steel reinforcement ($A_s E_s$).

2.2 CAN/CSA-S806_02 Design Guidelines

The CSA S806-02 gives the following expression to compute $V_{c,f}$ for sections having either the minimum amount of transverse reinforcement required or $d < 300mm$:

$$V_{c,f} = 0.035 \lambda \phi_c \left(f_c' \rho_f E_f \frac{V_f}{M_f} d \right)^{\frac{1}{3}} b_w d \quad (2)$$

where λ accounts for concrete density (set equal to 1 herein), ϕ_c is the resistance factor for concrete, f_c' is the specified compressive strength of concrete, V_f and M_f are the factored shear force and moment at the section of interest, b_w is the web width and d is the distance from the compression fiber to the centroid of the main tension reinforcement. For sections with $d > 300mm$ and with no transverse shear reinforcement, $V_{c,f}$ is calculated using:

$$V_{c,f} = \left(\frac{130}{1000 + d} \right) \lambda \phi_c \sqrt{f_c'} b_w d \geq 0.08 \lambda \phi_c \sqrt{f_c'} b_w d \quad (3)$$

The latter equation is derived from the corresponding formula given for steel reinforced sections, multiplied by 0.5.

2.3 Equation Proposed by Tureyen and Frosh

Due to the conservative predictions of equation (1), Tureyen and Frosh (2003) proposed a different design method to compute $V_{c,f}$, as follows:

$$V_{c,f} = \frac{2}{5} k \sqrt{f_c'} b_w d \quad (4)$$

where

$$k = \sqrt{2\rho_f n_f + (\rho_f n_f)^2} - \rho_f n_f \quad (5)$$

and $n_f = E_f/E_c$, E_c being the elastic modulus of concrete. It can be observed that through factor k , eq. (4) is a function of the axial stiffness $A_f E_f$.

3 PROPOSED SHEAR EQUATION

The proposed formula is a modified version of the Eurocode 2 (Eurocode 2, 1992) shear equation recommended for conventional steel RC members, which is:

$$V_c = \tau_{Rd} \cdot c \cdot (1.2 + 40\rho_s) \cdot b_w \cdot d \quad (6)$$

where τ_{Rd} is the design shear stress per unit area (equal to $0.053f'_c/\gamma_c$, γ_c being the strength reduction factor for concrete) and c is a factor depending on d .

A calibration was conducted in order to modify eq. (6) and extend it to FRP RC members; the following expression for $V_{c,f}$ has been proposed:

$$V_{c,f} = 1.3 \cdot \left(\frac{E_f}{E_s} \right)^{1/2} \cdot \tau_{Rd} \cdot c \cdot (1.2 + 40\rho_f) \cdot b_w \cdot d \quad (7)$$

Eq. (7) is also included in the Italian guidelines CNR-DT 203/2006.

4 VERIFICATION OF THE PROPOSED EQUATION

4.1 Experimental Database

In order to verify the proposed equation, a database composed of test results related to 79 specimens tested (beams and one way slabs) was used for comparisons, as given in Table 1.

Four specimens were reinforced with aramid FRP bars, 22 specimens reinforced with carbon FRP, and 53 specimens reinforced using glass FRP bars. All specimens had no transverse reinforcement and failed in shear. The concrete compressive strength, f'_c , ranged between 24.1 and 50.0 MPa (specimens with $f'_c > 50\text{MPa}$ were neglected not being typical of FRP RC members). The reinforcement ratio of tensile FRP bars, ρ_f , ranged between 0.0025 and 0.03; however, since CNR-DT 203 prescribes a minimum ρ_f equal to 0.01, experimental points below this threshold (dashed line in Figure 1) were not significant for the sake of the calibration. The effective depth, d , ranged between 150 and 970 mm, and the shear span to depth ratio, a/d , ranged between 1.82 and 5.80.

4.2 Comparison with Major Design Provisions

The predictions from equation (7) were compared with the values derived using the equations reported in section 2, after setting the strength reduction factors equal to the unity. It can be observed from Table 1 and Figure 1 that the trend line of CNR-DT 203 equation is very similar to that of CSA S-802 equation; the CNR-DT 203 line has the least mean value of V_{exp}/V_{pred} (i.e., 1.33) and coefficient of variation (i.e., 26 %), which is defined as the ratio of the standard deviation to the mean and is a measure of dispersion of a probability distribution. Thus, the proposed equation is found to be reliable for predicting the shear capacity of FRP RC members without shear reinforcement.

5 CONCLUSIONS

The paper presents the work at the basis of the Eurocode-like shear equation suggested by the CNR-DT 203 to compute the concrete contribution to the shear capacity of FRP RC members. Based on a wide experimental database, a verification of the proposed equation is carried out and a comparison with American and Canadian provisions is discussed. It is concluded that the proposed equation could give accurate predictions and yet enough conservative.

6 REFERENCES

- ACI Committee 440. (2003). "Guide for the Design and Construction of Concrete Reinforced with FRP Bars," ACI 440.1R-03, American Concrete Institute, Farmington Hills, Mich..
- CAN/CSA S806-02. (2002). "Design and Construction of Building Components with Fibre Reinforced Polymers", Canadian Standards Association, Rexdale, Ontario.
- CNR-DT 203/2006. (2006). "Istruzioni per la Progettazione, l'Esecuzione ed il Controllo di Strutture di Calcestruzzo armato con Barre di Materiale Composito Fibrorinforzato," *National Research Council*, Rome, Italy.
- El Sayed, A.K. et al. (2006). "Shear Strength of Concrete Beams Reinforced with FRP Bars: Design Method", *ACI Structural Journal*, V. 103, No 2, pp. 235-243.
- EN 1992-1-1 Eurocode 2 (1992). Design of concrete structures - Part 1-1: General rules and rules for buildings.

Razaqpur, A.G., and Isgor, O.B. (2006). "Proposed Shear Design Method for FRP-Reinforced Concrete Members without Stirrups", *ACI Structural Journal*, V. 103, No 1, pp. 93-102.

Tureyen, A. K., and Frosch, R. J. (2003). "Concrete Shear Strength: Another Perspective", *ACI Structural Journal*, V. 100, No. 5, pp. 609-615.

Table 1: Characteristics of Specimens Used and Comparison of Design Methods

Reference	f'_c [Mpa]	b_w [mm]	d [mm]	ρ_f	E_f [Gpa]	V_{exp} / V_{pred}			
						CNR	ACI	CSA	Tur-Fr.
Razaqpur	40.5	200	225	0.0025	145	0.87	5.80	1.30	2.19
	40.5	200	225	0.0050	145	1.05	3.77	1.34	2.08
	40.5	200	225	0.0063	145	1.02	3.00	1.25	1.89
	40.5	200	225	0.0050	145	2.16	7.72	2.41	4.26
	40.5	200	225	0.0050	145	1.05	3.77	1.47	2.08
Yost et al.	36.3	229	225	0.0131	40.3	1.22	3.56	1.24	1.73
	36.3	178	225	0.0170	40.3	1.21	2.96	1.23	1.66
	36.3	229	225	0.0197	40.3	1.25	2.80	1.28	1.70
	36.3	279	225	0.0215	40.3	1.01	2.15	1.04	1.37
	36.3	254	225	0.0243	40.3	1.05	2.08	1.09	1.42
Zhao & Maruyama	34.3	150	250	0.0151	105.0	1.26	1.93	1.30	1.79
	34.3	150	250	0.0302	105.0	0.96	0.99	1.06	1.38
	34.3	150	250	0.0227	105.0	0.97	1.15	1.03	1.36
Alkhajardi et al.	24.1	178	279	0.0230	40.0	2.01	2.72	1.48	2.23
	24.1	178	287	0.0077	40.0	1.86	5.33	1.37	2.39
	24.1	178	287	0.0134	40.0	1.80	3.40	1.27	2.06
Tairiq & Newhook	37.3	160	346	0.0072	42	2.01	8.43	1.67	2.99
	37.3	160	346	0.0072	42	2.35	9.85	1.95	3.49
	43.2	160	346	0.0110	42	1.30	4.41	1.22	1.85
	43.2	160	346	0.0110	42	1.38	4.70	1.29	1.97
	34.1	160	325	0.0154	42	1.64	3.69	1.63	2.06
	34.1	160	325	0.0154	42	1.51	3.40	1.51	1.90
	37.3	130	310	0.0072	120	1.44	3.66	2.01	2.30
	37.3	130	310	0.0072	120	1.34	3.40	1.88	2.14
	43.2	130	310	0.0110	120	1.14	2.36	1.81	1.78
	43.2	130	310	0.0110	120	1.27	2.61	2.00	1.97
	34.1	130	310	0.0154	120	1.42	1.91	2.39	1.94
	34.1	130	310	0.0154	120	1.48	1.99	2.50	2.03
	Benmokrane et al. ¹ (2004)	50.0	250	326	0.0087	130	0.86	2.23	1.37
50.0		250	326	0.0087	40.0	1.41	6.61	1.25	2.27
44.6		250	326	0.0124	130	1.14	2.09	1.95	1.75
44.6		250	326	0.0124	40	1.18	3.93	1.12	1.69
43.6		250	326	0.0172	130	1.24	1.80	2.36	1.84
Tur-Frosch	39.7	457	360	0.0096	40.5	1.25	4.42	1.07	1.74
	39.9	457	360	0.0096	37.6	1.13	4.17	0.96	1.58
	40.3	457	360	0.0096	47.1	1.22	4.04	1.15	1.72
	42.3	457	360	0.0192	40.5	1.22	2.82	1.34	1.59
	42.5	457	360	0.0192	37.6	1.40	3.39	1.49	1.83
42.6	457	360	0.0192	47.1	1.45	3.14	1.72	1.92	
Reference	f'_c [Mpa]	b_w [mm]	d [mm]	ρ_f	E_f [Gpa]	V_{exp} / V_{pred}			
						CNR	ACI	CSA	Tur-Fr.
Lubell et al.	40.0	450	970	0.0046	40	1.33	4.43	0.75	1.17
Yost et al.	38.0	305	192	0.0036	41.4	0.91	7.94	1.17	1.92
Mizukawa et al.	34.7	200	260	0.0130	130	1.18	1.81	1.22	1.73
Duranovic et al.	38.1	150	210	0.0131	45	1.27	3.70	1.31	1.87
	32.9	150	210	0.0131	45	1.17	2.99	1.14	1.61
Swamy-Aburawi	34.0	254	222	0.0155	34	1.24	3.34	1.06	1.67
Benmokrane et al. ² (2004)	40.0	1000	165	0.0039	114	0.96	4.99	1.31	2.11
	40.0	1000	165	0.0078	114	1.03	2.98	1.24	1.85
	40.0	1000	161	0.0118	114	1.08	2.30	1.07	1.80
	40.0	1000	162	0.0086	40	1.17	5.30	1.15	1.96
	40.0	1000	159	0.0170	40	1.23	3.44	1.15	1.84
	40.0	1000	162	0.0171	40	1.39	3.85	1.32	2.06
	40.0	1000	159	0.0244	40	1.22	2.75	1.17	1.80
	40.0	1000	154	0.0263	40	1.25	2.71	1.18	1.85
	36.3	229	225	0.0111	40.3	1.33	4.37	1.24	1.94
	36.3	229	225	0.0111	40.3	1.31	4.30	1.22	1.91
Yost et al. (2001)	36.3	229	225	0.0111	40.3	1.25	4.11	1.17	1.82
	36.3	178	225	0.0142	40.3	1.14	3.16	1.06	1.60
	36.3	178	225	0.0142	40.3	1.43	3.93	1.32	1.99
	36.3	178	225	0.0142	40.3	1.31	3.61	1.21	1.83
	36.3	229	225	0.0166	40.3	1.20	2.99	1.11	1.65
	36.3	229	225	0.0166	40.3	1.46	3.63	1.35	2.01
	36.3	229	225	0.0166	40.3	1.34	3.34	1.24	1.85
	36.3	279	225	0.0181	40.3	1.05	2.46	0.97	1.43
	36.3	279	225	0.0181	40.3	1.10	2.58	1.02	1.50
	36.3	279	225	0.0181	40.3	1.10	2.59	1.02	1.50
	36.3	254	224	0.0205	40.3	0.95	2.07	0.89	1.28
	36.3	254	224	0.0205	40.3	1.28	2.80	1.2	1.74
	36.3	254	224	0.0205	40.3	1.17	2.55	1.1	1.59
	36.3	229	224	0.0227	40.3	1.16	2.39	1.1	1.57
	36.3	229	224	0.0227	40.3	1.11	2.29	1.05	1.51
Deitz et al. (1999)	36.3	229	224	0.0227	40.3	1.10	2.27	1.04	1.49
	28.6	305	157.5	0.0073	40	1.21	4.67	1.19	1.85
	30.1	305	157.5	0.0073	40	1.23	4.99	1.38	1.92
	27	305	157.5	0.0073	40	1.37	5.01	1.47	2.04
	28.2	305	157.5	0.0073	40	1.30	4.94	1.42	1.97
	30.8	305	157.5	0.0073	40	1.19	4.90	1.33	1.86
Mean						1.33	3.59	1.49	1.96
Standard deviation						0.35	1.85	0.41	0.54
Coefficient of variation						26%	52%	28%	28%

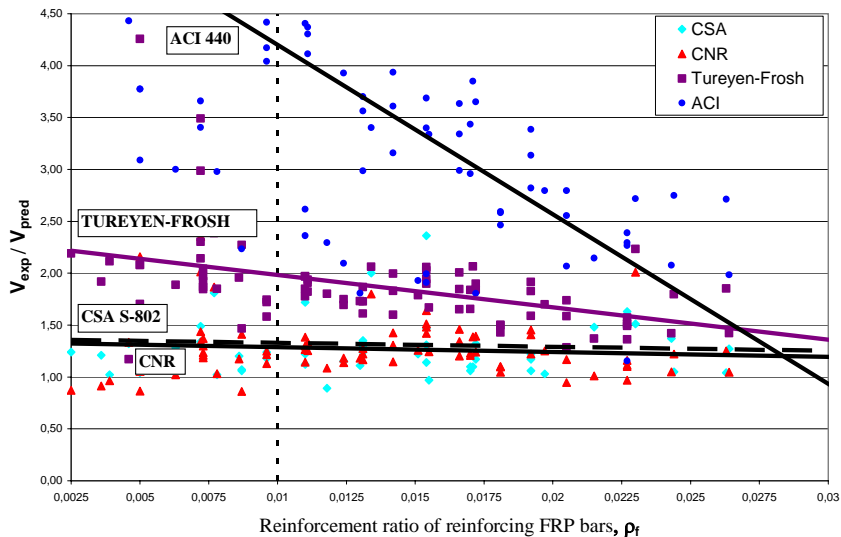


Figure 1: Comparison with Major Design Provisions

DUCTILITY AND SHEAR STRENGTH ENHANCEMENT BY FIBER SHEET WITH LARGE FRACTURING STRAIN

UEDA Tamon

(Professor, Hokkaido University, Sapporo, Japan)

Dhannyanto ANGGAWIDJAJA

(Graduate Student, Hokkaido University, Sapporo, Japan)

SENDA Mineo

(Graduate Student, Hokkaido University, Sapporo, Japan)

NAKAI Hiroshi

(Manager, Maeda Kosen Co. Ltd., Tokyo, Japan)

DAI Jianguo

(Project Researcher, Port and Airport Research Institute, Yokosuka, Japan)

ABSTRACT

Recently the authors have developed a jacketing method with fiber sheet whose fracturing strain is higher and stiffness is lower than those of commonly used fibers namely carbon aramid and glass. The fiber is Polyethylene Terephthalate (PET) and Polyethylene Naphthalate (PEN). In this paper results from a series of experiments on ductility and shear strength enhancement are presented. Fifteen specimens, modelled after a typical bridge pier, with PET and PEN sheet jacketing were tested under a reversed cyclic loading until the ultimate ductility was attained. The stiffness of PET and PEN sheet is smaller than that of carbon sheet to achieve a similar ultimate ductility. Two specimens tested for shear strength enhancement showed a higher shear strength and more ductile manner than a companion specimen with carbon fiber sheets. A good control of shear deformation by the un-fractured sheet is a primary reason to enhance the ductility and shear strength which cannot be predicted by the existing formula derived from results of tests with carbon and aramid fibers. Due to its good features and lower cost, the jacketing with PET and PEN sheet is adopted as a seismic retrofitting method for railway structures in Japan.

KEYWORDS

FRP sheet, jacketing, ductility, shear strength, large fracturing strain

1. INTRODUCTION

Major drawbacks with FRP strengthening for concrete structures are high cost and brittleness of the material. One reason why we have been unable to remove these drawbacks is the fact that we have been emphasizing on strength and stiffness of the material. To fully utilize concrete material properties besides strength/stiffness high fracturing strain is also vital to the reinforcing materials. A required strength/stiffness is not necessarily supplied by high strength/stiffness materials. However a high fracturing strain can be achieved only by materials with a high fracturing strain. Materials of a low strength/stiffness are generally equipped with a high fracturing strain at a low cost, while materials of a high strength/stiffness usually with a low fracturing strain are available at a high cost (see Figure 1). This is the background of our recent project to develop a seismic retrofitting method by jacketing fiber sheets whose fracturing strain is large. The fiber used in this study was Polyethylene Terephthalate (PET) and Polyethylene Naphthalate (PEN). The ultimate strength, fracturing strain, and elastic modulus in tension of PET are 923 MPa, 0.123 % and 6.7 GPa, while those of PEN are 1028 MPa, 0.045 % and 22.6 GPa, respectively.

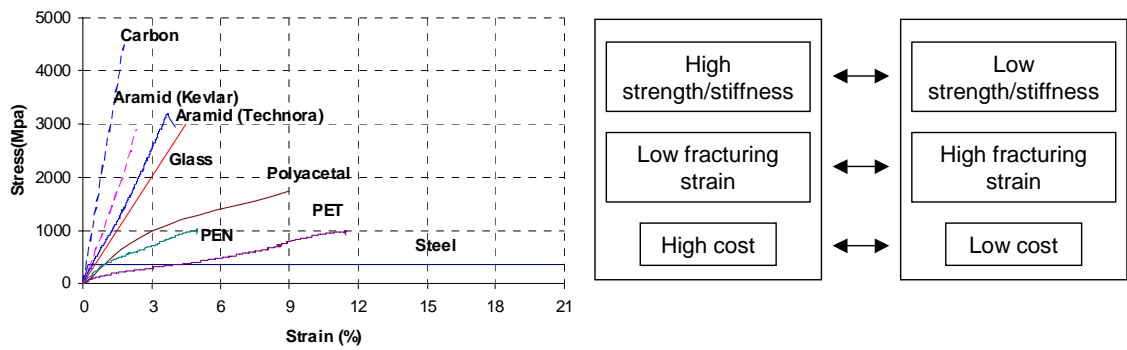
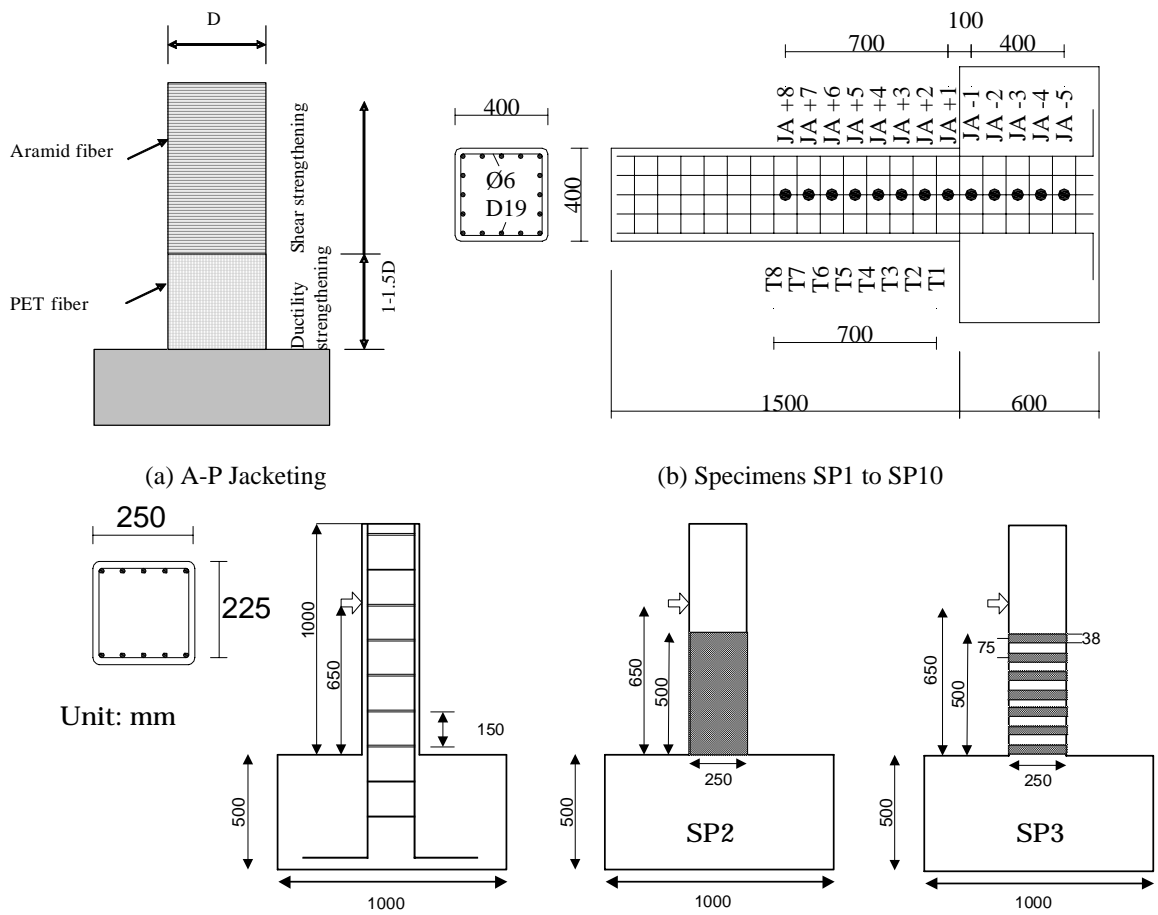


Figure 1: Comparison of strength, fracturing strain and cost of materials

2. EXPERIMENTAL OUTLINE

Two series of tests were conducted -- one for ductility enhancement and another for shear strength enhancement. The first series consists of 15 bridge pier specimens whose hinge zone was jacketed with fiber sheets with PET or PEN and the rest was jacketed with aramid fiber sheet (A-P Jacketing as shown in Figure 2 (a)) except a reference specimen. Ten and five specimens were with a cross section of 400 x 400 mm and 600 x 600 mm, respectively (see Table 1 and Figure 2 (b))(Anggawidjaja, et al. 2006a). Two specimens with a cross section of 250 x 250 mm were tested for the second series (see Figure 2 (c))(Anggawidjaja, et al. 2006b). Load-deformation curves (envelopes) of some of the specimens are shown in Figure 3.



(c) Specimens SP2s and SP3s
Figure 2: Specimens

Table 1: Specimens

Specimen	f_c'	a/d	ρ_t (%)	ρ_w (%)	ρ_f (%)	Fiber	V_c (kN)	V_s (kN)	V_f (kN)	V_{mu} (kN)	$\frac{V_c + V_s}{V_{mu}}$	μ^1	Cross-section
SP1	29.5	3	2.87	0.16	-	-	151	79	-	288	0.8	5.09	1 ²⁾
SP2	29.5	3	2.87	0.16	0.13	A2 ⁵⁾	151	79	213	288	0.8	11.84	1
SP3	29.5	3	2.87	0.16	0.38	PEN	151	79	201	288	0.8	10.65	1
SP4	29.5	3	2.87	0.16	0.37	PET	151	79	184	288	0.8	11.42	1
SP5	31.7	3	2.87	0.16	0.19	PET	155	79	90	290	0.8	7.98	1
SP6	31.7	4	2.87	0.16	0.12	PET	155	79	60	223	1.05	9.05	1
SP7	31.7	4	2.87	0.16	0.06	PET	155	79	30	223	1.05	8.46	1
SP8	31.7	4	2.87	0.16	-	-	155	79	-	223	1.05	7.40	1
SP9	31.7	4	3.59	0.16	0.12	PET	169	79	60	267	0.93	8.76	1
SP10	31.7	4	2.15	0.16	0.06	PET	151	79	30	177	1.3	10.41	1
SP11	31.7	4	2.82	0.2	0.25	PET	318	206	264	463	1.13	8.52	2 ³⁾
SP12	31.7	4	2.82	0.2	0.125	PET	318	206	132	463	1.13	7.54	2
SP13	34.5	3	2.82	0.2	0.29	PET	327	105	308	637	0.84	7.76	2
SP14	23.7	3	2.82	0.09	0.42	PET	289	83	441	612	0.61	4.12	2
SP15	31.1	3	2.82	0.09	0.42	PEN	316	83	469	641	0.62	6.87	2
SC1s	28.4	2.9	4.5	0.15	-	-	80	29	-	255	0.43	-	3 ⁴⁾
SC3s	29.0	2.9	4.5	0.15	0.032	Carbon	81.5	29	44	255	0.43	-	3
SP2s	35.4	2.9	4.5	0.15	0.67	PET	87	29	97	257	0.45	5.19	3
SP3s	36.7	2.9	4.5	0.15	0.35	PET	88	29	50	257	0.45	2.97	3

Note: 1) Ductility ratio ($=\delta_u/\delta_y$), 2) 400x400 mm, 3) 600x600 mm, 4) 250x250 mm, 5) Aramid of high strength type whose ultimate strength is 3246 MPa, fracturing strain is 4.1 % and elastic modulus is 79.5 GPa. 6) Notations: f_c' is concrete strength, a/d is shear span to depth ratio, ρ_t , ρ_w , ρ_f are ratios of tension reinforcement, stirrup and fiber sheet, V_c , V_s , V_f are concrete, stirrup and fiber sheet contribution in shear, V_{mu} is bending strength in terms of shear force.

3. ENHANCEMENT MECHANISM OF DUCTILITY AND SHEAR STRENGTH

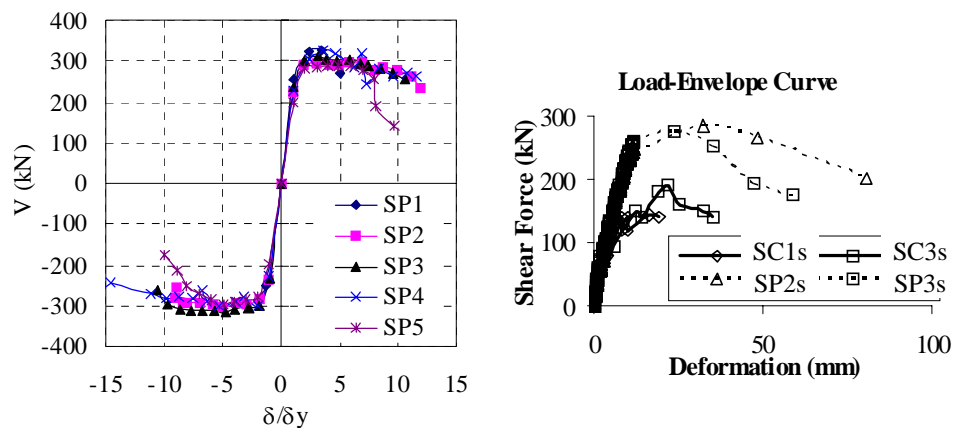
The ductility enhanced by PET jacketing increases with an increase in PET fiber ratio (comparing SP1, SP4 and SP5 in Table 1 and Figure 3 (a), and SP8, SP7 and SP6 in Table 1). PEN jacketing also increases the ductility (comparing SP1 with SP3 in Table 1). At ultimate deformation δ_u , no fracture was observed with PET and PEN fiber sheets, while the aramid fiber sheet fractured in SP2. No fracture or yielding of jacketed sheets can be considered to not only improve the ductility ratio, but also reduce negative slope of the falling branch in the load-deformation curve (see Figure 3 (a)).

A previous study on shear strength of concrete beams with shear reinforcement (Sato et al. 1997) indicates that shear strength depends on stiffness of both tension and shear reinforcement. If we apply this fact to reinforced concrete columns in which the flexural yielding takes place before the shear strength is reached, the following can be said. Once yielding of tension reinforcement, which means the reduction in stiffness, takes place, the potential shear strength starts to decrease. Yielding of shear reinforcement, which means not only reduction in the stiffness but also no increase in shear reinforcement component to carry shear force, further decreases the potential shear strength. Figure 4 (a) shows the shear force contribution of concrete, steel shear reinforcement and PET fiber sheet, the last two of which were calculated using their measured strains. The concrete component starts to decrease after the flexural yielding and decreases even faster after the shear reinforcement yielding. The load-carrying capacity decreases because the load-carrying capacity in shear becomes smaller than that in flexure. Small contribution of PET fiber sheet is visible only after the yielding of steel shear reinforcement in Figure 4 (a).

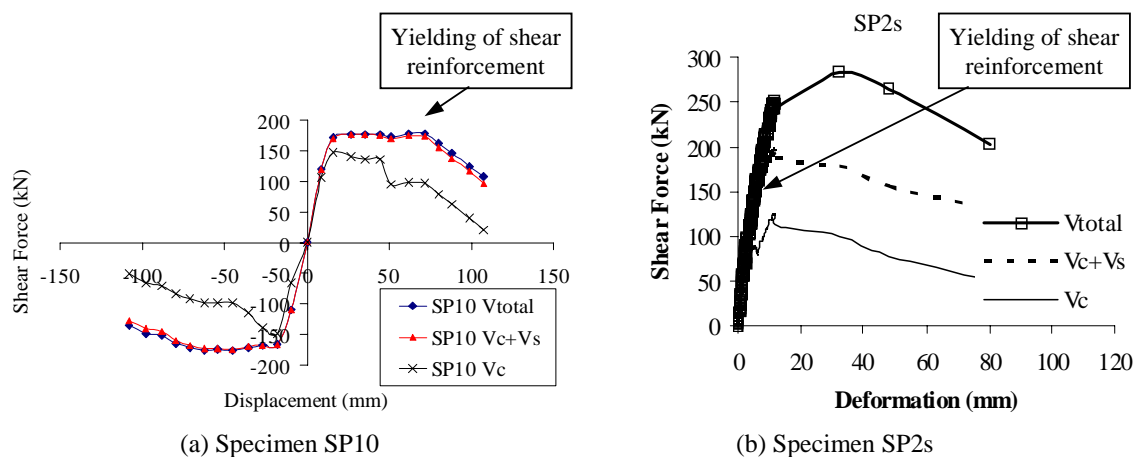
It seems that stiffness of both tension and shear reinforcement controls the potential shear strength. This means that FRP jacketing, which adds the stiffness of shear reinforcement, increases the potential shear strength resulting in enhancement of ductility and more ductile manner with falling load-carrying capacity. However, fracture of FRP would instantly eliminate the FRP contribution. PET fiber with a large fracturing strain can keep its contribution and contribute better than steel reinforcement which is likely to yield at ultimate deformation.

Similar observations can be made with specimens SP2s and SP3s, which were originally designed to fail in shear based on the JSCE formula for carbon and aramid fiber sheet jacketing. Both specimens showed shear failure after flexural yielding around 220 kN (see Figure 3 (b)). The load-deformation curves of SP2s and SP3s are compared with those of companion specimens with no jacketing (SC1s) and carbon fiber sheet (SC3s) with stiffness greater than those in SP2s and SP3s, which show rather brittle behavior and smaller shear strength. In specimen SC3s the carbon fiber sheet fractured. Shear force components in specimen SP2s are shown in Figure 4 (b). After yielding of steel shear reinforcement the concrete component increases with a smaller rate and the component of PET fiber sheet becomes more significant. The concrete component starts to decrease after the flexural yielding.

In order to estimate the ultimate deformation we have to predict shear deformation in hinge zone. The experimental results indicate that shear deformation increases with total deformation and more quickly after yielding of tension and shear reinforcement. It can be more than 10 % of the total deformation at ultimate deformation.



(a) Specimens SP1 to SP5 (b) Specimens SC1s, SC3s, SP2s and SP3s
Figure 3: Load-Deformation Curve (Envelope)



(a) Specimen SP10 (b) Specimen SP2s
Figure 4: Shear Force Contributions

5. REFERENCES

- Anggawidjaja, D., Ueda, T., Dai, J.G. and Nakai, H. (2006a). "Deformation capacity of RC wrapped with new reinforced-fiber polymer with large fracture strain". *Cement and Concrete Composites* (to be printed).
- Anggawidjaja, D., Senda, M., Ueda, T., and Dai, J.G. (2006b). "Shear capacity strengthening using high fracturing strain fiber material", *Proceedings of Tenth East Asia and Pacific Conference on Structural Engineering and Construction* (to be printed).
- Sato, Y., Ueda, T. and Kakuta, Y. (1997) "Shear strength of reinforced and prestressed concrete beams with shear reinforcement", *Concrete Library International of JSCE*, No.29, pp.233-247.

APPLICATION OF NEWLY DEVELOPED GFRP STIRRUPS FOR SHEAR REINFORCEMENT OF CONCRETE BEAMS

Jongsung Sim

(Professor, Hanyang University, Ansan, Kyeonggi-do, Korea)

Cheolwoo Park

(Assistant Professor, Kangwon National University, Samcheok, Korea)

Sungjae Park

(Ph. D Candidate, Hanyang University, Ansan, Kyeonggi-do, Korea)

Minkwan Ju

(Ph. D Candidate, Hanyang University, Ansan, Kyeonggi-do, Korea)

ABSTRACT

Recently, researches on high-durability concrete structure have remarkably been studied by adopting new construction material, fiber reinforced polymer (FRP) composites. In conjunction with these research trends, the shear capacity of RC beams reinforced with GFRP stirrup, which is developed in this study, was verified. Experimental variables were shear span to depth ratio and spacing of shear reinforcement. From the results, similar structural performance was found between the specimens reinforced with steel and GFRP stirrups with respect to crack pattern, failure mode, and shear capacity. It is anticipated that the adaptability of concrete structure shear-reinforced with GFRP stirrups can be considered in the future high performance concrete structures.

KEYWORDS

FRP composites, GFRP stirrup, high durability, shear capacity

1. INTRODUCTION

In recent years, fiber reinforced polymer (FRP) composite materials have been widely used in the field of construction for concrete structures because FRP reinforcement has many advantages, as it offers a high-strength, low-weight, superior resistant on the deteriorations such as corrosion, alkali reaction, de-icing salt, and freeze-thaw. Especially, the use of FRP bars to replace steel reinforcement in concrete structures is a new technique, which is a most effective way to prevent and to solve problems caused by the deteriorations.

FRP bars possess superior mechanical properties different from steel bars, for example, high tensile strength combined with low elastic modulus and elastic brittle stress-strain relationship. These properties might be reflected in structural design. Several experimental studies have been carried to verify the flexural and shear behavior of RC beams reinforced with FRP bars. As a result, few design guidelines have been published for the design and construction of concrete structures reinforced with FRP bars. However, these design guidelines emphasized the need for more research to verify the performance and behavior of RC beams reinforced with FRP bars for shear and flexure. Particularly the use of FRP as shear reinforcement for concrete structures has not yet been explored enough to establish a rational model to predict the performance and behavior of RC member with FRP stirrup.

In this paper, in order to verify shear performance and behavior of RC beams reinforced with GFRP stirrup, which is developed in this study, static four points loading tests were carried. Shear span to depth ratio (a/d), spacing of shear stirrup were variables.

2. EXPERIMENTS

2.1 Material properties and test variables

Fig. 1 shows the GFRP rebar developed in the study herein and the nominal diameter of both steel and GFRP stirrups are 10mm. Table 1 show mechanical properties of the materials used. A total of 12 reinforced concrete beams (i.e., 9 stirrup reinforced beams and 3 control beams) have been tested. The dimension of test beams is 180mm×230mm×2000mm (W×H×L). The stirrups are symmetrically placed as shown in Fig. 2. Designed compressive strength of concrete was 27MPa. In order to investigate the effects of shear reinforcing, three different reinforcing materials (non-stirrup, steel-stirrup, and GFRP-stirrup) and stir-up spacing (100mm and 200mm) were considered. In the testing shear span to depth ratios varied as $a/d = 1.7, 2.0,$ and 2.3 . More details on the specimens and variables are provided in Table 2 and Fig. 2.

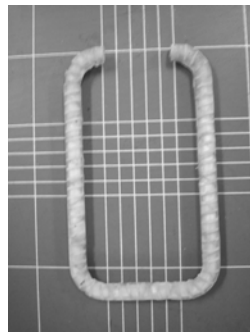


Fig. 1 Developed GFRP stirrup

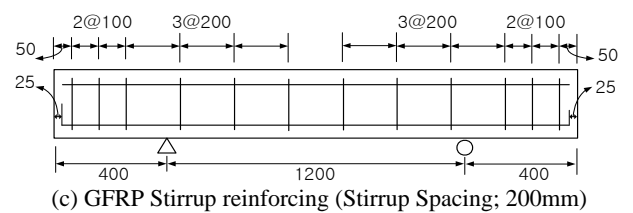
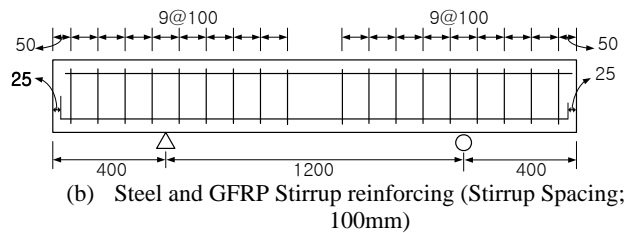
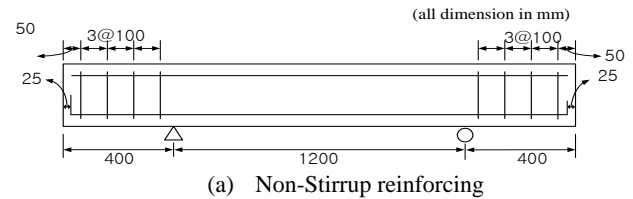


Fig. 2 Test specimen details

Table 1 Mechanical properties of materials

Materials	$\sigma_{tensile}$ [MPa]	$\epsilon_{ultimate}$	E [GPa]
Glass fiber	400.0	4.8	-
Epoxy resin	73.8	5.0	-
GFRP rebar	750.0	1.2	49
Steel rebar	300.0	-	200

Table 2 Test variables

Specimens	Span to depth ratio (a/d)	Spacing of shear stirrup (mm)	Type of shear strengthening
S1.7-CON (None)	1.7	-	None
S1.7-CON		100	Steel
S1.7-100		100	GFRP
S1.7-200		200	GFRP
S2.0-CON (None)	2	-	None
S2.0-CON		100	Steel
S2.0-100		100	GFRP
S2.0-200		200	GFRP
S2.3-CON (None)	2.3	-	None
S2.3-CON		100	Steel
S2.3-100		100	GFRP
S2.3-200		200	GFRP

2.2 Test set-up

Fig. 3 shows the experimental test set-up. Each RC beams was simply supported and loading was applied under the four-point bending configuration. The loading was controlled at a speed of 1 mm/min. One LVDT were used to measure the displacement of the specimens at mid-span during testing. Fig. 4 shows the loading condition according to the changing of the shear span to depth ratio ($a/d = 1.7, 2.0,$ and 2.3).

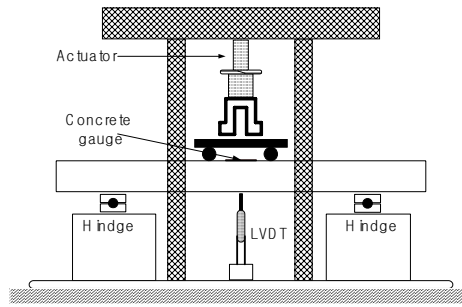
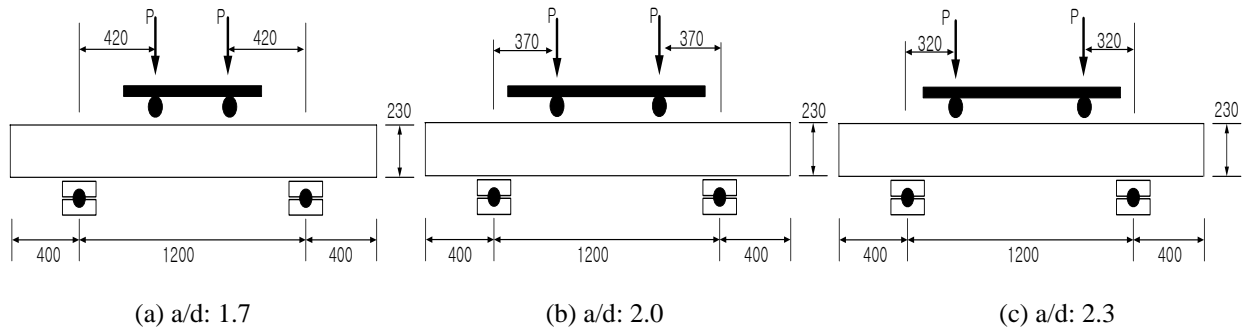


Fig. 3 Experimental test set-up



(a) $a/d: 1.7$

(b) $a/d: 2.0$

(c) $a/d: 2.3$

Fig. 4 Details of specimens according to the shear span to depth ratio

2.3 Test results and discussion

Though it is very difficult to compare directly the shear reinforcing capacity of the specimens since the material properties are completely different, in the study herein, the authors are willing to compare the test results as an initiative study on the application of GFRP stirrups. Table 3 summarizes the test results and Fig. 5 shows load-deflection curves according to the shear span to depth ratios. During the test, the GFRP stirrup of all specimens was not fractured and no debonding between the GFRP stirrups and concrete was observed. From the test results, as the shear span to depth ratio (a/d) of specimens increased shear failure load and shear failure angles decreased. Shear failure load of GFRP stirrup reinforcement specimen is similar to the specimens with steel stirrup that implies the application of the developed GFRP stirrup may provide as comparable shear reinforcing capacity as the steel stirrups. As the a/d ratio increased, the failure mode became governed by the interaction between bending and shear.

Table 3 Test results

Specimens		CON (NONE)	CON	Spacing (100mm)	Spacing (200mm)
S1.7	Load (kN)	96.3	135.9	141.4	135.4
	Displacement (mm)	5.7	11.6	16.5	9.1
	Failure mode	S	S	S	S
	Failure angle	42°	46°	47°	48°
S2.0	Load (kN)	95.2	127	119.8	91.4
	Displacement (mm)	5.22	13	17.5	5.2
	Failure mode	S	BS	S	S
	Failure angle	37°	-	45°	42°
S2.3	Load (kN)	88.9	107.9	105	91.9
	Displacement (mm)	10.6	10.4	12.6	8.1
	Failure mode	S	BS	FS	S
	Failure angle	36°	44°	43°	37°

* S: Shear failure mode BS: Bending and Shear Failure mode

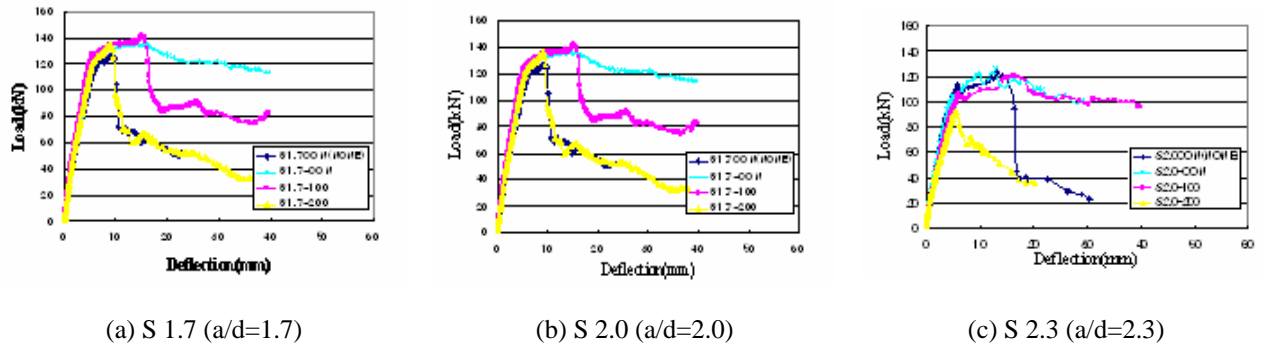


Fig. 5 Load-deflection curves according to a/d ratio

3. Conclusions

An experimental investigation was conducted on the application of the developed GFRP stirrups for the shear reinforcement in concrete beams. According to the results from this investigation, the following conclusions can be made:

1. From the static loading test, the crack pattern and failure behavior of RC beam specimens reinforced with GFRP stirrup were similar with that of RC beam specimens used steel stirrup. No obvious fractures and debonding of GFRP stirrups were observed during the test.
2. Below 2.0 of the a/d ratio, the ultimate loading of the specimens were similar. However, after the peak load, the strength drop of the specimens reinforced with the GFRP stirrup was more significant. This may be due to the bonding between concrete and GFRP stirrups and different material properties of GFRP comparing to steel.
3. When a/d was 2.3, the ultimate strengths of the specimens were decreased compared to the other a/d ratio. Particularly the specimen with GFRP stirrup and 200mm spacing the strength was even worse than the Non-stirrup specimens.
4. From this study, the application of the newly developed GFRP stirrup was investigated. Even though the mechanical properties of the GFRP is completely different from the steel, when it is used as a shear reinforcement in concrete beams based on the current design specifications, its shear reinforcing capacity seems to be applicable to the concrete structures. It is very obvious that definitely required are further researches on the design method and improvement of GFRP stirrups in manufacturing.

ACKNOWLEDGEMENTS

This research is funded from Korea Institute of Construction & Transportation Technology Evaluation and Planning [KICTTEP]. Authors thank their support.

REFERENCES

- A. Clader, A.R. Mari, "Shear design procedure for reinforced normal and high-strength concrete beams using artificial neural networks. Part I: beam without stirrups", *Engineering Structures* 26 (2004) 917~926.
- A. Clader, A.R. Mari, "Shear design procedure for reinforced normal and high-strength concrete beams using artificial neural networks. Part II: beam without stirrups", *Engineering Structures* 26 (2004) 927~936.

REPAIR OF CORROSION DAMAGED CONCRETE BEAMS WITHOUT SHEAR REINFORCEMENT USING CARBON FIBER REINFORCED POLYMER SHEETS

Abdullah Al-Saidy

(Assistant professor, Sultan Qaboos University, Muscat, Sultanate of Oman)

ABSTRACT

Strengthening/repair of existing reinforced concrete structures has become one of the important issues in the field of civil engineering. Corrosion of reinforcement in Oman and the Middle East region is a serious problem and is the main cause of concrete structures deterioration costing millions of dollars even though the majority of such structures are at the early age of their expected service life. This paper presents the experimental results of damaged/repared reinforced concrete beams. The experimental program consisted of reinforced concrete rectangular beam specimens reinforced with flexural reinforcement only without shear reinforcement and exposed to accelerated corrosion. The corrosion rate was varied between 5 to 7.5% which represents loss in cross sectional area of the steel reinforcement in the tension side. Damaged beams were repaired by bonding Carbon Fiber Reinforced Polymer (CFRP) U-straps and in some by CFRP sheets to the tension side to restore the strength loss due to corrosion. Test results showed that it is possible to use external shear reinforcement to enhance the strength of damaged concrete beams. In addition, combining U-straps and CFRP sheets is very effective to restore the lost strength in corrosion damaged beams.

KEYWORDS

Strengthening, rehabilitation, retrofitting, corrosion, advanced composite materials, CFRP sheets.

1. INTRODUCTION

The deterioration of reinforced concrete structures resulting from corrosion of steel reinforcement is a worldwide problem, and the cost of repairs is substantial. Reinforcement corrosion is induced primarily by the ingress of chloride (Cl^-), water, and oxygen into uncontaminated concrete. Fresh concrete protects the steel reinforcement from corrosion by the formation of a passive layer in the highly alkaline ($\text{pH}>13$) environment of fresh concrete. However, this passive layer will be destroyed by Cl^- ions which initiate the corrosion process. Corrosion damages reinforced concrete in three ways. First, it results in the reduction of effective cross – sectional area of the reinforcing bars. Second, it produces expansive corrosion products, causing cracking and spalling of the concrete cover. Third, it causes loss of bond between the concrete and the reinforcing steel. Hence, the serviceability as well as the ultimate capacity of the damaged reinforced concrete member is affected (Almusallam et al., 1996; Baweja et al., 1999; Umoto et al. 1984).

Repair or strengthening with fiber reinforced polymers (FRP) has gained some acceptance in recent years. It involves the external bonding of FRP sheets or plates to RC beams and slabs, or confinement of RC columns. Strengthening with FRP is simple and does not involve heavy equipments. Numerous studies have shown that repair and strengthening of corrosion damaged RC beams with FRP sheets or plates is efficient in restoring the strength of concrete members (Bonacci et al., 2000; Kutarba et al., 2004, Soudki and Sherwood, 2000).

This paper presents the research findings of an experimental study involving a case of damage due corrosion in the flexural reinforcement coupled with absence of shear reinforcement. This case represents a severe case of damage where it assumes that there is total damage in the stirrups and partial damage in the flexural reinforcement.

2. TEST PROGRAM

A total of 7 reinforced concrete beams were tested in this study as summarized in Table 1. Beam C0 was a control beam with no corrosion, while beams C (5%) and C (7.5%) were control beams with 5% and 7.5% corrosion (mass loss in reinforcement). Beams RU5 and RU7.5 were damaged beams with corrosion of 5% and 7.5%, respectively and then were repaired by applying six CFRP U-straps as shown in Figure 1. The remaining two beams, beams SUL5 and SUL7.5 were damaged with corrosion of 5% and 7.5%; then were strengthened by bonding one layer of CFRP sheet along the tension side of the beam followed by attaching CFRP U-straps as shown in Figure 1

Table 1 Beams description

Specimen designation	Corrosion level (mass loss%)	Remark
C0	0%	Control beam
C5	5 %	Control 5% corrosion beam
C7.5	7.5 %	Control 7.5% corrosion beam
RU5	5 %	5% corrosion with CFRP U-straps
RU7.5	7.5 %	7.5% corrosion with CFRP U-straps
SUL 5	5 %	5% corrosion with CFRP straps and sheet
SUL7.5	7.5 %	7.5% corrosion with CFRP straps and sheet

The specimens were 2.7 m long, 100 mm wide and 150 mm high. All beams were reinforced with two 10 mm diameter bars Grade 400 tensile reinforcement (Area of steel = 157 mm²). The reinforcing steel was extended 60 mm beyond the end of the concrete for the purpose of making external electrical connections for the accelerated corrosion process. The clear concrete cover was 20 mm on all sides of the specimen. No stirrups were used in all specimens.

Unidirectional carbon fiber sheets were used for the U-straps and the bottom longitudinal sheets. Thickness of the sheet was 0.11 mm (dry fibers), tensile strength of 3800 MPa, modulus of elasticity of 240 GPa, and ultimate elongation of 1.55%. The composite (fiber and epoxy) thickness of the CFRP sheet was 1 mm on average. The concrete had a 28-day compressive strength of 38 MPa with a maximum aggregate size of 10 mm. The concrete mix was proportioned as follows, aggregate : sand : water : cement = 60 : 67 : 16 : 25, with a water to cement ratio of 0.64. Reinforcing steel had yield strength of 460 MPa.

Bonding of the CFRP to the concrete was achieved by using epoxy adhesive. Prior to applying the epoxy and CFRP, the surface of the concrete was prepared by grinding the concrete in the area to receive the CFRP. The beams were tested after one week from applying the CFRP.

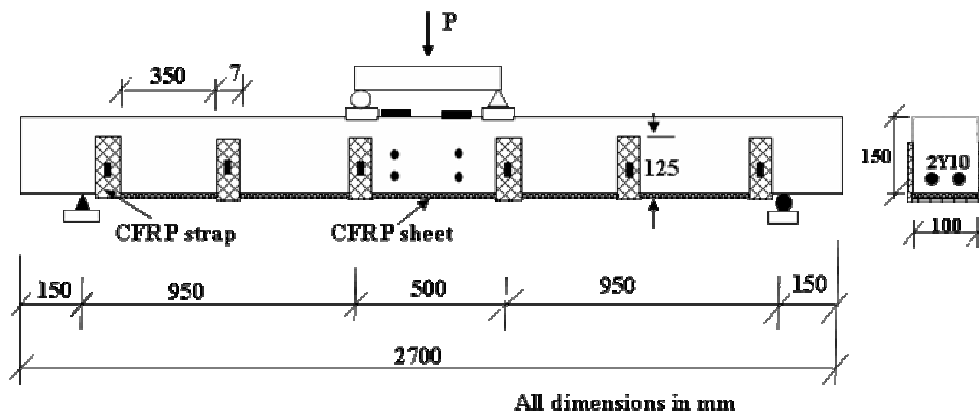


Figure 1. Test set-up and dimensions

The casting of each beam was done in three layers; after placing the first layer (at the level of the tensile steel bars) salt was spread along this layer except one beam (beam C0 -control beam). The amount of salt was approximately 1% by weights of cement. This was used to simulate chloride ions contamination and to accelerate corrosion. After 28 days curing in room conditions, the six beams were placed inside a tank which has salted water; the salt concentration was about 3% by weight of water. To induce corrosion in the reinforcement, the rebars were connected to a power (voltage) source where a current was applied to accelerate the corrosion process as shown in Figure 2. Stainless steel rebars were placed parallel to the beams in the tank to act as cathode and were connected to the negative charge of the power source. To obtain a theoretical 5% corrosion (or 5% mass loss in reinforcing bar) it was found that the time required to produce this mass loss was 14 days of continuous application of 487 mA current in each beam according to Farady's law.

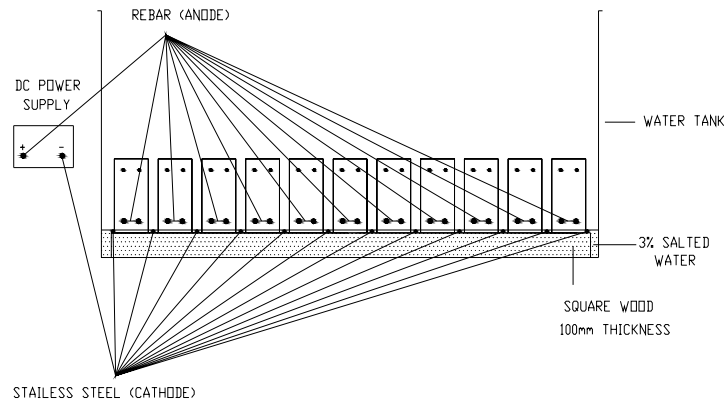


Figure 2. Schematic of accelerated corrosion set-up

3. TEST RESULTS AND DISCUSSION

3.1 Beams With 5% Corrosion

Following the accelerated corrosion phase, the beams were left for two days to dry. The beams were then repaired with CFRP and were left for a week for the CFRP to cure under room temperature. A four-point flexural test was carried out to all beams up to failure. The load - deflection curve for beams with 5% corrosion beams are shown in Figure 3a. Behavior of beam C0 (control beam with 0% corrosion) is of a typical under-reinforced beam exhibiting large deformation beyond the yield point before it failed by crushing of concrete. Beam C5 (5% corrosion) failed prematurely due to bond failure along the interface at the reinforcement and concrete (see Figure 4a). This clearly shows the importance of confinement provided by stirrups especially when corrosion is present. Note that the predicted load was approximately 14.0 kN. It is clear that bond failure caused this beam to fail prematurely when compared to the theoretical failure load that assumes complete bond between the concrete and steel reinforcement. Beam RU5 had 5% corrosion and repaired by external U-shaped CFRP straps. Adding U-straps improved the strength and ductility (deflection) as observed from the response of beam RU5 which failed by crushing of concrete. Adding CFRP sheet and U-shaped straps (beam SUL5) increased both strength and the stiffness of the repaired beam. The strength of beam SUL5 was higher by 37% above the uncorroded control beam (C0). Beam SUL5 also failed by crushing of concrete after a large deflection beyond the yielding load.

3.2 Beams With 7.5% Corrosion

The load - deflection curves for beams with 7.5% corrosion beams are shown in Figure 3b. Beam C7.5 had 7.5% corrosion, this beam failed prematurely due to bond failure for similar reasons as discussed earlier in beam C5. On the other hand, beam RU7.5 (repaired by external U-straps) showed an improved behavior by attaining adequate strength and ductility as a result of the confining effect of the U-straps. Failure of beam RU7.5 was due crushing of concrete. Following the accelerated corrosion phase, Beam SUL7.5 was severely cracked along the reinforcement on the side where the rebars were connected to the voltage source. It is believed that more moisture penetrated the beam through the cracks from the partially immersed bar ends. This produced higher concentration of corrosion on one side of the beam. This beam failed prematurely in a brittle manner as one of U-straps debonded and the crack along the beam opened up as shown in Figure 4b. This beam failed in shear-compression mode.

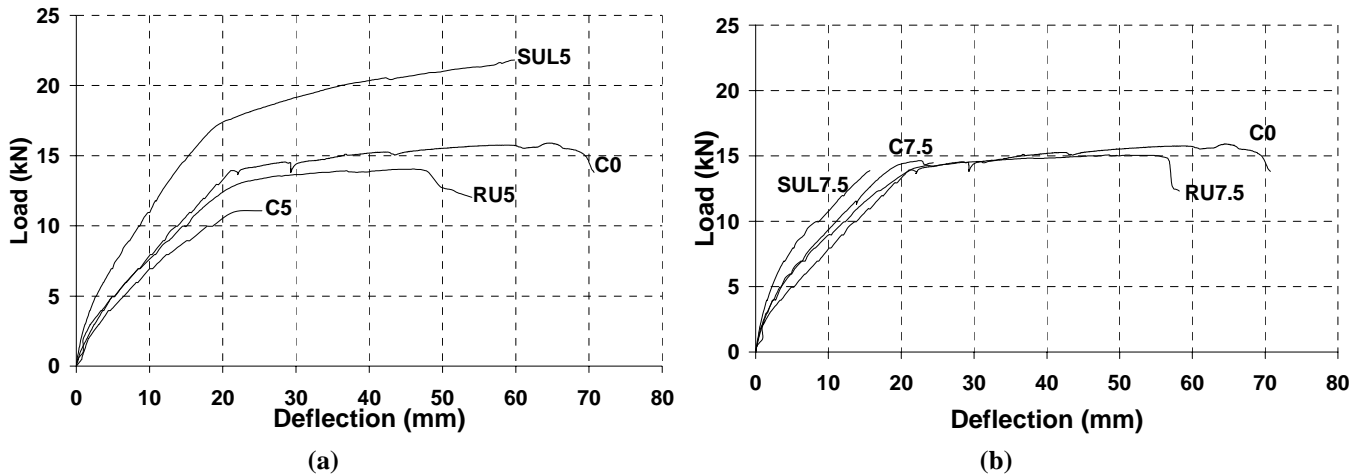


Figure 3. Load-deflection (a) 5% corrosion beams ; (b) 7.5% corrosion beams



Figure 4. (a) bond failure of beam C5 ; (b) shear-compression failure of beam SUL7.5

4. CONCLUSIONS

Corrosion of reinforcement weakens the strength of RC members as well as the bond between the reinforcing steel and the surrounding concrete. It was shown that stirrups are very critical in corrosion damaged beams to enhance the strength. The use of external CFRP U-straps can improve the performance of corrosion damaged beams by applying confining action. In addition, applying CFRP sheets to the tension side of beam increases the strength and stiffness considerably provided bond failure is prevented. However, if the cracks are wide and extensive probably continuous shear reinforcement is needed to prevent any brittle failure due to the lack of internal stirrups.

REFERENCES

- Almusallam, A., Al-Gahtani, A., Aziz, A. , Dakhil, F. and Rasheeduzzafar (1996). "Effect of reinforcement corrosion on flexural behavior of concrete slabs", *Journal of Materials in Civil Engineering*, pp 123 -127.
- Baweja, D., Ropert, H and Sirivivatnanan (1999)."Chloride-induced steel corrosion in concrete." *ACI Materials Journal*, V.96, No.3, pp 306-313.
- Bonacci, J. F. and Maaleej, M. (2000)."Externally bonded fiber reinforcement polymer for rehabilitation of corrosion damaged concrete beams." *ACI Structural Journal*, September –October, pp 703-711.
- Kutarba, M. P., Brown, J. R. and. Hamilton, H. R (2004). "Repair of Corrosion Damaged Concrete Beams with Carbon Fiber-Reinforced Polymer Composites." *Proceedings of COMPOSITES 2004*, Tampa, Florida USA.
- Soudki, K., and Sherwood, T. (2000). " Behaviour of reinforced concrete beams strengthened with carbon fiber reinforced polymer laminates subjected to corrosion damage." *Canadian Journal of Civil Engineering*, **27**, pp 1005-1010.
- Umoto, T, Tsuji, K., and Kakizawa, T. (1984). "Deterioration mechanism of concrete structures caused by corrosion of reinforcing bars". *Transactions of the Japan Concrete Institute*, **6**, pp 163-177.

SHEAR RETROFIT OF LOW STRENGTH REINFORCED CONCRETE SHORT COLUMNS WITH GFRP COMPOSITES

Alper Ilki

(Assoc.Prof.Dr., Istanbul Technical University, Istanbul, Turkey)

Idris Bedirhanoglu, Ismail Hakki Basegmez, Cem Demir

(Graduate Student, Istanbul Technical University, Istanbul, Turkey)

Nahit Kumbasar

(Emeritus Prof.Dr., Istanbul Technical University, Istanbul, Turkey)

ABSTRACT

In this experimental study, the behavior of shear critical reinforced concrete columns under constant axial load and reversed cyclic lateral loads is investigated. The specimens were constructed using low quality concrete, and insufficient transverse reinforcement, intentionally for reflecting the characteristics of relatively older existing buildings. Test results showed that the brittle shear behavior of the reference specimen was enhanced in different extents depending on the GFRP (glass fiber reinforced polymer) sheet retrofitting scheme. The retrofitted specimens, while not being able to reach flexural capacity due to the effects of diagonal compression stresses, exhibited much better performance with respect to reference specimen both in terms of strength and deformability.

KEYWORDS

Columns, Concrete, Fiber, Retrofit, Shear.

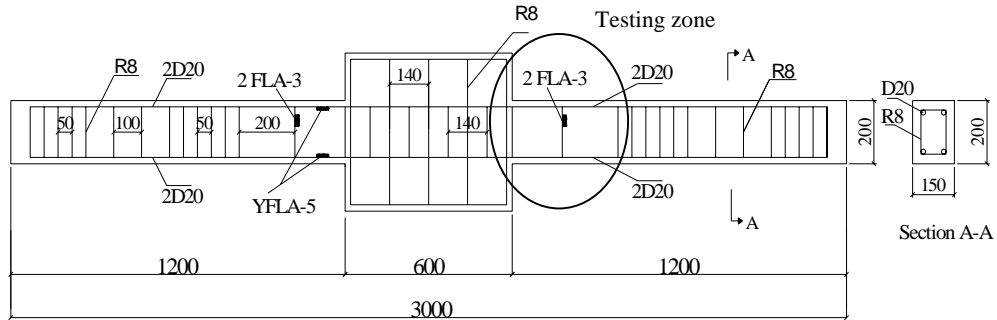
1. INTRODUCTION

Many existing buildings suffer severe seismic damage during earthquakes as a consequence of poor structural characteristics, such as low quality concrete and inadequate transverse reinforcement. The deficiencies related with low quality of concrete and inadequate transverse reinforcement, causing insufficient shear capacity, can be overcome by jacketing the structural members using fiber reinforced polymer composite sheets. Experimental research work on shear retrofit of concrete members with externally bonded fiber reinforced polymer composites are generally on beam specimens, which do not resist axial forces as well as shear stresses. Reversed cyclic shear tests on columns are limited, (Maruyama et al., 2001, Harmon et al., 2002, Furuta et al., 2003). In this experimental study, the behavior of shear critical reinforced concrete members under constant axial load and reversed cyclic lateral loads is investigated. Four specimens were tested after jacketing with GFRP sheets of different thickness and details, while one specimen was tested before retrofitting as the reference specimen. The specimens were constructed using low strength concrete ($f'_c \sim 10$ MPa), and insufficient transverse reinforcement (R8/200) intentionally for reflecting the characteristics of relatively older existing structures. The experimental findings are outlined by the damage patterns, load-displacement relationships, ductility characteristics, as well as attained transverse strains on FRP sheets, together with analytical shear strength predictions of the specimens.

2. TESTS AND COMPARISON WITH ANALYTICAL PREDICTIONS

The specimens, representing the column parts between the mid-heights of succeeding stories, were 3 m high and 150 mm \times 200 mm in cross-section. The longitudinal bars were 4D20 and transverse reinforcement in the testing region was R8/200. The net concrete cover thickness was 20 mm from outside of transverse reinforcement. The geometry and reinforcement details of the specimens and construction phases are presented in Figure 1 and 2, respectively.

The standard cylinder concrete compressive strength at the day of testing, number of GFRP plies, level of axial load (v), analytical and experimental shear strengths of the specimens are shown in Table 1. v is calculated by Eq. (1). Characteristics of steel reinforcement and GFRP sheets are given in Table 2. While LS-G-1/2 was jacketed with straps, all other retrofitted specimens were jacketed continuously in the shear span. It should be noted that for both cases, jackets were continuous around four sides.



* All Dimensions are in mm

Figure 1: Geometry and Reinforcement Details of the Specimens

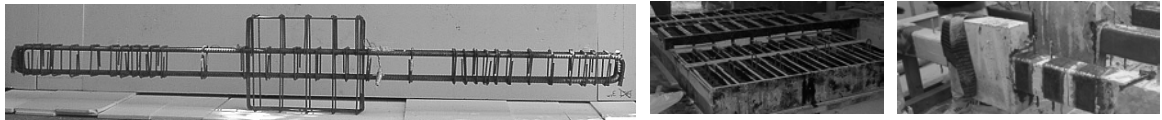


Figure 2: Specimen Construction and Retrofitting Phases

Table 1: Specimen Characteristics, Analytical and Experimental Shear Capacities

Specimen	j (days)	f'_{cj} (MPa)	FRP plies	f'_{ccj} ¹ (MPa)	v	V_c ² (kN)	V_s ³ (kN)	V_f ⁴ (kN)	$V_{r,analytical}$ ⁵ (kN)	V_{max} ⁶ (kN)	$V_{r,experimental}$ ⁷ (kN)
LS-0-1	332	10.9	0	10.9	0.19	18.3	31.1	0	49.4	63.3	46.5
LS-G-1/2	347	11.0	1 ⁸	11.4	0.19	18.3	31.1	12.0	61.3	66.2	66.0
LS-G-1	360	11.0	1	11.8	0.19	18.3	31.1	23.9	73.3	68.5	73.5
LS-G-2	370	11.0	2	12.9	0.19	18.3	31.1	47.8	97.2	74.9	80.0
LS-G-3	375	11.0	3	14.1	0.19	18.3	31.1	71.8	121.1	81.9	83.5

¹calculated as proposed by Ilki et al., 2004, ϵ_{hrup} is assumed as 0.004, ²calculated by Eq. (2), TS500, 2000, ³calculated by Eq. (3), ⁴calculated by Eq. (4), ⁵calculated by Eq. (5), ⁶ $V_{max}=0.22f'_{ccj}bd$, TS500, 2000, ⁷shear force corresponding to flexural failure is 106 kN, ⁸100 mm wide strips with 100 mm clear spacing between them

Table 2: Mechanical Characteristics of Steel and GFRP Reinforcement

Reinforcement	Diam. (mm)	Yield strength of steel bars f_y (MPa)	Thickness (mm)	Tensile strength of GFRP f_f (MPa)	Elasticity modulus of GFRP E_f (MPa)	Ultimate elongation of GFRP
Longitudinal bars	19.8	536	-	-	-	-
Transverse bars	7.8	370	-	-	-	-
GFRP sheets	-	-	0.23	1700	65000	0.028

$$v = \frac{N}{bhf'_{cj}} \quad (1)$$

$$V_c = 0.52f'_{cj}bd \left(1 + 0.07 \frac{N}{bh} \right), \quad f'_{cj} = 0.35\sqrt{f'_c} \quad (2)$$

$$V_s = \frac{A_{sw} df_{yw}}{s} \quad (3)$$

$$V_f = 2n_f t_f 0.004E_f h \quad (4)$$

$$V_r = V_c + V_s + V_f \quad (5)$$

In these tables and equations N , b , h , d , f'_{cj} , f_{ctj} are axial load, width, depth and effective depth of cross-section, concrete compressive and tensile strengths at the day of testing. V_c , V_s and V_f are contributions of concrete, transverse reinforcement and GFRP sheets to the shear resistance, and V_{max} is the maximum shear force permitted to prevent diagonal compression failure as given by TS500, 2000. A_{sw} , f_{yw} and s are cross-sectional area, yield strength and spacing of transverse reinforcement. n_f , t_f , f_f , ϵ_{hrup} and E_f are the number of plies, effective thickness, tensile strength, rupture strain and elasticity modulus of GFRP, and f'_{ccj} is the compressive strength of GFRP confined concrete. The measuring system included diagonal deformation measurements, GFRP strains, strains of longitudinal and transverse reinforcement as well as curvatures in potential plastic hinging zones, Figure 3. The envelopes of shear force-drift ratio relationships and appearance of specimens around drift ratio 0.035-0.040 are presented in Figure 4 and 5. As seen in these figures, significant enhancement was obtained in the behavior in terms of strength and deformability. However, although longitudinal bars yielded in all retrofitted specimens, none of them could reach their analytical flexural strength. The reference specimen prematurely failed in shear before longitudinal bars yielded. The transverse bars also yielded in all specimens. The yielding of transverse bars was retarded, with the increasing of number of GFRP plies. As it can be understood from Table 1 and Figure 4, the failure of retrofitted specimens was due to a combination of flexural and diagonal compression stresses.

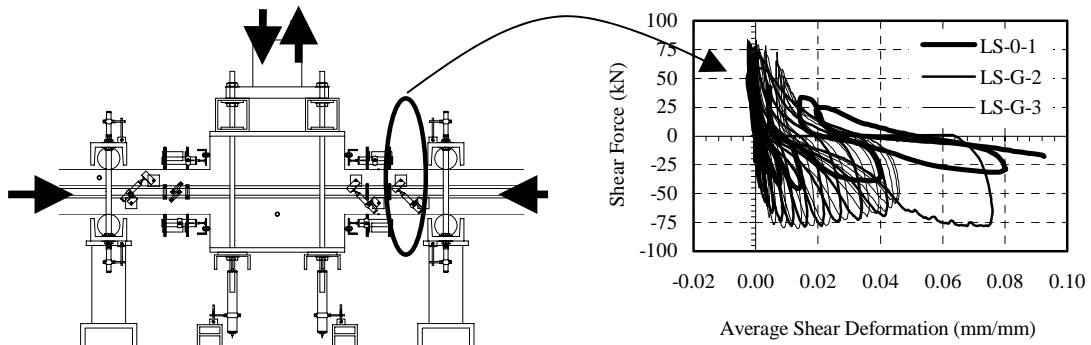


Figure 3: Loading and Measuring Setup and Average Strains Measured on Shear Span

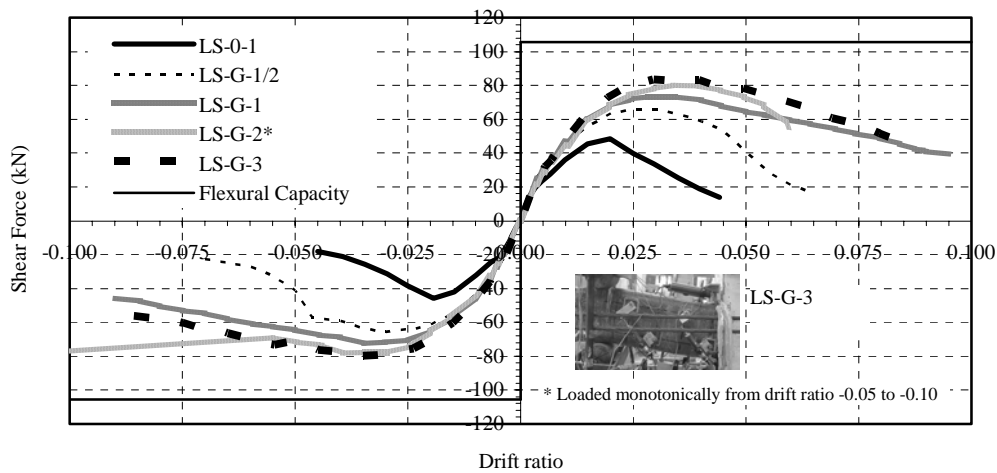
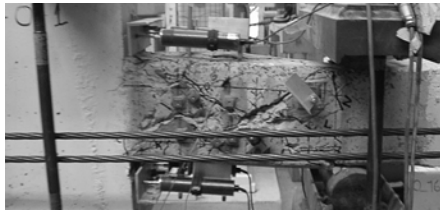
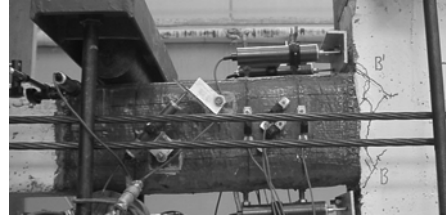
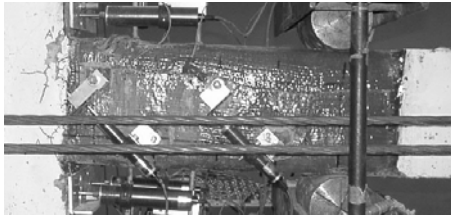


Figure 4: Shear Force-Drift Ratio Envelopes and Shear Force Corresponding to Flexural Capacity



(a) LS-0-1 ($\delta/L=-3.5$, $\delta=-15.75$ mm, $V=-27.5$ kN) (b) LS-G-1/2 ($\delta/L=-3.5$, $\delta=-15.75$ mm, $V=-63$ kN)



(c) LS-G-1 ($\delta/L=-4.0$, $\delta=-18.00$ mm, $V=-69$ kN) (d) LS-G-3 ($\delta/L=-3.5$, $\delta=-15.75$ mm, $V=-81$ kN)

Figure 5: Damages of Specimens at $\delta/L=-3.5$ and 4.0 (δ : drift, L: shear span)

At the end of the tests, the transverse GFRP sheets of LS-G-1/2 were totally fractured, while an approximately 50 mm wide part of GFRP jacket in the vicinity of stub was fractured in LS-G-1. The GFRP sheets were not fractured in LS-G-2 and LS-G-3. However, there was an apparent swelling in the cross-section close to the stub due to plastic compressive flexural and shear deformations.

3. CONCLUSIONS

Reinforced concrete columns representing typical deficiencies of relatively older buildings in Turkey were tested under constant axial and reversed cyclic shear forces before and after retrofitting with externally bonded FRP sheets. The original members were constructed using low strength concrete and inadequate transverse reinforcement. Consequently, the reference specimen failed prematurely in a brittle manner, due to shear effects. The retrofitted specimens, while not being able to reach flexural capacity, exhibited much better performance both in terms of strength and deformability. The failure of retrofitted specimens was due to combined effect of flexure and shear, particularly the diagonal compression stresses.

4. REFERENCES

- Furuta, T., Kanakubo, T., and Fukuyama, H. (2003). "Evaluation of shear capacity of RC columns strengthened by continuous fiber", *Proceedings of Sixth International Symposium on FRP Reinforcement for Concrete Structures*, Editor: K.H. Tan, National University of Singapore, Singapore, pp. 507-516.
- Harmon, T.G., Gould, N.C., Ramakrishnan, S., and Wang, E.H. (2002). "Confined concrete columns subjected to axial load, cyclic shear, and cyclic flexure-part I: analytical models". *ACI Structural Journal*, Vol. 99, No. 1, pp 32-41.
- Ilki, A., Kumbasar, N., and Koc, V. (2004). "Low strength concrete members externally confined with FRP sheets". *Structural Engineering and Mechanics*, Vol. 18, No. 2, pp 167-194.
- Maruyama, K., Nakai, H., Katsuki, F., and Shimomura, T. (2001). "Improvement of shear and ductility of reinforced concrete columns by wrapping of continuous fiber-reinforced polymer sheet". *Advanced Composite Materials*, Vol. 10, No. 2-3, pp 119-126.
- Turkish Standards Institute (2000). *TS500, Requirements for Design and Construction of Reinforced Concrete Structures*, Ankara, Turkey.

STATE-OF-PRACTICE OF FRP STRENGTHENED RC GIRDERS IN SHEAR

Abdeldjelil Belarbi

(Distinguished Professor, University of Missouri-Rolla, Rolla, Missouri, United States)

Ashraf Ayoub

(Assistant Professor, University of Missouri-Rolla, Rolla, Missouri, United States)

Sang-Wook Bae

(Research Associate, University of Missouri-Rolla, Rolla, Missouri, United States)

ABSTRACT

FRP systems are now becoming a widely accepted method of strengthening concrete structures. The acceptance and utilization of these new strengthening techniques depend on the availability of clear design guidelines, installation procedures and construction specifications. Standard specifications exist for all commonly used traditional materials in civil engineering structures. At this time, design specifications for FRP use are still under development. This paper presents an overview of the state-of practice of existing analytical and experimental studies on the use of FRP for shear strengthening of RC and PC girders. A summary of current design guidelines as a result of these studies will also be outlined. A statement of current research needs will then be provided.

KEYWORDS

Design guidelines, FRP, Shear, Strengthening.

1. INTRODUCTION

A significant portion of the U.S. infrastructure is in urgent need of strengthening and rehabilitation. There is an urgent need for innovative solutions that offer real advantages over traditional methods, particularly in terms of performance, simplicity of application, speed of execution, and ease of handling. FRP systems have been developed through extensive materials and structural testing under the guidance of practicing engineers, government officials, and university researchers. FRP systems have been used on a project-specific basis for the last two decades. They are now becoming a widely accepted method of strengthening concrete structures. The acceptance and utilization of these new strengthening techniques depend on the availability of clear design guidelines, installation procedures and construction specifications. Standard specifications exist for all commonly used traditional materials in civil engineering structures. At this time, design specifications for FRP use are still under development.

The results of several experimental investigations have shown that FRP systems can be effective for increasing ductility and strength to structural members such as columns and girders. As most of the research focused on strengthening of axial or flexural members, there are less experimental and analytical data on the use of FRP systems for shear strengthening of girders. Shear strengthening with FRP is still under investigation and the results obtained thus far are scarce and sometimes controversial. Even in traditional reinforced concrete members without FRP, the shear design is a complex challenge and uses more empirical methods as compared to axial and flexural design methods. Adding FRP to the equation, with its specific design issues, would bring another level of complication to the design. These FRP-related shear design issues and lack of comprehensive analytical and experimental models are the main motivation of several research studies worldwide. A thorough understanding of the shear design problem along with the development of design method for FRP shear strengthening is needed.

2. DESIGN ISSUES OF FRP STRENGTHENED RC AND PC GIRDERS IN SHEAR

It is well known that the shear behavior of RC girders is influenced by various factors such as tensile strength of concrete, longitudinal and transverse reinforcement indices, shear-span to depth ratio, member size, and axial forces. The number of parameters affecting the shear behavior increases if the RC/PC girder is strengthened with FRP composite materials. This is because FRP-strengthened girders show various types of failure modes including debonding, delamination, fracture of FRP, as well as peeling off of concrete cover with wide inclined cracks. It is, therefore, rather difficult, because of the failure mechanisms, to identify the material parameters controlling the behavior of FRP-strengthened girders at ultimate conditions.

Recently, a comprehensive research database was presented by Triantafillou and Antonopoulos (2000) and has been updated and enriched later by Bousselham and Chaallal (2004). This database includes more than 160 test results. The database was analyzed in terms of the following parameters: (a) properties of FRP composites, (b) shear-span to depth ratio a/d , (c) shear steel reinforcement ratio, (d) longitudinal steel reinforcement, and (e) scale effect. The analytical work was published with the objectives to synthesize the findings of the studies carried and to examine and analyze the parameters that have the greatest influence on the shear behavior of RC members strengthened with FRP laminates. The collected data was analyzed in order to assess the investigated test parameters. It was found that most of the experimental studies focused on determining the most effective shear strengthening scheme; while other influencing parameters, such as the longitudinal and transverse reinforcement ratio, the concrete strength, and the effect of pre-damage, has been investigated but only in a limited number of studies. Furthermore, in many studies, several parameters were varied simultaneously which made it difficult to decouple the effect of each parameter.

2.1. Existing Analytical Models

In current design methods, the total shear resistance of an RC beam, V_n , is expressed as the sum of the shear resisted by concrete, V_c , and that resisted by the transverse steel reinforcement, V_s . If the member is strengthened for shear with FRP laminates, an additional term, representing the contribution of FRP is added to the equation. To-date about thirteen analytical models have been developed to determine the shear resistance of RC member strengthened in shear with FRP sheets. The contribution of FRP to the shear resistance is often idealized as analogous to that of the steel shear reinforcement. However, it should be noted that FRP seldom reach their full strength due to the inherently different failure mechanisms. Most available models express the contribution of FRP to the shear capacity as a function of the effective strain of FRP, which is typically expressed as a fraction of the ultimate strain. The effective strain of FRP is largely dependent on the failure modes. The performance of the existing models has not yet been fully verified through a comprehensive comparison with available experimental data. Typically, each model tends to show a good agreement with the experimental data that was used to develop it, but is not verified against other data to identify the most promising model. Furthermore, current data do not address all of the parameters influencing the shear behavior of girders. Lastly, data derived from full-scale tests is not available to calibrate the current models for large-scale girders such as AASHTO-type structure.

2.2 Existing Design Guidelines and Standards

Currently, design guidelines for the use of FRP for strengthening of structurally deficient RC members are available in several countries. A brief discussion about all design guidelines mentioned above is presented in this section.

ACI 4402R-02 (2002): The ACI guidelines are the most thorough and complete specifications to date. The ACI 440-2R document provides strength reduction factors based on the expected failure mode, and is consistent with ACI 318-99. The document also specifically addresses environmental effects through reduction factors associated with various exposures. Fatigue and creep effects are addressed using prescribed FRP stress limits.

Canadian CAN/CSA S806-02 (2000): The Canadian specifications are the only formalized design codes addressing externally bonded FRP reinforcement for concrete. For strengthening applications, CSA S806 considers all possible failure modes rather than just concrete crushing. Durability is addressed through reference to CAN/CSA S478-95 Guideline of Durability in Buildings. Although a single limiting FRP tensile strain (0.007) is provided, delamination and debonding are addressed by directing the designers to “currently available information appropriate to the combination of sheets and adhesive”.

Japanese Recommendations for upgrading of concrete structures with use of CFRP sheets (JSCE, 2000): JSCE adopted a performance-based approach to the design of externally bonded FRP materials. In addition to verifying

flexural and shear capacity, flexural crack width and protection of the concrete substrate from chloride ion penetration are considered explicitly in the JSCE Recommendations.

European fib-TG 9.3 Bulletin 14 (2001): This document was produced by fib Task Group 9.3 and also represents a combination of guidelines and state-of-the-art research. The fib-Bulletin 14 recognizes the difference in expected performance between FRP material types and between preformed and wet lay-up FRP systems. Delamination and debonding are addressed using a simplified bilinear bond model and by also addressing the effects of the loss of composite actions between the FRP and concrete substrate.

ISIS Design Manual 4 (2001): This document provides considerable guidance and a number of design examples for the use of externally bonded FRP. The document, however, is written as a state-of-the-art report, referring to the recommendations of others rather than making its own design recommendations. The ISIS Design Manual 4 typically references to the recommendations of ACI 440.2R.

Great Britain Technical Report 55 (Concrete Society 2000): This report is similar to ISIS Design Manual 4 and fib Bulletin 14 in its approach and scope. The report, however, addresses more practical construction issues associated with the use of externally bonded FRP materials.

3. CURRENT PRACTICE AND FUTURE RESEARCH NEEDS

Based on the current state of knowledge, it is evident that further research investigations are needed to develop rational design guidelines for RC beams externally strengthened with FRP composite materials. Among others, the following surface to be the main controlling parameters that need further studies.

Properties of FRP Composite Materials: The determination of effective strain of FRP and its maximum limits are keys to the accurate prediction of its shear contribution. Although many empirical equations currently exist, they need to be evaluated through a larger set of experimental data.

Shear-span to Depth Ratio: The shear resistance of FRP can be affected by the shear-span to depth ratio. Several research studies showed that current empirical equations could not accurately predict the shear resistance of FRP for cases with low shear-span to depth ratio.

Transverse and Longitudinal Steel Reinforcement: Recent research studies showed that the interaction between transverse steel reinforcement and FRP exist. Boussselham and Chaallal, (2004) reported that the effect of increasing number of layers of FRP sheets decreases as the transverse steel reinforcement ratio increases. In addition, the effect of longitudinal steel reinforcement may also affect the contribution of FRP in shear resistance. To further investigate this, research studies must be carefully conducted to account for the effects of both transverse and longitudinal steel reinforcement.

Scale effect and Geometry: Since most previous experimental studies were performed on small scale RC beams, current design equations may not be accurate due to scale effects. In addition, failure modes of rectangular RC beams and T-beams may be different as briefly discussed. Thus, it is important to conduct additional experimental studies on full-scale T-sections.

FRP Strengthening Schemes and Control of Failure Mode: Numerous experimental works have been performed to investigate the effectiveness of the different types of FRP strengthening schemes, and the corresponding anchorage systems. As a result, it was found that the failure mode was dependent on the configurations of FRP composite materials. Zhang and Hsu (2005) recently reported that the R factor (the ratio of the effective strain to the ultimate strain of FRP) is more complex to define for FRP-rupture failure mode as compared to the case of FRP-debonding. Thus, using the concept of effective strain without information regarding failure mode may lead to unsafe design. Therefore, it may be necessary to control the failure mode of concrete structures with FRP by providing appropriate detailing of strengthening schemes at the design level, for example; anchorage provisions, minimum bond development length, minimum space of FRP strips.

Durability: Environmental factors also affect the failure mode since several research studies suggested that severe environmental conditions can degrade the mechanical properties of FRP as well as the interfacial bond strength, which may in turn affect the failure mode. Therefore, the long-term behavior of FRP-strengthened concrete structures is an important issue, which needs be addressed in the new design guidelines.

Fatigue: Research studies on RC structural elements retrofitted with FRP under large-amplitude cyclic loading or repeated low-amplitude fatigue loading are very few in comparison to monotonic loading. In addition, the research

work dedicated to fatigue performance is exclusively related to flexural strengthening. In contrast, limited studies have been carried out on the fatigue performance and behavior of shear strengthening. Research work to address the fatigue effect on shear behavior is therefore needed.

Prestressed vs. Non-Prestressed: A number of experimental research studies have been conducted with a focus on the behavior of RC members; however, there is very limited experimental data regarding the PC members strengthened in shear with FRP. Although Hutchinson and Rizkalla (1999) reported that the prediction by the analytical model proposed by the authors was in good agreement with the test results of 7 prestressed concrete beams strengthened with CFRP strips, the research regarding this parameter is still very limited and needs to be conducted.

Anchorage Details: It is known that for both flexure and shear strengthening of girders using FRP sheets without a carefully designed anchorage details at the ends of bonded FRP sheets, premature failure may occur due to debonding or peeling of the FRP sheets at its ends. An enormous amount of research effort has focused on the determination of the types, causes, and prevention of premature failure. To-date, several approaches have been tried to avoid peeling failures such as the use of mechanical anchorages at the ends of the FRP sheet, the use of additional wrapped sheets placed longitudinally at the top and bottom of girder web, and use of near surface mounted (NSM) FRP rebars. Some of these methods are simple and some are labor intensive. The current available design equations incorporate a limit on the effective FRP strains, which correspond to the maximum value at one of the following situations: (1) the control crack opening, (2) shear failure due to FRP debonding, and (3) shear failure combined with or followed by FRP rupture. The anchorage system should be reflected in newly developed design equation.

4. CONCLUDING REMARKS

FRP systems have shown great potential to be used for rehabilitation and retrofit of existing structures. They can be used to provide increased ductility, and shear and flexural strength to structural elements such as columns, beams/girders, slabs/decks and walls. The acceptance and utilization of these new strengthening techniques depend on the availability of clear design guidelines, installation procedures and construction specifications. A significant progress has been made in the last two decades and several design guidelines and documents have been developed worldwide, but there are still issues and research needs to be addressed to bring the comfort level for practicing engineers to use this FRP material as any other conventional material.

5. REFERENCES

- ACI Committee 440. (2002) "ACI 440.2R-02-Guide for the design and construction of externally bonded FRP systems for strengthening concrete structures, Farmington Hills, MI.
- Bousselham, A. and Chaallal, O. (2004). "Shear strengthening reinforced concrete beams with fiber-reinforced polymer: assessment of influencing parameters and required research." *ACI struc. J.*, 101(2), 219-227.
- Concrete Society (2000). "Design guidance on strengthening concrete structures using fibre composite materials: Technical Report 55, The Concrete Society, London.
- CSA-S806-02 (2002). "Design and construction of building components with fibre-reinforced polymer." Canadian standards Association, Rexdale, Ontario.
- fib-TG9.3 (2001). "Design and use of externally bonded fiber polymer reinforcement (FRP EBR) for reinforced concrete structures." *Bulletin 14*, July.
- Hutchinson, R. L., and Rizkalla, SH. (1999). "Shear strengthening of AASHTO bridge girders using carbon fiber reinforced polymer sheets." *Proc., 4th Int. Symp. on Fiber reinforced polymer reinforcement for reinforced concrete structures*. ACI publications SP-188, 945-56.
- ISIS Canada (2001). "Design Manual 4: Strengthening reinforced concrete structures with externally-bonded fiber reinforced polymers." The Canadian Network of Centers of Excellence on Intelligent Sensing for Innovative Structures, University of Manitoba, Winnipeg, Manitoba, Canada, Sep.
- JSCE (2000) "Recommendations for upgrading of concrete structures with use of CFRP sheet." Japanese Society of Civil Engineers.
- Triantafillou, T.C., and Antonopoulos, C.P. (2000). "Design of concrete flexural members strengthened in shear with FRP." *J. Compos. Construct*, 4(4), 198-205.
- Zhang, Z. and Hsu, C.-T. (2005). "Shear strengthening of reinforced concrete beams using carbon-fiber-reinforced polymer laminates." *J. of Comp. for Constr.*, 9(2), 158-169.

Strengthening of Concrete Beams in Shear with Mineral Based Composites Laboratory Tests and Theory

Björn Täljsten

*(Professor, Technical University of Denmark, Lyngby, Denmark
Luleå University of Technology, Luleå, Sweden)*

Katalin Orosz

(PhD Student, Technical University of Denmark and Norut Teknologi AS, Norway)

Thomas Blanksvärd

(PhD Student, Luleå University of Technology, Sweden)

ABSTRACT

Today, there are many different repair and strengthening methods that might be used to upgrade a concrete structure. One such method involves CFRP (Carbon Fibre Reinforced Polymer) bonding. This method has proven to be usable for many different types of retrofitting applications. Even so, there are some disadvantages while using epoxy resins as a bonding agent, i.e. diffusion closeness, thermal compatibility, working environment and the minimum temperature of assemble. It is therefore of interest to replace the epoxy adhesive with a mineral based bonding agent, e.g. polymer modified mortars with similar properties as the base concrete that also is more working environmental friendly. A combination between the polymer modified mortar and fibre reinforced polymers (FRP) can be used for repair and strengthening of civil structures. This paper presents a pilot study of RC beams strengthened in shear with mineral based bonding agents and CFRP grids. The project is a collaboration project among Luleå University of Technology, Norut Teknologi AS and Denmark Technical University and is also a part of the European funded project "Sustainable Bridges". The results so far show that comparable strengthening results as for epoxy bonded systems can be achieved with MBC strengthening systems. The strengthening effect of the beams was 40 – 100 % compared to the unstrengthened reference beam. The theoretical model describes the load carrying capacity fairly well.

KEYWORDS

CFRP grids, Strengthening, Shear, Laboratory tests, MBC, Mineral Based Strengthening, Carbon Fibre

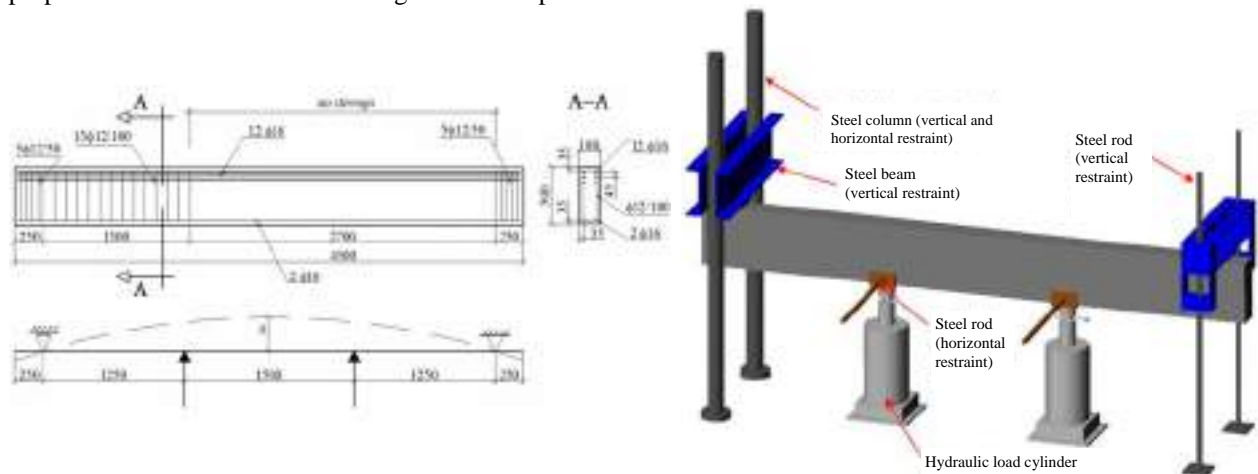
1. INTRODUCTION

Research with the use of short FRP fibres and cement based materials has been going on for some time now, see for example (Kesner et. al., 2003). However, experience with the use of long FRP fibres is limited. Research studying cement overlays with textiles of carbon fabrics embedded in cement based matrix to strengthen masonry walls has been carried out by (Kolsch, 1998). The strengthening system prevents partial or complete collapse of masonry walls in the critical out-of-plane direction during a seismic event. A study to improve the bond between carbon fibres and cementitious matrices has been done by (Badanoiu, 2001), where dry fibre fabrics were used. It was found that a pre-treatment with silica fume and high amounts of polymers improved the bond behaviour of carbon fibre to the cement. However, it was also stressed that more research is needed in this field. A very interesting pioneering work has been presented by (Wiberg, 2003). Large-scale tests of ordinary concrete beams strengthened with a cementitious fibre composite were reported. The composite used was made of polymer-modified mortar and a unidirectional sheet of continuous dry carbon fibres applied by hand. Both flexural and shear strengthening were tested. From the tests it was concluded that the method works, and that considerable strengthening effects can be achieved. In comparison with epoxy bonded carbon fibre sheets, the amount of carbon fibre needed to reach the

same strengthening effect for the cementitious strengthening system was more than double. The reason for this is mainly due to problems with wetting the carbon fibre. This is also emphasised by (Badanoiu & Holmgren, 2003), where it was found that the load capacity of the cementitious carbon fibre composite is influenced by the amount of fibres in the tow. If the cementitious matrix can penetrate into the interior of the carbon fibre tow, a higher number of filaments will be active during loading, and this will lead to an increase in load carrying capacity. To overcome this problem use of CFRP grids and a cementitious matrix might be used. In this paper a brief presentation of the tests carried out at Technical University of Denmark is presented.

2. TEST SET-UP

The test set up for the beam test is shown in Fig. 1. Five beams with the same geometry, concrete quality (average compressive strength 38 MPa), and steel reinforcement (average tensile strength 517 MPa for the rebars and 530 MPa for the stirrups) were tested, four of them strengthened with CFRP grids, while the first beam served as reference beam without CFRP strengthening. The properties of the grids are given in Fig. 1. The load was applied by two cylinders standing on the floor therefore the beams were turned upside down. Each of the cylinders provided a load of maximum 500 kN. The load was increased by approximately 10 kN/min/cylinder and the tests were load controlled. The pressure was translated into voltage by the data-logger and the optical measuring equipment. The measuring equipment comprised of transducers, strain gauges (on DTU2 and DTU5) and photogrammetric strain measuring equipment to measure the strains and crack propagation on the strengthened surfaces of each test beam. At failure, both data-logger and photo equipment were stopped, and the failure load was recorded. Numerous pictures were taken with a digital camera to keep track on the crack development during loading. However, due to limited space this is not presented in this paper. A great amount of longitudinal steel reinforcement ensured that the beams would not fail in bending. All the beams had a steel reinforcement for shear only in one side. The CFRP grids were applied using two types of mortars in two layers with a thickness of 10 mm on both sides of the beams. The CFRP grid was placed between the two layers of the mortar. Before applying the first layer of mortar a primer was applied to the sandblasted concrete surface to optimize the bond between concrete and mortar. In Fig. 1 the material properties for the mortar and CFRP grid used are presented.



MBC strengthening materials:

Mortar modulus of elasticity:

Cement I. $E_1=26.5$ GPa, with short glass fibres

Cement II. $E_2=18.0$ GPa

CFRP Grid properties (x: horizontal, y: vertical):

Grid 1. 70x72 mm; 230 g/m²,

$E_x = 341$ GPa, $\epsilon_{ux} = 1.3\%$, $E_y = 390$ GPa, $\epsilon_{uy} = 0.8\%$

Grid 2. 24x25 mm; 150 g/m²,

$E_x = 281$ GPa, $\epsilon_{ux} = 1.3\%$, $E_y = 380$ GPa, $\epsilon_{uy} = 1.4\%$

Grid 3. 42x43 mm; 390 g/m²,

$E_x = 407$ GPa, $\epsilon_{ux} = 1.1\%$, $E_y = 417$ GPa, $\epsilon_{uy} = 1.1\%$

Beam	CFRP	Mortar
DTU1 Ref.	-	-
DTU2	Grid 3	Cement I
DTU3	Grid 2	Cement I
DTU4	Grid 1	Cement II
DTU5	Grid 1	Cement I

Figure 1. Test set-up

3. EVALUATION

3.1. Theory

Studies on the shear strengthening of a RC beam by bonding FRP composites have been carried out since the early 1990's (Chen & Teng, 2003). In the early studies the shear capacity of the FRP strengthening was based on a very simplified stress distribution. In recent years a more advanced theory has been developed (Carolin & Täljsten, 2005). The theory provides a more detailed specification of the strain distribution in the bonded FRP. This is, of course, a decisive factor in the study since the strains in the CFRP material are proportional to the stresses. A well adopted approach for shear design is to use the truss or strut and tie model:

$$V_n = \underbrace{V_c}_{\text{Concrete}} + \underbrace{V_s}_{\text{Steel}} + \underbrace{V_f}_{\text{FRP}} \quad (1)$$

The derivation of V_c and V_s refers often on national codes or standards. For the term V_f the same approach as for the truss analogy may be used, with special consideration to the compatibility relationships for the studied FRP system. In this paper a simplified theory is presented for the contribution of the CFRP grid. A CFRP grid usually consists of a vertical and a horizontal tow. Both these tows contribute to the load carrying capacity, which in this paper is presented as a result vector, see Fig. 2.

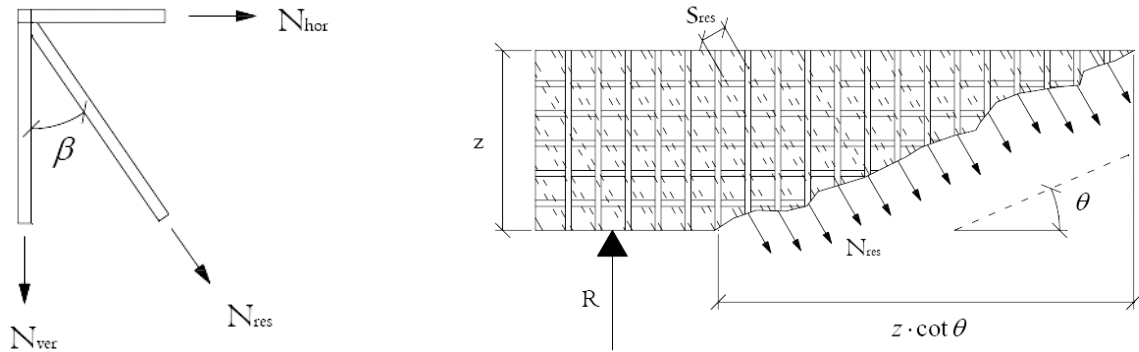


Figure 2. Relation between vertical and horizontal tow - left. The truss model - right

The direction and strength properties of the grid resultant are depending on the properties of each tow direction. This is expressed in equation (2)-(5).

$$N_{hor} = \frac{\varepsilon_{hor} \cdot E_{hor} \cdot A_{hor}}{s_{hor}} \quad (2)$$

$$N_{ver} = \frac{\varepsilon_{ver} \cdot E_{ver} \cdot A_{ver}}{s_{ver}} \quad (3)$$

$$N_{res} = \sqrt{N_{hor}^2 + N_{ver}^2} \quad (4)$$

$$\beta = \arctan\left(\frac{N_{hor}}{N_{ver}}\right) \quad (5)$$

Based on these considerations some of the existing design models can be used to determine the contribution from the CFRP grid, (Täljsten & Carolin, 2005). This equation is rewritten with the properties of the resulting tow, using $\eta = 0.4$ as the modification factor due to the parabolic form of the strain contribution over the section:

$$V_{FRP} = \frac{2 \cdot \eta \cdot N_{res} \cdot z \cdot \cos(\theta - \beta)}{s_{res} \cdot \sin \theta} \quad (6)$$

$$s_{res} = s_{ver} \cdot \cos \beta = s_{hor} \cdot \sin \beta \quad (7)$$

3.2. Results from tests

The load deflection curves from the tests are shown in figure 3 together with the calculated and experimental values, the calculation is carried out at a strain level of 10 %.

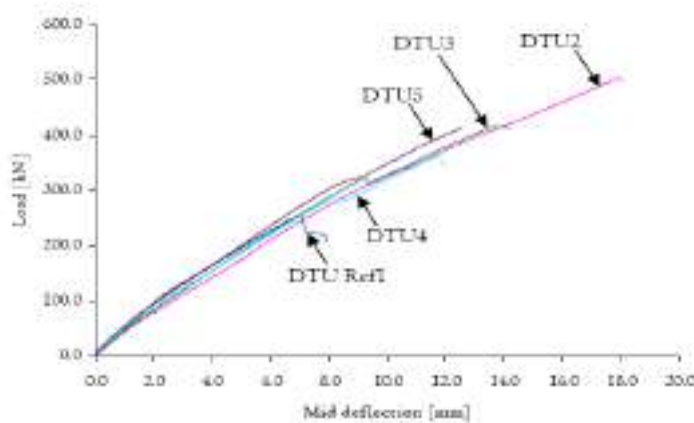


Figure 3a. Load-Deflection curves

Beam	Exp. [kN]	Calc. [kN]	V_{exp}/V_{cal}
DTU2	54	58	0.93
DTU3	54	42	1.29
DTU4	58	67	0.87
DTU5	54	45	1.20

Figure 3b. Experimental and calculated values

4. SUMMARY AND CONCLUSIONS

All five beams failed in shear. The strengthening effect was significant, the increase in load carrying capacity for the strengthened beams was approximately 40-100 % compared to the reference beam. The largest increase was achieved using the grid with the densest fibre area per cross-section and the mortar with short glass fibres. The theoretical approach gave a reasonable estimation of the shear strengthening effect, however it was difficult to exactly measure the strain in the tows and the scattering was large, therefore the theoretical evaluation is imperfect and further laboratory research together with more detailed analytical and numerical analysis is needed to improve the design model. Furthermore, a large test series is now ongoing at Luleå University of Technology in collaboration with Technical University of Denmark and Norut Teknologi A/S in Norway. Here we are not only investigating the structural behaviour of the strengthening system but also the effect of shrinkage and temperature.

ACKNOWLEDGEMENTS

The research presented in this paper has been funded by several organisations. Here Sto Scandinavia AB, the Norwegian Research Council through the strategic institute program RECON and Skanska Sverige AB should be acknowledged. Special thanks goes to the Master Students Morten Christiansen and Thorsten Jürgensen carrying out their work at Technical University of Denmark.

REFERENCES

- Badanoiu A., 2001, Improvement of the bond between carbon fibres and cementitious matrices, Technical report 2001:1, Concrete Structures, ISSN 1404-8450, Royal Institute of Technology, Department of Structural Engineering, 100 44 Stockholm, Sweden, p 44.
- Badanoiu A. and Holmgren J., Cementitious composites reinforced with continuous carbon fibres for strengthening of concrete structures, Journal of Cement & Concrete Composites, vol. 25, 2003, pp 387-394.
- Carolin A. and Täljsten B., Theoretical Study of Strengthening for Increase Shear Capacity, Journal of Composites for Construction, November/December 2005, pp 497-506.
- Chen, J. F. and Teng, J. G. (2003) Shear Capacity of Fiber-Reinforced Polymer-Strengthened Reinforced Concrete Beams: Fiber Reinforced Polymer Rupture, Journal of Composites for Construction, ASCE / May 2003, pp 615-625.
- Kolsch H., 1998, Carbon fibre cement matrix (CFCM) overlay system for masonry strengthening, Journal for composites for construction, Vol. 2, No. 2, May 1998, pp105-109.
- Kesner K.E., Billington S.L and Douglas K.S., 2003, Cyclic Response of Highly Ductile Fibre-reinforced Cement-Based Composites, ACI Materials and Journals - Technical Paper, September -October 2003, pp 381-390.
- Wiberg A., 2003, Strengthening of concrete beams using cementitious carbon fibre composites, Doctoral Thesis, ISSN 1103-4270, Royal Institute of Technology, Structural Engineering, 100 44 Stockholm, Sweden, p 140.

ANALYTICAL PREDICTION OF DEBONDING FAILURES IN RC BEAMS STRENGTHENED IN SHEAR WITH NSM FRP REINFORCEMENT

Andrea Rizzo

(PhD Student, Department of Innovation Engineering, University of Lecce, Lecce, Italy)

Laura De Lorenzis

(Assistant Professor, Department of Innovation Engineering, University of Lecce, Lecce, Italy)

ABSTRACT

The shear capacity of reinforced concrete (RC) members can be successfully increased using near-surface mounted (NSM) fiber-reinforced polymer (FRP) reinforcement. Tests on NSM-strengthened beams have shown that failure is controlled by diagonal tension associated to debonding between the NSM reinforcement and the concrete substrate. In absence of steel stirrups and/or when the spacing of the NSM reinforcement is large, debonding involves separately each of the bars crossed by the critical shear crack (type-I failure). The presence of steel stirrups, combined with a relatively small spacing of the reinforcement, may originate a debonding failure mechanism involving the lateral concrete covers of the steel stirrups (type-II failure). Thus, an analytical model able to encompass both failure modes must be developed. This paper extends a previous simplified model to predict the FRP contribution to the shear capacity when type-I failure occurs. The model, suitable for immediate design use, assumes a complete redistribution of the bond stresses along the failure interface at ultimate. Experimental results from previous test programs are compared to the model predictions.

KEYWORDS

Debonding failures, FRP, near-surface mounted reinforcement, RC beams, shear strengthening.

1. INTRODUCTION

An emerging method for shear strengthening of reinforced concrete (RC) members is the use of near-surface mounted (NSM) fiber-reinforced polymer (FRP) reinforcement, usually in the form of round bars or strips.

Tests conducted thus far on NSM-shear-strengthened beams have shown that failure is controlled by diagonal tension associated to debonding between the NSM reinforcement and the concrete substrate. In absence of steel stirrups and/or when the spacing of the NSM reinforcement is large, debonding involves separately each of the bars crossed by the critical shear crack (type-I failure). Recent experiments have also shown that the presence of steel stirrups, combined with a relatively small spacing of the reinforcement, may originate a debonding failure mechanism in which the lateral concrete covers of the steel stirrups detach from the core of the beam with the NSM reinforcement still embedded (type-II failure) (De Lorenzis and Rizzo 2006).

Few research programs on NSM FRP shear strengthening of RC beams are available in literature, as summarized in Table 1. Table 2 reports the main tests results. For all the cases reported, type-I failure occurred. Type-II failure is not treated in this paper and needs appropriate investigation.

At present, different approaches to compute the capacity of shear-strengthened beams are available in the literature, most of which are based on the generalization of the truss model. A model for beams strengthened in shear with NSM reinforcement, based on the model by De Lorenzis and Nanni (2001), is here formulated and applied to predict the test results reported in literature, when type-I failure occurs.

2. ANALYTICAL MODEL

The shear capacity (V_{tot}) of RC beams strengthened with NSM FRP systems can be calculated as the sum of the contributions of concrete (V_c), steel stirrups (V_s) and FRP system (V_{FRP}). The analysis developed herein focuses on the prediction of the FRP contribution.

2.1 Shear contribution for debonding failure mode

As follows, the simplified approach proposed in De Lorenzis and Nanni (2001) is generalized for any value of the angles formed by the shear crack and by the FRP strengthening with the horizontal direction. The formulation is suitable to account for any possible debonding failure mode, provided that it involves each NSM bar separately. A uniform shear stress τ_f at the failure interface is assumed in all the FRP bars intersected by the shear crack at ultimate, thus the FRP shear contribution V_{FRP} can be calculated multiplying τ_f by the total lateral surface of the minimum embedment lengths of all the bars crossed by the crack. This results in Eq (1)

$$V_{FRP} = 2l_{emb} p \tau_f \sin \alpha \quad (1)$$

where l_{emb} is the sum of the minimum embedment lengths of the bars intersected by the shear crack, p is the perimeter along which the bond stress acts (e.g. in the case of round bars, $p = \pi\phi$ where ϕ is the diameter of the bar), α is the angle of the FRP bars to the horizontal axis z (Figure 1), factor 2 accounts for the bars on both sides of the beam. Eq. (1) is valid provided that each embedment length $l_{emb,i}$ (i.e. the minimum length between $l_{s,i} - c_s/\sin\alpha$ and $l_{i,i} - c_i/\sin\alpha$ as shown in Figure 1) is smaller than the development length of the bars l_{dev} , i.e. of the value of bond length sufficient to cause failure in tension of the FRP bar prior to its debonding.. The next formulation assumes $l_{emb,i} < l_{dev}$ for each bar. For any given geometry of the beam, l_{emb} depends on α , θ (θ being the angle between the z -axis and the critical shear crack, see Figure 1) and the relative position between the shear crack and the strengthening system. For design purposes, the value of V_{FRP} corresponding to the most unfavourable crack position must be calculated, i.e. the minimum of l_{emb} and V_{FRP} ($l_{emb\ min}$ and $V_{FRP\ min}$) must be found. It is possible to demonstrate that $l_{emb\ min}$ is given by Eq. (2):

$$l_{emb\ min} = \left\{ n^* [\cot \theta + \cot \alpha] - (n^*)^2 \frac{s_f}{h_{net}} \right\} \frac{\sin \theta}{\sin(\alpha + \theta)} h_{net} \quad (2)$$

where h_{net} is the reduced height of the beam (Eq. (3)) obtained by subtracting the concrete cover thicknesses c_s and c_i (see Figure 1), s_f is the spacing of the bars measured along the longitudinal axis of the beam, and n^* is the number of the bars for which the minimum embedment length coincides with the one located above the crack, given by Eq. (4) where $|x|$ indicates the integer part of x ; r^* is provided by Eq. (5). Eq. (6) gives the minimum FRP shear contribution $V_{FRP\ min}$.

$$h_{net} = h - c_i - c_s \quad (3)$$

$$n^* = \left| r^* \right| - \left| \frac{r^*}{2} \right| \quad (4)$$

$$r^* = [\cot \theta + \cot \alpha] \frac{h_{net}}{s_f} \quad (5)$$

$$V_{FRP\ min} = 2l_{emb\ min} p \tau_f \sin \alpha . \quad (6)$$

2.2 Determination of the shear stress τ_f

Given the local bond -slip relationship, generally it is not conservative to use the maximum value of the bond stress as τ_f since the local bond stress-slip relationship is not sufficiently ductile. On the other hand, τ_f should be chosen properly in order to avoid an excessive crack opening with consequent loss of aggregate interlock. This control can be indirectly done by limiting the maximum strain in the bars as proposed in De Lorenzis and Nanni (2001). As follows, τ_f is determined based on the limitation of the ultimate slip s_u . This method allows to control the crack opening and to take the local bond -slip relationship into account.

When a bar is intersected by a shear crack, the crack width can be calculated if the slip at both loaded ends of the bar is known. At ultimate, the crack width is approximately given by the slip of the side of the bar that collapses first. In order to translate the limitation to this slip in terms of bond stress along the failure interface at ultimate, a reduced constant tangential stress, $\tau_{f, red}$, must be found, and this value can be reasonably obtained starting from the local bond-slip relationship and maintaining constant the fracture energy G_f (see Eq. (7)).

The obtained value can be directly used in Eq. (6) instead of τ_f to find $V_{FRP min}$. To sum up, the computation of $V_{FRP min}$ with the proposed model consists in the following steps: computation of h_{net} from Eq. (3); computation of r^* and n^* from Eq.s (4) and (5); computation of $l_{emb min}$ from Eq. (2); computation of $\tau_{f, red}$ from Eq. (7); computation of $V_{FRP min}$ from Eq. (6).

$$\tau_{f, red} = \frac{G_f}{s_u} = \frac{1}{s_u} \int_0^{s_u} \tau(s) ds \quad (7)$$

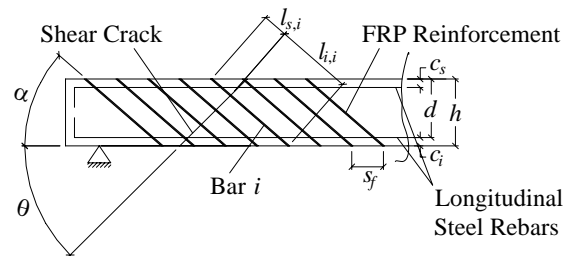


Figure 1: Calculation of the Embedment Lengths of the FRP Bars

3. COMPARISON BETWEEN THEORETICAL AND EXPERIMENTAL RESULTS

In this section, the model is applied to the beams tested by De Lorenzis and Nanni (2001), Barros and Dias (2006), Dias and Barros (2006) and Barros et al. (2006). Table 1 summarizes the main parameters. Figure 2a shows the bond-slip relationships reported in De Lorenzis (2002) and in Sena Cruz (2004) (curve 1 and 2-3, respectively); Figure 2b plots the reduced bond stress $\tau_{f, red}$ versus the maximum slip s_u , in the range of slips from 0 mm to 1.0 mm. There is a value of s_u , s_u^* , for which $\tau_{f, red}$ is maximum. This can be physically explained as follows. For slips smaller than s_u^* , the crack opening is limited and the bars are not stressed for their entire length; thus, a smaller value $\tau_{f, red}$ must be used. Conversely, for slips higher than s_u^* , part of the length of the bars, corresponding to the loaded ends, can result debonded; thus, $\tau_{f, red}$ must be reduced to take this into account.

Table 1 and Figure 3 compare the experimental results with predictions of the model. $\tau_{f, red}$ was found using the bond-slip relationship proposed by each author and assuming $s_u = 0.2$ mm. Figure 3a shows the results for the beams of Table 1. With few exceptions, predictions are conservative. Figure 3a also shows the results obtained using for τ_f the local bond strength, which is evidently unconservative. Figure 3b analyses the influence on results of s_u and h_{net} for the beam tests reported by De Lorenzis and Nanni (2001). It can be noted that the choice of s_u does not strongly affect the results as h_{net} does.

4. CONCLUSIONS

From results of the reported investigation, the following conclusions can be drawn:

- the proposed model uses simplifying assumptions that make it very easy to use for design purposes unlike more accurate but more onerous models accounting for bond-slip and evolution of bond stresses during opening of the critical shear crack;
- the proposed model with a properly reduced value of design bond strength (for example, maintaining constant the fracture energy and limiting the ultimate slip of the real bond-slip model in order to control the shear crack width) gives in most cases conservative predictions on the FRP shear contribution.

Obviously, further experimental investigations are necessary to validate the proposed formulation and extend it to the cases for which type-II failure occurs.

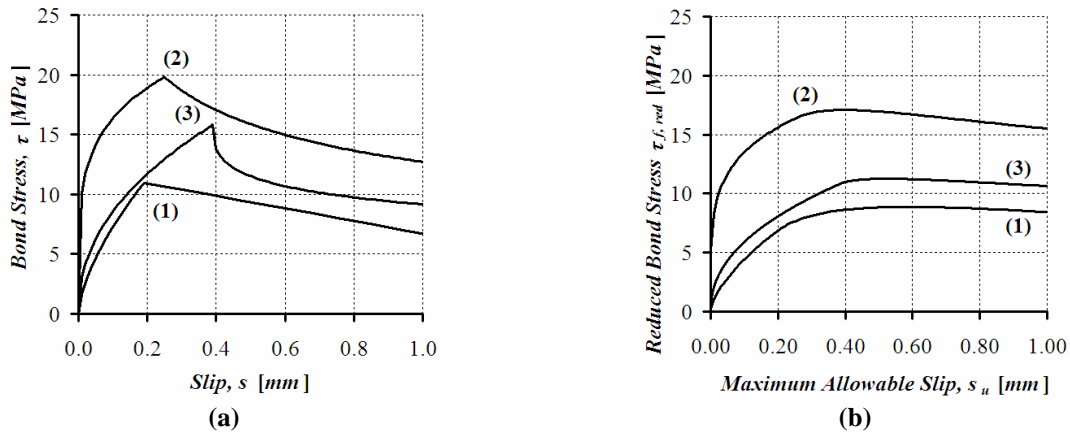


Figure 2: (a) Local τ - s Relationships Found by De Lorenzis (2002; curve 1), and Sena Cruz (2004; curve 2-3) for Joints Having the Same Characteristics of Those in the Shear-Strengthened Beams; (b) Reduced Bond Stress $\tau_{f,red}$ (eq. 7) versus Maximum Slip s_u .

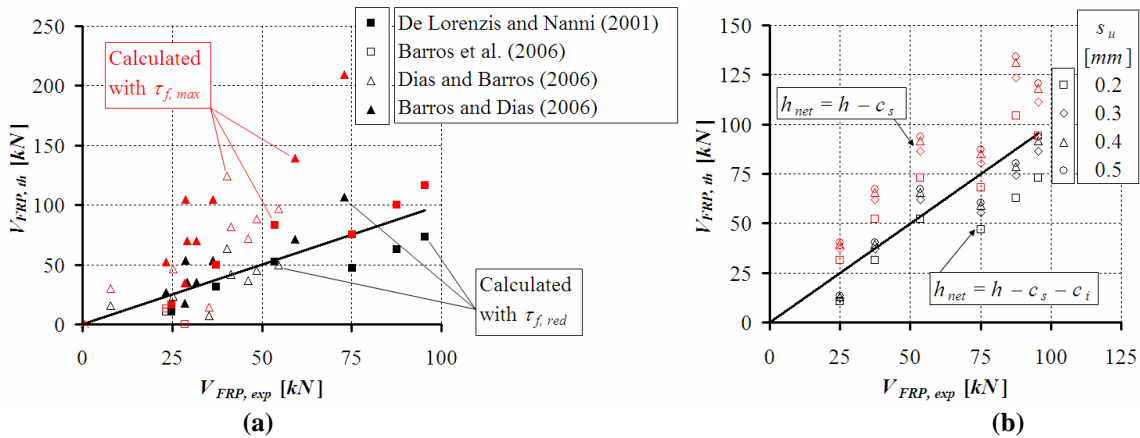


Figure 3: (a) Experimental and Theoretical Results; (b) Experimental and Theoretical Results for the Beam Tests Reported by De Lorenzis and Nanni (2001) Using Different Values of s_u and h_{net}

5. REFERENCES

- Barros, J. A. O., and Dias, S., (2006), "Near surface mounted CFRP laminates for shear strengthening of concrete beams", *Cement and Concrete Composites*, 28 (3), pp. 272-292.
- Barros, J. A. O., Ferreira, D. R. S. .M., Fortes, A. S. and Dias, S. J. E., (2006) "Assessing the effectiveness of embedding CFRP laminates in the near surface for structural strengthening", *Construction and Building Materials*, 20, pp. 478-491.
- Sena Cruz, J. M., (2004). "Strengthening of concrete structures with near-surface mounted CFRP laminate strips", PhD Thesis, Escola de Engenharia, Universidade do Minho, Portugal.
- De Lorenzis, L., and Nanni, A., (2001), "Shear strengthening of reinforced concrete beams with NSM fiber-reinforced polymer rods", *ACI Structural Journal*, 98(1), pp. 60-68.
- De Lorenzis, L., (2002), "Strengthening of RC structures with near-surface mounted FRP rods", PhD Thesis, University of Lecce, Italy.
- De Lorenzis, L., and Rizzo, A., (2006). "Behavior and capacity of RC beams strengthened in shear with NSM FRP reinforcement". *Proceedings of Second fib Congress*, Naples, Italy, CD-ROM
- Dias, S. J. E., and Barros, J. A. O., (2006), "NSM laminates for the shear strengthening of T Section RC Beams", private communication.
- Sena Cruz, J. M., and Barros, J.A.O. (2004), "Modeling of bond between near-surface mounted CFRP laminate strips and concrete", *Computers and Structures*, 82, pp. 1513-1521.

Table 1: RC Beams Strengthened in Shear with NSM Systems

Beam	Steel Stirrups Diameter/Spacing (mm)/(mm)	NSM System	Angle, α (degrees)	Spacing, s_f (mm)	Reduced Height, h_{net} (mm)
Source: De Lorenzis and Nanni (2001) Section: T (web width/height = 152/305 mm; flange width/height = 381/102 mm; $c_f/c_s = 50.8/0$ mm) NSM CFRP Shear Strengthening System: Round CFRP Bar (9.525 mm diameter; $E_f = 104.8$ GPa) + Epoxy Local bond parameters: $\tau_f = 10.96$ MPa; $s_m = 0.191$ mm (from Table 4.2 in De Lorenzis (2002))					
BV	None	None	-	-	-
B90-7	None	CFRP bars	90	177.8	254.0
B90-5	None	CFRP bars	90	127.0	254.0
B90-5A	None	CFRP bars anchored in the flange	90	127.0	355.6
B45-7	None	CFRP bars	45	177.8	254.0
B45-5	None	CFRP bars	45	127.0	254.0
BSV	9.525/355.6	None	-	-	-
BS90-7A	9.525/355.6	CFRP bars anchored in the flange	90	177.8	355.6
Source: Barros et al. (2006) Section: Rectangular (width/height = 150/150 mm; $c_f/c_s = 31.0/29.0$ mm) NSM CFRP Shear Strengthening System: CFRP Strip (width/thickness = 9.59/1.45 mm; $E_f = 158.0$ GPa) + Epoxy Local bond parameters: $\tau_f = 19.81$ MPa; $s_m = 0.25$ mm (from Table 1 in Cruz and Barros (2004))					
VB10	None	None	-	-	-
VBCV-10	None	CFRP strips	90	100.0	119.0
VBCI-15	None	CFRP strips	45	150.0	119.0
Source: Dias and Barros (2006) Section: T (web width/height = 180/300 mm; flange width/height = 450/100 mm; $c_f/c_s = 44.0/34.0$ mm) NSM CFRP Shear Strengthening System: CFRP Strip (width/thickness = 9.59/1.45 mm; $E_f = 166.6$ GPa) + Epoxy Local bond parameters: $\tau_f = 15.80$ MPa; $s_m = 0.39$ mm (from Table 3.3 in Sena Cruz (2004))					
2S-R	6/300	None	-	-	-
2S-3LV	6/300	CFRP strips	90	267.0	256.0
2S-5LV	6/300	CFRP strips	90	160.0	256.0
2S-8LV	6/300	CFRP strips	90	100.0	256.0
2S-3LI45	6/300	CFRP strips	45	367.0	256.0
2S-5LI45	6/300	CFRP strips	45	220.0	256.0
2S-8LI45	6/300	CFRP strips	45	138.0	256.0
2S-3LI60	6/300	CFRP strips	60	325.0	256.0
2S-5LI60	6/300	CFRP strips	60	195.0	256.0
2S-7LI60	6/300	CFRP strips	60	139.0	256.0
Source: Barros and Dias (2006) Section: Rectangular A-Beam (width/height = 150/300 mm; $c_f/c_s = (15.0+0.5\phi_{\text{longitudinal steel rebar (10 or 12 mm)})/18.0$ mm) Section: Rectangular B-Beam (width/height = 150/150 mm; $c_f/c_s = (15.0+0.5\phi_{\text{longitudinal steel rebar (10 or 12 mm)})/18.0$ mm) NSM CFRP Shear Strengthening System: CFRP Strip (width/thickness = 9.59/1.45 mm; $E_f = 166.6$ GPa) + Epoxy Local bond parameters: $\tau_f = 15.80$ MPa; $s_m = 0.39$ mm (from Table 3.3 in Sena Cruz (2004))					
A10_C	None	None	-	-	-
A10_VL	None	CFRP strips	90	200.0	262.0
A10_IL	None	CFRP strips	45	300.0	262.0
A12_C	None	None	-	-	-
A12_VL	None	CFRP strips	90	100.0	261.0
A12_IL	None	CFRP strips	45	150.0	261.0
B10_C	None	None	-	-	-
B10_VL	None	CFRP strips	90	100.0	112.0
B10_IL	None	CFRP strips	45	150.0	112.0
B12_C	None	None	-	-	-
B12_VL	None	CFRP strips	90	50.0	111.0
B12_IL	None	CFRP strips	45	75.0	111.0

Table 2: Experimental and Theoretical Results of the Beams of Table 1

Beam	Experimental Ultimate Shear V_{exp}^1 (kN)	Experimental FRP Contribution $V_{FRP exp}^1$ (kN)	Analytical FRP Contribution $V_{FRP d}^2$ (kN)	Δ_{min}^3 (%)
BV	90.29	-	-	-
B90-7	115.20	24.91	10.45	138.4
B90-5	127.66	37.36	31.35	19.2
B90-5A	185.70	95.41	73.15	30.4
B45-7	165.47	75.17	47.02	59.9
B45-5	177.92	87.63	62.70	39.8
BSV	153.23	-	-	-
BS90-7A	206.83	53.60	52.25	2.6
VB10	37.01	-	-	-
VBCV-10	65.61	28.60	0.00	-
VBCI-15	60.22	23.21	10.35	124.3
2S-R	246.00	-	-	-
2S-3LV	189.60	0.60	0.00	-
2S-5LV	214.20	25.20	23.88	5.5
2S-8LV	237.60	48.60	45.26	7.4
2S-3LI45	196.80	7.80	15.50	-49.7
2S-5LI45	230.40	41.40	41.70	-0.7
2S-8LI45	229.20	40.20	63.44	-36.6
2S-3LI60	224.40	35.40	7.47	373.9
2S-5LI60	235.20	46.20	36.84	25.4
2S-7LI60	243.60	54.60	49.50	10.3
A10_C	50.20	-	-	-
A10_VL	79.32	29.12	35.64	-18.3
A10_IL	78.95	28.75	53.46	-46.2
A12_C	58.25	-	-	-
A12_VL	117.56	59.31	71.28	-16.8
A12_IL	131.19	72.94	106.92	-31.8
B10_C	37.01	-	-	-
B10_VL	65.61	28.60	17.82	60.5
B10_IL	60.22	23.21	26.73	-13.2
B12_C	37.85	-	-	-
B12_VL	69.60	31.75	35.64	-10.9
B12_IL	74.25	36.40	53.46	-31.9

¹ Experimental data.
² $s_u = 0.2 \text{ mm}$.
³ $\Delta_{min} = \frac{V_{FRP exp} - V_{FRP min}}{V_{FRP min}}$.

Part XXII. Strengthening

FLEXURAL BEHAVIOUR OF REINFORCED CONCRETE BEAMS STRENGTHENED WITH NEAR SURFACE MOUNTED CFRP STRIPS

Renata Kotynia

(Assistant Professor, Technical University of Lodz, Lodz, Poland)

ABSTRACT

The paper presents test results of full-size simply supported reinforced concrete beams with rectangular cross section, strengthened for flexure with NSM CFRP strips. The specimens with different steel and CFRP reinforcement ratio were tested under four point monotonic loading. The aim of the test was to obtain the same flexural capacity for all tested beams. The structural performance and modes of failure of the tested beams are presented and discussed in this paper. Full composite action between the NSM CFRP strips and concrete was achieved. Results of the test indicated that the lower was steel reinforcement ratio and higher was CFRP ratio the lower was stiffness and ultimate load of strengthened beams. It was due to lower the axial stiffness $E_f A_f$ of NSMR CFRP strips than the stiffness of the steel reinforcement. If the elasticity modulus of NSMR strip is similar to the steel, the stiffness and load capacity of beams will be higher.

KEYWORDS

NSM, CFRP Strips, Flexural Strengthening, Debonding

1. INTRODUCTION

The research carried out up to now on RC members strengthened in flexure has indicated that externally bonded reinforcement (EBR) technique cannot utilize the full strength of the fiber reinforced polymer (FRP) reinforcement (Kotynia, 1999). Brittle failure due to premature FRP debonding and concrete cover separation has been the most dominant mode of failure (Teng et al., 2002). In order to improve the efficiency of this technique additional anchorage systems with U-jacket FRP sheets have been proposed (Kotynia and Kaminska, 2003). Moreover EBR FRP technique is susceptible to damage from collision, high temperature, fire and ultraviolet rays. To overcome these drawbacks, near surface mounted (NSM) strengthening technique has been proposed. Due to better anchorage of NSM FRP reinforcement bonded into pre-cut grooves opened in the concrete cover of the RC element, this technique is significantly more efficient than EBR system (Täljsten, 2005). Recent tests have pointed out several benefits of NSM technique such as: increase in the load carrying capacity of concrete structures in bending and shear, easy and cost effective (Barros and Fortes, 2005). The bond characteristic between NSM FRP reinforcement and concrete has been widely analysed (De Lorenzis and Nanni, 2001). Using the same axial stiffness of FRP to strengthen reinforced concrete beams, higher ultimate load has been achieved by the beams strengthened with the NSM CFRP strips than by the beams strengthened with EBR (El-Hacha and Rizkalla, 2004).

2. EXPERIMENTAL PROGRAM

Test carried out on RC beams strengthened with the NSM CFRP strips indicated that the average strain of the strip during debonding was 0.011 (Kotynia, 2005). This value has been assumed as a limit strain of the strip in the ultimate state. Based on this assumption, the test program of four beams has been proposed. The aim of the test was to obtain the same flexural capacity for all tested beams. Four rectangular concrete beams simply supported over 4200 mm clear span were tested in four-point flexure with a shear span of 1400 mm and a constant moment region of 1400 mm. Four different tension steel reinforcement ratios and three CFRP reinforcement ratios ($\rho_s = A_s/bh$, $\rho_f = A_f/bh$, where A_s and A_f are the total tension steel and CFRP reinforcement respectively, b and h are the width and height of the beam respectively) were used (Table 1). The beam P0 with the highest steel ratio

($\rho_s=1.57\%$) was unstrengthened in flexure and three other beams were strengthened with one, two or three CFRP strips $2.4 \times 15 \times 4050$ mm. Shear reinforcement consisted of the steel stirrups made of the deformed steel bars of nominal diameter 6 mm spaced at 100 mm and 200 mm. To install the NSM CFRP strips, longitudinal grooves (4 mm x 19 mm) were cut into the concrete cover on the tension side of the beams with a diamond blade. Details of the beams are shown in Figure 1. Experimental strength characteristic of steel and CFRP is shown in Table 2. Strains at the level of the longitudinal tension and compression steel were measured by the LVDT gauges, attached to the concrete side. Deflections were measured in five points of the beam's span. All measurements were recorded at every load level.

Table 1: Details of tested beams

Beam	Steel tension reinforcement		CFRP ratio		Concrete	
	Bars	ρ_s , (-)	Strips	ρ_{fr} , (-)	$f_{c,cube}$ (MPa)	f_c (MPa)
P0	2#20 + 1#10	1.57	-	-	48.0	41.3
P1	2#18	1.13	1 strip	0.08	48.7	41.5
P2	2#12 + 1#6	0.57	2 strips	0.16	43.0	37.7
P3	2#12	0.50	3 strips	0.24	49.2	43.5

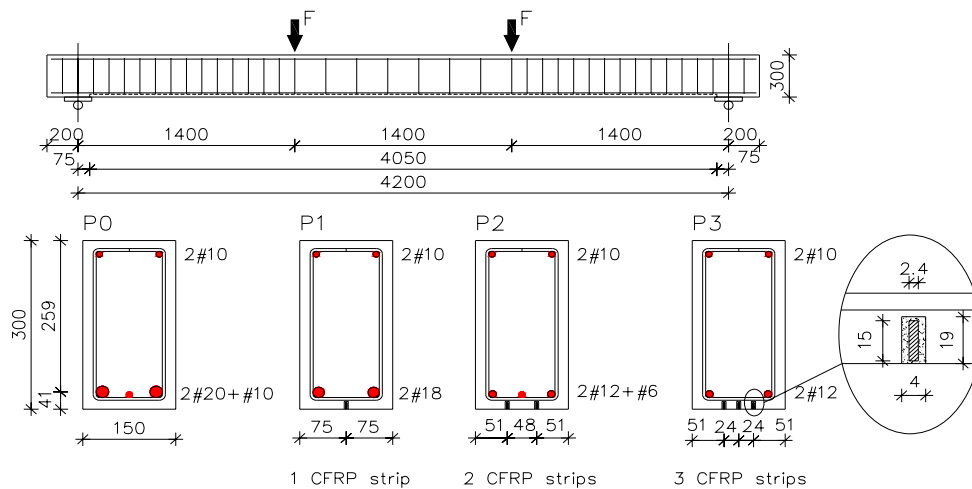


Figure 1: Details of tested beams, steel reinforcement and strengthening modes

Table 2: Properties of steel and CFRP reinforcement

Type	A, (mm)	f_y , (MPa)	E, (GPa)	f_u , (MPa)
Steel				
#10	80.9	425	210	655
#12	114.1	542	220	630
#18	252.9	563	210	669
#20	317.5	541	205	638
#6	29.5	437	207	501
CFRP				
XS1.52 4	29.5	-	163	2250

E – Elastic modulus; f_y – Yielding strength;
 f_u – Ultimate tensile strength

Table 3: Composition of concrete mix

Components	Amount (kg/m ³)
Cement 32,5R	350
Fly ash	60
Sand 0/2	711
Gravel 2/8	573
Gravel 8/16	451
Water	185
Total sum	2330

Composition of concrete mix is given in Table 3. Compressive strength of concrete determined on the cubic $f_{c,cube}$ (150 mm x 150 mm) and cylindrical f_c specimens is presented in Table 1.

3. TEST RESULTS

Two beams with the high steel reinforcement ratio (P0 and P1) failed due to concrete crushing (CC) in the compression zone (marked with a circle in Figure 2). Debonding of the NSM CFRP strips (SD) with the detached concrete cover below the steel was observed in the other two beams P2 and P3 (Figure 2). Full composite action between NSM CFRP strips and concrete was achieved throughout the tests since no slip was observed. The strip debonding was preceded by a typical flexure vertical crack of the beam and the internal concrete cracking followed by the formation of inclined and longitudinal cracks in the concrete surrounding the groove. The NSM CFRP strips debonded from the beam with the detached concrete cover below the steel. The ultimate loads, the average compression (ϵ_c) and CFRP strip's strains (ϵ_{fdb}) obtained during the beam's failure are summarized in Table 4.

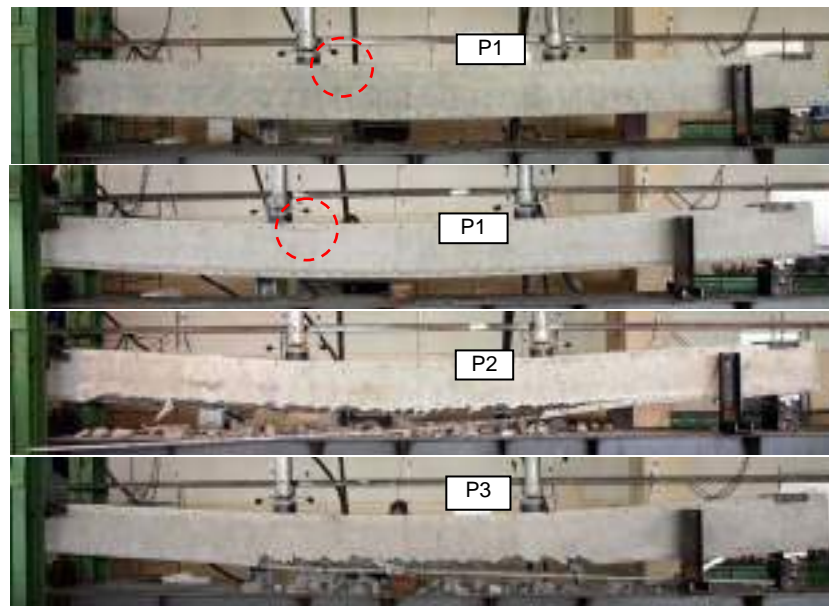


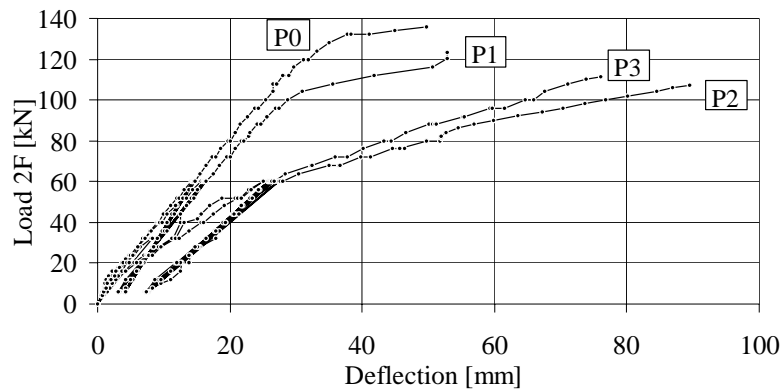
Figure 2. Failure of tested beams due to concrete crushing (P0, P1) and the strip debonding (P2, P3)

Table 4: Details of tested beams

Beam	Ultimate load $2F_u$, (kN)	Failure mode	Strain in tension steel level ϵ_t , (%)	CFRP strain ϵ_{fdb} , (‰)	Compression strain ϵ_c , (%)	Ultimate CFRP strain ϵ_{fu} , (%)	CFRP utilization $\epsilon_{fdb} / \epsilon_{fu}$
P0	136.0	CC	6.38	-	1.93	-	-
P1	123.4	CC	11.18	12.72	1.36	13.8	0.92
P2	107.0	SD	9.94	11.2	1.20		0.81
P3	111.2	SD	8.05	9.10	1.58		0.66

The test results indicated that the lower was the steel reinforcement the lower was the ultimate load. The reason of this decrease was lower modulus of elasticity of the CFRP strips than the modulus of the steel. The CFRP and steel elasticity modulus ratio was $E_f/E_s = 0.7$. Hence, the strengthening ratio should be analyzed in respect of total tension steel cross section area (A_s) and reduced FRP cross section area of the FRP strips ($A_f \times E_f/E_s$). To increase the strengthening ratio, NSM CFRP strips with higher elasticity modulus should be used. In case of the beam P0 a real stress-strain response of the steel bars (#20) turned out different than that assumed in the test program. Hence, the ultimate load for this beam was different than the remaining three beams. Tension strain measurements (ϵ_t) indicated that the higher was the CFRP ratio the lower was the strain of the debonded strip. It confirms the thesis about the effect of the axial stiffness of the NSMR FRP strip ($E_f A_f$) on the limit strain during its debonding (ϵ_{flim}). Hence, the strain utilization of the NSM CFRP ($\epsilon_{fdb} / \epsilon_{fu}$) increased from 66% to 92%. This is a satisfactory result in comparison with the FRP utilization in the EB FRP strengthened beams that was only 35% (Kotynia, 1999).

Comparison of the load-deflection response for all tested beams is shown in Figure 4. The deflection measurements confirm a decrease in the stiffness of the beams caused by the lower elasticity modulus of the NSM CFRP than the steel modulus. Beams with the lower steel ratio indicated higher deflections in failure.



Beam	Deflection v_{max} , (mm)
P0	49,71
P1	52,92
P2	89,53
P3	76,00

Figure 4. Load-deflection responses of tested beams

4. CONCLUSIONS

The test results indicated different ultimate loads for all tested beams. The reason of this effect was due to the low elasticity modulus of the NSM CFRP strips that caused decrease in the stiffness and ultimate loads of the strengthened beams. The higher was NSM CFRP ratio the lower was limit strain during its debonding and the strain utilization of the FRP. In order to increase the strengthening effect the NSM reinforcement with higher elasticity modulus should be used.

5. REFERENCES

- Barros, J.A.O. and Fortes, A.S. (2005). "Flexural strengthening of concrete beams with CFRP laminates bonded into slits". *Journal of Cement & Concrete Composites*, Vol. 27, pp. 471-480.
- De Lorenzis, L. and Nanni, A. (2001). "A Bond Between Near-Surface Mounted FRP Rods and Concrete in Structural Strengthening". *ACI Structural Journal*, Vol. 99, No. 2, pp. 123-132.
- El-Hacha, R. and Rizkalla, S. (2004). "Near-Surface-Mounted Fiber-Reinforced Polymer Reinforcements for Flexural Strengthening of Concrete Structures". *ACI Structural Journal*, Vol. 101, No. 5, pp. 717-726.
- Kotynia, R. (1999). "Ductility and Load Capacity of Reinforced Concrete Members Strengthened with CFRP Strips", Ph.D. thesis, Technical University of Lodz, Lodz, Poland.
- Kotynia, R. and Kaminska, M.E. (2003). *Ductility and failure mode of RC beams strengthened for flexure with CFRP*, Report No. 13, Technical University of Lodz, Lodz, Poland.
- Kotynia, R. (2005). Effectiveness of Near Surface Mounted CFRP Reinforcement for Strengthening of Reinforced Concrete Structures *Proceedings of the International Conference COBRAE 2005, Bridge Engineering with Polymer Composites*, EMPA, Dubendorf.
- Täljsten, B. (2005). Flexural Strengthening of Concrete Beams with Prestressed CFRP Near Surface Mounted Reinforcement (NSMR), *Proceedings of Third International Conference*, Editors: P. Hamelin, D. Biguard, E. Ferrier, E. Jacquelin, Lyon, pp. 3-10.
- Teng, J.G., Chen, J.F., Smith, S.T. and Lam, L. (2002). *FRP strengthened RC Structures*, Wiley, Chichester, U.K.

STRENGTHENING CHOICES FOR THE REPAIR & RETROFIT OF CONCRETE BRIDGE STRUCTURES WITH FRP

J. M. Eyre

(Graduate Structural Engineer, Costain Ltd, Maidenhead, UK)

T. J. Ibell

(Professor of Civil & Architectural Engineering, University of Bath, Bath, UK)

A. Nanni

(Jones Professor of Civil Engineering, University of Missouri-Rolla, Rolla, MO, USA)

ABSTRACT

At present there exist numerous, approved documents and guidelines across Europe, the US, Japan and Canada, giving detailed information on the various applications available that provide for the strengthening of concrete structures with Fibre Reinforced Polymers (FRP). Such guidelines offer a detailed overview of the principles involved in the design of strengthening for deficient beams, columns and slabs, but do not offer codified approaches for individual materials and techniques, or the necessary specialist bridge related criteria. The information and understanding gained from this study is intended for use in directing the generic approach to future FRP design strategies, through the unification of material, system & installation procedure selection and inspection & monitoring regimes.

Software has been developed by the authors to provide a rule-based, logic-programmed 'FRP Strengthening System – Selection Toolkit' defining the extent of required superstructure strengthening following diagnosis and recommendation for pre-installation treatment of the defects and degradation established from analysis of assessment and inspection results. The design process protocol incorporated in the software, consciously targets the concerns of largely inexperienced engineers in this field, particularly those of graduate level training, whilst also attempting to meet the knowledge demands of the Project Engineer or Department of Transportation Investigating Official, responsible for compilation of a preliminary strengthening scheme proposal, for later submission to tender.

KEYWORDS

Fibre Reinforced Polymer, Strengthening, Expert-system, Selection-criteria, Diagnosis.

1. INTRODUCTION

The failings of many of the guidelines, from the extensive range of those produced by the major European (Concrete Society Technical Report 55, Fib TG9.3 Committee 2001), US (ACI 440.2R-02) and Canadian Research committees/ national bodies, in providing truly useable and practical design assistance is in the provision of information relating to practical cases of 'whole' bridge or building strengthening/repair or retrofit. Particularly lacking are guidelines for the undertaking of adequate specification detailing.

Understandably, the industry still remains highly sceptical of new technologies, which further limits the take-up of FRP solutions. Most significantly because degradation cannot be fully anticipated and the associated risk is borne by clients, they are becoming increasingly aware of the durability and maintenance implications of the solutions they adopt. Experience with steel plate bonding and more than 20 years of use of carbon fibre in highly stressed applications for the aviation and automotive industries, has provided accepted criteria for comparable FRP techniques. Adhesives, for instance, have been shown to be equally effective for use with FRP in construction as in the above areas. Ultimately, the limitation of repair lies in the fatigue life of the embedded reinforcement and thus the success of externally bonded FRP relies on its ability to increase the stress range of the reinforcement.

2. AIMS & OBJECTIVES

If FRP techniques are to receive continued use and development, reliable performance of demonstration schemes must be assured and maintained. The foremost objective of this research work was therefore, to develop a design process protocol for the selection of suitable strengthening systems, for the retrofit of structurally defective and/or deteriorating concrete bridges. This objective has been reached through the production of a series of decision-tree's/ flow diagrams which are presented as design aids, along with a rule-based, logic-programmed, Expert-system, (referred to as the 'Toolkit' throughout this report where appropriate) titled; '**FRP Strengthening System – Selection Toolkit**', covering the following phases of selection and repair:

- *Deterioration and degradation processes* – Damage and crack analysis for selection of associated repair or protective treatment.
- *Strengthening option selection and elimination* – Balanced assessment of the merits or limitations of FRP over more traditional counterpart solutions, such as bonded steel plate, increased section size or additional prestress.
- *Structural re-calculation* – Analysis of the requirements for enhanced capacity – in shear, flexure, axial strengthening and/or ductility.
- *FRP material and system technique choice* – Suitability of material type. Namely carbon, aramid or glass, with epoxy, vinylester or polyester laminating resins/adhesives. Appropriate methods of application, principally wet-lay-up sheet, pre-cured plate or Near Surface Mounted reinforcement.
- *Structural Design* – Rule-based sequencing for shear, flexural, axial-strengthening or ductility retrofit. Extension of above phases, to include lengths, laps and splices, layering and the required geometry on the surface of the structure. Criteria for the selection of pre-stressed and mechanically anchored FRP are included to allow exploration for their suitability as appropriate solutions for less conventional defects. Flexibility is however in-built for future extension.

Cost is arguably one of the most influential factors when assessing the advantages of alternative methods and schemes. Detailed costing however is difficult to provide impartially and can become quickly outdated in a highly changeable environment, where new technology is continually emerging. For the benefit of preliminary design clarification, final unit costs are provided, developed from an accumulation of typical material-supply, labour and inclusive construction costs, for each of the phases of development highlighted above. Design costs cannot be accurately predicted under the scope of this work and thus are not included in the final cost report.

Work to tailor the expert system to cater directly for the needs of the Project Engineer, was also carried out after close consultation with MoDOT (Missouri Department of Transportation) area engineers, responsible for the Rolla precincts. Efforts have been made to manipulate criteria for selection throughout each stage, with refinements made to the Toolkits' user-form ordering, questioning and where appropriate, linking procedures and recommendations with MoDOT documentation for standard detailing, 'Special Job Provisions' and contractual requirements.

3. DEGRADATION DIAGNOSIS

The design of strengthening systems for concrete structures is largely achieved through the application of externally bonded reinforcement (abbreviated to EBR where appropriate). Such design is usually carried out as an iterative process of generation, evaluation and modification of trial and error solutions. In such early stages of development of composite technology, there exists little comprehensive guidance for use by inexperienced engineers for preliminary design of systems with FRP. The need to provide interactive, step-by-step guidance to this effect was considered from the project outset.

The most important use of the '**FRP Strengthening System – Selection Toolkit**' is to initiate appropriate thinking and direct/control preliminary design rationale and the generic approach. Overall, the suitability of a candidate bridge superstructure for flexural, shear or axial strengthening, is gauged, having provided an evaluation of the extent of the required strengthening and the sequential impacts of chosen options relating to construction, manpower, material and cost resources. The software does not attempt to prescribe a fixed solution to every eventuality at this stage, but does provide important and fundamental design considerations and practicality issues, specific to local and global conditions, environment and loading. The intention is for the programme to receive continued update to account for future modification and refinement to analysis approaches and as techniques and technologies advance.

Various alternative protective and partially curative techniques may be used to combat each form of chemical attack, based on the severity of their effects and the location and the nature of strengthening required. For diagnosis of observed defects and/or subsequent selection of appropriate remedial and compatible crack treatment; 'Pre-Installation Treatment 1,2 &3', 'Weaknesses', 'Cracks' and 'Substrate' of the 'FRP Strengthening System - Selection Toolkit' should be consulted. Questioning on the user-forms in the software, associated with the foregoing categories, corresponds to the stages of pre-installation treatment investigation and requires responses to establish the overall scheme priorities and limitations, progressively refined throughout each stage of treatment selection. Additionally the environmental and existing structural criteria is defined through responses to the 'Degradation Diagnosis' phase of questioning, giving options and reasoning for the potential environmental, chemical and mechanical defects present.

4. SELECTION

The knowledge base of the 'Toolkit' consists of two main knowledge modules pertaining to diagnosis & selection ('Pre-installation Treatment') and preliminary design ('FRP Strengthening'). Diagnostic information is stored in a spreadsheet format, database search being undertaken through 'If and Then' ruling and 'lookup' systems, written in Visual Basic. The benefit of relative simplicity in this form of data handling is in the ability for all routes through the program to be predefined by the author once a workable decision tree has been established. Problems of changes of the state of the variables with time are not of concern to this stage.

Taking the example of 'System' selection, a decision tree/network was used to create an Excel spreadsheet by compiling a rudimentary series of questions, asked in the associated user-form, to delineate the overall geometry, structure and construction methods used, but also to ensure compatibility with the previously selected repair, preparation and pre-installation conditions. Further questioning is designed to determine whether a bond or contact critical repair is necessary and hence what the stress-strain behaviour, eventual failure mode and ductility requirements are likely to be. 'System' options of Plate (Pre-cured Laminate), NSM or Sheet are subsequently progressively eliminated with applicable reasoning, based on their performance under the strengthening constraints presented. The results obtained at this point are entirely qualitative, with built in subjective preference by the single domain author. It is quite possible that substantial differences may be encountered in the rule base for different experts and indeed facilities are provided, encouraging customary changes to be made, through the 'expert inclusions' option at the base of each user-form.

5. STRUCTURAL ANALYSIS

Numerical calculations are now necessitated, some of which require iteration, whilst others require the solution of sets of equations. Again built on decision flow/ network diagrams, responses to most questioning and execution sequences are limited to 'True' and 'False', facilitating a rapid breakdown of the intricacies of design and division of the various routes to completion. Manufacturer's data is input by the user, allowing for testing and analysis with contemporary material solutions. The final result is an economical cross-section, which satisfies the design criteria. Responses given on user-forms called from the main-menu orientation page are written directly to the corresponding spreadsheet/ flow chart in the Excel platform, activating the execution of subsequent stages of calculation within the worksheet. Solutions and limits are then returned via message box captions to the screen or via the final report textboxes, giving details of the final system.

Where seemingly complex or involved questions arise and are queried, or guidelines are sought for a series of such questions by clicking on the available 'checkbox', numerous quick reference checklists have been compiled which offer elaborations on the type of response demanded, or underlying nature of the conditions attempting to be configured. Similarly where numerical input values are called for, options are given where possible, via a 'see chart' button function, which links the user to the worksheets corresponding to the calculation being undertaken, this option allows for more accurate initial estimations, however optimisation may be achieved through continual trial and error for all design parameters if complications arise.

American and British guidance is separated for the strengthening design stages, owing to the sometimes very different principles adopted. The highly prescriptive approach used in ACI-440.2R-02 generates a very concise program routine that has been adapted and applied to TR55 guidance by making alterations to the order of design development officially recommended. Mixing the views held in the separate codes, or differential schools of thought indiscriminately would almost certainly result in major shortcomings and inconsistencies.

6. COST ESTIMATION

The level of cost control included within the selection ‘Toolkit’ at this stage concentrates on the initial costs of repair. Included within this categorisation are; material, labour (supervisors, skilled and unskilled) and UK Highways Agency recommendations for start-up and preliminary design costs. It is argued that the single event repair, using correctly designed and constructed FRP systems together with the negligible probability of failure, results in near insignificant repair cost.

$$C_{repair} = \sum_{i=1}^n (1 - P_f(t_{r,i})) C_{maintenance}(t_{r,i}) \frac{1}{(1+r)^{t_{r,i}}}$$

(Source: cited in Throft-Christensen (2000) – Repair cost model)

The limited level of allowable strengthening or repair of structures with FRP, demanding an ultimately service-sustainable structural capacity following potential FRP failure, additionally eliminates failure costs of the consequences of injury or loss of life from bridge damage. It is also argued that, particularly in the US, where repair under live loading is permitted with nominal speed restrictions, user costs are minor factors of ultimate life cycle pricing. Hence:

$$W = B_{lifecycle} - C_{lifecycle} \quad \rightarrow \quad C_{lifecycle} = C_{initial} + C_{repair} + C_{user} + C_{failure}$$

$B_{lifecycle}$ = Benefit that can be gained from existing bridge after rehabilitation

The final cost report, at this stage ultimately follows the recommendations generated through project RI 02-022, ‘Cost-Effectiveness Analysis of FRP Strengthening’. Firstly a cost per square foot is extracted, based on a budget estimated per bridge span. Unit costs for material, labour, preparation and concrete repair are respectively adjusted by a corresponding ‘factor ratio’ equated to the; amount of FRP material for element in question divisible by the gross amount of material applied across the entire span.

7. CONCLUSIONS, POTENTIAL & FURTHER WORK

Preliminary design, involves the overall structural form of the artefact, satisfying a few key design constraints. This early stage of the design process for repair and retrofit works, is perhaps more closely linked with the conceptual design of a new structure, but is largely based around the adoption of key decisions, based on the criteria to be satisfied at the detailed design stage. As such, an expert system and the particular method chosen for the ‘Toolkit’ is entirely appropriate for providing a platform for integration of these related stages.

With the help of the ‘Toolkit’, design should now evolve with choices being made in a logical sequence. Where a stage in the design process is reached, requiring a complete analysis to be carried out, the expert designer will do this with the expectation that the structure is safe. The potential of the ‘Toolkit’ as a Value-Engineering tool and device used for ‘Early-warning’ of project shortcomings, is also significant, in providing advanced notification of potential or consequential constructional, technical or resourcing conflicts.

8. REFERENCES

- ACI 440.2R-02, (2002), *Farmington Hills, MI: American Concrete Institute, 2002*. “Guide for the Design and Construction of Externally Bonded Systems for Strengthening Concrete Structures,”
- American Association of State Highway and Transportation Officials (2003), *17th ed, AASHTO, Washington, D.C.* “Standard Specifications for Highway Bridges”
- FibTG9.3, (2001), “Externally bonded FRP reinforcement for RC structures”
- Technical Report No.55, (2001), *The Concrete Society, Berkshire RG45 6YS UK, (TR55)* “Externally bonded FRP Reinforcement for RC structures”
- De-Lorenzis L.A. and Nanni A. (2005), *Project RI 02-022, Preservation of Missouri transportation infrastructure Validation of FRP composite technology through field testing*, “Cost-Effectiveness Analysis of FRP Strengthening”
- Lynch R.J (2004), *Master Thesis, University of Missouri-Rolla, Rolla MO, U.S.A.*, “Provisional Design Guide in AASHTO Language for FRP Bridge Strengthening”.

NATURAL FIBRE COMPOSITES FOR STRENGTHENING OF GLUED-LAMINATED TIMBER IN TENSION PERPENDICULAR TO THE GRAIN

Alann André

*(Ph.D. student, Civil and Environmental Engineering –Structural Engineering
Luleå University of Technology, SE-971 87 Luleå, Sweden)*

Helena Johnsson

(Ph.D., Civil and Environmental Engineering –Timber Structure

Anders Carolin

(Ph.D., Civil and Environmental Engineering –Structural Engineering

ABSTRACT

This paper discusses strengthening of glued-laminated timber in tension perpendicular to the grain. Wood properties are often inappropriate for high performance structural applications. Major drawbacks like durability and high variability can be reduced by using glued-laminated timber. A further step to decrease the variability is to strengthen the cross-section to prevent tensile failure perpendicular to the grain. This has been widely investigated during the last decades by bonding fibre reinforced polymer (carbon, aramid and glass fibres) to timber or glulam beams, with mostly promising results. However, a great concern about environmental friendly materials showed up a few years ago. Mineral and petrol-based fibres are difficult to recycle and increase the amount of carbon dioxide in the atmosphere leading, for instance, to the preoccupant greenhouse effect. Natural fibres such as flax are on the contrary, recyclable and CO₂ neutral. Their low density and high specific mechanical properties provide great advantages for timber construction.

Specimens of glued-laminated timber with a volume of 0.01 m³ have been reinforced with fibre reinforced polymer (FRP) composites, and tested in tension perpendicular to the grain. Unidirectional laminates have been prepared with flax and glass fibres. Epoxy resin, which provides good bonding with hydroxyl groups in natural fibres, has been used. The results show that there is a potential in using natural fibres for strengthening timber structures.

KEYWORDS

Natural fibres, Strengthening, Tension perpendicular to the grain, Flax fibres composites, FRP composites

1. INTRODUCTION

Wood mechanical properties perpendicular to the grain are weak and dominate failure initiations while loading a timber member in bending. Besides, an important issue for a timber member is the failure mode. Compression failure in wood is ductile. Unfortunately, most of the failures occur in tension perpendicular to the grain and are brittle. This brittleness generates safety problems since it occurs suddenly. Indeed, brittle failures do not give adequate warning signals that may initiate evacuation.

On the timber front, significant benefits of combining FRPs with wood-based composites in a variety of end-use applications, including beams, has been demonstrated (Johnsson et al., 2005). With increased strength, reduced variability, and elimination of size effects, high-performance FRP-wood composites may present new commercial opportunities for both the FRP and the timber industry.

Natural fibres are light, renewable, CO₂-neutral and possess interesting specific mechanical properties (Bledzki and Gassan, 1998) which make them suitable to be used as polymer resins reinforcement for strengthening of structural elements made of wood (André, 2006). Flax is grown in abundance in Europe, from Finland to Italy, and in many other countries around the world. Temperate climate fits well to flax and European countries have focused their

natural fibre composite research principally on flax fibres because of its availability in Europe and its high performance in term of mechanical properties (Oksman, 2001).

2. EXPERIMENTAL METHODS AND MATERIALS

2.1 Materials

All glulam specimens were cut from spruce glulam beams supplied by Martinsons AB, Sweden. The beams were of strength class LT40 (BFS 2003:6, Swedish Construction Regulation), which is slightly similar to GL32c in ENV 1995-1-1: 2003 (Eurocode 5 – Design of timber structures). All specimens had the same volume $V = 0,01 \text{ m}^3$, which is the reference volume use in EN 408 to characterize the tensile strength perpendicular to grain of glued laminated timber.

Glass fibers were used to produce a reference FRP composite for the experiment. The glass fibre weave was unidirectional with a weight of 250 g/m^2 (GFRP-250). Flax fibers from Finflax, Finland, have been manufactured by Engtex, Sweden, to get two technical textiles (These products were derived from Project Texflax Contract N°: G5ST-CT-2001-50111). The first flax fibre weave was 185 g/m^2 (FFRP-185) and the other 230 g/m^2 (FFRP-230).

FRP composites were manufactured using epoxy as matrix (NM infusion 664) and the resin infusion processing technique. The FRP composites have been glued to the glulam specimens using the epoxy used previously. The glulam specimens have been randomly chosen before being glued to the FRP composites to evenly distribute the probability to have large defects. The steel plates, providing the interface specimen/tensile machine, have been glued to the wood with epoxy (StoBPE 465) as in figure 1.

2.2 Experimental methods

The test method is based on EN 408 and was modified to prevent failure at the connected area between the glulam reinforced FRP and the tensile test machine. The test set-up is shown in figure 1.

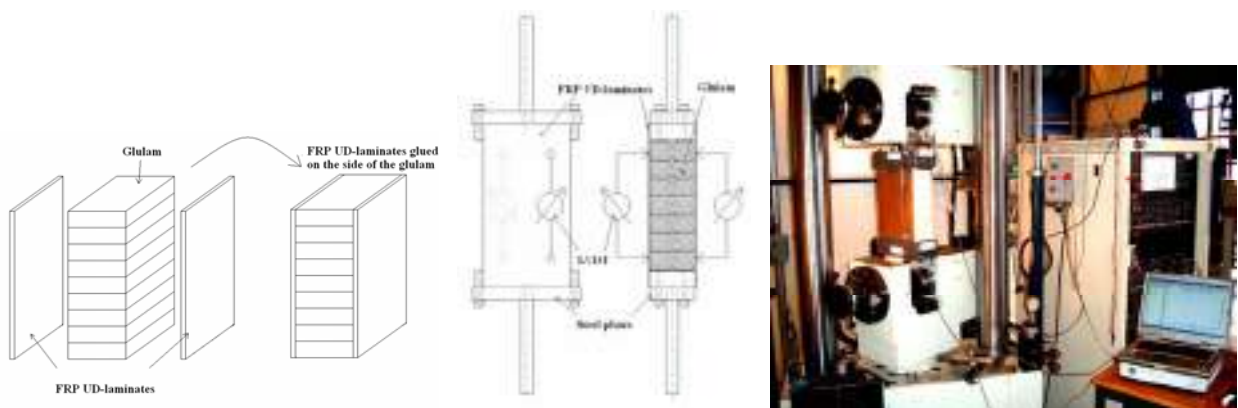


Figure 1: Test set-up

A total of 13 glulam specimens ($405 \text{ mm} \times 223 \text{ mm} \times 115 \text{ mm}$) were tensile tested to failure in this experimental program. The tensile testing equipment used was a Dartec Ltd RE 8991 machine with a 600kN load cell. The rate was $0,15 \text{ mm/min}$ for all specimens. Two Linear Variable Displacement Transducers (LVDT) were used to measure the displacement in the loading direction. The gauge length was 240mm.

All glued-laminated timber specimens had been previously conditioned at $(20 \pm 1) \text{ }^\circ\text{C}$ and $(30 \pm 10) \%$ relative humidity. Before all gluing, surfaces were sandblasted and cleaned from dust in order to ensure good bonding.

3. EXPERIMENTAL RESULTS

The tensile strength and modulus have been calculated for all specimens. Mean values and standard deviations are reported in table 1. To get better comparison values, specific properties have been determined using the density of

the materials calculated according to EN 408. A failure was considered as semi-ductile when the first crack along the section of the glulam did not lead to the final failure of the specimen.

Table 1: Absolute and Specific properties (Average values and standard deviation in parentheses)

Specimens	Number	Average density (kg/m ³)	Tensile Strength (MPa)	Specific Strength (MPa/g/m ³)	Tensile Modulus (MPa)	Specific Modulus (MPa/g/m ³)	Elongation at failure (%)	Failure mode
Unreinforced Glulam	4	422	0,73 (±0,27)	1,73	287,5 (±34,32)	681,3	0,38	Brittle
GFRP-250 Reinforced Glulam	5	439	1,80 (±0,36)	4,10	465,3 (±72,53)	1060	0,84	Semi-Ductile
FFRP-185 Reinforced Glulam	2	426	1,18 (±0,11)	2,77	459,7 (±6,43)	1079	0,45	Semi-Ductile
FFRP-230 Reinforced Glulam	2	433	1,49 (±0,29)	3,44	475,7 (±7,47)	1099	0,48	Semi-Ductile

Four load-deformation graphs corresponding to the four types of specimens are shown in figure 2. Failure occurred mostly in the middle section of the specimens. In some cases, failure occurs at the interface steel plate/specimen. These results were not taken into account.

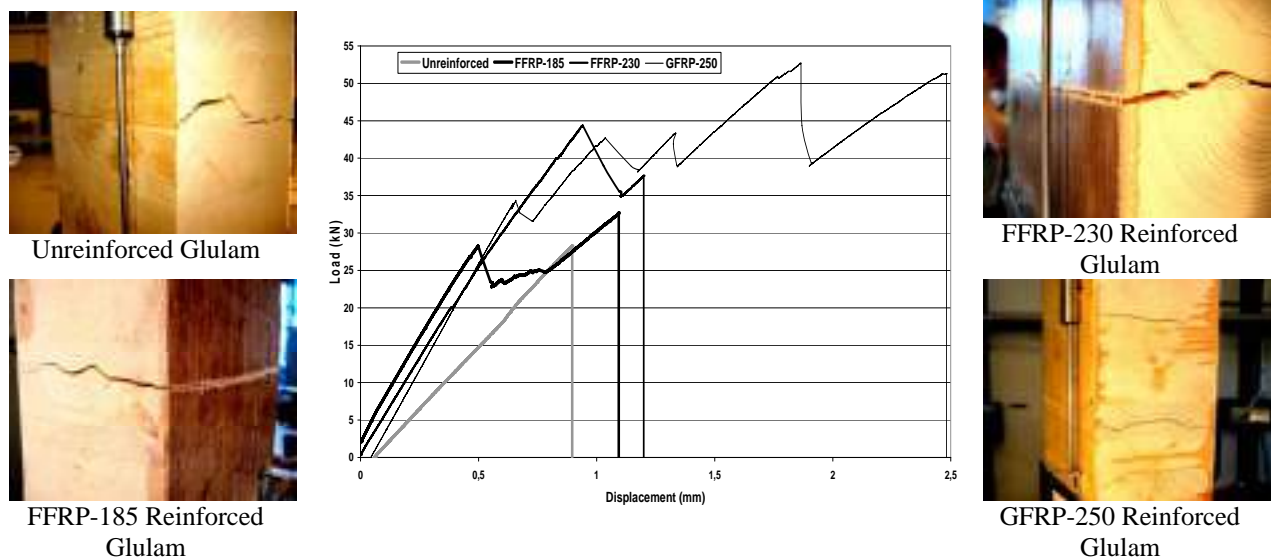


Figure 2: Typical load-displacement diagrams

4. DISCUSSION

A previous research study (Blass and Schmid, 1999) focused on the tensile strength perpendicular to grain of unreinforced glulam specimen. A total number of 153 specimens from different strength classes have been tensile tested. It was found that there was no significant difference in tensile strength perpendicular to grain among strength classes. The strength mean value was 0.77 MPa and the standard deviation 0.22.

The mean value for unreinforced glulam specimens in this investigation was 0.73 MPa with a standard deviation of 0.27. These results compare well to (Blass and Schmid, 1999), which show that the method used is accurate. However, just a few specimens have been tested so far and precaution must be taken regarding this conclusion on the test method.

For an approximate amount of FRP reinforcement of 0.7 % in volume (the thickness of the FRP layers were in between 1 mm and 1.5 mm), it has been shown an increase of the tensile strength by respectively 246%, 161% and 204% using GFRP, FFRP-185 and FFRP-230. Regarding the modulus of elasticity, the previous reinforcement devices led to an increase by respectively 161%, 160% and 165%.

We can see that a strengthening with GFRP provide a higher increase concerning the tensile strength than a FFRP reinforcement. This is probably due to the higher tensile strength of glass fibre, but also to the higher fibre content in GFRP laminates. However, no significant difference can be drawn regarding the modulus of elasticity between FFRP and GFRP reinforced glulam. Indeed, flax fibers have a lower tensile strength than glass fibers but the moduli of elasticity of both fibers are rather similar (André, 2006).

If taking into account the density of the materials, smaller differences in mechanical properties exist between unreinforced and FRP reinforced glulam due to the lower density of the unreinforced glulam specimens. For the same reason, it can be shown that the mechanical properties of FFRP reinforced glulam are closer to those of GFRP reinforced glulam. However, the small amount of FRP reinforcement (0.7 %) doesn't affect significantly the specific mechanical properties even if the density of flax fibers is much lower than the one of glass fibers (1.4 and 2.6 g/cm³ respectively (André, 2006))

Larger displacements are generally observed in the semi-ductile failures. The FRP provides local bridging where cracks in wood occur, confines the local rupture and arrests crack opening (See figure 2). For GFRP reinforced glulam, a number of cracks in the wood have been observed before final failure in the fibers. Concerning FFRP reinforced glulam, failure in the fibers often took place in the same section as the first and unique crack in the wood occurred.

5. CONCLUSION

The use of Fibre Reinforced Polymer (FRP) to reinforced glulam perpendicular to grain enhances its tensile properties. This has been observed both for glass fibers and flax fibers composites reinforced glulam.

It appears that the tensile strength is higher using glass fibers, but the weight of the glass fibers weave used is also higher than the ones made of flax fibers. The stiffness, however, seems to be rather similar, even with a lower amount of flax fibers.

Flax fibre reinforced glulam showed very promising properties if compared to glass fibre reinforced glulam. They appear as a possible alternative to glass fibers. However, only a few specimens have been tested with flax fibers reinforcement devices, and more experiments are needed to draw more significant conclusions.

For all specimens reinforced with fibre composites, semi-ductile failures are reported, which was one of the main objectives of this investigation.

It will be interesting to study moisture transmission in wood and in the FRP since humidity generates higher swelling and shrinking in the wood than it does in FRP. Internal stresses at the interface can appear due to this phenomenon and should be avoid to provide a good interface bonding between Glulam and FRP.

Another important point is to study the variation of the properties. More specimens will be tested to complete this pilot study and to be able to draw conclusions concerning the variation of the tensile properties.

6. REFERENCES

- André, A. (2006). "Fibres for Strengthening of Timber Structures" *ISSN: 1402-1528 ISRN: LTU-FR*
- Blass, H.J., and Schmid, M. (1999). "Tensile Strength Perpendicular to Grain of glued laminated Timber". *International Council for Research and Innovation in Building and Construction, Working Commission W18-Timber Structures (CIB-W18) – Meeting thirty-two, Graz, Austria.*
- Bledzki, A.K., and Gassan, J. (1998). "Composites reinforced with cellulose based fibres". *Progress in polymer science, Vol.24, pp221-274.*
- Johnsson, H., Johansson, T., and Carolin, A. (2005). "Glulam members strengthened by carbon fibre reinforcement". *Submitted for publication in RILEM Materials and Structures*
- Oksman, K. (2001). "High Quality Fibre Composites Manufactured by the resin Transfer Moulding Process". *Journal of reinforced Plastics and Composites, Vol.20, No. 07/2001, pp 621-627.*

PRESTRESSED SRP AND CFRP SHEETS FOR STRENGTHENING CONCRETE BEAMS

Daniel. B. Prentice

(Structural Design Engineer, Read Jones Christoffersen Ltd. Consulting Engineers, Calgary, Alberta, Canada)

Gordon Wight

(Associate Professor, Dept of Civil Engineering, Royal Military College of Canada, Kingston, Ontario, Canada)

ABSTRACT

Carbon Fibre Reinforced Polymer (CFRP) sheets, bonded to the tensile face of reinforced concrete (RC) beams, has become a widely accepted method of strengthening concrete beams and slabs. To use the material more efficiently and significantly reduce deflections, the sheets may be applied with a prestress. Despite the improvements that can be achieved by prestressing the CFRP sheets, the technique is seldom used because the process can be difficult and time-consuming due in part to the CFRP's susceptibility to damage from a mechanical prestressing system. Very recently, a Steel Reinforced Polymer (SRP) sheet system has been introduced for the strengthening of structures. While these sheets have much in common with CFRP sheets, they are tougher and cheaper than CFRP sheets. Because they are less susceptible to damage from lateral stresses, the SRP sheets appear to be very suitable for prestressing applications. This paper outlines an experimental program, investigating the behaviour of five 1.8m long RC beams strengthened with externally bonded non-prestressed and prestressed SRP or CFRP sheets. Prestressing anchorages were developed to tension the SRP and CFRP sheets. Bonded anchorage plates proved best for the CFRP while a mechanical anchorage technique was well suited for the SRP sheets. From these tests it appears that SRP sheets are a competitive alternative to CFRP in both non-prestressed and prestressed strengthening applications.

KEYWORDS

SRP, CFRP Sheets, Prestressing, Strengthening, Concrete Repair, Bonded, Mechanical Anchorages.

1. INTRODUCTION

Adapted from vehicle tire reinforcement technology, SRP systems offer slight ductility advantages over traditional FRP systems. Orthotropic steel cords are held together and bonded to the tension face of a reinforced concrete beam by an impregnation resin to compose SRP sheet strengthening. According to the manufacturer (Hardwire, 1999), the 3X2 cord configuration creates the best tensile properties for use in strengthening RC beams. Sikadur®330 is a typical resin used to impregnate the SRP strengthening sheet as it provides the high viscosity required to slowly penetrate filament voids and fully bond all steel filament cords together as a system. Sheet densities may also be specified as low, medium or high by varying the spacing between individual cords to suit certain applications. Application of SRP is similar to that of the FRP wet lay-up process.

Kim et al. (2005) performed preliminary testing of 1220mm long RC beams strengthened with high-density 3x2 SRP sheets. Observed failure modes were peeling failures where the line of failure either occurred in the concrete cover or in the epoxy layer. Ultimate strength was increased 34% with non-prestressed SRP strengthening. Prota et al. (2004), enhanced the flexural behaviour of 3700mm long RC beams with externally bonded high-density 3x2 SRP sheet strengthening. Test results were compared to CFRP sheet strengthened beams in the same experimental program. Similar cracking behaviour was observed between beams strengthened with SRP and CFRP sheets. Cracks during the service load range were reduced when SRP and CFRP sheet width was increased. All sheet-strengthened beams experienced a peeling failure in the concrete cover. Ultimate strength was increased in the SRP sheet-strengthened beams by 75-145% while the CFRP sheet-strengthened beams were increased by 95-173% over the control beam. High strength steel cords may exhibit yielding behaviour similar to high strength prestressing steel (Nanni et al., 2005). Casadi et al. (2005) utilized medium-density SRP to strengthen 13.4m long prestressed

concrete double-T girders in a decommissioned car park. When tested to failure, flexural capacity in the girders was increased by 12% with one SRP sheet. Nanni et al. (2005) are currently investigating SRP sheet strengthening on three 13m long spans of a 7.2m wide RC girder bridge. Four additional types of CFRP strengthening have also been applied to similar bridges within the same study. These include manual lay-up technique with U-wraps, precured laminates, near-surface mounted bars, and mechanically anchored laminates. Results from the study are still in progress and will be used to determine the long-term effects of strain distribution, debonding, crack opening, deflections and durability on these systems.

2. EXPERIMENTAL PROGRAM

The objective of this investigation was to investigate the behaviour of concrete beams strengthened with prestressed SRP and CFRP sheets. Prestressing anchorages for the SRP and CFRP Sheets were designed to transfer initial prestressing forces to actively strengthen RC beams. Anchorage plates were developed and tested until 30kN was safely transferred into the strengthening material. This level of prestress was approximately 10% of the ultimate strength of the SRP and CFRP sheets and ensured that the top concrete cover was not cracked during prestressing. The prestressing system, depicted in Figure 1, consisted of two welded steel plate assemblies at each beam end to serve the following functions:

1. Anchorage plates; transferred forces from two threaded rods to the strengthening sheet using either a bonded (CFRP) or a mechanical (SRP) anchorage technique.
2. Anchorage Brackets; provided a bearing area at each end of the beam to transfer the prestress force from the anchorage plate assembly to the beam. The brackets were anchored at each end of the beam specimen using full span threaded rod stabilizers.

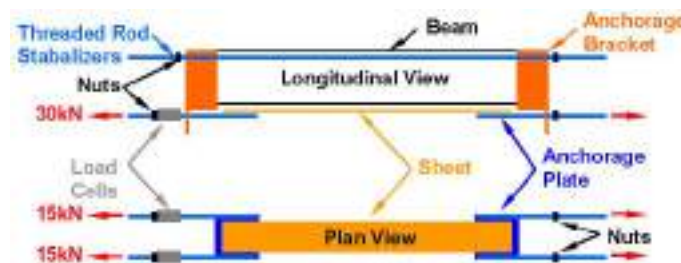


Figure 1: Prestressing Anchorage System

Five RC beam specimens were designed to resist 60kN at mid-span applied as two 30kN point loads. The unstrengthened beams, depicted in Figure 2 (left), were under-reinforced with two longitudinal 10M bars in the bottom tension zone to achieve flexural failure through steel yielding followed by concrete crushing. Two longitudinal 10M bars were placed in the top compression zone to resist tensile forces created from prestressing. Twelve 6M stirrups spaced at 50mm centre-to-centre provided shear reinforcement at each beam end. The strengthening scheme for these beams is summarized in Table 1 and detailed in Figure 2 (right). One unstrengthened beam (A1) was tested as a control specimen for this study. Remaining specimens (A2-A5) were strengthened with externally bonded SRP or CFRP sheets to compare the flexural behaviour of SRP to that of a leading strengthening material. Tension tests were also performed on coupons of Hardwire's high-density 3X2 SRP and MBrace's CF130/CF160 CFRP strengthening systems used in the comparison study. Strengthened beams were designed to resist approximately 120kN at mid-span anticipating a debond-failure by equating sheet stiffness.

Table 1: 1.8m Beam Strengthening Scheme

Specimen	Strengthening Type	Sheets	Thickness (mm)	Width (mm)	Area (mm ²)
A1, B1	Unstrengthened Control	-	-	-	-
A2, B2	Non-Prestressed CFRP	1.5	0.33	120	59.4
A3, B3	Non-Prestressed SRP	1	1.19	140	166.6
A4, B4	30kN Prestressed CFRP	1.5	0.33	120	59.4
A5, B5	30kN Prestressed SRP	1	1.19	140	166.6

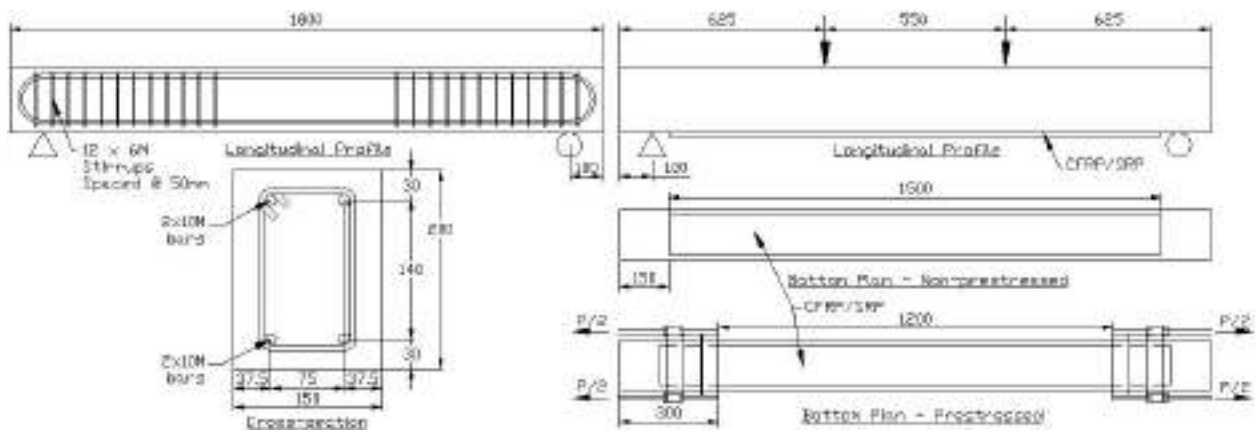


Figure 2: 1.8m Beam Design Specification (left) and Strengthening Scheme (right)

3. RESULTS

Anchorage systems were developed to transfer initial stresses to the SRP and CFRP sheets during prestressing operations. The susceptibility of carbon fibre to lateral stress damage necessitated that a bonded anchorage technique be developed to prestress the CFRP. The CFRP sheet was built up and bonded to steel plates prior to the event of prestressing to avoid damage from the concentrated stresses where the sheets terminate. The process of pre-bonding takes time and expertise that ultimately increases the overall cost of the strengthening required. The increased toughness of the high strength steel cord allows SRP sheets to be less vulnerable to lateral damage than CFRP sheets. A mechanical anchorage technique is therefore well suited for prestressing the SRP sheets. Mechanical anchorages for SRP sheets could save substantial time and money over the bonded anchorages for CFRP when strengthening with prestressed applications. The dry 3x2 Hardwire® was weaved through a series of two (2) 50mm long steel plates and clamped by a third floating plate using nuts tightened on threaded rods. Figure 3 depicts the application step of a prestressed SRP strengthened beam using the mechanical anchorage technique.



Figure 3: Prestressed SRP Strengthening Application with Mechanical Anchorage Technique

The flexural behaviour of 1.8m long non-prestressed and prestressed SRP and CFRP sheet-strengthened beams is summarized during the service range and at the ultimate condition in Table 2. The load-deflection curves for these beams are provided in Figure 3. The yielding point of the beams was chosen as the boundary that separates the service range from the ultimate condition. The service range represents the flexural behaviour before yielding and the service load was defined as the load equivalent to the yield load of the unstrengthened control beam (52kN). The cracking load was increased by 76% and 228% and deflections at the service load were reduced by 36% and 70% for the non-prestressed and prestressed strengthened beams, respectively, with the application of SRP or CFRP sheets. The ultimate condition was determined by investigating flexural behaviour during yield and at failure. Yield loads were increased to 60% and 92% for non-prestressed and prestressed strengthened beams, respectively, and the failure load of all strengthened beams was increased by 68-78%, using SRP or CFRP sheets. Behaviour was improved during the service range using non-prestressed sheets, and even more so when prestressed sheets were

used. Ultimate conditions were improved similarly with non-prestressed and prestressed sheets. SRP and CFRP sheets similarly improved the flexural behaviour of RC beams. It appears that strengthening with SRP sheets may be an alternative to CFRP sheets for non-prestressed and prestressed applications.

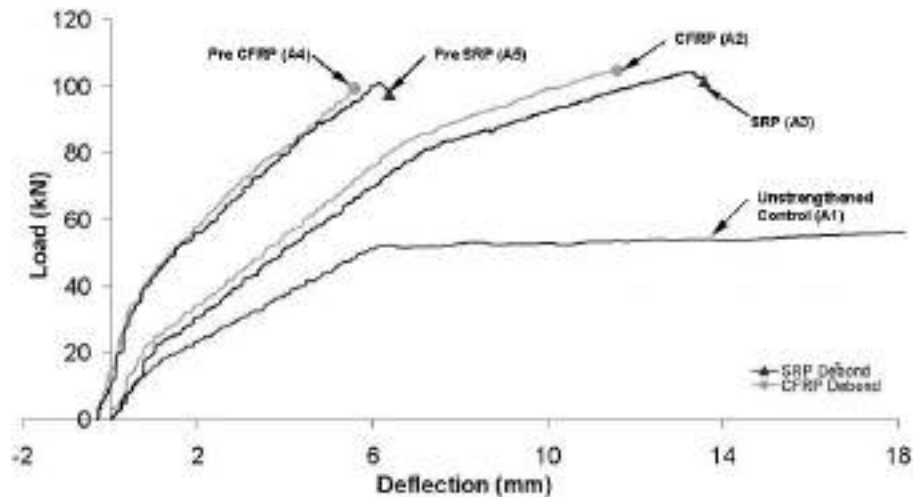


Figure 3: Load-Deflection Behaviour of 1.8m Beams Strengthened with SRP and CFRP Sheets

Table 2: Behaviour of 1.8m Beams Strengthened with SRP and CFRP Sheets

Beam Specimen	Cracking		Service		Yield Load (kN)	Failure	
	Load (kN)	Increase	Deflection (mm)	Reduction		Load (kN)	Increase
Control (A1)	12.5	---	6.1	---	52.1	59.0	---
CFRP (A2)	22.1	77%	3.7	39%	84.6	104.8	78%
SRP (A3)	21.7	74%	4.1	33%	80.9	104.3	77%
Pre CFRP (A4)	41.1	229%	1.8	70%	99.2	99.2	68%
Pre SRP (A5)	10.8	226%	1.9	69%	100.9	100.9	71%

4. CONCLUSIONS

Prestressing anchorages were developed to prestress SRP and CFRP sheets. In-situ tensile testing of bonded and mechanical anchorages on 1.8m long RC beams revealed the following conclusions.

1. Strengthening RC beams with prestressed SRP sheets can delay the formation of cracks, reduce deflections, and increase strength during yielding and at the ultimate conditions, more so than non-prestressed applications.
2. The effectiveness of externally bonded SRP sheets to strengthen RC beams is similar to CFRP sheets in both non-prestressed and prestressed applications.
3. It appears that the lateral stress resistance associated with steel cords make SRP sheets ideal for mechanical prestressing anchorages.

5. REFERENCES

- Casadi, P., Nanni, A., Alkhrdaji, T., Thomas, J., 2005: "Performance of Double-T Prestressed Concrete Beams Strengthened with Steel Reinforced Polymer", ASE, April.
- Hardwire, 1999: "Laminate Details Interactive Spreadsheet", Technical Data Sheet, www.hardwirellc.com, Hardwire LLC, Pocomoke City, MD.
- Kim, Y.J., Fam, A., Kong, A., El-Hacha, R., 2005: "Flexural Strengthening of RC Beams Using Steel Reinforced Polymer (SRP) Composites", Proceedings from FRPRCS-7 (ACI), Kansas City, MO, USA, Nov. 6-10, 1-17.
- Nanni, A., Casadei, P., Alkhrdaji, T., 2005: "Steel-reinforced Polymer: An Innovative and Promising Material for Strengthening Infrastructures", Concrete Engineering International, Vol. 9, No. 1, 54-56.
- Prota, A., Tan, K.Y., Nanni, A., Pecce, M., Manfredi, G., 2004: "Performance of RC Shallow Beams Externally Bonded with Steel Reinforced Polymer", Submitted to ACI Structural Journal.

FLEXURAL STRENGTHENING OF 48-YEAR OLD PEDESTRIAN BRIDGE REINFORCED CONCRETE GIRDERS

Raafat El-Hacha

(Assistant Professor, University of Calgary, Calgary, Alberta, Canada)

ABSTRACT

As an emerging technology, the use of Fiber-Reinforced Polymer (FRP) reinforcements in the civil infrastructure has seen an exceptionally rapid growth as an alternative replacement to steel reinforcement. FRP reinforcements have been used in various configurations using different techniques for strengthening and repairing concrete bridges to restore or increase their capacity. Externally bonded FRP reinforcements are currently the most commonly used techniques for flexural strengthening of concrete girders and slabs.

This paper provides experimental results of an investigation that evaluated the efficiency and feasibility of various systems for flexural strengthening of large-scale reinforced concrete girders dismantled from a 48-year old deteriorated pedestrian bridge. The strengthening system comprised externally bonded Carbon FRP (CFRP) including strips, plates and sheets. Another material known as Steel-Reinforced Polymer (SRP) was also used as externally bonded sheets. Four beams were strengthened with the above various strengthening systems using the same axial stiffness and tested under static monotonic loading up to failure. Two beams were tested without strengthening. A 25% increase in the yield load and about 32% to 42% increase in the ultimate strength were achieved. The SRP sheets were more effective at increasing the strength and ductility.

KEYWORDS

Carbon fiber reinforced polymer, externally bonded, flexure, girder, plates, sheets, static, steel, strips, strengthening.

1. INTRODUCTION

Forty percent of Canada's bridges were built in the 1950s and 1960s and many are reaching the end of their service design lives and require rehabilitation and strengthening. The civil engineering and construction industry are facing unexpected challenges due to the state of repair of concrete infrastructure worldwide, and Canada is no exception in which \$44 billion is required to renovate deteriorated infrastructure. Engineers all over the world are challenged and in search of new and affordable construction materials, cost-effective methods of extending the service life of deficient structures, as well as innovative approaches and systems to problem solving. Fibre-Reinforced Polymers (FRPs) have evolved as a promising form of reinforcement in new construction and rehabilitation projects. Various FRP systems for strengthening concrete structures have been widely accepted as practical substitutes to traditional strengthening techniques such as bonding steel plates, section enlargement, and external post-tensioning steel cables. Strengthening systems utilizing FRP reinforcements (sheets, strips, plates) externally bonded to the tension zone of concrete members are currently the most commonly used techniques for flexural and shear strengthening of concrete beams and slabs. Some FRP strengthening techniques could be more effective than others; however, their cost effectiveness is extremely important and could govern their use. The successful application of FRP for structural upgrade has motivated the development of other novel low-cost materials that exhibit excellent structural properties. One such material is composed of unidirectional knitted ultra high-strength steel wires forming cords (11 times stronger than typical steel plate) that are assembled into a fabric embedded or impregnated within a polymeric resin matrix and is referred to as Steel-Reinforced-Polymer, designated as (SRP). This paper investigates the feasibility and effectiveness of using various externally-bonded systems/materials to strengthen four full-scale G-type conventionally reinforced concrete girders dismantled from a deteriorated bridge near the city of Calgary that were cast in 1958 with 25% less flexural reinforcing steel bars. The structural performance under static loading including the behavior prior to cracking, post-cracking, yielding of steel and mode of failure of the strengthened girders will be evaluated and discussed.

2. EXPERIMENTAL INVESTIGATION

2.1 Specimens Details

A total of six girders provided by Alberta Transportation were tested under static load. The girders were dismantled from a pedestrian bridge near the city of Calgary and were 6.0 m (20 ft) long large-scale pre-cast G-type conventionally reinforced concrete girders fabricated in 1958. A cross-section showing details of the girder is shown in Figure 1. The girders are inverted open box channel with end blocks. The problems identified with these girders include the insufficient number of stirrups, lack of load sharing, and stringer legs spillings at the bottom. Spalling was noticed in the underside of the girders in localized sections, and some larger cracks were found on the girders before testing. Considering the age of these girders and the environment they were exposed to, they were in a decent shape. Though, in some places the clear cover was less than adequate and the flexural steel rebars were corroded.

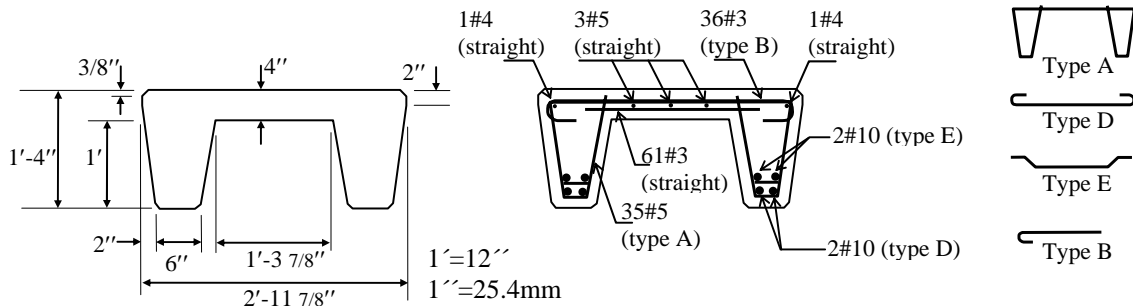


Figure 1: Details of the G-type reinforced concrete pedestrian girders

2.2 Material Properties

Concrete

The concrete compressive strength as specified on the drawings was 28 MPa (4 ksi). Concrete cores were extracted from the control girder and the actual compressive strength of the concrete was found 60 MPa (8.7 ksi). Also, the concrete compressive strength was determined from Schmidt hammer tests and was found to be 58 MPa (8.4 ksi).

Reinforcing Steel

The girders were reinforced with 32mm diameter steel bars with specified yield strength 350 MPa (51 ksi). Three samples of the reinforcing steel were removed from the end of the control girder and tested in uniaxial tension to determine the tensile properties. The yield strength and modulus of elasticity were found 300 MPa (43.5 ksi) and 200000 MPa (29001 ksi), respectively

Strengthening Materials

The externally bonded strengthening systems selected for this study were Carbon-Fiber Reinforced Polymers (CFRP) strips, CFRP sheets, CFRP plates, and Steel-Reinforced Polymer (SRP) sheets. The material properties of the different systems are given in Table 1. A two-part component epoxy adhesive, the main epoxy resin (component A) and the curing agent hardener (component B) was used. Sikadur 330 (mix ratio 4(A):1(B) by weight) was used for bonding the SRP and CFRP sheets, and Sikadur 30 (mix ratio 3(A):1(B) by volume) was used for bonding the CFRP plates and the CFRP strips to the bottom flange of the girders.

Table 1 – FRP material properties as reported by the manufacturers

FRP products (manufacturer and type)	Dimensions	Elastic Modulus (MPa)	Ultimate Tensile Strength (MPa)
Pultruded CFRP Strip (Hughes Brothers Alan 500 CFRP Tape)	t = 2.0 mm [†] w = 16 mm ^{††}	124000	2068
Pultruded CFRP Plate (Sika Carbodur [®] Type S 812)	t = 1.2 mm [†] w = 80 mm ^{††}	160000	2800
Unidirectional CFRP Sheet (Sika Wrap [®] Hex230C)	t = 0.381 mm [†]	61012	715
Unidirectional SRP Sheet (Hardwire [™] 3×2-23-12)	0.44 mm ² /mm [†]	206000	3170

[†] Net area per width ^{††} t: thickness ^{†††} w: width (as shipped by manufacturer and not necessarily entirely used)

2.3 Test Matrix

Four girders (B1, B2, B3, and B4) were strengthened with various strengthening systems using the same axial stiffness (AE) of the strengthening material (where A is the cross sectional area of the strengthening reinforcement and E is its elastic modulus) so as to achieve a 30% increase in the carrying capacity. The strengthening systems comprise externally bonded FRP reinforcements including different types of CFRP (strips, plates, and sheets) and SRP sheets. Two beams were tested without strengthening and served as unstrengthened control specimens for comparison purposes to compare the effectiveness of each technique in terms of percentage increase of the flexural strength and overall structural performance. Table 2 summarizes the test matrix.

Table 2 – Test matrix for the G-type reinforced concrete girders

Beam #	Externally Bonded Strengthening System
C1	Control beam without strengthening
C2	Control beam without strengthening
B1	Four CFRP strips per web (Hughes Brothers 500 Aslan CFRP Tape)
B2	One 80 mm wide CFRP plate per web (Sika Carbodur [®] Type S 812 Plate)
B3	Seven layers of 105 mm wide CFRP sheets per web (Sika Wrap [®] Hex230C Sheet)
B4	Two layers of 90 mm wide SRP sheets per web (Hardwire [™] Sheet)

2.4 Surface Preparation and Installation of the Strengthening Systems

The bottom surface of the concrete webs was leveled with a grinder to eliminate any ridges. To ensure good and strong bond, the surfaces were washed with a water pressure blaster and cleaned by air brushing to remove any debris and dust. Large amounts of concrete had spalled off near the ends of the girders and the reinforcing steel was exposed, therefore patching was done in these areas after removing loose concrete and oxidation from the reinforcing steel. The mortar used for the patching repair was a combination of oven-dried sand and the Sikadur 30 epoxy adhesive with a mix ratio of 1:1 by volume. The mortar was allowed to cure for 24 hours before strengthening was performed. Installation of the strengthening systems followed typical field conditions on the bottom flange beneath the girders. The epoxy was allowed to fully cure at room temperature for at least one week before testing the girders to failure. The anchorage system consisted of wrapping U shape unidirectional CFRP sheets (Sika Wrap[®] Hex230C) bonded to the webs of beams B1, B2 and B3, while for beam B4, the anchor consisted of SRP sheets. The anchors consisted of 28 pieces of 102×762 mm and 8 pieces of 305×762mm. The larger sheets were used at the ends of the webs, and the seven sheets were spaced at 600mm center-to-center through the length of each of the webs.

2.5 Test Setup, Procedure and Instrumentation

The girders were simply supported, simulating the majority of pedestrian bridges, with a span of 5.84m and tested under static monotonic loading up to failure. The girders were loaded at four-point bending with 1.2m spacing between the two concentrated point loads. The load was applied using a 500kN capacity actuator through an MTS controller-testing machine operating under displacement control mode at a constant loading rate of 2 mm/min. All girders were fully instrumented to monitor their behaviour during testing by measuring the deflection at midspan using Linear Strain Conversion devices (LSCs), strains in the concrete in the compression zone, and strain in the CFRP and SRP reinforcements using electrical resistance strain gauges. Horizontal LSC were also placed at midspan on each side of the girder to determine the strain in the concrete: one at 50 mm from top and one at 40 mm from bottom approximately at the level of the reinforcing steel bars. Crack widths were measured using crack comparator and their patterns were marked on the girders. Data were automatically collected and electronically recorded using a data acquisition system. Typical test set-up and instrumentation is shown in Figure 2.

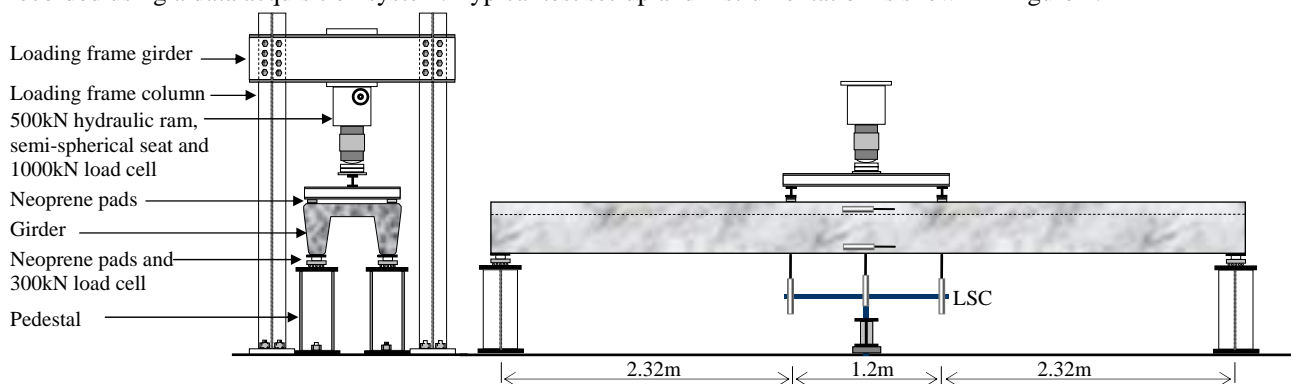


Figure 2: Test set-up and instrumentation of the G-type reinforced concrete girders

2.6 Test Results and Discussion

Beam C1 was loaded until a load of 287 kN which is 63% of the predicted load of 452 kN determined according to the provided information on the girders (Figure 1). Decision was made to test another control beam (C2) and the failure load recorded was 309 kN which is 68% of the predicted load. Testing of the second control beam confirmed the results of the first beam. However, to prove the accuracy of the given specifications and drawings for the theoretical predictions, the concrete cover was hammered off from part of the two webs to expose the reinforcing steel and it was discovered that only three steel bars in two layers were used in each web instead of four bars as shown on the drawings. Thus, these girders were cast with 25% less flexural reinforcing steel. This proved why the control beams yielded significantly lower flexural strength than calculated. The prediction of the ultimate load was recalculated based on the results of the materials (concrete and steel) tests and the accurate locations and number for the reinforcing steel bars and found to be 367 kN indicating 22% and 16% difference for beams C1 and C2, respectively. The load versus midspan deflection curves comparing the flexural behaviour of the beams are presented in Figure 3. The load-deflection behaviour is bilinear until failure. All beams exhibited similar behaviour with regard to cracking and their load-deflection followed almost similar paths until failure. Figure 4 shows the load versus strain in the CFRP and SRP reinforcements at midspan. None of the beams failed by rupture of the strengthening materials; as can be seen in Figure 4 at ultimate load the strain in the strengthening materials were less than the ultimate tensile strains. In beam B1, debonding at the interface of the CFRP strips and the epoxy took place at a load of 400 kN starting at the center of the span and as a result the load decreased slightly. This debonding stopped when it reached the nearest transverse anchor. This allowed the load to increase again as the imposed deflection increased and the FRP was “tightened”. Suddenly the anchor would separate allowing debonding up to the next anchor. Afterwards the load would repeatedly slowly increase until the next anchor separated. Finally the CFRP reinforcement tore away from the last anchor and debonded from the beam completely at a load of 417 kN. Similar behaviour was observed in beams B2, B3, and B4, debonding occurred at a load of 380 kN, 407 kN, and 428 kN; respectively, then the CFRP and SRP reinforcement tore away from the anchor at a load of 407 kN, 415 kN, and 435 kN, respectively in beams B2, B3, and B4. The debonding behaviour is illustrated by the jogs in the curves just before failure. The failure of the CFRP strengthened beams with CFRP sheet anchors was dramatic, as it literally tore the anchors off the corner of the web and the CFRP strips, plates, and sheets fell to the ground. The increase in the yield load was about 25% in all beams. After yielding, the strengthened beams continued to resist further increase in the applied load with a more gradual linear slope than the pre-yield portion of the curve. The increase in the load continued until failure. The ultimate strength increased by 35%, 32%, 34% and 42% in B1, B2, B3, and B4, respectively. However, the SRP sheets are more effective at increasing the strength and ductility.

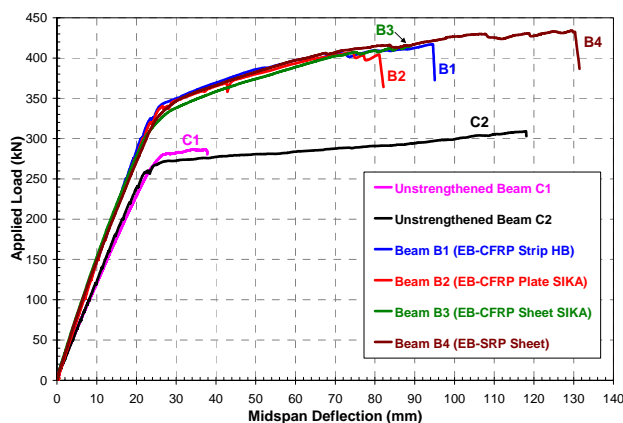


Figure 3: Load-midspan deflection curves for all beams

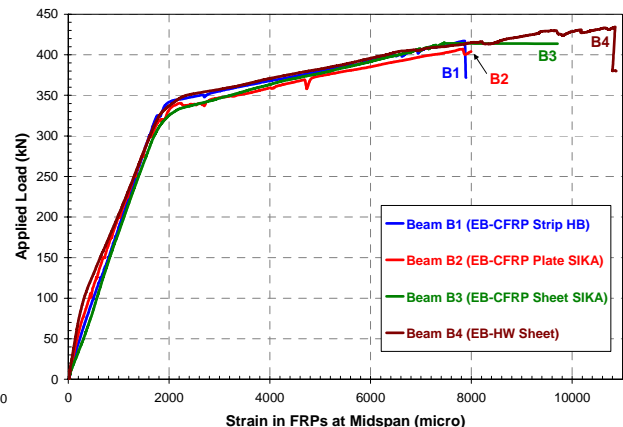


Figure 4: Load-FRP strain curves for all beams

3. CONCLUSIONS

Based on the results of this experimental study the following conclusions can be made:

- The ultimate strength gains achieved by the externally bonded reinforcements exceeded the initial goal of 30%.
- An increase in the yield load and ultimate load of 25% and up to 42%, respectively was achieved.
- All strengthened beams failed in a ductile manner accompanied by large deformation; however the beam strengthened with SRP sheets showed mores ductile behaviour and higher capacity than the other beams.

To summarize, this study has confirmed the structural benefits and feasibility of using externally bonded CFRP and SRP reinforcement to strengthen deficient reinforced concrete girders. However, the CFRP is particularly attractive since it is not susceptible to corrosion, and extremely lightweight making it easy to work with.

STRENGTHENING OF RC BEAMS WITH PRESTRESSED NEAR SURFACE MOUNTED CFRP RODS

Moataz Badawi

(PhD Candidate, University of Waterloo, Waterloo, Ontario, Canada)

Khaled Soudki

(Professor, CRC, University of Waterloo, Waterloo, Ontario, Canada)

ABSTRACT

The use of existing bridge structures are changing with time. The applied loads on these bridges have become larger and more frequent in the last decades as the population and their use have increased. Therefore, strengthening of such structures becomes a necessity. This paper presents experimental results of testing four reinforced concrete (RC) beams under monotonic loads. One beam is kept as a control beam representing the existing structure. The second beam is strengthened with near surface mounted (NSM) carbon fiber reinforced polymer (CFRP) rod. The other two beams are strengthened with NSM prestressed CFRP rod. Two different levels of prestressing are investigated. The test results show that using NSM CFRP rod without prestressing enhanced the flexural capacity (stiffness, yield and ultimate loads) compared to that of the control beam. Prestressing of NSM rods demonstrates a higher efficiency of using those expensive materials by achieving the ultimate capacity of the rod at failure. Beams strengthened with prestressed NSM CFRP rod have enhanced the flexural performance in terms of flexural stiffness, yield and ultimate loads with respect to both, the control beam and those strengthened with non-prestressed NSM CFRP rods.

KEYWORDS

NSM, CFRP, RC Beams, Prestressed

1. INTRODUCTION

The current service loads of the existing infrastructures such as bridges might be higher than the design loads at the time when they were constructed. This may be due to a population growth which leads to increased demands and volumes of traffic on these bridges. Design and construction errors could also be another cause of reduction in the capacity of these structures to carry the service loads. Thus, strengthening of bridge infrastructure is needed. Fiber reinforced polymer (FRP) has attracted structural engineers' concerns as a strengthening materials. The main advantage of using such materials, especially in cold climate countries is that they are not corrosive. In addition, they are very light materials compared to reinforcing steel (high strength to weight ratio). The FRP's have been extensively used and studied as externally bonded on the soffit of RC beams for flexural strengthening (Hassan and Rizkalla, 2002; Aidoo et al., 2004). Lately, an old technique has been re-adopted in the strengthening of RC structures using FRP materials, which is referred to as near surface mounted (NSM) reinforcement (Asplund, 1949). Several investigations have been carried out to study the effectiveness of NSM FRP (Blaschko and Zilch, 1999; De Lorenzis et al., 2004, Yost et al., 2004). These studies have shown comparatively a similar enhancement in the flexural response to those of the externally bonded FRP. To achieve a better use of FRP, prestressing and bonding the CFRP rod in a pre-cut groove in the RC beams is proposed and presented in this study. Only one study was reported in the literature using prestressed CFRP NSM strips as NSM conducted in Sweden (Nordin et al., 2001). It was found that prestressing increased the yield load with the ultimate load same as non-prestressed strengthened beam. This study presents a new North American experience of using *round* CFRP rods as prestressing materials for strengthening RC structures.

2. EXPERIMENTAL PROGRAM

Four large-scale reinforced concrete (RC) beams were designed and constructed. The beams had a cross section of 152×254mm and a total length of 3500mm. The compressive strength of concrete was 47MPa. The beams were reinforced with 2-No. 15M and 2-No. 10M for tension and compression reinforcement, respectively. Shear reinforcement was provided by 8 mm smooth stirrups spaced at 75 mm from center to center to ensure a flexural mode of failure. The specified yield strength of steel reinforcement was 400MPa. The geometry and reinforcement details of the RC beams are shown in Fig. 1. As given in Table 1, one beam was kept without strengthening as a reference beam, while the other three beams were strengthened with NSM CFRP with three levels of prestressing, namely, 0% (non-prestressed), 40%, and 50% of the tensile strength of the CFRP rods. The mechanical properties of the CFRP rod used were: a tensile strength of 1970MPa, a modulus of elasticity of 135.9GPa, and an ultimate strain of 1.45%. The CFRP rod that was used for strengthening was Aslan™ by Hughes Inc. It had a diameter of 9.4 mm and was placed in a near surface mounted groove having dimensions of 15 mm wide and 25 mm deep.

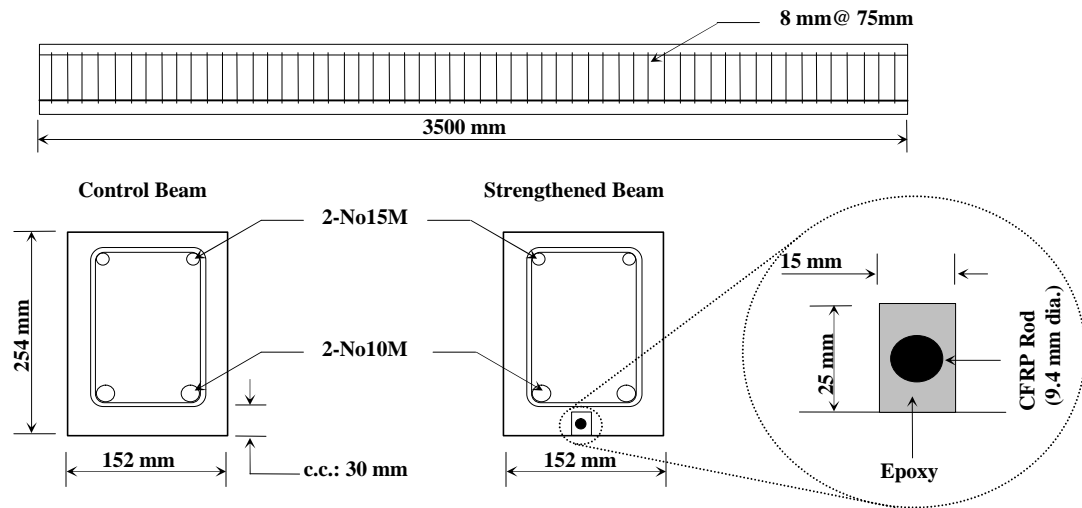


Figure 1: RC beam schematic

Table 1: Test matrix

Designation	Description	Prestressing Level (%)	Prestressing Force (kN)	Initial Strain ($\mu\epsilon$)
C	Control	-	-	-
PS-0	0% prestressed strengthened	0	0	0
PS-40	40% prestressed strengthened	40	55	5721
PS-50	50% prestressed strengthened	50	69	6933

The prestressed CFRP rods were tensioned using a clamp anchor developed at the University of Waterloo (Al-Mayah, 2004) and a prestressing set-up was designed for that purpose. After achieving the desired force in the CFRP rod, the NSM groove was completely filled with epoxy (Sikdur 30, creep resistant). To ensure a full filling of the epoxy in the groove, it was repeatedly added and pressed into the groove. After 7 days of curing, the prestressing force was released and transferred to the beam by means of bond.

The beams were instrumented with several strain gauges on concrete, reinforcing steel (compression and tension) and CFRP rod at the mid-span section. All the beams were monotonically loaded to failure under a four point-bending fixture with a clear and shear span of 3300 mm and 1100 mm, respectively, at a 1.5mm/min rate of loading. Figure 2 shows schematic drawing and photograph of the test set-up. Three linear variable differential transducers (LVDT's) were placed along the beam to measure the vertical deflections at a mid-span, a point load, and at a mid-shear-span section during testing.

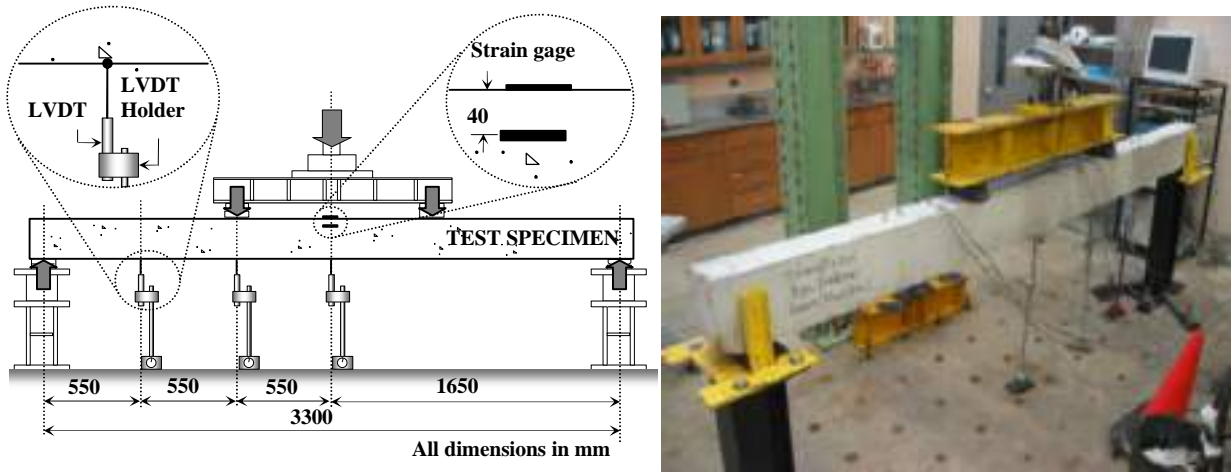


Figure 2: Test set-up

3. TEST RESULTS AND DISCUSSION

For the strengthened RC beams, the initial strain measurements at mid-span section in the CFRP rod were $0 \mu\epsilon$, $5721 \mu\epsilon$, and $6933 \mu\epsilon$ for 0%, 40% and 50% prestressed strengthened beams, respectively. Two modes of failure were obtained. A yielding in the tension reinforcement followed by a crushing in concrete was obtained for the control and non-prestressed strengthened beams (0% of prestressing). Beams strengthened with prestressed CFRP rods failed by a rupture in the CFRP rods after yielding of tension reinforcement steel. Figure 3 shows the plots of the load versus central vertical deflection for all tested beams illustrating the three stages of the behaviour of typical under-reinforced concrete beams (pre-cracking, pre-yielding and post-yielding stage). Table 2 gives the cracking, yield, ultimate loads of all strengthened beams with their percentages of the achieved increases in a comparison to those of the control beam. Strengthening RC beams with NSM CFRP rod was not only able to improve the flexural capacity of the strengthened beams in terms of cracking, yield, and ultimate loads but also was able to significantly increase the flexural stiffness with respect to those of the control beam. It is worthy noting that as the prestressing level of the CFRP rod increased, the flexural response of the strengthened RC beams was considerably improved.

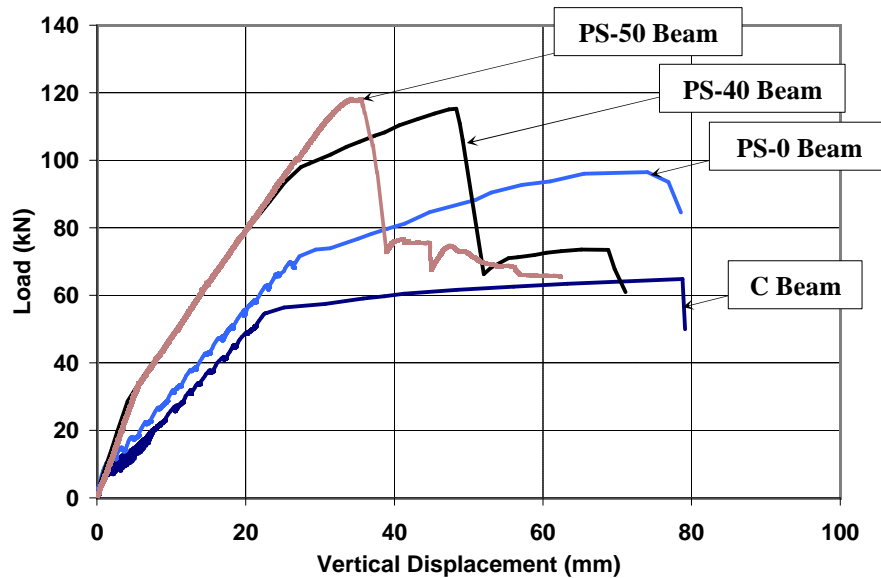


Figure 3: Load- deflection relationship

Table 2: Test results

Beam	Cracking load		Yield load		Ultimate load	
	Load (kN)	Increase (%)	Load (kN)	Increase (%)	Load (kN)	Increase (%)
Control	6.5	0	55	0	65	0
0% prestressed strengthened	10	54	71	29	95	46
40% prestressed strengthened	28.7	341	98	78	115	77
50% prestressed strengthened	33.1	409	116.6	112	118	81

4. CONCLUSION

A successful new experience in strengthening structures by using prestressed CFRP NSM rod to upgrade the flexural performance of RC beams is presented and investigated. Using NSM CFRP rod increased the flexural stiffness and capacity of all strengthened beams. Prestressing the CFRP rod before bonding in the NSM groove further enhanced the flexural performance. It also provided a better utilization of the mechanical properties of such material. By obtaining such results and performing further investigations, this method of strengthening might be considered to be useful in the field application.

5. ACKNOWLEDGEMENTS

The authors greatly acknowledge the technicians at University of Waterloo in particular Mr. Ken Bowman for his help and support through all stages of this study. Sika Canada is greatly appreciated for the material donations.

6. REFERENCES

- Aidoo, J; Harries, K.A.; and Pertou, M. F., "Behaviour of Reinforced Concrete Bridge Retrofit with CFRP and subjected to Monotonic and Fatigue Loading," *Proceedings of the 4th International Conference on Advanced Composite Materials in Bridges and Structures*, Calgary, Ontario, Canada, 2004
- Al-Mayah, A., "Interfacial Behaviour of CFRP-Metal Couples for wedge Anchor Systems," PhD Thesis, University of Waterloo, Waterloo, Ontario, Canada, 2004
- Asplund, S. O., "Strengthening Bridge Slabs with Grouted Reinforcement," *American Concrete Institute, Structural Journal*, 1949, pp. 397-406
- Balschko, M.; and Zilch, K., "Rehabilitation of Concrete Structures with Strips Glued into Slits," *Proceedings of the 12th International Conference on Composite Materials, Organization of the International Conference on Composite Materials*, Paris, France, 1999
- De Lorenzis L.; Nanni, A.; and LA Tegola, A., "Flexural and Shear Strengthening of Reinforced Concrete Structures with Near Surface Mounted FRP Rods," *Proceedings of the 3rd Advanced Composites Materials in Bridges and Structures*, Calgary, Ontario, Canada, 2004, August, 2000, pp. 521-528
- Hassan, T., and Rizkalla, S., "Flexural Strengthening of Prestressed Bridge Slabs with FRP Systems," *Prestressed Concrete Institute Journal*, 47, 2002, pp. 76-93
- Nordin, H.; Taljsten, B. and Collin, A., "Concrete Beams Strengthened with Prestressed Near Surface Mounted Reinforcement," *Proceedings of the International Conference on FRP Composites in Civil Engineering, Research Centre for Advanced Technology in Structural Engineering, Dept. of Civil Engineering and Structural Engineering, The Hong Kong Polytechnic University*, Hong Kong, 2001, pp. 1067-1075
- Yost, J. R.; Gross, S.P.; and Dinehart, D. W.; "Near Surface Mounted CFRP Reinforcement for Structural Retrofit of Concrete Flexural Members," *Proceedings of the 4th International Conference on Advanced Composites Materials in Bridges and Structures*, Calgary, Ontario, Canada, 2004.

STRENGTHENING OF STEEL BRIDGES UNDER LOW FREQUENCY VIBRATIONS

Lei Zhang

Post Doctoral Research Fellow, The Hong Kong Polytechnic University, Hong Kong China

L C Hollaway,

Professor of Composite Structures, University of Surrey, Guildford, Surrey, UK

J G Teng,

Chair Professor of Structural Engineering, The Hong Kong Polytechnic University, Hong Kong, China.

S.S. Zhang

Research Assistant, The Hong Kong Polytechnic University, Hong Kong, China.

ABSTRACT

A potential technique utilizing advanced polymer composites to rehabilitate a steel railway bridge open to traffic during the adhesive curing period is presented. The advanced polymer composites used for the upgrading system are manufactured from a factory-made hot melt pre-impregnated high modulus and ultra high modulus carbon fibres; the polymer system is an epoxy. The composite is bonded to the steel structural member with a compatible film adhesive; the two components are then fabricated in one operation onto the structure. The compaction is performed under a vacuum assisted pressure of 1 bar and two cure temperatures are used, one at 65⁰C for 16 hours and the other at 80⁰C for 4 hours; the length and time of cure are dependent parameters. The FRP structural and material characteristics and the beam test results are presented. It is shown that (i) some slight damage to the adhesive from the vibrational forces, during the cure period, did occur but the strain to failure of the high modulus CFRP composite took place well into the non-linear region of the steel beam and (ii) the high modulus carbon fibre composite supported 10% greater load than the ultra high modulus carbon fiber composite as a result of the low strain to failure of the latter carbon fibre. It is noticed, however, that half the thickness of the ultra high modulus CFRP composite is used compared with the high modulus CFRP. This allows the yielding of the steel beam to occur at a similar load value for the two upgrades and prevents a severe brittle failure of the composite beam.

KEYWORDS

Composites, carbon fibres, film adhesive, hot melt pre-impregnated composites.

1. INTRODUCTION

Many of the bridges world-wide are made of steel and a large percentage of these bridges are considered substandard and require upgrading or improvement from a strengthening/stiffening point of view. The main causes for the deterioration in steel bridges are a lack of proper maintenance, corrosion attack and fatigue sensitive details, (Tavakkolizadeh and Saadatmanesh 2003). In addition, many of the bridges require upgrading to enable them to meet present day traffic requirements. Clearly, a repair or rehabilitation option should be considered before a decision is taken to replace the structure, as the former option, in most cases, costs far less than the latter option and generally takes less time.

There is currently a considerable amount of research and investigative work being undertaken into the use of advanced polymer composites (APC) to upgrade and rehabilitate metallic structures, particularly steel bridges. (Luke 2001, Cadei *et al.* 2004). The excellent mechanical, fatigue and in-service properties of carbon fiber reinforced polymers (CFRPs) make them ideal candidates for the strengthening and rehabilitation of steel bridges.

A major problem which must be addressed when upgrading a steel railway bridge continuously traversed by trains, thus setting up vibrations in the structure during the polymerization process, is to know which type of adhesive should be used and its curing period. There are two techniques generally utilized in practice to rehabilitate

a structural steel member; these are (a) the wet lay-up method where the polymer of the matrix also acts as the adhesive polymer, and (b) the rigid plate method in conjunction with the two part adhesive joint system. The first procedure would generally be used on a curved member when it is not possible to use the rigid plate method. The second procedure is to manufacture, by the pultrusion or prepreg method, a rigid plate which is bonded to the straight beam by a two part adhesive polymer. The adhesives used in the two techniques are cold cure epoxies which polymerize at ambient temperature (i.e. the temperature of the environment at the time of upgrading the structure). Depending upon the site temperature, the adhesive will take 7 to 10 days to reach 90% polymerization. If a steel bridge structure on which these systems are used is under a vibration loading, the movement of the bridge, as a consequence of the passage of trains over the bridge, will impair the polymerization mechanism. Therefore, in this case, the cold cure adhesives are not desirable for the rehabilitation of steel railway bridges under vibrations.

The objective of this paper is to investigate the effectiveness of bonding a high modulus (H-M) CFRP prepreg to strengthen a structural steel system which, during polymerization, is under a continuous low frequency vibration. The strengthening characteristics of an ultra-high modulus (UH-M) CFRP prepreg is also compared with those of the H-M CFRP prepreg.

2 THE PRE-IMPREGNATION MANUFACTURING TECHNIQUE

Advanced Composite Group (ACG) Derbyshire UK has developed a pre-impregnation (prepreg) technique specifically for the civil engineering industry. The advanced polymer composite used for the prepreg is manufactured from a factory-made hot melt epoxy polymer system; the technique involves the prepreg composite and a compatible film adhesive. The construction site receives the prepreg and film adhesive both of which are stored at -20°C from the time of manufacture until use. Before cutting the two components to size, the materials are thawed for one hour. The adhesive film and the composite prepreg are then fabricated on to the beam by laminating the prepreg layers, as per design, with the adhesive film located correctly. A halar film and breather blanket cover the FRP composite on the beam and the whole composite system is surrounded in a vacuum sheet properly sealed at its extremities. A vacuum assisted pressure of 1 bar is applied and a heater blanket covers the whole composite. The prepreg cure temperature is 65°C for 16 hours, or it can be raised to 80°C applied for 4 hours. At the conclusion of the cure period the temperature is reduced to the environmental condition. The technique has been used in practice to encapsulate a curved steel section which had degraded badly, (Garden and Shahidi, 2002).

3 THE CURE PROCEDURE FOR THE PREPREG COMPOSITE

The site cure procedure of the prepreg and adhesive film has major advantages to offer compared to the pre-cast plate and two part adhesive system for the rehabilitation of structural systems in the civil engineering industry. The advantages are:

- (i) A much better control of the site fabrication and compaction operation. This will enable the adhesive thickness to be controlled to within high tolerances.
- (ii) The vacuum assisted pressure of 1 bar reduces any voids in the composite to a minimum.
- (iii) The elimination of any variation in cure temperature due to site conditions.
- (iv) The site cure at an elevated temperature enables a control to be made of the value of the glass transition temperature (T_g). The higher the cure temperature, the higher the T_g value will reach, but there is a limit irrespective of the temperature value of cure. This limiting value will vary from polymer to polymer.

As the cure is undertaken at an elevated temperature under controlled conditions on site the polymerization of the adhesive (and composite) will be completed much more quickly than the cold cure two part adhesive, which is dependent upon the environmental conditions. Furthermore, the cold cure adhesive used currently in construction will take 5 to 7 days, depending upon site temperature, to reach 90% polymerization. After this time, if the system is not post cured, polymerization will continue but over a very long time and will probably never reach 100%. The advantages that the site cure prepreg and film adhesive have over the other site bonding techniques have been demonstrated in (Photiou *et al* 2006) and can be exploited further when a structure is under vibrations whilst it is being rehabilitated.

4 THE REHABILITATION TECHNIQUE OF THE TWO STAGE CURE PROCEDURE.

The rehabilitation of structural members of a steel railway bridge is taken as an example of utilizing the factory-made hot melt pre-impregnated CFRP composite and compatible film adhesive. The following two scenarios are considered in the design of the laboratory tests presented in this paper:

- (i) The bridge is closed to rail traffic for 4 hours in a 24 hour period (ideally during the night shut-down period) whilst upgrading is in progress.
- (ii) The bridge is open to continuous rail traffic and is exposed to vibrations throughout.

5 THE COMPOSITE MATERIALS

Laboratory tests are conducted to evaluate the effectiveness of the rehabilitation technique based on the hot melt pre-impregnated site cure procedure. The main upgrading material system used is made from unidirectional high modulus CFRP prepregs, comprising of two double-ply laminates with ply thickness of 0.6 mm, the carbon fibers aligned with the longitudinal direction of the beam. Three single plies of GFRP are used with glass fibers positioned at $\pm 45^{\circ}$ to the longitudinal direction of the steel beam. The various layers are stacked as follows: firstly a single GFRP ply followed by one double-ply CFRP, followed by a single GFRP ply, followed by the other double-ply CFRP and finally another single GFRP ply. The first GFRP ply is adjacent to the adhesive film and hence separates the steel from the carbon fibers. The ultra high modulus CFRP composite is fabricated in the same way. The plate plan size of the prepregs are 60 x 1600 mm. The thickness of the adhesive film is about 110-120 μ m, and like the matrix material of the prepreg is made from a low temperature cure epoxy resin system. The specifications of the materials used are:

The high modulus CFRP - VTM264FRB/PANEX35-50K-600-35%RW (Uni-directionally aligned)

The $\pm 45^{\circ}$ biaxial GFRP - VTM264FRB/EBX602-32%RW

Adhesive film - VTA260/PK13-313g- (compatible film adhesive with the composite matrix VTM264FRB)

The ultra high modulus CFRP - VTM264FRB/K63712-600-35% RW (Uni-directionally aligned)

The mechanical properties of the composite materials and adhesive film are given in Table 1.

Table 1: Mechanical properties of FRP materials and adhesive film

Material	Tensile Strength MPa	Elastic Modulus GPa	Ultimate Strain (%)	Poisson's Ratio
UH-M CFRP (Unidirectional)	1120	270	0.4	0.32
HM-CFRP (Unidirectional)	2110	135	1.6	0.28
GFRP ($\pm 45^{\circ}$ to line of action of load)	215	16	1.7	0.15
Film Adhesive	32	3.7	0.9	0.37

6 THE UPGRADED BEAM PREPARATION

The beams are cut to a length of 2000 mm and a flat plate of dimensions 56 x 2000 mm is welded on to each of the compression flanges; this represents beams that had been degraded on the tension flange. The exposed tension flange of the beam is grit blasted to the Swedish Code SA 2^{1/2} Grade. Immediately before applying the adhesive film, the surface of the steel is solvent degreased using acetone to remove any contaminant materials.

The cure at 80°C for 4 hours The adhesive film and hot-melt prepreg laminates are laid on the two beams followed by the halar film, the breather blanket and the vacuum sheet and a vacuum assisted pressure of 1 bar is applied to both beams. The heating blanket temperature cure is raised to approximately 80°C. These beams represent the case of a bridge which is closed to traffic for 4 hours in a 24 hour period. After curing is completed the temperature of the heating blanket and the specimens are reduced to room temperature at a steady rate. The upgraded beams are then fully cured at that cure temperature and ready for testing. Steady static loads are applied up to the failure of the beams and comparisons are made with the control beam.

The cure at 65°C for 16 hours Two beams are prepared for the scenario of a bridge that is continuously traversed by rail traffic. The beams are prepared in the same way as that described for the first beam above. However, for these cases a heating cycle of approximately 65°C for 16 hours was used during which the beam specimens are exposed to loads varying between an upper and a lower limit throughout the 16 hours. Different load limits are employed in the

two tests, (i.e. 5 kN-40 kN and 5 kN-60 kN) under a frequency of 1 Hz. The beams, when cured, are statically tested to failure.

7 TEST LOADING TO FAILURE

Each beam is placed in the test rig on a clear span of 1700 mm. The two external loads are positioned at 200 mm on either side of the mid-span of the beam. Strain gauges are positioned at strategic positions on both sides of the beam at mid-span and down its sides. The test set-up and the cross section of the beam are shown in Figures 1a and 1b respectively. Displacement transducers are placed at mid span and a number of other locations. Two load cycles up to 20 kN and 40 kN are applied to the beam before taking it to failure under a steadily increasing displacement of 0.05 mm/s. Figure 2 shows the total load against central deflection for the H-M CFRP rehabilitated beams cured at 80°C and 65°C, the UH-M CFRP rehabilitated beam cured at 80°C and the control beam. Figures 3 and 4 illustrate the strain distributions in the pure bending region of beams rehabilitated with CFRP prepreg cured at 80°C and 65°C respectively.

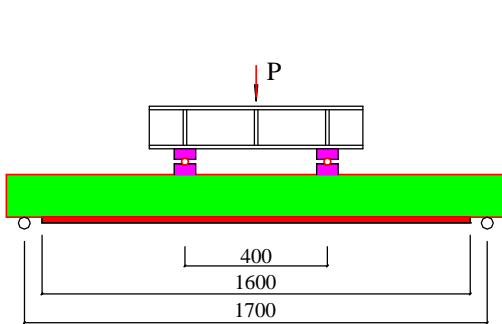


Figure 1a Loading arrangement

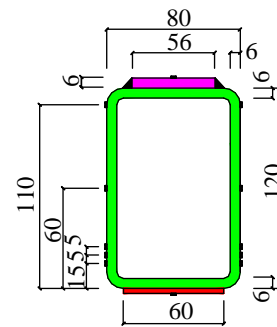


Figure 1b Cross section of steel beam

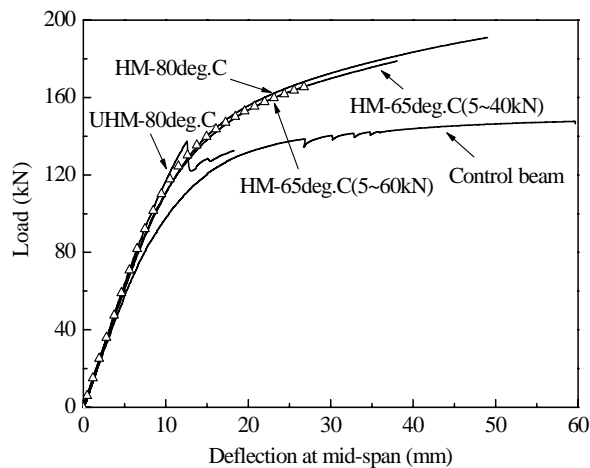


Figure 2 Total load~central deflection

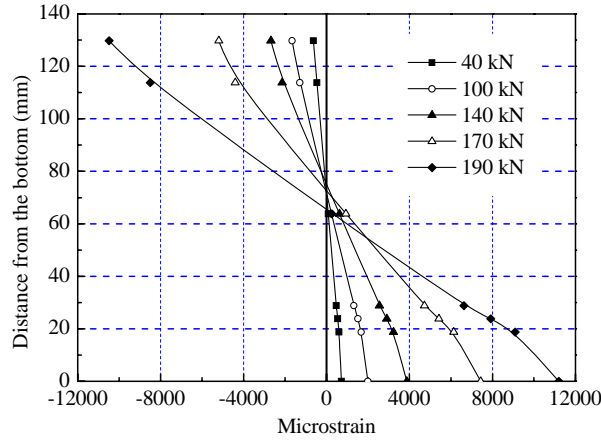


Figure 3 Strain Distributions for beam with HM- CFRP composite cure at 80deg.C

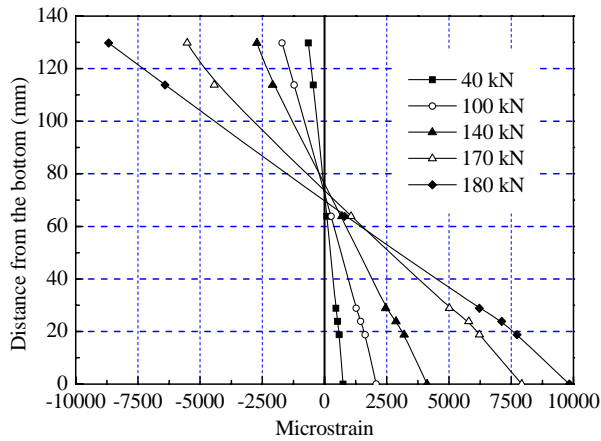


Figure 4 Distribution of strains for beam HM- CFRP composite cured at 65deg.C(5~40kN)

From Figure 2 the three upgraded beams have almost identical characteristics, with non-linear response from about 80 kN (the yield load) and this corresponds to the steel exhibiting softening response in the soffit of the beam. The load continues to increase in all four cases up to 138 kN, 160 kN, 178 kN and 190 kN for UH-M (80⁰C), H-M 65⁰C (N 5-60), H-M 65⁰C (N5-40) and H-M 80⁰C, respectively. The load deflection paths for the three beams with H-M CFRP prepreg upgrades follow a similar pattern irrespective of their cure temperature, but the beam with UH-M CFRP has a slightly stiffer characteristic compared to that of the beams with H-M CFRP upgrade. This indicates that the UH-M CFRP composite with a greater stiffness than that of the steel is stiffening the composite beam (i.e. the strengthened beams) in the elastic region of the original steel beam. The strain distributions in Figures 3 and 4 show shifts in the neutral axis, furthermore, it can be seen that the CFRP composite reached a large strain at failure. The composite on the upgraded beam in Figure 4 (when the FRP composite and adhesive film are cured at 65⁰C under vibration) failed at 10000 μ -strains and about 8500 μ -strains, under vibrations of 5-40 kN and of 5-60 kN respectively. These values are lower than the ultimate failure strain (about 12000 μ -strains) of the composite beam cured at 80⁰C and tested statically. This lower failure strain is believed to have been due to the detrimental effects of vibrations on the adhesive during the cure period.

The strain at failure (0.3%) of the UH-M CFRP composite cured at 80⁰C is a lower strain value than the axial tensile failure strain of the composite (0.4%); this result is consistent with other tests, (Photiou, *et al* 2006),

undertaken on upgraded UH-M CFRP steel beams. After failure of the UH-M CFRP composite the beam continues along the non-load-displacement path of the non-linear path of the control steel beam. However, the early brittle failure of these materials, albeit within the early period of the non-linear path of the steel beam, is not appropriate for the construction industry. The H-M CFRP beams again failed by strain rupture of the CFRP but these beams failed well into the non-linear region of the steel beams and at failure forced the steel beam into large deformations.

8 OBSERVATIONS

This paper has presented experimental results aimed at establishing the possibility of rehabilitating steel bridge beams, whilst under vibration forces, with bonded hot-melt pre-impregnated high and ultra high modulus carbon fiber composites. The composites are cured on site under a vacuum assisted pressure and at elevated temperature. It should be emphasized that one layer of GFRP prepreg is placed between the CFRP prepreg and the steel member; this facilitates a more uniform transfer of stress between the two materials. Preliminary conclusions are that:

- (i) Provided that the bridge can be closed for 4 hours in a 24 hour period, and that the adhesive film and prepreg composite can be cured on site at 80°C, the bonded system, comprising of one layer of film adhesive and the H-M composite, is the most efficient. The load sustained by the test beam with the adhesive film and prepreg composite cured on site at 80°C for four hours is 190 kN.
- (ii) The beam strengthened with the adhesive film and the H-M composite system cured at a temperature of 65°C for 16 hours under vibrations induced by loads of 5kN-40 kN at 1 Hz. is able to sustain a total load 181 kN.
- (iii) With the same manufacturing procedure as in item (ii) but with the upper value of the applied vibration load increased to 60 kN, the failure load of the strengthened beam decreases by 11% of that in item (ii).
- (iv) Due to the low strain to failure of the UH-M CFRP, the failure load of the strengthened beam is 138 kN and is the lowest of the four samples tested. However, it should be noticed that in this case, the thickness of UH-M CFRP prepreg is only half of that used for the H-M CFRP prepreg.
- (v) For the rehabilitation system, a most satisfactory upgrade can be achieved for steel members using the H-M CFRP prepreg and adhesive film.

9 REFERENCES

- Tavakkolizadeh, M. and Saadatmanesh, H. (2003). 'Strengthening of Steel-concrete Composite Girders Using Carbon Fiber reinforced Polymers Sheets'. *Journal of Structural Engineering, ASCE Vol129 No.1* , pp186-196.
- Luke, S. (2001), The use of carbon fibre plates for the strengthening of two metallic bridges of an historic nature in the UK. *Proc. CICE 2001 FRP Composites in Civil Engineering*, Ed. J-G Teng, Pub. Elsevier, London, pp 975-983.
- Cadei, J.M., Stratford, T.K., Hollaway, L.C., and Duckett, W.G., (2004), CIRIA Report C595 'Strengthening Metallic Structures Using Externally Bonded Fibre-Reinforced Polymers', London.
- Garden, H. and Shahidi, E., (2002). 'The Use of Advanced Composite Laminates As Structural Reinforcement In A Historic Building', In: *Advanced Polymer Composites For Structural Applications in Construction*, R A Sheno, S S J Moy, L C Hollaway. (Eds), Thomas Telford Publishing, 2002, pp.457-465.
- Photiou, N.K., Hollaway, L.C. and Chryssanthopoulos, M.K. (2006) 'Selection of CFRP systems for steelwork upgrading'. *Journal of Materials in Civil Engineering, ASCE*, In press.
- Photiou, N.K., Hollaway, L.C. and Chryssanthopoulos, M.K. (2006) 'Strengthening of an artificially degraded steel beam utilizing a carbon/glass CFRP plate' *Concrection and Building Materials Vol. 20 No.1, Feb/March 2006*, pp11-21

ACKNOWLEDGEMENTS

The authors gratefully acknowledge the financial support provided through a Kan Tong Po Visiting professorship jointly funded by a Kan Tong Po grant, the Royal Society and The Hong Kong Polytechnic University and through grants from The Hong Kong Polytechnic University (Project codes: BBZH and G-YX47. (Project codes: BBZH and G-YX47).

The authors also gratefully acknowledge the support received from Mr. E. Shahidi and the staff of Advanced Composite Group Ltd., Heanor, Derbyshire, UK, especially for the helpful discussions throughout these investigations.

STRUCTURAL STRENGTHENING WITH EXTERNALLY BONDED SCRP (STEEL CORD REINFORCED POLYMER)

Wine Figeys, Luc Schueremans, Dionys Van Gemert
*(PhD student, Prof. Dr., Prof. Dr., Civil Engineering Department, Katholieke Universiteit Leuven
Kasteelpark Arenberg40, B-3001 Heverlee, Belgium)*

Kris Brosens
(project engineer, Triconsult NV, Industriepark 1241/Bus 4, B-3545 Halen, Belgium)

ABSTRACT

One of the strengthening techniques is epoxy bonded external reinforcement. The additional reinforcement often exists of steel plates or carbon fiber reinforced polymer (CFRP). Steel plates have a low material cost but are heavy. On the contrary, CFRP is a lightweight, high strength flexible composite which can be easily applied. Steel plates are used for deformation problems and CFRP when the high strength or the flexibility of the fibers can be exploited. Steel cord reinforced polymer (SCRP) is a new material that consists of thin, uni-directional high-strength steel fibers. This innovative composite is intended to combine the advantages of steel plates and CFRP: the material cost can be relatively low compared to CFRP. Moreover, it can be flexible and SCRCP can be as strong as CFRP. In this paper, the search for a prototype of SCRCP is presented. Different types of SCRCP are investigated to develop an optimal type of SCRCP for the application as externally bonded shear reinforcement. The feasibility requirements, material lay-out, test set up and results and the resulting SCRCP choice are outlined.

KEYWORDS

Steel cord reinforced polymer (SCRCP), prototype, strengthening

1. INTRODUCTION

The use of externally bonded reinforcement is a common strengthening technique for civil engineering constructions nowadays. By adding additional reinforcement, it is possible to increase the capacity in bending or in shear and to enhance flexural stiffness (Brosens, 2001). Today, mostly steel plates and CFRP (carbon fibre reinforced polymer) sheets and laminates are applied as external reinforcement (Teng, 2001). Steel plates have a high stiffness and a low material cost compared to CFRP. On the other hand, CFRP is more flexible and easily applicable, unlike steel plates. CFRP is about 5 times stronger than standard steel. Each of these materials has its specific applications. A growing interest concerns the development of steel cord reinforced polymer (SCRCP), a new material that combines the advantages of steel plates and CFRP as external reinforcement (Casadei, P., et al., 2005; Prota, A., et al. 2005). In cooperation with the Belgian company Bekaert, this composite is developed. SCRCP consists of thin high-strength steel fibres. These fibres are bundled in cords and woven into unidirectional sheets. This new composite is intended to be a lower cost alternative for CFRP. The sheets have a high strength as well as a high stiffness. The composite remains quite flexible which makes SCRCP easy to apply (Figeys, 2004). Other requirements are discussed below. These requirements are used as a guideline to develop a prototype of SCRCP.

2. FEASIBILITY

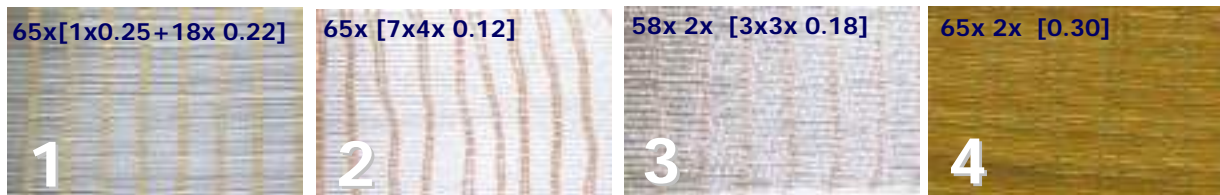
Requirements for SCRCP concern tensile strength and stiffness. Practical experience gives some extra requirements needed for an optimal prototype. The overall requirements are:

- **Evaluation of the material properties**, such as tensile strength and Young's modulus. Knowledge of these properties is necessary for calculation of the required cross-section of the external reinforcement.

- **Flexibility.** SCRP seeks an easy application. SCRP will be delivered on roll of 1m on site. If used as external shear reinforcement, even a higher foldability is necessary to wrap rectangular beams without any preparation and kept in place without special arrangements.
- **Sufficient impregnation.** Glue has to surround all fibers, so that force can be continuously transferred to the concrete. Together with a good impregnation, SCRP needs to stick to the concrete without extra auxiliary actions.
- **Bond strength.** Failure has to take place in the concrete. Concrete should be the weak link in the connection.
- **Rust-proof.** Steel plates need a special protective treatment for corrosion. It is not required for CFRP. All types of SCRP fibers have a protective layer of zinc or brass to protect the fibers from corrosion.
- **Bond behaviour.** The use of SCRP as externally bonded reinforcement requires the design of the anchorage length and the transferable force. Results of this study are presented in (Figeys, W., et. al, 2005).

2.1 Material properties

In a feasibility study, different kind of SCRP are studied, figure 1. The first type of SCRP consists of 65 steel cords. Each cord contains 19 filaments with a diameter of 0.22mm up to 0.25 mm. This type is presented as type 1. The compositions of the other types are mentioned in figure 1. Type 4 consists of single filaments, woven in a sheet with a synthetic textile and is coated with brass.



58x 2x [3x3x 0.18] is a weave with 58 stitches of 2 cords, each cord consist of 3 twists with 3 filaments with a diameter of 0.18mm .

Figure 1: Different prototypes of SCRP



Figure 2: Tensile test on SCRP: Single cord – impregnated SCRP – not-impregnated SCRP

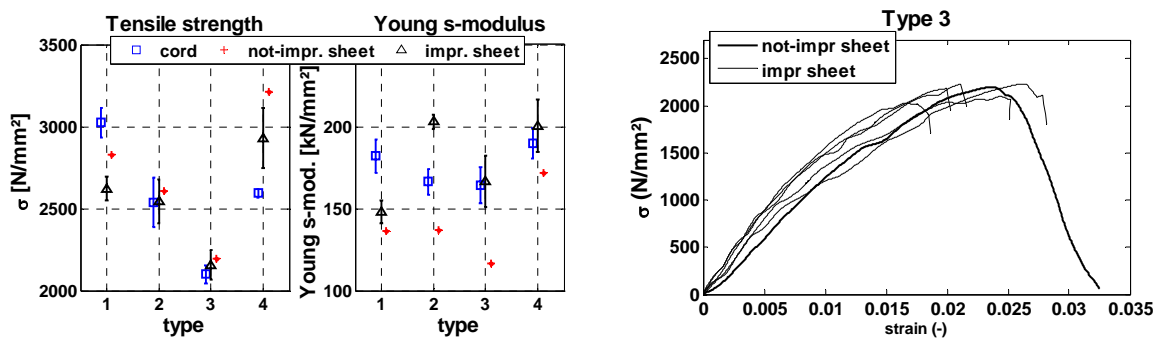


Figure 3: Test results of tensile tests on SCRP
Ultimate tensile stress – Young's modulus – Measured stress-strain behavior

The material properties are tested by means of tensile tests. The individual cords, the laminate itself and an impregnated laminate are tested. The tensile tests are deformation controlled, figure 2. From the test results, the tensile strength and the Young's modulus are calculated. Test results are presented in figure 3. The tensile strength is independent from the test set up. The tensile strength varies between 2000 and 3000 MPa. A correlation can be found between the Young's modulus and the test set-up. For all types of SCRPs, a lower Young's modulus is measured for not-impregnated SCRPs. Possibly, the different cords are not perfectly parallel which causes a different stress level in the cords. By failure, the cords break one after the other. Cords within a pre-impregnated SCRPs are subjected to a more uniformly distributed stress level. When reaching the tensile capacity, all cords break at the same moment. A ductile behavior is found, the high strength steel cords yield before failure. Because of this ductile behavior, lower safety factors can be used in the design.

3.2 Impregnation, flexibility and bond strength

Impregnation with a viscous adhesive, Epicol U of Resiplast, is tested by means of pull-off tests on SCRPs type 1, glued on a concrete surface. All test samples have failed in the concrete, not in the adhesive or in the connection between cylinder and SCRPs or between SCRPs and concrete. But in the laboratory, the work is more accurately done than on the site. Therefore, enhanced impregnation is necessary. Also the flexibility is investigated. Calculations show that type 1 of SCRPs is more than 100 times stiffer than CFRPs. A decrease in stiffness is necessary when SCRPs is used for wrapping. This can be reached if fewer filaments belong to a cord, if smaller diameters are used, or if the filaments are used single. From these conclusions, the other types 2, 3 and 4 of SCRPs are developed, figure 1. Laminates 2 and 3 are much more flexible because of the smaller diameter. Type 4 is composed of single filaments. These new types are much more flexible, but with a loss of steel section. The impregnation is improved compared to type 1. However, the development of a new adhesive is necessary for a sufficient impregnation on site. Another option is the use of pre-impregnated laminates.

3.3 Prototype 5

Prototype 5 is derived from the second type of SCRPs with an increased density. This higher density is reached because of the smaller width of the filament (type 5: 65mm, type 2: 95mm). This prototype is flexible and has an improved impregnation. Four filaments with a diameter of 0.12 mm are twisted together, 7 of these twist are bundled into cords. 65 cords belong to one sheet with a width of 65 mm, figure 4. In the same figure, it is shown that this SCRPs can be delivered on roll with a diameter of only 150 mm.

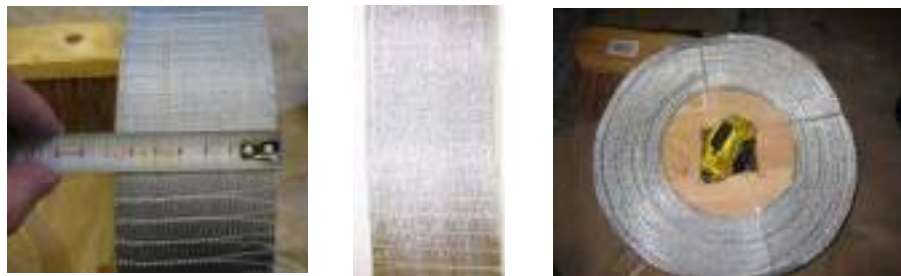


Figure 4: SCRPs type 5 - 65x [7x4x0.12] with increased density

4. CURVATURE

CFRPs is used for wrapping of columns to enhance the compressive strength of the column and as shear strengthening by wrapping of beams. However, preparation of the columns and beams is necessary for these applications. CFRPs can not take shear stresses so that it is only possible to wrap CFRPs to rounded corners. The radius of curvature has to amount at minimum 3 cm. The sharp concrete edges are rounded with epoxy mortar. Steel can take shear stresses so that a smaller radius of curvature is possible. In figure 5, the test set up is presented to measure the influence of the radius of curvature of a cord of type 2. A cord is put around cylinder A with a variable diameter and around cylinder B. The cord is fixed at cylinder C. The tests are deformation controlled for a diameter of cylinder A of 5 – 10 – 15 – 20 – 25 – 30 – 40 – 50 mm and a distance L of 500 mm. Using a larger diameter, the tensile strength equals 2621 N/mm². This value is comparable with the tensile strength obtained in the

test described before, figure 2. Only at a very small diameter ($\varnothing = 5$ mm), the cord fails at a lower force: the maximum tensile strength amounts 2147 N/mm². From the stress-strain diagram, it can be concluded that the cords tested with a smaller diameter do not yield, however with preserving the same Young's modulus. The material fails in a brittle way. Because of the possibility of a small radius of curvature, it is not necessary to round the edges of the concrete when SCRП is used as external reinforcement.

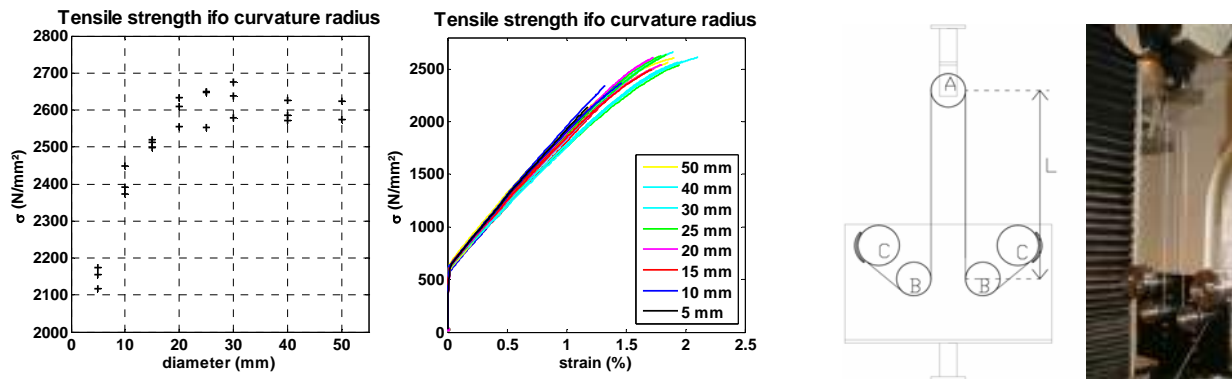


Figure 5: test set up and results of the influence of the radius of curvature on the tensile strength

5. CONCLUSION AND FUTURE RESEARCH

SCRП is a new material that can combine the advantages of steel plates and CFRP. It combines a relatively low material cost with a high strength and a flexible shape. For some applications (wrapping), it is necessary that SCRП has a low flexural stiffness, a sufficient impregnation and bond strength. Four types of SCRП are developed and tested. The sheets have high tensile strength and Young's modulus. A prototype is chosen. It is shown that SCRП is advantageous for wrapping: only a very small radius of curvature influences the tensile strength so that there is no need for preparation by rounding the edges. Further research concerns the durability of SCRП and the influence of SCRП on the anchorage of external reinforcement. The development of a new adhesive is necessary to improve impregnation. Also, pre-impregnated laminates might be an interesting option.

6. ACKNOWLEDGEMENT

The authors would like to thank the Flemish Institute for Promotion of Scientific and Technological Research in the Industry (IWT – Vlaams Instituut voor de Bevordering van Wetenschappelijk-Technologisch Onderzoek in de Industrie) for its financial support and NV Bekaert SA, represented by dr. ir. W. Dekeyser and ir. J. Gallens, for the collaboration and technical support.

7. REFERENCES

- Brosens, K., (2001). *Anchorage of externally bonded steel plates and CFRP laminates for strengthening of concrete elements*, doctoral thesis, Katholieke Universiteit Leuven.
- Figgeys, W. (2004). *Strengthening of reinforced concrete structures with bandweave (in Dutch: Versterking van gewapend beton met bandweefsel)*, Master of Science thesis, Katholieke Universiteit Leuven, 2004.
- Figgeys, W., Brosens K., et al. (2005). Strengthening of Concrete Structures using Steel Wire Reinforced Polymer”, *Proceedings of Fiber-Reinforced Polymer Reinforcement for Concrete Structures*, FRPRCS 7, Kansas City, pg. 743-762.
- Casadei, P., Nanni, A., et al. (2005). “Performance of double-T prestressed concrete beams strengthened with steel reinforced polymer”, *Proceedings of Fiber-Reinforced Polymer Reinforcement for Concrete Structures*, FRPRCS 7, Kansas City, pg. 763-778.
- Prota, A., et al. (2005). Performance of shallow RC beams with externally bonded steel reinforced polymer, in: *Structural Journal*, volume 103, nr. 2, pp. 163-170.
- Teng, J.G.; Chen, J.F.(2001). *FRP strengthened RC structures*, John Wiley & Sons, Weinheim.

WORLDS FIRST BRIDGE WITH SPRAYED FRP STRENGTHENING: REVISITED

N. Banthia

Professor and Distinguished University Scholar, The University of British Columbia, Canada

R. C. Tennyson

Chief Scientific Advisor, Fiber Optic Systems Technology Inc., Toronto, Ontario, Canada

A. Mufti

Professor and President of ISIS, The University of Manitoba, Winnipeg, Manitoba, Canada

ABSTRACT

An entirely new method of repair using Sprayed Fiber Reinforced Polymers (SFRP) has recently been developed at the University of British Columbia. The technique consists of spraying polymer and short, randomly distributed fibers concurrently on the surface of concrete to be repaired using a spray gun. A 2-dimensional random distribution of fibers is obtained on the application surface. In 2001, the technique was successfully applied to Safe Bridge on Vancouver Island for shear strengthening. The bridge was tested in 2001 before and after the application of spray using a fully loaded truck and the effectiveness of the spray was demonstrated. In 2005, the bridge was tested again to assess the durability of the SFRP coating. It was concluded that the SFRP coating has remained intact, and there are no signs of deterioration or debonding.

KEYWORDS

Strengthening, Sprayed Fiber Reinforced Polymers, Bridge, Load Testing.

1. INTRODUCTION

The vast majority of research and applications in the context of FRP strengthening have involved the use of laminates, plates or wraps bonded to the concrete surface (1-2). Recently, an entirely new method of repair using Sprayed Fiber Reinforced Polymer (SFRP) coatings, has been developed at the University of British Columbia (Banthia et al., 1996, 2000, 2002). The technique consists of spraying polymer and short, randomly distributed fibers concurrently on the surface of concrete to be repaired such that a 2-dimensional random distribution of fibers is obtained on the application surface (Figure 1). In the process, the resin and catalyst are fed separately into a spray gun, where they are mixed and then sprayed as a single compound. Two strands of roving are fed into a chopper unit mounted on top of the spray gun, wherein they pass between a pair of rollers and get chopped to a consistent length adjustable from 8 to 48 mm. Further details of the spray process, its optimization, etc. are given elsewhere (Banthia et al., 1996, 2000, 2002).



Figure 1: The Spray Process

2. REHABILITATION AND TESTING OF SAFE BRIDGE IN 2001

In 2001, the technique of sprayed composites was applied to the Safe Bridge on the Vancouver Island that needed shear strengthening (Figure 2). The 7.2 m long single span bridge was built in 1955, and has 11 precast channel beams each 0.35 m wide. The girders were cast from 35 MPa structural lightweight concrete and the average steel strength was of 356 MPa. The 9 m wide bridge includes a sidewalk separated from traffic by a concrete curb (Figure 2b). Like many other bridges in British Columbia and Alberta, the girders of Safe Bridge are considered shear deficient (CAN/CSA2000), and the purpose of applying the Sprayed FRP was to enhance their shear resistance. In order to demonstrate the effectiveness of sprayed composites at enhancing shear resistance, girders from an identical bridge that got replaced in 1999 after 50 years of service were tested in the laboratory (Banthia et al. 2002), Figure 3. Detailed results of the tests on full-scale girders are given in Refs.: (Banthia et al. 2002) and key results are given in Figure 4. Notice in Figure 4 that the Sprayed GFRPs performed superior to the GFRP wraps, and such curves formed the basis for the acceptance of SFRP retrofit technique for the Safe Bridge.



Figure 2a: The Safe Bridge, BC

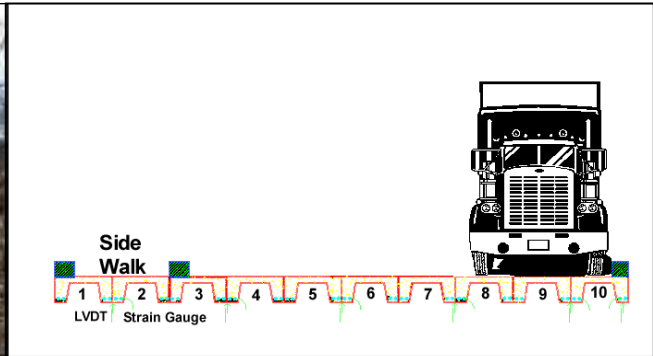


Figure 2b: Section of Safe Bridge



Figure 3: Laboratory Tests on Full-Scale Bridge Girders

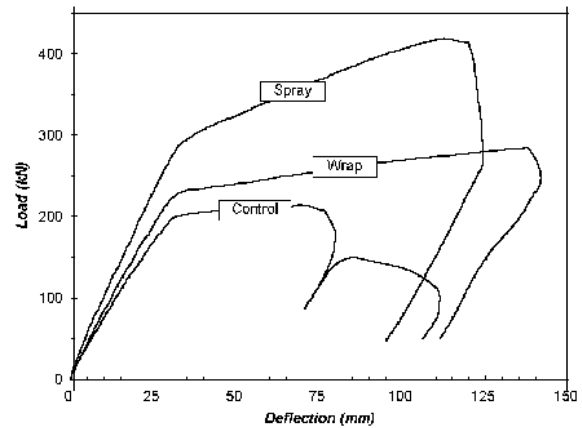


Figure 4: Results of Tests on Full-Scale Bridge Girders (Figure 3) with GFRP

Before the application of the spray, the bridge was instrumented by placing electrical resistance gauges on rebars of all girders. The bridge was then tested for its 'before spray' performance by using a 28 Ton dump truck (Figure 6). A 10 mm thick GFRP spray was then applied using the spray equipment mounted on a truck (Figure 7). After the spray, long gauge fiber optic sensors were installed on the bridge on selected girders (Figure 8), and the bridge was load tested again using the same dump truck (Figure 6). Results of the static and the roll tests performed before and after the placement of the spray are given in Table 1. Only the readings from the electrical resistance strain gauges were acquired. Notice the overall effectiveness of the spray.



Figure 5: Electrical Strain Gauges on the Rebar



Figure 6: Load Test on the Bridge Before and After Spray Application



Figure 7: GFRP Spray Application on the Bridge



Figure 8: Long Gauge Fiber Optic Sensors Installed on the Spray

Table 1: Comparison of Rebar Strains from Girder #6 (2001 Tests)

Property	Before Spraying	After Spraying	Reduction
Max. Rebar Strain (Static Tests)	101.76 x 10 ⁻⁶	65.55 x 10 ⁻⁶	36%
Max. Rebar Strain) (Roll Tests)	72.12 x 10 ⁻⁶	54.94 x 10 ⁻⁶	24%

3. LOAD TESTING OF SAFE BRIDGE IN 2005

In 2005, the Safe Bridge was tested again, but this time only the long gauge fiber optic sensors (FOSs) placed along the lengths of the girders were read. The long-gauge sensors actually measure the average displacement over their gage length L_s . Taking into account temperature effects, the total strain is given by,

$$\varepsilon_s = (\alpha + \beta)\Delta T + \frac{\int_0^{L_s} \varepsilon(z) dz}{L_s} \quad (1)$$

where ε_s = sensor strain, α = thermal coefficient of expansion for structure, β = thermal optic coefficient for fiber sensor ($\sim 8 \times 10^6/^\circ\text{C}$), $\Delta T = T - T_0$, where T = temperature at time of measurement, T_0 = temperature at the time of installation, and z = axial co-ordinate along sensor defined by $0 \leq z \leq L_s$. When monitoring bending strains, it is possible to estimate the maximum bending strain over the gage length from simple beam bending models, as described below.

If $M(z)$ = general bending moment function at location 'z' and if the axial location of maximum bending strain can be defined as ' z_m ', then the value ' z_m ' is calculated for our specific case by the condition:

$$\frac{dM(z)}{dz} = 0, \text{ and } \frac{d^2M(z)}{dz^2} < 0 \quad (2)$$

The relationship between the sensor average bending strain $\epsilon_s(y)$ and the maximum bending strain for the particular sensor location (y) relative to the neutral plane is given by

$$\frac{\epsilon_z(z_m)}{\epsilon_s(y)} = \frac{L_s M(z_m)}{\int_0^{L_s} M(z) dz} \quad (3)$$

Thus for a beam simply supported at its ends and subjected to concentrated load at the center (as in our case), the maximum bending strain is given by:

$$\frac{\epsilon_z(z_m)}{\epsilon_s(\theta)} = 2.0 \quad (4)$$

In other words, the maximum bending strain is 2.0 times the measured FOS strain. The FOS strains recorded on Girder 5 (Figure 2b) are given in Table 2. Note that the strains are not too different from those recorded in 2001 and hence there is no sign of FRP degradation or debonding.

Table 2: Rebar and FOS Strain (Girder #5)

Max. Rebar Strain from Electrical Resistance Strain Gages		Est'd Max. FRP Surface Strain from FOS
Before Spray (2001)	After Spray (2001)	After Spray (2005)
102 x 10 ⁻⁶	66* x 10 ⁻⁶	60** x 10 ⁻⁶

*Measured FOS strain of 33 x 10⁻⁶ concerted to maximum strain using Eqn. (4)

**Measured FOS strain of 30 x 10⁻⁶ concerted to maximum strain using Eqn. (4)

4. CONCLUDING REMARKS

A novel technique of rehabilitation and strengthening using sprayed fiber reinforced polymers is described along with its successful application to Safe Bridge in British Columbia. Full-scale load tests in 2001 and 2005 demonstrated that there's no degradation and debonding in the spray.

5. REFERENCES

- Banthia, N., Yan, C. and Nandakumar, N. (1996). *Proc. of ACMBS-II, CSCE*, Montreal, QC, Canada, pp 537-545.
 Banthia, N. and Boyd, A.J. (2000). *Can. J. of Civil Engineering*, Vol. 27, No. 5, pp 907-915.
 Banthia, N., Nandakumar, N. and Boyd, A., (2002). *Concrete International, ACI*, Vol. 24, No. 11, pp. 47-52.
CAN/CSA-S6-00, (2000) Published by CSA International, Canada, Dec. 2000.
 Meier, U., (1992) *Structural Engineering International*, Vol. 1, No. 12, 1992, pp 7-12.
 Neale, K. W. and Labossiere, P. (1997). *Japan Concrete Institute*, 1, 1997, pp. 25-39.

ANALYSIS OF POST-TENSIONED CONCRETE ROAD BRIDGE BEAMS STRENGTHENED BY CFRP TAPES USING FEM UNDER STATIC LOAD

Arkadiusz Mordak

(M.Sc., Ph.D. Student, Cracow Technical University, Cracow, Poland)

Zbigniew Manko

(Professor of Civil & Structural Engineering, Wrocław University of Technology, Wrocław, Poland)

ABSTRACT

The paper is presented the method and results of the FEM analysis and research, and also the main conclusions of a one-span post-tensioned concrete road bridge damaged by 1997 big flood performed under static field load before and after of its repair. There was a conception to make reinforcing by CFRP tapes glued on the bottom flanges of main beams or by overlaying a new concrete deck layer. The aim of the conducted bridge repair was to increase its load capacity to 300 kN (class C) according to the Polish Loads Standard (PN-85/S-10030). The results obtained for four different load schemes to determining the behavior of the analyzed span structure, which allowed for an assessment of the efficiency of the strengthening, as well as establishment of guidelines for future reference concerning this type of maintenance in the engineering practice. The conclusions were drawn from the passed analysis and tests can be helpful mostly for the assessment of behavior of such type of the bridge strengthening system by FRP tapes.

KEYWORDS

Bridge repair, FEM analysis, Static field load test, Post-tensioned concrete beam, CFRP tapes

1. INTRODUCTION

The subject of this study is the road bridge made of concrete spans with post-tensioned main beams over the Nysa Klodzka River situated in Klodzko (Upper Silesia, Poland). This paper is shown the range and the way of the conducted research and some of the results, given in the form of figures, acquired from measurements and FEM calculations of different quantities, e.g. displacements and strains as well as views showing the structure before and after strengthening by CFRP tapes. It also analysis of obtained results and main conclusions concerning testing conducted on this stage are presented. The research was conducted at two different stages of repair works, that is, before performing the main research on static field load tests (Manko, 2001), which was aimed to determine the efficiency of the applied repairing methods. The bridge load capacity before its repair, determined in expertise, was classified as class E, that is 150 kN in accordance with the Polish Loads Standard (PN-85/S-10030), mainly due to a very poor technical condition of the load-carrying structure of bridge span, resulting mostly from transverse cracks in the main beams. The main aim of the repair was to increase the object load capacity to class C (300 kN).

The aim of the conducted research was to determine the behavior of the span structure subjected to considerable static loads at various load schemes (Manko and Mordak, 1999). The research allowed to find out on which elements of the span load-carrying structure the biggest forces were exerted during the progress of repair works of the bridge. The inspection of spans and analysis of the obtained results performed each time after the accomplishment of repairs allow determining the influence of the same load on the quality and durability of this object in the process of strengthening as well as the efficiency and purposefulness of this process.

2. BRIEF BRIDGE DESCRIPTION AND RANGE OF CONDUCTED RESEARCH

The tests were carried out on the one-span road bridge (Figure 1). The examined span consists of four main beams integrated with the new reinforced concrete deck slab of B50 concrete class. The total width of the individual spans is constant along the bridge length and it is 6.50 m (Figure 2). The effective length of the span is 30.60 m. The span

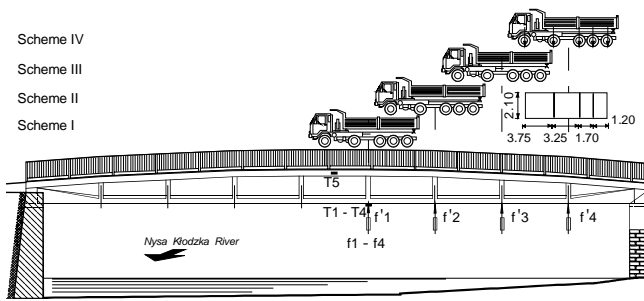


Figure 1: Side view of longitudinal section of road bridge in Klodzko and technical parameters of truck type LIAZ (top view) and localization of inductive gages (f1-f4 & f'1-f'4) and extensometers (T1-T5) on the span length during static field load tests of bridge

is simple-supported and made from post-tensioned concrete beams of length, L , of 31.60 m and are integrated with the RC deck slab over interior supports. The bridge was designed to serve under the II class load (150 kN) in accordance with the PN-66/B- 02015 (or D according to the actual Standard PN-85/S-10030). There are eight span interior crossbeams, all made as concrete. The bridge supports are in the form of massive concrete pier and abutments on spread foundation, fixed in a reinforced concrete footing. The foundation rests directly on the virgin soil. The main beams of the spans rest on single-roller and fixed steel bearings (Figure 1). The roadway was covered with bituminous pavement, 0.05 m thick, with incorporated insulation of an average thickness 0.01 m and 0.02 m thick protective concrete layer. The usable width of the bridge

amounts to 6.10 m which includes the 3.50 m wide roadway and a 1.30 m sidewalk on each side (Figure 2). The considering strengthening conception of the bridge span was accomplished by gluing the tapes made of carbon fibers CFRP SikaDur M1214 type (two for each beam) to the bottom flanges of the main beams (Meier and Deuring, 1991). The final results of the bridge acceptance inspection, conducted after the complete repair under the trial static and dynamic load (Manko and Mordak, 1999), allowed for a comprehensive evaluation of the efficiency of the main beams strengthening by applying CFRP tapes. Moreover, it enabled a comprehensive evaluation of the change of the spans structures behavior under the same load during different stages of repair works.

During the bridge repairs, the research was conducted at two different stages (phases). Figure 1 shows the load schemes on the tested span with the measurement points localization. The following quantities were made:

- four main beams deflections made by dial indicators with 1×10^{-5} m accuracy,
- vertical and horizontal displacements of the expansion and fixed bearings by dial indicators with 1×10^{-5} m accuracy,
- strains (indirectly – normal stresses) in the main beams, which were performed by strain gages (extensometers) and mechanical indicators,
- strains in the CFRP in half and 1/4 of the effective span of the main beams, which were performed by strain gages.

3. FEM ANALYSIS RESULTS

The program COSMOS/M was used for computation. Finite element analysis was used to model the behavior numerically to as to provide a valuable supplement to the field investigations, particularly in parametric studies. Modeling the complex behavior of reinforced concrete, which is both nonhomogeneous and anisotropic, is a difficult challenge in the finite element analysis of bridge engineering structures. Most early the finite element models of reinforced concrete included the effects of cracking based on a pre-defined crack pattern. With this approach, changes in the topology of the models were required as the load increased; therefore, the ease and speed of the analysis were limited.

Only recently we have attempted to simulate the behavior of reinforced concrete strengthened with FRP composites

using the finite element method on the basis of past experiences. A number of reinforced concrete beams strengthened with FRP tapes were tested in the laboratory. Therefore, it was decided to conduct own calculations on real assumptions with 3D SOLID elements, from the nonlinear contact elements of interface type. The FRP tapes were modeled with 2D plate elements in that study, however, and crack patterns of those beams were not predicted by the finite element analysis. The two-dimensional plate elements are surface-like elements, which have no actual thickness. Therefore, stress and strain results at the actual surfaces of the CFRP tapes were estimated by theoretical calculations. Some examples of FEM results are presented in Figures 3 and 4.

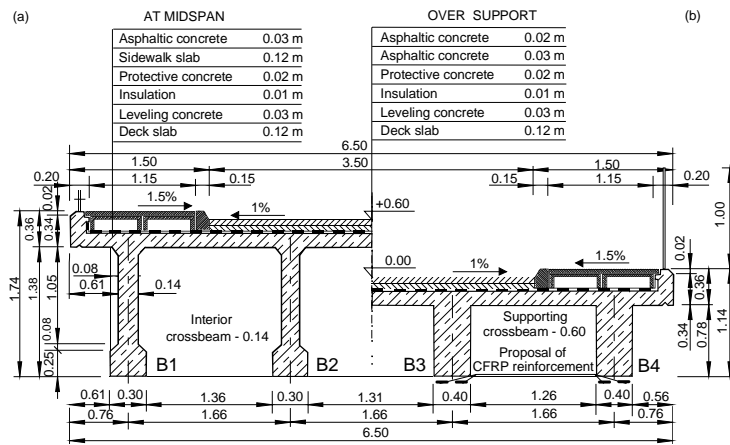


Figure 2: Cross-sections of post-tensioned concrete span at: (a) mispan (before repair), (b) support (after its renovation)

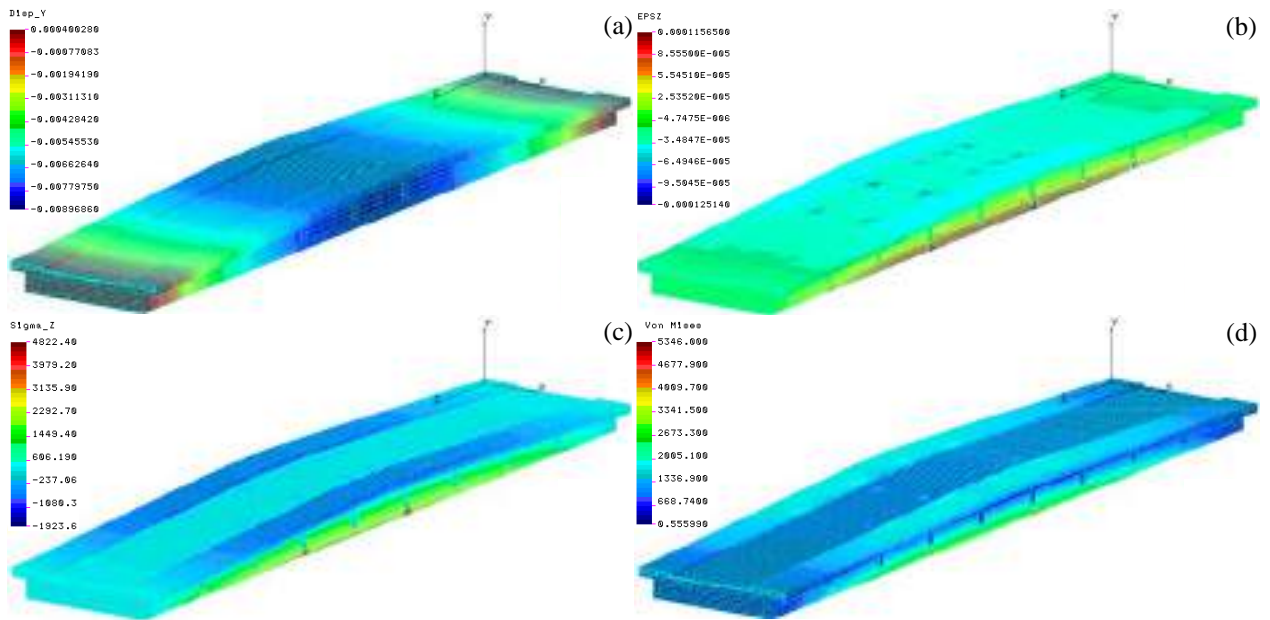


Figure 3: Some results of the bridge span calculation (before repair): (a) vertical displacements, (b) strains and (c) normal stress, in longitudinal direction, and (d) stresses according to von Mises criterion

4. CONCLUSIONS

The practical experience in the light of the conducted FEM calculations and research of the bridge span under the static load during the road bridge construction (I stage of tests), comprehensive analysis of displacement and strain (indirectly normal stress) load bearing structure results obtained from the measurements and comparison between them and calculated values (Figures 3–4) allowed for the following conclusions of general and detailed character:

1. The span structure made of post-tensioned concrete beams did not raise any reservations as far as average sizes of section forces, displacement and strain values obtained from research and were lower than calculated ones in almost all examined points and span structure sections. The causes of small differences between the results obtained both from calculations and measurements stay mainly from the calculations with assumed estimated

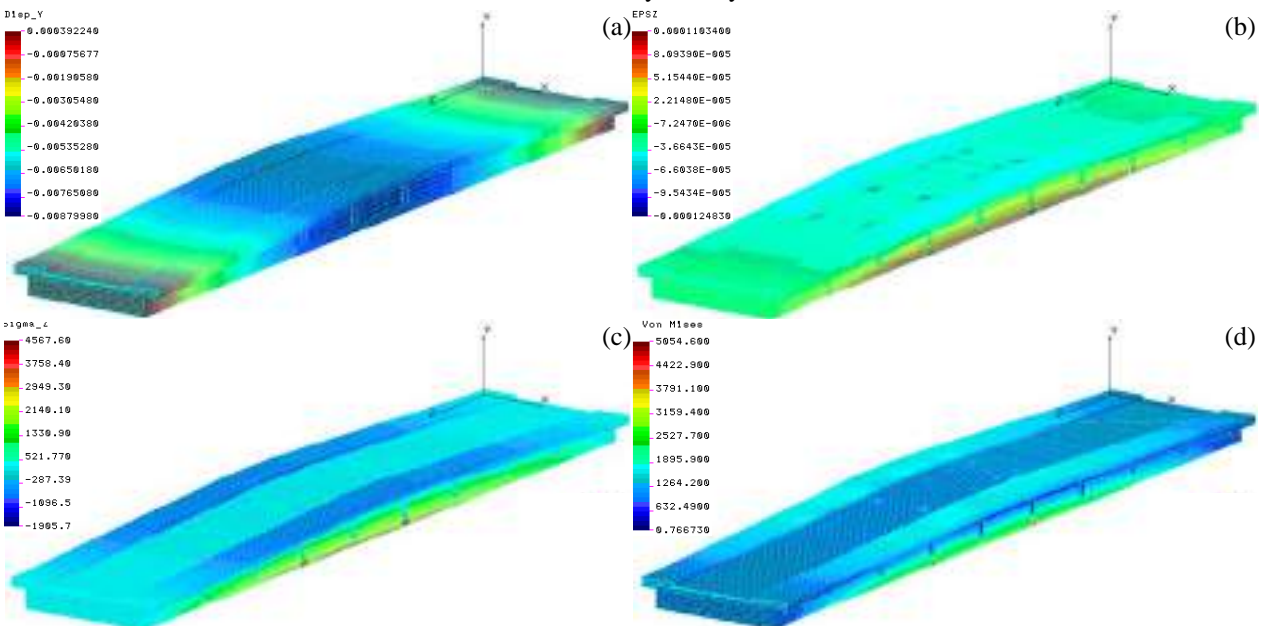


Figure 4: Some results of the bridge span calculation (after gluing CFRP tapes): (a) vertical displacements, (b) strains and (c) normal stress, in longitudinal direction, and (d) stresses according to von Mises criterion

Table 1: Results of the deflections at midspan of four beams B1–B4 obtained from the research and calculation (10^{-3} m) before and after reinforcement

Test stage	Result nature	B1	B2	B3	B4
Before repair	measured	5.82	6.37	6.86	7.39
	calculated	8.86	8.86	8.86	8.86
With CFRP	calculated	8.69	8.69	8.69	8.69
After repair	measured	5.16	5.19	5.48	5.55
	calculated	6.83	6.85	6.85	6.83

value of the span cross-section stiffness and cautious good estimation of interaction of the beams with the plate deck and pavement layers of the roadway at particular repair stages. They amount in range for deflections 18.74–34.32% (Table 1) and for strains 7.24–20.27%, it proves that the section has considerably higher span cross-section stiffness. The good interaction (interface type elements using) between the beams and the CFRP tapes can be caused such small differences. However, the applied of strengthening of the main beams with CFRP tapes did not bring about the significant changes in

deflections and strains values of main beams.

- The strains and displacements of the prestressed concrete beams during the bridge construction demonstrated basically elastic character. They were also lower than the expected values calculated theoretically and also the limit values were not exceeded. It means that construction work was conducted on a high level of technical quality and under constant control. As it was found during the research the minor displacements and permanent strains of the span were partially the beams permanent displacements and most frequently originated partially from the supports settlement and readings errors as well as measuring equipment errors (the change of air temperature and humidity during the time of measurements). Only to a small rate, they were caused by the permanent strains of the load bearing structure (less then 2% of total displacements). This shows a correctness of assumptions taken for calculation and static-strength analysis of this span or also the correctness of assumed analytical structure model with their real behavior in particular repairs phases.
- The grid model of variable load-capacity structure that was assumed at the first step of calculation in different repair phases in dependence of layers and strengthening tapes seems to be sufficient tool to determine the deflections and strains in tested structures on the engineering level. For the detailed analysis of interaction between particular pavement layers and structure components and the assumed strengthening manner is necessary to use more complex model which should be better reflecting a real interaction in a such type of span structures in the considered repair stages of bridge, especially on the contact section of concrete and CFRP tapes.
- As the effect of executed calculations by the FEM and the experimental tests on the real object was affirmed, that for the engineering aims the bridge structures analysis it is possible to carry out in the plane state of strains (the two-dimensional *2D* analysis) with the contact elements of the *interface* type between beams and tapes. In the some special cases, the calculations were possible also to execute in the *3D* space in aim of more detailed analysis. The modeling of bituminous parameters as elastic-plastic is recommended or as elastic-plastic material with reinforcement. Whereas the span as the bilinear elastic material is possible to analyzing (Kachlakev and al., 2001). The contact layers of *interface* type with non-linear proprieties should be considering between CFRP tape and concrete beam.

The conclusions concerning the behavior of such structures can be of great practical significance. As the most loaded span structure elements, which need a detailed study and analysis, one should concern the elements of the bridge deck plate where stresses caused by their direct load with stresses due to their interaction with main beams and crossbeams sum up. In the fact, above summary and main conclusions refer to structures of the tested span elements of preset geometric characteristics, particular element stiffness, and determined effective spans. However, it may be stated that spans strengthening constructed by lamels is not the best solution as far as this type of structures is concerned, mostly from the economical point of view. In order to use an expensive CFRP tapes to a higher extent, one should install on the beams already known prestressing devices for the CFRP tapes.

5. REFERENCES

- Kachlakev, D., Miller, T., Yim, S., Chansawat, K., and Potisuk, T. (2001). "Finite Element Modeling of Reinforced Concrete Structures Strengthened with FRP Laminates." Final Report SPR no. 316 for the Oregon Department of Transportation Research Group, California.
- Manko, Z. (2001). "Investigation of Prestressed Road Bridge Span over the Nysa Klodzka River in Matejko Street in Klodzko before its Modernization", *Proceedings of I Symposium on Bridge Diagnostics and Testing*, April 4–6, Opole, Poland, pp. 399-417.
- Manko, Z., and Mordak, A. (1999). "Research of Road Bridge over Nysa Klodzka River along Matejko Street in Klodzko after Repair." Scientific-Research Center for the Development of Bridge Industry MOSTAR, Wroclaw.
- Meier, U., and Dearing, M. (1991). The Application of Fiber Composites in Bridge Repair. *Strasse und Verkehr*, Vol. 9, pp. 7-11.

A REVIEW OF FRP-STRENGTHENED RC BEAM-COLUMN CONNECTIONS

S.T. Smith

(Senior Lecturer, Centre for Built Infrastructure Research, University of Technology Sydney, Australia)

R. Shrestha

(PhD candidate, Centre for Built Infrastructure Research, University of Technology Sydney, Australia)

ABSTRACT

Considerable research has been conducted over the last decade or so on the strengthening or repair of existing reinforced concrete (RC) structural elements such as beams, columns and slabs with externally bonded fibre reinforced polymer (FRP) composites. Very little research, by comparison, has been conducted on the strengthening of RC beam-column connections with FRP, with the majority scattered in various journals and conference proceedings. Fewer analytical studies have been undertaken and design recommendations proposed. This paper provides a concise but systematic review of experimental research on the strengthening of RC connections with FRP in addition to an evaluation of the effectiveness of the strengthening schemes.

KEYWORDS

Beam-Column Connections, External Bonding, FRP, Reinforced Concrete, Strengthening

1. INTRODUCTION

Extensive experimental, analytical and numerical studies have been conducted on the retrofit/repair/strengthening (herein referred to as *strengthening* unless noted otherwise) of reinforced concrete (RC) structural elements such as beams, columns and slabs with externally bonded FRP composites, and a comprehensive review is given in Teng et al. (2002). Surprisingly, very little research by comparison has been conducted on the strengthening of RC beam-column connections with FRP (the region where the beam frames into the column is referred to as the *joint* while *connection* refers to the joint region including with the beam/s and columns framing into it).

The need to strengthen and/or enhance the ductility of connections stems from gravity load designed frames of yesteryear being inherently weak within the connection region when subjected to seismic attack. The two most commonly occurring connection strengthening needs are shown in Figure 1 that are typical of both of external ("T") and internal ("+") connections in gravity load designed frames. In Figure 1a, a lack of transverse reinforcement in the form of horizontal steel ties in the joint region may mean the shear strength of the connection is unable to resist increased shear demand from seismic loading. Under seismic actions causing load reversal, anchorage failure of the bottom bars in the beam in Figure 1b may occur. Bottom bar failure, or pull-out, will lead to joint degradation and brittle failure in the beam at the face of the column.

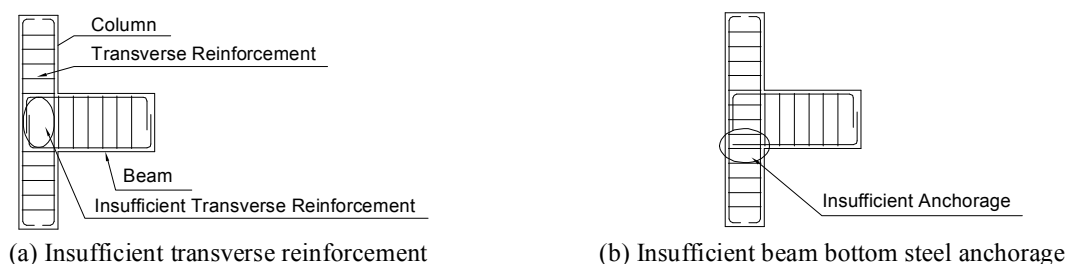


Figure 1: Typical external connection steel reinforcing details

Plain RC connections have been the subject of extensive experimental investigations, however, research on strengthening connections with FRP is much less. Prior to FRP, corrugated steel jacketing or fibre reinforced concrete coating have been used to strengthen connections. A comprehensive review of non-FRP strengthening solutions, as well as some FRP ones, is given in Engindeniz et al. (2005). The limited research on FRP strengthened connections is possibly due to the complex behavior of the connection, as well as difficulties in strengthening and complicated testing arrangements. This paper is a review of the limited experimental research available on strengthening connections with FRP and an evaluation of the effectiveness of the various strengthening schemes.

2. STRENGTHENING SCHEMES

Four different types of deficiencies have been introduced into connections that require strengthening with FRP. They are (1) insufficient transverse reinforcement in the joint region resulting in a deficiency of shear strength (*Shear Strengthening*), (2) insufficient anchorage of the longitudinal beam bottom reinforcement causing bar pull-out under load reversal (*Anchorage Strengthening*), (3) combination of inadequate transverse reinforcement and reinforcing bar anchorage (*Shear and Anchorage Strengthening*), and (4) formation of the plastic hinge in the beam too close to the joint region (*Plastic Hinge Relocation*).

Research has focused on testing two-dimensional connections, such as “-”, “T” and “+” shaped connections with in-plane loading. T-shaped connections have been more commonly tested as they are more susceptible to damage than “+” connections. Various strengthening schemes involving the application of externally bonded FRP in the connection region and adjacent beams and columns have been investigated, with connections being primarily subjected to cyclic loading of typically less than twenty push-pull cycles of increasing amplitude although limited investigations have applied monotonic loading. The only connections subjected to monotonic loading were those of Granata and Parvin (2001) and Li et al. (1999). Table 1 is a summary and categorization of the various types of connections tested, test layout, test criteria and FRP layout following an extensive review of the literature.

3. EFFECTIVENESS OF STRENGTHENING

The plain RC connections mainly failed in shear within the connection region (due to insufficient lateral reinforcement in the joint), anchorage failure of the beam longitudinal reinforcement, or plastic beam hinging. The FRP-strengthened connections typically failed by debonding or rupture of the FRP or the formation of plastic hinges generally in the beam outside of the FRP-strengthened region as the strong-column weak-beam principle was generally adhered to. Debonding occurred for unanchored FRP. Anchored FRP ruptured where anchorage involved mechanical bolting or wrapping FRP around the beam or column adjacent to the connection region.

Comparison of the ultimate load and maximum deflection to that of the control specimens from each study, as given in Figure 2 (based on available data), is one way to identify effective strengthening schemes. Energy dissipation is another indicator of strengthening effectiveness, however, limited published results prevented this quantity from being effectively compared. Based on the results of Figure 2 the following comments can be made. For shear strengthening, the anchored schemes of Gergely et al. (2000) (ref. B), Antonopoulos and Triantafillou (2003) (ref. C), and Tsonos and Styliandis (2002) (ref. D) were the most effective primarily because the FRP did not fail prematurely by debonding. For anchorage strengthening, the anchored schemes of Prota et al. (2001) (ref. J), Granata and Parvin (2001) (ref. K), and Mukherjee and Joshi (2004) (ref. L) were the most effective, again as the anchorage prevented FRP debonding. Both of the shear and anchorage schemes were effective although they appear difficult to implement in practice, while the plastic hinge relocation scheme and the ‘other’ strengthening scheme were not as effective as others. All strengthening schemes varied in complexity from simple relatively intuitive schemes to quite complicated ones. The degree of simplicity or complexity however does not necessarily reflect on the effectiveness of the scheme.

4. CONCLUSIONS

This paper has provided a review on and systematic characterisation of the strengthening of connections with FRP. Two main deficiencies of existing connections were identified, namely inadequate joint shear strength and inadequate anchorage of the bottom steel reinforcing bars for gravity load designed frames. The majority of research conducted to date has been experimental with less research on analytical modelling or development of design guidelines. Research efforts now need to be focused on the development of analytical models to calculate the connection shear strength for FRP strengthened connections that consider FRP rupture and debonding.

Table 1: Summary of test connections and strengthening schemes

Source ¹	Test Layout ²	Test Criteria	FRP Layout ³
Shear Strengthening			
A ^T		Effectiveness of FRP and anchorage scheme	
B ^T		Surface preparation, curing temperature and fibre orientation	
C ^T		Effectiveness of FRP and anchorage schemes	
D ^T		Effect of pre-cracking	
E ⁺		Vary connection transverse reinforcement ratios	
F ⁺		Effectiveness of FRP and anchorage scheme	
G ⁺ , H ⁺		Effectiveness of FRP and anchorage schemes	
Anchorage Strengthening			
I ⁻		Effectiveness of FRP and anchorage schemes	
J ⁺		Effectiveness of NSM bars and FRP sheets	
K ^T		Effectiveness of FRP and anchorage schemes	
L ⁺		Effectiveness of FRP and anchorage schemes	
Shear and Anchorage Strengthening			
M ^T		Effectiveness of FRP and anchorage schemes	
N ^T		Effectiveness of FRP and anchorage schemes	
Plastic Hinge Relocation			
O ^T		Effectiveness of FRP scheme	
Other (No Connection Deficiency)			
P ⁺		Effectiveness of FRP scheme	
Reference: A = Ghorbarah and Said (2001); B = Gergely et al. (2000); C = Antonopoulos and Triantafillou (2003); D = Tsonos and Stylianiadis (2002); E = Ouyang et al. (2003); F = D' Ayala et al. (2003); G = Mosallam (2000); H = Mosallam (2001); I = Geng et al. (1998); J = Prota et al. (2001); K = Granata and Parvin (2001); L = Mukherjee and Joshi (2004); M = El-Amoury and Ghorbarah (2002); N = Ghorbarah and El-Amoury (2005); O = Mahini et al. (2004); P = Li et al. (1999)			
¹ '-' shaped connections, 'T' shaped connections, '+' shaped connections			
² — Beam, — Column, ● Point of load application, ◆ Support			
³ # mechanical anchorage # anchorage provided by FRP wrapping.			

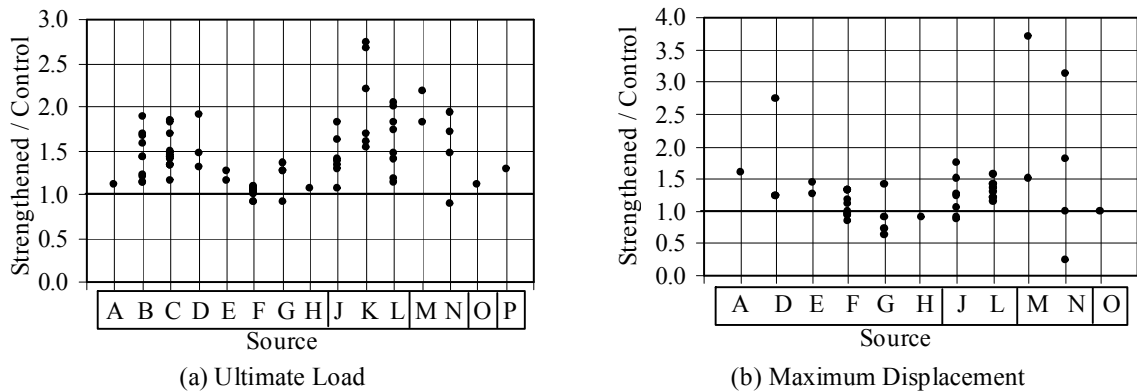


Figure 2: Comparison of strengthening effectiveness (strengthening categories differentiated)

5. ACKNOWLEDGEMENTS

This project was funded by Australian Research Council (ARC) Discovery Grant DP0559567. The financial assistance of the ARC is gratefully acknowledged. Professor J.G. Teng from the Hong Kong Polytechnic University, Hong Kong is thanked for his technical input.

6. REFERENCES

- Antonopoulos, C.P. and Triantafillou, C. (2003). "Experimental investigation of FRP-strengthened RC beam-column joints". *Journal of Composites for Construction, ASCE*, Vol. 7, No. 1, pp. 39-49.
- D'Ayala, D., Penford, A. and Valentini, S. (2003). "Use of FRP fabric for strengthening of reinforced concrete beam-column joints". *Proc. (CD-ROM), 9th Int. Conf. and Exhibition on Structural Faults and Repair*, UK, 4-6 July.
- El-Amoury, T. and Ghobarah, A. (2002). "Seismic rehabilitation of beam-column joint using GFRP sheets". *Engineering Structures*, Vol. 24, pp. 1397-1407.
- Engindeniz, M., Kahn, L.F. and Zureick, A.H. (2005). "Repair and strengthening of reinforced concrete beam-column joints: state of the art". *ACI Structural Journal*, Vol. 102, No. 2, pp. 1-14.
- Geng, Z.J., Chajes, M.J., Chou, T.W. and Pan, D.Y.C. (1998). "The retrofitting of reinforced concrete column to beam connections". *Composites Science and Technology*, Vol. 58, pp. 1297-1305.
- Gergely, J., Pantallides, C.P. and Reavely, L. (2000). "Shear strengthening of RCT-joints using CFRP composites". *Journal of Composites for Construction, ASCE*, Vol. 4, No. 2, pp. 56-64.
- Ghobarah, A. and El-Amoury, T. (2005). "Seismic rehabilitation of deficient exterior concrete frame joints". *Journal of Composites for Construction*, Vol. 9, No. 5, pp. 408-416.
- Ghobarah, A. and Said, A. (2001). "Seismic rehabilitation of beam-column joints using FRP laminates". *Journal of Earthquake Engineering*, Vol. 5, No. 1, pp. 113-129.
- Granata, P.J. and Parvin, A. (2001). "An experimental study on Kevlar strengthening of beam-column connections". *Composites: Part B*, Vol. 53, No. 2, pp. 163-171.
- Li, J., Bakoss, S.L., Samali, B. and Ye, L. (1999). "Reinforcement of concrete beam-column connections with hybrid FRP sheet". *Composite Structures*, Vol. 47, pp. 805-812.
- Mahini, S.S., Ronagh, H.R. and Smith, S.T. (2004). "CFRP-retrofitted RC exterior beam-column connections under cyclic loads". *Proc., 2nd Int. Conf. on FRP Composites in Civil Engineering*, Australia, 8-10 December, pp. 647-652.
- Mosallam, A.S. (2000). "Strength and ductility of reinforced concrete moment frame connections strengthened with quasi-isotropic laminates". *Composites: Part B*, Vol. 31, pp. 481-497.
- Mosallam, A.S. (2001). "Seismic repair and retrofit of reinforced concrete moment joints using composites". *Proc. (CD-ROM), 9th Int. Conf. and Exhibition on Structural Faults and Repair*, UK, 4-6 July.
- Mukherjee, A. and Joshi, M. (2004). "FRPC reinforced concrete beam-column joints under cyclic excitation". *Composite Structures*, Vol. 70, pp. 185-199.
- Ouyang, Y., Gu, X.L., Huang, Y.H. and Qian, Z.Z. (2003). "Seismic behavior of reinforced concrete beam-column joint strengthened with GFRP". *Proc. 6th Int. Symp. on FRP for RC Structures*, Singapore, 8-10 July, pp. 1107-1116.
- Prota, A., Nanni, A., Manfredi, G. and Cosenza, E. (2001). "Selective upgrade of beam-column joints with composites". *Proc. Int. Conf. on FRP Composites in Civil Engineering*, Hong Kong, 12-14 December, pp. 919-926.
- Teng, J.G., Chen, J.F., Smith, S.T. and Lam, L. (2002). *FRP-Strengthened RC Structures*. John Wiley & Sons, UK.
- Tsonos, A.G. and Stylianidis, K. (2002). "Seismic retrofit of beam-to-column joints with high strength fibre jackets". *European Earthquake Engineering*, Vol. 16, No. 2, pp. 56-72.

ANCHORAGE OF CARBON FIBER REINFORCED POLYMER SHEETS WITH AND WITHOUT HEIGHT TRANSITION

Sarah L. Orton

(PhD Candidate, University of Texas at Austin, USA)

James O. Jirsa

(Professor, University of Texas at Austin, USA)

Oguzhan Bayrak

(Assistant Professor, University of Texas at Austin, USA)

ABSTRACT

Debonding of CFRP sheets has been a serious limitation in the use of CFRP on reinforced concrete structures. Debonding is further magnified in cases where the CFRP must go through a height transition between surfaces of elements that are not in the same plane. Forty specimens were tested to investigate the use of carbon fiber anchors (anchors inserted into predrilled holes and fanned out over the CFRP sheet) and U-wraps (CFRP sheet wrapped around sides of beam) to develop the full rupture strength of a CFRP sheet with and without a height transition. Without any additional anchorage the CFRP sheet debonded at 40% of its capacity. Although the number and size of anchors is important, two rows of anchors, with the cross-sectional area of CFRP in each row equal to or greater than the area of the CFRP sheet, fully anchored the CFRP sheet. An equivalent anchorage using U-wraps required 5 times more CFRP. A height transition with a 1 to 2 transition slope reached only 40% of the CFRP capacity, while a 1 to 4 slope reached full capacity. Finally, surface preparation was unimportant when the CFRP was well anchored.

KEYWORDS

Carbon Fiber Reinforced Polymer Sheets, Anchorage, Carbon Fiber Anchors, Bonding

1. INTRODUCTION

CFRP sheets can be used to increase the capacity of reinforced concrete (RC) members (Teng et al., 2001). However, the capacity of the retrofitted member is limited by debonding of the CFRP sheets from the concrete. A study of behavioral trends of FRP retrofitted RC members found that FRP sheets debonded on average at 50% of their tensile capacity (Bonacci and Maalej, 2001). The bonding strength of CFRP is limited by the strength of the concrete because the debonding initiates from shear cracks within the concrete at a level just below the CFRP sheet or at the level of the internal reinforcement. Increasing the length of the CFRP sheet bonded to the concrete does not increase the bonding strength because there is an effective length beyond which bonding strength does not increase (Teng et al., 2001). Therefore, in order to more fully utilize the tensile capacity of the CFRP sheet some form of additional anchorage is needed.

Several different types of anchorage schemes have previously been studied, though a design methodology is still lacking (Ozdemir and Akyuz, 2005; Bramblett, 2000). In the series of tests presented in this paper, two of the most effective and easy to install anchorages, CFRP U-Wraps and CFRP anchors (Figure 1), are evaluated. Furthermore, a height transition (offset in the surface level of the CFRP) will accentuate the debonding problem of CFRP sheets. As illustrated in Figure 2, a height transition can occur when providing continuity of reinforcement that may not be continuous through a beam column joint using CFRP or when increasing the capacity of an infill shear wall whose width is less than that on the surrounding frame (Saatcioglu et al., 2005). The research presented in this paper provides data to develop a design methodology to fully utilize the capacity of the CFRP sheet with or without a height transition. The project was funded by the National Science Foundation.

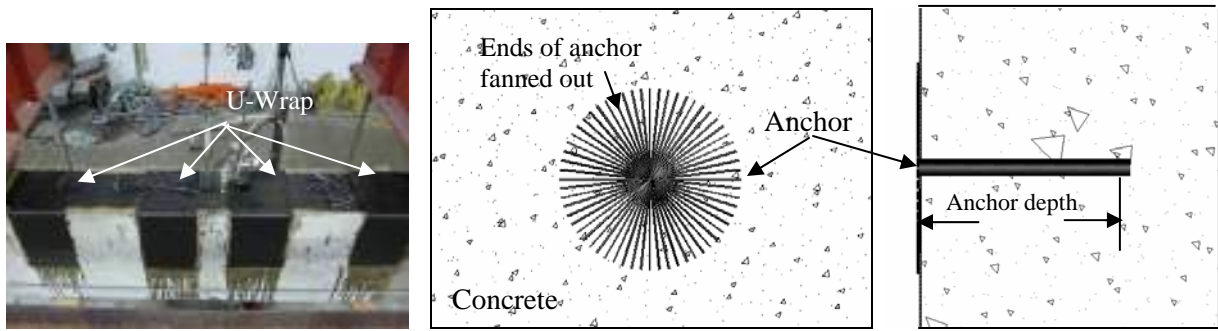


Figure 1: CFRP U-wrap and Anchor

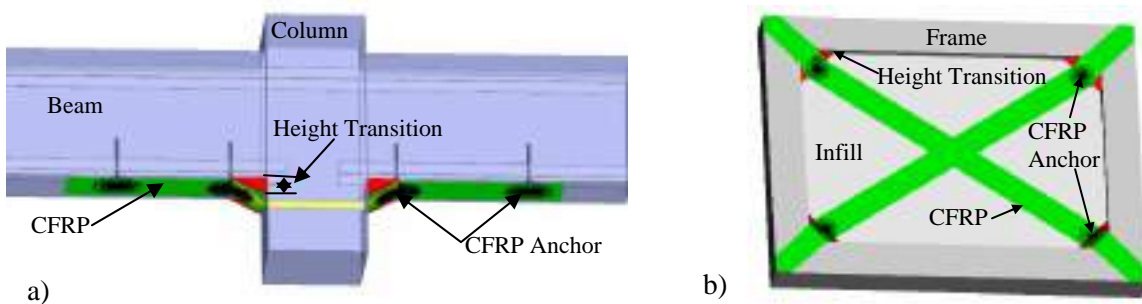


Figure 2: Use of CFRP at Height Transitions:
a) Provide Continuity of Reinforcement b) Increase Capacity of Infill Shear Wall

2. TEST SETUP AND PROGRAM

The specimen and test setup were designed to allow for a controlled evaluation of the anchorage of the CFRP sheet with and without a height transition (Figure 3). The test setup was designed to simulate a reinforced concrete beam in bending with a preexisting crack at midspan. The test specimens consisted of two blocks of reinforced concrete, measuring 16" plus transition height high, 32" long and 8" wide, connected only by a CFRP sheet. This created the crack to initiate debonding at a controlled point and ensured that the only tensile resistance is due to the CFRP sheet. The connected blocks were then loaded at midspan and simply restrained at each end thereby putting tension into the CFRP sheet. The transition slope was constructed using a polymer cement repair mortar with a bonding strength greater than the concrete substrate and suitable for overhead applications. Parameters varied included the slope of the transition (none, 1 to 2, 1 to 4), height of transition (0", 1", 2", 3"), anchorage of CFRP sheet (Anchors or U-wraps – size, number, spacing), surface preparation (grinding, sandblasting, none), and type of carbon fiber (unidirectional Tyfo® SCH-35 or SCH 41).

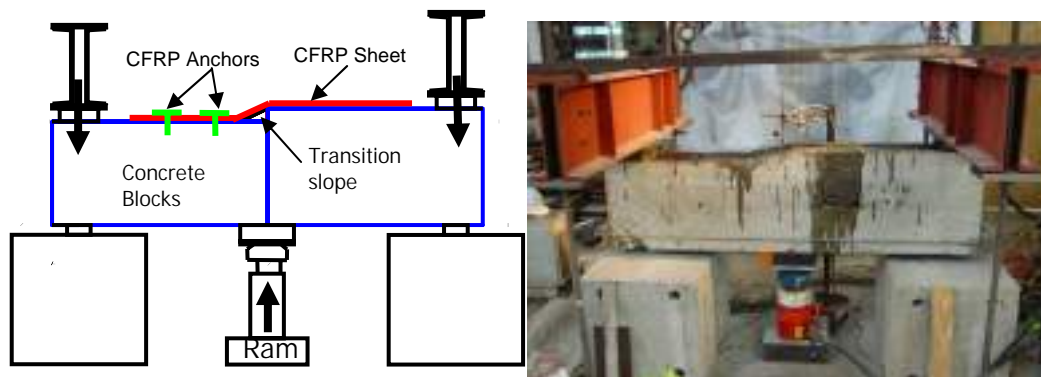


Figure 3: Test Setup

3. TEST RESULTS

3.1 Without Height Transition

In the first series of tests, presented in Table 1, the capacity of the anchorage system without a height transition between the blocks was studied. The results of tests 00-ng1 and 00-ns1 showed that without additional anchorage the CFRP sheet debonded at about 40% of its ultimate capacity (30 k). With additional anchorage the CFRP sheet was able to reach its ultimate capacity. A single layer of U-wrap only reached 75% of capacity with the longitudinal sheet debonding and the U-wrap failing in shear (00-us1). A double layer U-wrap provided adequate shear resistance and reached 99% of capacity (00-us2), but required 5 times more area of CFRP than the unanchored case.

Table 1: Test Results

Test #	Slope	Height difference	Type of Fabric	Anchorage	Tension in CFRP at Failure (kip)	Tension in CFRP (% of ultimate)	Area of CFRP (ft ²)	Failure Mode	
Without Height Transition									
00-ng1	none	0"	SCH-35	none		11.88	40%	2.00	Debonding
00-ns1	none	0"	SCH-35	none		10.56	35%	2.00	Debonding
00-us1	none	0"	SCH-35	U wraps 6" wide at 5" and 19"		22.36	75%	6.67	debond of flat FRP, shear of U wrap
00-us2	none	0"	SCH-35	Double U wrap 6" wide at 5" and 19"		29.58	99%	11.33	Fracture
00-2s1	none	0"	SCH-35 sheet SCH-41 anchors	5/8" anchor at 5" and 19"		21.39	71%	3.50	Fracture anchor, partly delimitate
00-4s1	none	0"	SCH-35	2 3/8" anchor at 5" and at 19"		21.16	71%	3.00	Fracture of 4.5" width, peeling of 1.5"
00-4s2	none	0"	SCH-35 sheet SCH-41 anchors	Two 1/2" anchors at 5" and 19"		25.14	84%	3.50	Fracture
00-4s3	none	0"	SCH-35 sheet SCH-41 anchors	2 < 5/8" anchors at 5" and 19"		31.41	105%	4.25	Fracture
00-6s1	none	0"	SCH-35	3 3/8" anchors at 5" and at 19"		31.94	106%	3.50	Fracture
With Height Transition									
22-ng1	1:2	2"	SCH-35	none		5.98	20%	2.67	peeling
22-us1	1:2	2"	SCH-35	U-wrap, 6" wide		12.94	43%	3.83	Fracture
22-6s1	1:2	2"	SCH-35 sheet SCH-41 anchors	3 3/8" anchors at 4" and at 21"		19.25	64%	3.17	Fracture
42-ns1	1:4	2"	SCH-35	none		12.78	43%	2.67	peeling
42-us3	1:4	2"	SCH-35	Double U-wrap at ramp and single at 21"		28.53	95%	6.17	Fracture
42-4s2	1:4	2"	SCH-35	2 3/8" anchors at 8" and at 21"		23.43	78%	3.17	Fracture around anchor
42-4s5	1:4	2"	SCH-41	2 < 5/8" anchors at 5" and 19"		26.33	88%	3.79	Fracture
42-6s2	1:4	2"	SCH-35	3 3/8" anchors at 8" and at 21"		33.60	112%	3.42	Fracture
42-6s3	1:4	2"	SCH-35 sheet SCH-41 anchors	3 3/8" anchors at 8" and at 21"		21.41	71%	3.42	Anchor Fracture
42-6s4	1:4	2"	SCH-35 sheet SCH-41 anchors	3 1/2" anchors at 8" and at 21"		33.84	113%	3.79	Fracture
42-6s5	1:4	2"	SCH-41	3 1/2" anchors at 8" and at 21"		30.45	102%	3.79	Fracture
42-6n1	1:4	2"	SCH-35 sheet SCH-41 anchors	3 3/8" anchors at 8" and at 21"		16.36	55%	3.42	Anchor Fracture
42-6n2	1:4	2"	SCH-41	3 1/2" anchors at 8" and at 21"		29.77	99%	3.79	Fracture
41-ns1	1:4	1"	SCH-35	none		7.86	26%	2.67	Peeling
43-ns1	1:4	3"	SCH-35	none		11.69	39%	2.67	Peeling
41-6s1	1:4	1"	SCH-35 sheet SCH-41 anchors	3 1/2" anchors at 8" and at 21"		34.38	115%	3.79	Fracture
43-6s1	1:4	3"	SCH-35 sheet SCH-41 anchors	3 1/2" anchors at 8" and at 21"		29.61	99%	3.79	Fracture

CFRP anchors also allowed the CFRP to reach ultimate capacity, but the number and size of anchors played a critical role. All anchors were inserted to a depth of 5 to 6 inches to ensure at least a 2" depth into the core of the concrete (concrete interior of the reinforcing steel) ensuring that failure did not occur by separation of the concrete cover. Two rows of one anchor of 5/8" diameter (full area of CFRP sheet per anchor) (00-2s1) reached only 71% of CFRP capacity. Two rows of two anchors of 1/2" diameter (1/2 area) reached 84% of CFRP capacity (00-4s2). Two rows of 3 anchors of 3/8" diameter (1/3 area) reached 100% capacity and lead to CFRP sheet rupture with only

an additional 1.5 sq ft area of CFRP (00-6s1). Each of the three 3/8" diameter anchors was able to develop about a 2" width of the 6" wide CFRP sheet. This test series of increasing anchor number and decreasing size indicates that smaller more closely spaced anchors are more effective. However, increasing the size of each anchor by 33% (2/3 area) allowed the CFRP sheet to reach 100% capacity with only two rows of two anchors (00-4s3), indicating that larger anchors are able to develop wider widths of a CFRP sheet.

3.2 With Height Transition

The effect of a height transition on the capacity of the CFRP sheet was considered in the next series of tests presented in Table 1. The steepness of a 1:2 transition slope proved detrimental to the capacity of the CFRP sheet with failure occurring at 64% of ultimate capacity (22-6s1). A shallower 1:4 allowed the CFRP to reach full capacity when adequate anchorage was provided (42-6s4, 42-6s5, 42-us2). Two types of CFRP fabric (Tyfo® SCH-35 and SCH-41) were donated by Fyfe Co. LLC. Both have the same tensile strength (143 ksi), and almost the same elastic modulus (11400 ksi and 13900 ksi respectively), but the SCH-35 fabric is regarded as a high grade fabric while the SCH-41 is not. The grade difference may have caused SCH-41 fabric to be weaker in cases where the CFRP is bent, such as in the anchors. Due to this weakness, the area of SCH-41 fabric had to be increased by 33% in order to achieve the same capacity in the anchors as the SCH-35 fabric (42-6s2, 42-6s4). Surface preparation was evaluated in 42-6n1 and 42-6n2 where a layer of plastic wrap was placed between the CFRP sheet and the concrete to eliminate bond. Test 42-6n1, with 3/8" diameter anchors, reached only 55% of capacity, but 42-6n2 with larger 1/2" anchors was able to reach 99% of capacity. The performance of 42-6n2 showed that with adequate anchorage, surface preparation was not necessary because the anchors transferred all the tensile force from the CFRP sheet into the concrete. The last set of tests studied the effect of the amount of height difference (1", 2", and 3") in the height transition with a 1:4 slope. When anchored with 1/2" anchors, the same full capacity of the CFRP sheet was reached regardless of height difference (41-6s1, 42-6s5, 43-6s1). When unanchored, the height difference affected the capacity though less than 45% of capacity was reached (41-ns1, 42-ns1, 43-ns1).

4. CONCLUSIONS

Anchorage of CFRP sheets enabled improved utilization of the tensile capacity of a CFRP sheet and thereby increased the capacity of a CFRP retrofit with or without a height transition.

- U-wraps fully anchored the CFRP sheet, but can require 5 times the amount of CFRP as the unanchored case.
- CFRP anchors fully anchored the CFRP sheet and require far less additional CFRP, as little as 75% more area of CFRP. Two rows of anchors with the area of CFRP fabric in each row equal to or greater than the area of the CFRP sheet fully anchored the CFRP sheet. Smaller more closely spaced anchors were more effective; however, increasing the area of CFRP used in the anchors increased the width of the CFRP sheet developed.
- The effect of a height transition was negated by the use of a 1:4 slope on the transition.
- The properties of carbon fiber fabric had an impact on the ultimate capacity in cases where the CFRP is bent.
- With proper anchorage, surface preparation to improve bond of the CFRP sheet to concrete was not necessary.
- The height difference did not affect the CFRP capacity when CFRP sheets were fully anchored.

5. REFERENCES

- Bramblett, R.M. (2000). "Strengthening of Reinforced Concrete Beams Using Carbon Fiber Reinforced Polymer Composites", Masters Thesis, The University of Texas at Austin, Texas, USA.
- Bonacci, J.F., and Maalej, F. (2001). "Behavioral Trends of RC Beams Strengthened with Externally Bonded FRP". *Journal of Composites for Construction*, May 2001, pp 102-113.
- Ozdemir, G., and Akyuz, U. (2005). "Tensile Capacities of CFRP Anchors", *7th International Symposium on Fiber-Reinforced Polymer (FRP) Reinforcement for Concrete Structures*, Editors: C.K. Shield, J.P. Busel, S.L. Walkup, and D.D. Gremel, pp. 39-56.
- Saatcoglu, M., Serrato, F., and Foo, S. (2005). "Seismic Performance of Masonry Infill Walls Retrofitted With CFRP Sheets". *7th International Symposium on Fiber-Reinforced Polymer (FRP) Reinforcement for Concrete Structures*, Editors: C.K. Shield, J.P. Busel, S.L. Walkup, and D.D. Gremel, pp. 341-353.
- Teng, J.G., Chen, J.F., Smith, S.T., and Lam, L. (2001). *FRP-Strengthened RC Structures*, John Wiley & Sons LTD, New York.

EFFECT OF FRP U-JACKETING ANCHORAGE ON FRP-CONCRETE INTERFACES UNDER FATIGUE LOADING

Kentaro Iwashita

(Researcher, Ibaraki University, Hitachi, Ibaraki, Japan)

Zhishen Wu

(Professor, Ibaraki University, Hitachi, Ibaraki, Japan)

Takashi Ishikawa

(Director, Japan Aerospace Exploration Agency (JAXA), Mitaka, Tokyo, Japan)

Yasumasa Hamaguchi

(Invited Researcher, Japan Aerospace Exploration Agency (JAXA), Mitaka, Tokyo, Japan)

ABSTRACT

This study aims to examine and investigate the effect of FRP U-jacketing anchorage on Fiber Reinforced Polymer (FRP) sheets-concrete interfaces under fatigue loading. Double-lap shear test specimens with the FRP U-jacketing anchorage are carried out under static and fatigue loading. The fatigue behavior of FRP sheets-concrete interface is finally characterized by the conducted amplitude tensile load (S) - the number of cycles (N) diagram at debonding on a semi logarithmic scale. The results demonstrate that the FRP U-jacketing anchorage increase the static bond strength and delay the occurring of initial FRP debonding under high fatigue load (high amplitude load) level, but it cannot enhance the fatigue strength of the FRP-concrete interface.

KEYWORDS

Fiber Reinforced Polymer (FRP) sheets, bond, fatigue loading, S-N curve, FRP U-jacketing anchorage

1. INTRODUCTION

The need to rehabilitate or upgrade the deteriorated and deteriorating civil infrastructure has been becoming a major and urgent problem worldwide. In contrast with the traditional strengthening methods such as overlaying and jacketing method, external cable method and bonded and jacketing steel plate method, the use of fiber reinforced polymers (FRP) represents an innovative and effective technology for strengthening of infrastructure. In recent years, repairing and strengthening concrete structures with externally bonded, epoxy-bonded FRP sheets to the tension face of structural element has been widely accepted for practical uses. But, recent studies have also reported a variety of FRP debonding problems. Therefore, it was found that the limit value of maximum load under fatigue loading is only about a half of maximum load under static loading (Ferrier et al. 1999, Wu et al. 2002, Tan et al. 2003, Iwashita et al. 2006). Recently, FRP U-jacketing anchorage is considered to be used as a countermeasures for enhancing the FRP-concrete bonding behavior around the ends of prestressed FRP sheets or around intermediate flexural cracks of the concrete structures strengthened with FRP sheets. The benefits associated with the FRP U-jacketing anchorage have been investigated by many researchers, but there is little research for discussing the effectiveness of this anchorage under fatigue loading. Moreover, for strengthening RC/PC structures, the evaluation of the fatigue performance of the FRP U-jacketing anchorage is considered to be very important one. Based on these considerations, this paper aims at investigating clearly the fatigue performance of FRP U-jacketing anchorage and the expanding effect on fatigue life of FRP-concrete interfaces.

Table 1 Summary of Material Properties

PBO fiber reinforced polymer sheets	Guaranteed tensile strength (GPa)	3.5
	Guaranteed tensile modulus of elasticity (GPa)	240
	Nominal thickness (mm/1 layer)	0.128
Epoxy resin	Guaranteed tensile strength (MPa)	51.9
	Guaranteed tensile shear strength (MPa)	25
	Guaranteed tensile modulus of elasticity (GPa)	3.43

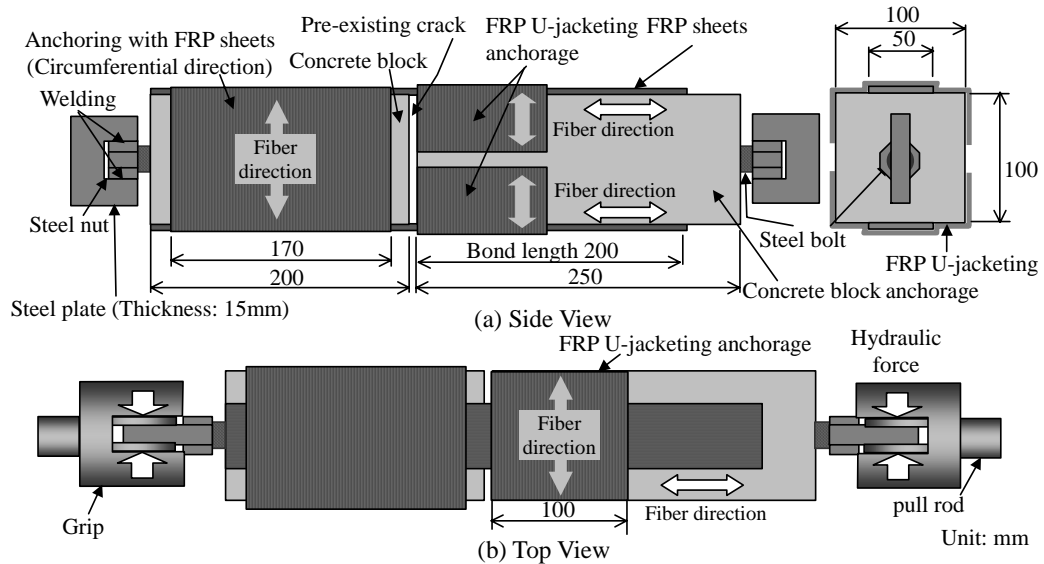


Fig. 1 Test Set-up and Details of The Prism Specimens

2. EXPERIMENTAL PROGRAMS

2.1 Composite Materials

The newly developed PBO (Poly-*p*-phenylene-benzobisoxazole) fiber sheets was chosen for this study. PBO fiber reinforced polymer (PFRP) sheets mainly present advantages such as high tensile strength and high stiffness-to-weight ratio as shown in Table 1. Density of reinforcing continuous fiber sheets are 200g/m^2 and fiber volume content (V_f) is decided to 50%.

2.2 Specimen Details and Test Set-Up

Specimens of FRP sheets-concrete double-lap bonding joints

In accordance with experimental method of JSCE Recommendations for Upgrading of Concrete Structures with Use of Continuous Fiber Sheets (JSCE, 2001), the prism specimens with 100mm width, 100mm thick and 500mm long are used in the investigation. The specimen is cut off at the position of the notch (Pre-crack). Before bonding of FRP sheets, the concrete surface preparation is treated with a diamond sander, and an epoxy primer is painted after wiping with cloth soaked with acetone. 2 layers FRP sheets whose size is 50mm width and 400mm span is impregnated with epoxy resin before bonded to concrete surface, and bonded to both sides of the concrete block along the axial direction after hardening of adhesive by the end of 24 hours. The tensile tests were started 7 days later. The details of the prism specimens are schematically shown in Fig. 1. The 28-day compressive strength of the concrete was 45.2MPa. The tensile load is applied by pulling both ends of the steel plate. A summary of the properties of PBO fiber sheets, the epoxy resin and the concrete is shown in Table 1.

Test Set-Up

The static and fatigue loads were applied to the specimen using an Instron 8502 series digital servohydraulic fatigue testing machine operating under load-control mode. Then, the load acting on the specimen and the position of lower grip were measured by using a load cell with 100kN capacity and LVDT set in the test machine. All static loads were applied with a speed of 1kN/min and all fatigue loads were applied with a rate of 5Hz. All data was recorded at

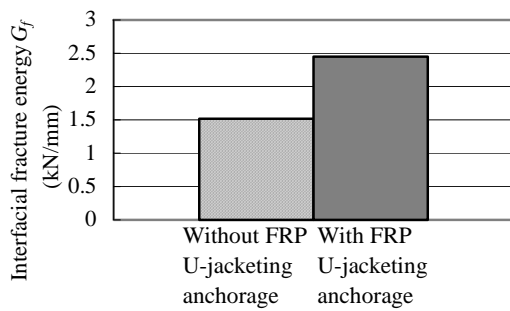


Fig. 2 Maximum load under static loading

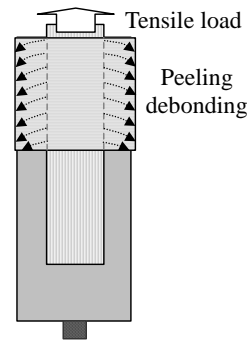


Fig. 3 Debonding Behavior of FRP U-jacketing anchorage

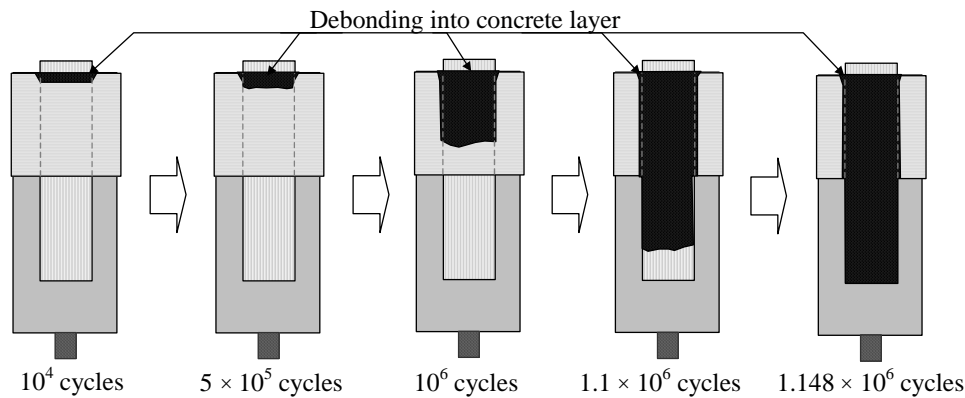


Fig. 4 Debonding Process of FRP Sheets and FRP U-jacketing Anchorage under Fatigue Loading

every 1000th cycle with Instron WaveMaker software. The variables of maximum repeated loads are set as 40%, 50% and 60% of the lowest value P_u among the maximum load investigated by the three static tests, and the minimum repeated load is set as 10% of P_u in all experiments. In case that the FRP debonding does not occur by the 2 millions cyclic loading, loading was stopped and tests were finished. The tests were carried out under a normal temperature condition (25-27°C).

3. RESULTS AND DISCUSSION

3.1 Effect of FRP U-jacketing Anchorage on Bond Strength under Static Loading

The results of prism tests under static loading are investigated for the determination of interfacial fracture energy (G_f). This value is calculated from the following equation.

$$G_f = \frac{P_{\max}^2}{8b^2 E_f t} \quad (1)$$

where P is the maximum transferable force in FRP sheet; E_f , b and t are modulus of elasticity, width and thickness of FRP sheets respectively. The average values of G_f are shown in Fig. 2. The average G_f value of without FRP U-jacketing specimens is nearly same as a standard value (JSCE, 2001, Wu et al., 2001) and a good reproducibility of these experiments was confirmed. From the results, average G_f value of specimens with FRP U-jacketing anchorage is higher than those without anchorage. It is found that the FRP U-jacketing anchorage can significantly increase the bond strength under static loading. On the other hand, peeling and debonding of the FRP U-jacketing sheets are occurred around crossing point of FRP and anchor FRP on the final stage as shown in Fig. 3, and FRP debonding reaches to the FRP ends.

3.2 Effect of FRP U-jacketing Anchorage on Bond Strength under Fatigue Loading

In case of 40%-10% of P_u fatigue loading specimen with FRP U-jacketing anchorage, it is confirmed by the impact echo tests that micro-debonding initiates at the tensile end of bonded FRP sheets, and propagates gradually to form a

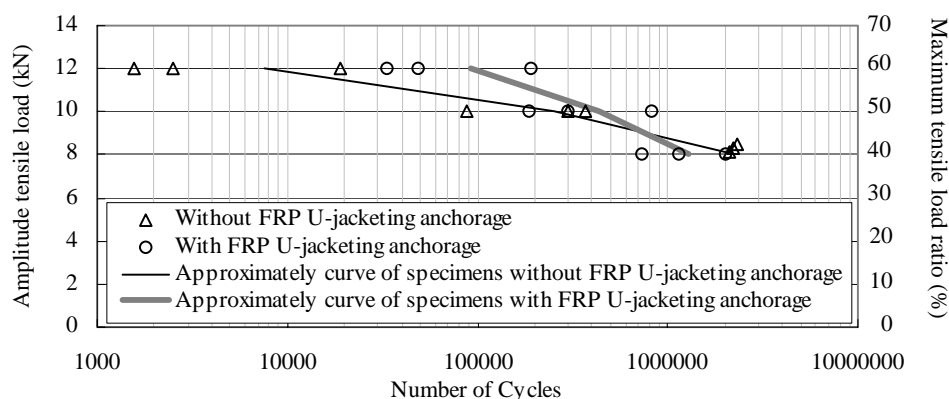


Fig. 5 Amplitude Tensile Load (S) - Number of Cycles (N) Curve.

macro-debonding by about 10^4 cycles as shown in Fig. 4. Once macro-debonding length grows to about 20-30 mm after about 5×10^5 cycles, debonding propagates towards the free end of bonded FRP sheet. Finally, a complete FRP sheet debonding occurs when debonding propagates to the FRP end. Fig. 5 shows the relationships between amplitude stress (S) and number of cycles (N) with a semi logarithmic scale. The results show that the FRP U-jacketing anchorage can delay the debonding failure occurred by fatigue loading under short-term fatigue loading before 10^6 cycles, but the effects are mitigated or disappeared on the specimens which have long-term fatigue life more than 10^6 cycles. Then, peeling and debonding of the FRP U-jacketing sheets occur around crossing point of FRP and anchor FRP after the final debonding as shown in Fig. 3, and FRP debonding reaches to the FRP ends. It is considered that the FRP U-jacketing anchorage can not expand the long-term fatigue life. On the other hand, the maximum load ratio of FRP sheets under fatigue loads of 10^6 cycles with or without a FRP U-jacketing anchorage is about 35% of one under static loading.

4. CONCLUSIONS

From the study carried out, bond strength and debonding processes under fatigue loading of FRP sheets with a FRP U-jacketing anchorage are examined. Based on the results of this study, the following conclusions are drawn:

1. It is found that the FRP U-jacketing anchorage can significantly increase the static and short-term bond strengths, before 10^6 cycles, but the effects are disappeared on the specimens which have long-term fatigue life more than 10^6 cycles.
2. The maximum load ratio of FRP sheets under fatigue loads of 10^6 cycles with or without a FRP U-jacketing anchorage is about 35% of one under static loading.

5. REFERENCES

- Ferrier, E., Nasserri, H., Hamelin, P. (1999) "Fatigue behavior of composite reinforcement for concrete structures", *Proceedings of fourth international symposium on fiber reinforced polymer reinforcement for reinforced concrete structures (FRPRCS-4)*, ACI International SP-188-48, Editors: Dolan, C.W., Rizkalla, S.H., Nanny, A., pp.535-545.
- Wu, Z.S, Iwashita, K., Ishikawa, T., Hamaguchi Y. (2002). "Bonding and debonding behavior of FRP sheets under fatigue loading". *Proceedings of 10th US-Japan workshop on composite materials*, Editors: Chang F.K., pp.810-818.
- Tan, K.H. (2003) "Effect of cyclic loading on bond strength of FRP reinforcement", *Proceedings of International Symposium on Latest Achievement of Technology and Research on Retrofitting Concrete Structures – Interface Mechanics and Structural Performance*, Kyoto, Japan, pp. 1-8 (Keynote paper).
- Iwashita, K., Wu, Z.S, Ishikawa, T., Hamaguchi Y., and Suzuki T. (2006). "Bonding and debonding behavior of FRP sheets under fatigue loading". *Journal of Advanced composite materials*, VSP publishers (Accepted).
- Japan Society of Civil Engineers (JSCE) (2001) "Recommendations for Upgrading of Concrete Structures with Use of Continuous Fiber Sheets", *Concrete Engineering Series 101*.
- Wu, Z. S., Yuan, H., Yoshizawa, H. and Kanakubo, T. (2001) "Experimental/Analytical Study on Interface Fracture Energy and Fracture Propagation Along FRP-Concrete Interface", *Fracture Mechanics for Concrete Materials: Testing and Applications*, ACI International SP-201-8, pp.133-152.

FRP Upgrade of Concrete Girders to Support Flood Loads

Abdelhakim Bouadi, Ph.D., P.E.

Senior Associate, Walter P Moore, Structural Diagnostics Services, Houston, Texas, USA

Eric Green, P.E.

Principal, Walter P Moore, Structural Diagnostics Services, Houston, Texas, USA

Narendra Gosain, Ph.D., P.E.

Senior Principal, Walter P Moore, Structural Diagnostics Services, Houston, Texas, USA

ABSTRACT

A medical facility building located in Houston, Texas incorporating a basement housing equipment and laboratories implemented a flood protection system consisting of multi-layered internal and external flood walls. Part of the flood protection system included strengthening of a portion of the existing basement roof to carry the weight of seven feet of water. The basement roof structure is formed by a reinforced concrete pan-joint system supported by girders. A review of the structure showed that the slab and joists had sufficient capacity to resist the loads due to the floodwaters. However, the girders did not have adequate flexural capacity and required strengthening. Several repair options were considered. The final option consisted in the use of Carbon Fiber Reinforced Polymer (CFRP) to strengthen the existing girders. CFRP was epoxy-bonded to the soffit of the girders. To simplify the retrofit, the design allowed for cracking and ensuing moment redistribution at the column supports. Construction was performed without any disruption to the existing mechanical, electrical, and plumbing (MEP) lines at the basement ceiling, and was completed in a timely fashion without any impact to building operations.

KEYWORDS

Fiber Reinforced Polymers, CFRP, Reinforced Concrete, Upgrade, Construction.

1. Introduction

A structural flood protection system was built around an existing medical facility located in Houston, Texas. The flood prevention system consists of two concentric and independent external (primary) flood walls and several internal (secondary) flood walls. Two types of internal floodwalls were installed. One internal wall divides the structure in half to prevent complete flooding of the building in the event of a failure of the primary flood walls. Other internal walls protect critical MEP rooms. Implementation of the flood protection system required construction of new reinforced concrete walls and strengthening of the existing reinforced concrete components.

2. Building Description

The facility built in the 1970s is a seven story building. The plan dimensions are approximately 250 feet x 190 feet. The building basement houses research equipment and laboratories. Due to existing site constraints, a roadway passes through the width of the structure at the ground level, with the basement roof functioning as the roadbed (Fig. 1).

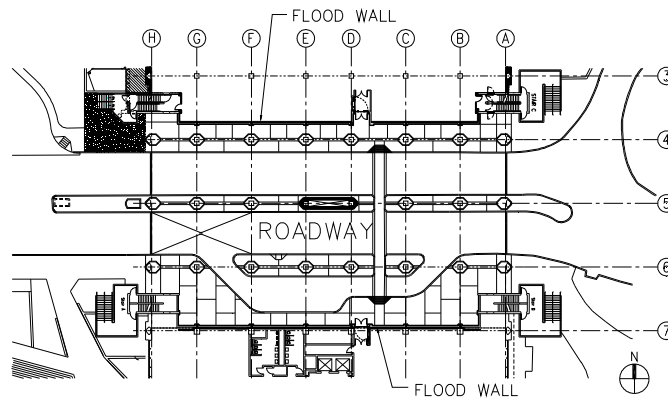


Figure 1: Plan View of Building and Flood Wall Location

The basement roof structure located between gridlines 4 and 7 is formed by a 5” reinforced concrete slab spanning between concrete joists that are located at 30 inches on center. This part of the structure was designed to resist the code-level loads due to vehicular traffic, including AASHTO defined concentrated loads and a uniform load of 250 psf. The joists are 16 inches wide, 25 inches deep and have a span of about 32 feet. The joists are supported by concrete girders that have a span of about 28 feet. The girders at gridline 7 are 40 inches wide and 47 inches deep. The girders at gridlines 4, 5 and 6 are 36 inches wide and 32 inches deep (Fig. 2). Reinforcing is shown in Table 1. All reinforcing bars were specified to conform to ASTM A615 with a yield strength of 60 ksi.

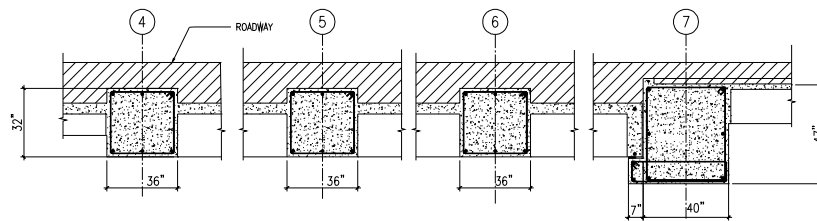


Figure 2: Girder Configuration at the Basement Ceiling

Table 1: Typical Girder Reinforcement

Gridline	Mid Span Bottom Reinf.	Top Reinf At Support	Top Reinf at Gridlines B and G
4	5 # 10	8 #10	4 #10 and 2 #9
5	6 #11	7 #11 and 3 #10	4 # 11 and 5 #10
6	6 # 11	4 # 11 and 6 # 10	4 # 11 and 5 #10
7	4 #10	4 #10 and 4 # 9	4 #10 and 2 #9

3. Primary Flood Protection at Roadway

3.1. Description

The primary flood protection system was formed by constructing two new 7-foot tall reinforced concrete walls located at the north and south sides of the road and strengthening of the basement roof to carry the loads imposed by seven feet of standing water (Fig. 3).

3.2. Analysis of the Existing Structure

The design of the existing basement roof structure was analyzed. At the time of the original construction, the structural system was designed for vehicular loads which included a service uniform live load of 250 psf. The addition of the flood system resulted in a service live load due to the flood water of about 440 psf. Although the design loads under flood conditions were significantly higher than the original design loads, the structural review indicated that the existing slabs and joists had adequate capacity to resist the higher loads. This was a result of the combined effects of lower load factors in the ACI 318-02 design code (ACI Committee 318, 2002), a higher concrete compressive strength and a conservative original design. However, while the girders had sufficient shear strength to carry the higher flood loads, they were found to have insufficient positive and negative flexural capacity.

Given the age of the structure, it was recognized that the actual concrete compressive strength was likely to be higher than the specified 4000 psi. The actual concrete strength based on field-measured values was found to be 4,500 psi.

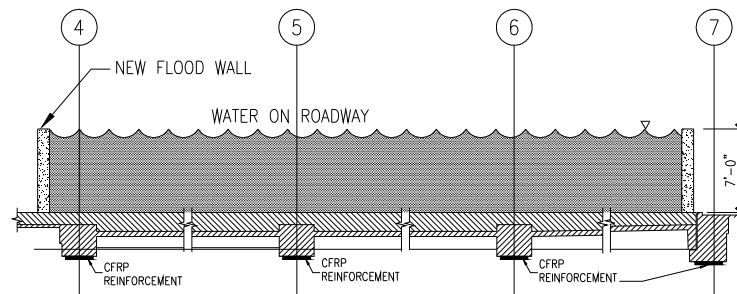


Figure 3: Section through Building at Roadway

4. Structural Upgrade

The first retrofit option considered the addition of bottom and top reinforcing bars in new concrete jackets connected to the existing girders with the use of dowels drilled and epoxied into the existing girders. The addition of the top reinforcement would require removal and replacement of the driving surface (topping slab). To develop the negative moment at the joints, the top reinforcement needed to be anchored into the column with the use of through bars or epoxy-doweled bars.

The use of the concrete jacket presented several construction challenges. The proposed dowel installation was labor intensive and time consuming. In addition, avoiding damage to the existing rebar during installation required a pre-construction phase consisting of locating the existing reinforcement. Additionally, the girders were located in the building basement which had extensive amount of mechanical ducts, pipes and mechanical or electrical equipments. Construction would require temporary disconnection and relocation of several critical pieces of mechanical, electrical and plumbing lines and equipment that would result in a temporary shut down of some building operations. This option was rejected because the expected operational disruption was unacceptable to the owner.

The second option considered the use of FRP epoxy-bonded to the underside of the beams to increase the flexural capacity. The use of FRP only was found not to be practical in increasing the negative moment capacity of the beams. Therefore we considered the use of moment redistribution at the supports where the imposed moment exceeded the negative flexural capacity of the girders. Although this redistribution remained within the limits allowed by the ACI code, the informed consent of the owner's representatives was solicited as moment redistribution might result in permanent deformation and concrete cracking in the event of a major flood.

After discussion, the owner's facility managers agreed to the use of a strengthening design that allowed for moment redistribution. This decision was based on several factors, including the fact that the alternative, using bonded reinforcing, would impact the building operations in an unacceptable manner during construction. Additionally, the

floor system would see full loads only in the event of a 500 year flood, an event which only has a 0.2% chance of occurring in any given year.

The final upgrade design consisted in the use of wet layup system of CFRP sheets having a thickness of 0.041 inches, an ultimate tensile strength of 127 ksi and an elastic modulus of elasticity of 10,500 ksi. The width of the sheets was in general equal to the girder width. The CFRP upgrade extended for an average of 16 feet centered on the girders. At the end, U-strips with Glass FRP anchors were added to prevent end-debonding. The upgrade was done following the general recommendations of ACI 440.2R-02 (ACI Committee 440, 2002).

5. Construction

The construction was performed without any disruption to the existing mechanical, electrical and plumbing lines at the basement ceiling, and was completed in a timely fashion without any impact to the building operations. The only area of the building that was closed during the construction process was the basement level where the actual work was performed.

As part of the construction quality control, it was required that an independent laboratory conduct a number of tests that included the preparation of coupon samples to verify the properties of the material. Due to the relatively recent introduction of the CFRP material into the market, the local testing laboratories were not trained in collecting or testing the material. In order to overcome this obstacle, the coupons were collected by the contractor in presence of the engineer and testing laboratory personnel. This created a level of reliability in the preparation of test coupons. The coupons were then submitted to an out-of-state independent specialty laboratory with prior experience in testing of CFRP coupons. The lack of testing laboratory personnel trained in the CFRP presented challenges for quality control, especially since the design was based on data provided by the manufacturer. The ability to verify the material properties is essential in order to validate the design. In addition several bond tests were carried by the contractor in presence of the engineer and testing laboratory personnel to verify proper adhesion.

6. Conclusions

The introduction of a new flood control system in a medical facility required upgrading existing concrete girders that form the roof structure of the basement and a support for a vehicular roadway. The upgrade was limited to an increase in the positive flexural capacity of the beams as the shear capacity was found to be adequate and the code permitted redistribution of the moment was used resulting in an acceptable negative moment capacity. While several repair options were considered, the final option consisted of the use of CFRP epoxy-bonded to the soffit of the girders. Construction was performed without any disruption to the existing mechanical, electrical or plumbing lines at the basement ceiling, and was completed in a timely fashion without any impact to building operations. The lack of FRP trained personnel in the local testing laboratories presented a challenge in verifying the properties of the FRP and in performing other specified tests. This was overcome by having the contractor collect sample in the presence of the engineer and the testing laboratory personnel and in having the testing laboratory submit the samples to an-out-state specialty laboratory experienced in conducting such tests.

7. References

- ACI Committee 318 (2002). *Building Code Requirements for Structural Concrete (ACI 318-02) and Commentary (ACI318R-02)*, Farmington Hills, MI.
- ACI Committee 440, 440.2R-02 (2002). *Design and Construction of Externally Bonded FRP Systems for Strengthening Concrete Structures*, American Concrete Institute, Farmington Hills, MI, 2002.

TESTS ON FRP-STRENGTHENED TIMBER JOINTS

K.I. Crews

(Professor, Centre for Built Infrastructure Research, University of Technology Sydney, Australia)

S.T. Smith

(Senior Lecturer, Centre for Built Infrastructure Research, University of Technology Sydney, Australia)

ABSTRACT

Surprisingly little research has been conducted on the strengthening of timber with fibre reinforced polymer (FRP) composites as opposed to the much more widely researched strengthening of concrete and to a lesser extent metallic structures. As with all FRP strengthening applications, the bond of the FRP to the substrate is of particular importance. A lack of understanding of the bond between FRP and timber is a major factor contributing to the reluctance of industry to utilise FRP for timber strengthening applications. This paper reports results of preliminary bond strength tests undertaken at the University of Technology Sydney (UTS) on FRP-strengthened timber joints. The aims of the tests were to observe the suitability of the test method, quality of the bond, bond strength and failure mode of the test specimens.

KEYWORDS

FRP, Bond, Strengthening, Timber, External Bonding

1. INTRODUCTION

There are some interesting similarities between the properties of timber and those of FRP's, in that both have orthogonal properties as a consequence of having an inherent fibrous structure set in a matrix binder. It can be argued that FRP is a manufactured product of "perfect" timber – where the fibre strength rather than the occurrence of strength reducing characteristics that occur naturally in wood (e.g. knots), govern the strength of a structural member. It is therefore somewhat surprising that combinations of the two products have not been more widely researched and as a result the bond interaction between FRP and timber is not generally understood.

Most work on FRP-strengthened timber to date has focused on the bonding of FRP composites to selected faces of timber beams. Research by Meier (1995), Tingley et al. (1996), Chajes et al. (1996), Gilfillan et al. (2004), and Dagher (2005) has demonstrated that FRP bonded tension face plates (or tension and compression faces) can significantly increase the bending strength and stiffness of a timber beam, whilst Milner (1999) demonstrated the effectiveness of FRP's to overcome inherent weaknesses in the finger joints of glued laminated timber beams. Experimental work undertaken by Greenland *et al.* (1999) at UTS also explored this issue as part of a detailed program of research on the viability of externally bonded FRPs for improving the tensile capacity of stress laminated T system webs, but this same work also highlighted some of the difficulties associated with bonding failures which can occur between the FRP and the timber substrate.

2. PREVIOUS RESEARCH AT UTS

The work undertaken to date at UTS has focused on characterising the flexural performance of Australian Radiata Pine products strengthened with carbon FRP (CFRP) composites. Pilot tests have been conducted on solid (sawn) and reconstituted (Laminated Veneer Lumber - LVL) sections of Radiata Pine to determine the short term properties of the CFRP, the bending strength and stiffness of timber elements, and improved bending strength, stiffness and ductility, with reduced variability, of FRP-strengthened timber elements. Further pilot studies investigated the short term behaviour of T beams (for use in stress laminated timber decks) constructed of LVL webs and solid Radiata Pine flanges with and without FRP web strengthening (Greenland 2001). Whilst Greenland developed models for

predicting linear-elastic and nonlinear behaviour of the FRP composite LVL beams as a structural system, the fundamental behaviour of the bond and the bond-slip relationship of the FRP-strengthened timber were not addressed.

3. TESTS ON BOND BEHAVIOUR OF FRP AND TIMBER

Vick (1997) investigated the durability of epoxy bonds and presented details of a primer system developed by the US Department of Agriculture (USDA) to improve epoxy durability. It was concluded that epoxy bonds develop bonds to timber that are as strong as the timber itself, as long as the bonds remain dry and that epoxy adhesives could equal the structural durability of resorcinolic adhesives when the USDA primer was used. The effectiveness of adhesion between FRP and timber was evaluated using a cyclic delamination test as noted in ASTM D2559-03 (2003) *Standard Specification for Adhesives for Structural Laminated Wood Products for Use Under Exterior (Wet Use) Exposure Conditions*. Once the specimens were exposed to the severe stresses from repeated water soaking and drying, the bonds tended to degrade and delamination occurred.

One of the variables that affects the behaviour of a composite FRP/timber element, are the shear properties of the bond/interface. Because the transfer of stress between timber and the fibre composite is achieved via the development of shear stresses in the adhesive bond, it is important that the strength properties of the adhesive in shear be understood and quantifiable for use in numerical models. In particular, the way in which load is transferred between the FRP and timber needs to be understood, namely; will the behaviour of the strengthened section be governed by the strength of the timber or FRP, or is it governed by the ability of the adhesive to transfer shear stresses from the timber into the FRP?

The strength properties of adhesive bonds in shear can be determined using either compression or tension methods. The majority of studies on the bond between timber and fibre composites have involved testing the shear strength of the adhesive through a (modified) compressive method, based on ASTM D905-03 (2003): *Standard Test Method for Strength Properties of Adhesive Bonds in Shear by Compression Loading*.

While ASTM D905-03 (2003) is primarily concerned with obtaining the shear strength of an adhesive, it is arguable that the critical factor in developing reliable bonds in FRP-to-timber composites is to ensure that the failure mode occurs as a wood fibre failure, rather than in the adhesive itself. This would be evident by the proportion of wood on the failure surface – a high amount of wood on the failure surface indicating that the adhesive itself may be less critical than other factors. Given that high proportions of wood failure are desirable, the results of such tests do not necessarily indicate the true value of the shear strength of the adhesive, since ASTM D905-03 specifically notes that wood failure is very common in joints made with strong adhesives, and when high proportions of wood are evident on the failure surface, the measured strength is lower than the true adhesive strength.

Preliminary tests on 10 specimens have been undertaken at UTS using specimens (as indicated in Figure 1) made from the following materials:

- Radiata pine (solid, sawn timber, dressed surface finish)
- ATL type I prefabricated carbon fibre composite
- ATL epoxy “Techniglu CA”

The ATL type I composite carbon fibre, consisted of 2 layers of a 580g/m² unidirectional carbon fibre prepreg plates which, when cured, formed 1.6mm thick carbon fibre laminates. When tested in accordance with the 1995 version of ASTM D3039 (2006) *Standard Test Method for Tensile Properties of Polymer Matrix Composite Materials*, the following properties were obtained from testing of 10 specimens: average ultimate strength 726 MPa, with a coefficient of variation (CoV) of 4.1%; and average Modulus of Elasticity 78,200 MPa with a CoV of 10.3%.

The cut timber and fibre composites were glued together using ATL Techniglu CA epoxy adhesive after the bonding surfaces of both the pine and fibre composites were lightly sanded in accordance with the adhesive manufacturer’s directions. The test specimens were 50mm wide blocks, with a set up similar to that in Figure 1 where the block on the left side is fixed while load is applied to the block on the right side.

Whilst the tests methods used for the determination of strength properties in shear were primarily sourced from the 1994 version of ASTM D905-03 (2003), cross reference was also made to AS1321.3 (1976) *Bond Strength of Cured Wood-to-Wood Adhesives in Shear* and to the block-shear test method specified in the 1987 version of AS1328

(1998) *Glued-Laminated Structural Timber*. The ASTM D905-03 (2003) test method for specimens containing the FRP required some modifications, which was the same as those made by some other researchers testing the interface properties between various timbers and fibre composites (e.g. Davalos et al. 1992).

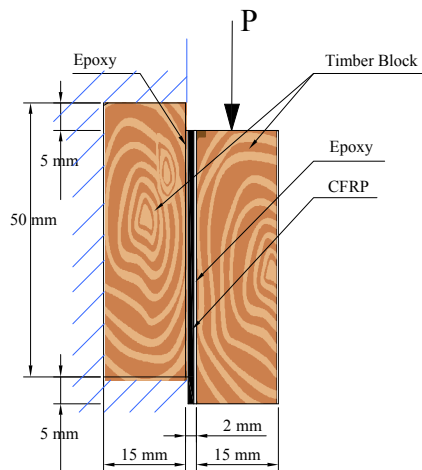


Figure 1. Side elevation of a typical test specimen

Table 1. Test results

Specimen	Ultimate Load (kN)	Shear Stress (MPa)
S03-1	21.1	10.6
S03-2	16.75	8.4
S03-3	10.8	5.4
S03-4	12.2	6.1
S03-5	20.4	10.2
S03-6	20.4	10.2
S03-7	9.0	4.5
S03-8	14.0	7.0
S03-9	16.4	8.2
Average		7.8
Standard Deviation		2.2
CoV (%)		28.4%
5% exceedence		4.9

The purpose of this test is to determine the strength of the adhesive-to-timber interface, assuming that the shear stress is constant throughout the depth of the “glue line”. Whilst some effort was made for the wood specimens to be fabricated so as to avoid significant growth characteristics, such as knots, the inherent variability of timber is still reflected in the test results. This simplification will need to be addressed in future tests with larger pieces of timber that will inevitably include knots, since such a “smeared” average, will not consider the effects of knots. Failure modes can be described as brittle.

4. RESULTS AND DISCUSSION

The results of the preliminary tests are presented in Tables 1 and 2. In Tables 1 and 2, the shear block test result for the FRP-timber specimens are given as well as a typical shear strength of the timber and manufacturers data for the epoxy alone in Table 2. It is evident the shear strength of the timber and epoxy are higher thus leading to failure at the FRP-to-timber interface in the timber.

Table 2. Summary results of shear block tests

Summary	Shear Test Result	Timber	Epoxy
Average Shear Stress (MPa)	7.8	14	10 - 12
Standard Deviation	2.2	1	-
CoV (%)	28%	7.1%	-
5 th Percentile (MPa)	4.9	12.7	-

Failures of the block shear specimens can be characterised into three types of failure: Failure within the glue line, failure within the wood, and failure partly within and partly adjacent to the glue line in the wood. The main type of failure that occurred in these tests was the third one, with a significant proportion of the failure surface showing wood failure. The results of the shear tests indicate that the shear strength of the timber-to-FRP interface is less than the shear strength of the (solid) timber and the epoxy. However, it must be noted that only a very small number of specimens were tested and a far greater number of specimens would need to be tested to report conclusively. Due to the high variability of these test results, conclusions about the shear strength of the bond, in particular whether the bond is likely to be a critical influence on limit state behaviour of reinforced beams, are difficult to draw with confidence based on the small number of specimens tested. However, failure surfaces typically showed greater proportions of wood failure than adhesive failure indicating that the properties of the bond are controlled by the properties of the Pine tested rather than the properties of the adhesive used. Other influences on the results are: surface preparation, knots, and size effects of knots on small test specimen

It should be noted that most glued timber products that are used in high performance structural applications (e.g. plywood, glulam and LVL), rely upon mechanical interlock of the glue with the timber fibres, occurring at a microscopic level. In the manufacture of plywood and LVL the sheets of ply are heated (to activate the resorcinol glue and also soften the timber) and squeezed together under a pressure of 1MPa in order to force the epoxy into the microfibrils of the timber. This results in what is really a mechanical bond, rather than adhesion, between the glue and the timber. Such glue lines tend to be very thin as a result and gap filling glues or epoxies are seldom used in structural applications. Therefore, in applying FRP strengthening to timber, we need to recognize that the same type of structural bond is not possible and as a result the connection is predominantly adhesive rather than mechanical. Furthermore, it is possible that some of the natural growth characteristics of timber, such as knots, may in fact act like aggregate in concrete, and in doing so, create difficulty for the epoxy to penetrate the substrate material. These are all issues that will need to be addressed in future research.

5. FUTURE RESEARCH

Considerably more tests will need to be conducted in the future to systematically characterise the influence of many variables (e.g. species of timber, grade of timber, surface preparation, moisture condition etc) on the FRP-to-timber bond strength. The test set-up outlined in this paper appears adequate for conducting future testing. Ultimately a bond-slip relation of FRP-strengthened timber joints that can be used in numerical simulations is required. Such a relation may be best determined by fitting strain gauges at the epoxy-timber interface. Care must be taken to ensure the strain gauges do not disturb the distribution of bond stresses.

6. REFERENCES

- AS1321.3 (1976). *Methods for the Sampling and Testing of Adhesives - Bond Strength of Cured Wood-to-Wood Adhesives in Shear*. Standards Australia, Homebush, Australia.
- AS1328 (1998). *Glued-Laminated Structural Timber*. Standards Australia, Homebush, Australia.
- ASTM D905-03 (2003). *Standard Test Method for Strength Properties of Adhesive Bonds in Shear by Compression Loading*. American Society for Testing and Materials, Philadelphia, USA.
- ASTM D2559-03 (2003). *Standard Specification for Adhesives for Structural Laminated Wood Products for Use Under Exterior (Wet Use) Exposure Conditions*. American Society for Testing and Materials, Philadelphia, USA.
- ASTM D3039 (2006). *Standard Test Method for Tensile Properties of Polymer Matrix Composite Materials*. American Society for Testing and Materials, Philadelphia, USA.
- Chajes, M.J., Kaliakin, V.N. and Meyer, A.J. Jr. (1996). "Behaviour of engineered wood-CFRP beams". *Proc., First International Conference on Composites in Infrastructure, ICCI'96*, Arizona, USA, 15-17 January.
- Dagher, H.J. (2005). "Current state of reinforced wood technology: New products, codes and specifications". *Proc., Third International Conference Advanced Engineered Wood Composites*, Maine, USA, 10-14 July.
- Davalos, J.F., Salim, H.A. and Munipalle, U. (1992). "Glulam-GFRP composite beams for stress-laminated T-system bridges". *Proc., Advanced Composite Materials in Bridges and Structures*, Eds. Neale and Labossiere, Canadian Society for Civil Engineering, Sherbrooke, Canada.
- Gilfillan, J.R., Gilbert, S.G. and Patrick, G.R.H. (2004). "Improving the structural performance of timber beams with FRP composites: a review", *Proc., FRP Composites in Civil Engineering, CICE 2004*, Ed. R. Seracino, Adelaide, Australia, 8-10 December, pp. 705-711.
- Greenland, A.G., Crews, K.I. and Bakoss, S.L. (1999). "Enhancing timber structures with advanced fibre reinforced plastic composite reinforcements". *Journal of Structural Engineering, Engineers Australia*, Vol. SE2, No. 2 & 3.
- Greenland, A.G. (2001). *Applications Of Advanced Fibre Reinforced Plastic Composites To Engineered Timber Structures*. Master of Engineering Thesis, University of Technology Sydney, Australia.
- Meier, U. (1995). "Strengthening of structures using carbon fibre / epoxy composites". *Construction and Building Materials*, Vol. 9, No. 6, pp. 341-351.
- Milner, H.R. (1999). "Reinforced glulam". *Proc., ACUN-1 International Composites Meeting - Composites: Innovations and Structural Applications*, University of New South Wales, Sydney, Australia, 23-25 February
- Tingley, D.A. and Cegelka, S. (1996). "High-strength-fibre-reinforced-plastic reinforced wood". *Proc., International Wood Engineering Conference*, New Orleans, USA, 28-31 October, Vol. 3 pp. 3-57 to 3-66.
- Vick, C.B. (1997). "More durable epoxy bonds to wood with hydroxymethylated resorcinol coupling agent". *Adhesives Age*, Vol. 40, No. 8, pp. 24-29.

RECENT DEVELOPMENTS ON THE USE OF INORGANIC POLYMER FOR HIGH TEMPERATURE / HIGH STRENGTH COMPOSITES

James W. Giancaspro, Ph.D.
(Assistant Professor, University of Miami, Coral Gables, FL, USA)

P. N. Balaguru, Ph.D.
(Program Director, National Science Foundation, Washington D.C., USA)

ABSTRACT

Composite materials have become commonplace in the civil engineering community over the past decade. Typically, organic polymers are used as the matrix for binding the high strength fibers and the composite to other structural materials such as concrete, brick, and wood. High temperature resistance is one concern in using organic matrices, especially for structures that could possibly be exposed to fire. The results reported in this paper deal with the use of an inorganic polymer matrix for both making composite plates and strength/stiffness enhancement of structural materials. The room-temperature curing matrix, called Geopolymer, can resist temperatures up to 1000°C. Several applications of this polymer, including its use in strengthening reinforced concrete and wood beams, as well as its performance after high-temperature exposure are summarized in this paper.

KEYWORDS

Concrete, Fire Protection, High-Temperature, Inorganic, Wood

1. INTRODUCTION

When high service temperatures are expected, composites made using inorganic matrices can be utilized. One such resin is Geopolymer, a member of the Polysialate family of inorganic matrices known for their low curing temperatures, high temperature resistance, and low cost. Geopolymer is a two-part system consisting of an alumina liquid and a silica powder that cures at a reasonably low temperature of 150°C (302°F). In addition, hardeners can be added to facilitate room temperature curing. Once cured, the matrix can withstand temperatures up to 1000°C without producing smoke. Geopolymer matrix composites have excellent potential in many applications where high-use temperatures are anticipated such as engine exhaust systems, or where fire safety is a critical design parameter such as in aircraft or high-rise buildings. It is compatible with carbon, glass, Kevlar[®], steel, cellulose materials such as wood, and a host of other inorganic materials such as clay bricks and concrete (Lyon, et al., 1997).

Processing requirements and mechanical properties of carbon/carbon composites, ceramic matrix composites made with silicon carbide, silicon nitride and alumina fibers, and carbon/Geopolymer composites were compiled by Papakonstantinou et al. to study the relative performance of Geopolymer composites. The extensive and in-depth study yielded promising results that indicate that carbon/Geopolymer composites have mechanical properties that are better than most fire-resistant composites (Papakonstantinou et al., 2001).

The effectiveness of Geopolymer has been demonstrated successfully in a number of civil engineering applications including high-temperature resistant composite panels and strengthening of beams made from reinforced concrete and timber. Each of these applications is described briefly in the following sections.

2. HIGH-TEMPERATURE EXPOSURE

A considerable amount of testing has been carried out to evaluate polysialate matrix composites for mechanical properties, behavior after high temperature exposure, and durability under various exposure conditions (Foden, 1999; Lyon et al., 1997, Hammell, 2000). In this research program, the effect of temperature exposure on the mechanical properties of Geopolymer composites was investigated. Carbon composite plates were fabricated using the procedure and equipment that are utilized for organic composites. Hence, economical, commercially available fabrication equipment and knowledge such as vacuum assisted impregnation can be utilized for composites made with polysialates. Once cured, the plates were cut with a diamond blade saw to yield composite specimens about 120-mm in length, 12-mm in width, and a thickness of either 3- or 6-mm depending on the number of plies used. Three-point flexure tests on the composite specimens were conducted over a simply supported span of 100 mm with a central load. The load-deflection responses were obtained for virgin samples and samples exposed to 200°, 400°, 600°, and 800°C for one hour in a furnace. Examination of the test results in Figure 1 reveals that even after one hour of exposure to 800°C, the polysialate composite retains 63% of its original load carrying capacity.

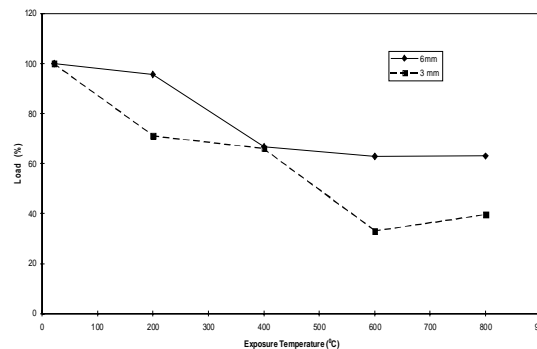


Figure 1: Residual Flexural Strength After Temperature Exposure for 3- and 6-mm Thick Specimens

3. STRENGTHENING OF REINFORCED CONCRETE BEAMS

The focus of this investigation was to compare the behavior of the inorganic matrix that is brittle to a ductile organic matrix when used to bond carbon fiber sheets to reinforced concrete beams. The experimental program consisted of strengthening four reinforced concrete beams using the inorganic carbon composite (Kurtz and Balaguru, 2001). All four beams were tested as simply supported beams under four-point flexure loading conditions. This experimental study simulated an earlier study in which beams were strengthened in the same way using an organic matrix. The results from both programs were then examined to compare the performance of the two types of matrices. The primary response variables used for comparison included:

- Differences in failure mode
- Magnitude of strength increase over their respective controls
- Magnitude of stiffness increase over their respective controls
- Deflection and ductility
- Crack patterns

The normalized load-deflection curves for all beams are shown in Figure 2. From these curves, it can be seen that the load-deflection behavior of beams strengthened with inorganic matrix are similar to the beam strengthened with organic matrix. The beams IS3 and OS, with about the same carbon fiber areas, had comparable strength, stiffness, and ductility.

The results indicated that the inorganic matrix is just as effective in increasing the strength and stiffness of reinforced concrete beams as the organic matrix, with a minor reduction in ductility. The failure mechanism changed from sheet delamination for the organic system to sheet rupture for the inorganic system. This change in mechanism is attributed to the brittleness of the inorganic matrix that results in crack formation in the composite and a minimum build-up of strain along the interface of the composite and concrete.

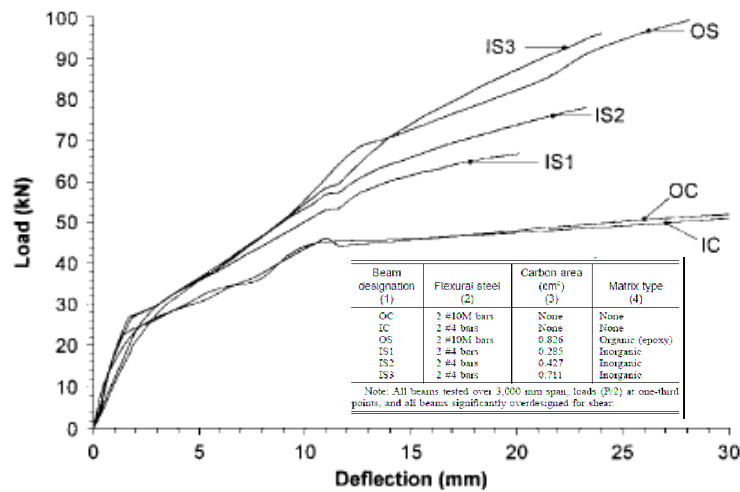


Figure 2: Comparison of Load-Deflection Response for Beams Reinforced with Inorganic and Organic Composite

4. STRENGTHENING OF WOOD BEAMS

Currently, high strength carbon and glass composites are being used to strengthen timber beams and to fabricate sandwich panels with high specific strengths. Organic polymers are typically used as the matrix for binding the fabrics and adhesion to wood. Unfortunately, organic matrices are often flammable and leave wooden structural elements susceptible to rapid damage and collapse in the event of a fire. In this study, structural sandwich beams were fabricated using the inorganic matrix. Carbon and glass fiber facings were laminated onto end-grain balsa wood and oak beams and tested in flexure to examine the effect of density on the mechanical properties of the resultant sandwich beam. The primary variables investigated were:

- Density of core material – balsa (56 to 163 kg/m³) and oak (560 to 826 kg/m³)
- Beam thickness – four depths of 6, 13, 19, and 25 mm (1/4, 1/2, 3/4, and 1 in.)
- Type of reinforcement – 12k high modulus carbon tows (640 GPa), woven carbon fabric with glass in the fill direction made using 3k tows, unidirectional carbon tape made using 3k tows, and 2k alkali-resistant glass (AR-Glass) tows
- Amount of reinforcement – between zero and four carbon tows; one or two woven carbon tapes; one or two unidirectional carbon tapes; zero, four, or eight AR-Glass tows
- Location of reinforcement – only on the tension face (T) or on both the tension and compression faces (T,C)

One hundred and thirty beams were tested in flexure to determine the load-deflection response of these sandwich beams. Typical load-deflection responses are presented in Figure 3. The beams were analyzed as reinforced wood beams using the concepts of composite action and flexure theory for linearly elastic and elastic-plastic materials. The influence of density on flexural strength, stiffness, toughness, and specific strength were also evaluated. Using the results from the flexure tests, a number of interesting observations were made. First, it was found that lower density cores provided better performance and exhibited the largest increases in most categories. Flexural theory using linear elastic material behavior provides good prediction in the linear range. However, non-linear analysis is needed to predict the strength accurately. As the wood density reduces, the shear stiffness plays a major role in the failure mechanism. No delamination failures were present, as the bond between the inorganic carbon composite and both types of wood cores is strong enough to prevent delamination.

The reinforced balsa beams displayed significantly higher increases in stiffness and toughness than the strengthened oak beams. The flexural strength of the plain wood cores is strongly related to the density and the strength can be predicted very well with a simple linear regression model. In general, there is no linear relationship between maximum capacity and density. Similarly, a linear relationship does not exist between deflection at maximum load and density for the strengthened beams.

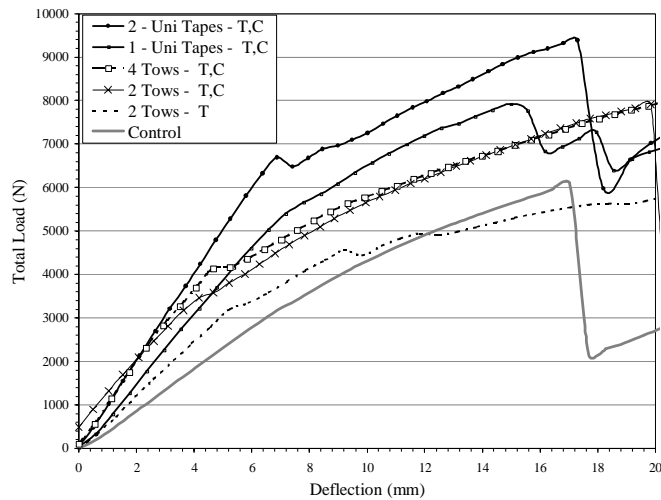


Figure 3: Load-Deflection Response for Oak Beams (25mm Thick x 64mm Width) Reinforced with Carbon

5. CONCLUSIONS

Using the analysis of the results presented in the aforementioned studies, the following conclusions can be drawn.

- The Geopolymer composite system is viable in terms of composite fabrication and the bonding the system to common construction materials.
- The matrix also protects fire susceptible materials. For example, after 1 hour of heat exposure at 800°C, the residual flexural strength of a Geopolymer-carbon composite decreased only by 37%. Note that carbon fibers start to oxidize at 400°C.
- Reinforced concrete beams strengthened using inorganic composite behave similar to those beams strengthened with organic composite. The major difference is that none of the beams strengthened with inorganic-polymer composites failed by delamination of composite.
- As expected, the strengthening system is more effective for weak wood such as balsa, as compared to strong wood such as oak.

6. REFERENCES

- Foden, A. J. (1999). "Mechanical properties and material characterization of Polysialate structural composites." Ph.D. Thesis, Rutgers, the State University of New Jersey, USA.
- Hammell, J. A. (2000). "The influence of matrix composition and reinforcement type on the properties of polysialate composites." Ph.D. Thesis, Rutgers, the State University of New Jersey, USA.
- Kurtz, S., and Balaguru, P.N. (2001). "Comparison of Inorganic and Organic Matrices for Strengthening of RC Beams with Carbon Sheets," *Journal of Structural Engineering*, January, 35-42.
- Lyon, R.E., Balaguru, P., Foden, A.J., Sorathia, U., and Davidovits, J. (1997). "Fire-resistant aluminosilicate composites." *Fire and Materials*, 21, 61-73.
- Papakonstantinou, CG, Balaguru, PN, and Lyon, RE, (2001). "Comparative study of high-temperature composites," *Composites Part B: Engineering*, 32(8), 637-49.

INFLUENCE OF FATIGUE AND AGGRESSIVE ENVIRONMENT ON THE PERFORMANCE OF RC BEAMS REINFORCED WITH CFRP MATERIALS

Marco Arduini

CEO - Co-Force s.r.l. – via Pindemonte, 16 – 42100 Reggio Emilia – Italy

Mariano Romagnolo

Autostrade S.p.A. – via Bergamini, 50 – Roma – Italy

Antonio Nanni

Prof. and Chair Dept. Civil, Arch. & Environ. Eng., University of Miami – Miami – USA – nanni@miami.edu

ABSTRACT

The strengthening of RC beams with CFRP laminates has been extensively studied, and design recommendations have been published in many countries (ACI 440, CNR-DT200, CEB-FIP 01, etc.). Few data are available for Near Surface Mounted (NSM) FRP strengthening techniques or for concrete beams that are repaired first using cementitious mortars and then reinforced with FRP materials.

A specific experimental campaign, with more than 200 beams, has been carried out to investigate many factors that can affect design in the common practice, such as concrete compressive strength, concrete fracture energy, FRP reinforcement ratio, FRP type, repair technique (plating, NSM, new concrete cover), fatigue, and aggressive environment. Tests on 4-point bending showed the good performance of FRP strengthening, as the minimum increment in peak bending load was 110 percent, and the maximum was 430 percent. The influence of fatigue, if the peak cyclic load is kept below 30 percent of ultimate quasi-static load, is negligible in the overall performance. Saltwater contact and temperature variation have a more significant effect in reducing ultimate capacity, especially because the internal steel reinforcement corrodes, and the interface adhesion strength degrades. The effect of concrete cover replacement was also investigated—the influence of high strength shrinkage-compensated cementitious mortar is negligible because the interface adhesion with the original concrete is similar to the epoxy-concrete adhesion. Moreover, the internal steel reinforcement is protected against aggressive environments.

KEYWORDS

CFRP laminates, CFRP rods, experimental results, Near Surface Mounted, plating, repair mortar

1. INTRODUCTION

The strengthening of reinforced and prestressed concrete (RC and PC) beams with FRP laminates applied by manual lay-up has been studied and reported in recent years and now has become accepted worldwide. Many tests have been reported using laboratory experimentation.

In practice, the FRP reinforcement can be applied on very old beams, for example, with concrete covers that are degraded or in very poor condition. Sometimes, the concrete cover is so degraded that it is removed, internal steel rebars are sandblasted, and new cementitious mortar is applied to recreate the alkaline environment around the steel rebars. After the curing of the mortar, FRP reinforcement is applied to upgrade the load capacity. In this case, two potential interface failures can develop—between FRP and the new mortar and between the new mortar and the original concrete. Conversely, precast PC beams are generally made with high strength concrete C50 to C70, and surfaces are smooth and pore-free because of the high amount of mold-releasing agents. In this case, FRP must be attached to the surface after a thorough sandblasting; otherwise, delamination can occur because the resin cannot penetrate into the concrete surface. In a sense, strengthening a low-quality concrete member is easier because of the ease in opening micro-pores during sandblasting.

2. EXPERIMENTAL CAMPAIGN

The experimental campaign takes into account four different strengthening technologies:

- **Type P:** CFRP plating using epoxy resin in the tensile face of the concrete beam;
- **Type C+P:** concrete cover replacement and adhesion of CFRP laminates;
- **Type NSM:** grooving of the concrete cover, application of epoxy resin, and embedment of CFRP rods (NSM technique); and
- **Type INT:** concrete cover replacement and embedment of NSM CFRP rods in the new mortar.

The campaign can be divided in three parts:

- **Part A:** 42 groups of beams were prepared, cured in a lab environment for 2 months, and then tested to failure without any preliminary type of degradation (Arduini et al. 2004);
- **Part B:** 34 groups of beams were prepared, cured in a lab environment for 2 months, subjected at 10,000 cycles under a 4-point bending configuration, and then tested to failure; and
- **Part C:** 35 groups of beams were prepared, cured in a lab environment for 2 months, placed in an aggressive environment for one year, and then tested to failure.

Concrete, steel reinforcing bars, and CFRP laminates used in this research program had mean and characteristic properties as reported in Table 1. Symbols used in Table 1 represent the following:

- SFR: cementitious mortars + short hooked steel fibers (7 percent by weight of dry mix, $L=3\text{cm}$);
- f_{ck} and f_b : cylinder characteristic compressive strength and splitting mean strength, respectively; and
- G_f and E_{ci} : fracture energy according to Rilem TC50-FMC and characteristic initial elastic tangent modulus.

The CFRP sheets were 300 gr/m^2 unidirectional sheets. The generic characteristic value, f_k , is related to mean value, f_m , obtained in the experimental campaign using the formula $f_k=f_m-\alpha\text{ std}$, where std represents the standard deviation, $\alpha=1.4$ for steel and concrete, and $\alpha=3$ for CFRP materials (according to ACI 440-2).

Four-point bending tests under a quasi-static load were carried out on 1-m clear span. Five progressive cycles were applied according to the following steps: at first visible crack, 30 percent of steel yield, 70 percent of steel yield, at steel yield, and around 1.3 steel yield. Two LT transducers provided the mid-span deflection, and strain gauges were mounted on concrete in the compressive zone, on tensile steel reinforcement, and on the CFRP sheets at the mid-span section. Concrete beams had a 2 cm concrete cover and 10 stirrups, 6 mm in diameter and equally spaced to avoid shear failure.

Table 2 presents all relevant information related to specimen characteristics of Part B. The first column shows the group name, which is a combination of the following parameters:

- Type of concrete used to cast the beam—C20 means that the concrete cylinder characteristic compressive strength = 20 MPa
- Reinforcement configuration: SAB means sand blasting (Type P), TIXO and S1 mean new concrete cover using high strength shrinkage compensated cementitious mortars (Type INT or Type C+P), SFR means high strength shrinkage compensated high ductility concrete, and TAS means NSM reinforcement;
- Type of reinforcement used: 1C5 means 1 layer of high modulus 300 gr/m^2 unidirectional carbon fiber sheet named C5-30 according to Table 1, 1B7 means 1 pultruded CFRP bar 7.5 mm in nominal diameter, and LAM means a smooth pultruded CFRP lamina; and
- The number and the diameter of internal steel rebars: 2F6 means 2 steel rebars, 6 mm in diameter.

The second column shows the number of samples tested. The following two columns show tensile reinforcement characteristics, such as steel tensile reinforcement ratio (ρ_s), defined as the steel area divided by the product of concrete cross-section width and steel reinforcement depth ($A_s/(bd)$), and the FRP reinforcement ratio (ρ_f), defined as the CFRP area divided by the product of concrete cross-section width and steel reinforcement depth ($A_s/(bd)$). The fifth column reports the FRP reinforcement dimensions, and the sixth column indicates the type of FRP reinforcement adopted. The seventh column describes the type of cementitious mortar used to replace the original bottom concrete cover. The last three columns summarize the main experimental results obtained from 4-point bending tests in terms of maximum total applied load F_{max} , mid-span deflection at failure δ_{max} , and mode of failure as visually observed during the test. Five different failure modes were observed, as shown in Figure 1.

To observe the influence of fatigue loads on bending capacity of strengthened RC beams, some groups of samples were duplicated and subjected to 10,000 bending cycles. The minimum load was kept constant to 0.5 tons, and the maximum load was fixed equal to 1/3 of F_{max} reported in Table 2 for each group of similar specimens. The frequency was kept constant equal to 1Hz. After the cyclic conditioning, beams were tested to failure. Table 2 summarizes the main experimental results as obtained. To observe the influence of aggressive environment on bending capacity of strengthened RC beams, some groups of samples of Part A were duplicated and subjected to one-year exposure to sea water and external temperature variation (from -10°C to $+45^\circ\text{C}$). The sea water level was monitored every week to guarantee that the tensile face of the beam was partially immersed in the water (water edge

condition). CFRP sheets were not protected by UV coating to facilitate the interface degradation. After the natural external exposure, beams were subjected to an additional 20 cycles in climatic chamber from -10°C to +55°C over a 10-day period of time, and then tested in bending to failure. Table 3 summarizes the main experimental results obtained.

Table 1: Mechanical characteristic properties of constituents

Concrete Type	f_{ck} MPa	f_b MPa	G_f N*m/m ²	$E_{ci}^{(3)}$ GPa	Reinforcement	Diameter or thickness mm	f_{tk} MPa	E_f GPa	ϵ_u %
SFR	53	3.6	6760	28.3	CFRP 7-Rod	7.5	1704	197	0.9
C63	63	3.8	130	33.7	CFRP 12-Rod	12	1194	130	1.0
C40	40	3.7	N/A	46.2	CFRP-Laminate	25 x 1.4	2650	160	1.6
C33	33	3.5	N/A	40.9	C5-30- sheet	0.165	2560	400	0.7
C20	20	2.8	N/A	33.8	AM- sheet	0.165	2961	404	1.0
TIXO ⁽¹⁾	58	2.5	149	27.0	Steel rods	6	534 ⁽⁴⁾	200	N/A
S1 ⁽²⁾	58	2.8	752	25.0					

Table 2: Part B (preliminary fatigue cycles)

Group Name	N ^o	ρ_s %	ρ_f %	CFRP type and dimension	Reinf. Type	Mortar type	F_{max} [kN]	δ_{max} [mm]	Failure mode
C20-SAB-1C5	2	0.23	0.07	1 layer 0.1x1m C5-30	P	NO	34.6	9.0	FRP rupture
C60-SAB-1C5	2	0.23	0.07	1 layer 0.1x1m C5-30	P	NO	35.9	7.6	FRP rupture
SFR-SAB-1C5	2	0.23	0.07	1 layer 0.1x1m C5-30	P	NO	48.6	9.1	FRP rupture
C20-SAB-1AM	1	0.23	0.07	1 layer 0.1x1m AM	P	NO	39.3	13.3	Peeling + crushing
C60-SAB-1AM	1	0.23	0.07	1 layer 0.1x1m AM	P	NO	30.0	6.6	Peeling
SFR-SAB-1AM	1	0.23	0.07	1 layer 0.1x1m AM	P	NO	47.6	11.8	Peeling + crushing
C20-SAB-3C5	2	0.23	0.21	3 layers 0.1x1m C5-30	P	NO	45.9	5.7	Peeling
C60-SAB-3C5	2	0.23	0.21	3 layers 0.1x1m C5-30	P	NO	55.6	6.0	Peeling
SFR-SAB-3C5	2	0.23	0.21	3 layers 0.1x1m C5-30	P	NO	72.7	8.2	Peeling
C20-SAB-3AM	1	0.23	0.21	3 layers 0.1x1m AM	P	NO	44.3	6.1	Peeling + crushing
C60-SAB-3AM	1	0.23	0.21	3 layers 0.1x1m AM	P	NO	60.3	7.3	Peeling
SFR-SAB-3AM	1	0.23	0.21	3 layers 0.1x1m AM	P	NO	64.1	7.7	Peeling
C20-TIXO-1C5	3	0.23	0.07	1 layer 0.1x1m C5-30	C+P	Tixo 3cm	34.4	7.0	FRP rupture
C60-TIXO-1C5	3	0.23	0.07	1 layer 0.1x1m C5-30	C+P	Tixo 3cm	35.9	7.1	FRP rupture
C33-S1-1C5	3	0.23	0.07	1 layer 0.1x1m C5-30	C+P	S1 3cm	37.5	8.7	Delamin.+FRP rupture
C60-S1-1C5	3	0.23	0.07	1 layer 0.1x1m C5-30	C+P	S1 3cm	36.4	7.1	Peeling
C33-NOR-1C5	2	0.23	0.07	1 layer 0.1x1m C5-30	C+P	NOR 3cm	34.0	7.4	FRP rupture
C60-TAS-1B7	2	0.23	0.21	1 Mbar ϕ 8 L=1.0m	NSM	Putty	59.1	20.1	crushing + Rod slippage
SFR-TAS-1B7	2	0.23	0.21	1 Mbar ϕ 8 L=1.0m	NSM	Putty	55.4	14.2	crushing + Rod slippage
C20-TAS-LAM	1	0.23	0.15	1/2 Laminate L=1.0m	NSM	Putty	33.2	10.2	crushing + Rod slippage
C60-TAS-LAM	1	0.23	0.15	1/2 Laminate L=1.0m	NSM	Putty	40.0	11.0	Laminate slippage
SFR-TAS-1B12	1	0.23	0.47	1 Mbar ϕ 12 L=1.0m	NSM	Putty	65.9	10.2	crushing + Rod slippage
C20-TIXOF-1B7	2	0.23	0.19	1 Mbar ϕ 8 L=1.0m	INT	Tixo 3cm	39.0	11.9	crushing + Rod slippage
C33-S1-1B7	2	0.23	0.19	1 Mbar ϕ 8 L=1.0m	INT	S1 3cm	43.0	12.5	crushing + Rod slippage
C60-TIXO-3B7	2	0.23	0.58	3 Mbar ϕ 8 L=1.0m	INT	Tixo 3cm	68.0	7.1	Mortar delamination
C60-S1-3B7	2	0.23	0.58	3 Mbar ϕ 8 L=1.0m	INT	S1 3cm	68.5	8.4	Mortar delamination
C33-TIXO-1B12	1	0.23	0.43	1 Mbar ϕ 12 L=1.0m	INT	Tixo 3cm	52.1	7.9	Rod slippage
C33-S1-1B12	1	0.23	0.43	1 Mbar ϕ 12 L=1.0m	INT	S1 3cm	50.8	9.1	Rod slippage

3. CONCLUSIONS

An experimental program consisting of more than 200 RC beams strengthened with external CFRP sheets or NSM CFRP rods was presented. Different types of concrete, FRP, and concrete over rehabilitation mortar were taken into account together with fatigue to show an environmental attack.

Experimental data shows good performance of the strengthening, and the minimum increment in peak bending load was 110 percent, while the maximum was 430 percent. The influence of fatigue, if the peak cyclic load is kept below 30 percent of ultimate load, is negligible in the final overall performance. Salt water contact and temperature variation have a more significant effect in reducing ultimate capacity, especially because the internal steel

reinforcement can corrode together with the degradation of the interface adhesion. The effect of concrete cover replacement was also investigated. The influence of the cementitious mortar layer is negligible because the interface adhesion with concrete is similar to the epoxy-concrete adhesion.

In design guidelines, the safety factor should not be related to FRP properties only, but needs to be calibrated on the interface adhesion properties and related to concrete properties.



Figure 1 – Different failure modes

Table 3: Part C (one year aggressive environment)

Name	N ^o	ρ_s %	ρ_f %	CFRP type and dimension	Reinf. Type	Mortar type	F _{max} [kN]	δ_{max} [mm]	Failure mode
C20-SAB-1C5	2	0.23	0.07	1 layer 0.1x1m C5-30	P	NO	30.3	6.8	Delamin.+FRP rupture
C60-SAB-1C5	2	0.23	0.07	1 layer 0.1x1m C5-30	P	NO	24.5	4.3	Delamination
SFR-SAB-1C5	2	0.23	0.07	1 layer 0.1x1m C5-30	P	NO	42.8	6.9	Delamin.+FRP rupture
C20-SAB-1AM	1	0.23	0.07	1 layer 0.1x1m AM	P	NO	33.2	9.5	Delamination
C60-SAB-1AM	1	0.23	0.07	1 layer 0.1x1m AM	P	NO	28.5	5.4	Delamination
SFR-SAB-1AM	1	0.23	0.07	1 layer 0.1x1m AM	P	NO	40.0	6.5	Delamination
C20-SAB-3C5	2	0.23	0.21	3 layers 0.1x1m C5-30	P	NO	28.2	3.2	Peeling
C60-SAB-3C5	2	0.23	0.21	3 layers 0.1x1m C5-30	P	NO	61.7	6.0	Peeling
SFR-SAB-3C5	2	0.23	0.21	3 layers 0.1x1m C5-30	P	NO	43.9	8.2	Peeling+FRP rupture
C60-SAB-3AM	1	0.23	0.21	3 layers 0.1x1m AM	P	NO	46.6	4.7	Peeling
SFR-SAB-3AM	1	0.23	0.21	3 layers 0.1x1m AM	P	NO	61.4	7.2	Peeling
C20-TIXO-1C5	3	0.23	0.07	1 layer 0.1x1m C5-30	C+P	Tixo 3cm	34.8	7.8	FRP rupture
C60-TIXO-1C5	3	0.23	0.07	1 layer 0.1x1m C5-30	C+P	Tixo 3cm	35.8	6.6	FRP rupture
C33-S1-1C5	3	0.23	0.07	1 layer 0.1x1m C5-30	C+P	S1 3cm	38.9	8.9	FRP rupture
C60-S1-1C5	3	0.23	0.07	1 layer 0.1x1m C5-30	C+P	S1 3cm	34.3	5.5	FRP rupture
C33-NOR-1C5	2	0.23	0.07	1 layer 0.1x1m C5-30	C+P	NOR 3m	32.9	7.3	FRP rupture
C20-TAS-1B7	2	0.23	0.21	1rod ϕ 8 L=1.0m	NSM	Putty	42.6	16.5	crushing + Rod slippage
C60-TAS-1B7	2	0.23	0.21	1rod ϕ 8 L=1.0m	NSM	Putty	61.1	19.8	crushing
SFR-TAS-1B7	2	0.23	0.21	1 rod ϕ 8 L=1.0m	NSM	Putty	55.1	15.5	crushing + Rod slippage
C20-TAS-LAM	1	0.23	0.15	1Lam25x1.4mmL=1m	NSM	Putty	34.5	16.8	crushing
C60-TAS-LAM	1	0.23	0.15	1Lam25x1.4mmL=1m	NSM	Putty	30.3	6.8	Laminate slippage
SFR-TAS-1B12	1	0.23	0.47	1rod ϕ 12 L=1.0m	NSM	Putty	53.9	7.3	Rod slippage
C20-TIXO-1B7	2	0.23	0.19	1rod ϕ 8 L=1.0m	INT	Tixo 3cm	41.6	14.4	crushing + Rod slippage
C33-S1-1B7	2	0.23	0.19	1rod ϕ 8 L=1.0m	INT	S13cm	44.8	13.1	Rod slippage
C60-TIXO-3B7	2	0.23	0.58	3rods ϕ 8 L=1.0m	INT	Tixo 3cm	64.8	7.7	Rod slippage
C60-S1-3B7	2	0.23	0.58	3rods ϕ 8 L=1.0m	INT	S1 3cm	75.44	7.8	Mortar delamination
C33-TIXO-1B12	1	0.23	0.43	1rod ϕ 12 L=1.0m	INT	Tixo 3cm	55.6	8.0	Rod slippage
C33-S1-1B12	1	0.23	0.43	1rod ϕ 12 L=1.0m	INT	S1 3cm	55.9	10.0	Rod slippage

4. REFERENCES

Arduini M., Romagnolo M., and Nanni A., (2004). "Influence of concrete quality on the performance of FRP strengthened RC beams: Experiments". Proc. 4th International Conference on Advanced Composite Materials in Bridges and Structures, Calgary, Alberta, 20-23, 2004.

BOND STRENGTH OF CARBON FIBER REINFORCED POLYMERS ON CONCRETE AND MASONRY

Umit Serdar Camli

(Graduate Student, Middle East Technical University, Ankara, Turkey)

Baris Binici

(Assistant Professor, Middle East Technical University, Ankara, Turkey)

ABSTRACT

This study presents the results of an experimental program conducted to determine the strength of carbon fiber reinforced polymers (CFRPs) bonded to low and normal compressive strength concrete and masonry units that are finished with or without plaster. In the experimental program, a total of 51 specimens with different types of anchorages (strip and embedded anchors) were tested. Test results showed that ultimate strength of CFRPs bonded to plaster finished specimens were significantly lower than those without plaster finish. It was found that ultimate strength of surface bonded CFRPs with the use of embedment at the free end and FRP dowels that act as shear connectors can result in strength enhancements as high as three times of those without any special anchorage. Based on slip measurements, a simple and effective strength model is calibrated and proposed for strip type anchorages.

KEYWORDS

bond strength, concrete, masonry, plaster

1. INTRODUCTION

Widespread utilization of FRPs has started in Turkey for seismic and non-seismic retrofit applications (i.e. strengthening of beams and columns for shear and in and out of plane strengthening of masonry infill panels with surface bonded FRPs). Furthermore a significant increase in FRP applications is expected in the upcoming years as a result of the introduction of FRP retrofit design guidelines in the draft version of the Turkish Seismic Code. Although use of FRPs are promising due to their advantages such as being light weight, high strength and easy to apply, a number of additional parameters require further investigation for their successful use in certain countries depending on the construction practice. For example, plaster finishing on concrete structural elements and masonry infill panels are commonly used in Turkey and special attention is needed when designing and bonding FRPs. Furthermore, low concrete strength (10 to 15 MPa) that may be observed in some of the deficient structural elements has the potential to adversely affect the success of the FRP retrofit. In addition, application of FRPs in retrofit of masonry infill walls to strengthen in and out of plane resistance necessitates knowing the bond strength of FRP to masonry, generally in the form of hollow clay tiles.

The objective of this paper to examine the strength of CFRPs bonded to low strength concrete and masonry finished with and without plaster. In addition, embedded type anchors are investigated, which can have the potential to enhance strength of surface bonded FRPs to concrete. To achieve this objective, an extensive experimental program was conducted. Based on the results of experiments, a simple analytical model calibrated using experimental results is proposed.

2. EXPERIMENTAL PROGRAM

A simple test setup that was successfully used in previous studies (Binici and Bayrak 2004, Dolan et. al. 1998) to examine bond strength of CFRP bonded to concrete was employed. Sideway and plan views of the experimental setup is shown in Figure 1. The test specimens were built by bonding two symmetrically located CFRP laminates horizontally along the center line of two similar concrete prisms or masonry, referred hereafter as hollow clay tile

(HCT). Load was applied using a hydraulic jack through the centerline of two prisms such that two blocks are pushed against each other while imposing shear stresses at the CFRP-block interfaces. Two steel plates were located on loading faces of the specimens to avoid local failures of the specimens and to distribute stresses uniformly. Special attention was given to eliminate any possible eccentricities on CFRP laminates that could cause premature failures. Displacements were continuously monitored using four dial gages that were located at the outer edges of the blocks as shown in Figure 1.

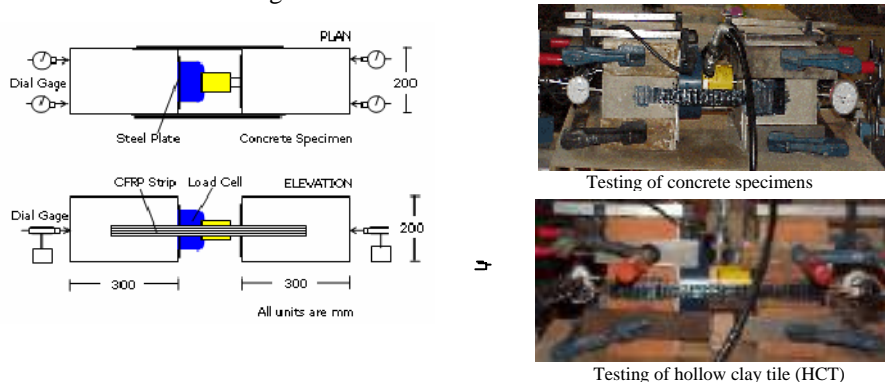


Figure.1 Test Setup

For low strength concrete, target compressive strength was 10 MPa, whereas for normal strength concrete, target uniaxial compressive strength of 30MPa was employed. The uniaxial compressive strength was found as 6 MPa considering the gross area of HCTs. Carbon fiber reinforced polymers (CFRPs) have been used throughout the test program. The ultimate tensile strength of CFRP having a thickness of 0.165 mm was 3430 MPa with a rupture strain of 0.015 according to manufacturer's report.

Prior to application of the CFRPs, surfaces of concrete, HCT blocks, or plaster finished surfaces were cleaned from dust by air-blowing. Then, CFRP sheets, cut to predetermined length and width, were impregnated into epoxy resin and bonded on the sides of the blocks. Wooden plywood sheets covered with plastic nylon were attached and C-clamps were used to keep the CFRP sheets in correct position while curing of the epoxy. After curing of epoxy, wooden blocks were removed and testing equipment was attached without moving the specimens.

Three types of CFRP application details that were used for the test specimens are shown in Figure 2. For strip anchors, CFRP sheets were bonded to the sides of concrete or masonry blocks without any special attachment detail (Figure 2a). For embedded anchors, different details were used for concrete and HCT units. In concrete specimens, free end of the CFRP was embedded in a hole drilled in concrete prisms (Figure 2b). For hollow clay tile applications, it was aimed to attach CFRP dowels as shear connectors to arrest the CFRP debonding process. CFRP anchor dowels were prepared by rolling CFRP sheets around a steel wire and impregnating them into epoxy (Figure 2c). These CFRP dowels were then passed through the predrilled holes and fanned out on the CFRP strips. The effect of embedment depth for concrete specimens and number of CFRP dowels hollow clay tiles were taken as test parameters to observe the enhancement of bond strength for CFRP-adherent interface. In the experimental program, 51 double shear push out tests were performed to systematically investigate the effect of parameters, such as strength of the concrete prisms or HCTs (f_c), presence of plaster, CFRP width (b_{fcp}), CFRP bond length (L_{fcp}), embedment depth (d_{fcp}), anchor type (strip, and embedded anchors).

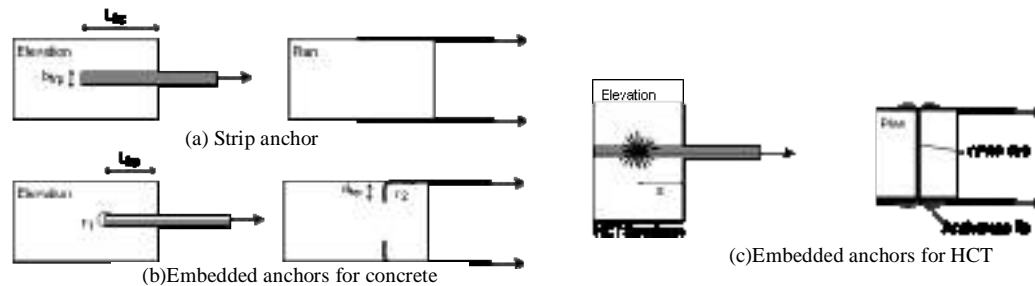


Figure 2. Anchorage types used in the experimental program

3. TEST RESULTS

The summary of experimental results in the form of normalized strength (P_{test}/P_{frp} where P_{frp} is the uniaxial tensile strength of bonded CFRP sheet) versus bond length are presented in Figure 3. Results of strip anchor tests showed that with increasing bonded length, L_{frp} , load carrying capacity increased up to a certain length (~100 mm) beyond which no strength enhancement occurs. The corresponding maximum strength was found as 40% and 34% of the uniaxial load carrying capacity of the CFRPs for 25 mm and 50 mm wide strips, respectively. From this group of tests, it was evident that increase in width of the CFRP laminates resulted in a decrease of normalized strength. The failure mode for all specimens in this group was debonding of the CFRP from the concrete surface while a thin concrete layer remained attached to the debonded CFRP sheet.

CFRPs bonded to HCT specimens had comparably lower strength compared to concrete specimens with similar details. Maximum normalized strength of 31% was obtained for a CFRP width of 25 mm and 75 mm bond length among all specimens. The effective bond length, which differed due to the discontinuities of the surface of masonry units, was found to be between 75 and 100 mm according to normalized strength-CFRP bond length behavior of test results. All the test specimens with strip anchors on HCT exhibited debonding from the HCT surfaces with a small chunk of tile remaining attached on CFRPs. Results of CFRP bonded to HCT specimens indicated that discontinuities on HCT texture and weak nature of HCTs due to presence of cores are the important factors that can prevent successful bonding of CFRPs, resulting in lower ultimate bond strength. Therefore, texture of the masonry units, which are different than that of concrete surfaces, were observed to significantly influence the bond strength of CFRPs.

Results of tests on specimens with plaster finish showed that presence of a low strength (~5MPa) thin plaster layer (~10 mm) adversely affected the ultimate strength, which was found to be about 10 to 20 % of the CFRP uniaxial tensile strength. As the strength of plaster was same for all three groups, similar strength values were obtained irrespective of concrete or masonry compressive strength. Results of experiments conducted on embedded anchors revealed that embedment enables the strength of CFRPs to be developed up to about 65% of their ultimate strength irrespective of the embedment depth and concrete strength. However, it was not possible to fully utilize the strength of CFRPs due to stress concentrations occurring around smoothed corners. In the presence of plaster, strength was three to four times that of the specimens without any special anchors and compressive strength of blocks did not affect the ultimate shear capacity of anchorages. It was also observed that presence of plaster reduced the strength by about 30% for specimens with embedded anchors. The strength of CFRPs bonded to HCTs equipped with CFRP dowels were comparable to the strength of CFRPs bonded to concrete using embedded anchors.

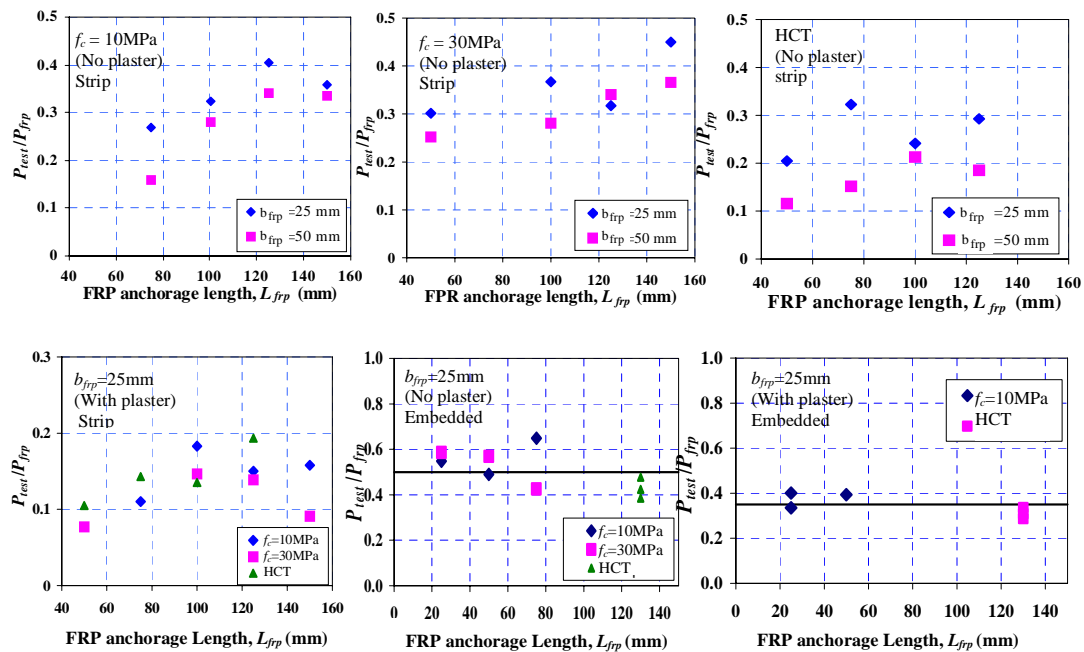


Figure 3. Test Results for Strip and Embedded Type CFRP Anchors

4. STRENGTH MODEL

Based on the examination of test results and employing an effective bond stress law following equation is proposed to estimate the strength of FRPs (P_u) bonded to concrete and masonry:

$$P_u = \sqrt{\tau_f \delta_u} \sqrt{E_{frp} t_{frp} b_{frp}} \tanh\left(\frac{\tau_f}{\delta_u \sqrt{f_c}} \frac{L_{frp}}{L_e}\right) \quad (1)$$

where δ_u is the ultimate slip displacement, E_{frp} is the modulus of elasticity, t_{frp} is the thickness, b_{frp} is the width of FRPs and ($L_e = \sqrt{E_{frp} t_{frp} / \sqrt{f_c}}$) is the effective bond length similar to that given by Chen and Teng (2001) beyond which no strength enhancement is obtained. It is interesting to observe that presence of “tanh” term in Equation 4 conveniently helps to incorporate the effective length concept into the formulation. In this study, shear strength ($\tau_f = \omega f_c^{0.19}$) originally proposed by Savioa et. al. (2003) is adopted to estimate surface shear strength of concrete bonded joints as it is simple and has proved to yield satisfactory strength estimations. In their original model, for FRPs bonded to concrete ω was proposed to be 3.5. For HCTs and plastered surfaces ω is taken as 2 in this study. The maximum measured slip at onset of debonding is assumed to be a function of compressive strength, ratio of anchor length to effective length and a width ratio. A nonlinear regression analysis is then performed based on a database of 103 experiments (including this study and others) that reported slip displacements to estimate δ_u for different cases in form: $\delta_u = f_c^\alpha \left(\frac{L_{frp}}{L_e}\right)^\beta \left(\frac{b_{frp}}{b_c}\right)^\gamma$, where b_c is the width of the concrete block. Constants α , β and γ are then found from nonlinear regression analysis. Values of α , β are found to be -0.4 and 0.8, respectively, irrespective of the material type or presence of plaster. On the other hand, γ is 0.4, 0.5, and 0.9 for concrete HCT, and plastered surfaces, respectively. The average of estimated to experimental bond strength ratios was found to be 0.99 with a standard deviation of 0.2. The model estimations of bond strength was also compared with strength results obtained from 159 experiments reported in the literature. The ratio of estimated to test capacities was found to be 1.03 with a standard deviation of 0.2 (Camli, 2005). Furthermore, the recommended ultimate normalized strength values for embedded anchors with and without plaster are shown in Figure 3 with a straight line.

5. CONCLUSIONS

The experimental results presented herein show that bond strength is more sensitive to anchorage length and width compared to concrete or masonry compressive strength. Increasing the bond length up to effective bond length, load carrying capacity of the anchor increased and remained constant beyond the effective length. Increasing bonded width resulted in a decrease of the normalized load carrying capacity of the anchors. This phenomenon remained valid for low strength concrete and masonry. Lower bond strengths were observed for hollow clay tile specimens due to weak tile texture and discontinuities on the tile surface. The presence of a thin plaster layer resulted in bond strength as low as one third of the similar specimens without any plaster. Based on these results, it is possible to say that FRP applications without any anchors on plaster finished surfaces should be conducted with special care. If possible, FRP dowels should always be supplied to secure the bonded FRP sheets on the plastered surfaces. A simple strength model, whose parameters were calibrated based on the experiment presented in this study and those in the literature, was verified by the tests results of other researchers.

6. REFERENCES

- Binici B., and Bayrak, O. (2004). “Strength of carbon fiber reinforced polymers bonded to concrete.” *11th US-Japan Conference on Composite Materials*, September 9-11, Yamagata University, Yonezawa, Yamagata, Japan.
- Chen, J.F. and Teng, J.G. (2001). “Anchorage strength models for FRP and steel plates bonded to concrete.” *ASCE, Journal of Structural Engineering*, Vol.127, No.7, pp 784-791.
- Dolan, B., Hamilton, H.R., and Dolan, C. (1998). “Strengthening with FRP lamina.” *ACI, Concrete International*, Vol. 20, No.6, 1998, 51-56.
- Camli, U.S. (2005). “Anchorage strength of fiber reinforced polymers.” M.Sc Thesis, Middle East Technical University, 89 p.
- Savioa M., Farracuti B., Mazzotti D. (2003). “Non-linear bond-slip for FRP concrete interface”, *Proc. of 6th International Symposium on FRP Reinforcement for Concrete Structures*, Singapore, pp 183-192.

COMPRESSIVE STRESS-STRAIN MODELS OF FRP-CONFINED CONCRETE

Liu Mingxue

(PhD candidate, Key Laboratory for Structural Engineering and Vibration of Education Ministry, Department of Civil Engineering, Tsinghua University, Beijing 100084, China)

Qian Jiaru

(Professor, Key Laboratory for Structural Engineering and Vibration of Education Ministry, Department of Civil Engineering, Tsinghua University, Beijing 100084, China)

ABSTRACT

To establish compressive stress-strain models of concrete confined by fiber reinforced polymer (FRP), test results of 304 FRP-confined concrete cylinders have been collected from open literatures. The study of the test results shows that when the fiber characteristic value of FRP sheet confined concrete cylinders is less than 0.18, the axial compressive stress-strain curve has an ascending branch as well as a descending branch. When the FRP tube and the concrete core of FRP tube confined concrete cylinders are axially loaded together, most of the existing models underestimate the initial modulus and overestimate the ultimate strain of concrete. Two compressive stress-strain models of FRP-confined concrete are proposed in this paper. One is hardening model which consists of a parabolic section and a straight line, the other is softening model which has a parabolic section only. Influences of fiber characteristic value, FRP laminate structure and loading method on the models have been taken into account.

KEYWORDS

fiber reinforced polymer (FRP), concrete cylinder, experimental database, compressive stress-strain model

1. INTRODUCTION

To give a favorable prediction of compressive stress-strain relationship of FRP-confined concrete (FCC), based on the experimental database built by Lam, L., and Teng, J.G. (2002, 2003) and 116 test results (Berthet et al., 2005; Fam and Rizkalla, 2001; Huang et al., 2002; Jin et al., 2003; Karabinis and Rousakis, 2002; Lam and Teng, 2004; Li et al., 2005; Lu, 2005; Tao et al., 2005), a new experimental database which has 304 FRP confined concrete cylinders (FCCC) has been developed. Based on the new database and the existing models, two improved compressive stress-strain models of FCC, one is hardening model and the other is softening model, are proposed in this paper. Influences of FRP laminate structure and loading method are taken into account. Two loading methods were adopted in existing tests, loading method 1(LM1) was to apply the axial force to the concrete core only and loading method 2(LM2) was to apply the axial force to the FRP tube and concrete core simultaneously.

2. PROPOSED STRESS-STRAIN MODELS

2.1 Equations of Proposed Models

As shown in Figure 1, the stress-strain relationship curve of the hardening model has an ascending branch which consists of a parabolic section and a straight line. The stress-strain relationship curve of the softening model has an ascending branch and a descending branch and it has a parabolic section only. In the Figure, f_{cc} is the peak strength of FCC, f'_{co} is the axial compressive strength of unconfined concrete, ϵ_{cc} is the peak strain of FCC, f_0 is the stress at the intersection point of the straight line and the stress axis, ϵ_1 is the strain where the parabolic section meets the straight line with a smooth transition, E_1 is the elastic modulus of FCC, E_2 is the slope of the straight line.

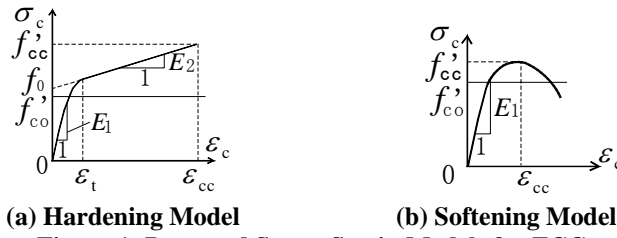


Figure 1: Proposed Stress-Strain Models for FCC

The hardening model adopts the equations proposed by Lam and Teng (2003), as given by the following expressions:

$$\sigma_c = E_1 \varepsilon_c - \frac{(E_1 - E_2)^2}{4f_0} \varepsilon_c^2 \quad (0 \leq \varepsilon_c \leq \varepsilon_t) \quad (1)$$

$$\sigma_c = f_0 + E_2 \varepsilon_c \quad (\varepsilon_t \leq \varepsilon_c \leq \varepsilon_{cc}) \quad (2)$$

$$\varepsilon_t = \frac{2f_0}{E_1 - E_2} \quad (3)$$

$$\varepsilon_{cc} = \frac{f'_{cc} - f_0}{E_2} \quad (4)$$

Among the total 304 test results, 271 are FRP tube confined concrete cylinders (FTCCs) and FRP sheet confined concrete cylinders (FSCCs) whose fiber characteristic values (f_r/f'_{co}) are not less than 0.18. Except one FTCC specimen of Fam and Rizkalla (2001), for which pultruded FRP tube was used, the stress-strain curves of them are all hardening type. With the exclusion, a total of 270 test results are adopted for developing the hardening model. In the expression of f_r/f'_{co} , $f_r = 2f_h t/D$, t is the thickness of FRP wrap, D is the diameter of concrete cylinder, f_h is the hoop tension strength of FRP wrap. Generally, the rupture strain and the strength of FRP measured in FCCC test are lower than those from flat coupon tensile test, split-disk test, classical lamination theory, and manufacturer data (Lorenzis and Tepfers, 2003; Lam and Teng, 2004). But in FTCC tests (Huang et al., 2002; Li et al., 2005; Lu, 2005) whose FRP tubes were cross-ply filament-wound FRP tube (CPFT), and the narrow ring specimens used to evaluate the mechanical properties of FRP tubes in split-disk test were cut from the tube, the rupture strains of FRP measured by FCCC test were higher than those from split-disk test. By analyzing the test results, f_h is $1.75 f_{h,ftp}$ in this case and is $f_{h,ftp}$ in the rest cases. Then, the applicable ranges of Equations (1, 2) are $f_r/f'_{co} \leq 2.2$ for FTCCs and $0.18 \leq f_r/f'_{co} \leq 2.2$ for FSCCs, respectively.

The softening model is given by the following expression:

$$\sigma_c = E_1 \varepsilon_c - \frac{E_1^2}{4f'_{cc}} \varepsilon_c^2 \quad (5)$$

The peak strain ε_{cc} of the softening model is $2f'_{cc}/E_1$. Other four parameters need to be defined are: elastic modulus E_1 of FCC, peak strength f'_{cc} of FCC, stress f_0 , and slope E_2 of the straight line.

2.2 Determination of Parameters of Proposed Models

Under LM2 condition, E_1 of concrete of FTCCs is given by the following equation:

$$E_1 = (E_c + \rho E_{c,ftp}) / (1 + \rho) \quad (6)$$

Where, the elastic modulus of unconfined concrete $E_c = 4730\sqrt{f'_{co}}$ (Lam and Teng 2003), $E_{c,ftp}$ is the axial compression elastic modulus of FRP tube, ρ is the section area ratio of FRP tube to concrete core. Except LM2 condition E_1 equals to E_c .

As the number of layer of FRP sheet or the thickness of FRP tube exceeds a certain value, the confinement efficiency of FRP decreases. The peak strength f'_{cc} of 270 hardening type FCC specimens can be predicted by a parabolic equation, as given by the following expression:

$$f'_{cc} = [1 + 2.721(f_r / f'_{co}) - 0.522(f_r / f'_{co})^2] f'_{co} \quad (7)$$

The statistics correlation coefficient R^2 of Equation (7) is 0.8201.

The value of f_r/f'_{co} was less than 0.18 for other 33 FSCC specimens. Among them, 21 specimens (Berthet et al 2005; Demers and Neale 1994; Jin et al. 2003; Karabinis and Rousakis 2002; Xiao and Wu 2000) had softening type stress-strain curve. By analyzing those 21 test results, the peak strength f'_{cc} of softening model is given by the following equation:

$$f'_{cc} = [1 + 0.87(f_r / f'_{co})]f'_{co} \quad (8)$$

The statistics correlation coefficient R^2 of Equation (8) is 0.3479. The average ratio of the test results to the calculated values of Equation (8) is 1.006 with a standard deviation of 0.059.

The stress f_0 can be predicted by the following equation:

$$f_0 = (1 + 0.303f_r / f'_{co})f'_{co} \quad (9)$$

The statistical correlation coefficient R^2 of Equation (9) is 0.2455. The average ratio of the test results to the calculated values of Equation (9) is 1.017 with a standard deviation of 0.142.

The expression of E_2 of concrete confined with CPFT is given by:

$$E_2 = [0.0144 + 0.0438(f_r / f'_{co})]E_1 \quad (10)$$

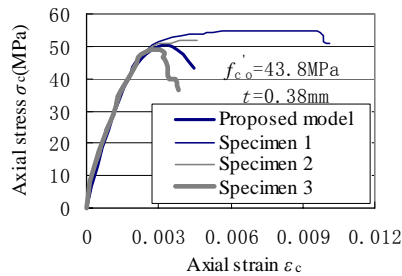
And E_2 of concrete confined with other type of FRP laminate structure is given by:

$$E_2 = (0.02 + 0.08\sqrt{f_r / f'_{co} - 0.18})E_1 \quad (11)$$

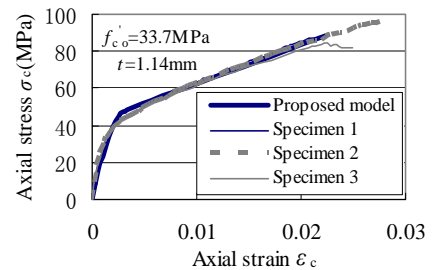
The statistics correlation coefficient R^2 of Equations (10, 11) is 0.8215 and 0.2948, respectively.

3. COMPARISON OF PROPOSED MODELS WITH TEST RESULTS

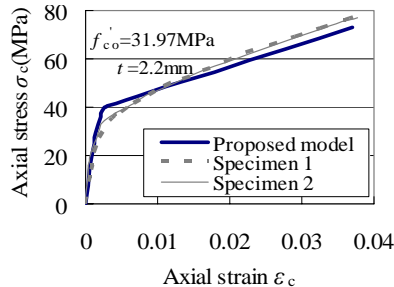
The proposed FRP confined concrete stress-strain models are compared with the test results obtained by Xiao and Wu (2000) on FSCCs, as shown in Figure 2(a, b); by Samaan et al. (1998) on FTCCs, as shown in Figure 2(c); by Lu (2005) on FTCCs, as shown in Figure 2(d). It can be seen from Figure 2 that the predictions have good agreement with the test results of FCC with various FRP laminate structures and loading methods.



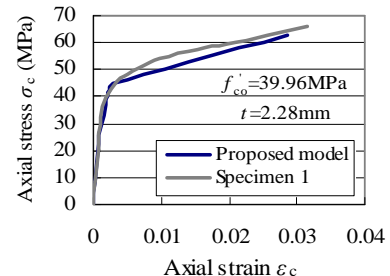
(a) FSCC, $f_r/f'_{co} = 0.178$ (Softening Model)



(b) FSCC, $f_r/f'_{co} = 0.693$ (Hardening Model)



(c) FTCC (CPFT, LM1), $f_r/f'_{co} = 0.523$ (Hardening Model)



(d) FTCC (CPFT, LM2), $f_r/f'_{co} = 0.217$ (Hardening Model)

Figure 2: Comparison of Proposed Models with Test Results

4. CONCLUSIONS

The following conclusions can be drawn from this study:

- The compressive strength of FRP-confined concrete is relevant to the fiber characteristic value. Influence of FRP laminate structure and loading method on it is not significant.
- The fiber characteristic value, the FRP laminate structure and the loading method affect the peak strain of FRP confined concrete.
- The proposed hardening model and softening model have good agreement with the test results of FRP confined concrete cylinders with various FRP laminate structures and loading methods.

5. ACKNOWLEDGEMENT

The work presented in this paper has received financial support from the National Natural Science Foundation of China for Distinguished Young Scholars (Project No. 50329802). The authors wish to express their sincere gratitude to the organization.

6. REFERENCES

- Berthet, J.F., Ferrier, E., and Hamelin, P. (2005). "Compressive behavior of concrete externally confined by composite jackets. Part A: experimental study". *Construction and Building Materials*, Vol. 19, pp 223-232.
- Demers, M, and Neale, K. W. (1994). "Strengthening of concrete columns with unidirectional composite sheets". *Development in Short and Medium Span Bridge Engineering '94, Proceedings of 4th International Conference on Short and Medium Bridges*, Editors: Mufti, A. A., Bakht, B., and Jaeger, L. G., Canadian Society for Civil Engineering, Montreal, pp 895-905
- Fam, A.Z. and Rizkalla, S.H. (2001). "Behavior of axially loaded concrete-filled fiber-reinforced polymer circular tubes". *ACI Structural Journal*, Vol. 98, No. 3, pp 280-289.
- Huang, L.N., Zhang, D.X., Wang, R.G. et al. (2002). "Research on the stress-strain relation of the GFRP-confined concrete column under the axial compression". *Journal of Wu Han University of technology*, Vol. 24, No. 7, pp 31-34. (in Chinese)
- Jin, X.N., Pan, J.L., Liu, G.Y., and Lai, W.H. (2003). "Stress-strain curves of concrete confined by fiber reinforced plastics under axial compression". *Journal of Building Structures*, Vol. 24, No.4, pp 47-53. (in Chinese)
- Karabinis, A.I., and Rousakis, T.C. (2002). "Concrete confined by FRP material: a plasticity approach". *Engineering Structures*, Vol. 24, pp 923-932.
- Lam, L., and Teng, J.G. (2002). "Strength models for fiber-reinforced-plastic-confined concrete". *Journal of Structural Engineering*, ASCE, Vol. 128, No.5, pp 612-622.
- Lam, L., and Teng, J.G. (2003). "Design-oriented stress-strain model for FRP-confined concrete". *Construction and Building Materials*, Vol.17, pp 471-489.
- Lam, L., and Teng, J.G. (2004). "Ultimate condition of fiber reinforced polymer-confined concrete". *Journal of Composites for Construction*, ASCE, Vol. 8, No. 6, pp 539-548.
- Li, G.Q., Tores, S., Alaywan, W., and Abadie, C. (2005). "Experimental study of FRP tube-encased concrete columns". *Journal of Composite materials*, Vol. 39, No.13, pp 1131-1145.
- Lorenzis, L. D., and Tepfers, R. (2003). "Comparative study of models on confinement of concrete cylinders with fiber-reinforced polymer composites". *Journal of Composites for Construction*, ASCE, Vol. 7, No. 3, pp 219-237.
- Lu, G.C. (2005). "Study on behavior of concrete-filled FRP tubes under axial compression". MS thesis, Tsinghua University, Beijing, China. (in Chinese)
- Samaan, M., Mirmiran, A., and Shahawy, M. (1998). "Model of concrete confined by fiber composites". *Journal of Structural Engineering*, ASCE, Vol. 124, No.9, pp 1025-1031.
- Tao, Z., Gao, X., Yu, Q., and Zhuang, J.P. (2005). "Stress-strain relation of FRP-confined concrete". *Engineering mechanics*, Vol. 22, No.4, pp 187-195. (in Chinese)
- Xiao, Y., and Wu, H. (2000). "Compressive behavior of concrete cylinders confined by carbon fiber composite jackets". *Journal of Materials in Civil Engineering*, ASCE, Vol. 12, No.2, pp 139-146.

ACCELERATED REPLACING AND CONSTRUCTION OF CONCRETE BRIDGE DECKS USING THIN CFRP STIFFENED PLATES

Lijuan Cheng

(Assistant Professor, Department of Civil & Environmental Engineering, University of California, Davis, CA, USA)

ABSTRACT

This paper presents a hybrid fiber reinforced polymer (FRP)-concrete deck system using thin carbon FRP stiffened plate for both deck replacement and new construction applications. The plate has a nominal thickness of 6 mm and has extruded stiffeners and shear ribs at the surface. The objective of this study is to fully characterize the structural behavior of the deck system through full-scale experiments and numerical simulations. This paper discusses the major results on interfacial characterization, short-term behavior of flexure and shear, and long-term fatigue response. Satisfactory performance was observed from the tests with a close correlation between the experimental results and analytical simulations using nonlinear finite element method and typical constitutive material models for FRP composites and nonlinear concrete.

KEYWORDS

Bridge deck, stiffened plate, fiber reinforced polymer (FRP) composites, finite element analysis (FEA)

1. INTRODUCTION

Many reinforced concrete bridges that were built before 1940's in the United States are either approaching the limit of their functional service-life or currently undergoing critical deck deterioration with serious capacity loss in the superstructure. Partially or fully replacing these concrete decks has been very expensive and also unavoidably causes traffic disruption and delays (Sprinkel, 1993). Due to this fact, accelerated replacing methods with least amount of traffic disruption have attracted much attention through the use of high performance materials such as advanced fiber reinforced polymer (FRP) composites and exploration of novel concepts on deck system design. FRP composites are known to have light weight, greatly improved corrosion resistance and long-term durability, potentially low maintenance and life-cycle costs. Their hybrid use with conventional concrete in bridge decks in the form of thin continuous plates has recently been explored, not only as reinforcing products in replacement of corrosion-prone steel, but also as stay-in-place permanent formwork to allow for rapid construction (Dieter et al., 2002, Matsui et al., 2001, Harik et al., 1999, Hall and Mottram, 1998). This paper presents a steel-free concrete deck system reinforced with carbon FRP (CFRP) stiffened thin plate (Cheng et al., 2005), which was sand treated on the contacting surface and installed with small interfacial shear ribs with a spacing of 152 mm (Figure 1). The objective of this study is to fully characterize the structural response at both component and system levels through full-scale experiment and numerical simulations, and to develop a simplified design approach that can facilitate the routine design of the system as well.

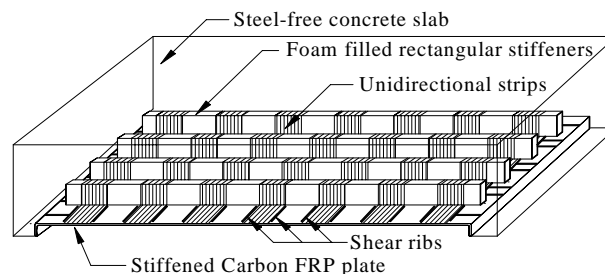


Figure 1: Steel-free deck system using thin CFRP stiffened plate

2. EXPERIMENTS

The CFRP plate consists of a 6 mm thick bottom plate and adhesively bonded rectangular stiffeners filled with foam material. The bottom plate is composed of 8 layers of unidirectional carbon fabric (305 g/m²) and 4 layers of E-glass chopped strand mat (458 g/m²) in a symmetric lay-up scheme of [C/E/C₂/E/C]_s. The rectangular stiffeners contain primarily unidirectional carbon fabric and foam core and are adhesively bonded onto the bottom plate. Transverse restraining strips made of one layer of unidirectional carbon fabric are overlaid across the plate width. To enhance the shear interaction between the concrete slab and the plate, the top surface of the plate is sand treated and additionally installed with interfacial shear ribs made of sand-epoxy paste. The steel-free slab is constructed from normal weight concrete with a nominal design compressive strength of 34.5 MPa at 28 days.

Eight specimens (610 mm wide, 2.254 m long) with varying spacing of interfacial stiffeners and ribs were constructed and tested to characterize the interfacial response between the slab and CFRP plate. All specimens were simply supported by a roller at one end, a pin at the other, and quasi-statically loaded at mid-span via a double-rod hydraulic actuator through an elastomeric pad from the top. Flexural specimens SF1–5 cast with steel reinforced concrete blocks at both ends (simulating fixity condition to supporting girders) behaved quite linear-elastically up to failure. The flexural cracks in SF1, SF2, and SF3 (with a rib spacing of 152mm, 305mm, and infinite, respectively) first grew vertically near the bottom at mid-span and then propagated diagonally toward the load point due to the combined flexural and shear stresses followed by a sudden diagonal failure crack with a similar load capacity of 310 kN (due to the restraining effect provided from the concrete end blocks). For the effect of the stiffener spacing, SF4 (spacing of 610 mm) and SF5 (no stiffener) had an ultimate capacity about 17% and 43%, respectively, lower than that of the control panel SF1 (spacing of 305 mm). The compressive strains in concrete and tensile strains in CFRP composites were all well within the code and design limit. Shear bond specimens SB1, SB2, and SB3 (with a rib spacing of 152 mm, 305 mm, and infinite, respectively) included no end blocks so as to allow for the slippage at the slab-plate interface under quasi-static cycles. Flexural-shear type of crack and horizontal debonding was observed in SB1 and SB2, but SB3 failed in a more flexure mode with the debonding occurred much earlier. The ultimate capacities of SB3 showed 37% lower than SB1 and SB2 due to the absence of interfacial ribs (Figure 2a).

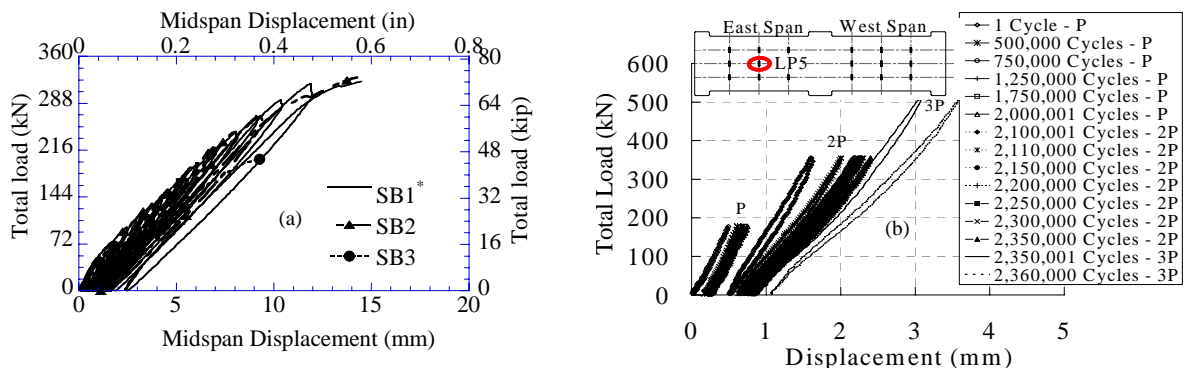


Figure 2: Test results on (a) static; (b) fatigue

The fatigue specimen was constructed from two continuous spans of 1.22 m wide slabs to allow for continuity with a set of CFRP mesh layers placed near the top surface of the slab over the middle one-third region as tensile reinforcement. The specimen is simply supported and loaded in a sinusoidal waveform by two 1.83 mm apart patch loads of 84 kN via two hydraulic actuators to simulate one axle of the AASHTO truck wheel load (2004). The specimen underwent 2.1 million cycles of fatigue service load and 250,000 cycles of doubled fatigue service load and 10,000 cycles of tripled fatigue service load, after which the specimen was monotonically loaded up to failure. Hairline cracks were observed on top surface of the slab above the middle negative bending moment region at the end of the 2 million cycles of service load where the crack width satisfied the serviceability limit state per code requirement. No tensile crack was observed on the vertical sides of the specimen. The structure suffered no stiffness degradation during the first 2 million cycles of service load but a substantial degradation of 37.6% was found during the subsequent 250,000 cycles of doubled service load (336 kN) and 44% during the further 10,000 cycles of tripled service load (504 kN), indicating the higher the magnitude of the wheel load, the larger the amount of degradation in the system. The residual displacement in the system under all the fatigue load conditions was

found to be insignificant (as shown in Figure 2b), which displayed a largely elastic and stable manner, indicating no slippage at the slab-deck interface (Cheng and Karbhari, 2006a).

3. ANALYSES

The functionality of the deck system arises from the intrinsic continuity and shear stress transfer between the FRP structural formwork and the concrete cast on top. This is maintained through both a sand roughened surface on the panel, and through raised ribs. An analytical model of the deck takes advantage of symmetry, and uses ABAQUS (2003) with the deck panel modeled using 4-node double curved general-purpose shell elements with reduced integration points (S4R) and the concrete by 8-node linear brick elements (C3D8). Linear elastic orthotropic properties are used for the FRP composite, while a “damaged” plasticity formulation is used to model the nonlinear response of concrete. This uses the ABAQUS formulation incorporating isotropic damaged elastic response in combination with isotropic tensile and compressive plasticity to represent inelastic behavior of concrete. The validity of the analytical model is shown in Figure 3 through the comparison with the experimental observations as previously discussed.

Main parameters influencing the inclined cracking behavior of the FRP-concrete deck is studied using the finite element model, including the tensile strength of concrete, the shear span-to-depth ratio, the amount of carbon fiber reinforcement, and the spacing of the ribs. Other geometrical and material parameters are remained constants during the parametric study. The analysis results are summarized in charts and plots which are readily to be used as design aids (Cheng and Karbhari, 2006b). Furthermore, they provide a basis for the development of simplified design formulae and equations as discussed in the following section.

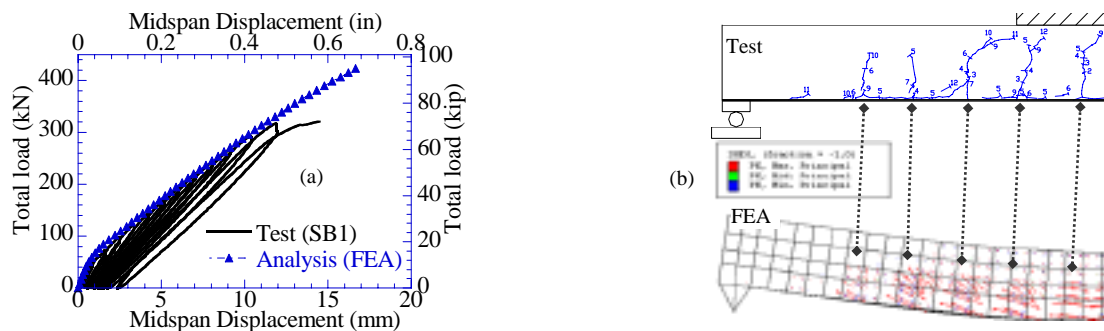


Figure 3: Verification of FEA model for SB1: (a) load-displacement response; (b) crack pattern

4. SIMPLIFIED DESIGN APPROACH

During the construction stage before the concrete sets, the composite deck panel itself shall be designed to carry the concrete deck load, the composite deck dead load, and the construction live load. The maximum stress and strain levels in the deck for bending and shear can be computed by elastic theory with its sectional properties and using moment and deflection coefficients determined from structural analysis based on classic beam theory.

Since the integrity of the deck system depends on shear-bond between the FRP plate and the concrete, the level of shear bond needs to be checked. This can be done using results from parametric studies (as previously discussed) or through use of simplified formulae. The three approaches reported by ACI (1995), Schuster (1972) and Zsutty (1968) were used in the study and a regression analysis was conducted between non-dimensional quantities, for cases corresponding to the rib spacing of 152 mm–305 mm. Since the number of cases for comparison was limited, a reduction of 15% in the regression line was used as recommended by Porter and Ekberg (1976) with a confidence level of 95%. The resulting design equation based on Zsutty’s formula was found to have the best R^2 values (indicating how well the model fits the data, i.e., a value close to 1.0 indicates that almost all the variability has been accounted for). Equation (1) below is recommended for design, where V_u =shear load, b =deck width, d' =distance from extreme compressive fiber to deck centroid, ρ_c =reinforcement ratio, L' =shear span length, f'_c =concrete strength, s =rib spacing. Constants m and k are determined from empirical fit to analysis data, with a value of 0.750 and 0.366 for cases with $s=152$ mm ($R^2=0.92$), and 1.511 and 0.770 for $s=305$ mm ($R^2=0.91$).

$$V_u s / bd' = m \left(f_c' \rho_c d' / L' \right)^{1/3} - k \quad (1)$$

The flexural capacity of the deck system can be obtained from compatibility of strains and equilibrium of internal forces along the section, following the similar principle as that for reinforced concrete structures. The controlling strain herein is either the maximum compressive strain of 0.003 in concrete or the allowable tensile strain of 0.005 in CFRP. The nominal moment strength, M_u , is obtained as a simple summation of internal moments of all the tensile and compressive forces on the cross section that is considered. The deflection limit state is to be checked following conventional elastic theory using transformed sections for FRP components and cracked and uncracked cases being considered. Derivation of these design equations is presented elsewhere (Cheng and Karbhari, 2006b).

5. CONCLUSIONS

This paper presents the experimental investigation of the hybrid FRP-concrete deck system and the appropriate analytical simulations that are developed for the system. The results showed that the system exhibited fairly good ultimate flexural capacity with typical concrete failure instead of catastrophic FRP brittle failure. The spacing of the interfacial stiffeners and shear ribs at the plate surface appeared to be sufficient in transferring the shear from the slab to the reinforcing plate. Fatigue was found to be a non-governing limit state for the slab design based on the fact that no damage was observed in the test after 2 million cycles of fatigue service load. Design charts and simplified equations were developed for use of this type of deck system. Development of an automatic design optimization procedure and studies on long-term durability due to creep, shrinkage, temperature, and moisture effects are currently under progress. Other anticipated future work involves the estimation of life-cycle cost of the deck system and its general applications in bridge systems using conventional concrete and steel girders.

6. REFERENCES

- AASHTO LRFD Bridge Design Specifications (2004). 3rd Edition, American Association of State Highway and Transportation Officials, Washington, D.C.
- ABAQUS/Standard User's Manual (2003). Version 6.4, ABAQUS Inc.
- ACI 318-95 (1995), Building Code Requirements for Reinforced Concrete (ACI 318-95) and Commentary (ACI 318R-95), American Concrete Institute, Detroit.
- Cheng, L., Zhao, L., Karbhari, V.M., Hegemier, G.A., and Seible, F. (2005). "Assessment of a Steel-Free Fiber Reinforced Polymer-Composite Modular Bridge System." *Journal of Structural Engineering*, 131(3): 498-506.
- Cheng, L., and Karbhari, V.M. (2006a). "Fatigue Behavior of a Steel-Free FRP-Concrete Modular Bridge Deck System." *Journal of Bridge Engineering*, in press.
- Cheng, L., and Karbhari, V.M. (2006b). "Design and Analysis of FRP Structural Formwork Based Steel-Free Modular Bridge System." *International Journal of Structural Engineering and Mechanics*, Techno-Press, in review.
- Dieter, D.A., Dietsche, J.S., Bank, L.C., Oliva, M.G., and Russell, J.S. (2002). "Concrete Bridge Decks Constructed with Fiber-Reinforced Polymer Stay-in-Place Forms and Grid Reinforcing." *Transportation Research Record 1814*, Paper No. 02-3205, pp. 219-226.
- Hall, J.E., and Mottram, J.T. (1998). "Combined FRP Reinforcement and Permanent Formwork for Concrete Members." *Journal of Composites for Construction*, 2(2): 78-86.
- Harik, I., Alagusundaramoorthy, P., Siddiqui, R., Lopez-Anido, R., Morton, S., Dutta, P., and Shahrooz, B. (1999) "Testing of Concrete/FRP Composite Deck Panels." *The 5th Construction Materials Congress*, ASCE Materials Engineering Division, pp. 351-358.
- Matsui, S., Ishizaki, S., and Kubo, K. (2001). "An Experimental Study on Durability of FRP-RC Composite Deck Slabs of Highway Bridges." *Third International Conference on Concrete under Severe Conditions: Environment & Loading*, Vancouver, Canada, June 18-20, pp. 933-940.
- Porter, M.L., and Ekberg, C.E., Jr. (1976). "Design Recommendations for Steel Deck Floor Slabs." *Journal of the Structural Division*, ASCE, 102(11): 2121-2136.
- Schuster, R.M. (1972). "Composite Steel-Deck-Reinforced Concrete Systems Failing in Shear-Bond." *Preliminary Report, the 9th Congress of the International Association for Bridge and Structural Engineering*, Zurich, Switzerland, pp. 185-191.
- Sprinkel, M.M. (1993). *Concrete Bridge Protection and Rehabilitation*, Washington, DC: Strategic Highway Research Program, National Research Council.
- Zsutty, T.C. (1968). "Beam Shear Strength Prediction by Analysis of Existing Data." Proceedings, *Journal of the American Concrete Institute*, 65(11): 943-951.

Part XXIII. Strengthening of Metals

BENDING STRENGTH OF CFRP-STRENGTHENED CIRCULAR HOLLOW STEEL SECTIONS

J. Haedir, M.R. Bambach, X.-L. Zhao and R. Grzebieta
(*Department of Civil Engineering, Monash University, Melbourne, Victoria, Australia*)

ABSTRACT

Circular hollow sections (CHS) have been widely employed in structural and energy absorbing applications. Due to greater strength and ductility requirements, it may result in very thin-walled steel sections that are susceptible to local buckling. The use of new materials in the form of carbon fibre reinforced polymer (CFRP) sheets has been increasingly applied with great advantage in strengthening of existing structures today. Furthermore, CFRP may also be applied to minimise the effects of local buckling of thin-walled steel tubes. There are limited international design guidelines that cater for the use of FRP in steel structures, and hence research is needed to provide engineers with a design method to use this new material with safety and cost efficiency. This paper presents an experimental study to assess the influence of slenderness on the bending strength of thin-walled CHS steel tubes strengthened with CFRP for use in design. The effects of fibre orientations are also examined by having both longitudinal and hoop wrappings of steel tubes. It has been proved that by using CFRP in both the longitudinal and hoop orientations enhanced the capacity of slender sections to behave as compact or non-compact sections. The study shows that greater strength and ductility can be achieved in thin-walled circular steel tubes strengthened with CFRP, thus the use of this innovative material have potential for cost efficient design and in retrofitting steel structures for strength and seismic enhancement.

KEYWORDS

Thin-walled steel sections, Steel tubes, Bending, Local buckling, Carbon fibre reinforced polymer

1. INTRODUCTION

External bonding of carbon fibre reinforced polymers (CFRP) has been applied to the strengthening of reinforced concrete beams and columns widely throughout the last decade (Hollaway and Cadei, 2002). More recently the benefits of FRP with steel in structural applications have been explored, particularly with the use of FRP for strengthening of flexural members (Miller et al., 2001, Sen et al., 2001, Tavakkolizadeh and Saadatmanesh, 2003, Patnaik and Bauer, 2004, Schnerch et al, 2005, Colombi and Poggi, 2006, Photiou et al., 2006). Investigations on the use of carbon fibre sheets in strengthened circular hollow sections were reported by Jiao and Zhao (2004), Teng and Hu (2004) and Seica et al. (2006). In the design of most structural steel sections, it is often needed to provide an optimum amount of material to achieve structural economy. Thin-walled steel tubes with circular sections have seen an increased usage in the application to tubular structures in steel construction mainly due to the economy they offer in construction and design. Local buckling may govern the design of thin steel sections when subjected to compressive loads by bending moments. The research into the local buckling behaviour of thin-walled steel in contact with fibre reinforced polymer has until now been limited. To control the problems related to local buckling of the steel tube, external CFRP reinforcement can be utilised as it has the effect of improving the buckling behaviour. Therefore, carbon fibre reinforced polymers are efficient when local buckling can be restrained in the design of thin-walled structural components. This study is aimed at examining the use of CFRP in both the longitudinal and hoop directions in improving the strength of slender CHS in pure bending to behave as compact or non-compact sections. A detailed experimental programme based on the behaviour of circular hollow steel tubes wrapped with CFRP sheets under pure bending is conducted herein. This paper focuses on the effectiveness of utilising CFRP sheets for flexural strengthening of steel tubes with thin-walled sections. The paper concludes by pointing out future research that is needed to be undertaken which involves extending the current study to examine the enhanced local buckling strength of CFRP-strengthened steel tubes with varying slenderness.

2. EXPERIMENTS

2.1 Test Series and Parameters

The experimental programme consisted of testing five cold-formed grade C350 circular hollow steel (CHS) sections. Four of the tube sections were strengthened and denoted as CF-SL2, whilst one of the sections, denoted as SL2, was tested without any CFRP wrapping, as given in Table 1. The steel tubes were cut from a single 6.5 m long tube, as shown in Figure 1. The outer dimensions of the cross-section were d_o and the total length, L . The measured steel thickness was denoted as t . The required diameter-to-thickness ratios were obtained by machining all the tubes to the specific thickness. The total length of each tube was 1500 mm, while the machined length, L_m was 800 mm. The ends of the tubes were filled with a very stiff plaster to prevent premature buckling occurring at the transition from the un-machined to the machined steel section, which allow the development of the full bending moment. A length of about 400 mm was made unfilled in the mid-span of the tube, and this was considered to be the deformation length, L_f for all the test tubes. The non-dimensional section slenderness for all of the steel sections was greater than the AS4100 limit of 120 (Standards Australia, 1998), hence all of the sections were designated slender. It is likely that this section would experience local buckling prior to the attainment of the full yield moment. All tubes had a length-to-diameter ratio (L_f/d_o) between 3 and 5. This value was chosen to be adequate for development of local buckles without end effects in the tube behaviour.

Table 1. Geometric Properties for Bare Steel and CFRP-Strengthened Tubes

Specimen	Measured dimensions		$\frac{d_o}{t}$	$\frac{d_o}{t} \left(\frac{f_y}{250} \right)$	$\frac{L_f}{d_o}$	Number CFRP layers		Fibre layout procedure
	d_o (mm)	t (mm)				Longitudinal (L)	Hoop (H)	
SL2	84.73	1.11	76.0	139.1	4.72	0	0	-
CF-SL2A	84.74	1.12	75.6	138.3	4.72	1	2	1H, 1H, 1L
CF-SL2B	84.59	1.12	75.8	138.7	4.73	2	2	1L, 1H, 1L, 1H
CF-SL2C	84.70	1.07	78.9	147.8	4.72	1	0	1L
CF-SL2D	84.75	1.12	75.4	141.2	4.72	1	1	1L, 1H

The steel tubes were surface ground and cleaned before applying CFRP sheets to provide adequate bonding between the steel surface and the adhesive. The tubes were wrapped using the lay-up method, and cured for a minimum period of two weeks in the laboratory, at ambient temperature. Each longitudinal and hoop carbon fibre layer had an overlap of 35 mm and 60 mm respectively, so that premature failure at the joints could be substantially minimised. The overlap for the longitudinal CFRP layer was less than the CFRP layer in the hoop direction due to the fact that the width of the CFRP layers was smaller than the circumference of the tube. Three circumferentially oriented fibres were needed to wrap the steel section along the axial direction, as illustrated in Figure 1.

The principle parameters that were examined in this study consisted of fibre orientations in the longitudinal (L) and hoop (H) directions, number of CFRP layers and fibre layout procedure. In laying out the carbon fibre sheets, each tube was wrapped by variation of the fibre orientations, mainly aiming at improvement of the buckling load for a given number of fibre layers. In tube CF-SL2A, two fibre layers were used to form the first two layers in the hoop direction, followed by one fibre layer applied in the longitudinal direction. A similar layout sequence was applied to the other tubes with a different number of CFRP layers, as shown in Table 1.

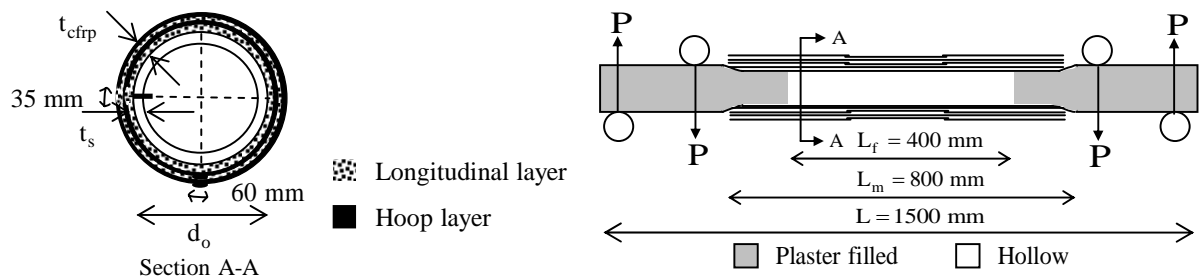


Figure 1. CFRP Strengthening Orientations of Tube CF-SL2B

2.2 Material Properties

Carbon fibre reinforced polymer and adhesive materials

The normal modulus carbon fibre used in the present study was manufactured by MBACE. The carbon fibre was in the form of unidirectional CFRP sheets. Araldite 420 epoxy resin was used to impregnate the carbon fibre sheets. Based on the mechanical properties specifications, the CFRP sheet had a nominal thickness of 0.17 mm per layer, a tensile strength of 3800 N/mm² and a Young's modulus of 240000 N/mm².

Steel properties

Coupon tests were conducted to determine the stress-strain relationship of the steel. Tensile coupons were cut from the tube at 90° measured circumferentially from the longitudinal seam weld. The mean yield strength for the steel was approximately 465 N/mm², with the average ultimate strength at 504 N/mm². It can be noted that the CFRP tensile strength is very high and it is meant to provide improved local buckling capacity to the thin steel section. Hence, the initiation of local buckling of the tube would likely occur after the carbon fibre reaches its failure strain.

2.3 Test Set-up and Procedures

The apparatus for the testing programme was arranged in such a way that a pure bending moment distribution could be applied over the mid-span of the tubes without incurring significant axial forces. The load was applied through the extension of the two hydraulic jacks that were connected to the load application wheels. The applied bending moment was obtained from the recorded angular rotations and forces from the load cells connected to the jacks. Strain gauges were used to measure the compressive and tensile surface strains of the tube at the mid-span section, which were useful in the determination of yielding and local buckling of the steel tube.

3. EXPERIMENTAL RESULTS

3.1 Moment-Rotation

Figure 2 gives a complete picture of the moment-rotation variations of all tested tubes. Two inclinometers were mounted to the top side of the tube to measure the rotations. The results indicate that increasing the number of fibre layers leads to a greater ultimate moment. It is worth noting that tubes CF-SL2A and CF-SL2B exhibit a more ductile behaviour at failure than tubes SL2, CF-SL2C and CF-SL2D. It can be observed from Figure 2 that tubes CF-SL2A and CF-SL2B behave in a manner suggestive of the response of a compact section, in which the plastic moment capacity of the steel section would be achieved. This shows quite clearly how the increase in the number of hoop fibre layers can have a marked effect on the plastic rotation capacity of the tube sections. Local buckling occurs inelastically for tubes CF-SL2C and CF-SL2D, and this is representative of the characteristic of a non-compact section. However, the tubes do not possess adequate rotation capacity for plastic design.

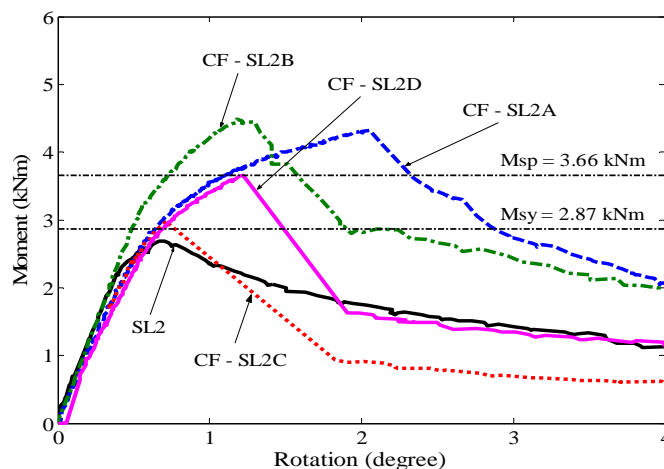


Figure 2. Moment-Rotation of Bare Steel and CFRP-Strengthened Tubes

3.2 Failure Modes

The failure modes for the same size cross-sections which were both bare steel and CFRP-strengthened tube are given in Figure 3. The local buckling shape is restrained by the carbon fibre in the hoop direction, and this has a significant effect on the buckling strength as evidenced by the attainment of the full plastic moment in Figure 2. Consequently, the slender CHS behaves as a non-compact CHS. The hoop layers of tube CF-SL2D appeared to fail in a crushing mode, whilst brittle failure of the longitudinal layers was evident in tube CF-SL2C.



Figure 3. Failure Modes of Bare Steel Tube SL2 and CFRP-Strengthened Tube CF-SL2D

4. CONCLUSIONS AND FURTHER RESEARCH

This paper has presented a background behind the use of carbon fibre reinforced polymers to improve the bending capacity of circular hollow steel sections used in steel structures. An exploratory experimental programme involving the testing of five circular steel tubes, including one bare steel and four CFRP-strengthened tubes, has been conducted. The experiments have highlighted the possible benefits of the use of CFRP in enhancing the overall behaviour of the thin steel section. This is attributed to the restraint offered by the carbon fibre for the ovalisation of the steel tube, for which the CFRP in the hoop direction plays an important role. It has been shown that slender CHS in pure bending may behave as compact or non-compact CHS with CFRP strengthening in both the longitudinal and hoop directions. Further research is currently ongoing at Monash University to test CFRP-strengthened steel tubes with compact and non-compact sections under bending conditions. This will allow the utilisation of CFRP in the design of composite sections, in particular CFRP-strengthened circular steel tubes.

5. REFERENCES

- Colombi, P. and Poggi, C. (2006). An experimental, analytical and numerical study of the static behaviour of steel beams reinforced by pultruded CFRP strips, *Composites Part B: Engineering*, Vol. 37, No. 1, pp. 64-73.
- Hollaway, L.C. and Cadei, J. (2002). Progress in the technique of upgrading metallic structures with advanced polymer composites, *Progress in Structural Engineering and Materials*, Vol. 4, No. 2, pp. 131-148.
- Jiao, H. and Zhao, X.L. (2004). CFRP strengthened butt-welded very high strength steel (VHS) circular steel tubes, *Thin-Walled Structures*, Vol. 42, No. 7, pp. 963-978.
- Miller, T.C., Chajes, M.J., Mertz, D.R. and Hastings, J.N. (2001). Strengthening of a steel bridge girder using CFRP plates, *Journal of Bridge Engineering*, ASCE, Vol. 6, No. 6, pp. 514-522.
- Patnaik, A.K. and Bauer, C.L. (2004). Strengthening of steel beams with carbon FRP laminates, *Proceedings of the 4th International Conference on Advanced Composite Materials in Bridges and Structures*, Calgary, Alberta, July 20-23.
- Photiou, N.K., Hollaway, L.C. and Chryssanthopoulos, M.K. (2006). Strengthening of an artificially degraded steel beam utilising a carbon/glass composite system, *Construction and Building Materials*, Vol. 20, No. 1-2, pp. 11-21.
- Schnerch, D., Dawood, M. and Rizkalla, S. (2005). Strengthening steel-concrete composite bridges with high modulus carbon fiber reinforced polymer (CFRP) laminates, *Proceedings of the 3rd International Conference on Composites in Construction (CCC 2005)*, Lyon, France, July 11-13.
- Seica, M.V., Packer, J.A., Guevara Ramirez, P., Bell, S.A.H. and Zhao, X.L. (2006). Rehabilitation of tubular members with carbon reinforced polymers, *Proceedings of the 11th International Symposium and IIV International Conference on Tubular Structures*, Québec, Canada Aug 31 - Sep 2.
- Sen, R., Liby, L. and Mullins, G. (2001). Strengthening steel bridge sections using CFRP laminates, *Composites Part B: Engineering*, Vol. 32, No. 4, pp. 309-322.
- Standards Australia. (1998). *Australian Standard, Steel Structures, AS4100-1998*, Sydney, Australia.
- Tavakkolizadeh, M. and Saadatmanesh, H. (2003). Strengthening of steel-concrete composite girders using carbon fiber reinforced polymer sheets, *Journal of Structural Engineering*, Vol. 129, No. 1, pp. 30-40.
- Teng, J.G. and Hu, Y.M. (2004). Suppression of local buckling in steel tubes by FRP jacketing, *Proceedings of the 2nd International Conference on FRP Composites in Civil Engineering*, Adelaide, Australia, Dec 8-10, pp. 749-753.

BOND AND SPLICE BEHAVIOR OF HIGH MODULUS CFRP MATERIALS BONDED TO STEEL STRUCTURES

M. Dawood

(Graduate Research Assistant, North Carolina State University, Raleigh, NC, USA)

S. Rizkalla

(Distinguished Professor of Civil Engineering and Construction, North Carolina State University, Raleigh, NC, USA)

ABSTRACT

Research on the use of CFRP materials for retrofit and strengthening of steel bridges and structures has increased in recent years. In order to implement these types of strengthening systems to longer span members, it is important to establish an effective method to splice adjacent lengths of CFRP laminates. This paper describes an experimental program to investigate the bond behavior of carbon fiber reinforced polymer (CFRP) laminates with the objective of developing an effective bonded splice joint. The experimental program was conducted in two phases. In the first phase, the effectiveness of three different CFRP splice joint configurations was evaluated using double lap shear coupon tests. In the second phase, steel beams were strengthened with CFRP laminates which incorporated a bonded splice joint located at the midspan of each of the beams. The test results demonstrate that debonding of the CFRP splice plate was the primary mode of failure for the tested joints. The research also indicated that the use of a reverse tapered joint configuration can significantly increase the splice joint capacity. The findings indicate that careful detailing can significantly increase the capacity of bonded CFRP splice joints.

KEYWORDS

CFRP, steel bridges, splice joints, bond behavior, reverse taper

1. INTRODUCTION

Recently, considerable research has been conducted on the use of carbon fiber reinforced polymer (CFRP) materials for rehabilitation and strengthening of steel bridges and structures (Al-Saidy et al., 2005, Mertz & Gillespie, 1996, Sen et al., 2001, Tavakkolizadeh and Saadatmanesh, 2003). The previous research indicates that externally bonded CFRP laminates can be used to increase the ultimate strength of steel girders and to restore the lost capacity and stiffness of damaged or deteriorated girders. However, due to the relatively low modulus of elasticity of conventional CFRP materials as compared to steel, large amounts of strengthening materials are required to achieve a significant increase of the elastic stiffness. The use of high modulus CFRP (HM CFRP) materials has been demonstrated to be a more effective technique to increase the stiffness of steel beams (Rizkalla and Dawood, 2006).

Similarly to reinforced concrete beams, for steel beams reinforced with externally bonded CFRP materials, the bond stresses at the interface between the beam and the strengthening materials, including both shear and peeling components, must be carefully considered to prevent premature debonding failures (Buyukozturk et al., 2003). Bond stresses are particularly critical at lap-spliced connections between CFRP laminates. The behavior of these splices is dramatically affected by the bond behavior and the bond stress distribution between CFRP laminates. There have only been a limited number of studies which investigate the behavior of spliced connections of CFRP laminates under flexural loading. Stallings and Porter tested eight reinforced concrete beams strengthened with various configurations of externally bonded CFRP splice joints (2003). They recommend that in order to prevent debonding of the CFRP splice plate, the maximum strain in the main CFRP plate immediately prior to the splice should not exceed a limiting value. To the authors knowledge there have not been any studies investigating the splice behavior of steel beams reinforced with CFRP laminates.

2. EXPERIMENTAL PROGRAM

An experimental program was conducted in two phases to investigate the bond and splice behavior of CFRP laminates. In the first phase three double-lap shear coupons with three different joint configurations, shown schematically in Figure 1(a) – (c), were tested. The objective of the first phase was to determine the effectiveness of implementing a reverse taper detail at various critical locations throughout the spliced joint. The splice coupons were 35 mm wide and were fabricated from 4 mm thick CFRP laminates with a modulus of elasticity of 460 GPa and an ultimate strain of 0.00334 as reported by the manufacturer. For all three joint configurations, strains were measured at various locations along the splice joint using electrical resistance strain gauges.

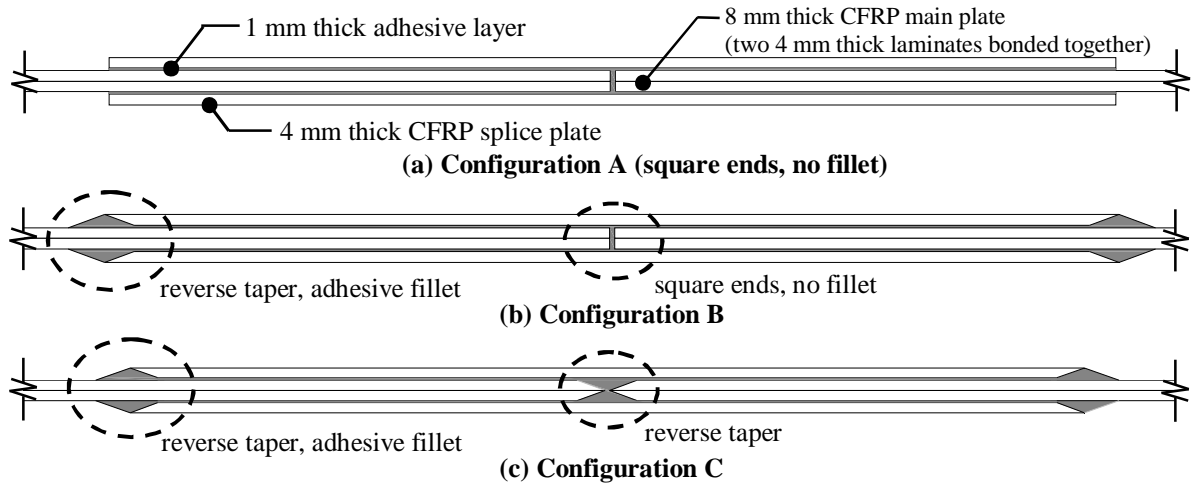


Figure 1: Double-lap shear coupon joint configurations and instrumentation

In the second phase of the experimental program, two steel beam tests were conducted to investigate the behavior of spliced joints under flexural loading conditions. The typical test beam is shown schematically in Figure 2. The beams each consisted of a standard wide-flange steel beam. A steel channel was welded to the top flange of the steel beam to simulate the presence of a reinforced concrete deck. The test beam was strengthened by bonding a 100 mm wide by 4 mm thick HM CFRP laminate to the tension flange. The laminate was left discontinuous at the midspan of the beam as shown in Detail A of Figure 2. Continuity of the strengthening system was provided by bonding an 800 mm long CFRP splice plate at the joint location which overlapped 400 mm on either side of the CFRP main plate. All of the plate ends were left square without incorporating a reverse taper to serve as a reference for future tests which will incorporate different joint details. Due to the high level of uncertainty associated with the bond behavior, two such beams were tested to provide repeated test data for a given splice configuration. The strengthened beams were loaded monotonically to failure in four point bending using a hydraulic actuator. The longitudinal strain in the CFRP splice plate and the main plates was measured at several locations using electrical resistance strain gauges.

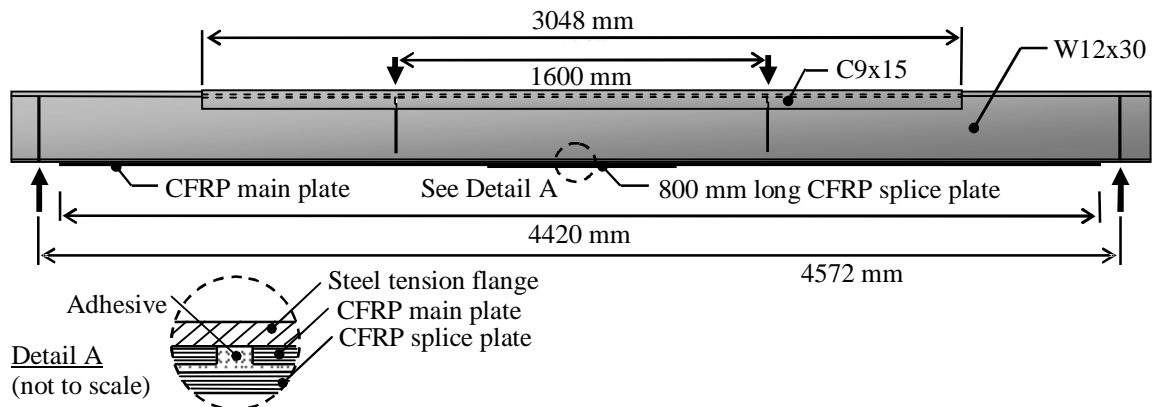


Figure 2: Typical steel test beam configuration

3. EXPERIMENTAL RESULTS

The measured load-strain behavior at the surface of the splice plate at the center of the joint is shown for the three double lap-shear joint configurations in Figure 3. The initial stiffness of all three joint configurations was similar up to a load level of 40 kN. At the 40 kN load level a sudden increase of the measured strain was observed for joint configurations A and B which was likely due to cracking of the adhesive due to a stress concentration near the square plate end within the center of the joint. Cracking of the adhesive resulted in a corresponding loss of stiffness of the joint as shown in Figure 3(a). Joint C did not exhibit a similar increase of strain which suggests that cracking did not occur and that the reverse taper was effective in reducing the stress concentration near the plate end. Joint A failed suddenly due to debonding of the CFRP splice plates at a load level of 90 kN. Failure occurred primarily by separation of the adhesive from the CFRP laminates as shown in Figure 3(b). Joint B exhibited additional cracking at a load level of 144 kN and ultimately failed by debonding of the splice plates at a load level of 160 kN. Joint C failed at a load level of 190 kN suddenly due to debonding of the splice plates and did not exhibit any cracking throughout the entire loading range. The experimental results demonstrate that the presence of the reverse taper and the adhesive fillet details can approximately double the capacity of a bonded splice joint.

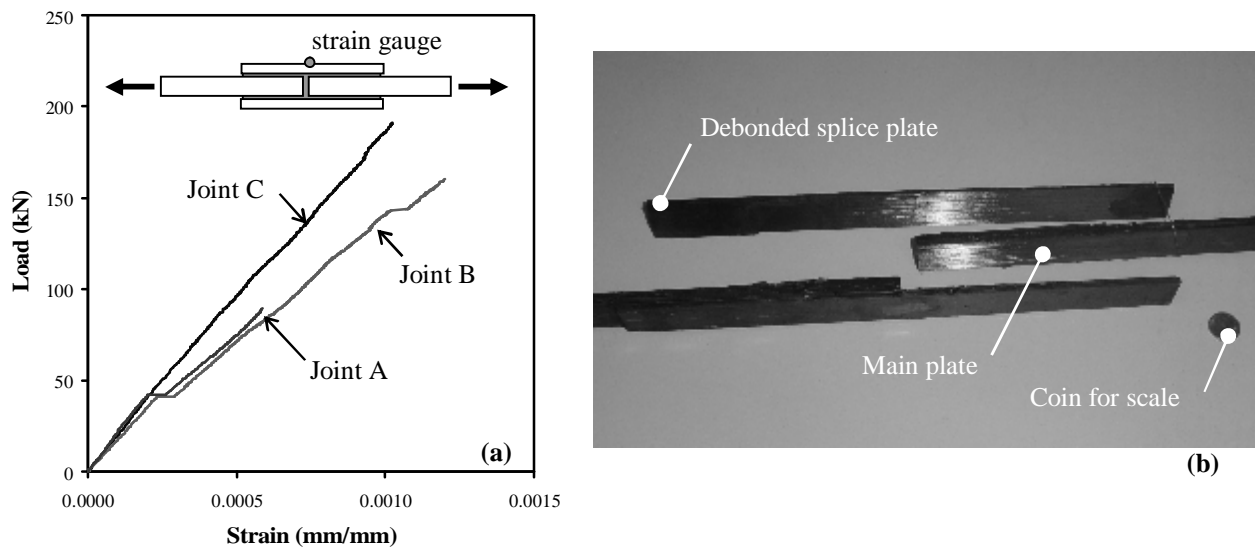


Figure 3: (a) Measured load-strain behavior for double-lap shear coupon tests (b) Debonding failure

Failure of the two tested beams occurred due to debonding of the splice plates prior to yielding of the tension flanges of the steel beams. The total measured load immediately prior to debonding was 177 kN and 205 kN for each of the beams respectively which corresponds to approximately 37 percent and 43 percent of the estimated yield load of the strengthened beams, respectively. The yield load was determined based on a non-linear moment curvature analysis. The longitudinal strain distribution along the length of the splice plate, which was measured during the second beam test, is shown in Figure 4(a) for various load levels. The measured strain profile from the first test closely matched that shown in Figure 4 and therefore is not presented in this paper.

The average shear stress along a given interval of the adhesive layer can be determined from the measured strains by considering equilibrium of forces and is proportional to the slope of the strain profile. The calculated bond shear stress distribution along the length of the splice plate is shown in Figure 4(b). Significant shear stress concentrations were calculated at localized regions near the end of the CFRP splice plate and near the center of the splice joint which can be observed in Figure 4(b). The maximum calculated shear stress in the adhesive at a load level of 205 kN was 20 MPa near the end of the CFRP splice plate and 7.3 MPa near the center of the splice. At the same load level, the calculated shear stress at a distance of 200 mm to 300 mm away from the splice plate end was only 0.9 MPa. This significant concentration of stresses near the plate ends is likely the cause of the premature debonding failure which was observed during both flexural tests. This highlights the need to investigate various details to help reduce the stress concentration near the plate ends.

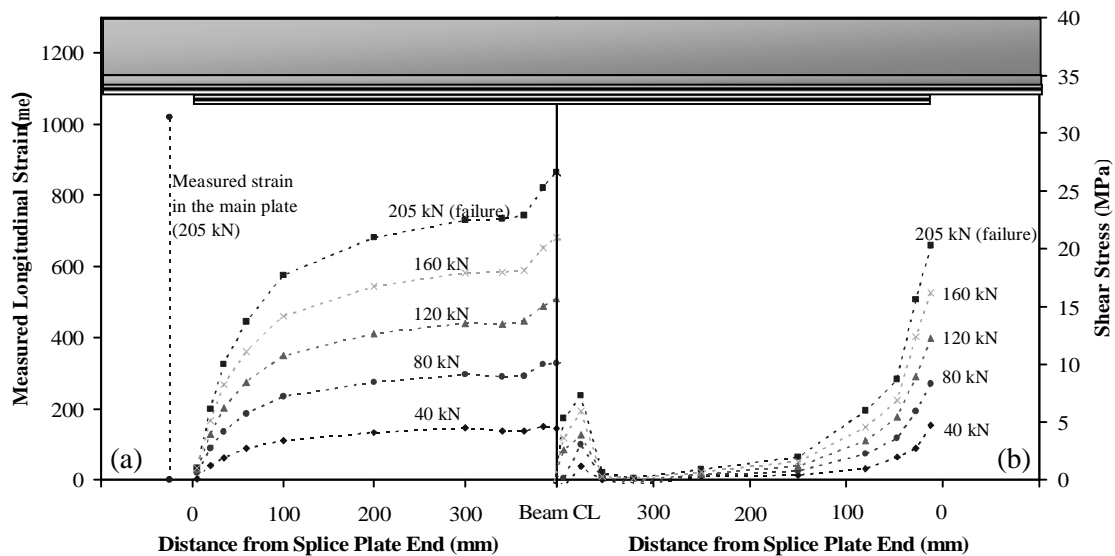


Figure 4: (a) Measured splice plate longitudinal strain (b) Calculated adhesive shear stress

4. CONCLUSIONS

This paper describes an experimental program which was conducted to investigate the bond and splice behavior of CFRP laminates. Initial lap-shear coupon test results indicate that a reverse tapered detail near plate ends can significantly reduce the bond stress concentrations at these locations and consequently increase the ultimate capacity of the spliced joints. The results of the beam tests indicated the presence of significant stress concentrations near the plate ends which resulted in premature debonding failure of the CFRP splice plates.

ACKNOWLEDGEMENTS

The authors would like to acknowledge the contributions of Mr. Akira Nakagoshi of Mitsubishi Chemical FP America Inc. and the support provided by the National Science Foundation (NSF) Industry/University Cooperative Research Center (I/UCRC) for Repair of Buildings and Bridges with Composites (RB²C).

REFERENCES

- Al-Saidy, A.H., Klaiber, F.W. & Wipf, T.J. (2004). Repair of steel composite beams with carbon fiber-reinforced polymer plates. *Journal of Composites for Construction*, 8 (2), 163-172.
- Buyukozturk, O. Gunes, O. & Karaca, E. (2004). Progress in understanding debonding problems in reinforced concrete and steel members strengthened using FRP composites. *Construction and Building Materials*, 18, 9-19.
- Mertz, D.R. & Gillespie Jr., J. W. (1996). Rehabilitation of steel bridge girders through the application of advanced composite materials (Contract NCHRP-93-ID011). Washington, D.C.: Transportation Research Board.
- Miller, T.C., Chajes, M.J., Mertz, D.R. & Hastings, J.N. (2001). Strengthening of a steel bridge girder using CFRP plates. *Journal of Bridge Engineering*, 6 (6), 514-522.
- Rizkalla, S. and Dawood, M. (2006). High modulus carbon fiber materials for retrofit of steel structures and bridges. Accepted for publication in the proceedings of *ACUN-5 International Composites Conference "Developments in Composites : Advanced, Infrastructural, Natural and Nano-composites"*. July 11-14, 2006. Sydney, Australia.
- Sen, R., Libby, L. & Mullins, G. (2001). Strengthening steel bridge sections using CFRP laminates. *Composites Part B: Engineering*, 39, 309-322.
- Stallings, J.M. and Porter, N.M. (2003). Experimental investigation of lap splices in externally bonded carbon fiber-reinforced plastic plates. *ACI Structural Journal*, 100 (1), 3-10.
- Tavakkolizadeh, M. & Saadatmanesh, H. (2003). Strengthening of steel-concrete composite girders using carbon fiber reinforced polymer sheets. *Journal of Structural Engineering*, 129 (1), 30-40.

CFRP-ALUMINUM ALLOY COMPOSITE STRUCTURES: A NEW TYPE OF COMPOSITE STRUCTURES IN FUTURE

Lieping Ye

(Professor, Department of Civil Engineering, Tsinghua University, Beijing, China)

Peng Qian

(PhD Graduate, Department of Civil Engineering, Tsinghua University, Beijing, China)

Peng Feng

(Lecturer, Department of Civil Engineering, Tsinghua University, Beijing, China)

ABSTRACT

High-strength, light-weight and durable materials are always desired by structure engineer. Although CFRP (carbon fiber reinforced-polymer) meets the demands, but its anisotropy makes the connection of structural elements considerably weak which is the main cause that make its high strength not be utilized fully. However, Al (aluminum alloy) is now becoming the structural material in civil engineering in recent years also due to its light-weight and anti-corrosion properties. Although it has reasonable strength as normal steel, but its low modulus makes it deformation control difficult that results in limiting its application in large span structures. The combination of CFRP and Al, which can make the high-strength being fully developed and make the connection being easy between elements, will be expected as a new type in composite structures in future. The state of the art of CFRP-Al composite in aero and space structures, and aluminum structures in civil engineering are firstly reviewed in this paper. CFRP-Al composite pipes, which can be used as elements in long-span space truss structures, under axial compressive and flexural loading were studied by tests. It is shown that CFRP can significantly increase the load capacity and the stiffness of pure Al members. The results of the experimental study have showed that this new composite will have potential benefits for the structures in future.

KEYWORDS

CFRP, Al (aluminum alloy), composite structures, light weight, anti-corrosion.

1. INTRODUCTION

The larger breathing space is always the dream of people all the while. There are two basic ways to obtain it by structural engineer: one is to use the appropriate structure styles, another is to use the light weight materials. These may be considered the main motives behind the introduction of CFRP (carbon fiber reinforced polymer) and Al (aluminum alloy) to be used as structural material in civil engineering. As compared with the Al, CFRP yields more high performance and offers more specific strength, stiffness and resistance (Hollaway, 2001). However CFRP is an anisotropic material, which has high strength and elastic module along the fiber direction and low strength in the transverse direction (Feng and Ye, 2002). So in the design of the CFRP and the CFRP composite structures, two directions have to be considered. Besides adding to the complications and difficulties in the design process of CFRP structures due to the anisotropic, the connections between elements are always the weak position in the structural and can not be easy solved with proper design. Al is a light weight, corrosion resistant material, which is widely applied in the aviation, railway and automobile (Mazzolni, 1985). Since 1940s, Al was introduced in the construction of bridges in North America and Europe, including footbridges, highway bridges, railway bridges and float bridges. At the same time, Al building structures, such as the long-span dome, springs up and becomes widely used all over the world for its light weight, easy manufacture, and anti-corrosion properties. Besides that, Al is also used in the construction of frames, water channels, roof boardings, walls, and communication towers, and so on. However, comparing with steel, the elastic module of Al, for example type of T6061 T6, is about 1/3 of it. The

deflection and the buckling often restrict the use of Al in structures. Therefore, FRP-Al composite structures are suggested here to use their common strong points and can overcome their individual weakness, weak connection for CFRP and lower modulus for Al. By combination of FRP and aluminum, FRP high strength can be made useful in the longitudinal direction to improve the stiffness and stable bearing capacity of Al components; and using aluminum in connections instead of FRP further ensures the reliability and strength at the junction between components. Moreover, the combination can make full use of the advantages of two materials that is the light-weight and anti-corrosion. In this paper, the state of the art of the CFRP-Al composite is firstly reviewed. Then, the experimental researches on CFRP-Al composite elements in compressive and bending are stated. The results show that FRP-Al composite elements have potential benefits for structures in future.

2. CFRP-AL COMPOSITE STRUCTURES

Al structures have the advantages of light weight and corrosion resistant, which were firstly used in the construction of bridges. The first pure Al bridge, which is a 29.72m long railway bridge, was built across the Glass River near New York in 1946. It was also used in the retrofit for existing bridges that Al bridge decks replace steel or concrete decks (Napier et al, 1998; Hag-Elsafi and Alampalli, 2002). For building structures, Al can reduce the structures self weight, which will improve the structures ultimate span and make the construction easy and fast. In addition, Al structures are glossy without painting, anti-corrosion, and non-magnetic. Due to these advantages, Al long-span space structures have been used in some special environments. In China, the applications of Al structures have gained attention in recent years, such as the dome structure of Shanghai international gymnastic center (Figure 1), glass ellipsoid Al of Shanghai science and technology museum, and a non-magnetic latticed structure roof (Figure 2).



Figure 1: International Gymnastic Center



Figure 2: Non-Magnetic Latticed Structure Roof

Comparing with the pure Al structures, CFRP-Al composite structures can be used to get more light and handy building structures. This kind of composite structures has been widely used in aviation industry, like the construction of commercial airplanes, military airplanes and spaceships (Harris et al, 2002). F-22 fighter, manufactured by Lockheed Martin, is a typical composite structure which is composed of 39% titanium alloy, 24% aluminum alloy and 39% FRP. Its tail fin manufactured by Al honeycomb core and CFRP stressed-skin structures. In the plane wing, the main skeleton structure is made up of Al and FRP is used as stressed skin. CFRP-Al composite structures have been used in manufacturing transportation and communication. Many automobile actuating arms made of CFRP-Al composite, can not only reduce the weight, but also improve the strength and stiffness of the rods (Lee et al, 2004).

FRP repairing the cracked Al structures was studied by Pantelides et al (2003). But the idea of the combination of CFRP and Al for civil engineering structures is different. CFRP and Al are used in a reasonable configuration to realize the longer span structures. So many feasible combination styles of CFRP and Al can be designed. Honeycomb panels made of FRP skins and Al honeycomb shown in Figure 3 can be used as lightweight walls and roof structures. CFRP-Al composite beams show in Figure 4, made by sticking CFRP sheets on the tensile and compressive wings of Al profiles, can make full utilization of CFRP high longitudinal strength. They are lighter than pure Al beams but heavier than pure CFRP beams, while the composite beams become cheaper, easier to manufacture, and have good ductility and fatigue resistance. The connection style of metal can be used to avoid the complexity of CFRP connection. CFRP-Al composite pipes and tubes, which are used to construct long-span space structures, were developed and studied in this paper. The CFRP sheets are wrapped and adhered with epoxy resin on the Al pipe's surface. The manufacture process is listed in Figure 5. By the combination, FRP high strength can be fully utilized in longitudinal direction to improve the stiffness and stable bearing capacity of aluminum pipes, and the aluminum connections can be employed instead of the CFRP ensures the reliability and strength at junction

between components. Moreover, aluminum can also supply enough bearing capacity in transverse direction to overcome the low strength of CFRP in this direction. With the development of science and technology, the establish of outer space structures are becoming more and more. Besides same requirements as the ordinary structures, some special requirements in outer space are demanded As all the building materials have to be sent from the earth, the whole structure must be light, handy, and modular. CFRP-Al c composite structures can meet all the requirements.

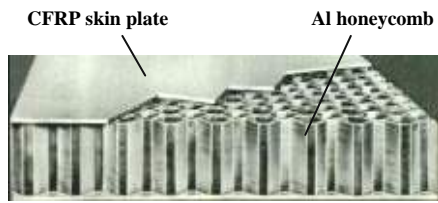


Figure 3: CFRP-Al Sandwich Panel

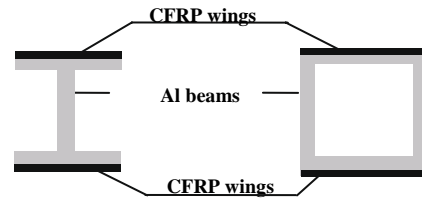


Figure 4: CFRP-Al Composite Beams

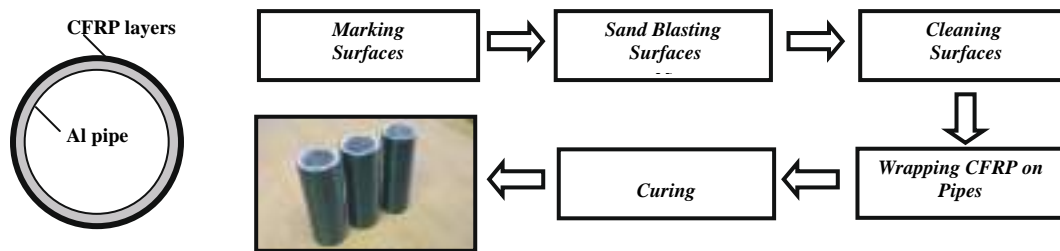


Figure 5: Manufacture Process of FRP-Al Composite Pipes

3. EXPERIMENTAL STUDY ON CFRP-AL MEMBERS

3.1 Axial Compressive Tests

Two sets of composite pipes were tested under axial loading. Twelve specimens in Set 1 are short pipes. Their bearing strength enhanced obviously with CFRP layer numbers increasing which can be seen from in Figure 6. And ten specimens in Set 2 with large slenderness and different CFRP layer numbers were tested to investigate their buckling load-capacity. Their buckling strength were enhanced significantly to the pure Al pipes, the flexural stiffness and deformation capacity were enhanced both. Figure 7 shows the curves of the transverse deflection for the vertical load for the long pipes with the slenderness ratio about 120. Based on the tests and a series of finite element analysis, the buckling behaviors of composite pipes were studied, a formula of stability factor was presented (Qian, 2006).

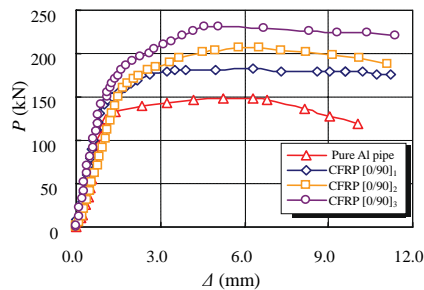


Figure 6: Load-Axial Deflection Curves of Set 1

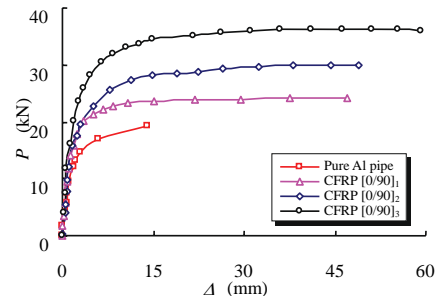


Figure 7: Load-Lateral Deflection Curves of Set 2

3.2 Bending Tests

Two sets of the square tube specimens with different width-thickness ratio were tested under bending. Their load-deflection curves are shown in Figure 8. It can be seen that the strength and stiffness of the composite members are

higher than those of pure Al members while the ductile failure mode is remained. Based on the tests, it was found the initial stiffness of the composite member can be determined by the sum of the Al and CFRP.

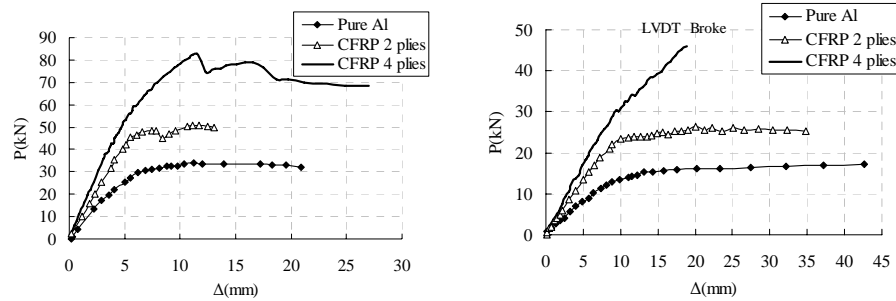


Figure 8: Load-Deflection Curves of the Flexural Specimens

4. SUMMARY

Since 1940s, Al has been applied and developed and had found its application in civil engineering, especially in the construction of bridges and space structures. It has potential benefits because of its high specific strength, high specific stiffness, corrosion resistant and easy processing properties. But Al has its own inherited faults. Its elastic module is only 1/3 of steel and the distortion of aluminum structures is usually large, so the aluminum structures are scarcely used. In order to avoid Al inherited faults and get the more light and handy structures, CFRP-Al composite components and structures are suggested in this paper. The experiment study shows that the combination not only improves components stiffness but also bearing capacity.

ACKNOWLEDGEMENTS

The authors are grateful to the Natural Science Foundation of China for their support to the research presented here through a national key project on the application of FRP composites in civil engineering in China (Project No. 50238030).

REFERENCES

- Feng, P., Ye, L. P. (2002). "FRP structures and FRP composite structures in structural engineering". *Proceeding of 2nd National Conference on FRP Application Technologies in Civil Engineering*. Beijing, Tsinghua University Press, pp51-63 (in Chinese).
- Hag-Elsafi, O., Alampalli, S., (2002) "Cost-effective rehabilitation of two aluminum bridges on Long Island, New York", *Practice Periodical on Structural Design and Construction*, Vol.7, No.3, pp111-117.
- Harris, C. E., Starnes Jr., J. H., Shuart, M. J. (2002). "Design and manufacturing of aerospace composite structures, state-of-the-art assessment". *Journal of Aircraft*, Vol.39, No.4, pp 545-560.
- Hollaway, L.C. (2001). "The evolution of and the way forward for advanced polymer composites in the civil infrastructure". *Proceedings of the International Conference on FRP Composites in Civil Engineering*, Editors: Teng, J.G. Hong Kong, Elsevier Science Ltd. pp27-40.
- Lee, D. G., Kim, H. S., Kim, J. W., et al. (2004). "Design and manufacture of an automotive hybrid aluminum/composite drive shaft". *Composite Structures*, Vol.63, No.1, pp87-99.
- Mazzolani, F.M. (1985). *Aluminum alloy structures*, Pitman, Boston.
- Napier, C. S., McKeel, W. T., Sprinkel, M. M. (1998). "Bridging the centuries: Moving Virginia's bridge program into the 21st century", <http://www.tfrc.gov/pubrds/septoct98/century.htm> , 08/01/2005.
- Pantelides, C. P., Nadauld, J., Cercone, L. (2003). "Repair of cracked aluminum overhead sign structures with glass fiber reinforced polymer composites". *Journal of Composites for Construction*, Vol.7, No.2, pp118-126.
- Qian, P. (2006). "Research on FRP and FRP-aluminum alloy composite members under axial force". Ph.D. thesis, Tsinghua University, Beijing, China (in Chinese).

EXPERIMENTAL STUDY ON CFRP-ALUMINUM ALLOY COMPOSITE PIPES UNDER AXIAL COMPRESSIVE LOAD

Peng Qian

(PhD Candidate, Department of Civil Engineering, Tsinghua University, Beijing, China)

Lieping Ye

(Professor, Department of Civil Engineering, Tsinghua University, Beijing, China)

Peng Feng

(Lecturer, Department of Civil Engineering, Tsinghua University, Beijing, China)

ABSTRACT

An innovated element, Al(aluminum alloy) pipe wrapped with CFRP (carbon fiber reinforced polymer), is presented for large-span structures and special structures in favor of their common advantages of light-weight and corrosion-resistance. Outside CFRP layers can enhance strength and stiffness of Al pipes for compression, while Al pipes provide convenient and strong connections between elements. Two sets of composite pipes were tested. Twelve specimens in Set 1 are short pipes, whose bearing strength increments with CFRP layer numbers varying were investigated. And ten specimens in Set 2 with large slenderness and different CFRP layer numbers were tested to investigate their buckling load-capacity. It was shown that the bearing strength and the buckling strength were enhanced significantly to the pure Al pipes. Their stiffness and deformation capacity were improved also.

KEYWORDS

CFRP, aluminum, composite pipe, axial loads, buckling

1. INTRODUCTION

Al (aluminum alloy) is a light-weight, long-endurance material widely used in many engineering fields. The research on Al structures for bridges and buildings has developed all over the world since 1930s (Mazzoloni, 1985). However, Al structures are limited for its low elastic module which is about 1/3 of steel although the strength is almost same as the common steel. Hence, the concept to combine FRP (fiber reinforced polymer) with high module and Al was proposed to improve Al element performance. FRP has found its applications in civil engineering and is gradually becoming a common structural material in recent 20 years (Ye and Feng, 2006). Comparing with aluminum alloy, FRP has higher tensile strength and elastic modulus in fiber direction, which can be used to enhance performance of Al elements. However, the performance of FRP in transverse and shear is weak. The strengths ratio between the two directions can be up to 25 and 5 respectively to tension and compression (Feng and Ye, 2002). It is resulted in that the high strength and the high stiffness of FRP can not be transferred through the joint without significant weight penalty where various major stress directions occur. If the FRP components are laminated structures, delamination may appear at the joint (Qian and Ye, 2004). The limitation for joints makes the FRP structure design complicated and difficult, which restricts the full utilization of its high strength and stiffness. It is favored that the combination of FRP and Al will counterbalance this as the connection between Al members is convenient and effective. Therefore, FRP-Al composite structures are presented for large-span structures and special structures. The FRP tubes and the aluminum elements in latticed structures can be taken place by the FRP-Al composite elements. The kind of composite structures has been widely used in aviation industry, like the construction of commercial airplanes, military airplanes and spaceships. F-22 fighter, manufactured by Lockheed Martin, is a typical composite structure which is composed of 39% titanium alloy, 24% aluminum alloy and 39% FRP. And its tail fin is manufactured by aluminum alloy honeycomb core and CFRP stressed-skin structures (Harris et al, 2002). Automobile actuating arms made of CFRP-aluminum alloy composite, can not only reduce the weight of rods, but also improve the strength and stiffness of rods (Lee et al, 2004).

As a typical example of the new conceptual composite elements in structural engineering, CFRP-Al composite pipes under compressive load, which is the most common case in spatial truss structures, are investigated in this paper. CFRP sheets were wrapped and adhered on out-surface of Al piped in longitudinal and transversal alternately. The longitudinal direction fiber is utilized to improve stiffness, strength and stable bearing capacity of Al pipes. The transversal fibers can provide a confinement and prevent the local buckling. The more effective connections between elements than pure FRP components' can be inherited from Al pipes. Thus, the common merits of FRP and Al, light-weight and anti-corrosion, can be utilized but their shortcomings separately may be overcome. In order to investigate the axial compressive behaviors of CFRP-Al composite pipes, two sets of specimens, twelve in Set 1 and ten in Set 2, were tested. The pipes were analyzed by finite element software. The theoretical formula based on Euler Theory were presented and compared with the results of tests and FEA. A design approach for CFRP-Al composite pipes in compression was suggested.

2. EXPERIMENTAL PROGRAM

T6061-T6 Al circular pipes with an outside diameter of 49.7mm and a nominal thickness of 3.1mm were used. The mechanical parameters are obtained by short column compression tests and tensile strength tests respectively as listed in Table 1. From table 1 it is evident that the yield strains and stresses both in compression and tension are quite close to each other. Since during investigation all the components are in compressive state so all the analytic parameters are taken from the stocky column tests in compression. The CFRP were wrapped on the outside surface of the Al pipes, which were treated by sand blasting and cleaned. The unidirectional fiber sheets made of T30 carbon fiber and epoxy resin were laminated layer by layer. The elastic parameters of the CFRP laminates were obtained by tensioning the one-layer plates with different fiber orientations: 0, 90 and 45, according to *Test method for tensile properties of oriented fiber reinforced plastics* (Chinese Standard GB3354-82), as listed in Table 2.

Table1: Aluminum Alloy and Mechanical Parameters

Test	σ_y (MPa)	ϵ_y	$f_{0.2}$ (MPa)	$\epsilon_{0.2}$	E (MPa)	ν
Compression	259	3881	291	6224	69800	0.36
Tension	270	3965	291	6317	70300	/

Table2: CFRP Laminate Mechanical Parameters

E_1 (MPa)	E_2 (MPa)	G_{12} (MPa)	ν_{21}
7.15×10^4	3.37×10^3	1.53×10^3	0.36

Table3: Set 1-Short Pipes

Specimens	Al Pipes Outer Diameter - Thickness (mm)	CFRP Thickness (mm)	CFRP Ply
SACP-1,2,3	49.7 - 3.0	/	/
SACCP1-1,2,3	49.7 - 3.0	1.4	[0°/90°] ₁
SACCP2-1,2,3	49.7 - 3.0	2.4	[0°/90°] ₂
SACCP3-1,2,3	49.7 - 3.0	3.7	[0°/90°] ₃

Table4: Set 2-Long Pipes

Specimens	Length (mm)	Al Pipes Outer Diameter - Thickness (mm)	CFRP Thickness (mm)	CFRP Ply
ACCP60-0	950	49.7 - 3.1	/	/
ACCP60-2	950	49.7 - 3.1	2.7	[0°/90°] ₂
ACCP60-3	950	49.6 - 3.0	3.5	[0°/90°] ₃
ACCP70-1	1100	49.6 - 3.1	1.5	[0°/90°] ₁
ACCP70-2	1100	49.6 - 3.0	2.7	[0°/90°] ₂
ACCP70-3	1100	49.7 - 3.1	3.5	[0°/90°] ₃
ACCP120-0	1950	49.7 - 3.1	/	/
ACCP120-1	1950	49.6 - 3.0	1.5	[0°/90°] ₁
ACCP120-2	1950	49.6 - 3.1	2.7	[0°/90°] ₂
ACCP120-3	1950	49.6 - 3.1	3.5	[0°/90°] ₃

Two sets of specimens were tested. Set 1 which is 12 short pipes with the length of 150 mm is to investigate the axial compressive loading capacity of composite elements. According to the layers number and the ply orientation the specimens can be divided into four groups as listed in Table 3, including a group of controlling specimens without CFRP named SACP and three groups of CFRP-Al composite pipes named SACCP. Set 2 includes 10 long specimens divided into three groups by slenderness ratio as listed in Table 4, in which two pure Al pipes of ACCP60-0 and ACCP120-0 act as the controlling specimens.

3. TEST RESULTS

3.1 Set 1: Short Pipes

The controlling specimen, SACP, was loaded increasing linearly with vertical displacement before reaching the yield strain of aluminum. After yielding, the end of the pipe began bulging outward, and the transverse deformation kept on increasing until its failure state reached along with a decrease in the load resistance. An elephant-foot buckling appeared as shown in Figure 3. And some tiny longitudinal cracks can be found on the surface near the pipe end. The composite specimens, SACCP1, SACCP2 and SACCP3, show the similar loading failure process with SACP besides the cracking sounds started emitting always when the pipes closed to the yield load and continued to the rupture of the carbon fiber. There was no obvious bulging, and the yield load and the maximum load rise with the increase of CFRP reinforcement. For SACCP1, two cross layers CFRP wrapped, the failure mode after Al yield is same as SACP without CFRP as the CFRP layer can not provide enough lateral confinement to restrict the lateral expansion of aluminum near the pipe end. But the confinement effect on the aluminum pipes is enhanced to make the ultimate failure mode after Al yield transferred with the increase of CFRP layer amount: SACCP2 were concaved inner and bulged a little on the opposite side; and there were concavity and no obvious bulge in SACCP3. In the test there was no debonding observed at the interfaces between Al and CFRP. The failure modes are shown in Figure 1.



(a) SACP and SACCP1 (b) SACCP2 (c) SACCP3

Figure 1: Failure Modes of Pipes in Set 1

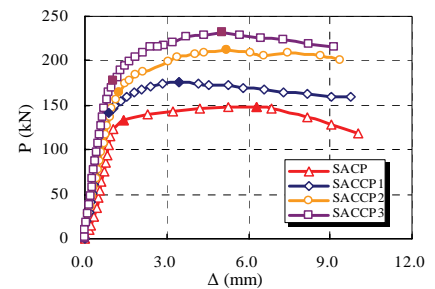


Figure 2: Load-deformation Relations of Set 1

At the same time, the yield loads and the ultimate loads rise almost linearly to the CFRP layer amount increase: the mean yield loads of SACCP1, SACCP2 and SACCP3 are 119%, 139.8% and 150% of SACP respectively, the maximum load capacity are 119.8%, 144% and 154.6% respectively. Figure 3 shows the axial load and the vertical displacement relations obtained from the tests. The values of the curve are taken as the mean of three specimens. It also can be seen that the stiffness of the pipes increase slightly with the increase of CFRP layers before yield and increase considerably after yield. Therefore, the CFRP reinforcements have two different contributions to the composite pipes: the longitudinal fibers enhance the pipe's load carrying capacity directly, and the annular fibers supply the radial restriction and change the failure modes after yield which resulted with the increase in the load carrying capacity indirectly.

3.2 Set2 : Long Pipes

All long pipes in Set 2 under the axial compressive load buckled integrally before Al yield. The lateral displacement in the middle of pipes is not obvious but goes up quickly when a certain axial load arrives. ACCP70-1, the first

specimens in Set 2, tested on a ball and socket support at the ends which restricted the ends from free rotation in the test and is not a hinge. After it, the setup was developed into hinge supports. The relations between the axial load P and the lateral displacement Δ for each slenderness group are shown in Figure 3 except for ACCP70-1. It can be found that the maximum load capacity can be enhanced obviously with the increase of CFRP layers. The bending rigidities of ACCP60 and ACCP70 decrease quickly after buckling because Al yield come immediately, while ACCP120 shows a slow degradation rate.

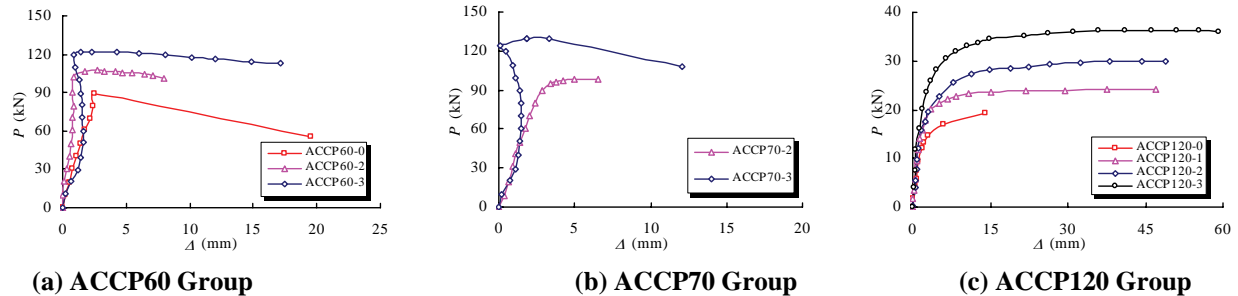


Figure 3: Load-lateral Displacement Relations of Set 2

4. CONCLUSIONS

Based on the tests of the CFRP-Al composite pipes under axial compressive load, the following conclusions can be drawn.

- (1) There was no debonding found between CFRP layer and Al in tests. CFRP-Al composite is an effective concept to build axial compressive elements.
- (2) The bearing strength of CFRP-Al composite pipes can be improved considerably which rise with the increase of the CFRP layers. It comes from two parts: the longitudinal fibers enhance the longitudinal and flexural stiffness and strength directly; and the annular fibers provide the radial restriction to change the failure mode.
- (3) The stable strength of CFRP-Al composite pipes can be improved considerably which rise with the increase of the CFRP layers.

ACKNOWLEDGEMENTS

The authors are grateful to the Natural Science Foundation of China for their support to the research presented here through a national key project on the application of FRP composites in civil engineering in China (Project No. 50238030).

REFERENCES

- Feng, P., Ye, L. P. (2002). "FRP structures and FRP composite structures in structural engineering". *Proceeding Of 2nd Academic And Communicative Meeting On The National FRP Application Technology In Civil Engineering*. Tsinghua University Press, Beijing, pp27-40 (in Chinese).
- Harris, C. E., Starnes Jr., J. H., Shuart, M. J. (2002). "Design and manufacturing of aerospace composite structures, state-of-the-art assessment". *Journal of Aircraft*, Vol.39, No.4, pp 545-560.
- Lee, D. G., Kim, H. S., Kim, J. W., et al. (2004). "Design and manufacture of an automotive hybrid aluminum/composite drive shaft". *Composite Structures*, Vol.63, No.1, pp87-99.
- Mazzolani, F.M. (1985). *Aluminum alloy structures*, Pitman, Boston.
- Qian, P., Ye, L. P. (2004) "Experimental study of CFRP tubes under uniaxial loading". *China Industrial Construction*., Vol. 34, No. 4, pp211-14 (in Chinese).
- Ye, L.P., Feng, P. (2006). "Applications and development of fiber-reinforced polymer in engineering structures". *China Civil Engineering Journal*, Vol. 39, No. 3, pp25-37 (in Chinese).

REHABILITATION OF CRACKED ALUMINUM STRUCTURES WITH GFRP COMPOSITES CONSIDERING FATIGUE

Chris P. Pantelides

(Professor, University of Utah, Salt Lake City, Utah, USA)

Justin D. Nadauld

(Engineer, Reaveley Engineers & Associates, Salt Lake City, Utah, USA)

ABSTRACT

Cracks develop in the welds between branch and chord members of aluminum overhead sign structures due to fatigue stresses by wind-induced vibration. The cracks propagate to complete fracture of the welds which causes signs to fall. The original design of aluminum overhead sign structures did not consider fatigue as a limit state. A rehabilitation method for cracked aluminum welded connections using Glass Fiber Reinforced Polymer (GFRP) composites is investigated. The paper presents results from constant amplitude fatigue tests of aluminum welded connections with no known cracks, cracked aluminum connections from actual sign structures rehabilitated with GFRP composites, and aluminum connections with 90% of the weld removed that were rehabilitated with GFRP composites. The fatigue limits of the welded connections and rehabilitated connections are established for various stress ranges including the constant amplitude fatigue limit threshold. The fatigue tests show that the rehabilitated connection from actual sign structures exceeded the fatigue limits of the welded connection with no known cracks. The repaired connection with 90% of the weld removed satisfied the constant amplitude fatigue limit. A cumulative damage index is established which can be used to develop a fatigue reduction factor for the rehabilitation design using GFRP composites.

KEYWORDS

Aluminum, Connections, Fatigue, FRP composites, Rehabilitation

1. INTRODUCTION

A large percentage of fatigue cracks in aluminum structures are caused by wind-induced vibration of members that are too slender (Sharp et al., 1996). Cracks develop and propagate at the welded connections between branch (diagonal) and main chord members of overhead sign structures as shown in Figure 1. The truss considered here, commonly referred to as a "tri-chord", has three chords and is shown in Figure 1 with a typical connection after it has been repaired using GFRP composites. This research is concerned with the fatigue performance of specimens rehabilitated with GFRP composites using the method developed by Pantelides et al. (2003). The connection tested in fatigue consists of two branch members attached to a main chord; the branches are oriented at an angle 42 degrees from the chord axis, as shown in Figure 2. The members consist of 6mm thick round aluminum tubing; the chord diameter is 102mm and that of the branches 64 mm. Aluminum alloy ASTM 6061-T6 was used as the tubing material; the mechanical properties of the aluminum and the GFRP composite architecture are given by Pantelides et al. (2003). The typical rehabilitated and repaired connection was strengthened with a GFRP layup consisting of two layers of unidirectional tendon (ultimate strength = 517MPa) and two layers of bear tubular weave braid (ultimate strength = 207MPa). The test units were obtained from structures in service for many years, so 1 million fatigue cycles were considered sufficient. Four stresses were used to obtain stress versus number of cycles to failure fatigue curves. The highest stress corresponded to the static design limiting stress of 83MPa, followed by 59MPa, and 39MPa; the lowest stress level was 19MPa, which is 1.4 times the constant amplitude fatigue limit threshold of the connection with the specific details of 13MPa, as specified in the *Standard Specifications for Structural Supports for Highway Signs, Luminaires and Traffic Signals* (AASHTO, 2001). The frequency of the fatigue cycles used was 2 Hz as shown in Figure 2, at a stress ratio $R=0.2$, defined as the ratio of the minimum to maximum stress applied.



Figure 1: Overhead sign structure rehabilitated with GFRP composites and close up of partially cracked weld

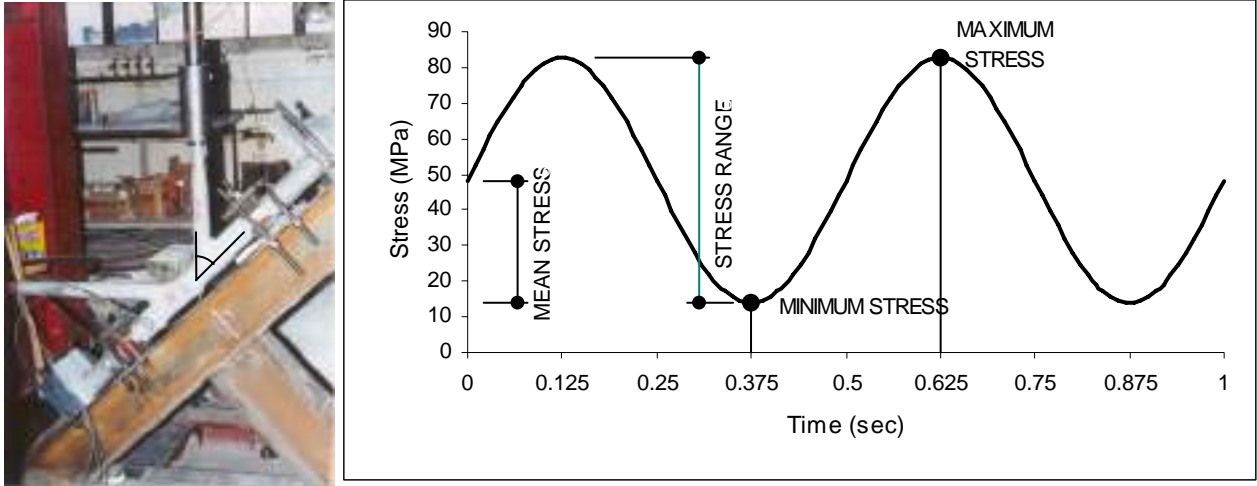


Figure 2: Test setup for fatigue testing with constant amplitude fatigue

2. EXPERIMENTAL RESULTS AND CUMULATIVE DAMAGE MODEL

Constant amplitude fatigue tests were carried out for three series of aluminum connections obtained from the field: (i) aluminum connections with no known cracks, identified as AL; (ii) cracked aluminum connections rehabilitated with GFRP composites, identified as R; and (iii) aluminum connections with 90% of the weld removed and subsequently repaired with GFRP composites, identified as WRR. A cumulative damage model is defined, in terms of the initial and residual stiffness of the structure as:

$$D_i = 1 - k_i / k_o \quad (1)$$

where D_i = cumulative damage at cycle (i), k_o = initial structure stiffness, and k_i = structure stiffness at cycle (i). The cumulative damage index of Eq. (1) is a measure of the loss of stiffness of the test unit in the fatigue tests; it provides a way to compare the results of fatigue tests for the three series. In the fatigue tests carried out, the number of cycles to failure was indicated as N_f . Two failure modes were observed in Series AL: (1) fracture through the throat of the weld, and (2) crack formation at the throat of the weld through the base metal that propagated to fracture of the chord. Two failure modes were observed in Series R: (1) cracking through the throat of the weld and GFRP tensile failure, as shown in Figure 3 for unit R1 tested at 83 MPa maximum stress, and (2) cracking through the toe of the weld, followed by cracking through the throat of the weld and GFRP tensile failure, as shown in Figure 4 for unit R2 tested at 59 MPa maximum stress. The cumulative damage index for test unit R1 is shown in Figure 3; the weld fractured at 5000 cycles, which is marked by the increase in cumulative damage, and the GFRP failed in tension at 6763 cycles. The stages of failure for unit R2 are shown in Figure 4; weld fracture occurred at 12000 cycles and GFRP tensile failure at 69194 cycles. Two main failure modes were observed in Series WRR: (1) adhesive failure with GFRP composite tearing, and (2) GFRP composite tensile failure.

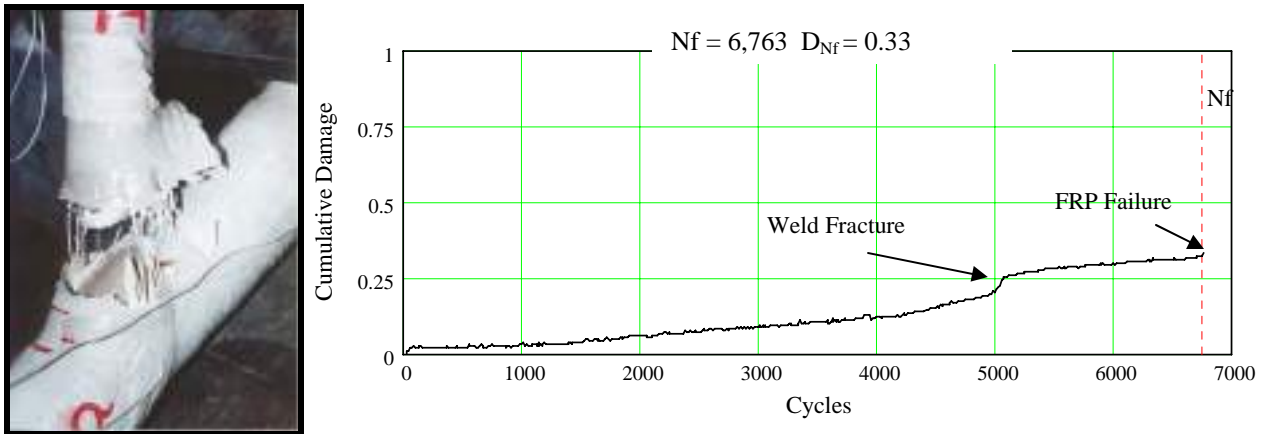


Figure 3: Weld fracture and GFRP composite tensile failure for fatigue test of R1 and cumulative damage index D_i

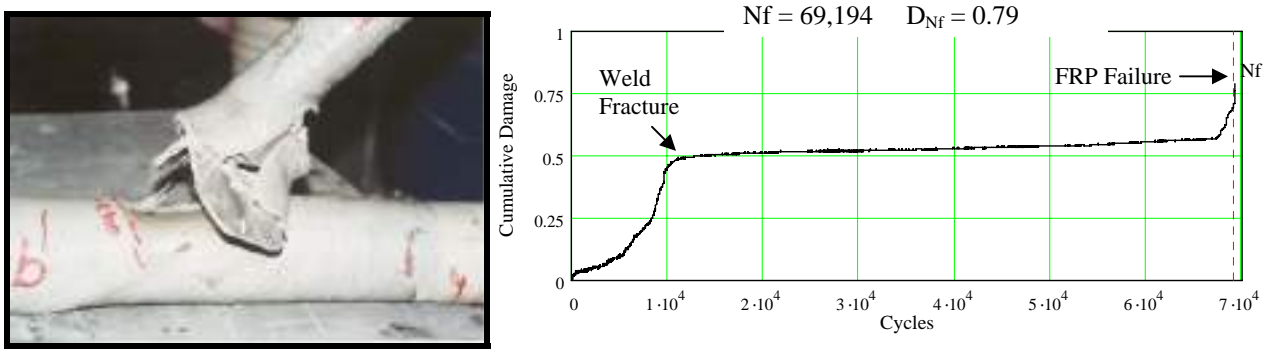


Figure 4: Fracture of weld, base material and GFRP for fatigue test of R2 and cumulative damage index D_i

Figure 5 shows the S-N curves for all fatigue tests. The connections of Series AL and the GFRP rehabilitated connections of Series R show similar behavior with Series R showing slightly better fatigue behavior for the lower maximum stress levels. The units with the weld 90% removed and repaired with GFRP composites, Series WRR did not perform as well as Series AL and Series R in the high maximum stress levels; however, Series WRR performed as well as Series AL in the lowest maximum stress. It should be stressed that the lowest maximum stress of 19MPa is still 1.4 times the constant amplitude fatigue limit threshold specified by AASHTO (2001). Given this fact, and the fact that Series R, and WWR reached 1 million cycles, it can be concluded that rehabilitation of the aluminum joints with GFRP composites concerning fatigue resistance was successful.

3. CONCLUSIONS

Constant amplitude fatigue tests were carried out for three series of aluminum connections obtained from actual overhead sign structures: (i) aluminum connections with no known cracks; (ii) cracked aluminum connections rehabilitated with GFRP composites; and (iii) aluminum connections with 90% of the weld removed and subsequently repaired with GFRP composites. Four maximum stresses were used to obtain stress to number of cycles to failure fatigue curves. The highest maximum stress corresponded to the static design limiting stress and the lowest maximum stress corresponded to 1.4 times the constant amplitude fatigue limit threshold of the connection with the specific details.

Two failure modes were observed for the aluminum connections with no known cracks in the fatigue tests: (1) fracture through the throat of the weld, and (2) crack formation at the throat of the weld through the base metal that

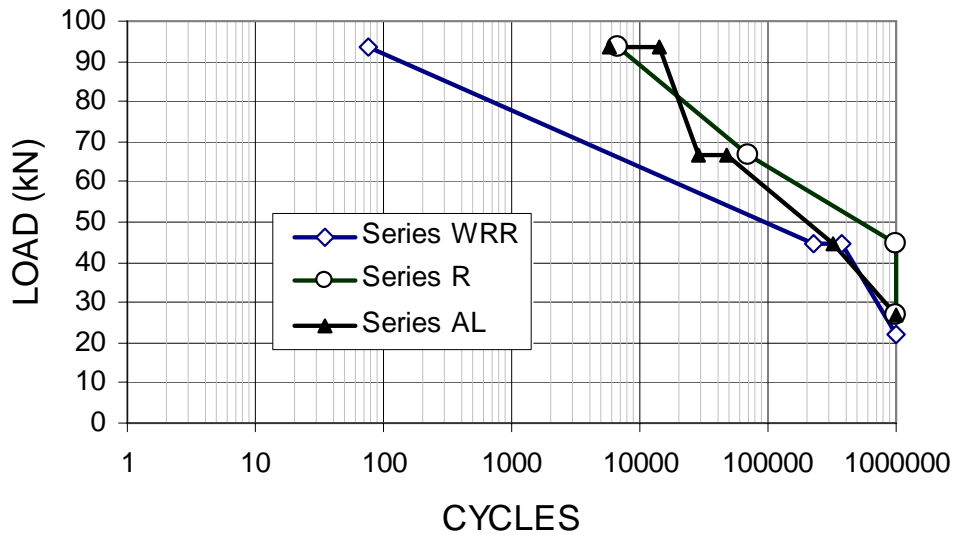


Figure 5: S-N curves for AL, R, and WRR specimens

propagated to fracture of the chord. Two failure modes were observed for cracked aluminum connections rehabilitated with GFRP composites: (1) cracking through the throat of the weld and GFRP tensile failure, and (2) cracking through the toe of the weld, followed by cracking through the throat of the weld and GFRP tensile failure. For aluminum connections with 90% of the weld removed and subsequently repaired with GFRP composites two failure modes were observed: (1) adhesive failure with GFRP composite tearing due to a short bond length, and (2) GFRP composite tensile failure. The cracked aluminum connections rehabilitated with GFRP composites exceeded the fatigue limit of the aluminum welded connections with no known cracks. The GFRP repaired connections with 90% of the weld removed satisfied the constant amplitude fatigue limit threshold.

A cumulative damage index was established which can be used to detect damage and compare between tests; it can also be used to develop a fatigue reduction factor for the rehabilitation design of cracked aluminum connections using GFRP composites. The fatigue test results agree with the results of the static tests and confirm that the GFRP repaired connections behave as well as the aluminum connections with no known cracks for the range of loading expected in service. The repair technique with GFRP composites is adequate and can be used in construction.

4. ACKNOWLEDGMENTS

The writers would like to thank the New York State DOT and Utah DOT for financial support and Air Logistics Corporation for the in-kind support. The writers would like to thank Harry L. White of NYSDOT; Doug Anderson of UDOT; and Dr. Larry Cercone, Franz Worth, and Steve Bazinet of Air Logistics Corp. In addition, the writers would like to thank Professor Lawrence D. Reaveley, Chris Delahunty, and Oliver Burt, of the Civil and Environmental Engineering Department of the University of Utah.

5. REFERENCES

American Association of State Highway and Transportation Officials (AASHTO). (2001). *Standard Specifications for Structural Supports for Highway Signs, Luminaires and Traffic Signals*, 4th Edition, Washington, D.C.

Pantelides, C. P., Nadauld, J., and Cercone, L. (2003). "Repair of cracked aluminum overhead sign structures with glass fiber reinforced polymer composites". *Journal of Composites for Construction*, Vol. 7, No. 2, pp 118-126.

Sharp, M. L., Nordmark, G. E., and Menzemer, C. C. (1996). *Fatigue Design of Aluminum Components and Structures*, McGraw-Hill, New York.

EFFECTIVENESS OF DIFFERENT COMPOSITE MATERIALS FOR REPAIR OF STEEL BRIDGE GIRDERS

Amr Shaat

(Doctoral Candidate, Queen's University, Kingston, Ontario, Canada)

Amir Fam

(Associate Professor and Canada Research Chair in Innovative and Retrofitted Structures, Queen's University, Kingston, Ontario, Canada)

ABSTRACT

Steel-concrete composite bridge girders damaged due to corrosion or fatigue cracks can be repaired by adhesively bonded carbon fiber reinforced polymer (CFRP) sheets. This paper describes the results of the first phase of an experimental study on beams of 1960 mm span length. Each beam is composed of W150 x 22 steel section acting compositely with a 75 mm thick by 465 mm width concrete slab to simulate an actual bridge girder condition. A severe damage was introduced by saw-notching the steel tension flange through the entire thickness at mid-span. Two different types of CFRP sheets were then applied to the tension flange to restore the stiffness and strength capacities of the undamaged control beam. The beams were tested to failure in four-point bending. The findings of this study indicate that proper selection of composite material properties and immediate application of FRP sheets after steel surface preparation are crucial for a successful repair.

KEYWORDS

Repair, Steel, Bridge, CFRP, Sheets.

1. INTRODUCTION

Fatigue and corrosion are main reasons for deterioration of steel bridges. The repair cost of steel structures, in most cases, is far less than the cost of replacement of the whole structure. Traditional methods of repair such as welding or bolting steel plates have a number of shortcomings, including the added self weight of steel plates, long installation time, and the need for an elaborate and expensive shoring system. The use of FRP materials for repair and strengthening of structures has been shown to be both time and cost effective. Steel-concrete composite bridge girders damaged due to corrosion or fatigue cracks can be repaired by epoxy bonding CFRP sheets, particularly due to their excellent corrosion resistance and fatigue properties (Shaat et al., 2004). Artificial degradation techniques such as complete removal of the tension flange at mid-span were previously utilized to simulate fatigue cracks or section loss (Liu et al., 2001). Efficiency of repair material is highly dependent on its elastic modulus, compared to the steel modulus (Hollaway and Cadei, 2002, and Buyukoztruk et al., 2004)

2. EXPERIMENTAL PROGRAM

The effectiveness of bonding two different types of CFRP sheets, namely Type 1 CFRP and Type 2 CFRP, in restoring both the stiffness and strength of steel beams acting compositely with concrete slabs was examined. Four steel-concrete specimens were loaded to failure through four-point bending tests, including an intact (un-notched) control specimen (B1). The tension flanges of three specimens were notched at mid-span throughout the entire flange thickness and width to simulate severely damaged bridge girders. The three notched specimens were then repaired by bonding either Type 1 CFRP for beam (B2) or Type 2 CFRP for beams (B3 and B4). Both the number of layers and width of each layer for both types of CFRP sheets were designed to achieve the same forces at failure when the sheets rupture. The load carrying capacity as well as the initial stiffness was measured and compared to

control beam B1, to evaluate the effectiveness of this repair technique in restoring the original capacity. The following is a brief description of the materials used, fabrication process, test setup and instrumentations.

2.1 Materials

Four W150x22 hot rolled steel sections with 400 MPa nominal yield strength were used for the steel beams. A 75 mm thick by 465 mm wide concrete slab with an average compressive strength of 50 MPa was cast on top of the steel section which had steel shear connectors embedded into the slab. Type 1 CFRP consisted of a 0.54 mm thick lamina, which has tensile strength and modulus of 510 MPa and 230 GPa, respectively. Type 2 CFRP consisted of a 0.89 mm thick lamina, which has tensile strength and modulus of 1130 MPa and 107 GPa, respectively. Fourteen layers of 150 mm wide sheets were used in case of Type 1 CFRP for beam B2, and five layers of 115 mm wide sheets were used in case of Type 2 CFRP for beams B3 and B4 to achieve the same strength. A glass-FRP (GFRP) lamina, 1.46 mm thick, with tensile strength and modulus of 269 MPa and 14 GPa, respectively, was placed between the steel surface and CFRP layers in all beams to prevent galvanic corrosion between steel and CFRP. Tyfo S epoxy resin was used for both GFRP and CFRP sheets to bond the fibres together and to the steel surface.

2.2 Fabrication of Test Beams

The steel beams were first cut to 2030 mm long sections. The entire flange width and thickness at mid-span of the tension flange was cut using a saw with a 1.4 mm thick blade. Conventional 41 mm long and 9.5 mm diameter Nelson studs were welded in pairs at a longitudinal spacing of 60 mm along the compression flange. A 150 x 150 x 5 mm welded wire mesh reinforcement was provided at mid-thickness of the concrete slab. Concrete was then pored, consolidated and cured for about 90 days. The bottom surface of the steel tension flange was sand blasted. FRP sheets were immediately applied on beams B2 and B3, within 24 hours, whereas the notched flange of beam B4 was covered with a thin layer of oil for a period of 22 months, to avoid corrosion, before cleaning it again with acetone and applying the FRP sheets. This was done to investigate the effect of delayed application of FRP after sand blasting on bond.

2.3 Test Setup and Instrumentations

All Four beams were tested using a simply supported configuration with a span of 1960 mm between the centerlines of the supports. The beams were monotonically loaded using four-point bending, as shown in Figure 1, with a distance of 400 mm between the two applied loads. Two linear potentiometers (LPs) were placed on both sides of the beams at mid-span to measure the vertical deflection. The longitudinal strains along the tension flange were measured using several 5 mm long electric resistance strain gauges, spaced as shown in Figure 1. Another strain gauge was attached to the lower side of the steel compression flange at mid-span. Displacement-type strain gauge transducers (PI gauges) installed over a gauge length of 100 mm were also attached to the top of concrete slab and the steel tension flange, as shown schematically in Figure 1. The load was applied using stroke control at a rate of 0.75 mm/min, up to failure. A data acquisition system was used to monitor and record test data.

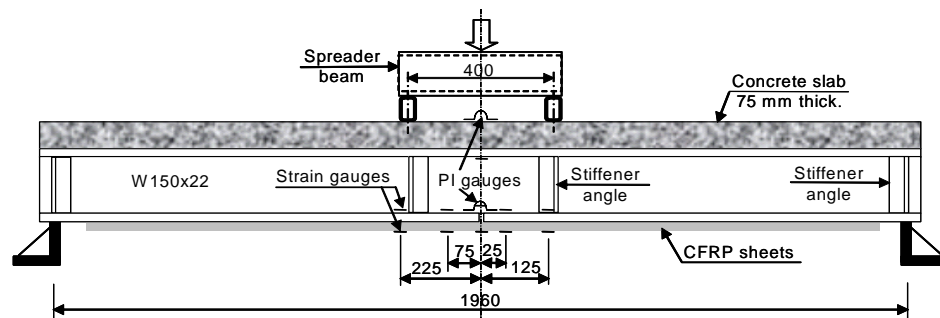


Figure 1: Test setup

3. TEST RESULTS AND DISCUSSION

This section presents the test results in terms of load-deflection and load-strain curves.

Figure 2(a) shows the load versus mid-span deflection of the three repaired beams, compared to the intact control beam. The figure shows that beam B2 with Type 1 CFRP sheets resulted not only in restoring the elastic stiffness and ultimate load of the undamaged beam but also exceeding them by 26% and 10%, respectively, as listed in Table 1. On the other hand, Type 2 CFRP sheets in B3 could not fully compensate for the loss of the entire steel flange. Figure 2(b) shows that the behavior of the intact beam was essentially linear up to first yielding of the steel section at a load level of 305 kN, based on strain gauge readings. Specimen B2 showed an extension of the linear part of the curve, beyond the observed yielding point of B1. Repaired beam B2 reached a significantly higher capacity ($P=394$ kN) than the intact beam B1 before the 14 layers of Type 1 CFRP sheets ruptured due to reaching their maximum tensile strength. The load then dropped to 33% of its maximum value (i.e. to $P=129$ kN) which emphasizes the significant contribution (67%) of the CFRP laminate, compared to a damaged and unrepaired specimen. On the other hand, specimens B3, which was repaired with Type 2 CFRP, reached maximum strength of 311 kN, which corresponds to 87% of the strength of the intact beam B1. The CFRP sheets were then completely debonded, which could be attributed to their lower modulus of elasticity compared to steel, unlike Type 1 CFRP. Moreover, the very low strength level of beam B4 (179 kN) is attributed to the long time interval between sand blasting and CFRP application. Beams B3 and B4 started to react nonlinearly upon initiation of CFRP sheets debonding at load levels of 185 and 104 kN, respectively. Figure 2(b) shows that yielding starts at about 2000 μ strain for the control intact beam B1 and that ultimate rupture strain of Type 1 CFRP sheets in tension occurs at 2200 μ strain, whereas debonding of Type 2 CFRP occurred at 5100 and 3600 μ strain for beams B3 and B4, respectively.

Table 1: Summary of Test Results

Beam I.D.	B1	B2	B3	B4
Maximum Load (kN)	357	394	311	179
Elastic stiffness (kN/mm)	34	43	29	31
% age increase in maximum load	---	+10	-13	-50
% age increase in elastic stiffness	---	+26	-15	-9

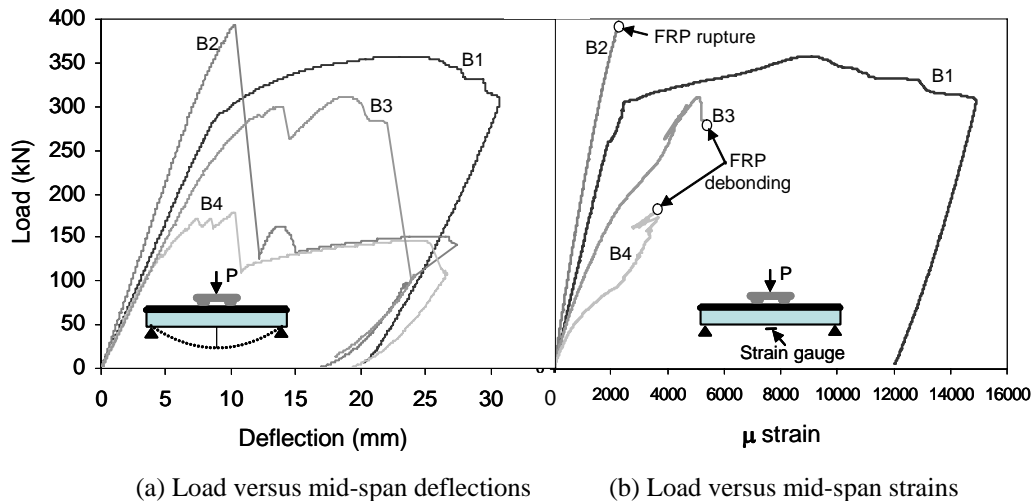


Figure 2: Behavior of Test Specimens

4. FAILURE MODES

The typical failure mode of the intact control beam was yielding of the steel tension flange followed by concrete crushing. In the specimen repaired with Type 1 CFRP, sheets were ruptured as shown in Figure 3(a) when their strains reached the maximum rupture strain of 2200 μ strain. On the other hand, the specimens repaired with Type 2 CFRP sheets were debonded at the interface between GFRP and steel, as shown in Figure 3(b). The loss of the CFRP sheets in both specimens resulted in very high strains above the notch, which led to expanding the notch and development of a crack propagating within the web, as shown in Figure 3(c).

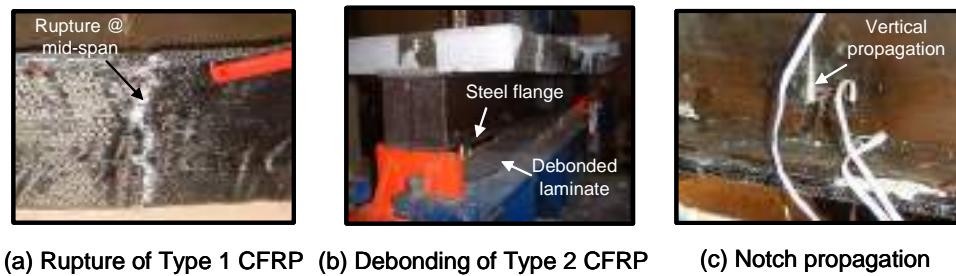


Figure 3: Modes of Failure

5. CONCLUSIONS

The findings of this study indicate that CFRP materials can effectively be used for repair of cracked steel-concrete composite beams. The following conclusions can be drawn:

1. The original strength and stiffness of the undamaged beams can be fully restored by bonding high modulus CFRP sheets. In this study, the specimen repaired with 14 layers of Type 1 CFRP recovered all the loss in strength and stiffness and even achieved an increase of 10% and 25%, respectively, when compared to the intact control beam.
2. The beam repaired with Type 2 CFRP recovered only 87% and 85% of the original strength and stiffness of the intact beam. This lack of efficiency for Type 2 CFRP was due to the premature debonding mode of failure which could be due to its low value of elastic modulus.
3. Immediate application of CFRP sheets on steel surface after sand blasting is very crucial to achieve the highest possible bond strength.
4. No debonding between FRP and steel was observed for the specimen repaired with the high modulus CFRP, which confirms that debonding failure could not only be dependent on surface preparation procedure but also on the stiffness of FRP.

6. ACKNOWLEDGMENT

The authors wish to acknowledge the financial support provided by the Natural Sciences and Engineering Research Council of Canada (NSERC). The authors also wish to thank Fyfe.Co.LLC and Mitsubishi Chemical for providing the FRP materials.

7. REFERENCES

- Buyukozturk, O., Gunes, O., and Karaca, E., (2004), "Progress on understanding debonding problems in reinforced concrete and steel members strengthened using FRP composites" *Journal of Construction and Building Materials*, Vol. 18, pp 9-19.
- Hollaway, L.C. and Cadei, J., (2002) "Progress in the technique of upgrading metallic structures with advanced polymer composites", *Journal of Progress in Structural Engineering and Materials*, Vol. 4, No. 2, pp 131-148.
- Liu, X., Silva, P. F., and Nanni, A., (2001) "Rehabilitation of steel bridge members with FRP composite materials." *Proceedings of the International Conference on Composites in Construction*, Editors: Figueiras J, Juvandes L, Furia R, Porto, Portugal, pp. 613-617.
- Shaat, A., Schnersch, D., Fam, A., and Rizkalla, S., "Retrofit of steel structures using fiber-reinforced polymers (FRP): State-of-the-art." The 83rd annual meeting of the Transportation Research Board (TRB), Washington, D.C., (2004) CD-ROM (04-4063).

EXPERIMENTAL AND NUMERICAL ANALYSIS OF THE STRUCTURAL RESPONSE OF FRP-STRENGTHENED COLD-FORMED STEEL COLUMNS

Ben Young

Associate Professor, Dept. of Civil Engineering, The University of Hong Kong, Pokfulam Road, Hong Kong

Nuno Silvestre¹, Dinar Camotim²

¹Assistant Professor, ²Associate Professor, Dept. of Civil Engineering, ICIST/IST, Technical University of Lisbon, Av. Rovisco Pais, 1049-001 Lisboa, Portugal

ABSTRACT

This paper reports the results of an experimental and numerical investigation on the non-linear behavior and load-carrying capacity of CFRP-strengthened cold-formed steel lipped channel columns. The experimental program involved two test series, comprising a total of 19 short and long fixed-ended lipped channel columns – while the former buckle in local-plate modes, the latter exhibit distortional buckling. The columns were strengthened with carbon fiber sheets glued at different outer surface locations (web, flanges or lips) and having fibers oriented either longitudinally or transversally – since the aim of the study is to assess the influence of the CFRP sheets on the column structural response, bare steel specimens were also tested. The experimental results, which consist of non-linear equilibrium paths (applied load vs. axial shortening) and ultimate strength values (most of them associated with local-plate and/or distortional failure mechanisms), are subsequently used to calibrate and validate geometrically non-linear numerical analyses based on shell finite element models, carried out with the code ABAQUS and adopting an elastic-plastic constitutive law to describe the steel material behavior. Finally, on the basis of both the experimental and numerical results obtained, some relevant conclusions are drawn concerning the most effective CFRP sheet location and fiber orientation to strengthen columns affected by local-plate and distortional buckling.

KEYWORDS

Cold-formed steel columns; Carbon fiber sheets; FRP-strengthening; Local-plate failure; Distortional failure; Ultimate strength

1. INTRODUCTION

Given the considerable stiffness of cold-formed steel members, their strengthening by means of FRP composite requires the use of expensive high-strength fibers, a fact that strongly affects the economical viability of this procedure. However, the increasingly competitive cost of carbon fibers, together with their quite high stiffness and strength properties, has altered this situation – indeed, carbon fiber sheets have been shown to be particularly well suited to reinforce steel plates. As far as the strength is concerned, the failure of CFRP-reinforced cold-formed steel members may stem from (i) local (local-plate and/or distortional) or global buckling of the steel-CFRP member, (ii) rupture or debonding of the CFRP sheet or (iii) a combination of both. Thus, an efficient (safe and economical) design of such members must be based on an in-depth knowledge concerning all these potential failure modes. The objective of this work is two-fold: (i) to report the results of an experimental investigation aimed at assessing how the CFRP-strengthening influences (enhances) the non-linear behavior and load-carrying capacity of cold-formed steel lipped channel columns and also (ii) to use these results to calibrate and validate numerical analyses performed in the code ABAQUS and based on shell finite element member discretisations.

2. EXPERIMENTAL INVESTIGATION

The tests were conducted on fixed-ended cold-formed steel lipped channel columns strengthened with carbon fiber sheets (CFS), which are glued to their outer surfaces in different locations (web, flanges, lips) and with the fibers oriented longitudinally or transversally – for reference purposes, a few bare steel columns were also tested. The specimens were brake-pressed from high strength zinc-coated grades G450 and G550 structural steel sheets (i) with nominal 0.2% proof (yield) stresses equal to 450 and 550 MPa, and (ii) conforming to the Australian Standard AS 1397 (1993). All the column

specimens have nominal web width $B_w=125\text{ mm}$, flange width $B_f=102\text{ mm}$ and lip width $B_l=14\text{ mm}$ and the test program comprises two test series: (i) one involving 9 short columns ($L=600\text{ mm}$) made of G550 steel sheets with nominal thicknesses $t=1.0\text{ mm}$ and (ii) the other consisting of 10 long columns ($L=2200\text{ mm}$) made of G450 steel sheets with nominal thicknesses $t=1.5\text{ mm}$ – the cross-section dimensions (see Fig.1(a)) and lengths effectively measured for each column specimen are shown in Tables 1 and 2. The column specimen end sections were welded to 25 mm thick steel plates, subsequently bolted to the bearing plates – this procedure ensures full contact between the column specimen ends and the bearing plates, *i.e.*, full warping restraint. The column specimen labeling provides information about the test series and the location and orientation of the CFS: (i) the first letter indicates whether the specimen belongs to the short (“S”) or long (“L”) column test series, (ii) the following letters indicate if the specimen has no strengthening (“NIL”), CFS located in the web (“W”), CFS located in the web and flanges (“WF”) or CFS located in the web, flanges and lips (“WFL”), and (iii) the numbers specify whether the CFS are oriented longitudinally (“0”) or transversally (“90”). Finally, the letter “R” identifies a repeated test.

The material properties of the cold-formed steel column specimens were obtained through tensile coupon tests – the coupons were extracted from the specimen central web regions, in the longitudinal direction, and their dimensions conformed to the Australian Standard AS 1391 (1991) for tensile testing of metals: 12.5 mm wide coupons of gauge length 50 mm . The values measured in the coupon tests are given next, for the short and long columns (nominal 0.2% proof stresses $\sigma_{0.2,s}=550\text{ MPa}$ and $\sigma_{0.2,l}=450\text{ MPa}$): (i) static 0.2% proof stresses $\sigma_{0.2,s}=610\text{ MPa}$ and $\sigma_{0.2,l}=521\text{ MPa}$, (ii) Young’s moduli $E_s=207\text{ GPa}$ and $E_l=218\text{ GPa}$, (iii) static tensile strengths $\sigma_{u,s}=626\text{ MPa}$ and $\sigma_{u,l}=546\text{ MPa}$ and (iv) elongations after fracture $\varepsilon_{f,s}=9.2\%$ and $\varepsilon_{f,l}=11.4\%$ (based on the 50 mm gauge length). As for the CFS thickness and material properties, the values provided by the fabricators were adopted – they read: (i) thickness $t_{CFS}=0.11\text{ mm}$, (ii) tensile strength $\sigma_{u,CFS}=4200\text{ MPa}$, (iii) tensile modulus $E_{CFS}=235\text{ GPa}$ and (iv) elongation after fracture $\varepsilon_{f,CFS}=1.8\%$. Moreover, the (single) CFS were attached to the outer surfaces of the zinc-coated cold-formed steel columns by means of an epoxy resin with tensile strength and modulus equal to $\sigma_{u,r}=30\text{ MPa}$ and $E_r=3.5\text{ GPa}$ – after attaching the CFS, the column specimens were completely cured for 7 days.

Fig. 1(b) shows the failure mode of a short column specimen and also provides an overall view of the test rig and experimental set-up employed – (i) the DARTEC servo-controlled hydraulic testing machine used to compress the column specimens, (ii) the two steel plates welded to the specimen ends, (iii) the rigid flat bearing plate connected to the testing machine upper support (and bolted to the specimen top end plate) and restrained against flexural (minor/major axis) and twist rotations, and (iv) the lower special bearing, bolted to the specimen bottom end plate and subsequently restrained against flexural and twist rotations

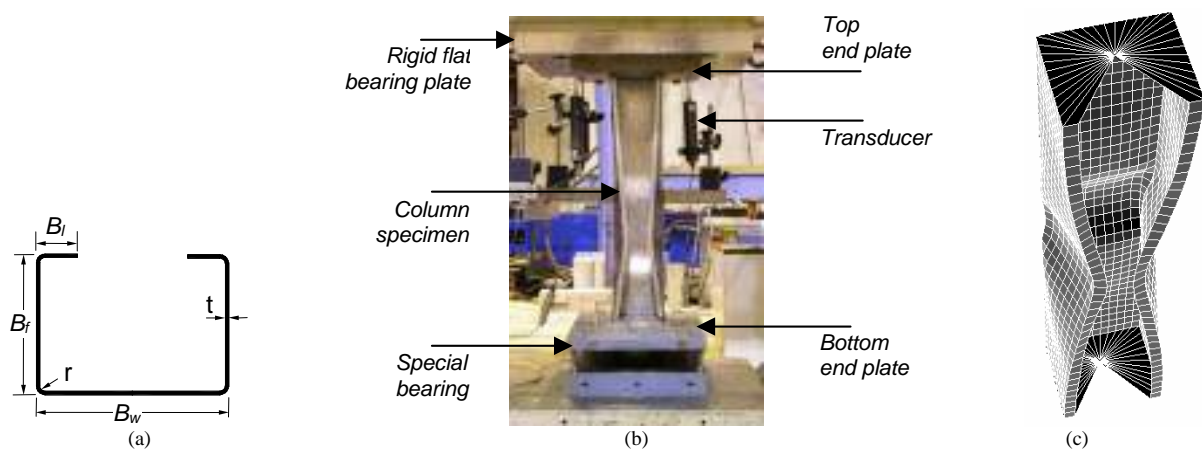


Figure 1: (a) Cross-section geometry, (b) experimental set-up and test view and (c) FEM failure mode (S-F-90)

Table 1: Measured dimensions and experimental/numerical ultimate strengths of the short column specimens

Specimen	B_w (mm)	B_f (mm)	B_l (mm)	t (mm)	r (mm)	L (mm)	P_{Exp} (kN)	P_{Num} (kN)	P_{Num}/P_{Exp}
S-NIL	124.1	101.9	13.8	1.071	3.0	600	54.9	55.3	1.007
S-W-0	124.1	101.9	13.7	1.074	3.0	600	55.9	57.0	1.020
S-F-0	124.0	102.0	13.7	1.075	3.0	600	56.0	58.1	1.038
S-WF-0	123.6	101.9	13.7	1.068	3.0	602	60.2	62.1	1.032
S-WFL-0	124.0	101.9	13.7	1.070	3.0	599	61.4	62.3	1.015
S-W-90	124.1	102.0	13.6	1.068	3.0	600	55.6	54.9	0.987
S-F-90	123.7	101.9	13.8	1.073	3.0	601	56.4	57.1	1.012
S-WF-90	124.1	101.9	13.7	1.061	3.0	601	63.2	59.3	0.938
S-WF-90-R	124.1	101.9	13.8	1.073	3.0	600	62.4	59.3	0.950
Mean	124.0	101.9	13.7	1.070	3.0	---	---	---	1.000
COV	0.002	0.000	0.005	0.004	0.000	---	---	---	0.035

Table 2: Measured dimensions and experimental/numerical ultimate strengths of the long column specimens

Specimen	B_v (mm)	B_f (mm)	B_l (mm)	t (mm)	r (mm)	L (mm)	P_{Exp} (kN)	P_{Num} (kN)	P_{Num}/P_{Exp}
L-NIL	126.3	102.6	13.8	1.552	3.0	2199	85.2	91.3	1.072
L-NIL-R	126.6	102.8	13.6	1.553	3.0	2200	86.7	91.3	1.053
L-W-0	126.4	102.7	13.8	1.556	3.0	2202	95.5	99.3	1.040
L-F-0	126.4	102.6	13.9	1.560	3.0	2199	90.1	92.0	1.021
L-WF-0	125.8	102.7	13.8	1.556	3.0	2201	98.6	100.3	1.017
L-WFL-0	125.7	102.8	13.8	1.555	3.0	2200	102.1	100.5	0.984
L-WFL-0-R	126.4	102.8	13.7	1.553	3.0	2200	100.4	100.5	1.001
L-W-90	125.6	102.7	13.7	1.549	3.0	2200	88.1	89.0	1.010
L-F-90	125.4	102.6	13.7	1.567	3.0	2199	92.6	88.2	0.952
L-WF-90	125.2	102.7	13.8	1.559	3.0	2199	100.9	100.5	0.996
Mean	126.0	102.7	13.8	1.556	3.0	---	---		1.015
COV	0.004	0.001	0.006	0.003	0.000	---	---		0.036

(by means of vertical and horizontal bolts that lock the bearing in position, once full contact is achieved) – these special bearings materialize fixed-ended supports, with the upper one allowing for longitudinal translations (to apply the compressive force). Three displacement transducers were used to measure the vertical motion of the top end plate, thus monitoring (i) the axial shortening of the column specimen and (ii) the effective absence of flexural rotations. Displacement control was used to drive the hydraulic actuator at a constant speed of 0.2 mm/min in all cases – this loading arrangement made it possible to continue column specimen tests beyond the ultimate load level, *i.e.*, to determine the post-ultimate equilibrium path descending branch. A data acquisition system was used to record the applied load and displacement transducer readings at regular intervals throughout the duration of the tests – the static loads were recorded by pausing the applied straining for 1.5 min and, in order to assess the column specimen ultimate strengths as accurately as possible, the recording frequency was increased at the onset of collapse (*i.e.*, when a considerable column axial stiffness reduction was detected).

All the experimental ultimate strength values (P_{Exp}) obtained, concerning the short and long cold-formed steel lipped channel columns with and without CFS-strengthening, are given in Tables 1 and 2. It should be noted that all (short and long) column failures were due to local-plate/distortional buckling mode interaction, as illustrated experimentally and numerically in Figs. 1(b)-(c), for the case of the column specimen S-F-90. Then, the excessive column wall deformations caused by the buckling-triggered collapse, clearly visible in Fig. 1(b), also cause the occurrence of CFS debonding in the post-failure stages. In order to assess the reliability of the experimental set-up and procedure, three tests were repeated – the differences between the ultimate strengths determined for each pair of (supposedly) identical column specimens were 1.3% (S-WF-90), 1.8% (L-NIL) and 1.7% (L-WFL-0). Finally, curves providing the variation of the column axial shortening with the applied load (P vs. u) for the column specimens S-WFL-0 and L-WFL-0/L-WFL-0-R are shown in Figs. 2(a) and 2(b), respectively.

3. NUMERICAL INVESTIGATION

The finite element code ABAQUS (HKS, 2002) was used to simulate the non-linear behavior and estimate the ultimate loads of the cold-formed steel lipped channel columns with and without CFS-strengthening. All columns were discretised into meshes of S4R shell finite elements (4-node elements with reduced integration) and the corners were not taken into account in the modeling. In order to simulate the column fixed support conditions, rigid plates (modeled using 3-node rigid elements R3D3) were attached to the column end sections and their centroidal translations and rotations were prevented – only the axial translation of one end section was left free, in order to enable the application of the compressive load. The short and long column meshes involved $15\text{ mm} \times 10\text{ mm}$ (length-width) and $30\text{ mm} \times 10\text{ mm}$ finite elements, which correspond to (i) 1462 and 2250 elements, (ii) 1505 and 2625 nodes, and (iii) 8622 and 15342 degrees of freedom, respectively. Moreover, the numerical analyses were based on (i) the mean measured values of the cross-section dimensions, given in Tables 1 and 2, (ii) the nominal lengths $L=600\text{ mm}$ and $L=2200\text{ mm}$ and (iii) the material properties obtained from the tensile coupon tests (steel) or provided by the fabricators (CFS). The CFS-strengthened walls were modeled as double-ply plates (one steel and one CFS ply) and, in order to have an indication concerning the CFS collapse, both the Maximum Stress and Tsai-Hill failure criteria (Jones 1999) were incorporated in the finite element analysis – these simple models were adopted because the tests showed that the CFS behave elastically until the columns reach their ultimate strengths (CFS debonding takes place afterwards).

Initially, column bifurcation analyses were performed in order to evaluate the buckling loads and identify the corresponding buckling modes – these analyses showed that (i) the short columns buckle in 5 half-wave local-plate modes and (ii) the long columns buckle in 3 half-wave distortional modes. Then, since there is no available information concerning the column initial geometric imperfections (they were not measured), the approach employed involved the performance of several preliminary (elastic) non-linear analyses, each incorporating initial imperfections (i) equally combining the normalized first local-plate and distortional buckling mode shapes and (ii) having different overall amplitudes. The criterion adopted to choose the imperfection to be included in the test simulation (geometrically and physically non-linear analysis) was the coincidence (or

close vicinity) of the initial portions of the experimental and numerical equilibrium paths (P vs. u) – the imperfection amplitudes reached by this approach were found to be almost always very near the column wall thickness. In order to follow the experimental procedure as closely as possible, (i) the non-linear numerical analyses were carried out by means of an incremental-iterative procedure with an arc-length control strategy, (ii) axial displacements were imposed at the column free end section and (iii) the applied load was deemed equal to the reactive force at the other (fully fixed) column end section – it was found that the adoption of this procedure (instead imposing load and reading displacements) precluded the occurrence of numerical difficulties related to the strong local-plate/distortional buckling mode interaction problems (mostly in the long column analyses). All the numerical column ultimate strength values (P_{Num}) are shown in Tables 1 and 2. Moreover, Figs. 2(a) and 2(b) also show the FEM based P vs. u curves for the S-WFL-0 and L-WFL-0/L-WFL-0-R columns.

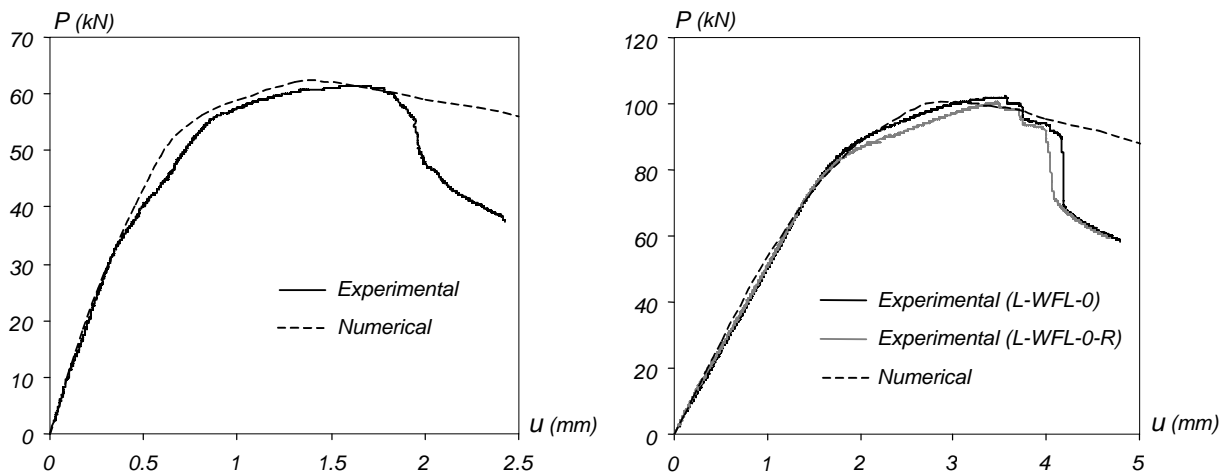


Figure 2: Axial shortening vs. axial load curves for columns (a) S-WFL-0 and (b) L-WFL-0/L-WFL-0-R

The observation of the experimental/numerical results presented in Tables 1-2 and Figs. 2(a)-(b) shows that:

- (i) The experimental and numerical ultimate strength values are in very good agreement – the maximum differences are 5.0% (short columns) and 7.2% (long columns). Moreover, the ratio P_{Num}/P_{Exp} mean and COV values read (i₁) 1.000 and 0.035 (short columns) and (i₂) 1.015 and 0.036 (long columns).
- (ii) In the short columns, the CFS-strengthening of only the web or flanges (0° or 90°) barely affects the ultimate load. On the other hand, the CFS-strengthening of both the web and flanges (0° or, to a larger extent, 90°) leads to non-negligible ultimate load increases (up to 15.1%). This seems to indicate that the local-plate post-buckling behavior of this particular short lipped channel column involves equally the web and flange transverse bending (thus, both have to be stiffened).
- (iii) In the long columns, the CFS-strengthening of only the web (for 0°) or the flanges (for 90°) causes visible ultimate load increases (11.7% and 8.7%) – this increase is even higher if both are CFS-strengthened (15.7% and 18.4% for 0° and 90°), even though a higher increase would be achieved by considering 0° and 90° orientations in the web and flanges.
- (iv) The CFS-strengthening of the lips causes no relevant ultimate load increases in either short (mostly) or long columns.
- (v) The Maximum Stress and Tsai-Hill criteria always predicted the CFS failure after the ultimate load was reached, thus confirming the experimental evidence that debonding only occurs in the equilibrium path descending branch.

4. CONCLUDING REMARKS

Due to space limitations, it is not possible to present and discuss here all the available results. For more detailed information, the reader is referred to previous (Silvestre *et al.* 2004) and subsequent (to be published in the near future) work by the authors.

5. REFERENCES

- Australian Standard (1993), *Steel Sheet and Strip -- Hot-Dipped Zinc-Coated or Aluminium/Zinc-Coated* (AS 1397), Standards Association of Australia, Sydney.
- Australian Standard (1991), *Methods for Tensile Testing of Metals* (AS 1391), Standards Association of Australia, Sydney.
- Hibbit, Karlsson and Sorensen Inc. (HKS) (2002). *ABAQUS Standard* (version 6.3-1).
- Jones, R.M. (1999). *Mechanics of Composite Materials*, Taylor & Francis, Philadelphia.
- Silvestre, N., Camotim, D. and Young, B. (2004). "Buckling behaviour of cold-formed steel members strengthened with carbon fibre sheets", *Proceedings of 2nd International Conference on Steel & Composite Structures* (ICSCS'04 – Seoul, 2-4/9), Editors: C.-K. Choi, H.-W. Lee and H.-G. Kwak, p. 148. (full paper in CD-ROM Proceedings – pp. 412-427)

EXPERIMENTAL AND NUMERICAL STUDY OF THE DEBONDING MECHANISMS IN STEEL ELEMENTS STRENGTHENED BY CFRP STRIPS

Pierluigi Colombi

(Associate Professor, Politecnico di Milan, Milan, Italy)

Paolo Dubini

(Research Fellow, Politecnico di Milano, Milan, Italy)

Giulia Fava

(PhD Student, Politecnico di Milano, Milan, Italy)

Carlo Poggi

(Full Professor, Politecnico di Milano, Milan, Italy)

ABSTRACT

A series of double and single lap joints was tested to characterize their debonding strength for a given adhesive type. The critical value of the interfacial stresses in the shear lap specimen was obtained by a back-analysis, using an approach based on Volkersen's and Goland and Reissner's analyses for adhesively bonded joints. The analytical methods were critically reviewed, mainly focusing on the drawback of the main assumptions. The experimental results were discussed and the influence on the joint strength of some parameters was investigated.

KEYWORDS

CFRP, Double Shear Lap, Single Shear Lap, Debonding, Adhesive.

1. INTRODUCTION

Steel structures and infrastructures may be structurally inadequate due to a possible change in use, an increase of the loading intensity or the safety requirements. The use of fiber reinforced polymers (FRP) is particularly effective in strengthening steel members under axial, flexural and fatigue loading. The advantages compared to traditional techniques such as welding or bolting of steel plates. Some of these are: a) in can be readily implemented on field; b) since the plates are lightweight there is no need of heavy support framework; c) traffic disruption is kept to a minimum. The rehabilitation of metallic beams typically consists in bonding carbon fiber reinforced polymers (CFRP) to the tensile flange in order to provide additional stiffness and strength. Nevertheless, the bond between the FRP and the metal usually represents the weakest link in a strengthened element. In particular, shear and peel adhesive stresses can lead to premature FRP debonding. In order to reduce the interface stresses, the FRP plate should be beveled to 45° or mechanically clamped to the metallic substrate.

In the present study, a series of double and single lap joints was tested to characterize the debonding strength for a given adhesive type. The critical value of the interfacial stresses was obtained by a back-analysis, using an approach based on Volkersen's and Goland and Reissner's analyses (CIRIA C595). The analytical models were critically reviewed with particular reference to the main assumptions on the shear stress boundary condition at the reinforcement end. From the experimental results, a critical stress was first computed through a back analysis and the influence of some parameters (like the shear lap geometry, the mechanical properties and the surface treatments of the adherents) on the joint strength was also highlighted.

2. DOUBLE SHEAR LAP TESTS

The specimens were designed conforming to the requirements of ASTM Standard D 3528. The double shear lap specimens were prepared using two CFRP strips bonded to two steel plates by the epoxy resin. The steel surfaces were treated by an abrasive disk and degreased by a solvent. Specimen dimensions are shown in Figure 1 and Table 1.

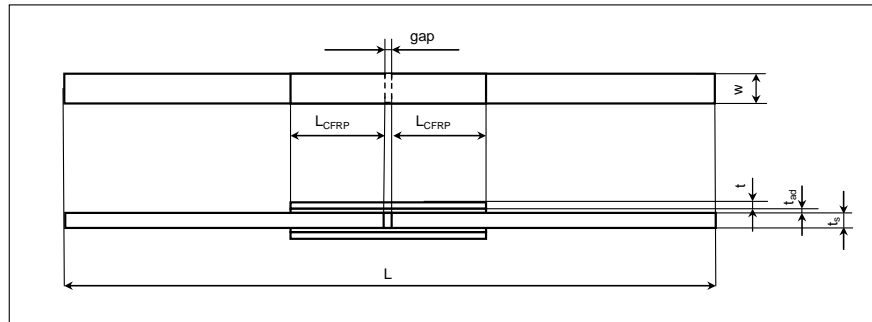


Figure 1. Double shear lap specimens (not to scale)

Table 1. Geometrical properties of the double shear lap specimens

	L [mm]	L _{CFRP} [mm]	gap [mm]	w [mm]	t _{steel} [mm]	t _{CFRP} [mm]	t _{adhesive} [mm]
A1	401	63	3	25.7	5.9	1.4	0.63
A2	400	62	2	22.9	6.0	1.4	0.72
B1	403	124	4	24.3	6.1	1.4	0.90
B2	402	123	3	24.3	6.0	1.4	0.75
C1	403	184	4	26.6	6.0	1.4	0.86
C2	401	184	2	22.0	6.0	1.4	0.89

The steel plates were made by Fe E 275. The nominal Young's modulus was assumed equal to 210000 MPa and the tensile strength of (minimum value) 430 MPa with a Poisson ratio equal to 0.3.

The steel plates were joined using two CFRP cover plates (Sika[®] CarboDur[®]). Tensile tests were performed to evaluate the Young's modulus (197.1 GPa). As reported by the supplier, the nominal value of the tensile strength is greater than 2800 MPa (SIKA Corporation, 2006). The Poisson's ratio of the overlays was assumed equal to 0.3.

The overlays were bonded to the steel plates using a thixotropic epoxy resin (Sikadur[®] 30). The supplier provided a nominal value of the Young's modulus equal to 4500 MPa and a tensile and shear strengths (after a curing period of 7 days at 35 °C) equal to 35 MPa and 22.5 MPa, respectively (SIKA Corporation, 2006). The Poisson's ratio of the adhesive was assumed equal to 0.35.

Uniaxial tension tests were performed under displacement control (0.2 mm/min) with a servo-hydraulic testing machine (MTS) with a load cell axial capacity of 100 kN. In specimens A1, B1 and C1 strain gauges were installed to monitor the load transfer from the steel substrate to the cover plates and to control the bond conditions between the two adherents since, after debonding, the strain in the relevant strain gauge suddenly drops to zero. In particular, specimen A1 was equipped with 2 strain gauges, while specimens B1 and C1 with 3 strain gauges. In each of the three specimens, a strain gauge was located on the gap.

During the loading process, a non-linear response, due to the non-linear behavior of the adhesive, was registered from a load level of about 12 kN to failure. The specimens failure was due to composite debonding which started at the end of the reinforcement moving toward the gap, as observed from the strain gauge response. In general, the fracture surface presented cohesive delamination of the adhesive layer in the gap zone, adhesive delamination of the steel-adhesive interface at the reinforcement ends and partial composite delamination in the middle of the joint. Up to a load of 12 kN, a linear strain gauge response was registered and then, the experimental data were consistent with the analytical results of a direct linear-elastic analysis (Albat and Romilly, 1999).

The critical value of the interfacial stresses in the shear lap specimen was obtained by a back-analysis, using an approach based on Volkersen's theory of a shear lap test specimen (CIRIA C595). Once the failure load is determined, the peak shear and peel stress in the adhesive layer (at the free edge along the centerline) are analytically calculated. The delamination strengths is then evaluated as the maximum principal stress in the adhesive layer and reported in Table 2.

Table 2. Summary of results from the double shear lap tests

	P_{failure} [kN]	ΔL [mm]	A_{bond} [mm ²]	τ_{max} [MPa]	σ_{max} [MPa]	$\bar{\sigma}$ [MPa]
A1	41.75	0.86	1612.8	53.98	28.92	70.35
A2	39.00	0.85	1419.8	56.88	30.47	74.12
B1	42.54	0.95	3075.2	55.45	29.71	72.26
B2	39.56	0.88	2927.4	51.45	27.57	67.04
C1	49.25	1.15	4857.6	58.33	31.25	76.01
C2	39.85	0.99	4066.4	57.06	30.57	74.36

From Table 2, an adhesive average strength of 72.36 MPa is found. On the other hand, considerable stress variation exists near bondline terminations, where stress singularity points exist due to material and geometrical discontinuity. Apart from these regions, Volkersen's model is found to be satisfactory. However, the Volkersen solution considers a constant shear stress through the adhesive layer which is not consistent with the real distribution at the interfaces. Moreover, the boundary condition at the cover plates termination is violated since a non-zero shear stress is estimated. Finally, in Volkersen's model only shear deformation in the adhesive layer is assumed, while the effect of the adherend shear deformation is ignored. As a result, Volkersen's solution overestimates the maximum shear stress.

3. SINGLE LAP-SHEAR TESTS

The specimens were designed conforming to the requirements of ASTM Standard 1002-99. Five single lap-shear specimens were prepared using two aluminum plates bonded together by the epoxy resin (Sikadur[®] 30). The nominal Young's modulus of the aluminum plates was assumed equal to 72 GPa. The specimens are characterized by different dimensions and surface treatments; as reported in Figure 3 and Table 3.

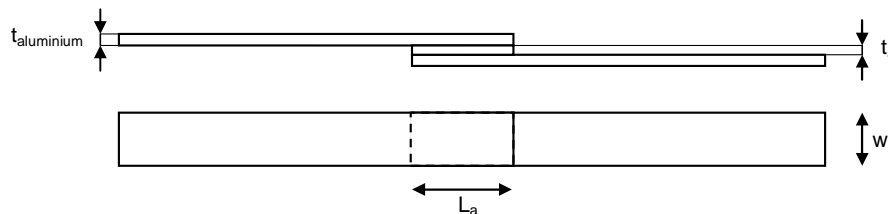


Figure 3. Single shear lap specimens (not to scale)

Table 3. Geometrical properties of the single shear lap specimens

	L_a [mm]	w [mm]	$t_{\text{aluminium}}$ [mm]	t_{adhesive} [mm]	# spec.	Surface treatment
1	70	20	2.2	0.3	2	None
2	60	20	1.8	0.4	3	Solvent
3	34	35	2.0	0.4	3	Solvent
4	60	20	1.8	0.4	3	Sandblast + Solvent
5	34	35	2.0	0.4	3	Sandblast + Solvent

For single shear lap specimens with alignment tabs, uniaxial tension tests were performed under displacement control (0.2 mm/min) with a servo-hydraulic testing machine (MTS) with a load cell axial capacity of 100 kN. No strain gauges were installed. The adhesive strength was obtained by a back-analysis, using an approach based on Goland and Reissner's model. At first, based on the failure load, peak shear and peel stress in the adhesive layer (at the free edge along the centerline) are analytically calculated. Then the adhesive strength is determined as the maximum principal stress in the adhesive (Table 4).

Table 4. Summary of averaged results from the single shear lap tests

	P_{failure} [kN]	A_{bond} [mm ²]	τ_{max} [MPa]	σ_{max} [MPa]	$\bar{\sigma}$ [MPa]
Set1	2.66	1400	16.69	28.64	36.32
Set2	3.39	1200	21.63	37.47	47.35
Set3	5.01	1200	21.57	41.25	50.47
Set4	5.31	1190	32.28	53.89	69.00
Set5	7.51	1190	31.33	58.65	72.24

Comparing the results reported in Tables 2 and 4, the adhesive strength does not seem to be particularly influenced either by the material of the adherents nor by the geometry of the shear lap. Conversely, the surface treatment plays an essential role in increasing the adhesive strength. The treatment by an abrasive disk or sandblasting help to increase the surface roughness and hence improve bond strength (from 36.32 MPa to 71.42 MPa) while solvents are used to obtain a rough and clean, chemically active surface.

On the other hand, in Goland and Reissner's model the strong singularities occurring at the corners of the interface between the adherents and the adhesive are not considered, while these points are believed to be the most likely fracture initiation point.

4. CONCLUSIONS

A series of double and single lap joints was tested to characterize the adhesive properties and to evaluate the force transfer and debonding mechanism. The critical value of the interfacial stresses in the shear lap specimen was obtained by a back-analysis, using an approach based on Volkersen's and Goland and Reissner's models. The analytical methods for adhesively bonded joints were reviewed, and some limitations were detected, mainly concerning the fact that only the cohesive failure in the adhesive along the centerline is considered, while the possibility of interfacial failures is not taken into account. Finally, the adhesive strength is found to be noticeably influenced by the surface treatment, but not by the material of the adherents or by the shear lap geometry.

4. ACKNOWLEDGEMENT

The financial support from the research project RELUIS (Italian Network of Seismic Engineering Labs) is gratefully acknowledged. Thanks are expressed to Sika Italia for supplying the CFRP strips and the adhesive. The authors thank Mr. G. Cersosimo for providing the single lap specimens .

5. REFERENCES

- Albat A.M. and Romilly D.P. (1999) "A direct linear-elastic analysis of double symmetric bonded joints and reinforcements", *Composites Science and Technology*, Vol. 59, pp 1127-1137.
- Cadei J., Stratford T.J., Hollaway L.C., and Duckett W.G. (2004) "Strengthening metallic structures using externally bonded fibre-reinforced polymers. CIRIA C595, London, U.K.
- Colombi P. and Poggi C. (2006) "An experimental, analytical and numerical study of the static behaviour of steel beams reinforced by pultruded CFRP strips", *Composites: Part B*, Vol. 37, pp. 64–73.
- SIKA Corporation. (2006). Technical data Sheets <http://www.sika.it/con/con-prod/con-prod-index.htm> 15/03/06
- Taljsten B. (1997) "Strengthening of beams by plate bonding", *J Mater Civ Eng*, Vol 9(4), pp 206-212.

EXPERIMENTAL STUDY ON FATIGUE BEHAVIOR OF TENSILE STEEL PLATES STRENGTHENED WITH CFRP PLATES

Zheng Yun Lingping Ye Xinzheng Lu

(Department of Civil Engineering, Tsinghua University Beijing 100084)

Q.R.Yue

(Central Research Institute of Building and Construction, MCC Group Beijing 100088)

Abstract

Fatigue experiments of six steel plates strengthened with CFRP plates are presented in this paper. The specimens are loaded in tension. The factors that may influence the effect of strengthening are discussed, including the amount of strengthening CFRP plates, the one face or two faces mode strengthening and the stress range. Experimental results show that the fatigue lives of steel plates can be greatly increased with externally bonded CFRP plates when they are compared with un-strengthened specimens.

Keywords

CFRP, Steel plate, Tensile, Fatigue life, Strengthening

1. INTRODUCTION

Due to the light weight, high strength, good durability and excellent fatigue performance, Carbon Fibre Reinforced Polymer (CFRP) is widely used in last decade to strength concrete structures. And in recent years, more attentions have been given on strengthening steel structural elements with CFRP. Most of such steel strengthening researches are focused on the enhancement of static load capacity. Very limited work can be found in the existing literatures on the fatigue strengthening [Zheng et al. 2005]. Colombi et al. (2003) suggested that CFRP patching would be a good solution for strengthening steel structural elements with fatigue damage, and prestressed CFRP patches would have a better performance on interfacial debonding. However, in practices, prestressed CFRP strengthening is not widely welcomed due to the inconvenience of construction. Tavakkolizadeh & Saadatmanesh (2003) studied the fatigue strength of 21 specimens made of W127×4.5 steel beams. The clear spans of all specimens were 1220mm and were all tested under four-point bending with 200mm spacing between the loading points. For all stress ranges considered in their work, this strengthening technique improved the fatigue lives of the strengthened specimens by about 2.6~3.4 times higher than those of un-strengthened specimens. Sean et al. (2003) reported their fatigue experiments on 21 specimens with edge notches and 8 specimens with center holes. Though their test results scattered greatly,

CFRP strengthening still shows a promising increase on the fatigue lives of steel elements. However, the above existing works have a common drawback that the initial faults in the steel elements are not real fatigue damages, but mechanical cutting notches or holes. Hence, in this work, pre-cracking cycle loads were imposed firstly on the steel plates to give a same level of real fatigue damage. And then the specimens were tested under different levels of tension load to get a more realistic simulation of fatigue strengthening.

2. EXPERIMENTAL TEST SETUP AND SPECIMENS

The steel plates used in this study is made of 16Mn whose yield strength is 435MPa. The size of the steel plates are 700mm in length, 100mm in width and 10mm in thickness, as shown in Figure 1a. The initial cracks are introduced by cutting 2 notches with a length of 2mm on opposite sides of the 2mm hole in diameter which is located at the centers of the plates, as shown in Figure 1b. Two kinds of CFRP plates with different thickness and stiffness are adopted in the tests. One is 1.0mm thick with a normal modulus of 165GPa and another is 1.4mm thick with a higher modulus of 320GPa. The adhesive used was a two-part thixotropic epoxy resin adhesive (Araldite 2015), with a shear modulus of 0.9 GPa.

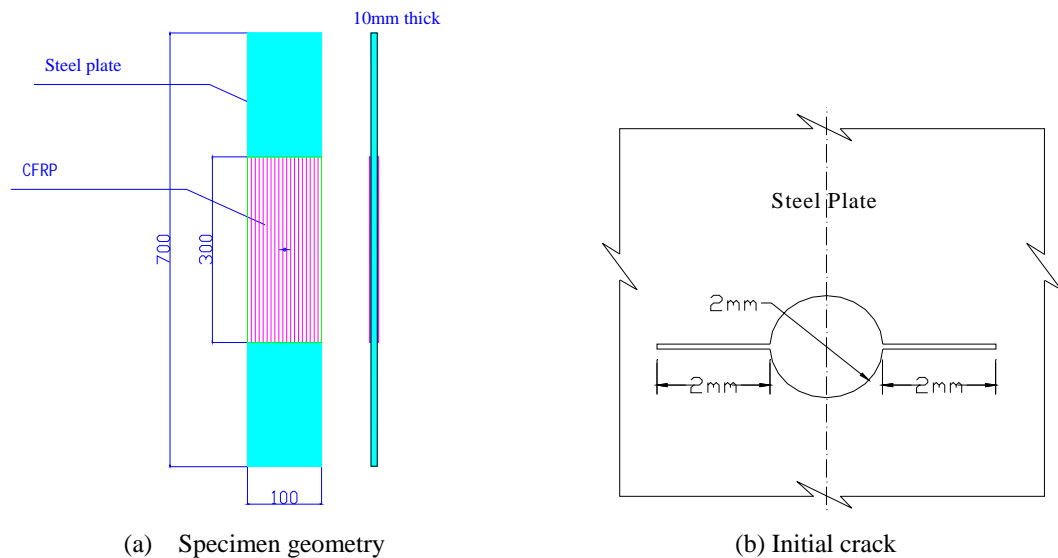


Figure 1 Specimen Geometry

The six specimens tested in this work were shown in Table 1. Following 3 parameters are considered: stress range, strengthening method and stiffness of CFRP. Specimens PC120 and PC90 are un-strengthened control ones with different stress range of 120MPa and 90 MPa. Specimen PS120 and PD120 were both tested under a stress range of 120MPa but the former one was strengthened with high modulus CFRP on single side whilst the later one was strengthened on both side. Specimen PD90 has the same strengthening scheme with PD120 but was tested under a stress range of 90MPa. Specimen PD120a has the same strengthening scheme and stress range with PD120 but normal modulus CFRP is used. Pre-crack cycle load with a stress range of 200MPa were give to all specimens to guarantee the fatigue cracks would propagate from the initial notches and to induce a 10mm length of fatigue cracks along the two notches on opposite sides of the hole. CFRP strengthening was installed after pre-cracking load. Then the fatigue testing of all the specimens was conducted under the cyclic tensile loads. A constant amplitude sine wave of 500 times/min frequency with stress ratio of 0.4 was applied.

Table 1 Specimen Details

Specimen numbers	Stress range /MPa	N_{max}/N_{min} /kN	Repaired Mode	CFRP Type	Stiffness Ratio (S)
PC120	120	200/80	Without strengthening	None	0
PC90	90	150/60	Without strengthening	None	0
PS120	120	200/80	Single Side	High Modulus	0.22
PD120	120	200/80	Double sides	High Modulus	0.43
PD90*	90	150/60	Double sides	High Modulus	0.43
PD120a	120	200/80	Double sides	Normal Modulus	0.16

Note: Stiffness ratio (S) is defined as: $S = \frac{\sum E_{CFRP} t_{CFRP}}{E_{Steel} t_{Steel}}$.

Table 2 Test results of fatigue lives of specimens

Stress Range (MPa)	Specimen	Repairing Mode	Stiffness Ratio (S)	Fatigue Lives ($\times 10^4$)	Increased life (%)
120	PC120	/	0	18.2	Baseline
	PS120	Single side	0.21	46.4	155
	PD120	Double Sides	0.43	100.0	450
	PD120a	Double Sides	0.16	65.0	260
90	PC90	/	0	48.4	Baseline
	PD90	Double Sides	0.43	331.2	580

3. EXPERIMENTAL RESULTS

The fatigue lives of all the specimens were listed in Table 2. It can be shown that fatigue lives of strengthened specimens were increased by 155~580% over un-strengthened specimens.

Figure 2 shows comparisons on the propagation of fatigue cracks. Different strengthening modes are compared in Figure 2a which illustrates that double bonded specimen (PD120) results in a much slower crack propagation speed than un-strengthened one (PC120) and the single side boned one (PS120), even though the interfacial debonding of PD120 was much worse than other two specimens due to poor quality installation of CFRP plates. Figure 2b shows a better example on the increment on fatigue life because no interfacial failure happened in the specimens. The strengthened specimen PD90 has an additional 3 million cycles longer fatigue life than the un-strengthened specimen PC90. Figure 2c shows the influence of stiffness of CFRP plates to the fatigue life. Higher stiffness results in a longer fatigue life. Figure 2d shows the influence of the stress range to the fatigue life. Larger stress range will heavily reduce the fatigue life.

4. CONCLUSIONS

In this study, the fatigue behavior of six steel plates strengthened with external bonded CFRP plates was investigated. It is shown that, (1) the fatigue life of strengthened specimens was increased by 155~580% over un-strengthened specimens, which indicated that fatigue life can be improved effectively by external bonded CFRP to the steel structures with fatigue crack; (2) The strengthening is more effective when CFRP plates with higher modulus are bonded to both sides of the steel plates; (3) De-bonding of CFRP from steel plate took place so early during the test of specimen PD120 that the retrofitted effect is not good. Therefore the quality control of bonding technique is very

important and some measures should be made.

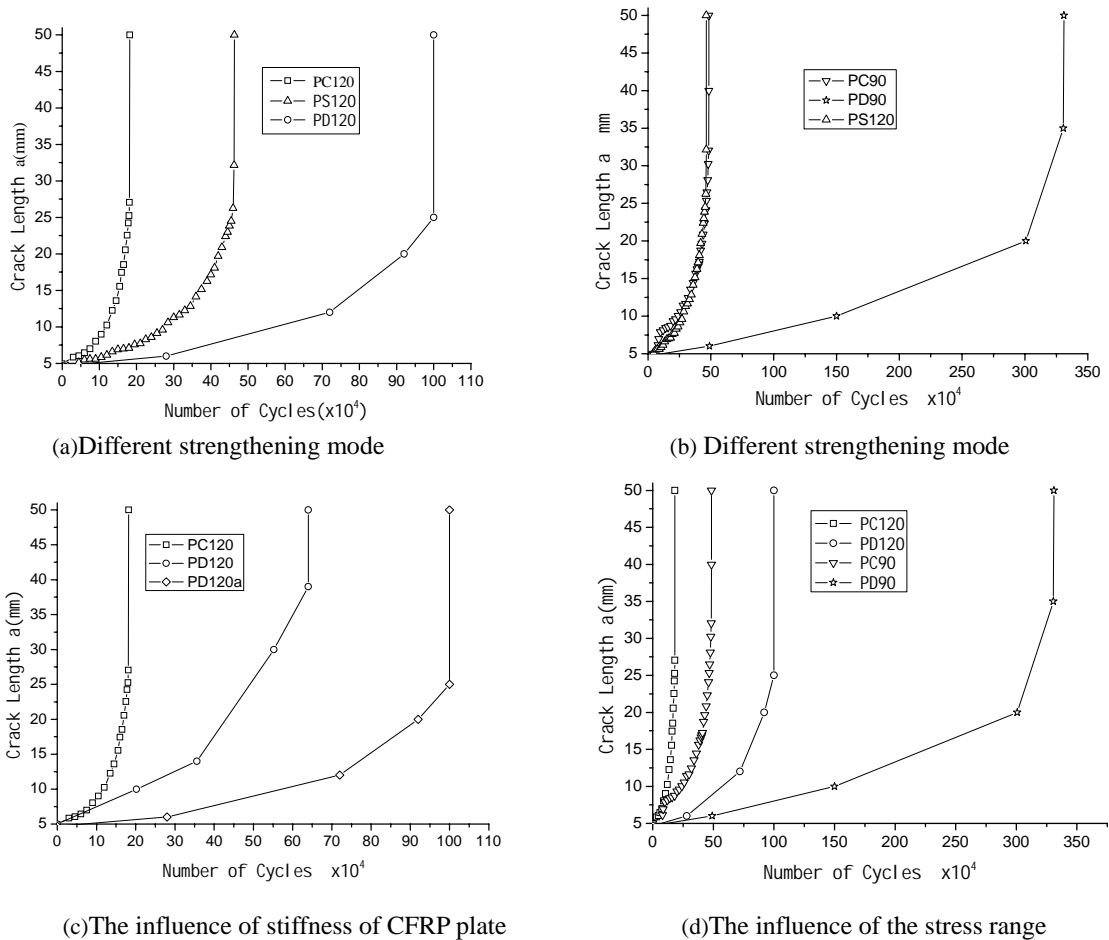


Figure 2 Fatigue crack propagation curves

5. ACKNOWLEDGEMENT

The authors are very appreciated to the key project No. 50238030 granted by Natural Science Foundation of China to support to the research presented here.

6. REFERENCES

- Zheng Yun, Ye Lieping and Yue Qingrui(2005). "Progress in research on steel structures strengthened with FRP", *Industrial Construction*, Vol.35, No.8, pp 20~25.
- P. Colombi, A. Bassetti and A.Nussbaumer(2003). "Analysis of cracked steel members reinforced by pre-stress composite patch", *Fatigue Fract Engng Mater Struct*, Vol.26, pp 59~66
- M. Tavakkolizadeh and H. Saadatmanesh(2003). "Fatigue Strength of Steel Girders Strengthened with CFRP patch". *Journal of Structural Engineering*, Vol.129, No.2, pp 186-196
- Sean C. Jones and Scott A. Civjan, P.E (2003). "Application of Fiber Reinforced Polymer Overlays to Extend Steel Fatigue Life", *Journal of Composites for Construction*, Vol.7, No. 4, pp 331-338

PRELIMINARY BOND-SLIP MODEL FOR CFRP SHEETS BONDED TO STEEL PLATES

S.Fawzia, X.L. Zhao, R. Al-Mahaidi

Department of Civil Engineering, Monash University, Clayton, Victoria 3800, Australia

S.H. Rizkalla

North Carolina State University, Raleigh, North Carolina, USA

ABSTRACT

Carbon fiber reinforced polymer (CFRP) sheets have established a strong position as an effective method for innovative structural rehabilitation. However, the use of externally bonded CFRP in the repair and rehabilitation of steel structures is a relatively new technique that has the potential to improve the way structures are repaired. An important step toward understanding bond behaviour is to have an estimation of local bond stress versus slip relationship. The current study aims to establish the bond-slip model for CFRP sheets bonded to steel plate. To obtain the shear stress versus slippage relationship, a series of double strap tension type bond tests were conducted. This paper reports on the findings of the experimental studies. The strain and stress distributions measured in the specimens for two different bond lengths. The results show a preliminary bi-linear bond-slip model may be adopted for CFRP sheet bonded with steel plate.

KEYWORDS

FRP Sheet, Bonding, Bond-Slip Model, Slip, Shear Stress.

1. INTRODUCTION

Successful use of carbon fiber-reinforced polymer (CFRP) materials for strengthening concrete structures has already been established [e.g. ACI Committee 440F 2002, Teng et al 2002, Oehlers and Seracino 2004, Pham and Al-Mahaidi 2006]. However, the development of the system for strengthening steel structures with CFRP materials is limited. More strengthening materials are needed to achieve a significant strength increase as steel is much stronger than concrete, especially in tension. But as more strengthening material is added the bond stresses become more critical. There have been relatively fewer studies on the bond stress and slip relationship between CFRP sheet and steel structures.

The bond-slip relationship relating the interfacial shear stress to the interfacial slip for steel structure strengthened by CFRP plate was recently studied by Xia & Teng (2005). In this paper a local bond-slip relationship is proposed from the experimental results for CFRP sheets bonded to steel structure. The possibility of finding local bond-slip relationship using long bond length (say twice the effective bond length or higher) is strictly related to the consideration of the distribution of slip and bond shear stress along the bond length.

2. EXPERIMENTAL PROGRAM

2.1 Bond specimen and surface preparation

The tensile specimen was composed of mild steel plate bonded with three layers of CFRP sheet on both sides. Figure 1 shows the schematic specimen configuration. A careful, meticulous approach is necessary when dealing with bonding since it may be difficult to verify the quality of the bond. Moreover, due to the local effect of bond stresses, any local defect of the bond may result in complete debonding of the applied strengthening material. The steel plate was 6mm thick and 900 mm long in total. The steel plate was grinded at 45° by angle grinder (FH38A36S-BF41). After grinding, the steel plate was cut into two pieces and then added together by applying small amount of adhesive at the cross section. After that the plate was cleaned by Acetone. Adhesive was first applied on the surface of steel plate by brush. Then a piece of fiber sheet, which had been cut beforehand into prescribed sizes using scissors, was placed with the fiber side down onto the coating and generally smoothed down by hand. After that, the surface of the sheet was rolled over along the longitudinal direction of the fibers using a ribbed roller to impregnate resin into the fibers and removed any air bubbles. Rolling was continued until the resin was squeezed out between the fibers. Same steps were followed to bond two more layers of fibers. The specimen was cured at least one week and then postcured for 24 hours at 70°C.

2.2 Material properties

Measured modulus of elasticity, tensile stress and thickness of CFRP sheet are 250 GPa, 1710MPa and 0.176mm, respectively. The modulus of elasticity and tensile stress of adhesive are 1900MPa and 32 MPa, respectively.

2.3 Instrumentation

Sixteen strain gauges were attached to each test specimen. Figure 1 shows the location of each gauge. Ten strain gauges were placed along the length at every 25mm on one side of the CFRP sheet to capture the longitudinal strain development along the bond length. Four strain gauges were placed on the backside of the specimen at every 50mm to act as “backup” gauges and for comparison with the primary gauge readings. Two additional strain gauges were attached to the steel plate before the initiation of the CFRP sheets and were used to determine the actual load applied to the steel plate during testing.

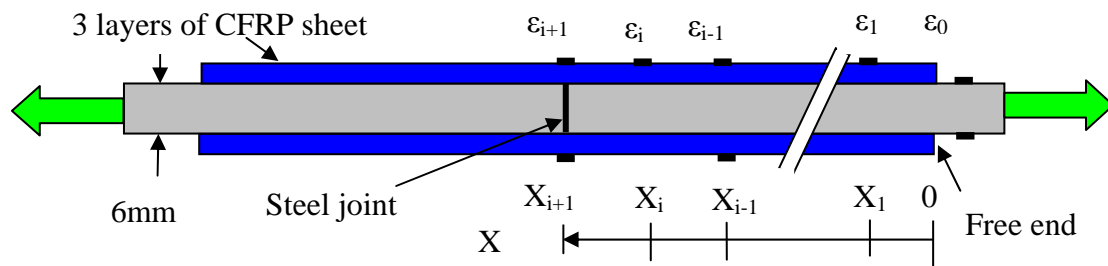


Figure 1: A Schematic of specimen and strain gauge locations

2.4 Failure mode and test results

Test results, together with the failure modes are presented in Table 1.

Table 1: Test results

Test specimen	S1	S2	S3	S4	S5	S6
Bond length (mm)	250	250	250	200	200	200
Overall thickness of specimen (mm)	9.50	9.75	9.82	9.28	9.38	9.46
Ultimate load (kN)	89.6	97.2	77.5	92.6	71.6	99.6
Failure mode	Bond	Bond	Bond	Bond	Bond	Bond

3. Strain and interfacial stress distribution

The data obtained from the strain gauges at the top layer of CFRP was used to create strain versus distance (from the steel joint) plots. The top strain is different from the average composite strain as the strain could vary across the layers of the composite. This variation was measured experimentally for circular tube strengthened by CFRP sheet [Fawzia et al.2004]. In this study it was assumed that the measured strain was representing the average CFRP strain. The distributions of strain along the bond length for different load levels are plotted in Figure 2 for Specimen S6. The distance in the figure is measured from the joint location, At low load levels, the distributions show a gradual decline from the peak near the steel joint to the other end. As the load increases up to 98.3kN, the strain values increase and the peak strain gradually shifts away from the joint. At low levels, the distributions have the largest slope near the steel joint. As the load increases, the maximum slope shifts away from the joint. This means that redistribution of the bond stress along the bond length occurs as a result of changes in the state of bond.

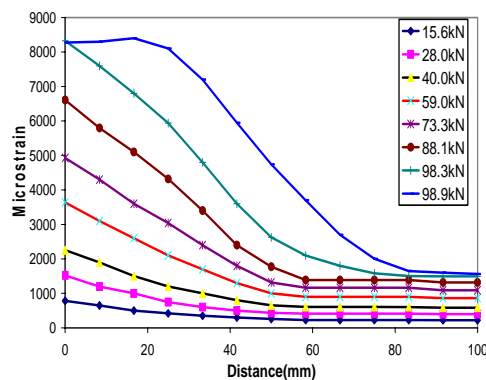


Figure 2: CFRP strain distribution

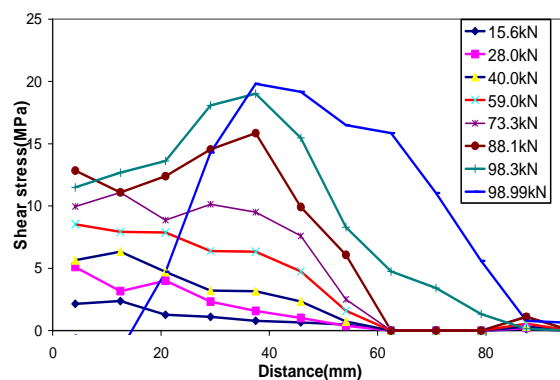


Figure 3 : Shear (bond) stress distribution

The average experimental shear stress between the two strain gauges were calculated using the relationship $\tau = \frac{E_f (\varepsilon_{f,i+1} - \varepsilon_{f,i}) t_f}{X_{i+1} - X_i}$, where E_f and t_f are the CFRP elastic modulus and thickness respectively and $\varepsilon_{f,i+1}$, $\varepsilon_{f,i}$ are the CFRP strains and X_{i+1} , X_i are the distance between strain gauges according to Figure 1. The shear stress distribution along the distance away from the “steel joint” is shown in Figure 3. It should be pointed out that there is a gap between the two steel plates. The location of the “steel joint” is equivalent to the “loaded edge” in the set up of testing bond between CFRP plate and steel (Xia and Teng 2005). The theoretical stress distribution for bond between CFRP and concrete can be found in H.Yuan et al. (2004). The theory shows that at loaded edge the shear stress is zero when it reaches peak load indicating occurrence of debonding. It can be seen from Figure 3 that when the load is less than 59kN, the peak shear stress is located at the steel joint. The location of the peak shear stress moves away from the “steel joint” as the load increases further. The shear stress at the steel joint becomes zero when the maximum load occurs indicating the occurrence of debonding.

The shear stress distribution along the distance away from the “steel joint” is shown in Figure 3. It should be pointed out that there is a gap between the two steel plates. The location of the “steel joint” is equivalent to the “loaded edge” in the set up of testing bond between CFRP plate and steel (Xia and Teng 2005). The theoretical stress distribution for bond between CFRP and concrete can be found in H.Yuan et al. (2004). The theory shows that at loaded edge the shear stress is zero when it reaches peak load indicating occurrence of debonding. It can be seen from Figure 3 that when the load is less than 59kN, the peak shear stress is located at the steel joint. The location of the peak shear stress moves away from the “steel joint” as the load increases further. The shear stress at the steel joint becomes zero when the maximum load occurs indicating the occurrence of debonding.

4. BOND-SLIP MODEL

The measured strain distribution along the bond length was used by integration to calculate local slips. Actually this local slip is the relative displacement between the CFRP sheet and the steel plate. Calculated bond stresses and slips are combined to obtain the local bond-slip curves. Bond-slip curves obtained from experimental data can be approximated as a bi-linear shape (Lu et al., 2005). These curves have a linear ascending branch followed by a linear descending branch. A schematic view is presented in Figure 4 which can be defined by three parameters δ_1 , τ_f and δ_f . The initial stiffness of the bond-slip curve is high, representing linear elastic state. Initiation of interfacial softening stage means load continues to increase as the length of the softening zone increases. The ultimate load is first attained at the end of this stage and starts propagation of debonding. These three stages can be identified from load-displacement behaviour. The local bond slip relationship is reasonably consistent between different locations on the same specimen.

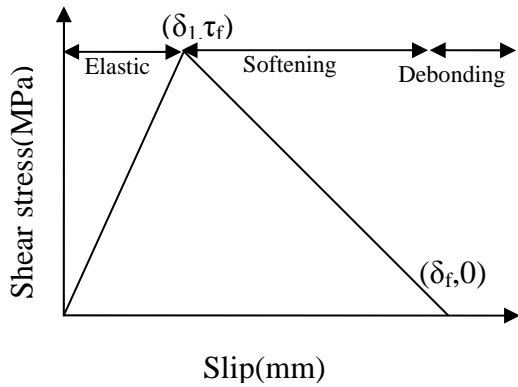


Figure 4 Bond slip model approximation

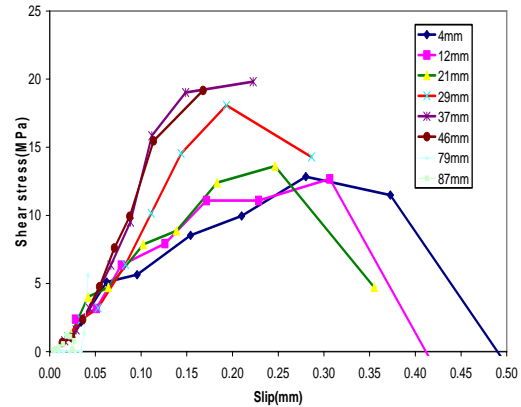


Figure 5 Bond slip curve (Specimen S6)

Figure 5 shows the stress vs slip curves (specimen S6) with bond length of 200mm. It seems that a bi-linear model may be adopted to represent the bond-slip relationship for CFRP sheet bonded with steel plate. However, the three parameters (δ_1 , τ_f and δ_f) in bond-slip model are to be determined after processing all the test data. These will be compared with those given by Xia & Teng (2005) in the near future.

5. CONCLUSIONS

The following conclusions can be drawn from this paper.

1. Strain distribution profiles show that strain level is significant over a limited bond length.
2. When debonding occurs at most highly stressed end, less or almost zero stress is transferred at that end and the maximum shear stress location shifts towards the unloaded end of the specimen.
3. The bond-slip curve may be approximated as a preliminary bilinear model. More reliable peak shear stress and slip values will be produced after analysing more test data.
4. The limitations of such bilinear model mentioned elsewhere in the paper are Depend on the values of δ_1 , τ_f and δ_f . One type of CFRP, One type of adhesive, Bond failure happened around 53% of FRP rupture strain, Only two types of bond length has considered.

6. REFERENCES

1. ACI Committee 440 (2002), Guide For The Design And Construction Of Externally Bonded FRP Systems For Strengthening Concrete Structures. American Concrete Institute, Detroit MI.
2. Fawzia, S., Zhao, X. L., Al-Mahaidi, R. and Rizkalla, S. (2004). Investigation Into The Bond Between CFRP And Steel Tubes, The Second International Conference on FRP Composites in Civil Engineering, CICE2004, December, Adelaide., pp733-739.
3. H. Yuan, Teng, J. G., Seracino, R., Z.S. Wu and J. Yao. (2004). Full-Range Behaviour Of FRP - To-Concrete Bonded Joints. Engineering Structures. Vol.26: pp553-565.
4. Lu, X.Z., Teng, J.G. Ye, L.P. and Jiang, J.J. (2005) Bond-Slip Models For FRP Sheets/Plates Bonded To Concrete. Engineering Structures. Vol.27: pp 920-937.
5. Oehlers, D.J. and Seracino, R. (2004), Design Of FRP And Steel Plated RC Structures – Retrofitting Beams And Slabs For Strength, Stiffness And Ductility, Elsevier, Oxford, UK
6. Pham, H. B. and Al-Mahaidi, R. (2006), “Prediction Models For Debonding Failure Loads Of CFRP Retrofitted RC Beams”, Journal of Composites for Construction, Vol. 10, No. 1, pp. 48-59
7. Teng, J. G., Chen, J. F., Smith, S. T. and Lam, L. (2002). FRP-Strengthened RC Structures, John Wiley and Sons Ltd, UK.
8. Xia, S. H. and Teng, J. G. (2005). Behaviour of FRP-to-Steel Bonded Joints. Proceedings of the International Symposium on Bond Behaviour of FRP in Structures (BBFS 2005). International Institute for FRP in Construction, Hong Kong: pp 419-426.

FLEXURAL STRENGTHENING OF COMPOSITE STEEL-CONCRETE GIRDERS USING ADVANCED COMPOSITE MATERIALS

Raafat El-Hacha

(Assistant Professor, University of Calgary, Calgary, Alberta, Canada)

Nora Ragab

(Master Student, University of Calgary, Calgary, Alberta, Canada)

ABSTRACT

Composite steel-concrete girders are used widely in bridge and building construction as the main structural elements in flexure. The load-carrying capacity of an under-strength or deficient steel-concrete composite girders can be improved by epoxy bonding fiber reinforced polymers (FRP) laminates to its tension flange. This paper presents the results of an experimental study that investigated the behaviour of steel-concrete composite girders strengthened in flexure using various advanced composite materials tested under static loading. The different strengthening materials used in this investigation included unidirectional intermediate and high modulus Carbon Fiber Reinforced Polymer (CFRP) plates, unidirectional CFRP sheets and the newly developed unidirectional Steel Reinforced Polymer (SRP) sheets. The primary objective of this investigation was to assess the flexural behaviour of the strengthened beams and examine the effectiveness of the different strengthening materials. Test results are very promising and showed that epoxy bonded CFRP sheets or plates and SRP sheets significantly improved the stiffness and increased the ultimate load carrying capacity of the steel-concrete composite girders. The effect of strengthening on the elastic stiffness and ultimate strength was more profound for beam with high modulus CFRP plate.

KEYWORDS

Carbon fiber reinforced polymer, composite, concrete, externally bonded, flexure, high-modulus, sheets, plates, steel

1. INTRODUCTION

Many researchers conducted experimental and analytical studies on concrete beams and slabs strengthened in flexure using externally bonded FRP sheets or strips, however; research on steel-concrete composite girders is limited and only few studies are reported in the literature. Tests conducted by Mertz and Gillespie (1993) on small-scale steel beams strengthened in flexure with CFRP plates showed about 20% increase in the flexural stiffness and more than 50% increase in the ultimate strength. Sen et al., (1994 and 2001) loaded large-scale steel-concrete composite girders past yielding before being repaired using unidirectional CFRP plates and the results showed an increase in the ultimate strength from 11 to 52% depending on the mode of failure, thickness of the CFRP plates, the anchorage at the ends of the plates, and the yield strength of the steel beams. The effect of the number of layers of CFRP sheets on the behaviour of large-scale composite girders has been investigated by Tavakkolizadeh and Saadatmanesh (2003a) and the test results showed an increase in the ultimate strength by 44, 51 and 76% using 1, 3 and 5 layers, respectively. Tests showed that the CFRP sheets not only extended the fatigue life of a steel beam by more than three times, but also decreased the crack growth rate significantly (Tavakkolizadeh and Saadatmanesh, 2003b). To simulate field corrosion, steel composite beams were damaged by removing 50 and 75% of their bottom flange then repaired using CFRP plates to restore their original strength. Test results showed that 50% of the elastic flexural stiffness can be restored and the ultimate strength was fully restored (Al Saïdy et al., 2004). Recently, high modulus and ultra-high modulus CFRP strips have been used to strengthen large-scale steel composite girders, and test results showed an increase in the ultimate flexural capacity by 16 and 45%, respectively; however, the flexural stiffness increased only by 10% and 36% due to the high elasticity modulus of the strips (Schnerch et al., 2005).

This paper investigates the feasibility and effectiveness of using various materials including high-modulus FRP to strengthen large-scale steel-concrete composite girders, simulating the majority of the highway bridges, tested under static loading. The structural performance of the strengthened steel beams will be examined and discussed.

2. EXPERIMENTAL INVESTIGATION

2.1 Specimens Details

A total of five 6.2m long steel-concrete composite girders made of steel I-beams and 56 mm thick by 435 mm wide reinforced concrete slabs were fabricated and tested. Shear stud connectors welded to the top flange of the steel beams were used to provide the shear connection between the concrete slab and the steel beams. Two longitudinal rows of shear studs were used with a 90 mm transverse spacing between rows of studs. The studs were spaced at 50 mm apart in the longitudinal direction. Figure 1 shows details of a typical beam specimen.

2.2 Material Properties

Concrete

The specified 28-d compressive strength of the concrete was 40 MPa. The actual concrete strength at the day of testing determined as the average of three standard concrete cylinders was 40.3, 39.1, 37.0, 39.0, and 36.5 MPa for beams B1, B2, B3, B4, and B5, respectively.

Steel

The steel beams were standard W200×19.3 Grade G40.21-M345W hot rolled I-sections with average yield and ultimate tensile strengths obtained from tension tests of 414 MPa and 532 MPa, respectively. The interface shear reinforcement along the top flange of the steel beam and the reinforced concrete slab was provided by shear connector. The shear connectors were 6.0 mm diameter and 28.5 mm length with yield and ultimate tensile strengths of 345 MPa and 414 MPa, respectively. The composite concrete deck slab reinforcement consisted of a welded wire fabric steel mesh type 152.4 × 152.4 MW28.3 × MW28.3 with a nominal diameter of 6.0mm.

Strengthening Materials

The externally bonded strengthening systems selected for this study were carbon FRP sheets, carbon FRP plates, and steel-reinforced polymer (SRP) sheets. The material properties of the different systems are given in Table 1. A two-part component epoxy adhesive, the main epoxy resin and the curing agent hardener, was used. Sikadur 330 was used for bonding the SRP and CFRP sheets, and Sikadur 30 was used for bonding the CFRP plates to the bottom flange of the steel girders.

Table 1 – FRP material properties as reported by the manufacturers

FRP products (type)	Dimensions	Elastic Modulus (MPa)	Ultimate Tensile Strength (MPa)
Unidirectional SRP Sheet (Hardwire™ 3×2-23-12)	0.44 mm ² /mm [†]	206000	3170
Pultruded CFRP Plate (Sika Carbodur type S 812)	1.2 mm [‡]	160000	2800
Unidirectional CFRP Sheet (Sika Wrap® Hex230C)	0.381 mm [‡]	61012	715
Pultruded High Modulus CFRP Plate (Sika Carbodur® type H 514)	1.4mm [‡]	300000	1300

[†] Net area per width [‡] Thickness

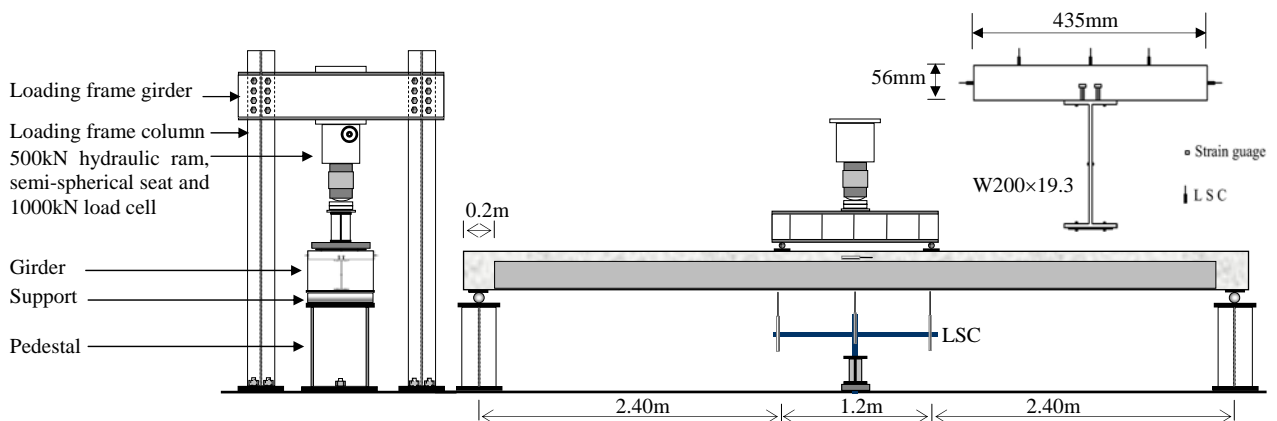


Figure 1: Test set-up and instrumentation of the steel-concrete composite girders

2.3 Test Matrix

One beam (B1) was tested without strengthening and served as unstrengthened control specimen. Four beams (B2, B3, B4, and B5) were strengthened with various systems designed to achieve a 30% increase in the ultimate load carrying capacity over the control beam. Table 2 summarizes the test matrix.

Table 2 – Test matrix for the composite girder specimens

Beam #	Strengthening System
B1	Control beam without strengthening
B2	Beam strengthened using two layers of 82mm wide SRP sheets
B3	Beam strengthened using one layer of 80 mm wide CFRP plate
B4	Beam strengthened using five layers of 98 mm wide CFRP sheets
B5	Beam strengthened using one layer of 25 mm wide HM-CFRP plate

2.4 Surface Preparation of Steel Beam and Installation of the Strengthening Systems

To ensure good and strong bond, the bottom surface of each steel beams was prepared by sand blasting and cleaned by air brushing to remove any dust. Before applying the strengthening materials an organic solvent (acetone) was used to clean the surface from any other bond inhibiting materials. Installation of the strengthening systems followed typical field conditions on the bottom flange beneath the steel I-beams using the dry lay-up technique. The epoxy was allowed to fully cure at room temperature for at least one week before testing the beams. The anchorage system consisted of a steel plate bolted to the bottom flange of the beam at both ends of the strengthening materials.

2.5 Test Setup, Procedure and Instrumentation

The 6.2m long girders were simply supported with a span of 6.0m between supports and tested under four-points bending static loading with 1.2m spacing between the two concentrated point loads. The load was applied using a 500kN capacity actuator through an MTS controller-testing machine operating under displacement control mode. The control beam (B1) was tested under a monotonically increasing load up to failure at a constant loading rate. To study the behavior of the strengthened beams after being loaded to the service condition and past the yield load, the Diagnostic Cyclic Load testing protocol was adopted in beams B2, B3, B4 and B5 (Nanni and Mettemeyer, 2001). All beams were fully instrumented to monitor their behaviour by measuring the deflection at midspan using Linear Strain Conversion devices (LSCs), strains in the concrete in the compression zone, and strain in the steel and in the CFRP and SRP reinforcements using electrical resistance strain gauges. During testing, the data were automatically collected and electronically recorded using a data acquisition system connected to a personal computer. Typical test set-up and instrumentation is shown in Figure 1.

2.6 Test Results and Discussion

The load versus midspan deflection curves comparing the flexural behaviour of the five beams are presented in Figure 2. For beams B2, B3 and B4, the strengthening effect is mainly affecting the post-yielding response since the stresses in the composite materials are less than those in the bottom steel flange due to their lower modulus of elasticity than steel. For the same beams, the improvement in the stiffness in the elastic range prior to yielding of the bottom steel flange is not significant due to the smaller elastic modulus of the strengthening materials compared with the steel section, however; the strengthening effect was more evident for beam B5 strengthened with a high modulus CFRP plate as shown by the significant increase in stiffness in the elastic range and ultimate strength when compared to beams B2, B3 and B4. The effectiveness of the FRP materials was more pronounced after yielding. As expected from the design, the beams achieved the required percentage increase in strength (30%) as can be seen for beams B2 and B3 the increase in strength was 29%, and 35%, respectively, except for beam B4 the increase in strength was 23% because the applied area of CFRP sheets of 187mm^2 (or 5 layers of 98mm) was less than the required 272mm^2 (8 layers of 89.25mm) in order to achieve 30% increase in strength. The use of higher modulus CFRP plate resulted in the highest stiffness increase. Beam (B5) strengthened with HM-CFRP plate demonstrated strength increases up to 49%. All strengthened beams had minimal losses in ductility compared to the control beam.

The load-deflection behaviour is bilinear until failure. No degradation in the stiffness was noticed due to the unloading/loading cycles which became slightly nonlinear after yielding. As well, after yielding, the strengthened beams continued to resist further increase in the applied load with a more gradual linear slope than the pre-yield portion of the curve. The increase in the load continued until failure. Failure of beams B2, B3 and B4 occurred by crushing of the concrete near one of the load points, while beam B5 strengthened with HM CFRP plate failed by rupture of the plate that occurred within the constant moment region. Ductility is slightly reduced with the addition of composite materials. No debonding or delamination between the FRP and the steel beam was observed in any of the beams, indicating that the surface preparation was adequate and the bonding was strong enough.

3. CONCLUSIONS

On the basis of the experimental study presented, the following conclusions can be made:

- No bond failure was observed between the composite materials and the steel surface in all specimens.
- The effect of FRP bonding on the elastic stiffness was not significant for beams strengthened with intermediate modulus CFRP sheets or plates and SRP sheets.
- Test results showed significant increases in the stiffness prior to yield as well in the ultimate strength for the beam with HM-CFRP plate indicating the possibility to increase service loadings. This is very important when strengthening bridge to meet the more stringent limits imposed on serviceability (live load deflections) and ultimate strength of current codes.
- Crushing of the concrete was the dominating mode of failure except for the beam with HM-CFRP plate it was by rupture of the plate in the constant moment region.
- In general, all strengthened beams failed in a ductile manner accompanied by large deformation; however the beam strengthened with HM-CFRP plates showed less ductile behaviour but higher capacity.

To summarize, this study has confirmed the structural benefits and feasibility of using externally bonded intermediate modulus CFRP plates and sheets and SRP sheets to strengthen steel-concrete composite girder. However, the results indicated that high-modulus CFRP plates are more effective at increasing the strength and stiffness and are well suited for use in the repair and strengthening of steel structures.

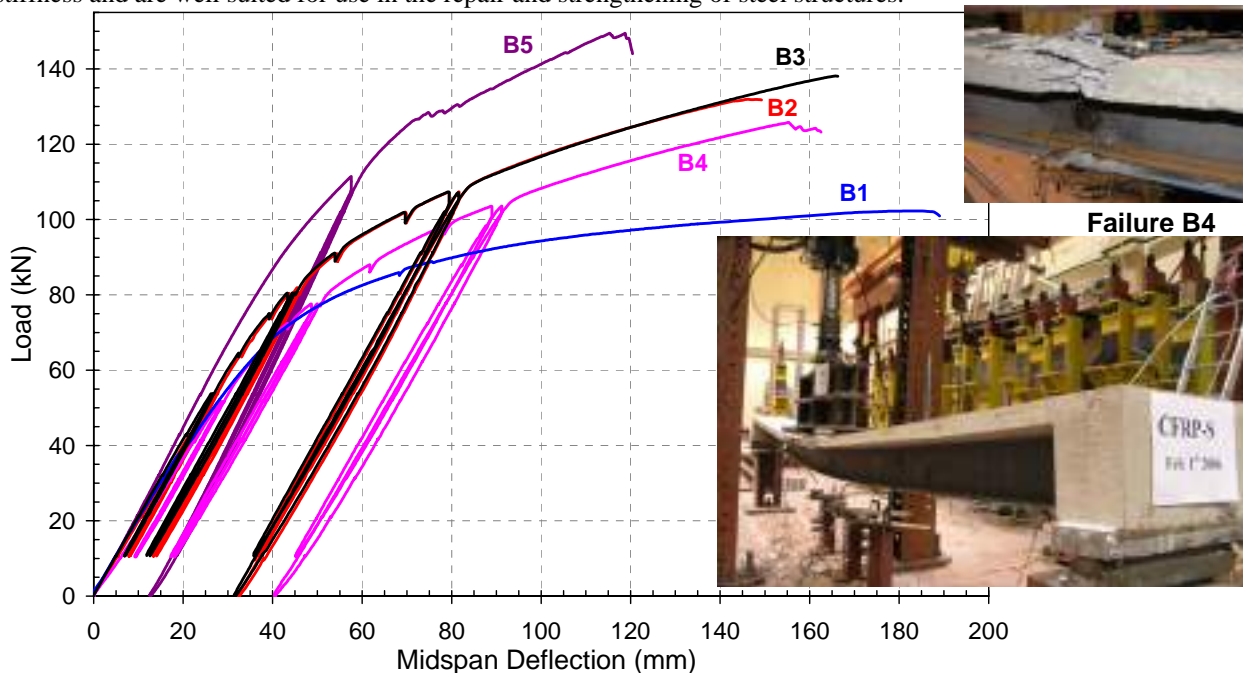


Figure 2 Load-midspan deflection curves for all steel-concrete composite girders

4. REFERENCES

- Mertz, D., Gillespie, J., (1993), "Rehabilitation of Steel Bridge Girders through the Application of Advanced Composite Material", *Transportation Research Board*, Washington, D.C., NCHRP 93-ID11:1-20.
- Sen, R., Liby, L., Mullins, G., (2001), "Strengthening Steel Bridge Sections Using CFRP Laminates", *Composites: Part B*, 32:309-322.
- Tavakkolizadeh, M., and Saadatmanesh, H., (2003a), "Strengthening of Steel-Concrete Composite Girders Using Carbon Fiber Reinforced Polymers Sheets", *J. Struct. Engrg.*, Volume 129, Issue 1, pp. 30-40 (January 2003).
- Tavakkolizadeh, M., and Saadatmanesh, H., (2003b), "Fatigue Strength of Steel Girders Strengthened with Carbon Fiber Reinforced Polymer Patch", *J. Struct. Engrg.*, Volume 129, Issue 2, pp. 186-196 (February 2003).
- Al-Saidy, A.H., Klaiber, F.W. and Wipf, T.J. (2004), Repair of Steel Composite Beams with Carbon Fibre-Reinforced Polymer Plates, *Journal of Composites for Construction*, ASCE, 8(2), pp.163-172
- Schnerch, D., Dawood, M., and Rizkalla, S., "Strengthening Steel-Concrete Composite Bridges with High Modulus Carbon Fiber Reinforced Polymer (CFRP) Laminates", *Proceedings of the Third International Conference on Composites in Construction (CCC 2005)*, Lyon, France, July 11-13, 2005, pp. 283-290.
- Nanni, A., and Mettemeyer, M., (2001), "Diagnostic Load Testing of a Two-Way Post-Tensioned Concrete Slab", *Practice Periodical of Structural Design and Construction*, ASCE, (6) (2001), 73-82.

AUTHOR INDEX

A

Abdul-Fattah, H. 523
Abro, A.M. 223
Ahmed Said, H.O. 75
Ahmed, E.A. 87
Alagusundaramoorthy, P. 363, 399
Al-Gadhib, A.H. 539
Alhassan, M.A. 429
Alliche, A. 511
Al-Mahaidi, R. 71, 235, 425, 737
Alrousan, R.Z. 429
Al-Saidy, A. 597
Al-Shawaf, A. 71
André, A. 627
Anggawidjaja, D. 589
Ansley, M. 155
Aram, M.R. 475
Araújo, M.D. 323
Arduini, M. 685
Argudo, J. 543
Arockiasamy, M. 29
Ascione, F. 211, 441
Ascione, L. 227
Asprone, D. 123
Atadero, R.A. 255
Ayoub, A. 55, 605

B

Badawi, M. 639
Bae, S. 605
Bakht, B. 299
Bakis, C.E. 307, 535
Baky, H.A. 527
Balaguru, P.N. 681
Baluch, M.H. 539
Bambach, M.R. 701
Bank, L.C. 151, 409
Banthia, N. 653
Baratta, A. 367, 371
Basegmez, I.H. 601
Bayrak, O. 543, 563, 665
Bedirhanoglu, I. 601
Belarbi, A. 55, 605
Benedetti, A. 227
Benmokrane, B. 87, 147, 287, 307, 319
Bergström, M. 335
Binici, B. 689
Bisby, L.A. 499
Blanksvärd, T. 609
Borazghi, H. 147
Borri, A. 227, 375

Bottoni, M. 215
Bouadi, A. 673
Bousselham, A. 577
Bradberry, T.E. 307
Brosens, K. 649
Bruno, D. 383
Burgueño, R. 107
Burtscher, S.L. 483

C

Cai, C.S. 251
Camli, U.S. 689
Camotim, D. 421, 725
Campione, G. 197
Cao, S. 193
Carolin, A. 243, 627
Carrazedo, R. 495
Casadei, P. 375
Castori, G. 375
Černý, M. 259
Ceroni, F. 17
Chaallal, O. 577
Chen, J. 67, 391
Cheng, L. 697
Choo, C.C. 239
Choppali, U. 143
Colombi, P. 275, 729
Corb, I. 371
Corbi, O. 367
Cosenza, E. 405
Crawford, J.V. 203
Crews, K.I. 677
Cronin, K. 339
Czaderski, C. 475

D

Dai, J. 39, 589
Darchis, F. 171
Davaran, A. 47
Dawood, M. 705
Debaiky, A.S. 147
Deifalla, A. 581
Demir, C. 601
Devitofranceschi, A. 123
Diab, H.M. 25
Dubini, P. 729

E

Ebaugh, S. 375
Ebead, U.A. 527
El-Gamal, S. 319
El-Hacha, R. 635, 741
El-Ragaby, A. 319
El-Salakawy, E.F. 87, 287, 319

Elsayed, W. 527
Enochsson, O. 387
Erki, M.A. 131
Erp, G.V. 457
Esmaeili, J. 47
Eyre, J.M. 623

F

Faella, C. 219
Fam, A. 163, 721
Fang, Z. 471
Fangueiro, R. 323
Fatemi, H. 47
Fava, G. 275, 729
Fawzia, S. 737
Feng, P. 139, 343, 709, 713
Feo, L. 227, 441
Ferrier, E. 487
Fico, R. 585
Figeys, W. 649
Fitzwilliam, J. 499
Foster, S.J. 183, 437
Frassine, R. 227

G

Galati, D. 95
Galati, N. 103, 231, 491
Gaudagnini, M. 159, 311
Gemert, D.V. 649
Ghobarah, A. 581
Giancaspro, J. 681
Godat, A. 527
Gosain, N. 673
Greco, F. 383
Green, E. 673
Griffith, M.C. 515
Gross, S.P. 203, 307
Grzebieta, R. 701
Gu, D.S. 547

H

Haedir, J. 701
Hamaguchi, Y. 669
Hamed, E. 519
Hamelin, P. 487
Hamilton III, H.R. 315
Hamoush, S. 523
Hanai, J.B.D. 495
Harichandran, R.S. 107
Harik, I.E. 239
Harries, K.A. 59, 91, 283, 339, 379
Harte, A.M. 271
Hejll, A. 331

Hii, A.K.Y. 235
Hiroshi, N. 589
Hollaway, L.C. 1, 643
Honickman, H. 163
Hordijk, D. 35
Hu, Y.M. 503
Huang, Y. 347
Huang, Z. 567

I

Ibell, T.J. 623
Ilki, A. 601
Imjai, T. 159, 311
In, C.W. 339
Ishikawa, T. 669
Issa, M.A. 429
Iwashita, K. 669

J

Jalali, S. 323
Jamwal, A.S. 179
Ji, H.S. 359
Jiang, T. 187
Jin, Y. 479
Jing, D. 193
Jirsa, J.O. 543, 563, 665
JNewhook, J.P. 307
John, M. 355
Johnson, R. 79
Johnsson, H. 627
Ju, M. 295, 593

K

Kalayci, S. 247
Karbhari, V.M. 43, 255
Katz, A. 279, 303
Kaul, R. 207
Keller, T. 291, 351
Key, P.W. 457
Khalid, A.A. 167
Kim, I. 563
Kim, S.D. 339
Klamer, E.L. 35
Kleinman, C.S. 35
Klowak, C. 299
Korynia, R. 619
Kumbasar, N. 601
Kurita, M. 175

L

Labossiere, P. 559
Lees, J. 467
Leng, Q. 479
Li, B. 555
Li, G. 355, 449
Li, H. 471
Li, T. 343, 417

Lignola, G.P. 405
Liu, H. 425
Liu, M. 693
Liu, R. 413
Lonetti, P. 383
Lorenzis, L.D. 95, 613
Lu, X. 391, 733
Lv, Z.T. 547

M

Ma, Z.J. 143, 359
Maher, A. 461
Mahini, S.S. 571
Malik, A.R. 183
Mallat, A. 511
Mancusi, G. 211
Manfredi, G. 227, 405, 585
Manko, Z. 111, 119, 657
Maragakis, E.M. 79
Maricherla, D. 449
Maruyama, K. 551
Masmoudi, R. 445
Matsumoto, A. 551
Matta, F. 151
Mazzotti, C. 215
McNeal, M. 523
Meggers, D. 135
Michael, A.P. 315
Mineo, S. 589
Minnaugh, P.L. 283
Miraglia, N. 197
Mirmiran, A. 127, 247, 555
Mohamed, H. 445
Mohiuddin, J. 539
Monti, G. 227
Mordak, A. 111, 119, 657
Motavalli, M.
Mufti, A. 299, 653

N

Nadauld, J.D. 717
Nanni, A. 103, 123, 151, 227,
231, 491, 585, 623, 685
Nardo, A.D. 219
Nassif, H. 461
Navada, R. 43
Neale, K.W. 527
Newman, N. 55
Nishizaki, I. 99, 453
Nossoni, G. 107

O

Oehlers, D.J. 531
Oh, H. 295
Omar, T. 457
Ombres, L. 51
Orosz, K. 609

Orton, S.L. 665
Ospina, C.E. 307, 535
Otoom, O.F.A. 437
Ouyang, Z. 263, 395, 433
Ozkul, O. 461

P

Pantelides, C.P. 717
Papia, M. 197
Park, C. 593
Park, S. 593
Parretti, R. 123, 585
Parvin, A. 179
Paultre, P. 559
Pecce, M. 17
Peng, H. 479
Pereira, C.G. 323
Phong, N.H. 551
Piazza, M. 227
Pilakoutas, K. 159, 311
Plunkett, J. 135
Poggi, C. 227, 275, 729
Porter, M. 379
Prakash, S.S. 363, 399
Prentice, D.B. 631
Prota, A. 123, 405, 585
Proulx, J. 559
Purdue, J.D. 115

Q

Qian, J. 693
Qian, P. 709, 71
Qu, Z. 391
Quiertant, M. 327, 487

R

Rabinovitch, O. 519
Raftery, G. M. 271
Ragab, N. 741
Ragaby, A.E. 287
Rahman, M.K. 539
Ravindrarajah, R.S. 207
Realfonzo, R. 219
Reeve, B. 91
Ringelstetter, T.E. 151
Rizkalla, S. 83, 705
Rizkalla, S.H. 737
Rizzo, A. 103, 613
Robert, M. 147
Rocca, S. 231, 491
Rodd, P.D. 271
Romagnolo, M. 685
Ronagh, H.R. 571
Rosario, J.A.B.D.L.D. 507
Rosenboom, O. 83
Rotter, J.M. 391
Roy, N. 559

Roy, R.J. 147
Rusinowski, P. 387

S

Sacco, E. 227
Saiidi, M.S. 79
Sarmad, A. 461
Savoia, M. 215
Saxena, P. 63
Schaumann, E. 351
Schueremans, L. 649
Scott, P. 467
Sekijima, K. 551
Seracino, R. 515
Shaat, A. 721
Shahawy, M. 29
Shan, B. 567
Shang, S. 479
Shao, Y. 171
Shawkat, W. 163
Shi, Y. 555
Shield, C.K. 409
Shimomura, T. 99, 175, 551
Shrestha, R. 661
Shyu, C.T. 131
Silva, N.F. 421
Silvestre, N. 421, 725
Sim, J. 295, 593
Sivakumar, M. 29
Smith, S.T. 207, 437, 661, 677
Sohn, H. 339
Son, B.J. 359
Soudki, K. 639
Stao, Y. 39
St-Georges, E. 559
Suksawang, N. 461
Sumiyoshi, K. 39

Sun, N. 193

T

Taillade, F. 327
Takeda, N. 99
Täljsten, B. 331, 335, 387, 609
Tamon, U. 589
Tanaka, H. 175
Tanovic, R. 131
Tazawa, H. 175
Teng, J.G. 67, 187, 643
Tennyson, R.C. 653
Thiagarajan, G. 307
Tian, Y. 543
Tomiyama, T. 453
Tommaso, A.D. 227
Tourneur, C. 327
Toutanji, H. 63

U

Uddin, N. 115, 223
Ueda, T. 11, 39

V

Vaidya, U. 115, 223
Vallée, T. 351
Vanevenhoven, L.M. 409
Vyas, J.S. 155

W

Waldron, P. 159, 311
Wan, B. 263, 395, 433
Wang, J. 21
Wang, M. 479
Wang, Y. 135
Weber, A. 267
Widianto, 543

Wight, R.G. 131, 631
Willis, C.R. 515
Wu, G. 547
Wu, Y. 347
Wu, Z. 25, 75, 547, 669

X

Xia, S.H. 515
Xiao, Y. 567
Xie, A. 131

Y

Yalim, B. 247
Yang, Q. 515
Yao, J. 67
Ye, L. 139, 343, 391, 709,
713, 733
Yishizuka, Y. 99
Yokota, H. 39
Yost, J.R. 203
Young, B. 725
Yuan, H. 413
Yue, Q. 733

Z

Zhang, L. 643
Zhang, S.S. 643
Zhang, Y. 251, 291
Zhao, L. 63, 155
Zhao, X. 71, 425, 701, 737
Zheng, R. 127
Zheng, Y. 733
Zhou, E. 135
Zhuo, J. 417
Zorn, A. 91

KEYWORD INDEX

A

Accelerated bridge construction 151
Accelerated durability test 267
Acoustic emission 143
Active sensing 339
Additives 1
Adhesion 441
Adhesive 59, 87, 91, 275, 729
-- bonding 39, 271, 531
-- joints 291
Advanced composite materials 597
Aggregate interlock 235
Al (aluminum alloy) 709
Aluminum 713, 717
Amount of carbon dioxide emissions 175
Analysis 239
Anchor 87
Anchorage 665
-- strength models 63
Anti-corrosion 709
Arches 375
Axial loads 179, 713

B

Baseline-free nondestructive testing 339
Beam-column connections 661
Beams 449, 471, 527
Beam-strengthening 279
Behavior 577
Bend capacity 311
Bending 701
-- loading 167
Bent concrete surface 413
Blast loading 127
Blast mitigation 123
Bolting 531
Bond 35, 43, 55, 63, 87, 95, 263, 283, 307, 347, 395, 433, 433, 669, 677
-- behavior 705
-- behavior and strength 17
-- configuration 39
-- length 63
-- strength 107, 511, 689
Bonded 631
-- joints 441
Bonding 519, 665, 737
Bond-Slip Model 737
Boundary element (BE) method

425

Bridge deck 151, 251, 299, 351, 697
Bridge rehabilitation 29
Bridge repair 657
Bridges 111, 123, 147, 287, 653, 721
Buckling 171, 405, 713

C

Cantilever 299
Carbon 507
-- epoxy 327
-- fiber anchors 665
-- fiber fabric 417
-- fiber laminates 29
-- fiber reinforced plastic 193
Carbon fiber reinforced polymer (CFRP) 35, 71, 183, 207, 235, 263, 275, 387, 395, 425, 429, 467, 471, 479, 483, 487, 547, 559, 635, 639, 673, 705, 709, 713, 721, 729, 733, 741
-- anchors 563
-- grids 609
-- laminates 685
-- reinforcement 315
-- rods 685
-- sheets 539, 543, 563, 597, 631, 665
-- strengthening 331
-- strips 119, 619
-- tapes 111, 657
Carbon fiber sheets 725
Carbon fibres 215, 259, 609, 643
Case study 175
Chloride 335
Cladding 163
Code provisions 219
Cohesive zone model 21
Cold-climate 331
Cold-formed steel columns 725
Columns 179, 183, 239, 409, 601
Composite curved beam 167
Composite pipe 713
Composite rebar 267
Composite sandwich panel 359, 363
Composite structures 211, 441, 709
Composite wedge 483
Composites 123, 163, 215, 259, 457, 643, 741

Compressive stress-strain model 693
Computational simulation 383
Concrete 17, 21, 207, 243, 279, 287, 311, 319, 323, 327, 391, 433, 449, 495, 507, 547, 601, 681, 689, 741
-- beam 67
-- bridge deck 295
-- bridges 259
-- columns 193, 405
-- confinement 315, 355
-- cylinder 693
-- jacketing 551
-- repair 631
Concrete-filled steel tubes 503
Confined concrete 179
Confinement 183, 187, 197, 207, 219, 231, 449, 487, 491, 495, 499, 503
Connections 717
Construction 673
-- guides 247
Continuous fiber rope 551
Core reinforced braided composite rod 323
Core reinforced braided fabric 323
Corrosion 311, 335, 597
-- resistance 139, 343, 453
Cost-efficiency 359, 363
Crack debonding 51
Crack propagation 425
Crack widths 159, 203, 307, 535
Cracking 107, 535
Creep 207, 211, 215, 567
Creep fracture propagation 25
Criticality 43
Curvature 335
Curved FRP bar 311
Cyclic loading 555, 559
Cycling test 143
Cylinder 449

D

Debond 29
Debonding 21, 35, 47, 59, 75, 83, 91, 107, 139, 275, 339, 383, 413, 619, 729
-- failures 71, 613
Deck 147, 287
-- slabs 319
Defect 43
Deflection 159, 203, 319

Degradation 335
Delamination 107
Deployable 457
Design 187, 239, 243, 487, 585
-- guidelines 11, 227, 605
-- methods 235
-- of strengthening 255
-- value 267
Deterioration 263, 179, 395
Development length 57
Diagnosis 623
Disbonds 327, 523
Distortional failure 725
Distortional post-buckling 421
Double shear lap 729
Double-lap shear 71
Ductility 47, 231, 315, 429, 491,
551, 571, 589
Durability 1, 267, 271, 275, 379,
453, 467
Dynamic analysis 127
Dynamic response 251
Dynamic tests 79

E

Earthquake damage 567
Eccentric loading 193
Eccentric loads 499
Effect 43
Effective bond length 71
Environmental aspect 175
Environmental impacts 303
Epoxy 167
-- Mortar 461
Existing civil constructions 227
Experimental database 693
Experimental results 685
Experimental validation 367
Expert-system 623
External bonding 437, 661, 677
Externally bonded 515, 635, 741
Externally pre-stressed 471
Extrapolation 267

F

Failure 239, 291
-- simulation 139
Far East 11
Fatigue 91, 139, 147, 283, 287,
717
-- life 425, 733
-- loading 669
-- test 155
-- testing 299
FEA 429, 441
FE-analysis 387
FEM analysis 657

Fiber 601
-- reinforced composite materials
323
-- reinforced plastics 271, 453
-- reinforced repair mortars 511
Fiberglass sheet piling 171
Fibre reinforced composite 159
Fibreglass 131
Fibre-reinforced polymer (FRP)
21, 39, 47, 51, 56, 63, 67, 79, 83,
95, 99, 107, 123, 127, 147, 151,
163, 179, 187, 197, 211, 219,
227, 239, 243, 251, 287, 319,
327, 347, 351, 355, 375, 379, 391,
433, 437, 445, 449, 495, 499,
503, 515, 519, 527, 531, 555,
567, 571, 585, 605, 613, 623,
661, 673, 677, 693
-- bridge 135
-- composite deck 155
-- composites 399, 421, 593, 627,
697, 717
-- confinement 405
-- deck panels 143
-- experimental 581
-- guideline 531
-- laminates 17, 279
-- poles 445
-- rebar 303
-- reinforcements 11, 367, 371,
535
-- repair systems 247
-- shape 11
-- sheets 75, 413, 577, 589, 669,
737
-- strengthening 383
-- structural Shapes 445
-- structures 175
-- U-jacketing anchorage 669
-- wraps 499
FRP/concrete bond 79
FRP-concrete interface 25
FRP-concrete structure 343
FRP-strengthening 231, 491, 725
Field load test 119
Field tests 111, 135
Filament Winding 445
Film adhesive 643
Finite element 359, 363, 433
-- analysis (FEA) 223, 697
-- modeling 103, 399, 437
Fire protection 681
Flax fibres composites 627
Flexural behaviour 445, 471
Flexural strength capacity 429
Flexural strengthening 39, 619
Flexure 91, 307, 527, 635, 741

Footbridge 99
Fracture energy release rate 43
Fracture mechanics 75
Full-scale test 539

G

Generalized beam theory (GBT)
421
Girder 635
Glass fiber 167
Glass-fibre reinforced polymer
(GFRP) 87, 299, 461
-- stirrup 593
Glass/polypropylene 223
Global buckling 409
Gradient method 475
Grids 355, 449

H

Hanger 457
Hardening 127
High durability 593
High strength concrete 203
High-modulus 741
High-temperature 681
Hollow core slab 539
Hollow sections 405
Hot melt pre-impregnated
composites 643
Hybrid 351
-- columns 555
-- constructions 1
-- FRP-steel core 359, 363
Hydraulic gate 453

I

Intermediate crack (IC) debonding
67
Impact traffic load 135
Infrastructure rehabilitation 1
Inorganic 681
-- epoxy 63
Interaction curves 219
Interface 67
-- models 383
-- region relative humidity (IRRH)
263
Interfacial fracture energy 413

J

Jacketing 589
Jackets 187
Joint 571
Jute fiber 167

L

Laboratory tests 371, 609

Large fracturing strain 589
Life cycle 335
-- cost 99
Life cycles assessment 303
Light-weight 709
-- concrete 351
-- structure 343
-- superstructure 139
Limit states 259
Live load model 295
Load bearing walls 399
Load capacities 171
Load distribution 251
Load rating 103
Load testing 653
Local buckling 409, 421, 701
Local reinforcement 197
Local-plate failure 725
Long-term behaviour 211
Low velocity impact 115
Load and Resistance Factor Design (LRFD) 255

M

Masonry 17, 375, 399, 519, 689
-- panel 371
-- vaults 367
-- walls 515
Material variability 255
MBC 609
Mechanical anchorages 631
Mechanical characterization 511
Mechanically fastened fiber reinforced polymers (MF-FRP) laminates 103
Mineral based strengthening 609
Modelling 405
Modified compression field theory (MCFT) 391
Modified virtual crack closure (VCCT) 433
Moisture 395
Moveable bridge 155
Moving traffic load 135

N

Natural fibres 627
Near surface mounted (NSM) 619, 639, 685
-- reinforcement 95, 613
Nondestructive testing 327
Nonlinear viscoelastic model 25
Near surface mounted (NSM) 619, 639
Numerical simulation 395

O

Openings 387
Out-of-plane loading 515

P

Parameters 577
Performance-based design 559
Permanent framework 343
Physico-chemical characterization 511
Pier 123
Plaster 689
Plasticity 495
Plates 635, 741
Plating 685
Polymer composites 1
Polypropylene jacket 115
Polyurethane 163
Post-tensioned 507
-- concrete beam 657
Practical application 11
Pre-stressed 417, 639
-- CFRP 475
-- concrete (PC) 83, 99, 471
-- concrete beam 111, 119, 475
-- slab 539
Pre-stressing 483, 631
-- force 479
-- tendons 467
Prismatic columns 231, 491
Probabilistic 243
Probability and reliability analysis 295
Prototype 649
Pull-off testing 59
Pull-out testing 95
Pulsating load 295
Pultruded composites 171
Pultruded shapes 211, 215
Pultruded structural shapes 131
Pultrusion 291, 409, 441

Q

Quality control/assurance (QC/QA) 59

R

Reactive powder concrete 183
Refurbishments technique 371
Rehabilitation 563, 597, 717
Reinforced 507
Reinforced concrete (RC) 51, 83, 123, 159, 231, 235, 247, 347, 379, 437, 491, 527, 531, 555, 563, 571, 585, 661, 673
-- beams 47, 429, 577, 613, 639
-- bridge column 559
-- columns 187, 219, 487, 499

Reinforced masonry 379
Reinforcement 375, 379, 417, 487
Repair 523, 543, 721
-- and Retrofit 127
-- mortar 685
-- stages 111
Repairing techniques 461
Research 11
-- need 577
Residual performance 567
Residual thickness of concrete (RTC) 263
Resistance factors 255
Retrofit 283, 601
Retrofitting 243, 347, 399, 531, 597
Reverse taper 705
Rib 449
Road bridge 119

S

Safety 155
-- concept 267
Sandwich 351
-- panel 163
Scarf 523
Seismic loading 547
Seismic retrofit 559, 567
Seismic retrofitting 551
Seismic strengthening 227
Selection-criteria 623
Serviceability 203, 535
Shallow depth patch 107
Sharp corners 197
Shear 391, 437, 527, 577, 581, 585, 601, 605, 609
-- capacity 593
-- failure 343
-- strength 589
-- strengthening 613
-- stress 737
Shearography 327
Sheets 635, 721, 741
Shelters 457
Short span bridge 131
Shrinkage 107
Single shear lap 729
Slab-column connection 543
Slabs 387, 527, 535
Slenderness 499
Slip 95, 737
Smear crack 75
Smoothed corners 197
S-N curve 669
Solution uptake 467
Spalling resistance 413
Span effect 75

Splice joints 705
Sprayed fiber reinforced polymers 653
Spun-cast piles 315
Square cross-section 197
Square cylinders 355
Standard 11
Static 635
-- field load test 657
-- loads 111, 119, 577
-- testing 299
Steel 275, 635, 721, 741
-- bridges 705
-- cord reinforced polymer (SCRCP) 649
-- fiber reinforced polymer (SFRP) 283
-- plate 733
-- reinforced polymers (SRP) 123, 375, 631
-- tubes 701
Stiffened plate 697
Stiffener 449
Stiffness 335
-- degradation 143
Strain gradient 193
Strain rate 79
Strains 319
Strarch 457
Strength 291, 547
Strengthen 471

Strengthening 21, 67, 259, 347, 387, 391, 429, 437, 475, 479, 519, 527, 539, 543, 577, 581, 597, 605, 609, 623, 627, 631, 635, 649, 653, 661, 677, 733
-- effect 331
Stress-concentration 197
Stretching 479
Strips 635
Structural analysis 371
Structural health monitoring (SHM) 331, 335, 339
Subzero temperature 71
Supporting conditions 519
Surface flaws 247
Surface preparation 59
Sustained load 203
Swelling 467

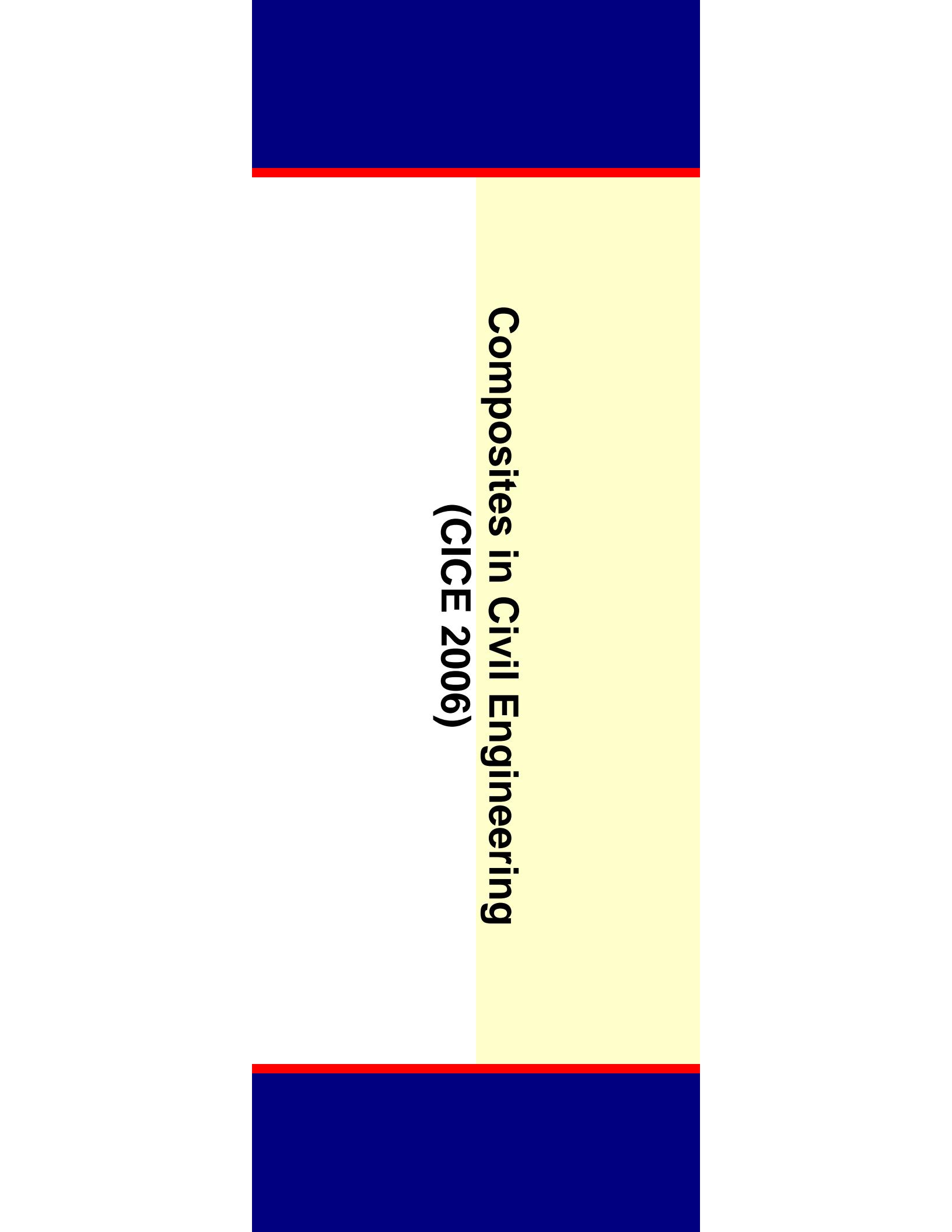
T
Thickness/depth (T/d) ratio 429
Temperature 35
Tensile 523, 733
-- strength 311
Tension perpendicular to the grain 627
Testing 319, 347
-- procedure 17
Tests 503
T-girders 581
Theoretical model 503

Theoretical setup 367
Thermal stresses 35
Thermoplastic 147
-- composite 115, 223
Thin-walled members 421
Thin-walled steel sections 701
Timber 677
-- Pile 461
Time dependent behaviour 207
Time-reversal acoustics 339
Torsion 235, 581
Truss 457
Two-dimensional 523
Two-way shear 543

U
Ultimate strength 725
Upgrade 673

V
Vehicle bridge interaction 251
Very cold temperatures 143

W
Weather resistance 453
Wed-bonded 571
Wedge anchorage 483
Wide-flange profiles 409
Wood 271, 681
WSGG anchor 417



**Composites in Civil Engineering
(CICE 2006)**



Organized by

and



Sponsored by



ISBN: 0-615-13586-2

CICE2006 Secretariat
Department of Civil and Environmental Engineering
Florida International University (FIU)
10555 West Flagler Street, Miami, FL 33174, USA
Phone: 305-348-2314
Fax: 305-348-2802
E-mail: cice2006@fiu.edu